

# UC Berkeley

## UC Berkeley Electronic Theses and Dissertations

### Title

Experimental and Analytical Studies on the Seismic Behavior of Conventional and Hybrid Braced Frames

### Permalink

<https://escholarship.org/uc/item/41m3t7wg>

### Author

Lai, Jiun-Wei

### Publication Date

2012

Peer reviewed|Thesis/dissertation

# **Experimental and Analytical Studies on the Seismic Behavior of Conventional and Hybrid Braced Frames**

**by**

**Jiun-Wei Lai**

A dissertation submitted in partial satisfaction of the

requirements for the degree of

Doctor of Philosophy

in

Engineering – Civil and Environmental Engineering

in the

Graduate Division

of the

University of California, Berkeley

Committee in charge:

Professor Stephen A. Mahin, Chair

Professor Bozidar Stojadinovic

Professor Douglas S. Dreger

Spring 2012

# **COPYRIGHT**

Experimental and Analytical Studies on the Seismic  
Behavior of Conventional and Hybrid Braced Frames

Copyright©2012 by Jiun-Wei Lai

All rights reserved.

# ABSTRACT

Experimental and Analytical Studies on the Seismic  
Behavior of Conventional and Hybrid Braced Frames

by

Jiun-Wei Lai

Doctor of Philosophy in Engineering – Civil and Environmental Engineering

University of California, Berkeley

Professor Stephen A. Mahin, Chair

This dissertation summarizes both experimental and analytical studies on the seismic response of conventional steel concentrically braced frame systems of the type widely used in North America, and preliminary studies of an innovative hybrid braced frame system: the Strong-Back System. The research work is part of NEES small group project entitled “International Hybrid Simulation of Tomorrow’s Braced Frames.”

In the experimental phase, a total of four full-scale, one-bay, two-story conventional braced frame specimens with different bracing member section shapes and gusset plate-to-beam connection details were designed and tested at the NEES@Berkeley Laboratory. Three braced frame specimens were tested quasi-statically using the same predefined loading protocol to investigate the inelastic cyclic behavior of code-compliant braced frames at both the global and local level. The last braced frame specimen was nearly identical to one of those tested quasi-statically. However, it was tested using hybrid simulation techniques to examine the sensitivity of inelastic behavior on loading sequence and to relate the behavior observed to different levels of seismic hazard.

Computer models of the test specimens were developed using two different computer software programs. In the software framework OpenSees fiber-based line elements were used to simulate global buckling of members and yielding and low-cycle fatigue failure at sections. The LS-DYNA analysis program was also used to model individual struts and the test specimens using shell elements with adaptive meshing and element erosion features. This program provided enhanced ability to simulate section local buckling, strain concentrations and crack development. The numerical results were compared with test results to assess and refine the ability of the models to predict braced frame behavior. A series of OpenSees numerical cyclic component simulations were then conducted using the validated modeling approach. Two hundred and forty pin-ended struts with square hollow structural section shape were simulated under cyclic loading to examine the effect of width-to-thickness ratios and member slenderness ratios on the deformation capacity and energy dissipation characteristics of brace members.

The concept of a hybrid system, consisting of a vertical elastic truss or strong-back, and a braced frame that responds inelastically, is proposed herein to mitigate the tendency of weak-story mechanisms to form in conventional steel braced frames. A simple design strategy about member sizing of the proposed Strong-Back System is provided in this study. To assess the ability of the new Strong-Back System to perform well under seismic loading, a series of

inelastic analyses were performed considering three six-story hybrid braced frames having different bracing elements, and three six-story conventional brace frames having different brace configurations. Monotonic and cyclic quasi-static inelastic analyses and inelastic time history analyses were carried out. The braced frame system behavior, bracing member force-displacement hysteresis loops, and system residual drifts were the primary response quantities examined. These indicated that the new hybrid system was able to achieve its design goals.

Experimental results show for the same loading history that the braced frame specimen using round hollow structural sections as brace members has the largest deformation capacity among the three types of bracing elements studied. Beams connected to gusset plates at the column formed plastic hinges adjacent to the gusset plate. The gusset plates tend to amplify the rotation demands at these locations and stress concentrations tended to result in early fractures of the plastic hinges that form. To remedy this problem, pinned connection details used in the last two specimens; these proved to prevent failures at these locations under both quasi-static and pseudo-dynamic tests. Failure modes observed near the column to base plate connections in all of the specimens suggest the need for further study. Both OpenSees and LS-DYNA models developed in this study predict the global braced frame behavior with acceptable accuracy. In both models, low-cycle fatigue damage models were needed to achieve an acceptable level of fidelity. Shell element models were able to predict local behavior and the mode of failures with greater but not perfect confidence. OpenSees analysis results show that the proposed hybrid braced frames would perform better than conventional braced frames and that the story deformations are more uniform. Finally, future research targets are briefly discussed at the end of this dissertation.

## **DEDICATION**

To my parents, family members, teachers and friends.

## ACKNOWLEDGMENTS

This doctoral dissertation would not have been written without the support of many individuals, and the author wants to express his deepest appreciation to them. Only some of them are particularly mentioned here.

Above all things, the author would like to thank his principal research advisor, Professor Stephen A. Mahin for his support and patience. Without his advice, help and encouragement, this dissertation would not have been possible. The author heartily acknowledges Professors Bozidar Stojadinovic and Douglas S. Dreger (from the Department of Earth and Planet Science) for serving as the members of dissertation committee and providing advice on this work. Constructive suggestions regarding this research work from Professors James M. Kelly, Abolhassan Astaneh-Asl, and Ming Gu (from the Department of Mathematics) during the qualifying examination are also deeply appreciated.

Financial support of this research was provided in part by the National Science Foundation under grant number NSF-0619161, NEESR-SG: "International Hybrid Simulation of Tomorrow's Braced Frame Systems." This support is greatly appreciated.

Laboratory assistance provided by NEES@Berkeley Laboratory and the Department of Civil and Environmental Engineering is appreciated. In particular, the assistance by managers of NEES@Berkeley Laboratory, Don Clyde and Dr. Shakhzod Takhirov, is greatly acknowledged. The author would also like to thank the engineers and technicians at both the NEES@Berkeley Laboratory and Davis Hall Structural Laboratory, including Wesley Neighbour, Donald Patterson, David MacLam, Nathaniel Knight, Jose Robles, Robert Cerney, Bill MacCracken, and Jeff Higginbotham. Full-scale specimen preparation assistance by a number of students, including Yuichi Maeda, Carl Misra and Charbel Moubarak is greatly appreciated. Special thanks are also directed to Dr. Andreas Schellenberg, Dr. Selim Gunay, and Kung-Juin Wang for their help on the hybrid simulation tests. Library assistance provided by Charles James and NISEE staff is gratefully appreciated. The assistance of Claire Johnson in proofreading this dissertation is also appreciated.

The author would like to show his gratitude to the Herrick Steel Corporation for donating four full-scale specimens, providing lab fabrication manpower, and shop drawing supports; California Erectors for providing the second specimen lab fabrication manpower; Schuff Steel Company for providing test specimens; and Iron Workers Union Local 378 for donating manpower for specimen fabrication. Without their generous help, the full-scale testing program would not have been possible. Finite element analysis software supported by ARUP Engineers is gratefully acknowledged.

Many researchers and engineers around the world including Professor Charles Roeder, Professor Keh-Chyuan Tasi, Rafael Sabelli, Walterio A. López, Dr. Patxi Uriz, Frances Yang, Ronald O. Hamburger, and Brett R. Manning provided valuable suggestions and comments along this research project. Although not all of these suggestions were incorporated into this study, the author would like to thank for their time on reviewing and providing professional advice.

The author personally would like to acknowledge the financial support provided by several sources, including the Graduate Student Scholarship from the Department of Civil and Environmental Engineering, William H. and Helena I. S. Popert Research Fellowships in Civil Engineering, Tse-Wei Liu Memorial Fellowship, and Dr. and Mrs. James C.Y. Soong

Fellowships from Graduate Division, the Byron and Elvira Nishkian Professorship in Structural Engineering, and the Scholarships for Studying Abroad Ph.D. Students from Taiwanese government. Without this generous financial support, the author could not have focused on the research and complete this academic dissertation smoothly.

In addition, the author must also thank his friends at UC Berkeley, Chui-Hsin Chen, Chin-Long Lee, Hong Kim, Yuli Huang, Frank McKenna, Dimitrios Konstantinidis, Tony Yang, Troy Morgan, Tracy Becker, Juan Carlos Reyes Ortiz, Wael M. Hassan, and Ken Orgozalek, for providing thoughtful suggestions and many useful discussions along this long journey.

While this dissertation is due to the contributions of many, the findings, conclusions and recommendations are those of the author alone.

Finally, the author would like to thank to his parents and family members. Without their constant support and love, this dissertation would have never been possible. He would like to share with them the joy of completing this doctoral degree and hope this dissertation makes them proud.



# TABLE OF CONTENTS

ABSTRACT.....	1
ACKNOWLEDGMENTS .....	I
TABLE OF CONTENTS .....	III
LIST OF FIGURES .....	VII
LIST OF TABLES .....	XLVI
1 INTRODUCTION .....	1
1.1 Background and Research Motivation .....	1
1.2 Research Objectives and Scope .....	3
1.3 Overview and Organization of Dissertation.....	4
2 LITERATURE REVIEW .....	6
2.1 Bracing Component .....	6
2.1.1 Issues Related to Net Reduced Section .....	6
2.1.2 Limitations on Slenderness Ratio and Width-to-Thickness Ratio .....	8
2.1.3 Experimental Studies on Brace Components .....	14
2.1.4 Analytical Modeling of Bracing Component .....	17
2.2 Gusset Plate Connection .....	18
2.2.1 The 30° Design Concept .....	18
2.2.2 Stability Issue .....	24
2.2.3 Connection Shape and Seismic Detail .....	25
2.3 Braced Frame System .....	26
2.3.1 Experimental Work on Braced Frame Systems .....	26
2.3.2 Frame Action in Braced Frame System .....	28
2.4 Steel Braced Frame Behavior during Past Earthquakes.....	28
2.4.1 Past Earthquakes in the United States .....	28
2.4.2 Past Earthquakes in Japan .....	31
2.5 Concluding Remark .....	34
3 EXPERIMENTAL PROGRAM AND SPECIMEN DESIGN .....	35

3.1	Background .....	35
3.2	Experimental Program at University of California, Berkeley.....	36
3.3	Selection and Design of Test Setup .....	43
3.4	Test Setup at NEES@Berkeley Facility .....	45
3.5	Description of Test Specimens .....	50
3.6	Loading Sequence for Quasi-Static Tests .....	61
3.7	Instrumentation .....	62
3.8	Specimen Construction Sequence.....	67
3.8.1	Specimen TCBF-B-1 .....	67
3.8.2	Specimen TCBF-B-2.....	74
3.8.3	Specimen TCBF-B-3.....	83
3.8.4	Specimen TCBF-B-4.....	87
3.9	Relation of specimen Design to Prototpye Design .....	93
3.9.1	Model (Prototype) Building .....	93
3.9.2	Seismic Forces.....	94
3.10	Experimental Controls .....	104
3.10.1	Quasi-Static Tests.....	104
3.10.2	Hybrid Simulation.....	104
4	EXPERIMENTAL RESULTS OF FOUR SPECIMENS.....	107
4.1	Material Properties.....	107
4.2	Quasi-Static Test Results of First Three Specimens.....	111
4.2.1	Specimen TCBF-B-1 (Square HSS Braces, Quasi-Static Test) .....	111
4.2.2	Specimen TCBF-B-2 (Round HSS Braces, Quasi-Static Test).....	181
4.2.3	Specimen TCBF-B-3 (Wide Flange Braces, Quasi-Static Test).....	264
4.3	Hybrid Simulation Test Results of Specimen TCBF-B-4 (Square HSS Braces).....	335
4.3.1	Key Response Quantities .....	337
4.3.2	Main Observations .....	392
5	DISCUSSION OF EXPERIMENTAL RESULTS .....	404
5.1	Quasi-static Test Results .....	404
5.1.1	Specimen Global Behavior.....	405
5.1.2	Brace Behavior.....	426

5.1.3	Column Behavior .....	439
5.1.4	Beam Behavior .....	440
5.1.5	Panel Zone Behavior .....	442
5.1.6	Gusset Plate Behavior .....	443
5.1.7	Test Setup Behavior .....	443
5.2	Hybrid Simulation Results .....	443
5.2.1	Specimen Global Behavior.....	445
5.2.2	Brace Behavior .....	454
5.2.3	Column Behavior .....	458
5.2.4	Beam Behavior .....	459
5.2.5	Panel Zone Behavior .....	460
5.2.6	Gusset Plate Behavior .....	460
5.2.7	Test Setup Behavior .....	461
5.2.8	Performance of Servo-Hydraulic Control System .....	461
5.3	Concluding Remarks .....	463
6	ANALYTICAL MODELLING USING OPENSEES AND LS-DYNA.....	465
6.1	Calibration using Data Derived From Previous Strut Tests.....	465
6.2	Prediction of Quasi-static Test Results .....	471
6.3	Predicting the Hybrid Simulation Results.....	476
6.4	Comparison of Square HSS Brace Cyclic Behaviors using OpenSees.....	486
6.5	Prediction of Strut and Braced Frame Specimen Behaviors using LS-DYNA.....	498
6.5.1	LS-DYNA Analysis of Individual Struts .....	498
6.5.2	LS-DYNA Analysis of Quasi-static TCBF Test Specimens.....	505
6.6	Concluding Remarks .....	512
7	HYBRID BRACED FRAMES: THE STRONG-BACK SYSTEM .....	513
7.1	Introduction .....	513
7.2	Previous Study .....	514
7.3	The Proposed Hybrid Braced Frame System.....	517
7.4	Analytical Study of the Strong-back System .....	521
7.4.1	Example Building.....	521
7.4.2	Seismic Force-Resisting Systems and Design Strategies.....	522

7.4.3	Modeling .....	531
7.4.4	Ground Motions .....	531
7.5	Response of Hybrid Strong-back System .....	533
7.5.1	Monotonic Pushover Results.....	533
7.5.2	Quasi-static Cyclic Results.....	533
7.5.3	Nonlinear Response History Analysis Results.....	536
7.6	Discussion .....	542
7.6.1	Pushover Analysis.....	542
7.6.2	Dynamic Analysis .....	542
7.7	Concluding Remarks.....	582
8	CONCLUSIONS AND RECOMMENDATIONS .....	583
8.1	Experimental Phase.....	583
8.2	Analytical Phase.....	586
8.3	Recommendations for Future Research .....	588
	REFERENCES.....	589
	APPENDICES.....	598

## LIST OF FIGURES

Figure 2.1	Net section failure mode in a brace without reinforcing plates (extracted from Figures 9 and 16 of Yang and Mahin, 2005) .....	7
Figure 2.2	Other possible net section reinforcing schemes .....	8
Figure 2.3	Illustration of Whitmore effective width for bolted (Whitmore, 1952) and welded connections (Astaneh-Asl, 1982).....	19
Figure 2.4	Dimension of gusset plate specimens in the preliminary tension tests (extracted from Fig. 10 of Wyss, 1923).....	20
Figure 2.5	The Warren truss specimen tested by Wyss in 1923 (extracted from Figs. 17 and 22 of Wyss, 1923).....	21
Figure 2.6	Illustration of rigid core in a gusset plate (extracted from Fig. 22 of Wyss, 1923) ...	22
Figure 2.7	The stress trajectories of preliminary test specimens (extracted from Figs. 33 and 34 of Wyss, 1923).....	23
Figure 2.8	Illustration of stress distribution in a gusset plate (extracted from Fig. 38 of Wyss, 1923) .....	23
Figure 2.9	Illustration of characteristic length of equivalent unit strips within the Whitmore effective width for bolted and welded connections .....	24
Figure 2.10	Illustration of typical and elliptical yield line patterns to accommodate brace out-of-plane buckling (where $t_g$ is thickness of gusset plate) .....	25
Figure 2.11	Connection details of beam end moment release .....	28
Figure 2.12	Brace failures observed in the 1971 San Fernando Earthquake .....	30
Figure 2.13	Brace failures observed in the 1994 Northridge Earthquake.....	30
Figure 2.14	Global buckling of braces during 1995 Hyogoken-Nanbu (Kobe) Earthquake (extracted from AIJ, 1995).....	32
Figure 2.15	Connection failures in 1995 Hyogoken-Nanbu (Kobe) Earthquake (extracted from AIJ, 1995) .....	33
Figure 2.16	Bolt failures in 1995 Hyogoken-Nanbu (Kobe) Earthquake (extracted from AIJ, 1995) .....	33
Figure 2.17	Brace connection failures observed in the 2011 Great Eastern Japan Earthquake Disaster .....	34

Figure 3.1	Different specimen types for each testing facility in the experimental phase of the NEES research project .....	36
Figure 3.2	Test matrix of the 2D braced frame specimens in the research project.....	38
Figure 3.3	Overview of specimen SCBF-1 before test (Uriz, 2005) .....	39
Figure 3.4	Overview of TCBF-1 specimens during the test .....	39
Figure 3.5	Application of stacked chevron braced frame in a building structure.....	40
Figure 3.6	Application of two-story split-X braced frame in a building structure .....	41
Figure 3.7	Application of two-story diamond shape braced frame in a building structure .....	42
Figure 3.8	Possible testing configurations at the University of California, Berkeley during the specimen design phase.....	44
Figure 3.9	Overview of the final test setup.....	46
Figure 3.10	Construction of reconfigurable reaction wall before pre-stressing .....	46
Figure 3.11	Atlas 1.5 M-lb actuators at both floor levels .....	47
Figure 3.12	The built-up floor beam after painting .....	47
Figure 3.13	Load transfer beams below strong floor before erection.....	48
Figure 3.15	Lateral stability frame (the orange cantilever beam and three blue HSS columns) in the test setup view from south-east side of lab .....	49
Figure 3.14	Four load transfer beams below the strong floor after pre-stressing.....	49
Figure 3.16	Dimension of test specimen.....	52
Figure 3.17	Member sizes of test specimen TCBF-B-1 .....	52
Figure 3.18	Member sizes of test specimen TCBF-B-2 .....	53
Figure 3.19	Member sizes of test specimen TCBF-B-3 .....	53
Figure 3.20	Member sizes of test specimen TCBF-B-4 .....	54
Figure 3.21	Specimen TCBF-B-1 before test .....	56
Figure 3.22	Specimen TCBF-B-2 before first trial.....	56
Figure 3.23	Specimen TCBF-B-3 before test .....	57
Figure 3.24	Specimen TCBF-B-4 before hybrid simulation .....	57
Figure 3.25 (a)	The sub-assemblages of specimens TCBF-B-1 and TCBF-B-2 .....	58
Figure 3.25 (b)	The sub-assemblages of specimens TCBF-B-3 and TCBF-B-4.....	58
Figure 3.25 (c)	The sub-assemblages of specimens TCBF-B-2 and TCBF-B-3 .....	59
Figure 3.25 (d)	The sub-assemblages of specimens TCBF-B-3 and TCBF-B-4.....	59

Figure 3.26	The ¾ inch one-piece gusset plate after tack welding to column flange.....	60
Figure 3.27	Detail view of reinforcing plate of TCBF-B-2 specimen.....	60
Figure 3.28	Cyclic loading protocol for TCBF-B-1, TCBF-B-2 and TCBF-B-3 specimens .....	61
Figure 3.29	The 1.5 million pound load cell.....	64
Figure 3.30	Baldwin 4 million pound universal test machine .....	64
Figure 3.31	Steel jacket for rotating the 1.5 M-lb actuator during the load cell calibration.....	65
Figure 3.32	Overview of the calibration setup during the load cell calibration .....	65
Figure 3.33	Reusable magnetic labels for TCBF-B specimens .....	66
Figure 3.34	Distribution of reusable magnetic labels on TCBF-B specimens .....	66
Figure 3.35	The 1-1/8 inch diameter all-thread anchor bolt .....	68
Figure 3.36	The lateral supporting tee section.....	68
Figure 3.37	Tee section sitting on the lateral supporting saddles .....	69
Figure 3.38	Steel angle kickers below the tee section .....	69
Figure 3.39(a)	Filler material used in the welding process.....	70
Figure 3.39(b)	Standard shim plates for the column base adjustment.....	70
Figure 3.40(a)	Specimen TCBF-B-1 lower beam-to-gusset plate connection details .....	71
Figure 3.40(b)	Specimen TCBF-B-1 lower beam-to-gusset plate connection weld details .....	71
Figure 3.41	Key construction steps of TCBF-B-1 specimen.....	72
Figure 3.42	Key welding processes of TCBF-B-1 specimen .....	73
Figure 3.43	Damaged specimen after cutting off the square HSS braces.....	75
Figure 3.44	Splicing the lower beam to one-piece gusset plates in TCBF-B-2 specimen.....	75
Figure 3.45	Key construction steps of TCBF-B-2 specimen.....	76
Figure 3.46	Key welding processes of TCBF-B-2 specimen .....	77
Figure 3.47(a)	Specimen TCBF-B-2 lower beam-to-gusset plate connection details .....	78
Figure 3.47(b)	Specimen TCBF-B-2 lower beam-to-gusset plate connection weld details .....	78
Figure 3.48(a)	Crack in the CJP weld at west column base (north-west corner).....	79
Figure 3.48(b)	Crack in the CJP weld at east column base (south-east corner) .....	79
Figure 3.49	Three-step crack detecting spray .....	80
Figure 3.50	Crack detecting spray applied in the CJP weld at east column base (south-east corner).....	80
Figure 3.51	The east column base (south-east corner) after gouging the cracked welds .....	81

Figure 3.52	The west column base after weld repairs .....	81
Figure 3.53	The east column base after weld repairs.....	82
Figure 3.54	The entire TCBF-B-2 specimen after whitewash painting.....	82
Figure 3.55	Lower beam to one-piece gusset plate connection detail .....	84
Figure 3.56	Roof beam, gusset plate and brace sub-assemblage of TCBF-B-3 specimen .....	84
Figure 3.57	Key construction steps of TCBF-B-3 specimen.....	85
Figure 3.58	Key welding processes of TCBF-B-3 specimen .....	86
Figure 3.60	Connection detail of the lower beam to one-piece gusset plates of TCBF-B-4 specimen .....	88
Figure 3.59	Damaged specimen after cutting off the wide flange braces.....	88
Figure 3.61	Grove prepared in the east side column flange near column base .....	89
Figure 3.62	A 0.55-in. thick cover plate welded to the south face of column web with filet welds at east side W12 × 96 column base.....	89
Figure 3.63	Two 0.55-in. thick vertical stiffener plates welded to the north face of column web with filet welds at east side W12 × 96 column base .....	90
Figure 3.64	The east side column base detail after repair and whitewash painting.....	90
Figure 3.65	Key construction steps of TCBF-B-4 specimen.....	91
Figure 3.66	Key welding processes of TCBF-B-4 specimen .....	92
Figure 3.67	Typical floor plan of the model building.....	93
Figure 3.68	Perspective View of the Model Building .....	93
Figure 3.69	Elevation of the Model Building (Y-direction).....	94
Figure 3.70	The snapshot of USGS Earthquake Ground Motion Parameters Java applet window.....	94
Figure 3.71	Typical member sizes distribution in Y direction .....	98
Figure 3.72	Member stress ratios distribution in Y direction .....	98
Figure 3.73	Target spectrum screenshot from the online ground motion selection tool on PEER web site .....	99
Figure 3.74	Screenshot of ground motion search interface .....	100
Figure 3.75	Snap shot of ground motion search results.....	100
Figure 3.76	The elastic response spectrum of scaled ground motions mapping on design spectrum and MCE spectrum.....	101



Figure 3.77	Original ground motion record and the scaled ground motions (NGA-960) .....	102
Figure 3.78	The hybrid modeling concept of TCBF-B-4 specimen .....	103
Figure 3.79	Experimental Control of Hybrid Simulation .....	105
Figure 4.1	Torch cutting the steel coupon from wide flange section.....	108
Figure 4.2	Torch cutting the steel coupon from HSS section.....	108
Figure 4.3	Steel coupons of TCBF-B-1 specimens .....	109
Figure 4.4	Steel coupons of TCBF-B-2, TCBF-B-3 and TCBF-B-4 specimens .....	109
Figure 4.5	Side view of specimen TCBF-B-1 .....	112
Figure 4.6	Actuator displacement histories of TCBF-B-1 specimen.....	113
Figure 4.7	Actuator force histories of TCBF-B-1 specimen.....	113
Figure 4.8	Base shear vs. roof displacement relationship of TCBF-B-1 specimen.....	114
Figure 4.9	Story shear vs. story deformation relationship of TCBF-B-1 specimen .....	114
Figure 4.10	Time history of the column axial forces in the first story of TCBF-B-1 specimen (location: 3-ft above column base plate).....	115
Figure 4.11	Roof displacement vs. first story column axial forces of TCBF-B-1 specimen.....	116
Figure 4.12	Time history of the first story column bending moments of TCBF-B-1 specimen (3- ft above column base plate and 3-ft below lower beam centerline) .....	116
Figure 4.13	Time history of the second story column bending moments of TCBF-B-1 specimen (3-ft above lower beam centerline and 3-ft below roof beam centerline).....	117
Figure 4.14	Time history of the first story column shear forces of TCBF-B-1 specimen.....	117
Figure 4.15	Time history of the second story column shear forces of TCBF-B-1 specimen ....	118
Figure 4.16	Time history of the sum of east and west column shear forces in both stories of TCBF-B-1 specimen .....	118
Figure 4.17	Column shear stress vs. shear strain relationships of TCBF-B-1 specimen (locations: EC1-B-N, EC2-B-N, WC1-B-N and WC2-B-N).....	119
Figure 4.18	Story shear component from columns vs. total story shear forces of TCBF-B-1 specimen .....	119
Figure 4.19	Time history of rosette type strain gauge readings in the first story column web of TCBF-B-1 specimen (location: R1, EC1-B-N) .....	120
Figure 4.20	Time history of rosette type strain gauge readings in the first story column web of TCBF-B-1 specimen (location: R5, WC1-B-N) .....	121

Figure 4.21	Time history of rosette type strain gauge readings in the second story column web of TCBF-B-1 specimen (location: R3, EC2-B-N) .....	122
Figure 4.22	Time history of rosette type strain gauge readings in the second story column web of TCBF-B-1 specimen (location: R7, WC2-B-N).....	123
Figure 4.23	Normalized maximum principal stress vs. normalized minimum principal stress in the first story column of TCBF-B-1 specimen (location: R1) .....	124
Figure 4.24	Normalized maximum principal stress vs. normalized minimum principal stress in the first story column of TCBF-B-1 specimen (location: R5) .....	124
Figure 4.25	Normalized maximum principal stress vs. normalized minimum principal stress in the second story column of TCBF-B-1 specimen (location: R3) .....	125
Figure 4.26	Normalized maximum principal stress vs. normalized minimum principal stress in the second story column of TCBF-B-1 specimen (location: R7) .....	125
Figure 4.27	Normalized P-M interaction diagrams of the first story columns of TCBF-B-1 specimen .....	126
Figure 4.28	Normalized P-V interaction diagrams of the first story columns of TCBF-B-1 specimen .....	126
Figure 4.29	Normalized P-M interaction diagrams of the second story columns of TCBF-B-1 specimen .....	127
Figure 4.30	Normalized P-V interaction diagrams of the second story columns of TCBF-B-1 specimen .....	127
Figure 4.31	The deflection time history at the center of beam span of TCBF-B-1 specimen (roof beam: W24 × 117, lower beam: W24 × 68).....	128
Figure 4.32	Time history of strain readings at both exterior ends of W24 × 68 lower beam of TCBF-B-1 specimen .....	129
Figure 4.33	Time history of strain readings at both exterior ends of W24 × 117 roof beam of TCBF-B-1 specimen .....	129
Figure 4.34	Time history of lower beam axial forces of TCBF-B-1 specimen .....	130
Figure 4.35	Time history of roof beam axial forces of TCBF-B-1 specimen.....	130
Figure 4.36	Time history of the lower beam end bending moment of TCBF-B-1 specimen ....	131
Figure 4.37	Time history of the roof beam end bending moment of TCBF-B-1 specimen .....	131
Figure 4.38	Lower beam estimated shear force time history of TCBF-B-1 specimen .....	132

Figure 4.39	Roof beam estimated shear force time history of TCBF-B-1 specimen .....	132
Figure 4.40	Estimated unbalanced force time history of TCBF-B-1 specimen roof beam .....	133
Figure 4.41	Estimated brace axial forces vs. brace axial deformations of the TCBF-B-1 specimen .....	134
Figure 4.42	Estimated brace axial forces vs. measured brace out-of-plane displacements of TCBF-B-1 specimen .....	134
Figure 4.43	Estimated brace axial force, brace axial deformation and measured brace out-of-plane displacement relationships of TCBF-B-1 specimen.....	135
Figure 4.44	Time history of the decomposed strain components of eastern side HSS brace in the first story of TCBF-B-1 specimen .....	136
Figure 4.45	Time history of the decomposed strain components of western side HSS brace in the first story of TCBF-B-1 specimen .....	136
Figure 4.46	Time history of the decomposed strain components of eastern side HSS brace in the second story of TCBF-B-1 specimen.....	137
Figure 4.47(a)	Time history of the decomposed strain components of western side HSS brace in the second story of TCBF-B-1 specimen.....	137
Figure 4.47(b)	Definition of the decomposed strain components.....	138
Figure 4.48	Estimated panel zone shear stress vs. shear strain relationships of TCBF-B-1 specimen .....	139
Figure 4.49	Time history of rosette type strain gauge readings in the lower panel zone of TCBF-B-1 specimen (location: R2) .....	140
Figure 4.50	Time history of rosette type strain gauge readings in the lower panel zone of TCBF-B-1 specimen (location: R6) .....	141
Figure 4.51	Time history of rosette type strain gauge readings in the roof panel zone of TCBF-B-1 specimen (location: R4) .....	142
Figure 4.52	Time history of rosette type strain gauge readings in the roof panel zone of TCBF-B-1 specimen (location: R8) .....	143
Figure 4.53	Normalized maximum principal stress vs. normalized minimum principal stress in the lower panel zone of TCBF-B-1 specimen (location: R2) .....	144
Figure 4.54	Normalized maximum principal stress vs. normalized minimum principal stress in the lower panel zone of TCBF-B-1 specimen (location: R6) .....	144

Figure 4.55	Normalized maximum principal stress vs. normalized minimum principal stress in the roof panel zone of TCBF-B-1 specimen (location: R4).....	145
Figure 4.56	Normalized maximum principal stress vs. normalized minimum principal stress in the roof panel zone of TCBF-B-1 specimen (location: R8).....	145
Figure 4.57	Time history of rosette type strain gauge readings in the one-piece gusset plate of TCBF-B-1 specimen (location: R9).....	146
Figure 4.58	Time history of rosette type strain gauge readings in the one-piece gusset plate of TCBF-B-1 specimen (location: R10).....	147
Figure 4.59	Time history of rosette type strain gauge readings in the one-piece gusset plate of TCBF-B-1 specimen (location: R11).....	148
Figure 4.60	Time history of rosette type strain gauge readings in the one-piece gusset plate of TCBF-B-1 specimen (location: R12).....	149
Figure 4.61	Time history of rosette type strain gauge readings in the one-piece gusset plate of TCBF-B-1 specimen (location: R13).....	150
Figure 4.62	Time history of rosette type strain gauge readings in the one-piece gusset plate of TCBF-B-1 specimen (location: R14).....	151
Figure 4.63	Time history of rosette type strain gauge readings in the one-piece gusset plate of TCBF-B-1 specimen (location: R15).....	152
Figure 4.64	Time history of rosette type strain gauge readings in the one-piece gusset plate of TCBF-B-1 specimen (location: R16).....	153
Figure 4.65	Time history of rosette type strain gauge readings in the one-piece gusset plate of TCBF-B-1 specimen (location: R17).....	154
Figure 4.66	Time history of rosette type strain gauge readings in the one-piece gusset plate of TCBF-B-1 specimen (location: R18).....	155
Figure 4.67	Time history of rosette type strain gauge readings in the one-piece gusset plate of TCBF-B-1 specimen (location: R19).....	156
Figure 4.68	Time history of rosette type strain gauge readings in the one-piece gusset plate of TCBF-B-1 specimen (location: R20).....	157
Figure 4.69	Normalized maximum principal stress vs. normalized minimum principal stress in the one-piece gusset plate of TCBF-B-1 specimen (location: R9) .....	158

Figure 4.70	Normalized maximum principal stress vs. normalized minimum principal stress in the one-piece gusset plate of TCBF-B-1 specimen (location: R10) .....	158
Figure 4.71	Normalized maximum principal stress vs. normalized minimum principal stress in the one-piece gusset plate of TCBF-B-1 specimen (location: R11) .....	159
Figure 4.72	Normalized maximum principal stress vs. normalized minimum principal stress in the one-piece gusset plate of TCBF-B-1 specimen (location: R12) .....	159
Figure 4.73	Normalized maximum principal stress vs. normalized minimum principal stress in the one-piece gusset plate of TCBF-B-1 specimen (location: R13) .....	160
Figure 4.74	Normalized maximum principal stress vs. normalized minimum principal stress in the one-piece gusset plate of TCBF-B-1 specimen (location: R14) .....	160
Figure 4.75	Normalized maximum principal stress vs. normalized minimum principal stress in the one-piece gusset plate of TCBF-B-1 specimen (location: R15) .....	161
Figure 4.76	Normalized maximum principal stress vs. normalized minimum principal stress in the one-piece gusset plate of TCBF-B-1 specimen (location: R16) .....	161
Figure 4.77	Normalized maximum principal stress vs. normalized minimum principal stress in the one-piece gusset plate of TCBF-B-1 specimen (location: R17) .....	162
Figure 4.78	Normalized maximum principal stress vs. normalized minimum principal stress in the one-piece gusset plate of TCBF-B-1 specimen (location: R18) .....	162
Figure 4.79	Normalized maximum principal stress vs. normalized minimum principal stress in the one-piece gusset plate of TCBF-B-1 specimen (location: R19) .....	163
Figure 4.80	Normalized maximum principal stress vs. normalized minimum principal stress in the one-piece gusset plate of TCBF-B-1 specimen (location: R20) .....	163
Figure 4.81	The actuator force vs. bracket deformation relationship at both floor levels during specimen TCBF-B-1 test.....	164
Figure 4.82	Slippage time history between specimen and test setup boundaries during specimen TCBF-B-1 test.....	165
Figure 4.83	The out-of-plane deformation time history of lateral supporting frame at different monitoring points during specimen TCBF-B-1 test.....	166
Figure 4.84	Western side of the upper gusset plate in the first story of TCBF-B-1 specimen ..	170
Figure 4.85	Western side of the upper gusset plate in the first story of TCBF-B-1 specimen ..	171
Figure 4.86	The bottom flange of east side lower beam of TCBF-B-1 specimen .....	171

Figure 4.87(a) The flaking of whitewash at second story gusset plate of the TCBF-B-1 specimen .....	172
Figure 4.87(b) The flaking of whitewash at the middle length of braces of the TCBF-B-1 specimen .....	173
Figure 4.88 The one-piece gusset plate at eastern side of TCBF-B-1 specimen .....	174
Figure 4.89 The column base at western side of TCBF-B-1 specimen .....	174
Figure 4.90 The lower beam-to-gusset plate splice at western side of TCBF-B-1 specimen....	175
Figure 4.91 The middle portion of a HSS brace at western side of TCBF-B-1 specimen in first story.....	175
Figure 4.92 The lower beam-to-gusset plate splice at eastern side of TCBF-B-1 specimen....	176
Figure 4.93 The gusset plate-to-column connection at eastern side of TCBF-B-1 specimen ...	176
Figure 4.94 The square HSS brace in the first story at eastern side of TCBF-B-1 specimen....	177
Figure 4.95 The square HSS brace in the first story at western side of TCBF-B-1 specimen ..	177
Figure 4.96 The cracks propagate in the square HSS brace at first story western side of TCBF-B-1 specimen .....	178
Figure 4.97 The flaking of whitewash on column web at eastern side of the TCBF-B-1 specimen .....	178
Figure 4.98 The square HSS braces at the first story of TCBF-B-1 specimen.....	179
Figure 4.99 The gusset-to-beam splice at eastern side of TCBF-B-1 specimen.....	179
Figure 4.100 Complete fracture of the square HSS brace at first story eastern side of TCBF-B-1 specimen .....	180
Figure 4.101 The cracks propagate in the square HSS brace at second story eastern side of TCBF-B-1 specimen .....	180
Figure 4.102 Specimen TCBF-B-1 after test (view from north side fisheye lens).....	181
Figure 4.103 Fracture of the column base flange CJP welds at west side of the TCBF-B-2 specimen .....	183
Figure 4.104 Specimen TCBF-B-2 after first trial.....	183
Figure 4.105 The west side column base of TCBF-B-2 specimen after repair with 1-in. thick stiffener plates and a 2-in. thick flange cover plate .....	184
Figure 4.106 Specimen TCBF-B-2 before second trial .....	184
Figure 4.107. Specimen TCBF-B-2 before test and after test.....	185

Figure 4.108	Actuator displacement time histories of TCBF-B-2 specimen.....	186
Figure 4.109	Actuator force time histories of TCBF-B-2 specimen .....	186
Figure 4.110	Base shear vs. roof displacement relationship of TCBF-B-2 specimen .....	187
Figure 4.111	Story shear vs. story deformation relationship of TCBF-B-2 specimen .....	187
Figure 4.112	Time history of the column axial forces in the first story of TCBF-B-2 specimen (location: 6-ft above column base plate).....	189
Figure 4.113	Roof displacement vs. first story column axial forces of TCBF-B-2 specimen (note that the vertical axis limit is from -600 kips to 800 kips; the horizontal axis limit is from -8-in. to 8-in.).....	189
Figure 4.114	Time history of the first story column bending moments of TCBF-B-2 specimen (3-ft above column base plate and 3-ft below lower beam centerline).....	190
Figure 4.115	Time history of the second story column bending moments of TCBF-B-2 specimen (3-ft above lower beam centerline and 3-ft below the roof beam centerline) .....	190
Figure 4.116	Time history of the first story column shear forces of TCBF-B-2 specimen.....	191
Figure 4.117	Time history of the second story column shear forces of TCBF-B-2 specimen ..	191
Figure 4.118	Time history of the sum of east and west column shear forces in both stories of TCBF-B-2 specimen .....	192
Figure 4.119	Estimated column shear stress vs. shear strain relationships of TCBF-B-2 specimen (locations: EC1-B-N, EC2-B-N, WC1-B-N and WC2-B-N) .....	192
Figure 4.120	Story shear component from columns vs. total story shear forces of TCBF-B-2 specimen .....	193
Figure 4.121	Time history of rosette type strain gauge readings in the first story column web of TCBF-B-2 specimen (location: R1).....	194
Figure 4.122	Time history of rosette type strain gauge readings in the first story column web of TCBF-B-2 specimen (location: R5).....	195
Figure 4.123	Time history of rosette type strain gauge readings in the second story column web of TCBF-B-2 specimen (location: R3) .....	196
Figure 4.124	Time history of rosette type strain gauge readings in the second story column web of TCBF-B-2 specimen (location: R7) .....	197

Figure 4.125	Maximum principal stress vs. minimum principal stress in the first story column of TCBF-B-2 specimen (location: R1) .....	198
Figure 4.126	Maximum principal stress vs. minimum principal stress in the first story column of TCBF-B-2 specimen (location: R5) .....	198
Figure 4.127	Maximum principal stress vs. minimum principal stress in the second story column of TCBF-B-2 specimen (location: R3) .....	199
Figure 4.128	Maximum principal stress vs. minimum principal stress in the second story column of TCBF-B-2 specimen (location: R7) .....	199
Figure 4.129	Normalized P-M interaction diagrams of the first story columns of TCBF-B-2 specimen .....	200
Figure 4.130	Normalized P-V interaction diagrams of the first story columns of TCBF-B-2 specimen .....	200
Figure 4.131	Normalized P-M interaction diagrams of the second story columns of TCBF-B-2 specimen .....	201
Figure 4.132	Normalized P-V interaction diagrams of the second story columns of TCBF-B-2 specimen .....	201
Figure 4.133	The deflection time history at the center of beam span of TCBF-B-2 specimen (roof beam: W24 × 117, lower beam: W24 × 68).....	202
Figure 4.134	Time history of strain readings at both exterior ends of W24 × 68 lower beam of TCBF-B-2 specimen .....	203
Figure 4.135	Time history of strain readings at both exterior ends of W24 × 117 roof beam of TCBF-B-2 specimen .....	203
Figure 4.136	Time history of lower beam axial forces of TCBF-B-2 specimen .....	204
Figure 4.137	Time history of roof beam axial forces of TCBF-B-2 specimen.....	204
Figure 4.138	Time history of the lower beam end bending moment of TCBF-B-2 specimen ..	205
Figure 4.139	Time history of the roof beam end bending moment of TCBF-B-2 specimen ....	205
Figure 4.140	Lower beam estimated shear force time history of TCBF-B-2 specimen .....	206
Figure 4.141	Roof beam estimated shear force time history of TCBF-B-2 specimen .....	206
Figure 4.142	Estimated unbalanced force time history of TCBF-B-2 specimen roof beam .....	207
Figure 4.143	Estimated brace axial forces vs. brace axial deformations of the TCBF-B-2 specimen .....	208



Figure 4.144	Estimated brace axial forces vs. measured brace out-of-plane displacements of TCBF-B-2 specimen .....	208
Figure 4.145	Estimated brace axial force, brace axial deformation and measured brace out-of-plane displacement relationships of TCBF-B-2 specimen.....	209
Figure 4.146	Time history of the decomposed strain components of eastern side HSS brace in the first story of TCBF-B-2 specimen .....	210
Figure 4.147	Time history of the decomposed strain components of western side HSS brace in the first story of TCBF-B-2 specimen .....	210
Figure 4.148	Time history of the decomposed strain components of eastern side HSS brace in the second story of TCBF-B-2 specimen.....	211
Figure 4.149	Time history of the decomposed strain components of western side HSS brace in the second story of TCBF-B-2 specimen.....	211
Figure 4.150	Estimated panel zone shear stress vs. shear strain relationships of TCBF-B-2....	212
Figure 4.151	Time history of rosette type strain gauge readings in the lower panel zone of TCBF-B-2 specimen (location: R2).....	213
Figure 4.152	Time history of rosette type strain gauge readings in the lower panel zone of TCBF-B-2 specimen (location: R6).....	214
Figure 4.153	Time history of rosette type strain gauge readings in the roof panel zone of TCBF-B-2 specimen (location: R4) .....	215
Figure 4.154	Time history of rosette type strain gauge readings in the roof panel zone of TCBF-B-2 specimen (location: R8) .....	216
Figure 4.155	Normalized maximum principal stress vs. normalized minimum principal stress in the lower panel zone of TCBF-B-2 specimen (location: R2) .....	217
Figure 4.156	Normalized maximum principal stress vs. normalized minimum principal stress in the lower panel zone of TCBF-B-2 specimen (location: R6) .....	217
Figure 4.157	Normalized maximum principal stress vs. normalized minimum principal stress in the roof panel zone of TCBF-B-2 specimen (location: R4).....	218
Figure 4.158	Normalized maximum principal stress vs. normalized minimum principal stress in the roof panel zone of TCBF-B-2 specimen (location: R8).....	218
Figure 4.159	Time history of rosette type strain gauge readings in the one-piece gusset plate of TCBF-B-2 specimen (location: R9).....	219

Figure 4.160	Time history of rosette type strain gauge readings in the one-piece gusset plate of TCBF-B-2 specimen (location: R10).....	220
Figure 4.161	Time history of rosette type strain gauge readings in the one-piece gusset plate of TCBF-B-2 specimen (location: R11).....	221
Figure 4.162	Time history of rosette type strain gauge readings in the one-piece gusset plate of TCBF-B-2 specimen (location: R12).....	222
Figure 4.163	Time history of rosette type strain gauge readings in the one-piece gusset plate of TCBF-B-2 specimen (location: R13).....	223
Figure 4.164	Time history of rosette type strain gauge readings in the one-piece gusset plate of TCBF-B-2 specimen (location: R14).....	224
Figure 4.165	Time history of rosette type strain gauge readings in the one-piece gusset plate of TCBF-B-2 specimen (location: R15).....	225
Figure 4.166	Time history of rosette type strain gauge readings in the one-piece gusset plate of TCBF-B-2 specimen (location: R16).....	226
Figure 4.167	Time history of rosette type strain gauge readings in the one-piece gusset plate of TCBF-B-2 specimen (location: R17).....	227
Figure 4.168	Time history of rosette type strain gauge readings in the one-piece gusset plate of TCBF-B-2 specimen (location: R18).....	228
Figure 4.169	Time history of rosette type strain gauge readings in the one-piece gusset plate of TCBF-B-2 specimen (location: R19).....	229
Figure 4.170	Time history of rosette type strain gauge readings in the one-piece gusset plate of TCBF-B-2 specimen (location: R20).....	230
Figure 4.171	Normalized maximum principal stress vs. normalized minimum principal stress in the one-piece gusset plate of TCBF-B-2 specimen (location: R9) .....	231
Figure 4.172	Normalized maximum principal stress vs. normalized minimum principal stress in the one-piece gusset plate of TCBF-B-2 specimen (location: R10) .....	231
Figure 4.173	Normalized maximum principal stress vs. normalized minimum principal stress in the one-piece gusset plate of TCBF-B-2 specimen (location: R11) .....	232
Figure 4.174	Normalized maximum principal stress vs. normalized minimum principal stress in the one-piece gusset plate of TCBF-B-2 specimen (location: R12) .....	232

Figure 4.175	Normalized maximum principal stress vs. normalized minimum principal stress in the one-piece gusset plate of TCBF-B-2 specimen (location: R13) .....	233
Figure 4.176	Normalized maximum principal stress vs. normalized minimum principal stress in the one-piece gusset plate of TCBF-B-2 specimen (location: R14) .....	233
Figure 4.177	Normalized maximum principal stress vs. normalized minimum principal stress in the one-piece gusset plate of TCBF-B-2 specimen (location: R15) .....	234
Figure 4.178	Normalized maximum principal stress vs. normalized minimum principal stress in the one-piece gusset plate of TCBF-B-2 specimen (location: R16) .....	234
Figure 4.179	Normalized maximum principal stress vs. normalized minimum principal stress in the one-piece gusset plate of TCBF-B-2 specimen (location: R17) .....	235
Figure 4.180	Normalized maximum principal stress vs. normalized minimum principal stress in the one-piece gusset plate of TCBF-B-2 specimen (location: R18) .....	235
Figure 4.181	Normalized maximum principal stress vs. normalized minimum principal stress in the one-piece gusset plate of TCBF-B-2 specimen (location: R19) .....	236
Figure 4.182	Normalized maximum principal stress vs. normalized minimum principal stress in the one-piece gusset plate of TCBF-B-2 specimen (location: R20) .....	236
Figure 4.183	The averaged axial strain time history in the tapered gusset plate at eastern side of TCBF-B-2 specimen .....	237
Figure 4.184	The bending strain time history in the tapered gusset plate at eastern side of TCBF-B-2 specimen .....	237
Figure 4.185	The actuator force vs. bracket deformation relationship at both floor levels during specimen TCBF-B-2 test.....	238
Figure 4.186	Slippage time history between specimen and test setup boundaries during specimen TCBF-B-2 test.....	239
Figure 4.187	The out-of-plane deformation time history of lateral supporting frame at different monitoring points during specimen TCBF-B-2 test.....	240
Figure 4.188	The reconfigurable reaction wall (RRW) tip deformation time histories during specimen TCBF-B-2 test.....	241
Figure 4.189	Whitewash flaking at the middle of the west side round HSS brace (Specimen TCBF-B-2).....	246

Figure 4.190	Flaking of whitewash near the CJP welds in the bottom flange of lower beam (Specimen TCBF-B-2).....	246
Figure 4.191	Yield pattern of the east column flange (Specimen TCBF-B-2).....	247
Figure 4.192	Yield pattern of the west column flange (Specimen TCBF-B-2).....	247
Figure 4.193	Global buckling of round HSS braces at both stories of TCBF-B-2 Specimen ...	248
Figure 4.194	Additional whitewash flaking in the braces (Specimen TCBF-B-2).....	248
Figure 4.195	Flaking of whitewash near gusset plate-to-column flange region (Specimen TCBF-B-2).....	249
Figure 4.196	Whitewash flaking at the corner of gusset plate-to-roof beam connection (Specimen TCBF-B-2).....	249
Figure 4.197	Local buckling of lower beam bottom flange at east side (the Specimen TCBF-B- 2) .....	250
Figure 4.198	Local buckling of lower beam top flange at west side (Specimen TCBF-B-2) ...	250
Figure 4.199	Column web yielding at the east side column in ground floor (Specimen TCBF-B- 2) .....	251
Figure 4.200	Crack near the flange CJP welds at west side column base (the Specimen TCBF- B-2) .....	251
Figure 4.201	Complete fracture near the flange CJP welds at west side column base (Specimen TCBF-B-2).....	252
Figure 4.202	Crack near the web CJP welds at west side column base (the Specimen TCBF-B- 2) .....	252
Figure 4.203	West side column base after repair (Specimen TCBF-B-2).....	253
Figure 4.204	East side column base after repair (Specimen TCBF-B-2) .....	253
Figure 4.205	Yielding in the column flange near 2-in.-thick cover plate (the Specimen TCBF- B-2) .....	254
Figure 4.206	Yield pattern between column base stiffener plates (Specimen TCBF-B-2) .....	254
Figure 4.207	Fracture of lower beam top flange (west side of Specimen TCBF-B-2).....	255
Figure 4.208	Partial fracture of lower beam bottom flange finger plate (east side of Specimen TCBF-B-2).....	255
Figure 4.209	Complete fracture of lower beam bottom flange finger plate (east side of Specimen TCBF-B-2) .....	256

Figure 4.210	Local buckling of column flange near 2-in.-thick cover plate (Specimen TCBF-B-2) .....	256
Figure 4.211	Local buckling of lower beam web at west side (Specimen TCBF-B-2).....	257
Figure 4.212	Local buckling of west side round HSS brace in the first story(Specimen TCBF-B-2) .....	257
Figure 4.213	Tearing of the vertical fillet welds at west column base (Specimen TCBF-B-2)..	258
Figure 4.214	Additional local buckling of west side round HSS brace in the first story (Specimen TCBF-B-2).....	258
Figure 4.215	Crack propagation into the web at east side lower beam (Specimen TCBF-B-2)	259
Figure 4.216	Crack initiates in the west side round HSS brace at the first story (Specimen TCBF-B-2).....	259
Figure 4.217	Additional tearing of fillet welds between cover plate and column flange (Specimen TCBF-B-2).....	260
Figure 4.218	Partial fracture of the west side brace in the first story (Specimen TCBF-B-2) ..	260
Figure 4.219	Complete fracture of the west side brace in the first story (the Specimen TCBF-B-2) .....	261
Figure 4.220	Crack in the lower beam web at west side near top flange (the Specimen TCBF-B-2) .....	261
Figure 4.221	Crack initiates in the east side round HSS brace at the first story (Specimen TCBF-B-2).....	262
Figure 4.222	Tearing of the vertical fillet welds at the west column base (the Specimen TCBF-B-2) .....	262
Figure 4.223	Necking of the east side round HSS brace in the first story before fracture .....	263
Figure 4.224	Complete fracture of the east side brace in the first story (the Specimen TCBF-B-2) .....	263
Figure 4.225	The entire side view of the TCBF-B-2 specimen after second trial.....	264
Figure 4.226	Column base connection detail of TCBF-B-3 specimen (four 7/8-in. gussets welded to the column flange and base plate).....	265
Figure 4.227	The lower beam to one-piece gusset plate pin connection detail of TCBF-B-3 specimen (eastern side of the W24 × 68 beam) .....	265
Figure 4.228	Specimen TCBF-B-3 before test and after test.....	266

Figure 4.229	Actuator displacement time history of TCBF-B-3 specimen .....	267
Figure 4.230	Actuator force histories of TCBF-B-3 specimen.....	267
Figure 4.231	Base shear vs. roof displacement relationship of TCBF-B-3 specimen .....	268
Figure 4.232	Story shear vs. story deformation relationship of TCBF-B-3 specimen .....	268
Figure 4.233	Time history of the column axial forces in the first story of TCBF-B-3 specimen (location: 3-ft above column base plate).....	269
Figure 4.234	Roof displacement vs. first story column axial forces of TCBF-B-3 specimen...	270
Figure 4.235	Time history of the first story column bending moments of TCBF-B-3 specimen (3-ft above column base plate and 3-ft below lower beam centerline).....	270
Figure 4.236	Time history of the second story column bending moments of TCBF-B-3 specimen (3-ft above lower beam centerline and 3-ft below the roof beam centerline) .....	271
Figure 4.237	Time history of the first story column shear forces of TCBF-B-3 specimen.....	271
Figure 4.238	Time history of the second story column shear forces of TCBF-B-3 specimen ..	272
Figure 4.239	Time history of the sum of east and west column shear forces in both stories of TCBF-B-3 specimen .....	272
Figure 4.240	Column shear stress vs. shear strain relationships of TCBF-B-3 specimen (locations: EC1-B-N, EC2-B-N, WC1-B-N and WC2-B-N).....	273
Figure 4.241	Story shear component from columns vs. total story shear forces of TCBF-B-3 specimen .....	273
Figure 4.242	Time history of rosette type strain gauge readings in the first story column web of TCBF-B-3 specimen (location: R1).....	274
Figure 4.243	Time history of rosette type strain gauge readings in the first story column web of TCBF-B-3 specimen (location: R5).....	275
Figure 4.244	Time history of rosette type strain gauge readings in the first story column web of TCBF-B-3 specimen (location: R3).....	276
Figure 4.245	Time history of rosette type strain gauge readings in the first story column web of TCBF-B-3 specimen (location: R7).....	277
Figure 4.246	Maximum principal stress vs. minimum principal stress in the first story column of TCBF-B-3 specimen (location: R1) .....	278

Figure 4.247	Maximum principal stress vs. minimum principal stress in the first story column of TCBF-B-3 specimen (location: R5) .....	278
Figure 4.248	Maximum principal stress vs. minimum principal stress in the first story column of TCBF-B-3 specimen (location: R3) .....	279
Figure 4.249	Maximum principal stress vs. minimum principal stress in the first story column of TCBF-B-3 specimen (location: R7) .....	279
Figure 4.250	Normalized P-M interaction diagrams of the first story columns of TCBF-B-3 specimen .....	280
Figure 4.251	Normalized P-V interaction diagrams of the first story columns of TCBF-B-3 ..	280
Figure 4.252	Normalized P-M interaction diagrams of the second story columns of TCBF-B-3 specimen .....	281
Figure 4.253	Normalized P-V interaction diagrams of the second story columns of TCBF-B-3 specimen .....	281
Figure 4.254	The deflection time history at the center of beam span of TCBF-B-3 specimen (roof beam: W24 × 117, lower beam: W24 × 68).....	282
Figure. 4.255	Time history of strain readings at both exterior ends of W24 × 117 roof beam of TCBF-B-3 specimen .....	283
Figure. 4.256	Time history of strain readings at both exterior ends of W24 × 68 lower beam of TCBF-B-3 specimen .....	283
Figure 4.257	Time history of lower beam axial forces of TCBF-B-3 specimen .....	284
Figure 4.258	Time history of the roof beam axial forces of TCBF-B-3 specimen.....	284
Figure 4.259	Time history of the lower beam end bending moment of TCBF-B-3 specimen ..	285
Figure 4.260	Time history of the roof beam end bending moment of TCBF-B-3 specimen ....	285
Figure 4.261	Lower beam estimated shear force time history of TCBF-B-3 specimen .....	286
Figure 4.262	Roof beam estimated shear force time history of TCBF-B-3 specimen .....	286
Figure 4.263	Estimated unbalanced force time history of TCBF-B-3 specimen roof beam ....	287
Figure 4.264	Estimated brace axial forces versus brace axial deformations of TCBF-B-3 specimen .....	288
Figure 4.265	Estimated brace axial forces versus measured brace out-of-plane displacements at the brace center point of each WF brace of TCBF-B-3 specimen.....	288

Figure 4.266	Estimated brace axial force, brace axial deformation and measured brace out-of-plane displacement relationships of TCBF-B-3 specimen.....	289
Figure 4.267	Time history of the decomposed strain components of eastern side wide flange brace in the first story of TCBF-B-3 specimen.....	290
Figure 4.268	Time history of the decomposed strain components of western side wide flange brace in the first story of TCBF-B-3 specimen.....	290
Figure 4.269	Time history of the decomposed strain components of eastern side wide flange brace in the second story of TCBF-B-3 specimen.....	291
Figure 4.270	Time history of the decomposed strain components of western side wide flange brace in the second story of TCBF-B-3 specimen.....	291
Figure 4.271	Estimated panel zone shear stress vs. shear strain relationships of TCBF-B-3....	292
Figure 4.272	Time history of rosette type strain gauge readings in the lower panel zone of TCBF-B-3 specimen (location: R2).....	293
Figure 4.273	Time history of rosette type strain gauge readings in the lower panel zone of TCBF-B-3 specimen (location: R6).....	294
Figure 4.274	Time history of rosette type strain gauge readings in the roof panel zone of TCBF-B-3 specimen (location: R4).....	295
Figure 4.275	Time history of rosette type strain gauge readings in the roof panel zone of TCBF-B-3 specimen (location: R8).....	296
Figure 4.276	Normalized maximum principal stress vs. normalized minimum principal stress in the lower panel zone of TCBF-B-3 specimen (location: R2).....	297
Figure 4.277	Normalized maximum principal stress vs. normalized minimum principal stress in the lower panel zone of TCBF-B-3 specimen (location: R6).....	297
Figure 4.278	Normalized maximum principal stress vs. normalized minimum principal stress in the roof panel zone of TCBF-B-3 specimen (location: R4).....	298
Figure 4.279	Normalized maximum principal stress vs. normalized minimum principal stress in the roof panel zone of TCBF-B-3 specimen (location: R8).....	298
Figure 4.280	Time history of rosette type strain gauge readings in the one-piece gusset plate of TCBF-B-3 specimen (location: R9).....	299
Figure 4.281	Time history of rosette type strain gauge readings in the one-piece gusset plate of TCBF-B-3 specimen (location: R10).....	300



Figure 4.282	Time history of rosette type strain gauge readings in the one-piece gusset plate of TCBF-B-3 specimen (location: R11).....	301
Figure 4.283	Time history of rosette type strain gauge readings in the one-piece gusset plate of TCBF-B-3 specimen (location: R12).....	302
Figure 4.284	Time history of rosette type strain gauge readings in the one-piece gusset plate of TCBF-B-3 specimen (location: R13).....	303
Figure 4.285	Time history of rosette type strain gauge readings in the one-piece gusset plate of TCBF-B-3 specimen (location: R14).....	304
Figure 4.286	Time history of rosette type strain gauge readings in the one-piece gusset plate of TCBF-B-3 specimen (location: R15).....	305
Figure 4.287	Time history of rosette type strain gauge readings in the one-piece gusset plate of TCBF-B-3 specimen (location: R16).....	306
Figure 4.288	Time history of rosette type strain gauge readings in the one-piece gusset plate of TCBF-B-3 specimen (location: R17).....	307
Figure 4.289	Time history of rosette type strain gauge readings in the one-piece gusset plate of TCBF-B-3 specimen (location: R18).....	308
Figure 4.290	Time history of rosette type strain gauge readings in the one-piece gusset plate of TCBF-B-3 specimen (location: R19).....	309
Figure 4.291	Time history of rosette type strain gauge readings in the one-piece gusset plate of TCBF-B-3 specimen (location: R20).....	310
Figure 4.292	Normalized maximum principal stress vs. normalized minimum principal stress in the one-piece gusset plate of TCBF-B-3 specimen (location: R9) .....	311
Figure 4.293	Normalized maximum principal stress vs. normalized minimum principal stress in the one-piece gusset plate of TCBF-B-3 specimen (location: R10) .....	311
Figure 4.294	Normalized maximum principal stress vs. normalized minimum principal stress in the one-piece gusset plate of TCBF-B-3 specimen (location: R11) .....	312
Figure 4.295	Normalized maximum principal stress vs. normalized minimum principal stress in the one-piece gusset plate of TCBF-B-3 specimen (location: R12) .....	312
Figure 4.296	Normalized maximum principal stress vs. normalized minimum principal stress in the one-piece gusset plate of TCBF-B-3 specimen (location: R13) .....	313

Figure 4.297	Normalized maximum principal stress vs. normalized minimum principal stress in the one-piece gusset plate of TCBF-B-3 specimen (location: R14) .....	313
Figure 4.298	Normalized maximum principal stress vs. normalized minimum principal stress in the one-piece gusset plate of TCBF-B-3 specimen (location: R15) .....	314
Figure 4.299	Normalized maximum principal stress vs. normalized minimum principal stress in the one-piece gusset plate of TCBF-B-3 specimen (location: R16) .....	314
Figure 4.300	Normalized maximum principal stress vs. normalized minimum principal stress in the one-piece gusset plate of TCBF-B-3 specimen (location: R17) .....	315
Figure 4.301	Normalized maximum principal stress vs. normalized minimum principal stress in the one-piece gusset plate of TCBF-B-3 specimen (location: R18) .....	315
Figure 4.302	Normalized maximum principal stress vs. normalized minimum principal stress in the one-piece gusset plate of TCBF-B-3 specimen (location: R19) .....	316
Figure 4.303	Normalized maximum principal stress vs. normalized minimum principal stress in the one-piece gusset plate of TCBF-B-3 specimen (location: R20) .....	316
Figure 4.304	The averaged axial strain time history in the tapered gusset plate at eastern side of TCBF-B-3 specimen .....	317
Figure 4.305	The bending strain time history in the tapered gusset plate at eastern side of TCBF-B-3 specimen .....	317
Figure 4.306	The actuator force vs. bracket deformation relationship at both floor levels during specimen TCBF-B-3 test.....	318
Figure 4.307	Slippage time history between specimen and test setup boundaries during specimen TCBF-B-3 test.....	319
Figure 4.308	The out-of-plane deformation time history of lateral supporting frame at different monitoring points during specimen TCBF-B-3 test.....	320
Figure 4.309	The reconfigurable reaction wall (RRW) tip deformation time histories during specimen TCBF-B-3 test.....	321
Figure 4.310	The whitewash flaking on the brace-to-gusset cover plates (the Specimen TCBF-B-3) .....	325
Figure 4.311	Whitewash flaking on the global buckled braces (west brace at the first story and east brace at the second story) .....	326
Figure 4.312	Whitewash flaking at the roof beam-to-column connection (west side).....	326

Figure 4.313	Local flaking of whitewash developed in the lower beam web near beam-to-gusset splice plate .....	327
Figure 4.314	Buckling shapes of all four wide flange braces, three of them buckled to the north side, only the east side brace at the first story buckled to the south side.....	327
Figure 4.315	Flaking of whitewash developed at the $2t$ gap region in the gusset plate .....	328
Figure 4.316	Whitewash flaking patterns shown on the column flanges near the column base plate (west column base).....	328
Figure 4.317	Whitewash flaking patterns shown on the column flanges near the column base plate.....	329
Figure 4.318	The closed view of flange local buckling at the west-side wide flange brace in the first story .....	329
Figure 4.319	The local yielding in the beam-to-gusset plate splices near the shot-slotted holes .....	330
Figure 4.320	Evidence of slippage between splice plate and the one-piece gusset plate .....	330
Figure 4.321	East column flange fractured near the base plate stiffeners (view from north-west side).....	331
Figure 4.322	East column flange fractured near the base plate stiffeners (the view from east side).....	331
Figure 4.323	West wide flange brace partially fractured near the middle of the brace (view from north-west side).....	332
Figure 4.324	West wide flange brace partially fractured near the middle of the brace (view from east side).....	332
Figure 4.325	Top flange of the west wide flange brace completely fractured near the middle of the brace (view from north-west side) .....	333
Figure 4.326	West wide flange brace completely fractured near the middle of the brace (view from north side).....	333
Figure 4.327	Crack tip in the web of east column near the column base .....	334
Figure 4.328	Specimen TCBF-B-3 after test .....	334
Figure 4.329	Specimen TCBF-B-4 before and after hybrid simulation .....	336
Figure 4.330	Actuator displacement time history of TCBF-B-4 specimen .....	337
Figure 4.331	Actuator force histories of TCBF-B-4 specimen.....	338

Figure 4.332	Base shear vs. roof displacement relationship of TCBF-B-4 specimen .....	339
Figure 4.333	Story shear vs. story deformation relationship of TCBF-B-4 specimen .....	339
Figure 4.334	Upper actuator force vs. lower actuator force relationship of the TCBF-B-4 specimen .....	340
Figure 4.335	Upper actuator displacement vs. lower actuator displacement relationship of TCBF-B-4 specimen .....	340
Figure 4.336	Time history of the column axial forces in the first story of TCBF-B-4 specimen (location: 3-ft above column base plate).....	341
Figure 4.337	Roof displacement vs. first story column axial forces of TCBF-B-4 specimen...	342
Figure 4.338	Time history of the first story column bending moments of TCBF-B-4 specimen (3-ft above column base plate and 3-ft below lower beam centerline).....	342
Figure 4.339	Time history of the second story column bending moments of TCBF-B-4 specimen (3-ft above lower beam centerline and 3-ft below the roof beam centerline) .....	343
Figure 4.340	Time history of the first story column shear forces of TCBF-B-4 specimen.....	343
Figure 4.341	Time history of the second story column shear forces of TCBF-B-4 specimen ..	344
Figure 4.342	Time history of the sum of east and west column shear forces in both stories of TCBF-B-4 specimen .....	344
Figure 4.343	Column shear stress vs. shear strain relationships of TCBF-B-4 specimen (locations: EC1-B-N, EC2-B-N, WC1-B-N and WC2-B-N).....	345
Figure 4.344	Story shear component from columns vs. total story shear forces of TCBF-B-4 specimen .....	345
Figure 4.345	Time history of rosette type strain gauge readings in the first story column web of TCBF-B-4 specimen (location: R1).....	346
Figure 4.346	Time history of rosette type strain gauge readings in the first story column web of TCBF-B-4 specimen (location: R5).....	347
Figure 4.347	Time history of rosette type strain gauge readings in the first story column web of TCBF-B-4 specimen (location: R3).....	348
Figure 4.348	Time history of rosette type strain gauge readings in the first story column web of TCBF-B-4 specimen (location: R7).....	349

Figure 4.349	Maximum principal stress vs. minimum principal stress in the first story column of TCBF-B-4 specimen (location: R1) .....	350
Figure 4.350	Maximum principal stress vs. minimum principal stress in the first story column of TCBF-B-4 specimen (location: R5) .....	350
Figure 4.351	Maximum principal stress vs. minimum principal stress in the first story column of TCBF-B-4 specimen (location: R3) .....	351
Figure 4.352	Maximum principal stress vs. minimum principal stress in the first story column of TCBF-B-4 specimen (location: R7) .....	351
Figure 4.353	Normalized P-M interaction diagrams of the first story columns of TCBF-B-4 specimen .....	352
Figure 4.354	Normalized P-V interaction diagrams of the first story columns of TCBF-B-4 specimen .....	352
Figure 4.355	Normalized P-M interaction diagrams of the second story columns of TCBF-B-4 specimen .....	353
Figure 4.356	Normalized P-V interaction diagrams of the second story columns of TCBF-B-4 specimen .....	353
Figure 4.357	The deflection time history at the center of beam span of TCBF-B-4 specimen (roof beam: W24 × 117, lower beam: W24 × 68).....	354
Figure. 4.358	Time history of strain readings at both exterior ends of W24 × 117 roof beam of TCBF-B-4 specimen .....	355
Figure. 4.359	Time history of strain readings at both exterior ends of W24 × 68 lower beam of TCBF-B-4 specimen .....	355
Figure 4.360	Time history of lower beam axial forces of TCBF-B-4 specimen .....	356
Figure 4.361	Time history of the roof beam axial forces of TCBF-B-4 specimen.....	356
Figure 4.362	Time history of the lower beam end bending moment of TCBF-B-4 specimen ..	357
Figure 4.363	Time history of the roof beam end bending moment of TCBF-B-4 specimen ....	357
Figure 4.364	Lower beam estimated shear force time history of TCBF-B-4 specimen .....	358
Figure 4.365	Roof beam estimated shear force time history of TCBF-B-4 specimen .....	358
Figure 4.366	Estimated unbalanced force time history of TCBF-B-4 specimen roof beam .....	359
Figure 4.367	Estimated brace axial forces versus brace axial deformations of TCBF-B-4 specimen .....	360

Figure 4.368	Estimated brace axial forces versus measured brace out-of-plane displacements at the brace center point of each HSS brace of TCBF-B-4 specimen.....	360
Figure 4.369	Estimated brace axial force, brace axial deformation and measured brace out-of-plane displacement relationships of TCBF-B-4 specimen.....	361
Figure 4.370	Time history of the decomposed strain components of eastern side HSS brace in the first story of TCBF-B-4 specimen .....	362
Figure 4.371	Time history of the decomposed strain components of western side HSS brace in the first story of TCBF-B-4 specimen .....	362
Figure 4.372	Time history of the decomposed strain components of eastern side HSS brace in the second story of TCBF-B-4 specimen.....	363
Figure 4.373	Time history of the decomposed strain components of western side HSS brace in the second story of TCBF-B-4 specimen.....	363
Figure 4.374	Estimated panel zone shear stress vs. shear strain relationships of TCBF-B-4 specimen .....	364
Figure 4.375	Time history of rosette type strain gauge readings in the lower panel zone of TCBF-B-4 specimen (location: R2).....	365
Figure 4.376	Time history of rosette type strain gauge readings in the lower panel zone of TCBF-B-4 specimen (location: R6).....	366
Figure 4.377	Time history of rosette type strain gauge readings in the lower panel zone of TCBF-B-4 specimen (location: R4).....	367
Figure 4.378	Time history of rosette type strain gauge readings in the lower panel zone of TCBF-B-4 specimen (location: R8).....	368
Figure 4.379	Normalized maximum principal stress vs. normalized minimum principal stress in the lower panel zone of TCBF-B-4 specimen (location: R2) .....	369
Figure 4.380	Normalized maximum principal stress vs. normalized minimum principal stress in the lower panel zone of TCBF-B-4 specimen (location: R6) .....	369
Figure 4.381	Normalized maximum principal stress vs. normalized minimum principal stress in the lower panel zone of TCBF-B-4 specimen (location: R4) .....	370
Figure 4.382	Normalized maximum principal stress vs. normalized minimum principal stress in the lower panel zone of TCBF-B-4 specimen (location: R8) .....	370

Figure 4.383	Time history of rosette type strain gauge readings in the one-piece gusset plate of TCBF-B-4 specimen (location: R9).....	371
Figure 4.384	Time history of rosette type strain gauge readings in the one-piece gusset plate of TCBF-B-4 specimen (location: R10).....	372
Figure 4.385	Time history of rosette type strain gauge readings in the one-piece gusset plate of TCBF-B-4 specimen (location: R11).....	373
Figure 4.386	Time history of rosette type strain gauge readings in the one-piece gusset plate of TCBF-B-4 specimen (location: R12).....	374
Figure 4.387	Time history of rosette type strain gauge readings in the one-piece gusset plate of TCBF-B-4 specimen (location: R13).....	375
Figure 4.388	Time history of rosette type strain gauge readings in the one-piece gusset plate of TCBF-B-4 specimen (location: R14).....	376
Figure 4.389	Time history of rosette type strain gauge readings in the one-piece gusset plate of TCBF-B-4 specimen (location: R15).....	377
Figure 4.390	Time history of rosette type strain gauge readings in the one-piece gusset plate of TCBF-B-4 specimen (location: R16).....	378
Figure 4.391	Time history of rosette type strain gauge readings in the one-piece gusset plate of TCBF-B-4 specimen (location: R17).....	379
Figure 4.392	Time history of rosette type strain gauge readings in the one-piece gusset plate of TCBF-B-4 specimen (location: R18).....	380
Figure 4.393	Time history of rosette type strain gauge readings in the one-piece gusset plate of TCBF-B-4 specimen (location: R19).....	381
Figure 4.394	Time history of rosette type strain gauge readings in the one-piece gusset plate of TCBF-B-4 specimen (location: R20).....	382
Figure 4.395	Normalized maximum principal stress vs. normalized minimum principal stress in the one-piece gusset plate of TCBF-B-4 specimen (location: R9) .....	383
Figure 4.396	Normalized maximum principal stress vs. normalized minimum principal stress in the one-piece gusset plate of TCBF-B-4 specimen (location: R10) .....	383
Figure 4.397	Normalized maximum principal stress vs. normalized minimum principal stress in the one-piece gusset plate of TCBF-B-4 specimen (location: R11) .....	384

Figure 4.398	Normalized maximum principal stress vs. normalized minimum principal stress in the one-piece gusset plate of TCBF-B-4 specimen (location: R12) .....	384
Figure 4.399	Normalized maximum principal stress vs. normalized minimum principal stress in the one-piece gusset plate of TCBF-B-4 specimen (location: R13) .....	385
Figure 4.400	Normalized maximum principal stress vs. normalized minimum principal stress in the one-piece gusset plate of TCBF-B-4 specimen (location: R14) .....	385
Figure 4.401	Normalized maximum principal stress vs. normalized minimum principal stress in the one-piece gusset plate of TCBF-B-4 specimen (location: R15) .....	386
Figure 4.402	Normalized maximum principal stress vs. normalized minimum principal stress in the one-piece gusset plate of TCBF-B-4 specimen (location: R16) .....	386
Figure 4.403	Normalized maximum principal stress vs. normalized minimum principal stress in the one-piece gusset plate of TCBF-B-4 specimen (location: R17) .....	387
Figure 4.404	Normalized maximum principal stress vs. normalized minimum principal stress in the one-piece gusset plate of TCBF-B-4 specimen (location: R18) .....	387
Figure 4.405	Normalized maximum principal stress vs. normalized minimum principal stress in the one-piece gusset plate of TCBF-B-4 specimen (location: R19) .....	388
Figure 4.406	Normalized maximum principal stress vs. normalized minimum principal stress in the one-piece gusset plate of TCBF-B-4 specimen (location: R20) .....	388
Figure 4.407	The actuator force vs. bracket deformation relationship at both floor levels during hybrid simulation .....	389
Figure 4.408	Slippage time history between specimen and test setup boundaries during hybrid simulation.....	390
Figure 4.409	The out-of-plane deformation time history of lateral supporting frame at different monitoring points during hybrid simulation .....	391
Figure 4.410	The reconfigurable reaction wall (RRW) tip deformation time histories during hybrid simulation .....	392
Figure 4.411	The whitewash flaking near the repaired column base .....	394
Figure 4.412	Global buckling of eastern side brace in the first story .....	395
Figure 4.413	Global buckling of western side brace in the second story .....	395
Figure 4.414	Local buckling of eastern side brace in the first story.....	396
Figure 4.415	Local buckling of western side brace in the second story .....	396



Figure 4.416	Local yielding in the beam-to-gusset plate splice .....	397
Figure 4.417	Additional flaking of whitewash near the lower beam splice plate.....	397
Figure 4.418	Panel zone yielding in the roof beam to column connection region .....	398
Figure 4.419	Cracks in the first story eastern side brace .....	398
Figure 4.420	Cracks in the second story western side brace .....	399
Figure 4.421	Crack propagation in the second story western side brace.....	399
Figure 4.422	Cracks developed in the first story western side brace.....	400
Figure 4.423	Cracks opening in the second story eastern brace .....	400
Figure 4.424	Completely fracture of the second story eastern side brace .....	401
Figure 4.425	Completely fracture of the second story western side brace .....	401
Figure 4.426	Completely fracture of the first story eastern side brace .....	402
Figure 4.427	Completely fracture of the first story western side brace.....	402
Figure 4.428	Local buckling of column flanges in the first story columns .....	403
Figure 5.1	Backbone curves of each specimen (both the cycle one and the cycle two in each load stage) .....	418
Figure 5.2	Total cumulative energy dissipation of each specimen (GB: global buckling, LB: local buckling, CF: first brace completely fracture) .....	418
Figure 5.3	Total energy dissipation in each excursion and total cumulative energy dissipation of TCBF-B-1 specimen .....	419
Figure 5.4	Total energy dissipation in each excursion and total cumulative energy dissipation of TCBF-B-2 specimen .....	419
Figure 5.5	Total energy dissipation in each excursion and total cumulative energy dissipation of TCBF-B-3 specimen .....	420
Figure 5.6	Total roof plastic displacement in each excursion and total cumulative roof plastic displacement of three specimens .....	421
Figure 5.7	Normalized energy dissipation in each excursion and cumulative normalized energy dissipation of three specimens .....	422
Figure 5.8	Story deformation ratio of TCBF-B-1 specimen.....	423
Figure 5.9	Story deformation ratio of TCBF-B-2 specimen.....	423
Figure 5.10	Story deformation ratio of TCBF-B-3 specimen.....	424
Figure 5.11	Story energy dissipation ratio of TCBF-B-1 specimen.....	424

Figure 5.12	Story energy dissipation ratio of TCBF-B-2 specimen .....	425
Figure 5.13	Story energy dissipation ratio of TCBF-B-3 specimen .....	425
Figure 5.14	Buckling shape of the first story eastern side brace of TCBF-B-1 specimen in compression excursions .....	429
Figure 5.15	Buckling shape of the first story western side brace of TCBF-B-1 specimen in compression excursions .....	429
Figure 5.16	Buckling shape of the second story eastern side brace of TCBF-B-1 specimen in compression excursions .....	430
Figure 5.17	Buckling shape of the second story western side brace of TCBF-B-1 specimen in compression excursions .....	430
Figure 5.18	Buckling shape of the first story eastern side brace of TCBF-B-2 specimen in compression excursions .....	431
Figure 5.19	Buckling shape of the first story western side brace of TCBF-B-2 specimen in compression excursions .....	431
Figure 5.20	Buckling shape of the second story eastern side brace of TCBF-B-2 specimen in compression excursions .....	432
Figure 5.21	Buckling shape of the second story western side brace of TCBF-B-2 specimen in compression excursions .....	432
Figure 5.22	Buckling shape of the first story eastern side brace of TCBF-B-3 specimen in compression excursions .....	433
Figure 5.23	Buckling shape of the first story western side brace of TCBF-B-3 specimen in compression excursions .....	433
Figure 5.24	Buckling shape of the second story eastern side brace of TCBF-B-3 specimen in compression excursions .....	434
Figure 5.25	Buckling shape of the second story western side brace of TCBF-B-3 specimen in compression excursions .....	434
Figure 5.26	Brace cumulative normalized energy dissipation and normalized energy dissipation of TCBF-B-1 specimen in each excursion.....	435
Figure 5.27	Brace cumulative plastic deformations and plastic deformations of TCBF-B-1 specimen in each excursion .....	435

Figure 5.28	Brace cumulative normalized energy dissipation and normalized energy dissipation of TCBF-B-2 specimen in each excursion.....	436
Figure 5.29	Brace cumulative plastic deformations and plastic deformations of TCBF-B-2 specimen in each excursion .....	436
Figure 5.30	Brace cumulative normalized energy dissipation and normalized energy dissipation of TCBF-B-3 specimen in each excursion.....	437
Figure 5.31	Brace cumulative plastic deformations and plastic deformations of TCBF-B-3 specimen in each excursion .....	437
Figure 5.32	Source of total energy dissipation in each excursion and total cumulative energy dissipation of TCBF-B-1 specimen .....	438
Figure 5.33	Source of total energy dissipation in each excursion and total cumulative energy dissipation of TCBF-B-2 specimen .....	438
Figure 5.34	Source of total energy dissipation in each excursion and total cumulative energy dissipation of TCBF-B-3 specimen .....	439
Figure 5.35	Demonstration of geometry amplification effect at the lower beam to gusset plate connections .....	441
Figure 5.36	The lower beam end rotation versus first story drift ratio relationships of each specimen .....	442
Figure 5.37	Ground motion time history for the hybrid simulation .....	444
Figure 5.38	Floor level displacement time histories of TCBF-B-4 specimen .....	451
Figure 5.39	Story force time histories of TCBF-B-4 specimen.....	451
Figure 5.40	Total energy dissipation in each time segment and total cumulative energy dissipation of TCBF-B-4 specimen .....	452
Figure 5.41	Total roof plastic displacement in each time segment and total cumulative roof plastic displacement of TCBF-B-4 specimen .....	452
Figure 5.42	Normalized energy dissipation in each time segment and cumulative normalized energy dissipation of TCBF-B-4 specimen.....	453
Figure 5.43	Story deformation ratio of TCBF-B-4 specimen.....	453
Figure 5.44	Story energy dissipation ratio of TCBF-B-4 specimen .....	454
Figure 5.45	Brace cumulative normalized energy dissipation and normalized energy dissipation of TCBF-B-4 specimen in each time segment.....	457

Figure 5.46	Brace cumulative plastic deformations and plastic deformations of TCBF-B-4 specimen in each time segment.....	457
Figure 5.47	Source of energy dissipation in each time segment and total cumulative energy dissipation of TCBF-B-4 specimen .....	458
Figure 5.48	The lower beam end rotation versus first story drift ratio relationships of TCBF-B-4 specimen .....	460
Figure 5.49	Synchronization subspace plot of top actuator during hybrid test .....	462
Figure 5.50	Synchronization subspace plot of bottom actuator during hybrid test .....	462
Figure 6.1	Simple strut tests at University of California, Berkeley (Yang and Mahin, 2005) ..	467
Figure 6.2	Loading protocols of simple strut tests (Yang and Mahin, 2005) .....	468
Figure 6.3	Demonstration of the fiber sections and element numbers used in OpenSees strut models .....	468
Figure 6.4	Axial force versus axial deformation relationship of specimen #4 from experiment and OpenSees simulation.....	469
Figure 6.5	Axial force versus out-of-plane displacement relationship of specimen #4 from experiment and OpenSees simulation.....	469
Figure 6.6	Axial force versus axial deformation relationship of specimen #5 from experiment and OpenSees simulation.....	470
Figure 6.7	Axial force versus out-of-plane displacement relationship of specimen #5 from experiment and OpenSees simulation.....	470
Figure 6.8	Demonstration of a braced frame model in OpenSees .....	472
Figure 6.9	Base shear versus roof displacement relationship of TCBF-B-1 specimen from experiment and OpenSees simulation (trial one).....	473
Figure 6.10	Base shear versus roof displacement relationship of TCBF-B-1 specimen from experiment and OpenSees simulation (trial two).....	473
Figure 6.11	Brace Axial Force versus axial deformation relationships of TCBF-B-1 specimen from experiment and OpenSees simulation (trial two).....	474
Figure 6.12	Base shear versus roof displacement relationship of TCBF-B-2 specimen from experiment and OpenSees simulation.....	474
Figure 6.13	Brace Axial Force versus axial deformation relationships of TCBF-B-2 specimen from experiment and OpenSees simulation.....	475

Figure 6.14	Base shear versus roof displacement relationship of TCBF-B-3 specimen from experiment and OpenSees simulation .....	475
Figure 6.15	Brace Axial Force versus axial deformation relationships of TCBF-B-3 specimen from experiment and OpenSees simulation .....	476
Figure 6.16	Displacement time histories of TCBF-B-4 specimen from elastic hybrid test and OpenSees simulation (pinned lower beam ends) .....	480
Figure 6.17	Displacement time histories of TCBF-B-4 specimen from elastic hybrid test and OpenSees simulation (semi-rigid lower beam ends) .....	480
Figure 6.18	Demonstration of semi-rigid lower beam ends in TCBF-B-4 specimen .....	481
Figure 6.19	Free vibration test results of TCBF-B-4 specimen .....	481
Figure 6.20	Displacement time histories of TCBF-B-4 specimen from DE and MCE hybrid test and OpenSees simulation (semi-rigid lower beam ends) .....	482
Figure 6.21(a)	Base shear versus roof displacement relationships of TCBF-B-4 specimen from DE hybrid test and OpenSees simulation (semi-rigid lower beam ends) .....	482
Figure 6.21(b)	Base shear versus roof displacement relationships of TCBF-B-4 specimen from MCE hybrid test and OpenSees simulation (semi-rigid lower beam ends) .....	483
Figure 6.21(c)	Base shear versus roof displacement relationships of TCBF-B-4 specimen from DE and MCE hybrid test and OpenSees simulation (the semi-rigid lower beam ends) .....	483
Figure 6.22	Brace axial force versus axial deformation relationships of TCBF-B-4 specimen from DE and MCE hybrid test and OpenSees simulation (semi-rigid lower beam ends) .....	484
Figure 6.23	Displacement time histories of simulated TCBF-B-4 specimen subjected to MCE ground motion and then DE ground motion (semi-rigid lower beam ends) .....	484
Figure 6.24	Base shear versus roof displacement relationships of simulated TCBF-B-4 specimen subjected to MCE ground motion and then DE ground motion (semi-rigid lower beam ends) .....	485
Figure 6.25	Brace axial force versus axial deformation relationships of simulated TCBF-B-4 specimen subjected to MCE ground motion and then DE ground motion (semi-rigid lower beam ends) .....	485

Figure 6.26	Assumed braced bay for the square HSS struts and the relationship between brace axial deformation and story drift.....	488
Figure 6.27	Normalized axial force versus normalized axial deformation and normalized out-of-plane deformation relationships of square HSS $6 \times 6 \times 3/8$ with $kL/r = 60$ .....	490
Figure 6.28	Normalized axial force versus normalized axial deformation and normalized out-of-plane deformation relationships of square HSS $16 \times 16 \times 5/8$ with $kL/r = 100$ .....	490
Figure 6.29	Normalized energy dissipation of selected square hollow structural sections until brace failure ( $kL/r = 40$ ).....	494
Figure 6.30	Normalized energy dissipation of selected square hollow structural sections until brace failure ( $kL/r = 60$ ).....	494
Figure 6.31	Normalized energy dissipation of selected square hollow structural sections until brace failure ( $kL/r = 80$ ).....	495
Figure 6.32	Normalized energy dissipation of selected square hollow structural sections until brace failure ( $kL/r = 100$ ).....	495
Figure 6.33	Normalized energy dissipation of selected square hollow structural sections until brace failure ( $kL/r = 150$ ).....	496
Figure 6.34	Normalized energy dissipation of selected square hollow structural sections until brace failure ( $kL/r = 200$ ).....	496
Figure 6.35	Normalized energy dissipation until brace failure of selected square hollow structural sections with different $kL/r$ ratios .....	497
Figure 6.36	Group comparisons of normalized energy dissipation of selected square hollow structural sections with different $kL/r$ ratios .....	497
Figure 6.37	Mesh pattern for the simple strut modelling in LS-DYNA.....	499
Figure 6.38	Illustration of simplified models for the simple strut modeling in LS-DYNA .....	499
Figure 6.39	Axial force versus axial deformation relationship of specimen #5 from experiment and LS-DYNA simulation .....	500
Figure 6.40	Axial force versus out-of-plane displacement relationship of specimen #5 from experiment and LS-DYNA simulation .....	500
Figure 6.41	Comparison between actual test and LS-DYNA simulation results at final cycle.	501
Figure 6.42	Crack initiation in HSS brace section wall simulated by LS-DYNA model.....	502
Figure 6.43	Complete fracture in the LS-DYNA strut model .....	502

Figure 6.44	Axial force versus axial deformation relationship of specimen #4 from experiment and LS-DYNA simulation .....	503
Figure 6.45	Axial force versus out-of-plane displacement relationship of specimen #4 from experiment and LS-DYNA simulation .....	503
Figure 6.46	Comparison between actual test and FE model under near-fault loading protocol	504
Figure 6.47	Comparison between actual test and FE model at the final stage of testing .....	504
Figure 6.48	Mesh layout in the LS-DYNA simulation for TCBF-B-1 specimen.....	506
Figure 6.49	Base shear versus roof displacement from LS-DYNA simulation for TCBF-B-1 specimen .....	507
Figure 6.50	Von Mises stress distribution of TCBF-B-1 specimen at the end of LS-DYNA simulation.....	507
Figure 6.51	Plastic strain distribution of TCBF-B-1 specimen at the end of LS-DYNA simulation.....	508
Figure 6.52	Base shear versus roof displacement from LS-DYNA simulation for TCBF-B-2 specimen .....	509
Figure 6.53	Von Mises stress distribution of TCBF-B-2 specimen at the end of LS-DYNA simulation.....	509
Figure 6.54	Plastic strain distribution of TCBF-B-2 specimen at the end of LS-DYNA simulation.....	510
Figure 6.55	Base shear versus roof displacement from LS-DYNA simulation for TCBF-B-3 specimen .....	511
Figure 6.56	Von Mises stress distribution of TCBF-B-3 specimen at the end of LS-DYNA simulation.....	511
Figure 6.57	Plastic strain distribution of TCBF-B-3 specimen at the end of LS-DYNA simulation.....	512
Figure 7.1	Illustration of different braced frame systems (Khatib, Mahin and Pister, 1988)....	517
Figure 7.3	Possible strong-back configuration details with buckling-restrained braces along the entire or partial height of the building .....	519
Figure 7.4	More possible strong-back configurations with different spine systems .....	520
Figure 7.5	Plan view of the example building and the two-dimensional model elevation.....	522
Figure 7.6	Elevation views of six different bracing configurations.....	524

Figure 7.7	Averaged spectrum of selected ground motion records .....	532
Figure 7.8	Base shear versus roof displacement relationships of six models .....	533
Figure 7.9	Base shear versus roof displacement relationships of each model under cyclic pushover .....	535
Figure 7.10	Maximum story drift ratios for each model under different hazard level ground motions .....	544
Figure 7.11	Residual story drift ratios for each model after different hazard level ground excitations .....	544
Figure 7.12	Maximum floor level accelerations for each model under different hazard level ground motions .....	545
Figure 7.13	Base shear versus roof displacement relationship of model V6 under NGA 1119 fault-normal component ground motion .....	546
Figure 7.14	Story drift ratio histories of model V6 under NGA 1119 fault-normal component ground motion .....	546
Figure 7.15	Fourth story to sixth story brace axial force versus axial deformation relationships of model V6 under NGA 1119 fault-normal component ground motion .....	547
Figure 7.16	First story to third story brace axial force versus axial deformation relationships of model V6 under NGA 1119 fault-normal component ground motion .....	548
Figure 7.17	Base shear versus roof displacement relationship of model V6 under NGA 1602 fault-parallel component ground motion .....	549
Figure 7.18	Story drift ratio histories of model V6 under NGA 1602 fault-parallel component ground motion .....	549
Figure 7.19	Fourth story to sixth story brace axial force versus axial deformation relationships of model V6 under NGA 1602 fault-parallel component ground motion .....	550
Figure 7.20	First story to third story brace axial force versus axial deformation relationships of model V6 under NGA 1602 fault-parallel component ground motion .....	551
Figure 7.21	Base shear versus roof displacement relationship of model X6 under NGA 1119 fault-normal component ground motion .....	552
Figure 7.22	Story drift ratio histories of model X6 under NGA 1119 fault-normal component ground motion .....	552



Figure 7.23	Fourth story to sixth story brace axial force versus axial deformation relationships of model X6 under NGA 1119 fault-normal component ground motion .....	553
Figure 7.24	First story to third story brace axial force versus axial deformation relationships of model X6 under NGA 1119 fault-normal component ground motion .....	554
Figure 7.25	Base shear versus roof displacement relationship of model X6 under NGA 1602 fault-parallel component ground motion .....	555
Figure 7.26	Story drift ratio histories of model X6 under NGA 1602 fault-parallel component ground motion.....	555
Figure 7.27	Fourth story to sixth story brace axial force versus axial deformation relationships of model X6 under NGA 1602 fault-parallel component ground motion .....	556
Figure 7.28	First story to third story brace axial force versus axial deformation relationships of model X6 under NGA 1602 fault-parallel component ground motion.....	557
Figure 7.29	Base shear versus roof displacement relationship of model X6-3 under NGA 1119 fault-normal component ground motion .....	558
Figure 7.30	Story drift ratio histories of model X6-3 under NGA 1119 fault-normal component ground motion.....	558
Figure 7.31	Fourth story to sixth story brace axial force versus axial deformation relationships of model X6-3 under NGA 1119 fault-normal component ground motion.....	559
Figure 7.32	First story to third story brace axial force versus axial deformation relationships of model X6-3 under NGA 1119 fault-normal component ground motion .....	560
Figure 7.33	Base shear versus roof displacement relationship of model X6-3 under NGA 1602 fault-parallel component ground motion .....	561
Figure 7.34	Story drift ratio histories of model X6-3 under NGA 1602 fault-parallel component ground motion.....	561
Figure 7.35	Fourth story to sixth story brace axial force versus axial deformation relationships of model X6-3 under NGA 1602 fault-parallel component ground motion .....	562
Figure 7.36	First story to third story brace axial force versus axial deformation relationships of model X6-3 under NGA 1602 fault-parallel component ground motion .....	563
Figure 7.37	Base shear versus roof displacement relationship of model SB6-3 under NGA 1119 fault-normal component ground motion .....	564

Figure 7.38	Story drift ratio histories of model SB6-3 under NGA 1119 fault-normal component ground motion.....	564
Figure 7.39	Fourth story to sixth story brace axial force versus axial deformation relationships of model SB6-3 under NGA 1119 fault-normal component ground motion.....	565
Figure 7.40	First story to third story brace axial force versus axial deformation relationships of model SB6-3 under NGA 1119 fault-normal component ground motion .....	566
Figure 7.41	Base shear versus roof displacement relationship of model SB6-3 under NGA 1602 fault-parallel component ground motion .....	567
Figure 7.42	Story drift ratio histories of model SB6-3 under NGA 1602 fault-parallel component ground motion .....	567
Figure 7.43	Fourth story to sixth story brace axial force versus axial deformation relationships of model SB6-3 under NGA 1602 fault-parallel component ground motion .....	568
Figure 7.44	First story to third story brace axial force versus axial deformation relationships of model SB6-3 under NGA 1602 fault-parallel component ground motion .....	569
Figure 7.45	Base shear versus roof displacement relationship of model SB6-3B under NGA 1119 fault-normal component ground motion .....	570
Figure 7.46	Story drift ratio histories of model SB6-3B under NGA 1119 fault-normal component ground motion .....	570
Figure 7.47	Fourth story to sixth story brace axial force versus axial deformation relationships of model SB6-3B under NGA 1119 fault-normal component ground motion .....	571
Figure 7.48	First story to third story brace axial force versus axial deformation relationships of model SB6-3B under NGA 1119 fault-normal component ground motion .....	572
Figure 7.49	Base shear versus roof displacement relationship of model SB6-3B under NGA 1602 fault-parallel component ground motion .....	573
Figure 7.50	Story drift ratio histories of model SB6-3B under NGA 1602 fault-parallel component ground motion .....	573
Figure 7.51	Fourth story to sixth story brace axial force versus axial deformation relationships of model SB6-3B under NGA 1602 fault-parallel component ground motion .....	574
Figure 7.52	First story to third story brace axial force versus axial deformation relationships of model SB6-3B under NGA 1602 fault-parallel component ground motion.....	575

Figure 7.53	Base shear versus roof displacement relationship of model SB6-3L under NGA 1119 fault-normal component ground motion .....	576
Figure 7.54	Story drift ratio histories of model SB6-3L under NGA 1119 fault-normal component ground motion .....	576
Figure 7.55	Fourth story to sixth story brace axial force versus axial deformation relationships of model SB6-3L under NGA 1119 fault-normal component ground motion .....	577
Figure 7.56	First story to third story brace axial force versus axial deformation relationships of model SB6-3L under NGA 1119 fault-normal component ground motion.....	578
Figure 7.57	Base shear versus roof displacement relationship of model SB6-3L under NGA 1602 fault-parallel component ground motion .....	579
Figure 7.58	Story drift ratio histories of model SB6-3L under NGA 1602 fault-parallel component ground motion .....	579
Figure 7.59	Fourth story to sixth story brace axial force versus axial deformation relationships of model SB6-3L under NGA 1602 fault-parallel component ground motion.....	580
Figure 7.60	First story to third story brace axial force versus axial deformation relationships of model SB6-3L under NGA 1602 fault-parallel component ground motion .....	581

## LIST OF TABLES

Table 2.1	Slenderness ratio and width-to-thickness ratio limitations .....	13
Table 3.1	Name, member size, material type and test method of the specimens .....	54
Table 3.2	Section properties of beams and columns.....	55
Table 3.3	Section properties of HSS braces (square and round) .....	55
Table 3.4	Section properties of wide flange braces .....	55
Table 3.5	Vertical distribution of seismic forces .....	96
Table 3.6	The site information of selected ground motion.....	101
Table 4.1	Material mechanical properties from mill certificates.....	110
Table 4.2	The major observations during specimen TCBF-B-1 test .....	169
Table 4.3	The major observations during specimen TCBF-B-2 test .....	245
Table 4.4	The major observations during specimen TCBF-B-3 test .....	324
Table 5.1	Loading Protocol Details of TCBF-B Specimens.....	405
Table 5.2	Base shear and roof displacement data of TCBF-B-1 .....	409
Table 5.3	Base shear and roof displacement data of TCBF-B-2 .....	412
Table 5.4	Base shear and roof displacement data of TCBF-B-3 .....	415
Table 5.5	Measured eccentricities of brace before test and buckling direction during the test.....	428
Table 5.6	Specimen failure characteristics (brace completely fractures) .....	428
Table 5.7	Input ground motion parameters.....	444
Table 5.8	Story shear and floor level displacement data of TCBF-B-4.....	448
Table 5.9	Specimen TCBF-B-4 brace failure characteristics (brace completely fractures) .....	456
Table 6.1	Input parameter details in OpenSees 2D model.....	467
Table 6.2	The dimensions of selected square hollow structural sections .....	489
Table 6.3	Normalized cumulative energy dissipation of selected square hollow structural sections under different $kL/r$ ratios .....	491
Table 6.4	Normalized cumulative energy dissipation of selected group of square hollow structural sections under different $kL/r$ ratios .....	493
Table 7.1	Six-story model building with different seismic force-resisting systems.....	524
Table 7.2	Model V6 Member Size Information.....	525
Table 7.3	Model X6 Member Size Information.....	526

Table 7.4	Model X6-3 Member Size Information .....	527
Table 7.5	Model SB6-3 Member Size Information .....	528
Table 7.6	Model SB6-3B Member Size Information.....	529
Table 7.7	Model SB6-3L Member Size Information.....	530
Table 7.8	Predefined ground motion search criteria.....	532
Table 7.9	Selected ground motion pairs for nonlinear dynamic response history analysis .....	532
Table 7.10	Prescribed roof displacements for cyclic pushover analyses.....	534
Table 7.11	Identification number list for all ground motions.....	536
Table 7.12	Fundamental and second mode periods of each model .....	537
Table 7.13	Mean responses of each model under selected ground motions .....	538
Table 7.14	Mean responses of each model under selected ground motions .....	539
Table 7.15	Mean responses of each model under selected ground motions .....	540
Table 7.16	Mean responses of each model under selected ground motions .....	541

# 1 Introduction

## 1.1 BACKGROUND AND RESEARCH MOTIVATION

Over the past few decades, steel concentrically braced frame systems are considered an efficient and economical lateral force-resisting systems to control the lateral deformation in building structures under wind loading or earthquake ground shaking. Already widely used in the United States, this kind of structural system has been increasingly employed in the Pacific west coast given that another design strategy—steel moment-resisting frames—have proved susceptible to large deformations during strong ground shaking. In addition to the larger displacements, significant damage observed in the 1994 Northridge earthquakes necessitated giving special attention to the beam-to-column connections in moment-resisting frames to avoid problems associated with brittle failures in these regions. However, a review of structural damage to the concentrically steel braced frame systems after several major earthquakes has identified some anticipated and unanticipated damages (Steinbrugge et. al., 1971; EERI, 1978; Tanaka et. al, 1980 and Kato et. al, 1980; SEAOC, 1991; Phipps et. al, 1992; AIJ, 1995; Bonneville and Bartoletti, 1996; EERI, 1997; Kelly et al., 2000). This damage has prompted many engineers and researchers in highly seismic zones to consider new approaches to improve the behavior of steel concentrically braced frame systems.

One of the key components that controls the system behavior of steel concentrically braced frame is the bracing member. Typically, this member will buckle under compression loads and yield under tension forces, which inherently make the behavior complex. The asymmetric hysteretic behavior under cyclic loadings with compression capacity degradation further limits the cyclic deformation capacity of individual braces. Given that such a complex cyclic behavior accompanies a wide range of different structural configurations, it is often difficult to proportion the braces within a braced frame system to achieve uniform brace demand-to-capacity ratios along the height of the braced bay. This variation has been shown to be one of critical factors causing the concentration of deformation on certain floor levels.

Another key component that affects the braced frame behavior is the connection. A significant number of failure modes associated with connections have been observed in both the laboratory and the field. Although these failure modes are often localized near the region of the connection, these failures have substantial effects on the braced frame global behavior. For instance, premature or brittle failures in the brace-to-gusset plate connections near the net section regions usually occurs before inelastic demands develop in the braces, meaning that the entire braced frame is essentially elastic when the connection fails.

Many strategies exist to improve the concentric steel braced frame behaviors; they vary from component level to system level. For example, one way to make changes at the component level is using devices such as buckling-restrained braces (Watanabe et al., 1988; Kalyanamaran

et al., 1998 and 2003; Chen et al., 2001; Mahin et al., 2004; Lai et al., 2004) or self-centering braces (Christopoulos et al., 2008; Tremblay et al., 2008). These kinds of braces have excellent and stable hysteresis behaviors but have drawbacks: they are usually more expensive than the conventional buckling braces and typically require paying proprietary fees. The more recently developed re-centering braces exhibit a flag-shaped pattern of hysteresis loops that almost re-centered to the un-deformed condition of structure. But most of this research has been conducted on small-scale models, and much more research needs to be conducted before field applications are viable.

Another way to improve the seismic behavior of steel concentric braced frame is to prevent local concentration of overall system deformation at one or a few stories by improving the distribution of inelastic demand along the entire height of the structure (Khatib et al., 1988). Although this concept was proposed several decades ago, the analytical and experimental state-of-the-art weren't adequate at that time. Recently this concept has been revived by several researchers (Sabelli, 2001; Tremblay, 2003; Tremblay and Merzouq, 2004; Tirca and Tremblay, 2004; Mahin and Lai, 2008; Yang et al., 2008 and 2010) and adopted in seismic retrofit projects and new steel constructions (Mar, 2010). Note that there are many other ways to improve the behavior of braced frame behaviors that will not be discussed herein.

Although many experimental studies of conventional buckling brace components and several braced frame specimens have been investigated over the past forty years (e.g., Black et al., 1980; Ballio and Perotti, 1987; Lee and Goel, 1987; Bertero et al., 1989; Tremblay, 2002; Yang and Mahin, 2005; Fell et al., 2006; Uriz and Mahin, 2008; Clark et al., 2008; Yang et al., 2008; Lumpkin et al., 2009; for a more detailed list see Chapter 2), the number of studies on the full-scale concentric braced frames is still limited. Many of these existing research efforts focused on investigating individual brace behavior by using reduced-scale brace specimens and some of the specimens tested initially used structural details rarely used in current practice. As for the braced frames, they were often single-story, one-bay small-scale specimens loaded at the top of one-story structures that focused on the brace-to-gusset plate connection behaviors. Through the improvement of test equipment and laboratory techniques, the cyclic behaviors of several large-scale multi-story braced frame specimens have been tested and studied. However, even with the improved testing set ups, these braced frame specimens have been typically loaded at roof level only, which does not represent real conditions. Moreover, quasi-static cyclic loading sequences were often used in these tests, and only a few of them were tested pseudo-dynamically to simulate the braced frame behaviors under actual ground motion records.

Most existing analytical investigations focused on the study of nonlinear cyclic behavior of structural components in braced frames; few of them tackled the inelastic behavior of large-scale specimens. Analytical studies of system level performances are comparatively rarer and often limited to conventional brace configurations, such as chevron bracing (inverted-V), V-shaped bracing, or split-X bracing configuration.

These observations have stimulated the experimental and analytical study of the nonlinear behavior of concentrically steel braced frame systems designed to current codes and structural details. The opportunity to improve and validate the design concepts for tomorrow's concentrically steel braced frame structures through developing innovative braced frame systems and validating practical computer models exists, with the added benefit of using these improved models under the framework of modern performance-based earthquake engineering to evaluate braced frame systems.

Conducted at the NEES Berkeley site, the experimental part of this research consisted of four full-scale one-bay two-story steel concentrically braced frames that were constructed and tested under a series of incremental cyclic loadings increasing in amplitude up to a maximum roof drift ratio about 4%. Hybrid simulations were also conducted to examine the braced frame system behavior under two selected hazard level ground motions, with maximum expected roof drift ratio up to 5% or more. Note that in a companion study (Chen and Mahin, 2010; Lai et al., 2010), nonlinear dynamic analyses showed that under the most severe hazard level (i.e., 2% probability of exceedance in 50 years), the median expected maximum story drift ratio was about 3.3%. In a previous analytical study with a 10% probability of exceedance in 50-year ground motions (Sabelli, 2000), the mean maximum story drift ratio in the concentrically steel braced frame could be as large as 3.9%, and the mean residual story drift ratio could be as large as 2.5%.

For the analytical portion, testing data obtained from previous individual brace components were first used to validate the analytical models at the component level. Next, the new data obtained from the full-scale braced frame specimens were used to confirm the validation of analytical model at the system level. With the calibrated and validated models in hand, forty compact square hollow structural sections selected from the steel design manual. These sections were numerically tested under prescribed cyclic loadings with various slenderness ratios to investigate the sensitivity of inelastic behaviors of brace components to actual width-to-thickness ratios and member slenderness ratios. Finally, a series of nonlinear dynamic response history analyses were performed to examine the dynamic behaviors of six braced frame systems, including the proposed Strong-Back System and hybrid braced frame system.

## 1.2 RESEARCH OBJECTIVES AND SCOPE

The fundamental goal of this research was to investigate the system performance of steel concentrically braced frame structures subjected to both quasi-static cyclic loadings and severe ground motions. Through experimental studies on full-scale specimens, the structural characteristics that control the system global behaviors can be identified and better understood. As mentioned previously, in the last forty years only a few large-scale steel braced frame specimens have been performed, and some of them had unrealistic lateral force distributions or loading boundary conditions in the test set up. Accordingly, reported herein is a new test program and a test set up that imposes a lateral force pattern on the braced frame specimen that better represents the lateral force distribution that occurs in a real seismic event. The hybrid simulation or pseudo-dynamic testing techniques introduced into the experimental program document the steel braced frame specimen cyclic behaviors under different hazard level input ground motions. The main objectives and scope of the test program are as follows:

- To obtain the experimental data on the behavior of key components such as bracing components, gusset plates, connections and braced frame systems.
- To provide full-scale braced frame testing data for developing and validating the improved analytical models in both OpenSees and LS-DYNA analysis tools.
- To devise improved design and analysis methods, proposing modifications where appropriate.
- To identify the improved design concepts and structural details.
- To confirm the improvements by both quasi-static cyclic loading tests and hybrid simulations of full-scale steel concentrically braced frame specimens.



In view of the observations from existing studies and past earthquakes, the analytical part of this research aims at scrutinizing the nonlinear behavior of braced frame systems specifically on several topics such as:

- The sensitivity of bracing component cyclic behaviors to slenderness ratios and sectional width-to-thickness ratios.
- Performance evaluation of different design configurations of steel concentrically braced frames.
- Proposal of a hybrid braced frame system—the Strong-Back System—and investigating the inelastic behavior of this system. A series of nonlinear dynamic response history analyses will be performed to examine the dynamic behaviors of the proposed Strong-Back System and hybrid braced frame systems.
- Initiating feasible design recommendations on the proposed system so that it can be incorporated into future design provisions.

### 1.3 OVERVIEW AND ORGANIZATION OF DISSERTATION

To achieve the above-mentioned research objectives, a series of experimental and analytical studies were carried out on various steel concentrically braced frame systems. To support this research, a review of relevant literature is presented in Chapter 2 that examines steel concentric braced frames related to analytical simulations of cyclic and dynamic response and the evolution of applicable building code provisions. This review identifies and discusses several key parameters, such as brace slenderness ratios and width-to-thickness ratios. Experimental studies from previous tests of components, connections, sub-assemblages, and complete braced frames are reviewed. Finally, observations based on reported damage to steel braced frame systems from past earthquakes, including the recent 2011 Great Eastern Japan Earthquake Disaster, are presented.

Chapter 3 describes the overall experimental aspects of the research. Beginning with an overview of the entire test program with an emphasis on the experimental program at Berkeley site, a newly developed full-scale test rig is introduced in detail, followed by detailed design descriptions of four full-scale braced frame specimens. Next the quasi-static loading sequences, specimen instrumentation plans, and construction sequences are presented for each specimen, concluding with a discussion of the design philosophy of hybrid simulation specimen.

Both quasi-static and hybrid simulation test results are present in Chapter 4. The first specimen considered was the braced frame specimen TCBF-B-1, which used square hollow structural sections (HSS) as bracing members. The second specimen considered, TCBF-B-2, used round HSS braces, and the third specimen, TCBF-B-3, used wide-flange bracing members. Finally, to investigate on the braced frame behavior under different hazard level ground shakings, the results of hybrid simulations of TCBF-B-4 specimen are presented where the same square HSS braces are those used as those used in the TCBF-B-1 specimen. Response quantities measured during the experiments were either plotted or tabulated in common formats. Selected still photos taken during the test are also shown at the end of each section.

Further test results are discussed in Chapter 5. Systematic comparisons between quasi-static test results are presented from global responses to local responses. Discussion on the hybrid simulation results are then conducted similarly.

Before conducting the analytical study on the proposed braced frame systems, a series of numerical modeling validations and calibrations were performed in OpenSees and LS-DYNA

using the test data obtained from previous experimental works and current studies. All these analytical modeling details and discussions are included in Chapter 6. Based on calibrated models, results of a simple parametric study on the square HSS bracing members are presented and discussed at the end of this chapter.

Based on current experimental study and extensive literature reviews, a new hybrid braced frame system was developed—the Strong-Back System—and is described in Chapter 7. Static pushover analyses and nonlinear dynamic response history analyses were conducted on six different predefined six-story models including the Strong-Back System to investigate system behaviors and to validate system performance analytically.

Chapter 8 contains the conclusions and summary of the current experimental and analytical study. Several topics not covered herein and investigated in current research are discussed and areas for future study are presented.

Detailed full-scale specimens and test rig design calculations, shop drawings, material mill certificate copies, instrumentation sensor lists, and experimental data reductions are presented in the Appendices, followed by a detailed reference list. Extra plots from the parametric study are also attached in this section.

## 2 Literature Review

This chapter briefly summarizes literature related to the current study. Relevant literature related to component-level studies is examined first, followed by information on connections and systems. Finally, some observations on the behavior of steel concentric braced frames during past earthquakes are presented. Because of the extensive literature that exists on these topics, only major references used to guide the overall scope of this study are discussed in this chapter. Additional references are presented throughout the report.

### 2.1 BRACING COMPONENT

#### 2.1.1 Issues Related to Net Reduced Section

Bracing members are critical components in braced frame systems. They often contribute 75% or more of the total system lateral stiffness and strength. The behavior of braces under tension forces is well understood. Special issues related to the tension behavior at the brace-to-gusset plate connection are reviewed below.

The hollow structural sections frequently used as braces are usually slotted at the end so that they can be welded to the gusset plate. This is a simple and economic approach, but the tip of the slot and the gap between slot tip and gusset plate edge typically form a reduced net section, which may cause premature brittle failure. In the very first “Steel Tips” about the seismic design of special concentrically steel braced frames, Becker (1995) noted that the reduced net section resulting from holes in bolted brace-to-gusset plate connections were identified as a potential problem. It was pointed out that the effective net areas at the connection needed to be checked in the design process and reinforced if necessary. Brittle failures at these locations were observed in past earthquakes (EERI, 1978; AIJ, 1995; EERI, 1997; Astaneh-Asl, 1998) and were generally attributed to poor detailing. Later, possible net reduced section issues in slotted HSS braces were identified, and the use of net section reinforcement side plates was demonstrated as an example (Cochran, 2000 and 2003).

The net reduced section failure mode (see Fig. 2.1) was studied in a series of simple strut tests (Yang and Mahin, 2005). A total of six specimens having end connections mimicking brace-to-gusset plate detailing were tested quasi-statically under different uniaxial loading protocols. In addition to conventional protocols having symmetrically incremented cycles of displacement, tension-dominated cyclic near-fault type excursions and compression-dominated near-fault type protocols were used to examine the cyclic behavior of braces with and without reinforcing cover plates at the net reduced section regions. Five square hollow structural section braces (HSS  $6 \times 6 \times 3/8$ ) and one extra strong pipe section brace (Pipe 6 XS) were employed in the experimental program. The results showed that net reduced section failures occurred when the braces were not reinforced at the net reduced section regions. The type of loading history and cross-sectional shape also had significant effects on the net section failures. For example, the tension-dominated loading histories typically triggered the net reduced section failure of an unreinforced brace earlier than the symmetrical histories, while the compression-dominated histories might not trigger this failure mode at all. The net section failure in the square HSS brace

typically happened earlier than the net section failure in the pipe section brace under the same loading history. While considerable yielding was noted in the unreinforced sections in the vicinity of the reduced net section, the small length of member yielding compared to the total length of the member resulted in a small (nearly brittle) ductility capacity for the braces in tension.



(a) Square HSS



(b) Pipe section

**Figure 2.1 Net section failure mode in a brace without reinforcing plates (extracted from Figures 9 and 16 of Yang and Mahin, 2005)**

Similar net reduced section failures were found in monotonic static loading tests (Korol, 1996; Cheng et al., 1998; Willibard et al., 2006; Packer, 2006), and the tear-out failure mode (block shear) along the weld lines also reported. Similar failures were noted under static and dynamic cyclic loading protocols (Fell, 2008; Fell and Kanvinde, 2010).

The first edition of AISC Seismic Provisions for Structural Steel Buildings (AISC, 1992) listed a minimum ratio of effective net section area to gross section area for bolted brace connections to account for the net section problem. To prevent connection local failures, five years later the second edition of AISC seismic provisions (AISC, 1997) extended the net section provisions from bolted connections to any types of bracing connections under tension forces. Later, the 2002 and 2005 editions (AISC, 2002; AISC, 2005) explicitly stated that the strength of the net section should be greater than the smaller of expected tensile strength of the brace and the maximum force that will develop in the brace. Reinforcing cover plates were mentioned as one scheme to overcome strength deficiencies at the net reduced section. In some instances, welds were wrapped around the gusset plate edges as reinforcement. These were not recommended by many in the United States because of possible poor fit up of the leading edge of the gusset plate and the end of the slot on the brace (making the weld effectiveness difficult to judge) and the potential for high stresses in this area (due to applied loads or weld shrinkage) that could lead to ductility reduction (Cheng et al., 1998) or crack initiation. Other possible reinforcing schemes (Fig. 2.2), while not prohibited by AISC, were not mentioned, including extended gusset plate details (Mitsui and Kurobane, 1981), pad attachments (Mitsui and Maeda, 1986), and modified hidden gap detailing (Packer, 2006; Martinez-Saucedo et al., 2008a and 2008b). The most recent version of the AISC Seismic Provisions (AISC, 2010) retains the basic requirements from the 2005 edition. As the specific issues of the behavior of the net reduced section region and

detailing to mitigate the effects of strength deficiencies are not the subject of this work, simple approaches (i.e., cover plates) will be used herein to avoid premature brittle failures in these regions.

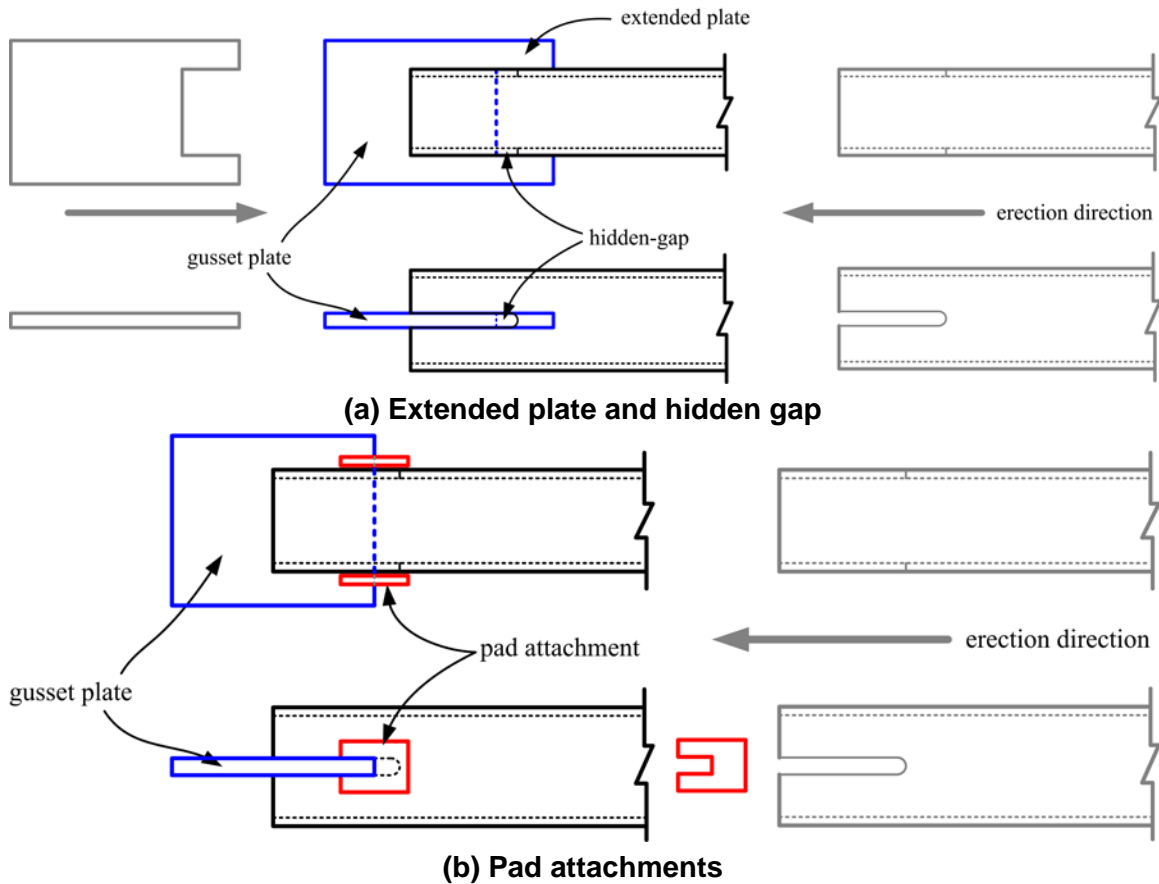


Figure 2.2 Other possible net section reinforcing schemes

### 2.1.2 Limitations on Slenderness Ratio and Width-to-Thickness Ratio

The behavior of braces under compression or cyclic loadings is typically governed by global stability (brace end boundary conditions and slenderness ratio) and local stability (width-to-thickness ratios and brace sectional shapes) issues. Various test results suggest that the slenderness ratio and width-to-thickness ratios should be limited to achieve adequate ductile behavior. For example, observations from shaking table tests of a 0.3-scale model of a six-story concentrically braced frame suggested that the  $P_{cr}/P_y$  and  $b/t$  ratios should be limited (Uang and Bertero, 1986). To prevent undesirable behavior, it was suggested that the  $P_{cr}/P_y$  ratio should be greater than 0.8, and  $b/t$  ratio should be less than 18 for square HSS braces. Based on those suggestions—along with an assumption that the limitation of  $b/t$  ratio is inverse proportional to

$\sqrt{F_y}$  and applying the allowable stress design (ASD) column design formula at that time for intermediate and stocky members—the  $kL/r$  and  $b/t$  ratio limitations could be derived. That is,

$$\frac{P_{cr}}{P_y} = \frac{F_a}{F_y} = \frac{1}{FS} \left[ 1 - \frac{\left(\frac{kL}{r}\right)^2}{2 C_c^2} \right] \geq 0.8 \quad (2.1)$$

$$C_c = \sqrt{\frac{2 \pi^2 E}{F_y}} \quad (2.2)$$

$$FS = \frac{3}{5} + \frac{3}{8} \frac{kL}{r} - \frac{1}{8} \frac{\left(\frac{kL}{r}\right)^3}{C_c^3} \quad (2.3)$$

where  $P_{cr}$  and  $P_y$  are allowable compression force and yield force of brace, respectively,  $F_a$  and  $F_y$  are allowable compression stress and yield strength of brace, respectively,  $FS$  is the safety factor,  $L$  is the brace length,  $r$  is the radius of gyration of the brace section,  $k$  is the effective length factor, and  $C_c$  is the slenderness ratio that separates the long and short columns for ASD column design.

The slenderness ratio limitation can then be found by solving the above equations; getting

$$\frac{kL}{r} \leq 0.8123 \cdot C_c = 0.8123 \cdot \sqrt{\frac{2 \pi^2 E}{F_y}} = \frac{615}{\sqrt{F_y}} \quad (2.4)$$

where  $E$  is the elastic modulus of elasticity of the steel. For the  $b/t$  ratio limitation,

$$\frac{b}{t} \leq 18 = \frac{x}{\sqrt{F_y}} \quad (2.5)$$

where the coefficient  $x$  remains to be determined. Assuming ASTM A500 grade B steel for the square HSS braces,

$$F_y = 46 \text{ ksi} \quad (2.6)$$

and  $x$  can be solved, resulting in the following  $b/t$  ratio limitation formula for square HSS braces:

$$\frac{b}{t} \leq \frac{122}{\sqrt{F_y}} \quad (2.7)$$

Note that  $b$  is the width of compression element as defined in AISC specification for structural steel buildings (Section B4.1 of AISC 360-10) and  $t$  is the wall thickness of compression element.

In the first edition of AISC seismic provisions (AISC, 1992), bracing members used in the concentrically steel braced frames could be compact or non-compact sections, but the overall  $L/r$  ratio had a limit.

$$\frac{L}{r} \leq \frac{720}{\sqrt{F_y}} \quad (2.8)$$

If  $k = 1.0$  in this case, this corresponds to  $P_{cr}/P_y = 0.65$  using the ASD column formula. The width-to-thickness ratio limits for round HSS and rectangular HSS sections were

$$\frac{OD}{t} \leq \frac{1300}{F_y} \quad (\text{Round HSS}) \quad (2.9)$$

$$\frac{b}{t} \leq \frac{110}{\sqrt{F_y}} \quad (\text{Rectangular HSS}) \quad (2.10)$$

where  $OD$  is outer diameter of round HSS sections. A 0.9 reduction factor applied was to the  $b/t$  ratio limit, as suggested by the shaking table test results (Uang and Bertero, 1986). However, this limitation was 16 % higher than the  $b/t$  limit ( $b/t \leq 95/\sqrt{F_y}$ ) proposed by other researchers (Tang and Goel, 1987), which was chosen simply to be half the limitation used in the plastic design ( $b/t \leq 190/\sqrt{F_y}$  from AISC, 1978).

In the 1997 version of the AISC Seismic Provisions (AISC, 1997), the slenderness ratio was limited as

$$\frac{kL}{r} \leq \frac{1000}{\sqrt{F_y}} \quad (2.11)$$

This further relaxed the  $P_{cr}/P_y$  ratio limitation to 0.46 (derived from the ASD column formula). The width-to-thickness ratio limits for round HSS and rectangular HSS sections were taken as the same as used in the 1992 Seismic Provisions.

In the 2002 version of Seismic Provisions (AISC, 2002), the slenderness ratio was limited as

$$\frac{kL}{r} \leq 5.87 \sqrt{\frac{E}{F_y}} = \frac{1000}{\sqrt{F_y}} \quad (2.12)$$

which is the same as the limit in 1997 Seismic Provisions, provided  $F_y$  is 50ksi. The width-to-thickness ratio limits for round HSS and rectangular HSS sections were changed to

$$\frac{D}{t} \leq 0.044 \frac{E}{F_y} = \frac{1276}{F_y} \quad (\text{Round HSS}) \quad (2.13)$$

$$\frac{b}{t} \leq 0.64 \sqrt{\frac{E}{F_y}} = \frac{109}{\sqrt{F_y}} \quad (\text{Rectangular HSS}) \quad (2.14)$$

where  $D$  is outer diameter of round HSS sections; these were essentially the same as 1997 seismic provisions. However, the limitation of slenderness ratio was reduced in the 2005 seismic provisions

$$\frac{kL}{r} \leq 4 \sqrt{\frac{E}{F_y}} = 4 \sqrt{\frac{29000}{F_y}} = \frac{681}{\sqrt{F_y}} \quad (2.15)$$

The resulting corresponding  $P_{cr}/P_y$  ratio limitation was 0.70, returning close to the limitation in 1992 Seismic Provisions. The width-to-thickness ratio limits for round HSS and rectangular HSS sections were the same as 2002 Seismic Provisions.

In the 2010 Seismic Provisions, the limitation of slenderness ratio of bracing members in SCBF changed to 200, but the previous limitation was retained for bracing member in ordinary concentric braced frames (OCBF). That is:

$$\frac{kL}{r} \leq 200 \quad (SCBF) \quad (2.16)$$

$$\frac{kL}{r} \leq 4 \sqrt{\frac{E}{F_y}} = \frac{681}{\sqrt{F_y}} \quad (OCBF) \quad (2.17)$$

Note that the noted slenderness limit is for V and inverted-V brace configurations in OCBF system. The 2010 AISC Seismic Provisions further stipulated the width-to-thickness limitations for round HSS and rectangular HSS sections are based on the ductility factor of the bracing members. The width-to-thickness limitations for highly ductile and moderately ductile members were different. For moderately ductile members, the same limitations as in the 2005 seismic provisions applied.

$$\frac{D}{t} \leq 0.044 \frac{E}{F_y} = \frac{1276}{F_y} \quad (Round\ HSS) \quad (2.18)$$

$$\frac{b}{t} \leq 0.64 \sqrt{\frac{E}{F_y}} = \frac{109}{\sqrt{F_y}} \quad (Rectangular\ HSS) \quad (2.19)$$

For highly ductile members, the width-thickness ratio limits were 14% smaller than the limits for moderately ductile members.

$$\frac{D}{t} \leq 0.038 \frac{E}{F_y} = \frac{1102}{F_y} \quad (Round\ HSS) \quad (2.20)$$

$$\frac{b}{t} \leq 0.55 \sqrt{\frac{E}{F_y}} = \frac{94}{\sqrt{F_y}} \quad (Rectangular\ HSS) \quad (2.21)$$

Note that the  $b/t$  ratio limitation for highly ductile rectangular HSS braces is very close to the proposed limitation from the study by Tang and Goel (1987). Table 2.1 summarizes the



slenderness ratio and width-to-thickness ratio limitations for square HSS, round HSS and also the wide flange braces listed in the seismic provisions from the first version to the current version.

**Table 2.1 Slenderness ratio and width-to-thickness ratio limitations**

Version of Seismic Provisions	$kL/r$		Section Shape			
	OCBF	SCBF	Square HSS	Round HSS	Wide Flange	
			$b/t$	$D/t$	Flange	Web
					$b/t$	$h/t$
<b>1992</b>	$\frac{720 k}{\sqrt{F_y}}$	N.A.*	$\frac{110}{\sqrt{F_y}}$	$\frac{1300}{F_y}$	N.A.	$\frac{P_u}{\phi_b P_y} \leq 0.125$ $\frac{520}{\sqrt{F_y}} [1 - 1.54 \frac{P_u}{\phi_b P_y}]$ $\frac{P_u}{\phi_b P_y} > 0.125$ $\frac{191}{\sqrt{F_y}} [2.33 - \frac{P_u}{\phi_b P_y}] \geq \frac{253}{\sqrt{F_y}}$
<b>1997</b>	$\frac{720^{**}}{\sqrt{F_y}}$	$\frac{1000}{\sqrt{F_y}}$	$\frac{110}{\sqrt{F_y}}$	$\frac{1300}{F_y}$	N.A.	(the same as 1992 version)
<b>2002</b>	$4.23 \sqrt{\frac{E}{F_y}}^{**}$	$5.87 \sqrt{\frac{E}{F_y}}$	$0.64 \sqrt{\frac{E}{F_y}}$	$0.044 \frac{E}{F_y}$	$0.30 \sqrt{\frac{E}{F_y}}$	$\frac{P_u}{\phi_b P_y} \leq 0.125$ $3.14 \sqrt{\frac{E}{F_y}} [1 - 1.54 \frac{P_u}{\phi_b P_y}]$ $\frac{P_u}{\phi_b P_y} > 0.125$ $1.12 \sqrt{\frac{E}{F_y}} [2.33 - \frac{P_u}{\phi_b P_y}]$
<b>2005</b>	$4 \sqrt{\frac{E}{F_y}}^{**}$	$4 \sqrt{\frac{E}{F_y}}$	$0.64 \sqrt{\frac{E}{F_y}}$	$0.044 \frac{E}{F_y}$	$0.30 \sqrt{\frac{E}{F_y}}$	$\frac{P_u}{\phi_b P_y} \leq 0.125$ $3.14 \sqrt{\frac{E}{F_y}} [1 - 1.54 \frac{P_u}{\phi_b P_y}]$ $\frac{P_u}{\phi_b P_y} > 0.125$ $1.12 \sqrt{\frac{E}{F_y}} [2.33 - \frac{P_u}{\phi_b P_y}] \geq$ $1.49 \sqrt{\frac{E}{F_y}}$
<b>2010 (moderately ductile members)</b>	$4 \sqrt{\frac{E}{F_y}}^{**}$	200	$0.64 \sqrt{\frac{E}{F_y}}$	$0.044 \frac{E}{F_y}$	$0.38 \sqrt{\frac{E}{F_y}}$	$1.49 \sqrt{\frac{E}{F_y}}$
<b>2010 (highly ductile members)</b>	$4 \sqrt{\frac{E}{F_y}}^{**}$	200	$0.55 \sqrt{\frac{E}{F_y}}$	$0.038 \frac{E}{F_y}$	$0.30 \sqrt{\frac{E}{F_y}}$	$1.49 \sqrt{\frac{E}{F_y}}$

(\*Note: in the 1992 seismic provisions, there was no specific terminologies for ordinary concentrically braced frames or special concentrically braced frames)

(\*\* Limitations for V or inverted-V brace configurations)

### 2.1.3 Experimental Studies on Brace Components

One of early experimental study on the effect of slenderness ratio and  $b/t$  ratio upon the inelastic local buckling of single-angle and double-angle braces was done by Mangat (1969) at the University of Windsor. The experiments were conducted under monotonic compression load on twenty-four pin-ended single-angle braces (sections varied from  $L3 \times 3 \times 3/16$  to  $L4 \times 4 \times 5/16$ ), thirty-two fix-ended single-angle braces (sections varied from  $L1-3/4 \times 1-3/4 \times 1/8$  to  $L3-1/2 \times 3-1/2 \times 5/16$ ), twenty-four pin-ended double-angle braces (sections varied from  $L1-3/4 \times 1-3/4 \times 1/8$  to  $L3-1/2 \times 3-1/2 \times 3/16$ ), and twenty-four fix-ended double-angle braces (sections varied from  $L1-3/4 \times 1-3/4 \times 1/8$  to  $L3-1/2 \times 3-1/2 \times 3/16$ ) with 4-ft and 1-ft in length. The  $b/t$  ratios of angles varied from 10.67 to 18.67, and the slenderness ratios were between 20 and 96. Based on these experiments several conclusions were drawn:

- The boundary conditions at single-angle brace ends did not affect to any degree the compression capacity. For  $16 < b/t \leq 18.67$  single-angle braces, local buckling will occur when the braces fail.
- Similar to single-angle braces, for  $16 < b/t \leq 18.67$  double-angle braces, local buckling will occur when the braces fail.
- The compression capacities of fix-ended double-angle braces with  $16 < b/t \leq 18.67$  were greater than that of pin-ended double-angles braces at about 14%.
- The number of bolts used at the connections did not have significant effects on the compression capacity of angle braces.

Although design recommendations were also provided for angle brace design, these were only for angle brace compression capacities with slenderness ratios between 20 and 96.

An early literature survey of existing research findings on the cyclic behavior of structural steel bracing systems was performed at University of California, Berkeley (Popov et al., 1976). About thirty publications, mostly from the United States and Japan, were reviewed and discussed extensively in this report; some alternative concepts of braced frame design were also proposed. The investigation suggested that more accurate and efficient analytical models, testing on braces of larger sizes, and improved design concepts were needed.

In Japan, cyclic behavior of conventional buckling braces was extensively investigated during the 1970s at Kyoto University (Wakabayashi et al., 1972; Shibata et al., 1973; Wakabayashi et al., 1973; Wakabayashi, 1973; Wakabayashi et al., 1976; Wakabayashi et al., 1977). Square and H-shaped sections were used in the relatively small-scale brace specimens (specimen length ranged from 7.6 in. to 36.5 in.) with different slenderness ratios varied from 40 to 160. Incremental cyclic displacement amplitudes were selected as loading protocol during the tests. The effect of brace-end fixities (restraints) was studied and represented through an amplification factor. Axial force versus axial deformation and axial force versus out-of-plane displacement hysteresis loops were examined and compared with empirical formula proposed in the studies. Comparisons between test results and the empirical theory were found to be satisfactory.

During this time period, several studies were underway in the United States at the University of Michigan, Ann Arbor. Sixteen hot-rolled steel bars of various lengths (specimen length ranged from 24 in. to 59 in.) were tested under static and quasi-dynamic cyclic loadings (Khan and Hanson, 1976) to verify the findings of theoretical studies of braces (Higginbotham, 1973). The slenderness ratios ( $kL/r$ ) of the brace specimens investigated in the experiments varied from 85 to 210, and all specimens had a nominal cross section of 1 in.  $\times$  0.5 in. It was

found that the experimental results generally agreed with existing theory. Net elongation phenomenon was observed under cyclic loading, and cyclic degradation of compressive strength was also noted. Quasi-dynamic loading effect on brace hysteretic response was found to be small but made the tension region response stiffer. Full-size bracing component tests were suggested to further develop design provisions.

Within a year after Khan and Hanson presented their work, Jain, Goel, and Hanson (1977) published a cyclic test report of twenty-four 1-in.  $\times$  1-in. cold-rolled steel tubes with a  $b/t$  ratio equal to 7.52. The tubular specimens covered a wide range of slenderness ratio from 30 to 140 and were tested statically and dynamically. Three loading frequencies, 1/60 Hz (static), 1/16 Hz (slow dynamic) and 1 Hz (fast dynamic), were applied in eighteen static tests and six dynamic tests on tubular specimens. It was found that the rate of loading did not have significant influences upon the test results (as shown in previous studies by Hanson). Brace residual elongations were found to be larger for smaller slenderness ratio specimens, and the slenderness ratio seemed to be the most important factor governing brace hysteretic behavior.

Based on the detailed literature survey on the braced frame systems (Popov et al., 1976), researchers at UC Berkeley conducted a series of cyclic axial loading tests on steel struts (Black et al., 1980). There were twenty-four commercially available steel struts selected to represent the common bracing members in braced frames. Larger and heavier sections were selected but within the capacity of test equipment. Eighteen out of twenty-four specimens were pinned at both ends with slenderness ratios of 40, 80, and 120. The remaining six specimens were fixed at one end and pinned at the other with slenderness ratios of 40 and 80. A total of eight different cross sectional shapes, including double-angles, double-channels, wide flanges, tees, thin-walled pipes, thick-walled pipes, thin-walled square tubes and thick-walled square tubes, were tested in the experimental program. The primary goals were to examine the effects of cross-sectional shapes, slenderness ratios, brace-end conditions, and load patterns on the hysteresis characteristic of the struts. The slenderness ratio was identified again as the most influential parameter influencing brace hysteretic behavior. Normalized hysteretic envelopes were proposed to compare specimen responses with different loading histories, and several design suggestions were made.

Behavior of tubular braces in the offshore platforms was also studied at UC Berkeley (Zayas et al., 1980a). Six tubular brace specimens representing one-sixth scale brace models for an offshore platform were subjected to inelastic cyclic loading. Different brace-end fixities (pinned and fixed), diameter-to-thickness ratios ( $D/t = 33$  and  $48$ ), and heat treatment procedures (annealed and un-annealed) were examined. Test results showed that the struts with lower diameter-to-thickness ratio performed better than the struts with higher diameter-to-thickness ratio, and brace-end conditions had significant effects on the responses. Since the manufacturing process of tubes at that time caused the steel to be highly work-hardened, the brittle failure occurred in the heat-affected zones of the welds at the ends of the un-annealed specimens. It was suggested the annealing process should be done for the tubes subjected to severe cyclic loading. Developing analytical models that could simulate local buckling of tube walls and experiments on large size specimens were mentioned for future study.

A series of quasi-static cyclic loading tests on seventeen double-angle braces with unequal legs were conducted at University of Michigan (Astaneh-Asl, 1982; Astaneh-Asl et al., 1985). The slenderness ratios of specimens ranging from 81 to 189 and the  $b/t$  ratios of angles varied from 4 to 20. Nine out of seventeen double-angle braces were designed to buckle out-of-plane, while the remaining eight were designed to buckle in plane. Modified design procedures

for double-angle braces under cyclic loading were proposed to improve the ductility performance. An improved design procedure for stitches in the out-of-plane buckled double-angle braces was presented to increase the ductility. One major conclusion suggested that a minimum free length equaled to twice the gusset plate thickness will improve the ductility of gusset plate under cyclic loading. It was noted that the longer free length may cause a stability problem in the gusset plate. Two plastic hinges instead of one may form in the same gusset plate, potentially reducing the ductility significantly. Several examples of this type of damage to steel buildings after earthquakes can be found (AIJ, 1995; EERI, 2011) and also observed in the laboratory after pseudo-dynamic tests (Tsai et al., 2008) of a full-scale buckling-restrained braced frame.

Because local buckling of bracing member typically has a significant effect on the hysteresis behavior, experimental tests on concrete filled-in -tube braces were performed (Goel and Liu, 1987; Liu and Goel, 1988). It was found that the filled concrete can successfully delay the crack initiation from local buckling of braces and improve the cyclic behavior. However, the filled concrete did not effectively delay initiation of local buckling in the brace members. In addition, the strength of concrete did not have any significant effect on the brace behavior. The improvement from concrete fill was not significant except for smaller  $b/t$  ratio braces (Lee and Goel, 1987).

It is interesting to note that the number of experimental studies in the United States on bracing members during the 1990s was relatively low, with most of research works focused on the analytical modeling of braces or braced frame behaviors. Meanwhile, the 1994 Northridge Earthquake and 1995 Kobe Earthquake brought out several issues for urgent study. Compared to other systems, braced frames performed about as expected.

However, researchers in at University of Toronto, Canada, performed five cyclic tests on square hollow structural section (HSS  $4 \times 4 \times 1/4$ ) braces with slenderness ratio 83 and  $b/t$  ratio 13.9 (Pons, 1997). The objective was to investigate on the brace-to-gusset plate connection details that were feasible for use in braced frames under severe cyclic loading. Several design comments were provided based on the experimental findings.

Another group of Canadian researchers conducted a series of experiments on nine square HSS braces (Shaback, 2001; Shaback and Brown, 2003) with different effective slenderness ratios (from 52 to 66) and width-to-thickness ratios (from 8.93 to 15.1). The selection of specimens was based on the Canadian code provisions. Similar to previous works done by many researchers, the effective slenderness ratio ( $kL/r$ ) was found to be the most important parameter that affected the behavior of brace. A statistically better equation to predict the fatigue life of braces was proposed based on their experimental results, accompanied by the suggestion that a more reliable fracture prediction model was required.

As the testing set ups have improved, so has the size of the specimens. Eleven square HSS braces with slenderness ratios varied from 69 to 90 and  $b/t$  ratios ranging from 8.1 to 28.3 were tested cyclically in a  $45^\circ$  single diagonal layout (Han et al., 2007). The net reduced section failure mode was found in the smallest  $b/t$  ratio specimen at the earlier loading stage without any local buckling observed in the section walls. This failure mode was noted in earlier laboratory tests (Yang and Mahin, 2005). Another interesting finding was that the energy dissipation capacity of braces increased with decreased  $b/t$  ratio, and a  $b/t$  ratio of 14 seemed to achieve the maximum energy dissipation capacity based on test results.

More recent experimental work on the brace components was done by researchers at University of California, Davis (Fell, 2008; Fell and Kanvinde, 2010). A total of nineteen braces

at two-third scale were tested statically and dynamically. The specimen sections included square HSS, standard pipe, and wide flange sections. Slenderness ratios of specimens varied from 63 to 153, two  $b/t$  ratios were selected (14.2 and 8.5) for square HSS specimens, two  $D/t$  ratios were used for the pipes, and  $b/t$  ratio equaled to 7.5 for wide flange braces. Two square HSS specimens were filled with grout and subjected to two different loading protocols (standard and near-fault compression dominated). One of major findings was that the fracture ductility of a brace is more related to the section compactness and less related to the brace slenderness or loading histories. Another finding was that the width-to-thickness ratio limitations of bracing members in the 2005 AISC seismic provisions needed to be reduced to insure adequate member deformation capacity. Similar to past studies, the loading rate and the effect of mortar fill did not have significant effects on the brace cyclic behavior.

Canadian researchers recently conducted thirty-four large-scale brace specimen tests (between 17-ft to 26-ft in length of working points) with a variety range of  $b/t$  ratios, two different  $kL/r$  ratios (40 and 60), and three different sectional shapes (nineteen square HSS, nine round HSS and six wide flange sections) that are commonly used in the field (Tremblay et al., 2008). All specimens were reinforced at the net section connection regions. Both out-of-plane and in-plane buckling braces were tested quasi-statically. It was found that the square HSS and round HSS with similar slenderness ratios and approaching to code-limited  $b/t$  (and  $D/t$ ) ratios had comparable cyclic behaviors until fracturing. The slenderness ratio seemed to affect the fracture performance of square HSS compared to round HSS braces. Also, the wide flange braces had better cyclic deformation capacities based on test observations.

#### **2.1.4 Analytical Modeling of Bracing Component**

There are many existing numerical models that simulate the behavior of brace components. Early models modified elastic truss elements to very simple representations of brace buckling, e.g., tension-only behavior, nonlinear elastic buckling, and ideal bilinear hysteretic behavior. Because these models did not represent observed brace cyclic behavior very well, more advanced modeling techniques were developed. Basically, these models can be categorized into three types: physical theory models, phenomenological models, and finite element models. The following paragraphs briefly review the relevant work, especially the computer simulations based models; more detailed literature reviews can be found elsewhere (Zayas et al., 1981; Uriz and Mahin, 2008).

##### **2.1.4.1 Physical Theory Models**

These models were very simple: only cross section properties and effective length of braces needed to be defined. Several early brace models of this type include the Point Hinge Model (Singh, 1977; Jian et al., 1978a), Elasto-Plastic Hinge Model (Wakabayashi et al., 1972), Higginbotham Model (Higginbotham, 1973), Refined Model (Ikeda and Mahin, 1984; Ikeda and Mahin, 1986), and Inelastic Beam-Column Element Model (Uriz et al., 2008). Some of these models were implemented into DRAIN-2D (Powell, 1972; Kannan and Powell, 1973) and OpenSees (McKenna, 1997) to simulate the cyclic buckling behavior of braces (Jain and Goel, 1978b; Ikeda and Mahin, 1984; Uriz et al., 2008). These preliminary models were only accurate in cases with braces with higher slenderness ratios and could not simulate the strength deterioration. Refined models were developed but still did not account for Bauschinger effects,

progressive cyclic degradation of strength, and local buckling of braces. Although more recent developed models—such as Inelastic Beam-Column Model—can simulate the Bauschinger effect including strength cyclic degradation within acceptable accuracy, they still cannot account for the effect of local buckling.

#### **2.1.4.2 Phenomenological Models**

The most common type of model, at least nine different models were proposed and developed in the past (Higginbotham, 1973; Nilforoushan, 1973; Singh, 1977; Roeder and Popov, 1977; Jain and Goel, 1978b; Marshall, 1978; Maison and Popov, 1980; Gugerli and Goel, 1982; Ikeda et al., 1984). Here, the shape of brace hysteresis loop segments based on the mathematical equations or empirical results were pre-defined. Although such models are computationally efficient, the rules can become very complicated and calibration against experimental results is required (Ikeda et al., 1984; Zayas et al., 1981; Uriz et al., 2008).

#### **2.1.4.3 Finite Element Models**

The most general among the three categories, in this model the entire brace is subdivided into numerous finite elements to define the three-dimensional geometry of the brace. The finite elements can be shell or solid elements. The material properties are defined for each element. The program and elements need to be able to represent the inelastic behavior of the steel and the large displacements associated with yielding, local buckling and lateral (global) buckling. However, this type of models is often computationally expensive and may not be suitable for simulating the response of large structures. Past studies typically applied the three-dimensional finite element models to component level models (Huang and Mahin, 2007 and 2010; Ding et al., 2008; Fell, 2008), sub-assembly structure (Field, 2003; Mahin et al., 2004; Yoo et al., 2008 and 2009; Huang and Mahin, 2010), and infrequently to simulate a complete structure.

## **2.2 GUSSET PLATE CONNECTION**

Connections are always critical components in any structural system. In concentrically braced frames, gusset-plate behavior plays an important role. Several papers and reports describe and summarize previous gusset plate research in detail (for example, Birkemoe, 1966; Rabinovitch, 1993; Astaneh-Asl, 1998; Chambers and Ernst, 2005; Dowswell, 2006). This section highlights a few of the findings.

### **2.2.1 The 30° Design Concept**

Currently, gusset plates are designed based on a rule of thumb called the Whitmore section (Whitmore, 1952). As can be seen in Fig. 2.3, the Whitmore effective section is determined by extending two lines at about 30° with respect to the longitudinal axis of the brace and beginning at the first row of bolts or gusset-to-brace weld at the tip of the gusset plate. The intersection of these two lines with a line perpendicular to the brace through the last row of bolts (or end of the

welds) defines the width of Whitmore section. The original definition of Whitmore effective width was initially applied to bolted connections and extended to welded connections by Astaneh-Asl (1982).

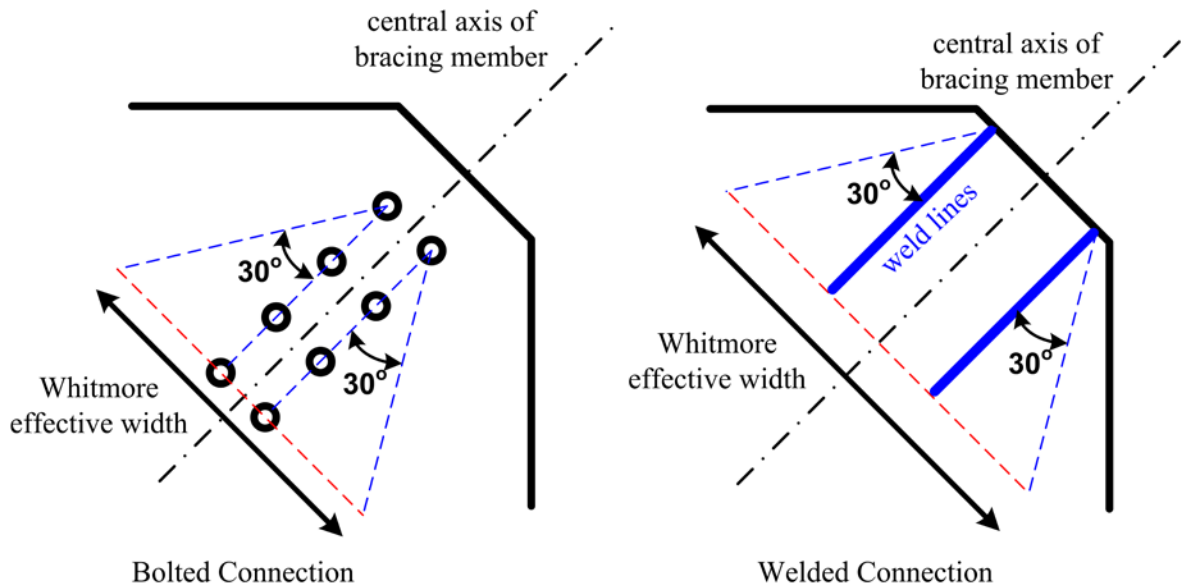


**Figure 2.3 Illustration of Whitmore effective width for bolted (Whitmore, 1952) and welded connections (Astaneh-Asl, 1982)**

In Whitmore's experimental study, a prototype bottom chord connection of a Warren truss model was tested to examine the stress distribution in the gusset plates. Strain gauges were used to measure the local strain distributions in the gusset plate. Tests were conducted under service load and did not continue to failure. The bending stresses in the gusset plate were not linearly distributed, and the neutral axis did not coincide with the centerline of the connecting members. Maximum bending stress did not occur at the extreme edges of the gusset but at an interior location. Shear-stress distributions did not follow the classic parabolic distribution. Whitmore concluded that standard beam theory could not be applied to gusset-plate design. The most rational method to determine the maximum normal stresses in the gusset plate was to use a spread out angle of  $30^\circ$  to define an effective section for estimating the maximum stress.

However, the concept of the  $30^\circ$  spread to determine an effective critical area was suggested about thirty years earlier. As noted by Dowswell (2006), stress analysis of iron truss gusset plates by Theophil Wyss in his 1923 doctoral dissertation at Swiss Federal Institute of Technology Zurich (Wyss, 1923) incorporated a similar idea. In the preliminary tension tests of two gusset plates, as shown in Fig. 2.4, Wyss tried to determine the stress distributions in the gusset plate specimens and investigated ideal shapes of gusset plates. Almost uniformly distributed stresses were found in the section cuts perpendicular to the loading direction for both  $20^\circ$  and  $12^\circ$  tapered specimens (gusset plate A and B in Fig. 2.4). Stress concentrations at the edges of the rivet holes—about 2.2 times the averaged stress—were also found in the tension tests. He concluded that the shape of gusset plate whereby the edges converge symmetrically to the direction of force is an optimum configuration for the gusset plate. It also provides smooth and gradual force transition in the connection region.



Probekörper.

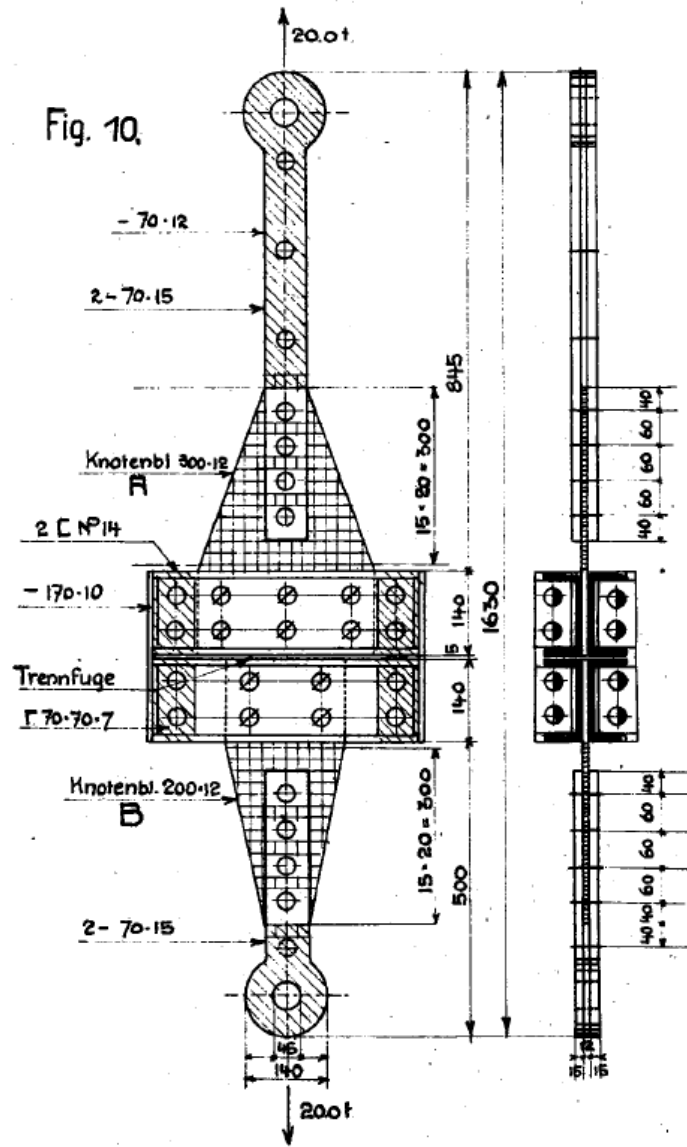


Figure 2.4 Dimension of gusset plate specimens in the preliminary tension tests (extracted from Fig. 10 of Wyss, 1923)

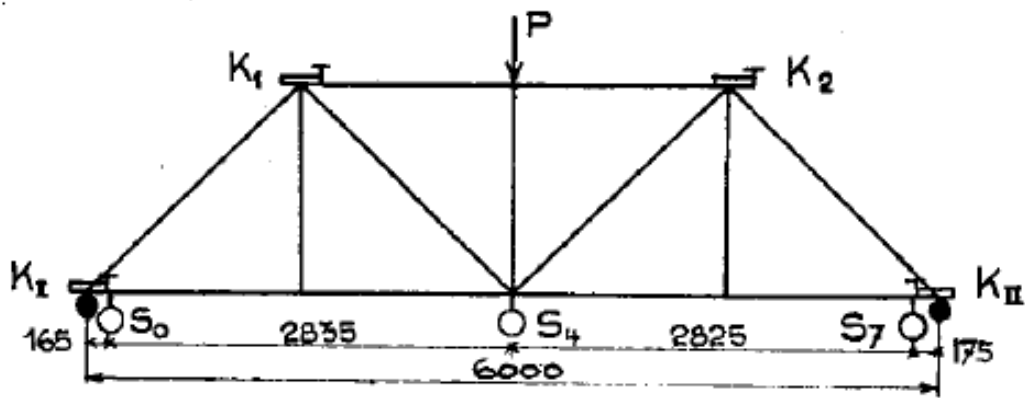
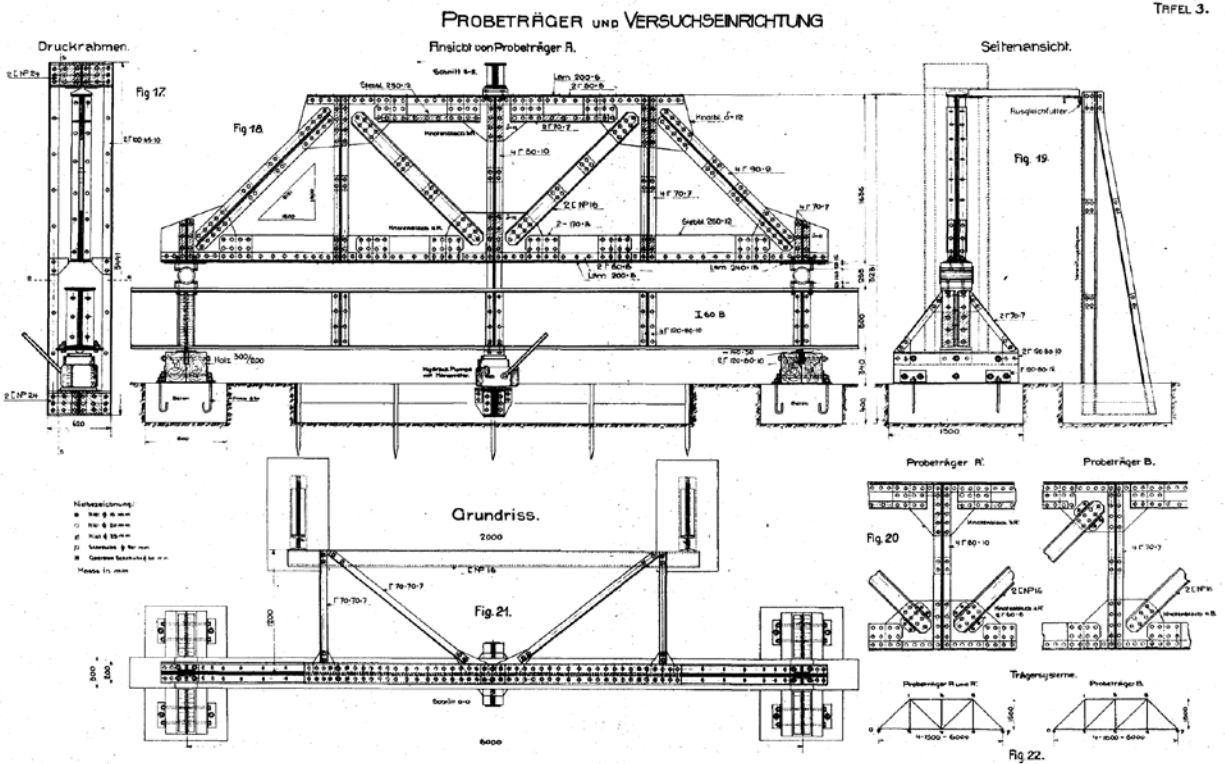


Abb. 17.

(a) Instrumentation points and loading point



(b) Shop drawings of test specimen and test frame

Figure 2.5 The Warren truss specimen tested by Wyss in 1923 (extracted from Figs. 17 and 22 of Wyss, 1923)

In the main experimental study performed by Wyss, a 6 meter span, 1.5 meter high, statically determinate Pratt truss (Fig. 2.5) was tested under simple loading and unloading at the node of top chord. In the study, he noted that the rigid core (rigid zone) in a gusset plate (see Fig. 2.6) affects the bending stiffness and moment capacity of the gusset plate. He also pointed out that the connection size also affects the deformations in the gusset plate. Elastic behavior of the gusset plate was studied based on the beam theory at the time and secondary stress effects were included.

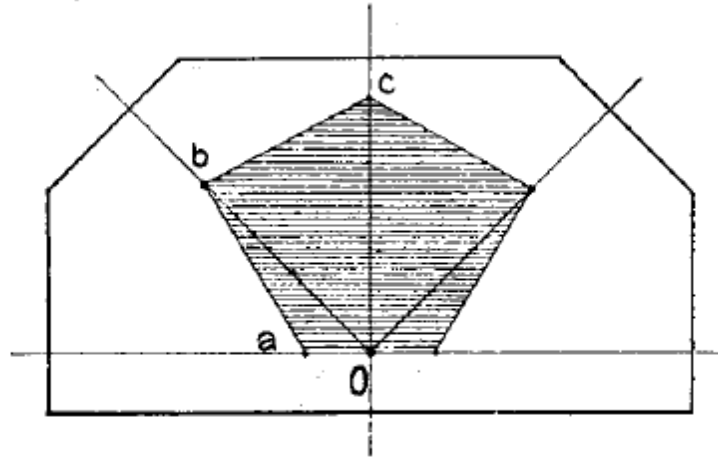


Abb. 22. Knotenblech mit starrem Kern.

Figure 2.6 Illustration of rigid core in a gusset plate (extracted from Fig. 22 of Wyss, 1923)

Based on the preliminary experimental results, Wyss drew the gusset plate stress trajectories under tension and shear forces as illustrated in Fig. 2.7. Normal stress, shear stress, and bending stress distributions along a section cut were also shown in Fig. 2.7. The relationship between stress along the course of stress trajectory  $\sigma_o$  and the normal stress  $\sigma_\alpha$  at the section cut was derived.

$$\sigma_o = \frac{\sigma_\alpha}{\cos^2 \alpha} = \frac{P}{F_{net}} \frac{1}{\cos^2 \alpha} \quad (2.22)$$

where  $\alpha$  is the angle between stress trajectory and the direction of applied force  $P$ , and  $F_{net}$  is the cross-section area along the section cut that perpendicular to the symmetric axis. He proposed a method to determine the width of the gusset plate given that allowable stress in the gusset plate is known as  $\sigma_{allowable}$ .

$$b' = \frac{P}{d \sigma_{allowable} \cos^2 \gamma} \quad ; \quad \gamma < 30^\circ \quad (2.23)$$

where  $\gamma$  is gusset plate tapered angle,  $b'$  is gusset plate width,  $d$  is thickness of gusset plate and  $P$  is the applied force. The  $\gamma = 30^\circ$  is assumed to be the critical tapered angle and  $\sigma_o = 1.33 \sigma_\alpha$  when this angle applied. Secondary stresses based on beam formulas were also derived and combined with primary stresses to determine the critical stresses in the gusset plate.

$$\sigma_o = \left( \frac{P}{F_{net}} \pm \frac{M}{W} \right) \frac{1}{\cos^2 \gamma} = \sigma_{max} \quad ; \quad \gamma < 30^\circ \quad (2.24)$$

where  $\gamma$  is gusset plate tapered angle,  $P$  is the applied force,  $F_{net}$  is the cross section area along the section cut that perpendicular to the symmetric axis,  $M$  is the bending moment applied to the gusset plate, and  $W$  is the elastic section modulus. For asymmetric gusset plates, he noted that the formulas can also apply to the situation only the 30 degree critical angle is introduced as shown in Fig. 2.8. This also came from his observations during the main experiments.

The method Wyss proposed in 1923 is similar to the concept of Whitmore's section as done in current practice. Except the 30° extension lines did not start at the first row of rivet holes, but at the edge of the channel sections, as illustrated in Fig. 2.8.

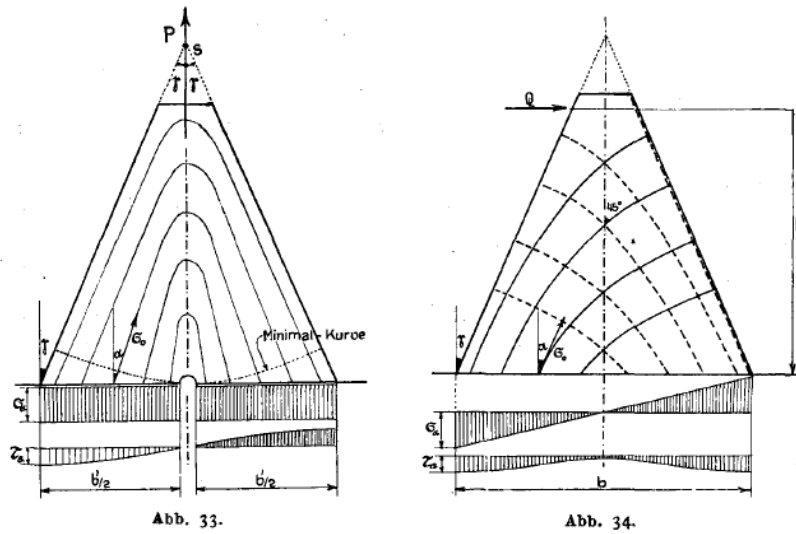


Figure 2.7 The stress trajectories of preliminary test specimens (extracted from Figs. 33 and 34 of Wyss, 1923)

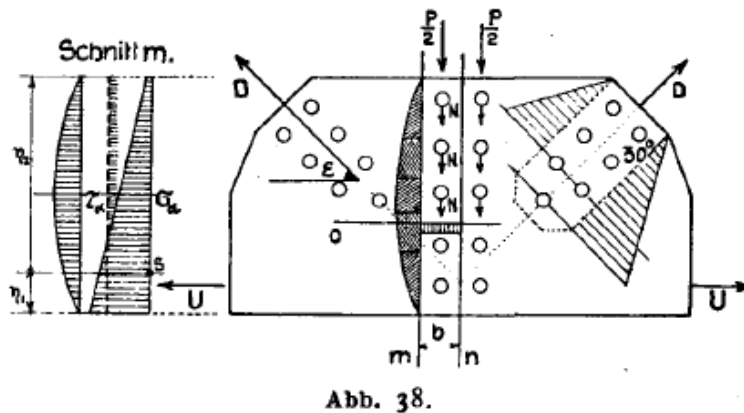


Figure 2.8 Illustration of stress distribution in a gusset plate (extracted from Fig. 38 of Wyss, 1923)

## 2.2.2 Stability Issue

For the gusset plate stability under compression, Thornton (1984) proposed a simple method to calculate the elastic buckling capacity of gusset plate using equivalent unit strips within the Whitmore effective section. The definition of the characteristic length of the strips is illustrated in Fig. 2.9, and the critical length to determine the buckling capacity is selected from the maximum among these characteristic lengths:  $L_t$ ,  $L_c$  and  $L_b$ . Typical column buckling formula were used with effective length factor  $k = 0.65$  to determine the buckling stress of the critical strip within the effective width. Several modified or generalized methods have also been proposed and investigated in later studies (Yam, 1994; Yam and Cheng, 2002; Lehman et al., 2004; Yoo, 2006; Dowswell, 2006).

A free edge buckling equation was proposed (Brown, 1988) as a design check equation to ensure the gusset plates yield before edge buckling. The general form of the edge buckling equation

$$\frac{a}{t} \leq \sqrt{\frac{\pi^2 E}{12(1-\nu^2)F_y k^2}} = 0.79 \sqrt{\frac{E}{F_y}} \quad (2.25)$$

where  $a$  is the gusset plate free edge length,  $t$  is the thickness of gusset plate,  $k$  is the effective length factor, and  $\nu$  is Poisson's ratio of steel. The 24 gusset plate monotonic compression tests conducted by Brown indicated that  $k = 1.2$  was the most appropriate value. Later, Astaneh-Asl (1989) proposed an equation for checking cyclic free edge buckling based on experimental results; the length-thickness limit was reduced about 5% for cyclic loading.

$$\left(\frac{a}{t}\right)_{cyclic} \leq 0.75 \sqrt{\frac{E}{F_y}} \quad (2.26)$$

Other methods were also proposed and investigated (Walbridge et al., 1998; Nast, 1999).

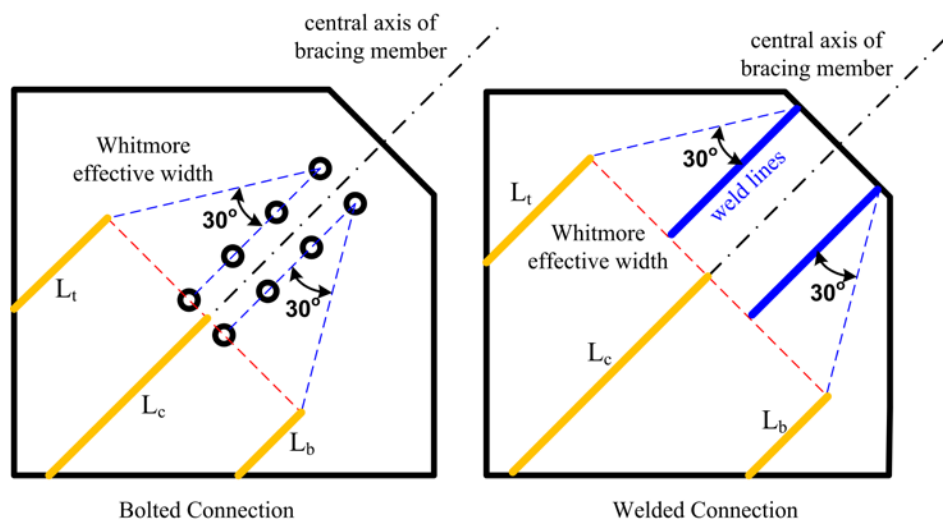


**Figure 2.9** Illustration of characteristic length of equivalent unit strips within the Whitmore effective width for bolted and welded connections

### 2.2.3 Connection Shape and Seismic Detail

The shape and dimension of gusset plates are usually determined by the force demands in the gusset plate-to-beam and gusset plate-to-column connection interfaces. Several methods are available to estimate the force demands in the connection interfaces, such as the KISS method (keep it simple and stupid, Thornton, 1992), the parallel force method (Ricker, not dated), the truss analogy method (Astaneh-Asl, 1989), and the uniform force method (Thornton, 1991), etc. Current AISC includes the uniform force method in the Manual of Steel Construction (AISC, 2005) as the preferred method. However, the constraints on this method sometimes result in awkward looking and excessively large gusset plates. Recently, a modified uniform force method was proposed (Muir, 2008) that provides a way to design gusset plates more economically and also retain the basic concept underlying the uniform force method. Geometric formulas for the gusset-plate design were also developed recently (Chambers and Bartley, 2007).

Detailing of gusset plates in special concentrically braced frames allowing out-of-plane buckling of braces typically follows a straight yield line pattern with  $2t_g$  in width (Astaneh-Asl, 1982; Astaneh-Asl et al., 1986), where  $t_g$  is the thickness of gusset plate as shown in Fig. 2.10. The clearance at both ends of brace allows the plastic hinges formed in the gusset plates without any restraints and reduces deformation concentrations in the gusset plate through spreading out the inelastic regions. Other yield patterns, such as elliptical yield line pattern, were also proposed (Roeder, 2007; Roeder et al., 2011) as an alternative design scheme (Fig. 2.10).

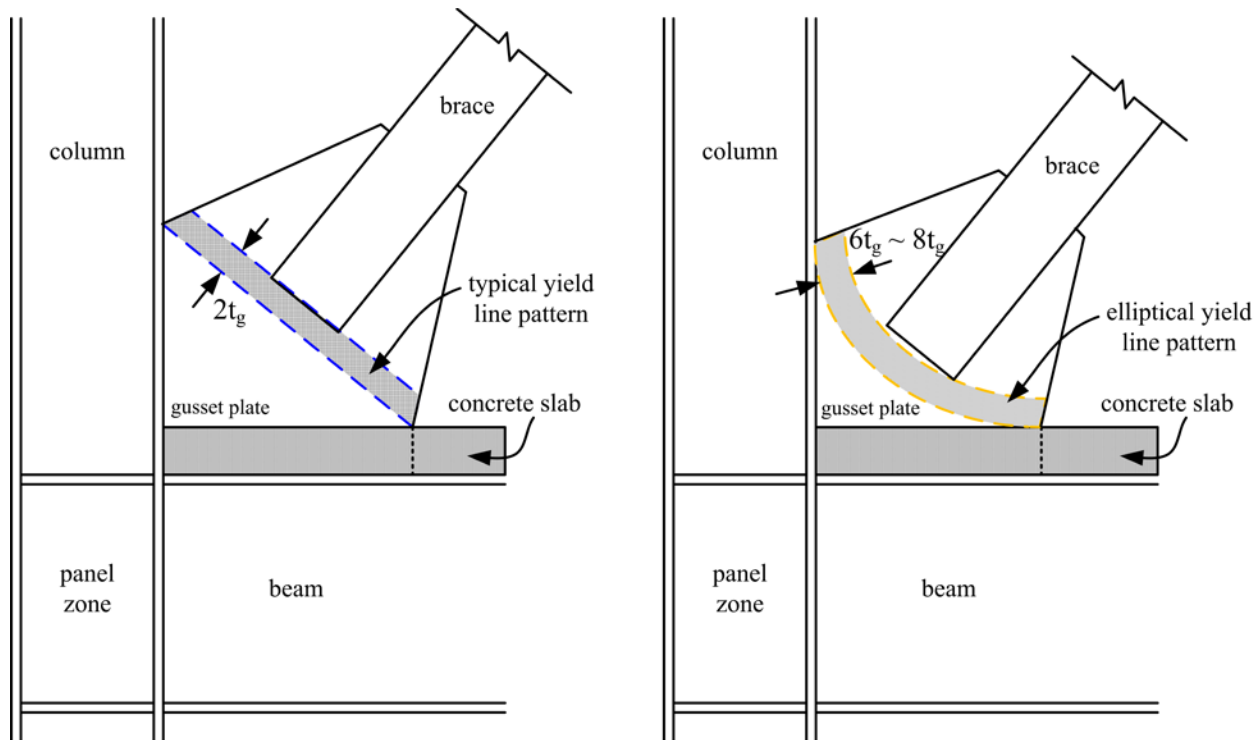


**Figure 2.10** Illustration of typical and elliptical yield line patterns to accommodate brace out-of-plane buckling (where  $t_g$  is thickness of gusset plate)

## 2.3 BRACED FRAME SYSTEM

### 2.3.1 Experimental Work on Braced Frame Systems

Early braced frame tests were conducted at Takenaka Technical Research Laboratory in Japan (Fujimoto et al. 1972; Tanabashi et al., 1973). The braced frame specimens were one-bay two-story and a reduced-scale (about 1/2-scale) braced frame models. Those specimens were tested cyclically in a two-million pound universal test machine. Both concentrically and eccentrically braced frames were studied in this project to compare the system's cyclic performance. Although the maximum story drift ratio imposed in the concentric braced frame specimen was only about 0.6% and the peak story shear was less than 150 kips, it provided valuable information about braced frame behaviors under cyclic loading.

Later on, four one-story one-bay X-braced frame tests under monotonic and cyclic loadings were conducted at Kyoto University (Wakabayashi et al., 1974). Pinched hysteresis loops were found in two cyclic loading tests. The base shear versus lateral displacement relationships were also found to be relatively unaffected by the gravity forces applied in the experiments.

One of the earliest shake table tests on steel braced frames were performed at UC Berkeley (Ghanaat, 1980). An existing three-story moment-resisting frame model was used as a base structure, and three different types of bracing members were used (rods, pipes, and double-angles) in a single-story X-configuration. The 0.6-scale model braced frame was then subjected to a series of ground shakings to investigate on the dynamic behavior of braced frames. Test results showed that the model structures with pipe braces and double-angle braces performed better than the structure with rod braces. Recommendations on the slenderness ratio limitations for braced frame systems were also made.

About the same time, two carefully prepared 1/6-scale X-braced frame specimens were tested at UC Berkeley as part of a research program on offshore platforms (Zayas et al., 1980b). All members were made from round tubular sections. Cyclic prescribed displacements were imposed at the tip of an X-braced frame to simulate earthquake effects. Results found that using compact sections as bracing members actually did not prevent the occurrence of local buckling under larger cyclic displacements. However, using members with lower  $D/t$  ratio helped delay local buckling and improved cyclic response of entire structure, suggesting that performing pseudo-dynamic tests on the X-braced frames would be desirable. Subsequently, these hybrid tests were performed (Mahin and Shing, 1985).

To examine the dynamic effect on the tubular braced frames used in offshore platforms and the failure mechanism, a two-dimensional 5/48-scale model was built and tested on the shake table at UC Berkeley (Ghanaat and Clough, 1982). The frame model results demonstrated that a moderate amount of energy dissipation was achieved under severe ground shakings. One major observation was that the damage of tubular braces was concentrated at the upper panel region, which was not observed in the cyclic testing conducted previously (Zayas et al., 1980b). Significant table-specimen interaction from pitching motion of the shaking table was reported.

Beginning in the early 1980s, the US-Japan cooperative earthquake research program initiated a series of studies to improve seismic safety. One of the core research topics was the testing of a six-story full-scale steel structure. The entire test program consisted of four testing phases. The first phase tested a concentrically steel braced frame (Foutch et al., 1986 and 1987; Roeder, 1989; Yamanouchi et al., 1989). This was the first time that a six-story full-scale braced

frame was tested using the pseudo-dynamic testing technique. For these experiments, each floor level was attached by at least one servo-controlled actuator to apply the required story displacements. Test results not only demonstrated the importance of the energy-dissipation mechanism and redundancy within the structure, it also showed how important were design details and ductility. Square HSS braces with  $b/t$  ratios varied from 9.9 to 22.8 and  $kL/r$  ratios ranging from 51.2 to 78.6 (assuming  $k = 0.7$ ) were installed in the Chevron brace configuration specimen. The brace connection details—different than current practices—were directly welded as fixed connections to the beams. Both in-plane and out-of-plane buckling of square HSS braces were observed in the tests. Maximum story drift of 1.9% occurred in the second story of the building, and the maximum base shear was about 720 kips. It was noticed that the HSS braces with higher  $b/t$  ratio (22.8) in the second and third story either completely fractured or partially tore during the final test.

Under the same research program, a reduced-scale six-story Chevron braced frame specimen was tested on the shake table at UC Berkeley and subjected to twenty earthquake ground motions (Uang and Bertero, 1986; Bertero et al., 1989). It represented a 0.3-scale model of the full-scale building tested in Japan. Slightly different  $b/t$  ratios of HSS braces were used in the model but similar observations were found. The stories with higher  $b/t$  ratio braces had larger column shear demand, and the braces ruptured at either the lower end or at mid-length of the brace, suggesting that limitations on both slenderness ratio and  $b/t$  ratio should be included in seismic design provisions.

Before testing on the full-scale six-story braced frame specimen mentioned above, six three-story 0.5-scale concentrically braced frame tests were conducted to understand the possible behavior of the lower story of a full-scale building (Fukuta et al., 1989). Gravity forces were applied on the top of each column line and lateral force applied at the roof level only. Both in-plane and out-of-plane buckling behavior of braces were studied. A Chevron brace configuration with braces of slenderness ( $L/r$ ) between 70 and 120 was selected. It was concluded that the specimens had stable hysteresis loops and were comparable to moment resisting frames, and that the hysteresis model proposed predicted the system behavior quite well.

Recently, a two-story one-bay Chevron configuration special concentrically braced frame test was performed at UC Berkeley (Uriz and Mahin, 2008). Relatively larger beam, column and brace member sizes were used in the braced frame specimen. No gravity forces were applied in the columns and only one actuator installed to apply lateral force at roof level. Both stories used HSS  $6 \times 6 \times 3/8$  braces, and reinforcing plates were welded at both sides of net section connection regions. Beam to column connections were designed as pin connections. From the cyclic loading test results, it was clear that the individual brace behaved as expected from the component tests (Yang and Mahin, 2005). Formation of a soft story mechanism at the lower story was observed. Significant cracks were initiated between shear tab and column flange and propagated through the column web, suggesting that further tests on different brace configurations (such as split-X and single-story diagonal) should be conducted to investigate the effect of brace configuration on the system behavior. Since the loading protocol affects the cyclic behavior of braces, frame tests with different loading protocols were recommended.



### 2.3.2 Frame Action in Braced Frame System

Frame action typically exists in a steel braced frame system. This framing action is an important factor in determining the behavior of braced frames following the deterioration and fracture of one or more braces.

Previous experiments have shown (Mahin et al., 2004) that the frame action in buckling restrained braced frames can induce distortional pinching forces in the gusset plate itself and can buckle the gusset plate when the brace is in tension. The pinching force can be reduced through using smaller and compact shaped gusset plates or by releasing the moment at the edge of gusset-to-beam interfaces (Thornton and Muir, 2009). Existing connection details often can help to achieve this goal. Figure 2.11 illustrates two examples that were designed to release the moment at the edge of gusset-to-beam interfaces.

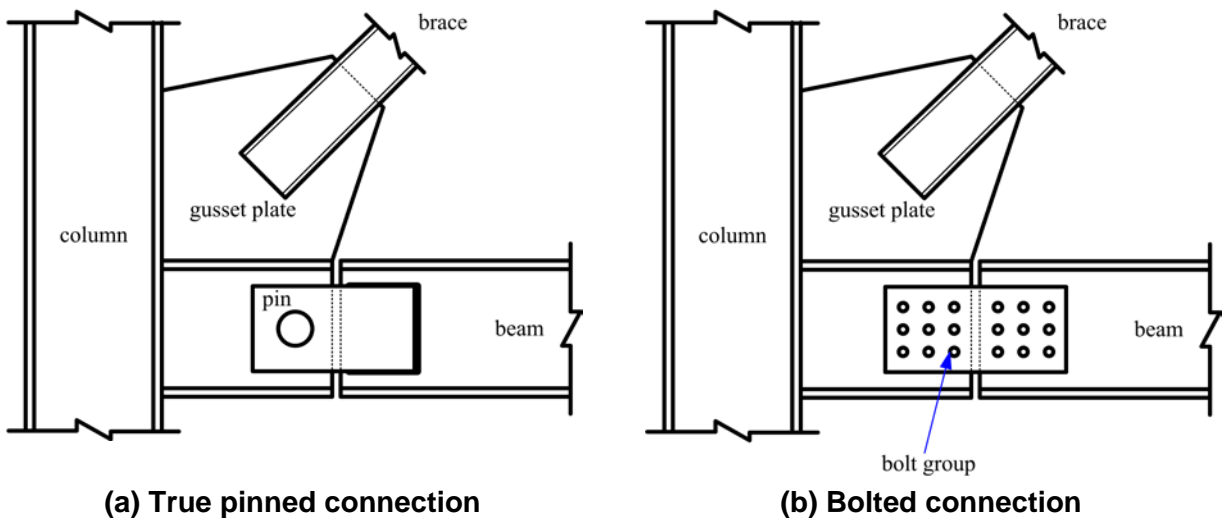


Figure 2.11 Connection details of beam end moment release

## 2.4 STEEL BRACED FRAME BEHAVIOR DURING PAST EARTHQUAKES

Past earthquakes usually provide opportunities to judge the adequacy of the building codes or design guidelines. Damage observations provide valuable information and stimulus for engineers and researchers to develop better structures to resist earthquakes. Several major seismic events are briefly discussed in the following sections.

### 2.4.1 Past Earthquakes in the United States

Damage to a light steel braced frame was reported in the magnitude 6.6 San Fernando Earthquake on February 9, 1971 (Steinbrugge et. al., 1971), where the out-of-plane buckling of steel flat-bars in the single story x-braced frame was observed. Figure 2.12 shows the braced bays after the earthquake. In another three-story chemical storage building, in-plane buckling of double-angle braces was observed after this earthquake (Fig. 2.12 right).

Significant damage of a two-story steel braced frame in Palo Alto was reported after the magnitude 6.9 1989 Loma Prieta earthquake that struck the San Francisco Bay Area (SEAOC, 1991) with on October 17. The building was built in 1985. The downtime after the earthquake needed for repair was about five months. Three failure modes were identified within fourteen braced frames on the perimeter of the building: (1) twisting of W12 steel beams at brace-to-beam intersections where the beams were not properly supported; (2) buckling of bracing members; and (3) weld failures at brace connections. It was believed that the twisting of the interstitial beam contributed to the loss of brace compression capacity in some braced bays and consequently increased the force demands in the other braced bays, which resulted in the brace buckling and weld failures. Another report listed the damages of four nearly identical two-story braced frames in Silicon Valley (Phipps et al., 1992). These buildings were constructed in 1973 and were used for administration and development purposes. Buckling of braces was reported after the earthquake, and the downtime of these four buildings was nine months. It was also noted that the slenderness of the buckled bracing members ranged from 110 to 160 in these cases.

Another major event occurred in Northridge, California, on January 17, 1994, where a magnitude 6.9 earthquake caused significant amount of damages to the steel structures. One of damaged steel concentrically braced frame was extensively examined and studied after the earthquake (Bonneville and Bartoletti, 1996). The building was a four-story stacked Chevron braced frame constructed in 1986 based on the 1980 Los Angeles Building Code (LABC). The foundation of this office building was sitting on medium dense to very dense soil, and the site was about 10.5 miles from the epicenter. The width-to-thickness ratios of square hollow structural section braces used in the braced frames varied from 27.1 to 31.4, and the slenderness ratio varied from about 54 to 66. No  $2t$  straight yield line details were introduced into the original design of brace-to-gusset plate connections. Several brace failure pictures after earthquake are shown in Figs. 2.13. Typical brace failure modes were local buckling of brace section walls, brace gross section fracture, and weld failures at brace-to-gusset plate connections. During the post-earthquake repairs, the square HSS braces were replaced by wide-flange braces and the  $2t$  straight yield line details were applied. The brace configuration changed to zipper system configuration (Khatib et. al., 1988), but the ground-story braces were designed to remain elastic.



(a) Out-of-plane buckling of steel flat-bars (source: NISEE e-Library by Steinbrugge, Karl V.)



(b) In-plane buckling of double-angle braces (source: NISEE e-Library by Steinbrugge, Karl V.)

Figure 2.12 Brace failures observed in the 1971 San Fernando Earthquake



(a) Local buckling of square HSS brace section wall (source: NISEE e-Library)



(b) Weld failures at brace-to-gusset plate connection (source: EERI, 1997)

Figure 2.13 Brace failures observed in the 1994 Northridge Earthquake

## 2.4.2 Past Earthquakes in Japan

The 1978 Miyagiken-Oki earthquake ( $M_s = 7.7$ ) was a major seismic event that severely damaged twenty-eight steel building structures in Sendai City (Tanaka et. al, 1980 and Kato et. al, 1980) and a number of steel buildings were slightly damaged. Among those buildings, eight of them collapsed and twenty had more than 3.33% residual drift angles. Structural failure modes such as brace connection failures, column base failures, interior wall failures, and exterior wall failures were observed (EERI, 1978). It was noted that most of severely damaged steel structures were only one or two-story braced frames. Post-earthquake investigations indicated that insufficient strength of brace connections, poor detailing of brace connection regions, and the over-estimation of post-elastic strength were critical factors. The EERI report pointed out that inadequate connection strength typically came from insufficient effective areas (i.e., net section areas), insufficient bolt shear strengths, poor workmanships, and poor done welds. This insufficient connection strength caused the premature failure of braces and had significant effects on the nonlinear behavior of the braced frame systems and the ultimate capacity of the systems, suggesting the urgent research needed in designing of brace connections and nonlinear behavior of the braced frames

The 1995 Hyogoken-Nanbu (Kobe) magnitude 6.8 earthquake resulted in a significant amount of damages to steel buildings. A post-earthquake reconnaissance team surveyed nine hundred and eighty-eight damaged steel buildings around the effective earthquake area (AIJ, 1995) and then categorized the survey results into four types based on the lateral force resistant system of the buildings:

- Moment frame in both directions (type R-R).
- Moment frame in one direction and braced frame in another direction (type R-B).
- Braced frame in both directions (type B-B).
- Other types not listed above.

Among the surveyed steel buildings, about 17% (168 out of 988) were steel braced frames and more than 50% (89 out of 168) of those braced frames were classified as severely damaged or totally collapsed. The severely damaged buildings typically had residual drifts of more than 1%, and significant fractures were noticed in the main structural components that proved difficult to repair. All collapsed steel braced frame buildings used single-story X-bracing configuration. For the severely damaged steel braced frame buildings, only 4% used the Chevron brace configuration, and 96% of them used the single-story X-bracing configuration. Section shapes used for the brace components were also included in the survey. Many total collapsed or severely damaged buildings used light-gauge steel braces such as round-bars, flat-bars, or angles. Several failure mode pictures are shown in Figs. 2.14, 2.15, and 2.16. Note that similar damages were found in both 1978 Miyagiken-Oki earthquake and the earthquakes in United States.



(a) Wide flange brace



(b) Double-tee single-story X

**Figure 2.14 Global buckling of braces during 1995 Hyogoken-Nanbu (Kobe) Earthquake (extracted from AIJ, 1995)**



**(a) Connection failure in a single-story X braced frame using round HSS braces**



**(b) Buckling of gusset plate**

**Figure 2.15 Connection failures in 1995 Hyogoken-Nanbu (Kobe) Earthquake (extracted from AIJ, 1995)**



**(a) Bolt failures in a double channel brace-to-gusset plate connection**



**(b) Bolt failures in a gusset plate-to-column connection**

**Figure 2.16 Bolt failures in 1995 Hyogoken-Nanbu (Kobe) Earthquake (extracted from AIJ, 1995)**

This was neither the first time nor the last time that brace connection failures occurred after the major earthquakes in Japan. In the 1922 Uruga Channel earthquake (Naito, 1926), brace connection in a five-story knee-braced frame in Tokyo City failed due to the shear rupture of fasteners. Recently, in the 2011 Great Eastern Japan Earthquake Disaster, brace connection failures were again observed in low-rise industrial buildings and a two-story parking structure in Sendai City. Several connection failure photos are shown in Fig. 2.17.



**(a) Brace connection fractures in a two-story parking structure**



**(b) Detail view of a brace connection fracture in a two-story parking structure**



**(c) Gusset plate buckling in a two-story parking structure**



**(d) Gusset plate net section failure in a low-rise industrial building**

**Figure 2.17 Brace connection failures observed in the 2011 Great Eastern Japan Earthquake Disaster**

(photo source: <http://iisee.kenken.go.jp> by Midorikawa, Dec. 2011)

## 2.5 CONCLUDING REMARK

Steel concentrically braced frame systems are considered to be efficient and economical lateral load resisting systems to control the lateral deformation in civil structures under wind loading or earthquake ground shaking. A review of structural damages to the braced frame systems after several major earthquakes—including recent earthquakes—has identified some anticipated and unanticipated damage. This damage has prompted many engineers and researchers around the world to consider new approaches to improve the behavior of braced frame systems. Extensive experimental studies over the last forty years of conventional buckling brace components and several braced frame specimens have been briefly reviewed above, highlighting that the number of studies on the full-scale concentric braced frames is still limited.

# 3 Experimental Program and Specimen Design

## 3.1 BACKGROUND

The NEES research project entitled, “International Hybrid Simulation of Tomorrow's Braced Frame Systems,” involved coordinated research at the University of Washington, Seattle, the National Center for Research in Earthquake Engineering (NCEE), Taipei, Taiwan, the University of Minnesota, Minneapolis, and the University of California, Berkeley. Researchers at each locale provided valuable experimental data and analytical results. A schematic drawing of the different types of specimens tested as part of the overall research program is shown in Fig. 3.1.

At the University of Washington, Seattle, more than thirty single-bay, one-story conventional concentric braced frame specimens and five single-bay one-story buckling restrained braced frame specimens were tested under unidirectional quasi-static cyclic loading. Three single-bay two-story conventional concentric braced frame specimens with a double-story-X bracing configuration and three single-bay, three-story concentric braced frame specimens with stacked double-story-X bracing configurations were similarly tested at NCEE (Powell et al., 2008; Roeder et al., 2011). To account for the three-dimensional and floor slab effects in the braced frame system, two-story, one-bay by one-bay, concentric braced frame specimens with conventional braces (in a single story-X braced configuration) and buckling restrained braces were tested under bi-directional cyclic loading in the MAST laboratory at the University of Minnesota (Palmer et al., 2011). At University of California, Berkeley, four single-bay two-story conventional concentric braced frame specimens having a V and inverted-V bracing configuration in the first and second story, respectively (i.e., an overall diamond-shaped configuration), were tested under unidirectional loading. In three specimens, unidirectional loading was applied quasi-statically at each floor level, and in one of the specimens hybrid simulation techniques were used to determine the deformation histories applied at each floor level. The tests conducted at the NEES shared-use experimental laboratory at UC Berkeley (NEES@Berkeley) are the subject of this report.

In this chapter, the design and construction of the specimens and test setup are described in detail, as is the instrumentation used to monitor the response of the specimens during testing. This chapter also discusses the selection of the quasi-static loading protocol used for three of the specimens and the assumptions utilized to develop and carry out the hybrid test of one specimen.



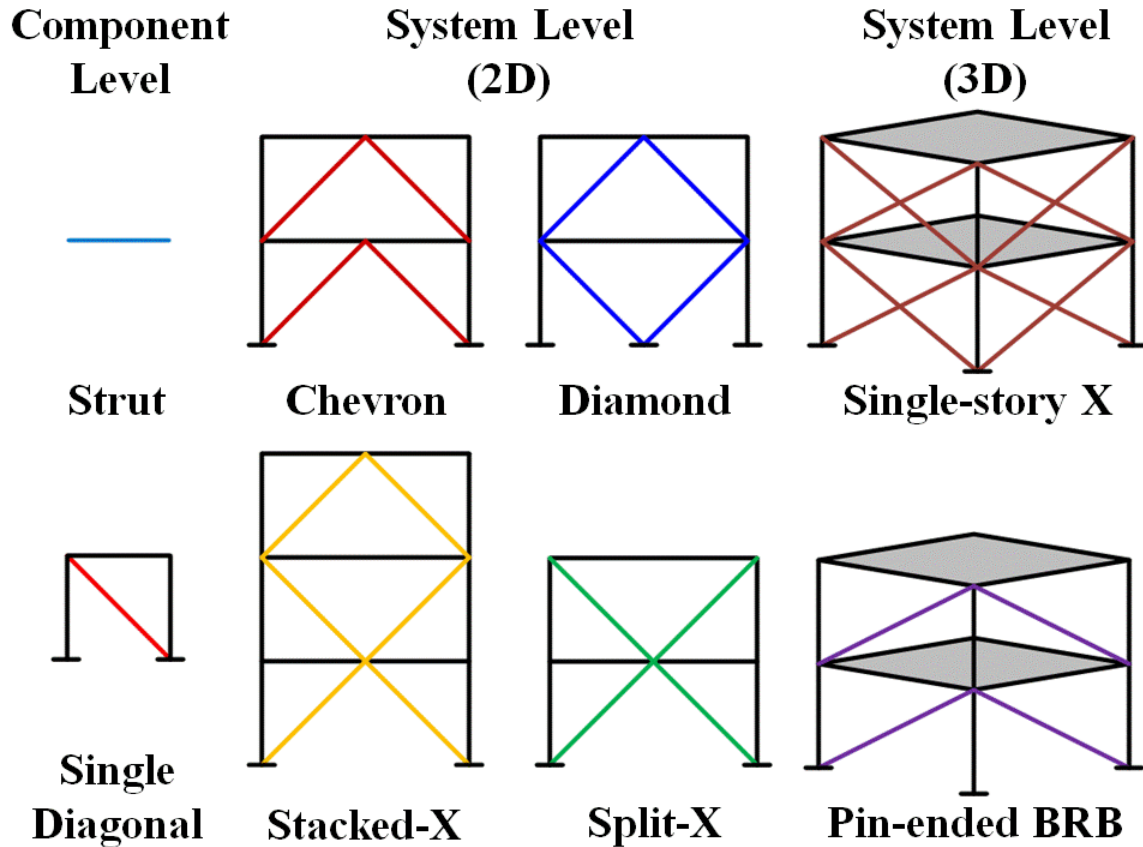


**Figure 3.1 Different specimen types for each testing facility in the experimental phase of the NEES research project**

### 3.2 EXPERIMENTAL PROGRAM AT UNIVERSITY OF CALIFORNIA, BERKELEY

As part of the overall NEES small group research project, testing of two-story tall specimens considered the test matrix graphically represented in Fig. 3.2. The two-story chevron brace configuration (Fig. 3.2(a)) with square HSS braces was tested previously at UC Berkeley in 2004 (Uriz, 2005). An overview of the test setup for this test is shown in Fig. 3.3. As noted previously, modern construction practices are moving away from stacked Chevron configuration, towards the Split-X configuration. Thus, the double story split-X brace configuration with square HSS braces and wide flange braces in Figs. 3.2(b) and 3.2(h), respectively, were tested at NCREE in 2007 and 2008 (Powell et al., 2008). Figure 3.4 illustrates the test setup for three two-story tall specimens tested at NCREE. For these specimens, testing was stopped before significant damage occurred in the beams and columns, and these members were reused for all tests; only the braces (and gusset plates) were replaced to enable subsequent tests. In these NCREE experiments, loads were only imposed at the roof level so that shears in both stories were identical.

In keeping with the test matrix, tests at UC Berkeley examined specimens with a two-story diamond-shape bracing configuration as illustrated schematically in Fig. 3.2 (c, f and i). In comparison with other specimens, these tests focus attention on the behavior of the floor levels where two braces intersect at a column line. To better represent the actual force distribution in

the structure when different sized braces occur in adjacent stories, servo-controlled actuators were installed for these tests at both floor levels.

Figures 3.5, 3.6 and 3.7 show some typical steel concentric braced frame building in California using the common brace configurations shown in the testing matrix.

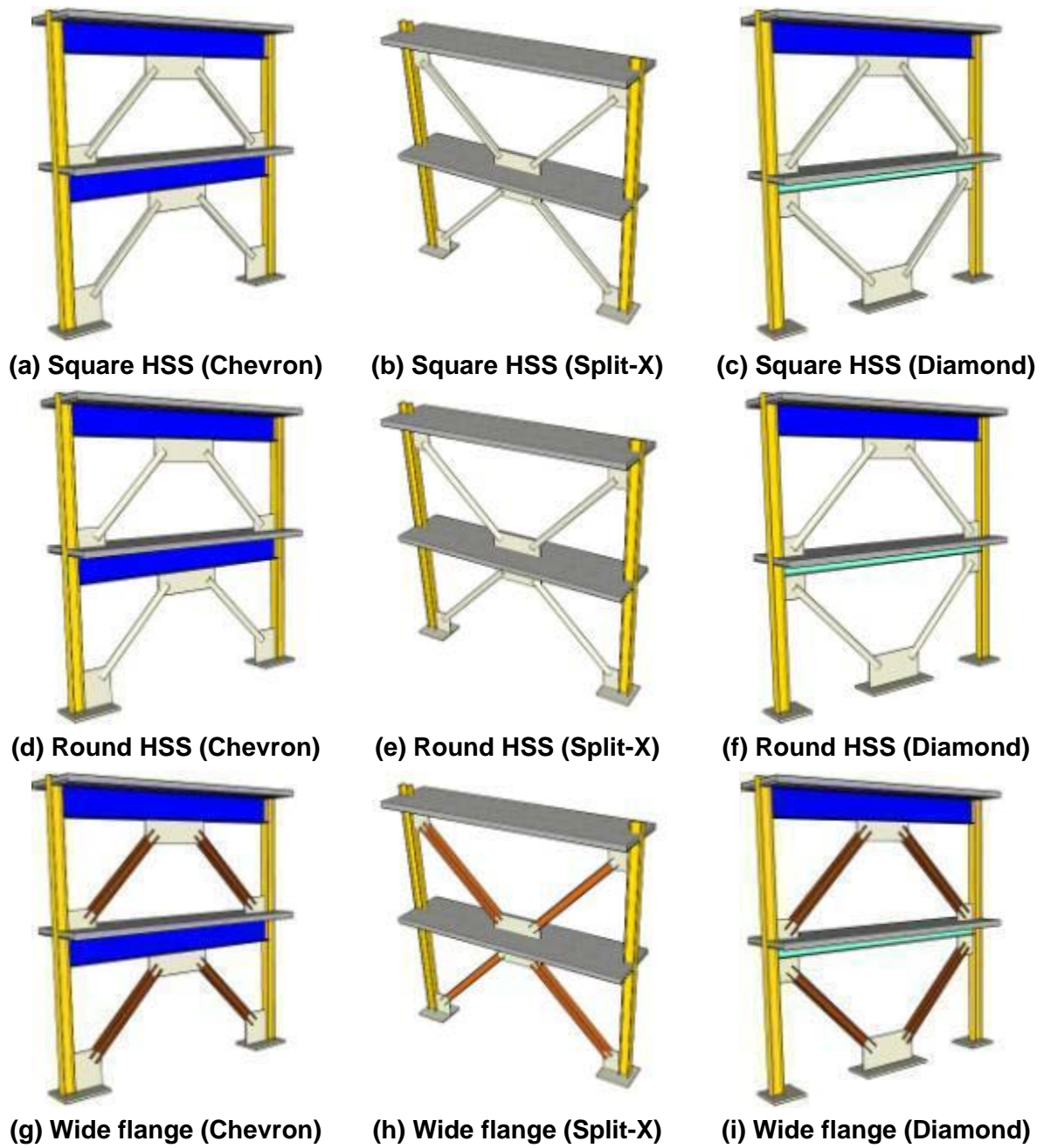


Figure 3.2 Test matrix of the 2D braced frame specimens in the research project



Figure 3.3 Overview of specimen SCBF-1 before test (Uriz, 2005)

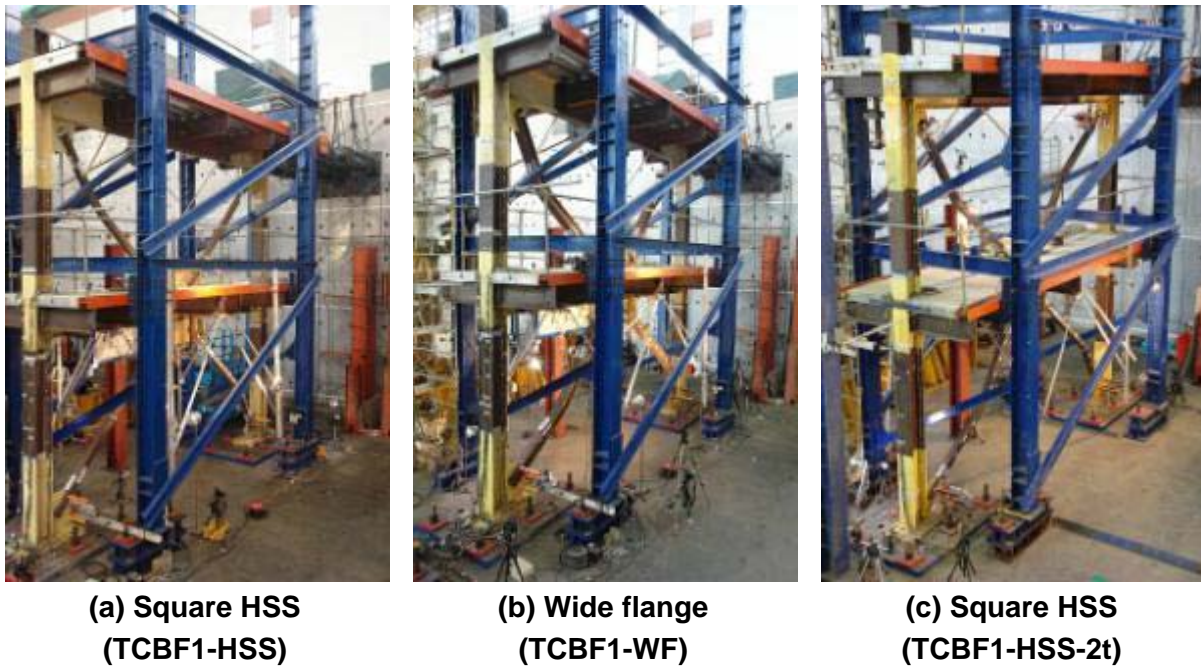


Figure 3.4 Overview of TCBF-1 specimens during the test

(Source: <http://exp.ncree.org/cbf/>)



(a) (Photo courtesy of Professor Stephen A. Mahin)



(b)

Figure 3.5 Application of stacked chevron braced frame in a building structure



(a) Ferry Landing, Oakland, California



(b) Skyline College, South San Francisco, California

Figure 3.6 Application of two-story split-X braced frame in a building structure



**(a) West Elm, Emeryville, California**



**(b) A two-story auditorium at Vista Grande Elementary School, Danville, California (Photo courtesy of Prof. Stephen A. Mahin)**

**Figure 3.7 Application of two-story diamond shape braced frame in a building structure**

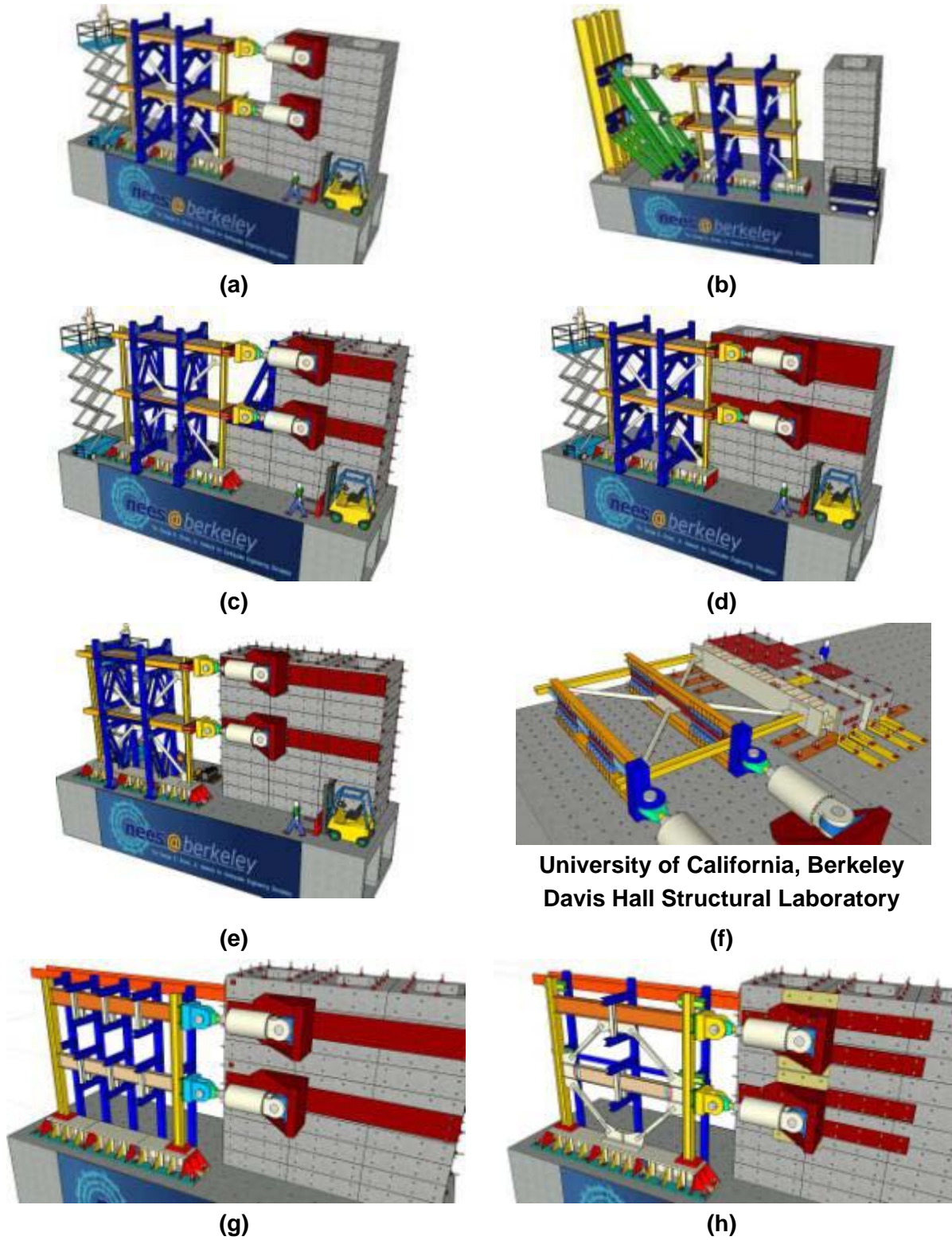
### 3.3 SELECTION AND DESIGN OF TEST SETUP

At the beginning of the specimen design process, several testing configurations were carefully considered and evaluated. Some of the design criteria, constraints, desirable conditions, prescribed loading capacities, and deformation capabilities considered are listed below:

- (1) The testing condition should be as close to the actual field conditions as possible.
- (2) The test setup should permit as large (in terms of base shear capacity and size) of framed specimen as possible.
  - a. As to the dimension range of framed specimen, a beam span between 20-ft and 30-ft in length and a story height between 9-ft and 12-ft were considered.
  - b. Previous tests had considered braced frames with capacities of approximately 1,000 kips.
- (3) Based on previous dynamic analyses for maximum considered events in near fault regions of California (Uriz and Mahin, 2004), a minimum target roof drift of about 5% maximum target was selected.
- (4) Use as small of lab footprint as possible to enable the reaction wall in the NEES@Berkeley lab to be shared with other research projects.
- (5) Limit loads on specimen to the capacity of the reaction wall and strong floor in the NEES@Berkeley lab.
  - a. Limit the maximum overturning moment and total web shear force that will develop in the two-cell box girder strong floor to less than 20,000 kip-ft and 1,500 kip, respectively (Aktan and Bertero, 1981).
  - b. The maximum concentrated uplift force per anchorage hole in the strong floor should be 100 kips or less (Skidmore et al., 1963 and 1964).
- (6) The weight of each member or component of the test setup should be less than the capacity of the overhead crane (24 kip) in the laboratory.
- (7) Use existing actuators, instrumentation, other equipment, and material to the extent possible.
- (8) Design specimen and setup considering simplicity, economy and ease of fabrication, erection and repair.
- (9) Design test set up considering:
  - a. Strength and stability in the in-plane and out-of-plane directions, including effects of possible specimen over-strength.
  - b. Reliability and accuracy of instrumentation and visual/photographic observation during tests.

Three-dimensional sketches illustrating the evolution of the test setup during the design process are shown in Fig. 3.8. The final setup used is described in the next section.





University of California, Berkeley  
Davis Hall Structural Laboratory

Figure 3.8 Possible testing configurations at the University of California, Berkeley during the specimen design phase

### 3.4 TEST SETUP AT NEES@BERKELEY FACILITY

The overview of the final configuration of the test setup is shown in Fig. 3.9. For the specimen to fit in the laboratory, and satisfy the other criteria outlined in Section 3.3, the specimen was designed to have a spacing between columns of 20 feet, and a distance of 9-ft between the mid-depth of beams. This geometry limited the base shear that could be imposed on the specimen to 900 kips, with 600 kips being applied at the top level and 300 kips at the lower level (i.e., considering an inverted triangular force distribution).

To develop the lateral reactions that could be imposed on the specimens during tests, a total of thirty reconfigurable reaction blocks (ten blocks per stack and each block is weight about 20 kips) were grouted and post-tensioned horizontally and vertically together to create an integrated reaction wall. Figure 3.10 shows a photo taken during the construction of the NEES@Berkeley reconfigurable reaction wall. Detailed calculations related to the reaction wall and adequacy of the floor system are presented in Appendix A.

Actuators for the tests were selected from among those available in the laboratory, considering the loads and displacement targets. While the specimen's design criteria limits the peak actuator force to about 600 kips, for accuracy in control during hybrid simulations, an actuator with a capacity 50% larger ( $1.5 \times 600 \text{ kips} = 900 \text{ kips}$ ) (Schellenberg et al, 2009). Thus, two Atlas 1,500 kip actuators with  $\pm 12$  inch stroke were used, with one installed at each floor level as shown in Fig. 3.11. With these actuators, a roof level displacement equal to about 5% of the specimen height can be imposed. Large brackets were installed on the reaction wall to attach the actuators. Due to the weight and size of the actuators, brackets were also installed on walls to help support the actuators during construction and testing. Detailed calculations and shop drawings for these brackets are presented in Appendices A and B, respectively.

To distribute the concentrated shear and axial loads applied at the base of a specimen to the strong floor, a heavy built-up floor beam (Fig. 3.12) was provided at the top of the strong floor top slab, and a series of relatively stiff load transfer beams (Figs. 3.13 and 3.14) were provided on the bottom side of the top slab. The floor beam and load transfer beams were connected by post-tensioned anchor rods. Detailed calculations and shop drawings for these details at the base of the specimen are presented in Appendices A and B, respectively.

Several different systems were considered to provide lateral restraint for the test specimen (Fig. 3.8). To improve access to the specimen during erection and repair, and to facilitate observation during testing, the lateral stability system shown in Figs. 3.9 and 3.15 was used. Detail design calculations for the lateral support frame are described in Appendix A. Shop drawings of the frame are provided in Appendix B.

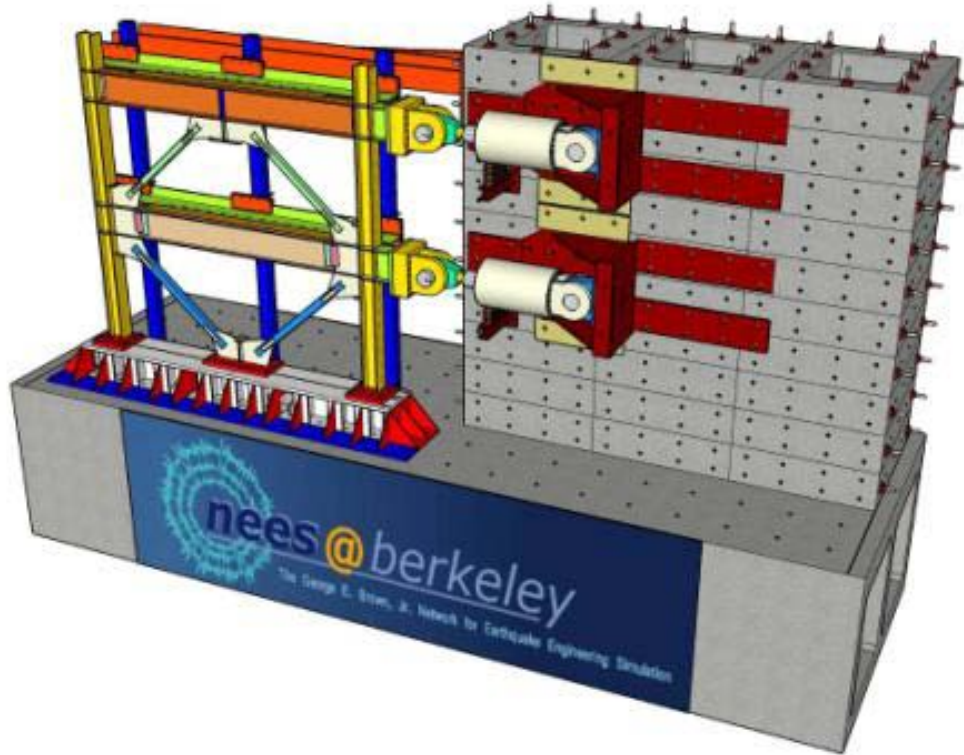


Figure 3.9 Overview of the final test setup



Figure 3.10 Construction of reconfigurable reaction wall before pre-stressing



Figure 3.11 Atlas 1.5 M-lb actuators at both floor levels



Figure 3.12 The built-up floor beam after painting



**Figure 3.13 Load transfer beams below strong floor before erection**



**Figure 3.14** Four load transfer beams below the strong floor after pre-stressing



**Figure 3.15** Lateral stability frame (the orange cantilever beam and three blue HSS columns) in the test setup view from south-east side of lab

### 3.5 DESCRIPTION OF TEST SPECIMENS

Four nearly identical braced frame specimens were designed, constructed and tested as part of this test program. Each test specimen consists of a two-story, single-bay concentric braced frame. As shown in Fig. 3.16, the story height is 9 feet measured from beam center line to center line of the top two beams (or from base to the centerline of the lower beam), and the bay width is 20 feet measured from column center line to center line. All specimens were detailed in compliance with the AISC Seismic Provisions for Structural Steel Buildings (AISC, 2005). Detailing provided was consistent with out-of-plane buckling of the braces. Specifics of the design process related to a prototype structure are described in Section 3.9. However, the basic design was arrived at by iteratively designing a structure, consistent with AISC Seismic Provisions and ASCE-7 (2005) requirements such that the ultimate base shear of the specimen did not exceed the 900 kips limit of the test setup considering an inverted triangular distribution of lateral forces.

To explore construction details that might speed field construction, special one-piece gusset plates were used at the ends of the lower floor beam where the beam intersects with two braces and the column (Fig. 3.9). The single piece gusset was shop welded to the column (Fig. 3.26), and attached by field welding to the braces and beam. Slotted stiffener (finger) plates were used to replicate the appearance and function of beam flanges that would have been present if the gusset was welded to a continuous beam extending from column to column.

The first three specimens were tested quasi-statically under cyclic loading excursions. These specimens were provided with square HSS, round HSS and WF bracing elements. The fourth specimen was the same as the first specimen with square HSS bracing, but it was tested using hybrid simulation techniques. Based on experience with the first two specimens, some of the details of the second two specimens were modified to improve behavior.

The specimen naming convention is TCBF-B- $\times$ , where TCBF stands for “Tomorrow’s Concentric Braced Frame”, B stands for “Berkeley” specimen, and the “ $\times$ ” stands for the specimen sequential number in the test program. The specimen name, member size, steel material type and test method of each specimen are listed in Table 3.1. The details of the specimens are shown in Figs. 3.17, 3.18, 3.19 and 3.20. Shop drawings for each specimen are summarized in Appendix C. Basic dimensional and engineering properties of sections used for beams, columns and braces are listed in Tables 3.2, 3.3 and 3.4. Photos in Figs. 3.21 to 3.24 show the entire side view of the completed specimens TCBF-B-1, TCBF-B-2, TCBF-B-3 and TCBF-B-4 before testing.

Photos of the fabricated sub-assemblages used to erect all four specimens are shown in Fig. 3.25. The gusset plates were all tapered and constructed from 3/4 inch thick plate. The  $2t_g$  separation from the end of the brace to the end of the taper on the gusset plate recommended in the AISC Seismic Provisions for out-of-plane brace buckling was used. One-piece gusset plates with two finger plates (see Fig. 3.26, flush the beam top and bottom flanges) welded on them and spliced to the W24  $\times$  68 lower beam. The one-piece gusset plates were welded to columns with double-side fillet welds (details are shown in Appendix C).

All of the braces were slotted and welded to the gusset plates per AISC requirements. Based on these requirements, reinforcing plates were welded to the braces at the net reduced section of the braces where the slot continued for a short distance past the end of the gusset plate (Fig. 3.27). This type of reinforcement was found to prevent premature failure of bracing components connected to gusset plates in this manner when loaded under loading histories with significant cycles of tensile deformation.

It should be noted that after testing of Specimens TCBF-B-1 and TCBF-B-3, the W24 × 117 roof beam, two W12 × 96 columns and 2-in.-thick base plates were re-used to reduce costs of constructing Specimens TCBF-B-2 and TCBF-B-4.



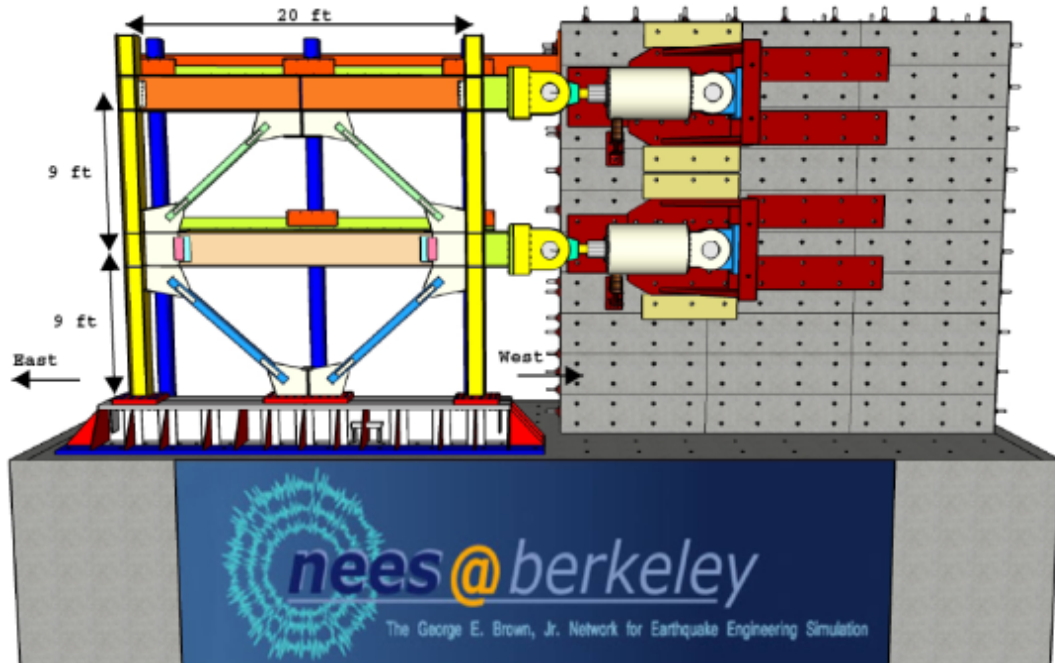


Figure 3.16 Dimension of test specimen

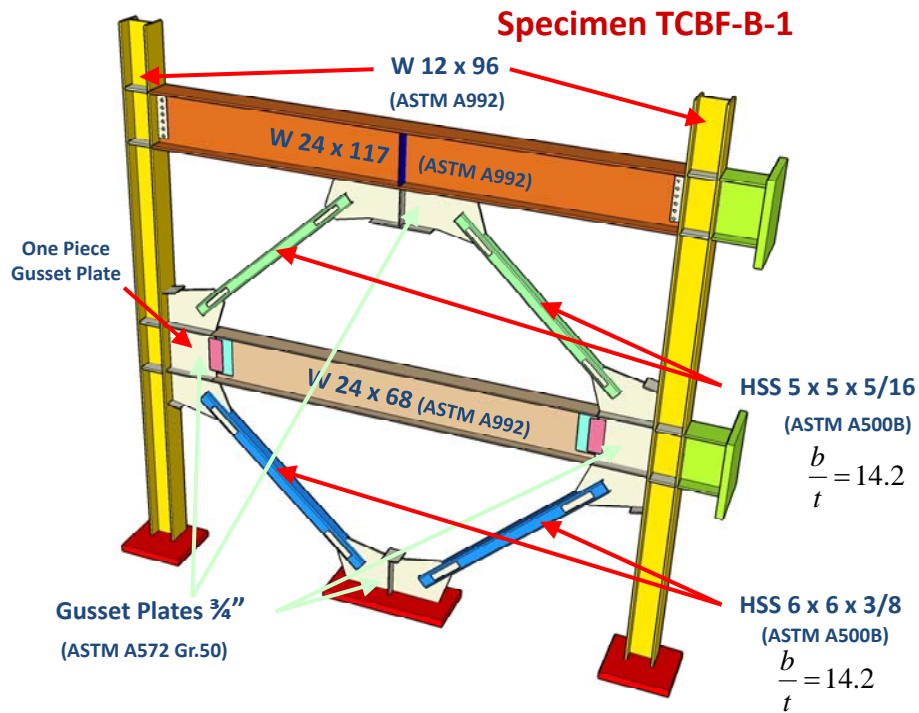


Figure 3.17 Member sizes of test specimen TCBF-B-1

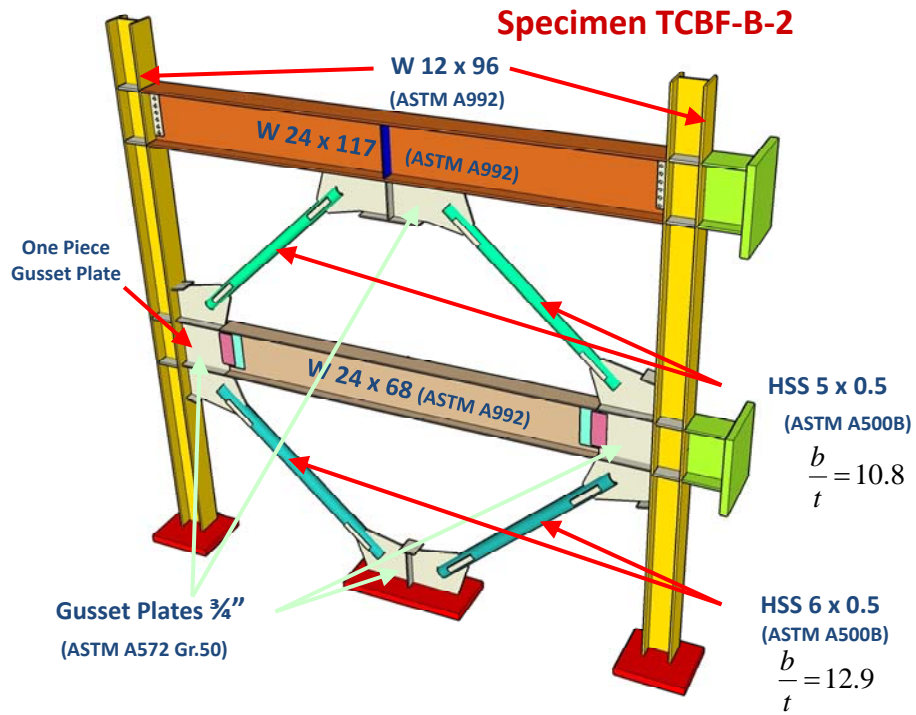


Figure 3.18 Member sizes of test specimen TCBF-B-2

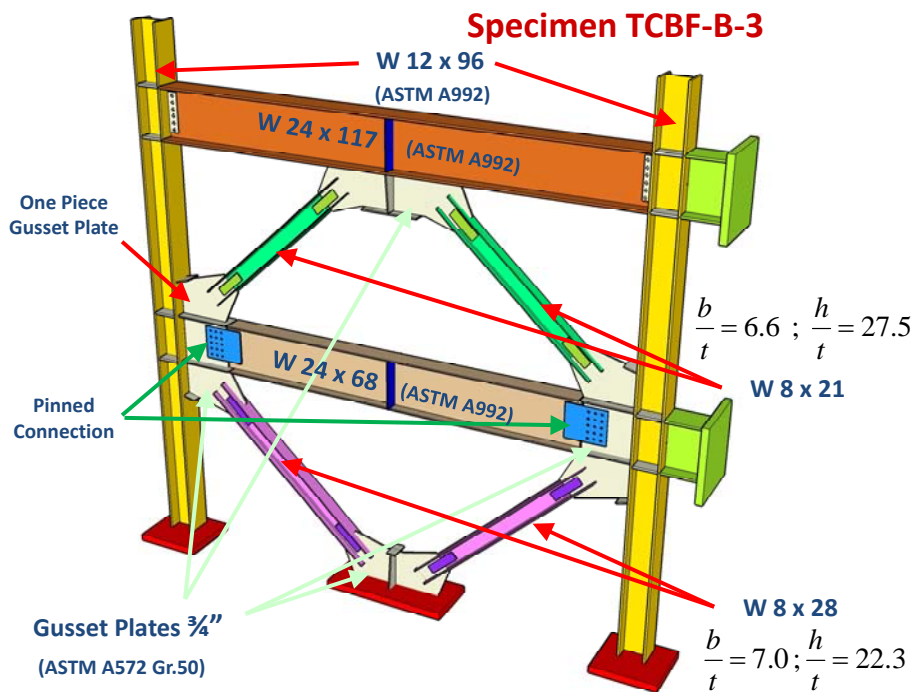


Figure 3.19 Member sizes of test specimen TCBF-B-3

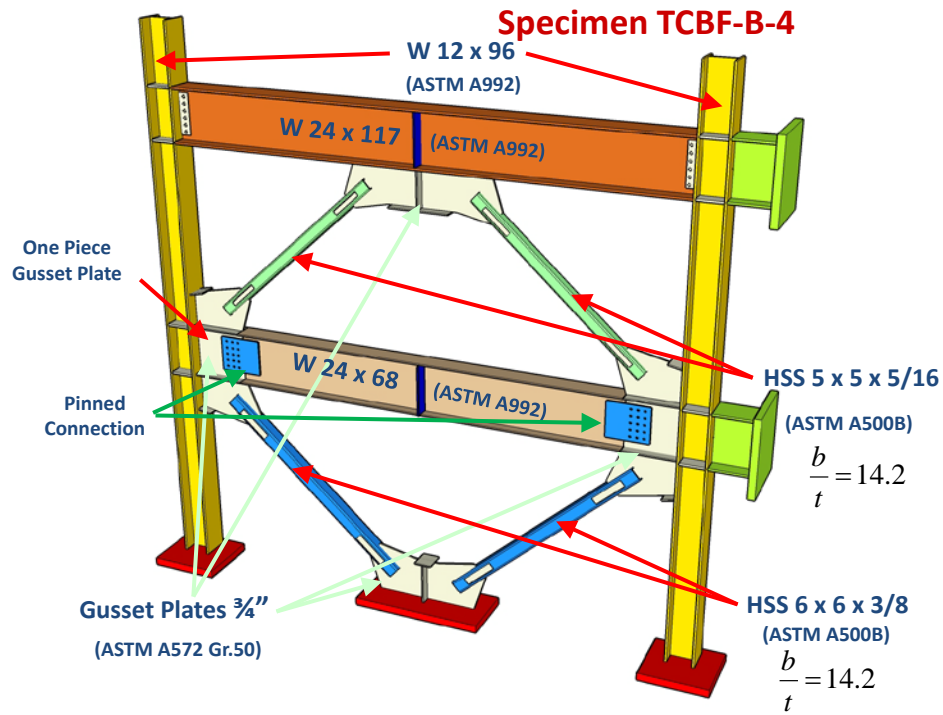


Figure 3.20 Member sizes of test specimen TCBF-B-4

Table 3.1 Name, member size, material type and test method of the specimens

Name	Column & Beam	Brace		Test Method
TCBF-B-1	W12 × 96 (Column) (ASTM A992)	HSS 5 × 5 × 5/16	ASTM A500B	Cyclic Loading
TCBF-B-2		HSS 6 × 6 × 3/8	ASTM A500B	Cyclic Loading
TCBF-B-3	W24 × 117 (Roof Beam) W24 × 68 (Lower Beam) (ASTM A992)	HSS 5 × 0.5	ASTM A500B	Cyclic Loading
TCBF-B-4		HSS 6 × 0.5	ASTM A500B	Cyclic Loading
		W 8 × 21	ASTM A992	Cyclic Loading
		W 8 × 28	ASTM A992	Cyclic Loading
		HSS 5 × 5 × 5/16	ASTM A500B	Hybrid Simulation
		HSS 6 × 6 × 3/8	ASTM A500B	Hybrid Simulation

**Table 3.2 Section properties of beams and columns**

Section	d (in)	t <sub>f</sub> (in)	b (in)	t <sub>w</sub> (in)	A <sub>s</sub> (in <sup>2</sup> )	I <sub>x</sub> (in <sup>4</sup> )	S <sub>x</sub> (in <sup>3</sup> )	Z <sub>x</sub> (in <sup>3</sup> )
W24 × 117	24.3	0.85	12.8	0.55	34.4	3540	291	327
W24 × 68	23.7	0.59	8.97	0.42	20.1	1830	154	177
W12 × 96	12.7	0.9	12.2	0.55	28.2	833	131	147

**Table 3.3 Section properties of HSS braces (square and round)**

Section	A <sub>s</sub> (in <sup>2</sup> )	B (in)	t (in)	I <sub>y</sub> (in <sup>4</sup> )	r <sub>y</sub> (in)	S <sub>x</sub> (in <sup>3</sup> )	Z <sub>x</sub> (in <sup>3</sup> )
HSS 6 × 6 × 3/8	7.58	6	0.375	39.5	2.28	13.2	15.8
HSS 5 × 5 × 5/16	5.26	5	0.3125	19	1.9	7.62	9.16
HSS 6 × 0.5	8.09	6	0.5	31.2	1.96	10.4	14.3
HSS 5 × 0.5	6.62	5	0.5	17.2	1.61	6.88	9.6

**Table 3.4 Section properties of wide flange braces**

Section	d (in)	t <sub>f</sub> (in)	b (in)	t <sub>w</sub> (in)	A <sub>s</sub> (in <sup>2</sup> )	I <sub>x</sub> (in <sup>4</sup> )	r <sub>x</sub> (in)	I <sub>y</sub> (in <sup>4</sup> )	r <sub>y</sub> (in)	S <sub>x</sub> (S <sub>y</sub> ) (in <sup>3</sup> )	Z <sub>x</sub> (Z <sub>y</sub> ) (in <sup>3</sup> )
W8 × 28	8.06	0.47	6.54	0.29	8.24	98	3.45	21.7	1.62	24.3 (6.63)	27.2 (10.1)
W8 × 21	8.28	0.4	6.27	0.25	6.16	75.3	3.49	9.77	1.26	18.2 (3.71)	20.4 (5.69)



Figure 3.21 Specimen TCBF-B-1 before test



Figure 3.22 Specimen TCBF-B-2 before first trial



Figure 3.23 Specimen TCBF-B-3 before test



Figure 3.24 Specimen TCBF-B-4 before hybrid simulation



Figure 3.25 (a) The sub-assemblages of specimens TCBF-B-1 and TCBF-B-2



Figure 3.25 (b) The sub-assemblages of specimens TCBF-B-3 and TCBF-B-4



Figure 3.25 (c) The sub-assemblies of specimens TCBF-B-2 and TCBF-B-3



Figure 3.25 (d) The sub-assemblies of specimens TCBF-B-3 and TCBF-B-4





Figure 3.26 The  $\frac{3}{4}$  inch one-piece gusset plate after tack welding to column flange



Figure 3.27 Detail view of reinforcing plate of TCBF-B-2 specimen

### 3.6 LOADING SEQUENCE FOR QUASI-STATIC TESTS

Specimens TCBF-B-1 through TCBF-B-3 were tested quasi-statically, with a prescribed history of roof displacement imposed. The displacement of the roof beam was monitored and controlled during the entire test process. However, the lower level actuator was force controlled. Throughout the tests, the force applied at the lower level was one-half of the instantaneous force measured in the load cell of the upper level actuator. This makes the lateral force pattern imposed on the specimen an inverted triangular distribution throughout the entire experiment. In this way, drifts in each story would evolve during the tests according to the damage occurring in each story.

The displacement protocol imposed at the roof was modified from the Appendix T of the AISC Seismic Provisions (AISC, 2005). This was used in order to compare the results with previous tests and tests conducted by others. However, because the specimens were special concentric braced frames, and were likely to buckle prior to the deformations at first yield of a buckling restrained braced frame for which Appendix T applies, an additional eight cycles corresponding to one half of the elastic design drift ( $6@0.5D_{be}$ ) and two cycles at the elastic design drift ( $2@D_{be}$ ) were added to the test protocol.

Figure 3.28 shows the cyclic loading protocol for the first three specimens in terms of roof displacement and roof drift ratio. The sign convention for imposed displacements and forces are that positive displacements and forces correspond to the actuator pushing the specimen to the east side of laboratory (Fig. 3.16), while negative values correspond to the actuator pulling the specimen to the west side of laboratory.

During the entire test process, the motion of the actuators was paused for a short time whenever major events such as fracture of braces, weld cracking or unanticipated flaking of whitewash were observed. The overall test was terminated following the cycle when both braces at the same story (typically the first story) completely fractured.

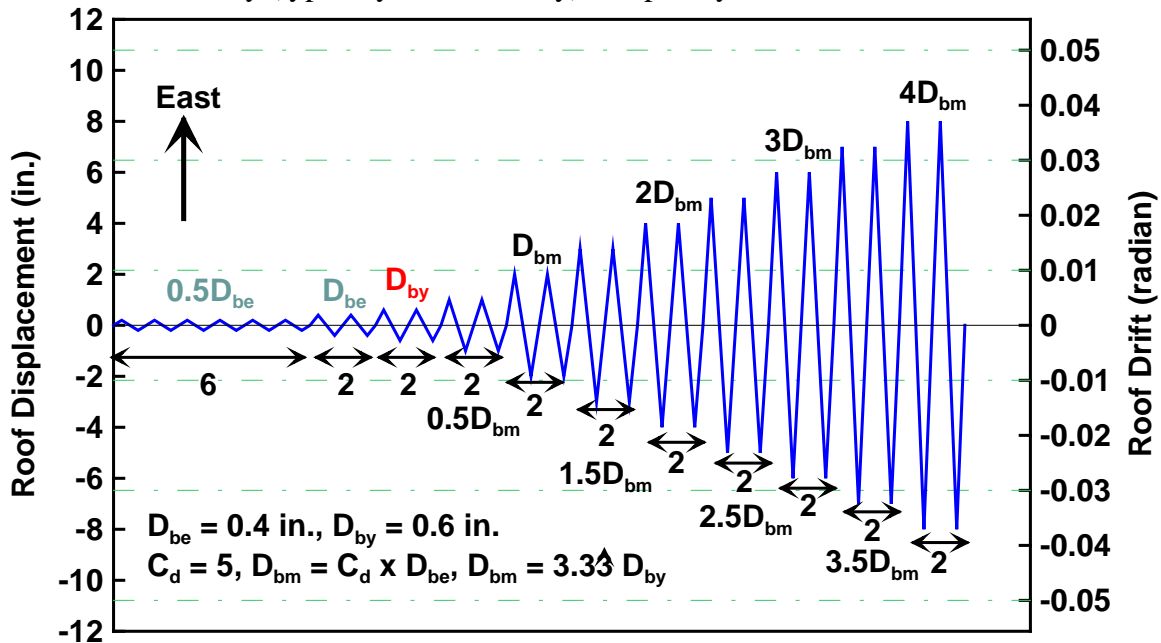


Figure 3.28 Cyclic loading protocol for TCBF-B-1, TCBF-B-2 and TCBF-B-3 specimens

### 3.7 INSTRUMENTATION

Each specimen was extensively instrumented with displacement transducers, tilt meters, strain gauges and load cells. The detailed location of instrumentation points, corresponding channel numbers, extension cable numbers, device serial numbers, device types, instrumentation ranges and detail descriptions for all four specimens are listed in Appendixes D, E, F and G.

Displacement transducers consisted of more than 75 digital encoders, linear variable differential transducers (LVDTs), Direct Current Displacement Transducers (DCDT) and wire pots. These were used to measure the floor level displacements, actuator displacements, longitudinal and lateral displacements of braces, local deformations of plastic hinge regions, and movement of the test set up (in-plane and out-of-plane). A set of brackets were installed on the out-of-plane displacement restraining system to provide support for displacement transducers measuring out-of-plane motion of the braces. Displacement transducers installed at the east end (with measuring target located at intersection of the center line of roof beam and the center line of east column exterior flange) of the first three specimens were used for external displacement control during the quasi-static tests. This was done to ensure the specimens were actually pushed and pulled to the displacements specified in the MTS-STC control software. For the last specimen (hybrid simulation specimen), the displacement transducer measuring targets were located at the west end of the specimen (i.e. at the actuator side) for safety reasons.

Two tilt meters were installed on the specimen. These were used to measure the rotation relative to an absolute vertical axis of the lower level beam-to-gusset plate connections.

Depending on the specimen, nearly 140 linear type strain gauges and rosette strain gauges were utilized. Many of the strain gauges were attached to portions of beams and columns where elastic behavior was expected. Engineering principles were then used to estimate curvatures, average axial strains, bending moments, shears and axial loads in these members. Strain gages were also attached to braces, gusset plates, panel zone regions and in plastic hinge regions to measure strains for subsequent comparison with numerical predictions.

The force acting in the 1,500 kip actuators were monitored by calibrated load cells (Fig. 3.29) between the rod head clevis and the actuator rod. Both load cells were calibrated before the experiment. The labs Baldwin 4,000 kip universal test machine (Fig. 3.30) was used to calibrate the load cell. This machine is calibrated to NIST standards on a regular basis. Figure 3.31 shows the steel jacket used for rotating the actuator to an upright position for calibration without the need to unscrew the load cell unit. Figure 3.32 shows a photo of overall setup during the calibration process.

The instruments and load cells were connected to three switch boxes using extension. These switch boxes are integrated into a high-speed data acquisition system programmed to scan every channel and record the data into a desktop computer under specified sampling rate defined before testing.

Reusable magnetic labels (Figs. 3.33 and 3.34) were used at column ends, beam ends and brace ends to easily identify the locations and orientations of specific photos during post processing. All of the specimens were painted with whitewash prior to testing to facilitate detection of yield patterns (see Figs. 3.21 to 3.24).

Thousands of digital photos in different views and angles were taken and stored in a desktop computer as a secondary observation tool (hand-held digital single-lens reflex camera was the primary observation tool). High quality videos were captured for the global response of the specimen through the entire experiment process and captured locally during the incipient fracture of bracing components. Four Canon EOS 5D Mark-II digital single-lens reflex (DSLR)

cameras were connected to data acquisition system and triggered to take still photos every 0.2 inch roof displacement (measured at the east end of specimen). Three Canon EOS D1 digital single-lens reflex cameras were connected to desktop computers and shot the still photos every 10 (or 15) seconds continuously throughout the entire test. The resolution of these DSLR cameras was very high, allowing for detailed post-test examination of behavior.

A three-dimensional Leica high definition laser scanner was also used to capture the specimen deformed shape throughout the cyclic loading tests. The resulting point clouds permit examination of the three-dimensional deformed shape of the specimen to within about 0.04 inch.



**Figure 3.29** The 1.5 million pound load cell



**Figure 3.30** Baldwin 4 million pound universal test machine



**Figure 3.31** Steel jacket for rotating the 1.5 M-lb actuator during the load cell calibration



**Figure 3.32** Overview of the calibration setup during the load cell calibration



Figure 3.33 Reusable magnetic labels for TCBF-B specimens



Figure 3.34 Distribution of reusable magnetic labels on TCBF-B specimens

## 3.8 SPECIMEN CONSTRUCTION SEQUENCE

### 3.8.1 Specimen TCBF-B-1

The first specimen (TCBF-B-1) was erected within a six hour period in the lab (this time does not including the welding process). First, the gusset plate assemblage at ground level was placed on the floor beam. Then, two columns were lifted and moved into position on the floor beam and temporarily secured by several 1-1/8 inch diameter all-thread anchor bolts (Fig. 3.35) at base. The HSS  $6 \times 6 \times 3/8$  braces were then inserted and bolted to the gusset plates at both ends with ASTM A307 erection bolts. The W24  $\times$  68 lower beam was then lifted up and spliced to the one-piece gusset plate using bolts. After the lower beam was fully bolted to the shear tabs at both ends, the yellow painted tee section (Fig. 3.36) that is part of the out-of-plane bracing system was then lifted up and positioned in three saddles (Fig. 3.37) connected at the elevation of the top flange of the lower beam to three vertical (blue) HSS columns. The tee section was bolted to a 14 feet long, 3/4 inch thick splice plate (made of ASTM A36 mild steel). This plate was in turn fillet welded along the center line of the lower beam's top flange. Three steel angle kickers were provided below the tee section and braced to the bottom flange at the middle span of the W24  $\times$  68 beam and also braced to the bottom continuity plates at the beam column joint panel zones as shown in Fig. 3.38.

In the next step, the W24  $\times$  117 roof beam was lifted and bolted to the shear tabs on the interior side of column flange at both ends. The HSS  $5 \times 5 \times 5/16$  braces for second story were then installed and bolted to the gusset plates. Finally, the lateral supporting tee section at roof level was placed on adjustable saddles and connected to the top flange of roof beam (similar to the lower beam).

Welding of beam-to-column connections, gusset plate-to-beam splices and gusset plate-to-brace connections were continued after the whole specimen was aligned to insure plumbness and fit up. Self-shielded, flux-cored wires for self-shielded arc welding were used in this specimen. All welding consumables were AWS E71T-8-H16 low hydrogen electrodes or equivalent filler metal (Fig. 3.39a). Ultrasonic inspection of welds was performed in the shop. Only visual inspection of welds was performed in the field (laboratory).

Complete joint penetration weld details were specified at the lower beam-to-gusset plate connections. The beam top and bottom flanges were 45° grooved, and welded to gusset plate finger stiffeners. Backing bars were used on the flange welds. Note that the backing bars on top flange and bottom flange welds did not remove after welding. The beam web was also 45° grooved and welded on one side. Beam-to-gusset plate shear tab with shim plate and bolt holes at beam side were used for fabrication and served as a backing plate. Figure 3.40 shows the lower beam-to-gusset plate connection and welding details.

All high strength fasteners and anchor bolts were tightened to the minimum required pretension forces specified in AISC manual using impact gun based on the torque table provided by the tool manufacturer. Standard shim plates (Fig. 3.39b) were used between base plates and top flange of floor beam to control the plumbness of the columns in the specimen within 1/16 inch out-of-plumb between column tip and column base. A laser level and a traditional level were used to check for plumbness. Figures 3.41 and 3.42 show the key construction steps and welding processes of this specimen.





Figure 3.35 The 1-1/8 inch diameter all-thread anchor bolt



Figure 3.36 The lateral supporting tee section



Figure 3.37 Tee section sitting on the lateral supporting saddles



Figure 3.38 Steel angle kickers below the tee section



Figure 3.39(a) Filler material used in the welding process



Figure 3.39(b) Standard shim plates for the column base adjustment



Figure 3.40(a) Specimen TCBF-B-1 lower beam-to-gusset plate connection details

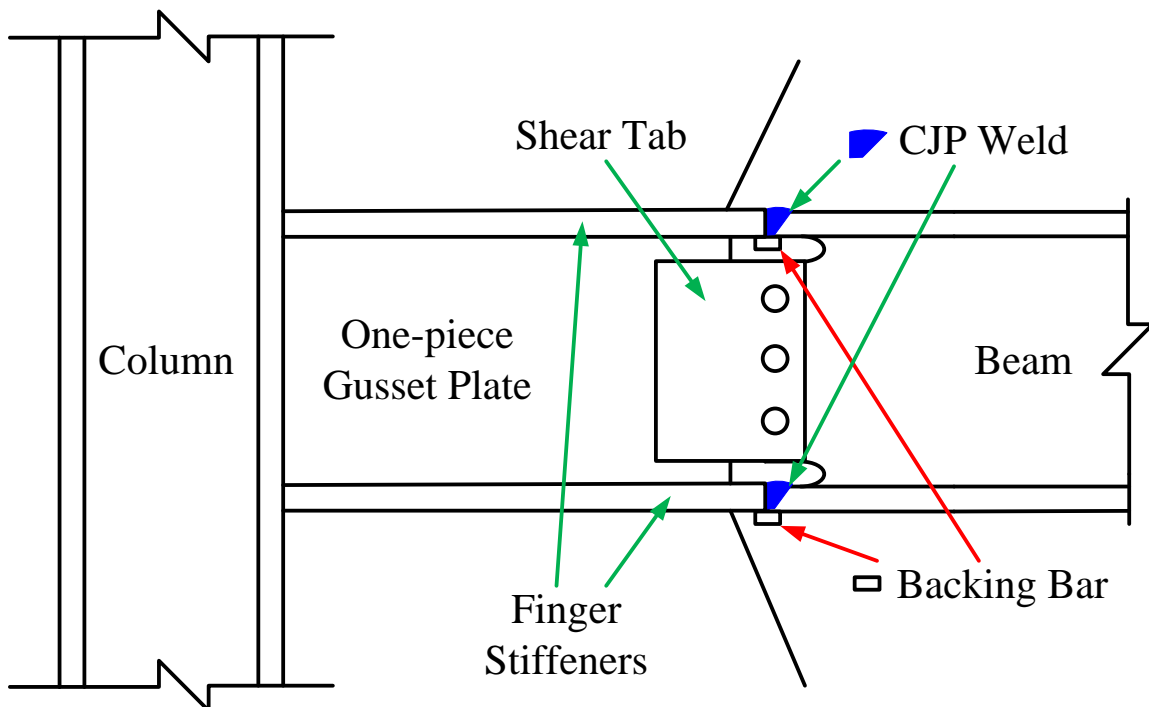
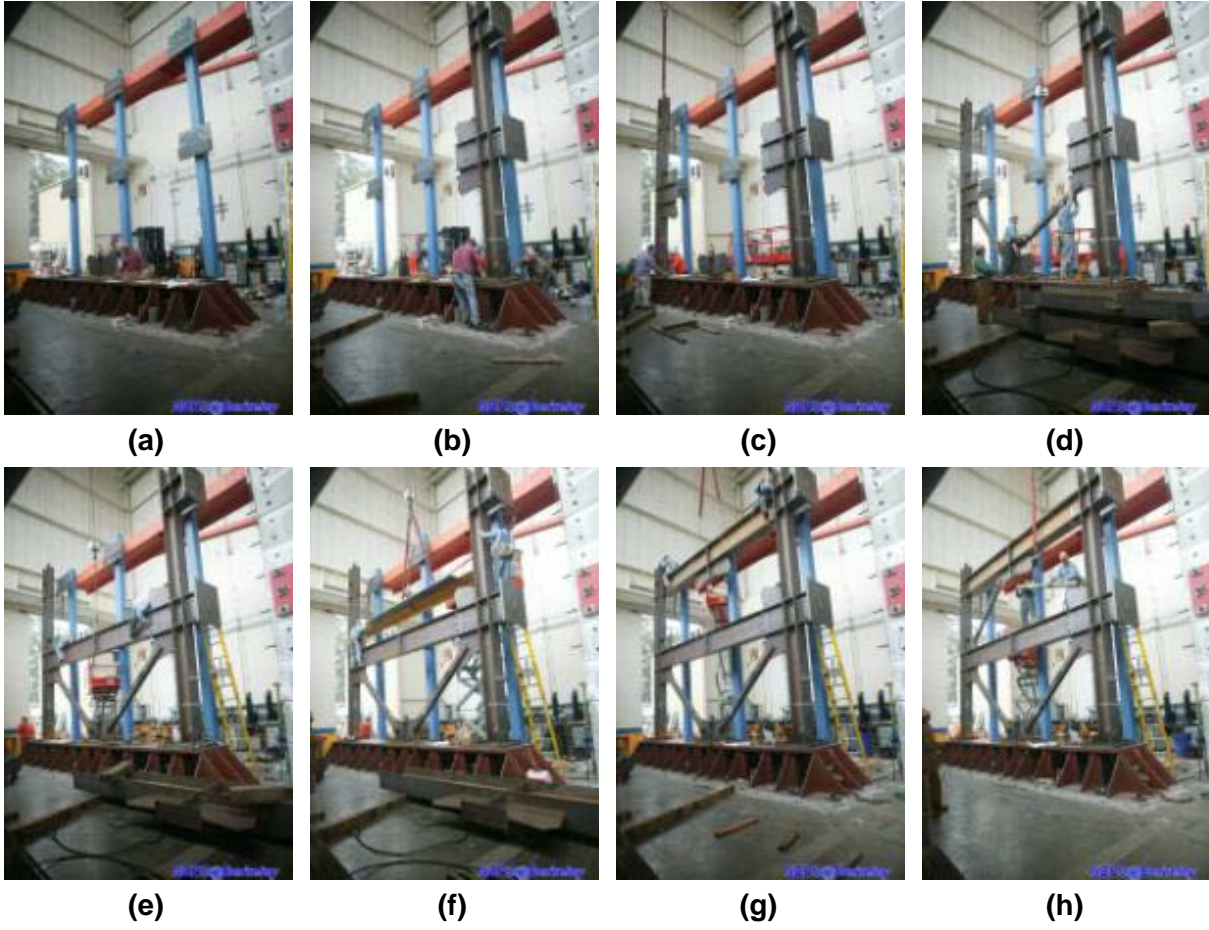
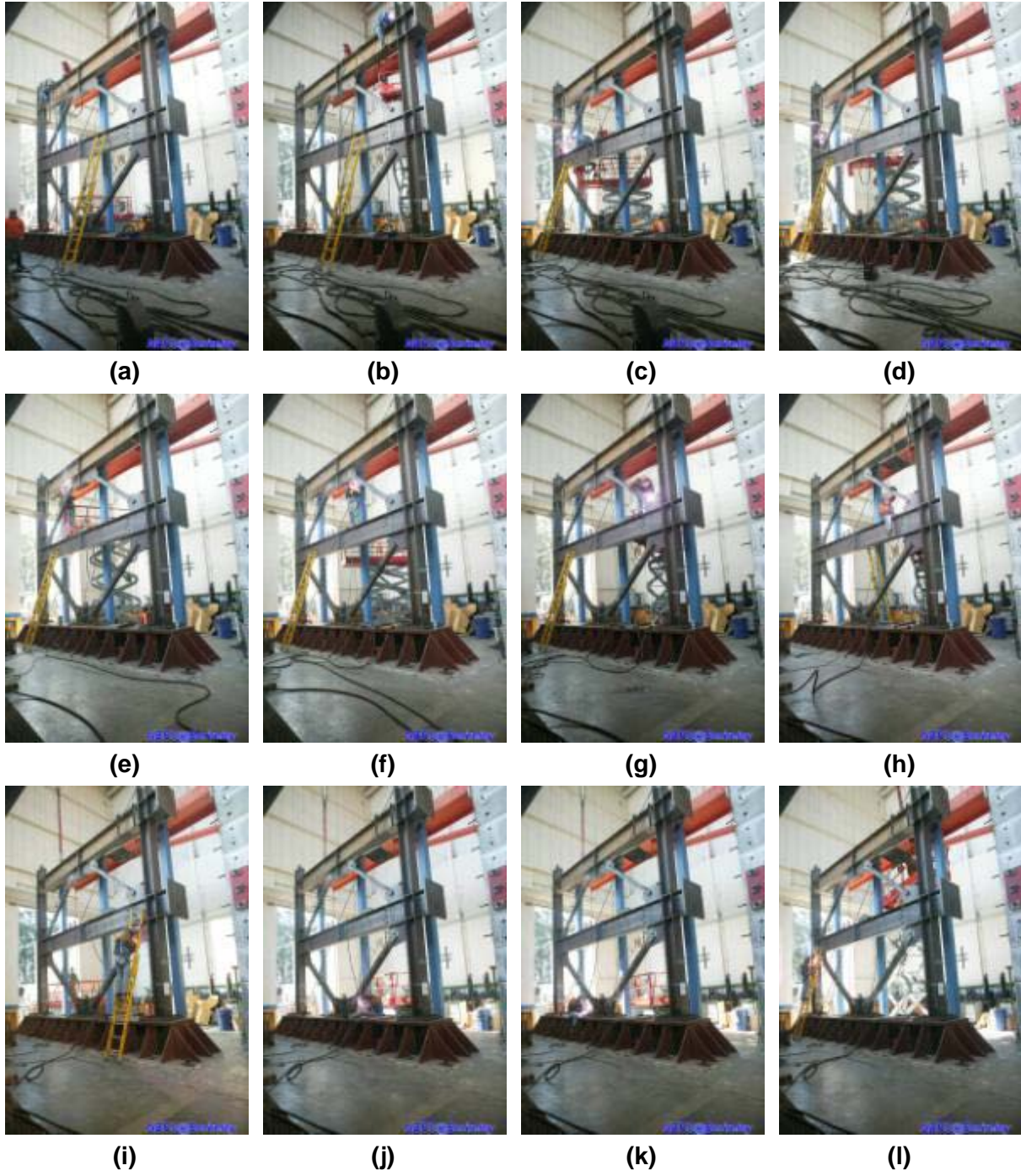


Figure 3.40(b) Specimen TCBF-B-1 lower beam-to-gusset plate connection weld details



**Figure 3.41 Key construction steps of TCBF-B-1 specimen**



**Figure 3.42 Key welding processes of TCBF-B-1 specimen**

### 3.8.2 Specimen TCBF-B-2

The second specimen (TCBF-B-2) reused the same W24 × 117 roof beam, W12 × 96 columns and the 2-in. thick base plates from TCBF-B-1 specimen. Only the W24 × 68 lower beam and 3/4 inch thick gusset plates were replaced. Round HSS braces were used instead of square HSS braces in this specimen.

After testing of the first specimen, the damaged square HSS braces were cut off from the frame specimen using the torch cutting tool. The specimen with the braces removed is shown in Fig. 3.43. The specimen without braces was straightened to a vertical position using two hydraulic actuators. The residual deformation at roof level was monitored from the position transducer installed during the first test. Manual control the movement of the actuator was used to straighten the specimen back to its original position. When the residual deformation was within an acceptable tolerance (about 1/8 inch out-of-plumb between column tip and column base in the in-plane direction, the actuators were locked and then the W24 × 68 lower beam and gusset plates were cut off using a torch cutting device. Air carbon arc equipment was used to remove the old welds and any base metal that was still sticking out. A hand grinder was then used to grind the surface to an acceptable surface condition for welding new materials to it. Some surface weld repairs were performed during this process.

After surface preparation was done, the gusset plate assemblages were then tack welded to the 2 inch thick base plate, roof beam and two columns. Next, the round HSS braces in both stories were connected to the gusset plates by erection bolts. Then, the new lower beam was bolted to the one-piece gusset plate at both ends (Fig. 3.44). Slightly trimming of the ends of W24 × 68 beam were done to fit the space between gusset plate assemblages. A simple alignment check was performed before welding process. Similar field welding procedures were used as the TCBF-B-1 specimen. Figs. 3.45 and 3.46 show some key construction steps and welding processes of the specimen. The one-piece gusset plates were welded to column using double-side fillet welds.

Similar to Specimen TCBF-B-1, the complete joint penetration weld details were also specified at the lower beam-to-gusset plate connections. The beam top and bottom flanges were 45° grooved, and welded to gusset plate finger stiffeners. Backing bars were used on the flange welds. Note that the backing bars on top flange welds did not remove after welding. Single-pass fillet welds were applied to bottom flange welds after removal of backing bar. The beam web was also 45° grooved and welded on one side. Beam-to-gusset plate shear tab with shim plate and bolt holes at beam side were used for fabrication and served as a backing plate. Figure 3.47 shows the lower beam-to-gusset plate connection and welding details.

Several small weld fractures were found at both column bases during the final surface inspection (Fig. 3.48) before whitewash painting. The three-step dye penetrant (cleaner/remover, penetrant and developer; see Fig. 3.49) crack detecting method was used to help determine the length of cracks (Figs. 3.50). Inferior welds and cracks were gouged using air carbon arc equipment. Two additional inches of gouging measured from the crack tips was done along the course of cracks or welds as illustrated in Fig. 3.51. Preheating before repair welding was also included in the repair weld procedure. The two column bases after weld repairs are shown in Figs. 3.52 and 3.53. The side view of entire TCBF-B-2 specimen after whitewash painting is shown in Fig. 3.54.



**Figure 3.43** Damaged specimen after cutting off the square HSS braces



**Figure 3.44** Splicing the lower beam to one-piece gusset plates in TCBF-B-2 specimen



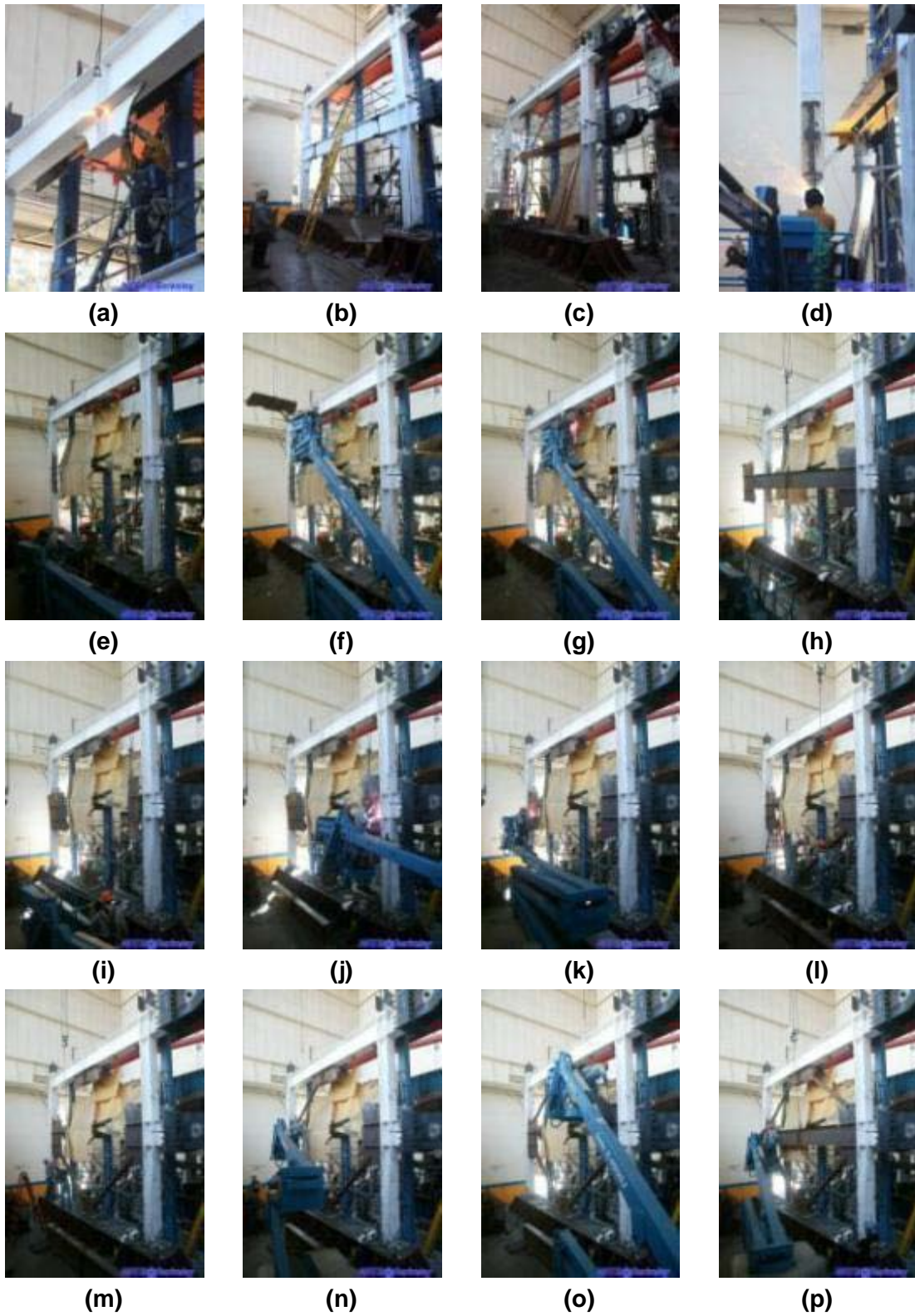


**Figure 3.45 Key construction steps of TCBF-B-2 specimen**

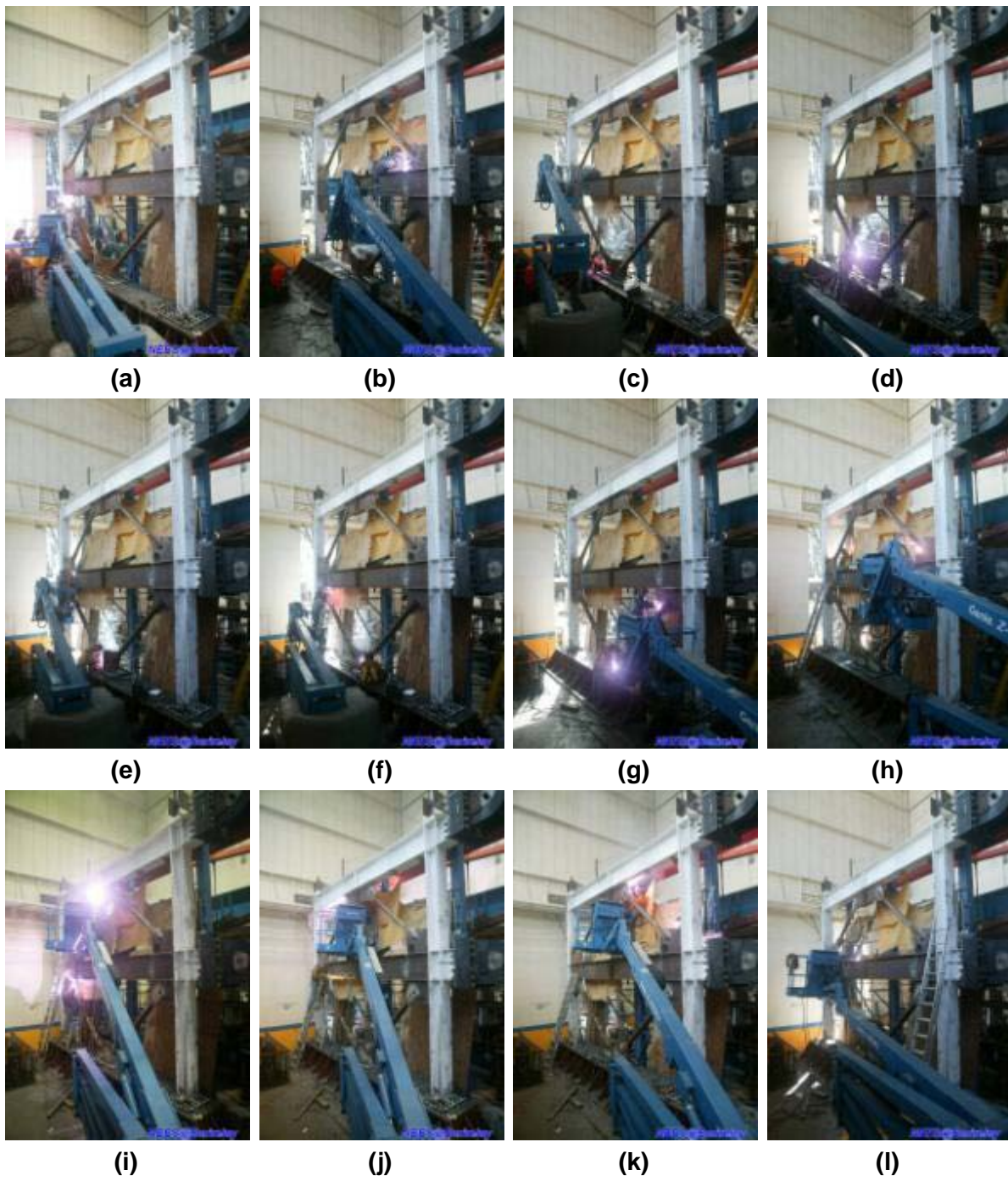


**Figure 3.46 Key welding processes of TCBF-B-2 specimen**



Figure 3.47(a) Specimen TCBF-B-2 lower beam-to-gusset plate connection details

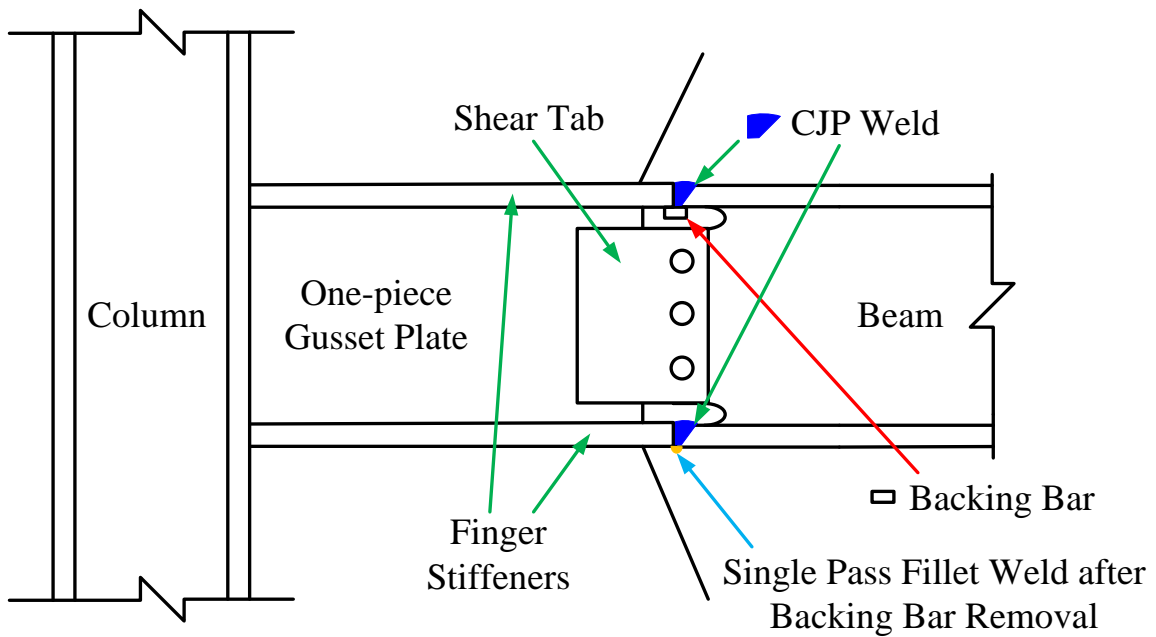


Figure 3.47(b) Specimen TCBF-B-2 lower beam-to-gusset plate connection weld details



Figure 3.48(a) Crack in the CJP weld at west column base (north-west corner)



Figure 3.48(b) Crack in the CJP weld at east column base (south-east corner)



Figure 3.49 Three-step crack detecting spray



Figure 3.50 Crack detecting spray applied in the CJP weld at east column base (south-east corner)



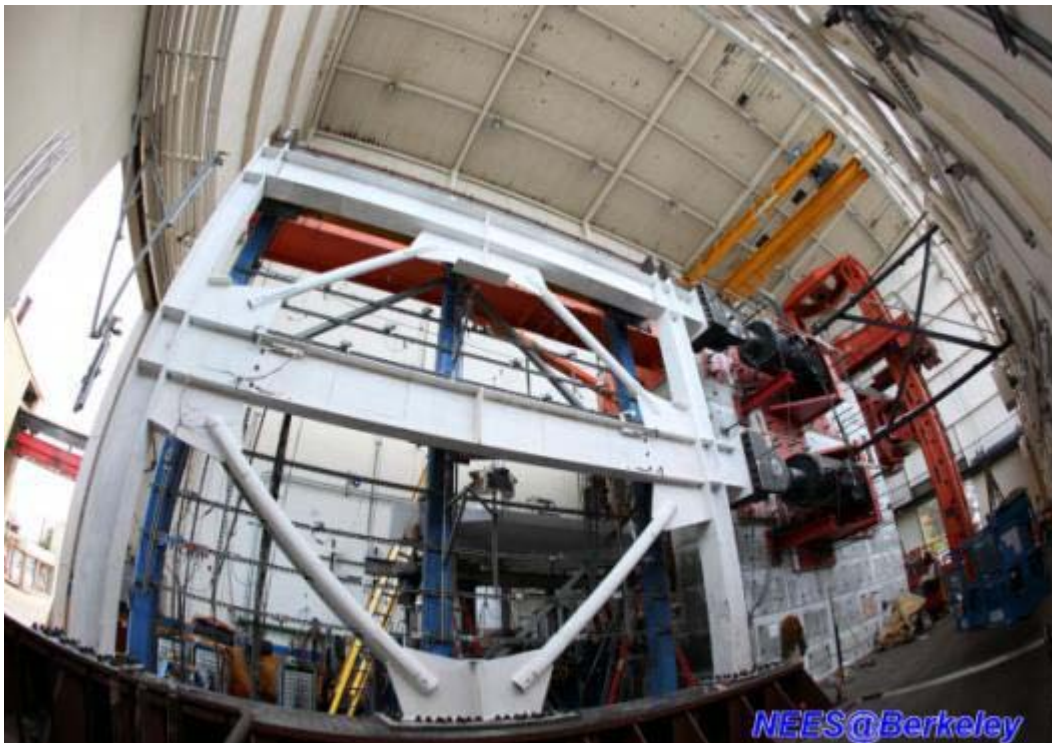
Figure 3.51 The east column base (south-east corner) after gouging the cracked welds



Figure 3.52 The west column base after weld repairs



**Figure 3.53** The east column base after weld repairs



**Figure 3.54** The entire TCBF-B-2 specimen after whitewash painting

### 3.8.3 Specimen TCBF-B-3

The third specimen (TCBF-B-3) with wide-flange braces was an entirely new specimen. It did not reuse the roof beam or columns from previous test. The specimen erection, not including the welding process, took about eight hours in the laboratory.

As before, two columns were initially lifted and moved to the position on the floor beam and temporarily secured by several 1-1/8 inch diameter all-thread anchor bolts at their base. Note that four gusset stiffeners were welded at base of each column for this specimen. Then, the gusset plate assemblage at ground level was placed on the floor beam. The first story W8 × 28 braces were then inserted and bolted to the gusset plates at both ends with ASTM A307 erection bolts.

The W24 × 68 lower beam was then lifted up and spliced to the one-piece gusset plate with fifteen tension control bolts at both ends (Fig. 3.55). Following the first two tests, it was decided (as will be discussed later in Chapter 4 and 5) to change the detail at the end of the beams where they attached to the gusset plates. Rather than fully welding the beam to the gusset plate, to simulate a continuous member, only the beam web was bolted to the gusset plate, to provide a more pin connection. After the lower beam was temporary connected to the gusset plates, the existing lateral supporting tee section (sitting on the saddles connected to vertical blue HSS columns at lower level which hold the entire tee section during the test) was then adjusted to bolt to a 14-foot long, 3/4-inch thick splice plate and fillet welded to the top flange center line of lower beam. Three steel angle kickers were provided below the tee section and braced to the bottom flange at the middle span of the W24 × 68 beam and also braced to the bottom continuity plates at the beam column joint panel zones.

Next, a sub-assemblage with W24 × 117 roof beam, top gusset plate and two W8 × 21 braces (see Fig. 3.56) were lifted and bolted to the shear tabs on the interior side of column flange at both ends. The W8 × 21 braces for second story were then bolted to the gusset plates. Finally, the lateral supporting tee section at roof level was connected to the top flange of roof beam.

The welding of beam-column connections, gusset plate-to-beam splices and gusset plate-to-brace connections were completed after aligning the specimen. Self-shielded, flux-cored wires for self-shielded arc welding were used in this specimen. All welding was accomplished using AWS E71T-8-H16 low hydrogen electrodes or equivalent filler metal. All high strength fasteners and anchor bolts were tightened to the minimum required pretension forces specified in AISC manual using tension control wrench and impact gun based on the torque table provided by the tool manufacturer. Standard shim plates were used between base plates and top flange of floor beam to control the plumb of the columns in the specimen within 1/16 inch out of plumb between column tip and column base. A laser level and traditional level were used to check for plumbness. Figures 3.57 and 3.58 show the key construction steps and welding processes of this specimen.





Figure 3.55 Lower beam to one-piece gusset plate connection detail



Figure 3.56 Roof beam, gusset plate and brace sub-assembly of TCBF-B-3 specimen

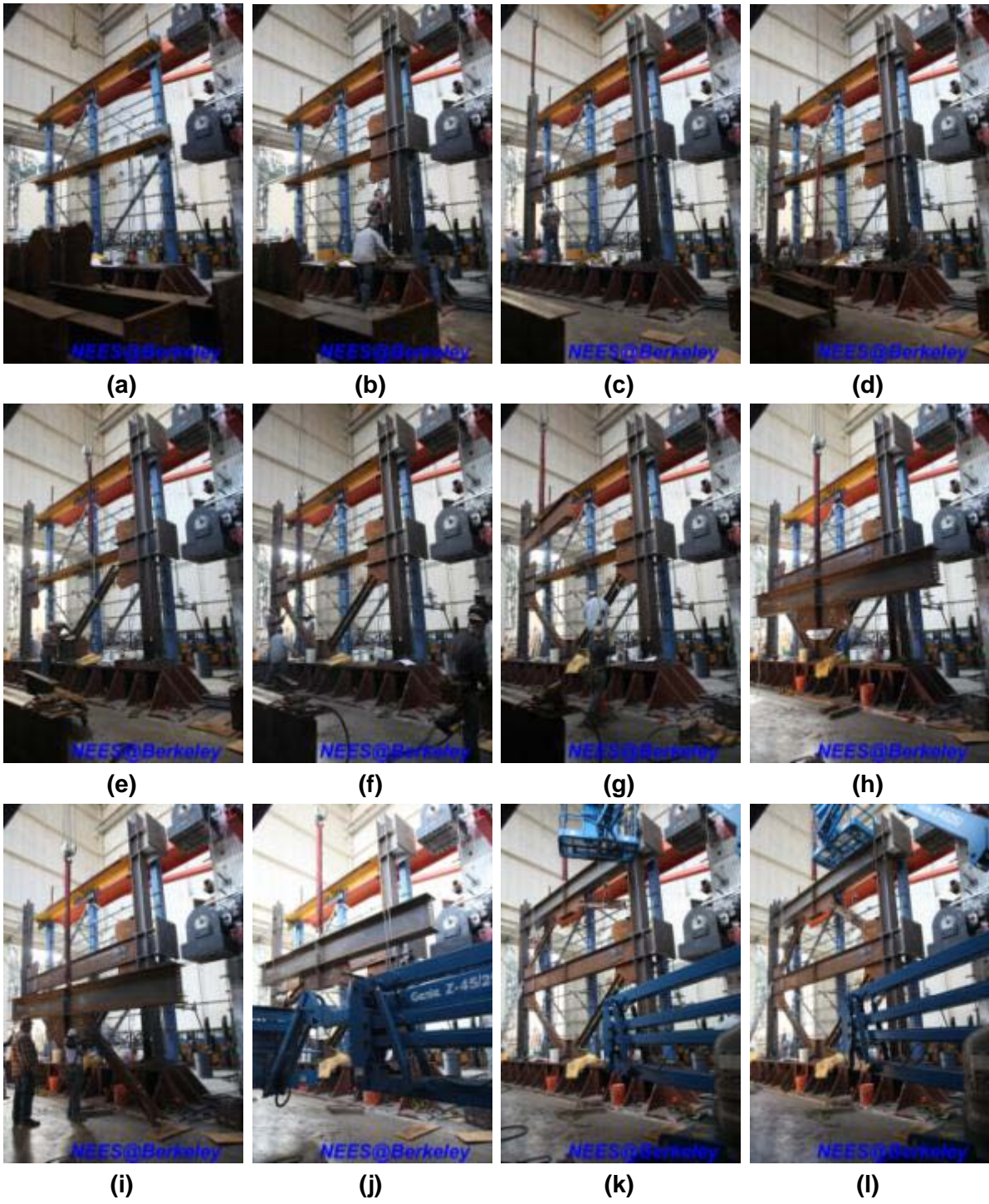


Figure 3.57 Key construction steps of TCBF-B-3 specimen

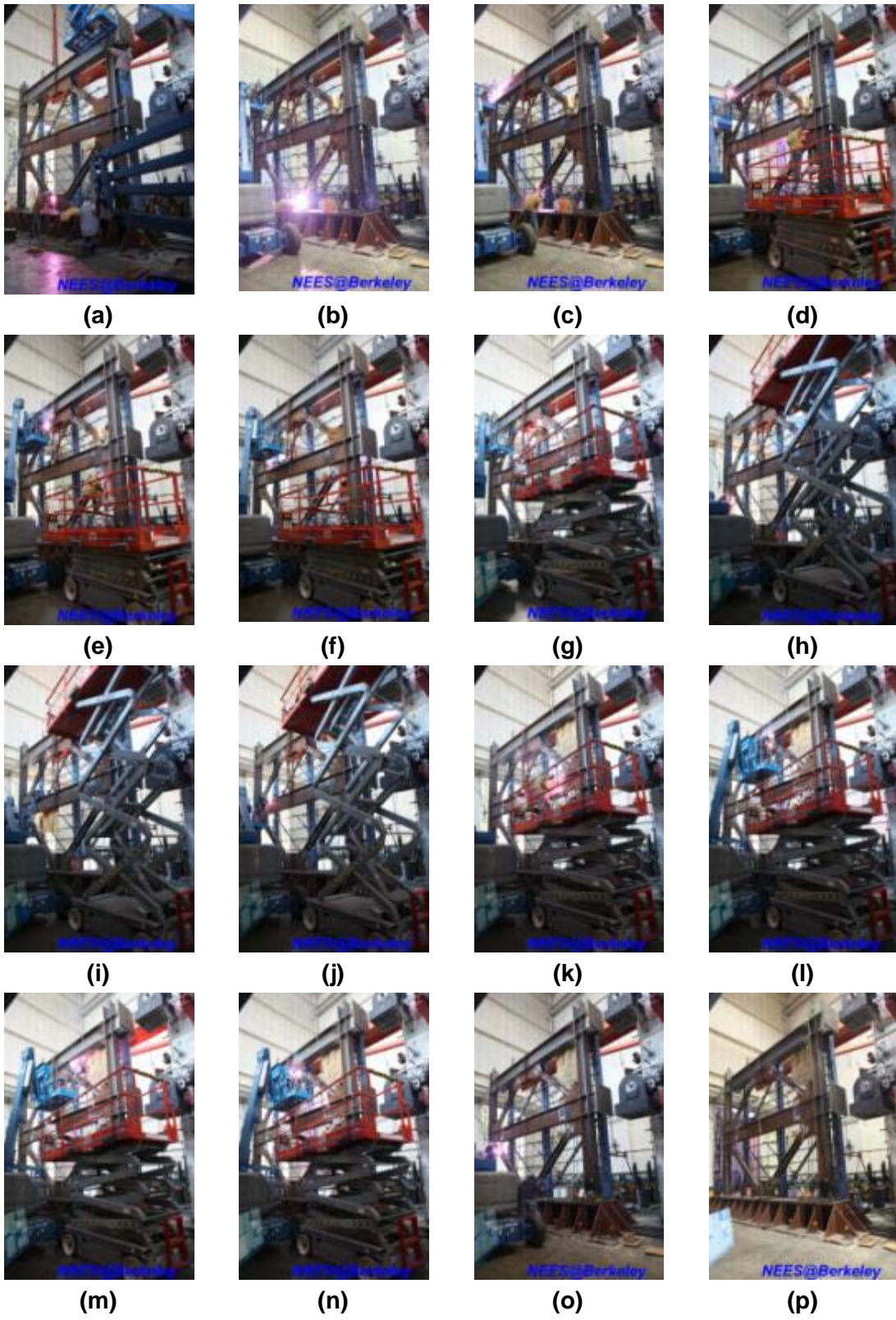


Figure 3.58 Key welding processes of TCBF-B-3 specimen

### 3.8.4 Specimen TCBF-B-4

The fourth specimen (TCBF-B-4) reused the W24 × 117 roof beam, W12 × 96 columns and the 2-inch thick base plates from TCBF-B-3 specimen. Only the W24 × 68 lower beam and ¾-inch thick gusset plates were replaced. Square HSS braces identical to those used in TCBF-B-1 were used in this specimen.

After testing of the TCBF-B-3 specimen, the damaged wide flange braces were cut off from the frame specimen (Fig. 3.59) using torch cutting tool. Then, the specimen without braces was straightened by the actuator at roof level. The residual deformation at roof level was monitored from the position transducer installed during the previous test. Manual control the movement of the actuator was conducted to straighten the specimen back to its original position. When the residual deformation was within an acceptable tolerance, the actuator position was locked.

Before welding the new sub-assemblages, air carbon arc equipment was used to remove the old welds and sticking out base metal. A hand grinder was also used to grind the surface to an acceptable surface condition for welding. Some surface weld repairs were performed during this process. After the surface preparation was done, the gusset plate assemblages were then tack welded to the 2-inch thick base plate, roof beam and two columns. Next, the square HSS braces in both stories were connected to the gusset plates by erection bolts. Then, the new lower beam was spliced to the one-piece gusset plate at both ends (Fig. 3.60). This detail was the primary difference between specimens TCBF-B-1 and TCBF-B-4. Slightly trimming of the ends of W24 × 68 beam were done to fit the space between gusset plate assemblages. Simple alignment check was performed before welding process. The remainder of the erection process and field welding used were similar to that used for the TCBF-B-1 specimen.

The east side column flange near the column base had fractured completely during the previous test and was repaired with complete joint penetration welds. The groove in the column flange prepared for complete joint penetration welds are shown in Fig. 3.61. In addition to the flange fracture repair, a repair had to be done for a fracture that extended into the column web near the base of the same column. Here, a cover plate and pair of vertical stiffener plates were attached to the column web to bridge over the fracture (Figs. 3.62 and 3.63). A weld access hole remained in the column web (see Fig. 3.62). The repaired column base after whitewash painting is shown in Figs. 3.64.

Figures 3.65 and 3.66 show some key construction steps and welding processes of the specimen.



Figure 3.60 Connection detail of the lower beam to one-piece gusset plates of TCBF-B-4 specimen



Figure 3.59 Damaged specimen after cutting off the wide flange braces



Figure 3.61 Grove prepared in the east side column flange near column base



Figure 3.62 A 0.55-in. thick cover plate welded to the south face of column web with fillet welds at east side W12 × 96 column base



Figure 3.63 Two 0.55-in. thick vertical stiffener plates welded to the north face of column web with fillet welds at east side W12 × 96 column base

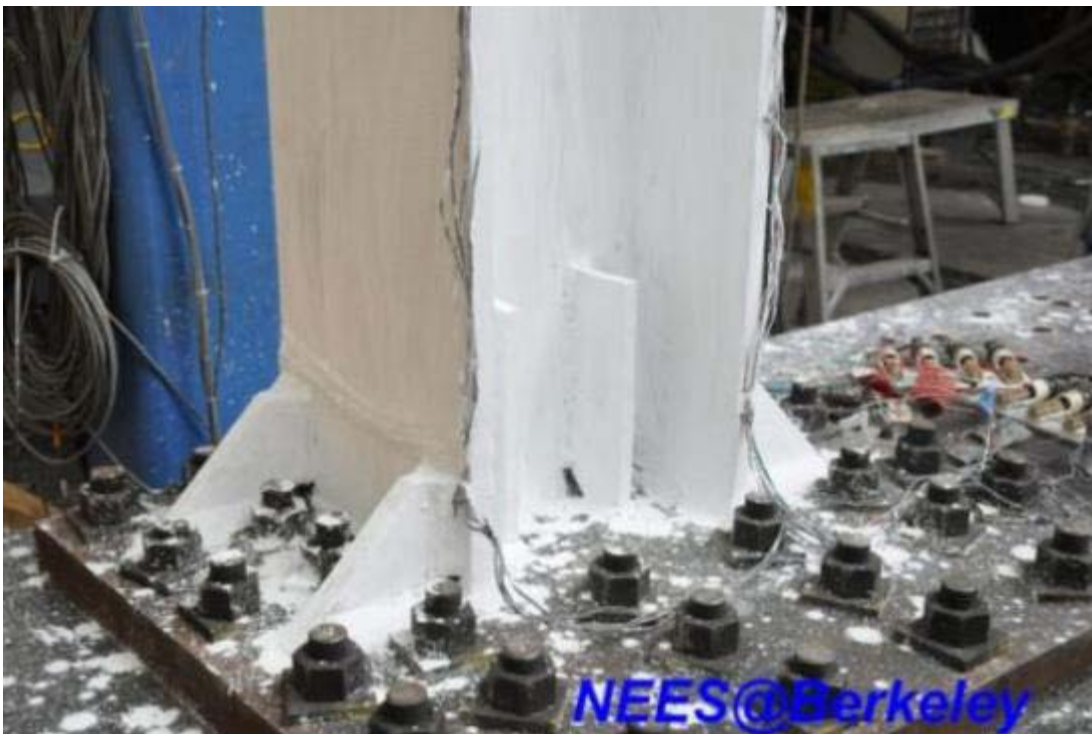
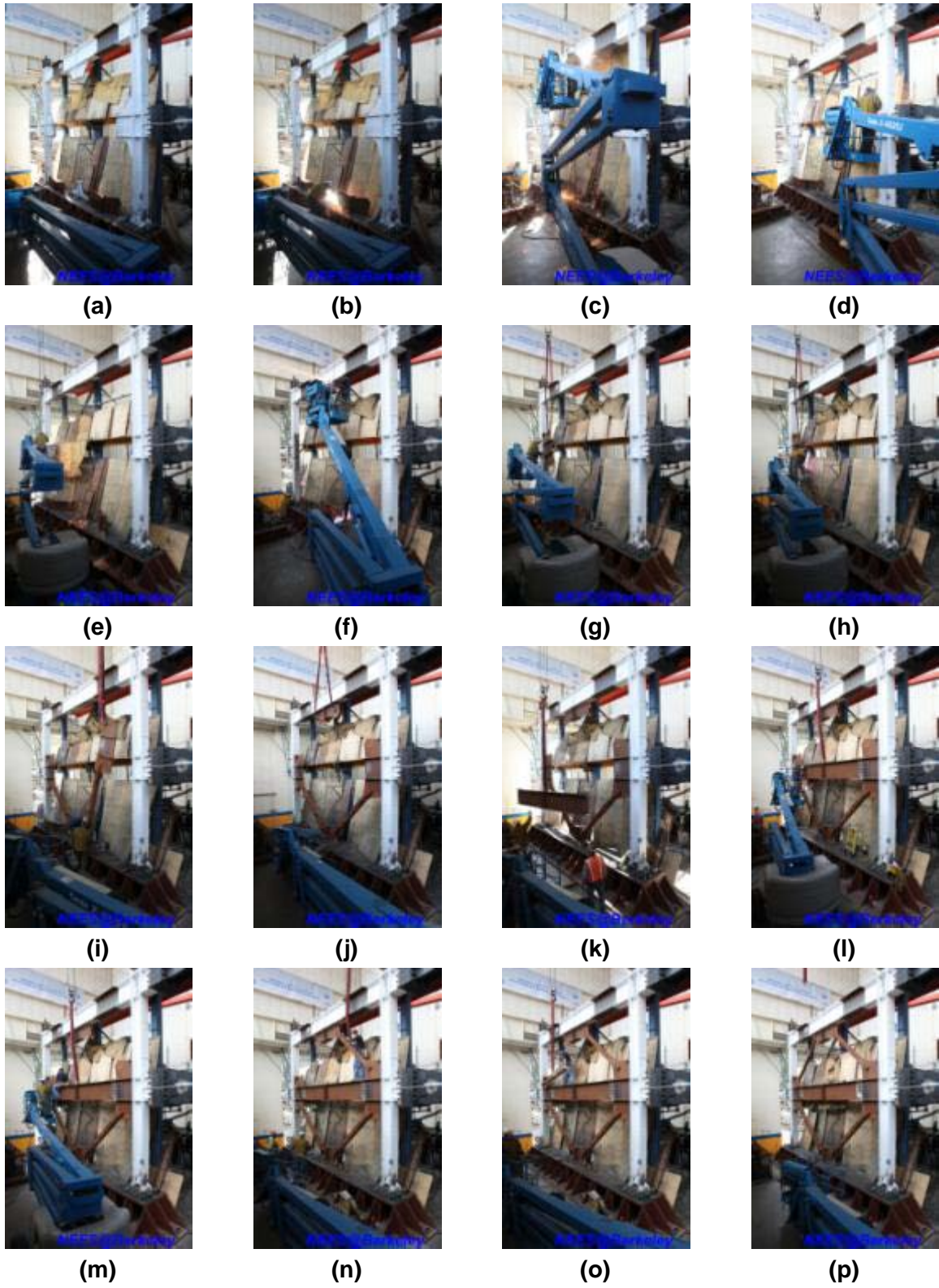


Figure 3.64 The east side column base detail after repair and whitewash painting



**Figure 3.65 Key construction steps of TCBF-B-4 specimen**





Figure 3.66 Key welding processes of TCBF-B-4 specimen

### 3.9 RELATION OF SPECIMEN DESIGN TO PROTOTPYE DESIGN

The test specimen designs were based on the constraints imposed by the laboratory test setup, and detailed according to AISC Seismic Provisions for Special Concentric Braced Frames. However, it is interesting to assess how these specimens might relate to an actual structure designed for a seismic region, like California. Moreover, to implement the hybrid tests a prototype structure is needed to identify the inertial and damping characteristics of the structure, as well as the properties associated with the gravity load resisting system. In this subsection, 2005 edition of the ASCE-7 building code is used along with the mechanical properties of the test specimens to identify characteristics of a prototype structure for which the specimen could be used to provide lateral load resistance

#### 3.9.1 Model (Prototype) Building

The model or prototype building was selected as a two-story building with special concentric braced frames in both directions. The typical beam span and story height were 20 feet and 9 feet in both X and Y direction. It is realized that these values are small compared to usual dimensions, but close enough that a larger scale factor need not be used. Typical floor plan, perspective view and the elevation considered in identifying the model building design are shown in Figs. 3.67, 3.68 and 3.69. The LRFD design method was used to select member sizes and the loading followed the ASCE-7-05 LRFD load combinations. The detailing and design basically followed the 2005 AISC Seismic Provisions. The braced bays in the Y direction (Fig. 3.69) were intentionally moved to the corner of the building to represent the actual testing configuration in the laboratory.

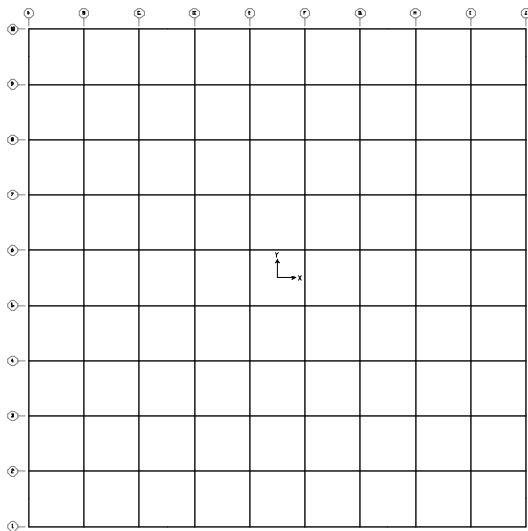


**Figure 3.67 Typical floor plan of the model building**

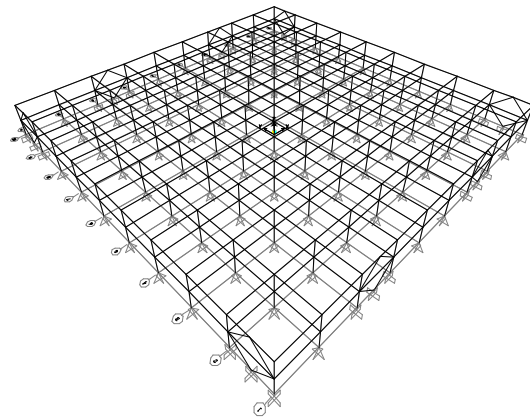


**Figure 3.68 Perspective View of the Model Building**

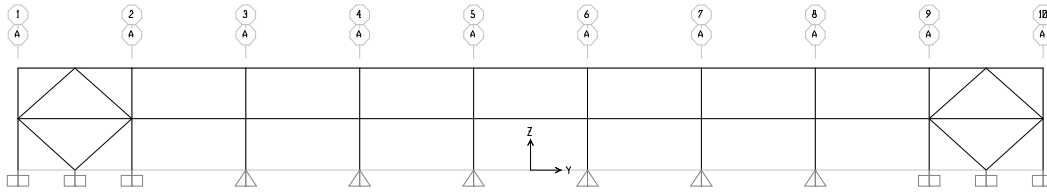


**Figure 3.69 Elevation of the Model Building (Y-direction)**

### 3.9.2 Seismic Forces

The model building location was assumed to be Berkeley, California (Zip code: 94720). According to the USGS Java software tool, Earthquake Ground Motion Parameters, Ver. 5.1.0 (see Fig. 3.70), the mapped MCE, 5% damped, spectral response acceleration parameter at 1 second and short periods can be determined:

$$S_1 = 0.787$$

$$S_5 = 2.014$$
(3.1)



**Figure 3.70 The snapshot of USGS Earthquake Ground Motion Parameters Java applet window**

Then the default site class D was selected per ASCE-7-05, Section 11.4.2, the site coefficients and acceleration parameters can be calculated as:

$$F_a = 1.0 \quad (3.2)$$

$$F_v = 1.5$$

$$S_{M1} = F_v \cdot S_1 = 1.181 \quad (3.3)$$

$$S_{MS} = F_a \cdot S_s = 2.014$$

$$S_{D1} = \frac{2}{3} \cdot S_{M1} = 0.787 \quad (3.4)$$

$$S_{DS} = \frac{2}{3} \cdot S_{MS} = 1.343$$

The selected occupancy category is taken as II, the importance factor is taken as 1.0 and the seismic design category is set as E. Per ASCE-7-05, Section 11.6 and ASCE-7-05, Fig. 22-15, characteristic periods in defining the design response spectrum can be calculated as:

$$T_0 = 0.2 \cdot \frac{S_{D1}}{S_{DS}} = 0.117 \quad (3.5)$$

$$T_S = \frac{S_{D1}}{S_{DS}} = 0.586 \quad (3.6)$$

$$T_L = 8 \quad (3.7)$$

Also from ASCE-7-05, Table 12.2-1, the design coefficients and factors for special steel concentrically braced frame were extracted:

$$R = 6; \Omega_o = 2; C_d = 5 \quad (3.8)$$

With the above information, the seismic base shear for the model building can be calculated using the following equations:

$$V = C_S \cdot W \quad (3.9)$$

$$C_S = \frac{S_{DS}}{(R/I)} = \frac{1.343}{6} = 0.224 \quad (3.10)$$

$$T_a = C_t \cdot h_n^x = 0.02 \cdot 18^{0.75} = 0.175 \quad (3.11)$$

$$T_a < T_L = 8 \text{ (second)}$$

The derived seismic response coefficient also needs to be within the limitations calculated from the following equations:

$$C_s (\text{limit 1}) = \frac{S_{D1}}{T (R/I)} = \frac{0.787}{0.175 \cdot 6} = 0.75 > C_s \quad (3.12)$$

$$C_s (\text{limit 2}) = 0.01 < C_s \quad (3.13)$$

$$C_s (\text{limit 3}) = \frac{0.5 \cdot S_{S1}}{(R/I)} = \frac{0.5 \cdot 0.787}{6} = 0.066 < C_s \quad (3.14)$$

$$C_u = 1.4 \quad (3.15)$$

It is clear that the derived seismic response coefficient 0.224 passed the limitation checks.

For the building weight calculation, it was assumed that the tributary floor dead load was 100 psf for both floor levels. Tributary live load for the roof level is 100 psf (roof garden) and 50 psf for the typical floor level (typical office building) based on the ASCE-7-05, Table 4-1. From the calculations shown below, the total weight of the model building shown in Fig. 3.67 is 6,480 kips and the seismic base shear is 1,451.5 kips. It will be shown below that the test specimen is adequate for these loads. Table 3.5 lists the vertical distribution of seismic forces in both X and Y direction.

$$W_1 = 100 \text{ psf} \times 180 \text{ ft} \times 180 \text{ ft} = 3240 \text{ kip}$$

$$W_2 = 100 \text{ psf} \times 180 \text{ ft} \times 180 \text{ ft} = 3240 \text{ kip} \quad (3.16)$$

$$W = W_1 + W_2 = 6480 \text{ kip}$$

$$V = C_s \cdot W = 0.224 W = 1451.5 \text{ kip}$$

**Table 3.5 Vertical distribution of seismic forces**

Floor Level	W <sub>x</sub> (kip)	h <sub>i</sub> (ft)	h <sub>x</sub> (ft)	W <sub>x</sub> h <sub>x</sub> <sup>k</sup> (k=1)	C <sub>vx</sub>	F <sub>x</sub> (kip)
<b>2F</b>	3,240	9	9	29,160	1/3	483.8
<b>Roof</b>	3,240	9	18	58,320	2/3	967.7
<b>Σ</b>	6,480	-	-	87,480	1.0	1,451.5

The seismic masses for each floor level for dynamic analysis are calculated using the following equations:

$$m_1 = \frac{3240 \text{ kip}}{386 \frac{\text{in}}{\text{sec}^2}} = 8.39 \frac{\text{kip} - \text{sec}^2}{\text{in}}$$

$$m_2 = \frac{3240 \text{ kip}}{386 \frac{\text{in}}{\text{sec}^2}} = 8.39 \frac{\text{kip} - \text{sec}^2}{\text{in}}$$
(3.17)

For the load combination, four basic combinations were used according to ASCE-7-05:

- ①.  $1.4 D$
- ②.  $1.2 D + 1.6 L$
- ③.  $1.2 D \pm 1.0E + L$ ; where  $E = E_h + E_v$
- ④.  $0.9D \pm 1.0E$ ; where  $E = E_h - E_v$

where  $E_h = \rho Q_E = 1.3 Q_E$ ;  $E_v = 0.2 S_{DS} D = 0.2686 D$ . If this is plugged into the original combinations, the load combinations then become:

- ①.  $1.4 D$
- ②.  $1.2 D + 1.6 L$
- ③.  $1.4686 D + 1.3 Q_E + L$
- ④.  $0.6314 D + 1.3 Q_E$
- ⑤.  $0.9314 D - 1.3 Q_E + L$
- ⑥.  $1.1686 D - 1.3 Q_E$

The load combinations (amplified) used to check column design are listed below:

$$(1.2 + 0.2 S_{DS})D \pm \Omega_o E + L$$

$$(0.9 - 0.2 S_{DS})D \pm \Omega_o E$$

Applying  $S_{DS}$  and  $\Omega_o$  values to the equations, we obtain:

- ①.  $1.4686 D + 2.0 Q_E + L$
- ②.  $0.6314 D + 2.0 Q_E$
- ③.  $0.9314 D - 2.0 Q_E + L$
- ④.  $1.1686 D - 2.0 Q_E$

The integrated structural analysis and design software, SAP2000 (Computers and Structures, 2009) was used in static analysis to check the stress state of the members and the deformation under the load combinations given above. Final member sizes in the exterior frame (Frame A) and interior frame (Frame B) in Y direction are identified in Fig. 3.71. The members are the same size as used for the test specimen. Note that square HSS braces were used in this

analytical model. Under the given load combinations, the maximum member stress ratio occurred in the square HSS brace in the first story and was equal to 0.935. The maximum column stress ratio was 0.590 in the W12 × 96 column in the same braced bay as shown in Fig. 3.72. The stress ratio in the W12 × 96 columns were also checked using the amplified load combinations to make sure they essentially remained elastic. The maximum stress ratio under these amplified load combinations was 0.864. The amplified story drift at first story (1.54%) and second story (1.25%) were less than the 2% code limit.

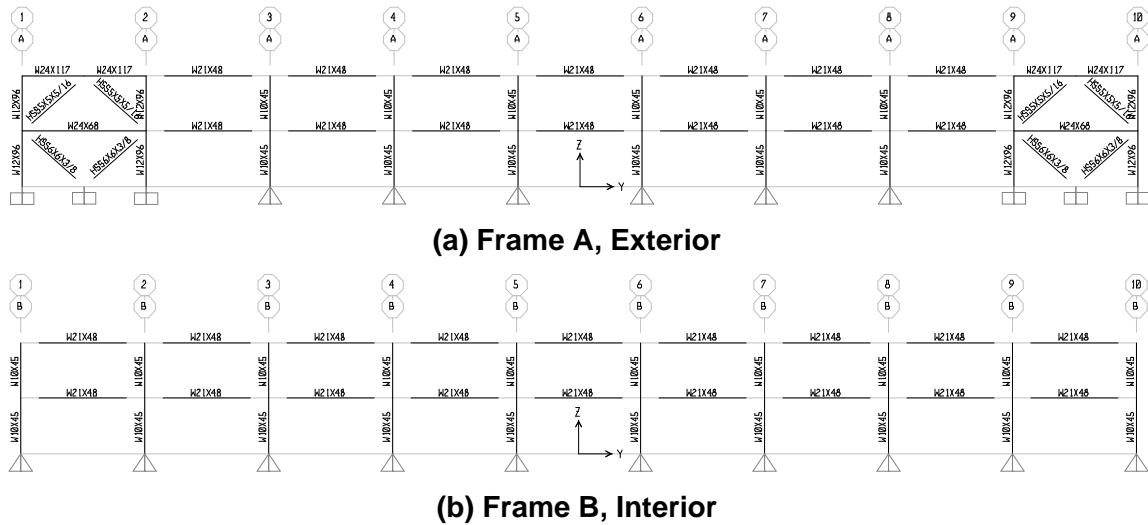


Figure 3.71 Typical member sizes distribution in Y direction

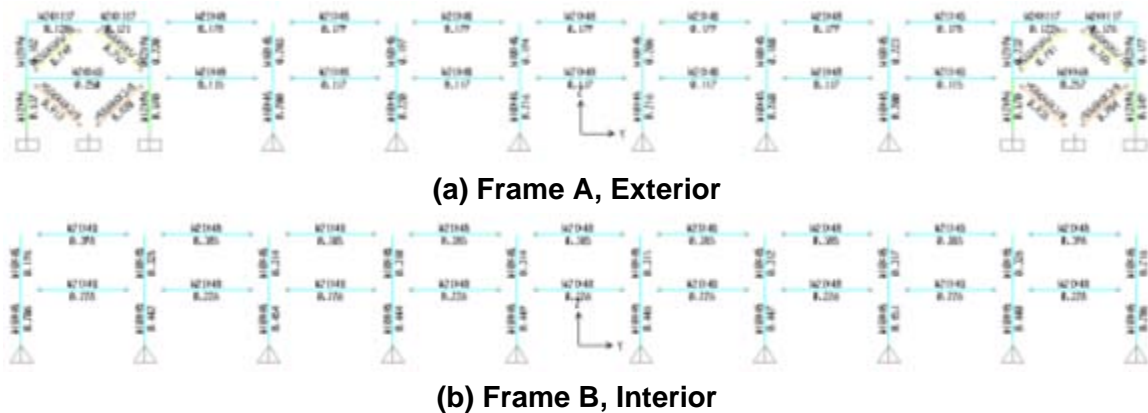
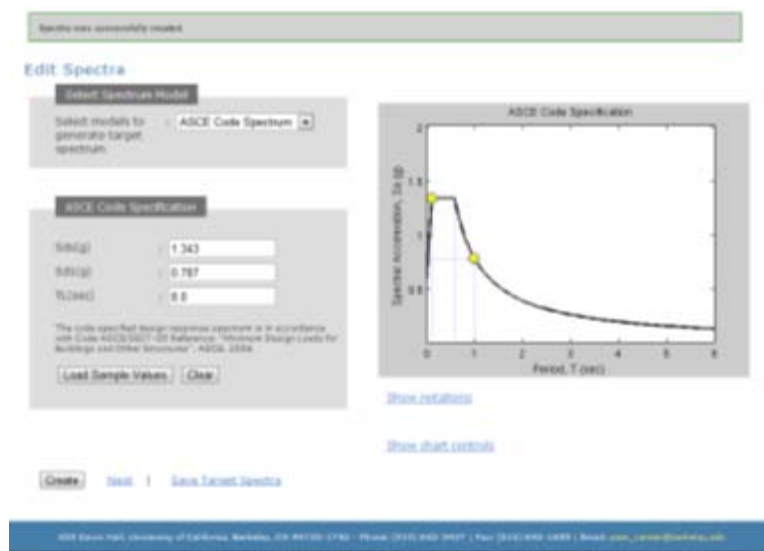


Figure 3.72 Member stress ratios distribution in Y direction

The computer model built in SAP2000 directly represents both TCBF-B-1 and TCBF-B-4 specimens because diagonal braces were the same sizes and the same section shapes (square HSS). For TCBF-B-2 and TCBF-B-3 specimens, only brace section shapes and bracing member sizes changed while the beam and column sizes remained the same. The selections of bracing member size for these two specimens were performed in a customized excel calculation

spreadsheet. All required weld sizes and bolt sizes for connections in three specimens were calculated in the same excel spreadsheet. Detail calculations are listed in Appendix H.

For the hybrid simulation, input ground motion record is required to conduct the experiments. The ground motion selecting and scaling tool in the PEER Ground Motion Database was used ([http://peer.berkeley.edu/peer\\_ground\\_motion\\_database/](http://peer.berkeley.edu/peer_ground_motion_database/)). To do this, values of  $S_{ds}$ ,  $S_{d1}$  and  $T_L$  were input to get the target spectrum as shown in Fig. 3.73. Then, type in the search criteria shown in Fig. 3.74 were used to find the representative ground motions from the database.



**Figure 3.73 Target spectrum screenshot from the online ground motion selection tool on PEER web site**



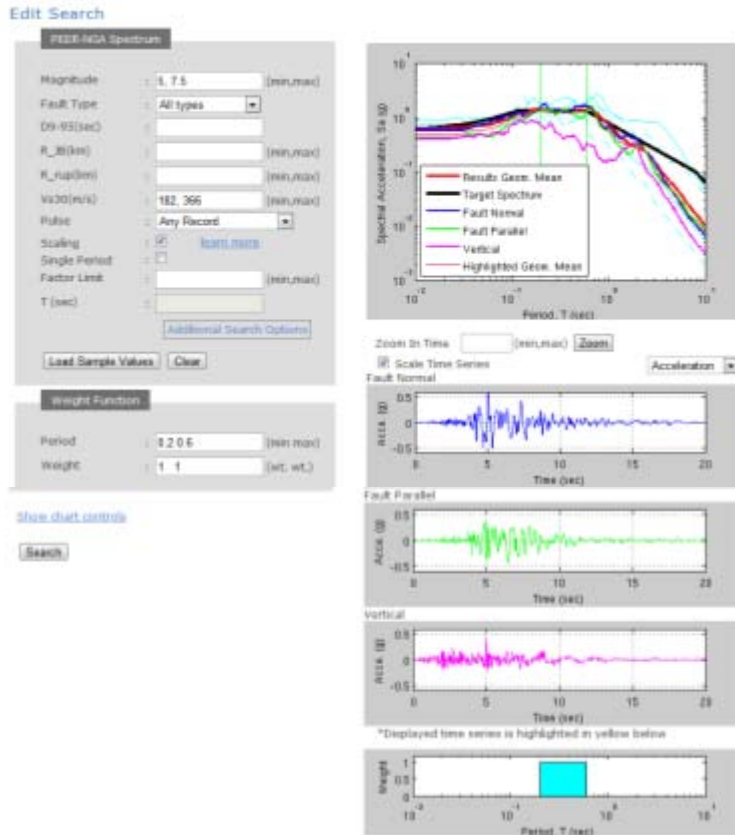


Figure 3.74 Screenshot of ground motion search interface

Results

\*Click on the record below to display Spectra and Time series  Plot Selected

Result#	Comp.	NSAF	MSF	ScaleF	Pulse	Tp(s)	DR- R(%)	Event	Year	Station	Mag	Mechanism	EQC
<input type="checkbox"/> 24	GM	1602	0.0052	0.9762	0.1	0.91	8.3	Duzce, Turkey	1999	Bolu	7.14	Strike-Slip	12.0
<input type="checkbox"/> 9	GM	558	0.0034	1.2346	0.0	—	7.0	Chalfant Valley-02	1985	Brothers Ranch	6.19	Strike-Slip	6.4
<input checked="" type="checkbox"/> 17	GM	960	0.0043	1.2545	0.0	—	6.1	Northridge-01	1994	Country - West Cam	6.89	Reverse	13.4
<input checked="" type="checkbox"/> 26	GM	182	0.0054	2.0173	1.1	4.2	4.8	Imperial Valley-06	1979	El Centro Arroyo #7	6.53	Strike-Slip	0.8
<input checked="" type="checkbox"/> 8	GM	814	0.0033	2.3531	0.0	—	4.1	Whittier Narrows-01	1987	Dorway - Birchdale	5.99	Reverse-Oblique	14.9
<input type="checkbox"/> 3	GM	1736	0.0025	2.6564	0.0	—	2.7	Northridge-06	1994	Sanitar - Converter Sta	5.28	Reverse	[6.5]
<input type="checkbox"/> 12	GM	328	0.0037	4.7887	0.0	—	15.3	Coalinga-01	1983	Parkfield - Cholame SWA	6.38	Reverse	43.8
<input type="checkbox"/> 30	GM	710	0.0055	6.0961	0.0	—	9.7	Whittier Narrows-02	1987	Inglewood - Union Oil	5.27	Reverse-Oblique	[23.0]
<input type="checkbox"/> 16	GM	3272	0.0042	8.2715	0.0	—	45.8	Chi-Chi Taiwan-06	1999	CHY033	6.20	Reverse	72.9
<input type="checkbox"/> 19	GM	1782	0.0049	8.5936	0.0	—	15.9	Hector Mine	1909	Forest Falls Post Office	7.13	Strike-Slip	74.9

Figure 3.75 Snap shot of ground motion search results

The search results are shown in Fig. 3.75. Note that the records are ordered from smaller scale factors to larger scale factors. The scale factor of the ground motion was limited to be below 3.0. Finally, the NGA #960 (Northridge-01, 1994) ground motion record was selected as

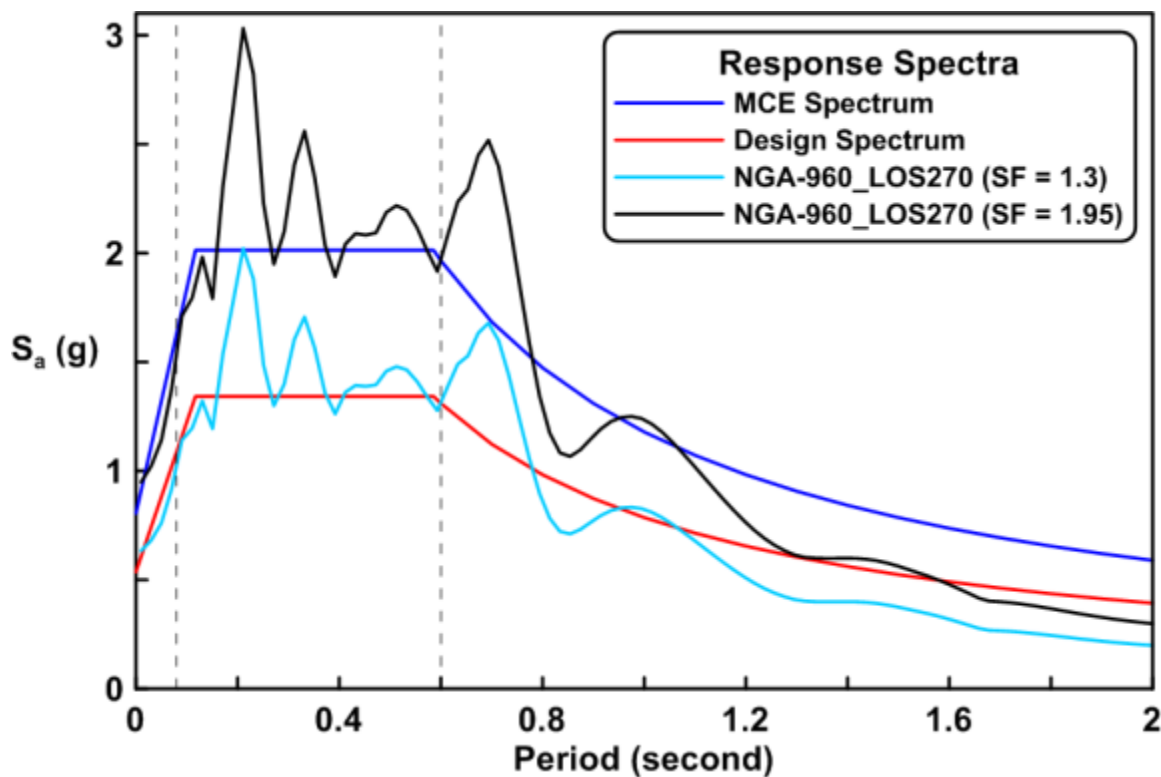
the input ground motion in hybrid simulation. Note that the  $V_{s30}$  value of the site where the ground motion was recorded also falls into the  $V_{s30}$  range listed in ASCE-7 for the site condition D. The scale factor for the selected ground motion to match the target spectrum is 1.3. Detail site information of the selected ground motion is listed in Table 3.6. The response spectrum of scaled ground motions are shown in Fig. 3.76 to compare with the design spectrum and the MCE spectrum. The original ground motion record and the scaled ground motions are plotted in Fig. 3.77 for reference.

Fig. 3.78 illustrates the hybrid modeling concept used on the TCBF-B-4 specimen. Only one-fourth of entire structure was modeled during the hybrid simulation.

**Table 3.6 The site information of selected ground motion**

Earthquake Record Name	NGA #	PGA (g)	Magnitude	$D_R$ (km)	Mechanism	$V_{s30}$ (m/s)	$\Delta t$ (sec)	Duration (sec)	Scale Factor
Northridge-01, 1994	960	0.396	6.69	12.4	Reverse	308.6	0.01	19.99	1.3

(Note that the PGA is from original unscaled ground motion)



**Figure 3.76 The elastic response spectrum of scaled ground motions mapping on design spectrum and MCE spectrum**

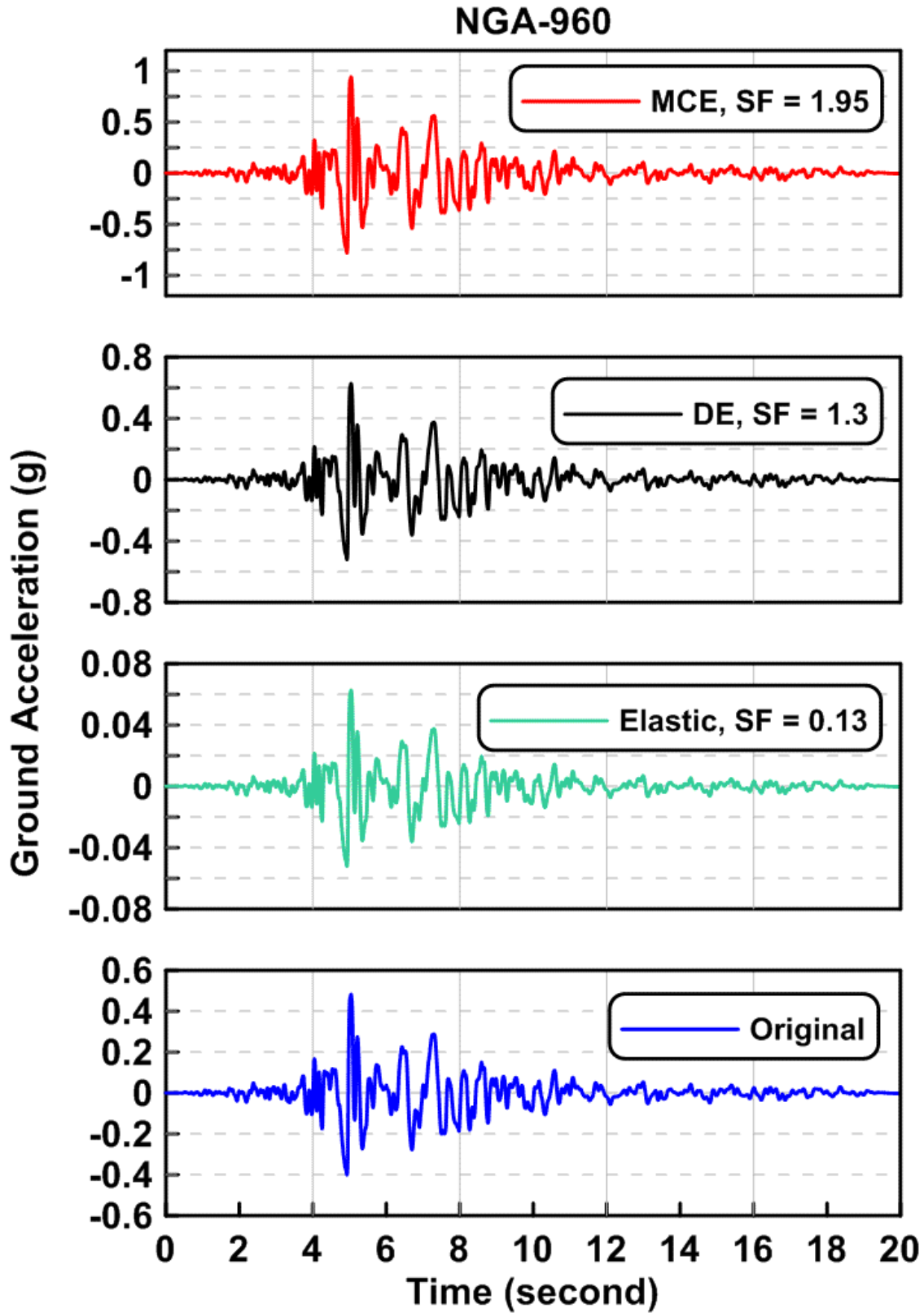


Figure 3.77 Original ground motion record and the scaled ground motions (NGA-960)

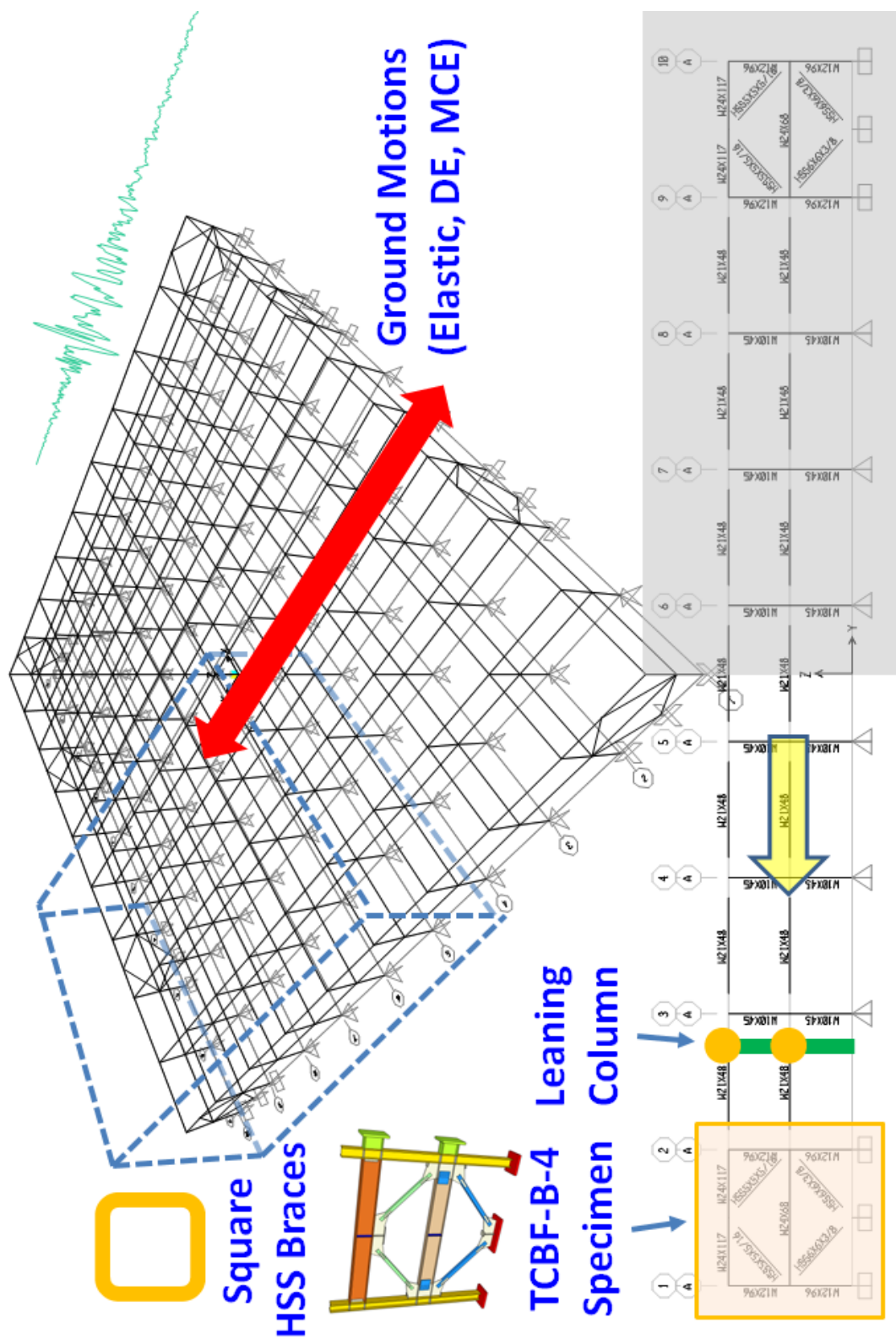


Figure 3.78 The hybrid modeling concept of TCBF-B-4 specimen

## 3.10 EXPERIMENTAL CONTROLS

### 3.10.1 Quasi-Static Tests

The displacement controlled actuator (roof level) was programmed to move with a constant velocity of 0.01 inch per second through the entire test. The  $\Delta t$  in the input binary file for MTS Structural Test System (STS) controller software was set equal to 1/64 second. The sampling rate for the proportional–integral–derivative (PID) control loop in the STS controller was set to 1024 Hz. The persistence value was set to be equal to 0.0078 second. The lower level actuator was force controlled, and set to impose one half the load cell force feedback of the roof level actuator through settings for the “master-slave matrix” in the STS controller software. Actuator displacement and force interlocks were also specified in the software to prevent any damages to the actuators and the test setup in the event of larger than anticipated responses. Real-time XY plots showing selected instrument channel readings were displayed on four Panasonic plasma display screens in the control room through the Real-time Data Viewer (RDV) software provided by NEES (Daugherty et al., 2011).

### 3.10.2 Hybrid Simulation

The Open-Source Framework for Experimental Setup and Control, OpenFresco (Schellenberg et al., 2009), was used for hybrid control and OpenSees was used for structural analysis during the hybrid simulation. Figure 3.79 illustrates experimental control concepts and the corresponding abstract components of the OpenFresco software architecture. Detailed OpenFresco software architecture discussions can be found in the report by Schellenberg et al. (2009).

One Simulink model (HybridControllerD3D3\_Vconst\_rec100Hz.mdl) and two tcl files (server.tcl and client.tcl) were prepared for the hybrid simulation. The Simulink model was built and uploaded to xPC target and the model utilized displacements for prediction and correction. Integration time step was set to 0.005 second in the Simulink model.

In the server.tcl file, the xPCtarget experimental control was specified through OpenFresco expControl command. No transformation was defined in this hybrid test. Actor experimental site was defined in this tcl file.

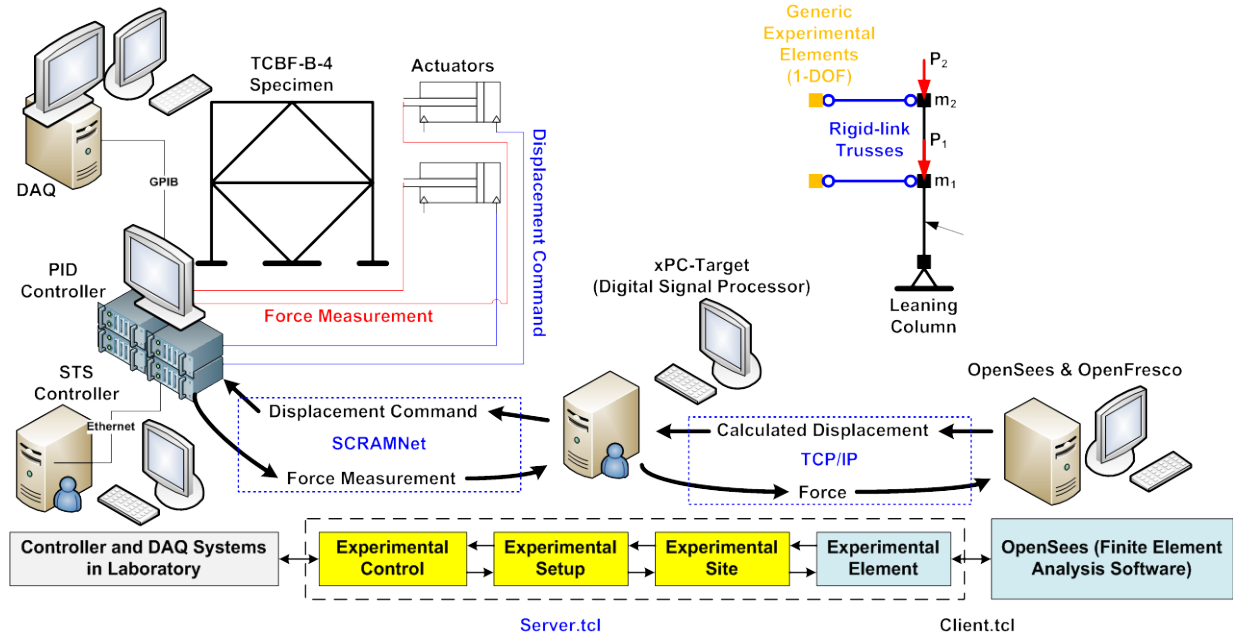


**Figure 3.79 Experimental Control of Hybrid Simulation**

As mentioned before, only one-fourth of entire prototype building was modeled during the hybrid test. A two-story physical specimen was built in the laboratory and a substructure was defined in OpenSees tcl file. In this client.tcl file, two generic experimental elements (1-DOF), two rigid-link trusses and a leaning column were defined (Fig. 3.79). P-delta effects were considered through introducing a leaning column in the OpenSees model. The section properties of the leaning column were derived from the gravity columns using the following equations.

$$A_{leaning\ column} = \sum_i A_{gravity\ columns} \quad (3.18)$$

$$I_{leaning\ column} = \sum_j I_{gravity\ columns} \quad (3.19)$$

Lump floor mass and concentrated point loads from gravity forces were assigned at the nodes of leaning column at each floor level as illustrated in Figures 3.78 and 3.79. Pinned boundary condition was assigned at the base of leaning column in OpenSees model. Rayleigh damping parameters were set be equal to 0.01 for mode one and 0.02 for mode two in the OpenSees model. Newmark method for hybrid simulation with fixed number of iteration was used. The  $\gamma$  factor and  $\beta$  factor in the Newmark integrator object were set to 0.5 and 0.25 (average acceleration method), respectively. The number of iterations was set to 10. And the analysis time step was set to 0.01 second. Shadow experimental site was defined in the client.tcl file.

Both actuators were displacement controlled and the actuator speed (displacement rate) was selected as 0.002 inch per second during the hybrid simulation. Similar to the settings used in the quasi-static tests, the sampling rate for the PID control loop in STS controller was set to

1024 Hz. The persistence value was set to be equal to 0.0078 second, the same as previous specimens. Actuator displacement and force interlocks were also specified in the STS software to prevent any possible damage to the actuators and the test set up. Real-time XY plots, selected instrument channel readings and specimen overview were displayed on four Panasonic plasma display screens in the control room. The RDV software was not used in the hybrid test.

## 4 Experimental Results of Four Specimens

### 4.1 MATERIAL PROPERTIES

All wide flange beams, wide flange columns and wide flange braces in the specimens were ASTM A992 steel sections. All braces using hollow structural sections (HSS) were ASTM A500 Grade B steel tubes for both square and round sections. The 3/4 inch thick gusset plates, 2 inch thick base plates, 2 inch stub beam end plates, 1/2 inch shear tabs, 5/8 inch finger plates, 5/8 inch continuity plates, 3/8 inch washer plates for all-thread anchor rods and brace reinforcing cover plates were made of ASTM A572 Grade 50 steel plates. The beam web stiffener plates, lifting lugs, shim plates and miscellaneous parts were made of ASTM A36 steel plates. High strength structural fasteners that satisfy the ASTM A490 standard were used at beam-column connections and one-piece gusset plate-to-beam splices. All-thread high strength anchor bolts (ASTM A193 Grade B7) were used at column base plates and a gusset-to-floor-beam base plate.

Steel tensile test coupons were sampled during the shop fabrication process as shown from Figs. 4.1 to 4.4. The material tensile test results extracted from the mill certificates are summarized in Table 4.1. The original mill certificates from steel fabricators are reproduced in Appendix I.





**Figure 4.1 Torch cutting the steel coupon from wide flange section**



**Figure 4.2 Torch cutting the steel coupon from HSS section**



Figure 4.3 Steel coupons of TCBF-B-1 specimens



Figure 4.4 Steel coupons of TCBF-B-2, TCBF-B-3 and TCBF-B-4 specimens

**Table 4.1 Material mechanical properties from mill certificates**

<b>Description</b>	<b>Heating Number</b>	<b>Yield Strength <math>F_y</math> (psi)</b>	<b>Tensile Strength <math>F_u</math> (psi)</b>	<b>Yield to Tensile Ratio</b>	<b>Elongation (%)</b>
W24 × 117 <sup>(1, 2)</sup>	30406710	52,400	68,500	0.76	25.3
W24 × 117 <sup>(3, 4)</sup>	30424590	51,850	71,350	0.73	24.6
W24 × 68 <sup>(1)</sup>	22477490	53,100	71,750	0.74	25.6
W24 × 68 <sup>(2, 3, 4)</sup>	316424	57,000	74,000	0.77	25
W12 × 96 <sup>(1, 2)</sup>	313889	57,500	74,500	0.77	26.5
W12 × 96 <sup>(3, 4)</sup>	338703	55,500	72,500	0.77	25.5
¾" plate <sup>(1)</sup>	M8G153	58,000	71,000	0.82	26
¾" plate <sup>(2, 3, 4)</sup>	284241	65,049	78,683	0.83	18
HSS 6 × 6 × 3/8 <sup>(1)</sup>	H080304	46,397	66,986	0.69	28
HSS 5 × 5 × 5/16 <sup>(1)</sup>	F3979	56,000	68,100	0.82	37
HSS 6 × 0.5 <sup>(2)</sup>	53786048	68,100	77,600	0.88	33
HSS 5 × 0.5 <sup>(2)</sup>	T82669	65,881	72,580	0.91	33.1
W8 × 28 <sup>(3)</sup>	291731	54,000	73,000	0.74	25
W8 × 21 <sup>(3)</sup>	207071031	54,027	78,320	0.69	33
HSS 6 × 6 × 3/8 <sup>(4)</sup>	L1084	58,710	69,163	0.85	37
HSS 5 × 5 × 5/16 <sup>(4)</sup>	23021M08	61,970	72,264	0.86	35
½" splice plate <sup>(3, 4)</sup>	B7J635	59,000	76,000	0.78	36
2" base plate <sup>(3, 4)</sup>	0500464	58,450	84,350	0.69	17.5
5/8" plate <sup>(3, 4)</sup>	M13742	56,500	70,500	0.80	24.5
7/8" plate <sup>(3, 4)</sup>	1W380	67,000	95,000	0.71	23
1-1/8-7 × 9" rod	225082	133,000	146,000	0.91	22

Description	Heating Number	Yield Strength $F_y$ (psi)	Tensile Strength $F_u$ (psi)	Yield to Tensile Ratio	Elongation (%)
3/8" washer plate	254334	56,700	76,600	0.74	32
7/8-9 × 3" bolt	NU844781	-	161,508	-	-
7/8-9 × 2-1/2" bolt	NU844781	-	164,351	-	-
7/8-9 × 2-3/4" bolt	IN391612	-	165,138	-	-

(Note: the numbers in the small bracket indicate the specimen number, for example, 1 indicates the TCBF-B-1 specimen, etc.)

## 4.2 QUASI-STATIC TEST RESULTS OF FIRST THREE SPECIMENS

For first three experiments, more than two hundred instrumentation points were monitored and recorded through the entire test process. Numerous photos and videos were also taken. The measured time history and hysteretic loops provided valuable data to compare the behavior of the specimens. The following subsections discuss the test results and describe the main observations for each cyclically tested specimen.

### 4.2.1 Specimen TCBF-B-1 (Square HSS Braces, Quasi-Static Test)

The test started at around 1:06 PM on Sunday, August 9, 2009. Before initiating the pre-defined loading, two complete cycles of 0.15 inch (about 25% yield roof displacement) peak roof displacement were imposed to check all instrument readings and the actuator control algorithms in the MTS Structural Test System. The side views of the entire specimen from the north-west side of the lab before and after test are shown in Fig. 4.5.



(a) Before test



(b) After test

Figure 4.5 Side view of specimen TCBF-B-1

#### 4.2.1.1 Key Response Quantities

Following paragraphs briefly describe the response quantities recorded during the experiments and the post-processed response quantities derived from the raw data. Detailed interpretations of individual response quantities are described in Chapter 5. Locations of strain gauges can be found in Appendix D.

##### 4.2.1.1.1 System Global Response

Figures 4.6 and 4.7 show two actuators displacement histories and two actuators load cell force feedback histories for TCBF-B-1 specimen. A hysteresis plot of the base shear versus controlled roof displacement is shown in Fig. 4.8. The corresponding relationships between story shear and story drift for the specimen are shown in Fig. 4.9.

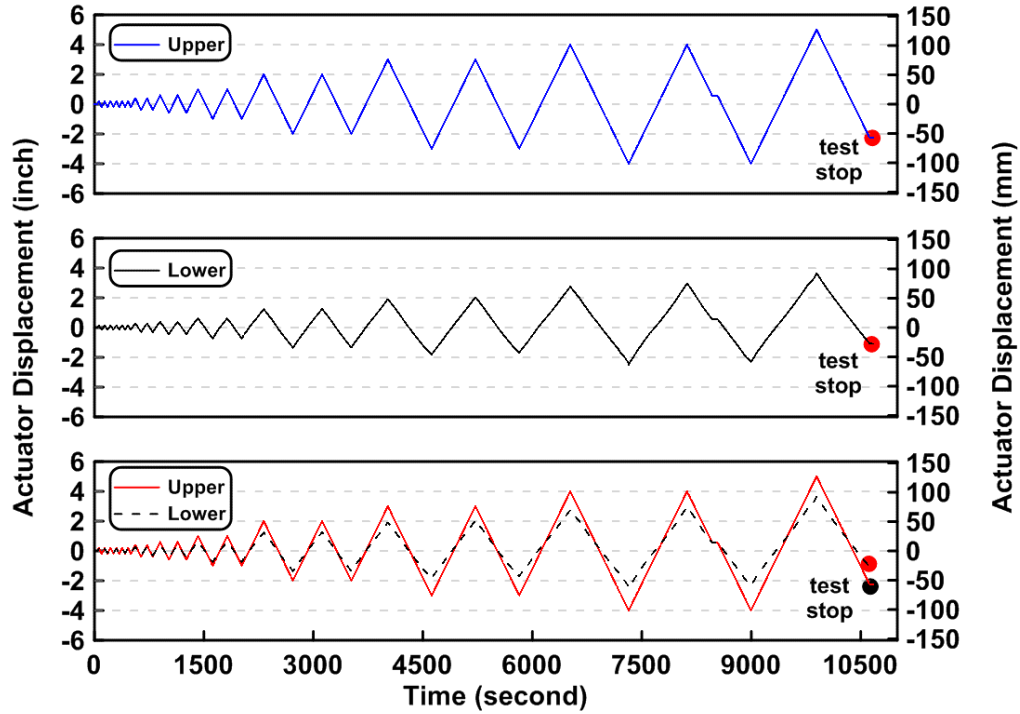


Figure 4.6 Actuator displacement histories of TCBF-B-1 specimen

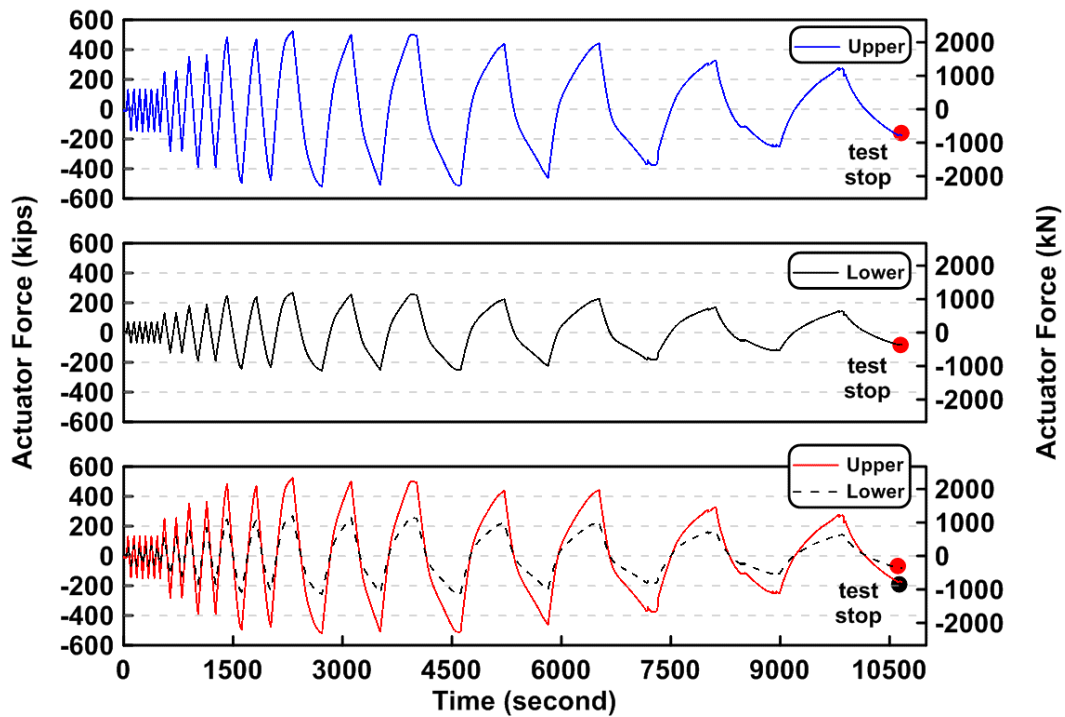


Figure 4.7 Actuator force histories of TCBF-B-1 specimen

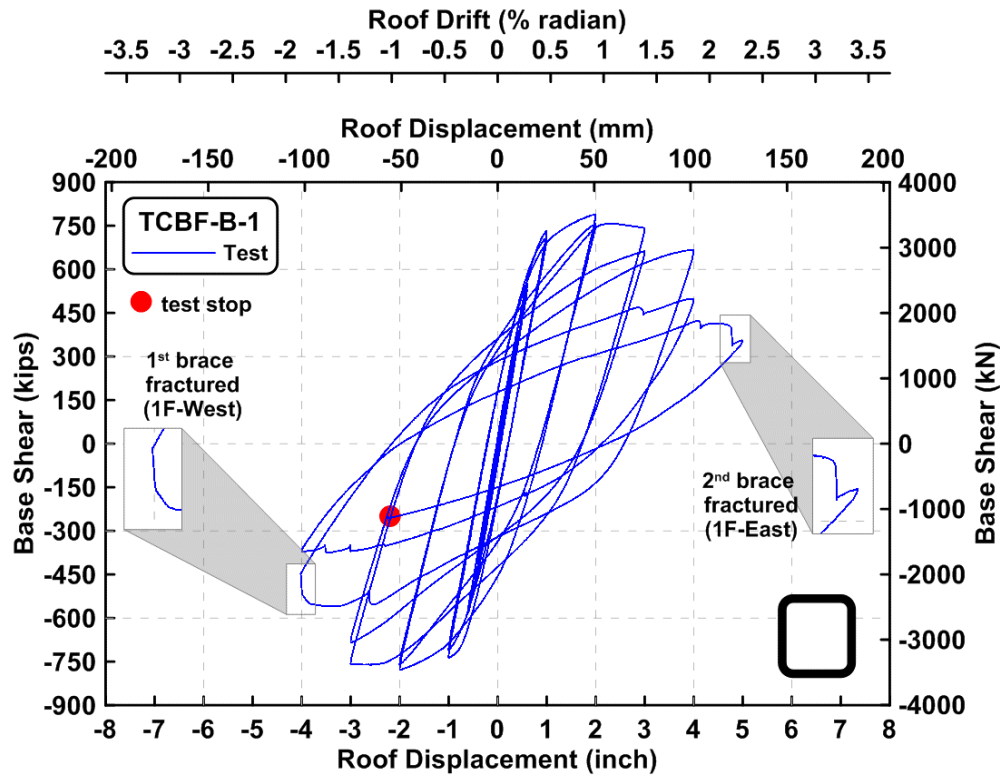


Figure 4.8 Base shear vs. roof displacement relationship of TCBF-B-1 specimen

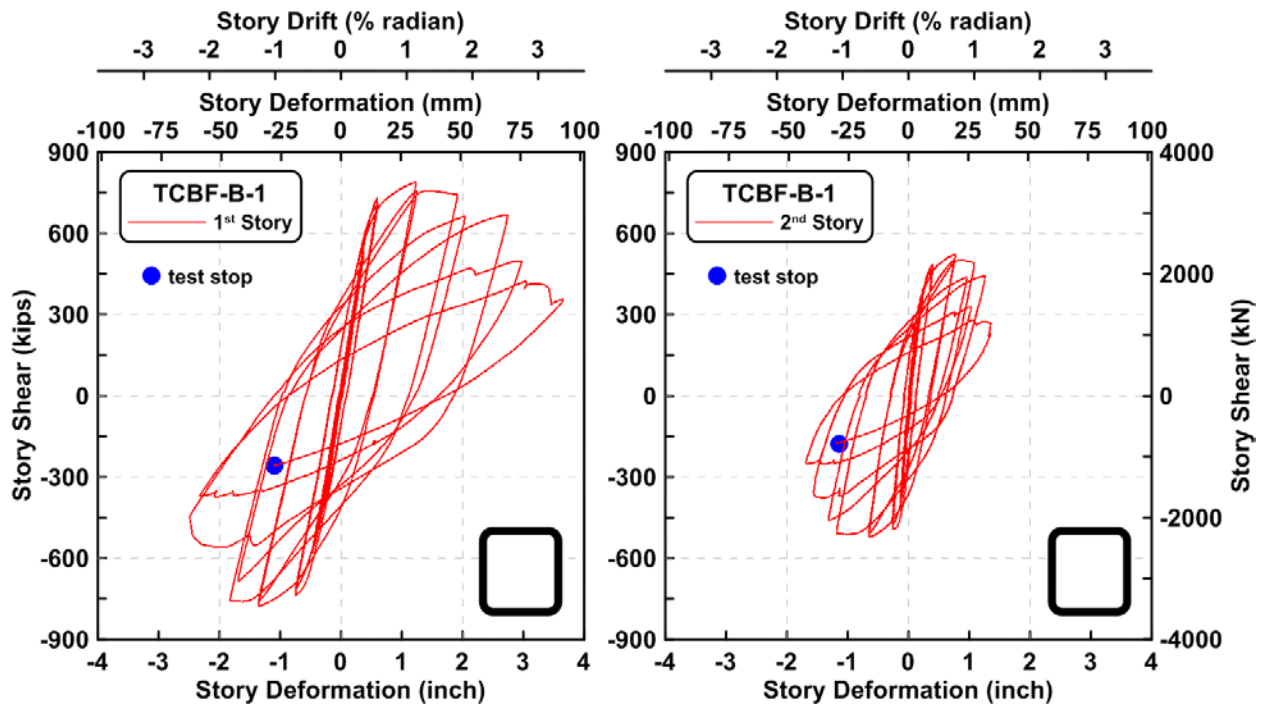


Figure 4.9 Story shear vs. story deformation relationship of TCBF-B-1 specimen

#### 4.2.1.1.2 Column Response

The time history of the axial forces in the first story W12 × 96 columns at the western and eastern sides of the specimen is plotted in Fig. 4.10. These are derived from strain gauge readings on the columns. The relationship between roof displacements and axial forces at both columns are shown in Fig. 4.11. The bending moment time history at the top and bottom ends of the column in each story are presented in Figs. 4.12 and 4.13. The moments drift with time as a result of the unequal distribution of drifts in the upper and lower stories. Derived column shear force time history in both story are plotted in the Figs. 4.14 and 4.15, respectively. Two column shear forces in each floor are added together and shown in Fig. 4.16. These are nearly identical during the first half of the test. The column web shear stress versus shear strain readings from strain rosettes are plotted in Fig. 4.17. It appears that web of the East column in the bottom story yields. The sum of the column shear force components versus the total story shear forces for each story are shown in Fig. 4.18. This slope of the graphs on these plots indicate that the braces take a much larger portion of the total base shear during early cycles with relatively small displacement amplitudes and a smaller portion during subsequent cycles where the braces have suffered various forms of damage. The derived rosette type strain gauge readings in the column web at each story are shown from Figs. 4.19 to 4.22. Normalized maximum and minimum principal stress relationships along with different yield criteria are plotted in Figs. 4.23 to 4.26. The normalized P-M and P-V interaction diagrams at column bases and column top ends are shown in Figs. 4.27 to 4.30. The P-M diagrams indicate the presence of yielding during later cycles.

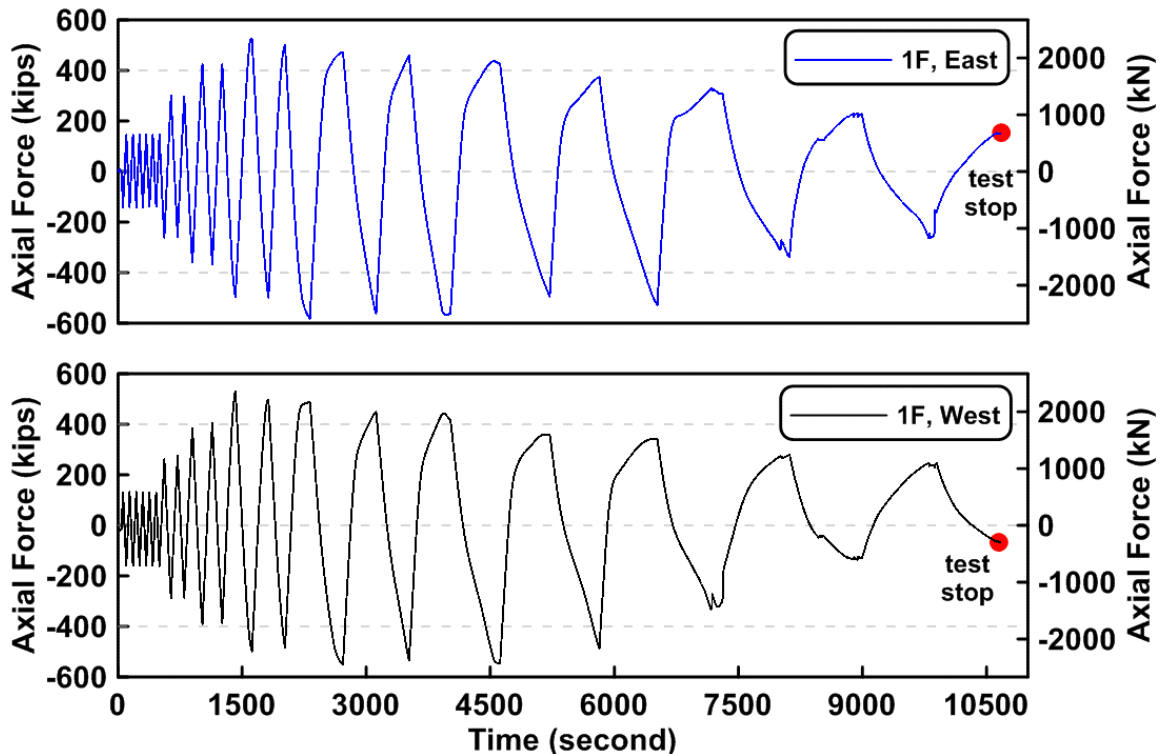


Figure 4.10 Time history of the column axial forces in the first story of TCBF-B-1 specimen (location: 3-ft above column base plate)



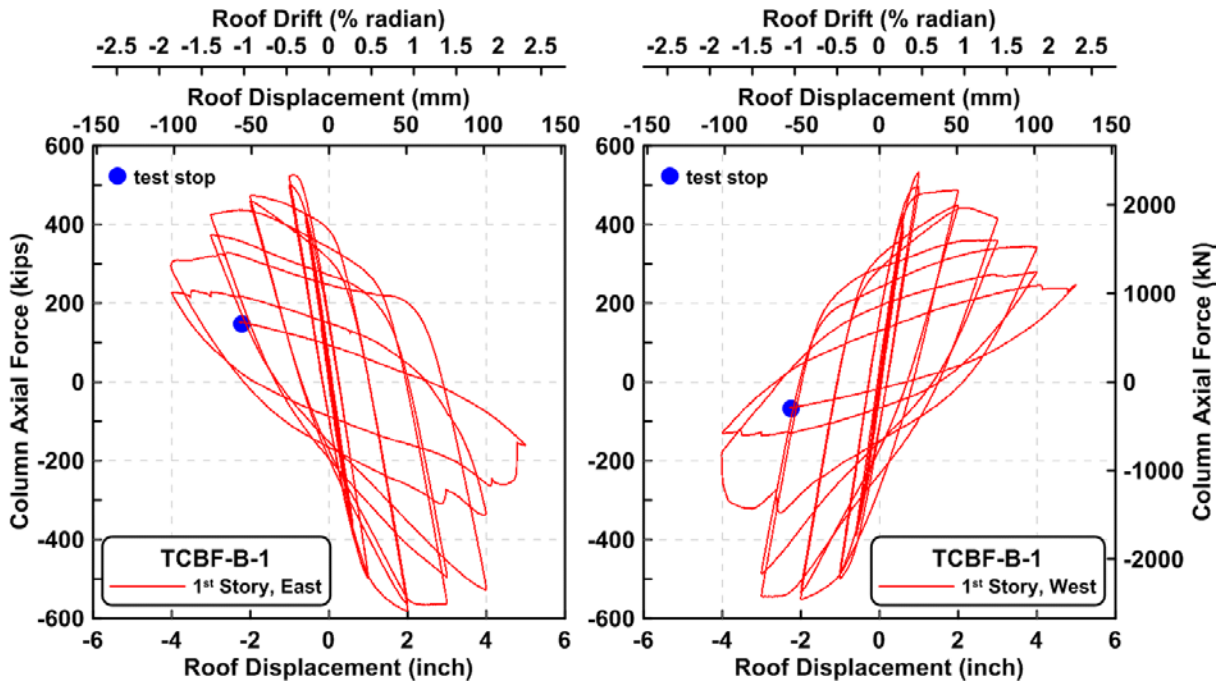


Figure 4.11 Roof displacement vs. first story column axial forces of TCBF-B-1 specimen

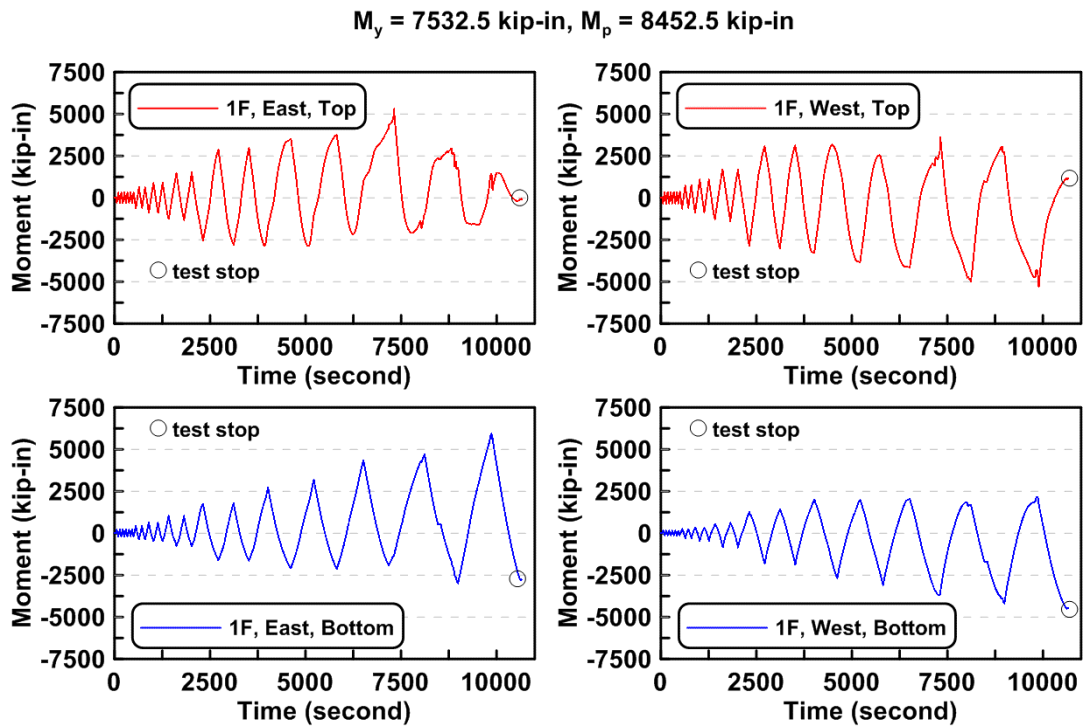


Figure 4.12 Time history of the first story column bending moments of TCBF-B-1 specimen (3-ft above column base plate and 3-ft below lower beam centerline)

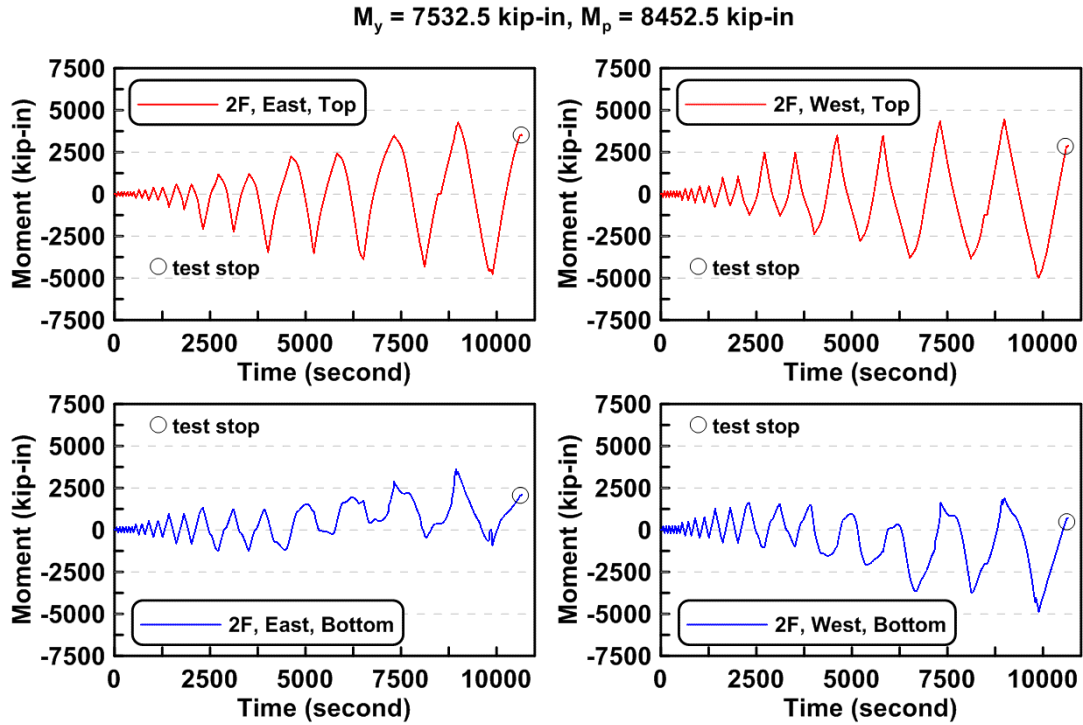


Figure 4.13 Time history of the second story column bending moments of TCBF-B-1 specimen (3-ft above lower beam centerline and 3-ft below roof beam centerline)

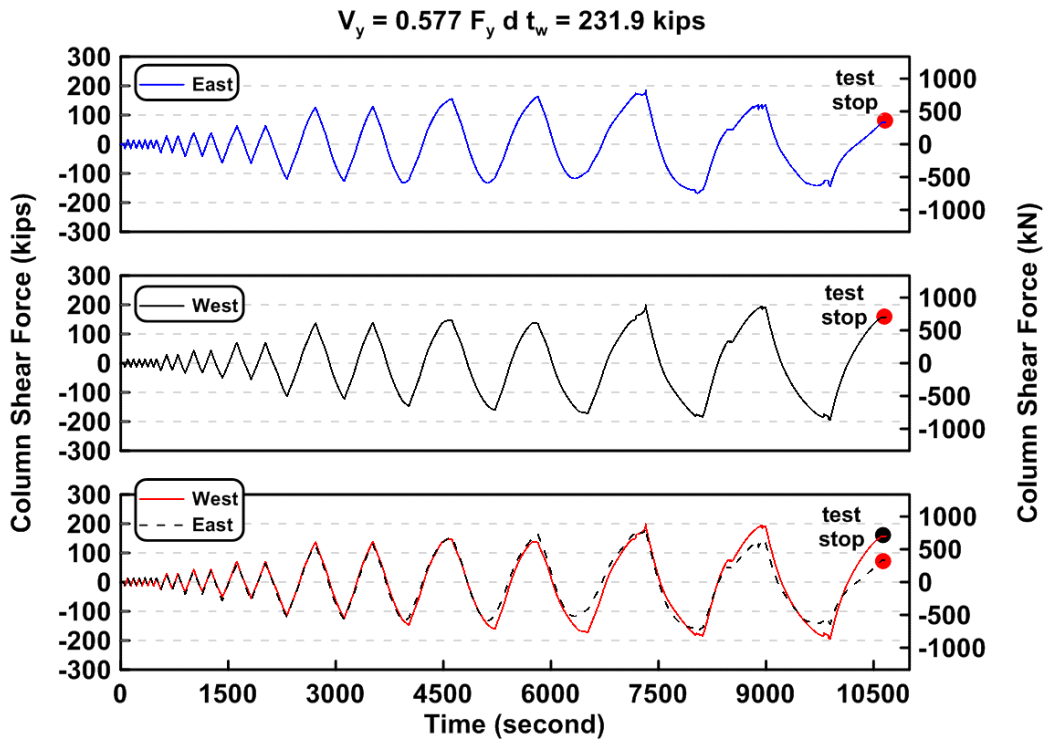


Figure 4.14 Time history of the first story column shear forces of TCBF-B-1 specimen

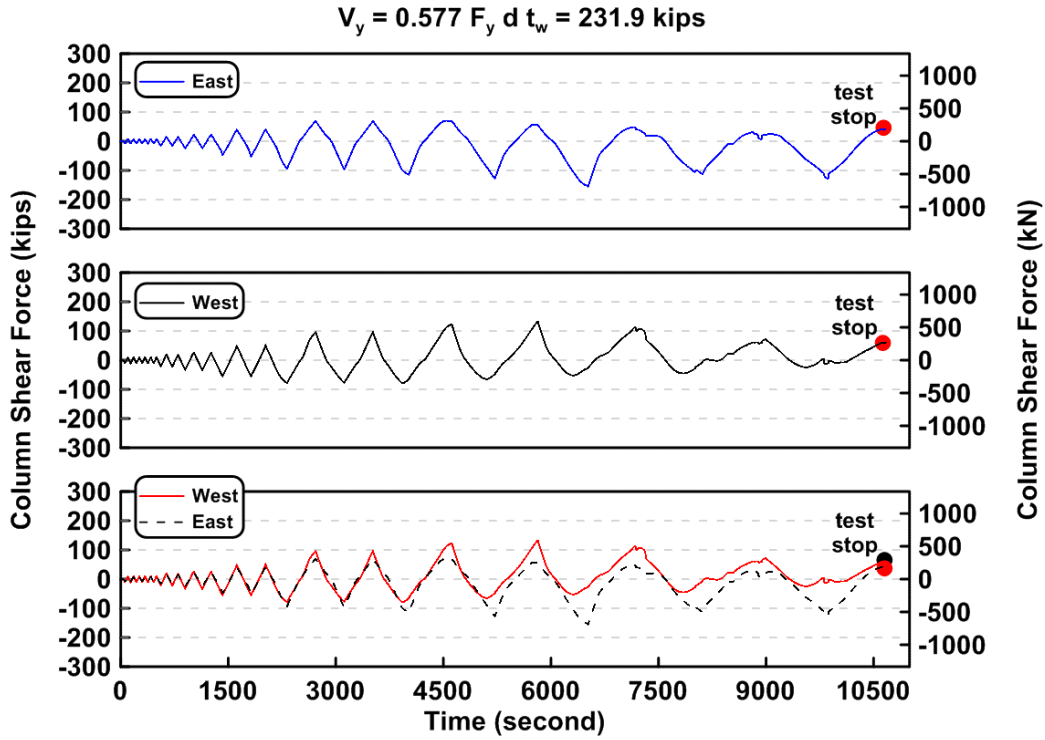


Figure 4.15 Time history of the second story column shear forces of TCBF-B-1 specimen

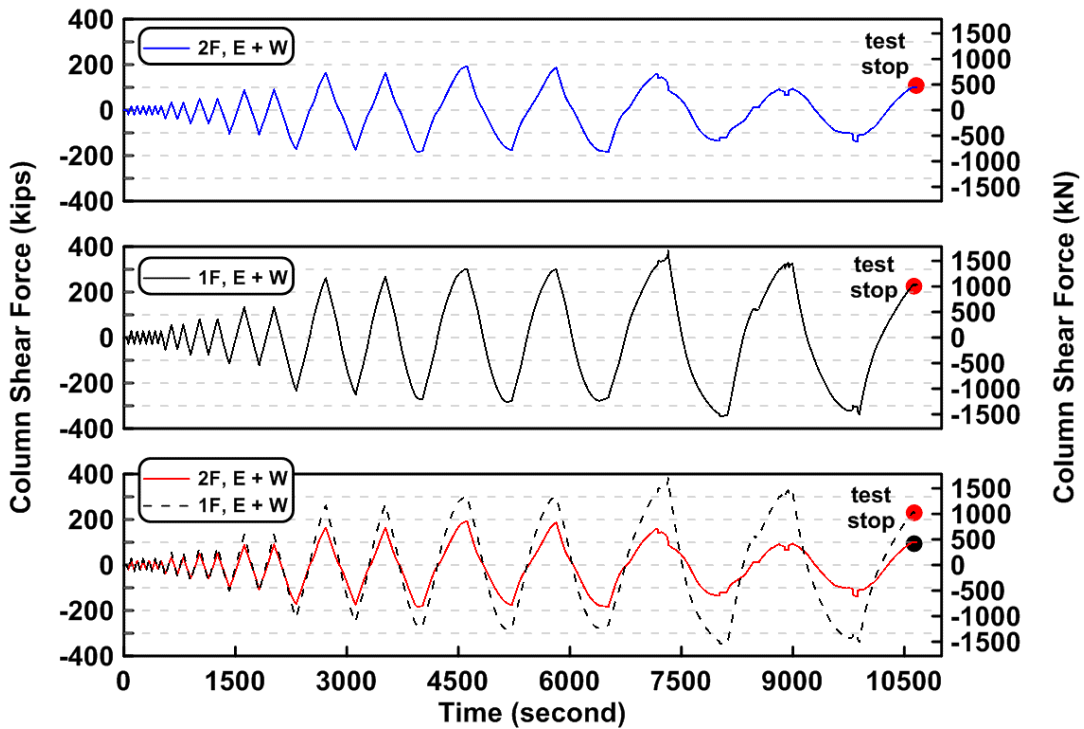


Figure 4.16 Time history of the sum of east and west column shear forces in both stories of TCBF-B-1 specimen

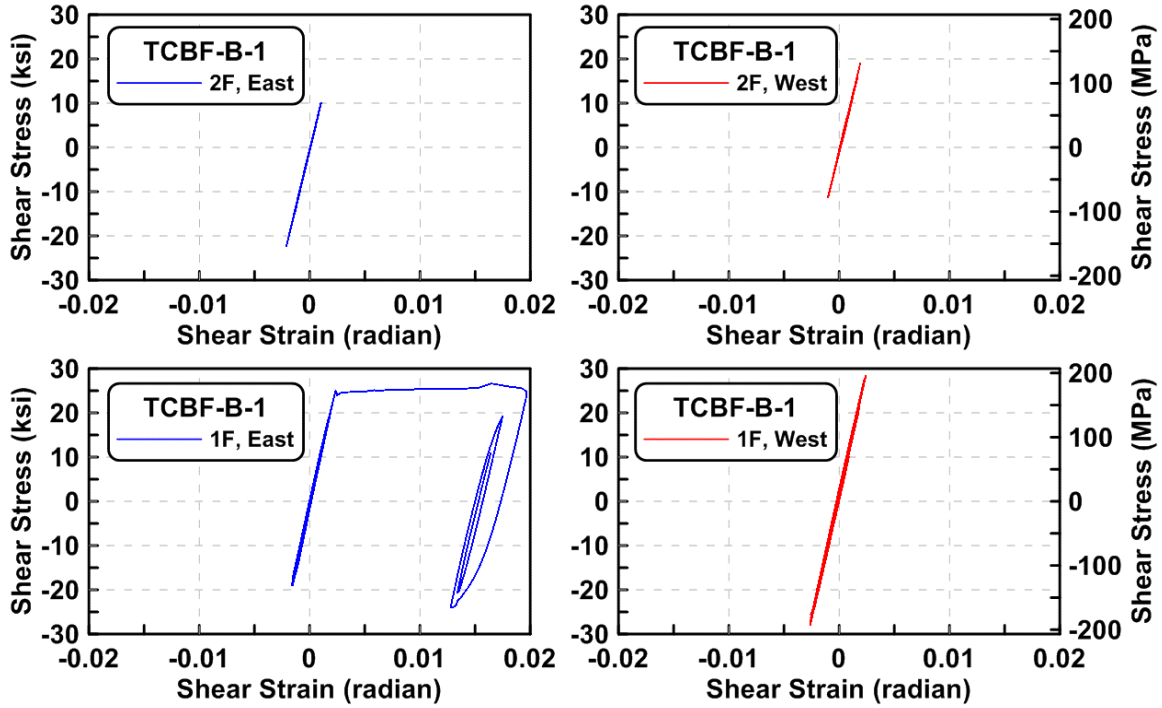


Figure 4.17 Column shear stress vs. shear strain relationships of TCBF-B-1 specimen (locations: EC1-B-N, EC2-B-N, WC1-B-N and WC2-B-N)

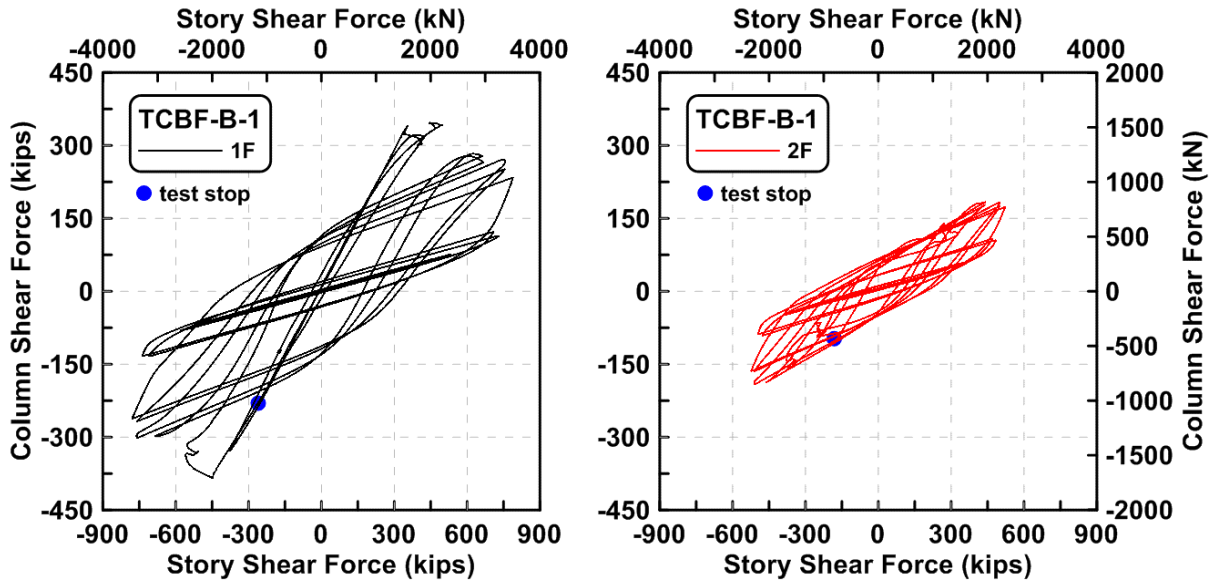


Figure 4.18 Story shear component from columns vs. total story shear forces of TCBF-B-1 specimen

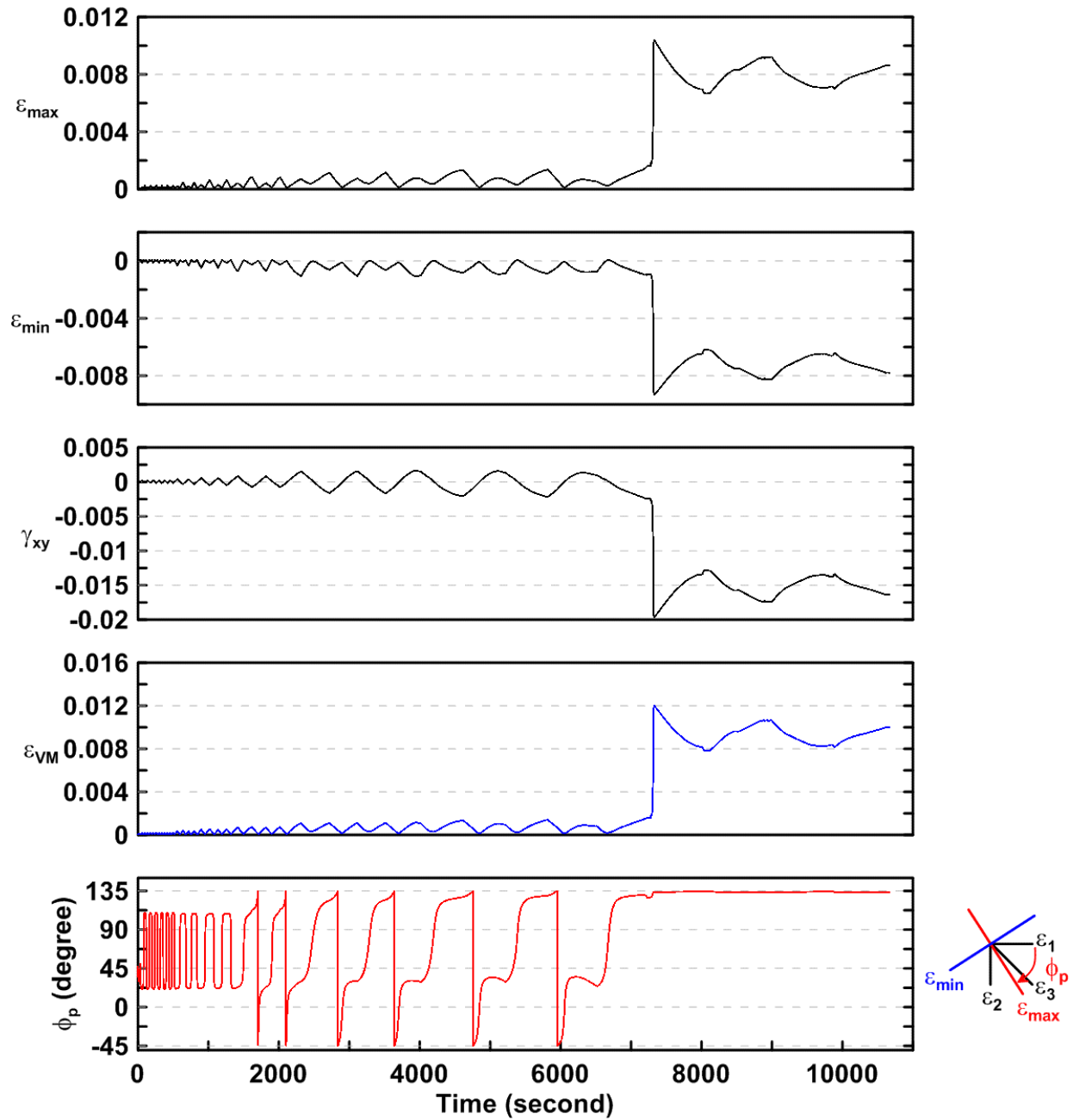


Figure 4.19 Time history of rosette type strain gauge readings in the first story column web of TCBF-B-1 specimen (location: R1, EC1-B-N)

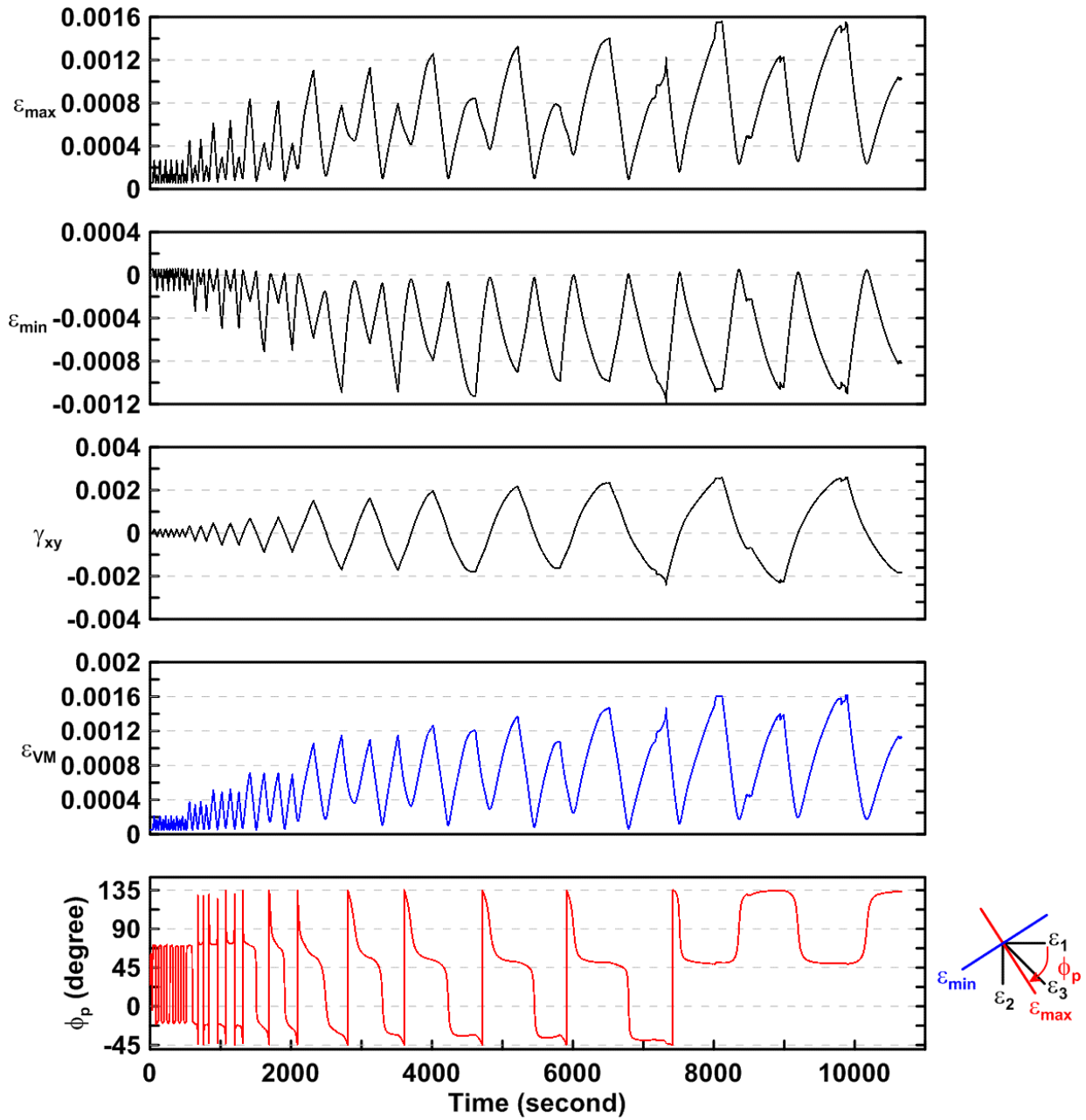


Figure 4.20 Time history of rosette type strain gauge readings in the first story column web of TCBF-B-1 specimen (location: R5, WC1-B-N)

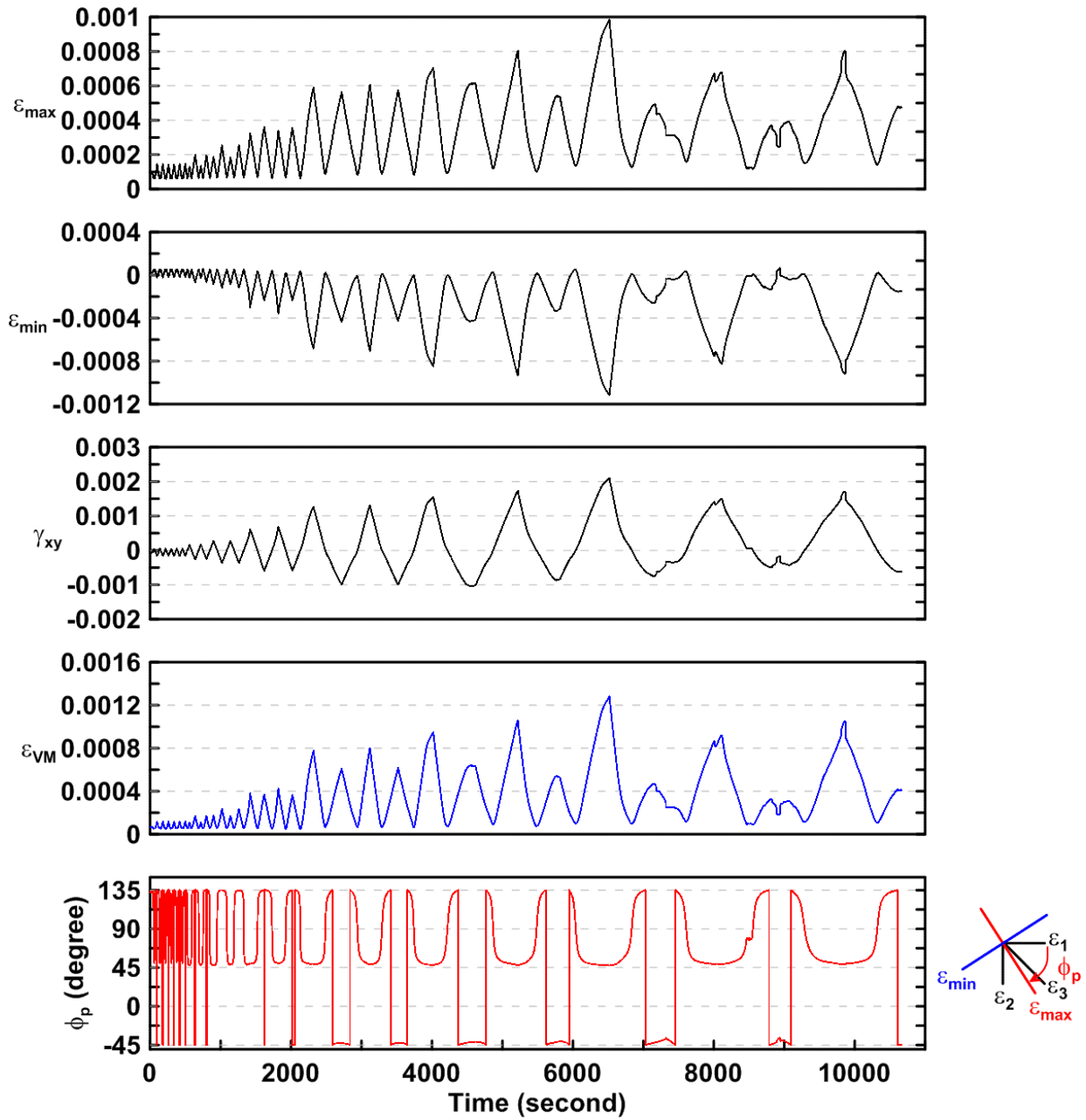


Figure 4.21 Time history of rosette type strain gauge readings in the second story column web of TCBF-B-1 specimen (location: R3, EC2-B-N)

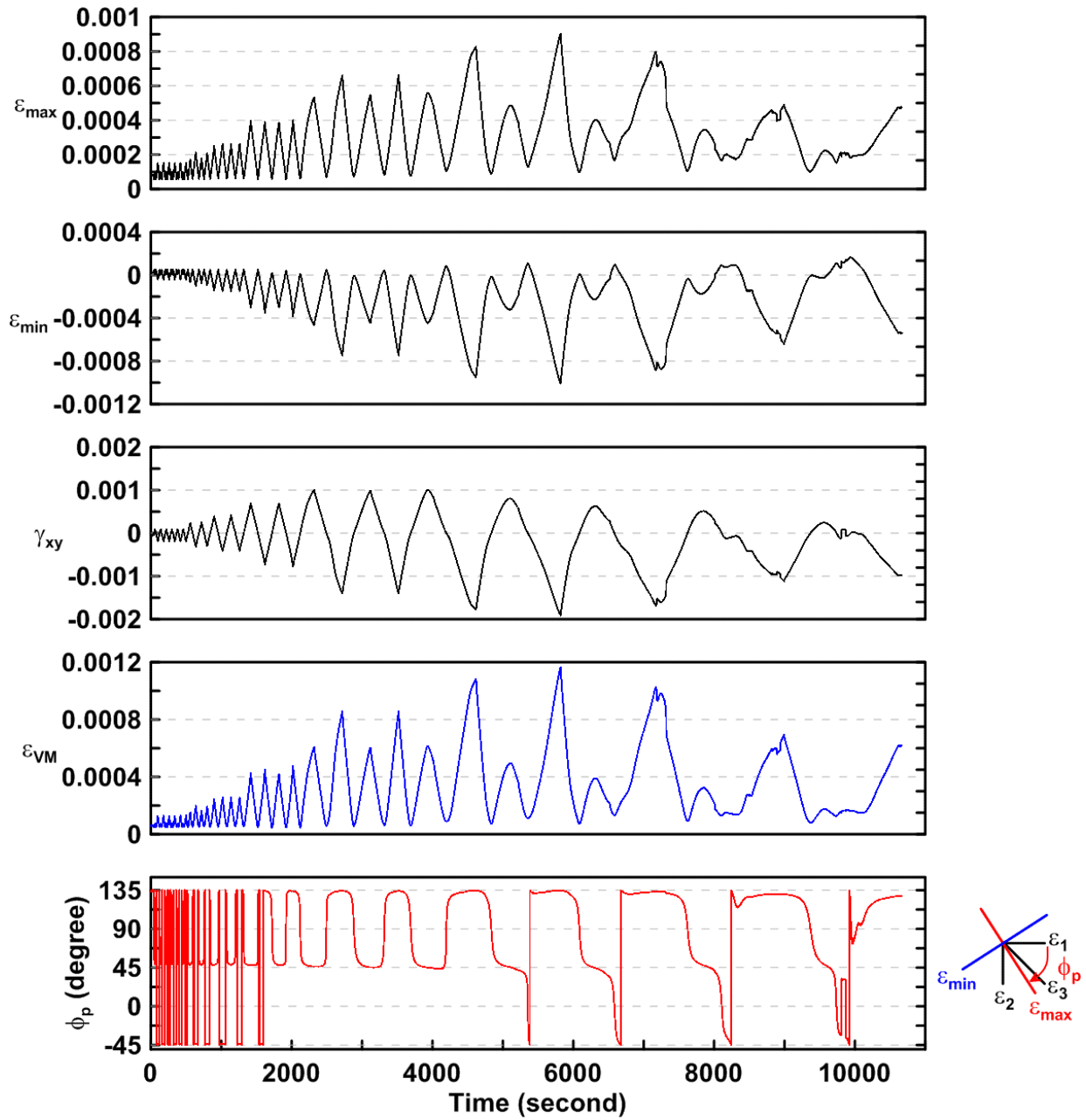


Figure 4.22 Time history of rosette type strain gauge readings in the second story column web of TCBF-B-1 specimen (location: R7, WC2-B-N)



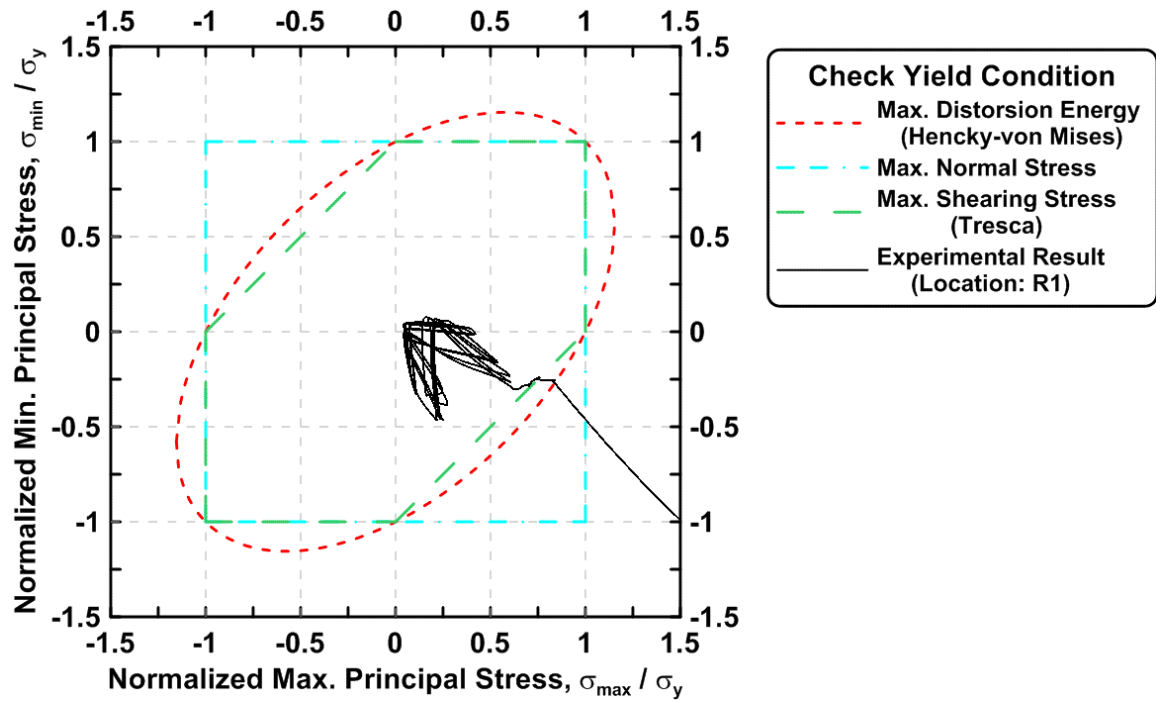


Figure 4.23 Normalized maximum principal stress vs. normalized minimum principal stress in the first story column of TCBF-B-1 specimen (location: R1)

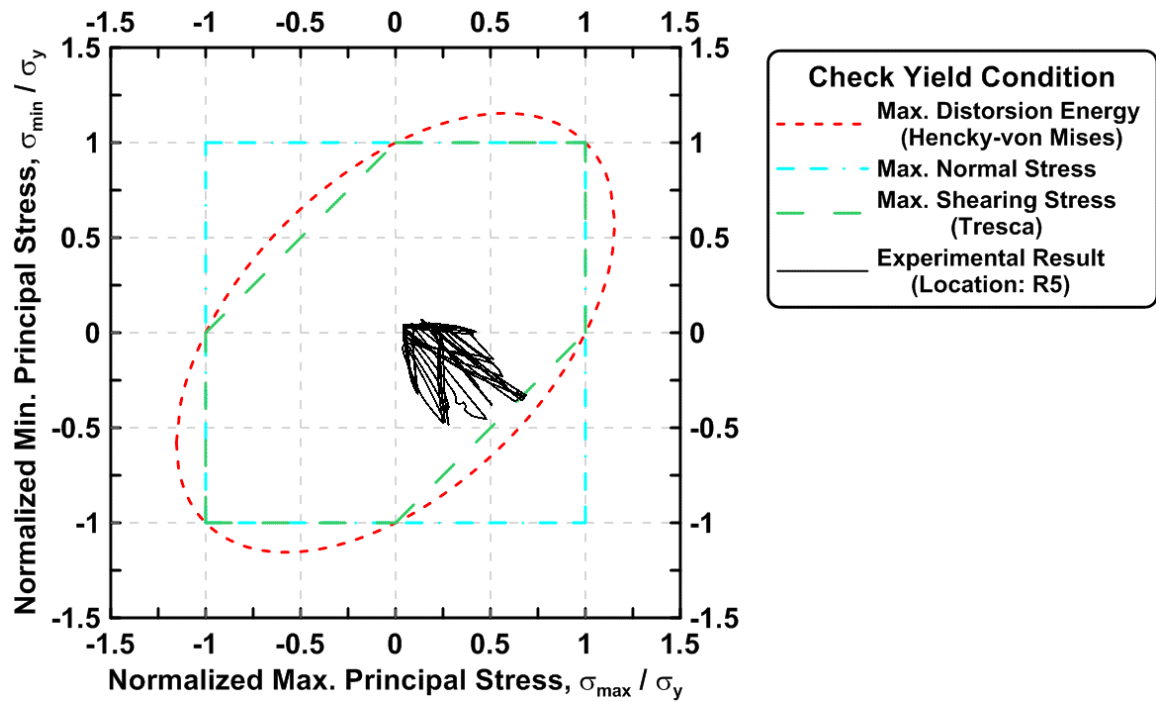


Figure 4.24 Normalized maximum principal stress vs. normalized minimum principal stress in the first story column of TCBF-B-1 specimen (location: R5)

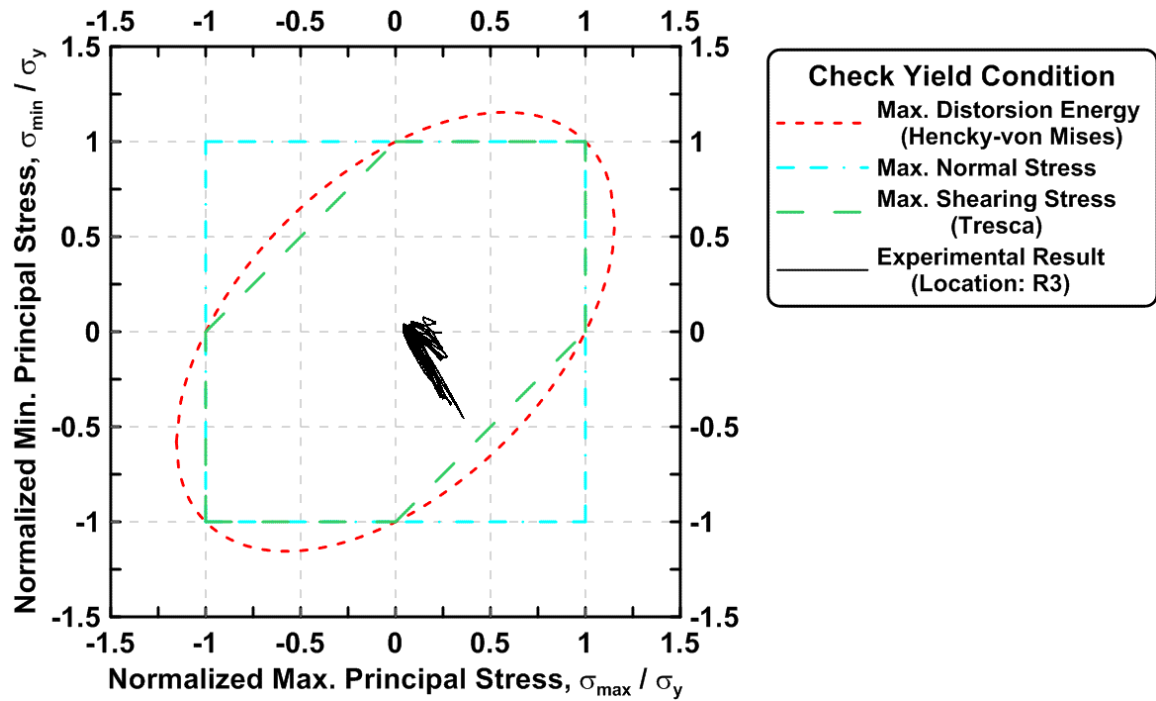


Figure 4.25 Normalized maximum principal stress vs. normalized minimum principal stress in the second story column of TCBF-B-1 specimen (location: R3)

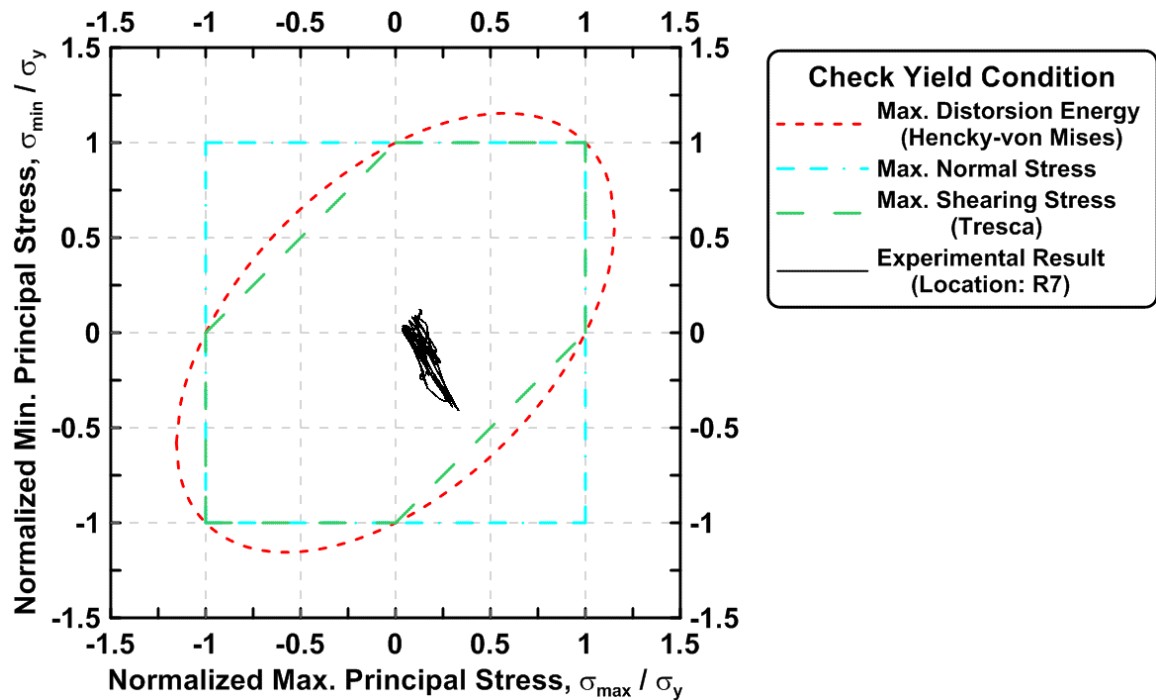


Figure 4.26 Normalized maximum principal stress vs. normalized minimum principal stress in the second story column of TCBF-B-1 specimen (location: R7)

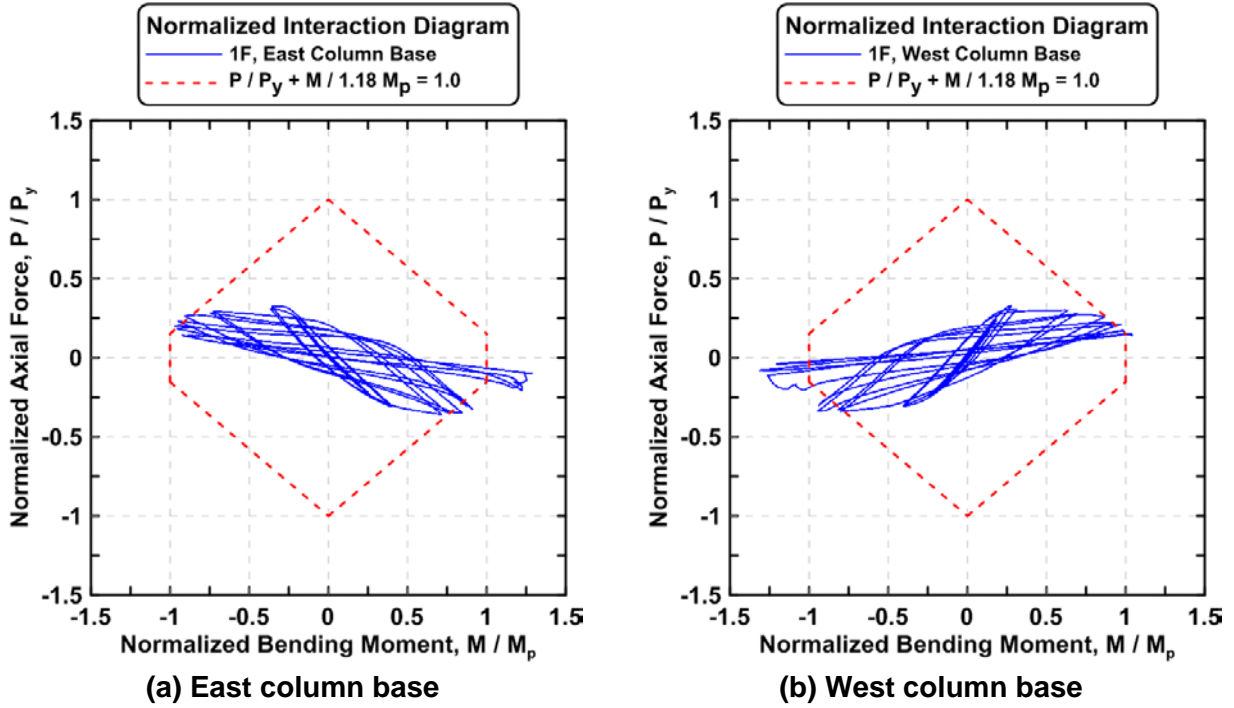


Figure 4.27 Normalized P-M interaction diagrams of the first story columns of TCBF-B-1 specimen

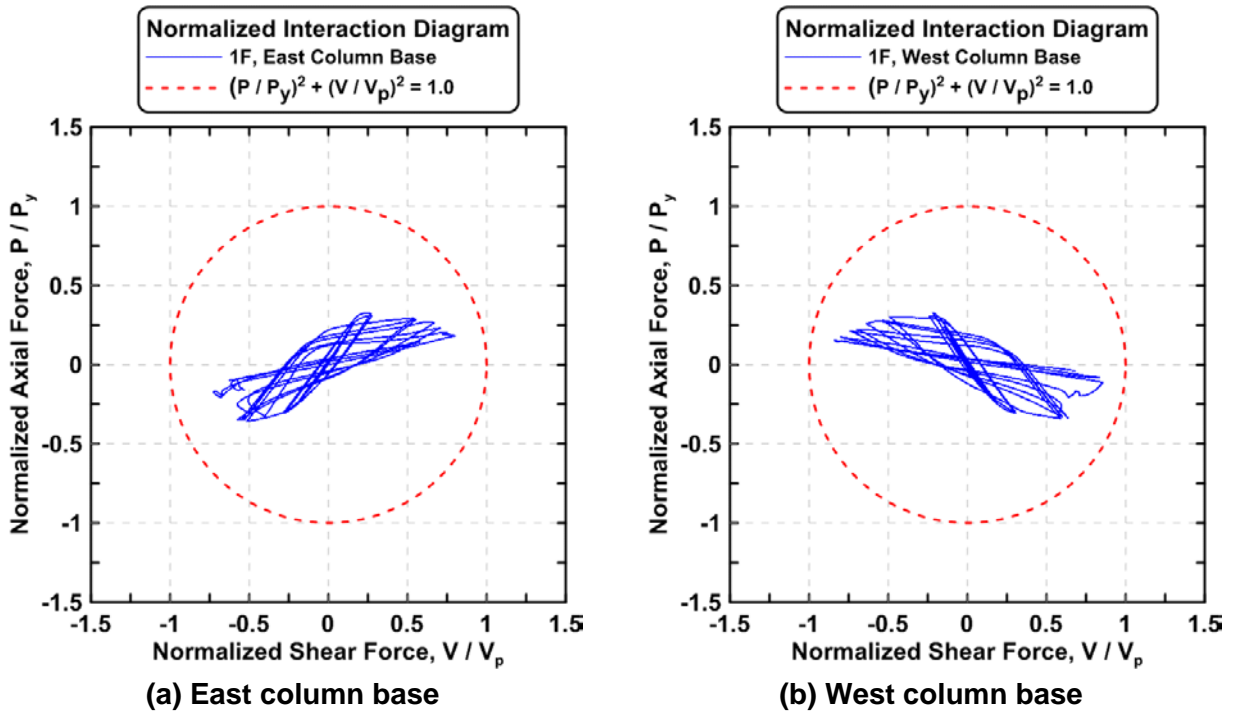


Figure 4.28 Normalized P-V interaction diagrams of the first story columns of TCBF-B-1 specimen

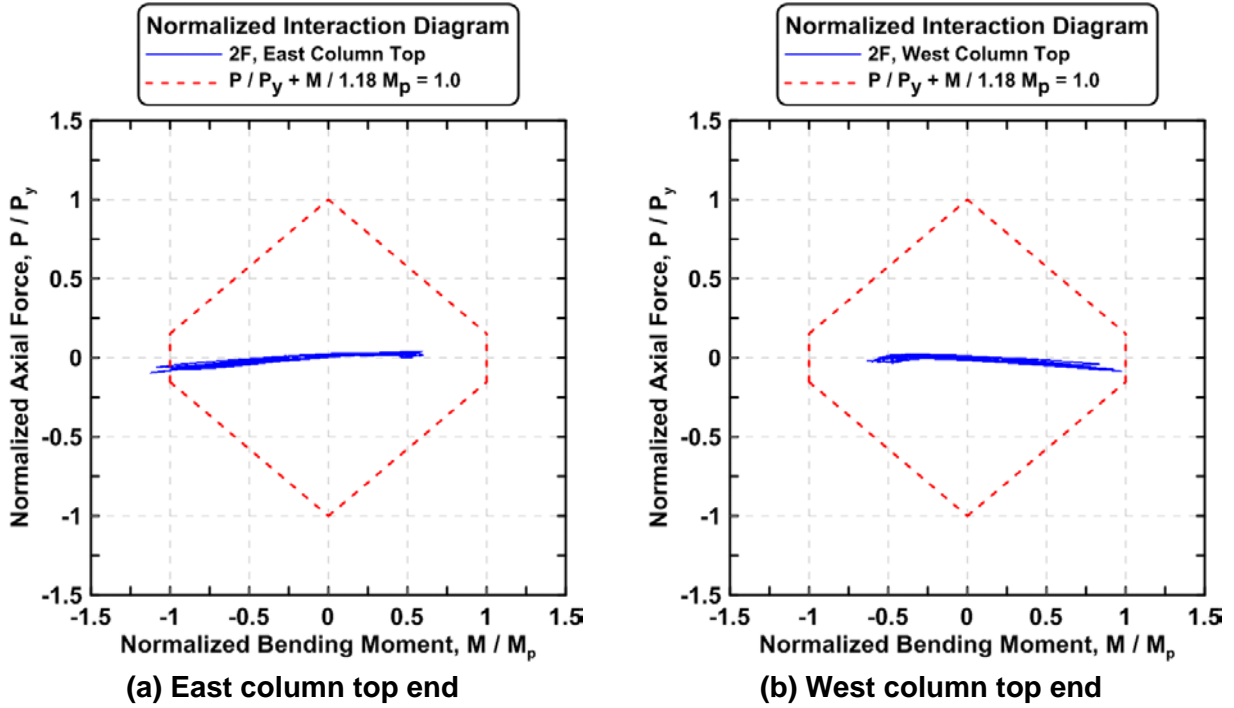


Figure 4.29 Normalized P-M interaction diagrams of the second story columns of TCBF-B-1 specimen

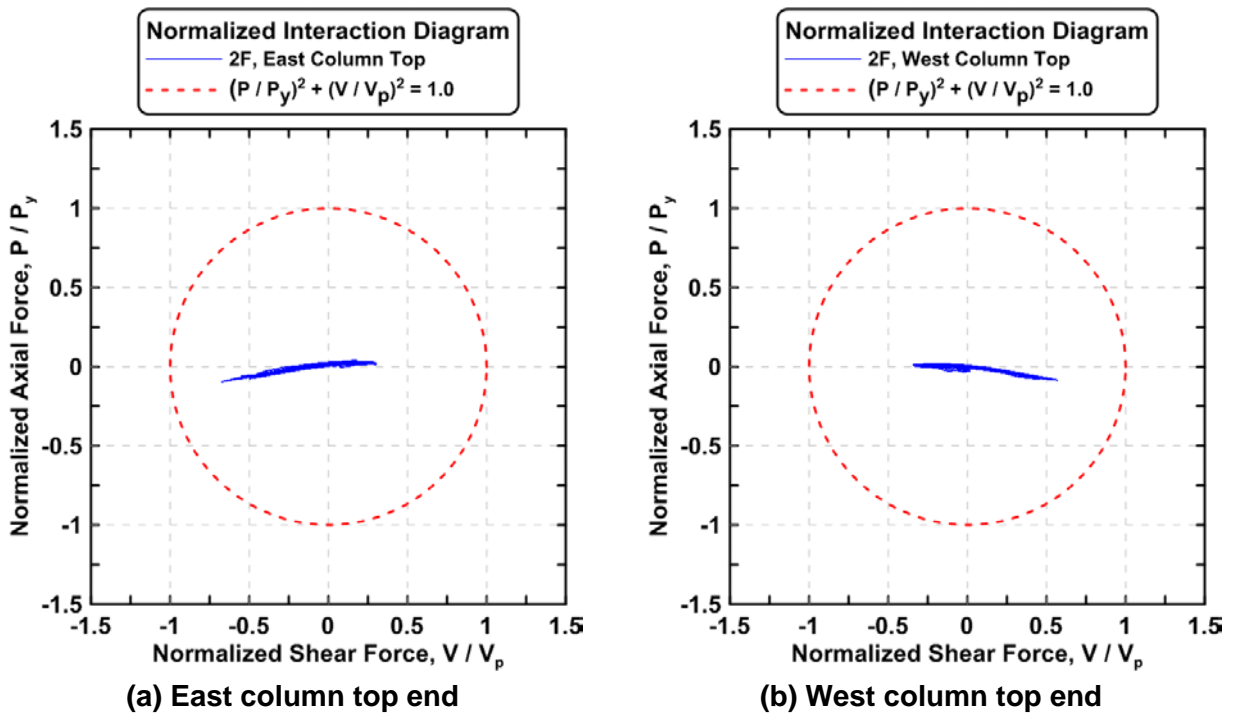


Figure 4.30 Normalized P-V interaction diagrams of the second story columns of TCBF-B-1 specimen

#### 4.2.1.1.3 Beam Response

The vertical deflection time history at the center of W24 × 117 roof beam and W24 × 68 lower beam are plotted in Figs. 4.31. Figs. 4.32 and 4.33 show the time history of strain readings at both ends of roof beam and lower beam, respectively. Both beam axial force time histories derived from linear type strain gauge at different locations of the beams are plotted in Figs. 4.34 and 4.35. The bending moment time histories of both beams are shown in Figs. 4.36 and 4.37. Estimated beam shear force time histories are illustrated in Figs. 4.38 and 4.39. Unbalanced force in the roof beam center is plotted in Fig. 4.40.

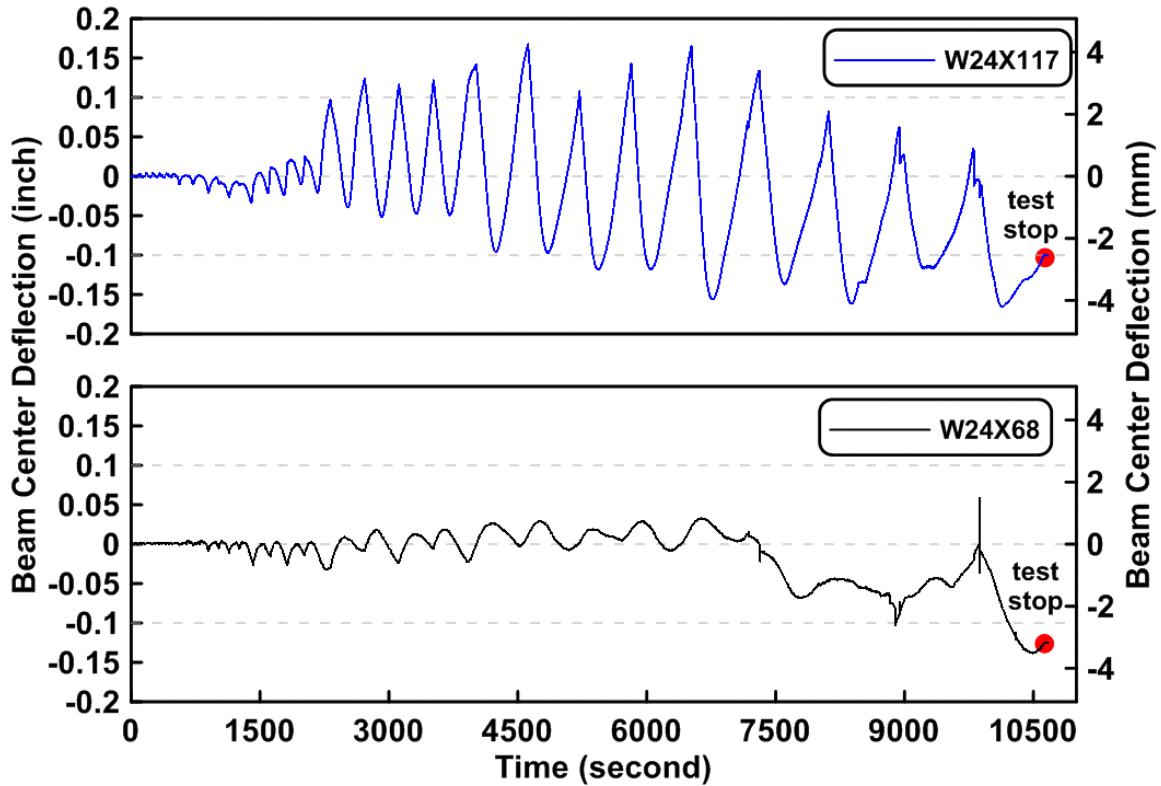
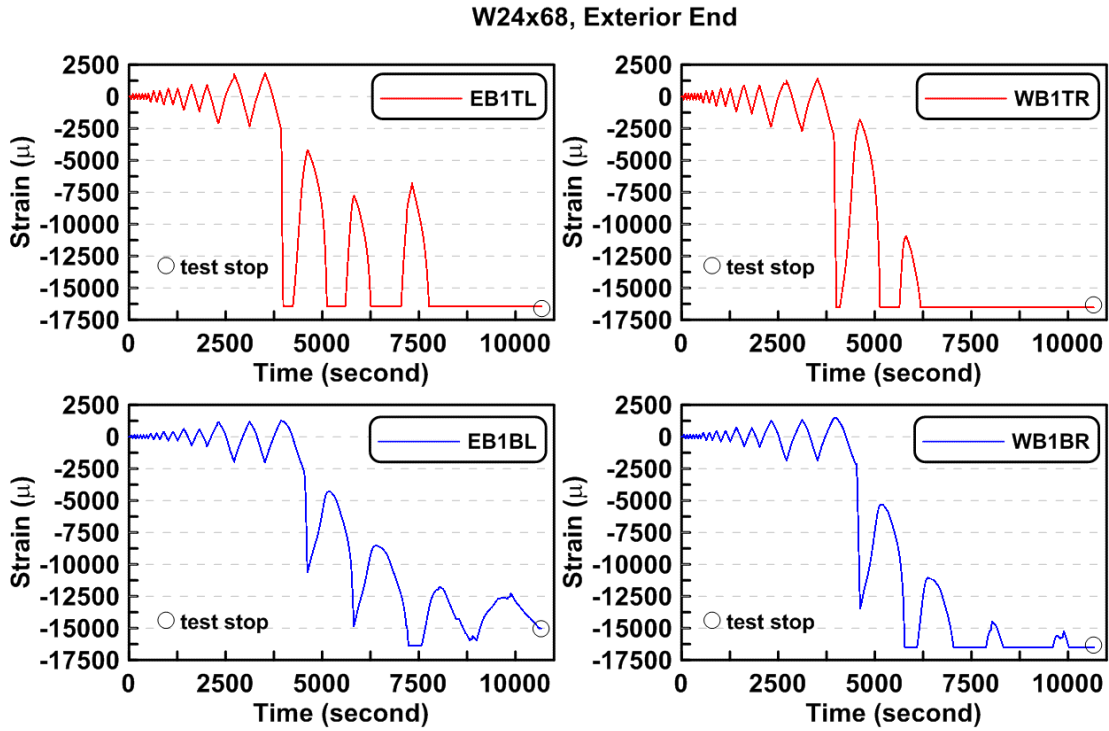
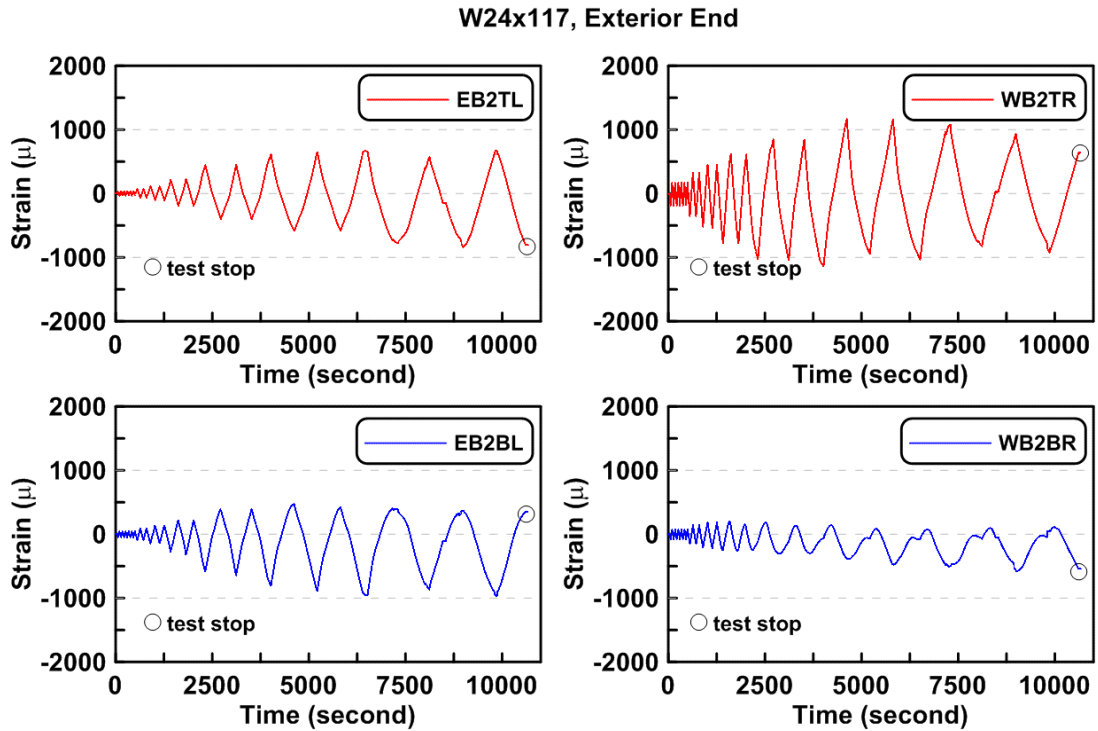


Figure 4.31 The deflection time history at the center of beam span of TCBF-B-1 specimen (roof beam: W24 × 117, lower beam: W24 × 68)



**Figure 4.32** Time history of strain readings at both exterior ends of W24 × 68 lower beam of TCBF-B-1 specimen



**Figure 4.33** Time history of strain readings at both exterior ends of W24 × 117 roof beam of TCBF-B-1 specimen

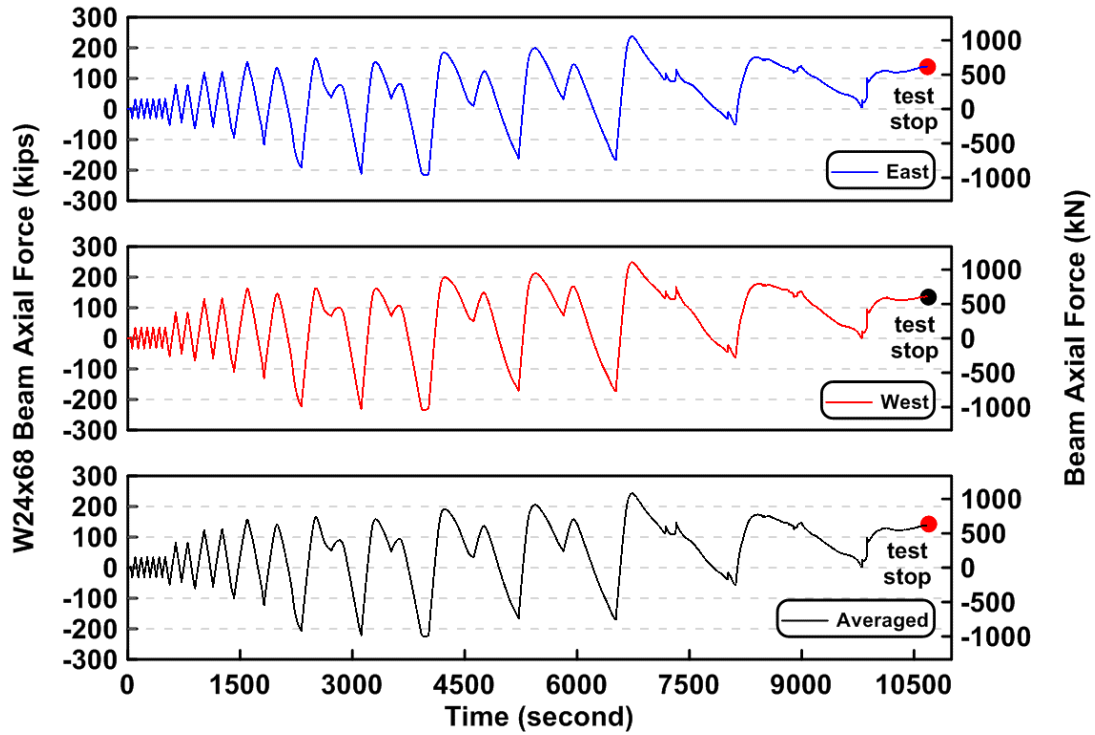


Figure 4.34 Time history of lower beam axial forces of TCBF-B-1 specimen

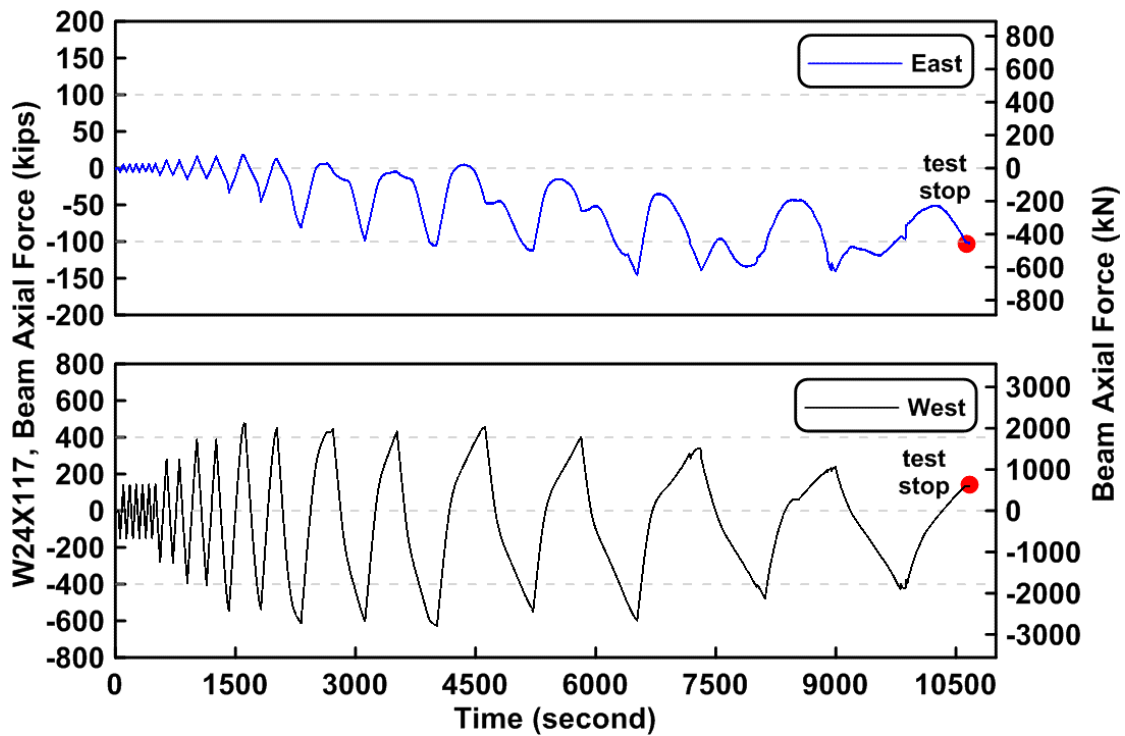


Figure 4.35 Time history of roof beam axial forces of TCBF-B-1 specimen

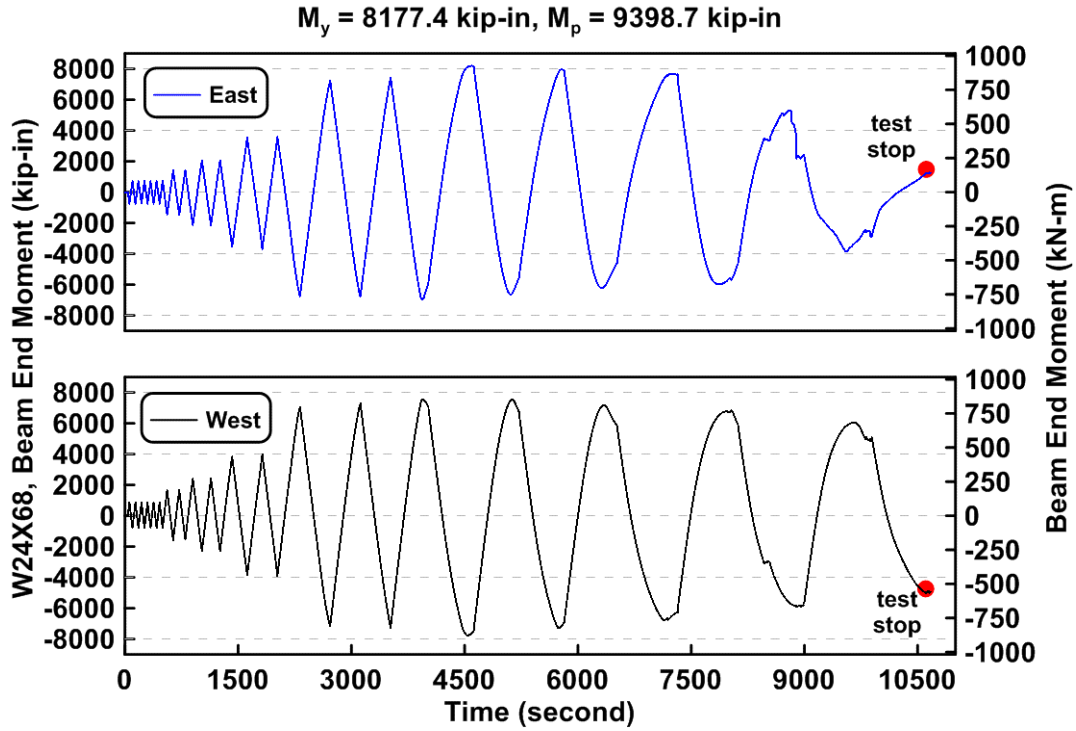


Figure 4.36 Time history of the lower beam end bending moment of TCBF-B-1 specimen

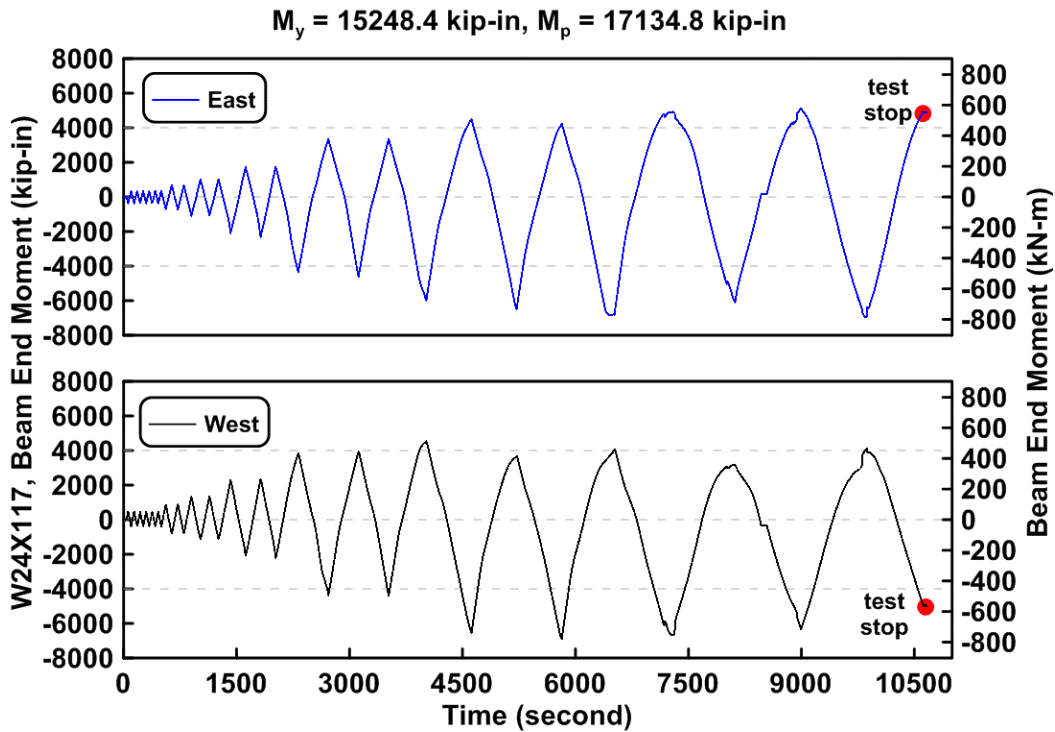


Figure 4.37 Time history of the roof beam end bending moment of TCBF-B-1 specimen



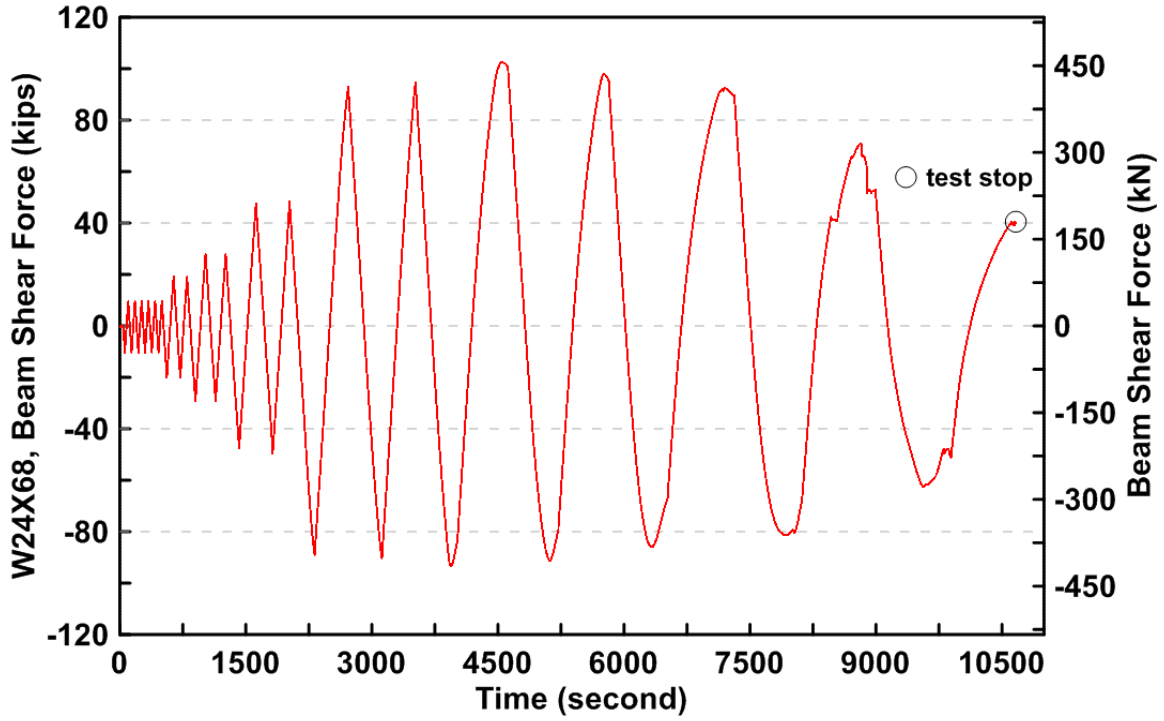


Figure 4.38 Lower beam estimated shear force time history of TCBF-B-1 specimen

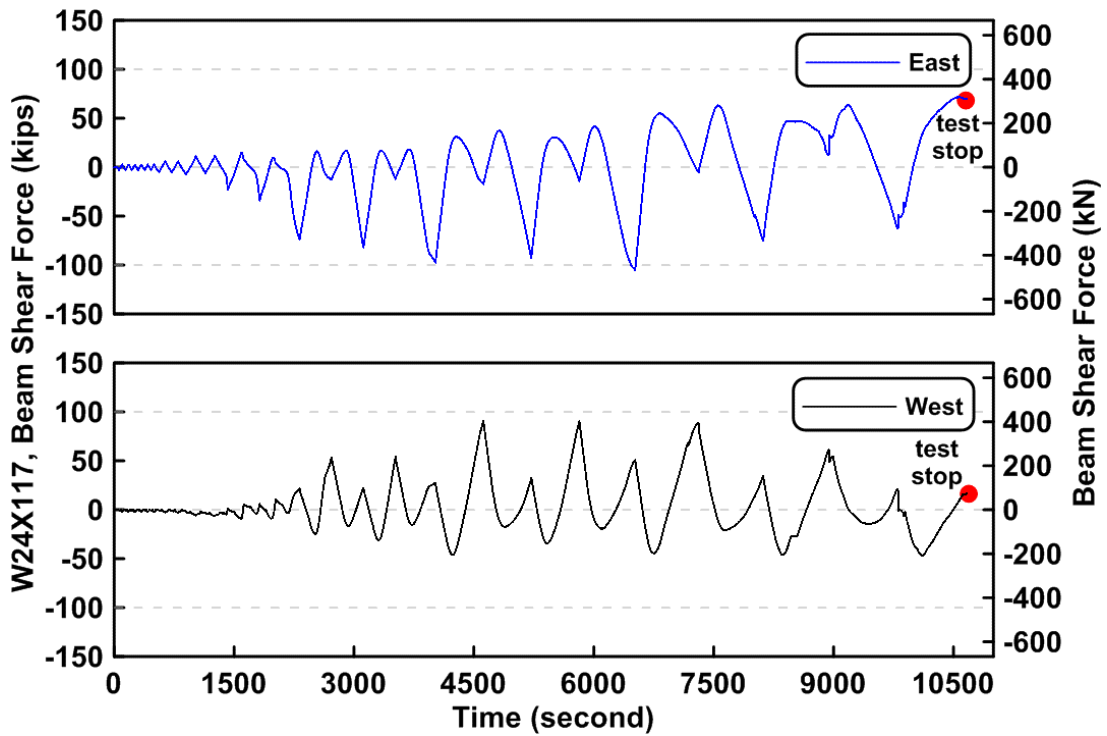


Figure 4.39 Roof beam estimated shear force time history of TCBF-B-1 specimen

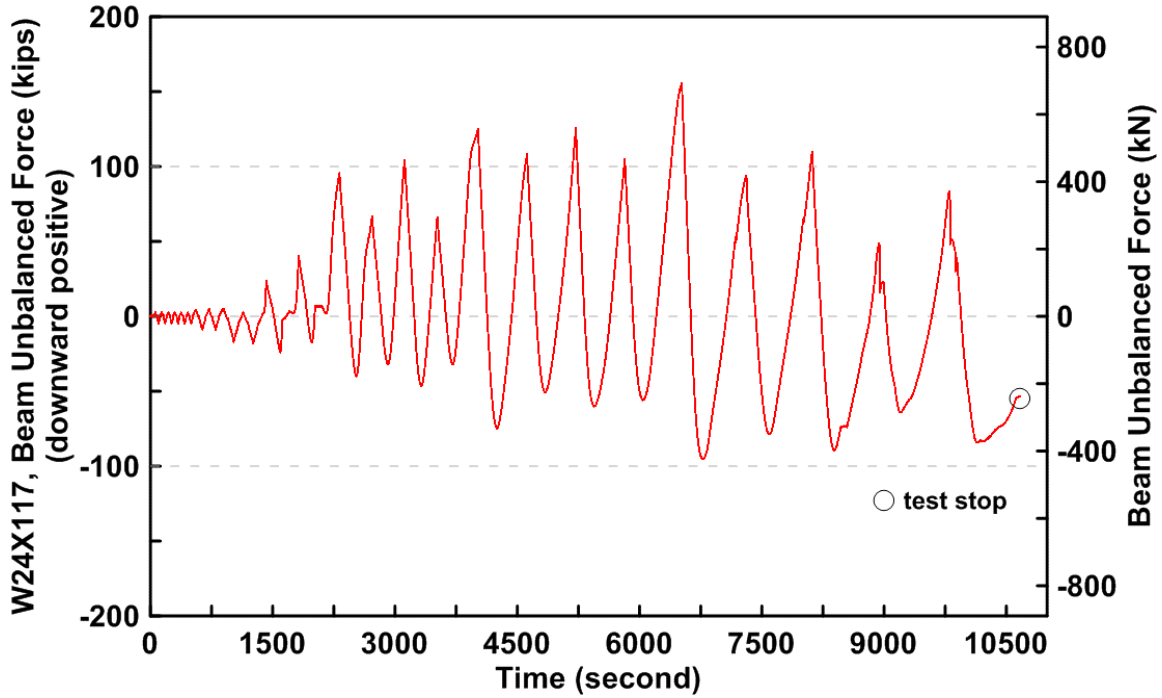


Figure 4.40 Estimated unbalanced force time history of TCBF-B-1 specimen roof beam

#### 4.2.1.1.4 Brace Response

The estimated brace axial forces versus brace axial deformations for each square HSS braces are shown in Fig. 4.41. The estimated brace axial forces versus measured brace out-of-plane displacements at the brace center point for each square HSS braces are shown in Fig. 4.42. Combined brace axial force, axial deformation and out-of-plane displacement relationships are shown in Fig. 4.43. The decomposed strain (axial strain, in-plane bending strain, out-of-plane bending strain and warping strain) time histories of each brace are plotted in Figs. 4.44 to 4.47(a). Figure 4.47(b) illustrates the definition of the decomposed strain components for the square HSS braces.

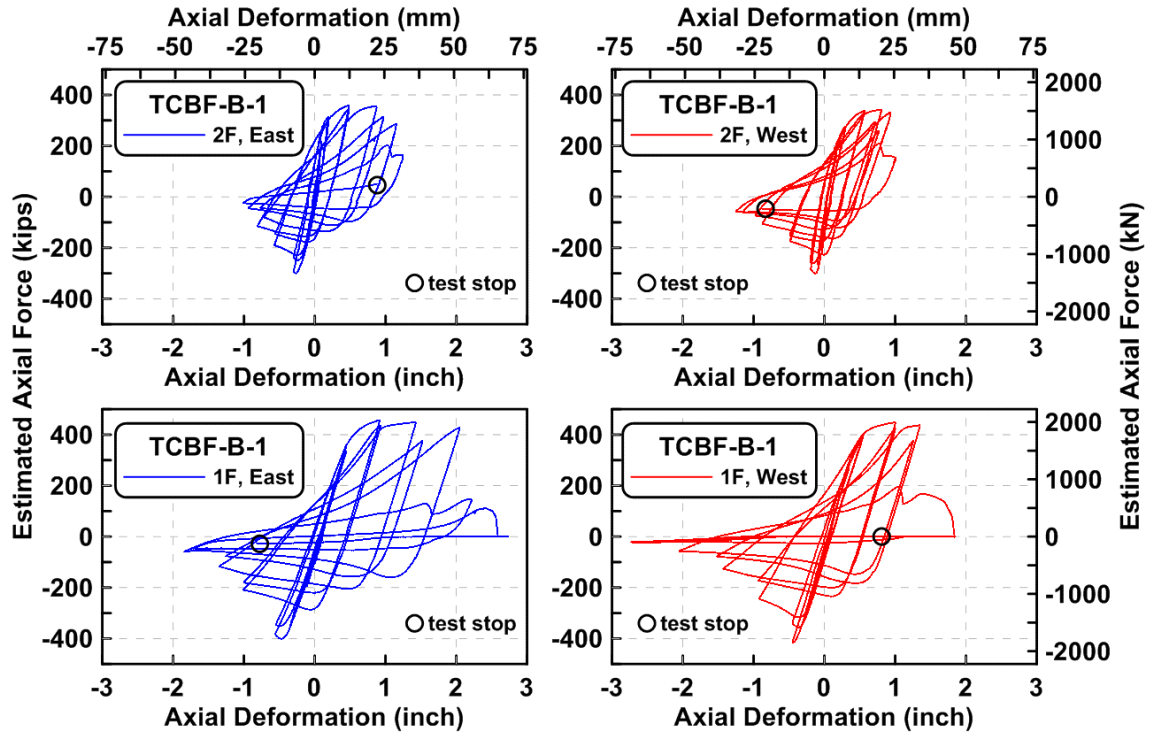


Figure 4.41 Estimated brace axial forces vs. brace axial deformations of TCBF-B-1 specimen

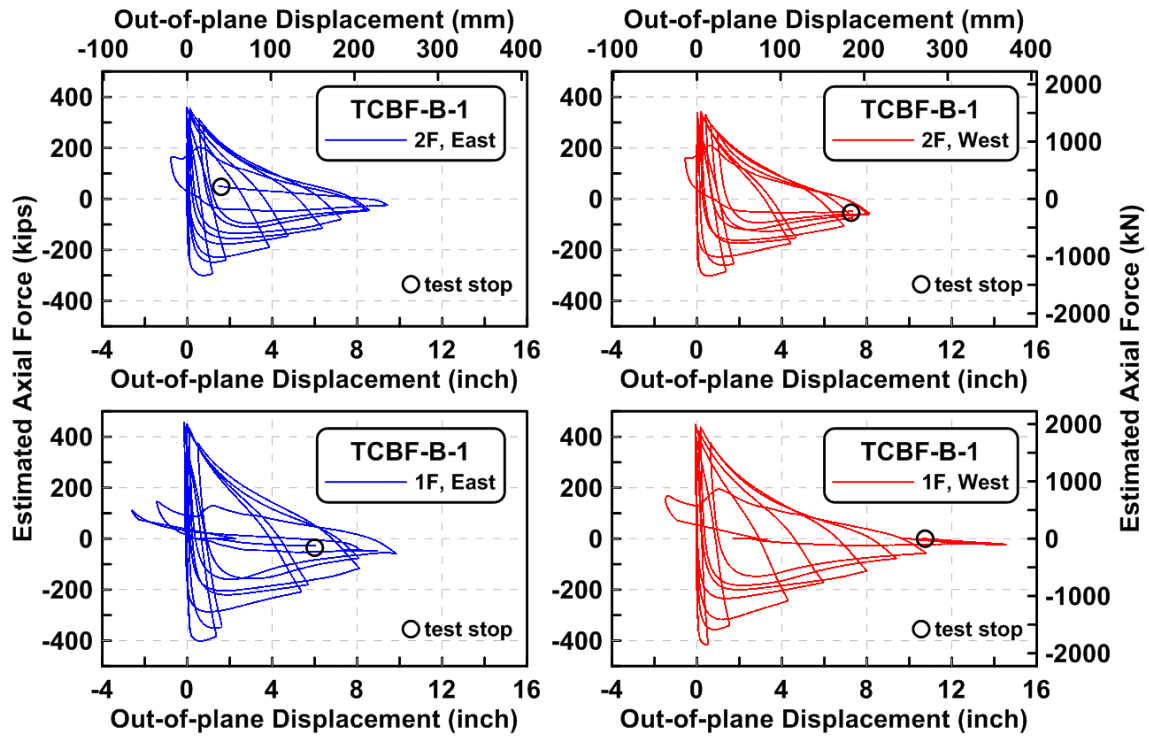


Figure 4.42 Estimated brace axial forces vs. measured brace out-of-plane displacements of TCBF-B-1 specimen

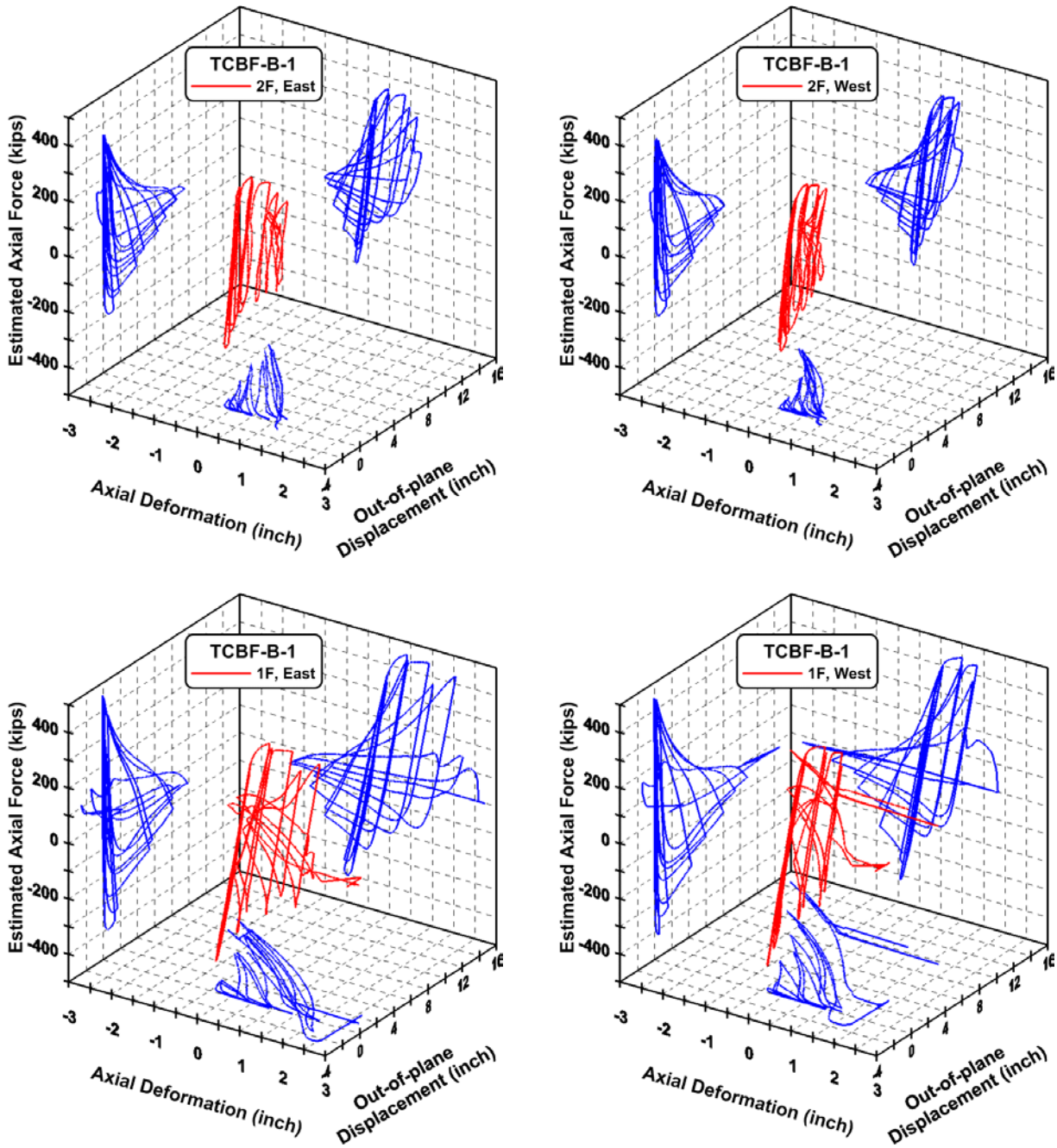


Figure 4.43 Estimated brace axial force, brace axial deformation and measured brace out-of-plane displacement relationships of TCBF-B-1 specimen

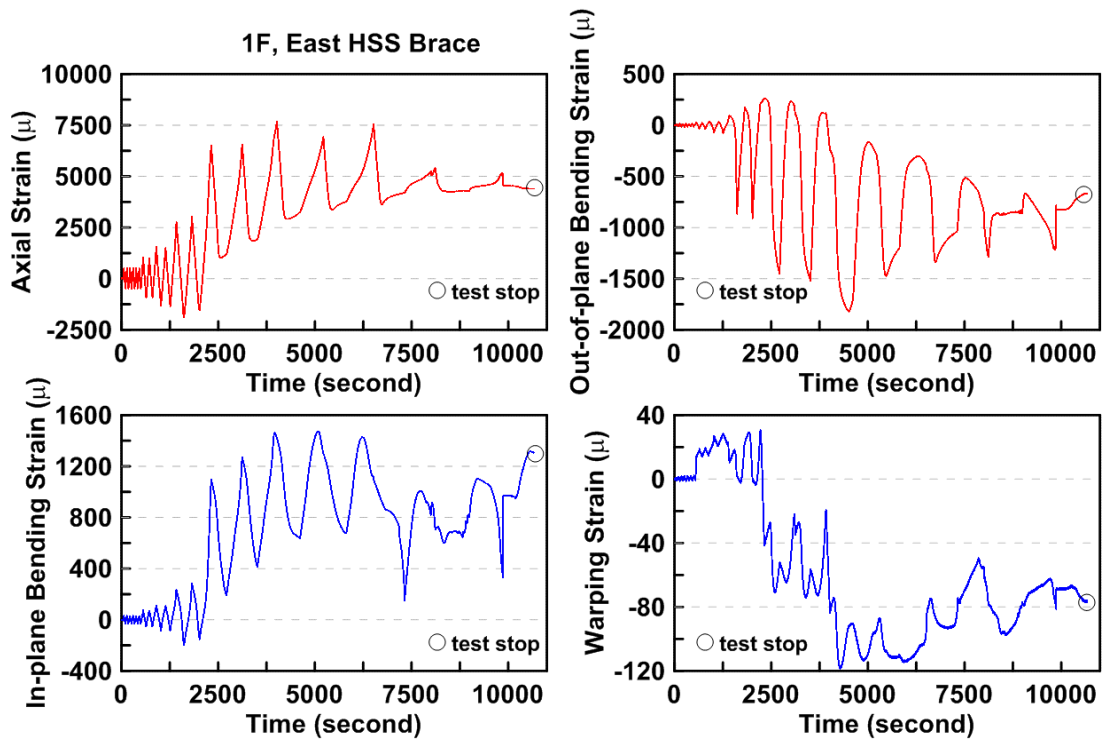


Figure 4.44 Time history of the decomposed strain components of eastern side HSS brace in the first story of TCBF-B-1 specimen

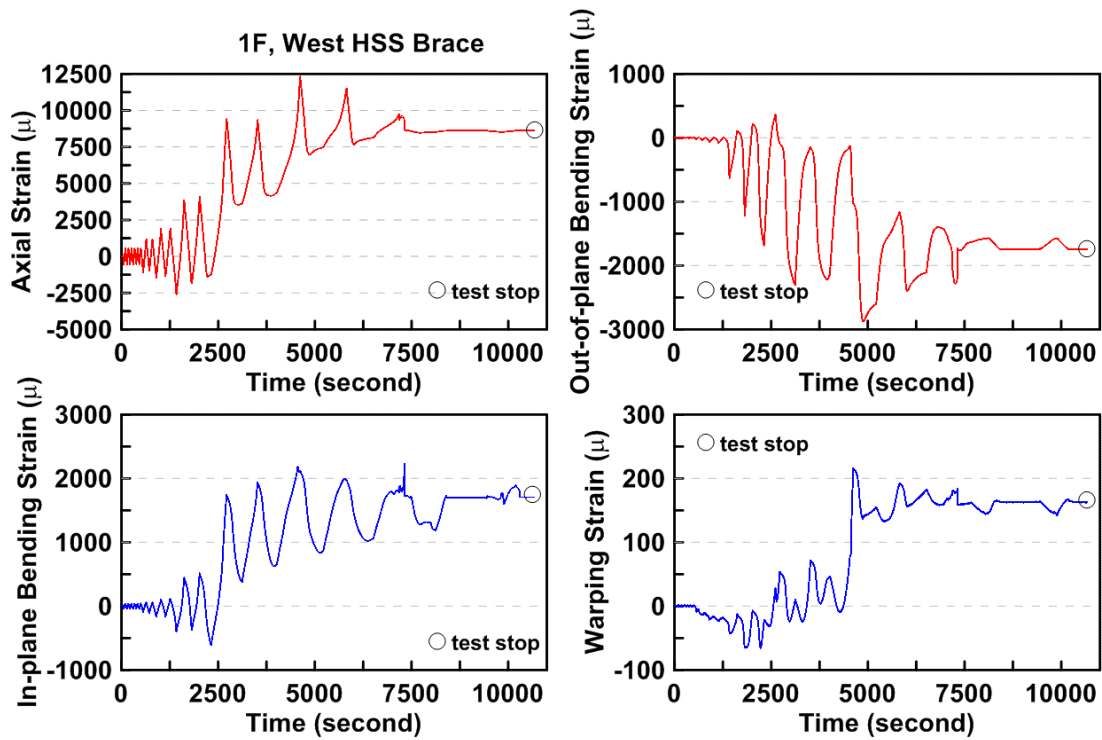


Figure 4.45 Time history of the decomposed strain components of western side HSS brace in the first story of TCBF-B-1 specimen

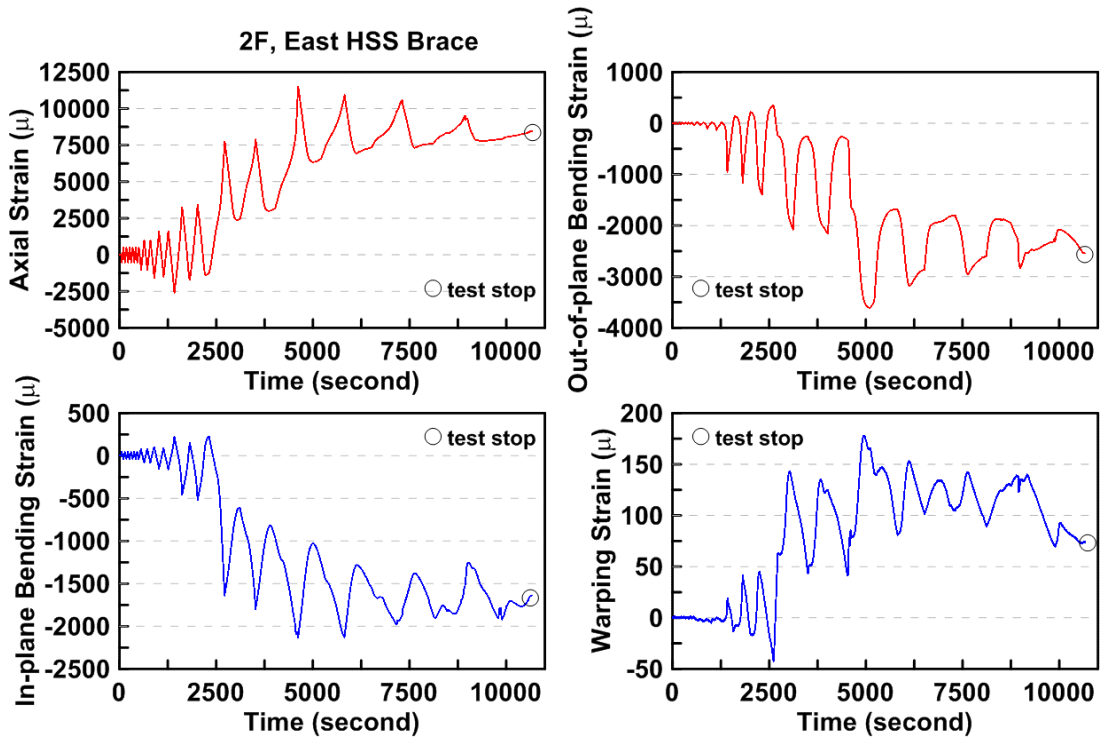


Figure 4.46 Time history of the decomposed strain components of eastern side HSS brace in the second story of TCBF-B-1 specimen

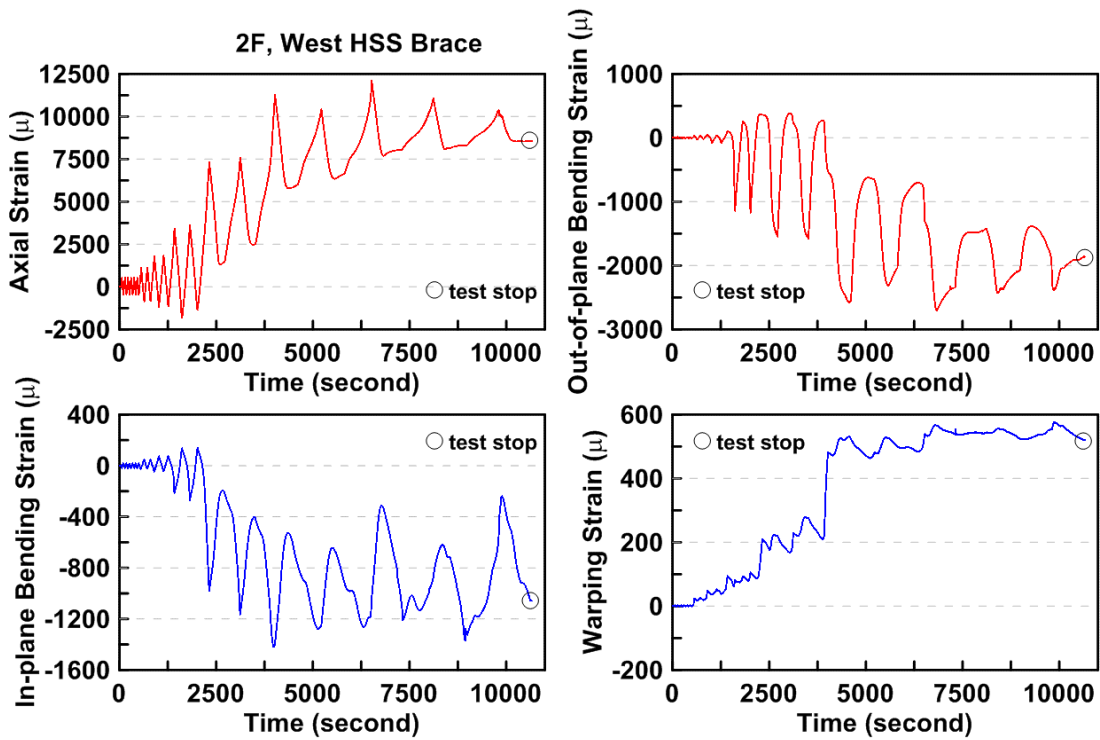
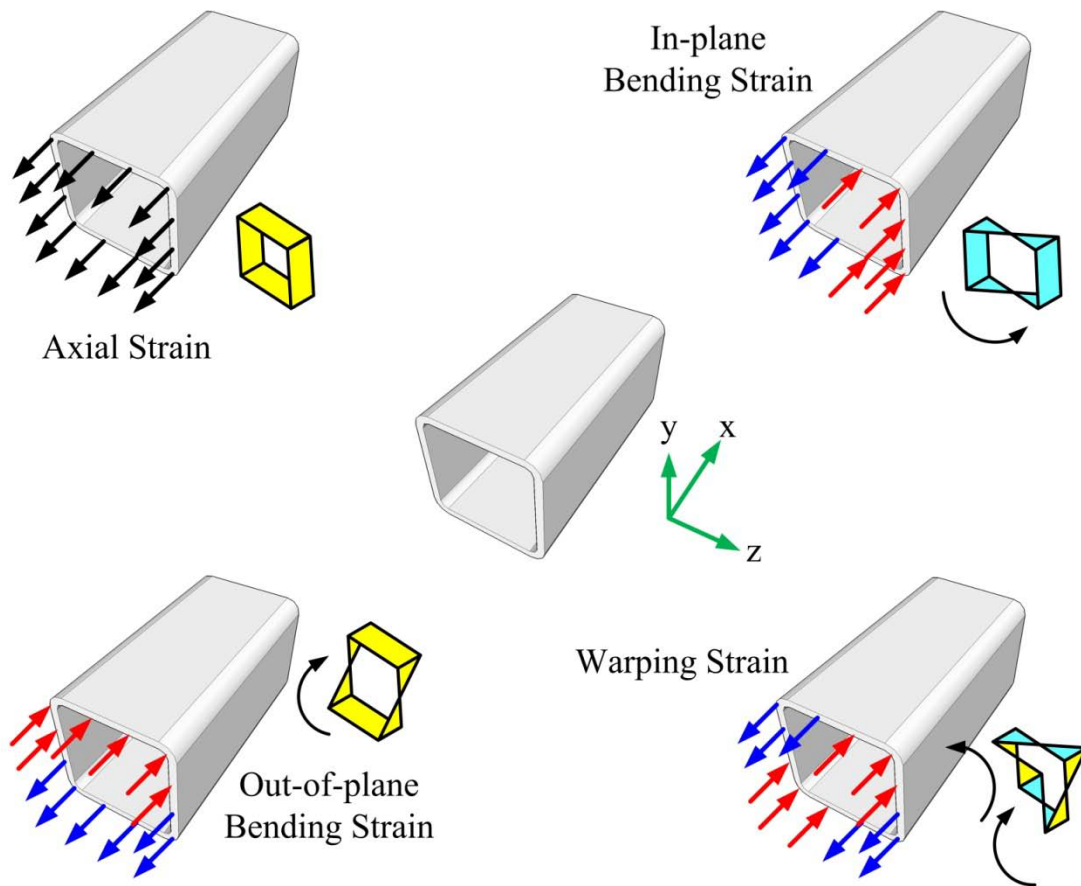


Figure 4.47(a) Time history of the decomposed strain components of western side HSS brace in the second story of TCBF-B-1 specimen



**Figure 4.47(b) Definition of the decomposed strain components**

#### **4.2.1.1.5 Panel Zone Response**

Estimated panel zone shear stress versus measured panel zone shear strain relationship for four locations are plotted in Figs. 4.48. This suggests that yielding occurs in the upper floor, East side panel zone. Time history of derived rosette type strain gauge readings in the panel zone area at each story are shown from Figs. 4.49 to 4.52. Normalized maximum and minimum principal stress relationships along with different yield criteria for the panel zone regions are plotted in Figs. 4.53 to 4.56.

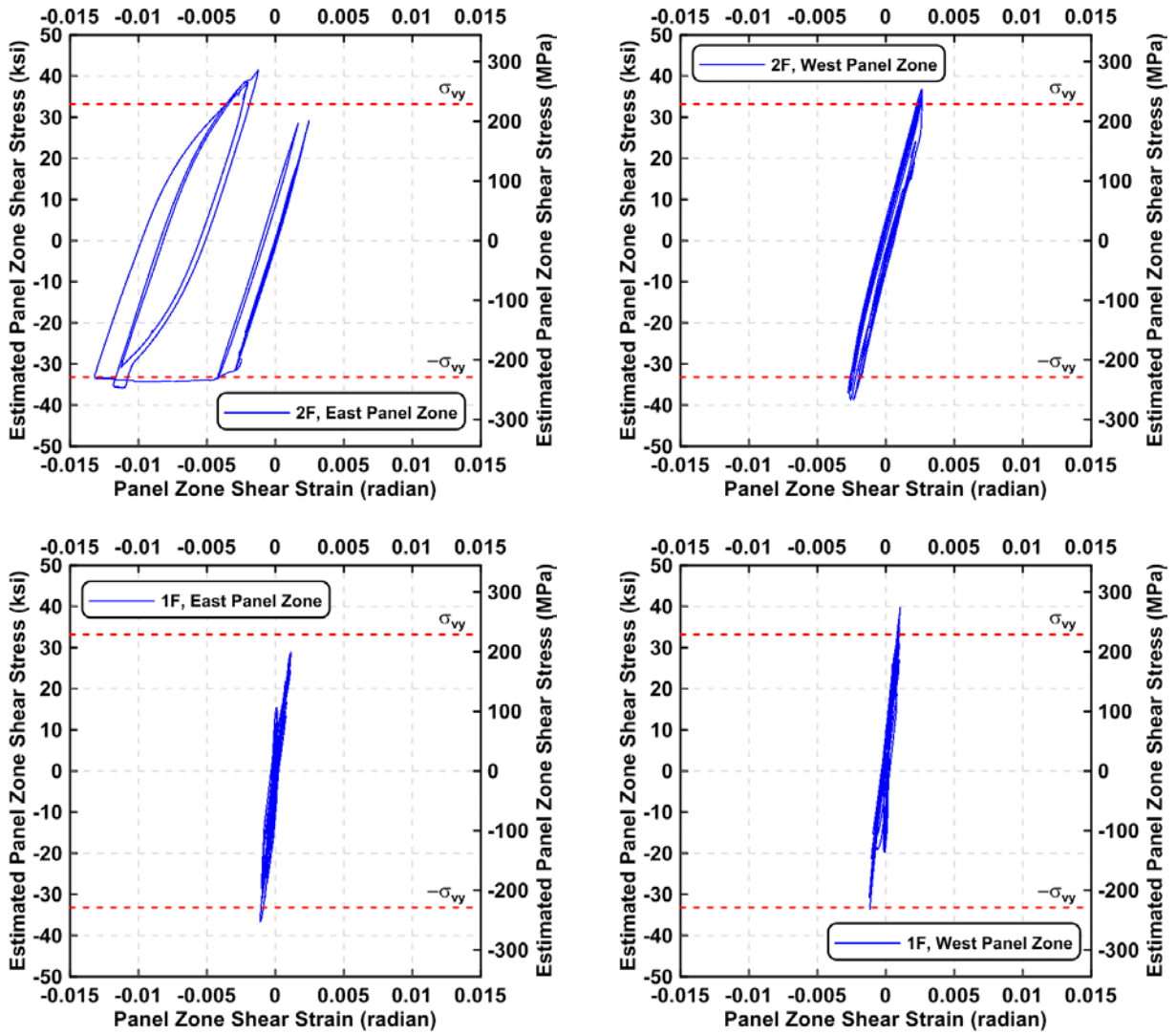


Figure 4.48 Estimated panel zone shear stress vs. shear strain relationships of TCBF-B-1 specimen



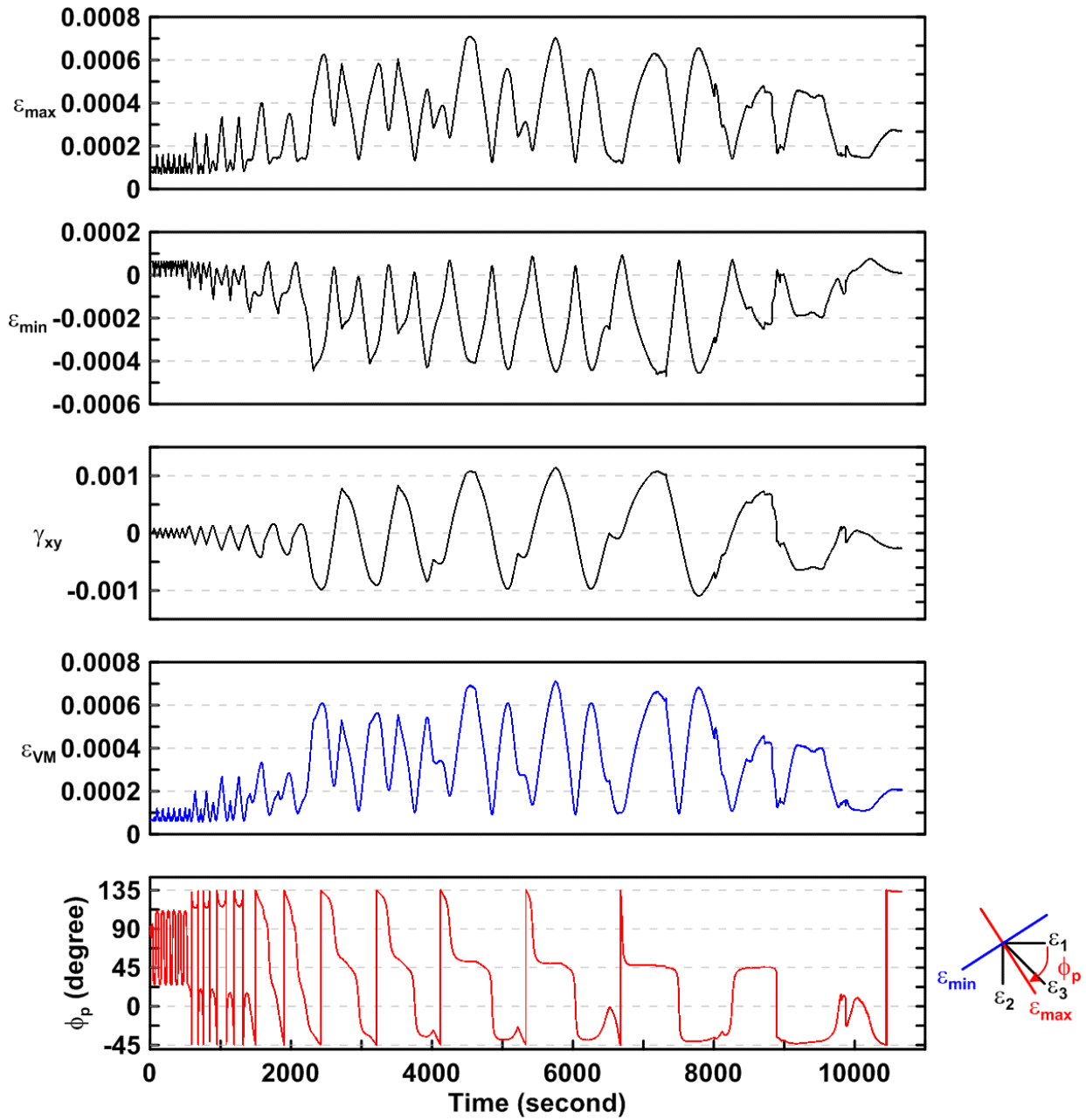


Figure 4.49 Time history of rosette type strain gauge readings in the lower panel zone of TCBF-B-1 specimen (location: R2)

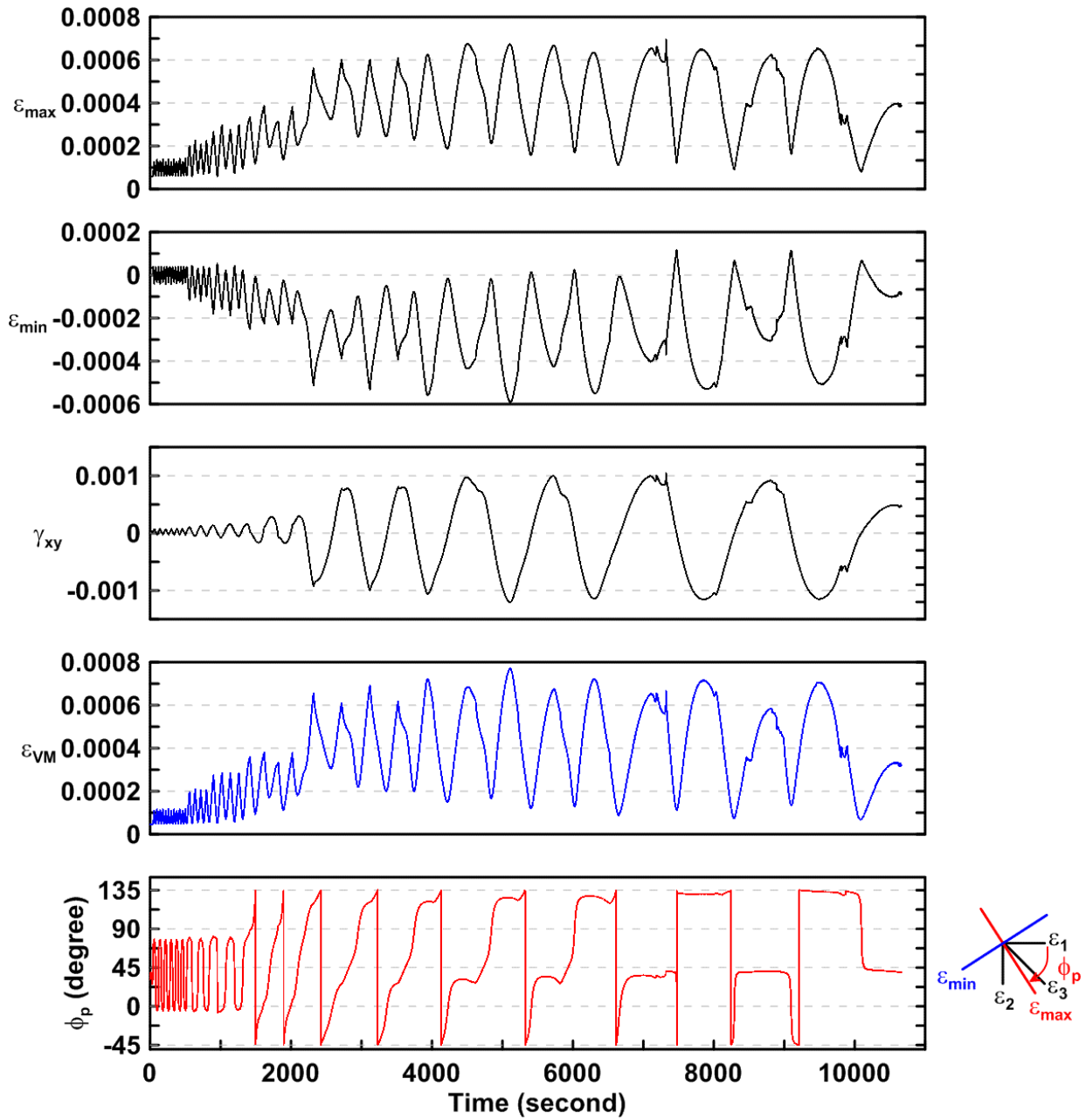


Figure 4.50 Time history of rosette type strain gauge readings in the lower panel zone of TCBF-B-1 specimen (location: R6)

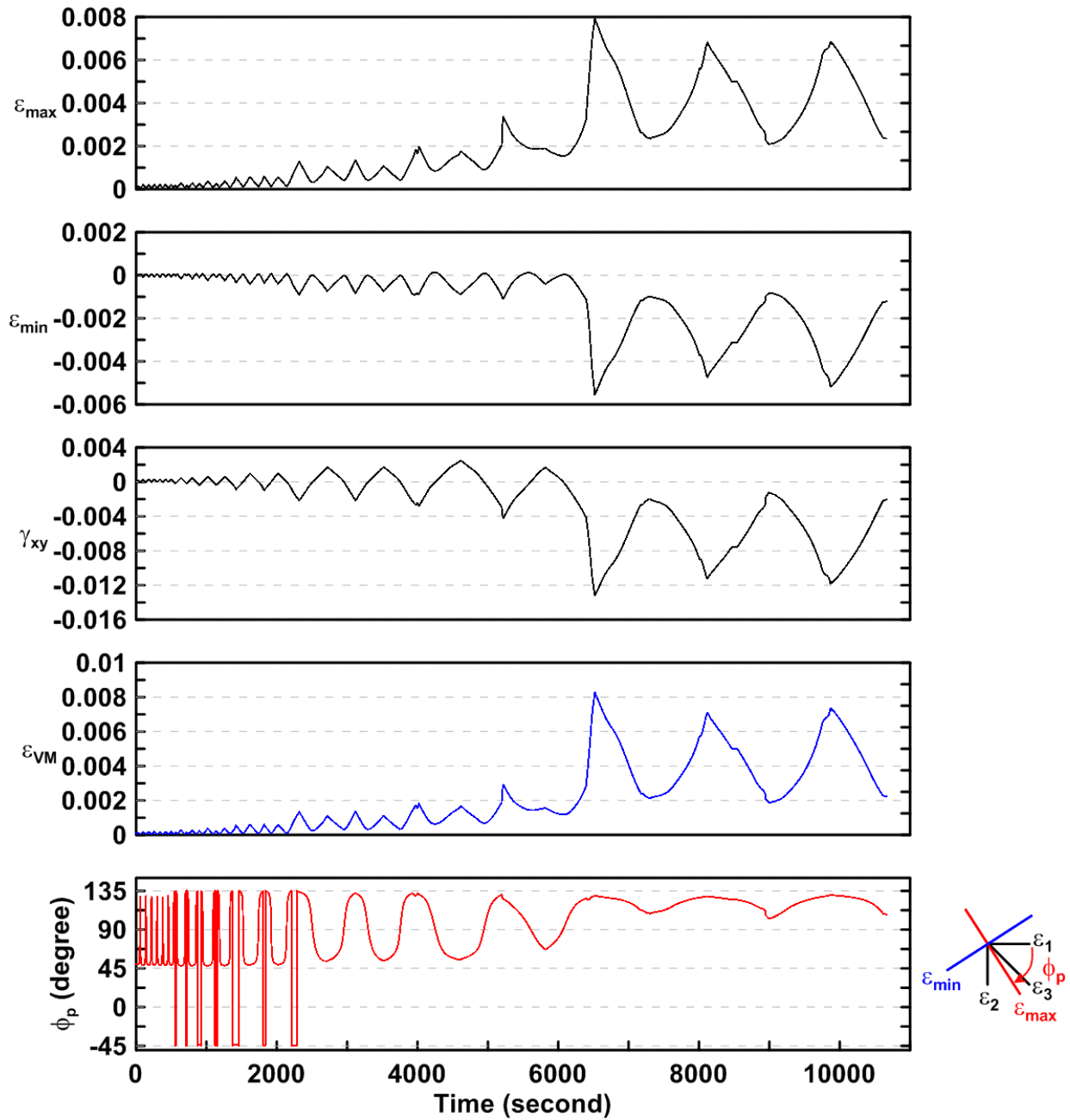


Figure 4.51 Time history of rosette type strain gauge readings in the roof panel zone of TCBF-B-1 specimen (location: R4)

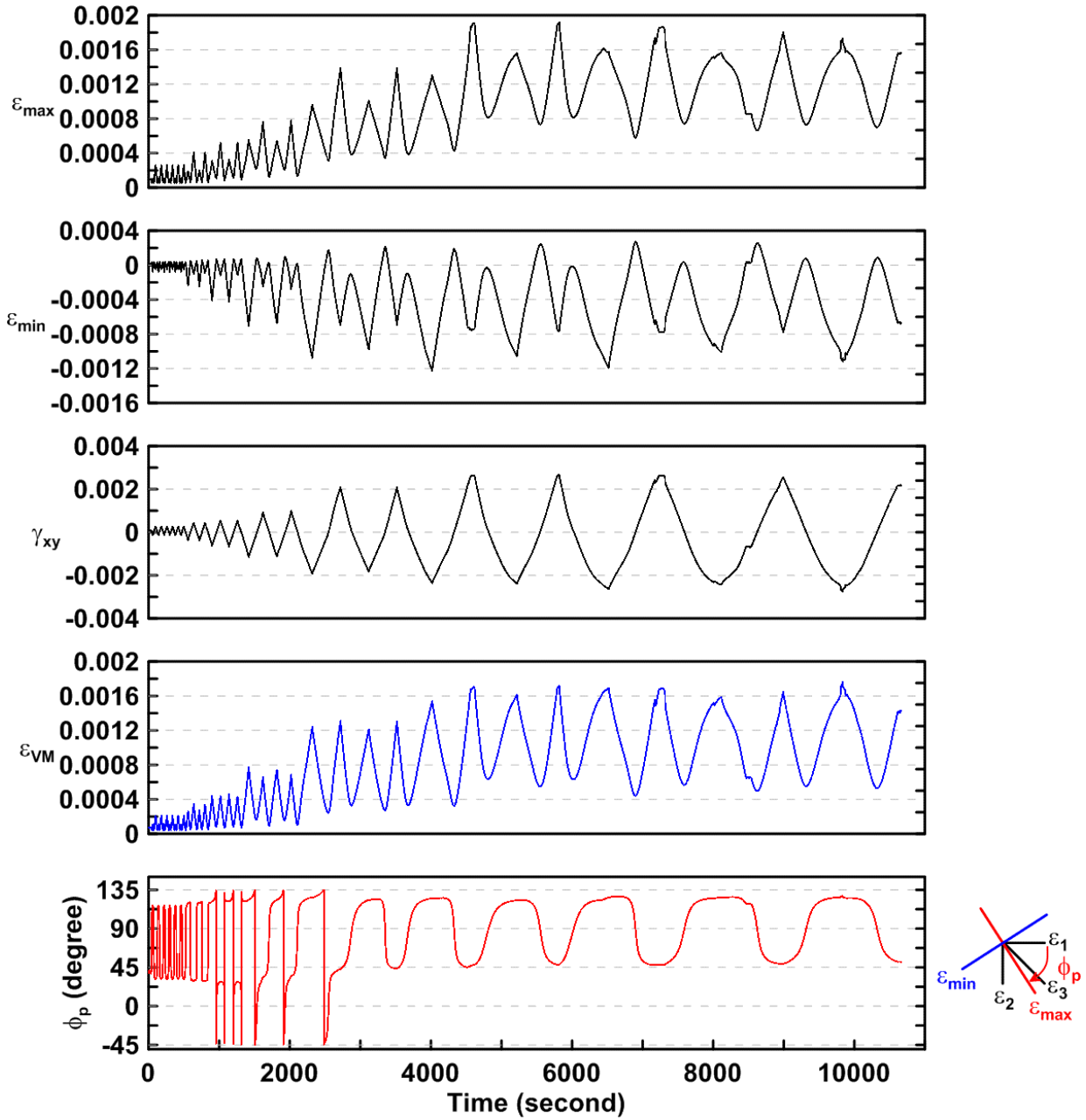


Figure 4.52 Time history of rosette type strain gauge readings in the roof panel zone of TCBF-B-1 specimen (location: R8)

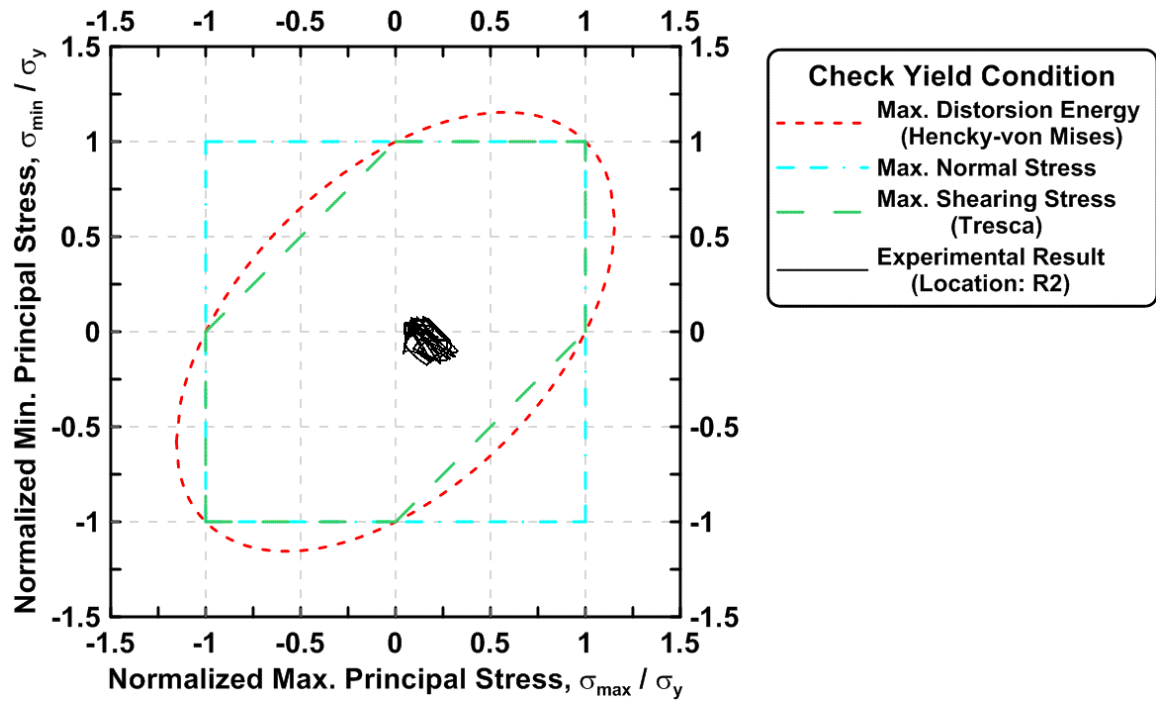


Figure 4.53 Normalized maximum principal stress vs. normalized minimum principal stress in the lower panel zone of TCBF-B-1 specimen (location: R2)

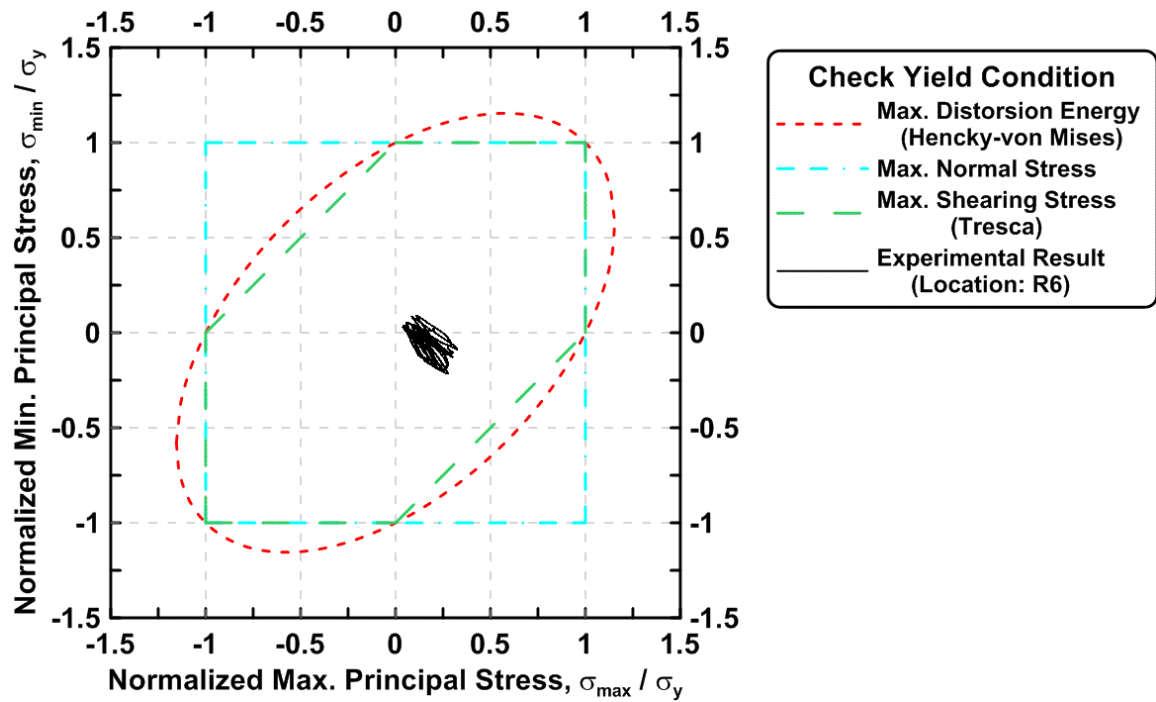


Figure 4.54 Normalized maximum principal stress vs. normalized minimum principal stress in the lower panel zone of TCBF-B-1 specimen (location: R6)

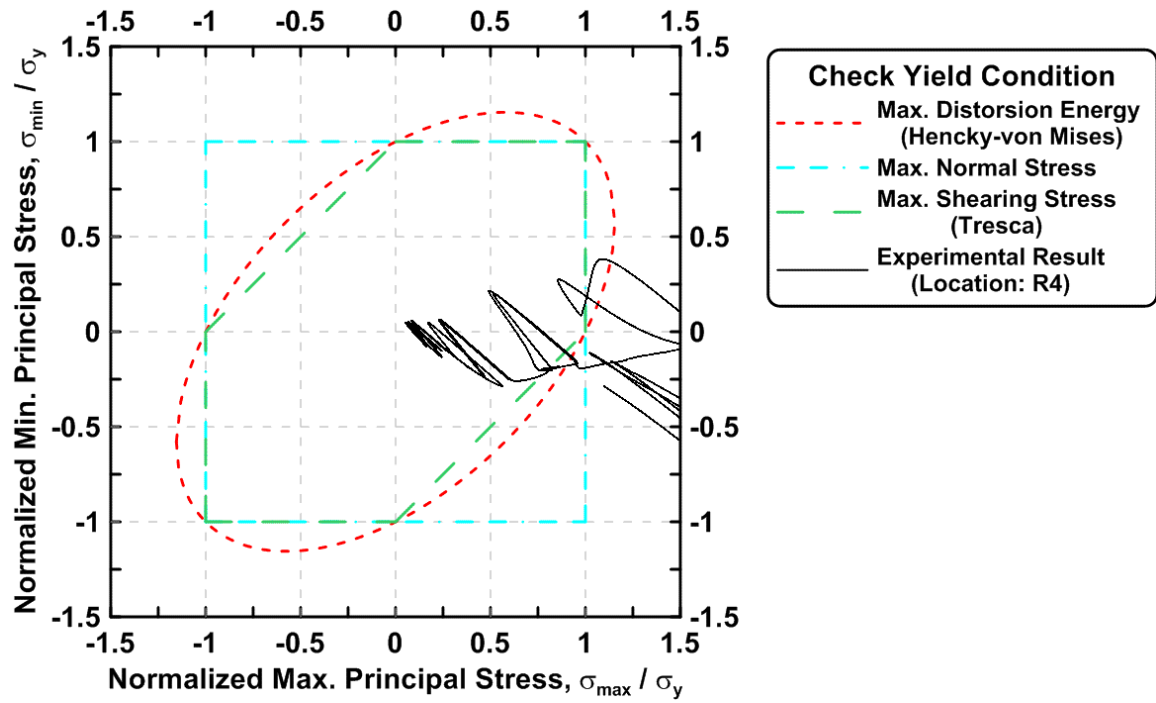


Figure 4.55 Normalized maximum principal stress vs. normalized minimum principal stress in the roof panel zone of TCBF-B-1 specimen (location: R4)

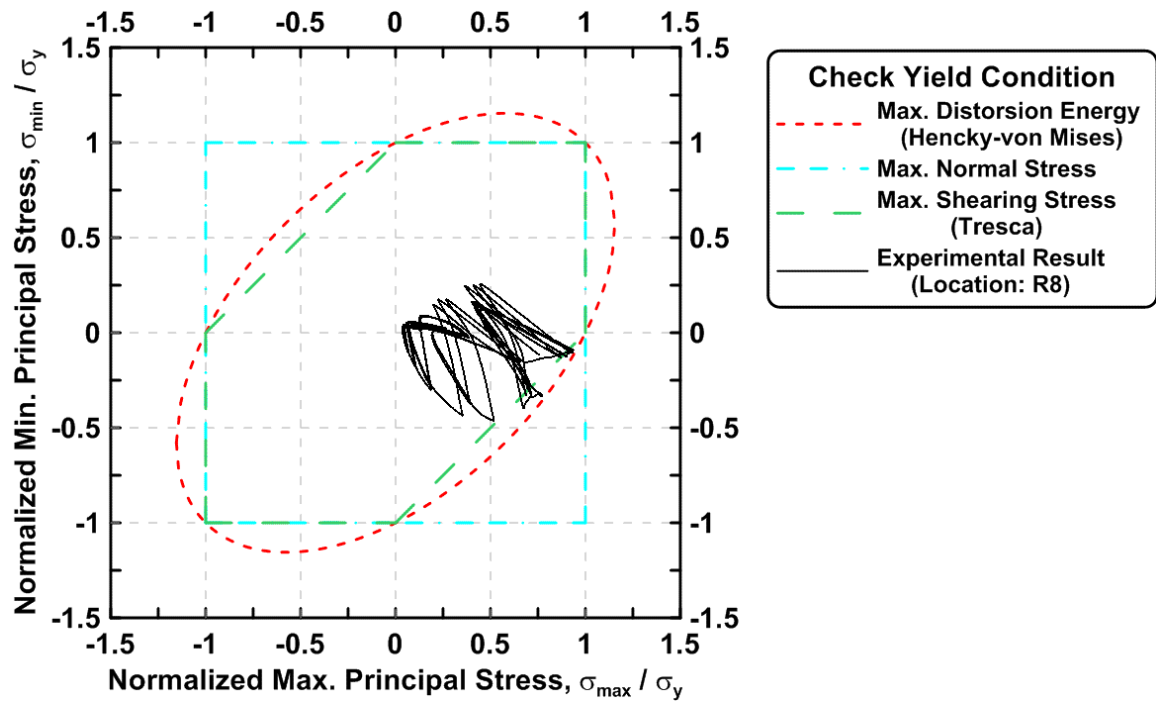


Figure 4.56 Normalized maximum principal stress vs. normalized minimum principal stress in the roof panel zone of TCBF-B-1 specimen (location: R8)

#### 4.2.1.1.6 Gusset Plate Response

The time history of derived rosette type strain gauge readings in the 3/4-inch thick one-piece gusset plate are shown from Figs. 4.57 to 4.68. Normalized maximum and minimum principal stress relationships along with different yield criteria for the rosettes on the gusset plate are plotted in Figs. 4.69 to 4.80.

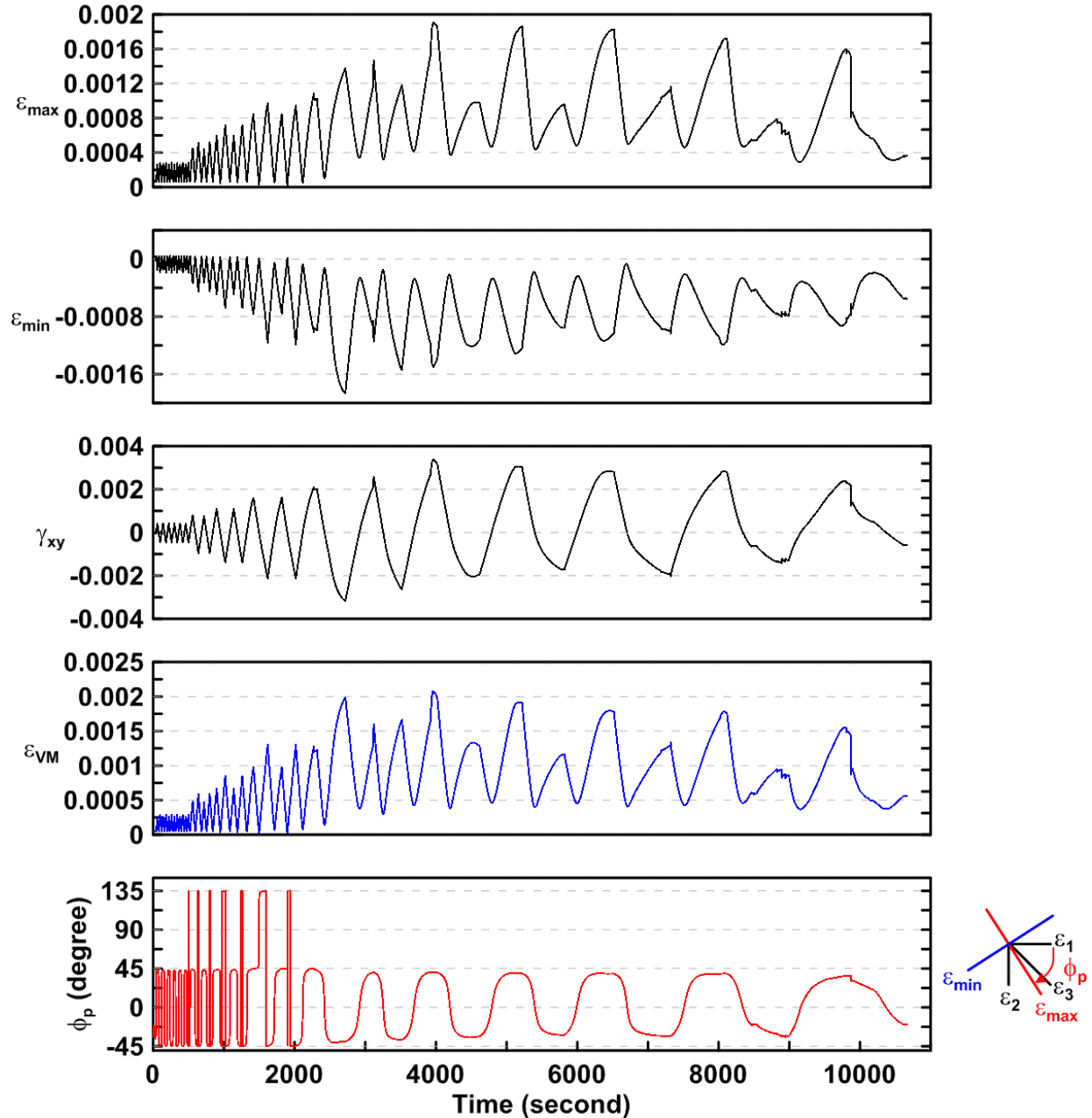


Figure 4.57 Time history of rosette type strain gauge readings in the one-piece gusset plate of TCBF-B-1 specimen (location: R9)

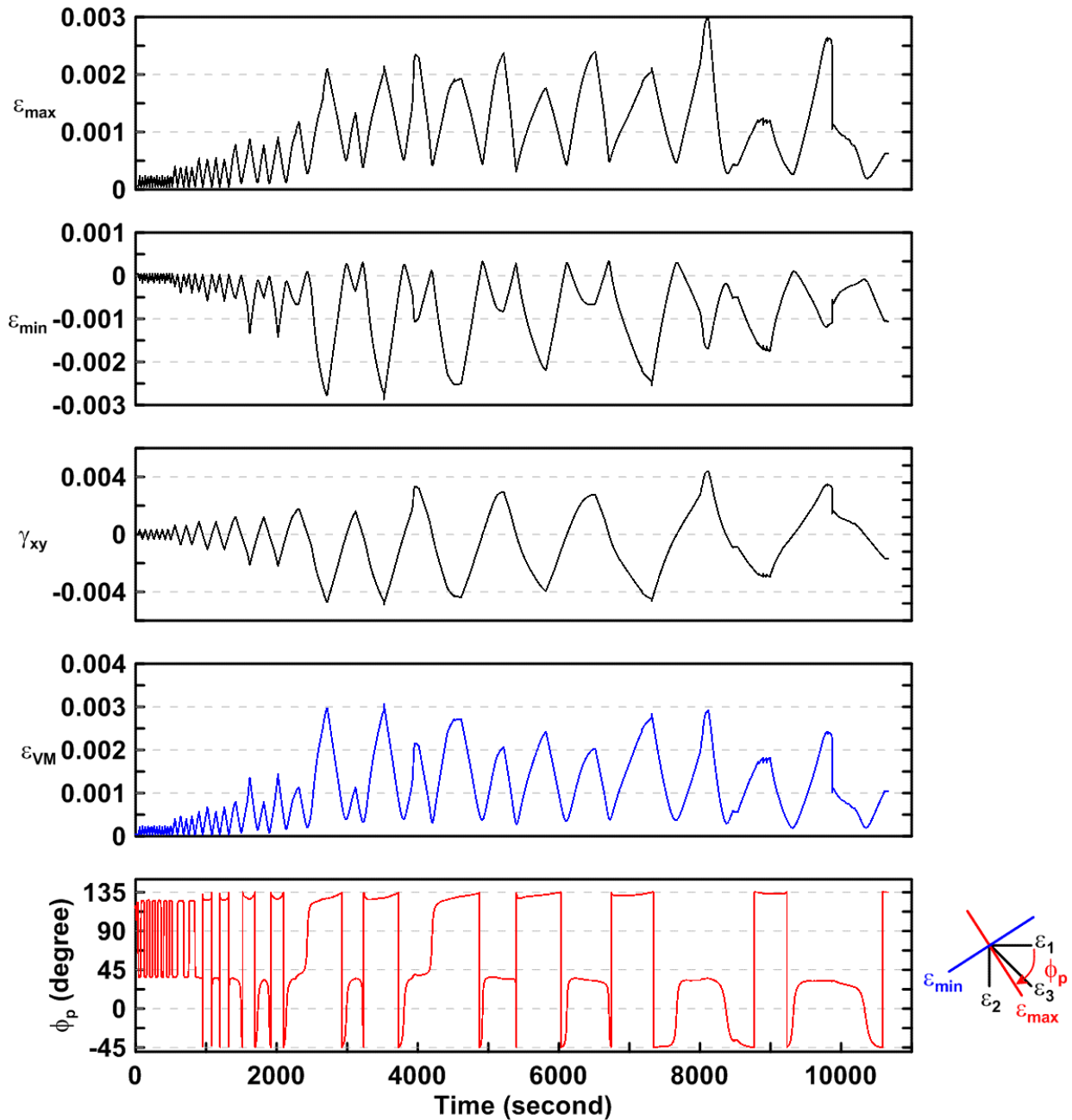


Figure 4.58 Time history of rosette type strain gauge readings in the one-piece gusset plate of TCBF-B-1 specimen (location: R10)



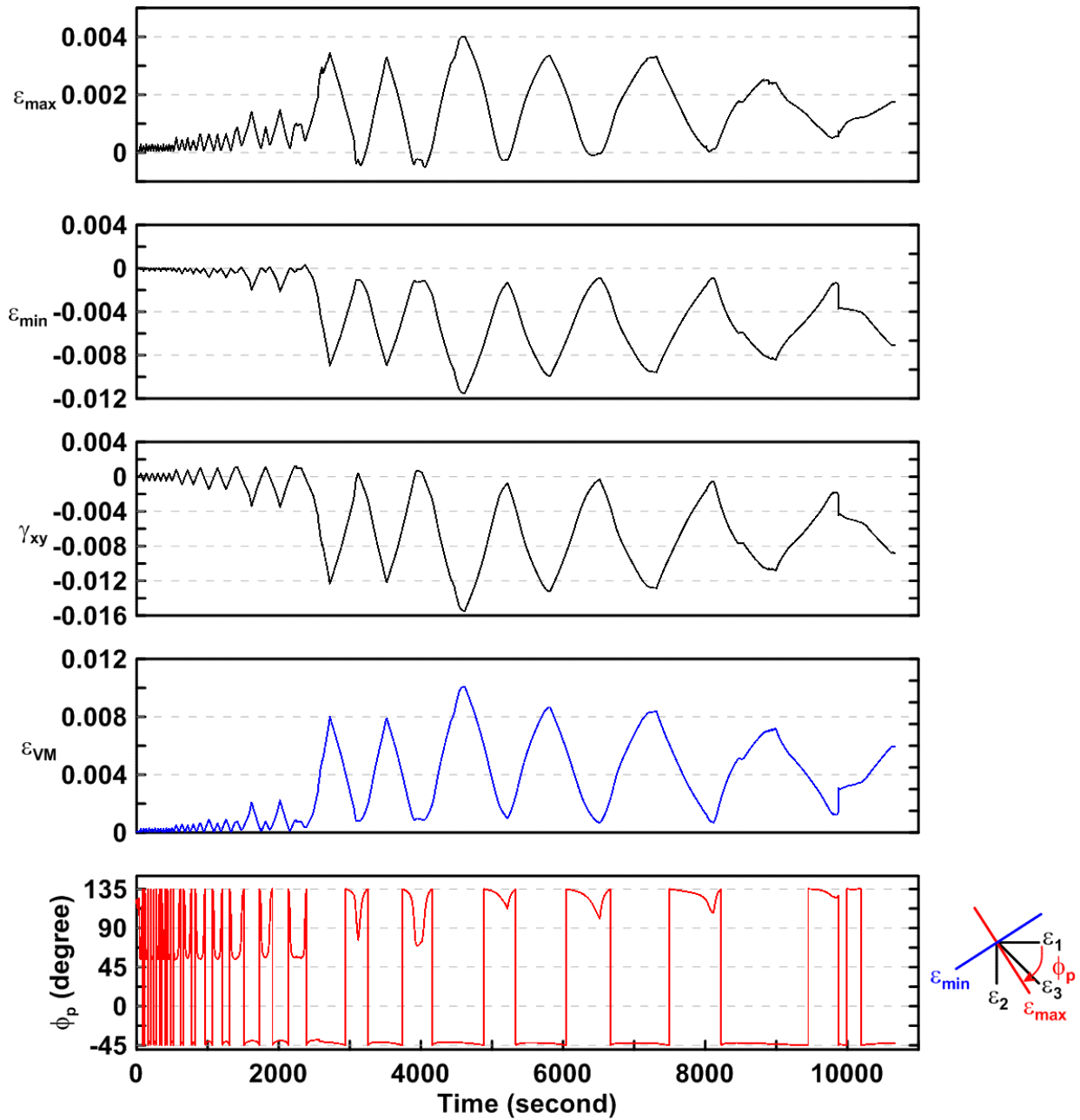


Figure 4.59 Time history of rosette type strain gauge readings in the one-piece gusset plate of TCBF-B-1 specimen (location: R11)

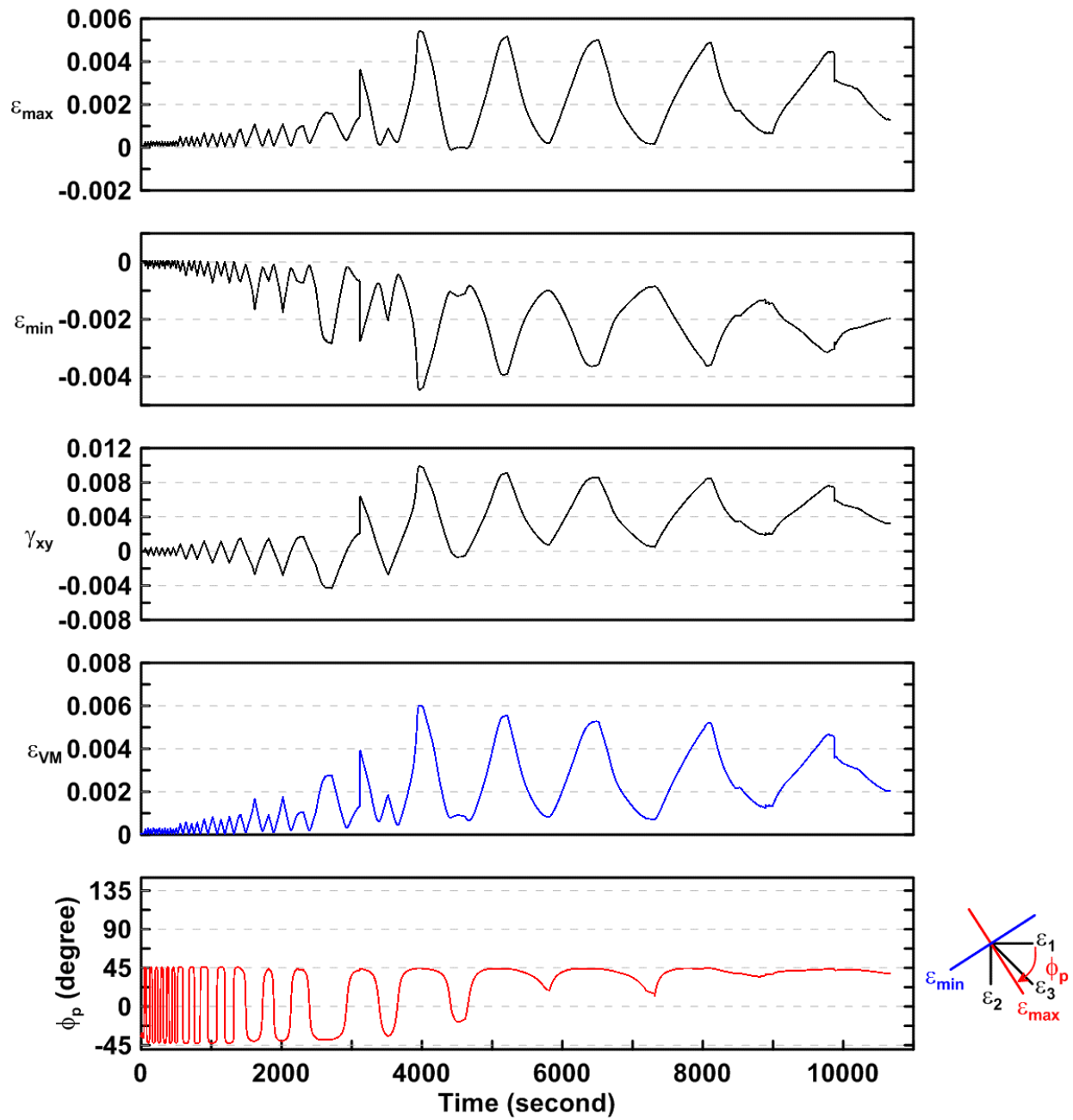


Figure 4.60 Time history of rosette type strain gauge readings in the one-piece gusset plate of TCBF-B-1 specimen (location: R12)

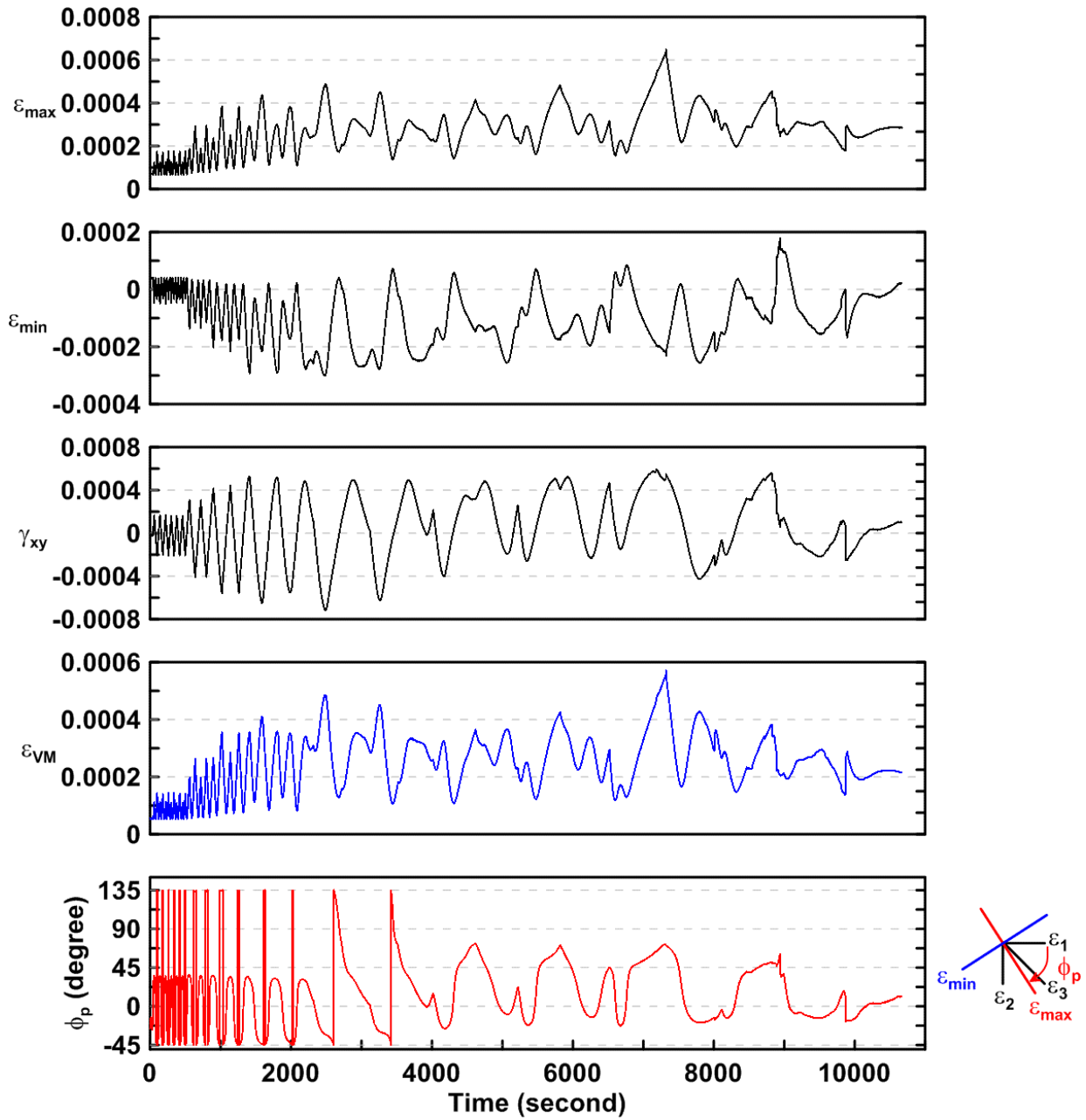


Figure 4.61 Time history of rosette type strain gauge readings in the one-piece gusset plate of TCBF-B-1 specimen (location: R13)

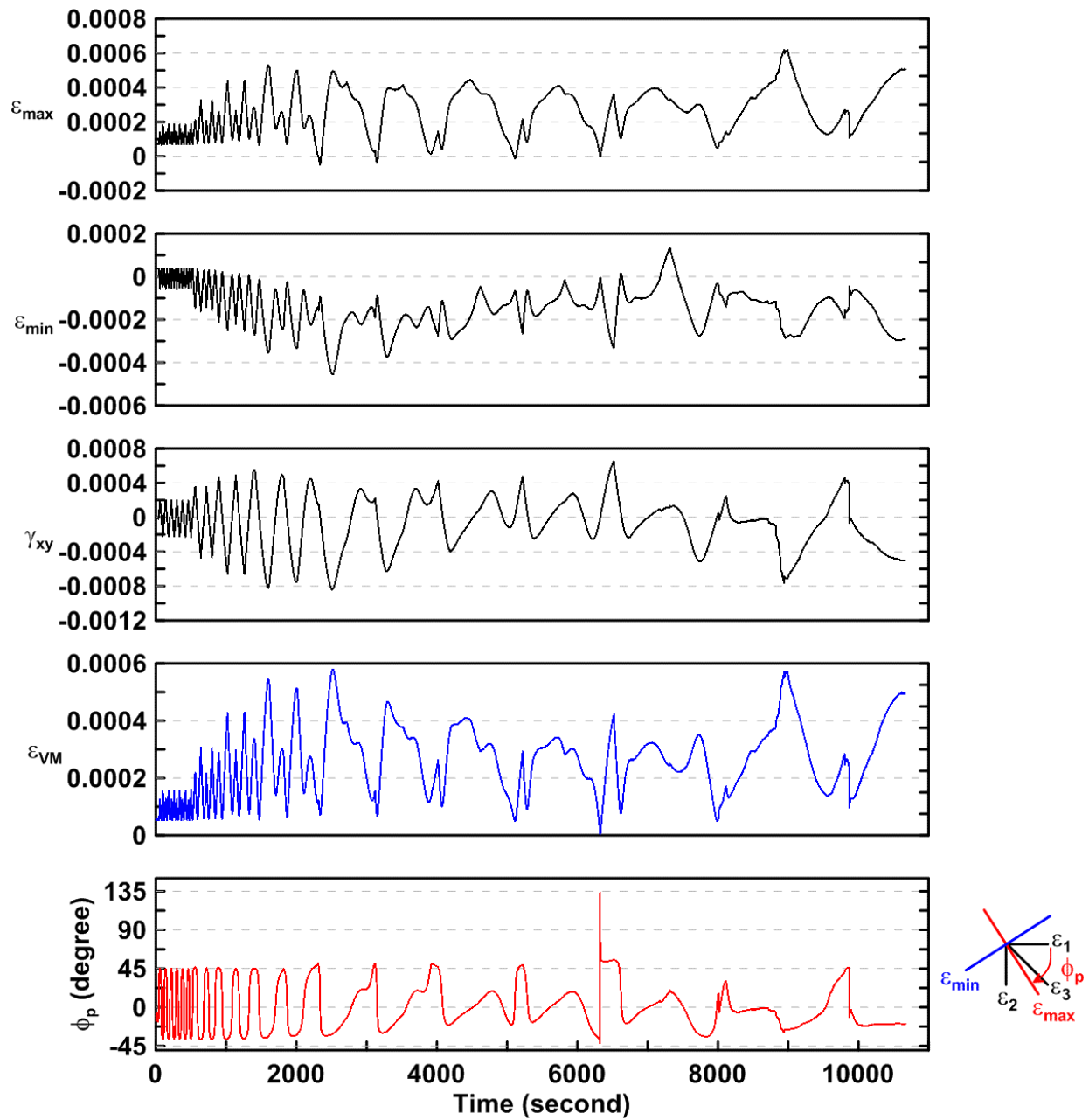


Figure 4.62 Time history of rosette type strain gauge readings in the one-piece gusset plate of TCBF-B-1 specimen (location: R14)

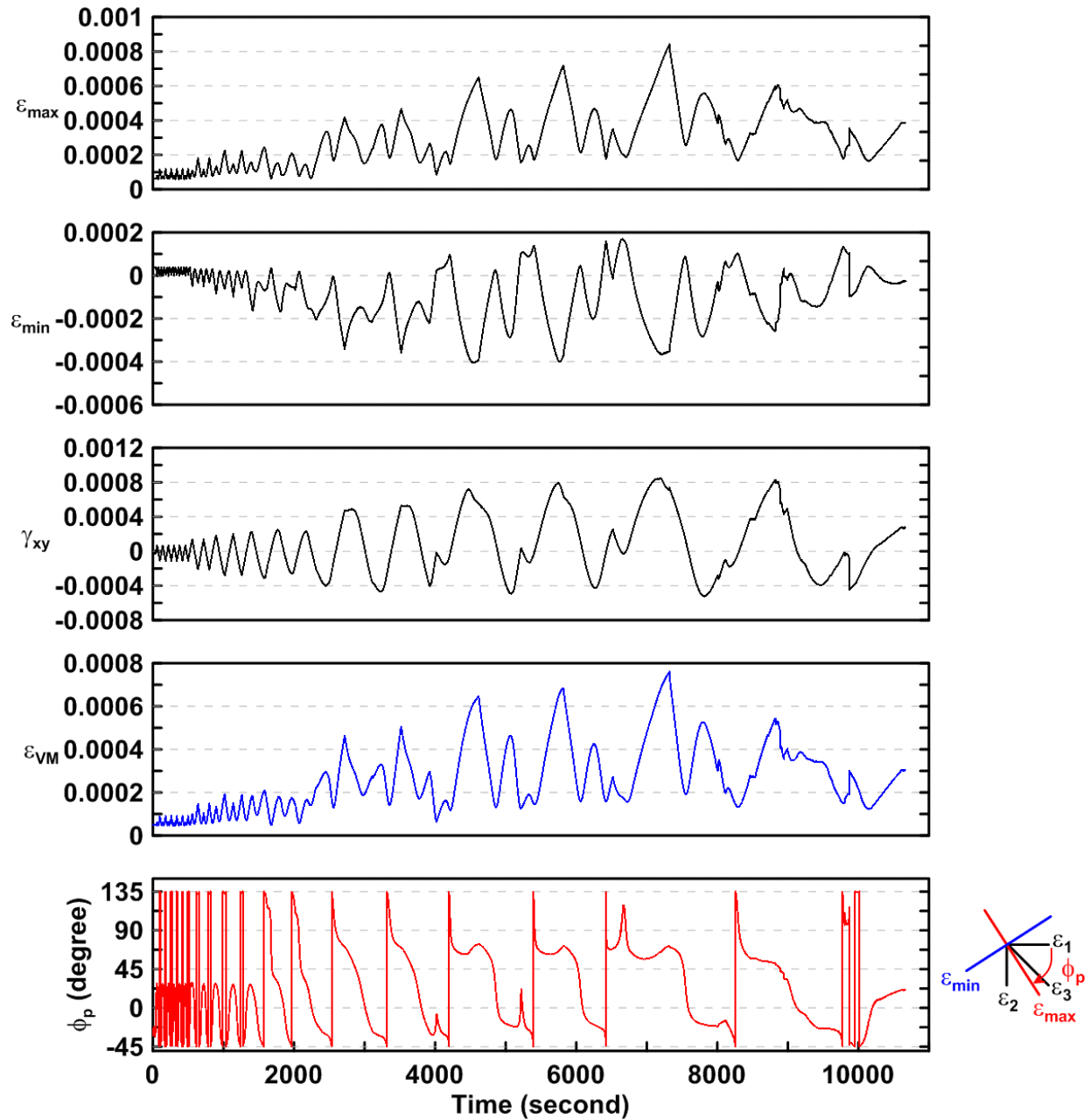


Figure 4.63 Time history of rosette type strain gauge readings in the one-piece gusset plate of TCBF-B-1 specimen (location: R15)

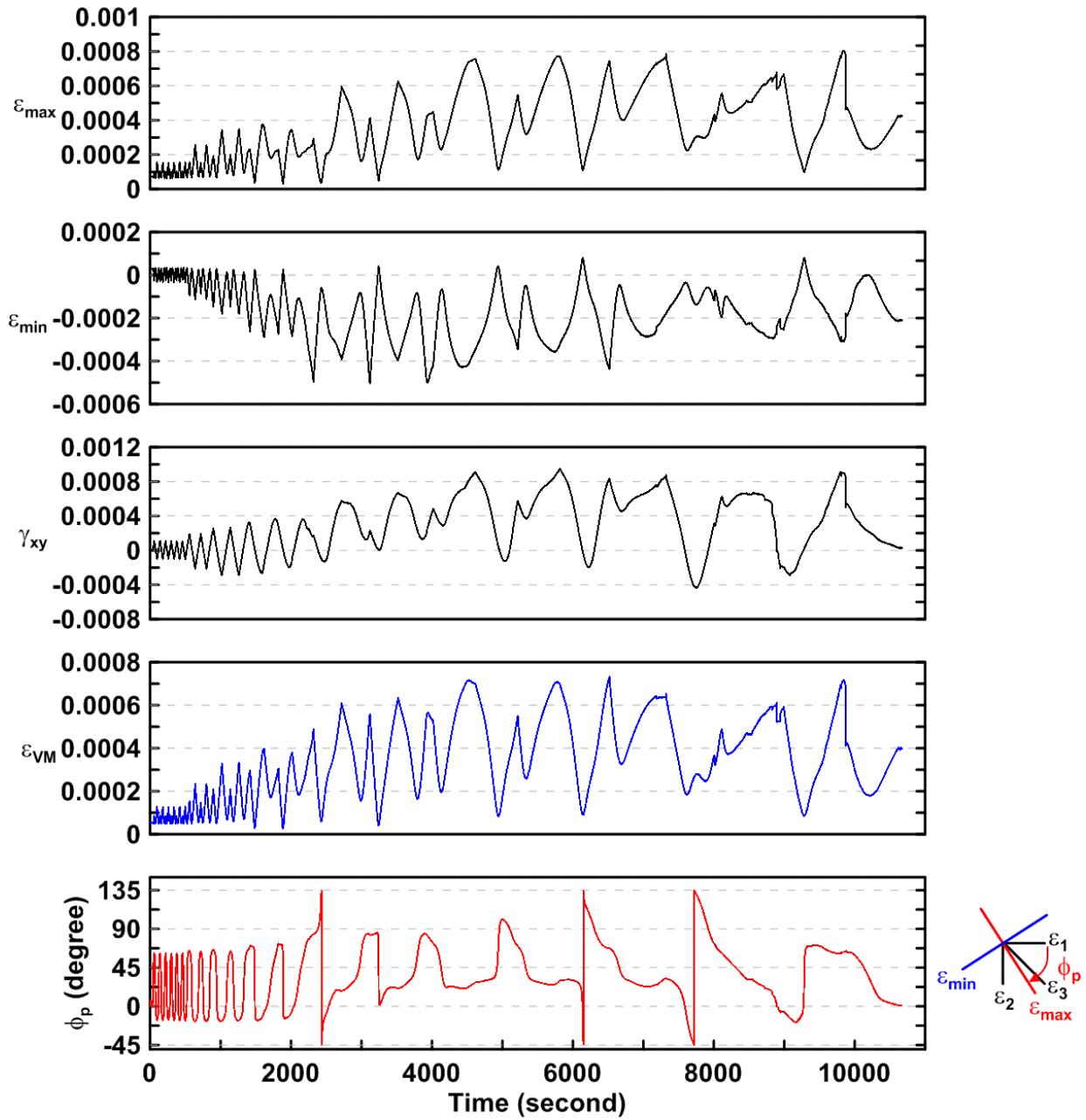


Figure 4.64 Time history of rosette type strain gauge readings in the one-piece gusset plate of TCBF-B-1 specimen (location: R16)

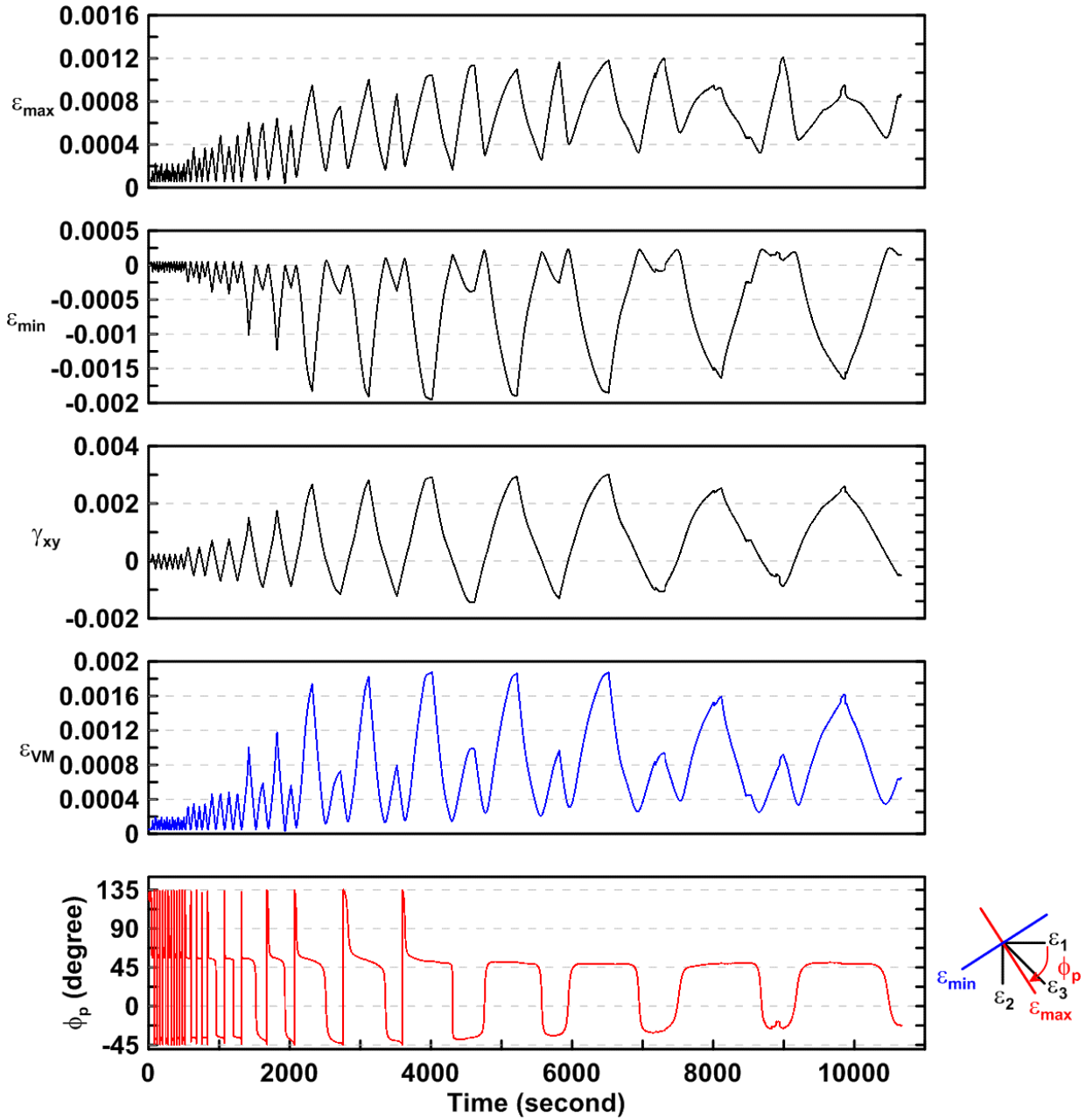


Figure 4.65 Time history of rosette type strain gauge readings in the one-piece gusset plate of TCBF-B-1 specimen (location: R17)

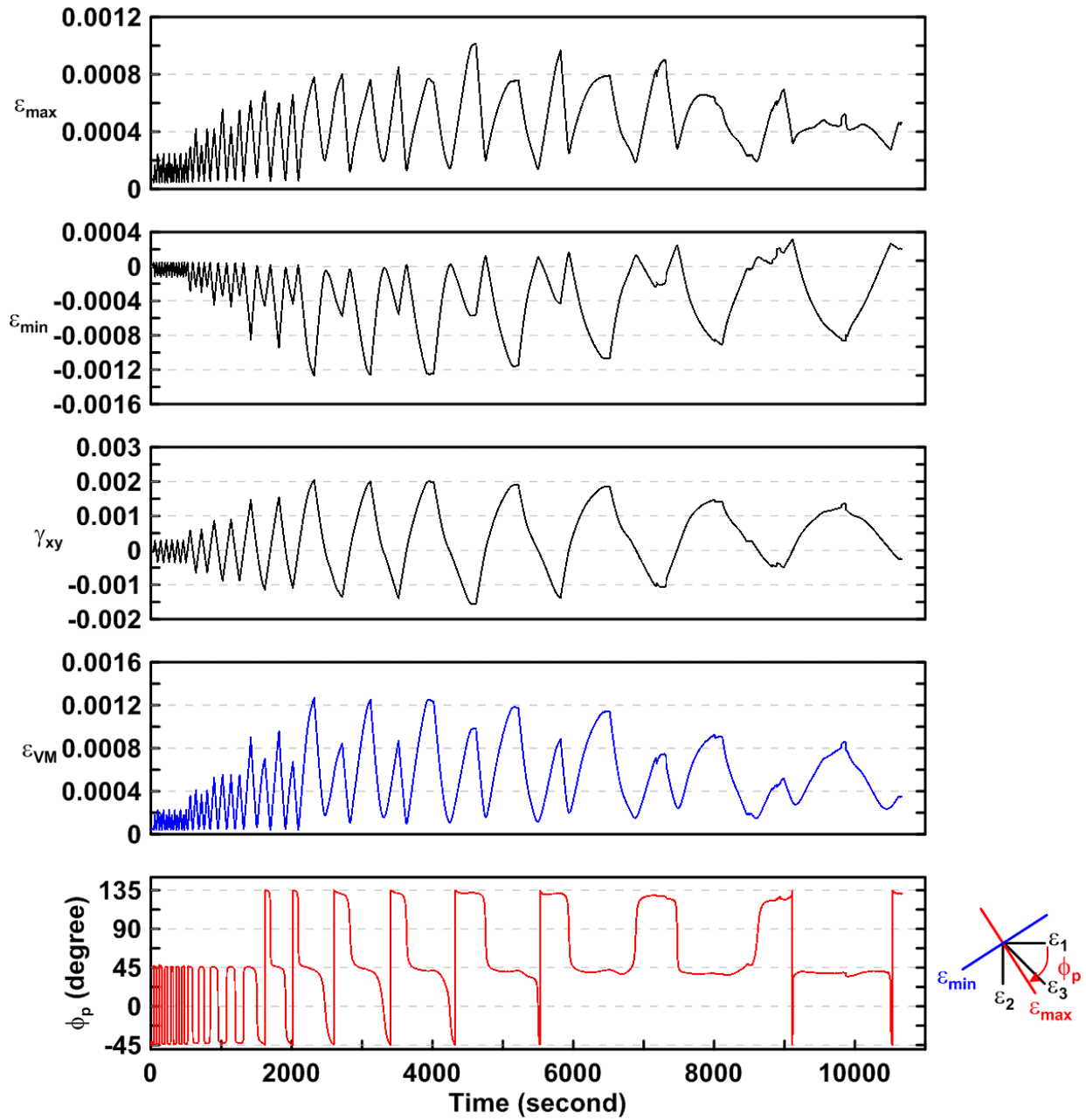


Figure 4.66 Time history of rosette type strain gauge readings in the one-piece gusset plate of TCBF-B-1 specimen (location: R18)



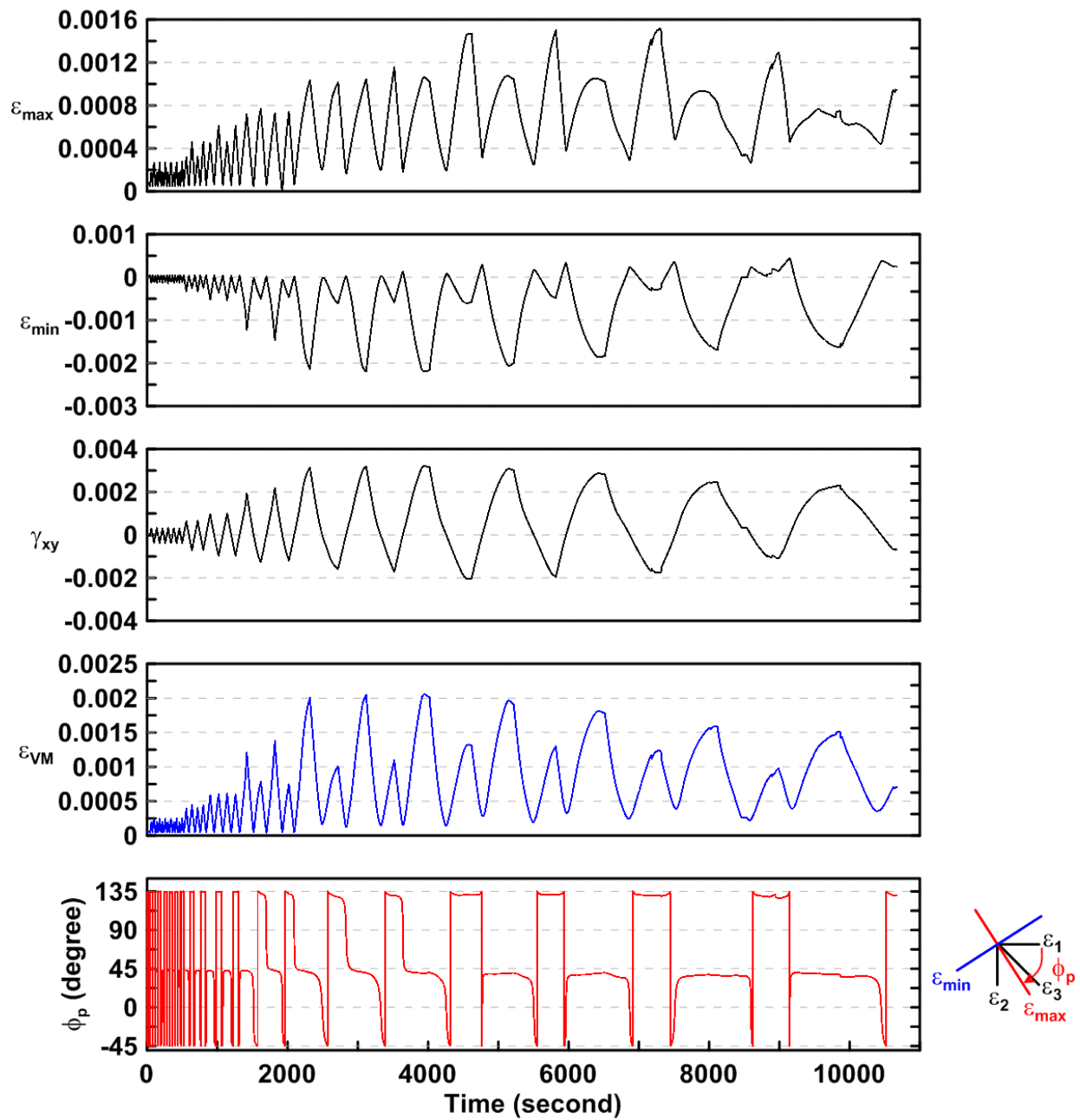


Figure 4.67 Time history of rosette type strain gauge readings in the one-piece gusset plate of TCBF-B-1 specimen (location: R19)

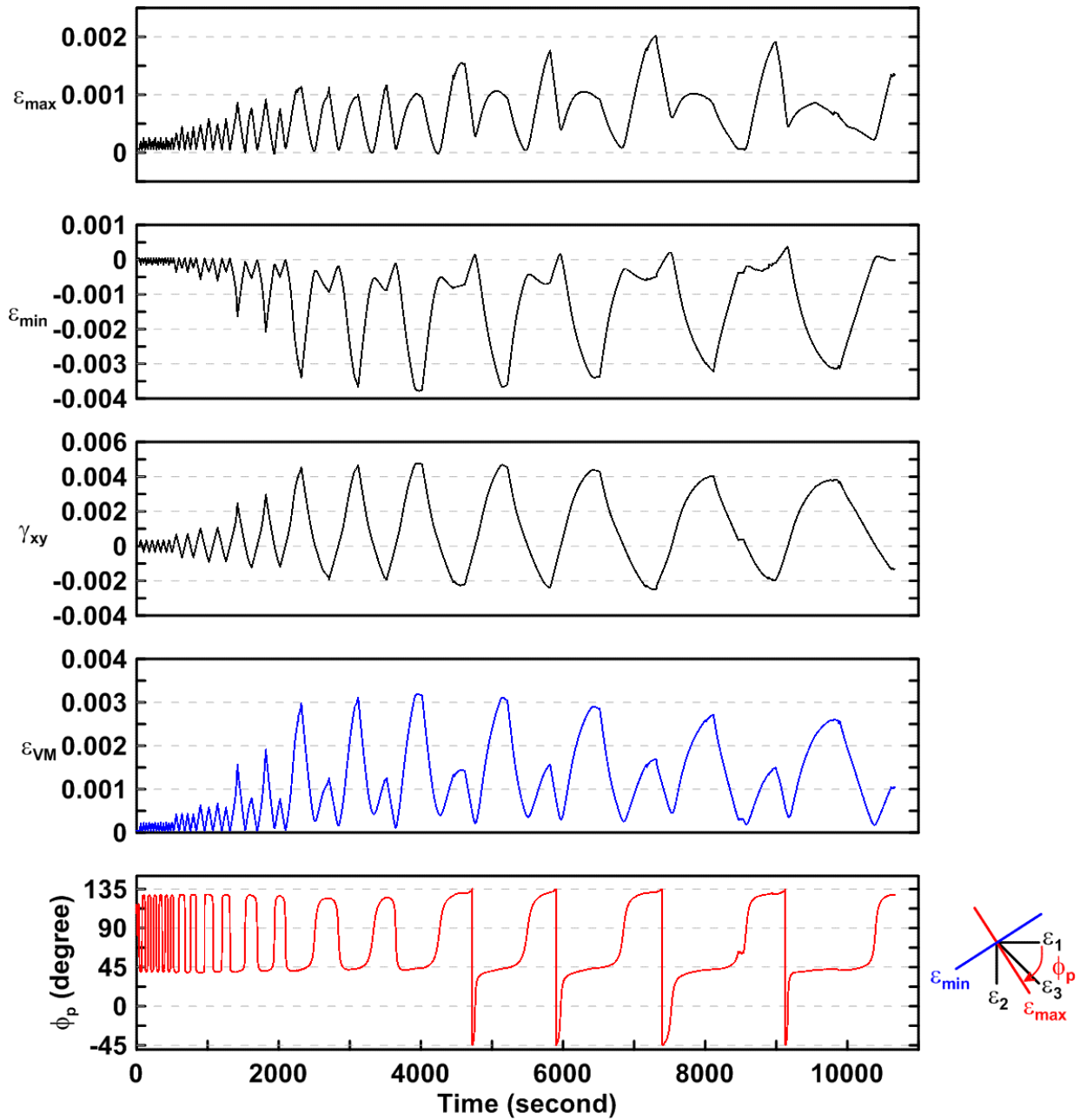


Figure 4.68 Time history of rosette type strain gauge readings in the one-piece gusset plate of TCBF-B-1 specimen (location: R20)

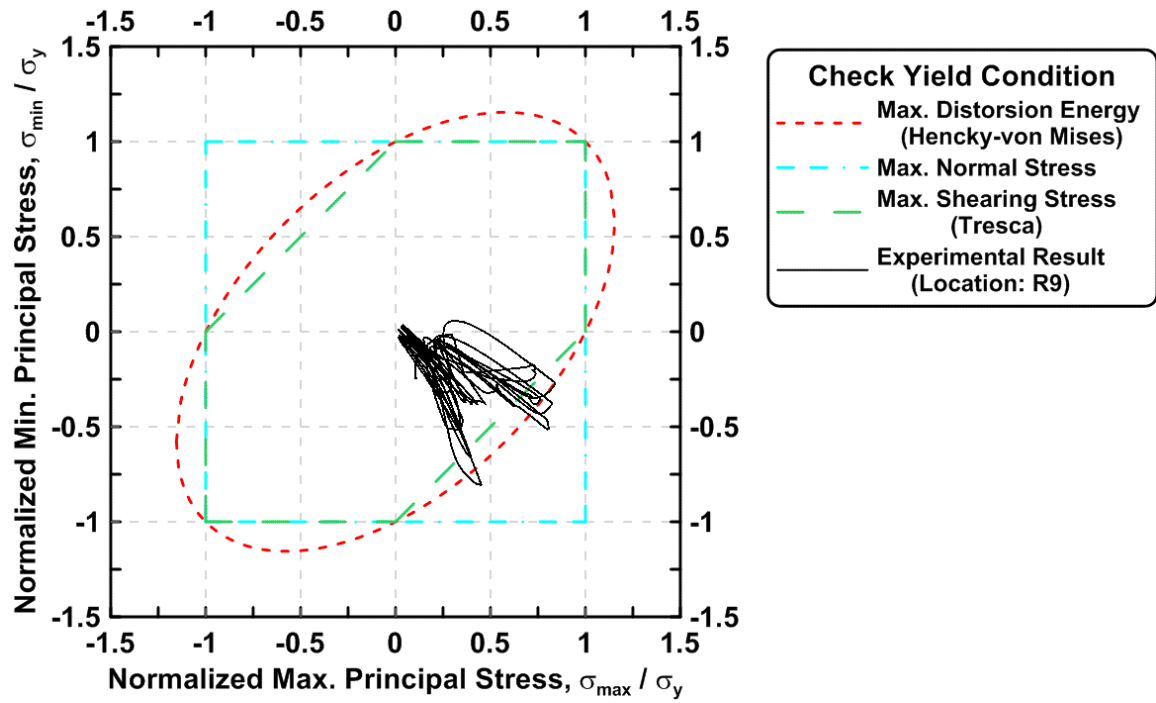


Figure 4.69 Normalized maximum principal stress vs. normalized minimum principal stress in the one-piece gusset plate of TCBF-B-1 specimen (location: R9)

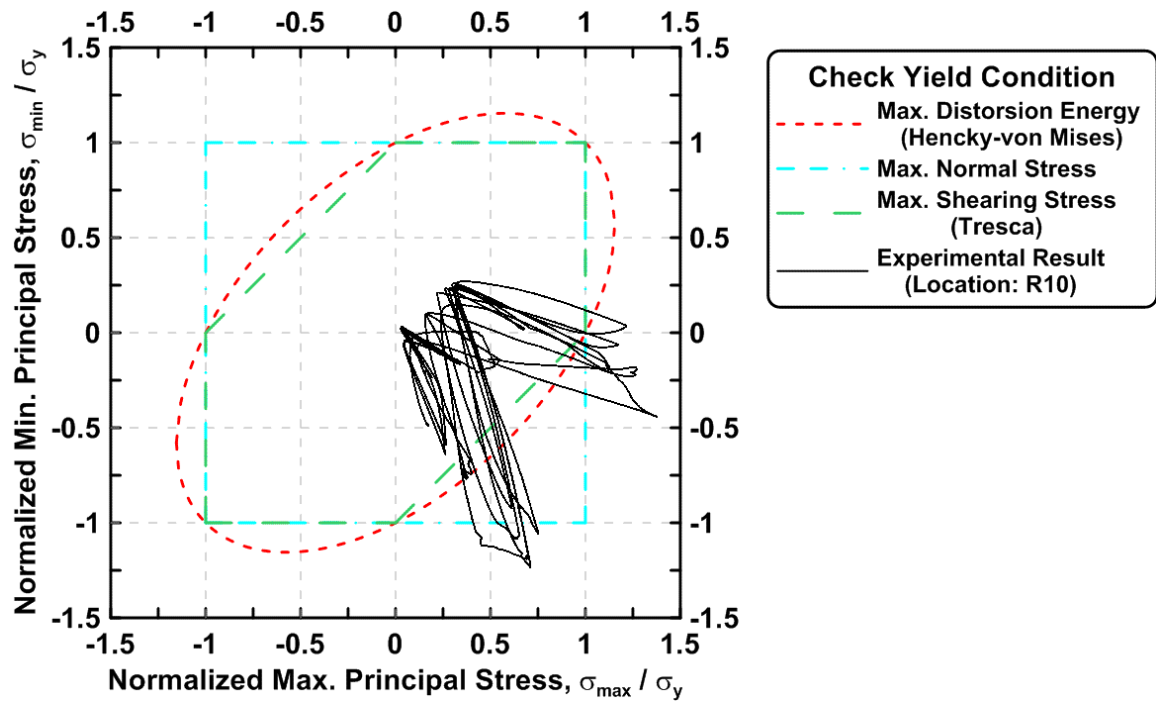


Figure 4.70 Normalized maximum principal stress vs. normalized minimum principal stress in the one-piece gusset plate of TCBF-B-1 specimen (location: R10)

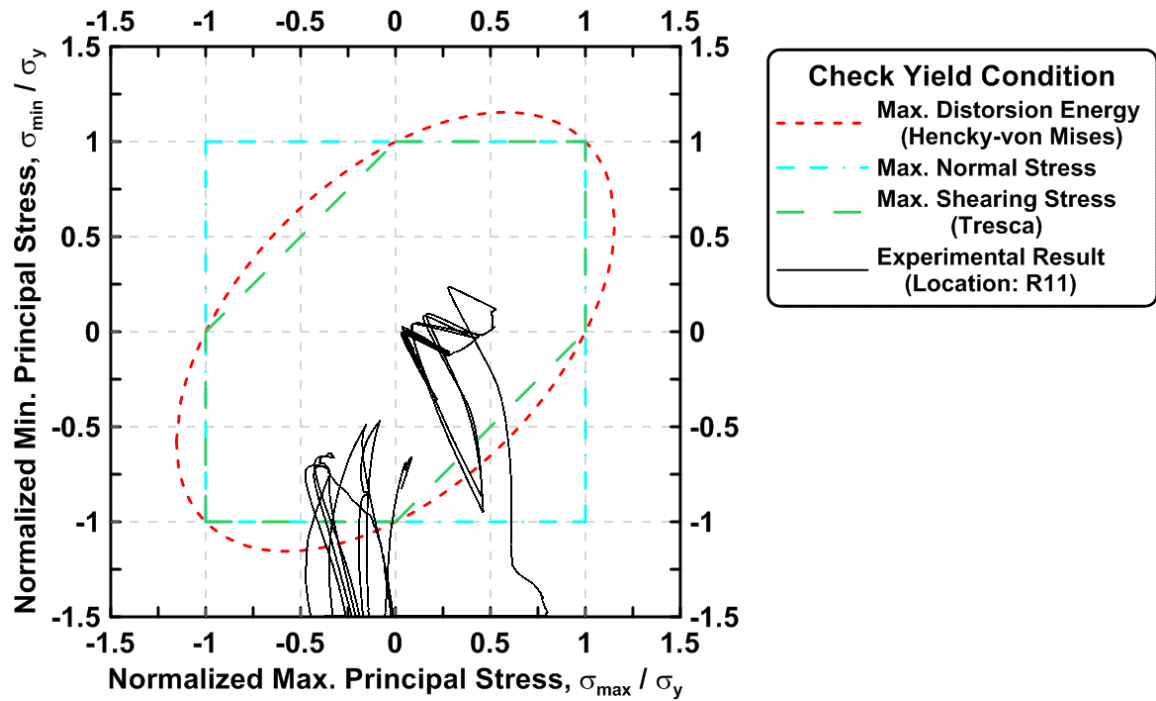


Figure 4.71 Normalized maximum principal stress vs. normalized minimum principal stress in the one-piece gusset plate of TCBF-B-1 specimen (location: R11)

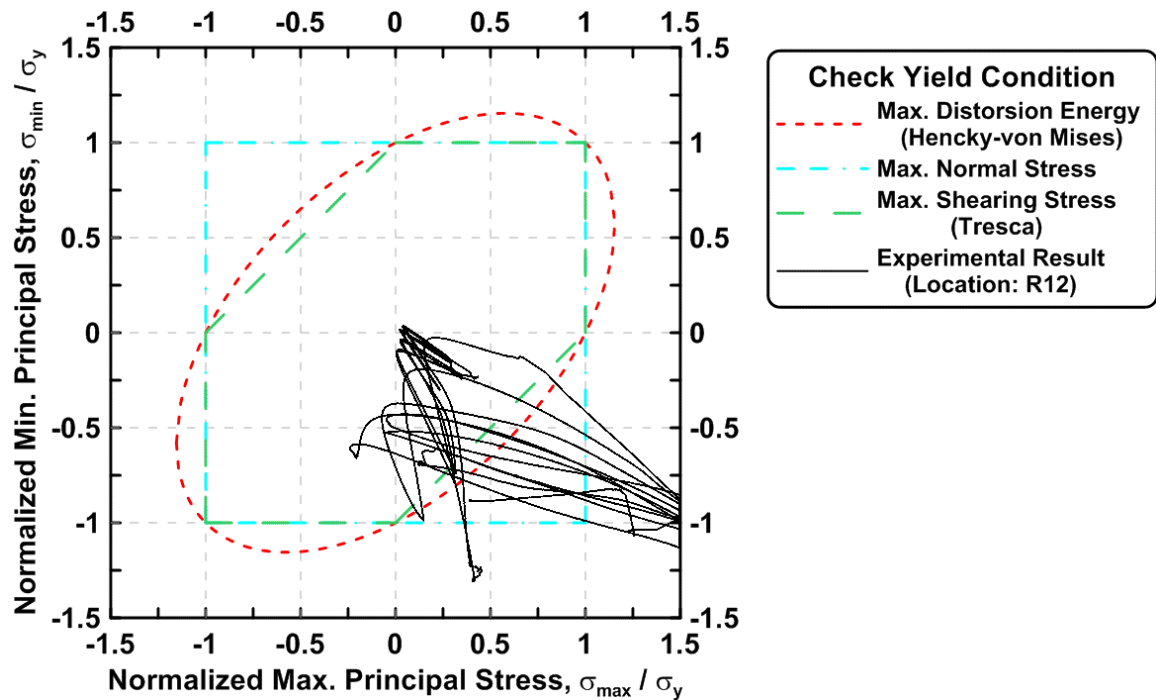


Figure 4.72 Normalized maximum principal stress vs. normalized minimum principal stress in the one-piece gusset plate of TCBF-B-1 specimen (location: R12)

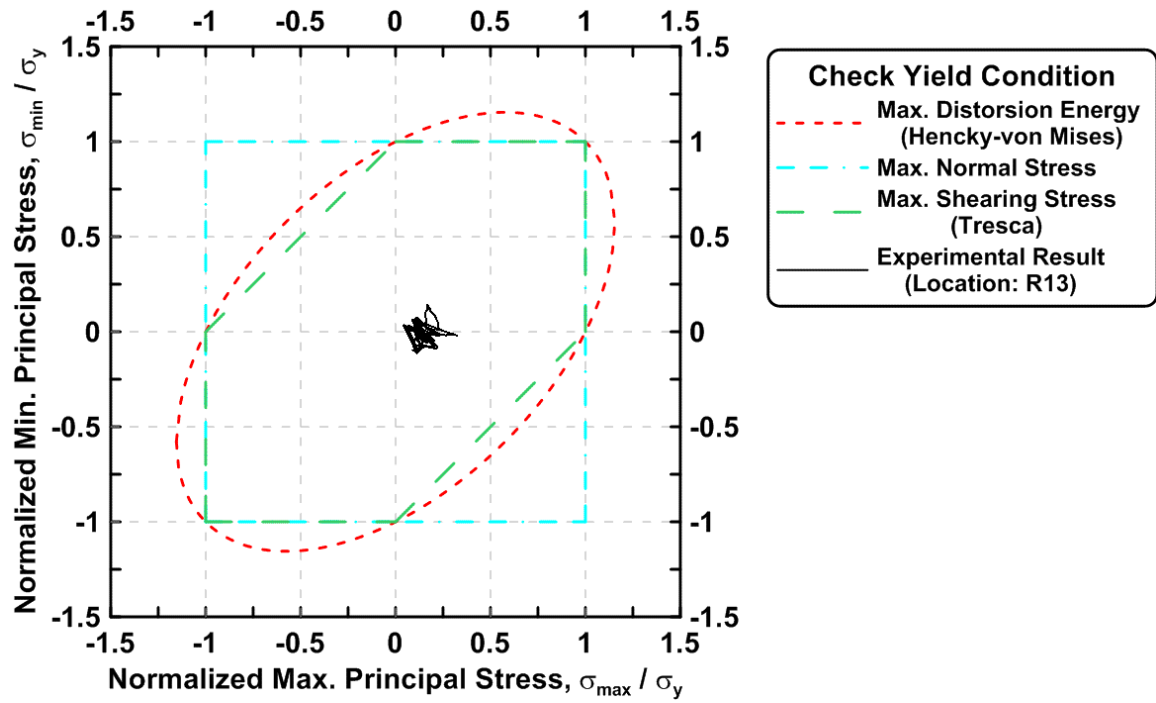


Figure 4.73 Normalized maximum principal stress vs. normalized minimum principal stress in the one-piece gusset plate of TCBF-B-1 specimen (location: R13)

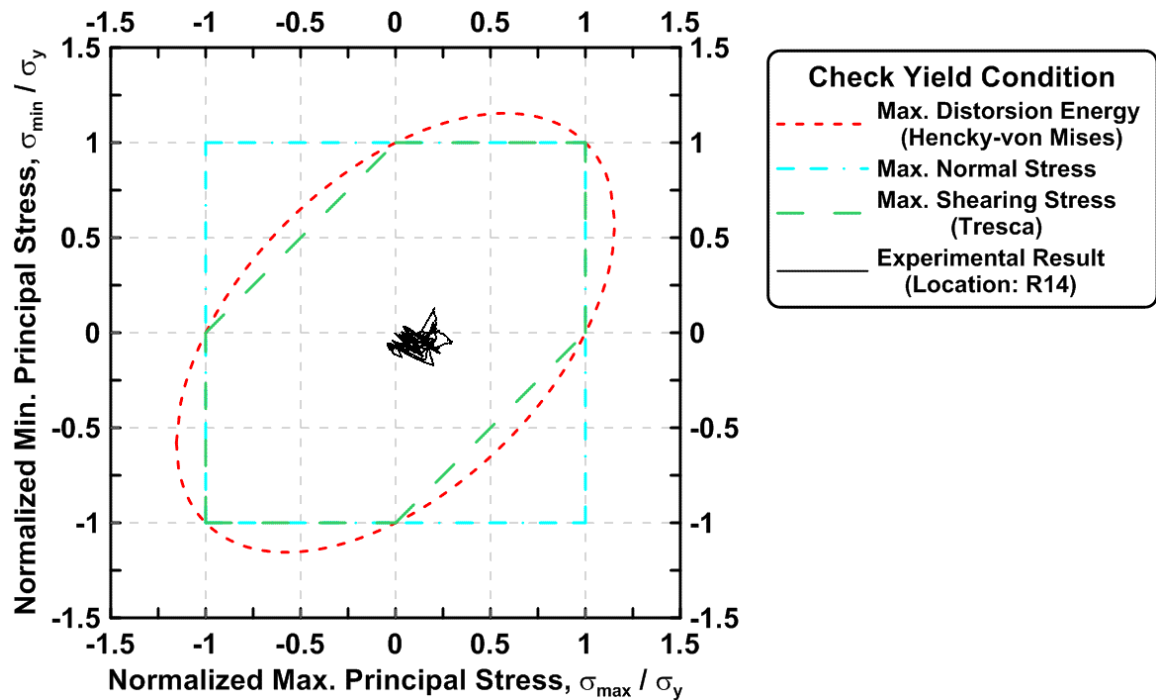


Figure 4.74 Normalized maximum principal stress vs. normalized minimum principal stress in the one-piece gusset plate of TCBF-B-1 specimen (location: R14)

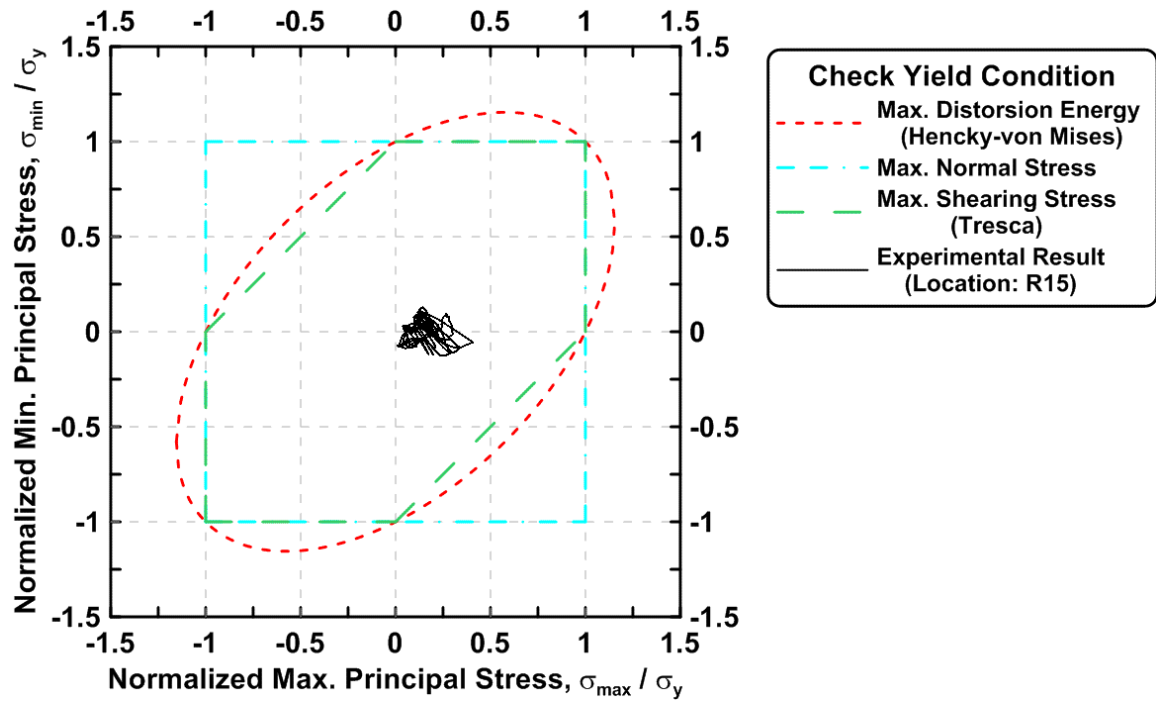


Figure 4.75 Normalized maximum principal stress vs. normalized minimum principal stress in the one-piece gusset plate of TCBF-B-1 specimen (location: R15)

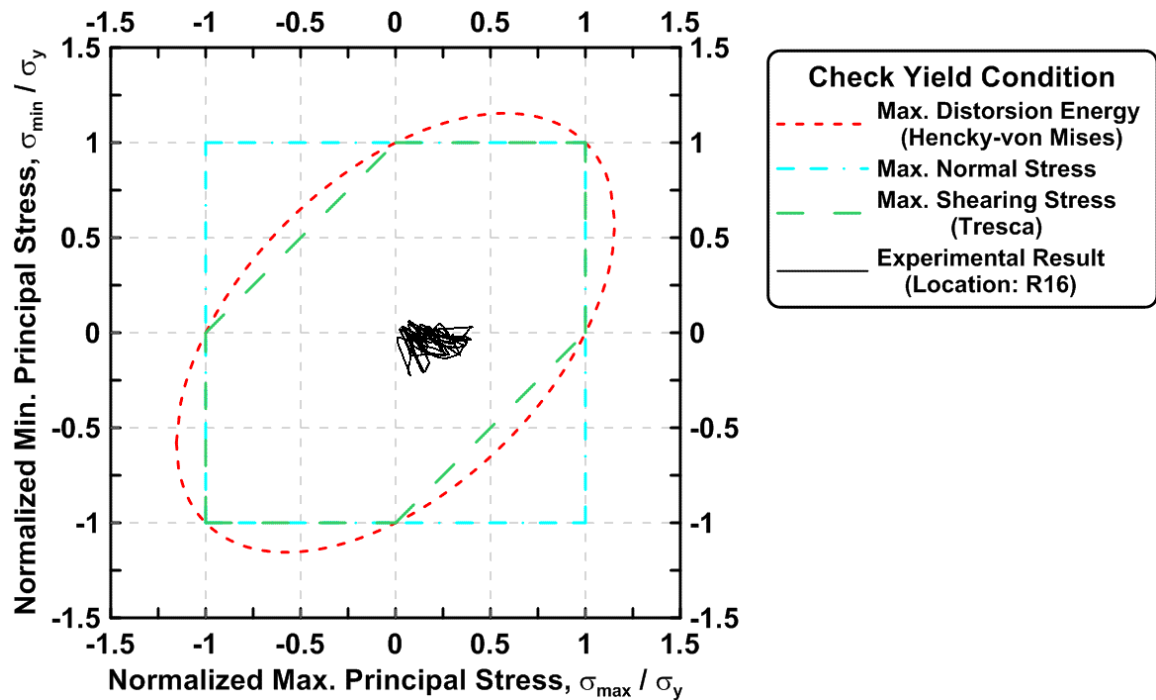


Figure 4.76 Normalized maximum principal stress vs. normalized minimum principal stress in the one-piece gusset plate of TCBF-B-1 specimen (location: R16)

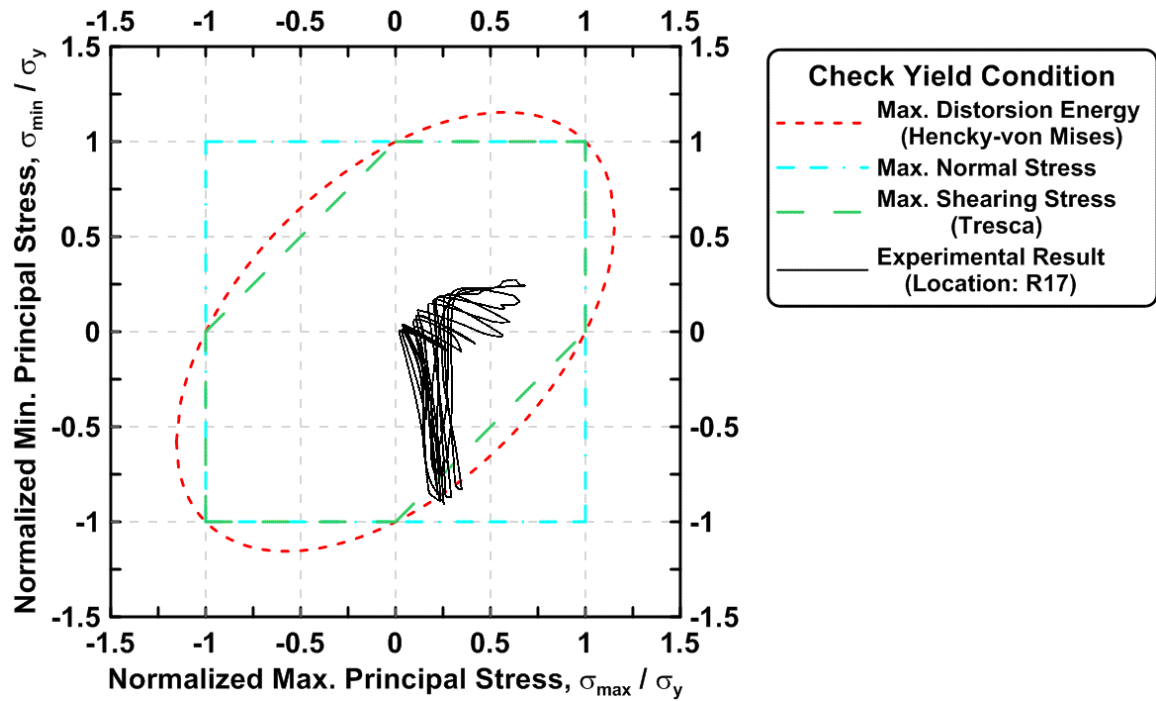


Figure 4.77 Normalized maximum principal stress vs. normalized minimum principal stress in the one-piece gusset plate of TCBF-B-1 specimen (location: R17)

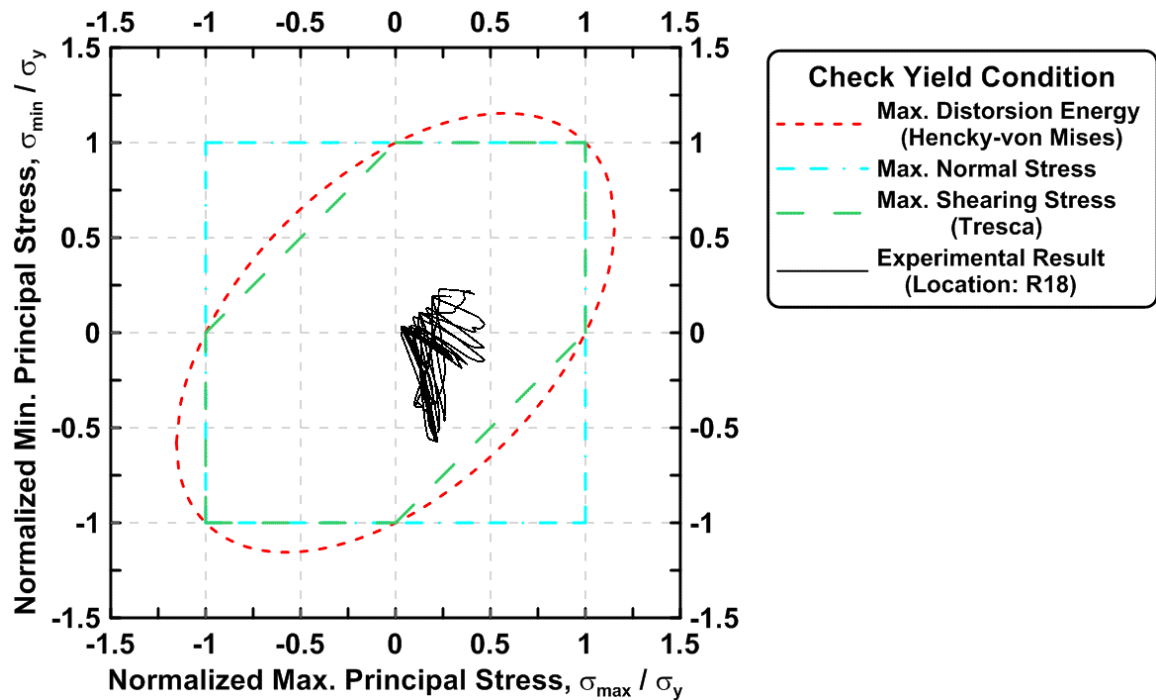


Figure 4.78 Normalized maximum principal stress vs. normalized minimum principal stress in the one-piece gusset plate of TCBF-B-1 specimen (location: R18)

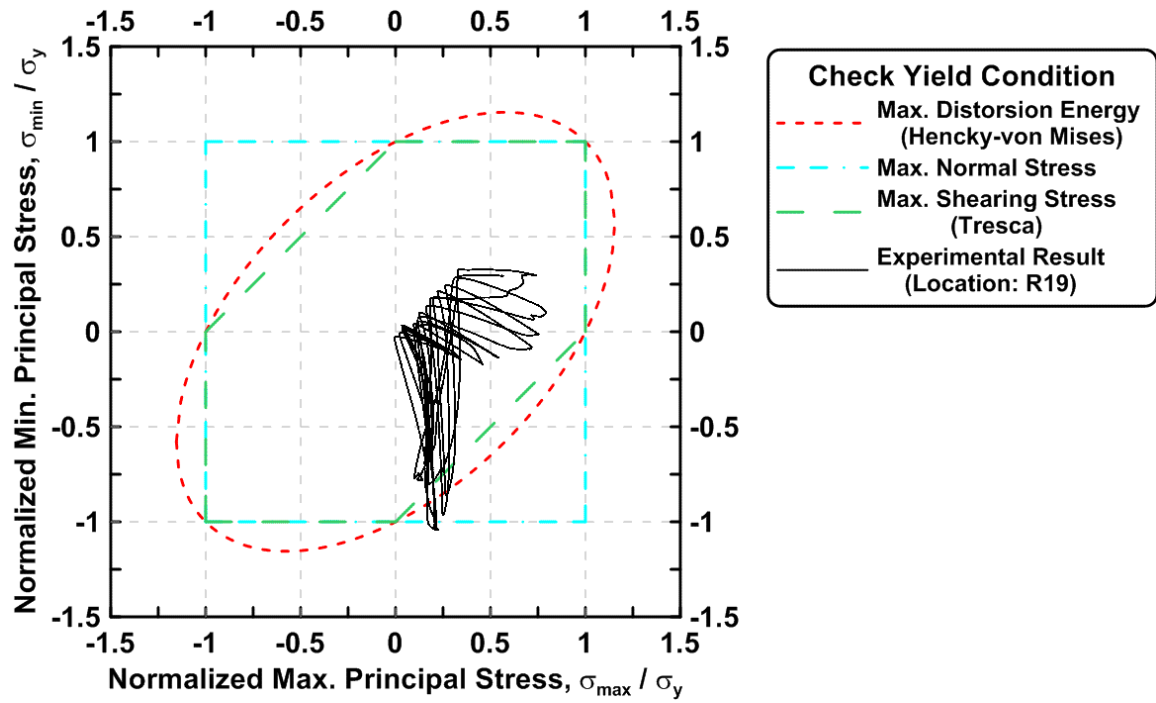


Figure 4.79 Normalized maximum principal stress vs. normalized minimum principal stress in the one-piece gusset plate of TCBF-B-1 specimen (location: R19)

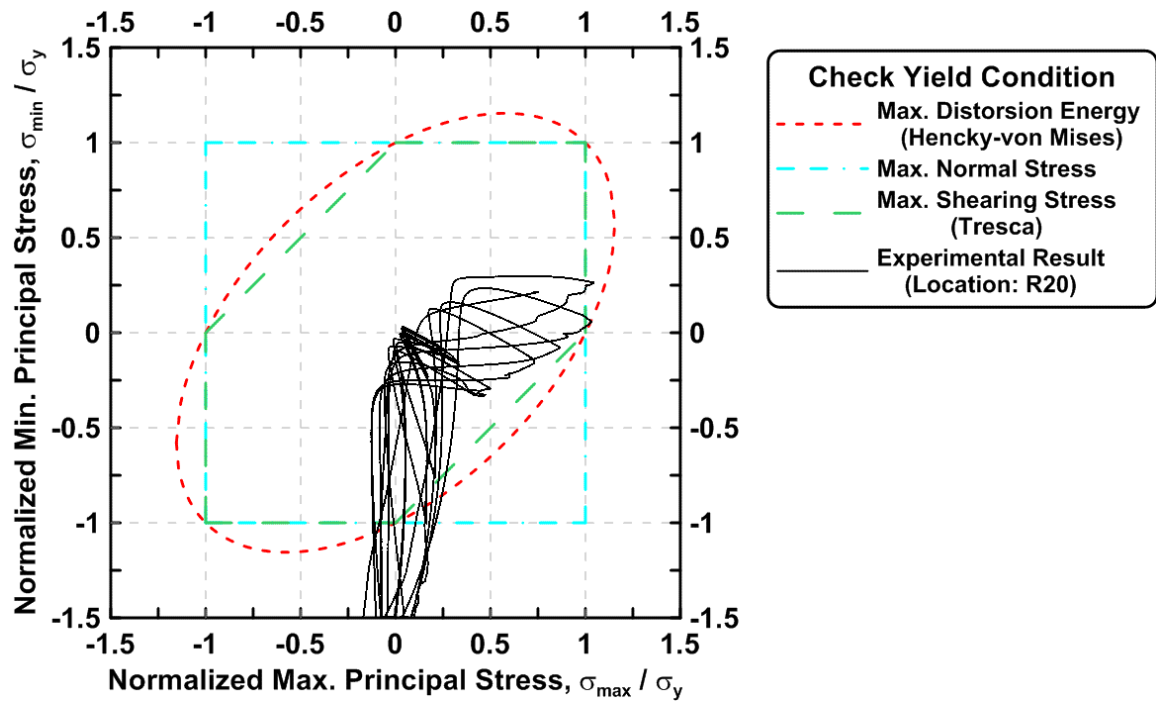


Figure 4.80 Normalized maximum principal stress vs. normalized minimum principal stress in the one-piece gusset plate of TCBF-B-1 specimen (location: R20)



#### 4.2.1.1.7 Test Setup Response

While the strong floor and reaction wall are relatively stiff, they do deform during the tests. To assess this, displacement transducers were attached to the laboratory building away from the reaction wall and used to measure the displacement of the brackets that supported the actuators in the direction of their applied load. The actuator bracket deformations versus actuator forces are plotted in Fig. 4.81. It can be seen that the reaction wall and strong floor are distorting relative to the building. The building of course is likely deforming as well. The relative displacement time history between base plates of the specimen and the floor beam, relative displacement time history between floor beam and strong floor, and relative displacement time history between integrated reconfigurable reaction wall and strong floor at northern and southern sides are shown in Fig. 4.82. The out-of-plane deformation time history of the lateral supporting frame with respect to the wall of the building at different locations are plotted in Fig. 4.83.

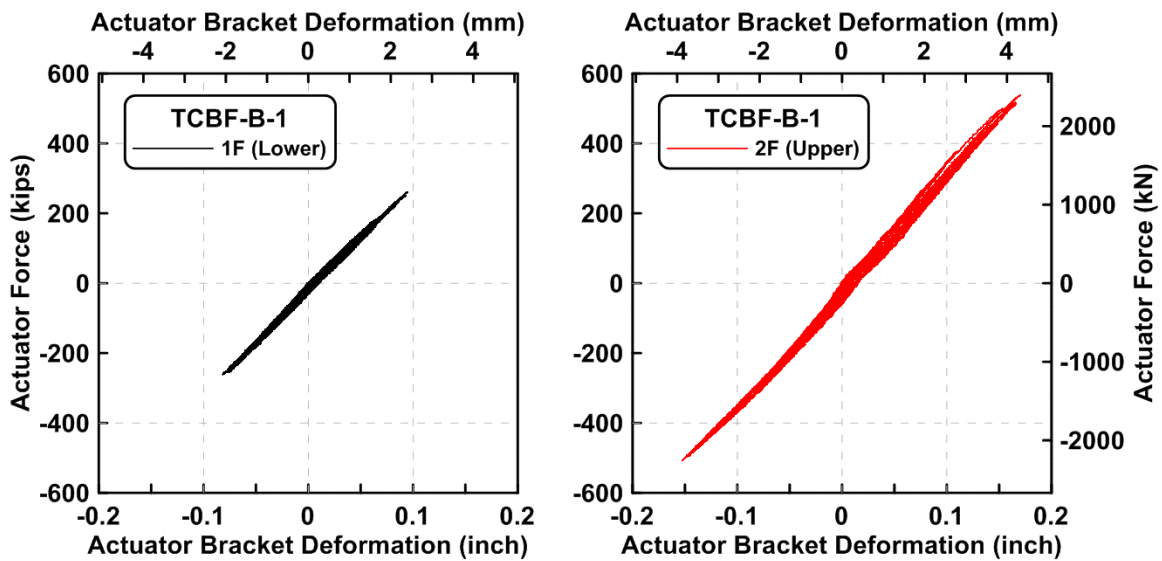


Figure 4.81 The actuator force vs. bracket deformation relationship at both floor levels during specimen TCBF-B-1 test

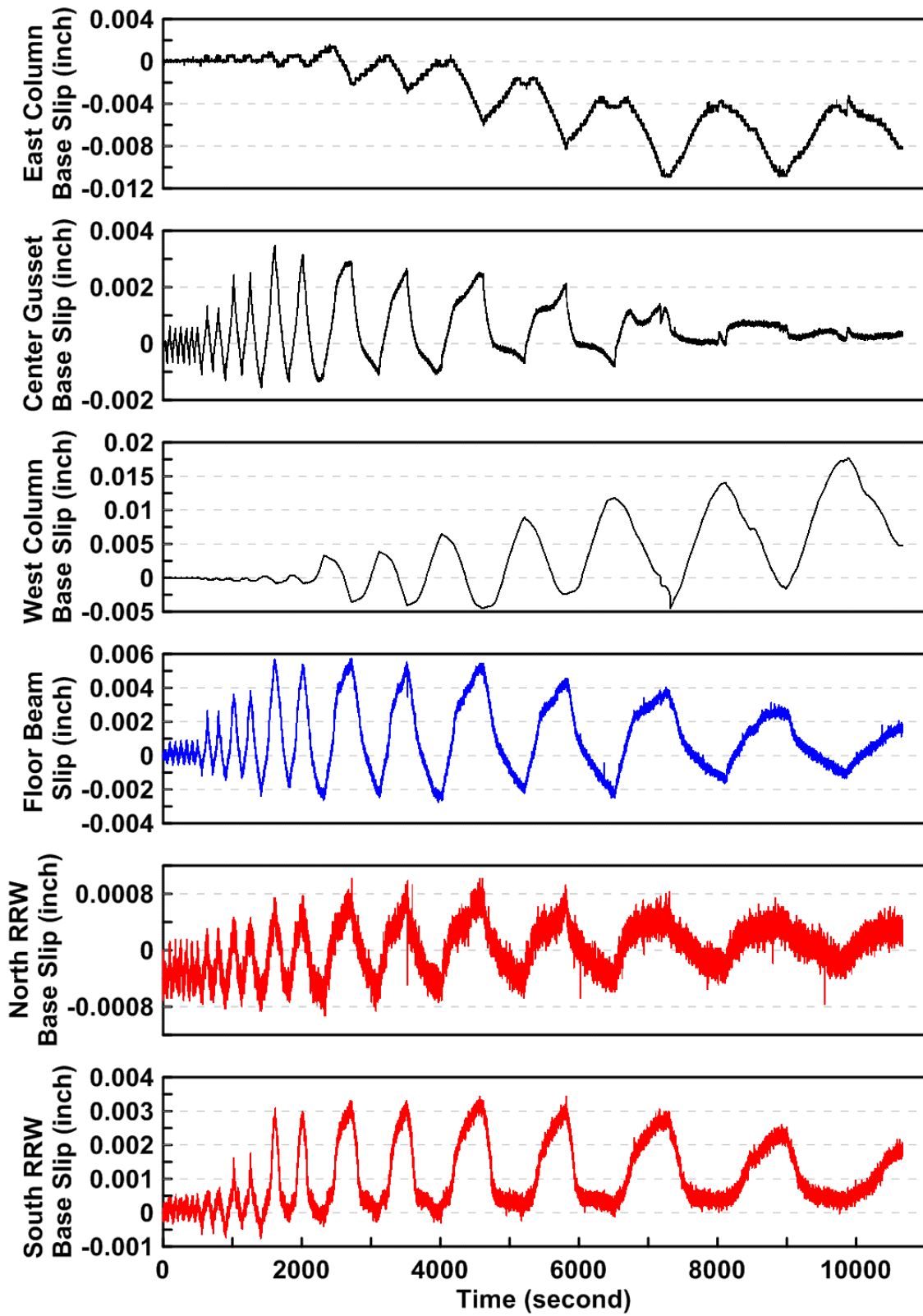


Figure 4.82 Slippage time history between specimen and test setup boundaries during specimen TCBF-B-1 test

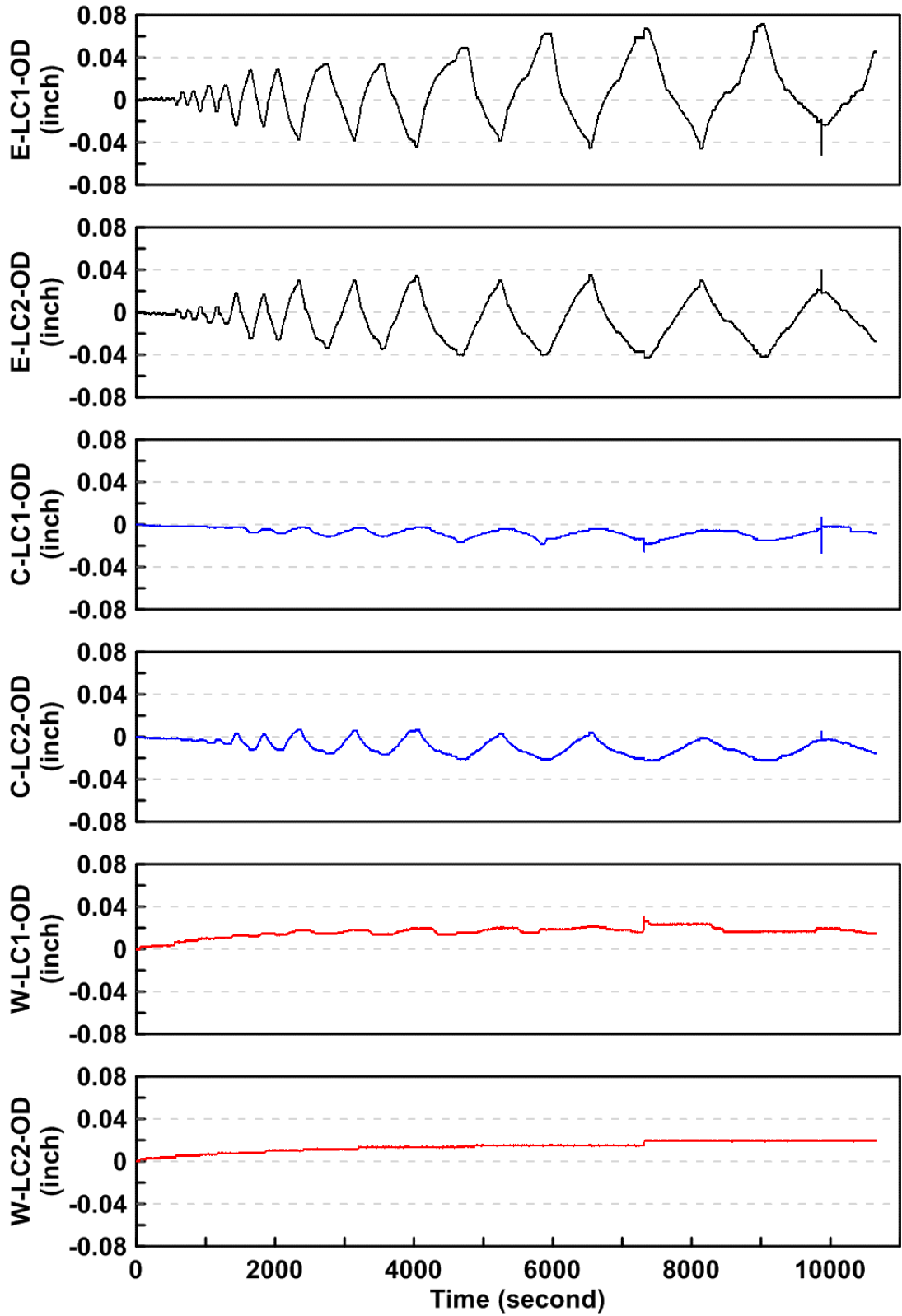


Figure 4.83 The out-of-plane deformation time history of lateral supporting frame at different monitoring points during specimen TCBF-B-1 test

#### **4.2.1.2 Main Observations**

As illustrated in the pre-defined loading protocol in Fig. 3.28, the experiment process was divided into several sets of loading steps (amplitudes or phases). Every loading step contained two complete cycles except that the first loading step ( $0.5D_{be}$ ) contained six complete cycles. Detailed information about each of these cycles is described sequentially below. Some key observations are illustrated on the testing protocol and listed with brief descriptions in Table 4.2.

##### **$\Delta = 0.5 D_{be} = 0.2$ inch (Roof Drift $\delta = 0.1$ %), from 1:06 PM to 1:14 PM**

The test began at 1:06 PM after two small cycles were completed and every instrument readings were carefully checked. During this loading amplitude, the entire frame remained elastic. No special findings were found anywhere through this loading step.

##### **$\Delta = 1.0 D_{be} = 0.4$ inch (Roof Drift $\delta = 0.2$ %), from 1:14 PM to 1:19 PM**

Very minor yielding (determined from visible flaking of whitewash) was noted near the tip of fillet welds at the brace-to-gusset plate connection at first-story gusset plate, as illustrated in Fig. 4.84.

##### **$\Delta = 1.0 D_{by} = 0.6$ inch (Roof Drift $\delta = 0.3$ %), from 1:19 PM to 1:27 PM**

Some local flaking of whitewash developed near the beginning of  $30^\circ$  tapered region of gusset plate at first story (Fig. 4.85).

##### **$\Delta = 0.5 D_{bm} = 1.0$ inch (Roof Drift $\delta = 0.5$ %), from 1:27 PM to 1:40 PM**

At the beginning of the first half cycle of the loading step, some local flaking of the whitewash developed near the backing bar on the bottom flange of middle beam at eastern side (Fig. 4.86). Additional flaking of the whitewash in the top and bottom flanges was found near the backing bar at both sides of lower beam. Some local flaking of whitewash developed near the  $30^\circ$  tapered region of eastern gusset plate at the second story (Fig. 4.87(a)). The braces at both stories started global buckling (all out-of-plane to the north), and the whitewash on braces began flaking (Fig. 4.87(b)). Additional flaking developed on the gusset plates.

##### **$\Delta = 1.0 D_{bm} = 2.0$ inch (Roof Drift $\delta = 0.9$ %), from 1:40 PM to 2:07 PM**

At the beginning of the first half cycle of this loading step, some flaking of whitewash developed on the one-piece gusset plate near gusset-to-column flange welds at eastern side and the lower beam web closed to the shear tab (Fig. 4.88). Additional flaking developed in panel zone area and the  $2t$  gap region on the gusset plates. Minor yielding was noted in the column flanges near the base plates (Fig. 4.89).

##### **$\Delta = 1.5 D_{bm} = 3.0$ inch (Roof Drift $\delta = 1.4$ %), from 2:07 PM to 2:47 PM**

Near the end of the first half cycle of this loading step, the top flange and web of lower beam at western side began localized buckling (Fig. 4.90). Local buckling of section walls was also found at the middle portion of the brace (Fig. 4.91). Additional flaking of whitewash developed on the gusset plate  $2t$  gap fold region. The bottom flange and web of lower beam at eastern side began localized buckling (Fig. 4.92). The lower beam formed plastic hinges at both ends. Additional flaking of whitewash developed on the column flanges near the base plate. At the beginning of the third half cycle of the loading step, lots of flaking of whitewash occurred on lower story column flanges near gusset plate stiffener plates, as shown in Fig. 4.93.

##### **$\Delta = 2.0 D_{bm} = 4.0$ inch (Roof Drift $\delta = 1.9$ %), from 2:47 PM to 3:40 PM**

Near the peak displacement of the loading step in the first half cycle, cracks initiated in the outside corners of HSS brace section at first story for both braces (see Figs. 4.94 and 4.95). When the specimen moved across zero roof displacement and continued moving to the west, the

cracks in the first-story western brace propagated from the outside corners to the center of the HSS brace section during the second half cycle of the load step as shown in Fig. 4.96. At around negative 2-in. roof displacement, a lot of flaking of whitewash occurred on the web of western and eastern columns at the first story (Fig. 4.97). The western brace at ground story completely fractured during the first half cycle of loading to a roof displacement of 3.8 in. to the west (Fig. 4.98). The eastern brace at the ground story had cracks on the outside corner of the HSS section around the middle portion of the brace but did not completely fracture. Crack initiated at the outside corner of HSS brace section at second story for both braces. The bottom flange at eastern side of lower beam fractured at the CJP weld line during the second cycle of this load step at roof displacement about 3.8 in. to the west (Fig. 4.99).

**$\Delta = 2.5 D_{bm} = 5.0$  inch (Roof Drift  $\delta = 2.3$  %), from 3:40 PM to 4:02 PM**

The eastern brace at first story completely fractured during the first cycle of  $2.5D_{bm}$  load step at a roof displacement corresponding to 4.7 in. to the east (Fig. 4.100). The cracks in the second story eastern brace propagated from outside corners to the center of the HSS brace section during the first cycle of  $2.5D_{bm}$  load step (Fig. 4.101) but did not completely fracture. The test was manually stopped (the yellow button of controller was pressed) at about 2.2 in. of roof displacement to the west (so that the specimen could be unloaded to about zero lateral displacement) after unloading the entire specimen. The entire side view of the specimen after test is shown in Fig. 4.102.

**Table 4.2 The major observations during specimen TCBF-B-1 test**

<b>Major Observations</b>	
1	No special findings through this loading step.
2	Very minor yielding (via. flaking of whitewash) was noted near the tip of fillet welds at brace-to-gusset connection at first story gusset plate.
3	Some local flaking of whitewash developed near the beginning of the 30° tapered region of gusset plates at first story.
4	Some local flaking of whitewash developed near the backing bar on the bottom flange of middle beam at eastern side.
5	Some local flaking of whitewash developed near the 30° tapered region of eastern gusset plate at second story. The braces at both story start global buckling and the whitewash on braces start flaking (all out-of-plane to the north side). Additional flaking develops on the gusset plates.
6	Some flaking of whitewash developed on the one-piece gusset plate near gusset-to-column flange welds at eastern side and the lower beam web closed to the shear tab. Additional flaking developed in panel zone area, and the 2t gap region on the gusset plates. Minor yielding was noted in the column flanges near the base plates.
7	The top flange and web of lower beam at western side start local buckling. The braces start local buckling at the middle portion of the brace. Additional flaking of whitewash developed on the gusset plate 2t gap fold region. The bottom flange and web of lower beam at eastern side start local buckling (Fig. 4.90). The lower beam formed plastic hinges at both ends. Additional flaking of whitewash developed on the column flanges near base plate.
8	Lots of flaking of whitewash occurred on lower story column flanges near gusset plate stiffener plates.
9	Crack initiated in the outside corner of HSS brace section at first story for both braces.
10	The cracks in the first story western brace propagated from outside corners to the center of the HSS brace section during the first cycle of the load step (Fig. 4.95).
11	Lots of flaking of whitewash occurred on the web of western and eastern columns at the first story.
12	The western brace at ground story completely fractured during the first half cycle of loading

	to a roof displacement of 3.8 inch to the west. The eastern brace at the ground story has cracks on the outside corner of the HSS section around the middle portion of the brace but did not completely fracture. Crack initiated at the outside corner of HSS brace section at second story for both braces.
13	The bottom flange at eastern side of lower beam fractured at the CJP weld line during the second cycle of $2.0 D_{bm}$ load step at roof displacement about 3.8 inch to the west (Fig. 4.99).
14	The eastern brace at first story completely fractured during the first cycle of $2.5 D_{bm}$ load step at roof displacement corresponded to 4.7 inch to the east (Fig. 4.100).
15	The cracks in the second story eastern brace propagated from outside corners to the center of the HSS brace section during the first cycle of $2.5 D_{bm}$ load step. Test stopped at about 2.2 inch of roof displacement to the west (to have specimen unload to about zero lateral displacement).

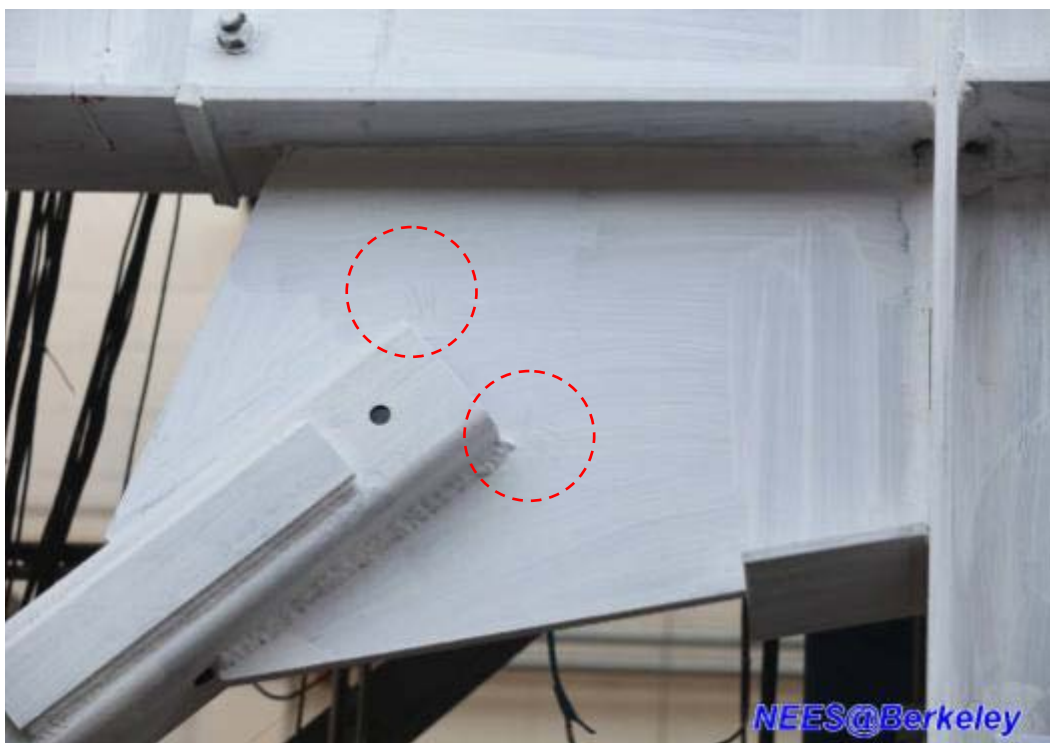


**Figure 4.84 Western side of the upper gusset plate in the first story of TCBF-B-1 specimen**

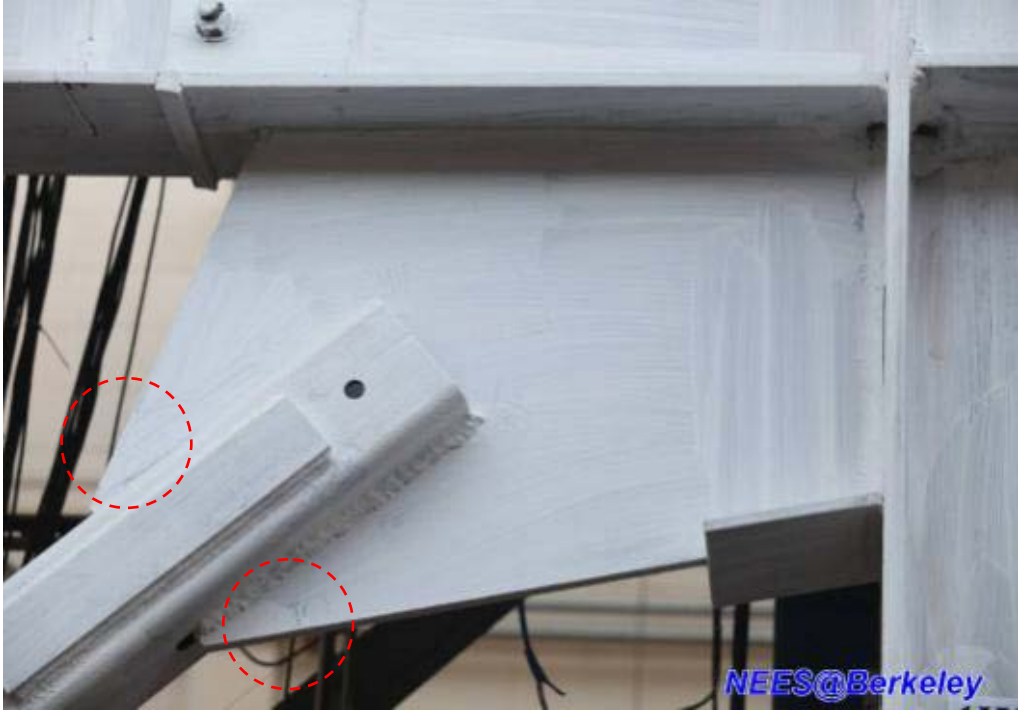


**Figure 4.85** Western side of the upper gusset plate in the first story of TCBF-B-1 specimen



**Figure 4.86** The bottom flange of east side lower beam of TCBF-B-1 specimen





**Figure 4.87(a) The flaking of whitewash at second story gusset plate of TCBF-B-1 specimen**



**Figure 4.87(b)** The flaking of whitewash at the middle length of braces of TCBF-B-1 specimen

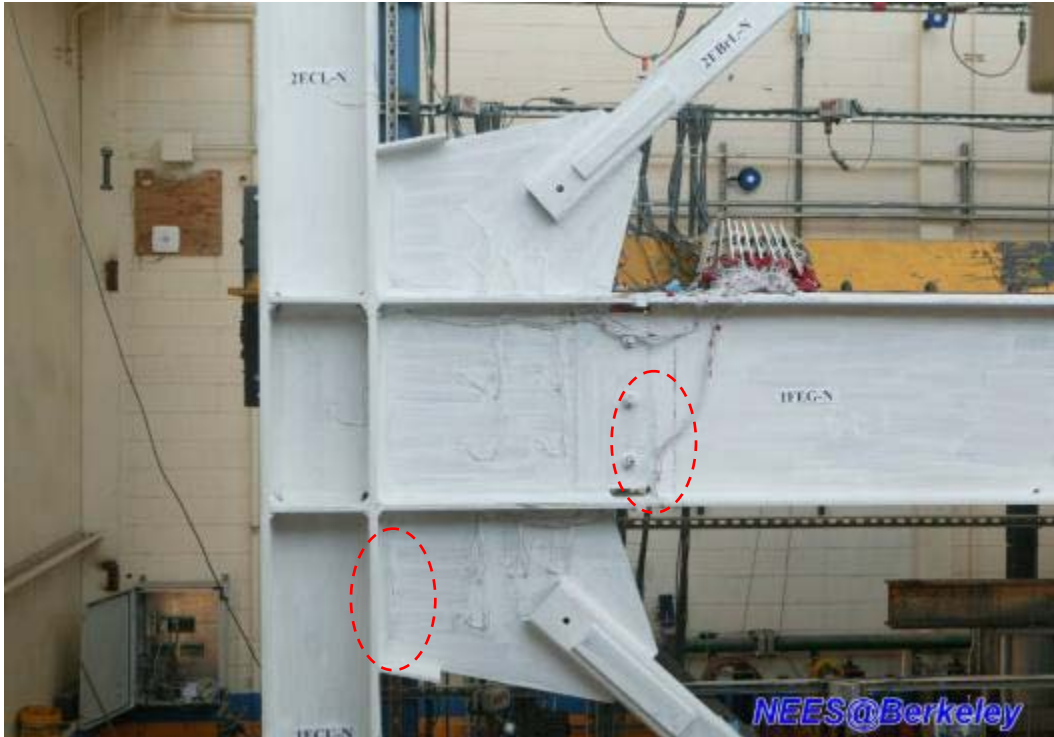


Figure 4.88 The one-piece gusset plate at eastern side of TCBF-B-1 specimen



Figure 4.89 The column base at western side of TCBF-B-1 specimen



Figure 4.90 The lower beam-to-gusset plate splice at western side of TCBF-B-1 specimen



Figure 4.91 The middle portion of a HSS brace at western side of TCBF-B-1 specimen in first story



**Figure 4.92** The lower beam-to-gusset plate splice at eastern side of TCBF-B-1 specimen



**Figure 4.93** The gusset plate-to-column connection at eastern side of TCBF-B-1 specimen



Figure 4.94 The square HSS brace in the first story at eastern side of TCBF-B-1 specimen



Figure 4.95 The square HSS brace in the first story at western side of TCBF-B-1 specimen



**Figure 4.96** The cracks propagate in the square HSS brace at first story western side of TCBF-B-1 specimen



**Figure 4.97** The flaking of whitewash on column web at eastern side of TCBF-B-1 specimen



Figure 4.98 The square HSS braces at the first story of TCBF-B-1 specimen

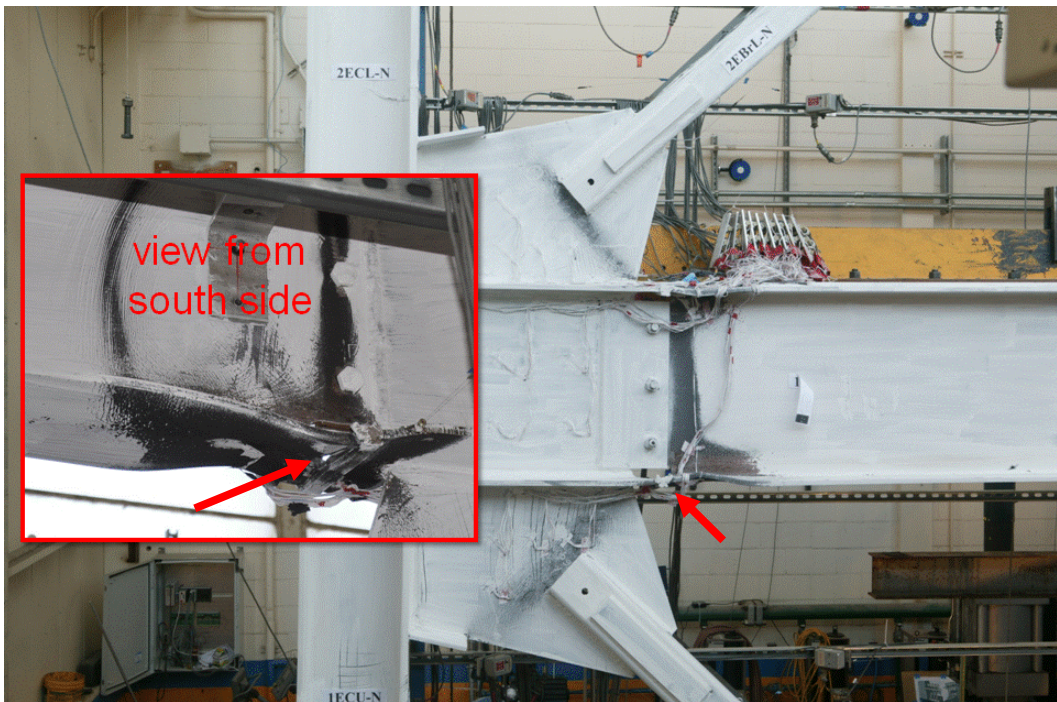


Figure 4.99 The gusset-to-beam splice at eastern side of TCBF-B-1 specimen





**Figure 4.100** Complete fracture of the square HSS brace at first story eastern side of TCBF-B-1 specimen



**Figure 4.101** The cracks propagate in the square HSS brace at second story eastern side of TCBF-B-1 specimen



**Figure 4.102 Specimen TCBF-B-1 after test (view from north side fisheye lens)**

#### **4.2.2 Specimen TCBF-B-2 (Round HSS Braces, Quasi-Static Test)**

Specimen TCBF-B-2 re-used the  $W24 \times 117$  roof beam, the  $W12 \times 96$  columns and 2-in.-thick base plates from the previous test. Before the first trial, some welding repairs were conducted at the column bases (see Figs. 3.51, 3.52, and 3.53). Before conducting the actual test, two complete cycles of 0.15-in. peak roof displacement was performed to check all instrument readings and the actuator control algorithms.

First trial of the braced frame with round HSS braces began at around 2:26 PM on Sunday, October 18, 2009. This test was similar to that carried out for TCBF-B-1. Because some of the channels recording the linear strain gauge readings saturated in the earlier test, the gain value was reduced from 200 to 50 for of the channels where high local strain developed in the data acquisition system. The entire side view of the specimen before first trial is shown in Figs. 3.22 and 3.54.

During the first trial at about 2-inch roof displacement (the second cycle of  $1.5 D_{bm}$  load step), the west side column base fractured (see Fig. 4.103). The test was paused for emergency repairs of the column base before continuing with the subsequent loading cycles. The entire side view of the specimen after first trial is shown in Fig. 4.104.

Column bases at both sides of the specimen were stiffened with four one-inch thick stiffeners at both sides of column flanges. The column base at the western side that had fractured was stiffened with two additional one-inch thick stiffeners at both sides of column web. In

addition, a two-inch thick flange cover plate was fillet welded to attach the fractured column flange to the base plate (Fig. 4.105).

The second trial began at 4:36 PM on Thursday, October 22, 2009. The entire side view of the specimen before the second trial is shown in Fig. 4.106. Fig. 4.107 shows the specimen before test and after the second trial.



**Figure 4.103** Fracture of the column base flange CJP welds at west side of TCBF-B-2 specimen



**Figure 4.104** Specimen TCBF-B-2 after first trial

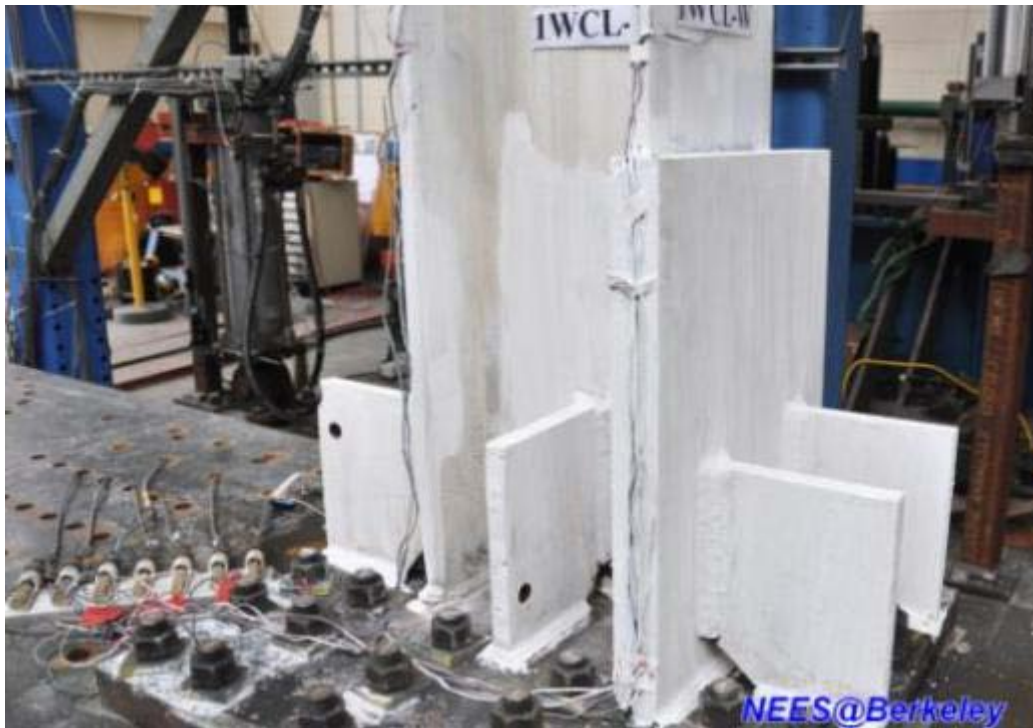


Figure 4.105 The west side column base of TCBF-B-2 specimen after repair with 1-in. thick stiffener plates and a 2-in. thick flange cover plate



Figure 4.106 Specimen TCBF-B-2 before second trial



(a) Before test



(b) After second trial

Figure 4.107. Specimen TCBF-B-2 before test and after test

#### 4.2.2.1 Key Response Quantities

The paragraphs below briefly describe the response quantities record in two test trials, and the post-processed response quantities derived from the raw data. Detailed discussion of the individual response quantities are described in Chapter 5.

##### 4.2.2.1.1 System Response

Figures 4.108 and 4.109 show the time history of the actuator displacements and actuator load cell force feedbacks for Specimen TCBF-B-2. The base shear versus controlled roof displacement of the specimen is shown in Fig. 4.110. The relationship between the story shear and story drift ratio for the specimen is shown in Fig. 4.111.

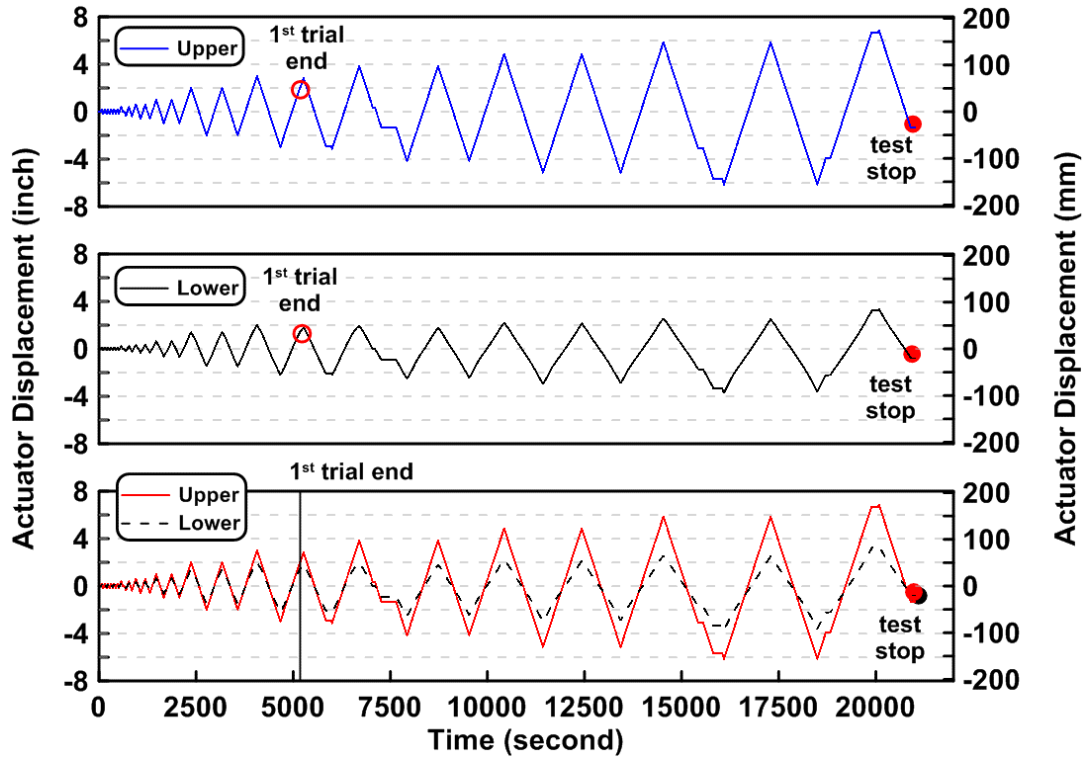


Figure 4.108 Actuator displacement time histories of TCBF-B-2 specimen

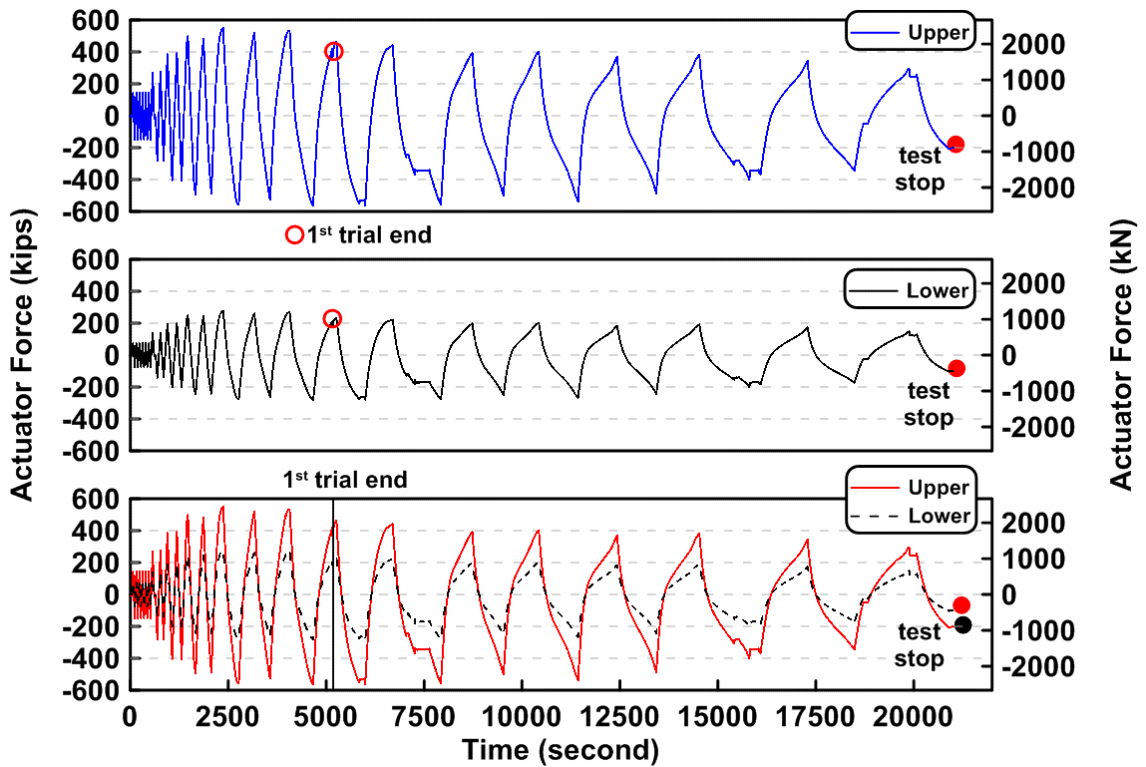


Figure 4.109 Actuator force time histories of TCBF-B-2 specimen

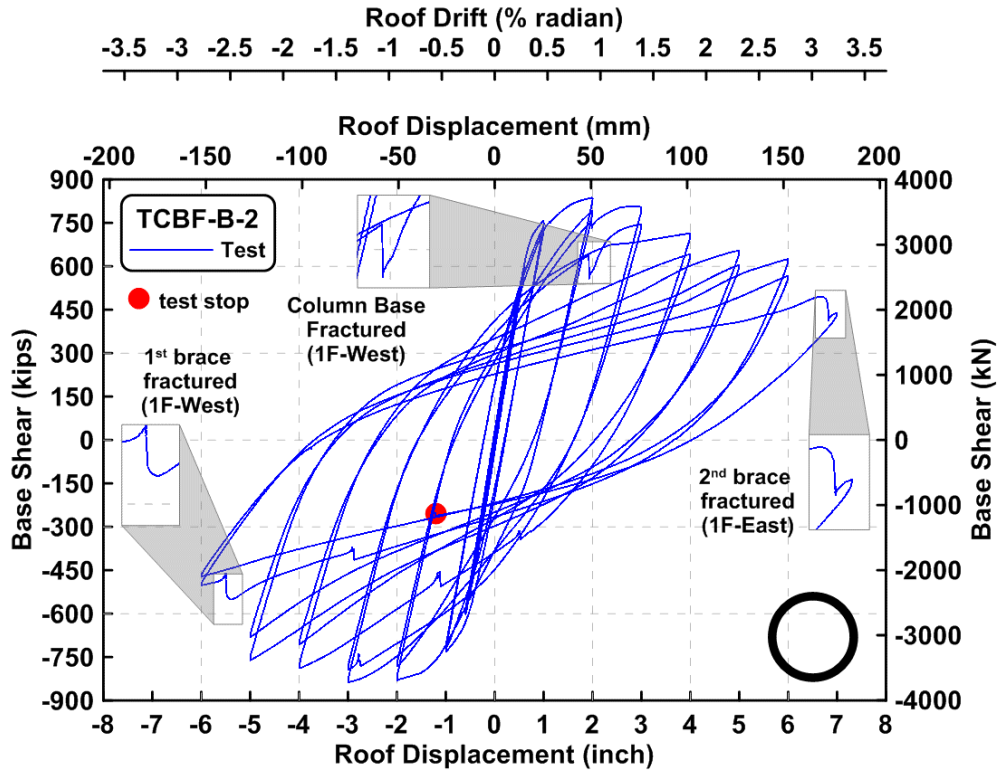


Figure 4.110 Base shear vs. roof displacement relationship of TCBF-B-2 specimen

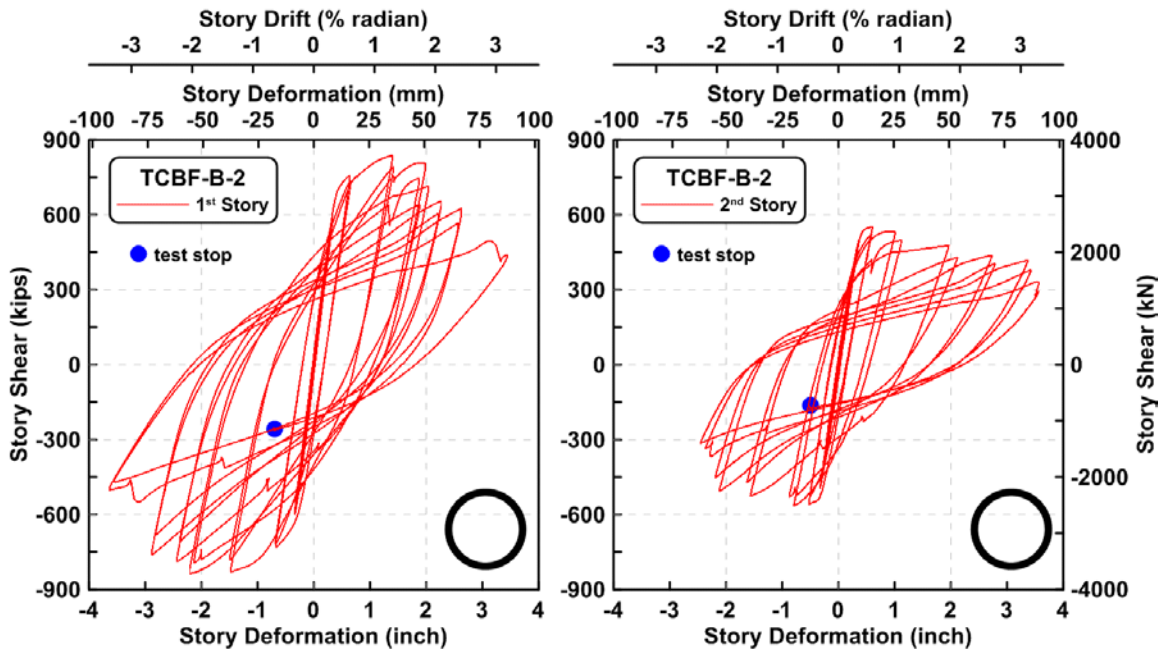


Figure 4.111 Story shear vs. story deformation relationship of TCBF-B-2 specimen



#### **4.2.2.1.2 Column Response**

The time histories of the axial forces in the  $W12 \times 96$  columns at the western and eastern sides of the specimen are plotted in Fig. 4.112. Note that because significant yielding occurred in the column where the lower set of strain gauges were installed (around 3ft above the column base plate), only the strain gauge readings at 6ft above the base plate were used in estimating the column axial forces in this case. The relationships between roof displacements and axial forces at both columns are shown in Fig. 4.113. The bending moment time history at the top and bottom ends of the column in each story are shown in Figs. 4.114 and 4.115. Estimated column shear force time histories in the upper and lower stories are plotted in Figs. 4.116 and 4.117, respectively. Estimated column shear forces in each floor were added together and the sum is plotted in Fig. 4.118. The estimated column web shear stress versus shear strain readings from strain rosettes are plotted in Fig. 4.119. The sum of the estimated column shear force components versus the total story shear forces for each story are shown in Fig. 4.120. The derived rosette type strain gauge readings in the column web at each story are shown from Figs. 4.121 to 4.124. Normalized maximum and minimum principal stress relationships along with different yield criteria are plotted in Figs. 4.125 to 4.128. The normalized P-M and P-V interaction diagrams at column bases and column top ends are shown in Figs. 4.129 to 4.132.

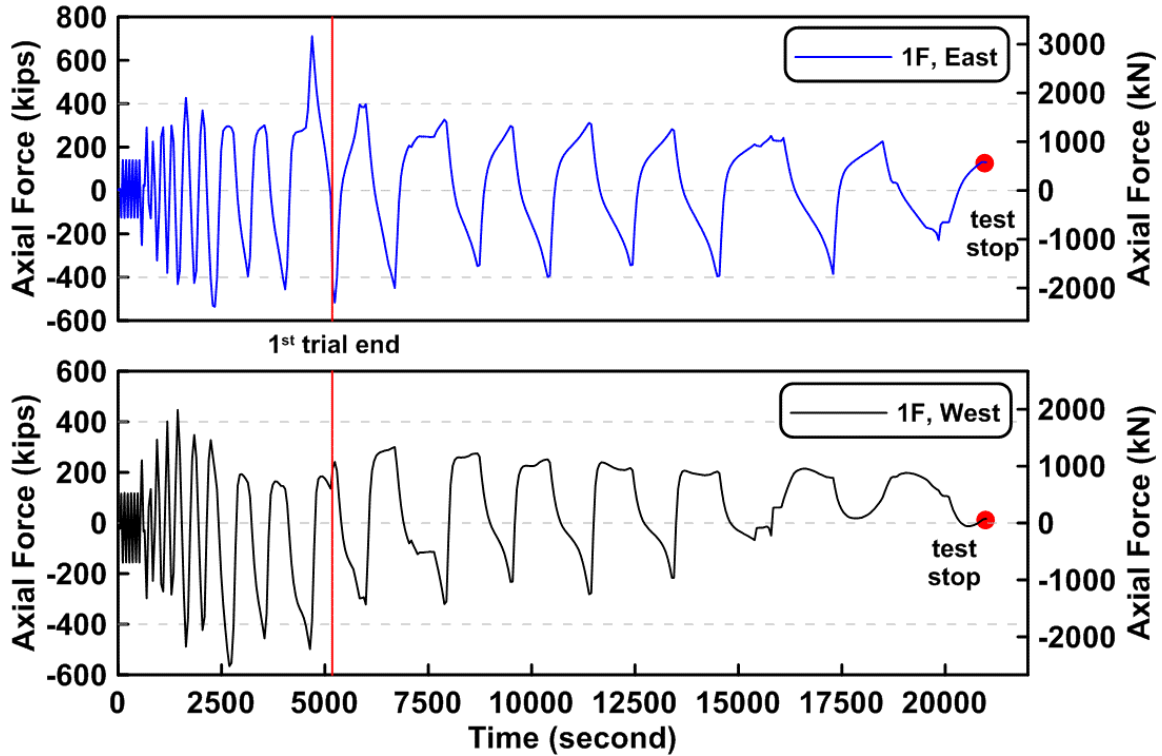


Figure 4.112 Time history of the column axial forces in the first story of TCBF-B-2 specimen (location: 6-ft above column base plate)

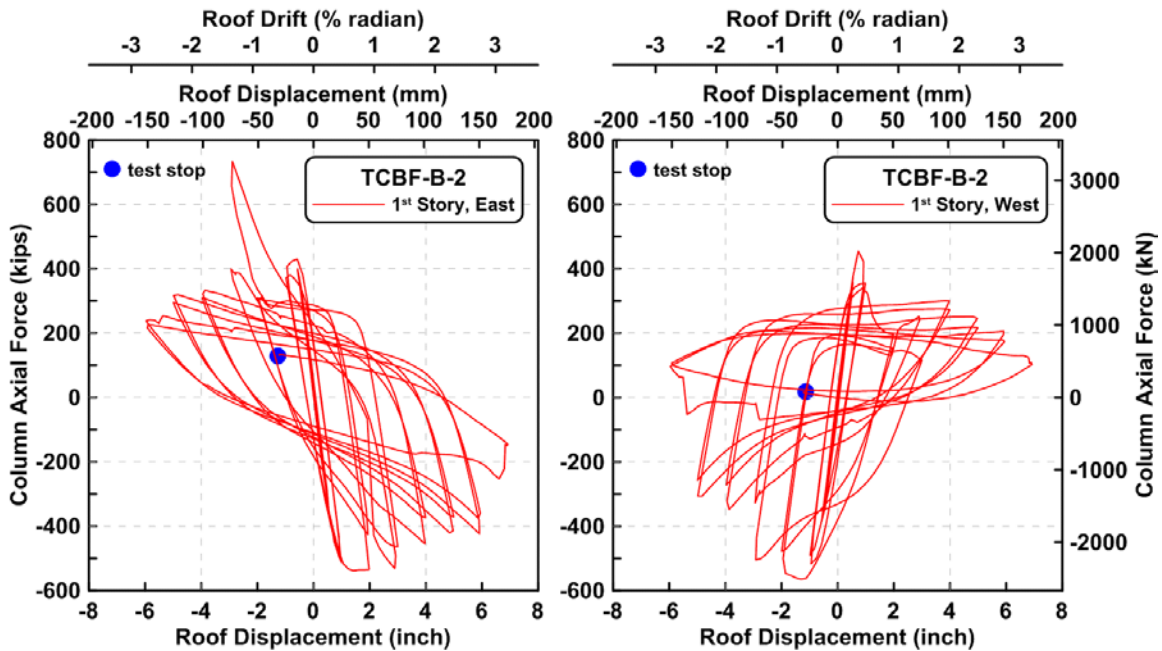


Figure 4.113 Roof displacement vs. first story column axial forces of TCBF-B-2 specimen (note that the vertical axis limit is from -600 kips to 800 kips; the horizontal axis limit is from -8-in. to 8-in.)

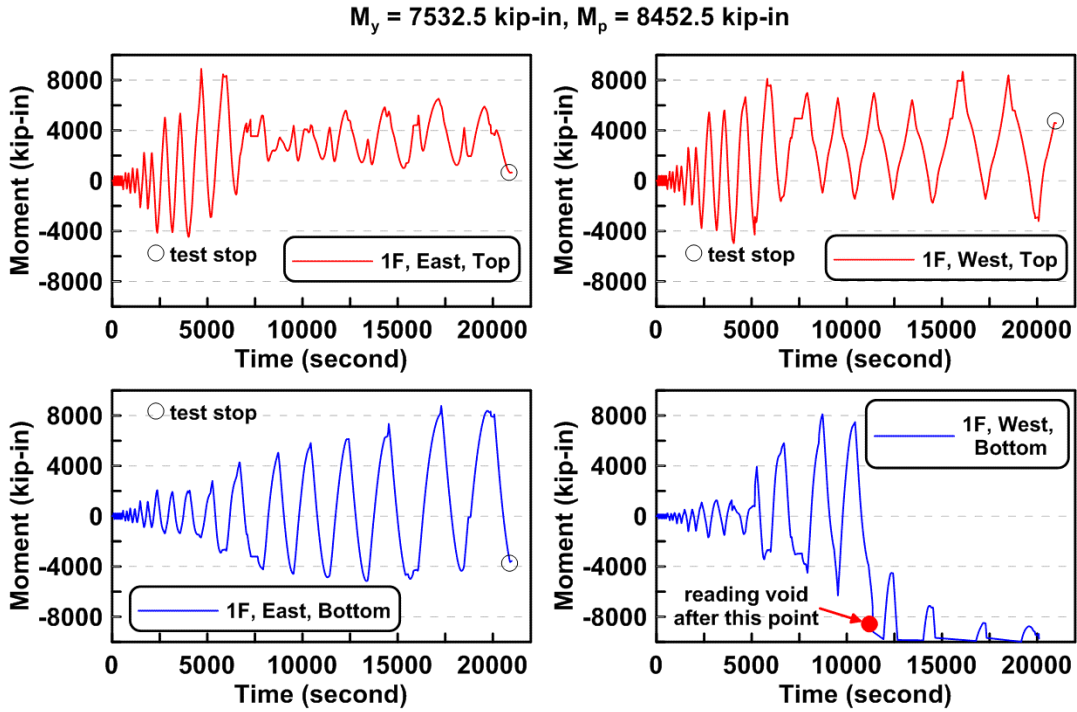


Figure 4.114 Time history of the first story column bending moments of TCBF-B-2 specimen (3-ft above column base plate and 3-ft below lower beam centerline)

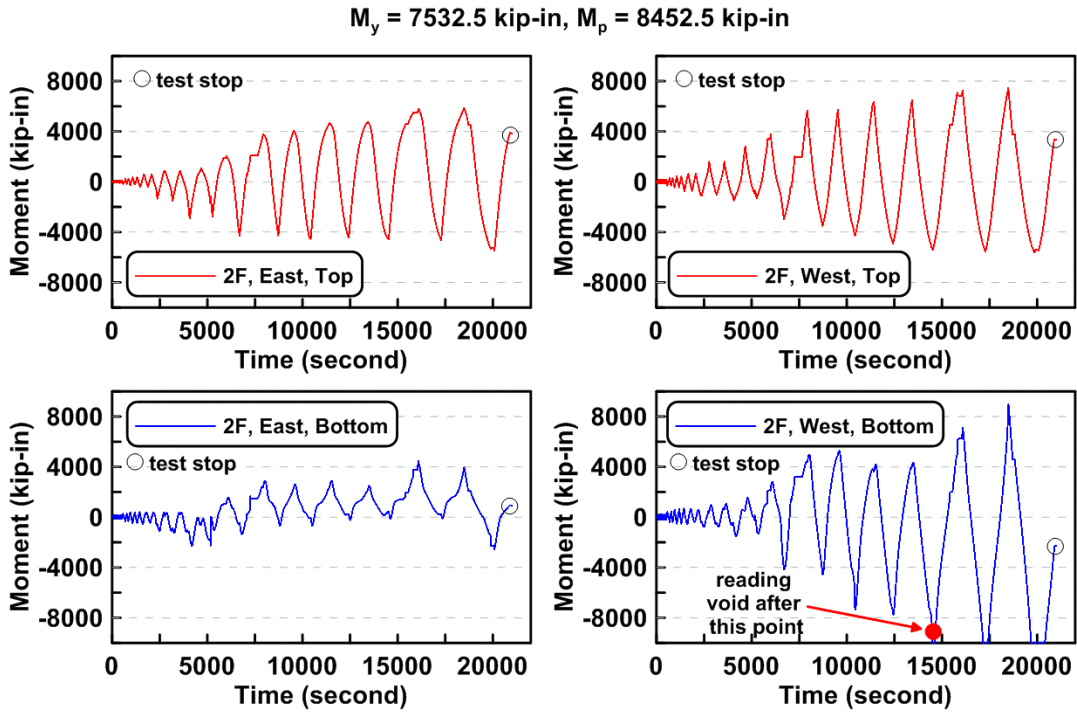


Figure 4.115 Time history of the second story column bending moments of TCBF-B-2 specimen (3-ft above lower beam centerline and 3-ft below roof beam centerline)

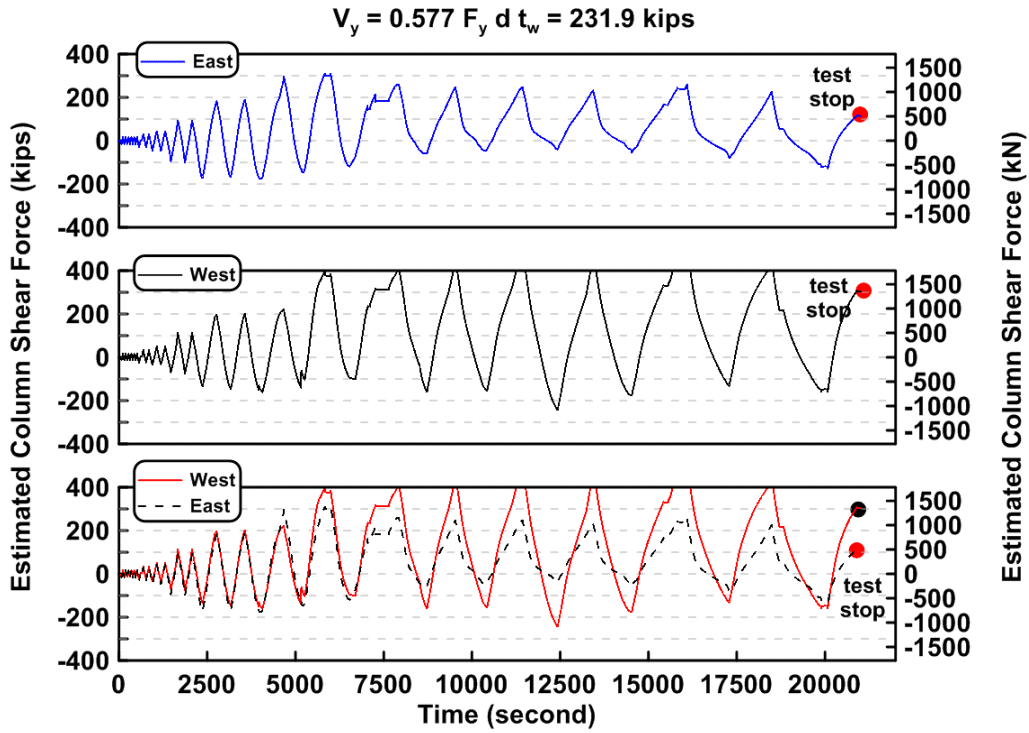


Figure 4.116 Time history of the first story column shear forces of TCBF-B-2 specimen

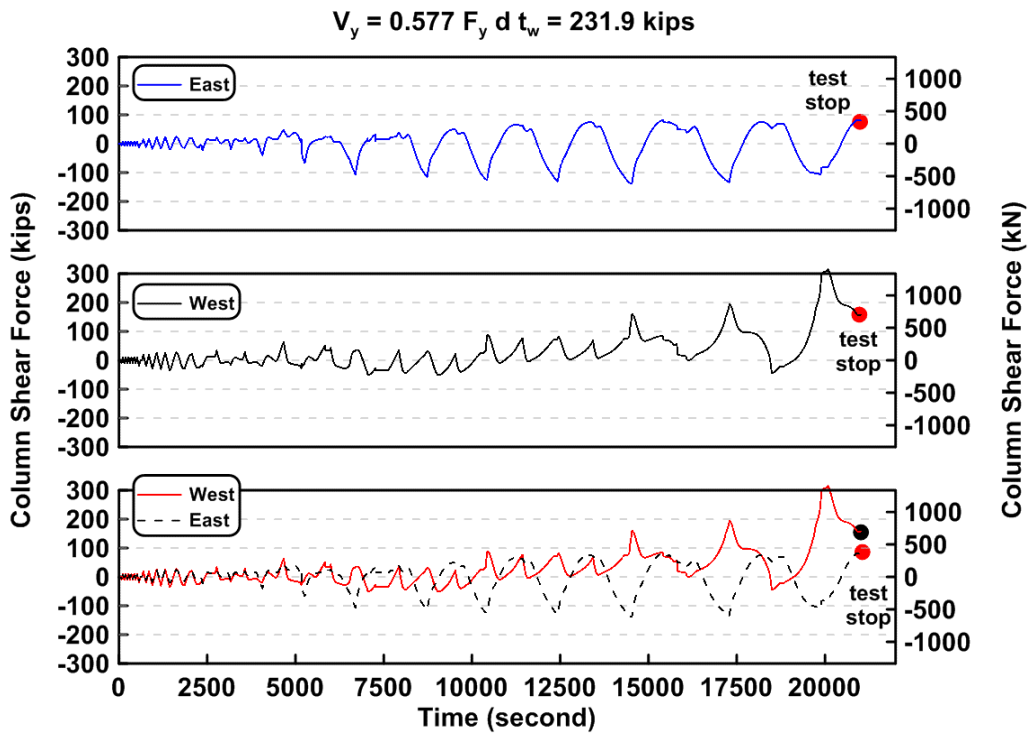


Figure 4.117 Time history of the second story column shear forces of TCBF-B-2 specimen

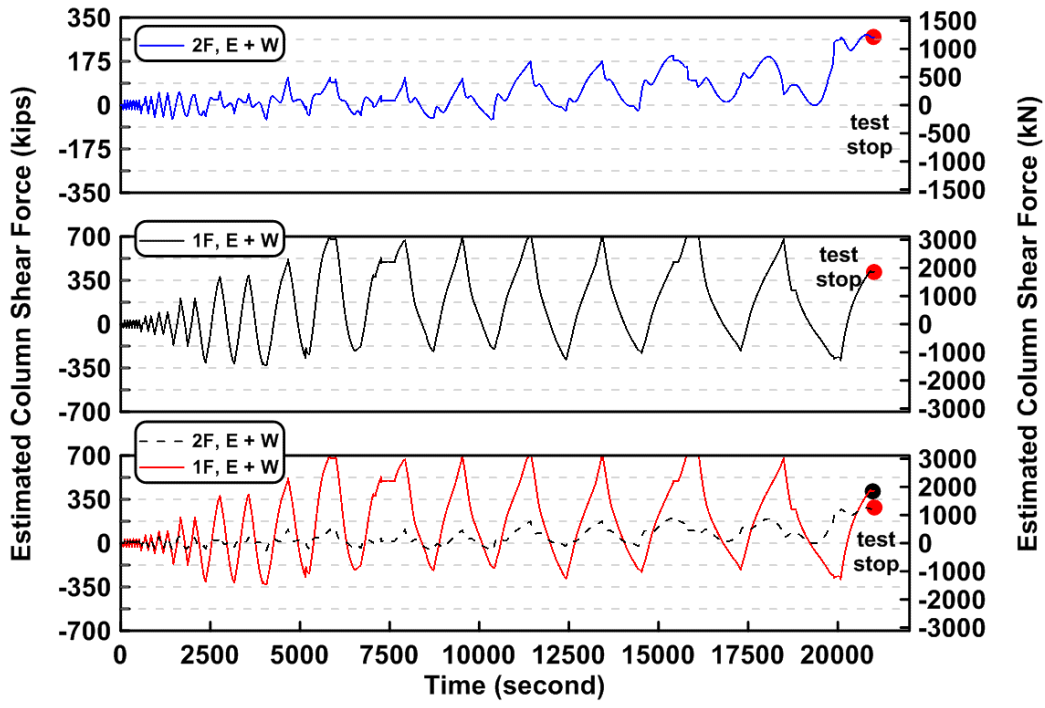


Figure 4.118 Time history of the sum of east and west column shear forces in both stories of TCBF-B-2 specimen

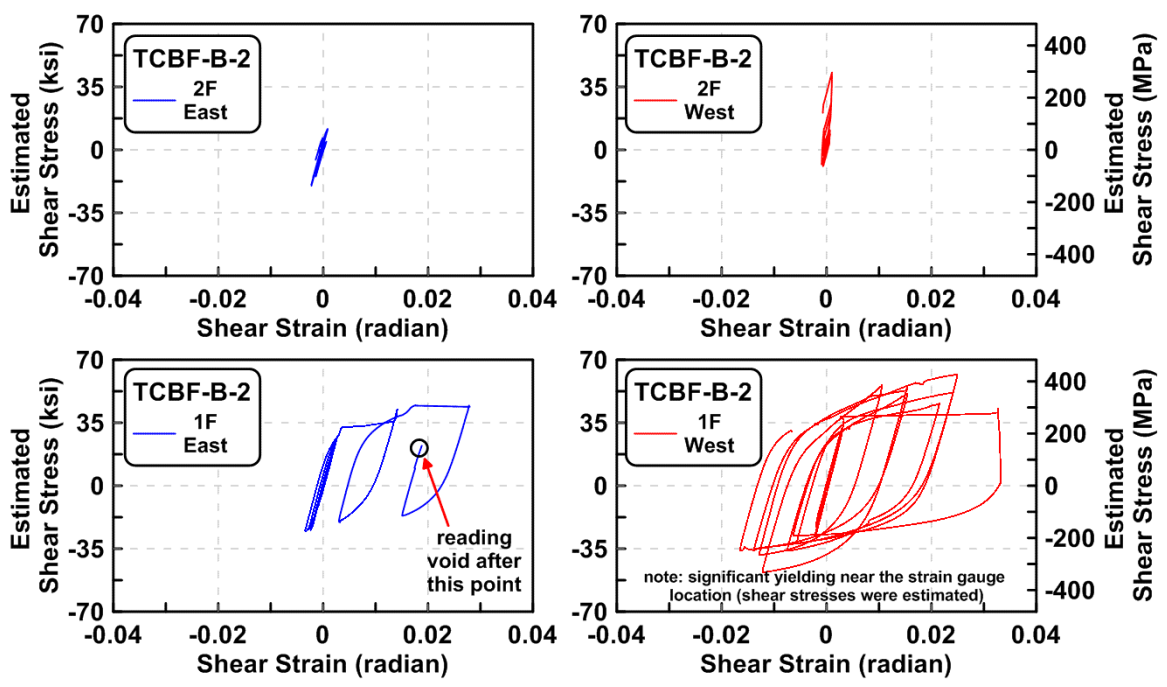


Figure 4.119 Estimated column shear stress vs. shear strain relationships of TCBF-B-2 specimen (locations: EC1-B-N, EC2-B-N, WC1-B-N and WC2-B-N)

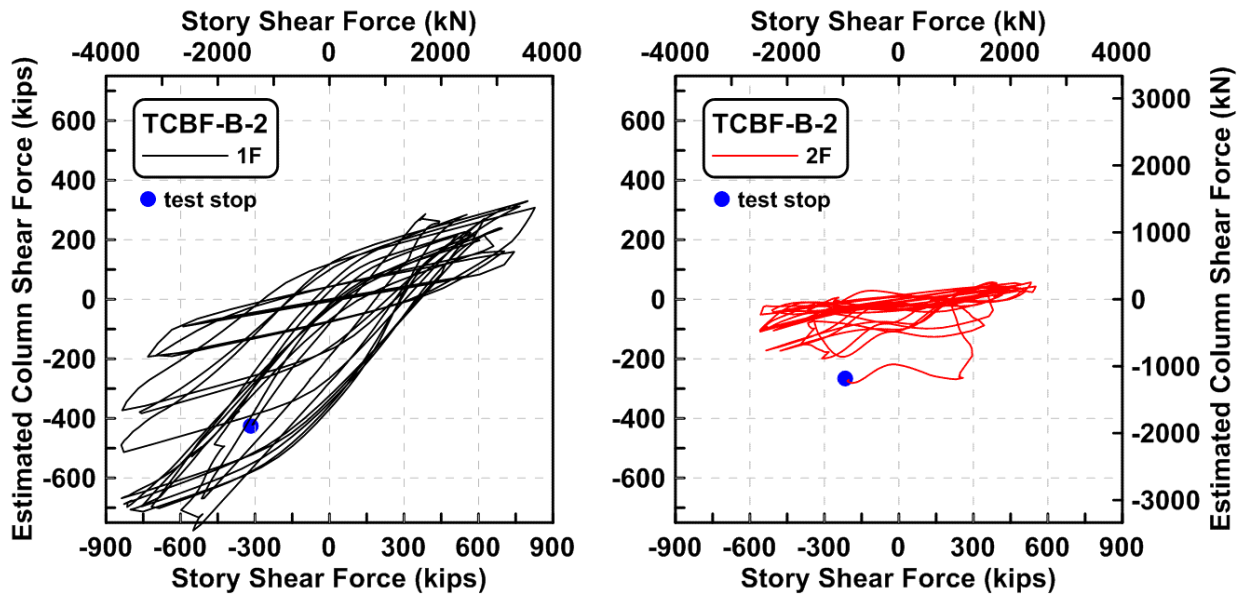


Figure 4.120 Story shear component from columns vs. total story shear forces of TCBF-B-2 specimen

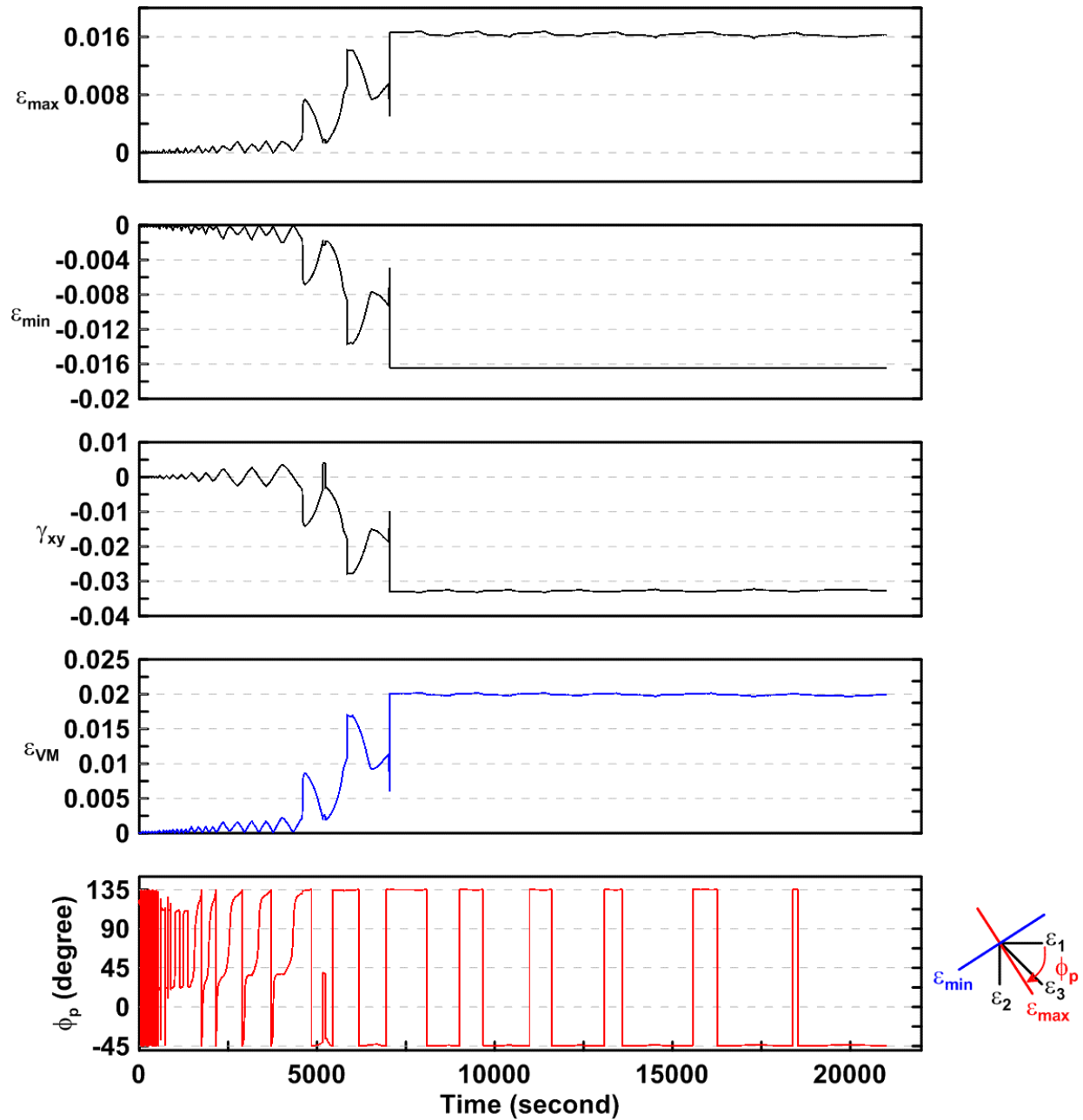


Figure 4.121 Time history of rosette type strain gauge readings in the first story column web of TCBF-B-2 specimen (location: R1)

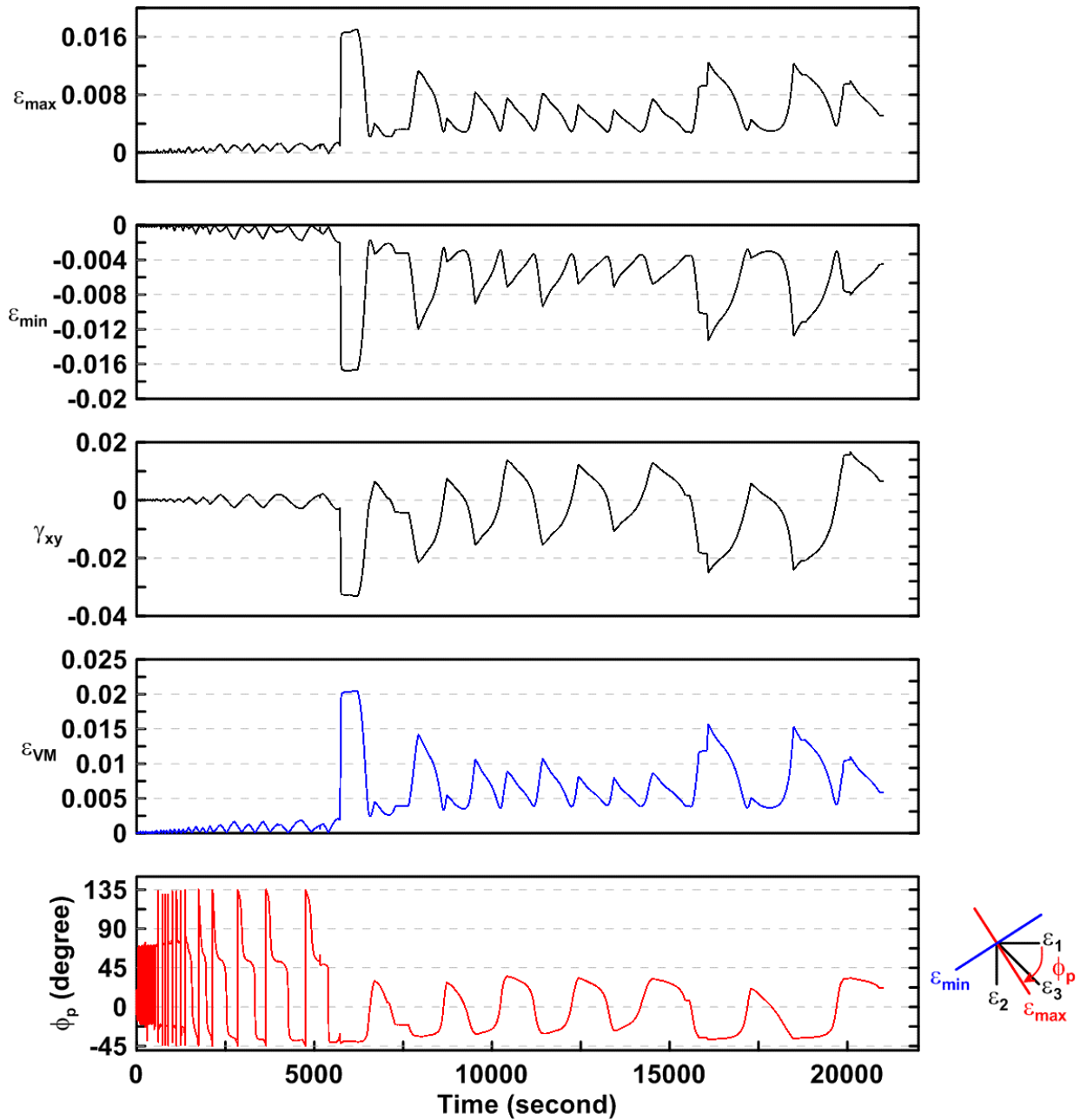


Figure 4.122 Time history of rosette type strain gauge readings in the first story column web of TCBF-B-2 specimen (location: R5)



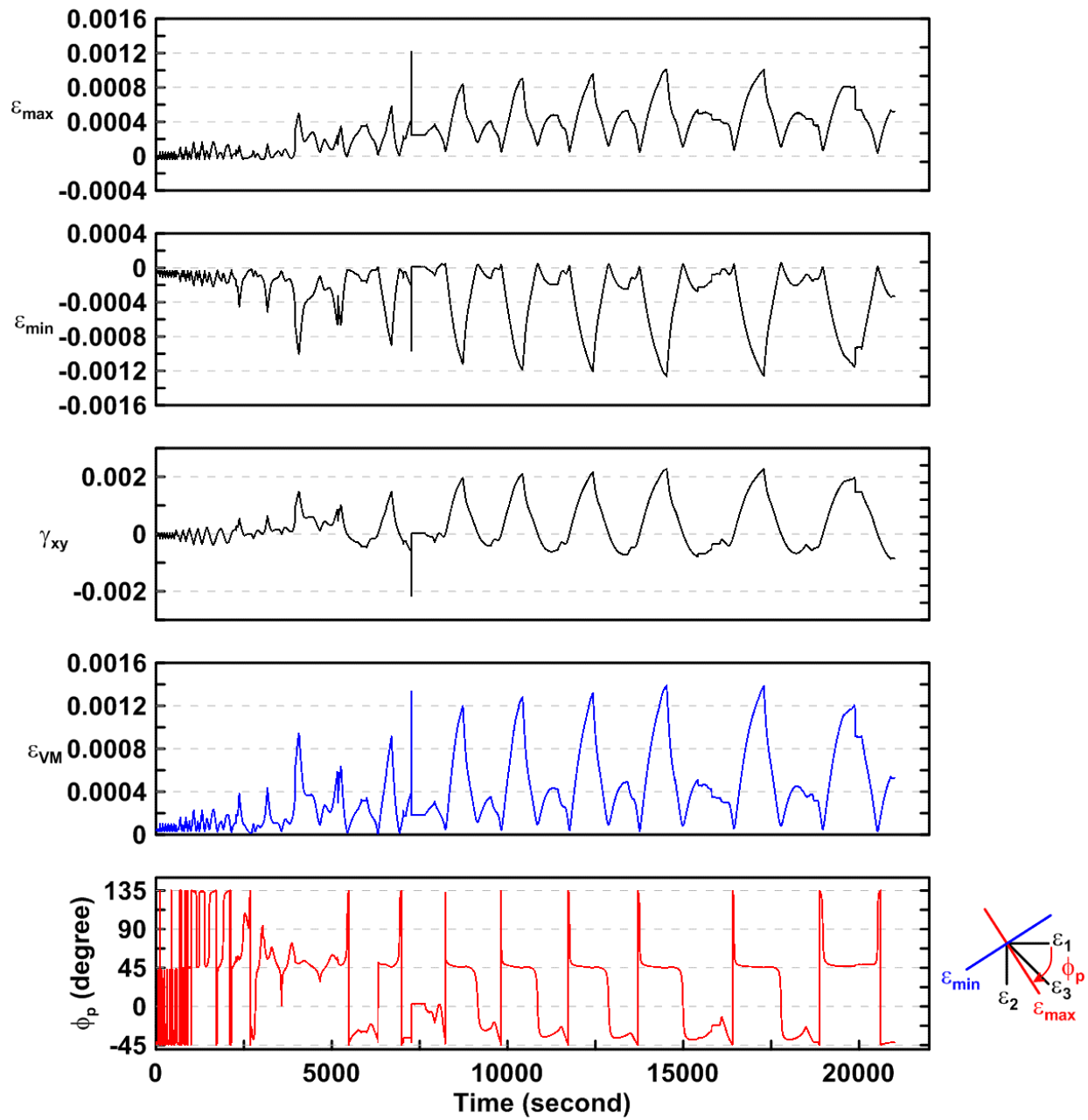


Figure 4.123 Time history of rosette type strain gauge readings in the second story column web of TCBF-B-2 specimen (location: R3)

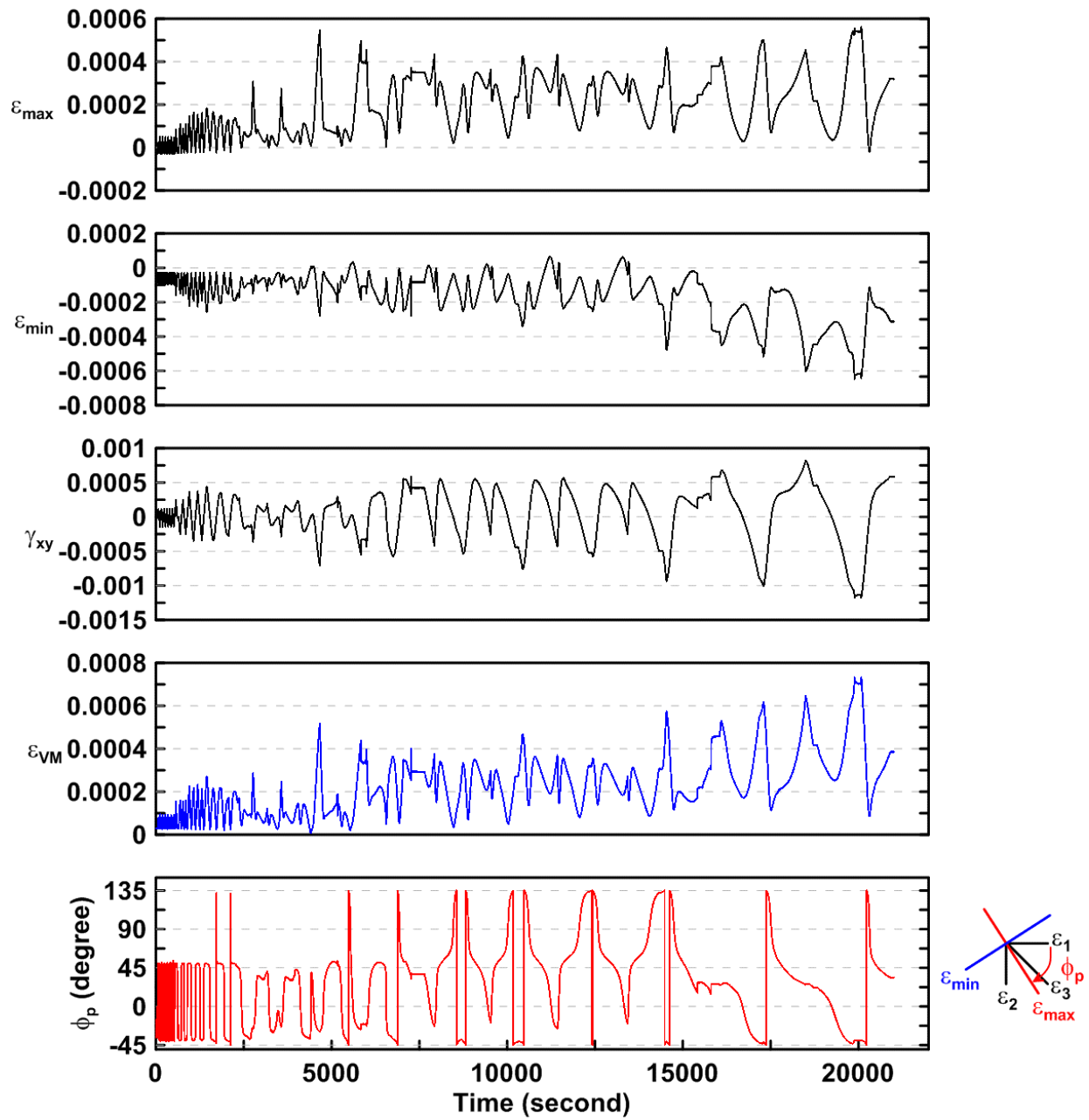


Figure 4.124 Time history of rosette type strain gauge readings in the second story column web of TCBF-B-2 specimen (location: R7)

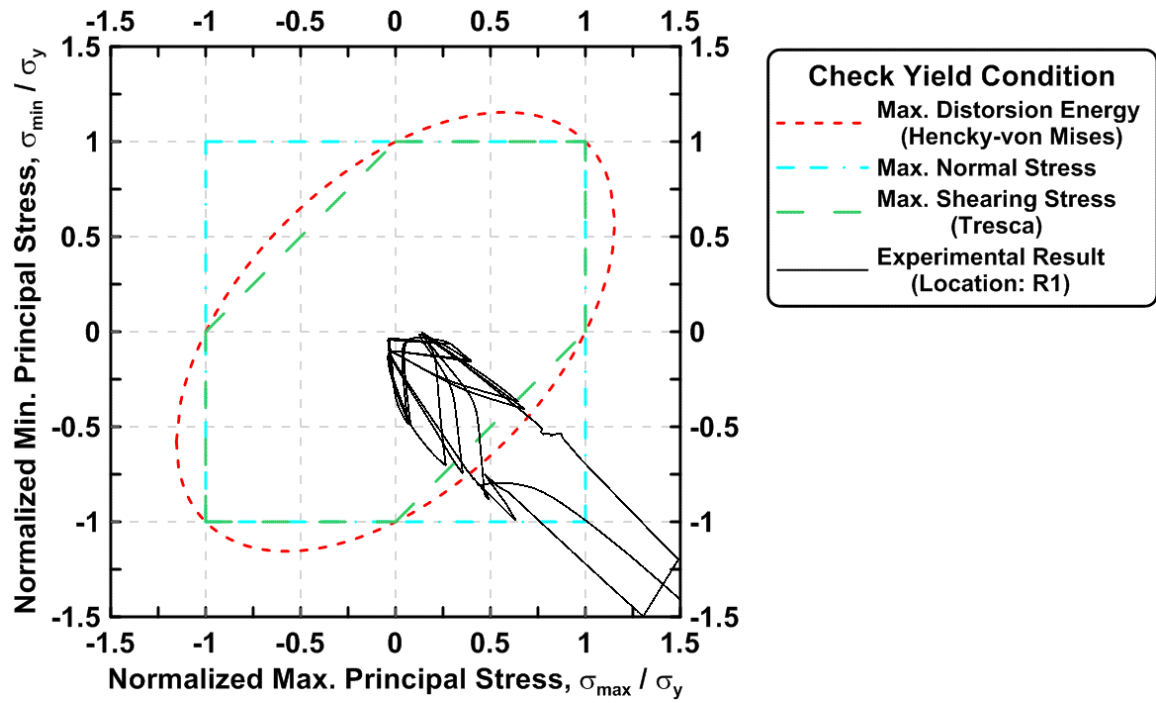


Figure 4.125 Maximum principal stress vs. minimum principal stress in the first story column of TCBF-B-2 specimen (location: R1)

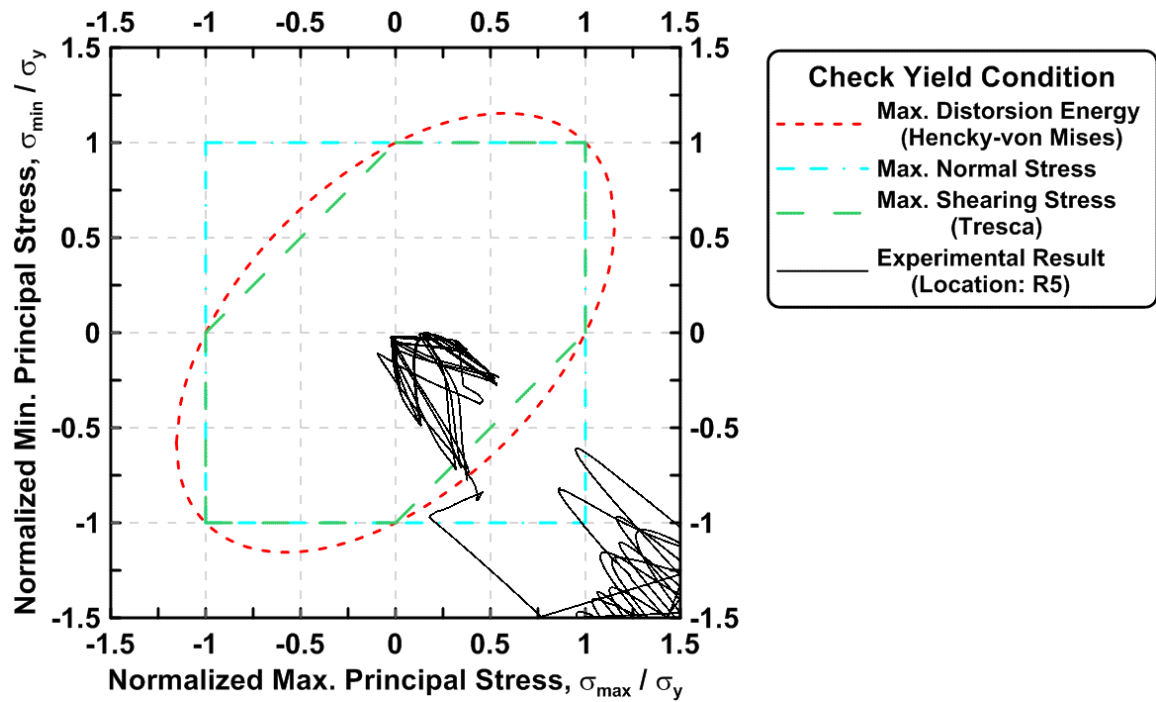


Figure 4.126 Maximum principal stress vs. minimum principal stress in the first story column of TCBF-B-2 specimen (location: R5)

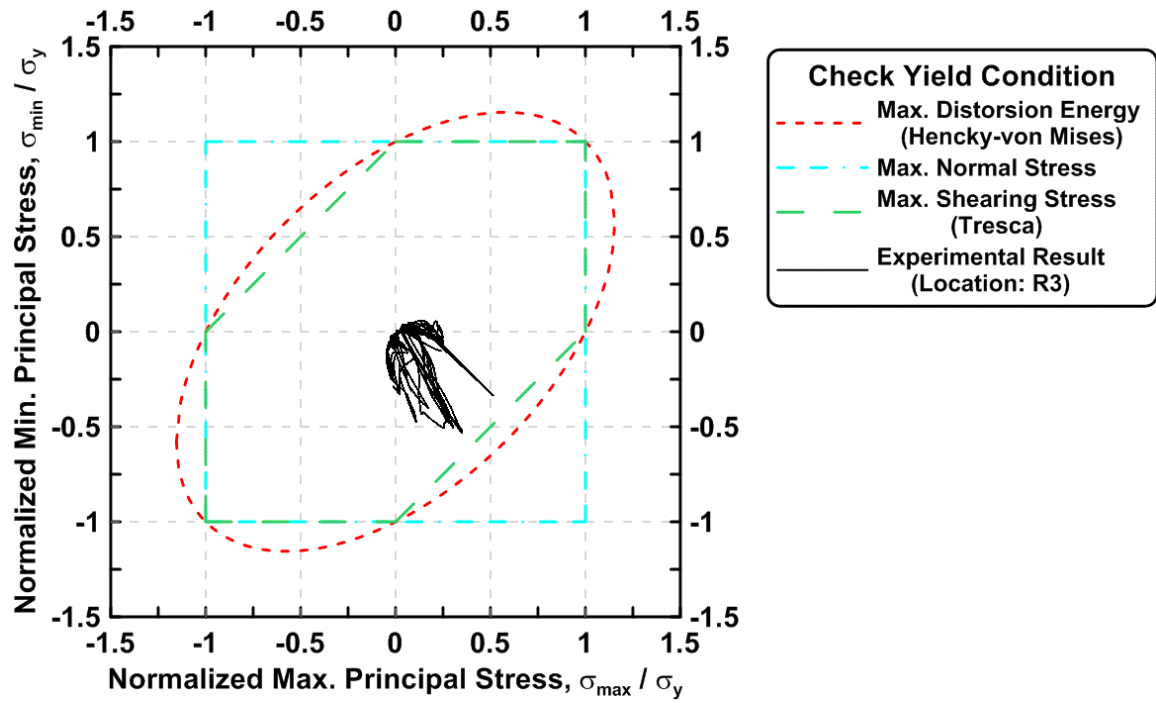


Figure 4.127 Maximum principal stress vs. minimum principal stress in the second story column of TCBF-B-2 specimen (location: R3)

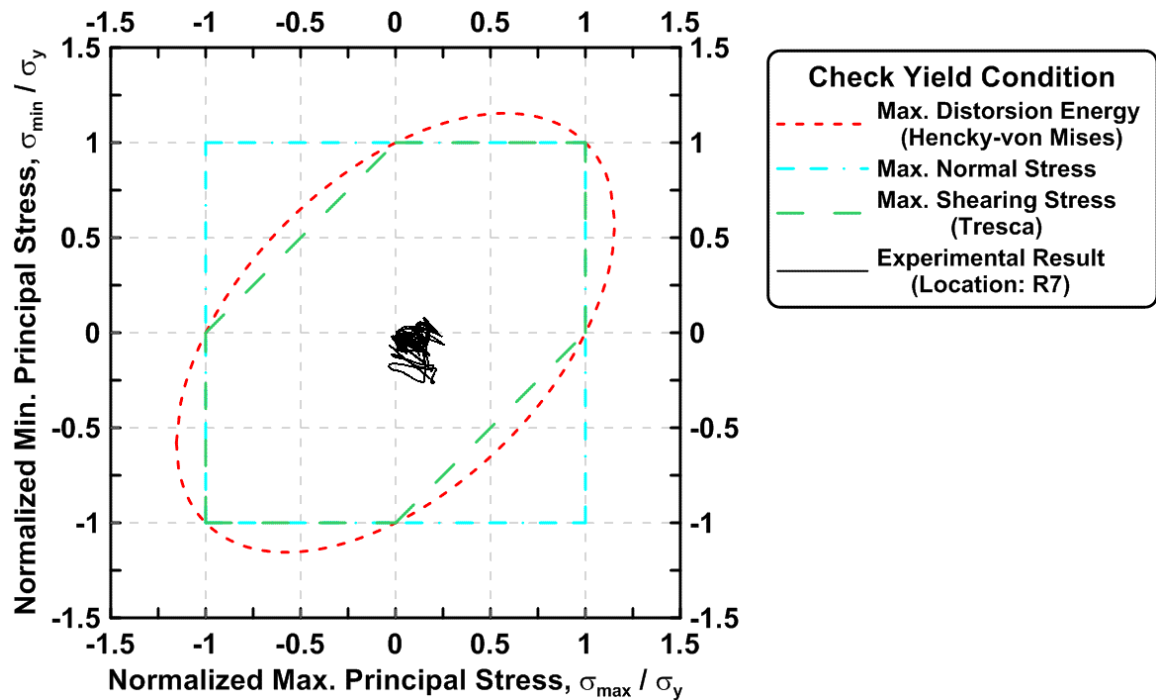


Figure 4.128 Maximum principal stress vs. minimum principal stress in the second story column of TCBF-B-2 specimen (location: R7)

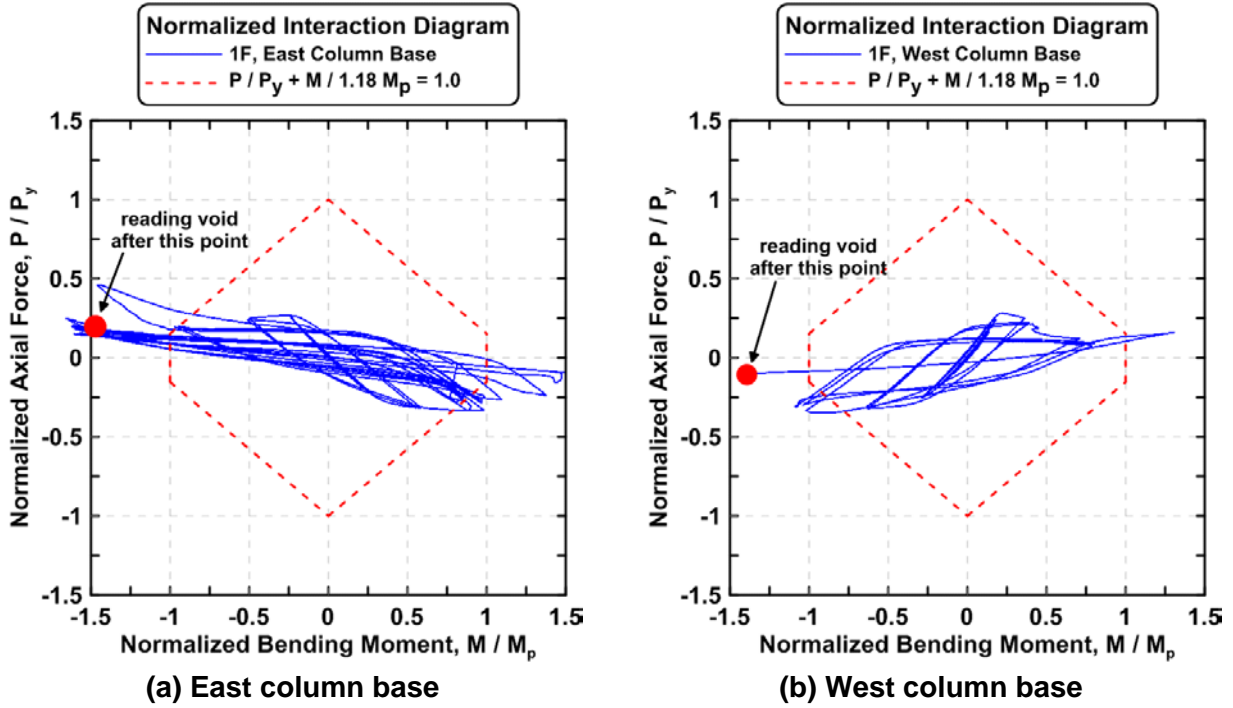


Figure 4.129 Normalized P-M interaction diagrams of the first story columns of TCBF-B-2 specimen

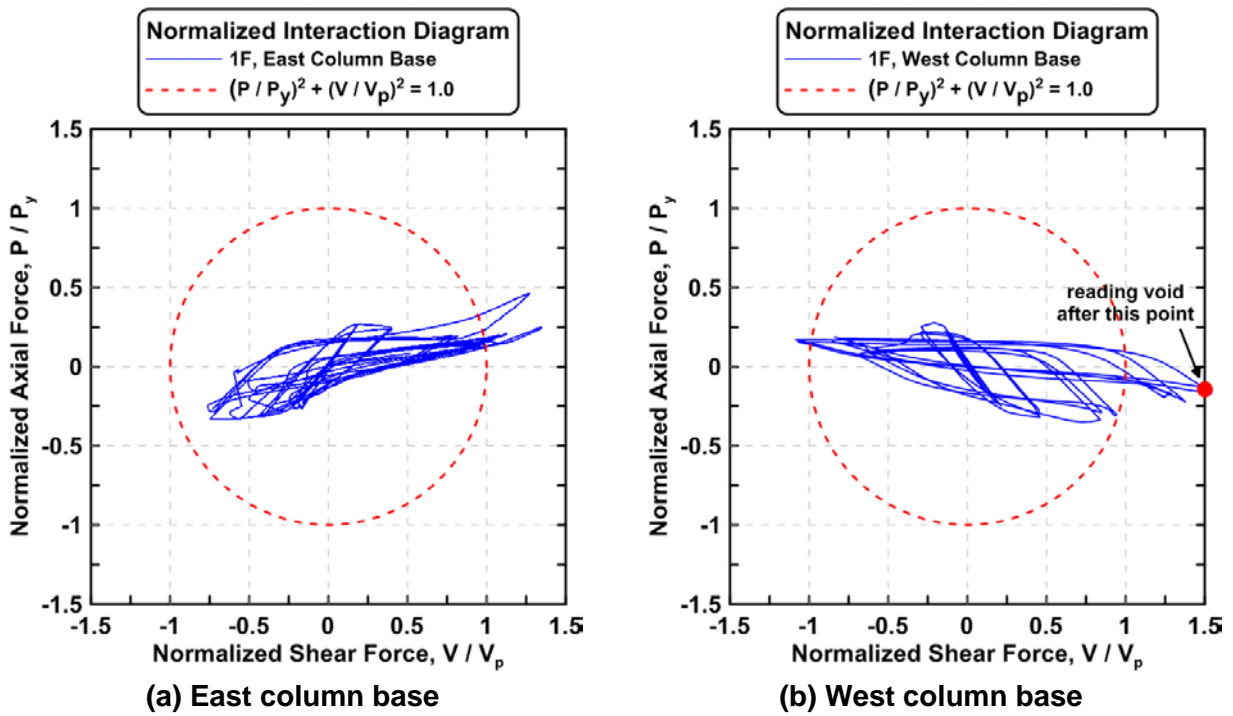


Figure 4.130 Normalized P-V interaction diagrams of the first story columns of TCBF-B-2 specimen

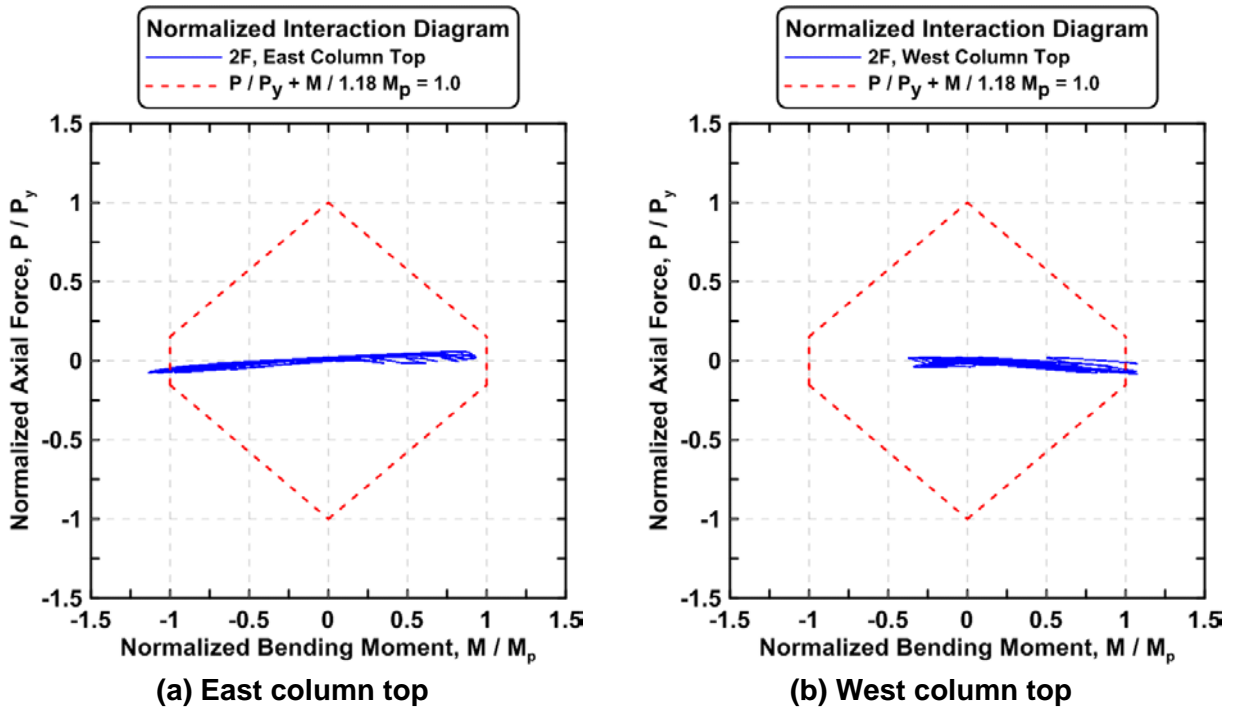


Figure 4.131 Normalized P-M interaction diagrams of the second story columns of TCBF-B-2 specimen

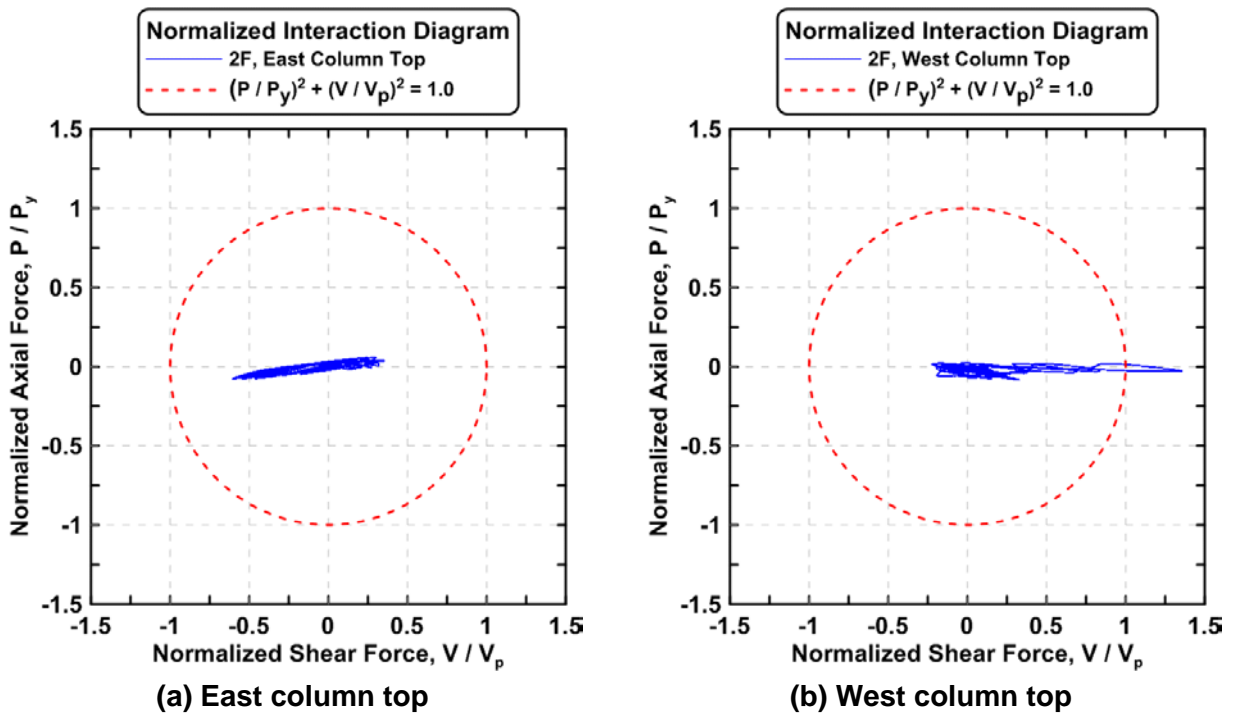


Figure 4.132 Normalized P-V interaction diagrams of the second story columns of TCBF-B-2 specimen

### 4.2.2.1.3 Beam Response

The vertical deflection time history at the center of the W24 × 117 roof beam and the W24 × 68 lower beam are plotted in Figs. 4.133. Figs. 4.134 and 4.135 show the time history of strain readings at both ends of the roof beam and lower beam, respectively. Both beam axial force time histories derived from linear strain gauges at different locations along the beams are plotted in Figs. 4.136 and 4.137. The bending moment time histories of both beams are shown in Figs. 4.138 and 4.139. Estimated beam shear force time histories are illustrated in Figs. 4.140 and 4.141. The estimated vertical unbalanced force at the center of the roof beam is plotted in Fig. 4.142.

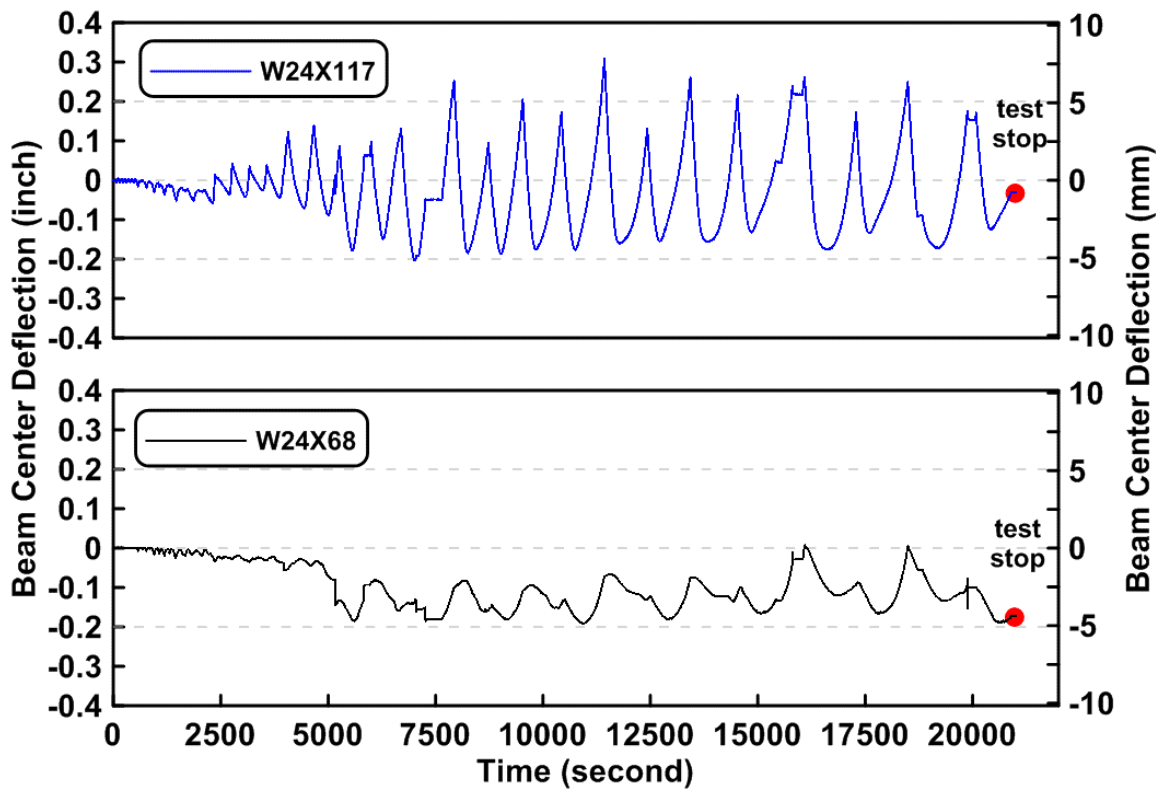
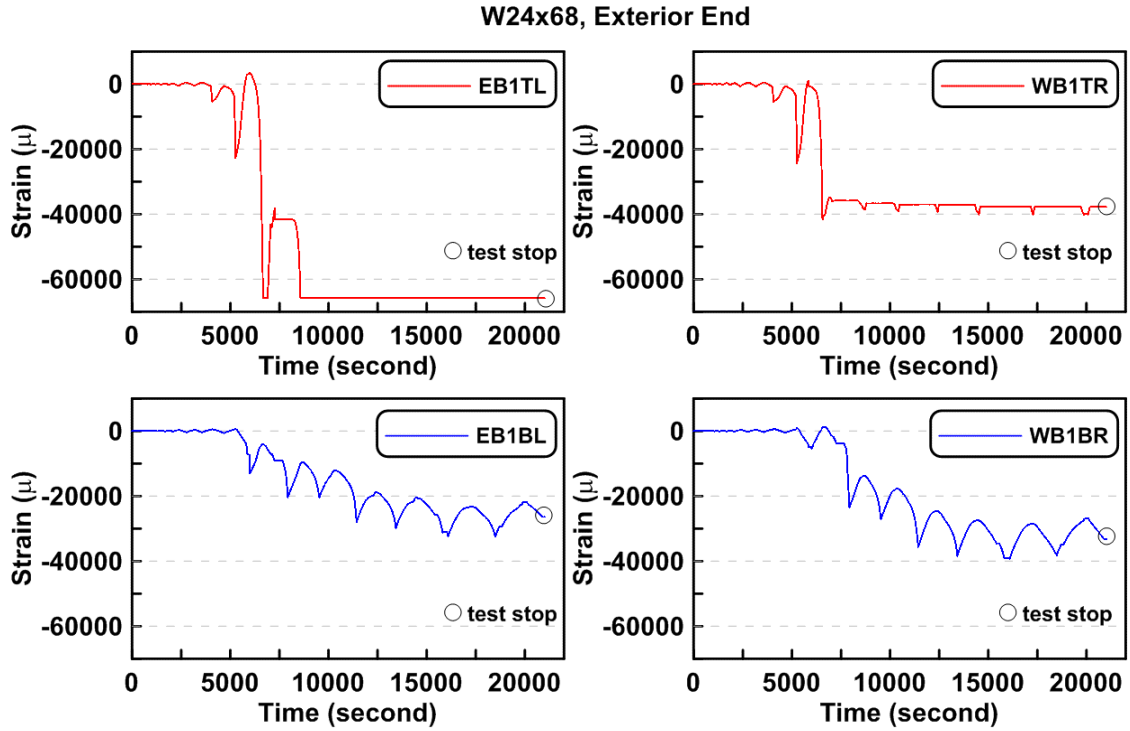
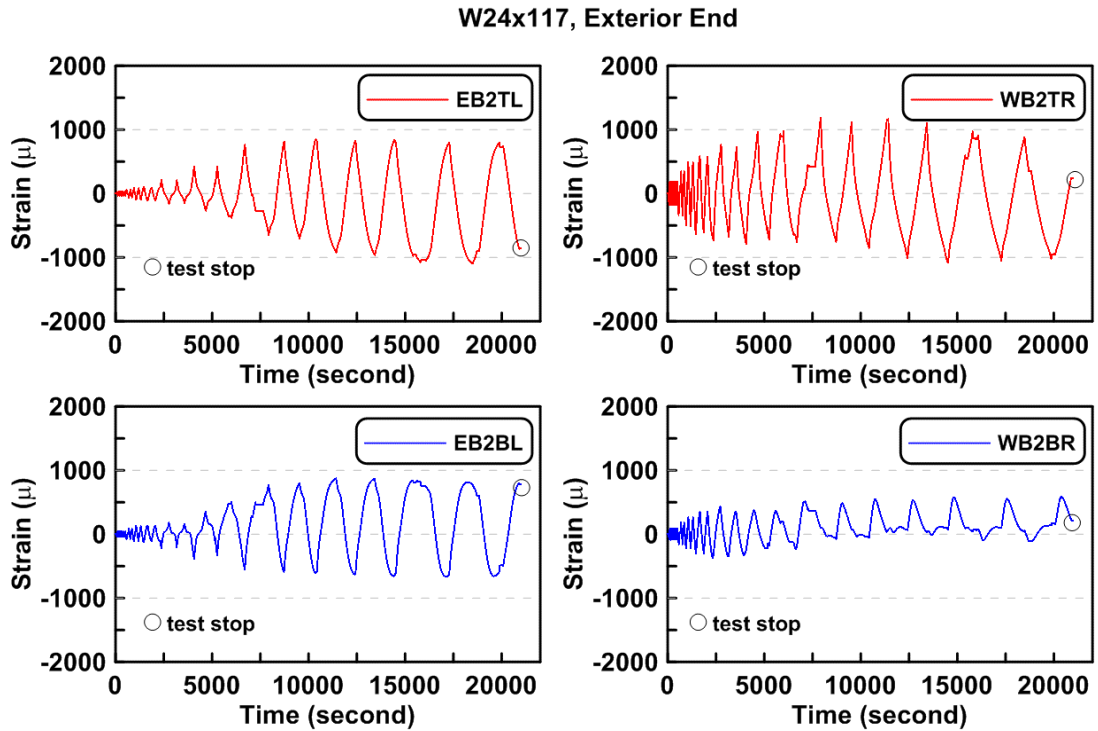


Figure 4.133 The deflection time history at the center of beam span of TCBF-B-2 specimen (roof beam: W24 × 117, lower beam: W24 × 68)



**Figure 4.134** Time history of strain readings at both exterior ends of W24  $\times$  68 lower beam of TCBF-B-2 specimen



**Figure 4.135** Time history of strain readings at both exterior ends of W24  $\times$  117 roof beam of TCBF-B-2 specimen



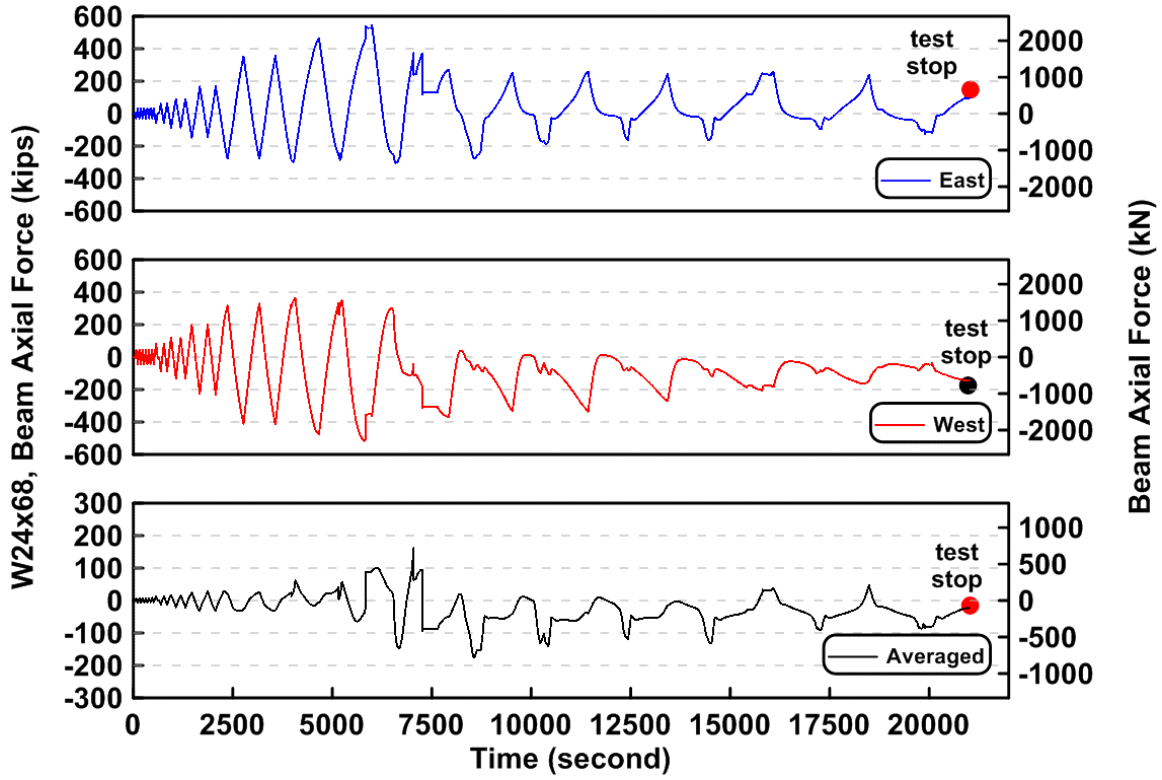


Figure 4.136 Time history of lower beam axial forces of TCBF-B-2 specimen

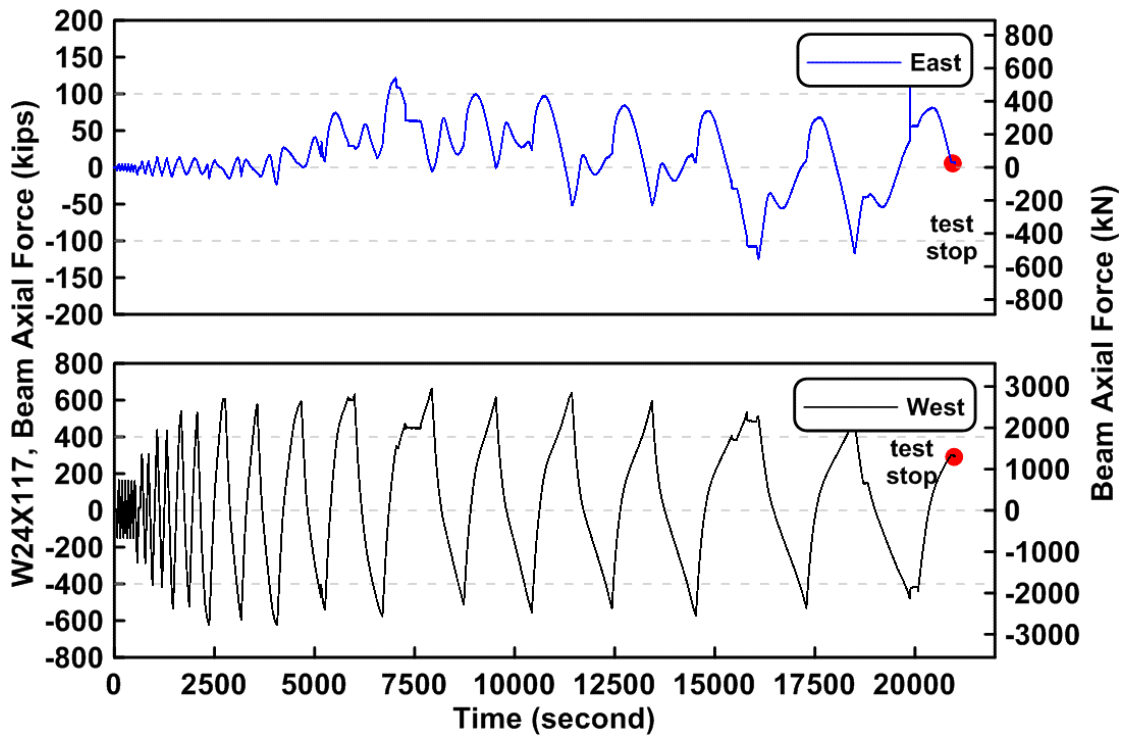


Figure 4.137 Time history of roof beam axial forces of TCBF-B-2 specimen

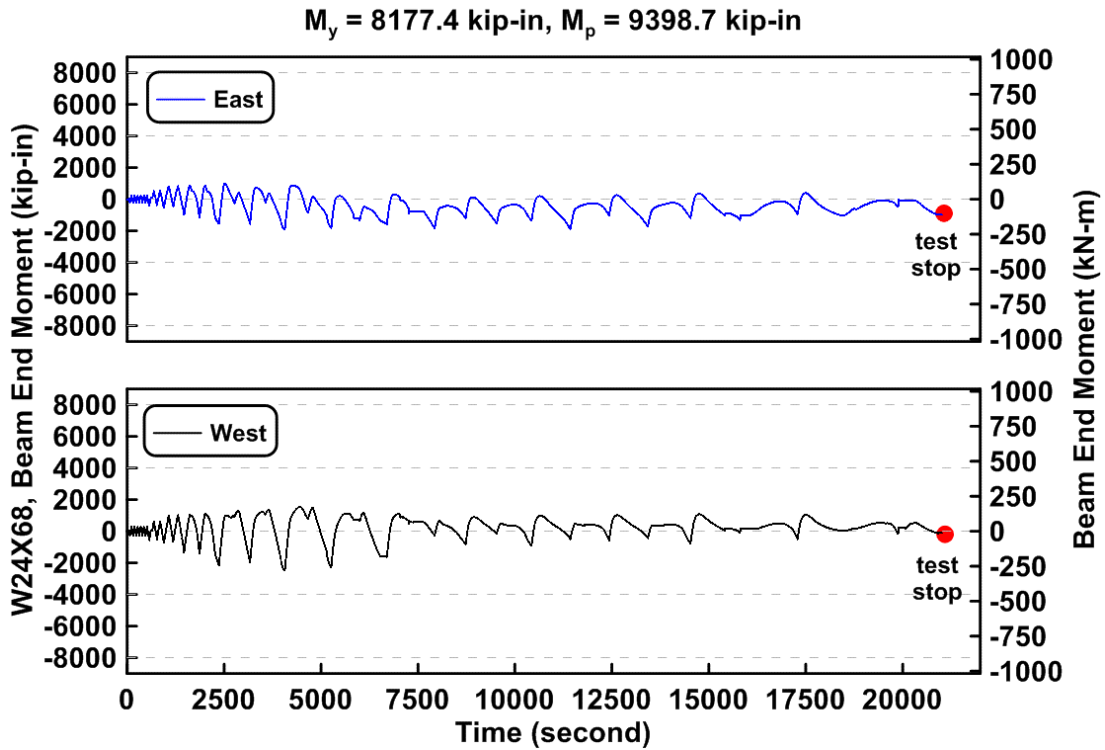


Figure 4.138 Time history of the lower beam end bending moment of TCBF-B-2 specimen

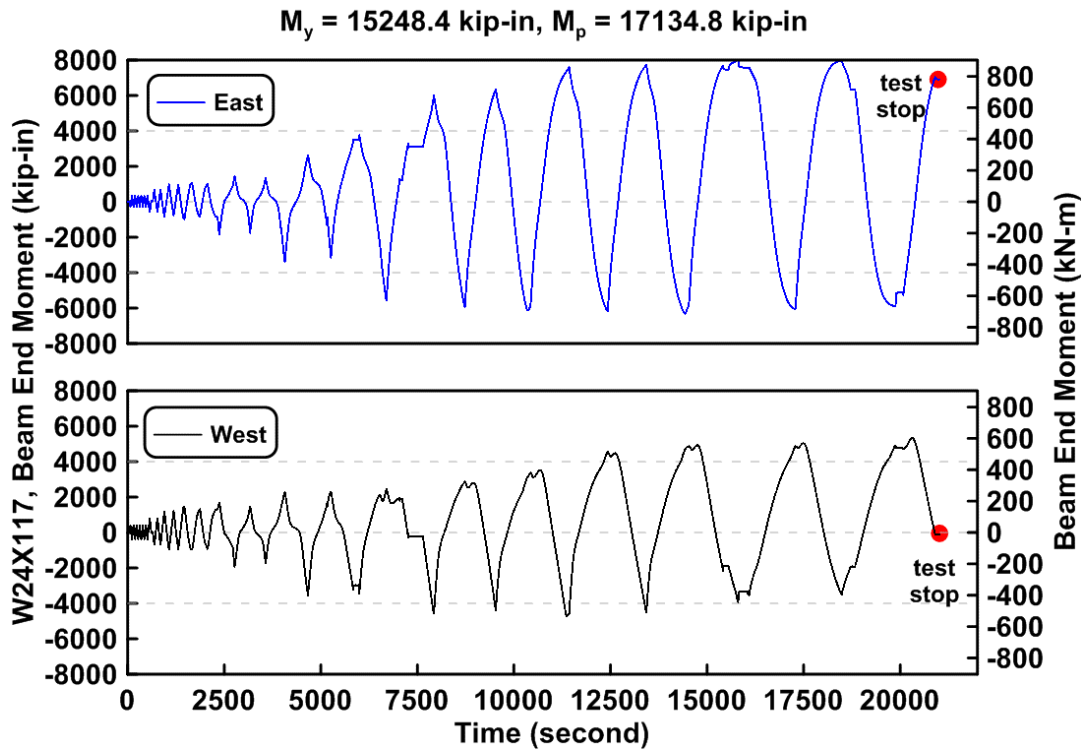


Figure 4.139 Time history of the roof beam end bending moment of TCBF-B-2 specimen

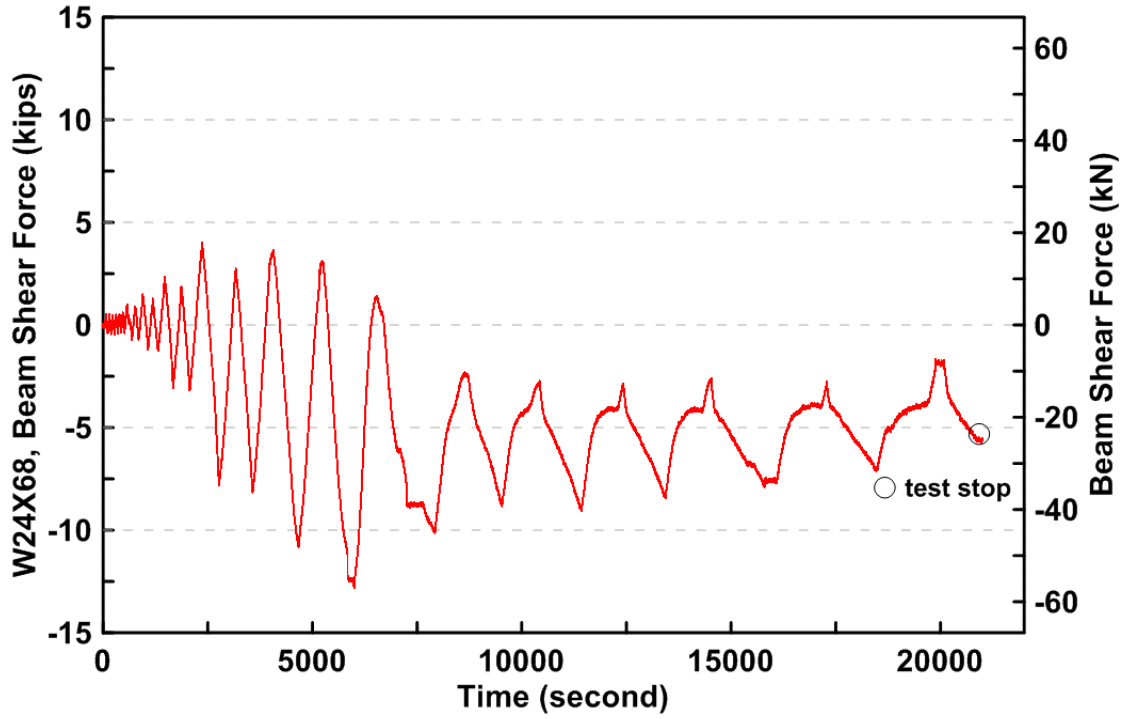


Figure 4.140 Lower beam estimated shear force time history of TCBF-B-2 specimen

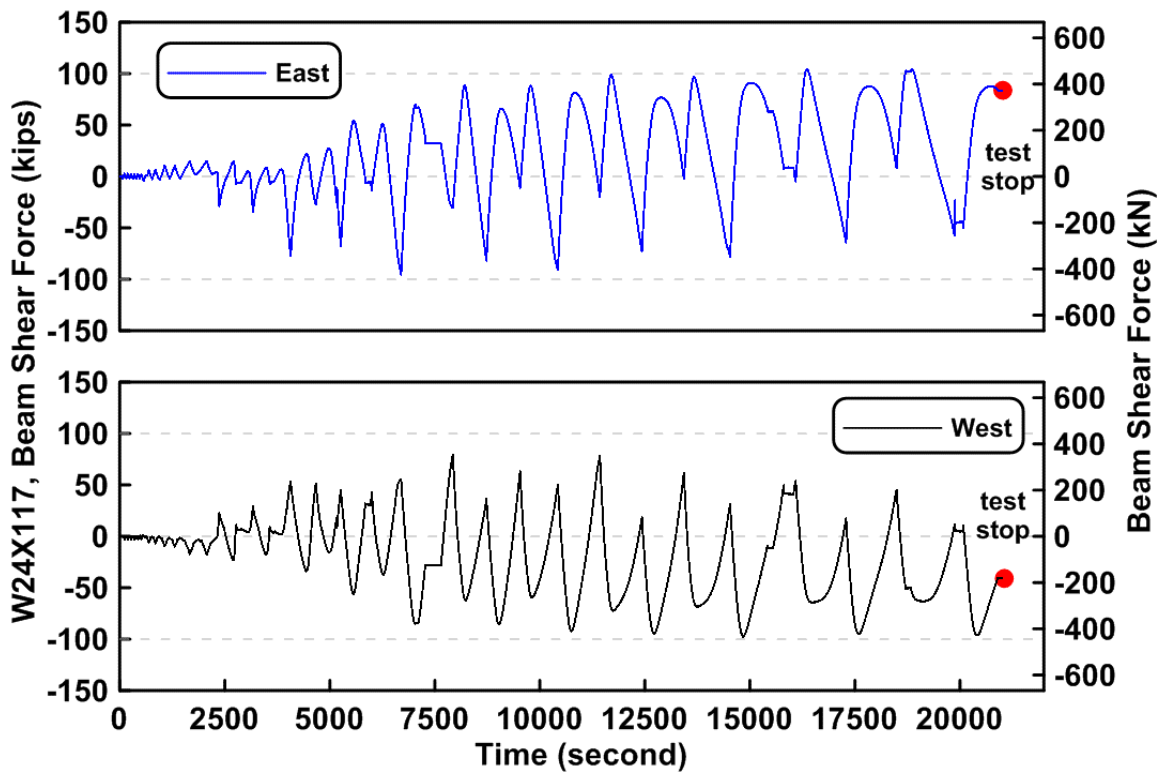


Figure 4.141 Roof beam estimated shear force time history of TCBF-B-2 specimen

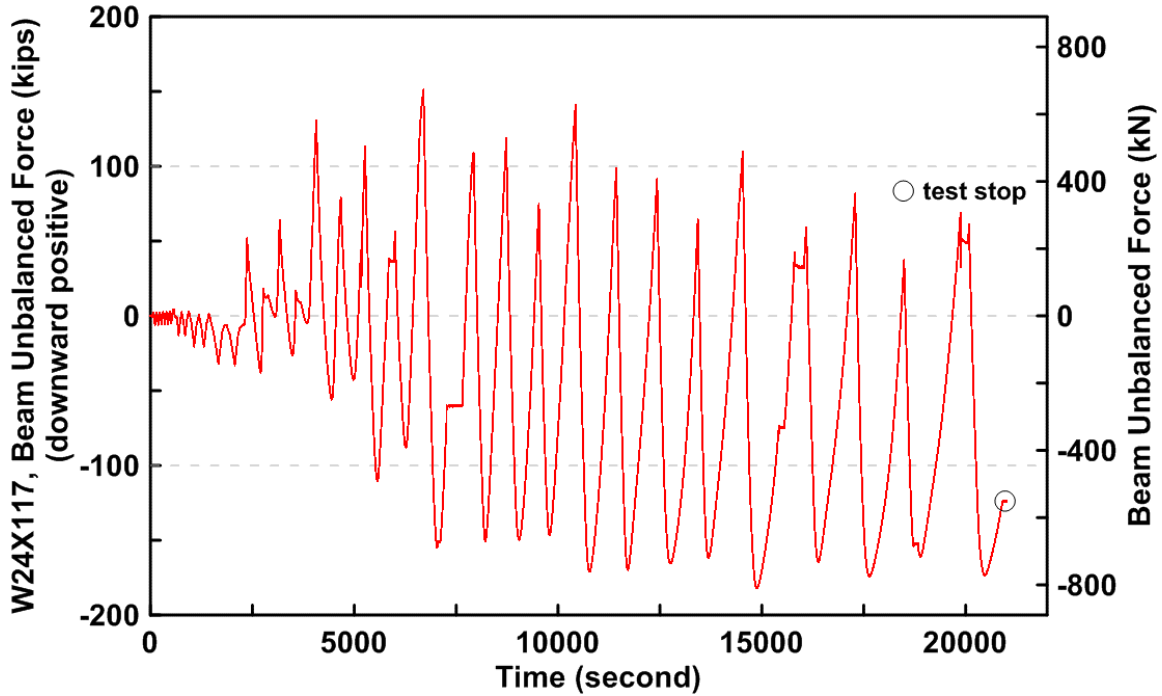


Figure 4.142 Estimated unbalanced force time history of TCBF-B-2 specimen roof beam

#### 4.2.2.1.4 Brace Response

The estimated brace axial forces versus brace axial deformations for each round HSS brace are shown in Fig. 4.143. The estimated brace axial forces versus measured brace out-of-plane displacements at the brace center point for each round HSS braces are shown in Fig. 4.144. Combined brace axial force, axial deformation and out-of-plane displacement relationships are shown in Fig. 4.145. The decomposed strain (axial strain, in-plane bending strain, out-of-plane bending strain and warping strain; definition of strain components are similar to that shown in Fig. 4.47(b) but assuming no warping strain for round HSS braces) time histories of each brace are plotted in Figs. 4.146 to 4.149.

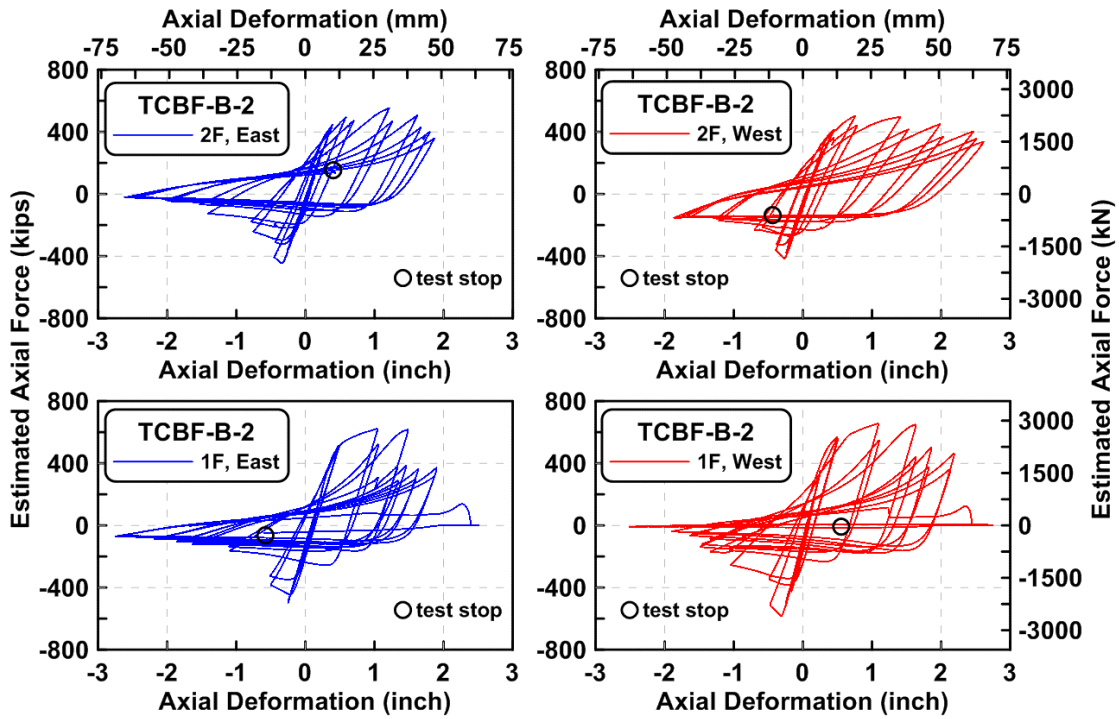


Figure 4.143 Estimated brace axial forces vs. brace axial deformations of TCBF-B-2 specimen

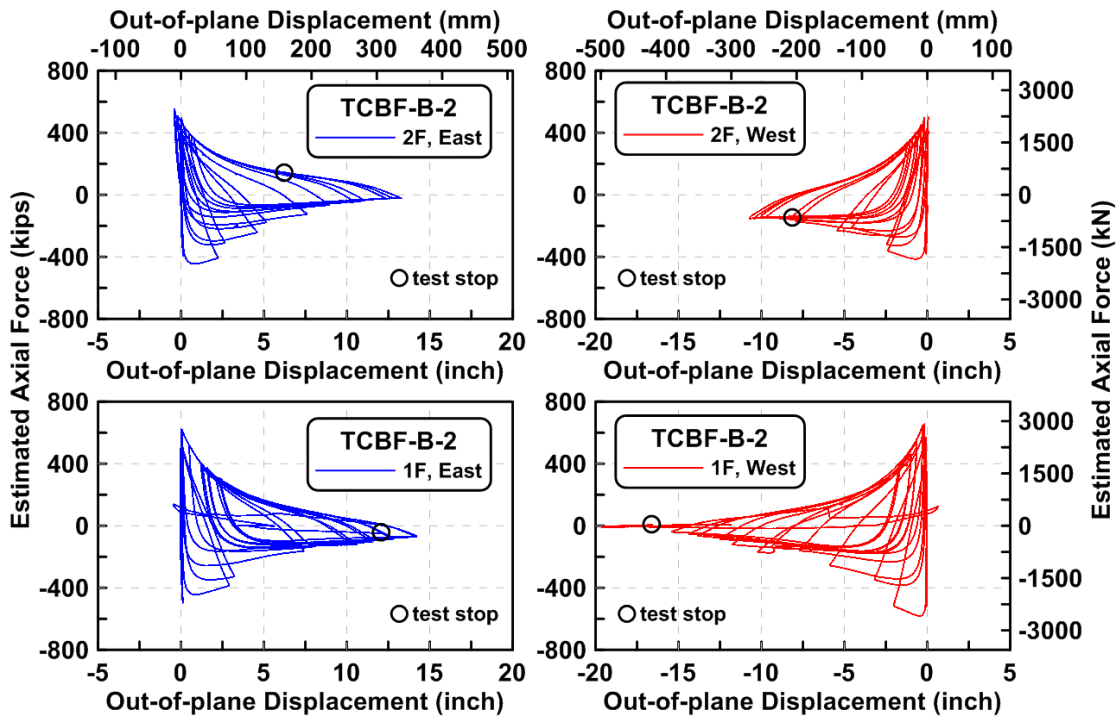


Figure 4.144 Estimated brace axial forces vs. measured brace out-of-plane displacements of TCBF-B-2 specimen

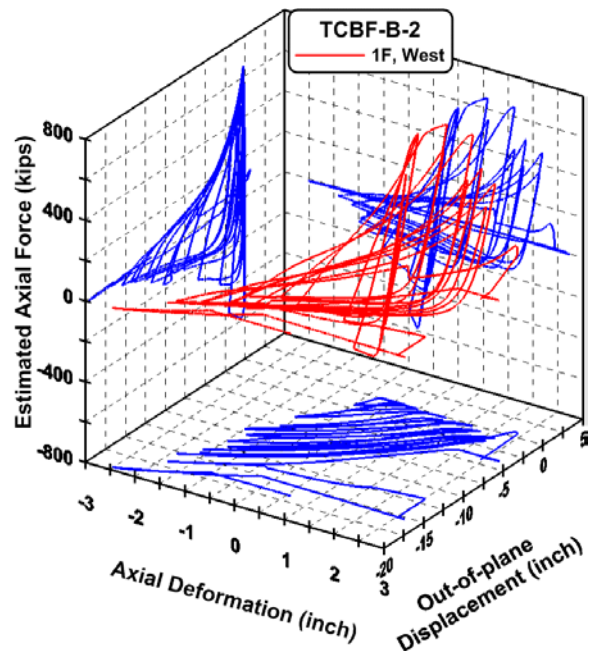
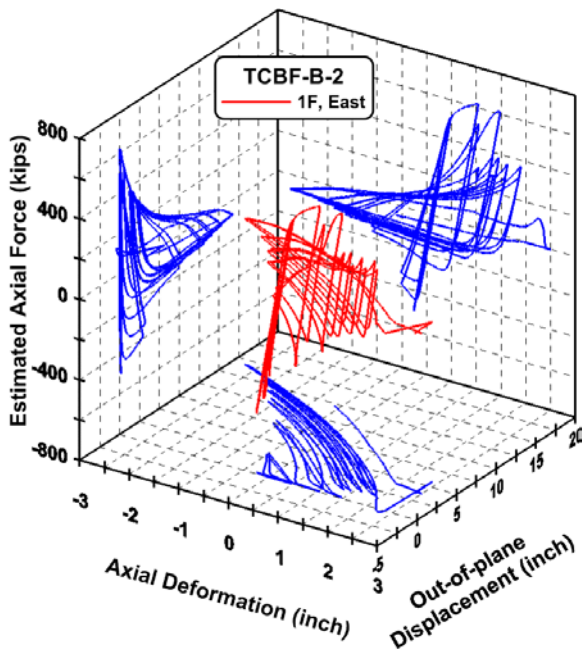
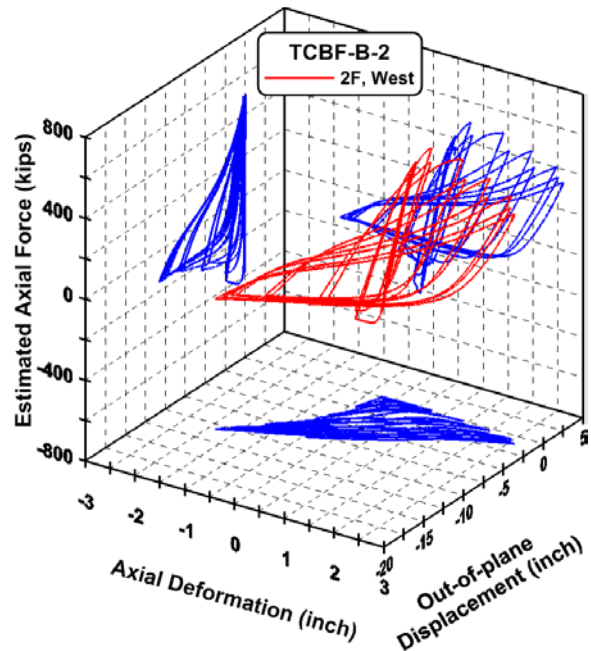
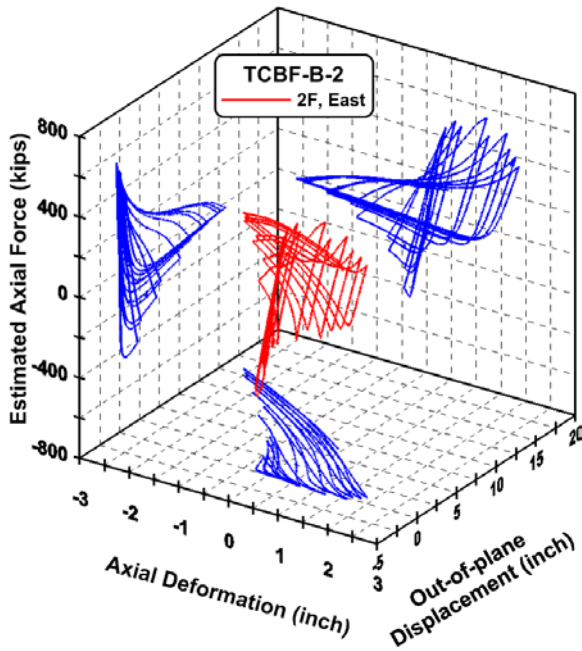


Figure 4.145 Estimated brace axial force, brace axial deformation and measured brace out-of-plane displacement relationships of TCBF-B-2 specimen

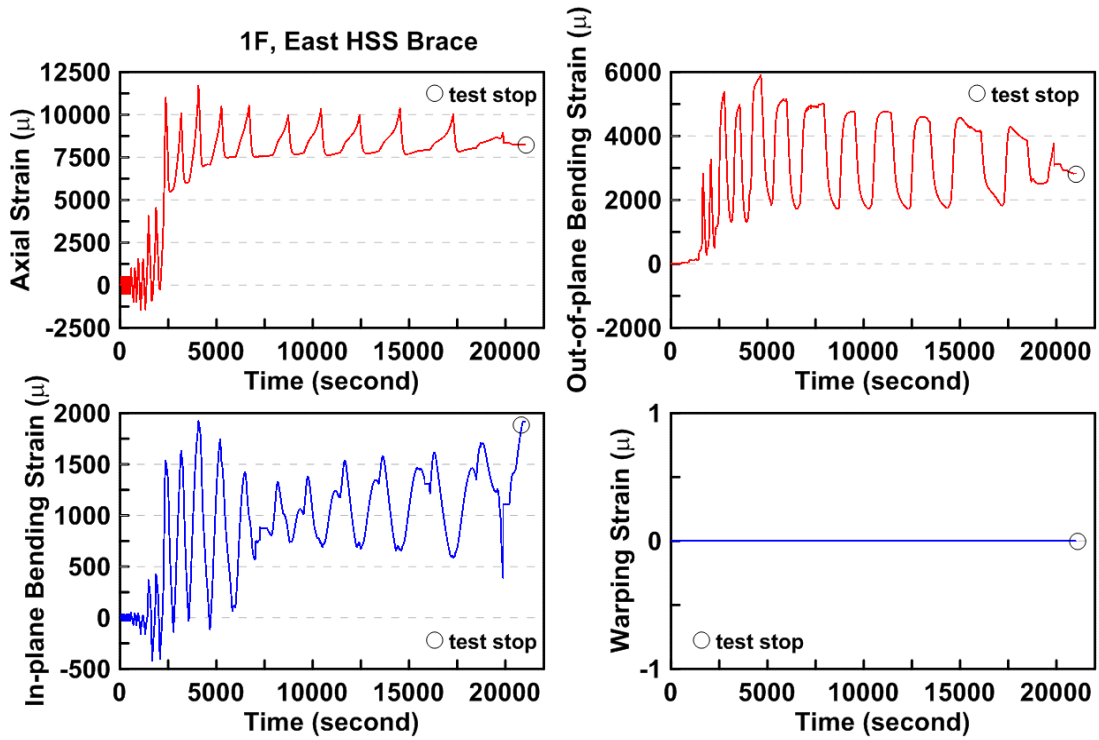


Figure 4.146 Time history of the decomposed strain components of eastern side HSS brace in the first story of TCBF-B-2 specimen

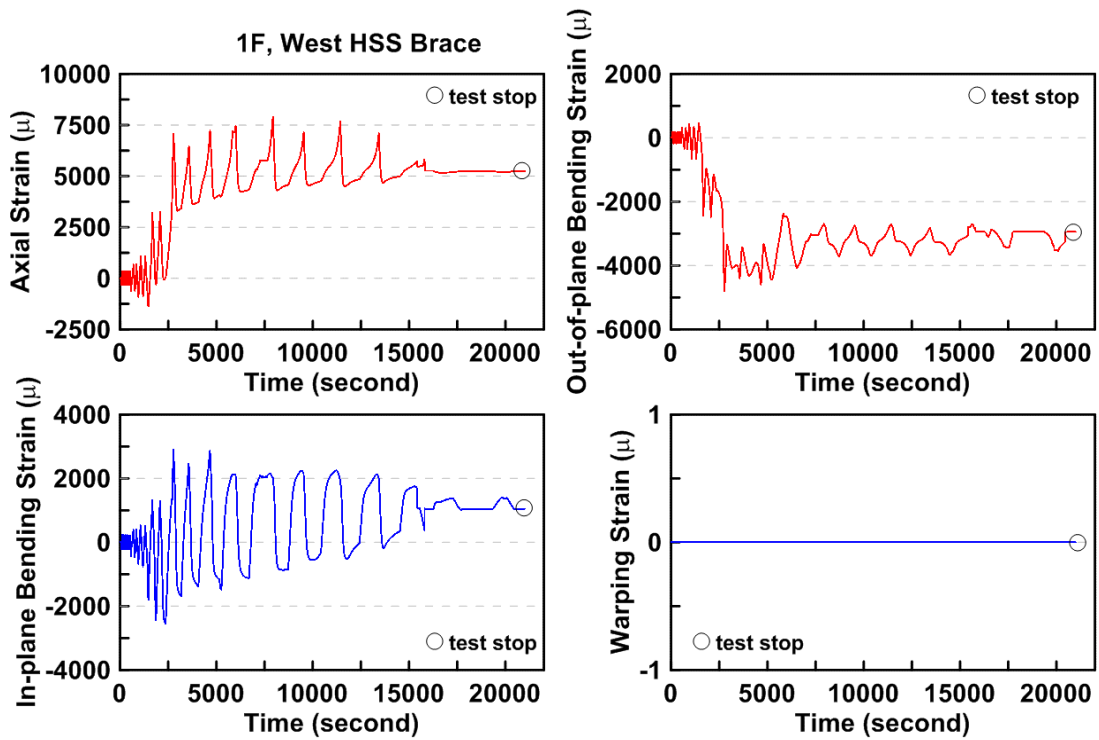


Figure 4.147 Time history of the decomposed strain components of western side HSS brace in the first story of TCBF-B-2 specimen

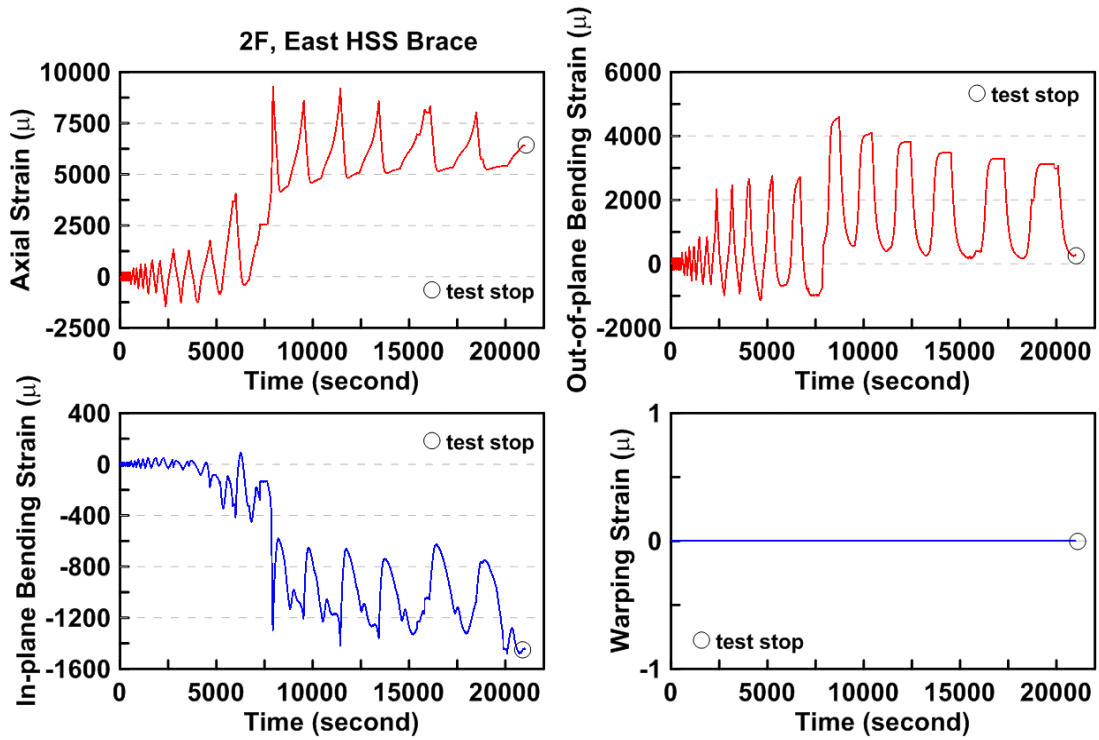


Figure 4.148 Time history of the decomposed strain components of eastern side HSS brace in the second story of TCBF-B-2 specimen

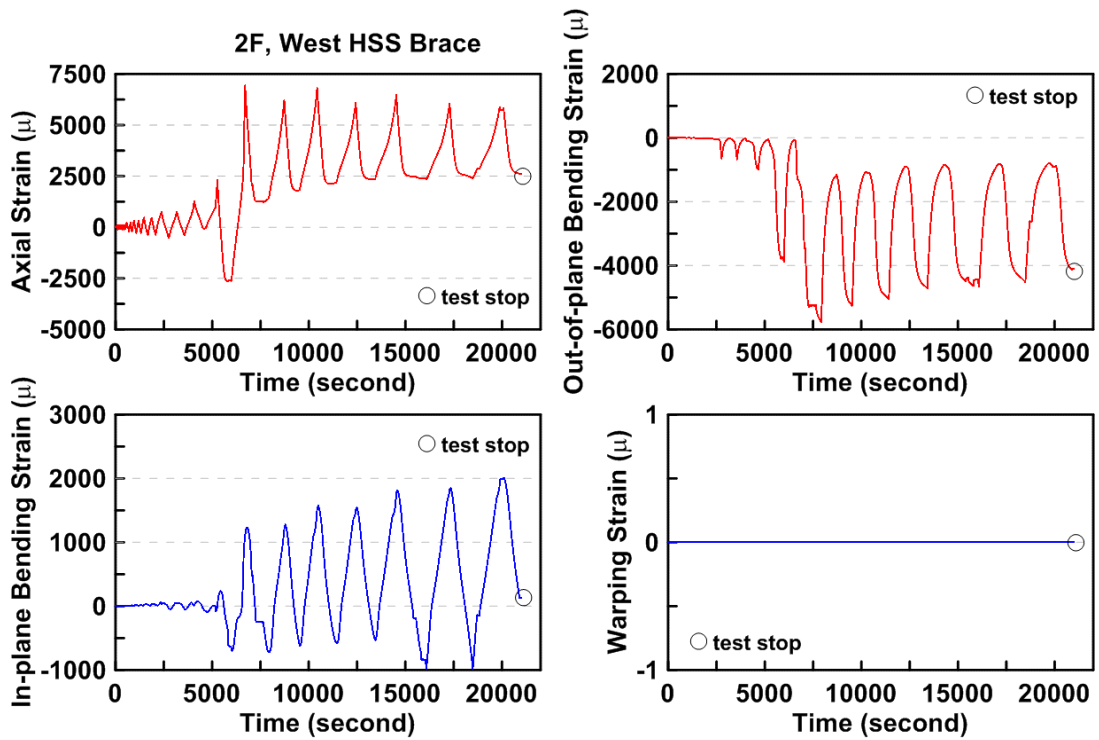


Figure 4.149 Time history of the decomposed strain components of western side HSS brace in the second story of TCBF-B-2 specimen



#### 4.2.2.1.5 Panel Zone Response

Estimated panel zone shear stress versus measured panel zone shear strain relationships for four locations are plotted in Figs. 4.150. Time history of derived rosette type strain gauge readings in the panel zone area at each story are shown from Figs. 4.151 to 4.154. Normalized maximum and minimum principal stress relationships along with different yield criteria for the panel zone regions are plotted in Figs. 4.155 to 4.158.

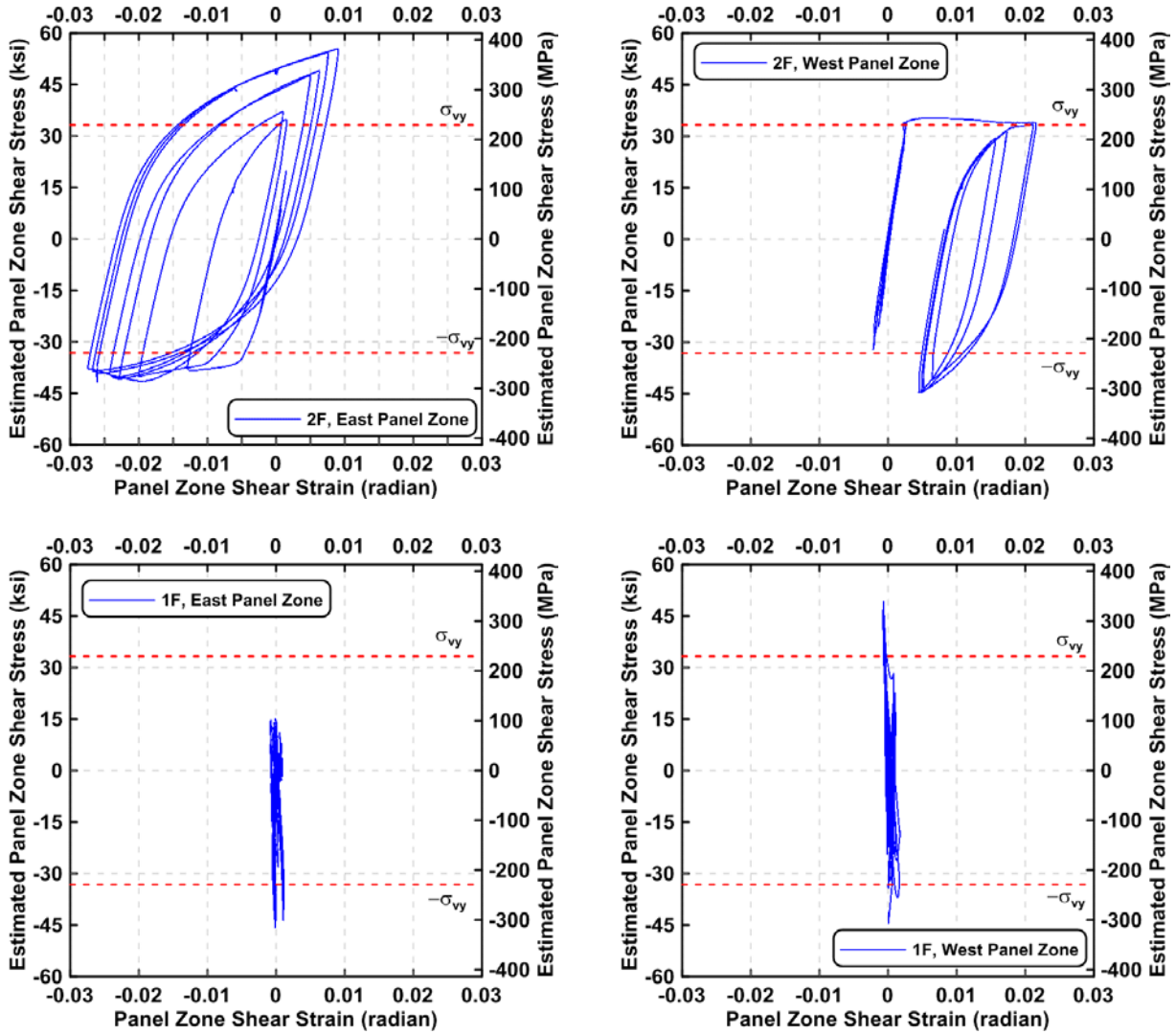


Figure 4.150 Estimated panel zone shear stress vs. shear strain relationships of TCBF-B-2

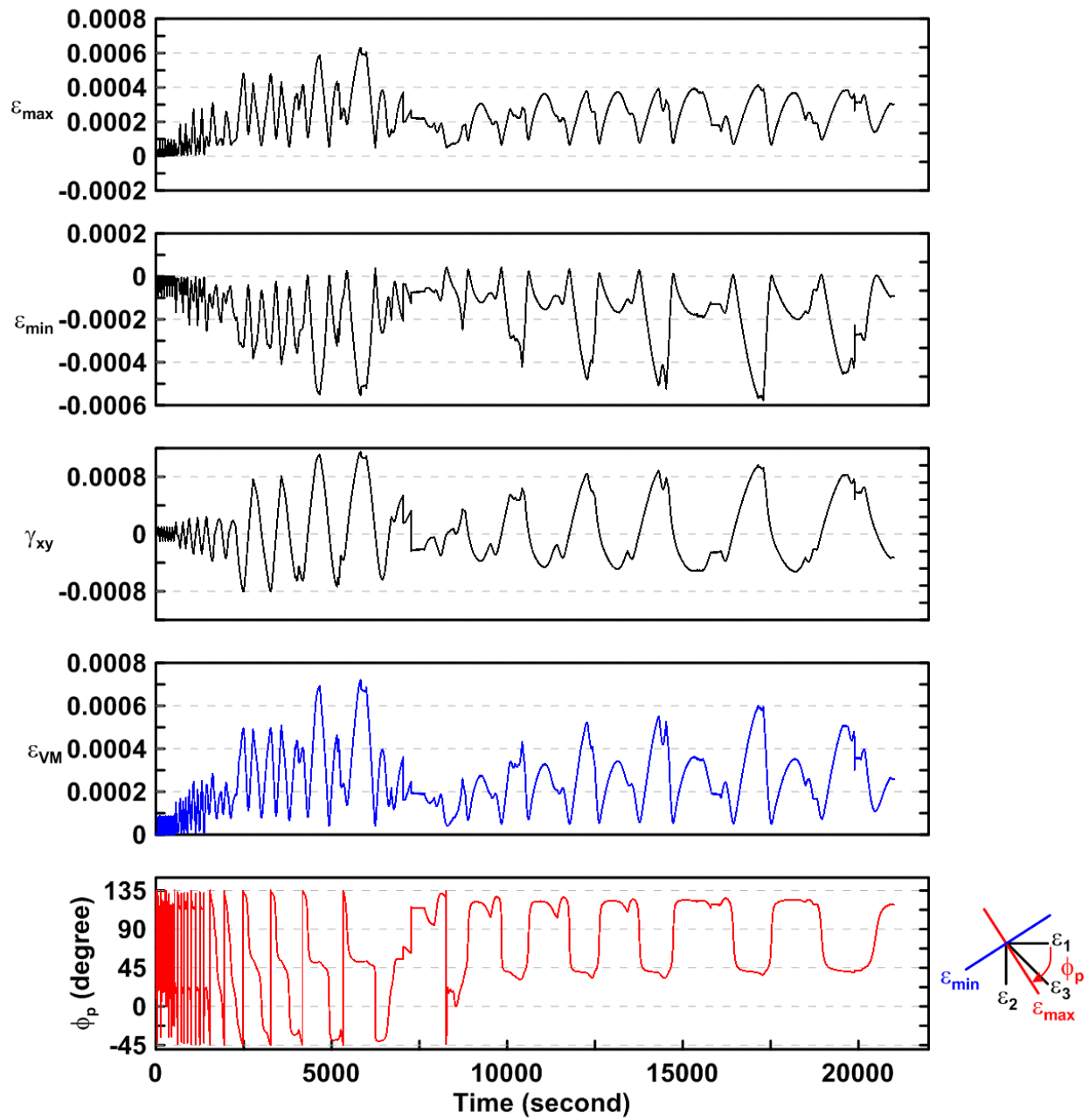


Figure 4.151 Time history of rosette type strain gauge readings in the lower panel zone of TCBF-B-2 specimen (location: R2)

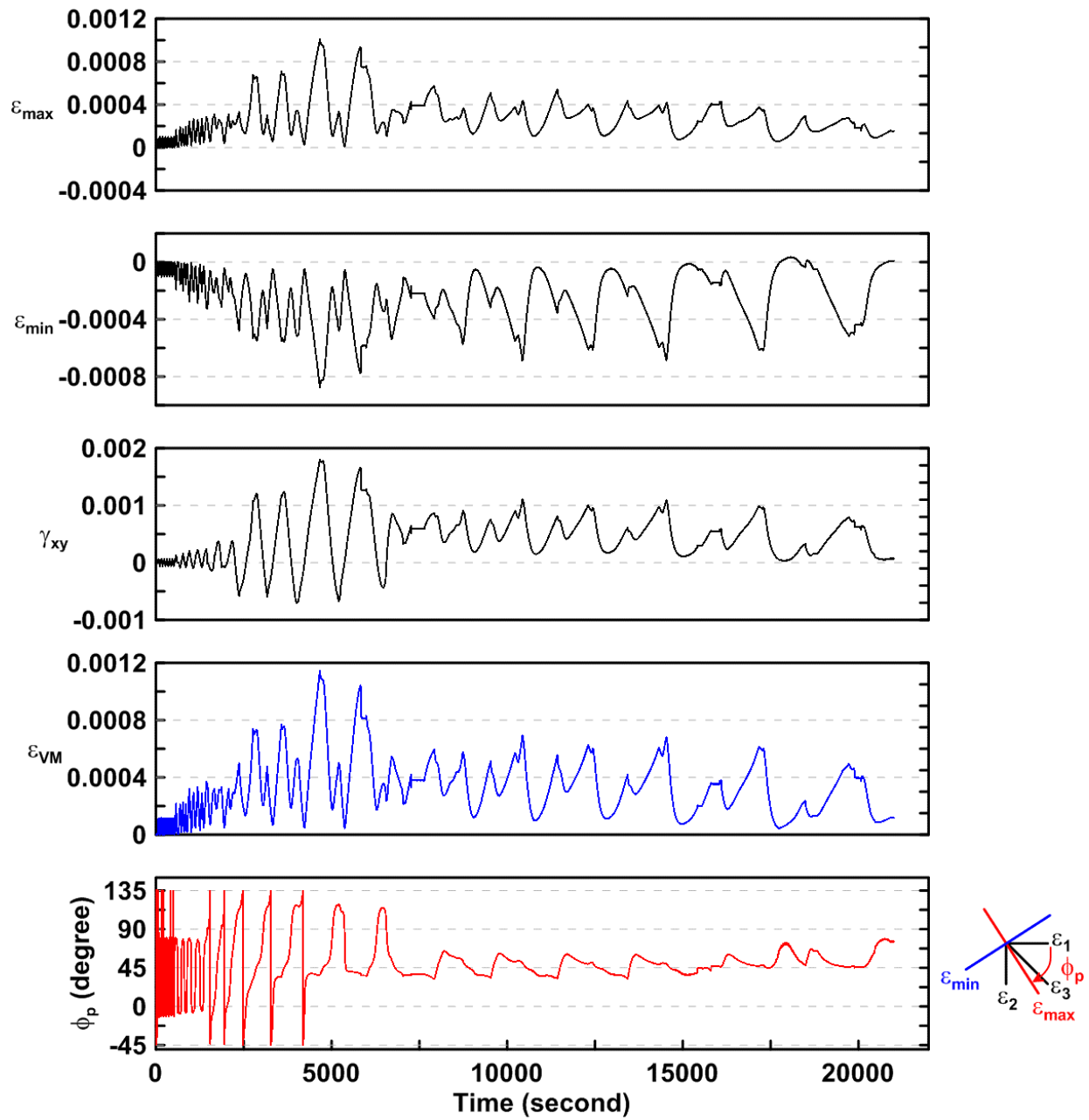


Figure 4.152 Time history of rosette type strain gauge readings in the lower panel zone of TCBF-B-2 specimen (location: R6)

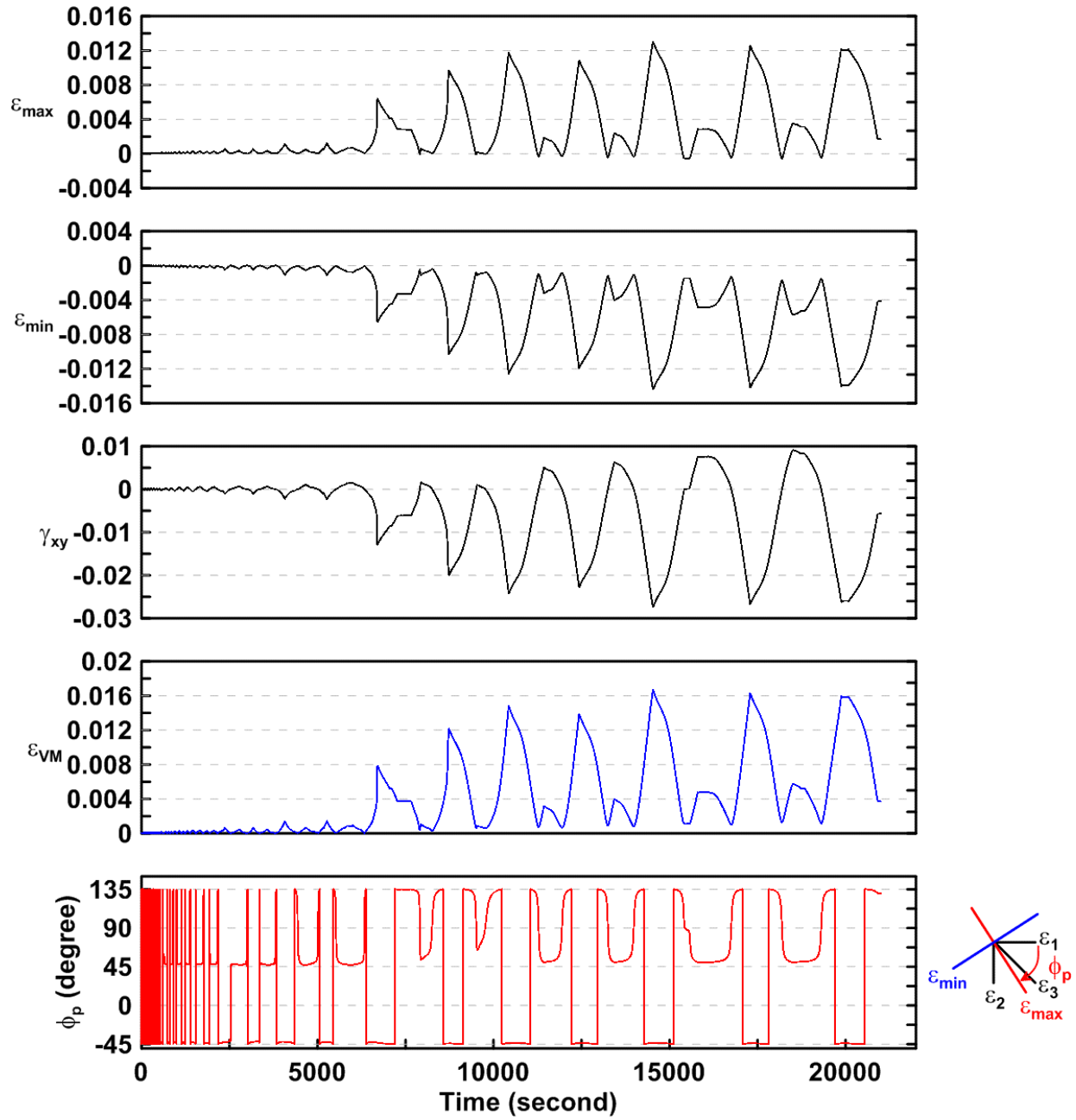


Figure 4.153 Time history of rosette type strain gauge readings in the roof panel zone of TCBF-B-2 specimen (location: R4)

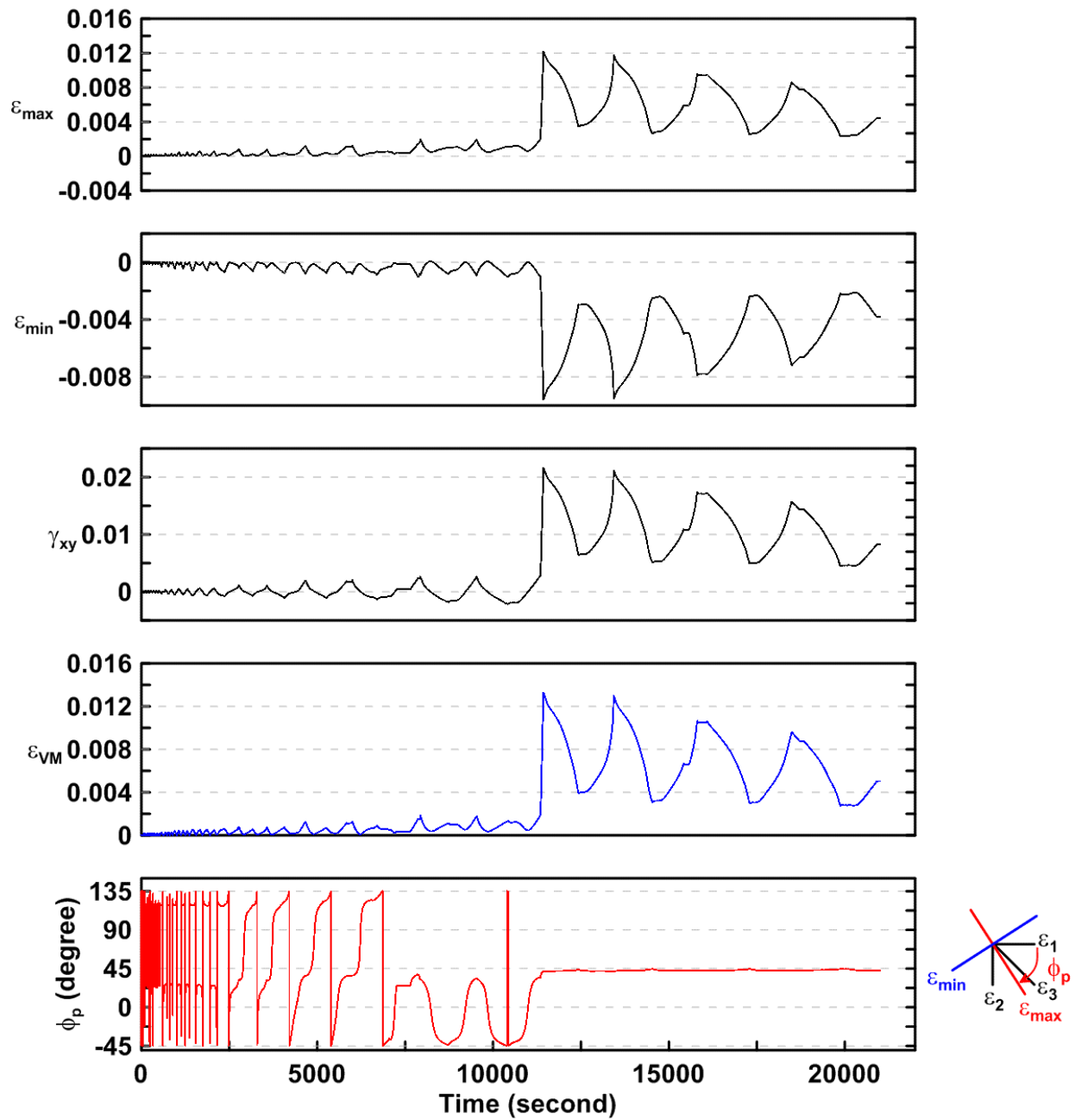


Figure 4.154 Time history of rosette type strain gauge readings in the roof panel zone of TCBF-B-2 specimen (location: R8)

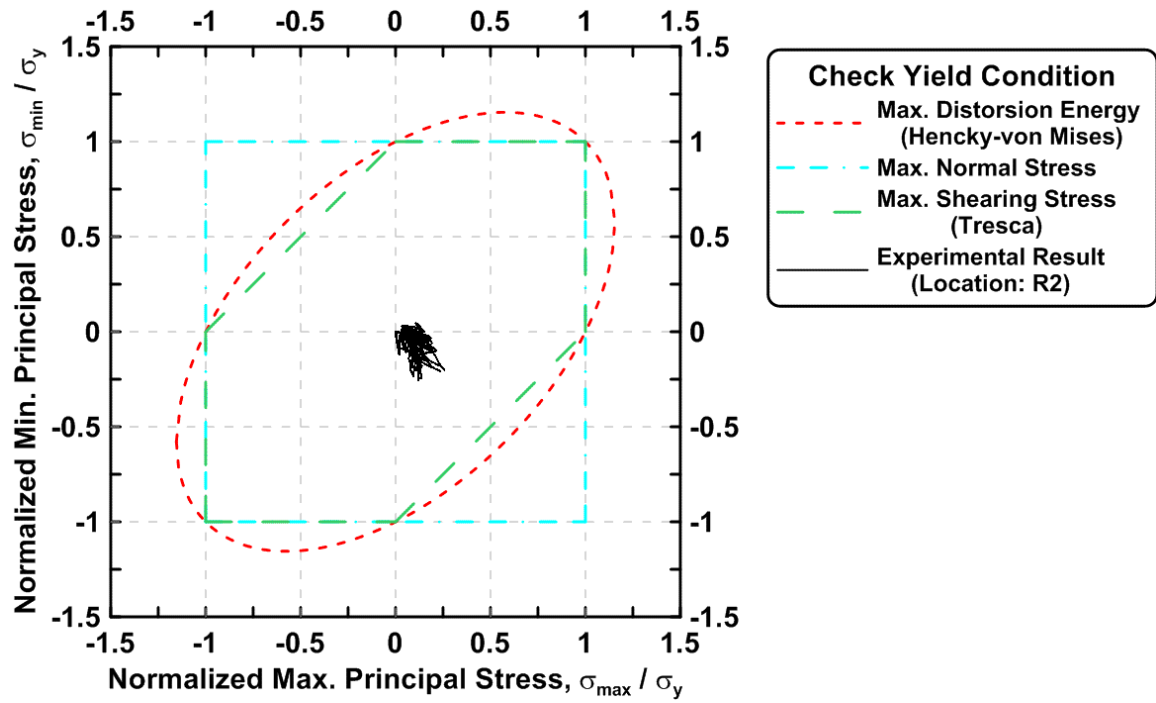


Figure 4.155 Normalized maximum principal stress vs. normalized minimum principal stress in the lower panel zone of TCBF-B-2 specimen (location: R2)

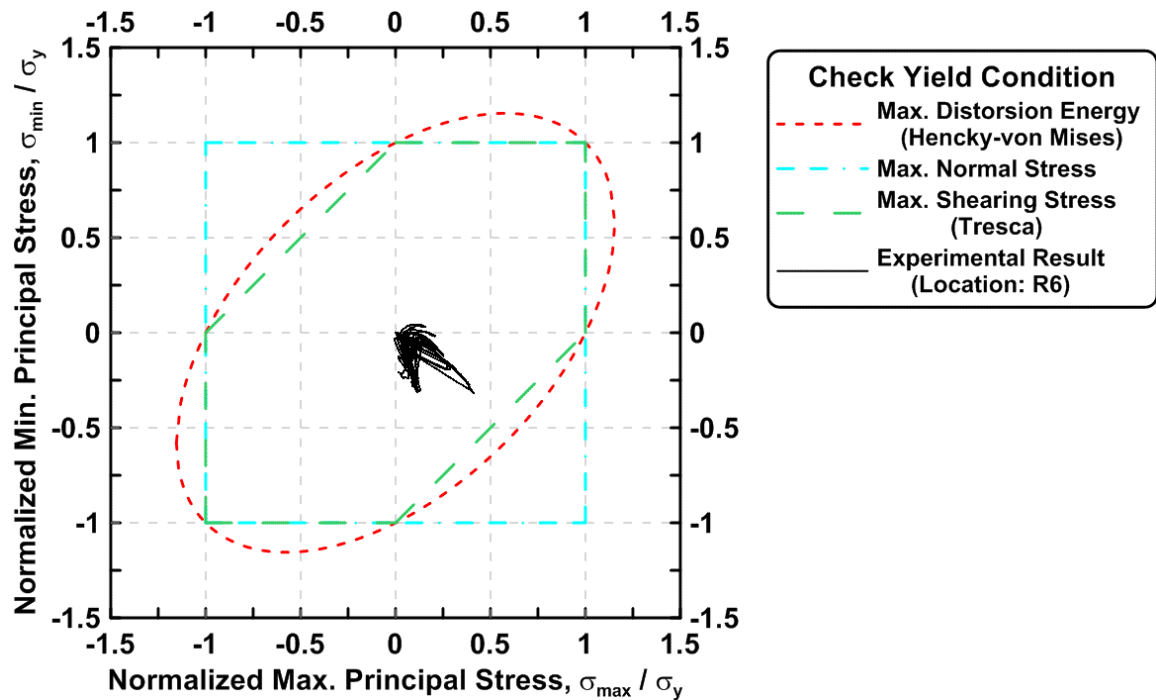


Figure 4.156 Normalized maximum principal stress vs. normalized minimum principal stress in the lower panel zone of TCBF-B-2 specimen (location: R6)

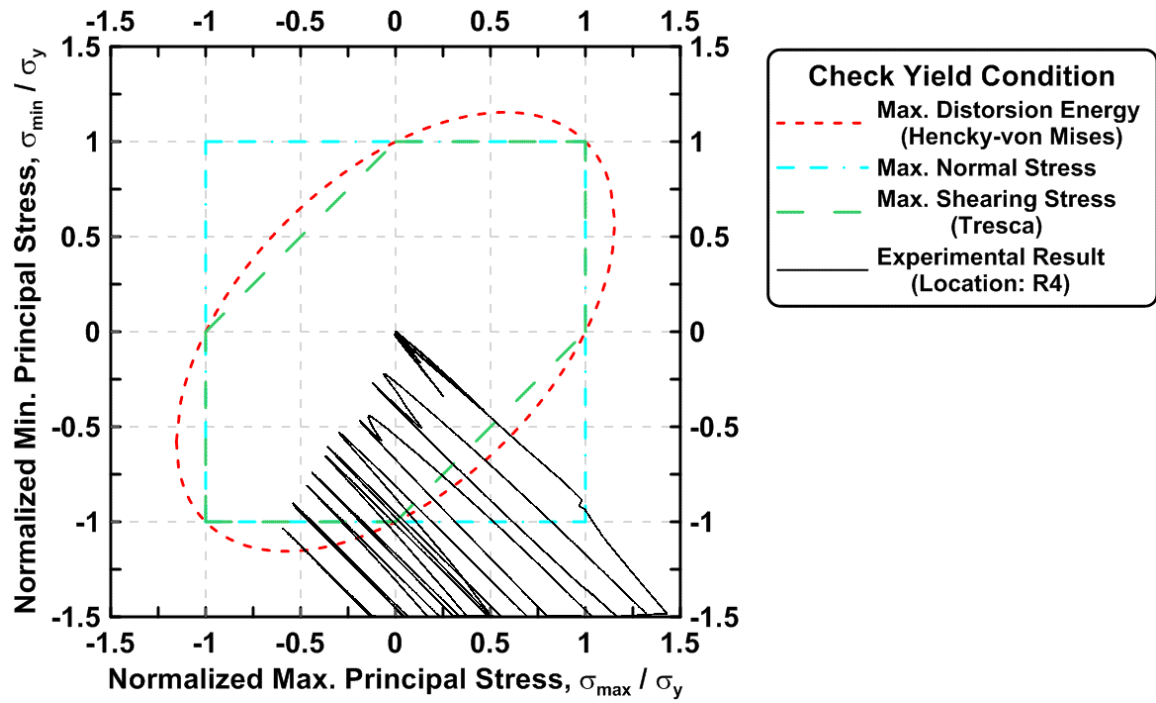


Figure 4.157 Normalized maximum principal stress vs. normalized minimum principal stress in the roof panel zone of TCBF-B-2 specimen (location: R4)

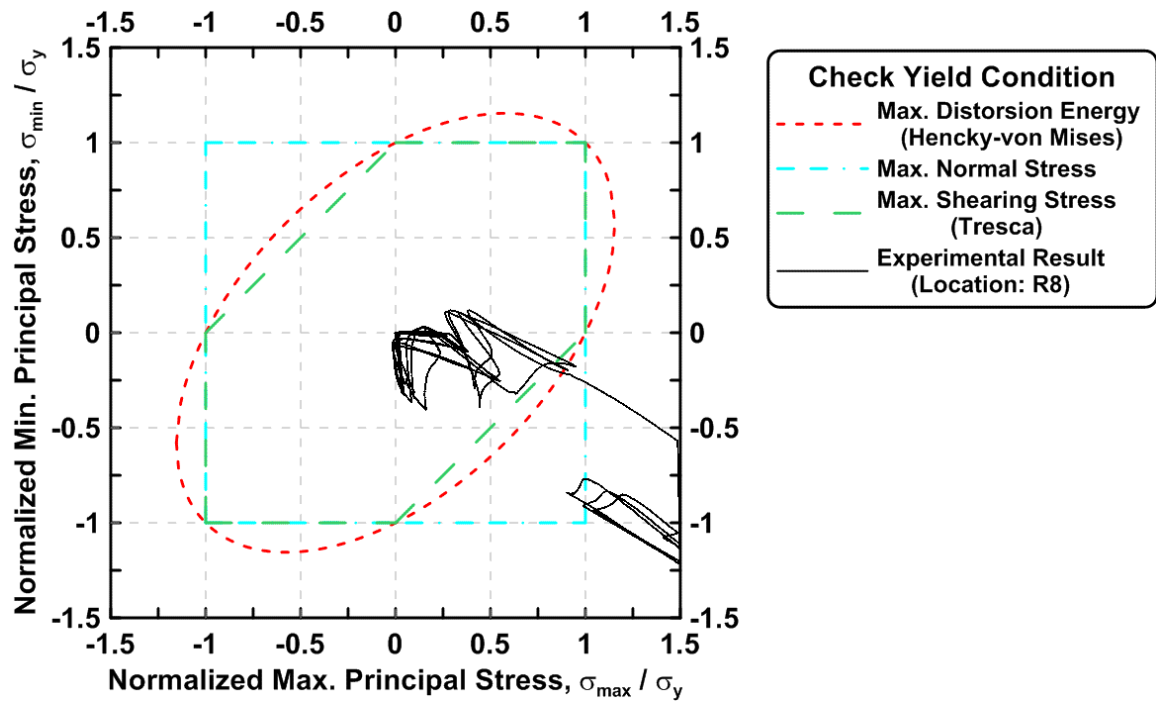


Figure 4.158 Normalized maximum principal stress vs. normalized minimum principal stress in the roof panel zone of TCBF-B-2 specimen (location: R8)

#### 4.2.2.1.6 Gusset Plate Response

The time history of derived rosette type strain gauge readings in the 3/4-inch thick one-piece gusset plate are shown from Figs. 4.159 to 4.170. Normalized maximum and minimum principal stress relationships along with different yield criteria for the rosettes on the gusset plate are plotted in Figs. 4.171 to 4.182. The averaged axial strain and bending strain time history in the tapered gusset plate at eastern side of the specimen are shown in Figs. 4.183 and 4.184, respectively.

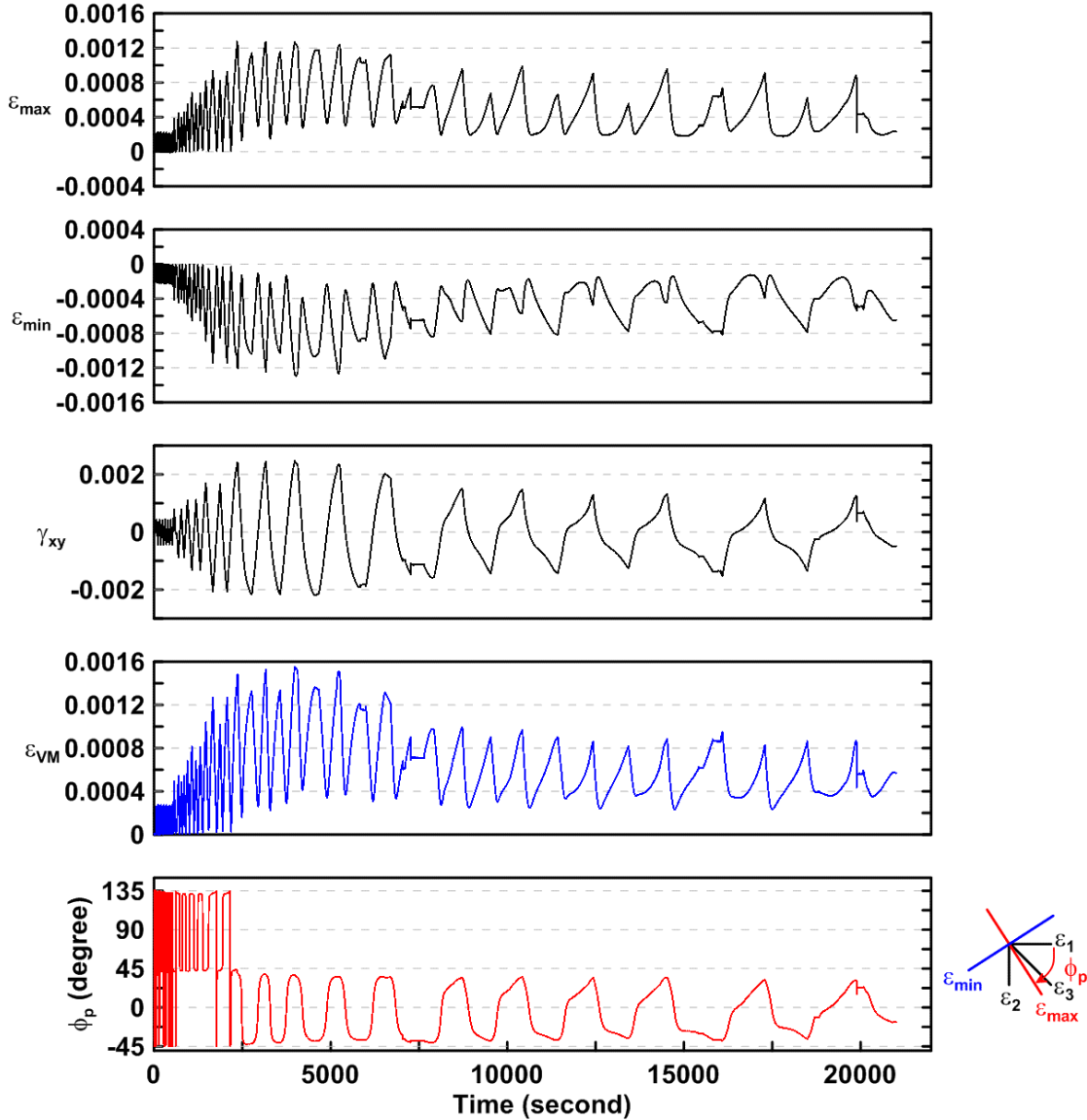


Figure 4.159 Time history of rosette type strain gauge readings in the one-piece gusset plate of TCBF-B-2 specimen (location: R9)



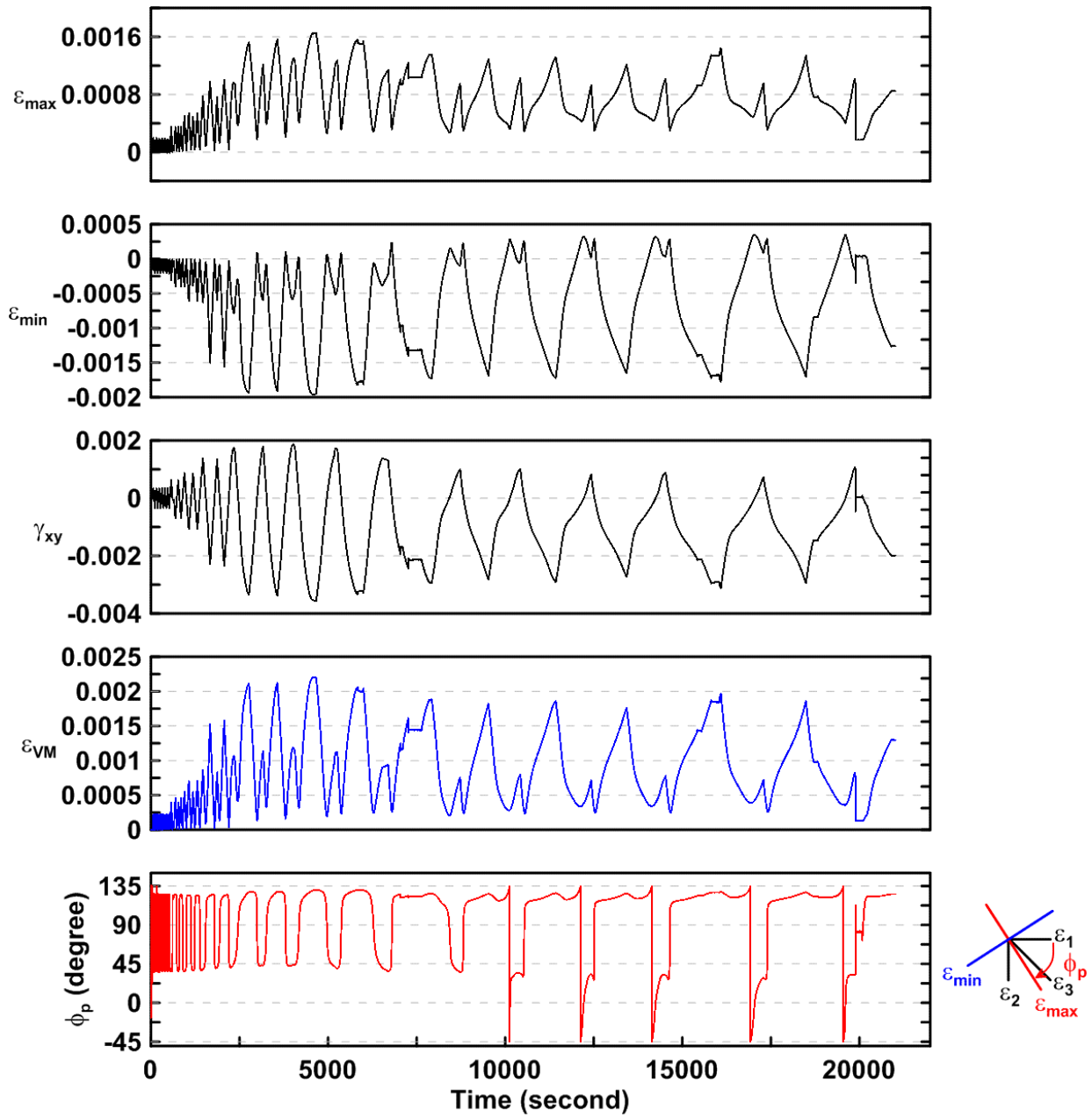


Figure 4.160 Time history of rosette type strain gauge readings in the one-piece gusset plate of TCBF-B-2 specimen (location: R10)

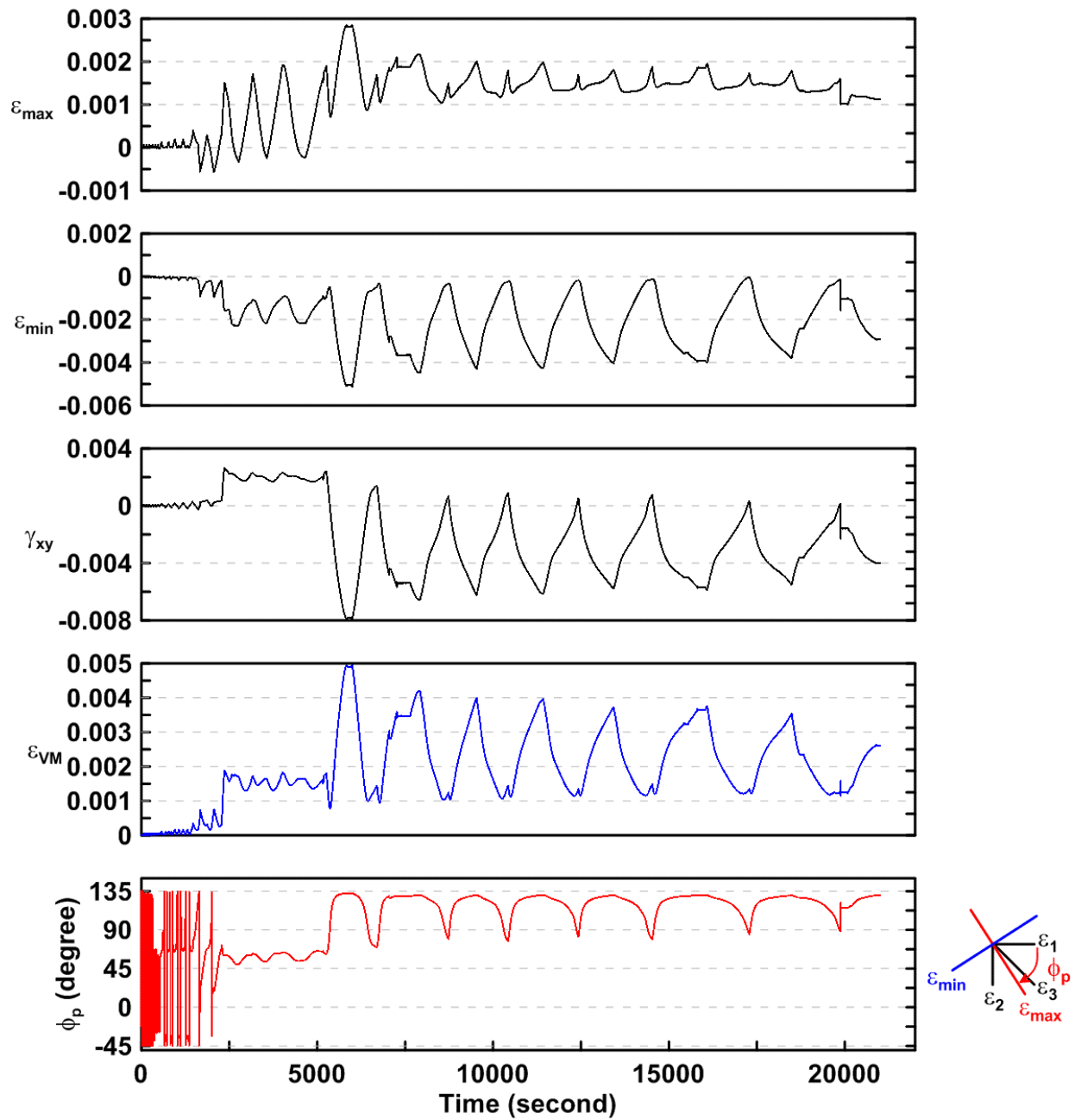


Figure 4.161 Time history of rosette type strain gauge readings in the one-piece gusset plate of TCBF-B-2 specimen (location: R11)

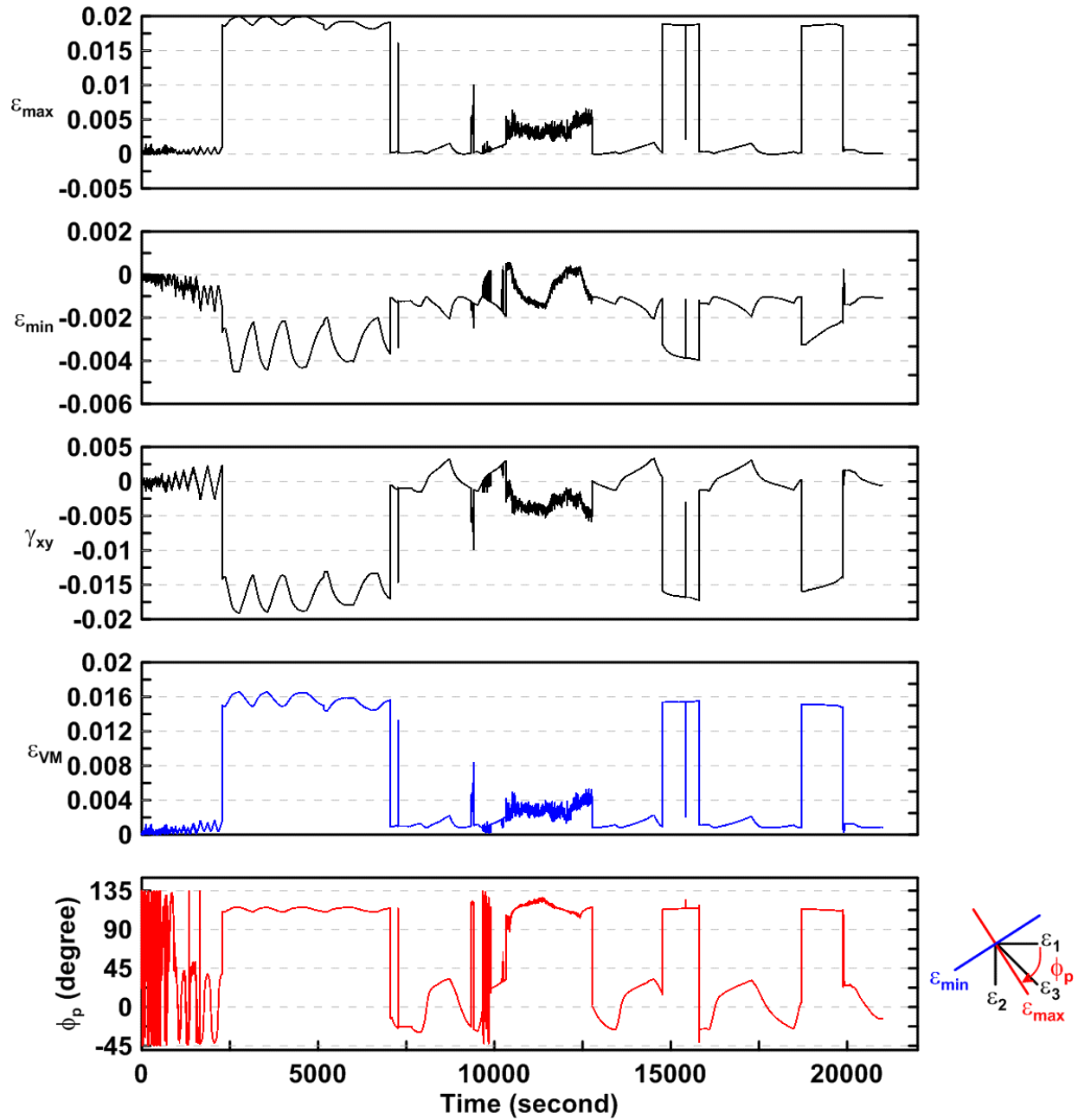


Figure 4.162 Time history of rosette type strain gauge readings in the one-piece gusset plate of TCBF-B-2 specimen (location: R12)

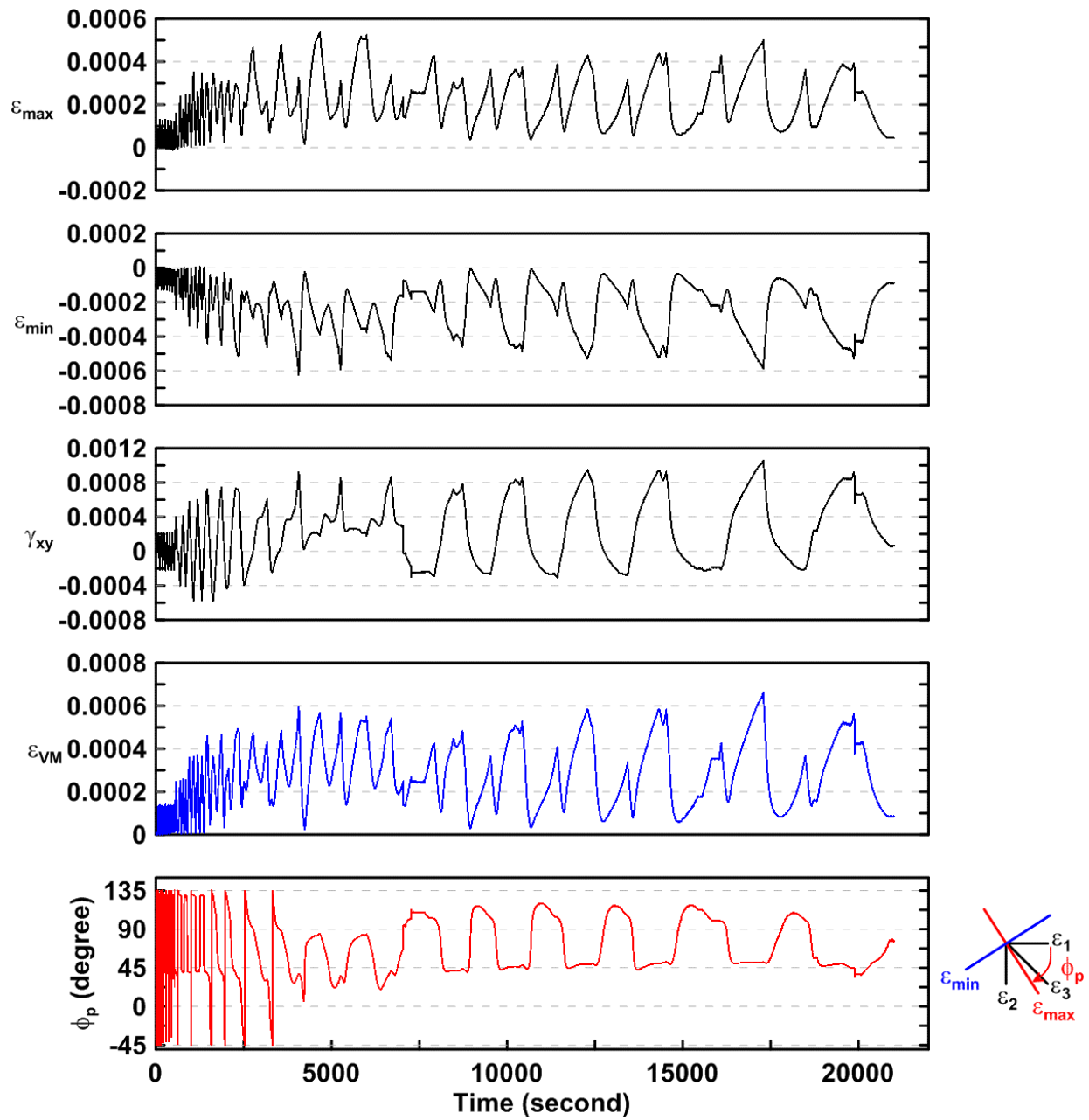


Figure 4.163 Time history of rosette type strain gauge readings in the one-piece gusset plate of TCBF-B-2 specimen (location: R13)

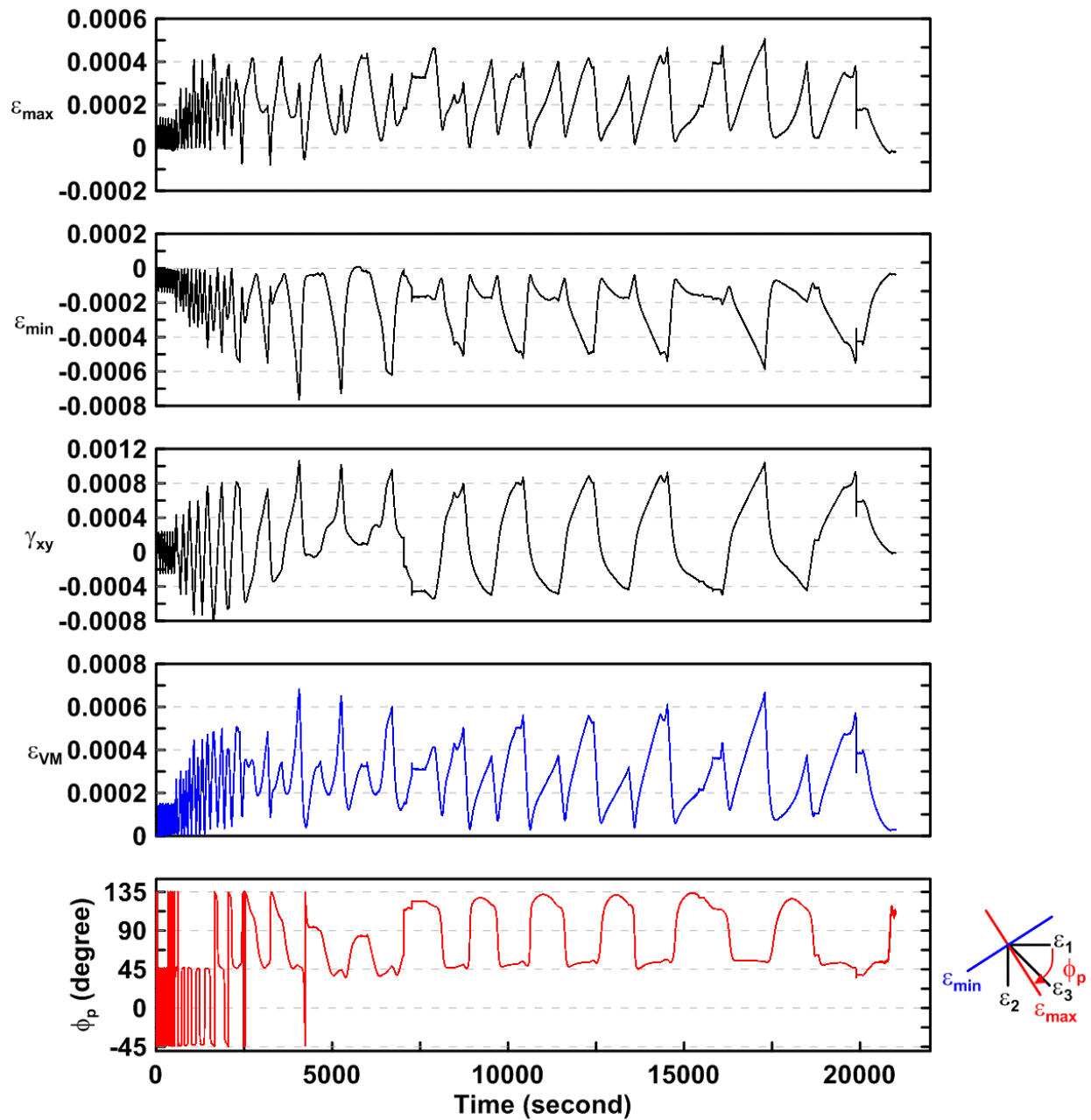


Figure 4.164 Time history of rosette type strain gauge readings in the one-piece gusset plate of TCBF-B-2 specimen (location: R14)

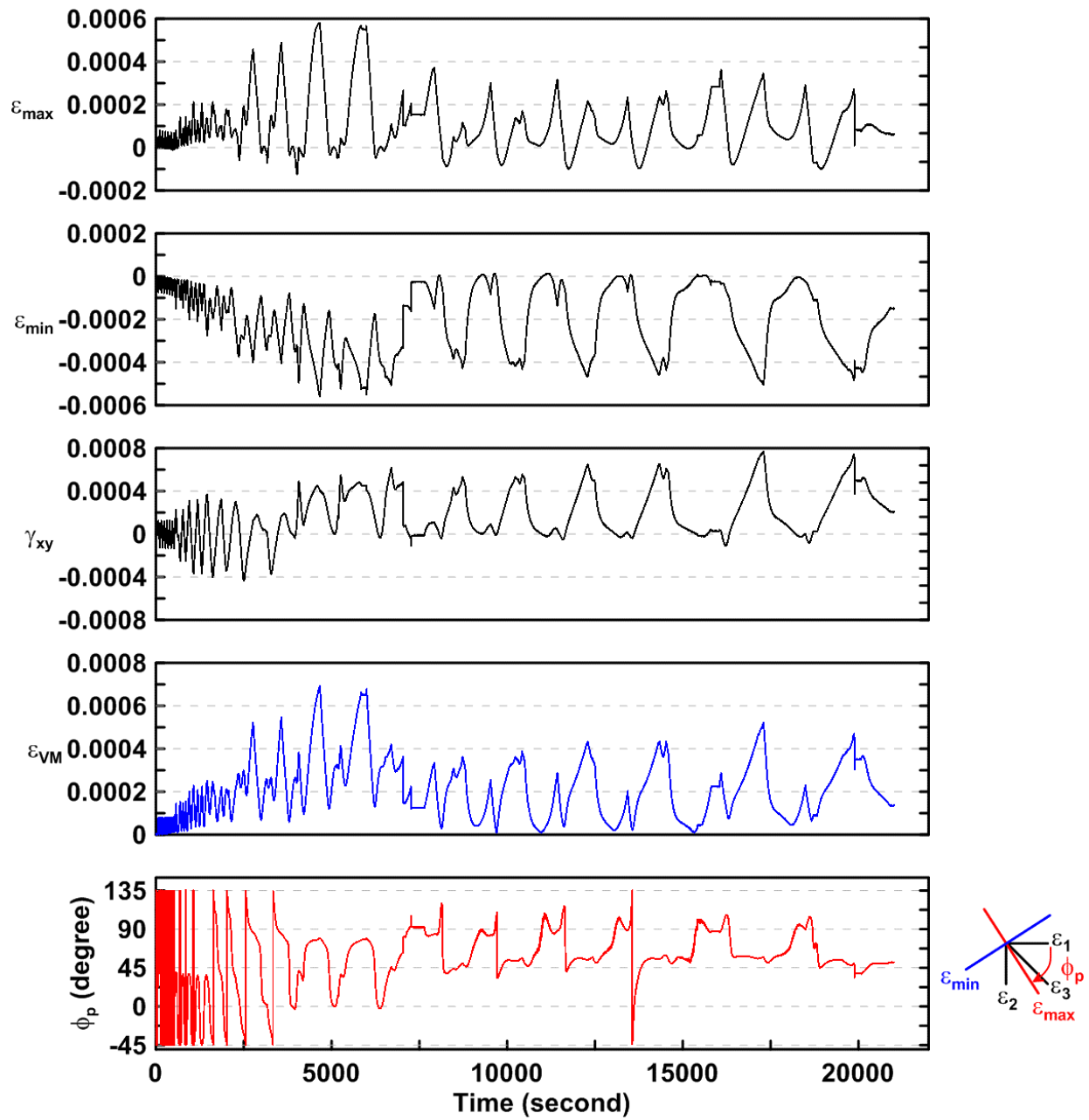


Figure 4.165 Time history of rosette type strain gauge readings in the one-piece gusset plate of TCBF-B-2 specimen (location: R15)

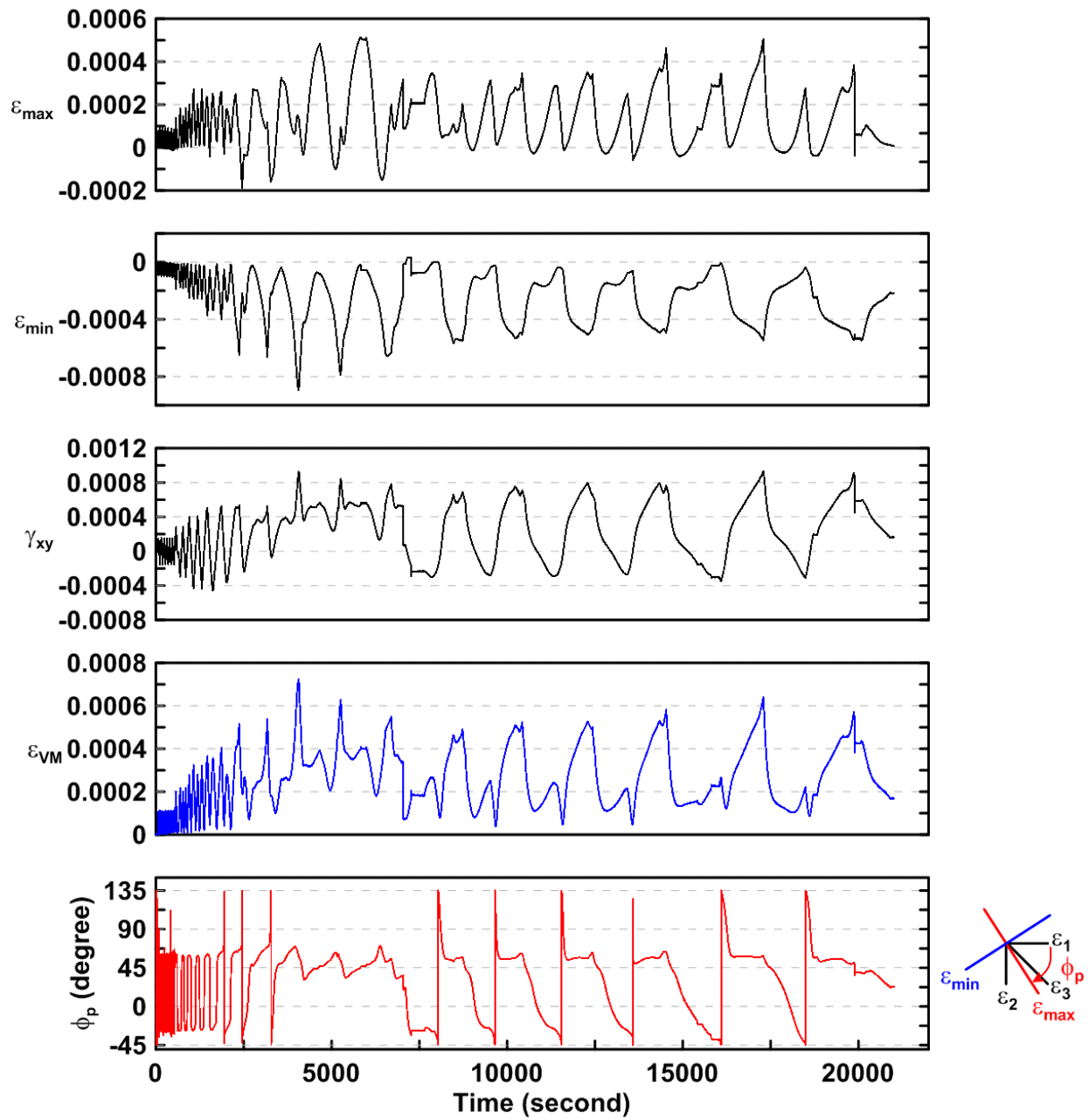


Figure 4.166 Time history of rosette type strain gauge readings in the one-piece gusset plate of TCBF-B-2 specimen (location: R16)

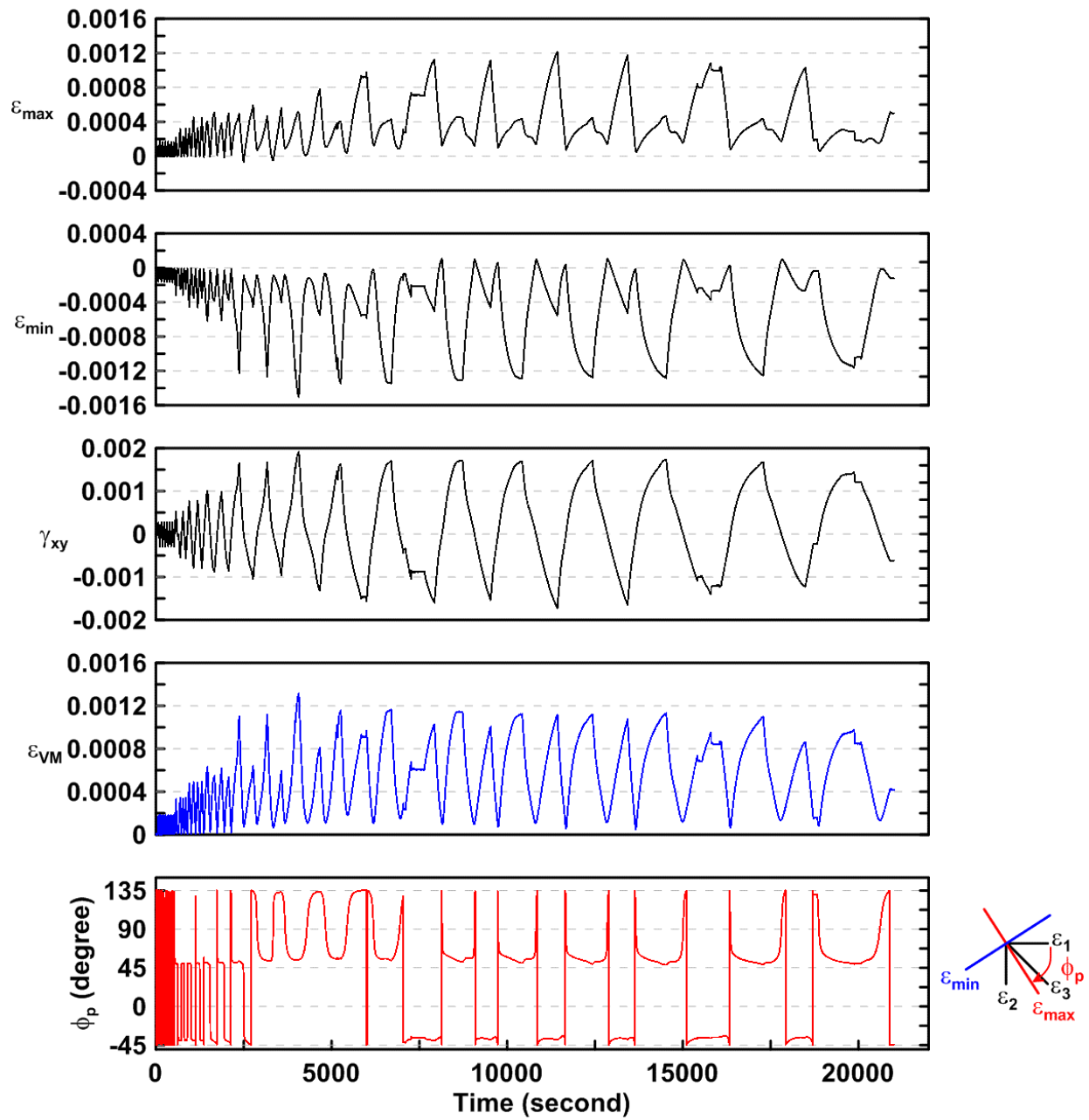


Figure 4.167 Time history of rosette type strain gauge readings in the one-piece gusset plate of TCBF-B-2 specimen (location: R17)



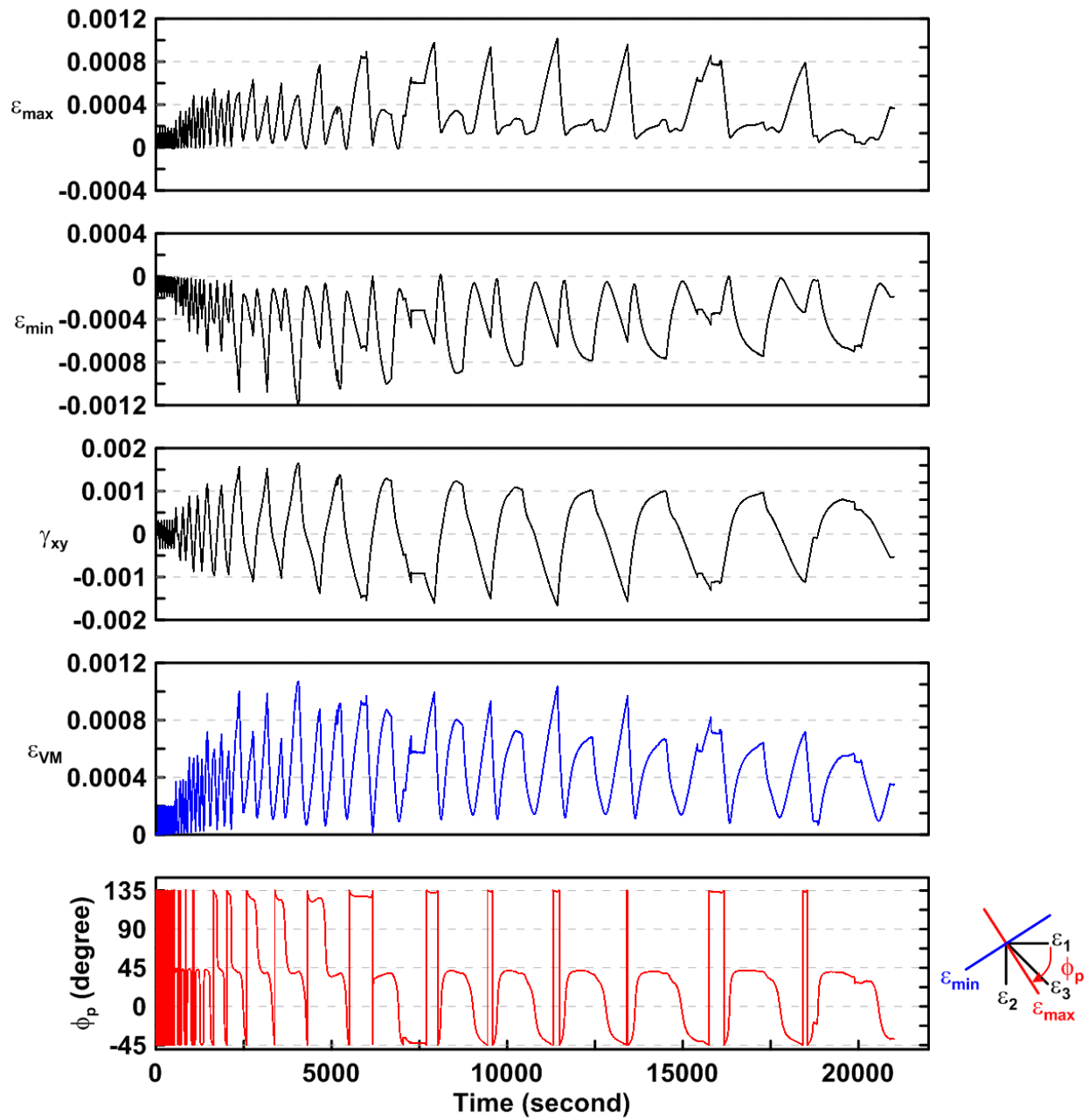


Figure 4.168 Time history of rosette type strain gauge readings in the one-piece gusset plate of TCBF-B-2 specimen (location: R18)

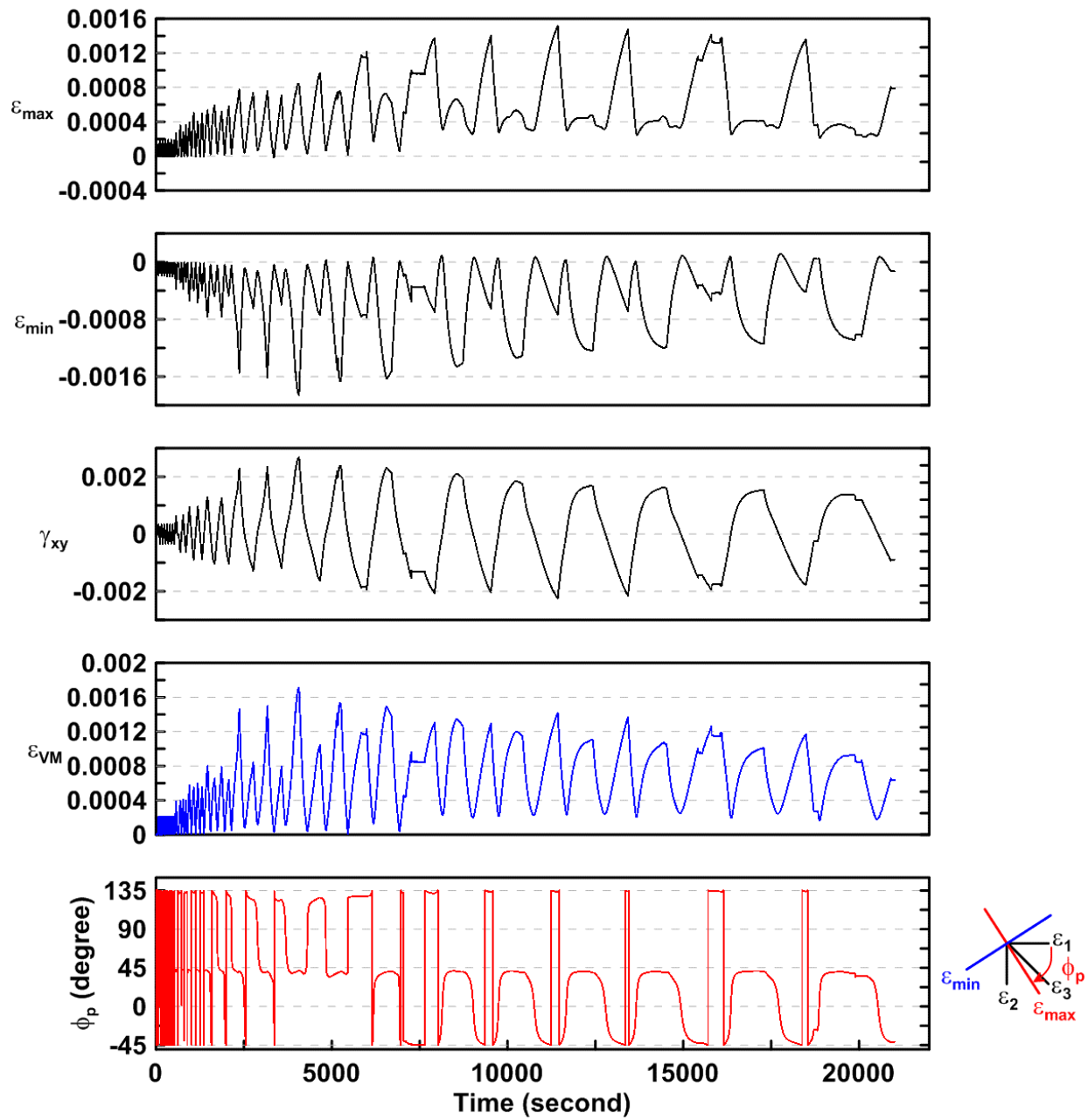


Figure 4.169 Time history of rosette type strain gauge readings in the one-piece gusset plate of TCBF-B-2 specimen (location: R19)

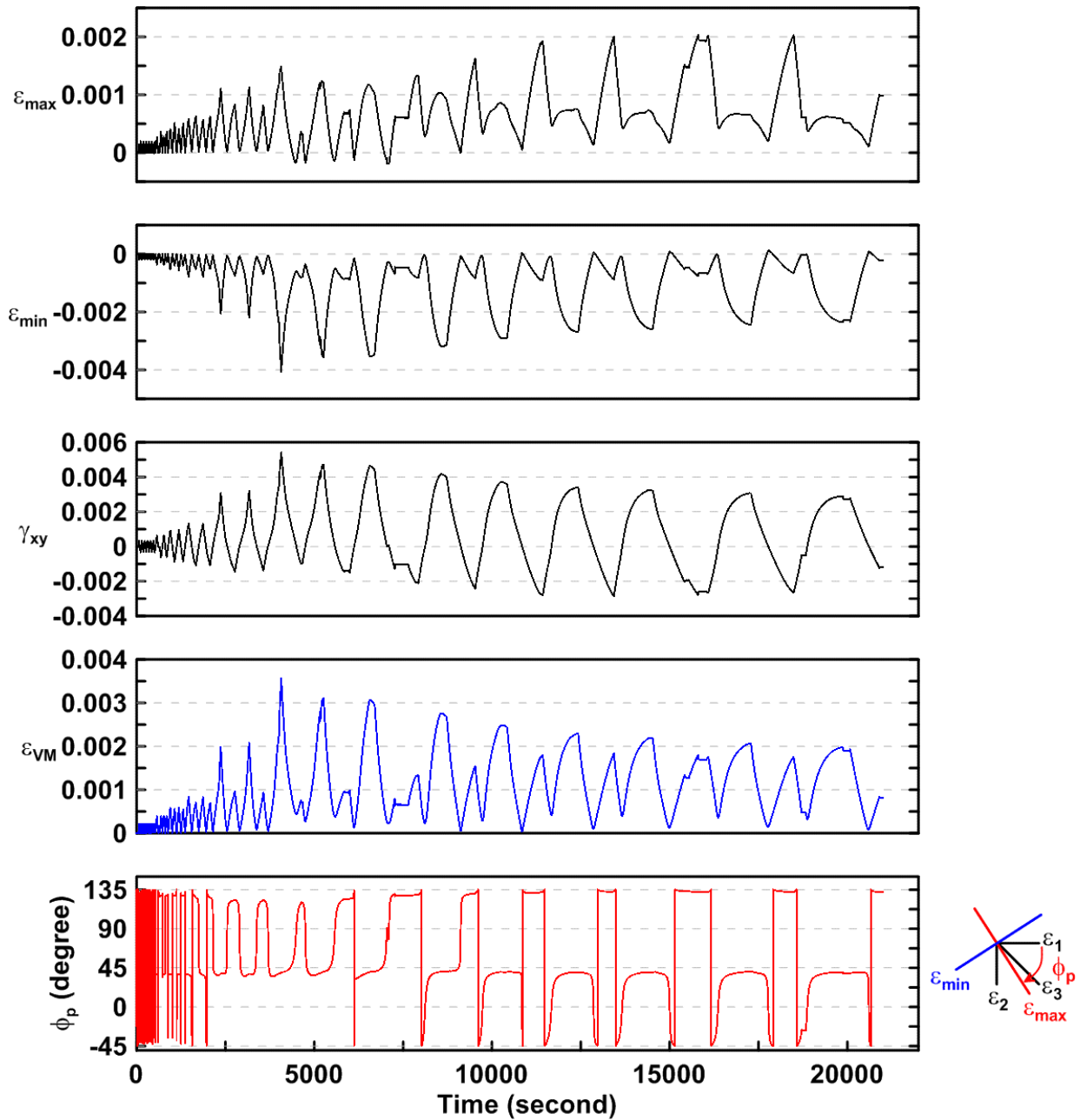


Figure 4.170 Time history of rosette type strain gauge readings in the one-piece gusset plate of TCBF-B-2 specimen (location: R20)

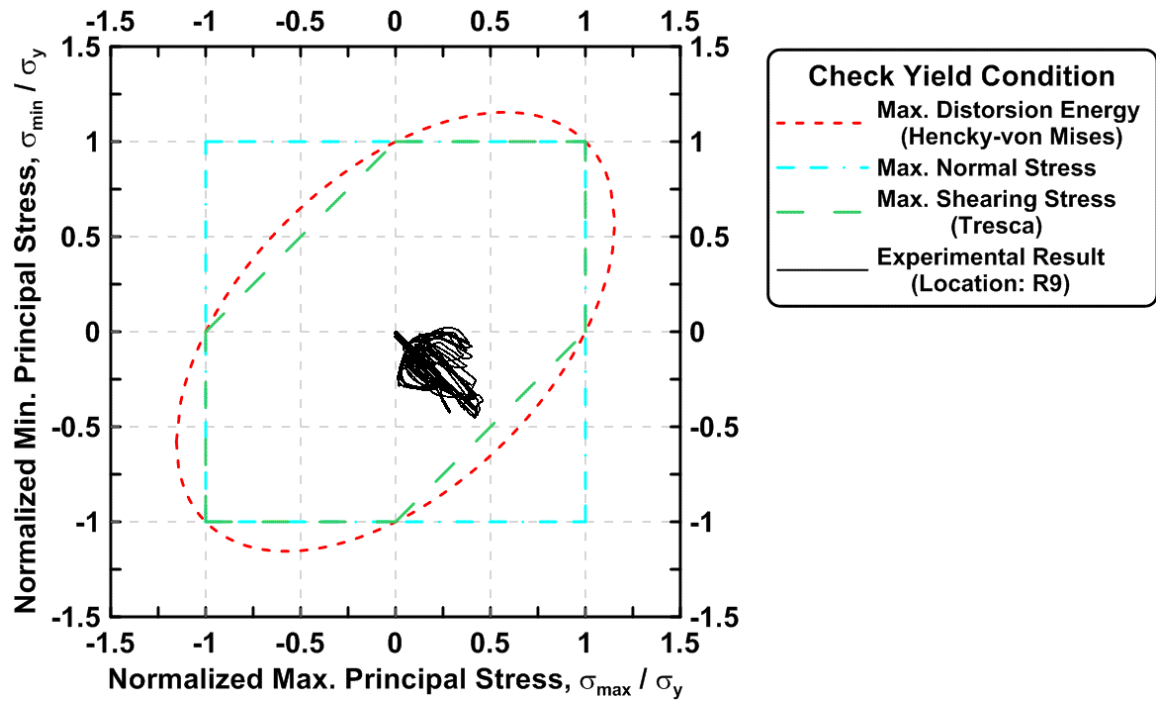


Figure 4.171 Normalized maximum principal stress vs. normalized minimum principal stress in the one-piece gusset plate of TCBF-B-2 specimen (location: R9)

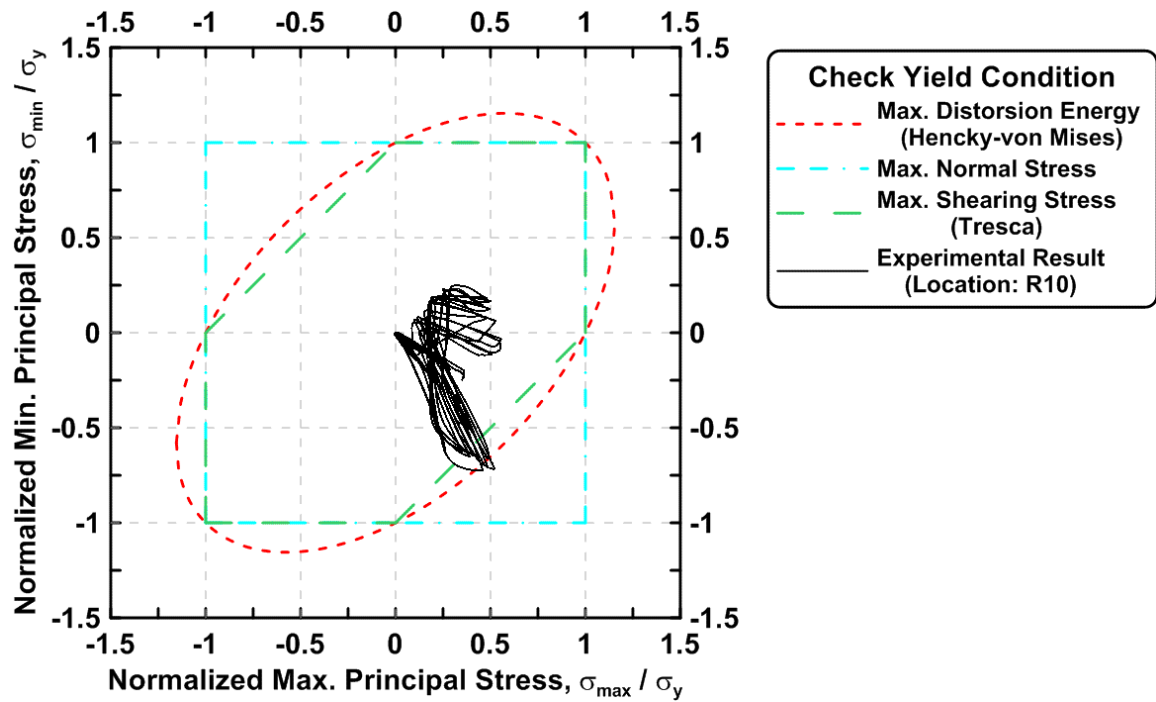


Figure 4.172 Normalized maximum principal stress vs. normalized minimum principal stress in the one-piece gusset plate of TCBF-B-2 specimen (location: R10)

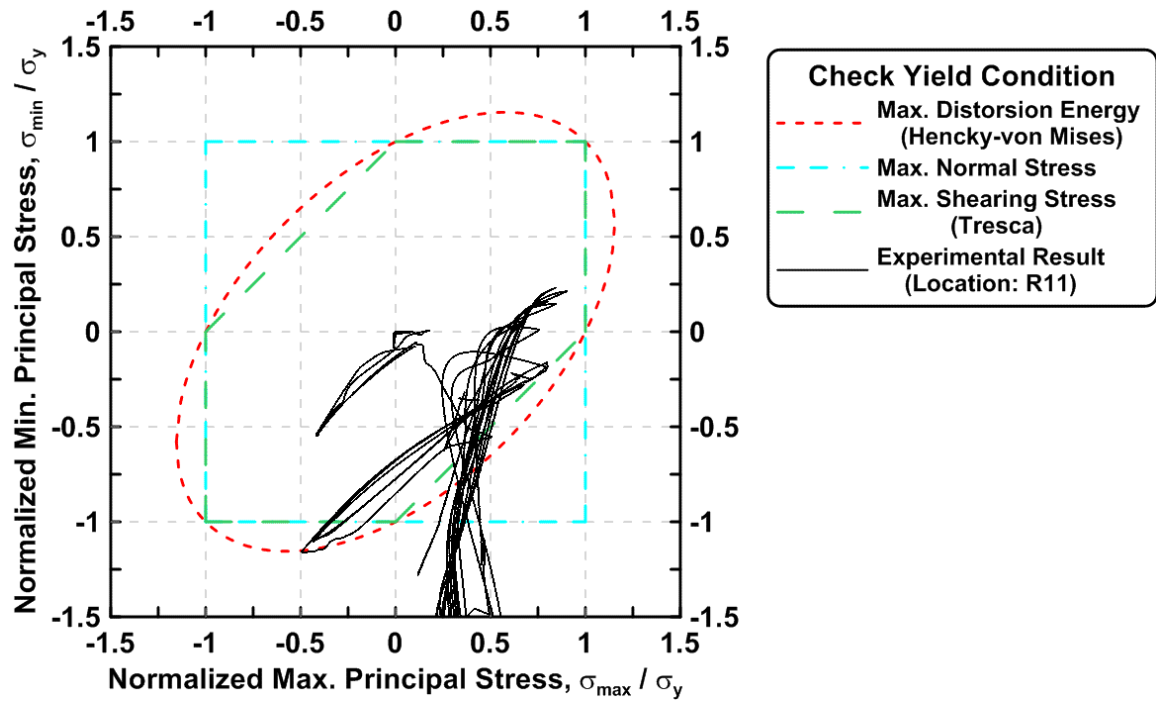


Figure 4.173 Normalized maximum principal stress vs. normalized minimum principal stress in the one-piece gusset plate of TCBF-B-2 specimen (location: R11)

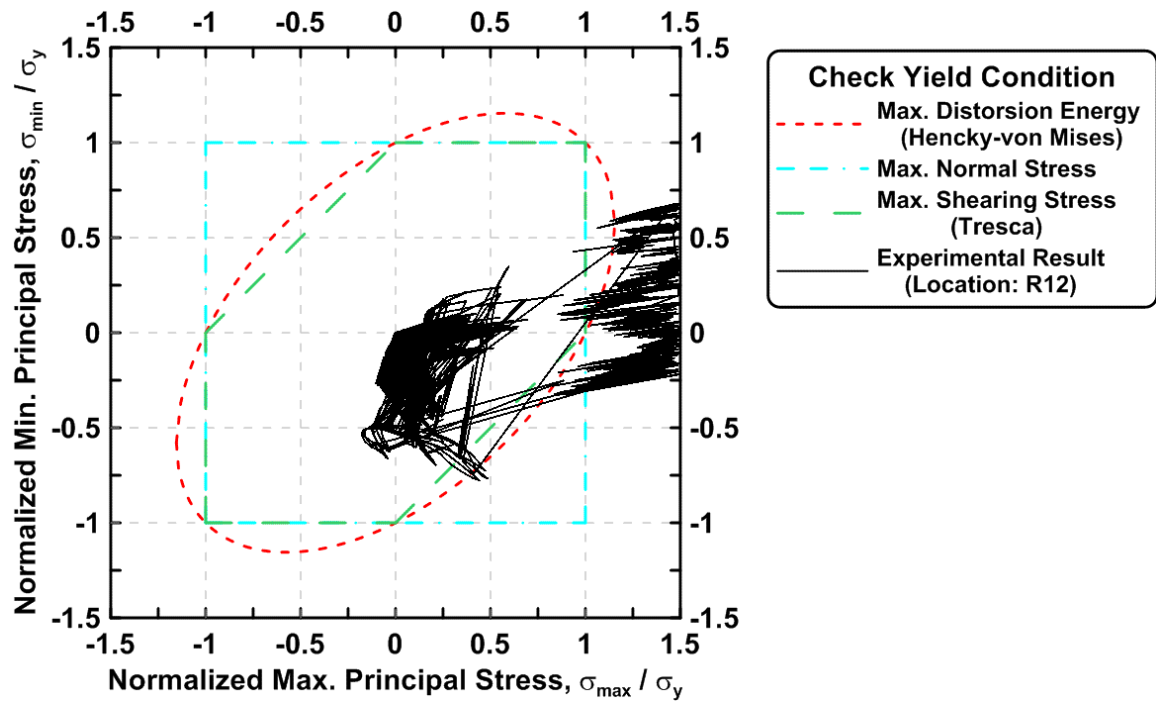


Figure 4.174 Normalized maximum principal stress vs. normalized minimum principal stress in the one-piece gusset plate of TCBF-B-2 specimen (location: R12)

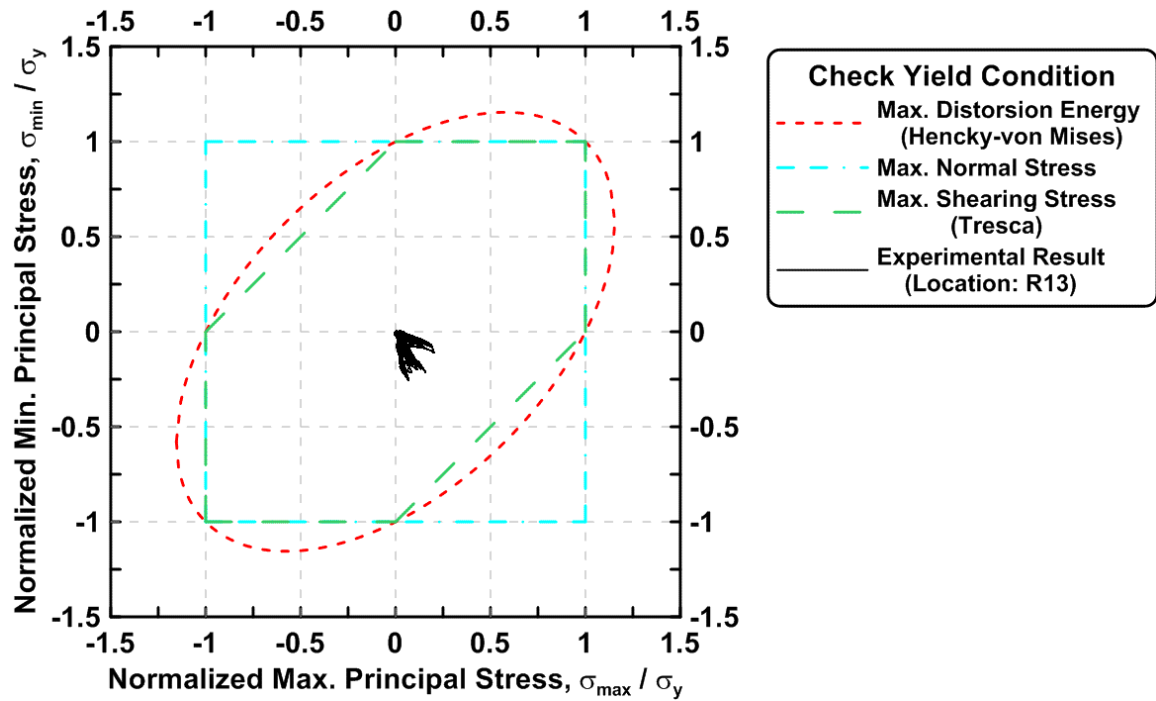


Figure 4.175 Normalized maximum principal stress vs. normalized minimum principal stress in the one-piece gusset plate of TCBF-B-2 specimen (location: R13)

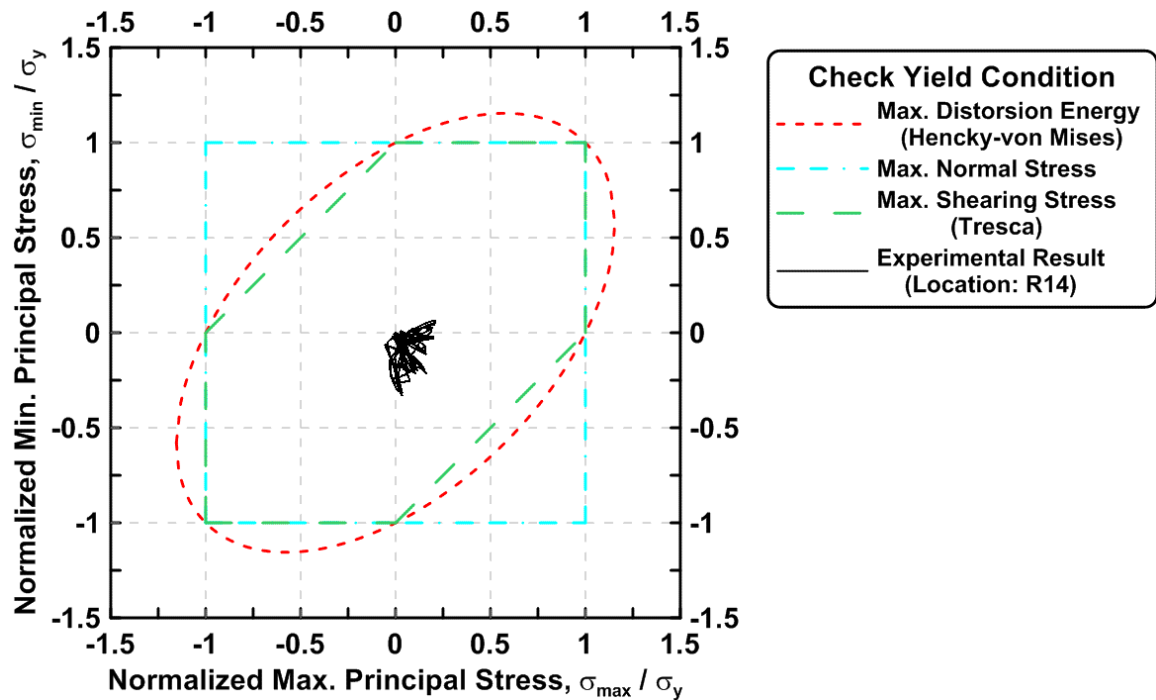


Figure 4.176 Normalized maximum principal stress vs. normalized minimum principal stress in the one-piece gusset plate of TCBF-B-2 specimen (location: R14)

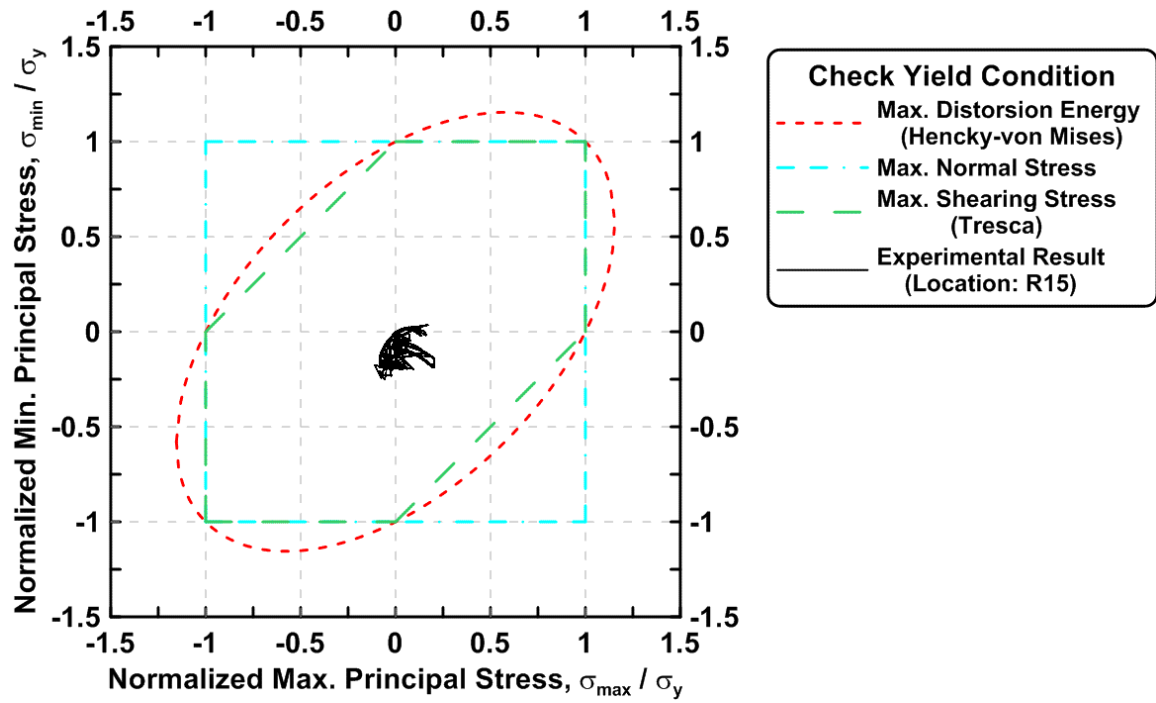


Figure 4.177 Normalized maximum principal stress vs. normalized minimum principal stress in the one-piece gusset plate of TCBF-B-2 specimen (location: R15)

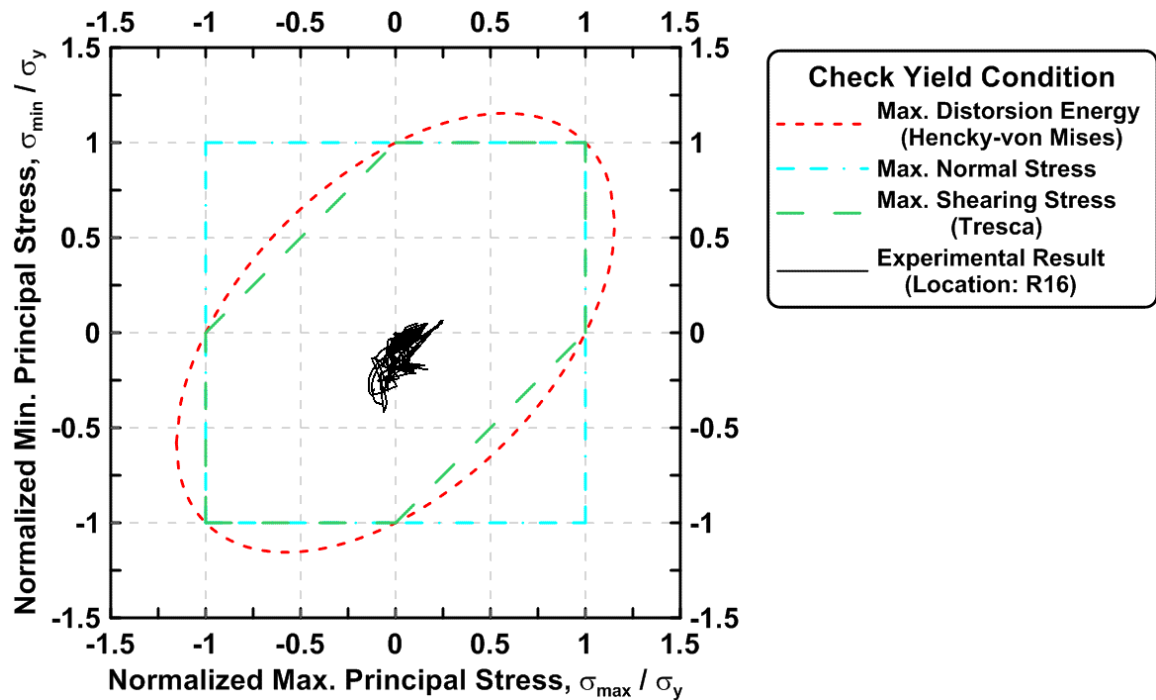


Figure 4.178 Normalized maximum principal stress vs. normalized minimum principal stress in the one-piece gusset plate of TCBF-B-2 specimen (location: R16)

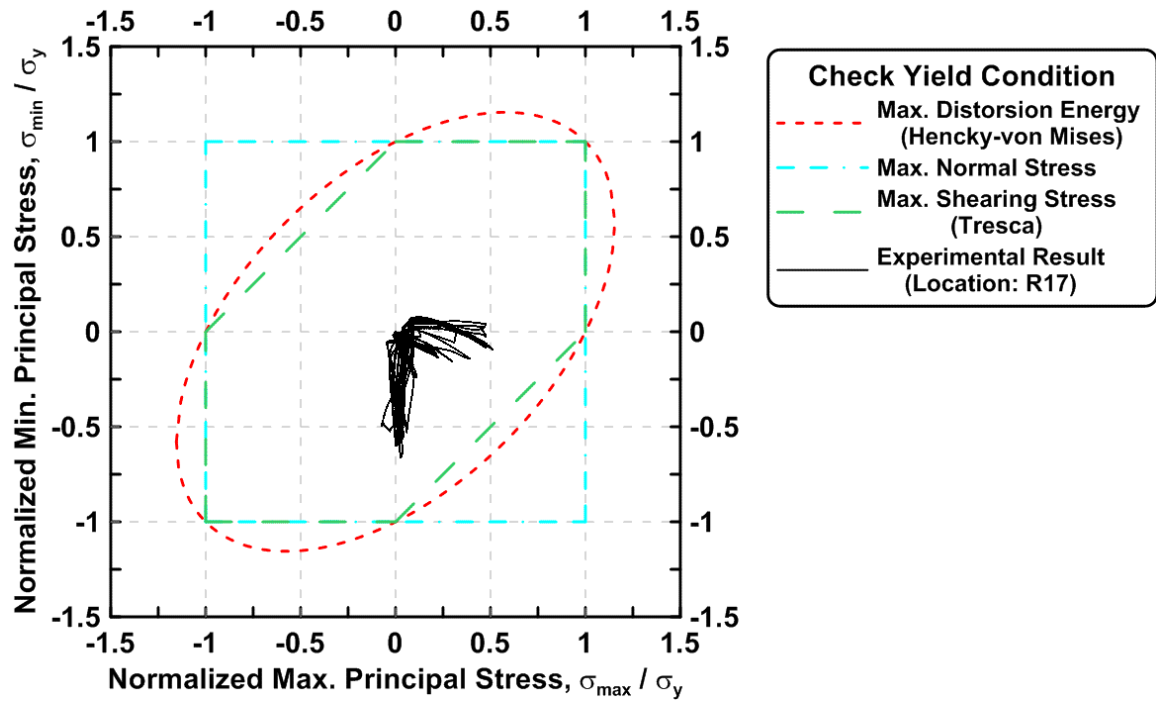


Figure 4.179 Normalized maximum principal stress vs. normalized minimum principal stress in the one-piece gusset plate of TCBF-B-2 specimen (location: R17)

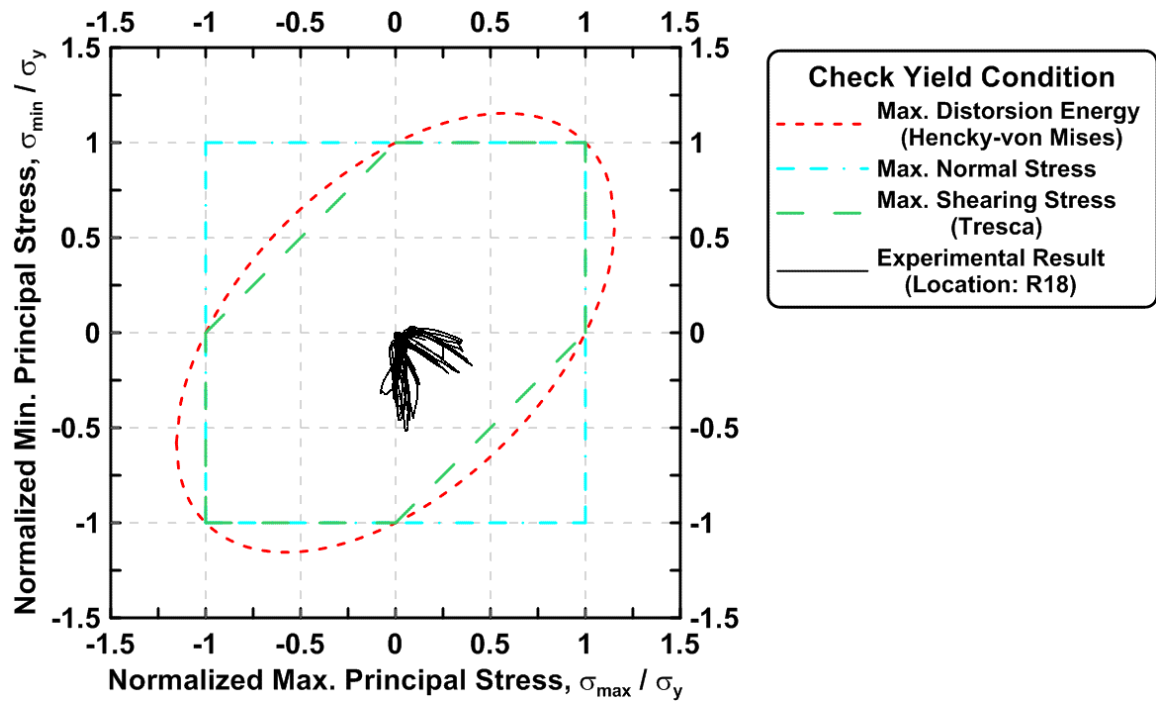


Figure 4.180 Normalized maximum principal stress vs. normalized minimum principal stress in the one-piece gusset plate of TCBF-B-2 specimen (location: R18)



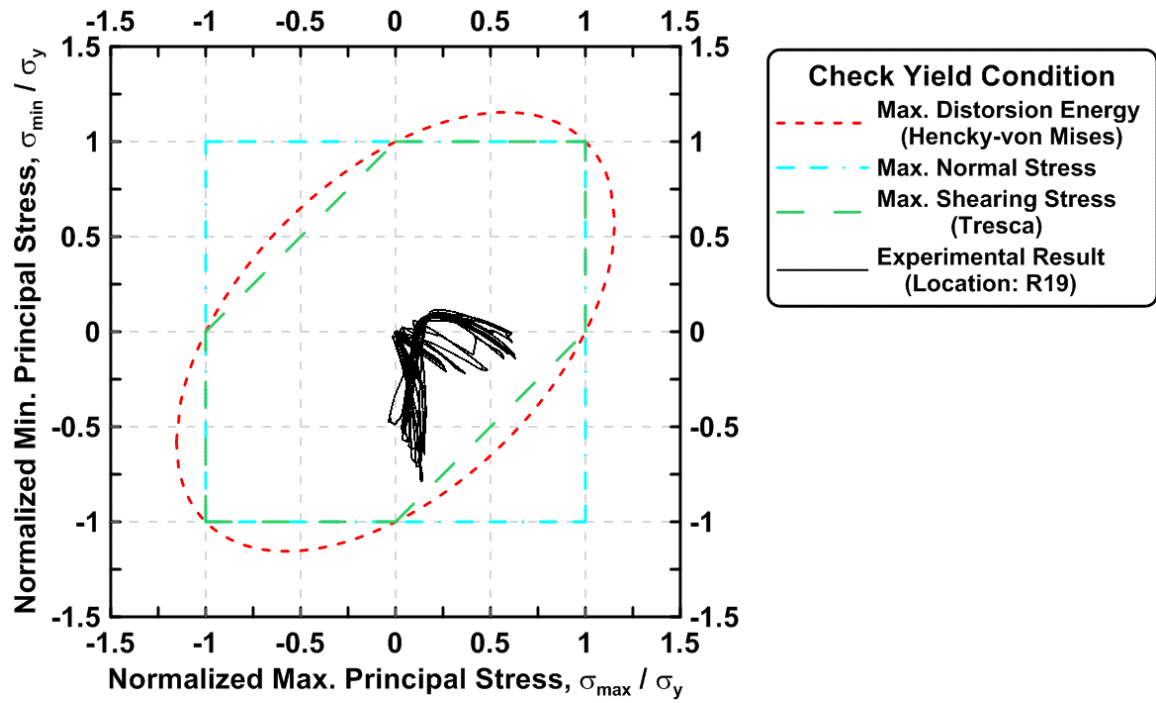


Figure 4.181 Normalized maximum principal stress vs. normalized minimum principal stress in the one-piece gusset plate of TCBF-B-2 specimen (location: R19)

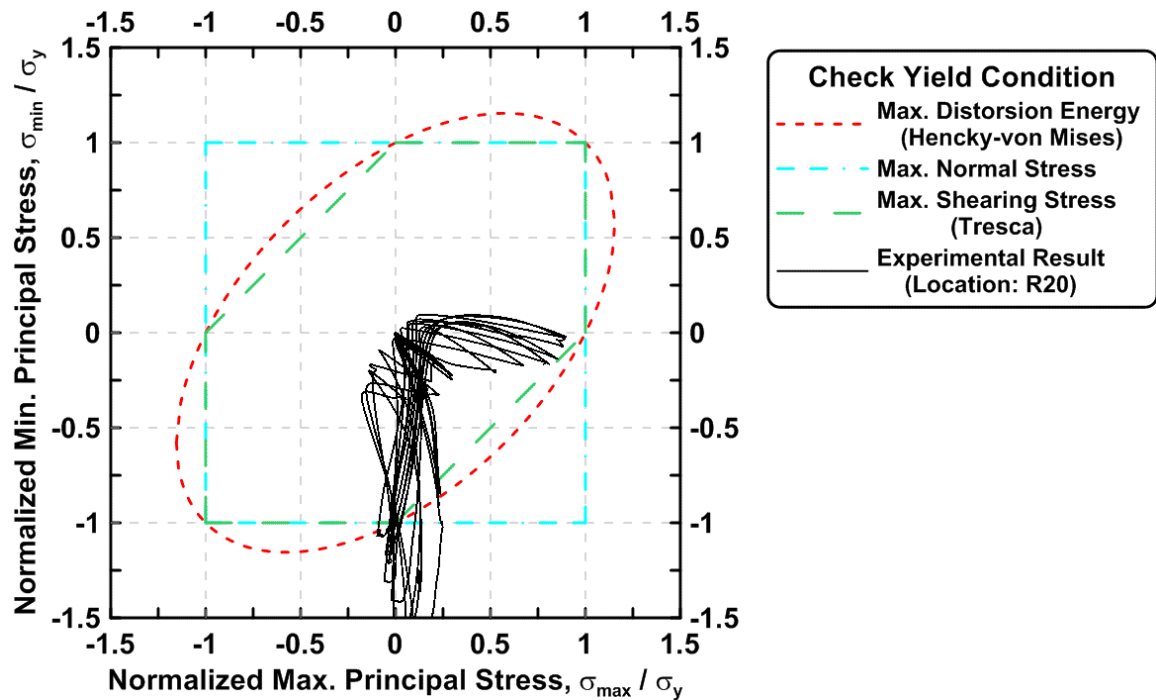


Figure 4.182 Normalized maximum principal stress vs. normalized minimum principal stress in the one-piece gusset plate of TCBF-B-2 specimen (location: R20)

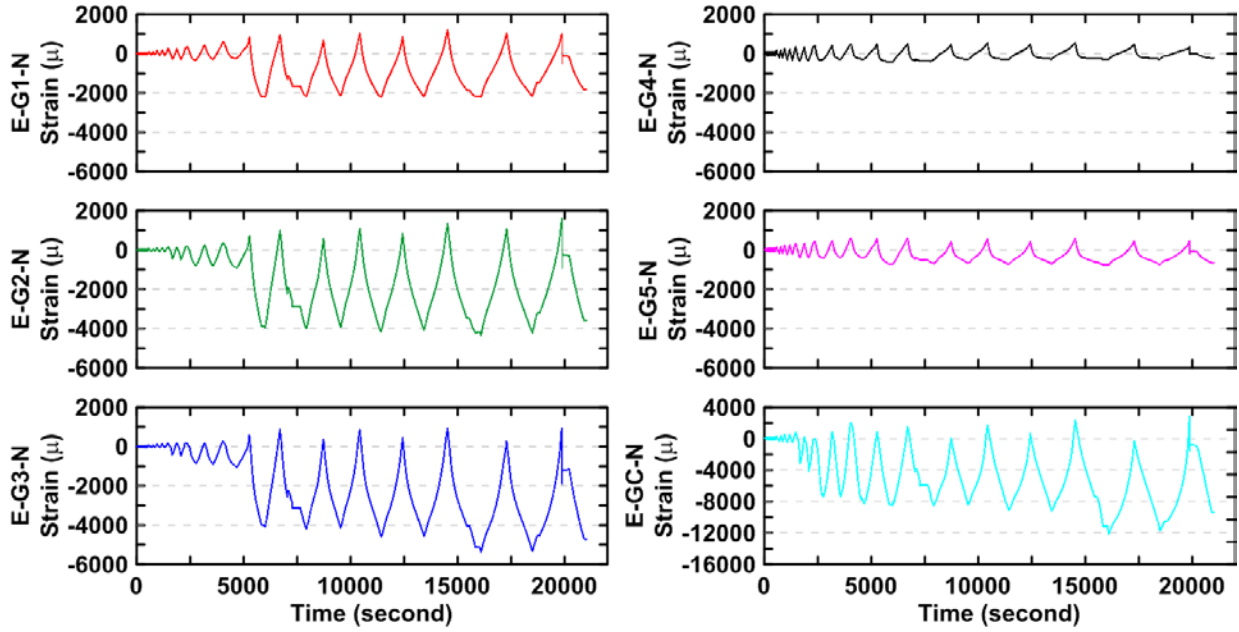


Figure 4.183 The averaged axial strain time history in the tapered gusset plate at eastern side of TCBF-B-2 specimen

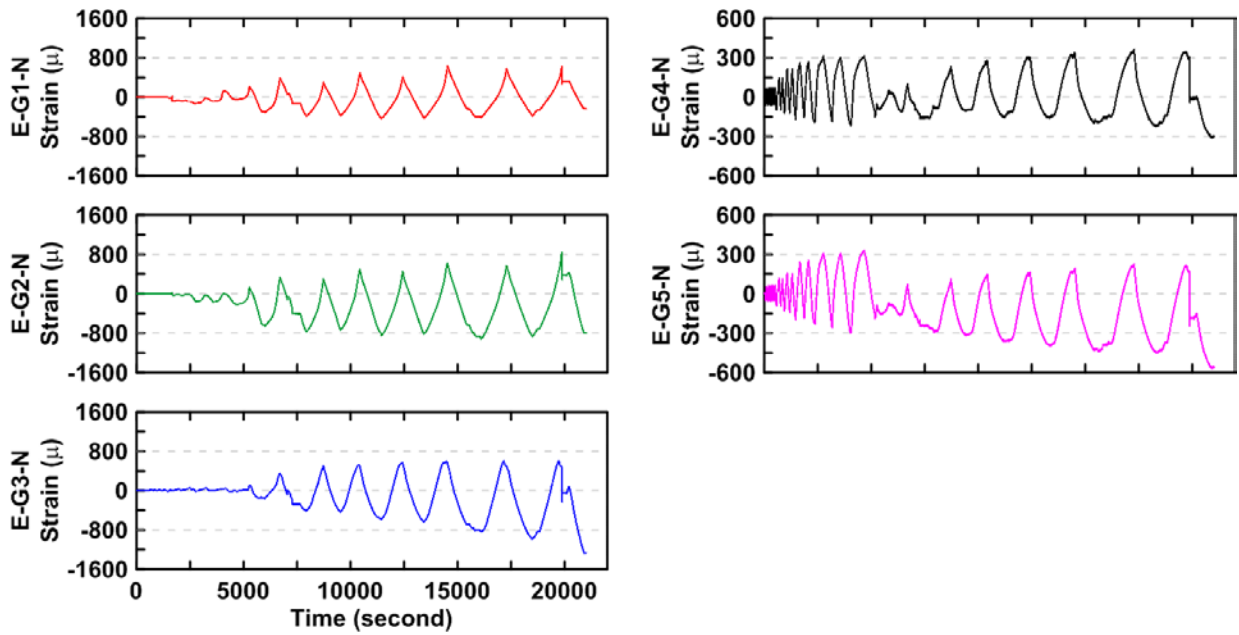


Figure 4.184 The bending strain time history in the tapered gusset plate at eastern side of TCBF-B-2 specimen

#### 4.2.2.1.7 Test Setup Response

The actuator bracket deformations versus actuator forces are plotted in Fig. 4.185. The relative displacement time history between base plates of the specimen and the floor beam, relative displacement time history between floor beam and strong floor, and relative displacement time history between integrated reconfigurable reaction wall and strong floor at northern and southern sides are shown in Fig. 4.186. The out-of-plane deformation time history of the lateral supporting frame with respect to the wall of the building at different locations are plotted in Fig. 4.187. The reconfigurable reaction wall (RRW) tip deformation time histories during the test are shown in Fig. 4.188.

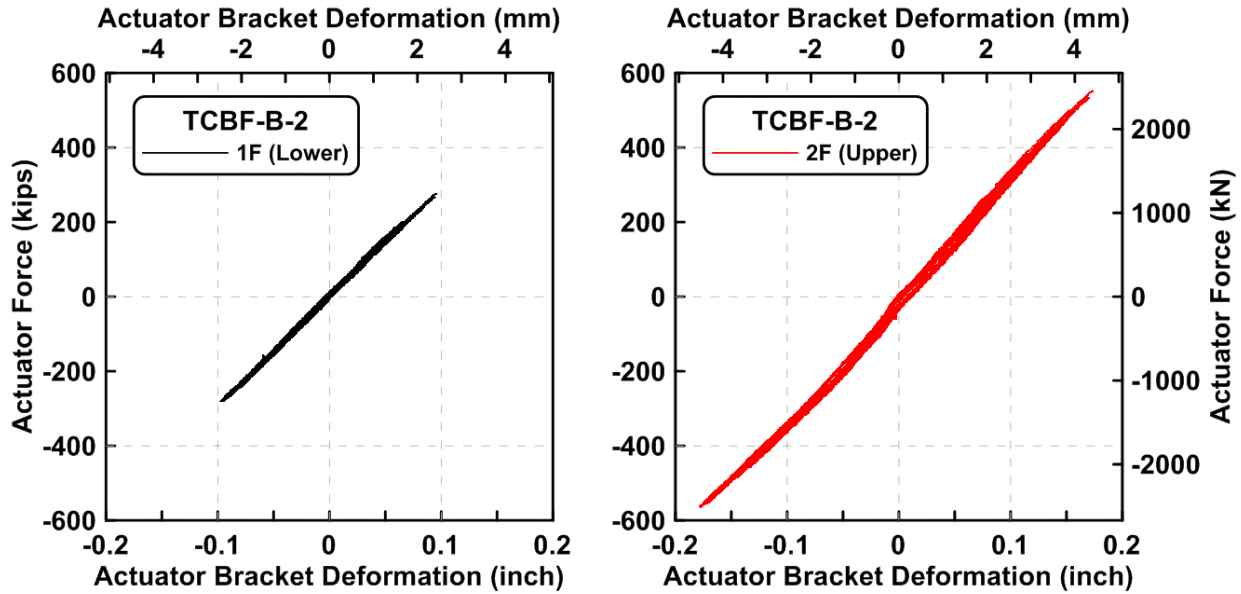


Figure 4.185 The actuator force vs. bracket deformation relationship at both floor levels during specimen TCBF-B-2 test

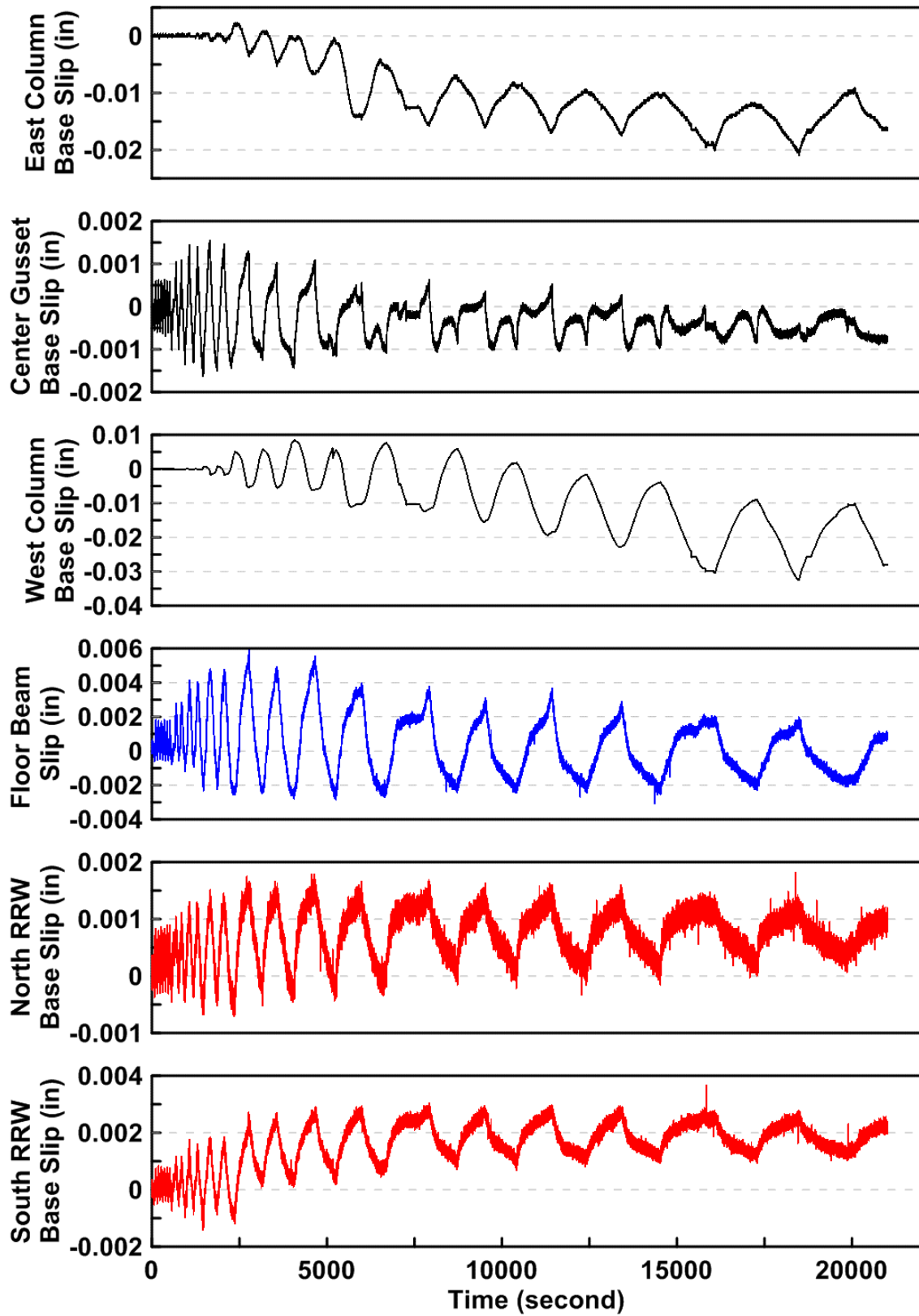


Figure 4.186 Slippage time history between specimen and test setup boundaries during specimen TCBF-B-2 test

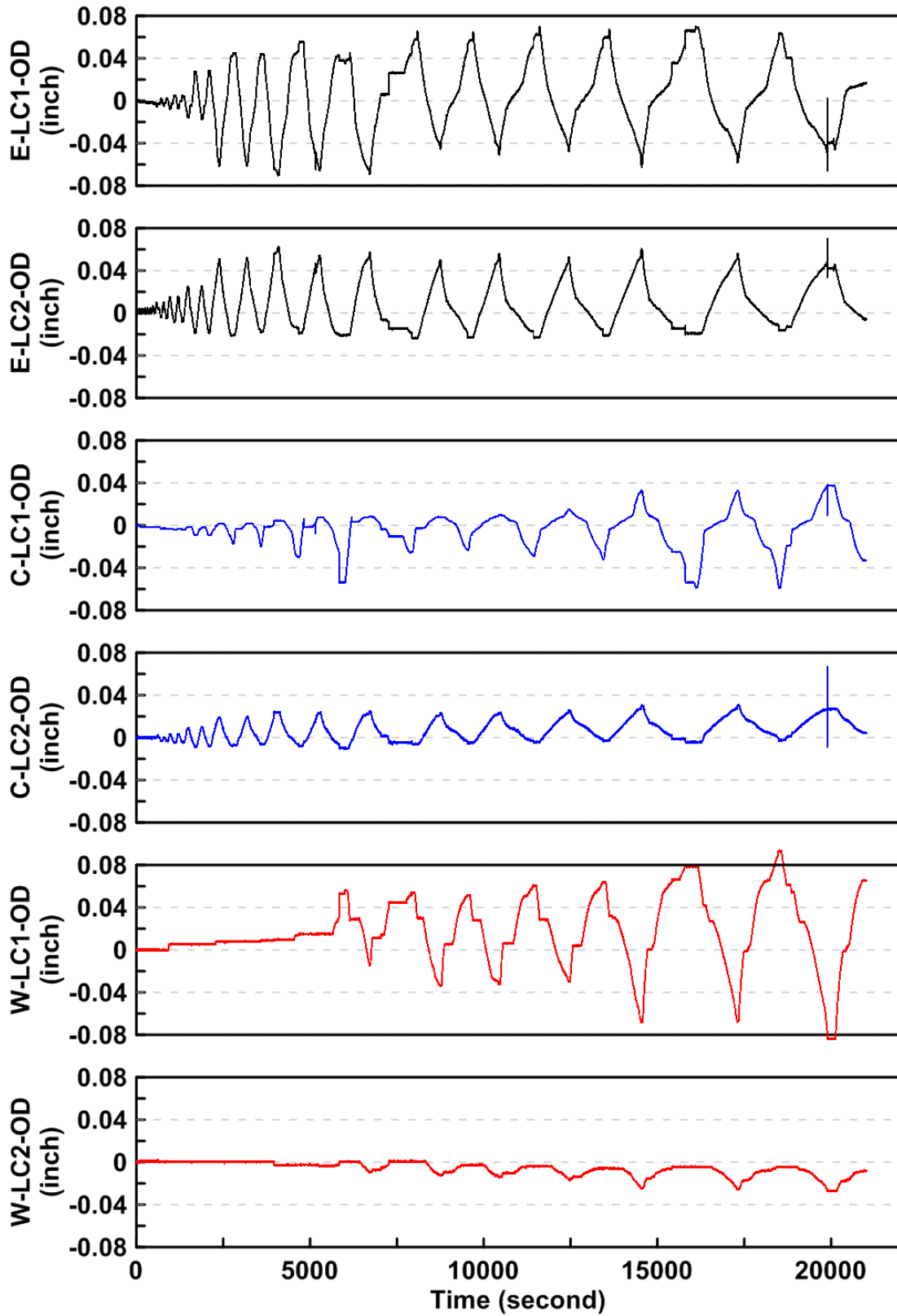


Figure 4.187 The out-of-plane deformation time history of lateral supporting frame at different monitoring points during specimen TCBF-B-2 test

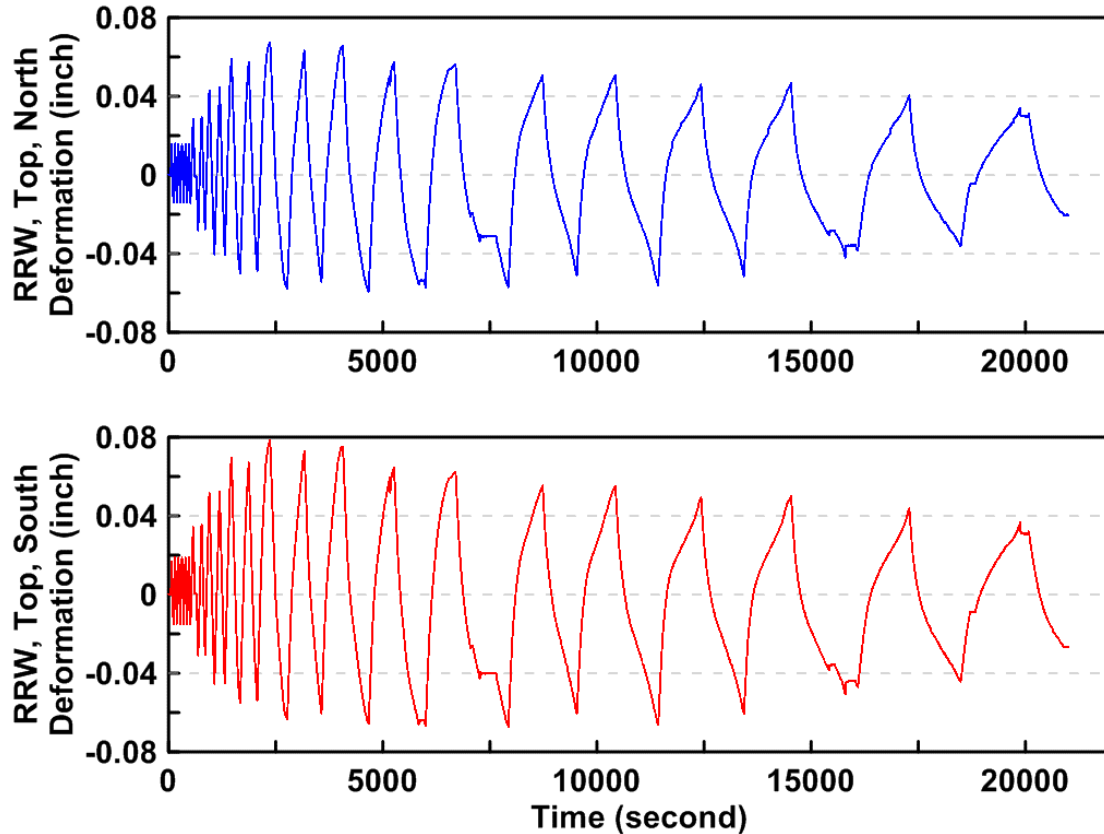


Figure 4.188 The reconfigurable reaction wall (RRW) tip deformation time histories during specimen TCBF-B-2 test

#### 4.2.2.2 Main Observations

As illustrated in the pre-defined loading protocol in Fig. 3.28, the experiment process was divided into several stages of loading (amplitudes or phases). Every loading stage contained two complete cycles, except the first loading stage contained six complete cycles. Detailed information about each of these cycles is described sequentially below. Table 4.3 illustrates and lists the major observations on the testing protocol along with brief descriptions.

##### **$\Delta = 0.5 D_{be} = 0.2$ inch (Roof Drift $\delta = 0.1$ %), from 2:26 PM to 2:34 PM**

After two small cycles were completed and all instrument readings were carefully checked, the formal loading protocol was started at 2:26 PM. During the first six low amplitude cycles, the entire frame remained elastic. No special observations were found anywhere through during this loading stage.

##### **$\Delta = 1.0 D_{be} = 0.4$ inch (Roof Drift $\delta = 0.2$ %), from 2:34 PM to 2:39 PM**

The entire frame essentially remained elastic; no special findings were found during this loading stage.

##### **$\Delta = 1.0 D_{by} = 0.6$ inch (Roof Drift $\delta = 0.3$ %), from 2:39 PM to 2:47 PM**

Some local flaking of whitewash developed near the beginning of 30 degree tapered region of gusset plate at first story (eastern side gusset plate on the north face) and also the tips of brace-to-gusset plate fillet welds.

**$\Delta = 0.5 D_{bm} = 1.0$  inch (Roof Drift  $\delta = 0.5$  %), from 2:47 PM to 3:00 PM**

At the beginning of the first half cycle of the loading cycle, the first story brace on the west side began global buckling out-of-plane to the south side of the specimen and the whitewash on the round HSS brace began flaking at the middle of the brace (Fig. 4.189). Some local flaking of whitewash developed near the beam splice welds in the bottom flange of the lower beam on the western side (Fig. 4.190). Similar whitewash flaking was found near the backing bar in the top flange of the lower beam on the western end. Some minor local flaking of whitewash developed near the 30° tapered region of the eastern gusset plate at the second story (near lower beam).

**$\Delta = 1.0 D_{bm} = 2.0$  inch (Roof Drift  $\delta = 0.9$  %), from 3:00 PM to 3:27 PM**

At the beginning of the first half cycle of the load step, some loud popping noises (probably from the base of the specimen) were heard at around one inch roof displacement while pushing the specimen to the east. Some yielding of the column flange was found at both east side and west side column base (Figs. 4.191 and 4.192). Note that the yield lines were not parallel to the base plate. Those were typical Luder's bands (Luder's lines) formed in the steel plates. The brace at top story east side began global buckling out-of-plane towards the north side of the specimen when the roof displacement approached to 2 inches to the east. The brace at upper story west side started global buckling (Fig. 4.193) out-of-plane towards the south side of the specimen as the roof displacement approached to 1 inch to the west in the second half cycle. Popping noises were heard again at the beginning of second load cycle at about 1-inch roof displacement towards the east. Additional flaking developed in the braces (Fig. 4.194), and in the  $2t$  gap region on the gusset plates. Some flaking of whitewash developed on the one-piece gusset plate near the gusset-to-column flange welds at eastern and western sides of the specimen (see Fig. 4.195). The lower beam web at both ends close to the shear tab also had some whitewash flaking. Local yielding was found at gusset plate tip between roof beam and the gusset below the bottom flange (Fig. 4.196).

**$\Delta = 1.5 D_{bm} = 3.0$  inch (Roof Drift  $\delta = 1.4$  %), from 3:27 PM to 4:03 PM on October 18, 2009 and 4:36 PM to 4:56 PM on October 22, 2009**

Additional flaking of whitewash in both columns (near the bases), gusset plates, braces and beam-to-gusset plate splices were found in this load stage. Loud popping noises were heard at the beginning of first load cycle at about 2-inch roof displacement towards the east. No load drop occurred at this time. As the specimen continued to move to the east, at about 2.8-inch roof displacement, the bottom flange of the lower beam at east side and the top flange of the lower beam at west side began local buckling near the beam-to-gusset plate splices (Figs. 4.197 and 4.198). As the first cycle of this stage was about to finish, vertical yield line patterns were observed in the east column web as shown in Fig. 4.199. The test was continued to the second load cycle. At around 1 inch roof displacement towards the east, cracks were detected near the CJP weld at western side of the column base as shown in Fig. 4.200. As the roof displacement continued to increase (moving to the east) up to about 2 inch roof displacement, a fracture near the outermost west side flange-to-base plate CJP weld was found (Fig. 4.201). A significant load drop occurred at this time. A crack was also found between the column web and the base plate at south side of the western column (Fig. 4.202). No significant cracks were found at the base of the eastern column. The test was paused to repair the column bases.

After a quick column base repair of both flanges of both column bases (see Figs. 4.203 and 4.204), the second trial continued to finish the remainder of the loading protocol. At the second half of the second cycle of the  $1.5D_{bm}$  load stage, about 2.8-inch to the west, a loud pop sound was heard from the top of the specimen. It remains uncertain where the sound came from (perhaps a crack initiating in one of the the lower beam-to-gusset plate splices). No significant load drop was observed this time. Yielding was found (via flaking of whitewash) in the west W12  $\times$  96 column flange where it connected to the 2-inch thick cover plate used for the repair at the column base, as shown in Fig. 4.205. Whitewash flaking between the two welded 1-inch thick stiffener plates was found at the eastern side of column base (Fig. 4.206). Additional flaking of whitewash developed on the gusset plate  $2t$  gap fold regions, beam-to-gusset plate splice regions, braces, and column web at both sides in the ground story.

**$\Delta = 2.0 D_{bm} = 4.0$  inch (Roof Drift  $\delta = 1.9$  %), from 4:56 PM to 5:49 PM**

Additional local buckling of the lower beam flanges (top flange at west side and bottom flange at east side) was observed at the beginning of this load stage. At the end of the first half cycle, corresponding to about 0.66-inch (negative side) roof displacement to the west, the top flange of beam-to-gusset plate splice at west side of the lower beam completely fractured (Fig. 4.207) and followed almost immediately by the partial fracture of the bottom finger plate (northern side of the net section) on the eastern end of the lower beam splice, as shown in Fig. 4.208. When the actuator continued pulling the specimen to the west at around 0.96-inch (negative side) roof displacement, the bottom finger plate on the east end of the lower beam splice completely fractured as illustrated in Fig. 4.209. The west side column flange near the 2-inch thick cover plate then began to buckle locally and the vertical fillet welds on both sides of the column flange tore (Fig. 4.210). Note that the round HSS braces at both stories had not buckled locally at this time. Local buckling of the lower beam web was also observed during this load step (Fig. 4.211).

**$\Delta = 2.5 D_{bm} = 5.0$  inch (Roof Drift  $\delta = 2.3$  %), from 5:49 PM to 6:56 PM**

When the roof displacement passed the peak roof displacement in the previous load step (which is 4 inch) at about 4.5-inch displacement, the brace at the western side of the first story (Fig. 4.212) and the eastern side brace at the top story buckled locally. The vertical fillet welds between the two-inch cover plate and the W12  $\times$  96 column flange at north-west corner of column base in the ground story continued to tear apart (Fig. 4.213). Additional local buckling of the western brace in the ground story was observed during the second load cycle at this stage (Fig. 4.214). Tearing crack (initiates at the tip of welding access hole) between beam flange and web was observed (Fig. 4.215) at the east end of the lower beam to gusset plate connection. After passing the negative peak roof displacement in the second load cycle, cracks initiated in the first story west side round HSS brace at the local buckled region (Fig. 4.216). Additional local buckling occurred in the lower story east side brace as the entire specimen passed the zero roof displacement at the end of this load step.

**$\Delta = 3.0 D_{bm} = 6.0$  inch (Roof Drift  $\delta = 2.8$  %), from 6:56 PM to 8:16 PM**

After passing the first positive peak roof displacement at this stage, additional cracking and tearing of the vertical fillet welds between 2-inch flange cover plate and column flange at the west side of the column base were observed on both sides of the exterior flange (Fig. 4.217). At about negative 2.71-inch roof displacement, the ground story brace on the west side partially fractured (Fig. 4.218). The round HSS brace completely fractured at a negative 5.29-inch roof displacement, as shown in Fig. 4.219. The western end of the lower beam web fractured from top the top flange and partially across the web towards the bottom of the beam (Fig. 4.220). After passing the first negative peak displacements in this load stage, cracks initiated in the ground



story east side brace at the center part of the brace (Fig. 4.221). The vertical fillet welds between the 2-inch flange cover plate and column flange at the west side column base torn all the way down from top to bottom of the weld lines (Fig. 4.222). After passing the second negative peak displacement, the test paused to take some detailed pictures.

**$\Delta = 3.5$  D<sub>bm</sub> = 7.0 inch (Roof Drift  $\delta = 3.2$  %), from 8:16 PM to 9:02 PM**

Before the specimen reached the peak roof displacement (about 6.9 inch) in this load stage, the east side round HSS brace at the ground story yielded significantly (via the necking of the round section) before the entire cross section fractured (Fig. 4.223). At about 7-inch roof displacement in the first half cycle at this stage, the eastern brace in the first story completely fractured (Fig. 4.224). The test was manually stopped at about negative one-inch to have a small residual roof deformation when unloaded based on the trend of unloading slope shown on the display screen. The entire side view of the specimen after test is shown in Fig. 4.225.

**Table 4.3 The major observations during specimen TCBF-B-2 test**

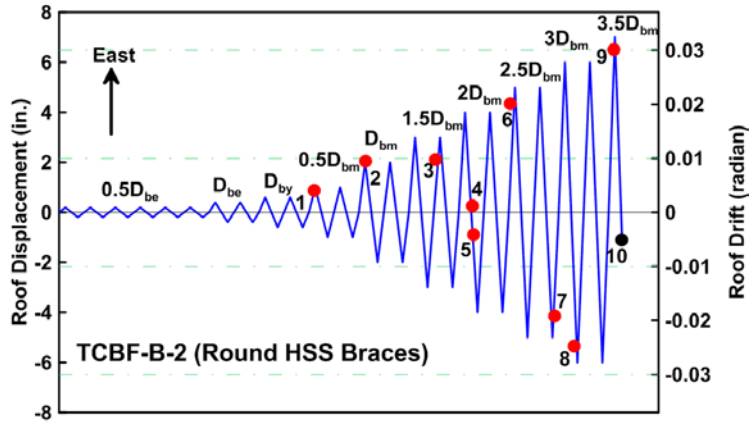
	
<b>Major Observations</b>	
1	The brace at first story west side began global buckling (out-of-plane to the south side).
2	The brace at second story east side began global buckling (out-of-plane to the north side).
3	The brace at second story west side began global buckling (out-of-plane to the south side).
4	A very loud noise heard this time but no load drop observed.
5	The flange-to-base plate weld at the west side of column base completely fractured. Test paused to repair column base (Figs. 4.201 and 4.203).
6	The top flange at western side of lower beam splices completely fractured at the CJP weld line (Fig. 4.207). The bottom flange at eastern side of lower beam splices partially fractured at net section of finger plate (Fig. 4.208).
7	The bottom flange at eastern side of lower beam splices completely fractured at net section of finger plate (Fig. 4.209). No local buckling of braces observed at this time.
8	The braces began local buckling at the middle portion of the brace (1F-West and 2F-East). The northern side vertical fillet weld between cover plate and column flange was torn.
9	Cracks initiated in the middle of round HSS brace at first story western brace at the local buckling region (Fig. 4.216).
10	Both northern and southern side vertical fillet welds between cover plate and column flange were torn and cracked.
11	The western brace at first story partially fractured.
12	The western brace at ground story completely fractured during the first cycle of $3.0 D_{bm}$ load step at roof displacement of 5.3 inch to the west. (Fig. 4.219)
13	Cracks developed in the middle of round HSS brace at first story eastern brace at the local buckling region. The vertical fillet welds between cover plate and column flange cracked all the way down to cover-plate-to-base-plate connection.
14	The eastern brace at first story completely fractured during the first cycle of $3.5 D_{bm}$ load step at roof displacement corresponded to about 7 inch to the east. (Fig. 4.224)
15	No local buckling or cracks in the second story braces were found. Test stopped at about 1.0 inch of roof displacement to the west.



Figure 4.189 Whitewash flaking at the middle of the west side round HSS brace (Specimen TCBF-B-2)



Figure 4.190 Flaking of whitewash near the CJP welds in the bottom flange of lower beam (Specimen TCBF-B-2)



Figure 4.191 Yield pattern of the east column flange (Specimen TCBF-B-2)

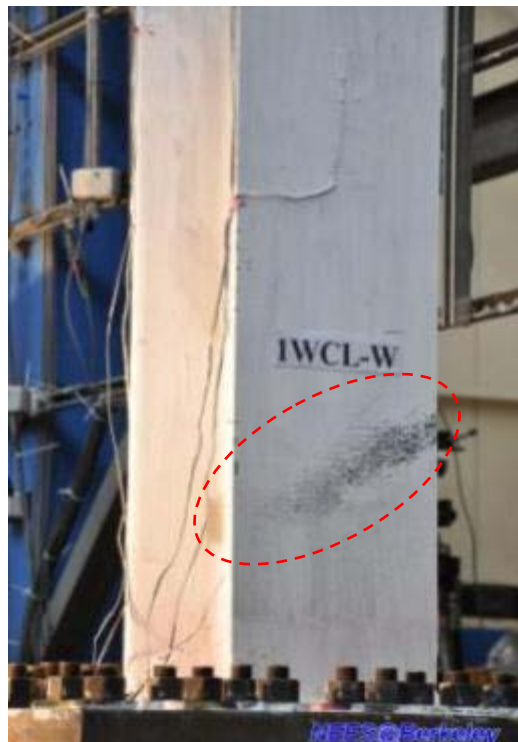


Figure 4.192 Yield pattern of the west column flange (Specimen TCBF-B-2)



Figure 4.193 Global buckling of round HSS braces at both stories of TCBF-B-2 Specimen



Figure 4.194 Additional whitewash flaking in the braces (Specimen TCBF-B-2)



**Figure 4.195 Flaking of whitewash near gusset plate-to-column flange region (Specimen TCBF-B-2)**



**Figure 4.196 Whitewash flaking at the corner of gusset plate-to-roof beam connection (Specimen TCBF-B-2)**



Figure 4.197 Local buckling of lower beam bottom flange at east side (Specimen TCBF-B-2)



Figure 4.198 Local buckling of lower beam top flange at west side (Specimen TCBF-B-2)



Figure 4.199 Column web yielding at the east side column in ground floor (Specimen TCBF-B-2)

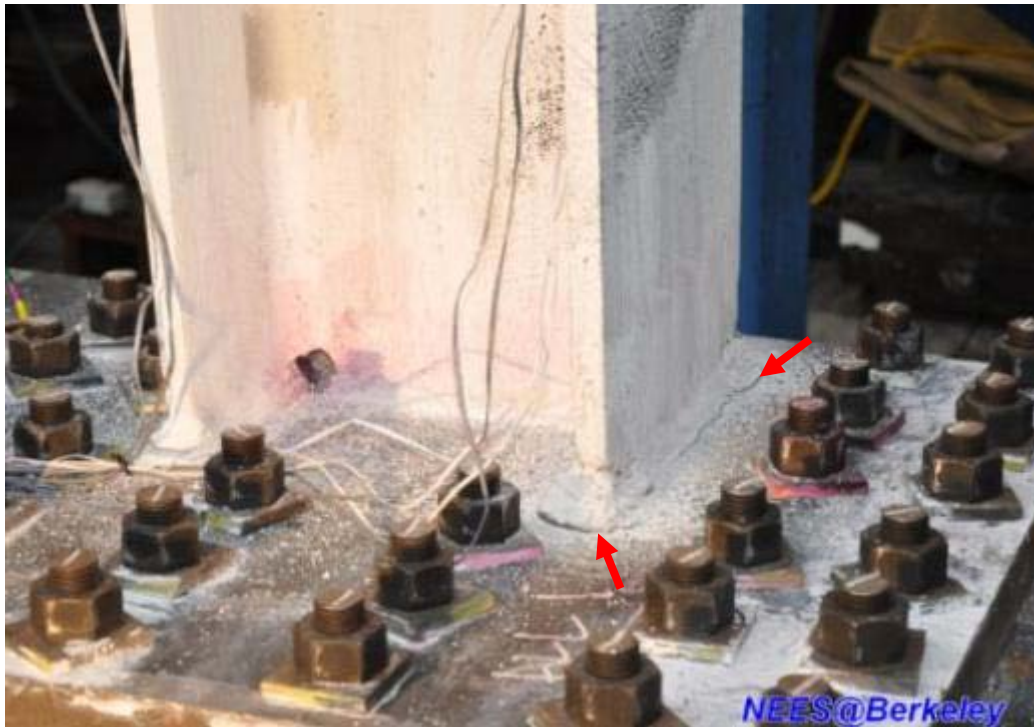


Figure 4.200 Crack near the flange CJP welds at west side column base (Specimen TCBF-B-2)





Figure 4.201 Complete fracture near the flange CJP welds at west side column base (Specimen TCBF-B-2)



Figure 4.202 Crack near the web CJP welds at west side column base (Specimen TCBF-B-2)



**Figure 4.203** West side column base after repair (Specimen TCBF-B-2)



**Figure 4.204** East side column base after repair (Specimen TCBF-B-2)



Figure 4.205 Yielding in the column flange near 2-in.-thick cover plate (Specimen TCBF-B-2)



Figure 4.206 Yield pattern between column base stiffener plates (Specimen TCBF-B-2)



Figure 4.207 Fracture of lower beam top flange (west side of Specimen TCBF-B-2)



Figure 4.208 Partial fracture of lower beam bottom flange finger plate (east side of Specimen TCBF-B-2)

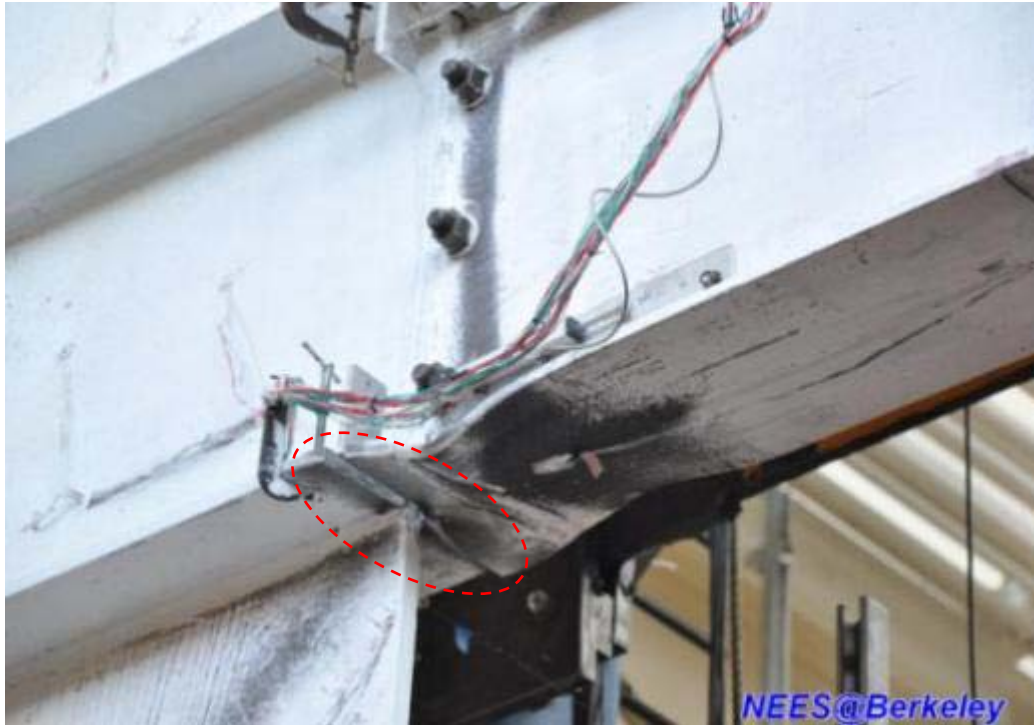


Figure 4.209 Complete fracture of lower beam bottom flange finger plate (east side of Specimen TCBF-B-2)



Figure 4.210 Local buckling of column flange near 2-in.-thick cover plate (Specimen TCBF-B-2)



Figure 4.211 Local buckling of lower beam web at west side (Specimen TCBF-B-2)



Figure 4.212 Local buckling of west side round HSS brace in the first story (Specimen TCBF-B-2)



Figure 4.213 Tearing of the vertical fillet welds at west column base (Specimen TCBF-B-2)



Figure 4.214 Additional local buckling of west side round HSS brace in the first story (Specimen TCBF-B-2)

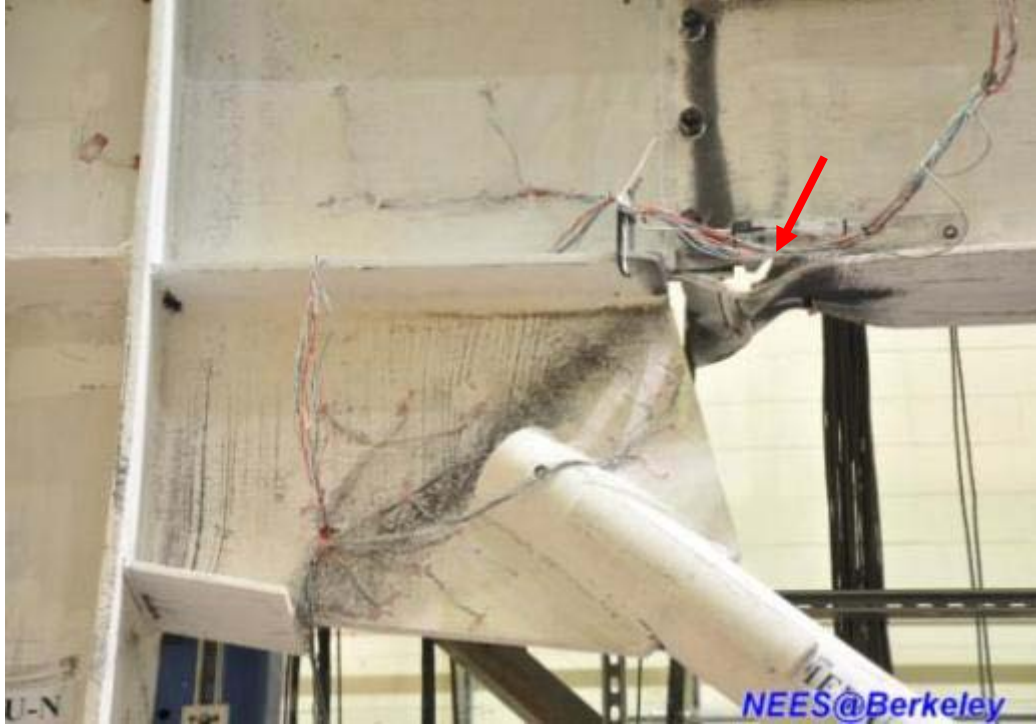


Figure 4.215 Crack propagation into the web at east side lower beam (Specimen TCBF-B-2)

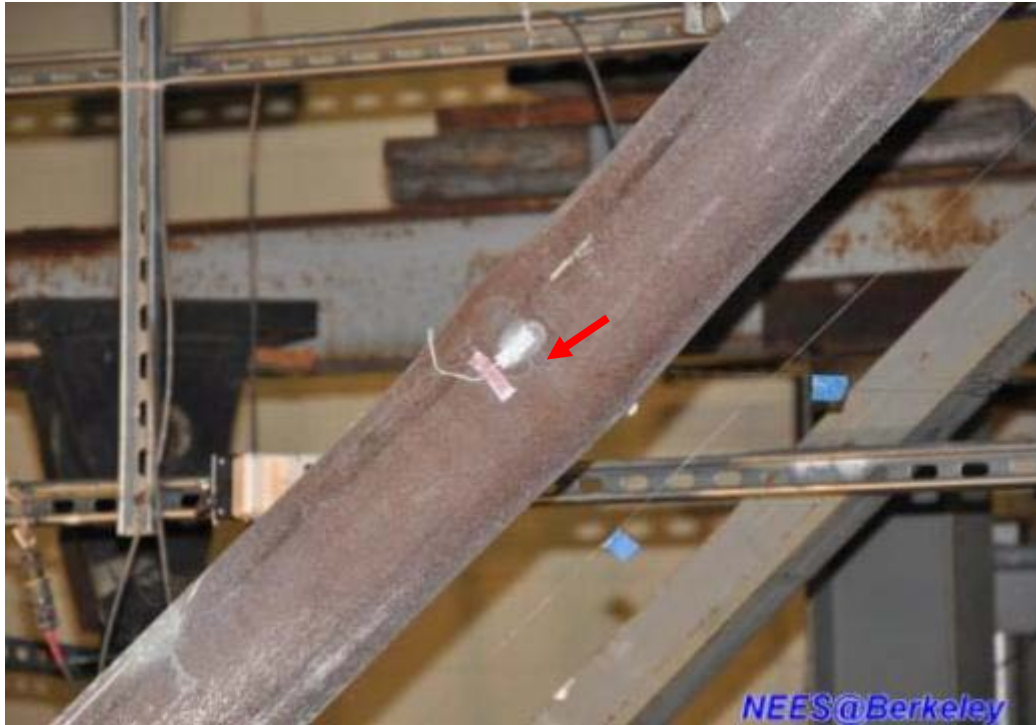


Figure 4.216 Crack initiates in the west side round HSS brace at the first story (Specimen TCBF-B-2)





Figure 4.217 Additional tearing of fillet welds between cover plate and column flange (Specimen TCBF-B-2)



Figure 4.218 Partial fracture of the west side brace in the first story (Specimen TCBF-B-2)

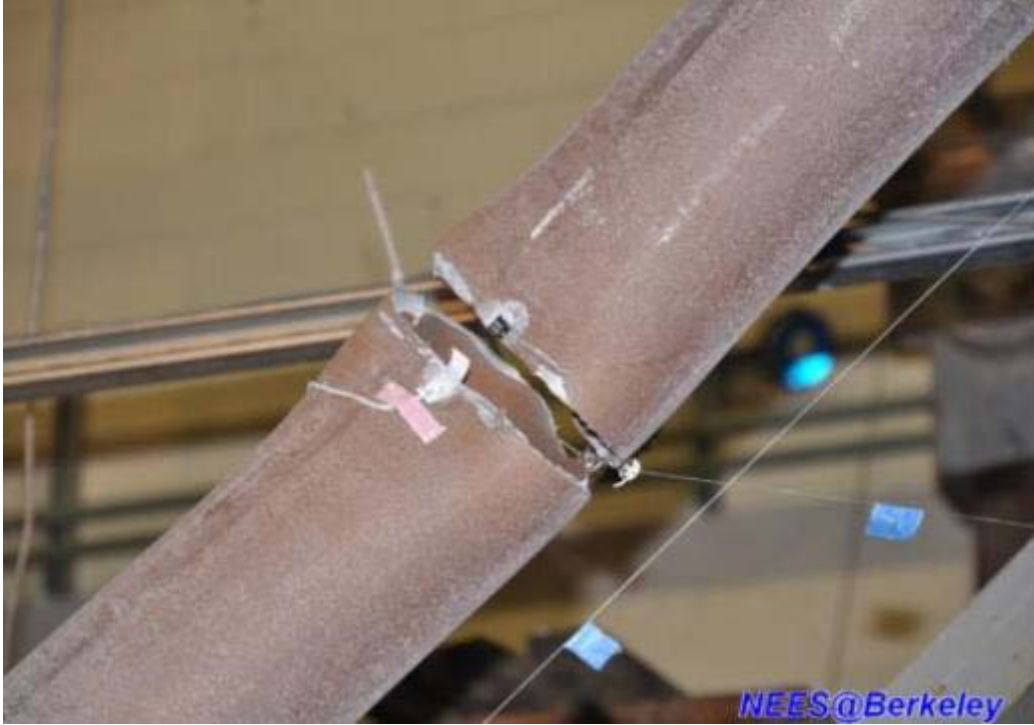
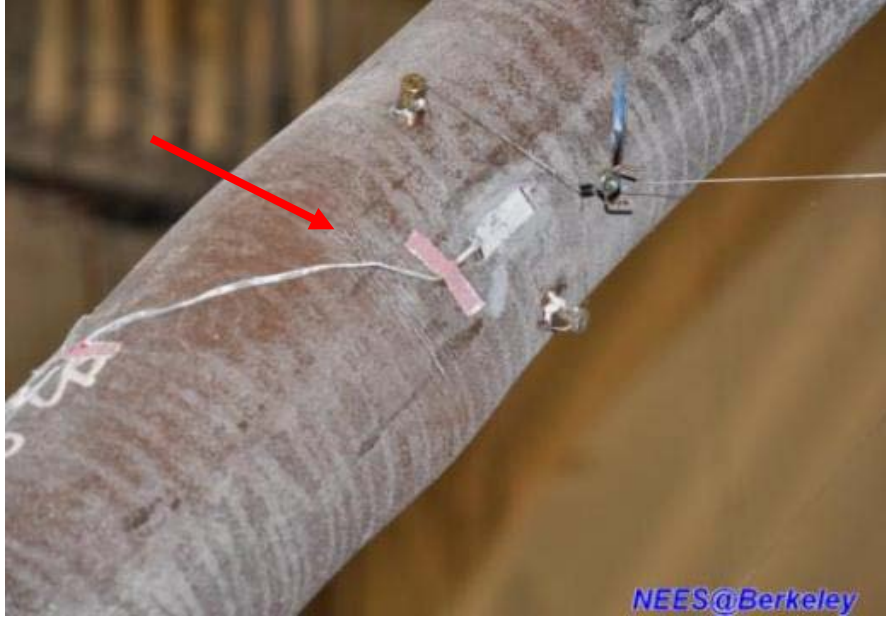


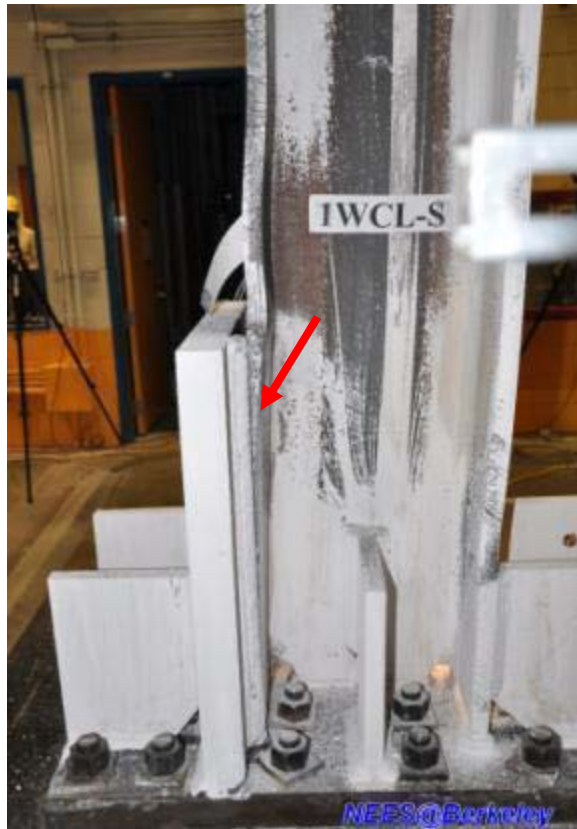
Figure 4.219 Complete fracture of the west side brace in the first story (Specimen TCBF-B-2)



Figure 4.220 Crack in the lower beam web at west side near top flange (Specimen TCBF-B-2)



**Figure 4.221** Crack initiates in the east side round HSS brace at the first story (Specimen TCBF-B-2)



**Figure 4.222** Tearing of the vertical fillet welds at the west column base (Specimen TCBF-B-2)



Figure 4.223 Necking of the east side round HSS brace in the first story before fracture



Figure 4.224 Complete fracture of the east side brace in the first story (Specimen TCBF-B-2)



**Figure 4.225** The entire side view of the TCBF-B-2 specimen after second trial

### **4.2.3 Specimen TCBF-B-3 (Wide Flange Braces, Quasi-Static Test)**

This specimen was entirely new and had wide flange braces. The roof beam size and column size remained the same as previous two specimens. To prevent premature in the column-to-base plate CJP welds, the column base connection detail was modified by adding four 7/8-in. thick gussets as shown in Fig. 4.226. At the same time, the lower beam to one-piece gusset plate connections were also modified to a pin connection (Fig. 4.227). To prevent the early local buckling and fracture of the lower beam where it connected to the gusset plates, a bolted connection was used to attach the beam web to the gusset plate (Fig. 4.227). The gain values in the portable data acquisition software were set to be 50 for all data channels (note that all channels in portable DAQ were connected to strain gauges).

The test began at around 11:01 AM on Monday, January 24, 2011. The entire side views of the specimen before and after test are shown in Fig. 4.228.



Figure 4.226 Column base connection detail of TCBF-B-3 specimen (four 7/8-in. gussets welded to the column flange and base plate)



Figure 4.227 The lower beam to one-piece gusset plate pin connection detail of TCBF-B-3 specimen (eastern side of the W24 x 68 beam)



(a) Before test



(b) After test

Figure 4.228 Specimen TCBF-B-3 before test and after test

#### 4.2.3.1 Key Response Quantities

The paragraphs below briefly describe the response quantities recorded in the test and the post-processed response quantities derived from the raw data. Detailed discussion of the individual response quantities are described in Chapter 5.

##### 4.2.3.1.1 System Response

Figures 4.229 and 4.230 show the time history of the actuator displacements and actuator load cell force feedbacks for specimen TCBF-B-3. The base shear versus controlled roof displacement of the specimen is shown in Fig. 4.231. The relationship between story shear and story drift for the specimen is shown in Fig. 4.232.

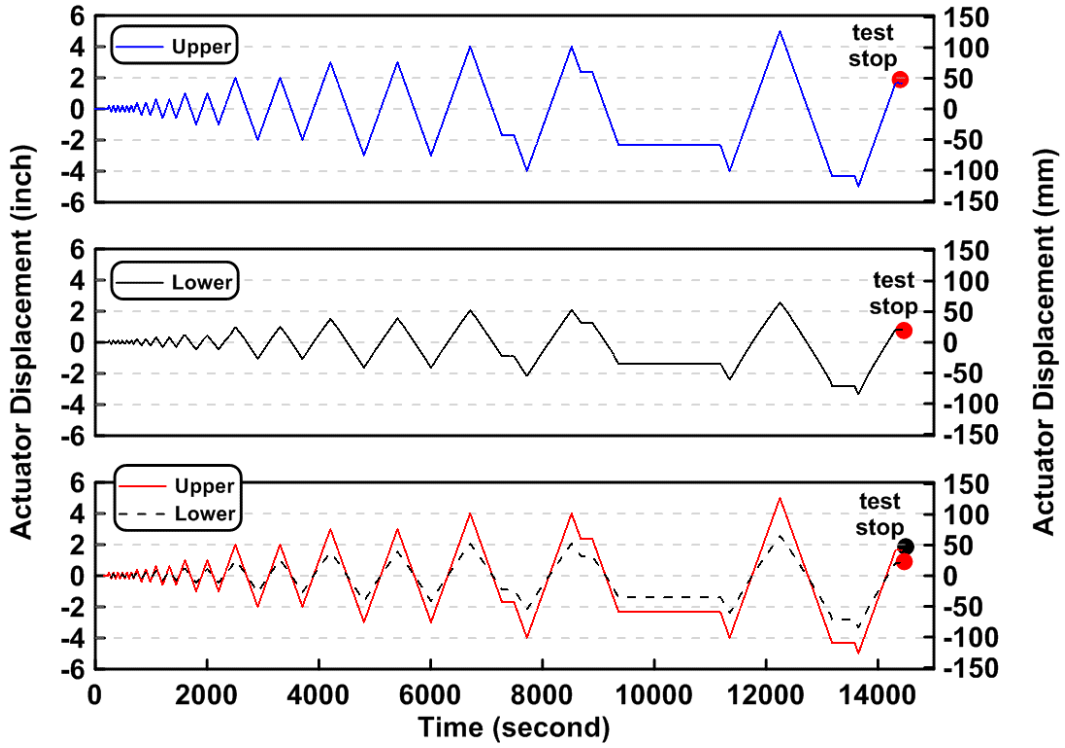


Figure 4.229 Actuator displacement time history of TCBF-B-3 specimen

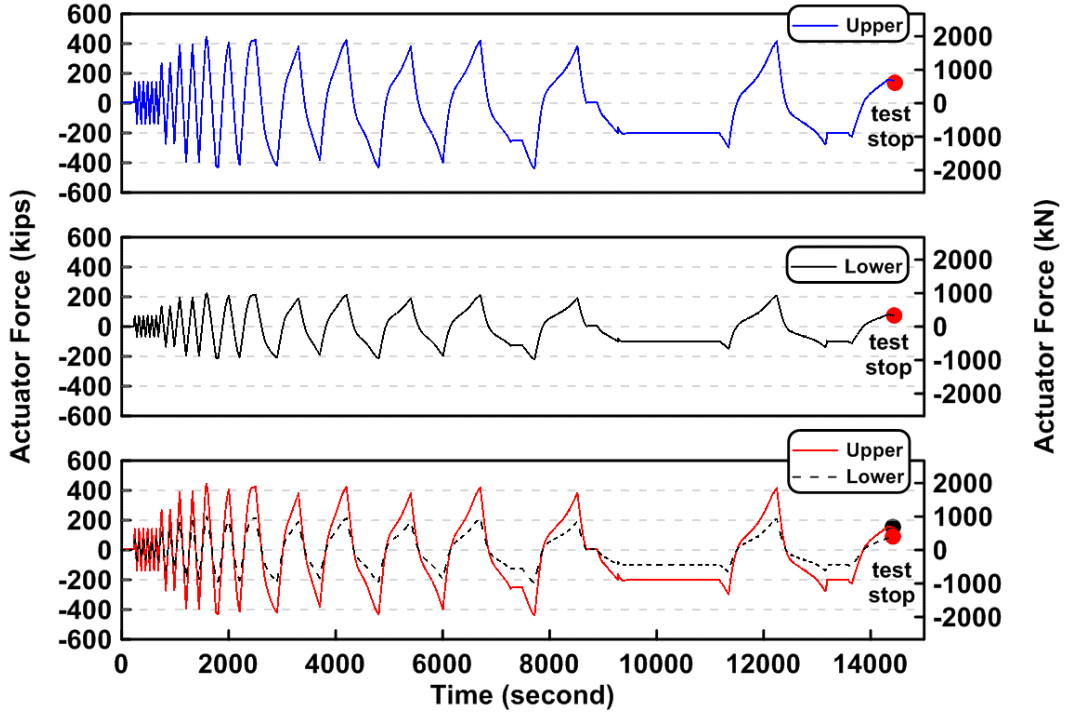


Figure 4.230 Actuator force histories of TCBF-B-3 specimen



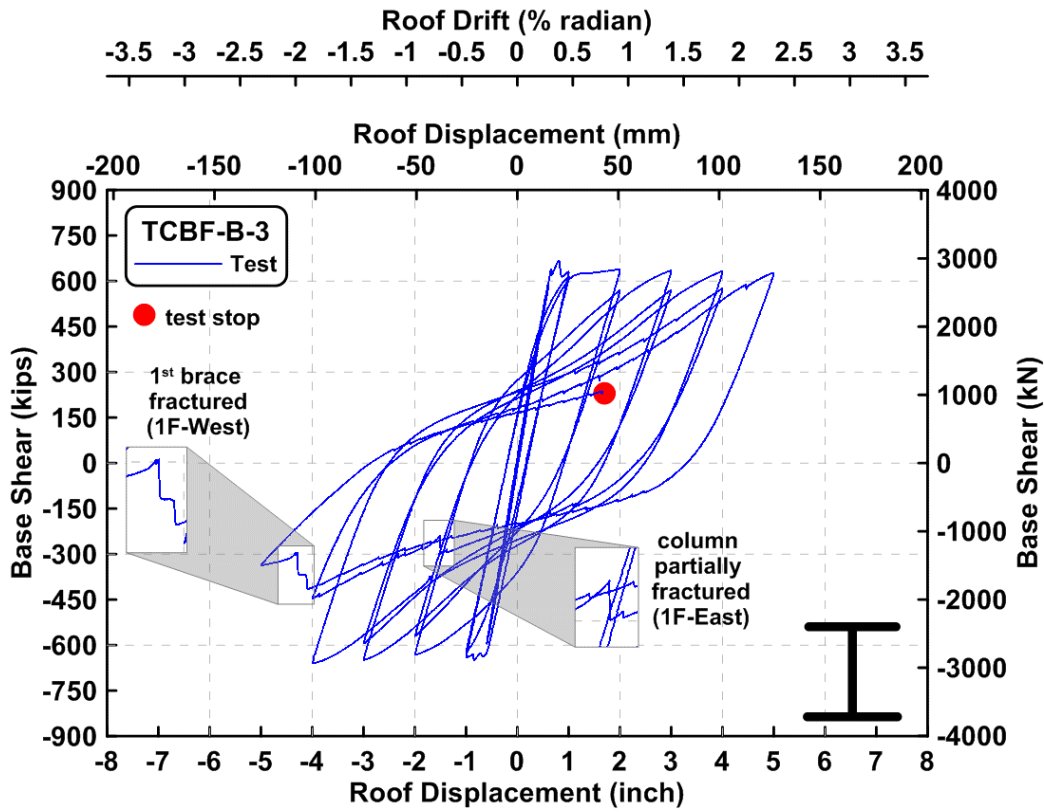


Figure 4.231 Base shear vs. roof displacement relationship of TCBF-B-3 specimen

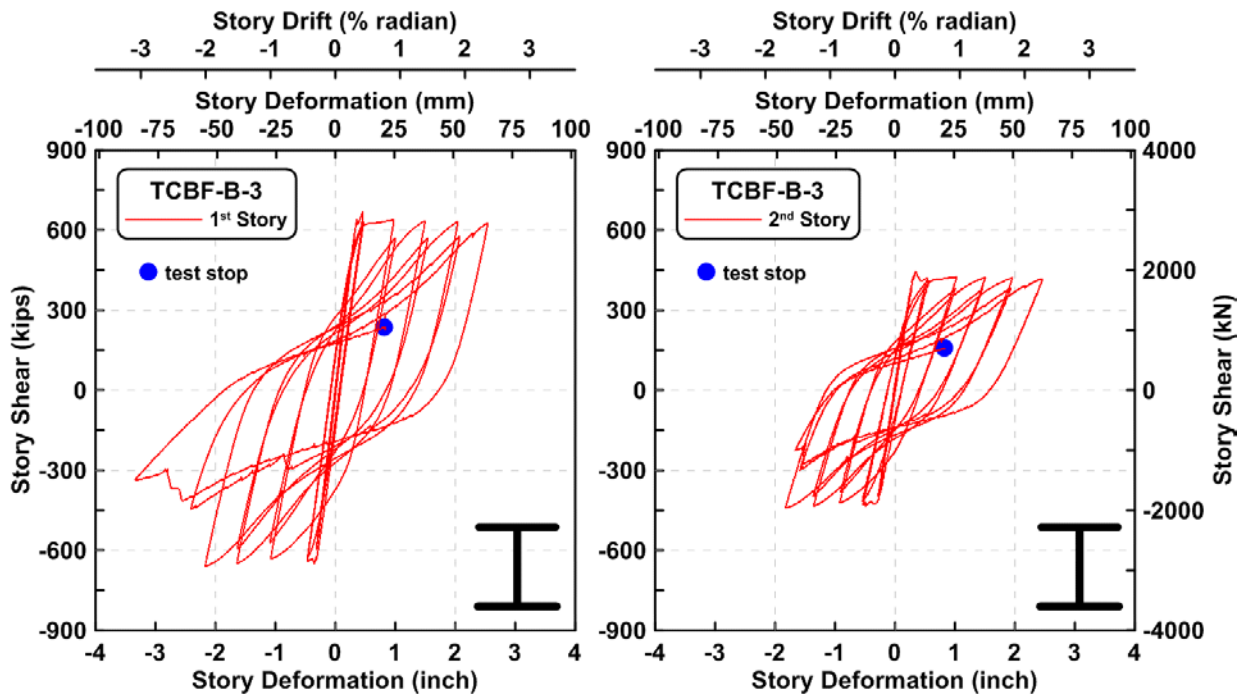


Figure 4.232 Story shear vs. story deformation relationship of TCBF-B-3 specimen

### 4.2.3.1.2 Column Response

The time history of the axial forces in W12 × 96 columns at western and eastern sides of the specimen is plotted in Fig. 4.233. The relationship between roof displacements and axial forces at both columns is shown in Fig. 4.234. The bending moment time history at the top and bottom ends of the column in each story is shown in Figs. 4.235 and 4.236. Derived column shear force time history in both stories are plotted in the Figs. 4.237 and 4.238, respectively. Two column shear forces in each floor were added together and are shown in Fig. 4.239.

The column web shear stress versus shear strain readings from strain rosettes is plotted in Fig. 4.240. The sum of the column shear force components versus the total story shear forces for each story are shown in Fig. 4.241. The derived rosette-type strain gauge readings in the column web at each story are shown in Figs. 4.242 to 4.245. Normalized maximum and minimum principal stress relationships along with different yield criteria are plotted in Figs. 4.246 to 4.249. The normalized P-M and P-V interaction diagrams at column bases and column top ends are shown in Figs. 4.250 to 4.253.

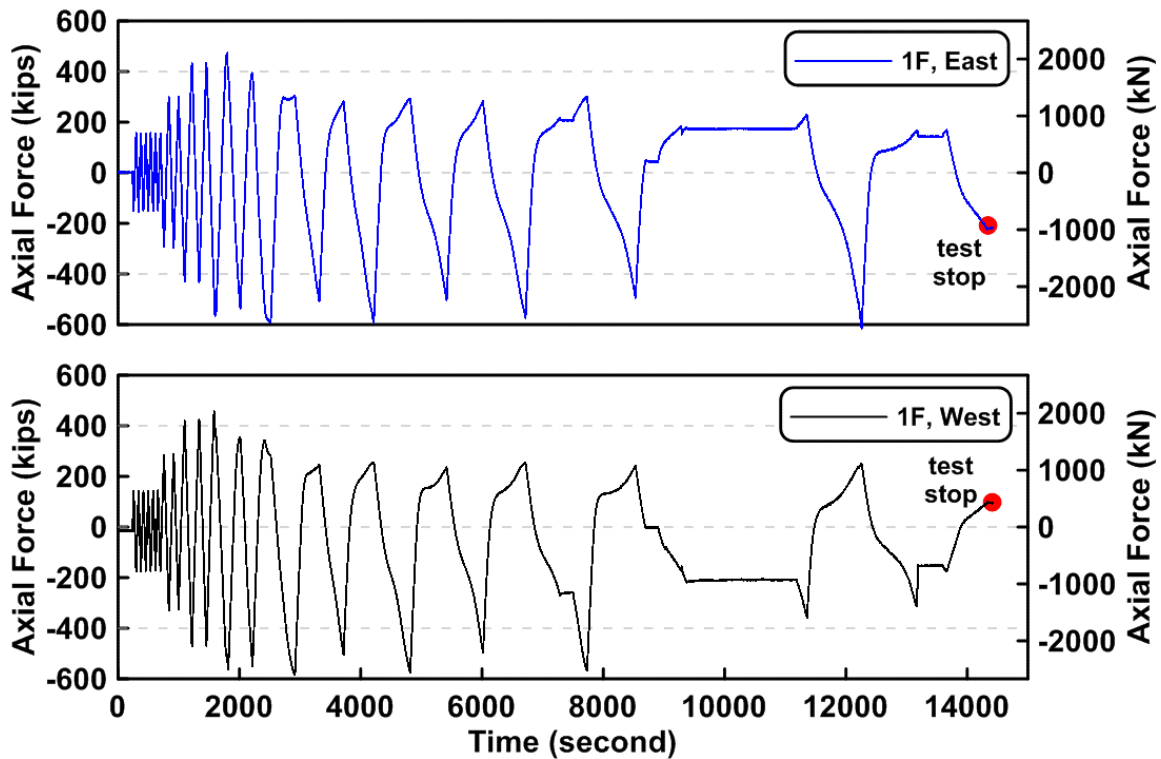


Figure 4.233 Time history of the column axial forces in the first story of TCBF-B-3 specimen (location: 3-ft above column base plate)

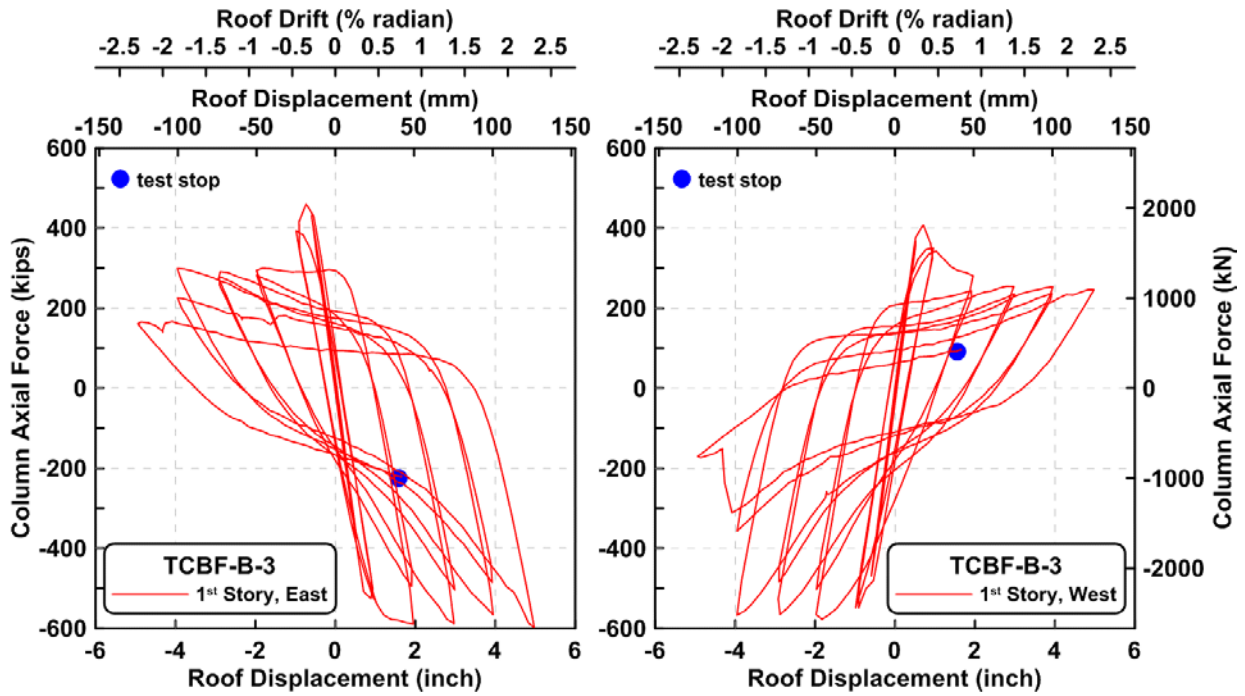


Figure 4.234 Roof displacement vs. first story column axial forces of TCBF-B-3 specimen

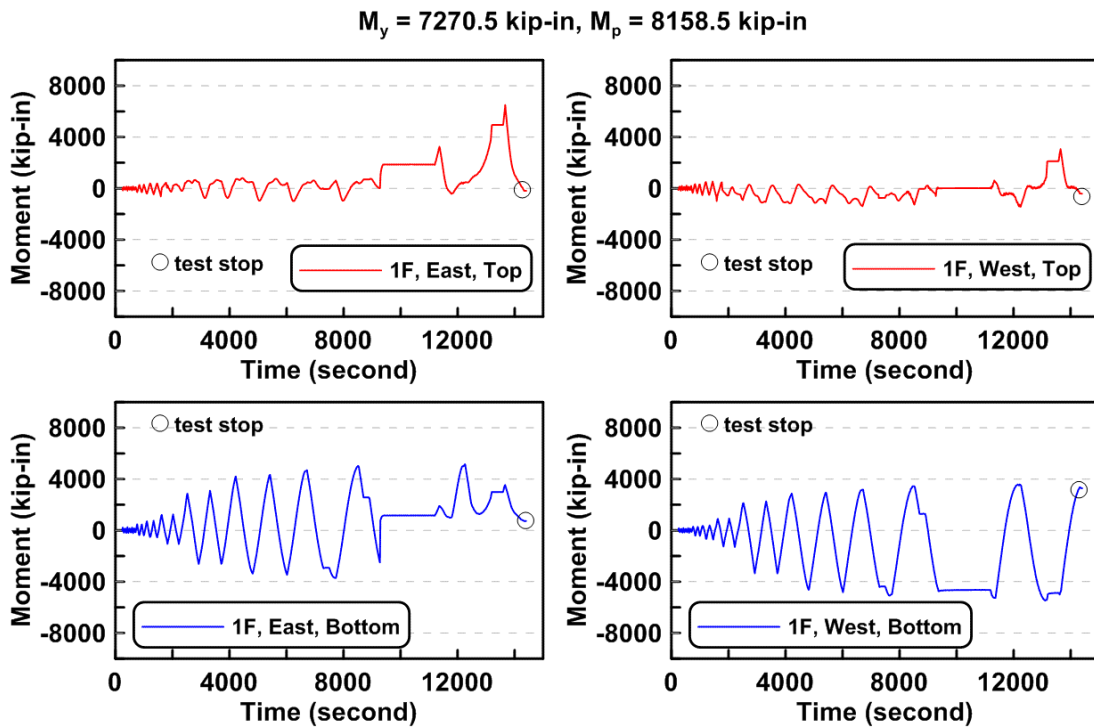


Figure 4.235 Time history of the first story column bending moments of TCBF-B-3 specimen (3-ft above column base plate and 3-ft below lower beam centerline)

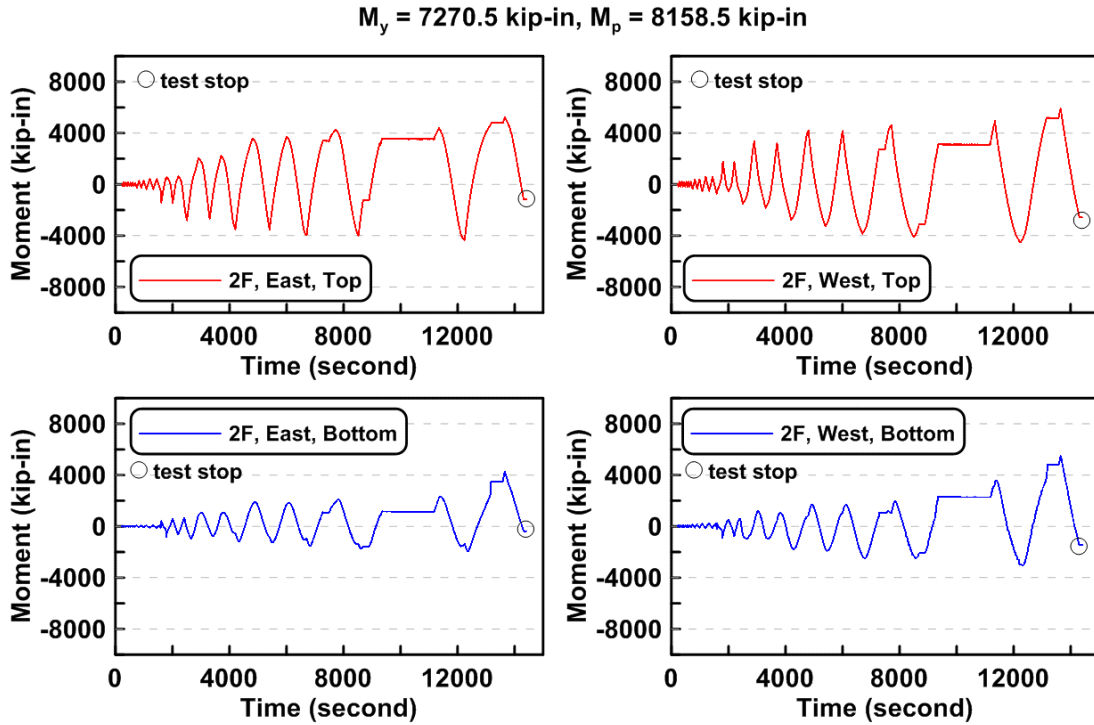


Figure 4.236 Time history of the second story column bending moments of TCBF-B-3 specimen (3-ft above lower beam centerline and 3-ft below roof beam centerline)

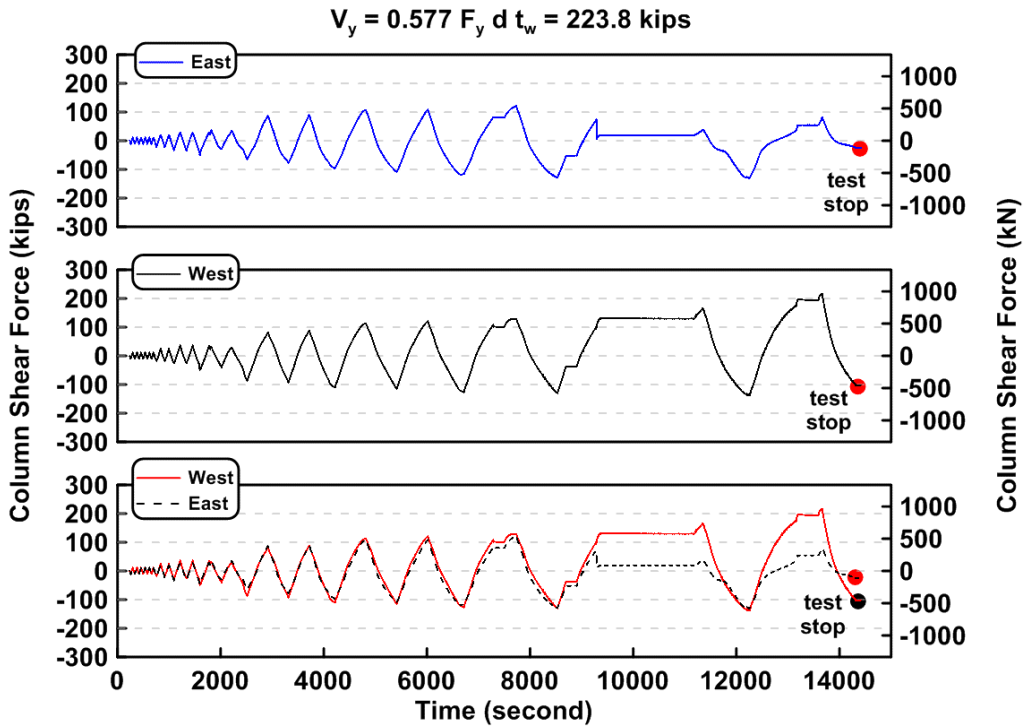


Figure 4.237 Time history of the first story column shear forces of TCBF-B-3 specimen

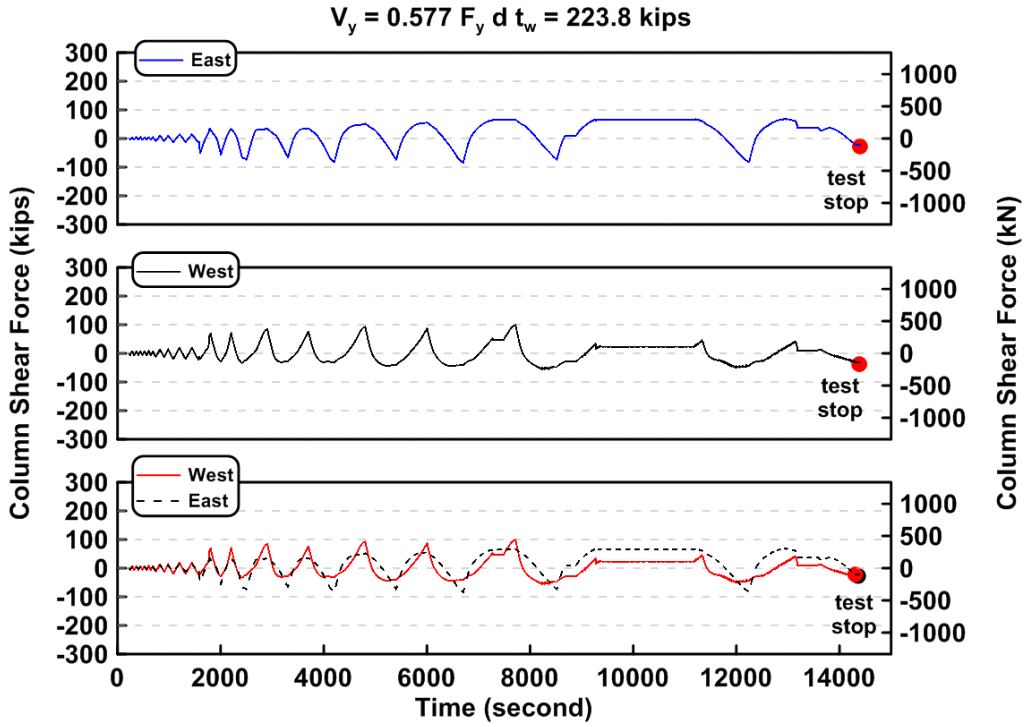


Figure 4.238 Time history of the second story column shear forces of TCBF-B-3 specimen

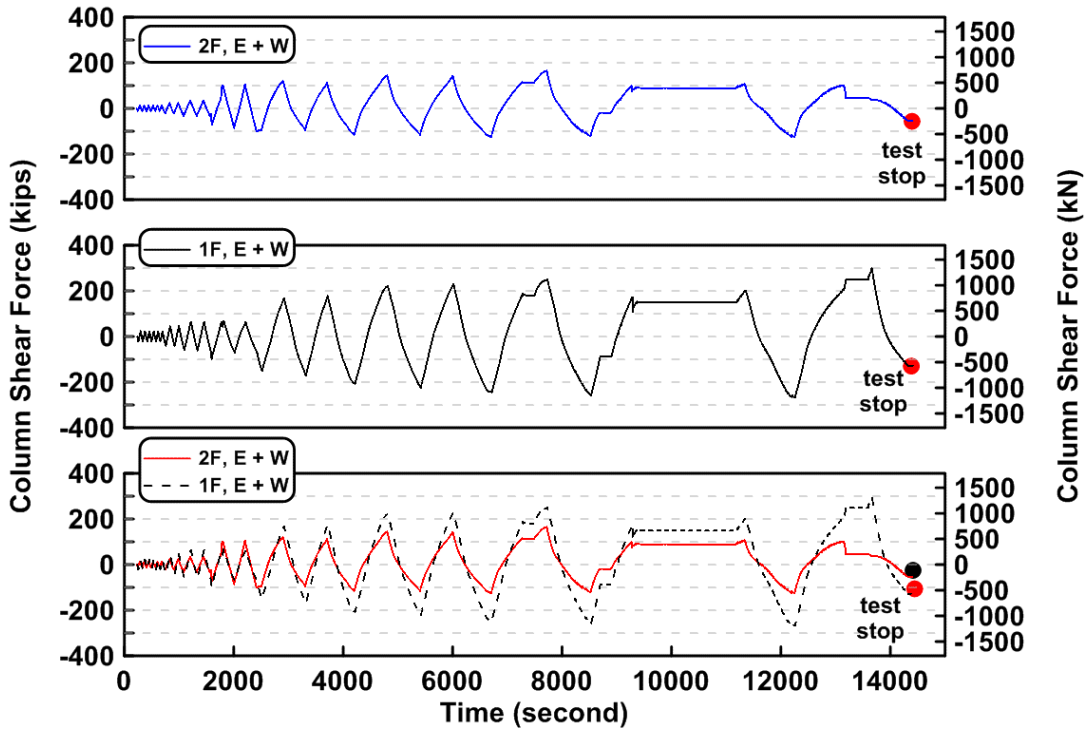


Figure 4.239 Time history of the sum of east and west column shear forces in both stories of TCBF-B-3 specimen

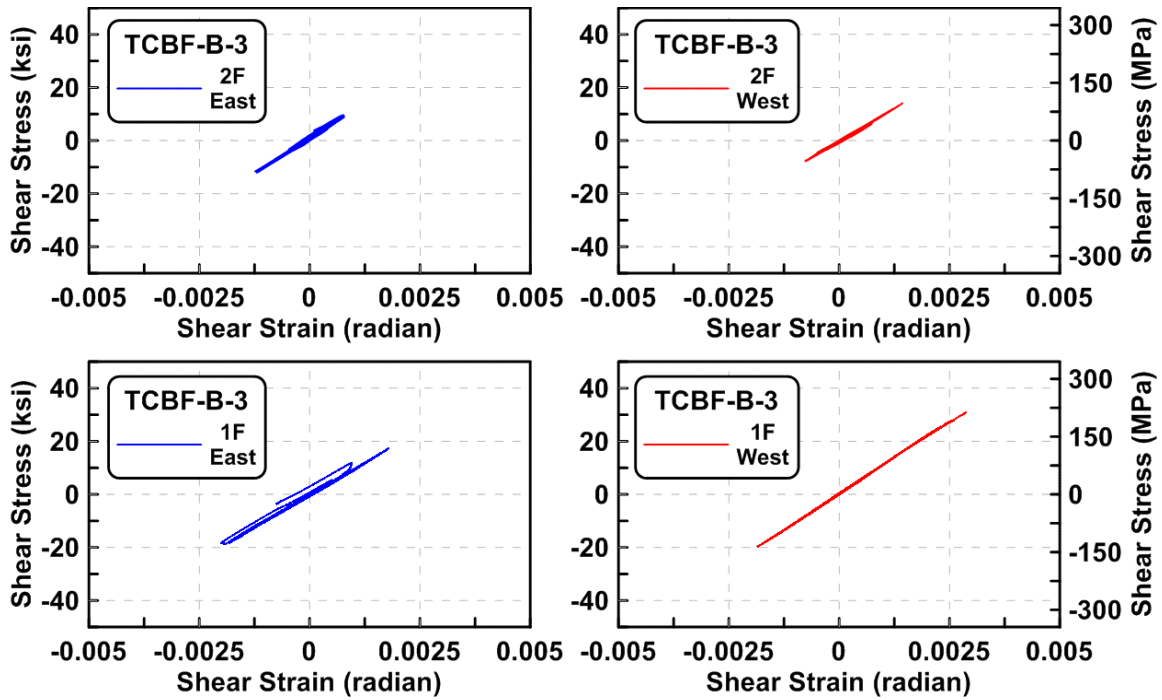


Figure 4.240 Column shear stress vs. shear strain relationships of TCBF-B-3 specimen (locations: EC1-B-N, EC2-B-N, WC1-B-N and WC2-B-N)

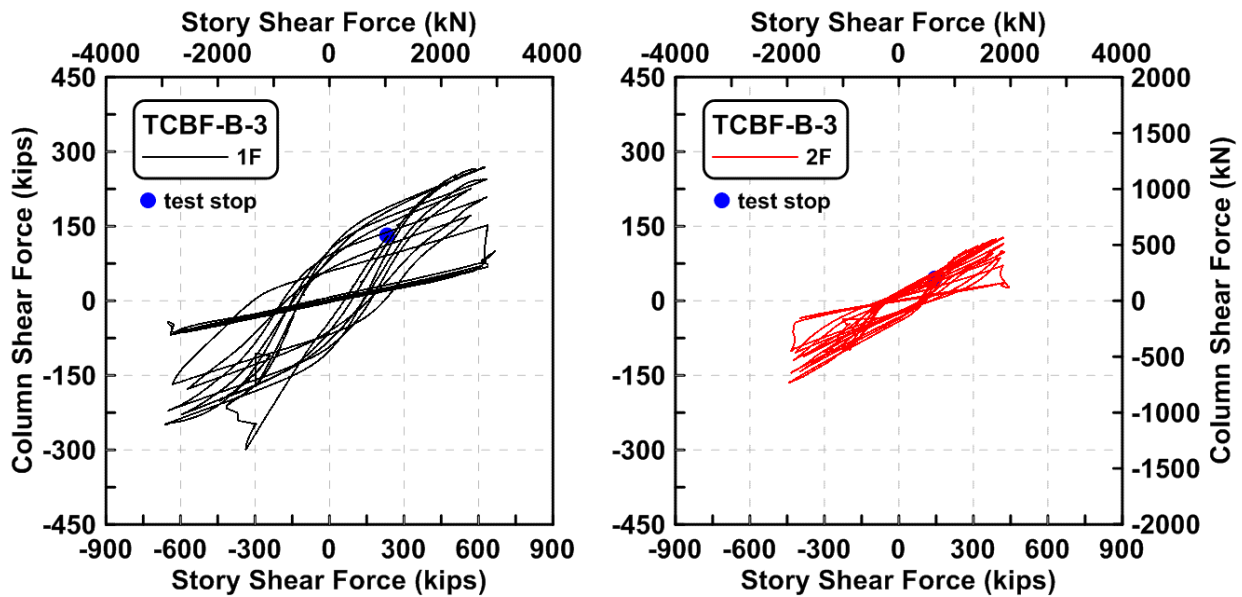


Figure 4.241 Story shear component from columns vs. total story shear forces of TCBF-B-3 specimen

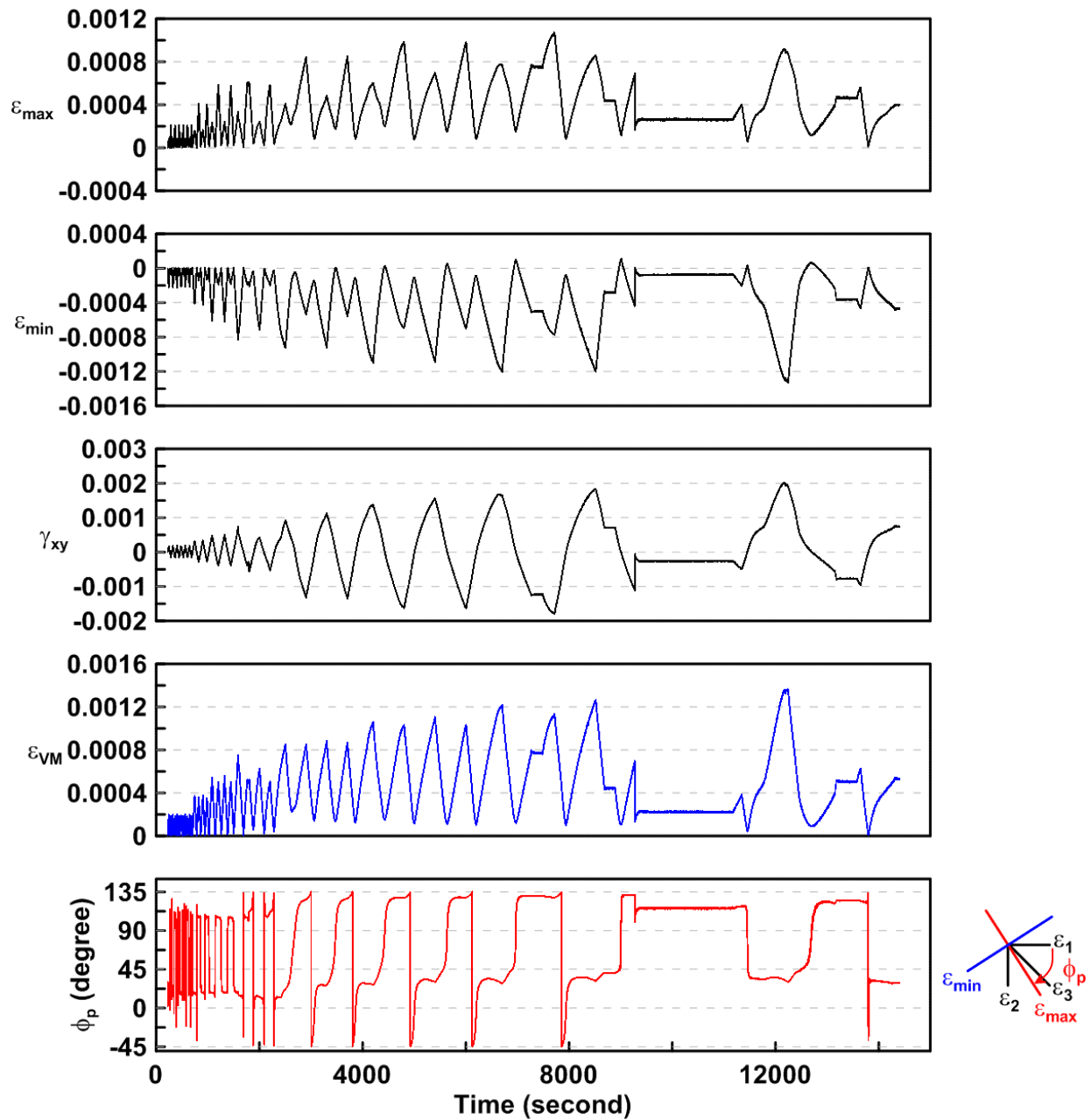


Figure 4.242 Time history of rosette type strain gauge readings in the first story column web of TCBF-B-3 specimen (location: R1)

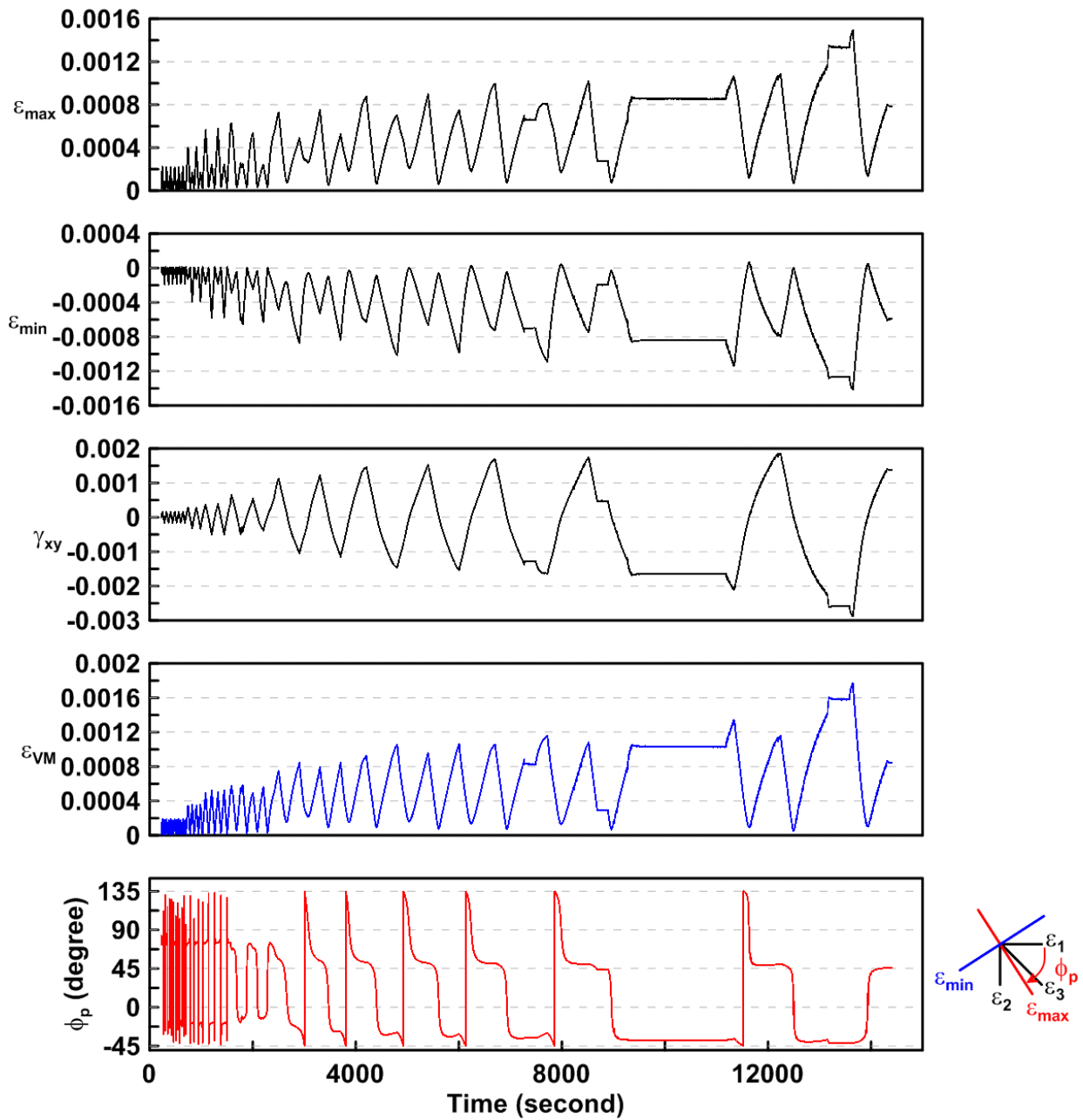


Figure 4.243 Time history of rosette type strain gauge readings in the first story column web of TCBF-B-3 specimen (location: R5)



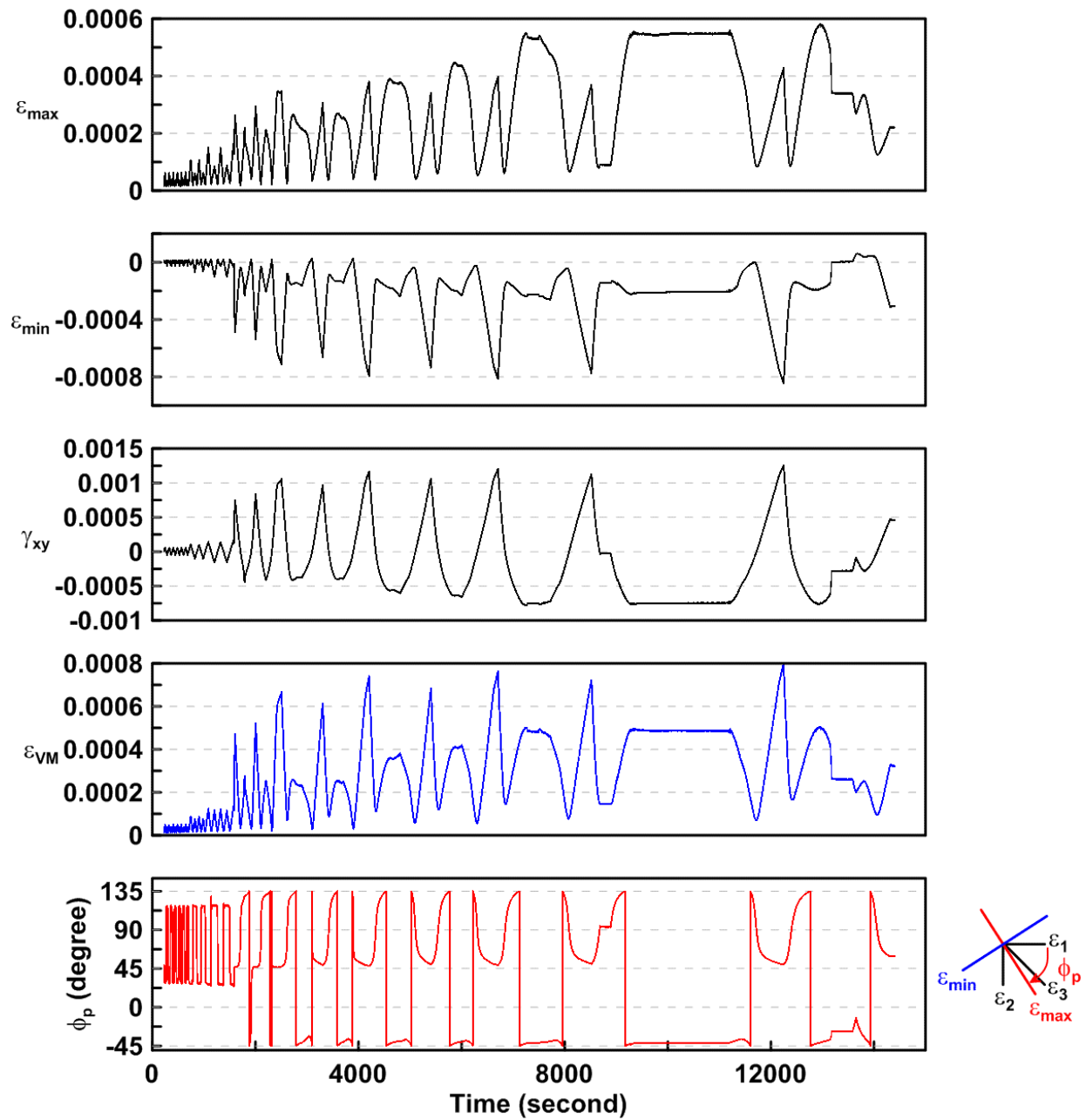


Figure 4.244 Time history of rosette type strain gauge readings in the first story column web of TCBF-B-3 specimen (location: R3)

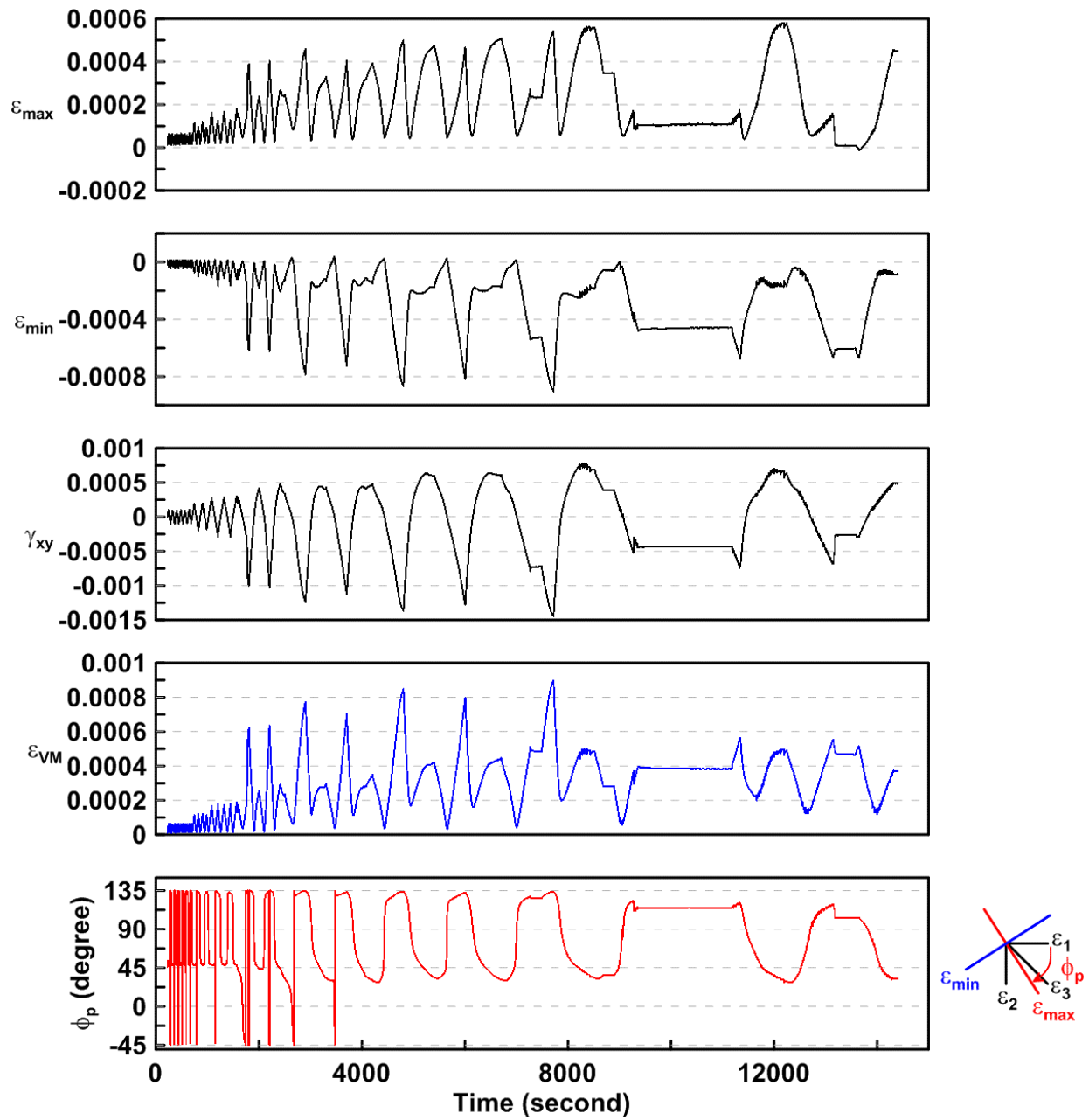


Figure 4.245 Time history of rosette type strain gauge readings in the first story column web of TCBF-B-3 specimen (location: R7)

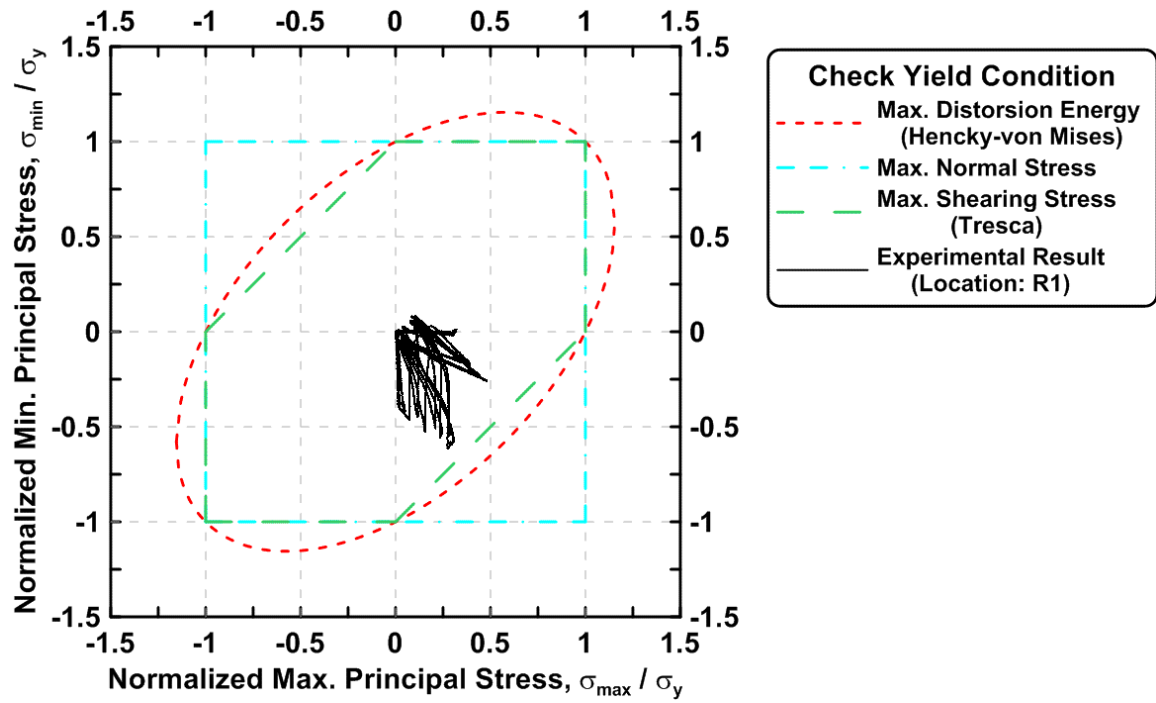


Figure 4.246 Maximum principal stress vs. minimum principal stress in the first story column of TCBF-B-3 specimen (location: R1)

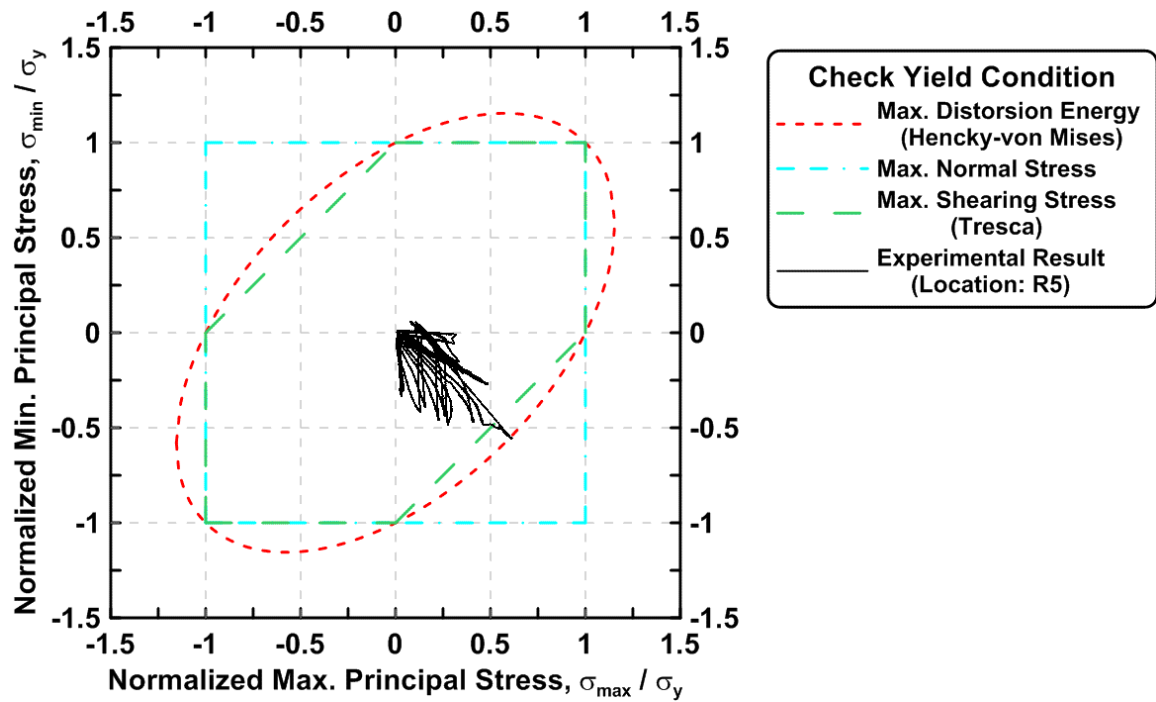


Figure 4.247 Maximum principal stress vs. minimum principal stress in the first story column of TCBF-B-3 specimen (location: R5)

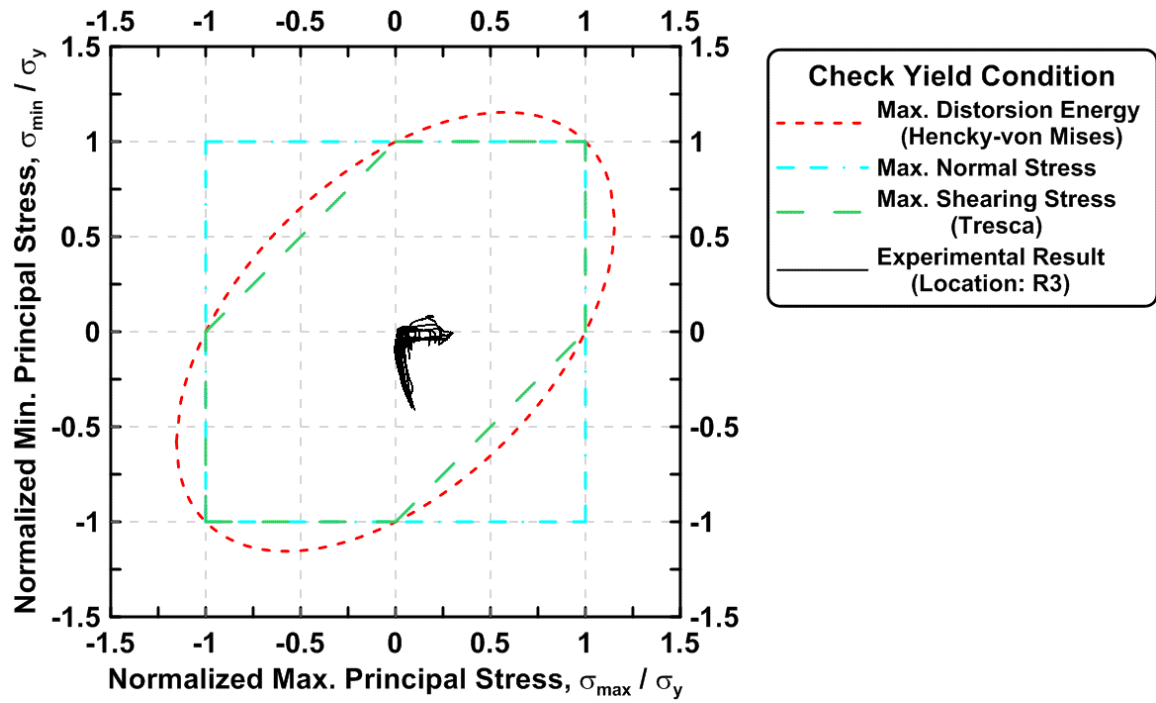


Figure 4.248 Maximum principal stress vs. minimum principal stress in the first story column of TCBF-B-3 specimen (location: R3)

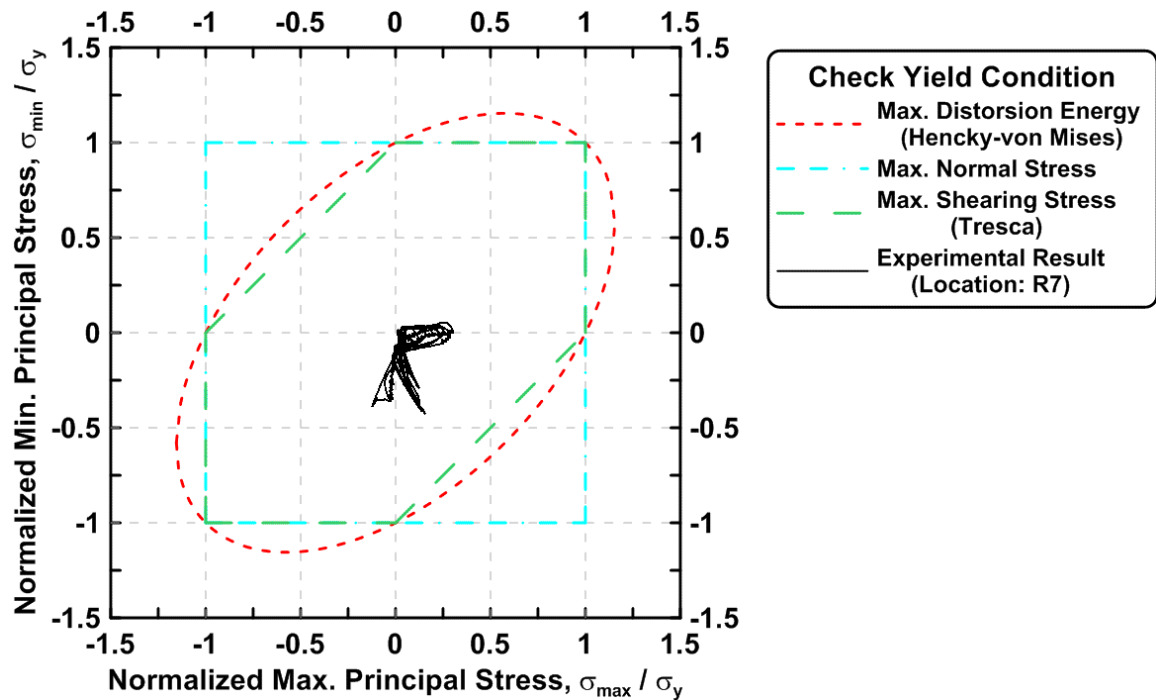


Figure 4.249 Maximum principal stress vs. minimum principal stress in the first story column of TCBF-B-3 specimen (location: R7)

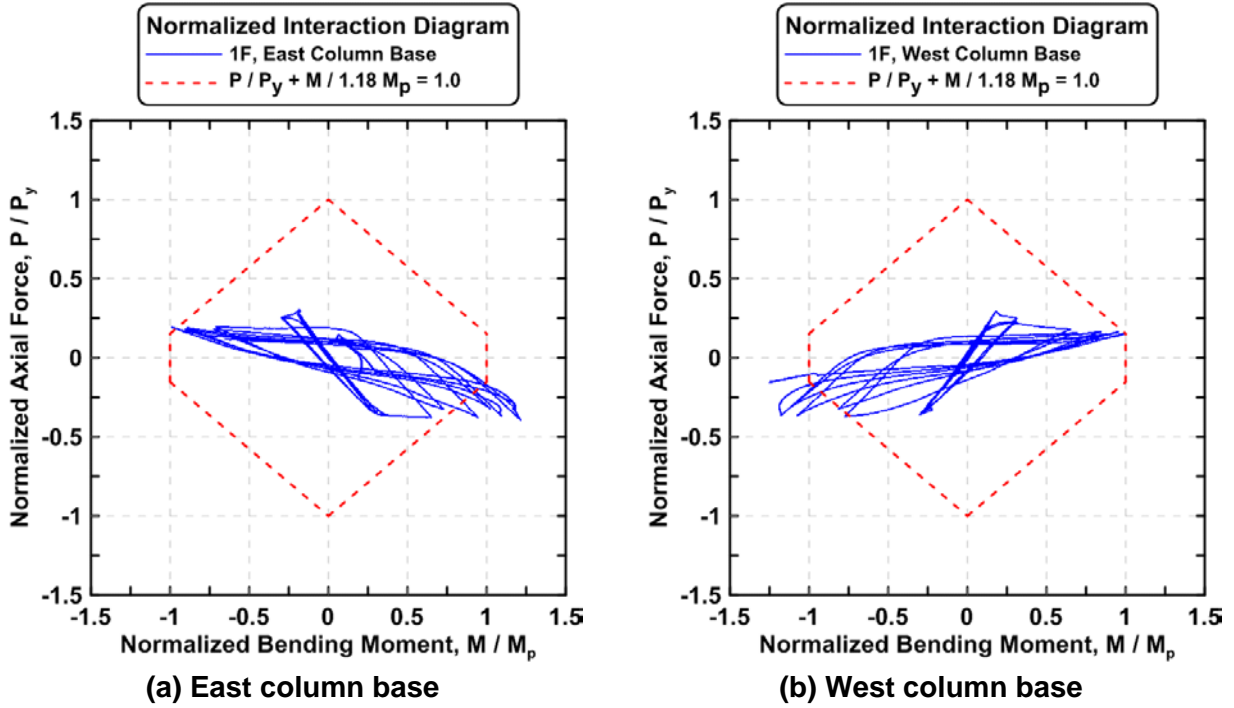


Figure 4.250 Normalized P-M interaction diagrams of the first story columns of TCBF-B-3 specimen

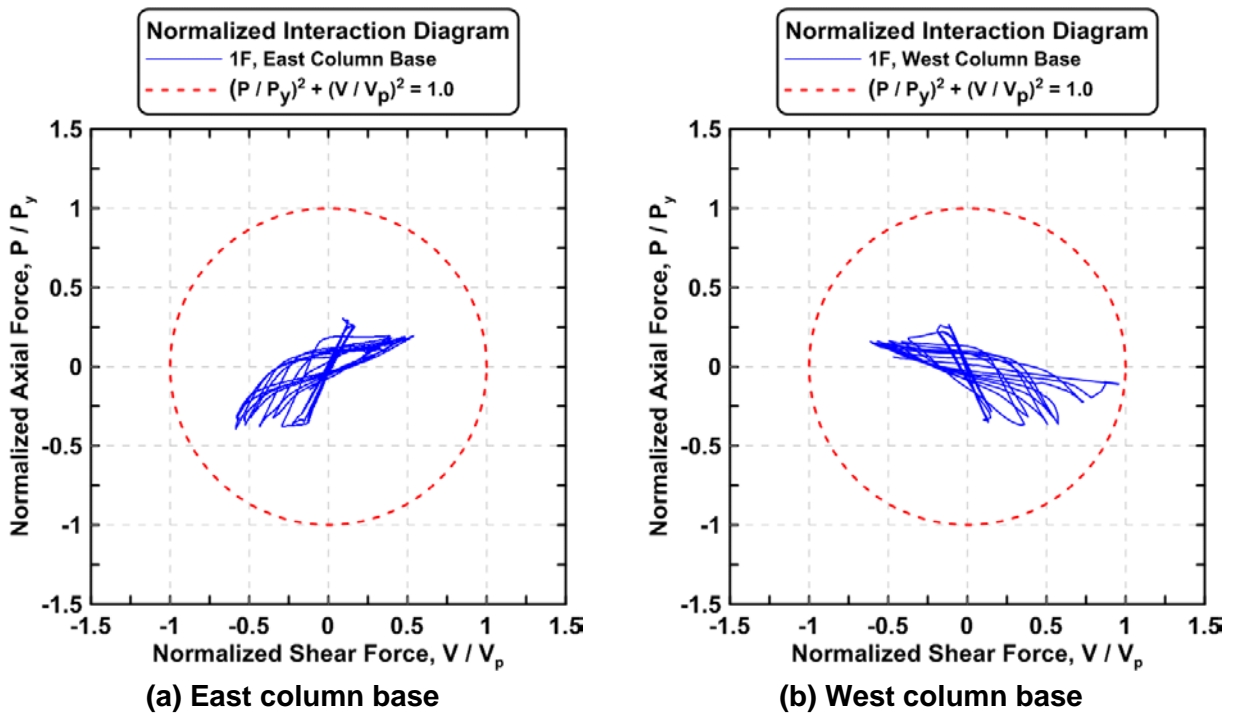


Figure 4.251 Normalized P-V interaction diagrams of the first story columns of TCBF-B-3

Specimen

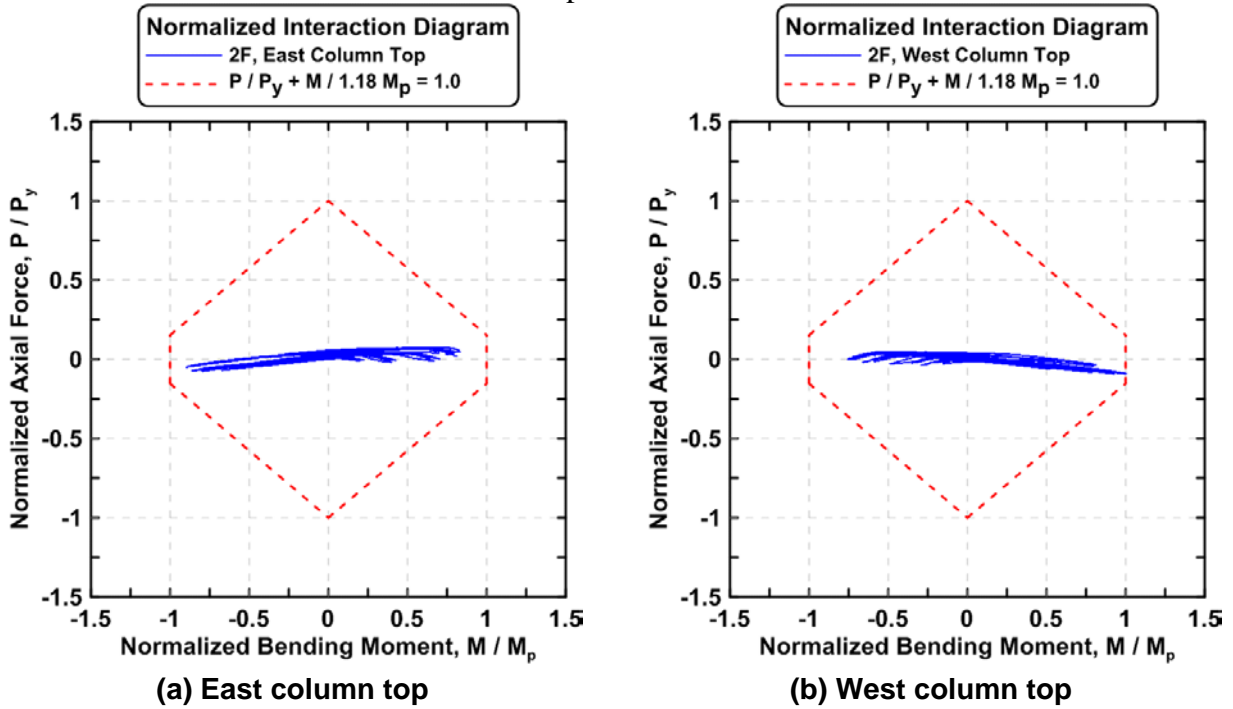


Figure 4.252 Normalized P-M interaction diagrams of the second story columns of TCBF-B-3 specimen

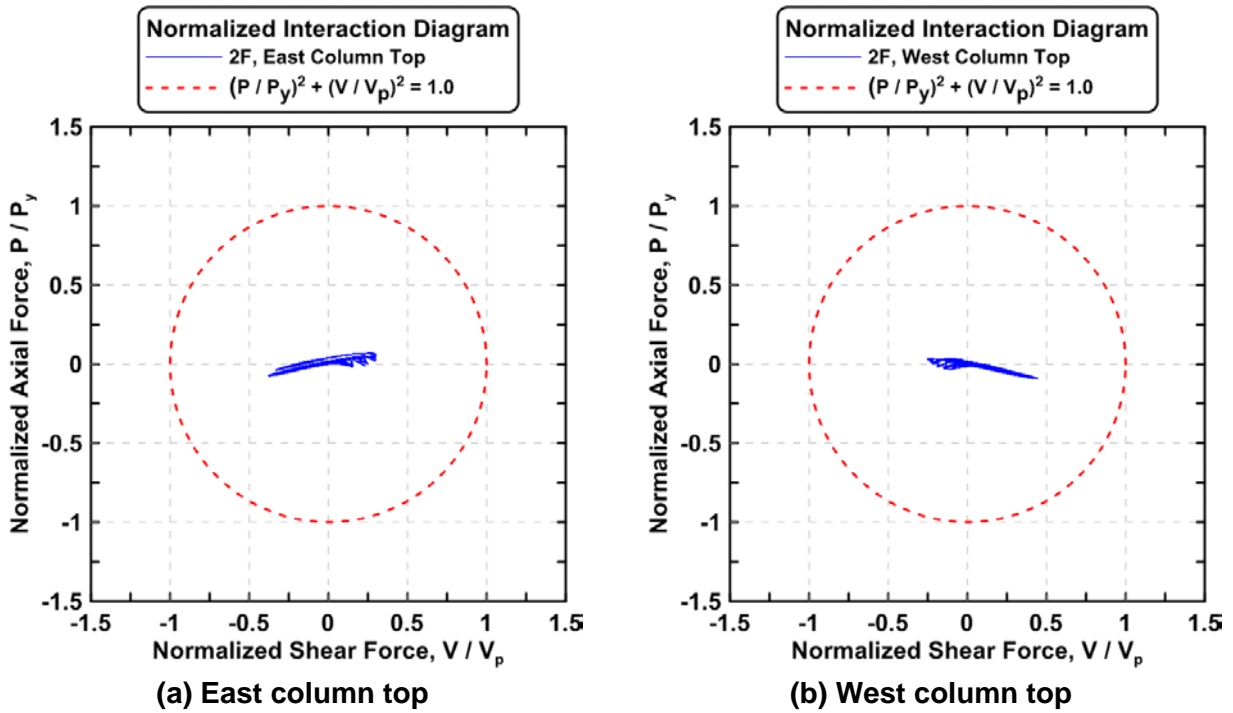


Figure 4.253 Normalized P-V interaction diagrams of the second story columns of TCBF-B-3 specimen

### 4.2.3.1.3 Beam Response

The vertical deflection time history at the center of W24 × 117 roof beam and W24 × 68 lower beam are plotted in Fig. 4.254. Figures 4.255 and 4.256 show the time history of strain readings at both ends of roof beam and lower beam, respectively. Both beam axial force time histories derived from linear type strain gauges at different locations of the beams are plotted in Figs. 4.257 and 4.258. The bending moment time histories of both beams are shown in Figs. 4.259 and 4.260. Estimated beam shear force time histories are illustrated in Figs. 4.261 and 4.262. Unbalanced force in the roof beam center is plotted in Fig. 4.263.

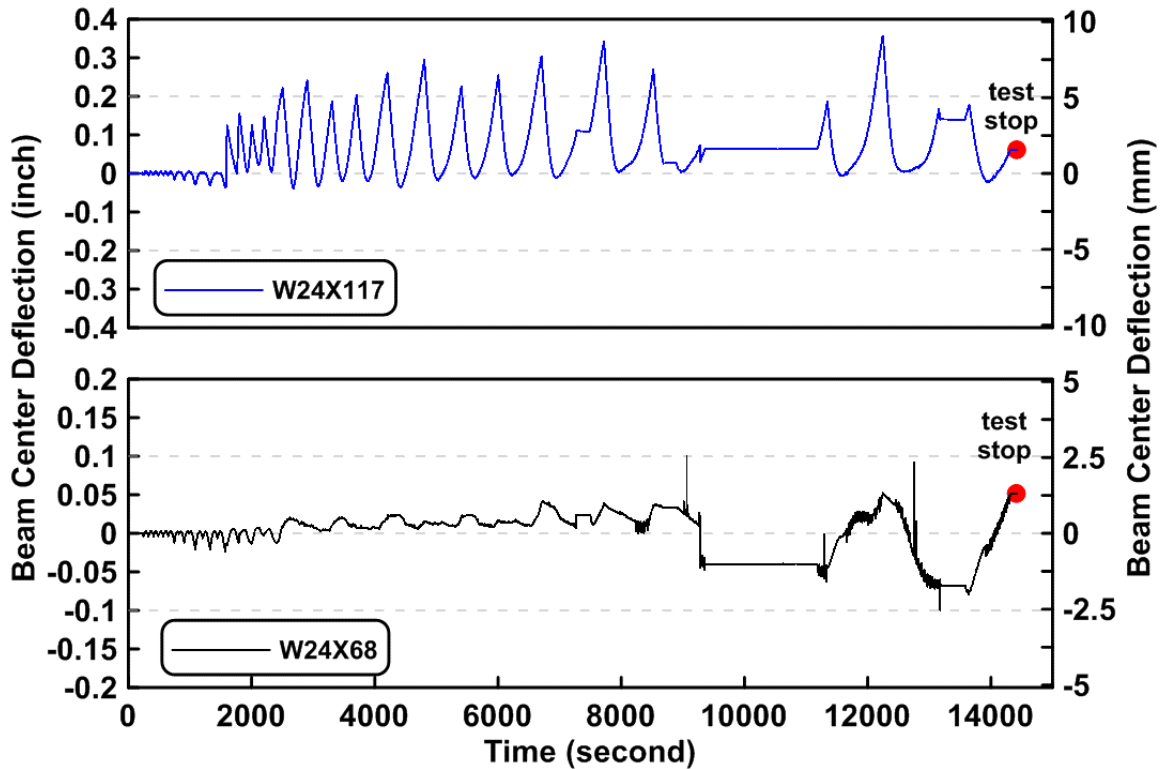


Figure 4.254 The deflection time history at the center of beam span of TCBF-B-3 specimen (roof beam: W24 × 117, lower beam: W24 × 68)

W24x117, Exterior End

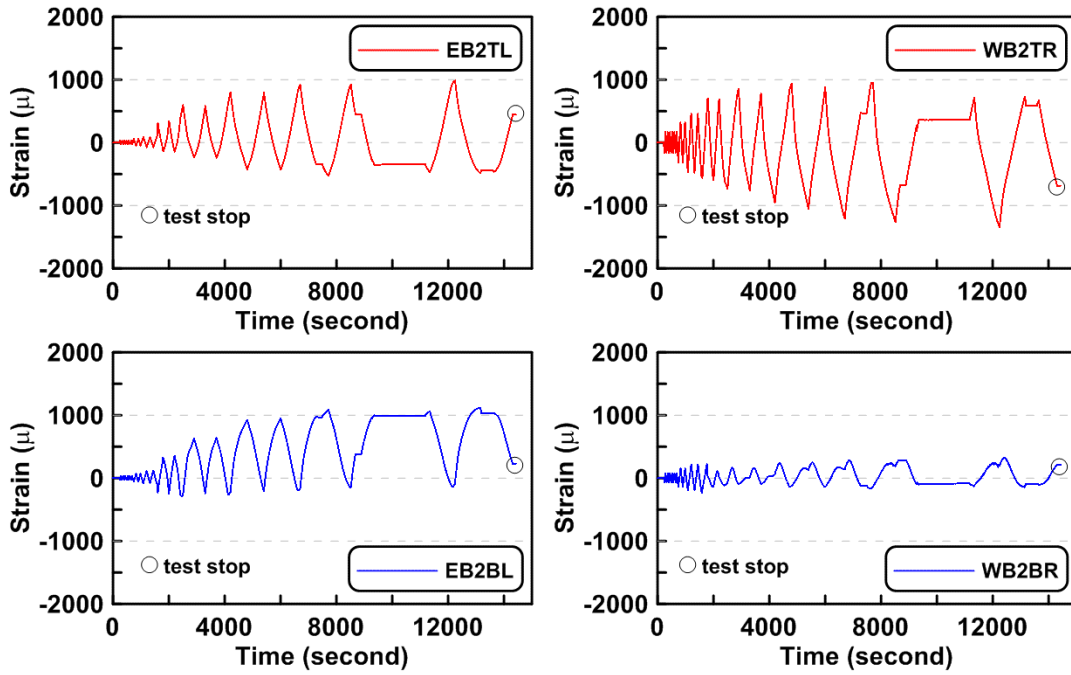


Figure. 4.255 Time history of strain readings at both exterior ends of W24 × 117 roof beam of TCBF-B-3 specimen

W24x68, Exterior End

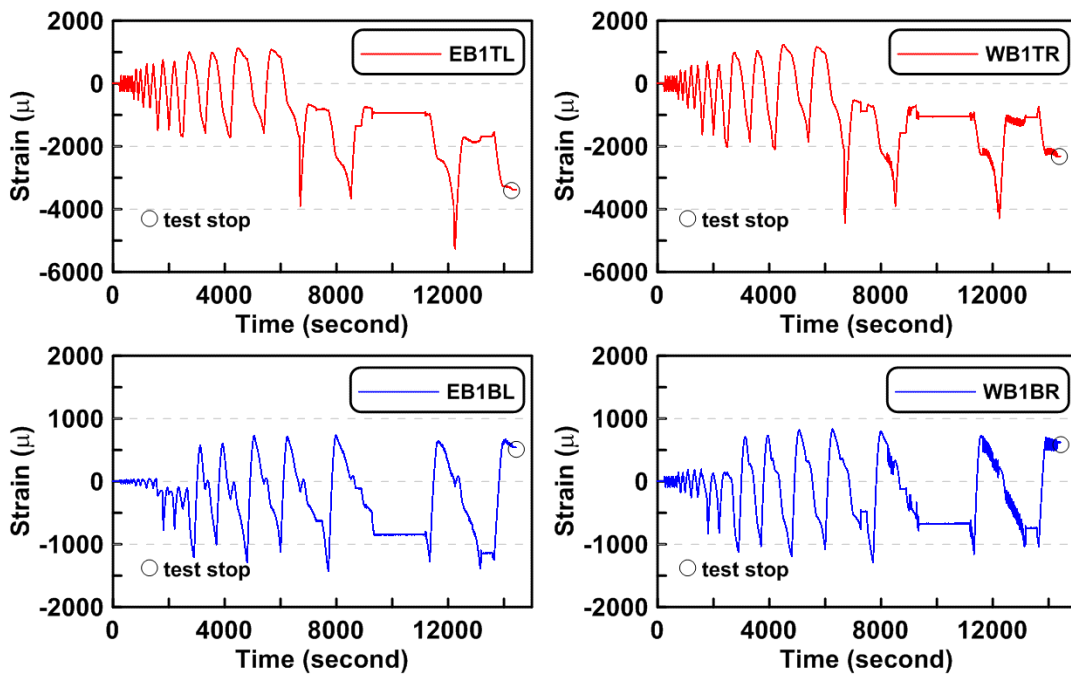


Figure. 4.256 Time history of strain readings at both exterior ends of W24 × 68 lower beam of TCBF-B-3 specimen



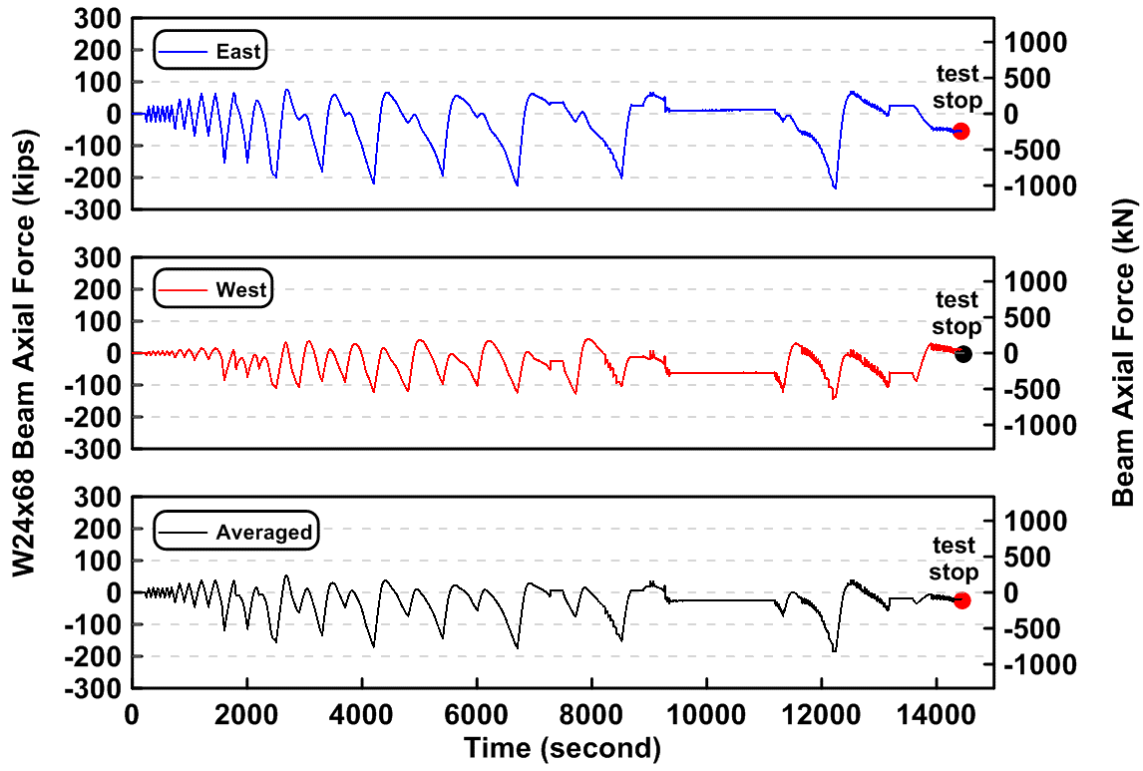


Figure 4.257 Time history of lower beam axial forces of TCBF-B-3 specimen

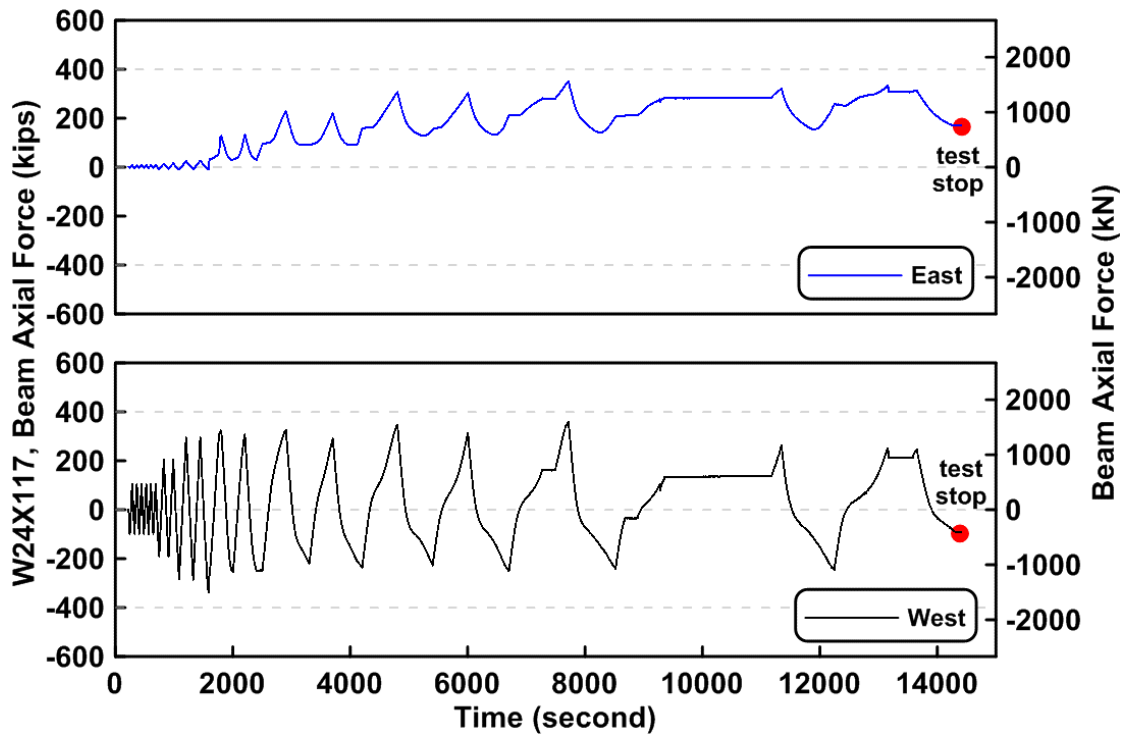


Figure 4.258 Time history of the roof beam axial forces of TCBF-B-3 specimen

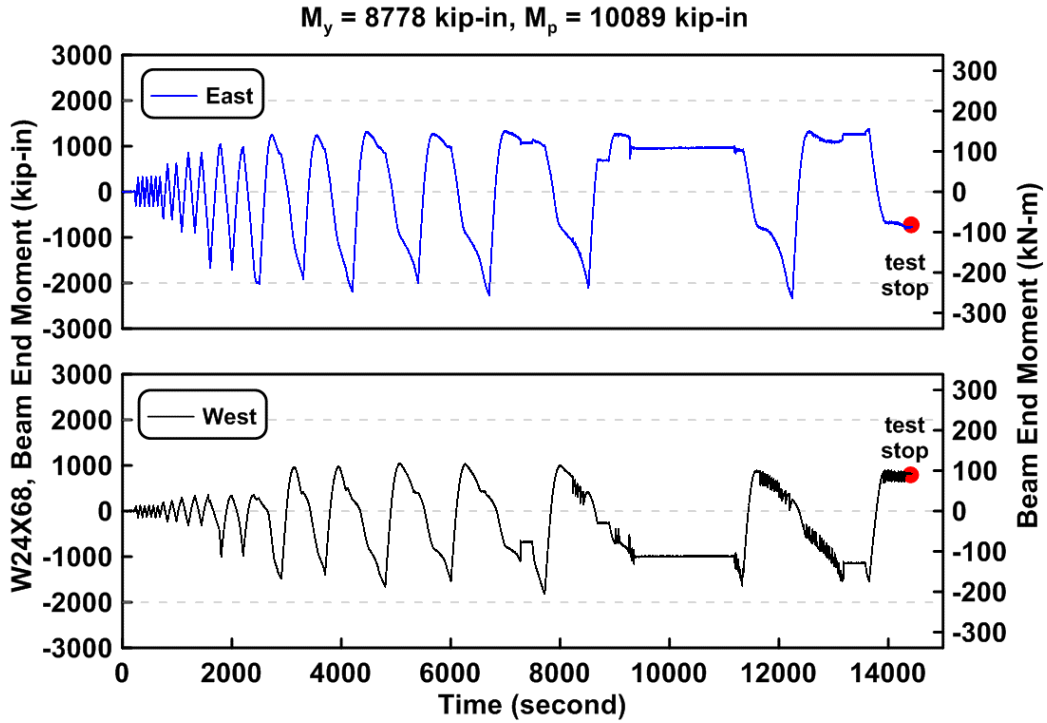


Figure 4.259 Time history of the lower beam end bending moment of TCBF-B-3 specimen

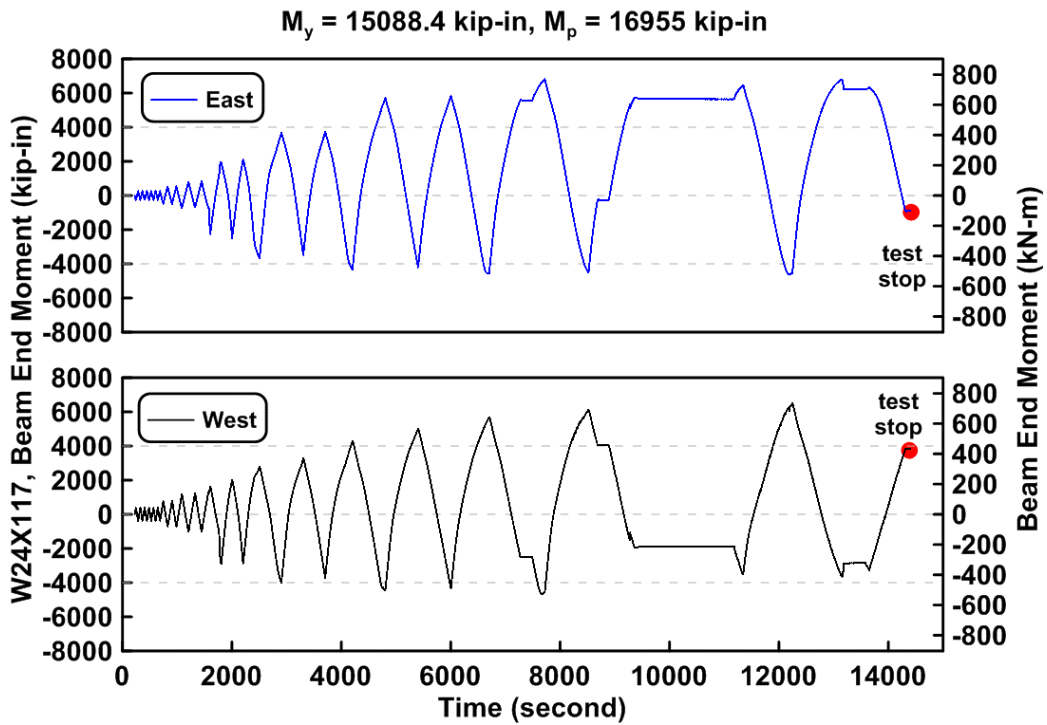


Figure 4.260 Time history of the roof beam end bending moment of TCBF-B-3 specimen

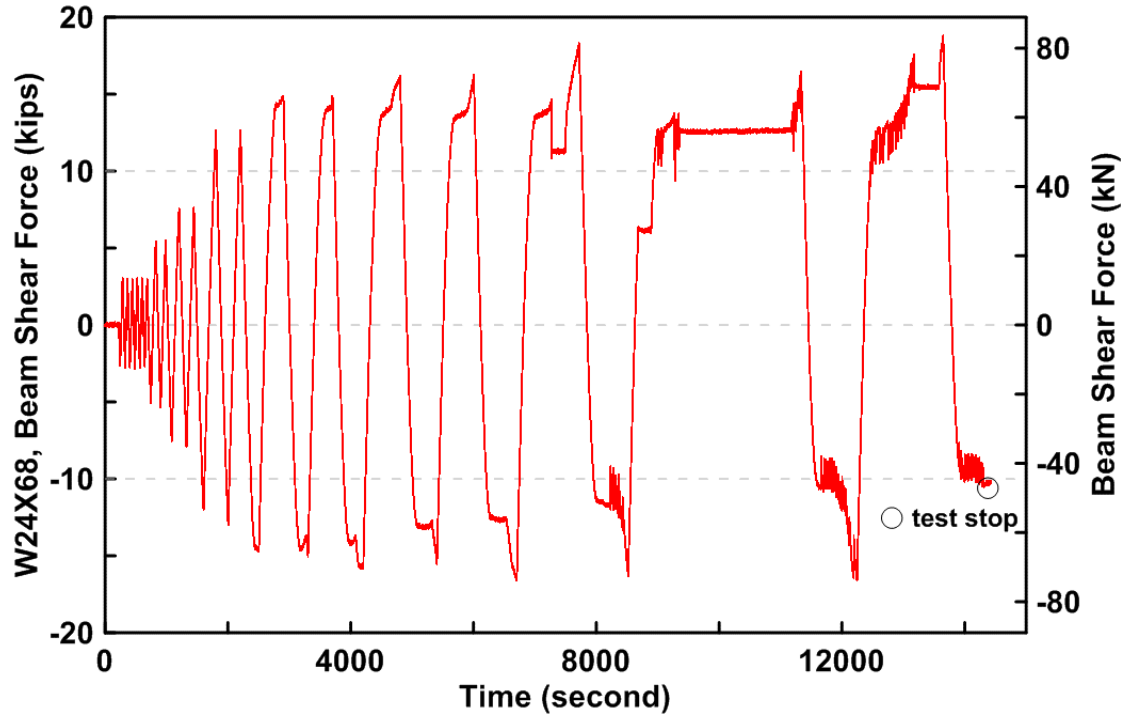


Figure 4.261 Lower beam estimated shear force time history of TCBF-B-3 specimen

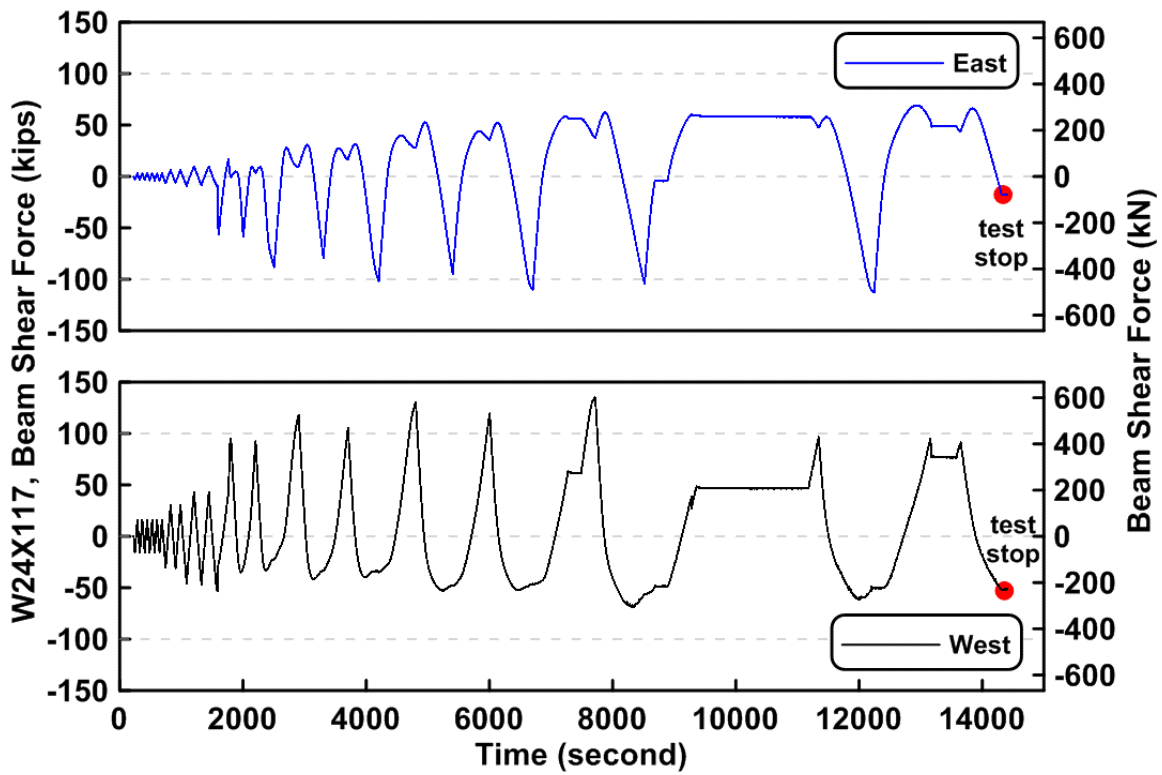


Figure 4.262 Roof beam estimated shear force time history of TCBF-B-3 specimen

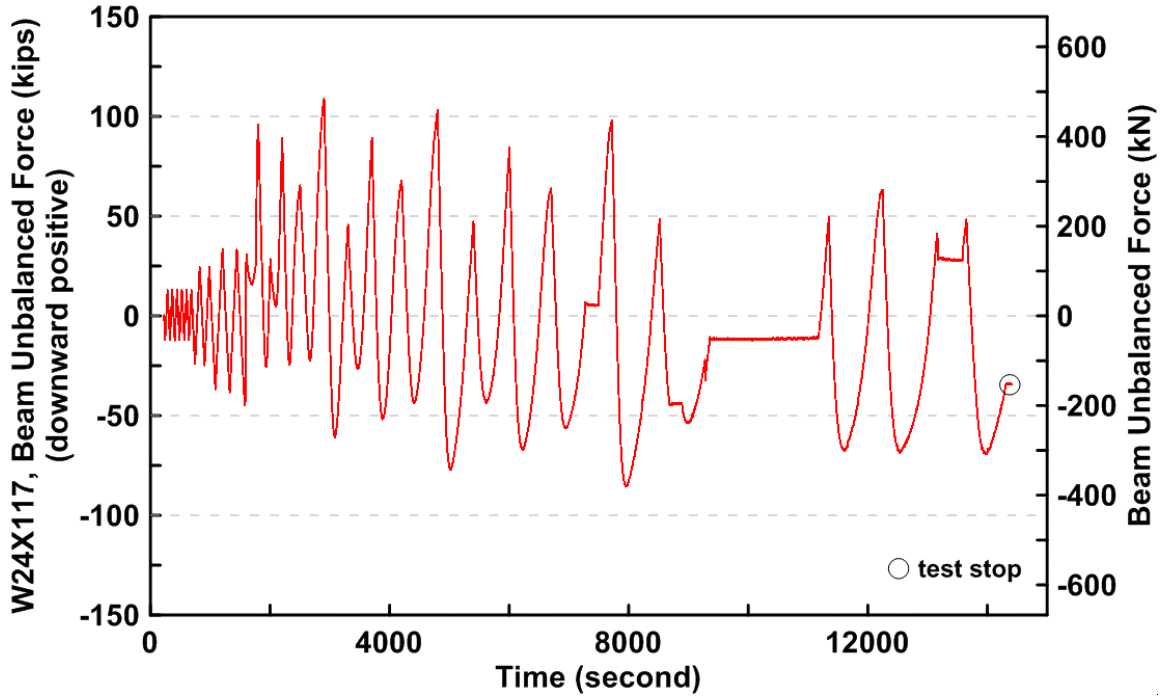


Figure 4.263 Estimated unbalanced force time history of TCBF-B-3 specimen roof beam

#### 4.2.3.1.4 Brace Response

The estimated brace axial forces versus brace axial deformations for each wide flange braces are shown in Fig. 4.264. The estimated brace axial forces versus measured brace out-of-plane displacements at the brace center point for each wide flange brace are shown in Fig. 4.265. Combined brace axial force, axial deformation, and out-of-plane displacement relationships are shown in Fig. 4.266. The decomposed strain (axial strain, in-plane bending strain, out-of-plane bending strain, and warping strain; definition of strain components are similar to that shown in Fig. 4.47(b)) time histories of each brace are plotted in Figs. 4.267 to 4.270.

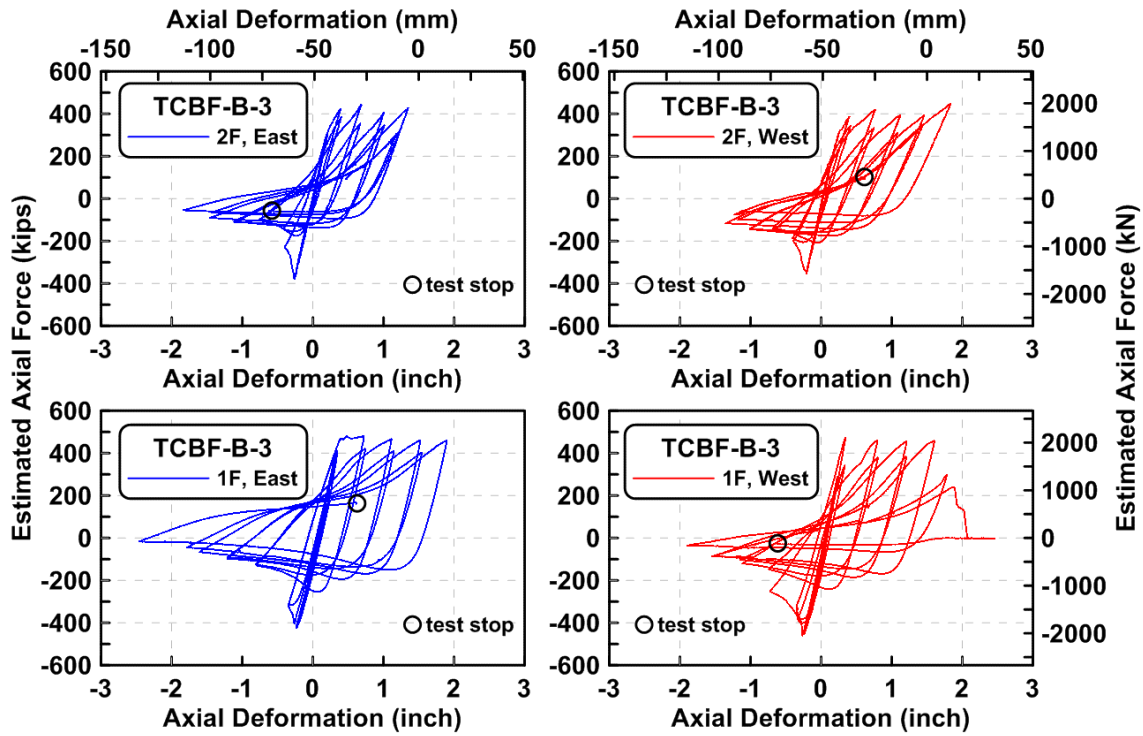


Figure 4.264 Estimated brace axial forces versus brace axial deformations of TCBF-B-3 specimen

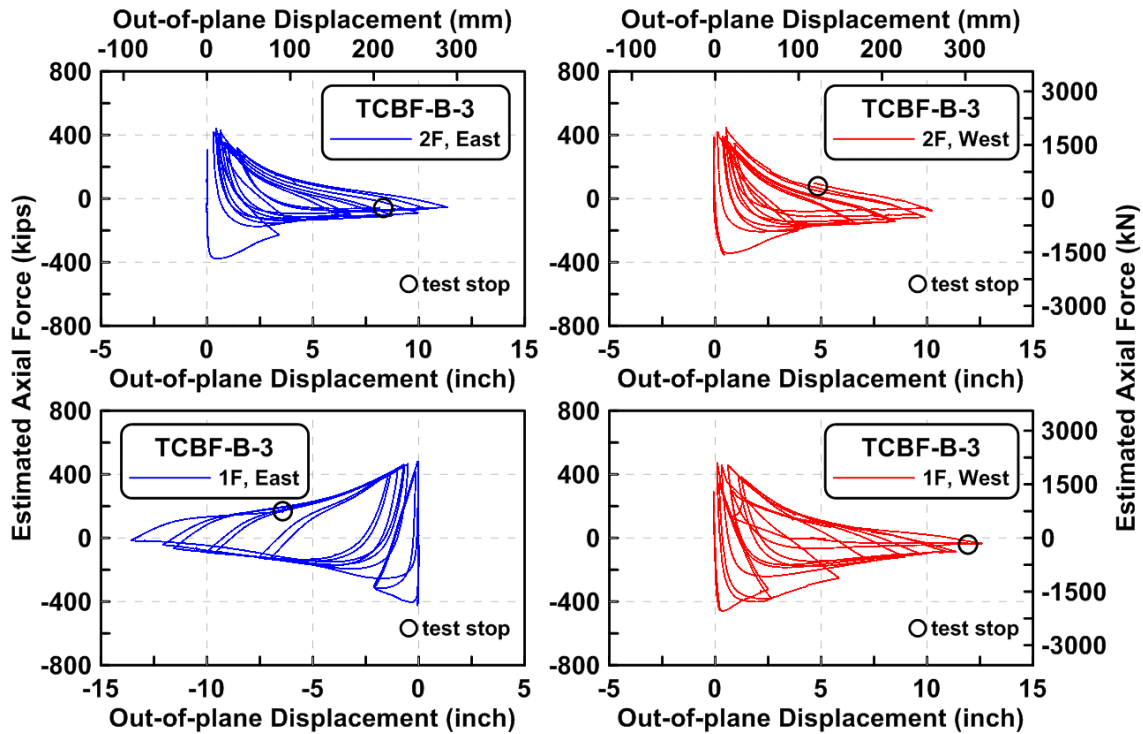


Figure 4.265 Estimated brace axial forces versus measured brace out-of-plane displacements at the brace center point of each WF brace of TCBF-B-3 specimen

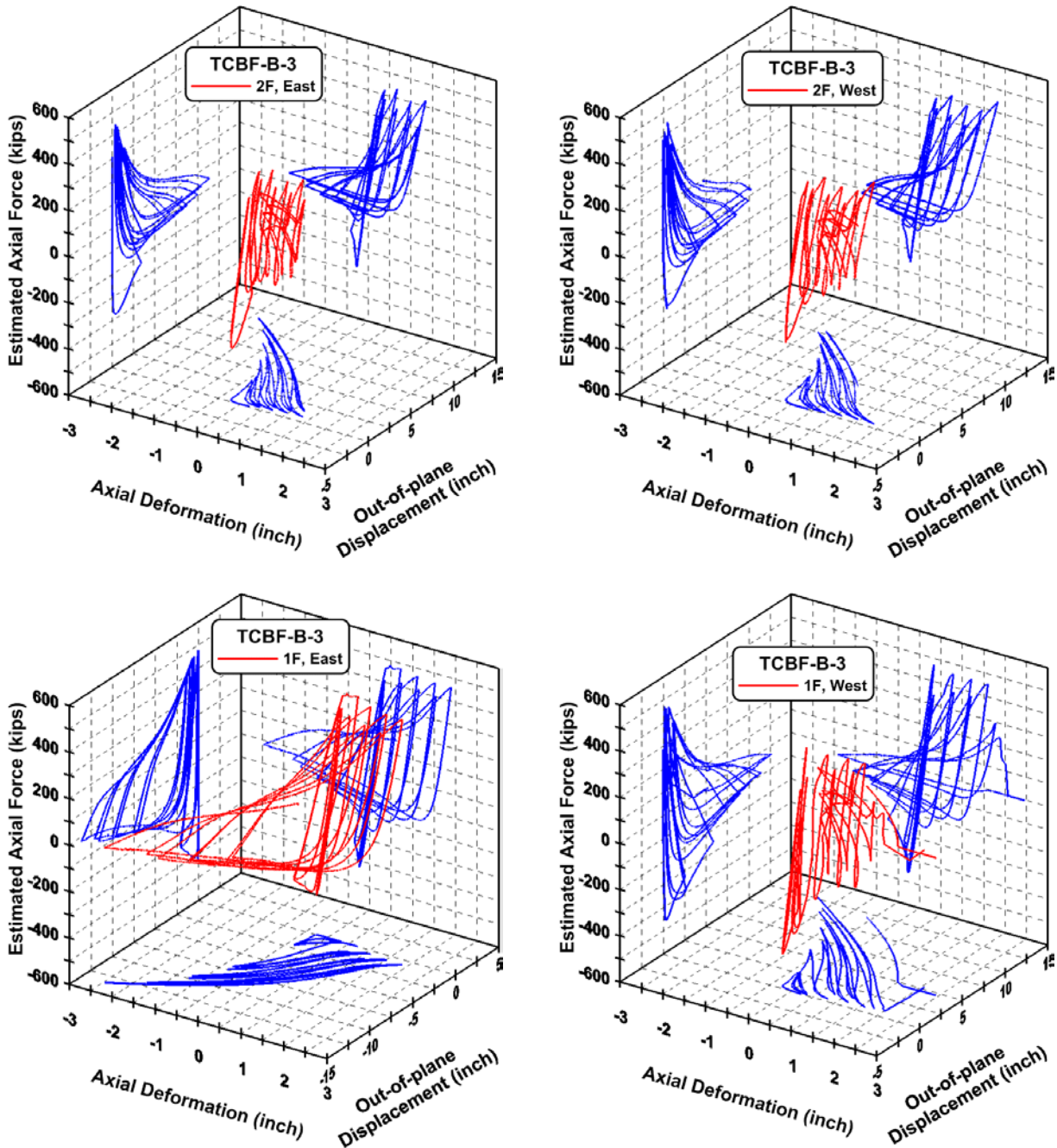


Figure 4.266 Estimated brace axial force, brace axial deformation and measured brace out-of-plane displacement relationships of TCBF-B-3 specimen

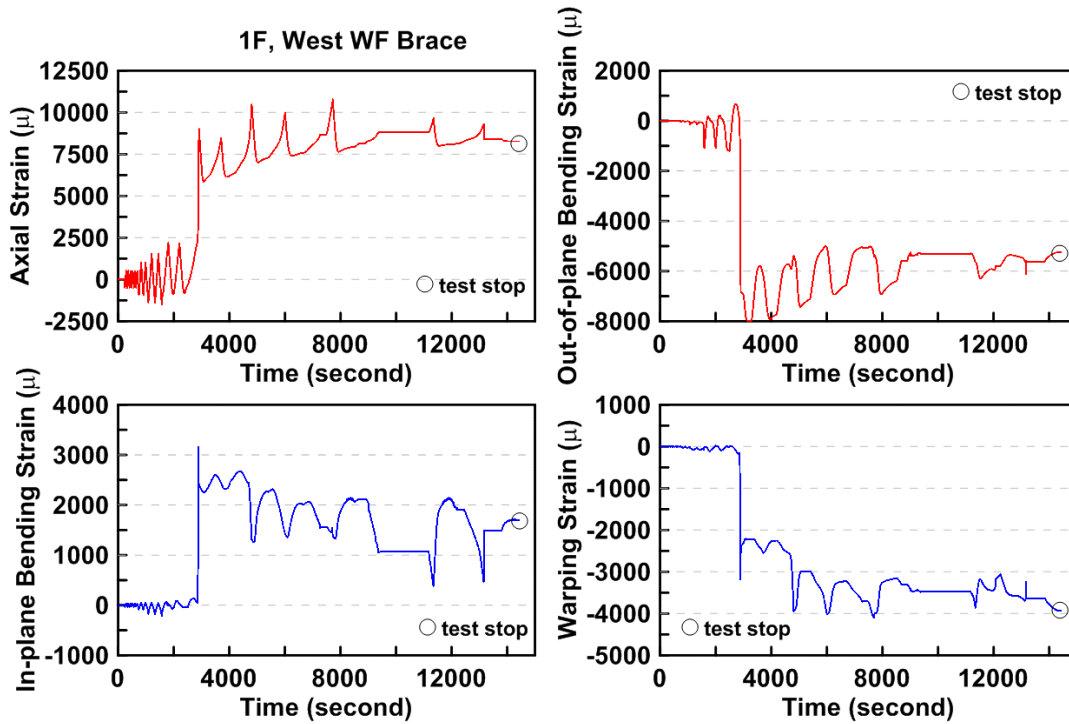


Figure 4.267 Time history of the decomposed strain components of eastern side wide flange brace in the first story of TCBF-B-3 specimen

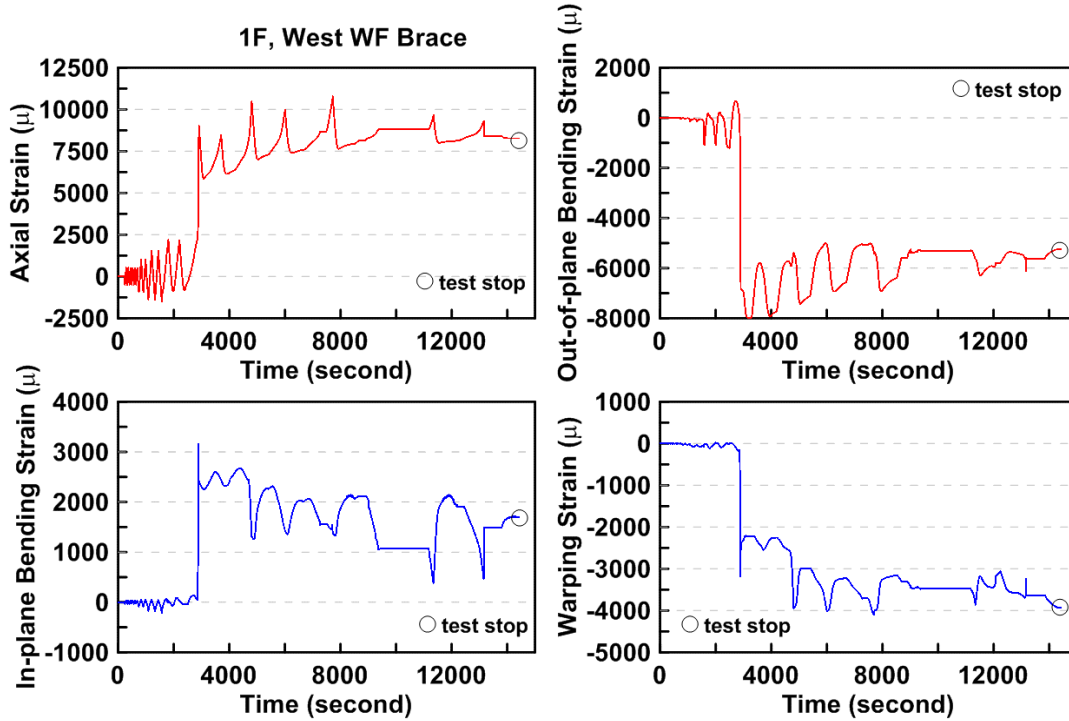


Figure 4.268 Time history of the decomposed strain components of western side wide flange brace in the first story of TCBF-B-3 specimen

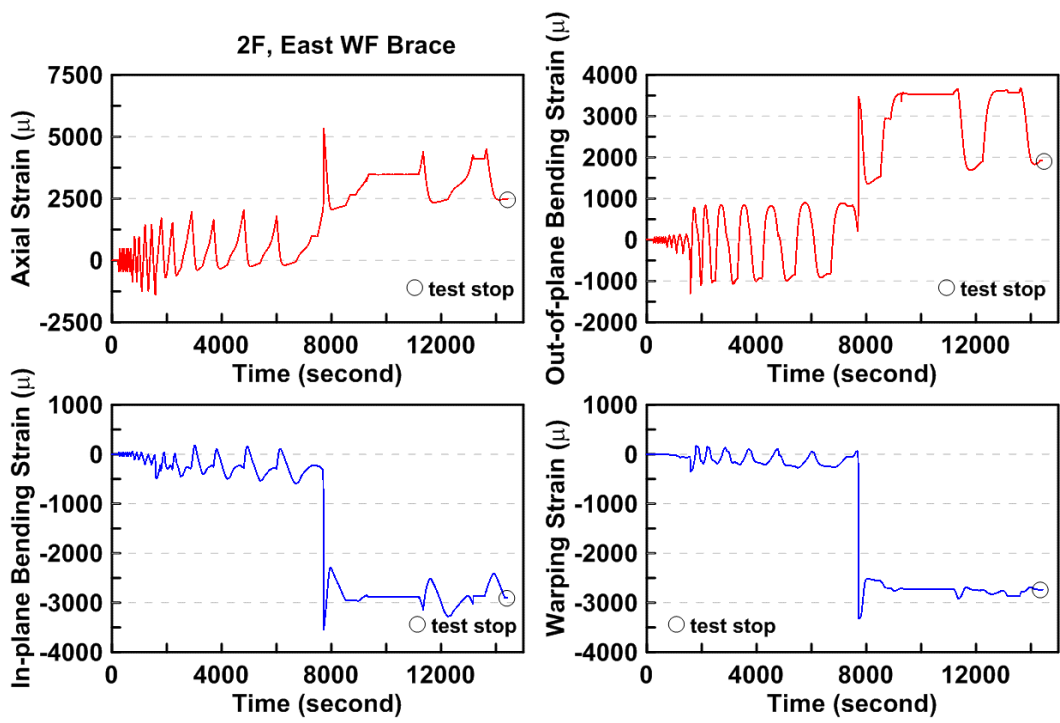


Figure 4.269 Time history of the decomposed strain components of eastern side wide flange brace in the second story of TCBF-B-3 specimen

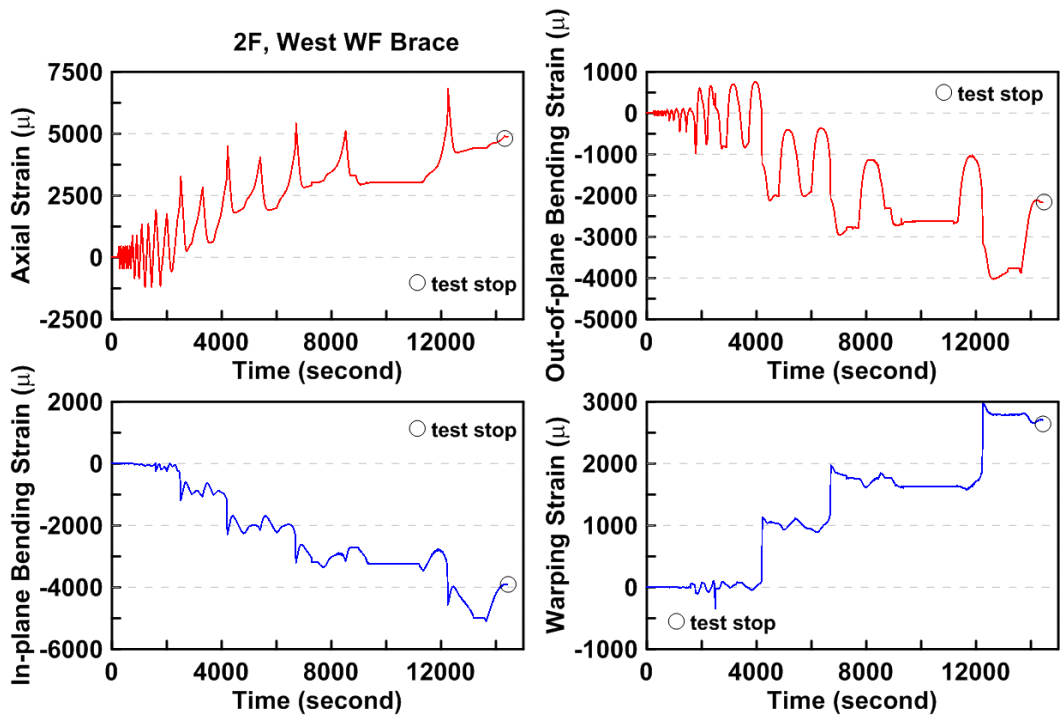


Figure 4.270 Time history of the decomposed strain components of western side wide flange brace in the second story of TCBF-B-3 specimen



#### 4.2.3.1.5 Panel Zone Response

Estimated panel zone shear stress versus measured panel zone shear strain relationship for four locations are plotted in Fig. 4.271. The time history of derived rosette-type strain gauge readings in the panel zone area at each story are shown from Figs. 4.272 to 4.275. Normalized maximum and minimum principal stress relationships along with different yield criteria for the panel zone regions are plotted in Figs. 4.276 to 4.279.

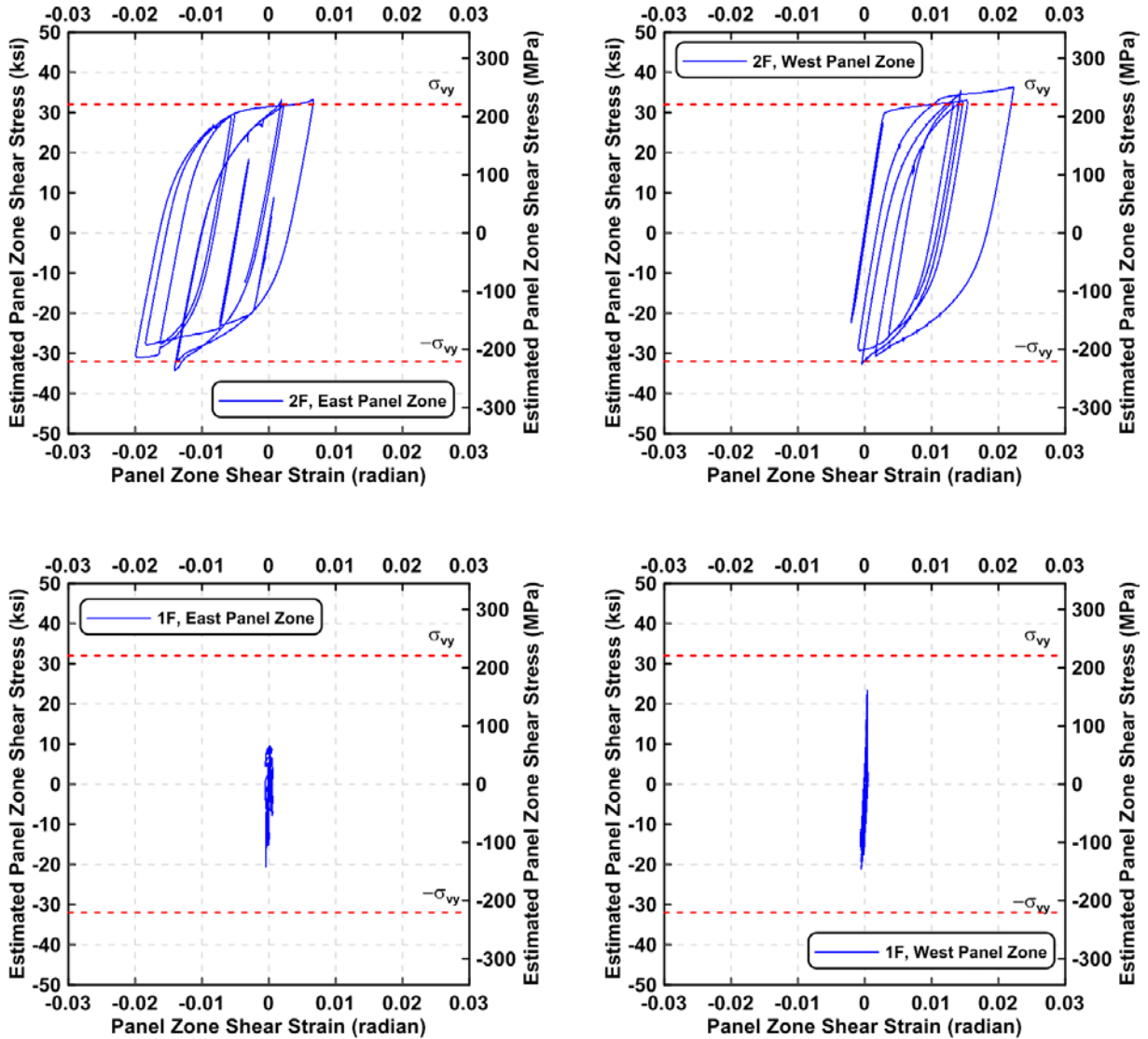


Figure 4.271 Estimated panel zone shear stress vs. shear strain relationships of TCBF-B-3

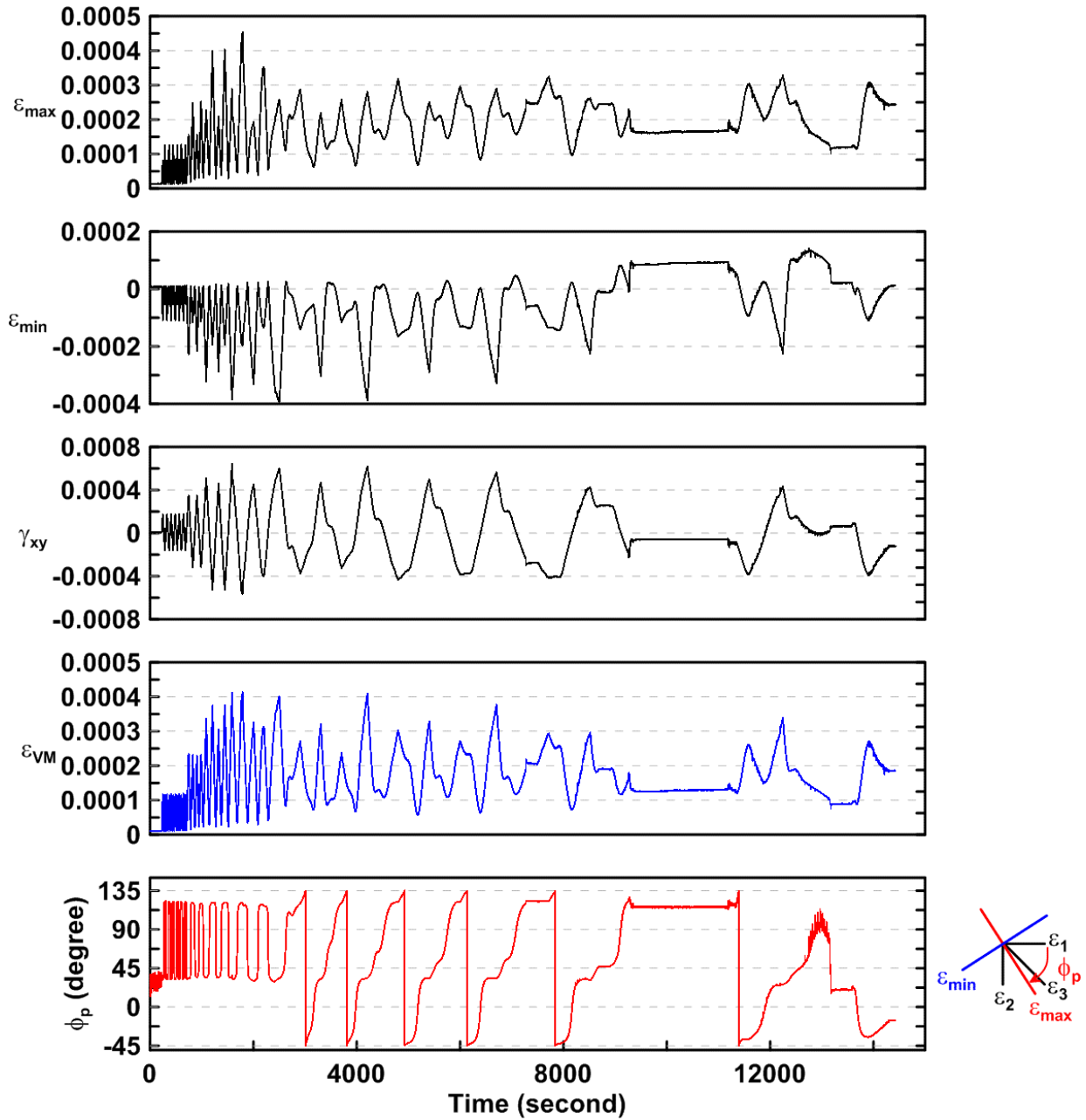


Figure 4.272 Time history of rosette type strain gauge readings in the lower panel zone of TCBF-B-3 specimen (location: R2)

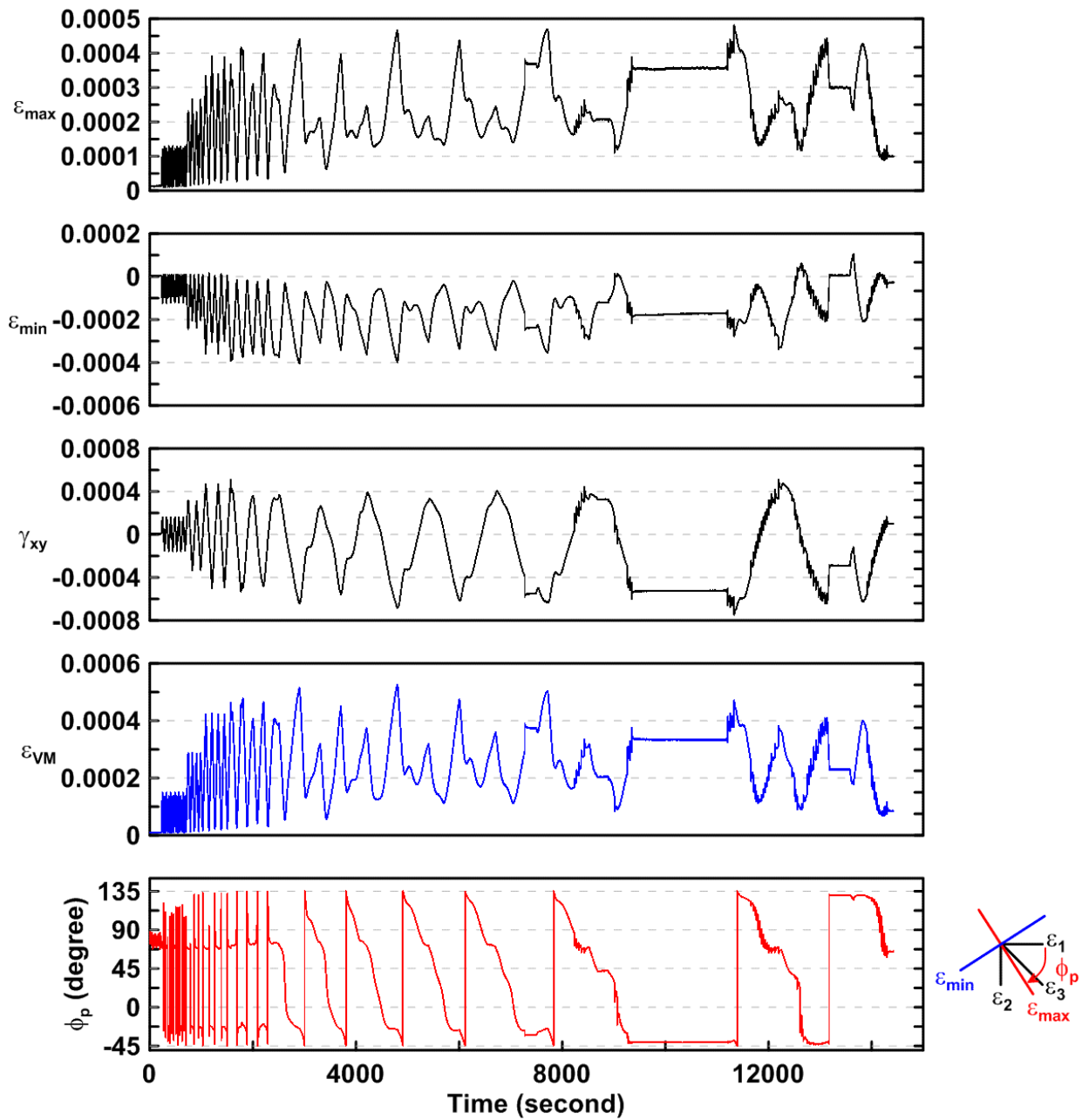


Figure 4.273 Time history of rosette type strain gauge readings in the lower panel zone of TCBF-B-3 specimen (location: R6)

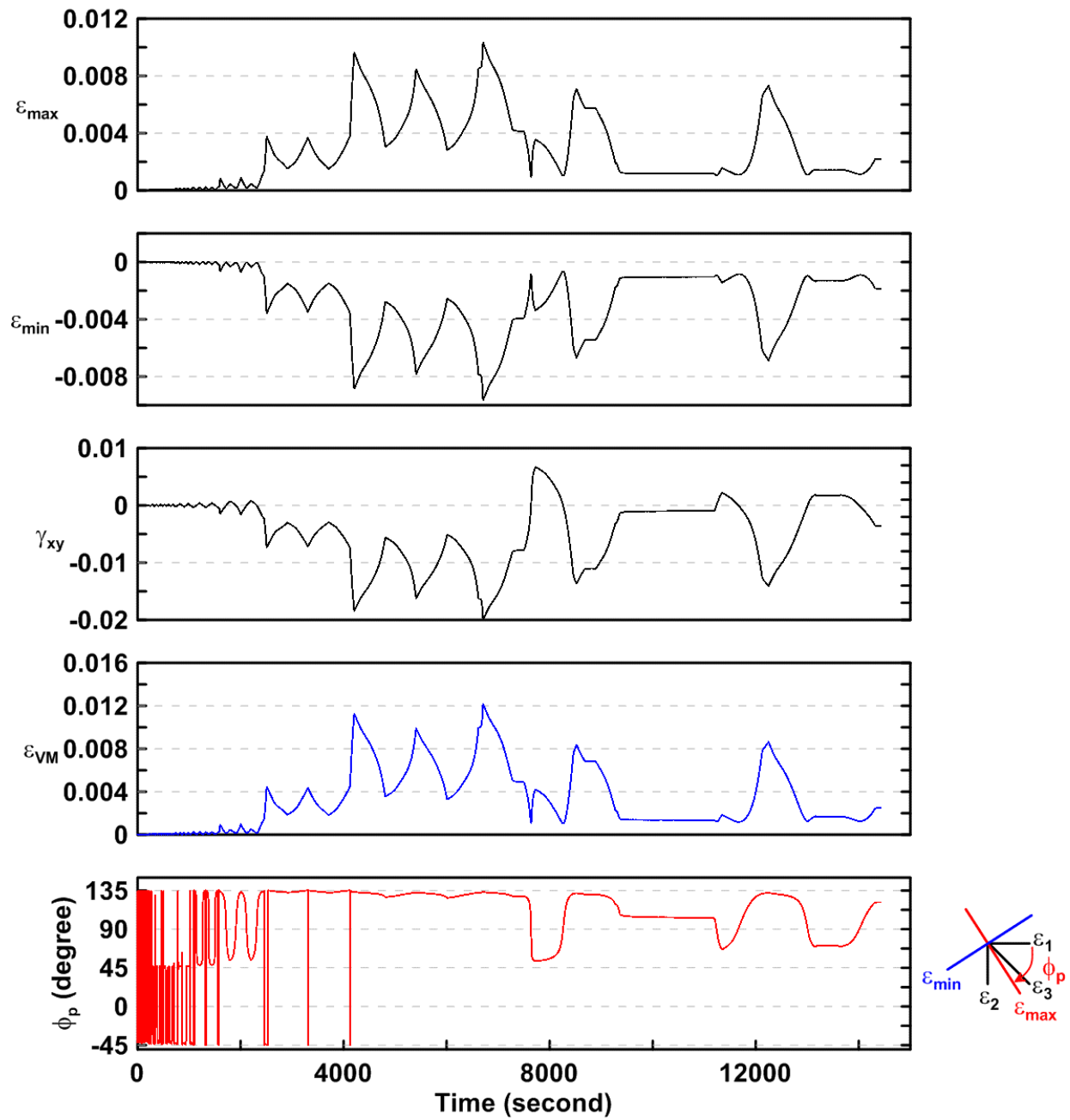


Figure 4.274 Time history of rosette type strain gauge readings in the roof panel zone of TCBF-B-3 specimen (location: R4)

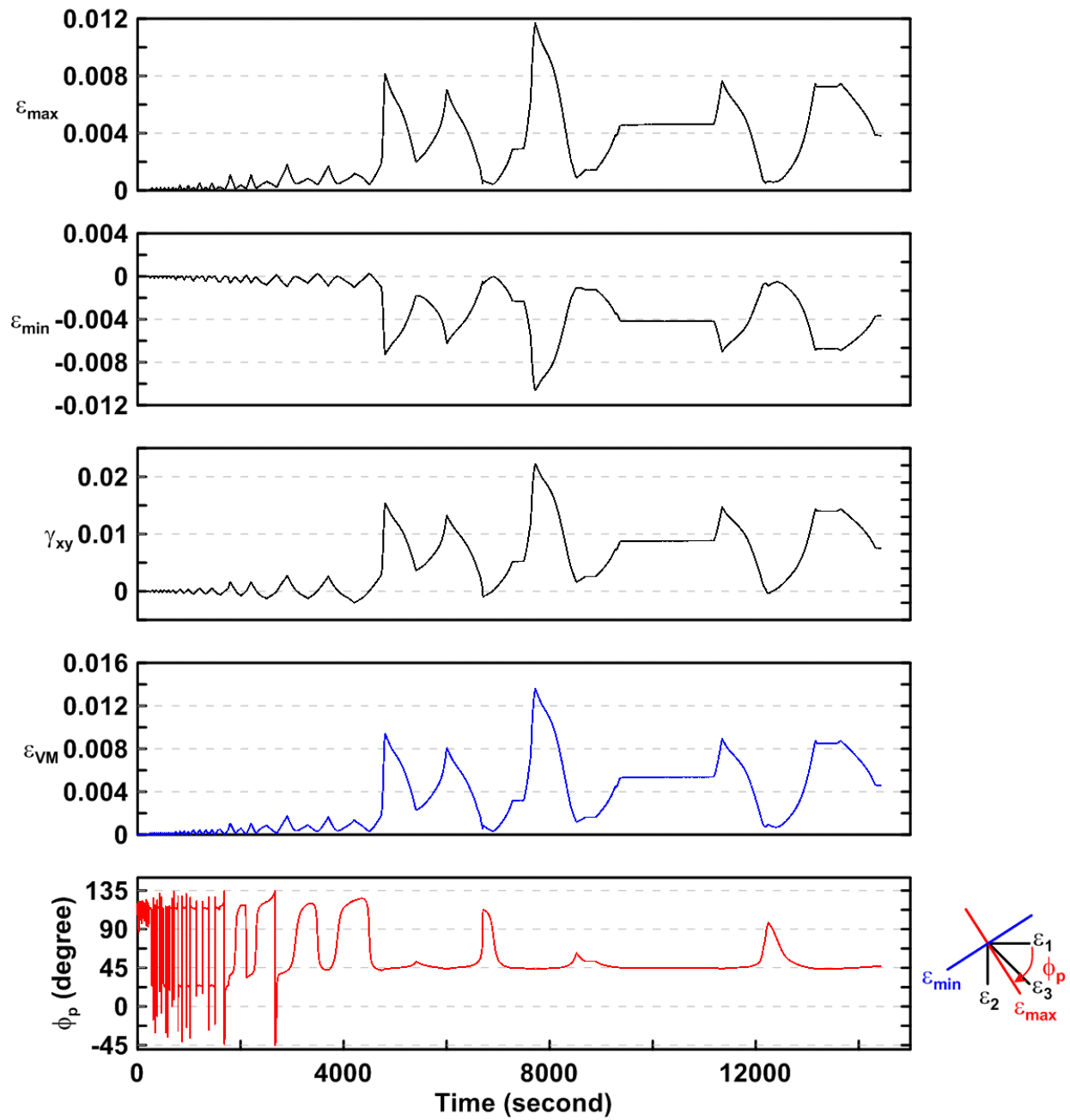


Figure 4.275 Time history of rosette type strain gauge readings in the roof panel zone of TCBF-B-3 specimen (location: R8)

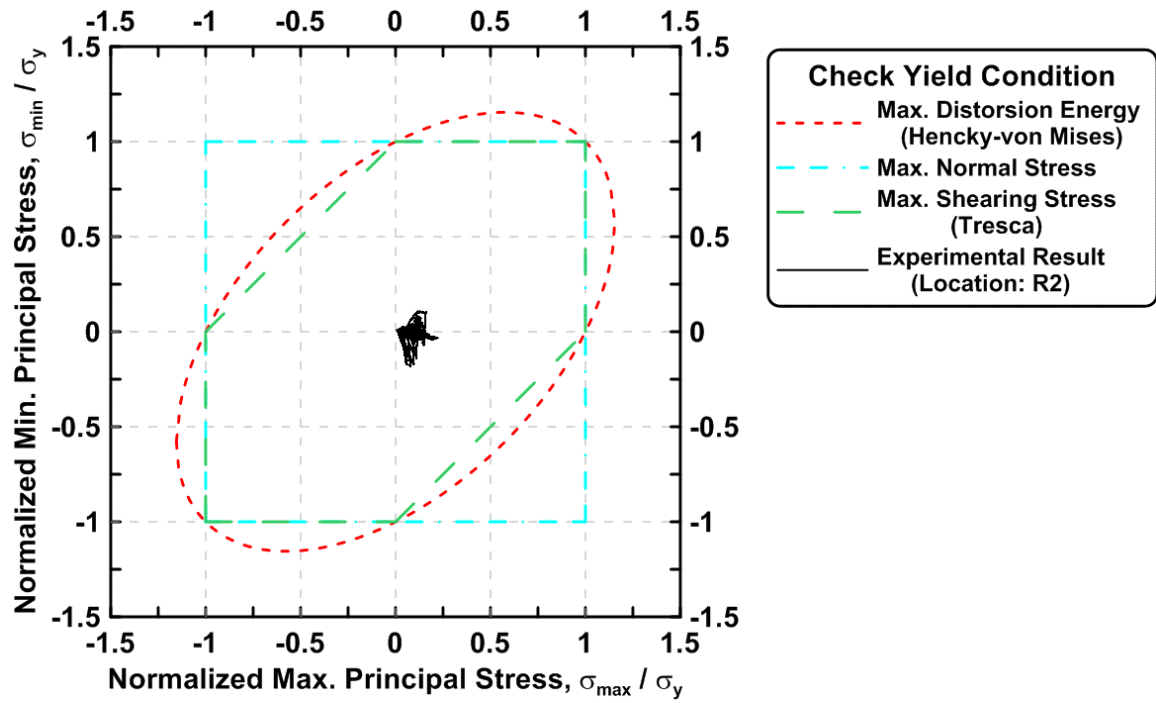


Figure 4.276 Normalized maximum principal stress vs. normalized minimum principal stress in the lower panel zone of TCBF-B-3 specimen (location: R2)

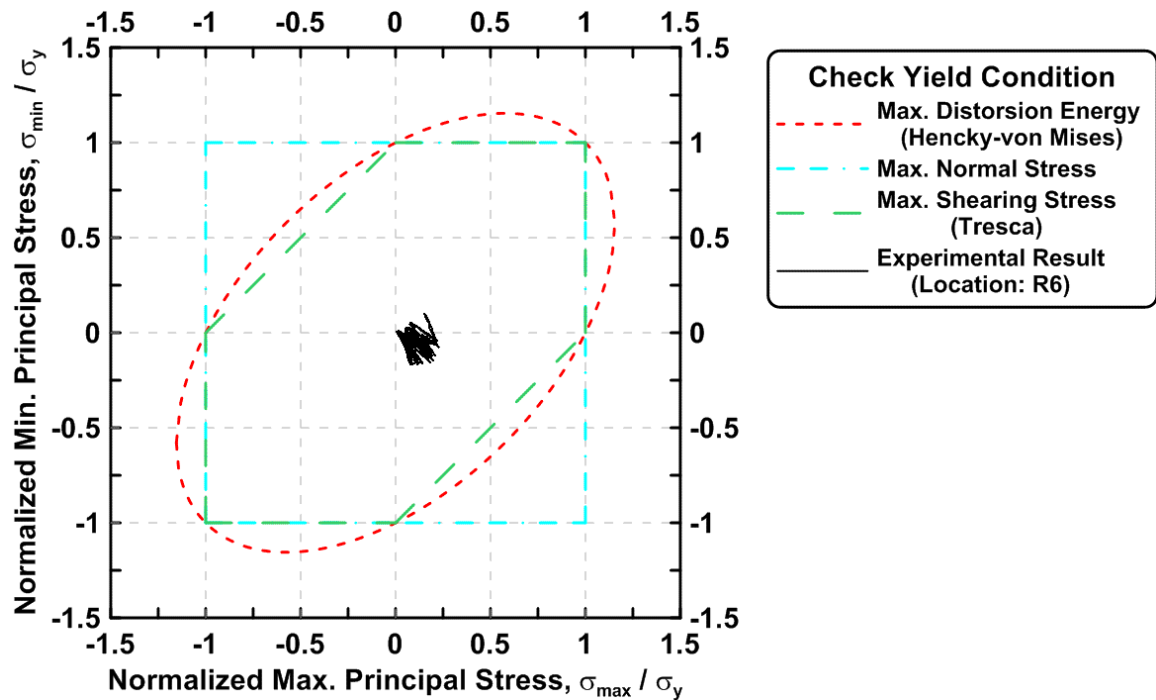


Figure 4.277 Normalized maximum principal stress vs. normalized minimum principal stress in the lower panel zone of TCBF-B-3 specimen (location: R6)

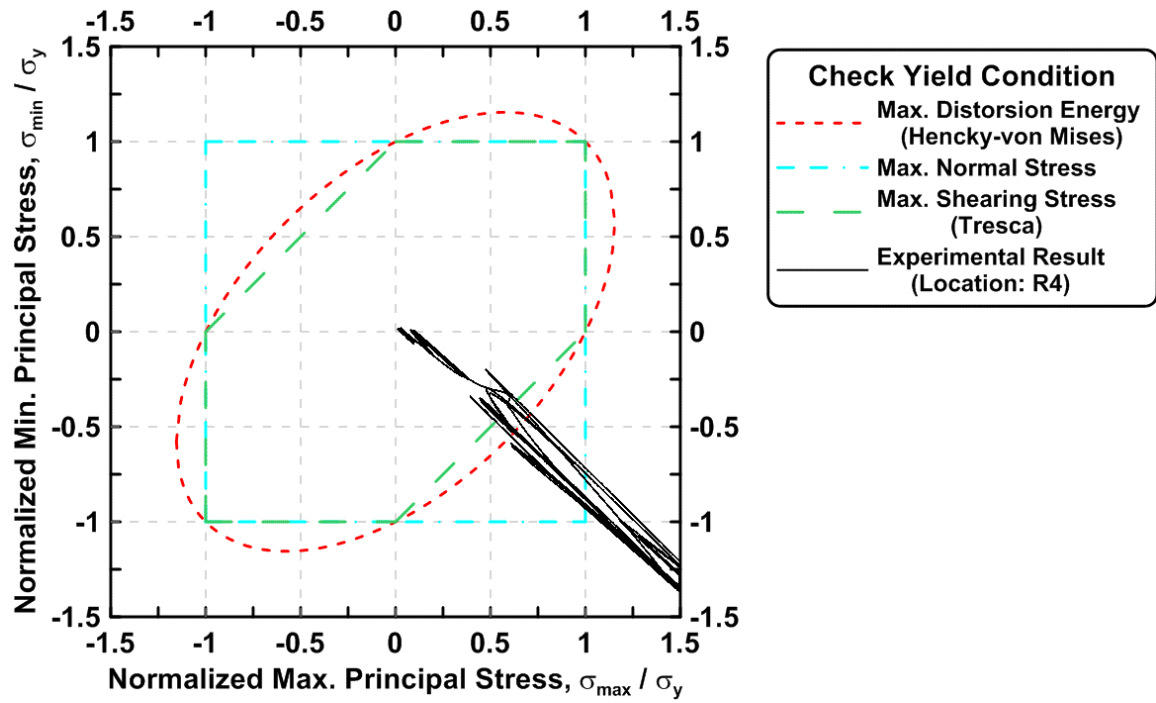


Figure 4.278 Normalized maximum principal stress vs. normalized minimum principal stress in the roof panel zone of TCBF-B-3 specimen (location: R4)

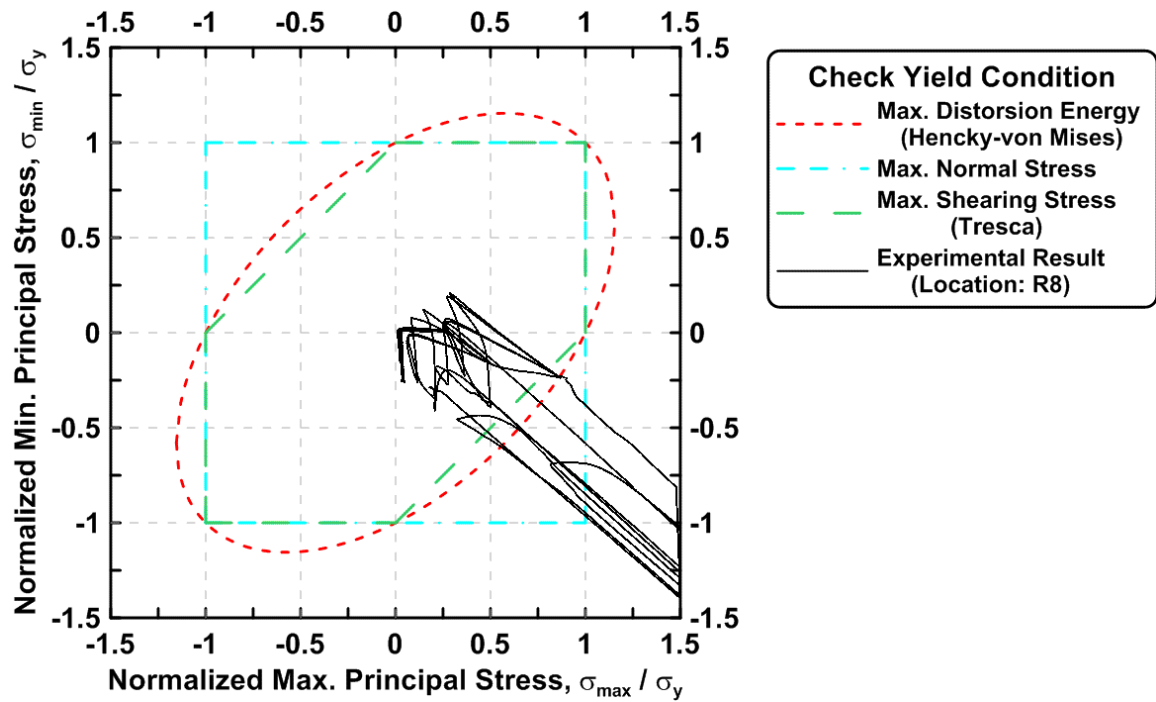


Figure 4.279 Normalized maximum principal stress vs. normalized minimum principal stress in the roof panel zone of TCBF-B-3 specimen (location: R8)

#### 4.2.3.1.6 Gusset Plate Response

The time history of derived rosette-type strain gauge readings in the 3/4-in.-thick one-piece gusset plate is shown in Figs. 4.280 to 4.291. Normalized maximum and minimum principal stress relationships along with different yield criteria for the rosettes on the gusset plate are plotted in Figs. 4.292 to 4.303. The averaged axial strain and bending strain time history in the tapered gusset plate at eastern side of the specimen are shown in Figs. 4.304 and 4.305, respectively.

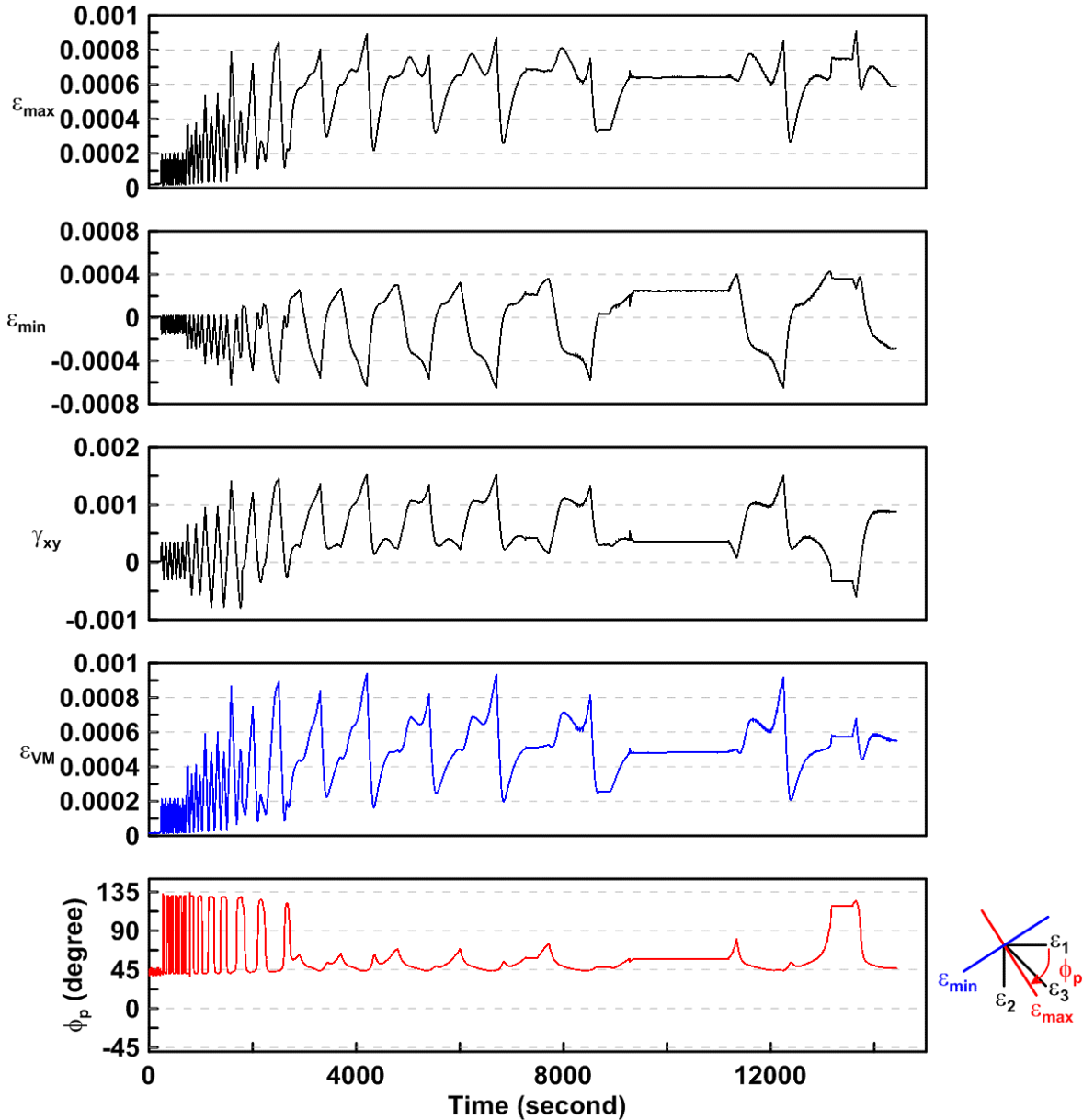


Figure 4.280 Time history of rosette type strain gauge readings in the one-piece gusset plate of TCBF-B-3 specimen (location: R9)



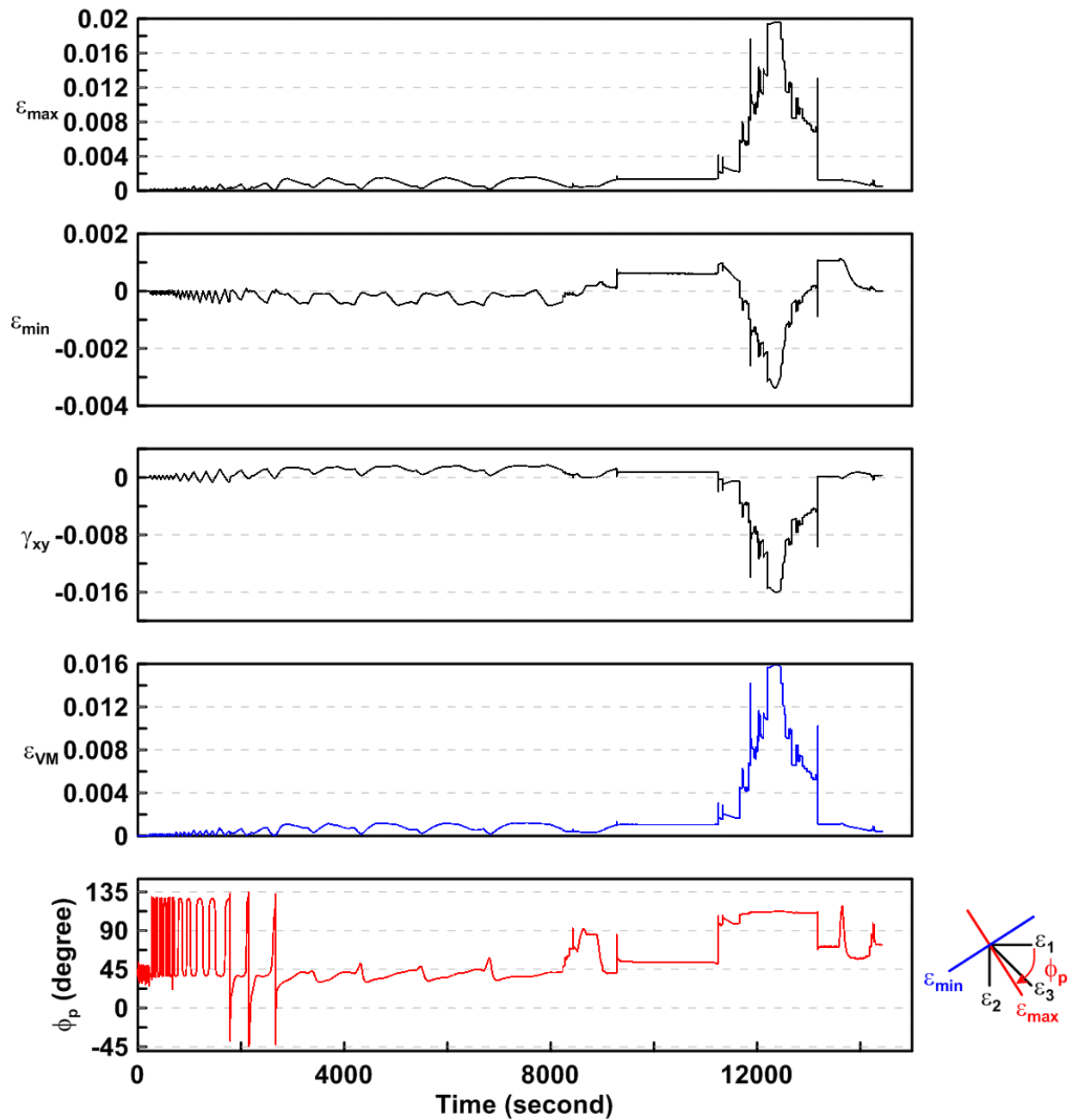


Figure 4.281 Time history of rosette type strain gauge readings in the one-piece gusset plate of TCBF-B-3 specimen (location: R10)

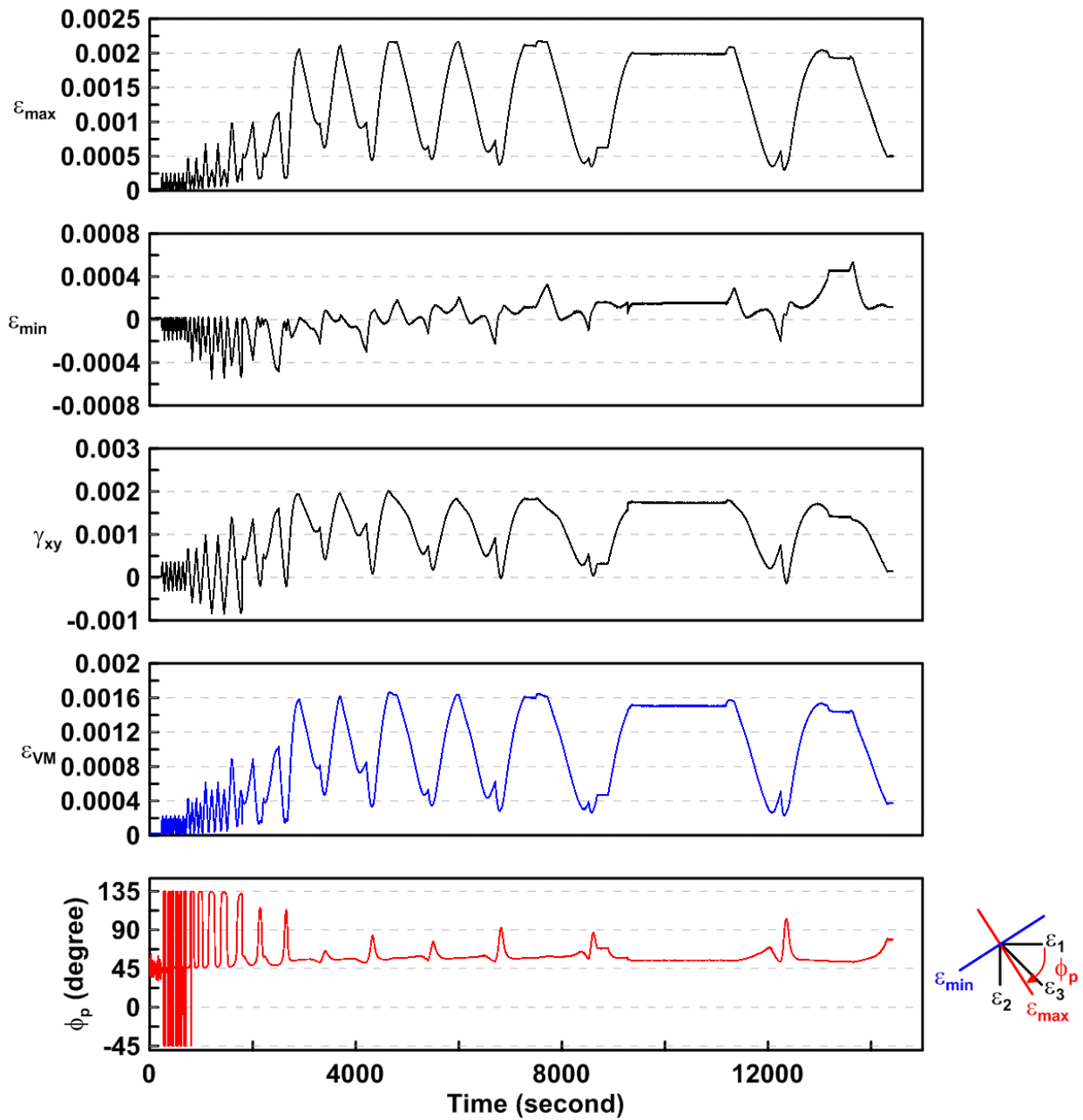


Figure 4.282 Time history of rosette type strain gauge readings in the one-piece gusset plate of TCBF-B-3 specimen (location: R11)

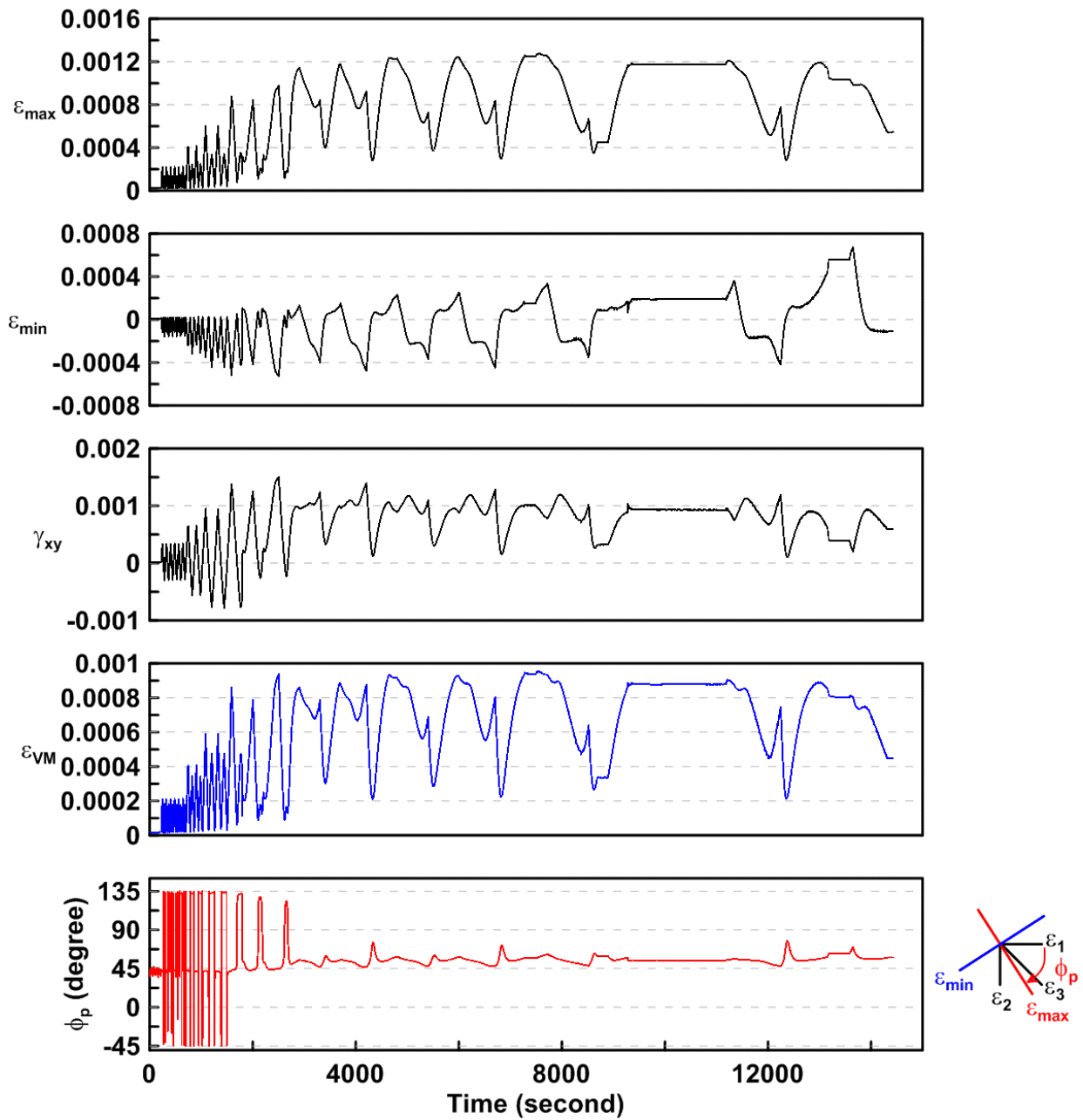


Figure 4.283 Time history of rosette type strain gauge readings in the one-piece gusset plate of TCBF-B-3 specimen (location: R12)

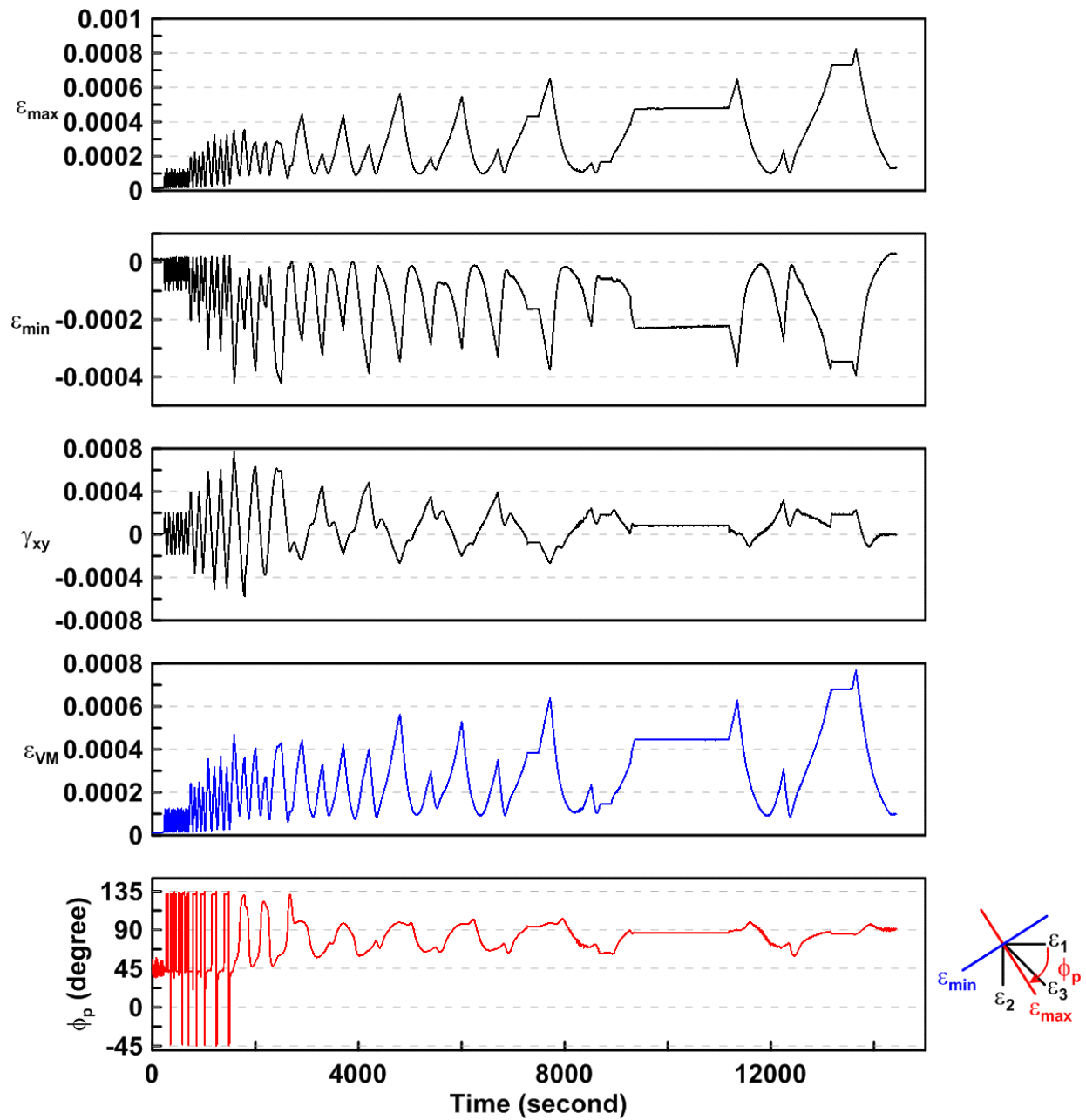


Figure 4.284 Time history of rosette type strain gauge readings in the one-piece gusset plate of TCBF-B-3 specimen (location: R13)

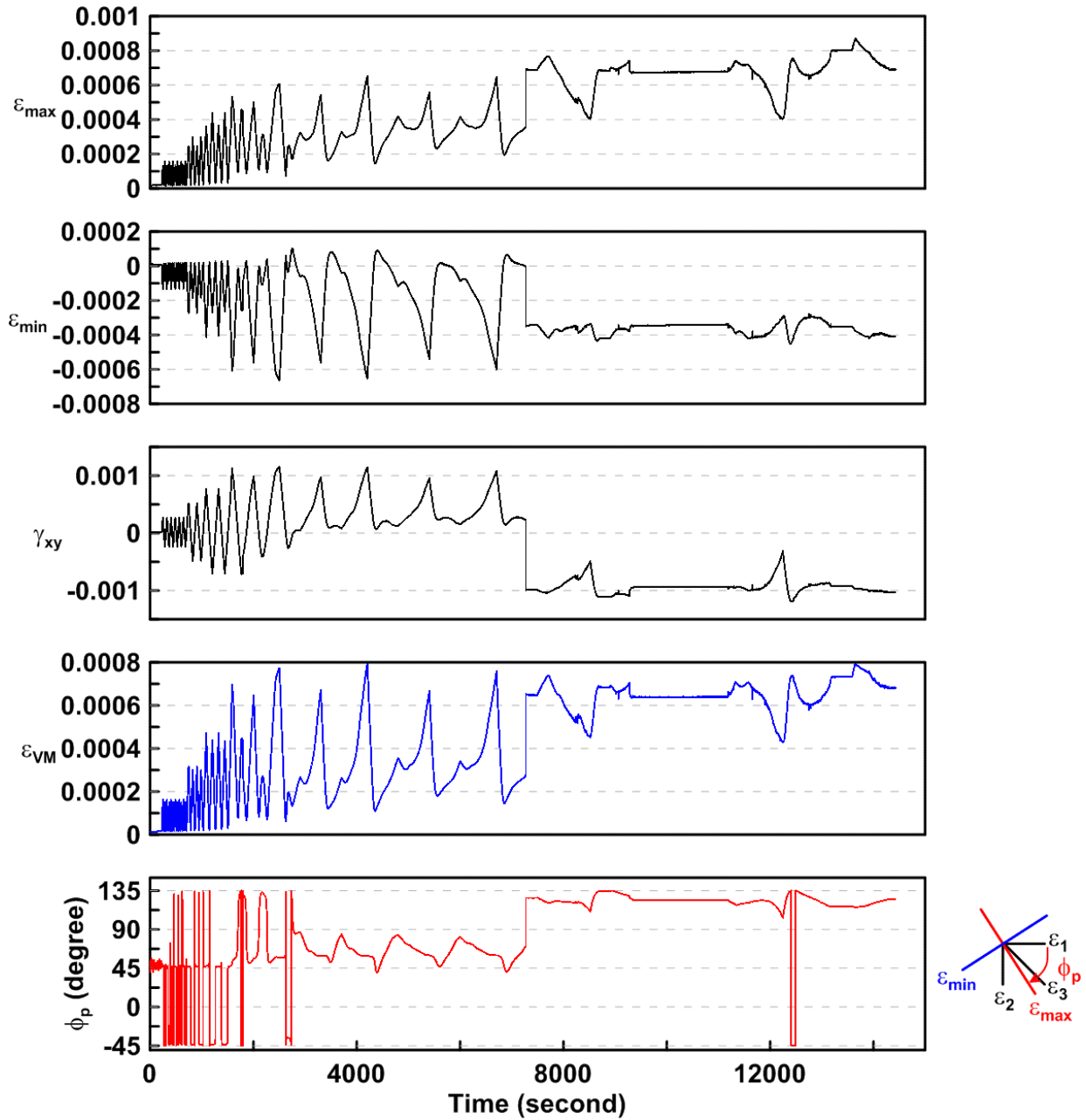


Figure 4.285 Time history of rosette type strain gauge readings in the one-piece gusset plate of TCBF-B-3 specimen (location: R14)

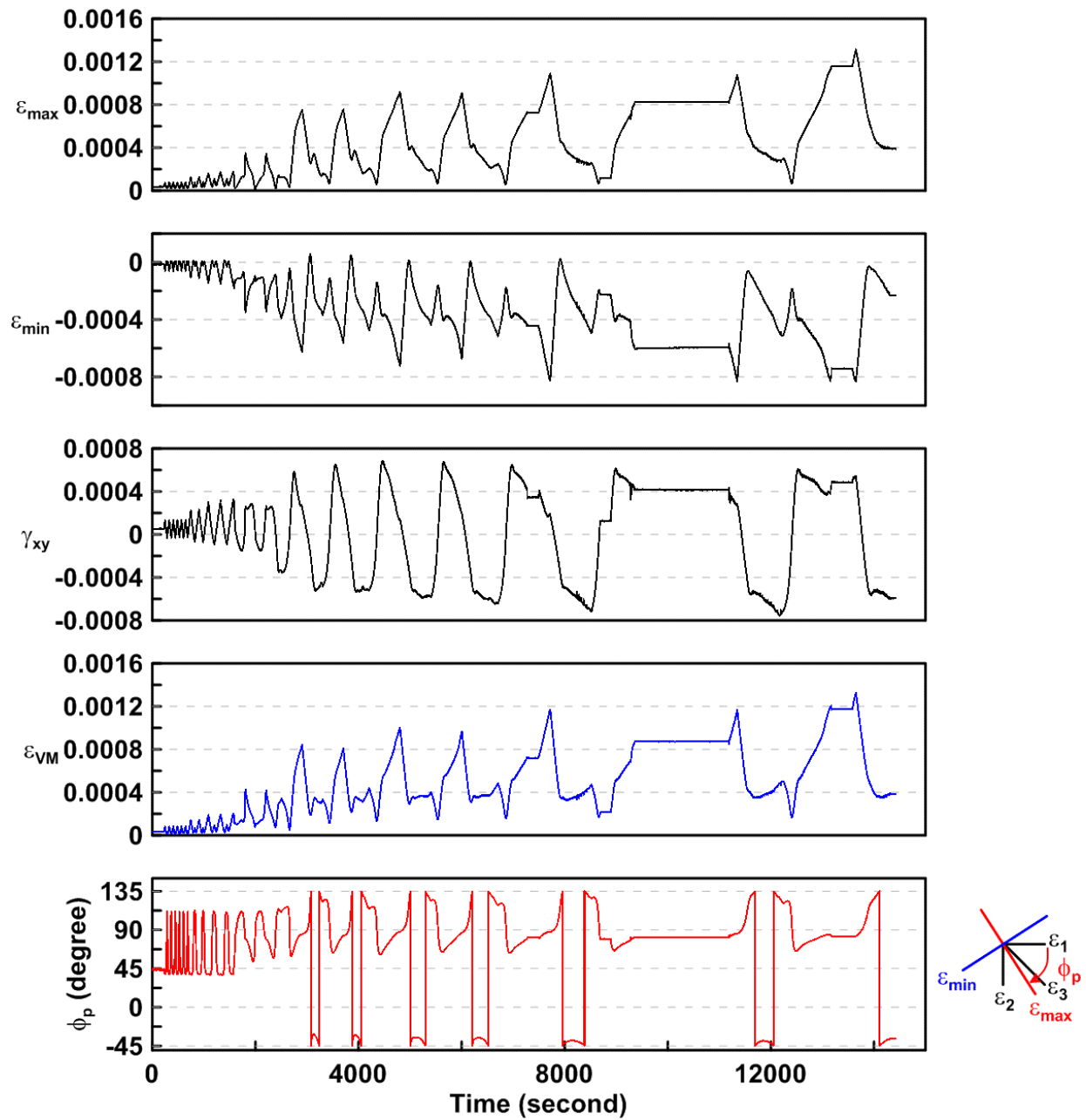


Figure 4.286 Time history of rosette type strain gauge readings in the one-piece gusset plate of TCBF-B-3 specimen (location: R15)

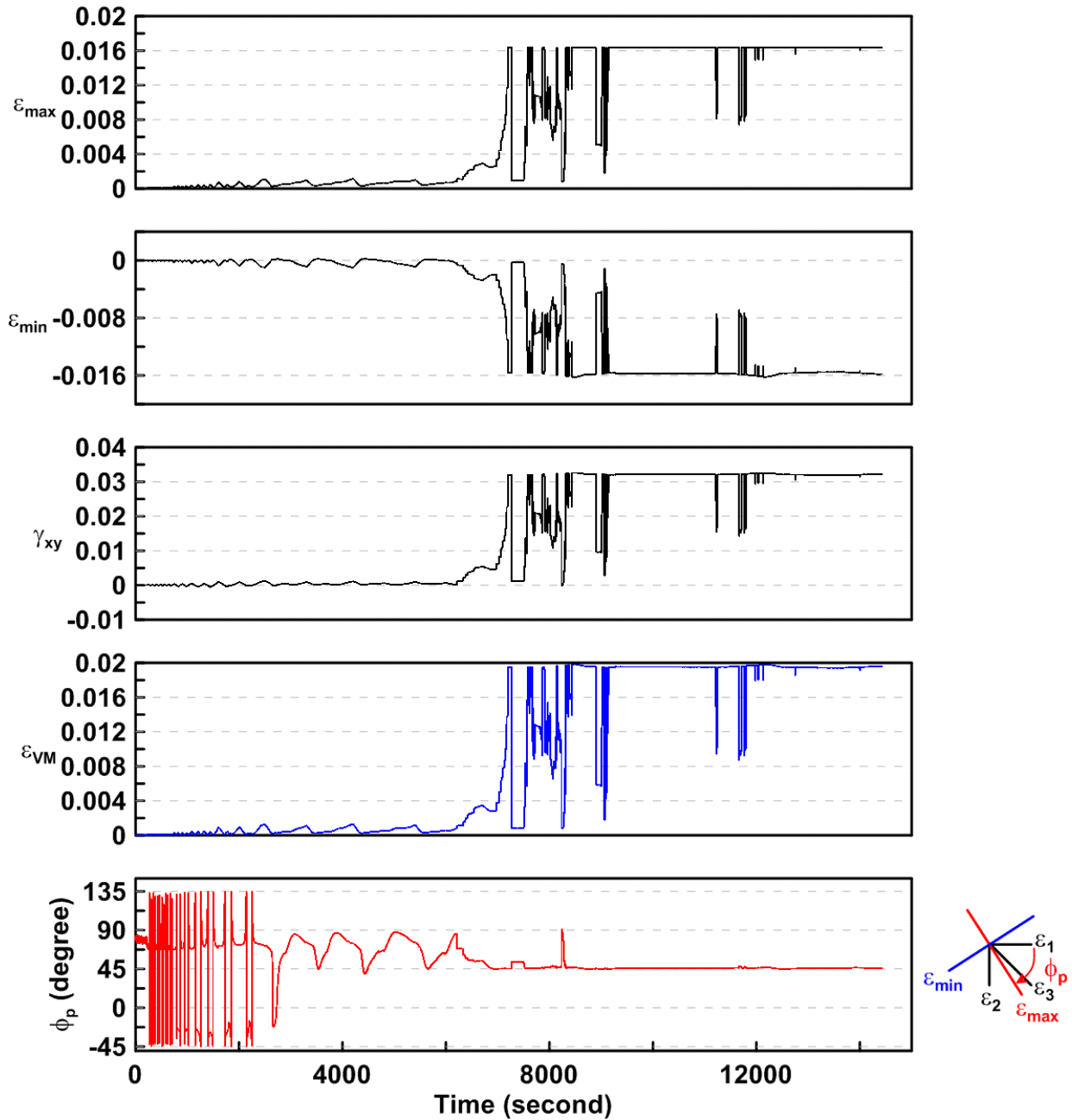


Figure 4.287 Time history of rosette type strain gauge readings in the one-piece gusset plate of TCBF-B-3 specimen (location: R16)

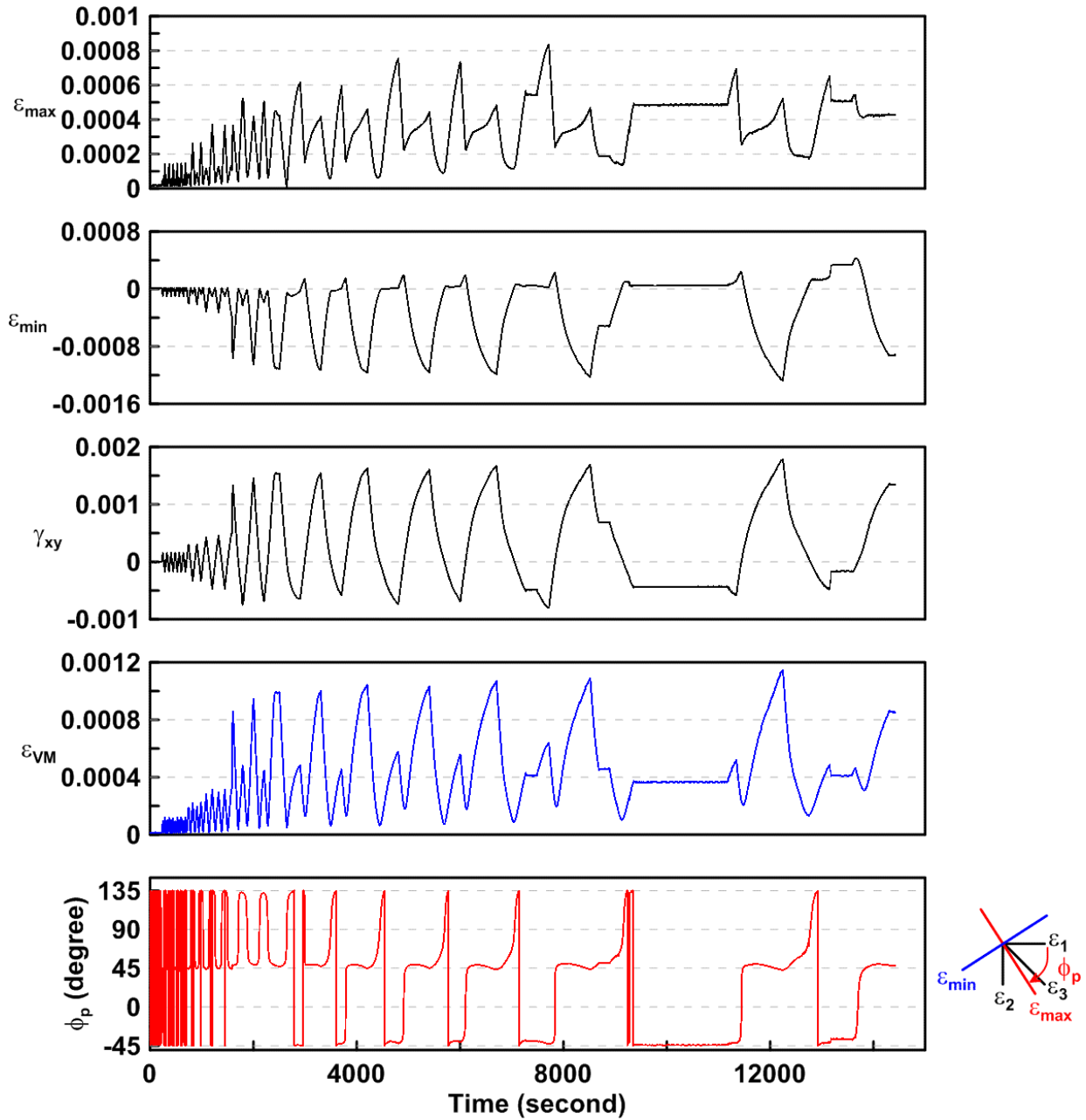


Figure 4.288 Time history of rosette type strain gauge readings in the one-piece gusset plate of TCBF-B-3 specimen (location: R17)



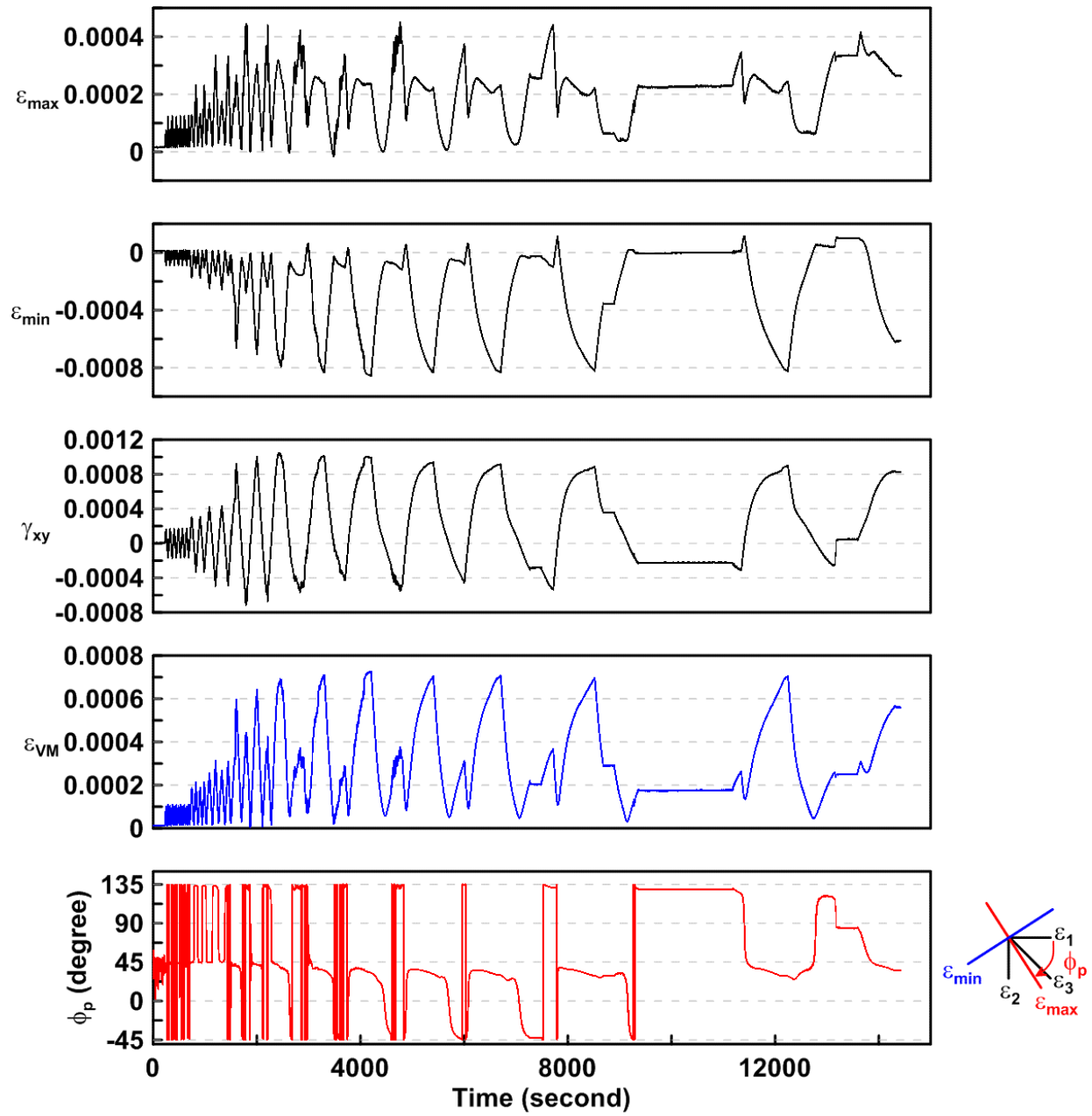


Figure 4.289 Time history of rosette type strain gauge readings in the one-piece gusset plate of TCBF-B-3 specimen (location: R18)

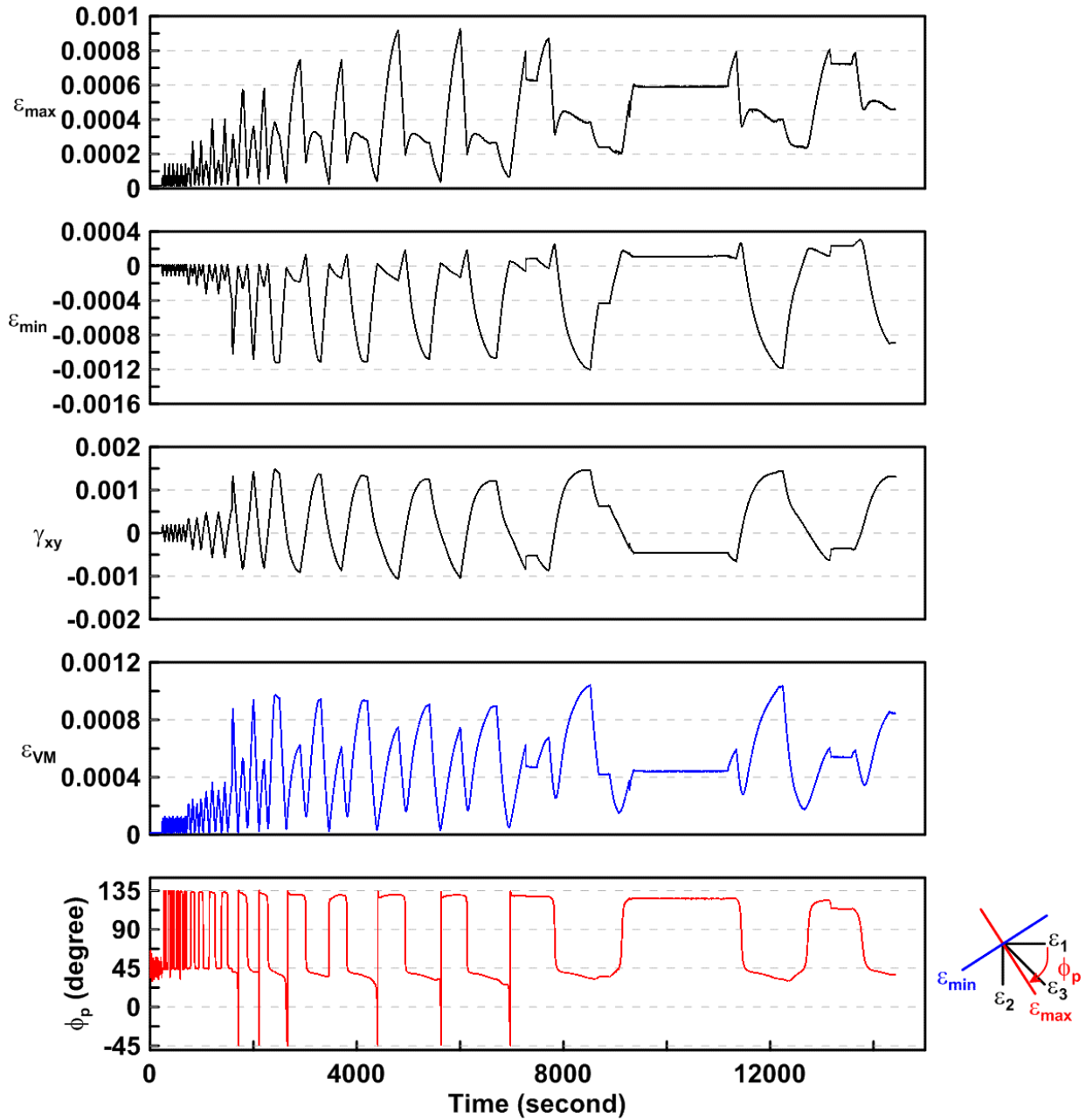


Figure 4.290 Time history of rosette type strain gauge readings in the one-piece gusset plate of TCBF-B-3 specimen (location: R19)

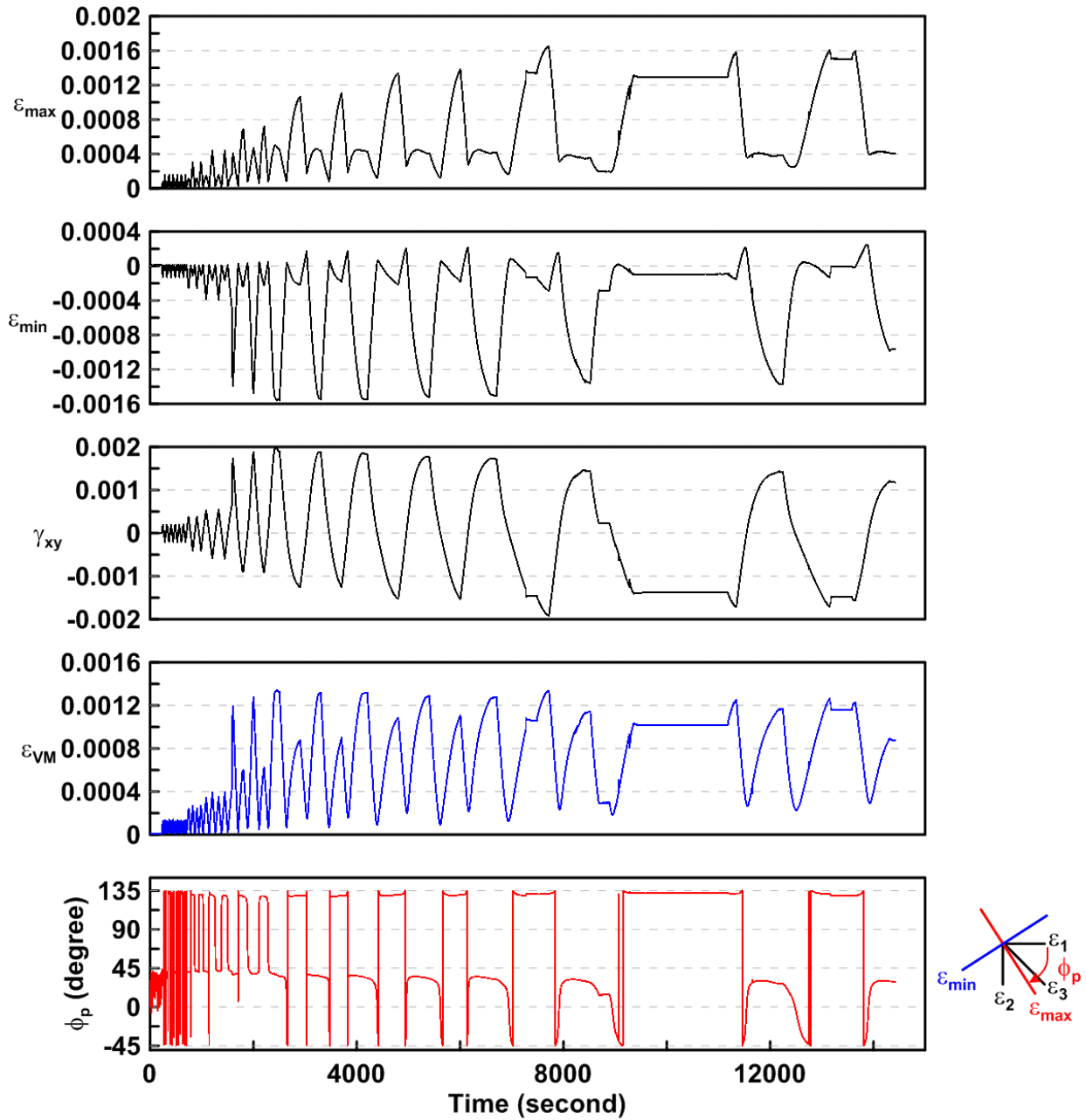


Figure 4.291 Time history of rosette type strain gauge readings in the one-piece gusset plate of TCBF-B-3 specimen (location: R20)

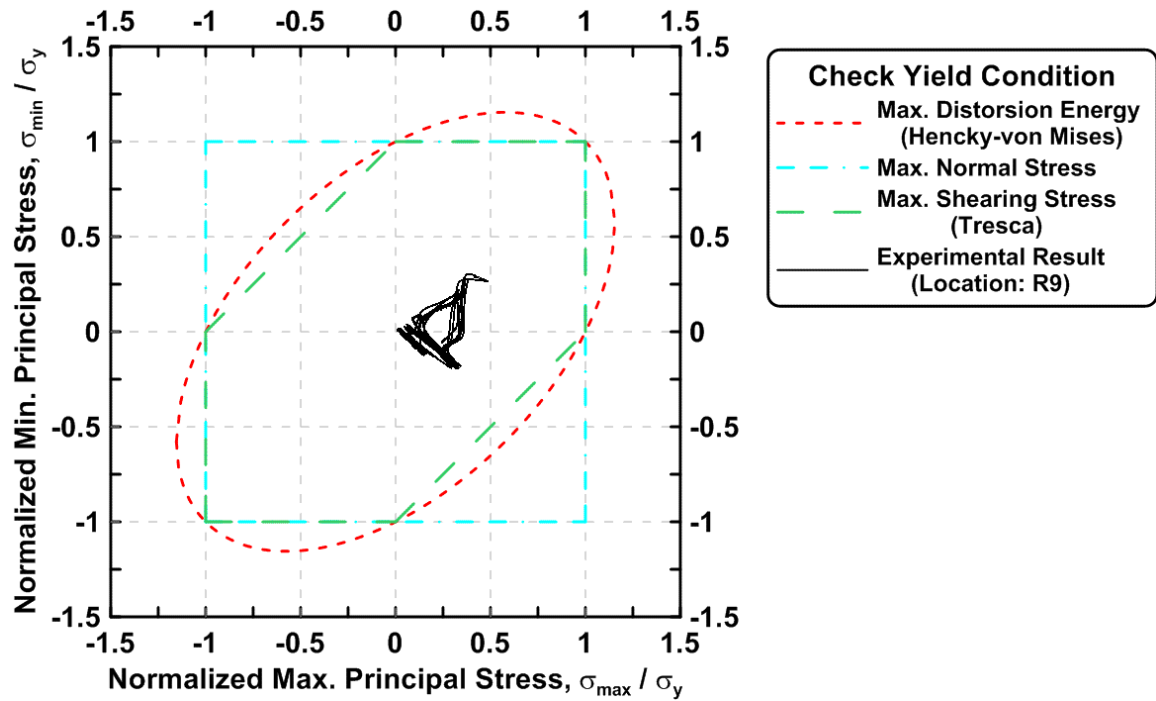


Figure 4.292 Normalized maximum principal stress vs. normalized minimum principal stress in the one-piece gusset plate of TCBF-B-3 specimen (location: R9)

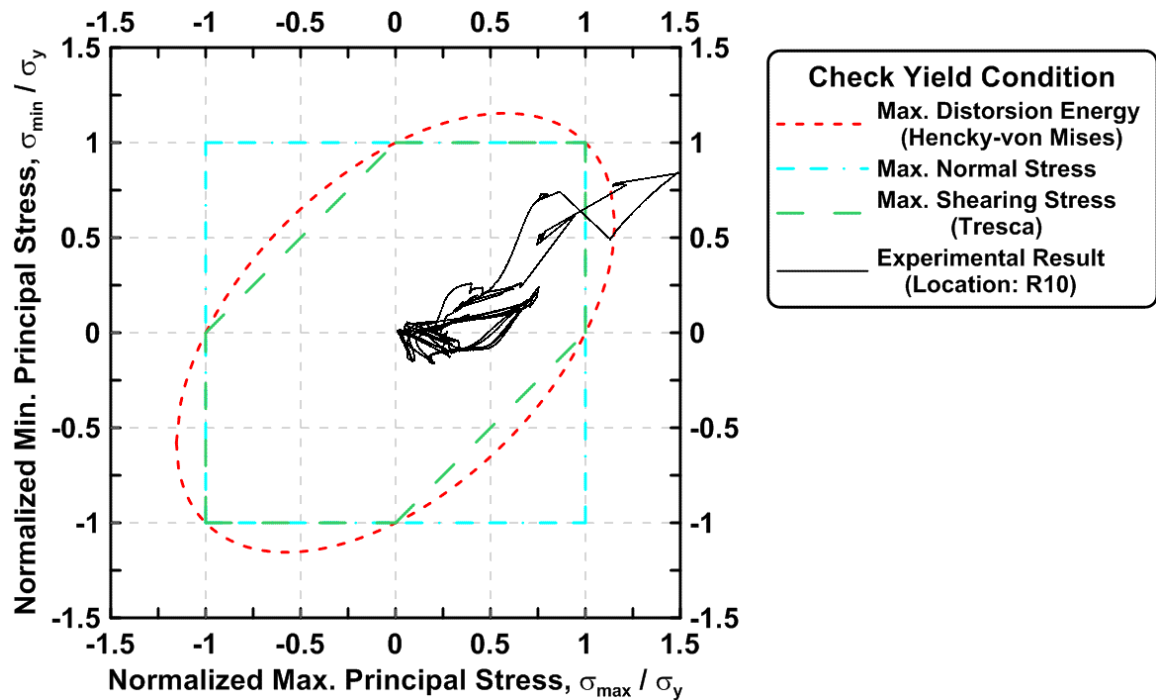


Figure 4.293 Normalized maximum principal stress vs. normalized minimum principal stress in the one-piece gusset plate of TCBF-B-3 specimen (location: R10)

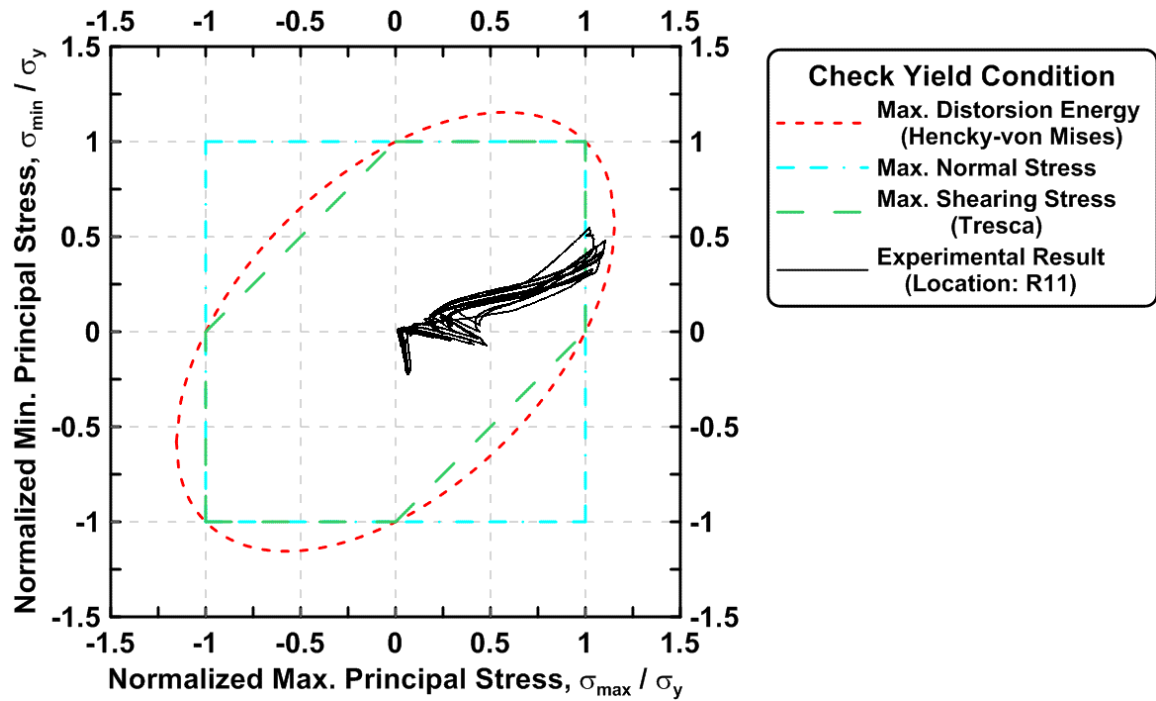


Figure 4.294 Normalized maximum principal stress vs. normalized minimum principal stress in the one-piece gusset plate of TCBF-B-3 specimen (location: R11)

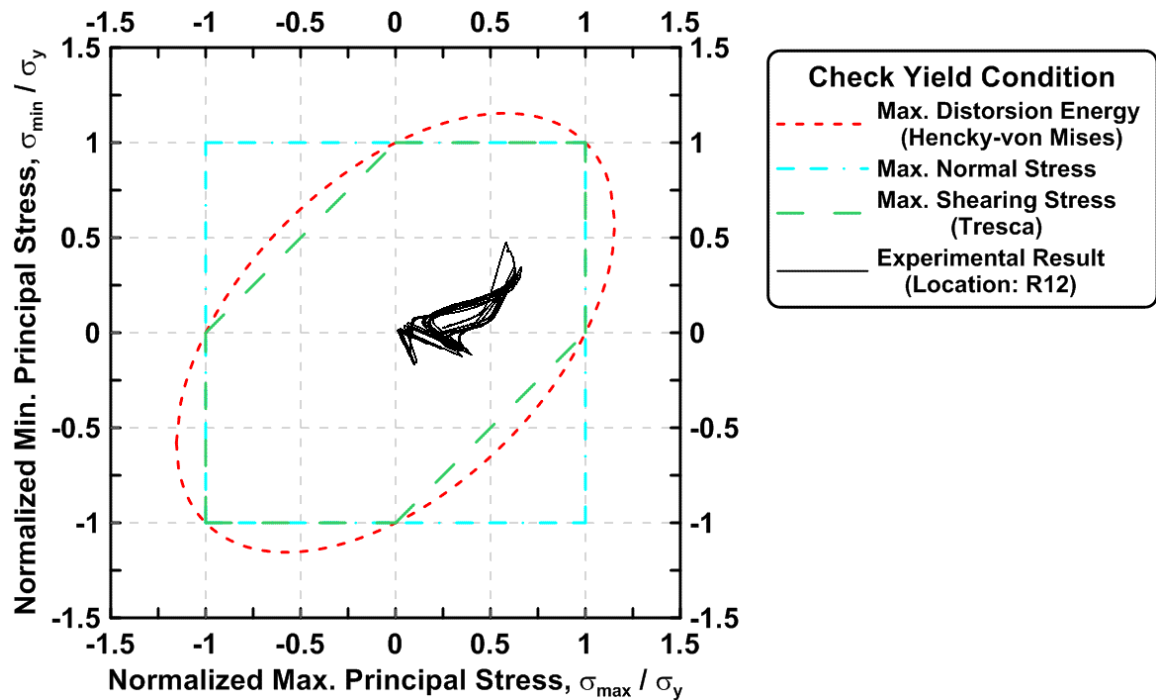


Figure 4.295 Normalized maximum principal stress vs. normalized minimum principal stress in the one-piece gusset plate of TCBF-B-3 specimen (location: R12)

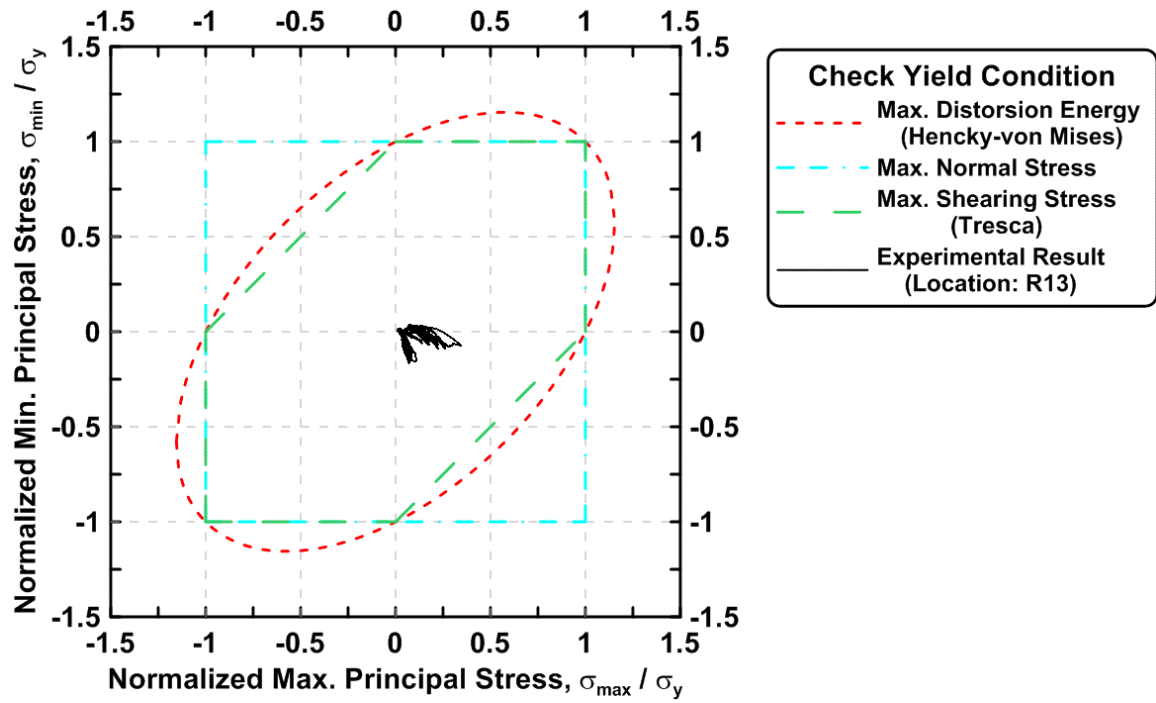


Figure 4.296 Normalized maximum principal stress vs. normalized minimum principal stress in the one-piece gusset plate of TCBF-B-3 specimen (location: R13)

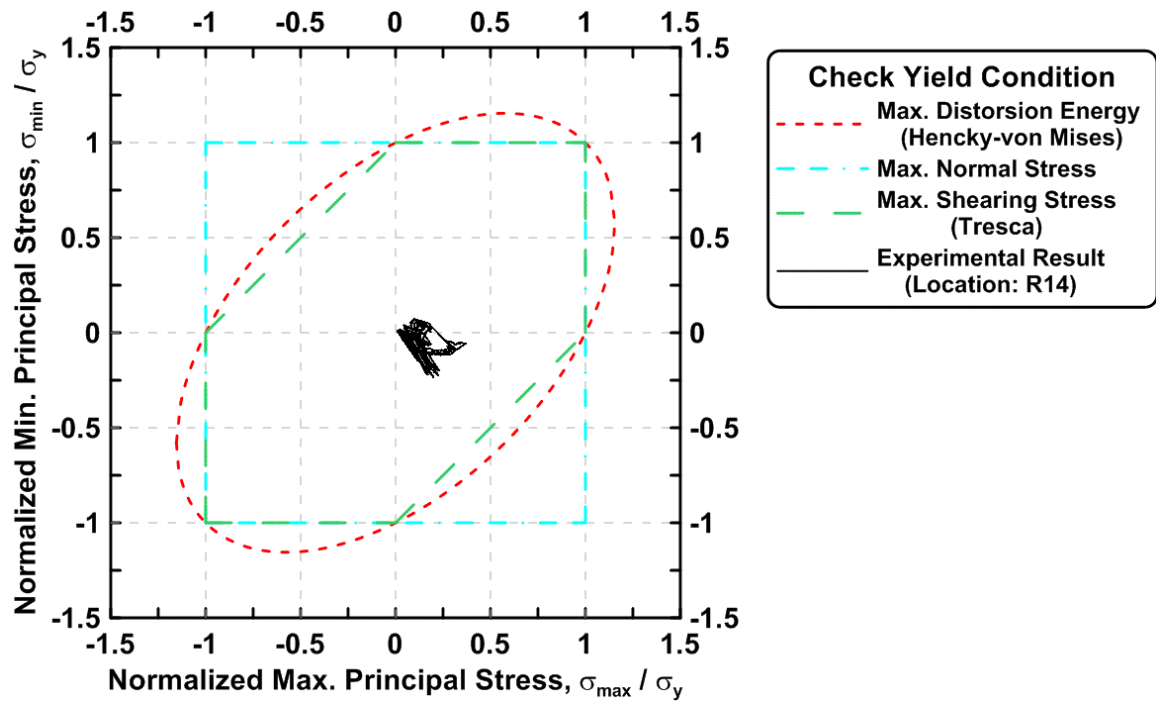


Figure 4.297 Normalized maximum principal stress vs. normalized minimum principal stress in the one-piece gusset plate of TCBF-B-3 specimen (location: R14)

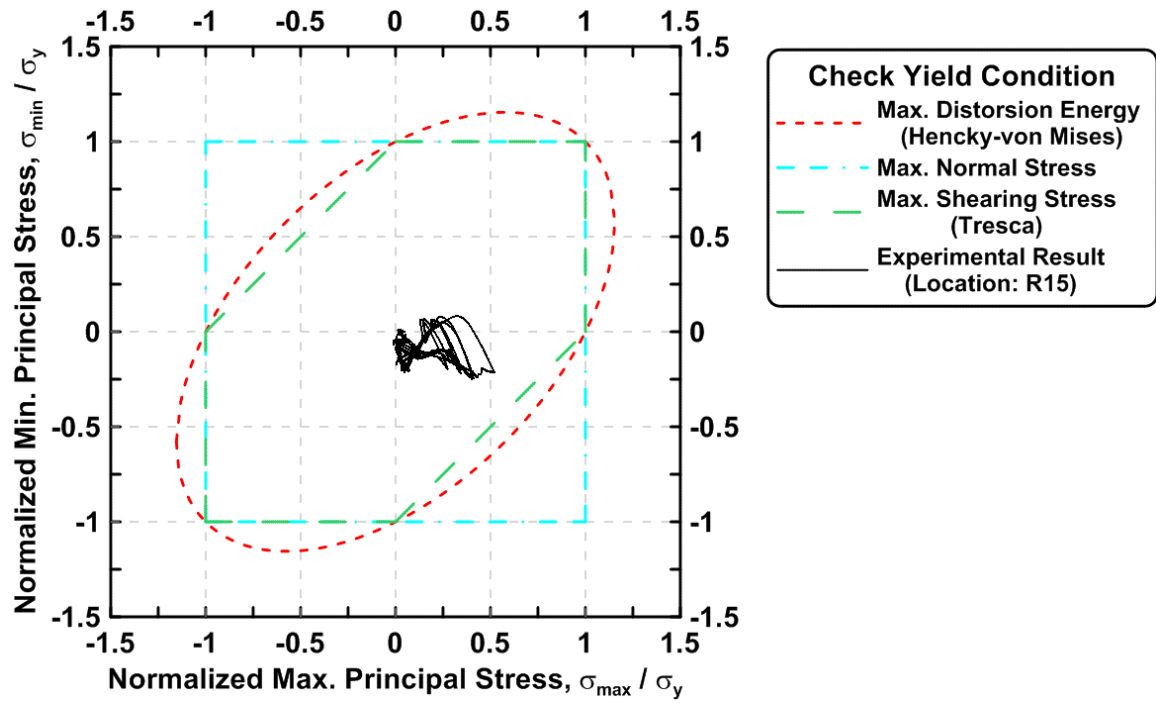


Figure 4.298 Normalized maximum principal stress vs. normalized minimum principal stress in the one-piece gusset plate of TCBF-B-3 specimen (location: R15)

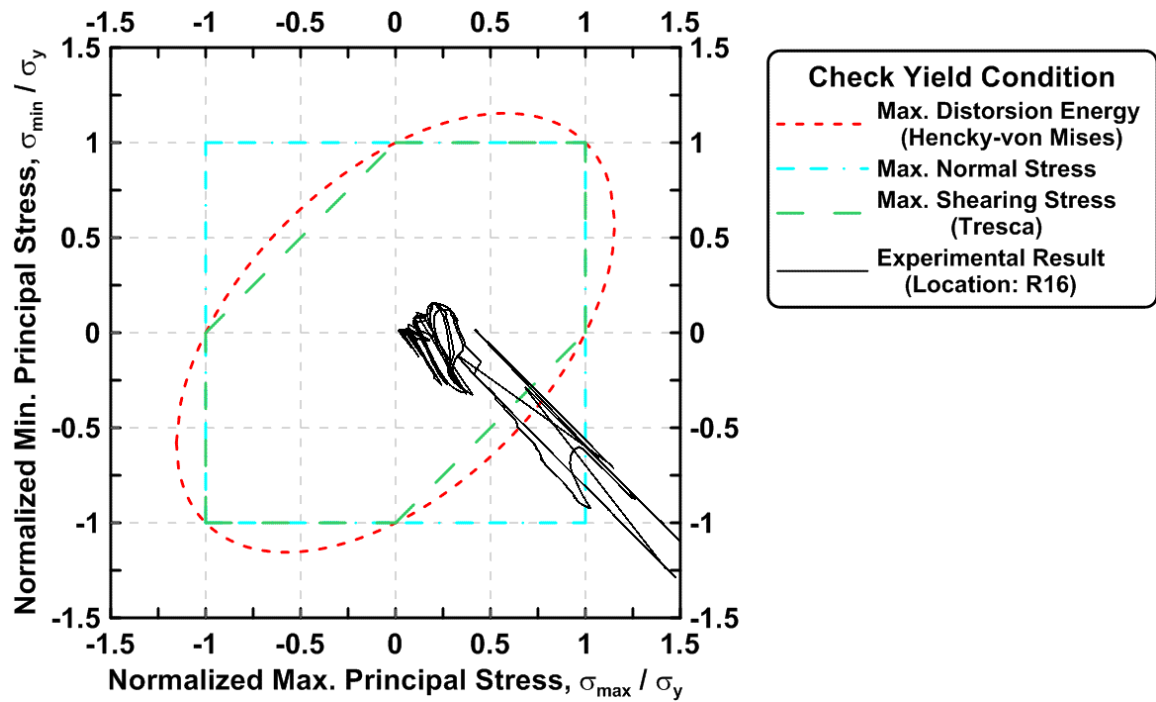


Figure 4.299 Normalized maximum principal stress vs. normalized minimum principal stress in the one-piece gusset plate of TCBF-B-3 specimen (location: R16)

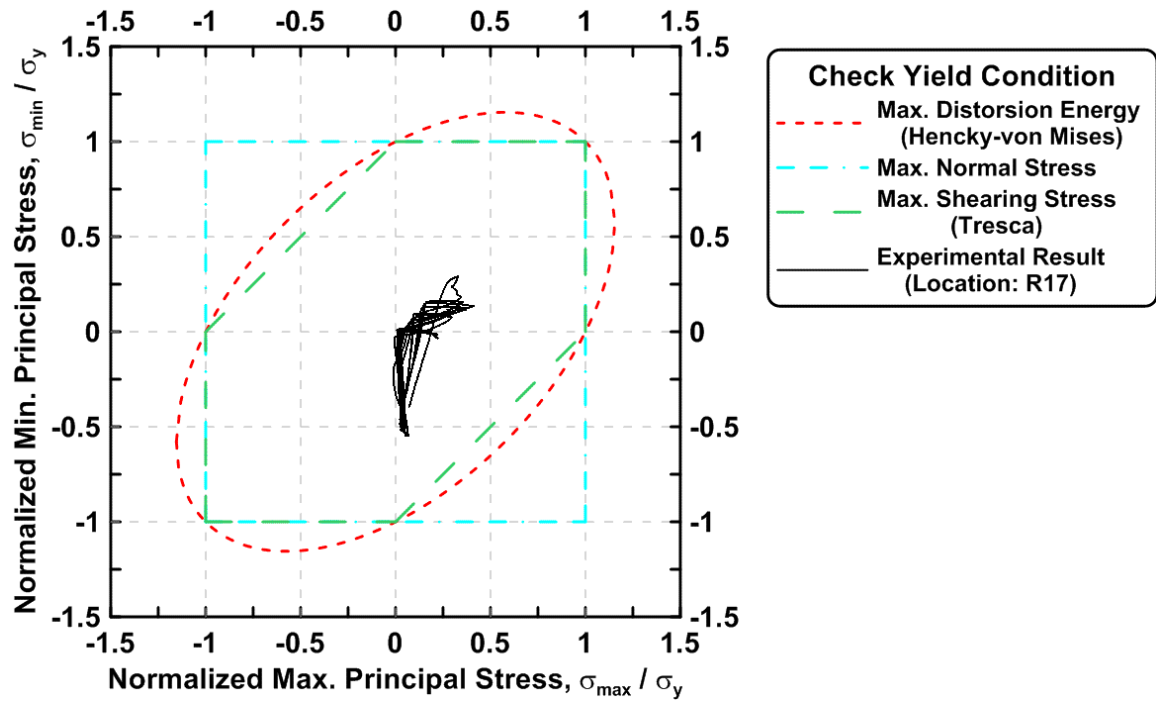


Figure 4.300 Normalized maximum principal stress vs. normalized minimum principal stress in the one-piece gusset plate of TCBF-B-3 specimen (location: R17)

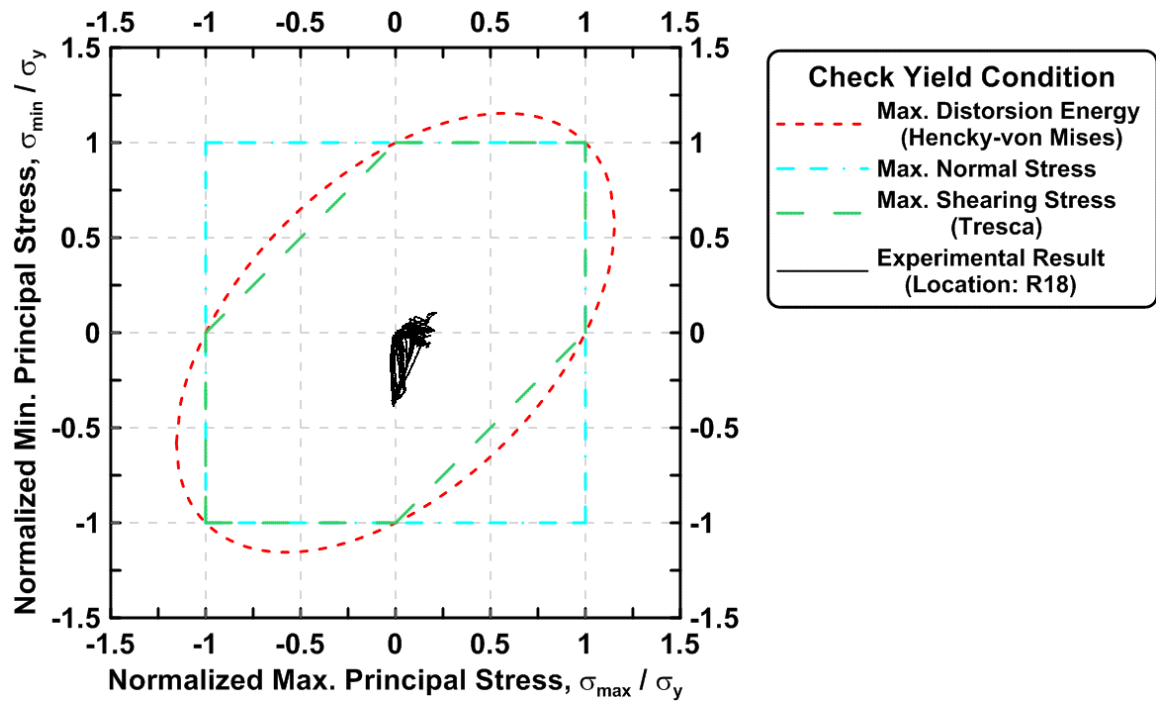


Figure 4.301 Normalized maximum principal stress vs. normalized minimum principal stress in the one-piece gusset plate of TCBF-B-3 specimen (location: R18)



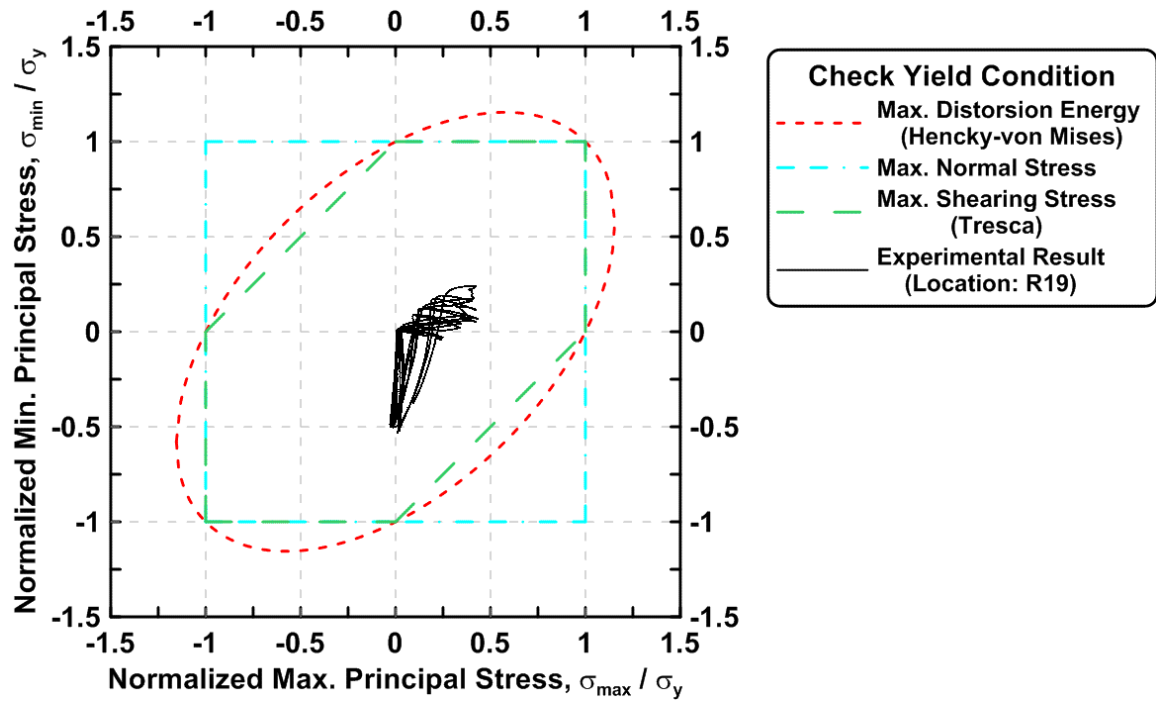


Figure 4.302 Normalized maximum principal stress vs. normalized minimum principal stress in the one-piece gusset plate of TCBF-B-3 specimen (location: R19)

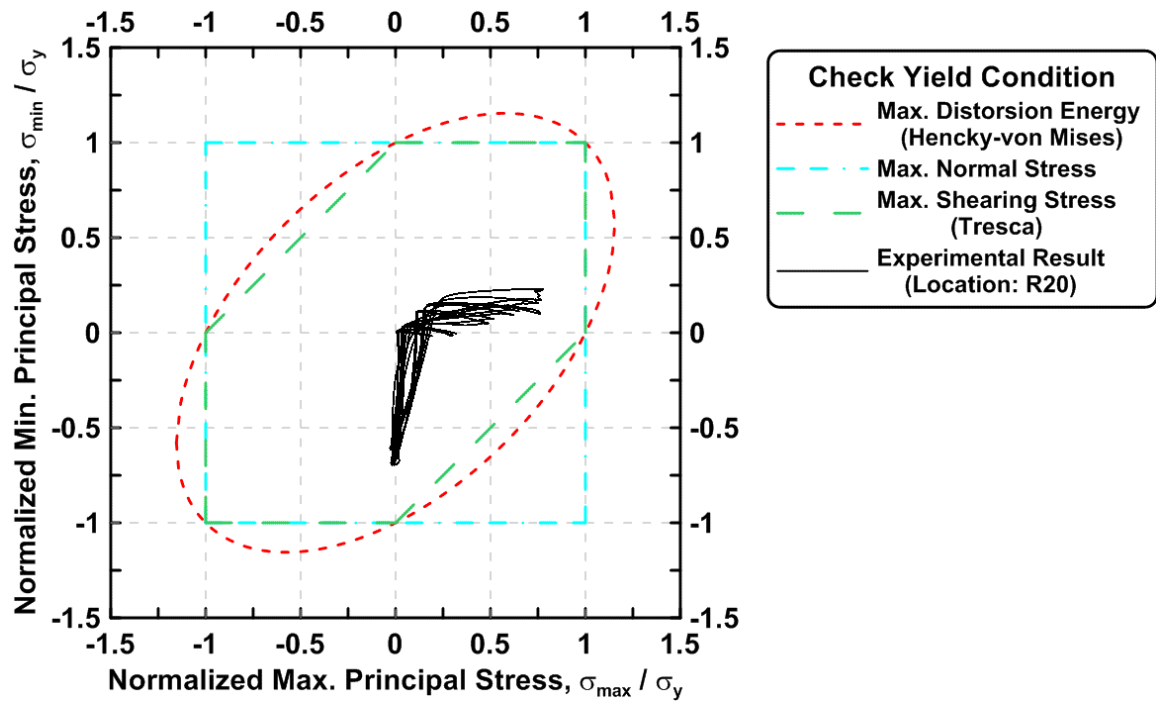


Figure 4.303 Normalized maximum principal stress vs. normalized minimum principal stress in the one-piece gusset plate of TCBF-B-3 specimen (location: R20)

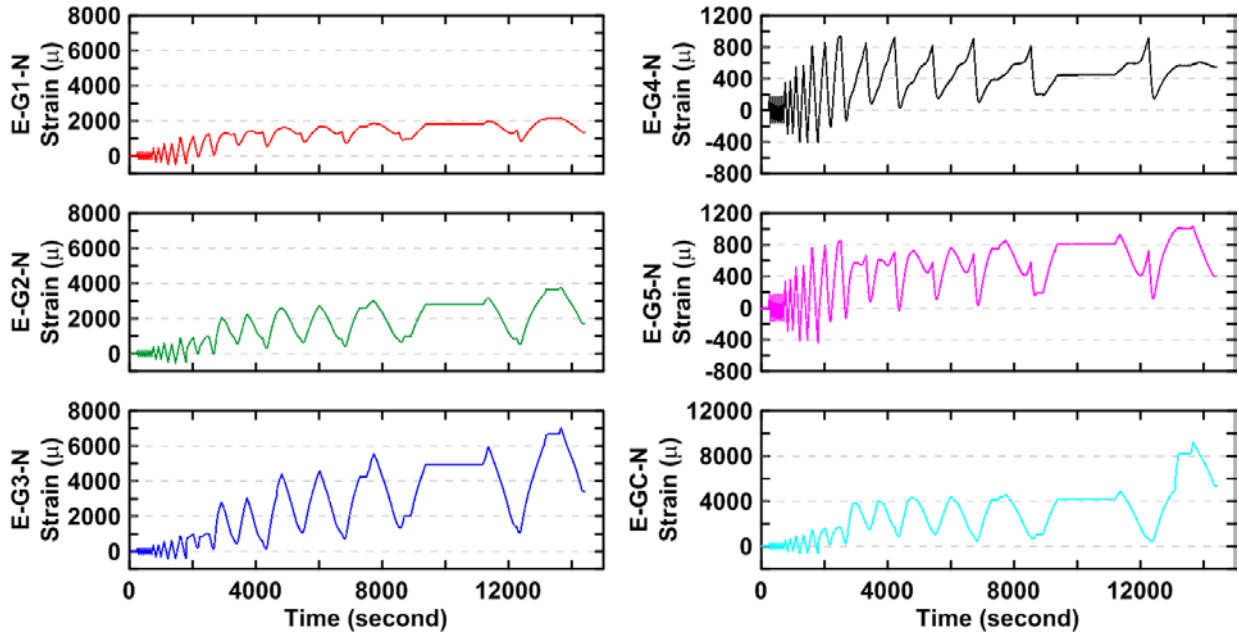


Figure 4.304 The averaged axial strain time history in the tapered gusset plate at eastern side of TCBF-B-3 specimen

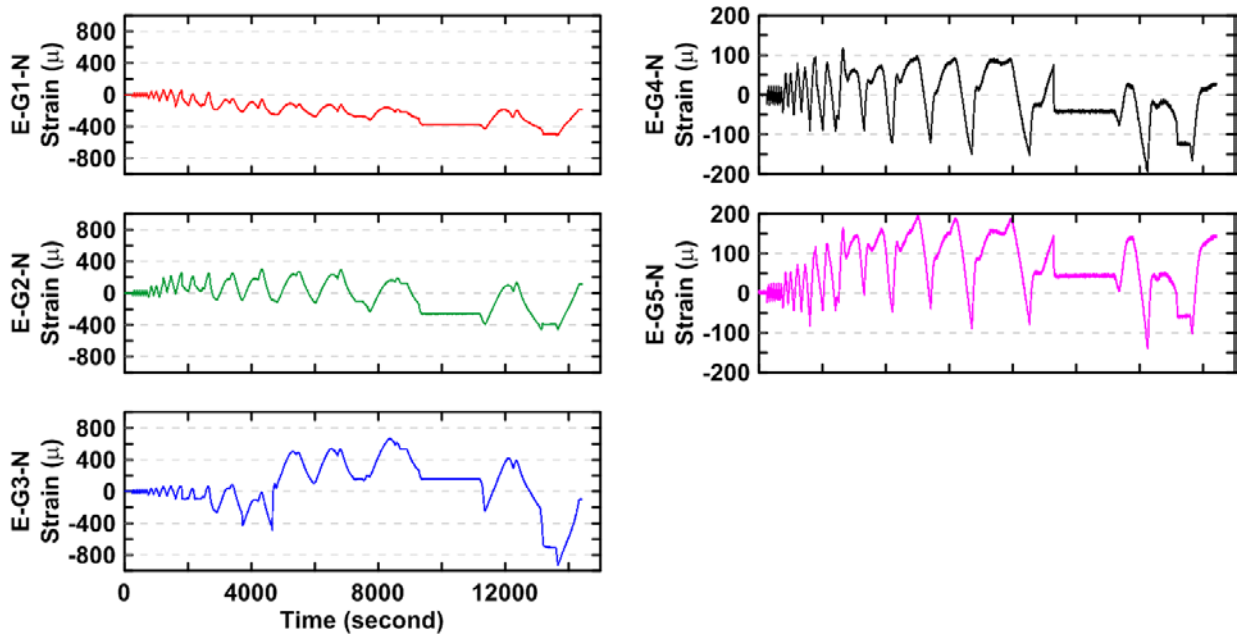


Figure 4.305 The bending strain time history in the tapered gusset plate at eastern side of TCBF-B-3 specimen

#### 4.2.3.1.7 Test Setup Response

The actuator bracket deformations versus actuator forces are plotted in Fig. 4.306. The relative displacement time history between base plates of the specimen and the floor beam, relative displacement time history between floor beam and strong floor, and relative displacement time history between integrated reconfigurable reaction wall and strong floor at northern and southern sides are shown in Fig. 4.307. The out-of-plane deformation time history of the lateral supporting frame with respect to the wall of the building at different locations is plotted in Fig. 4.308. The reconfigurable reaction wall (RRW) tip deformation time histories during the test are shown in Fig. 4.309.

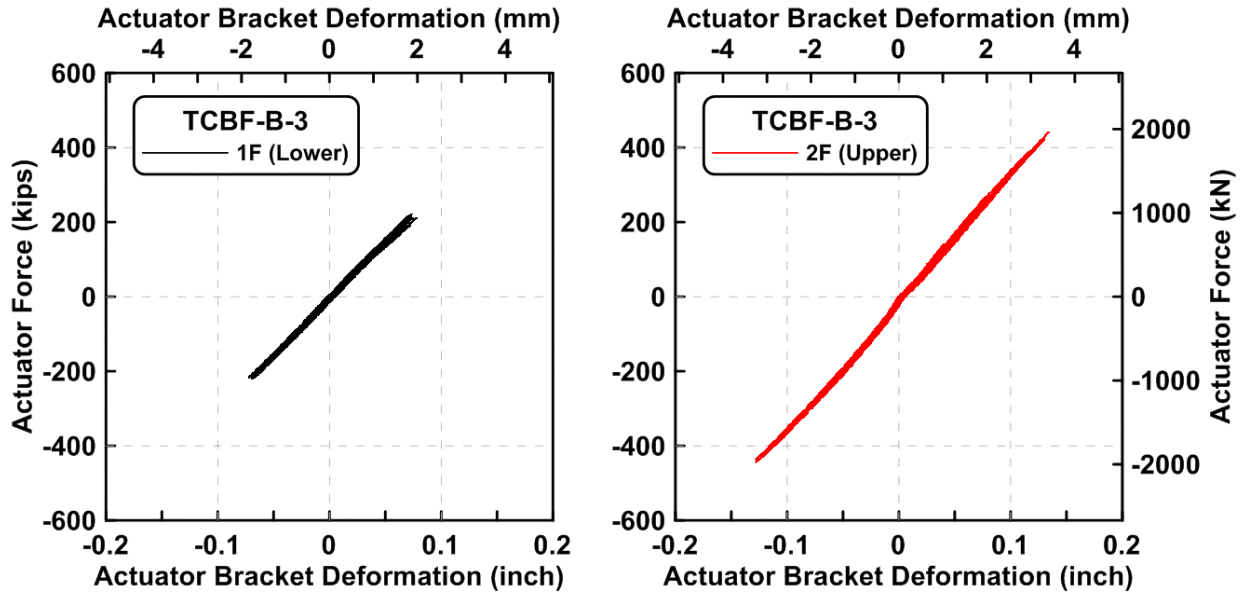


Figure 4.306 The actuator force vs. bracket deformation relationship at both floor levels during specimen TCBF-B-3 test

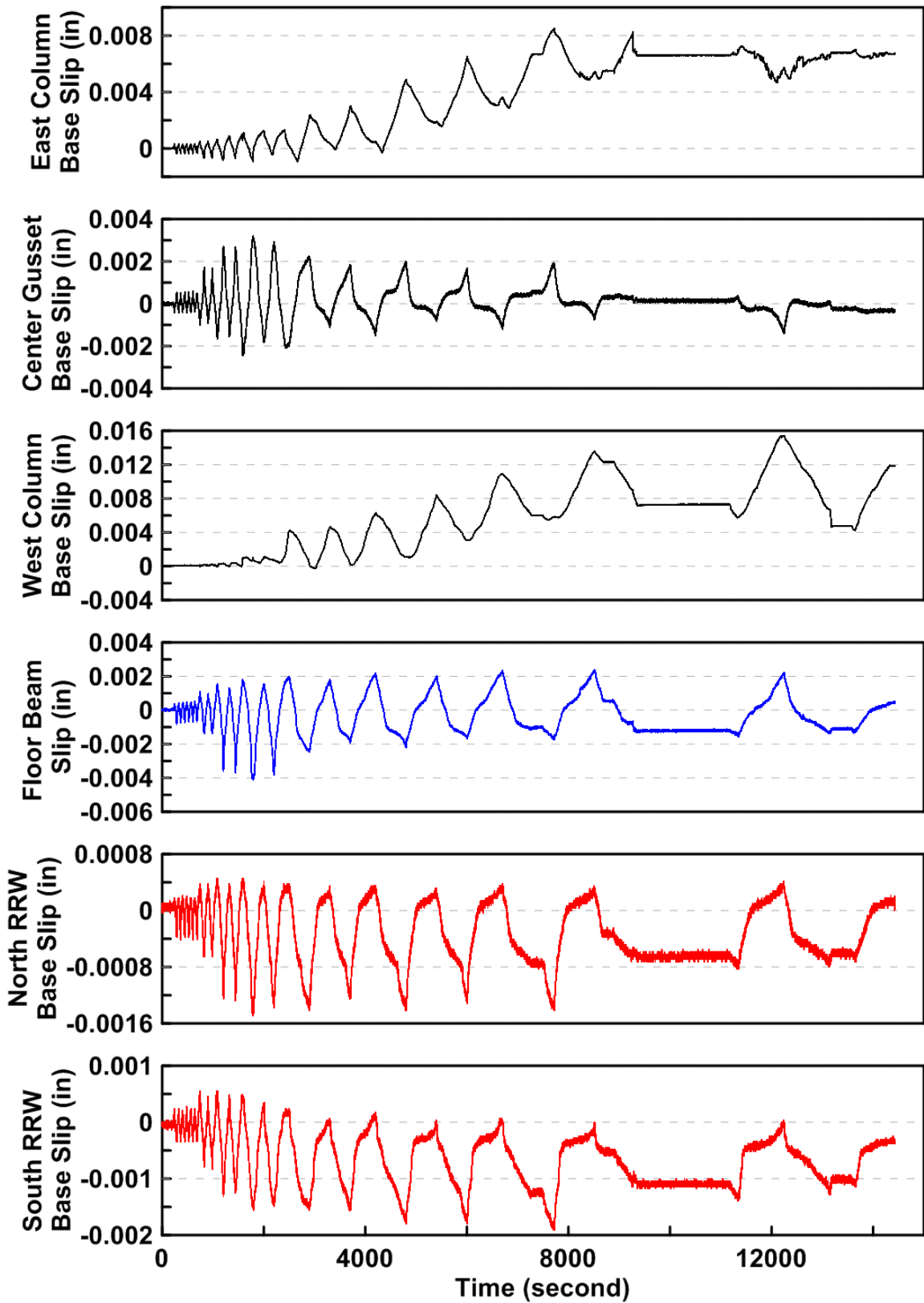


Figure 4.307 Slippage time history between specimen and test setup boundaries during specimen TCBF-B-3 test

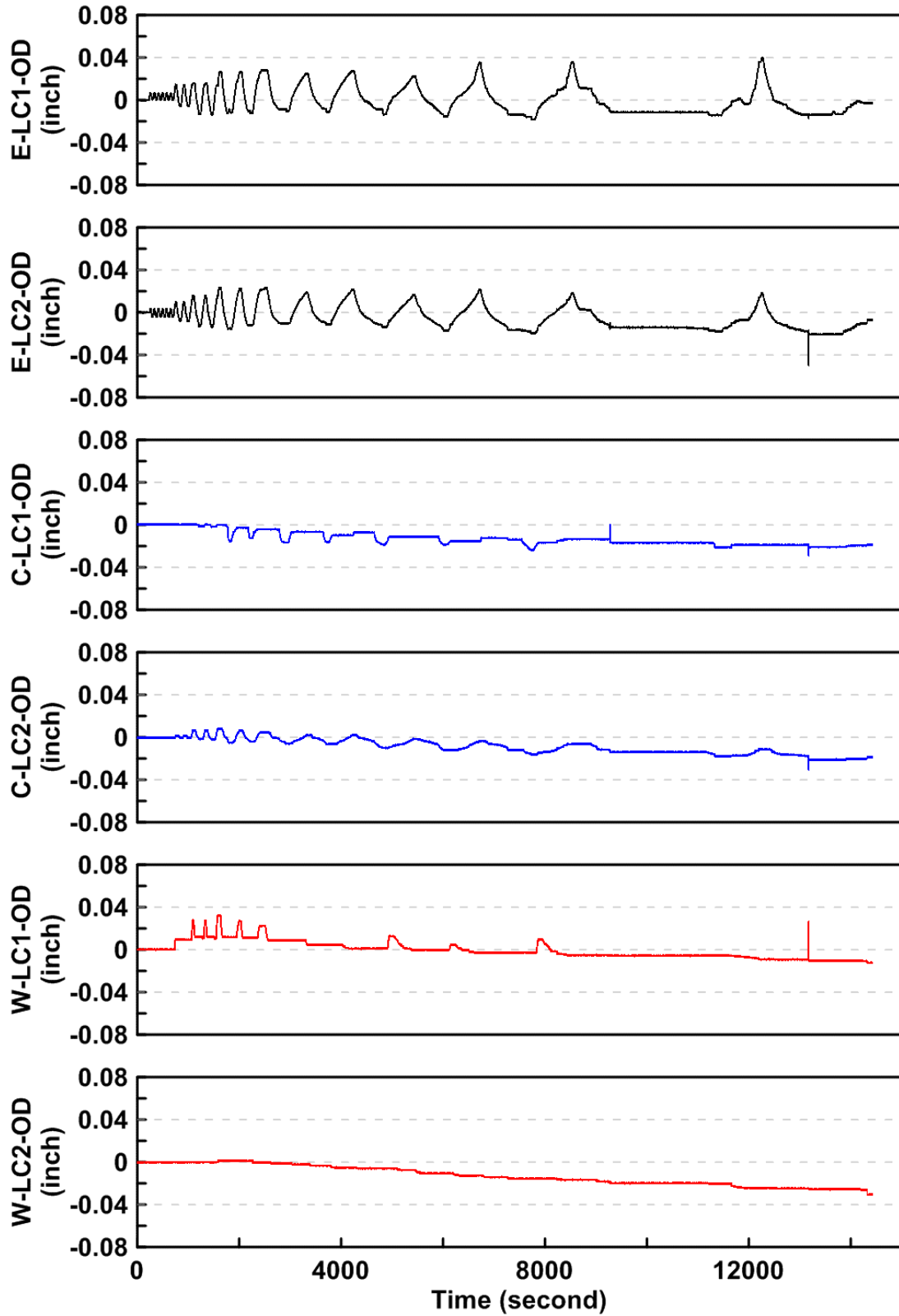


Figure 4.308 The out-of-plane deformation time history of lateral supporting frame at different monitoring points during specimen TCBF-B-3 test

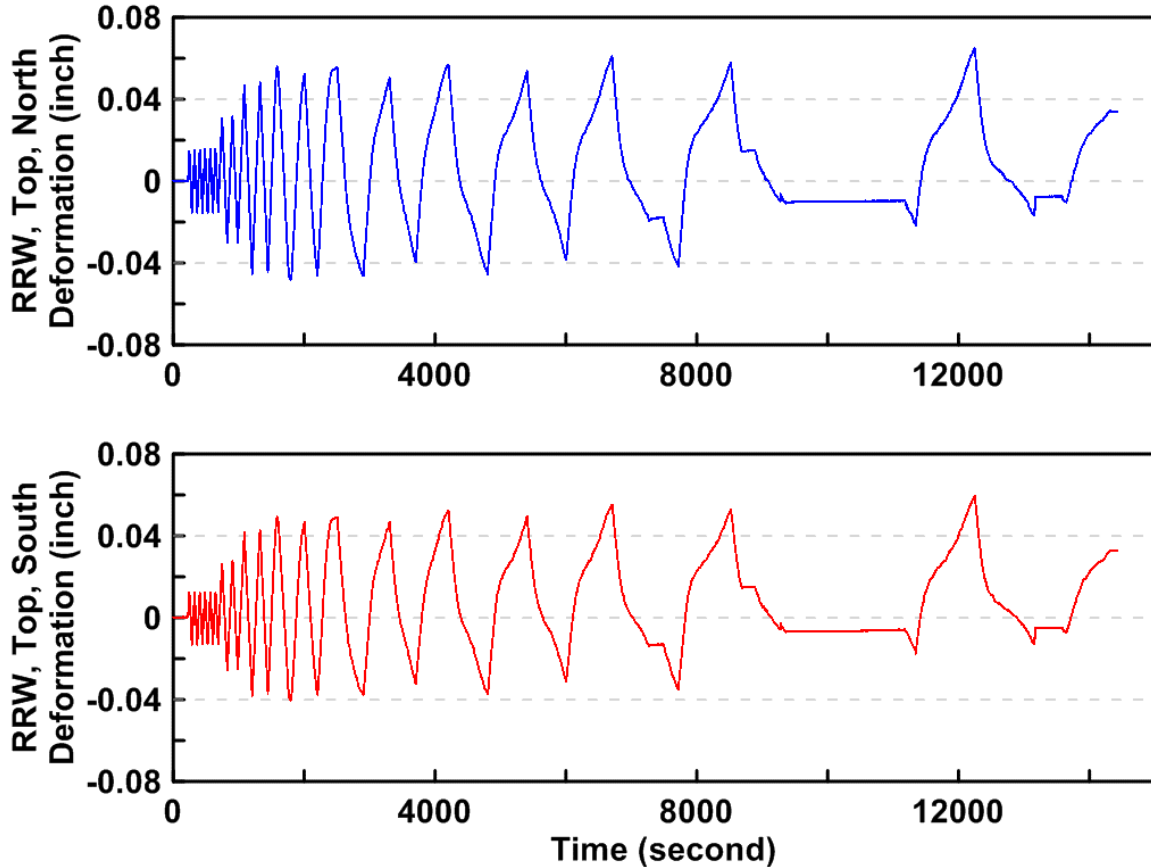


Figure 4.309 The reconfigurable reaction wall (RRW) tip deformation time histories during specimen TCBF-B-3 test

#### 4.2.3.2 Main Observations

Specimen TCBF-B-3 was subjected to the same pre-defined loading protocol shown in Fig. 3.28. Each loading stages contained two complete cycles at a given amplitude, except the first stage contained six complete cycles. Detailed information about each of these cycles is described sequentially below. Table 4.4 illustrates and lists the major observations on the testing protocol with brief descriptions.

##### **$\Delta = 0.5$ $D_{be} = 0.2$ inch (Roof Drift $\delta = 0.1$ %), from 11:01 AM to 11:09 AM**

Test started at 10:01 AM, after having completed two small cycles performed to check the operation of the data acquisition and control systems. During this low amplitude loading stage, the entire frame remained elastic. No special findings were found during this loading stage.

##### **$\Delta = 1.0$ $D_{be} = 0.4$ inch (Roof Drift $\delta = 0.2$ %), from 11:09 AM to 11:14 AM**

The entire frame essentially remained elastic; no special findings were found in this loading step.

##### **$\Delta = 1.0$ $D_{by} = 0.6$ inch (Roof Drift $\delta = 0.3$ %), from 11:14 AM to 11:22 AM**

Some local flaking of the whitewash occurred on the brace-to-gusset cover plates and near the brace erection holes at first story (western wide flange brace on the north face, see Fig. 4.310).

Minor whitewash flaking also occurred on the column web and column flange near the base plates.

**$\Delta = 0.5 D_{bm} = 1.0$  inch (Roof Drift  $\delta = 0.5$  %), from 11:22 AM to 11:35 AM**

At the beginning of the first half cycle of the loading step (approaching the positive peak displacement), the brace at first-story west side and the brace at second-story east side began global buckling out-of-plane both to the north side of the specimen and the whitewash on the wide flange brace began flaking at the middle of the brace (Fig. 4.311). Note that the whitewash flaking on the second-story brace occurred slightly above the brace midpoint. In the same loading cycle when the roof displacement was moving towards the negative peak displacement, the brace at first-story east side and the brace at second-story west side began global buckling out-of-plane to the south and north side of the specimen, respectively. Flaking of the whitewash on the wide flange braces occurred near the middle of the braces. Some local flaking of whitewash occurred on the roof beam web near the beam-to-column connection shear tab and also on the roof beam top flange near the beam-to-column connection CJP welds. Minor flaking also occurred in the panel zone region, as shown in Fig. 4.312. Some minor local flaking of whitewash occurred near the lower beam-to-gusset splice plates (Fig. 4.313).

**$\Delta = 1.0 D_{bm} = 2.0$  inch (Roof Drift  $\delta = 0.9$  %), from 11:36 AM to 12:03 PM**

Additional flaking of whitewash occurred in the gusset plates and the braces during this loading stage. Additional global buckling of all four braces occurred in the out-of-plane direction (Fig. 4.314). Yielding of the  $2t$  folding lines became easily visible in some gusset plates (Fig. 4.315). Some yielding of the column flange occurred at both east side and west side column bases (Figs. 4.316 and 4.317). Note that the yield lines in the column flanges were about  $45^\circ$  angle from the column line, indicating that Lüder's bands had developed in the column flanges.

**$\Delta = 1.5 D_{bm} = 3.0$  inch (Roof Drift  $\delta = 1.4$  %), from 12:03 PM to 12:43 PM**

When the roof displacement approached the first positive peak for this stage, the west-side wide flange brace in the ground story experienced localized buckling at the southern-side flanges near the midpoint of the brace (Fig. 4.318). Additional flaking of the whitewash in both columns (near the bases), gusset plates, wide flange braces, and beam-to-gusset plate splices occurred at this load stage. Severe local yielding was found in the beam-to-gusset plate splices near the corner shot-slotted holes (Fig. 4.319). The beam-to-gusset connections also slipped as expected as shown in Fig. 4.320.

**$\Delta = 2.0 D_{bm} = 4.0$  inch (Roof Drift  $\delta = 1.9$  %), from 12:44 PM to 2:18 PM**

Although loud popping noises were heard at the second excursion of the first load cycle at about 1.7-in. roof displacement to the west (heading to the negative 4 in. peak), no drop in load occurred at this time. The test was manually paused at about five minutes to inspect the specimen and then started. After moving back from the negative peak roof displacement in the first load cycle, the northern face of the east side brace at the second story began to locally buckled (about -2.6-in. roof displacement). Several loud popping noises were heard at the beginning of the second cycle in this load step. The test was again manually paused for about six minutes to inspect the specimen. No fractures associated with the popping noises were found, and testing resumed. The base shear was small (less than 10 kips) and the roof displacement was about 2.36 in. during the short pause. Again, no significant load drop occurred. When the roof displacement approached negative 2.32 in. during the second half of the second cycle in the loading stage, the east column exterior column flange fractured near the tip of base plate stiffeners (Figs. 4.321 and 4.322). The test was paused at about 1:35PM and resumed at around 2:05PM. Partial fracture of

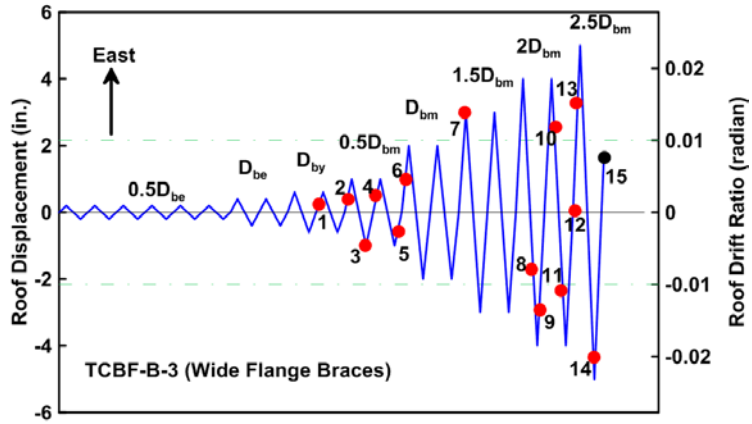
the west-side wide flange brace in the first story was noticed during this loading phase (Figs. 4.323 and 4.324).

**$\Delta = 2.5$  D<sub>bm</sub> = 5.0 inch (Roof Drift  $\delta = 2.3$  %), from 2:19 PM to 2:57 PM**

At the first cycle of this load stage when the roof displacement approached to 3.5 in., the top flange of the west-side brace in the lower story completely fractured (Fig. 4.325). Later at the negative 4.3-in. roof displacement (approaching to the first negative peak roof displacement in this load stage), the west-side brace in the first story completely fractured (Fig. 4.326). In this excursion, the crack tip in the east column web also moved toward the center of the web, and the crack opening became bigger (Fig. 4.327). The test was stopped at roof displacement equaled to 1.67 in. after completing the first cycle of this load step. This displacement was estimated to return the structure to a nearly plumb position after unloading. The entire side view of the specimen after test is shown in Fig. 4.328.

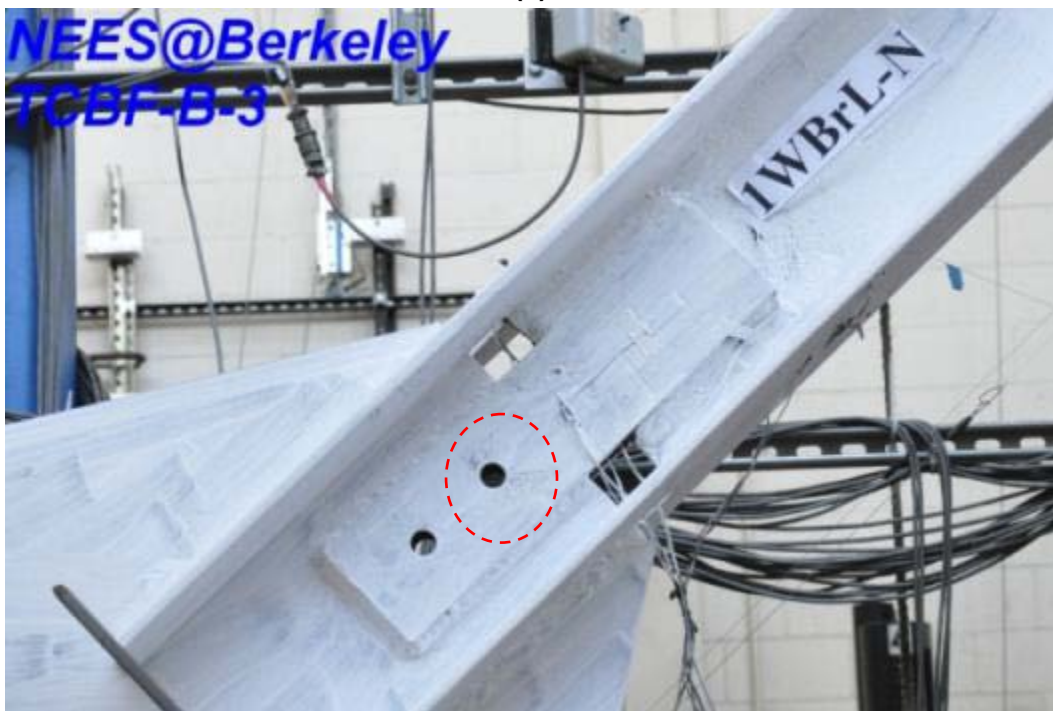


**Table 4.4 The major observations during specimen TCBF-B-3 test**

	
<b>Major Observations</b>	
1	Whitewash flaking on the brace-to-gusset cover plates and near the brace erection holes at first story (Fig. 4.310).
2	The brace at first story west side and the brace at second story east side began global buckling brace (see Fig. 4.311, buckled out-of-plane to the north side).
3	The brace at first story east side and the brace at second story west side began global buckling brace (out-of-plane to the south and north side, respectively).
4	Minor local flaking of whitewash developed near the column base at both east and west side.
5	Minor local flaking of whitewash developed near the corner of lower beam-to-gusset splice plates (Fig. 4.313).
6	Additional flaking of whitewash developed in the gusset plates and the braces. The 2t folding lines became visible in some gusset plates (Fig. 4.315).
7	The west-side wide flange brace in the first story local buckled at the southern-side flanges near the midpoint of the brace (Fig. 4.318).
8	Loud popping noises were heard but no load drop occurred at this time.
9	The northern face of the east side brace at the second story began locally buckled.
10	Test paused about six minutes to inspect the specimen. No significant load drop occurred.
11	The east column exterior column flange fractured near the tip of base plate stiffeners (Figs. 4.321 and 4.322). And a partial fracture of the west-side wide flange brace in the first story was noticed (Figs. 4.323 and 4.324).
12	The crack in the top flange of the west-side brace continued to propagate to the north side.
13	The top flange of the west-side brace in the first story completely fractured (Fig. 4.325).
14	The west-side brace in the first story completely fractured (Fig. 4.326). The crack tip in the east column web moved toward the center (Fig. 4.327).
15	Test stopped at roof displacement equaled to 1.67 inches.



(a)



(b)

Figure 4.310 The whitewash flaking on the brace-to-gusset cover plates (Specimen TCBF-B-3)



Figure 4.311 Whitewash flaking on the global buckled braces (west brace at the first story and east brace at the second story)



Figure 4.312 Whitewash flaking at the roof beam-to-column connection (west side)

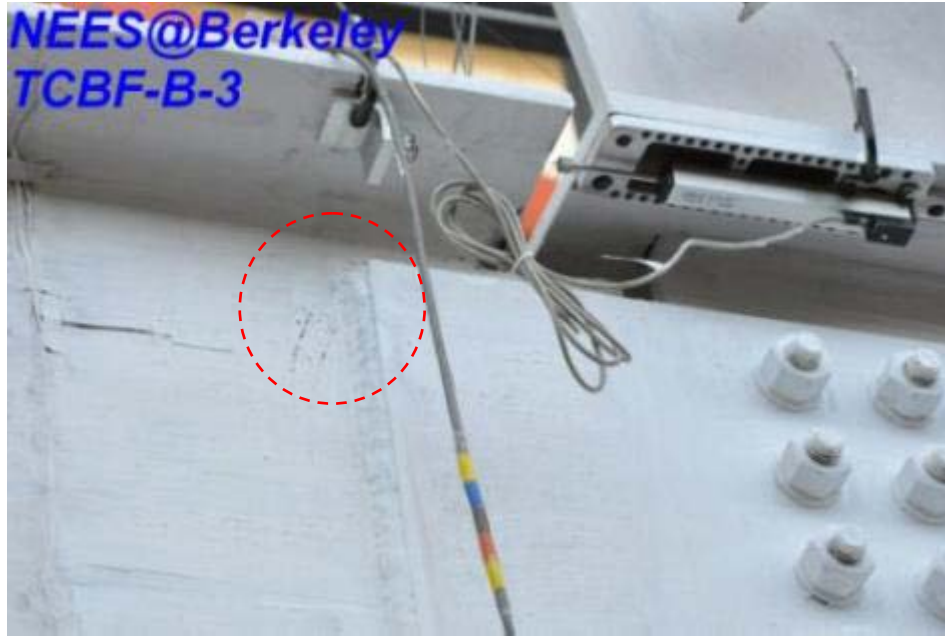


Figure 4.313 Local flaking of whitewash developed in the lower beam web near beam-to-gusset splice plate



(a)



(b)

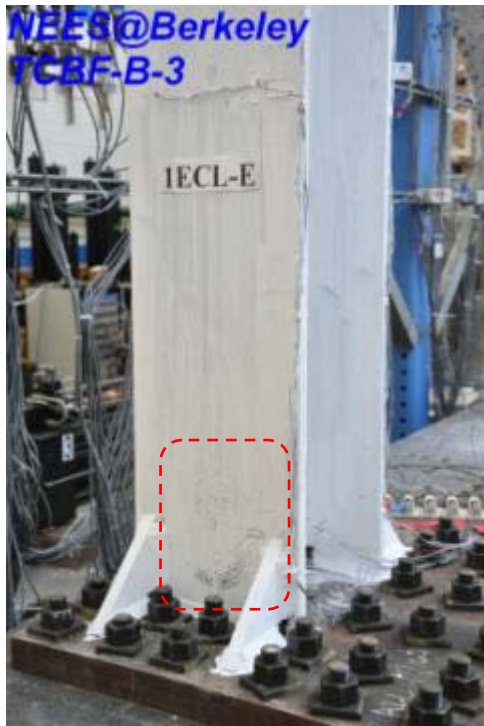
Figure 4.314 Buckling shapes of all four wide flange braces, three of them buckled to the north side, only the east side brace at the first story buckled to the south side



Figure 4.315 Flaking of whitewash developed at the  $2t$  gap region in the gusset plate



Figure 4.316 Whitewash flaking patterns shown on the column flanges near the column base plate (west column base)



(a) East column base



(b) West column base

Figure 4.317 Whitewash flaking patterns shown on the column flanges near the column base plate



Figure 4.318 The closed view of flange local buckling at the west-side wide flange brace in the first story

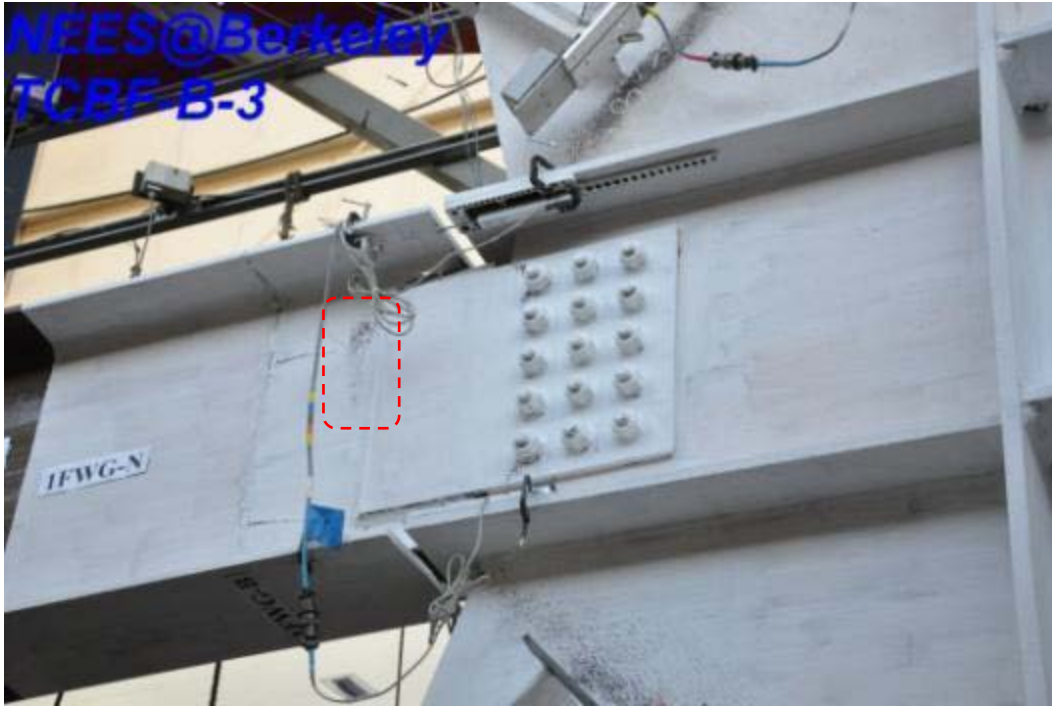


Figure 4.319 The local yielding in the beam-to-gusset plate splices near the shot-slotted holes



Figure 4.320 Evidence of slippage between splice plate and the one-piece gusset plate



Figure 4.321 East column flange fractured near the base plate stiffeners (view from north-west side)



Figure 4.322 East column flange fractured near the base plate stiffeners (view from east side)





Figure 4.323 West wide flange brace partially fractured near the middle of the brace (view from north-west side)



Figure 4.324 West wide flange brace partially fractured near the middle of the brace (view from east side)



Figure 4.325 Top flange of the west wide flange brace completely fractured near the middle of the brace (view from north-west side)



Figure 4.326 West wide flange brace completely fractured near the middle of the brace (view from north side)



Figure 4.327 Crack tip in the web of east column near the column base



(a) View from north-east side



(b) View from north-west side

Figure 4.328 Specimen TCBF-B-3 after test

### 4.3 HYBRID SIMULATION TEST RESULTS OF SPECIMEN TCBF-B-4 (SQUARE HSS BRACES)

This specimen re-used the roof beam, two W12 × 96 columns and base plates from TCBF-B-3 specimen. The east side column flange and web near the column base region were repaired with CJP welds. Stiffener plates and cover plates were also provided in this region as illustrated in Figs. 3.62 and 3.63. As with Specimen TCBF-B-3, pinned connections between the lower beam and the one-piece gusset plates were used in this specimen. Connection detail was the same as shown in Fig. 4.227 for TCBF-B-3 specimen.

Before running the design earthquake (DE) level ground motion, two one-tenth amplitude DE level ground motions were executed to check instrumentations, data readings, actuator control algorithms and to determine the adequate actuator speed. The hybrid test system was used to simulate a low amplitude free vibration test to derive the fundamental period and inherent damping of the specimen. Both actuators were displacement controlled and the actuator speed was selected as 0.002 inch per second and this setting did not change during the entire hybrid simulation.

The test began at 10:54 PM on Saturday, March 26, 2011. The entire side views of the braced frame specimen before and after hybrid simulations are shown in Figs. 4.329.



(a) Before test



(b) After elastic test



(c) After design earthquake (DE)



(d) After maximum credible earthquake (MCE)

Figure 4.329 Specimen TCBF-B-4 before and after hybrid simulation

### 4.3.1 Key Response Quantities

The paragraphs below briefly describe the response quantities record in the hybrid simulation and the post-processed response quantities derived from the raw data. Detailed discussion of the individual response quantities are described in Chapter 5.

#### 4.3.1.1 System Response

Figures 4.330 and 4.331 show the time history of the actuator displacements and actuator load cell force feedbacks for specimen TCBF-B-4. The base shear versus controlled roof displacement of the specimen is shown in Fig. 4.332. The relationship between story shear and story drift for the specimen is shown in Fig. 4.333. Upper actuator force versus lower actuator force relationship is shown in Fig. 4.334. Upper actuator displacement versus lower actuator displacement relationship is shown in Fig. 4.335.

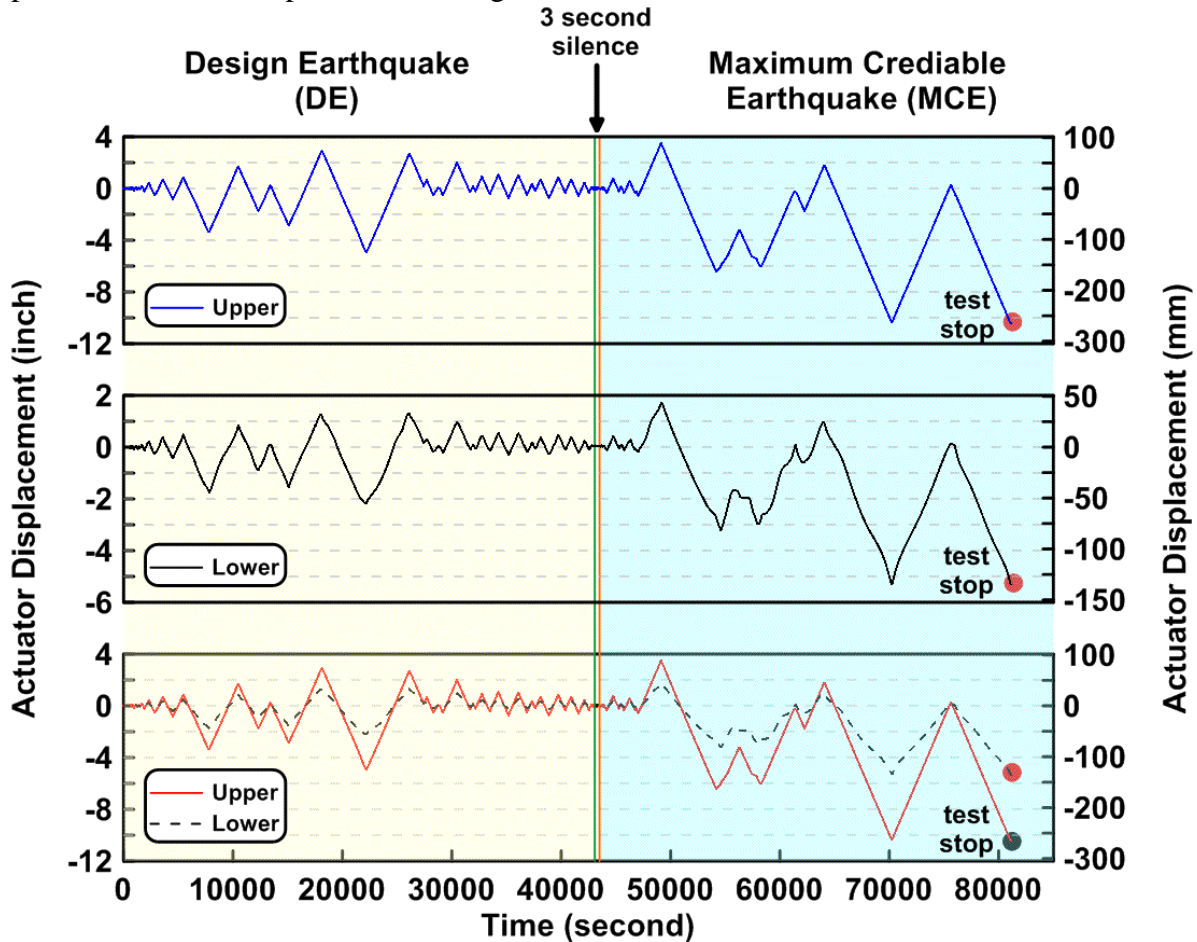


Figure 4.330 Actuator displacement time history of TCBF-B-4 specimen

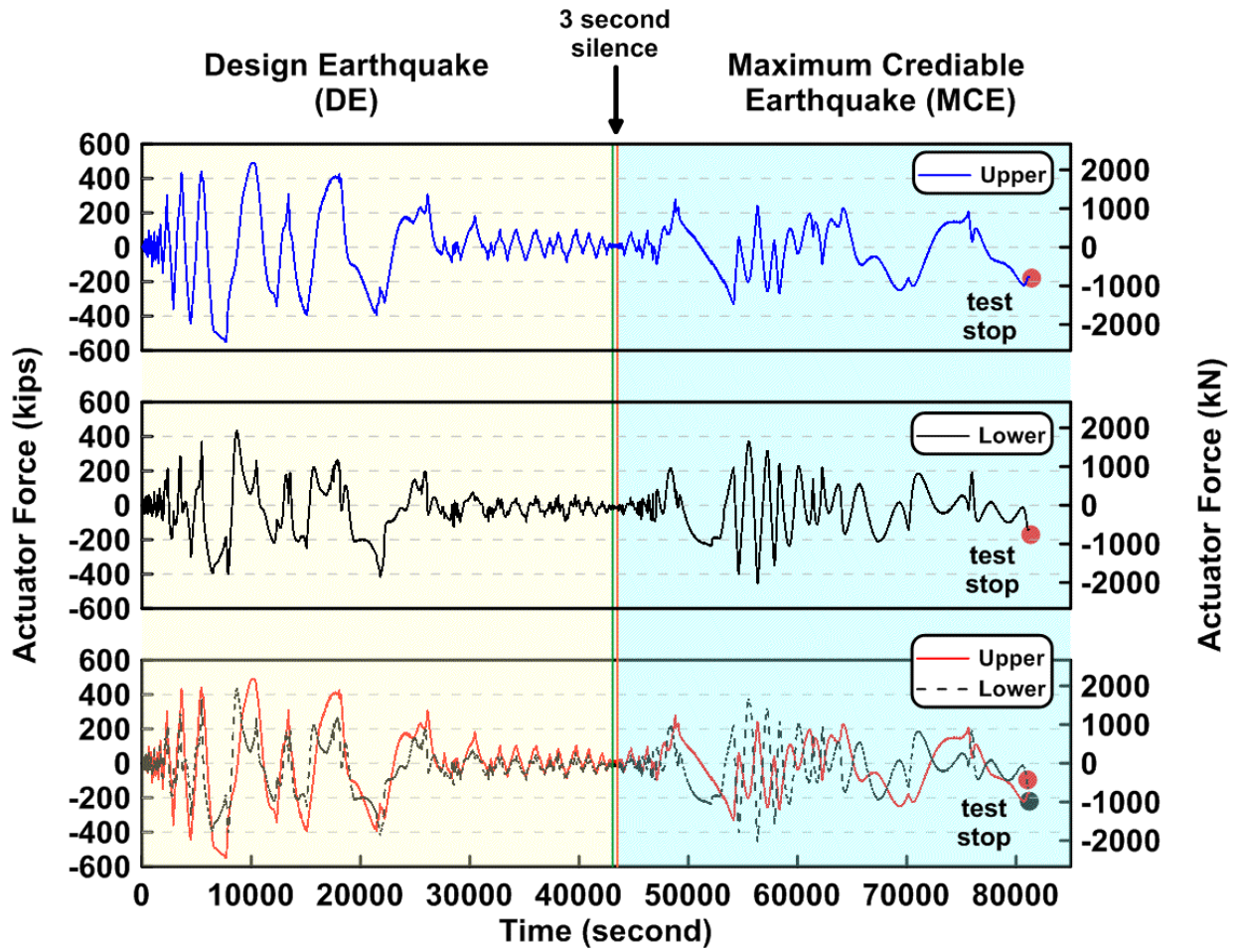


Figure 4.331 Actuator force histories of TCBF-B-4 specimen

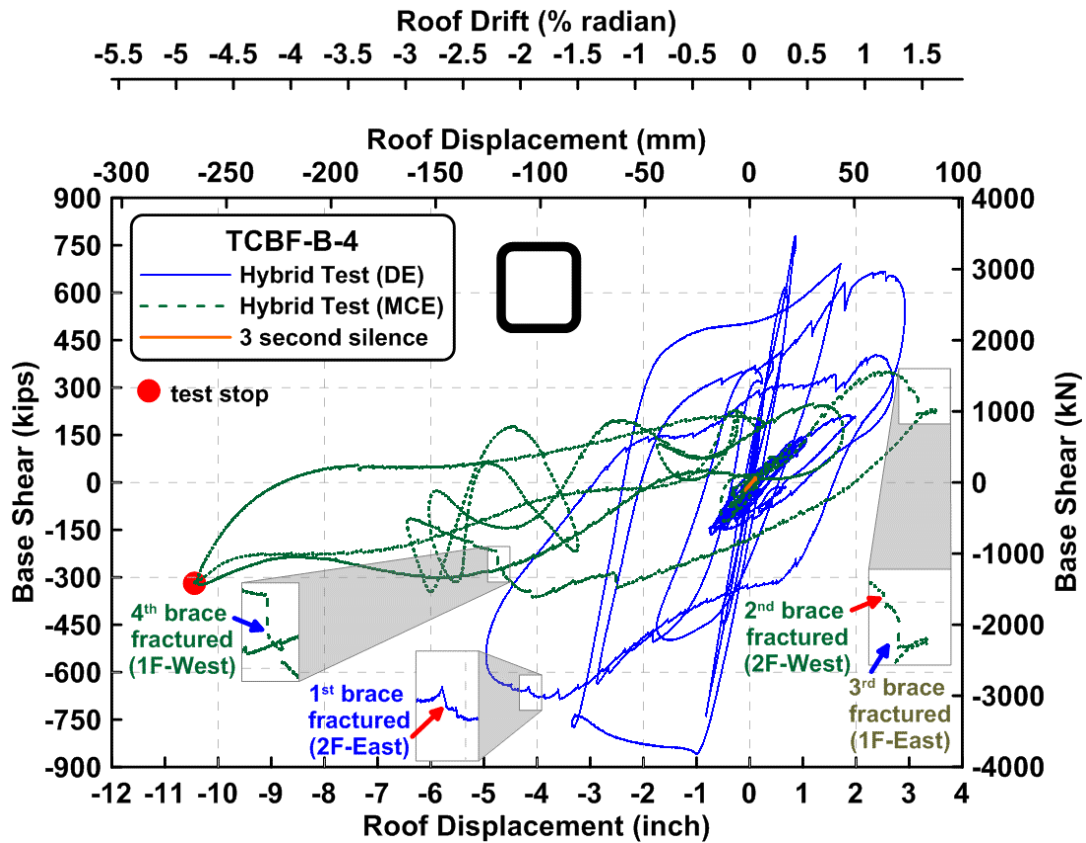


Figure 4.332 Base shear vs. roof displacement relationship of TCBF-B-4 specimen

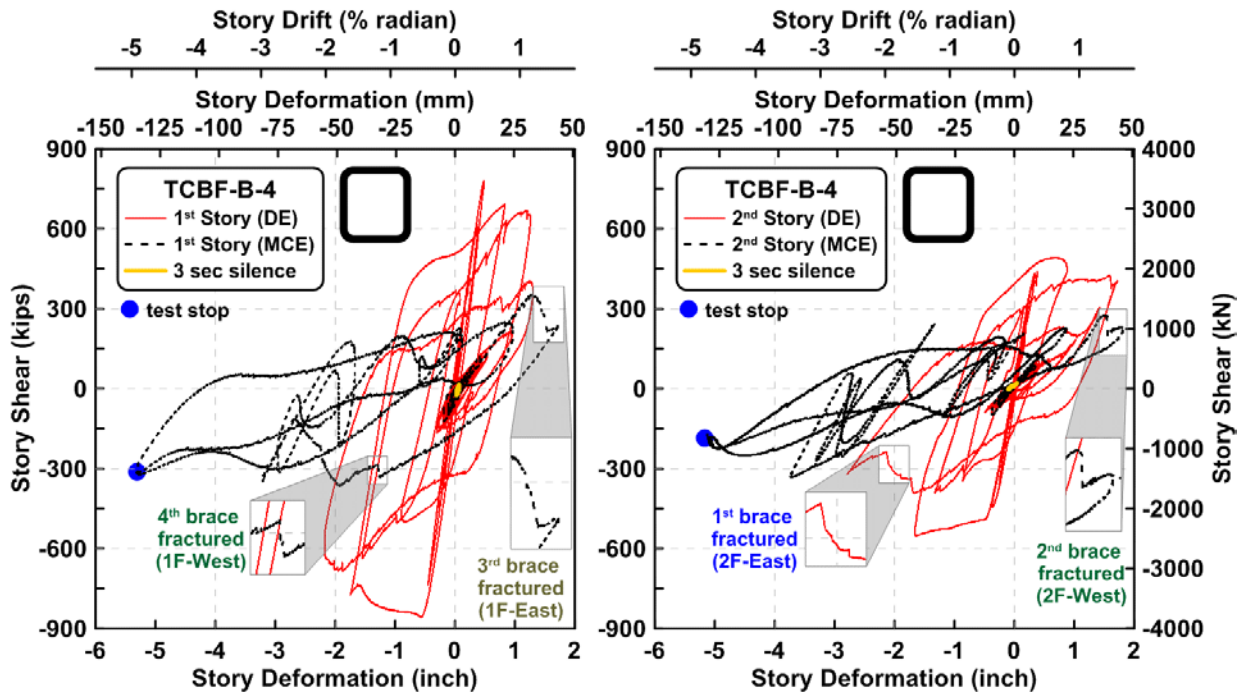


Figure 4.333 Story shear vs. story deformation relationship of TCBF-B-4 specimen



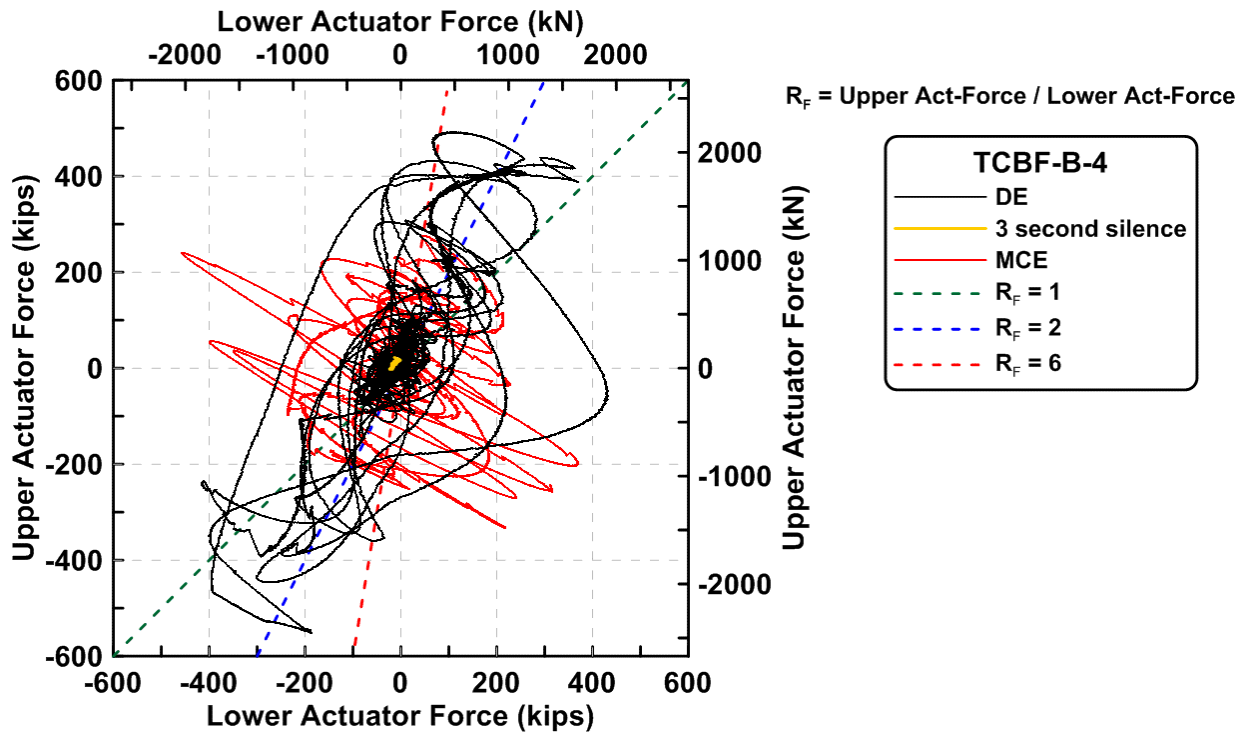


Figure 4.334 Upper actuator force vs. lower actuator force relationship of TCBF-B-4 specimen

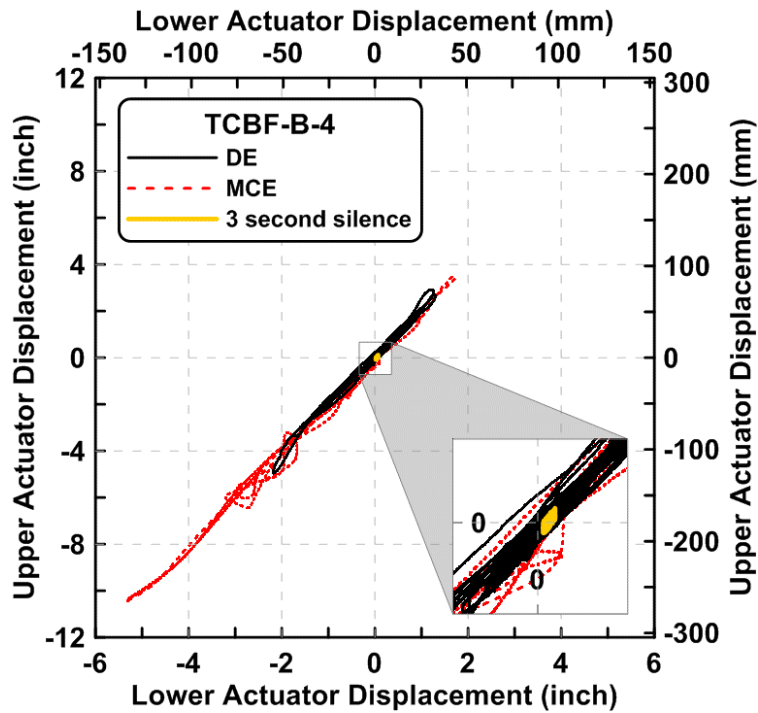


Figure 4.335 Upper actuator displacement vs. lower actuator displacement relationship of TCBF-B-4 specimen

### 4.3.1.2 Column Response

The time history of the axial forces in W12 × 96 columns at western and eastern sides of the specimen is plotted in Fig. 4.336. The relationship between roof displacements and axial forces at both columns are shown in Fig. 4.337. The bending moment time history at the top and bottom ends of the column in each story is shown in Figs. 4.338 and 4.339. Derived column shear force time history in both stories are plotted in the Figs. 4.340 and 4.341, respectively. Two column shear forces in each floor were added together and are shown in Fig. 4.342. The column web shear stress versus shear strain readings from strain rosettes is plotted in Fig. 4.343. The sum of the column shear force components versus the total story shear forces for each story is shown in Fig. 4.344. The derived rosette-type strain gauge readings in the column web at each story are shown from Figs. 4.345 to 4.348. Normalized maximum and minimum principal stress relationships along with different yield criteria are plotted in Figs. 4.349 to 4.352. The normalized P-M and P-V interaction diagrams at column bases and column top ends are shown in Figs. 4.353 to 4.356.

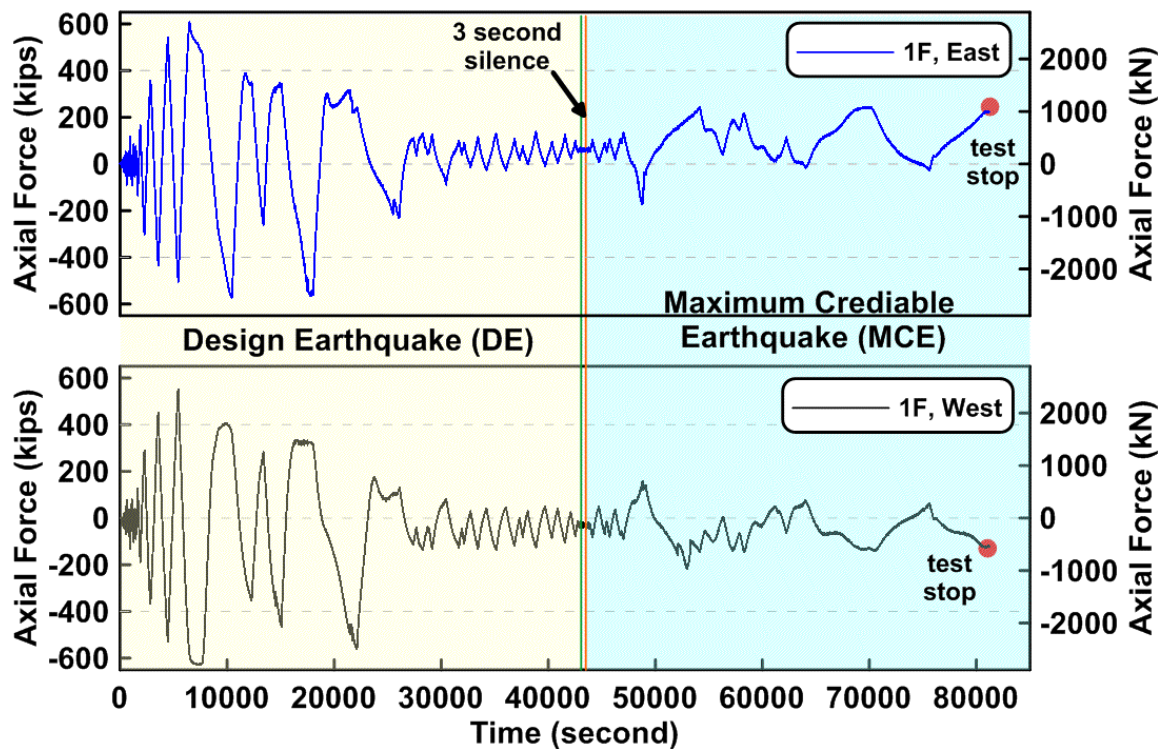


Figure 4.336 Time history of the column axial forces in the first story of TCBF-B-4 specimen (location: 3-ft above column base plate)

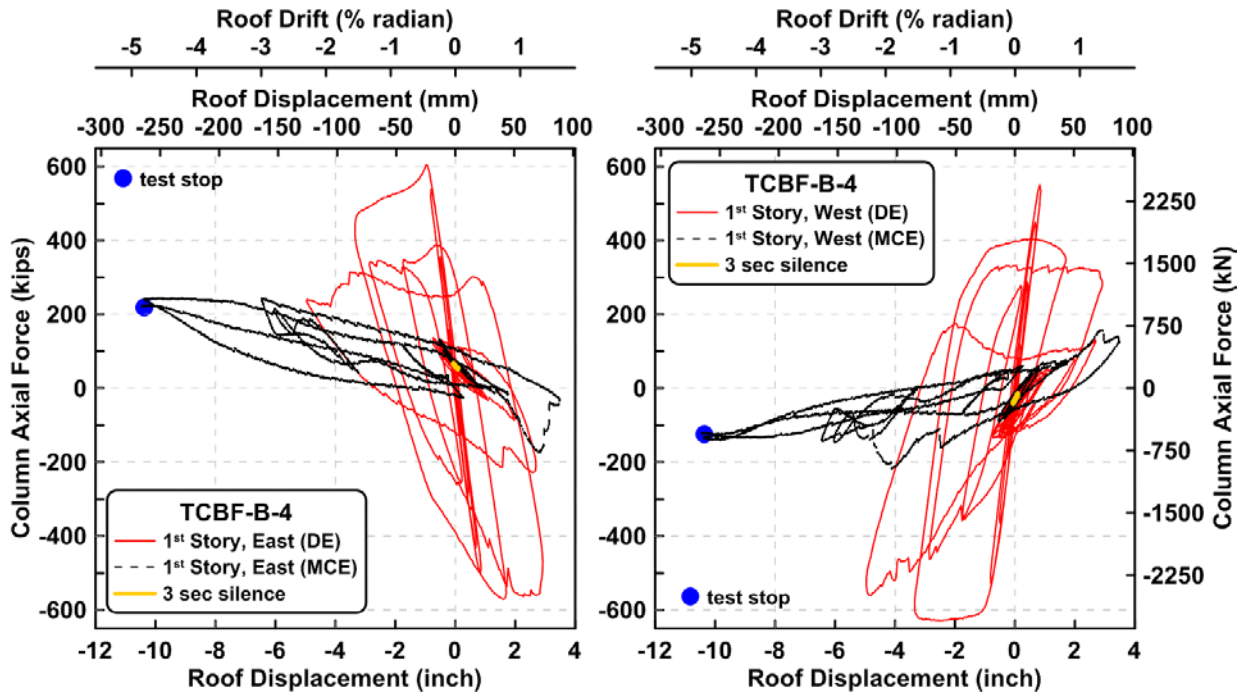


Figure 4.337 Roof displacement vs. first story column axial forces of TCBF-B-4 specimen

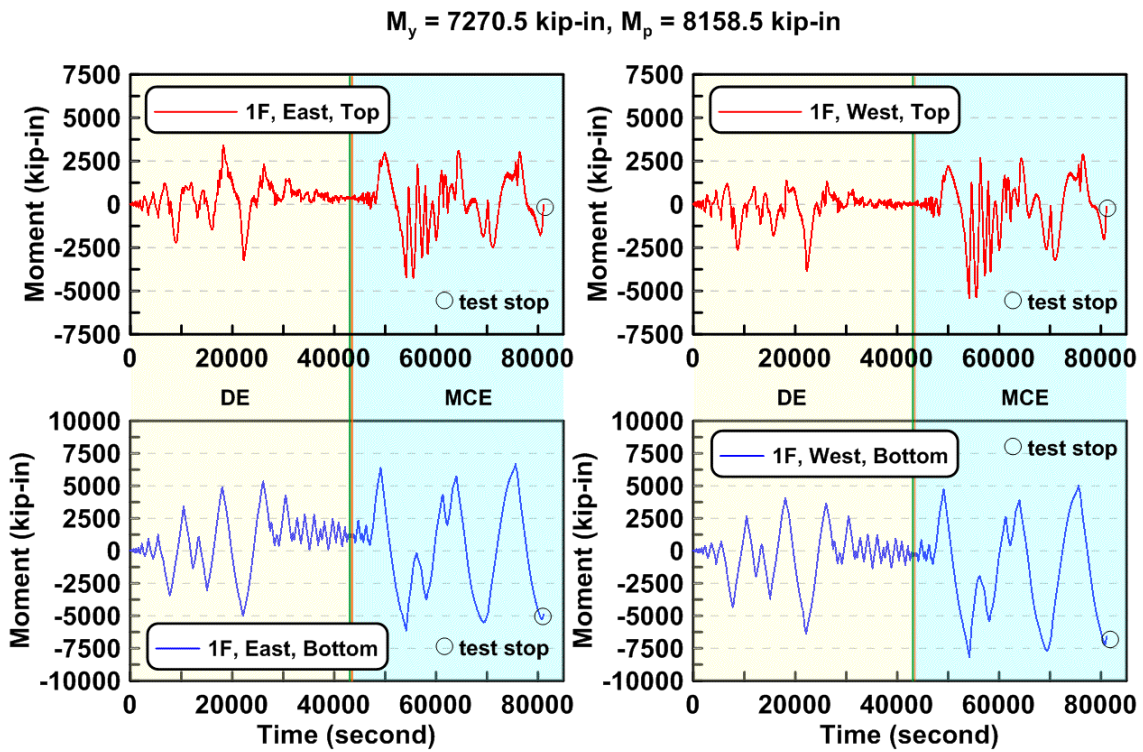


Figure 4.338 Time history of the first story column bending moments of TCBF-B-4 specimen (3-ft above column base plate and 3-ft below lower beam centerline)

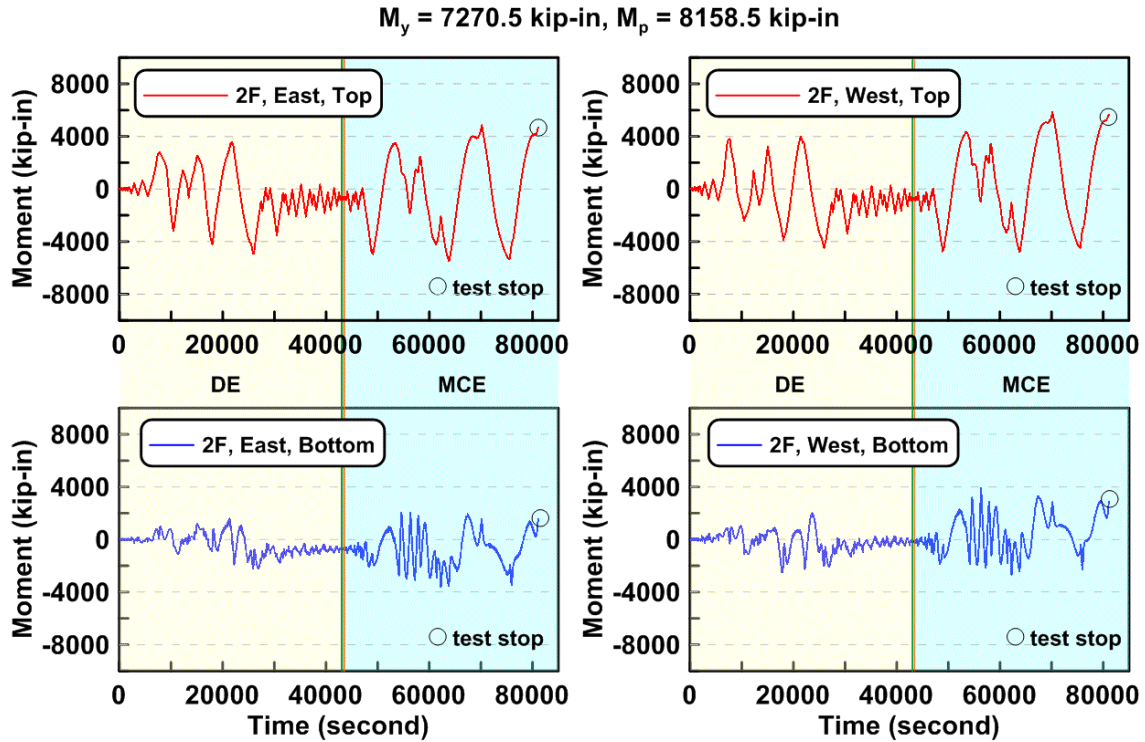


Figure 4.339 Time history of the second story column bending moments of TCBF-B-4 specimen (3-ft above lower beam centerline and 3-ft below roof beam centerline)

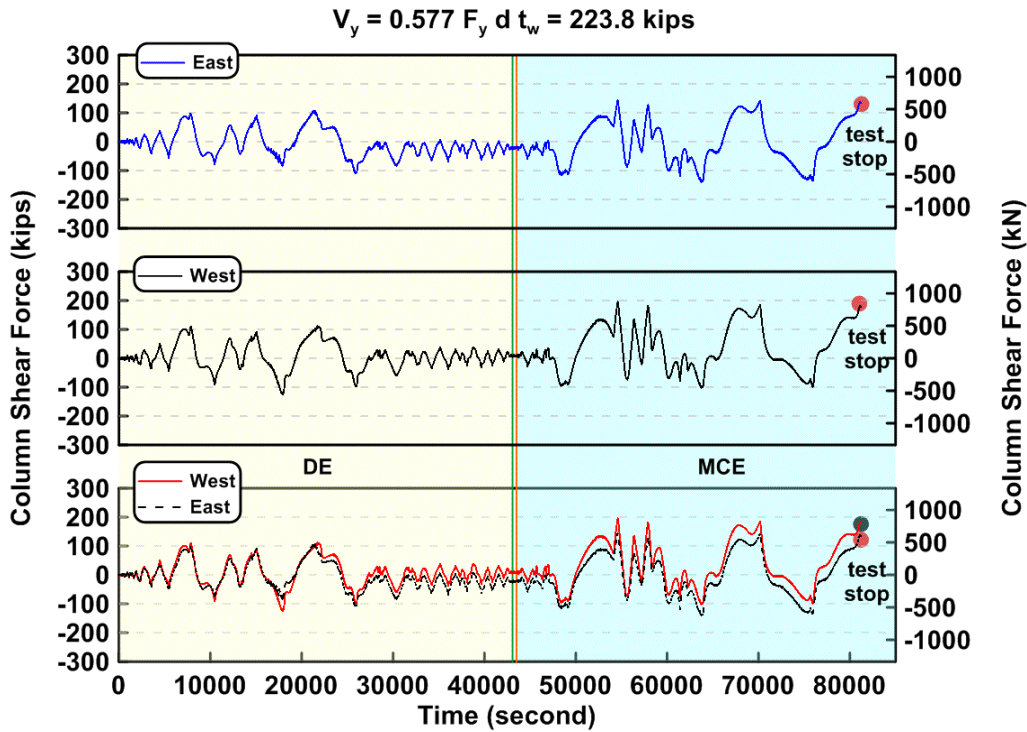


Figure 4.340 Time history of the first story column shear forces of TCBF-B-4 specimen

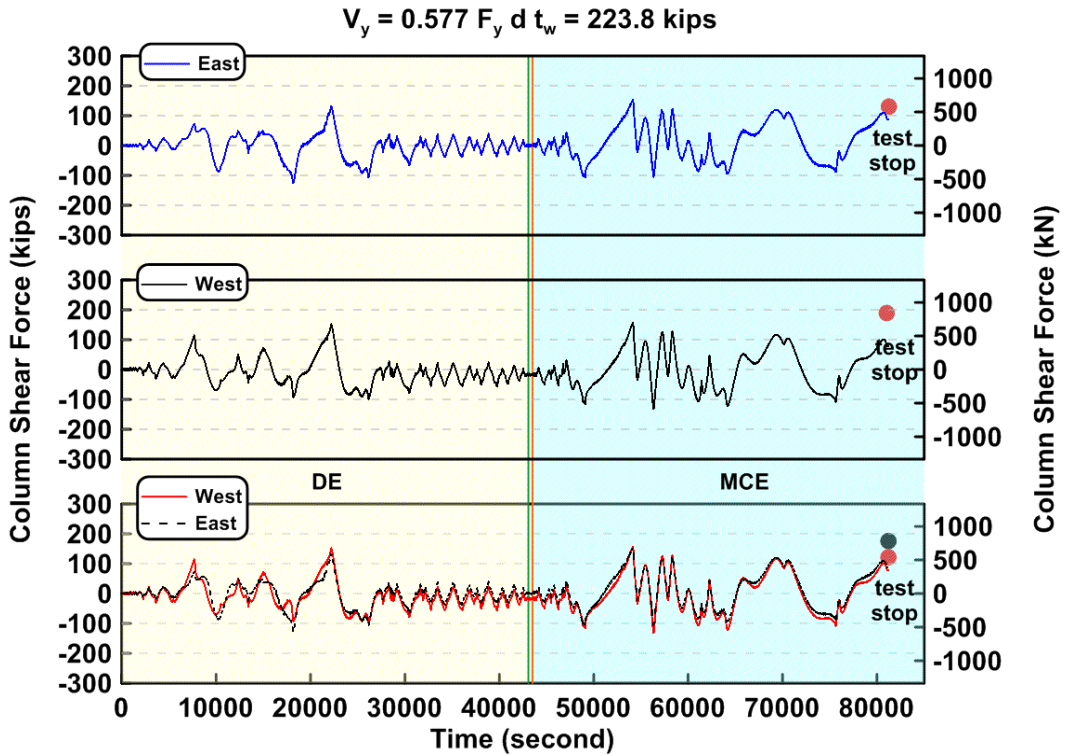


Figure 4.341 Time history of the second story column shear forces of TCBF-B-4 specimen

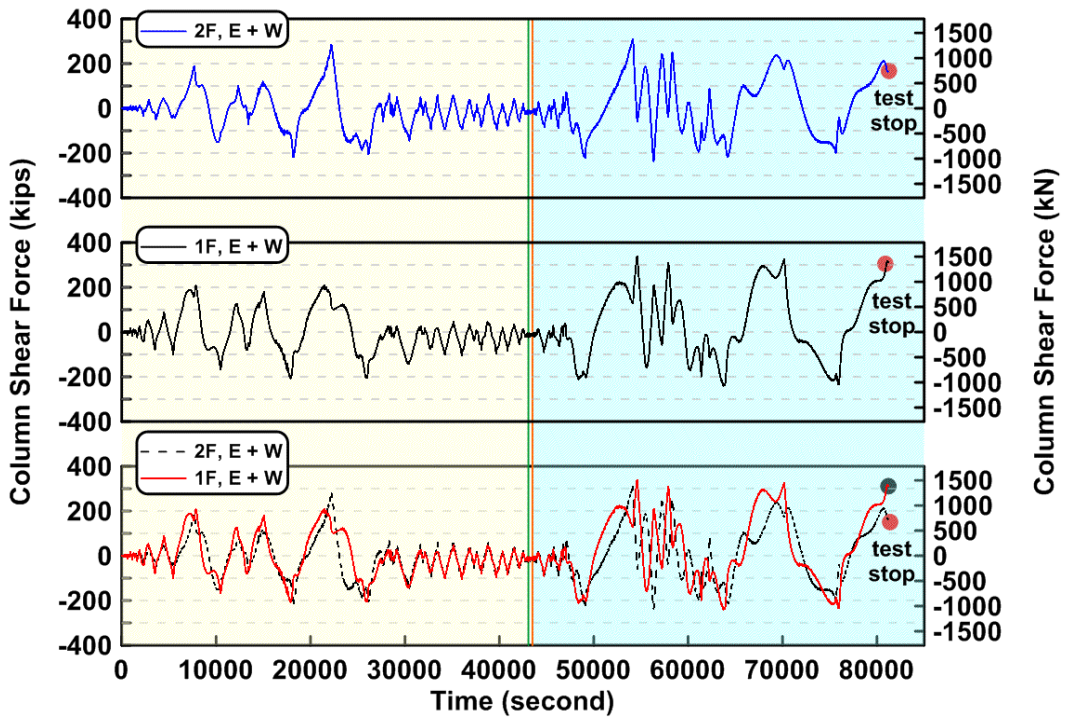


Figure 4.342 Time history of the sum of east and west column shear forces in both stories of TCBF-B-4 specimen

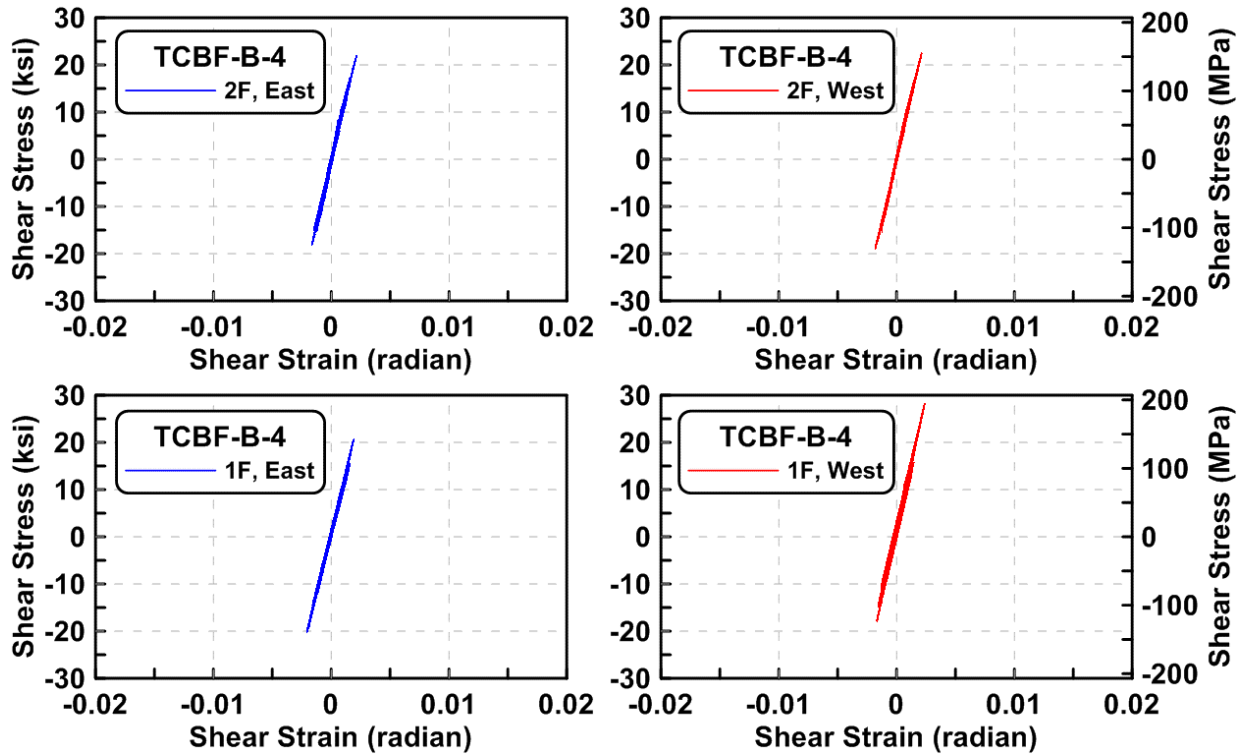


Figure 4.343 Column shear stress vs. shear strain relationships of TCBF-B-4 specimen (locations: EC1-B-N, EC2-B-N, WC1-B-N and WC2-B-N)

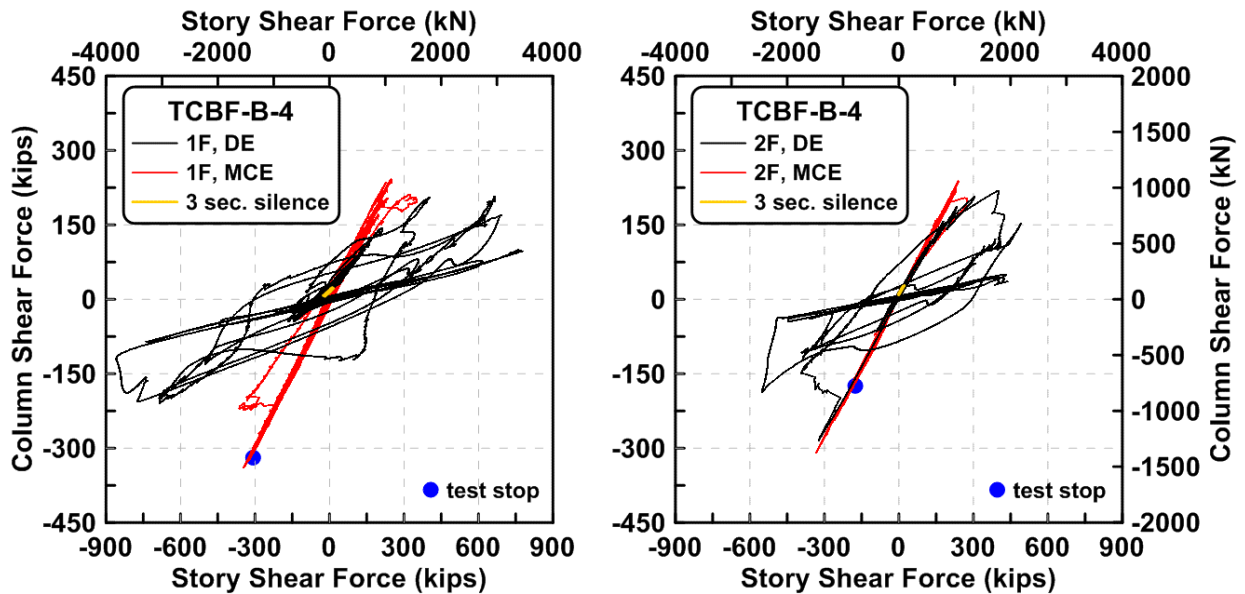


Figure 4.344 Story shear component from columns vs. total story shear forces of TCBF-B-4 specimen

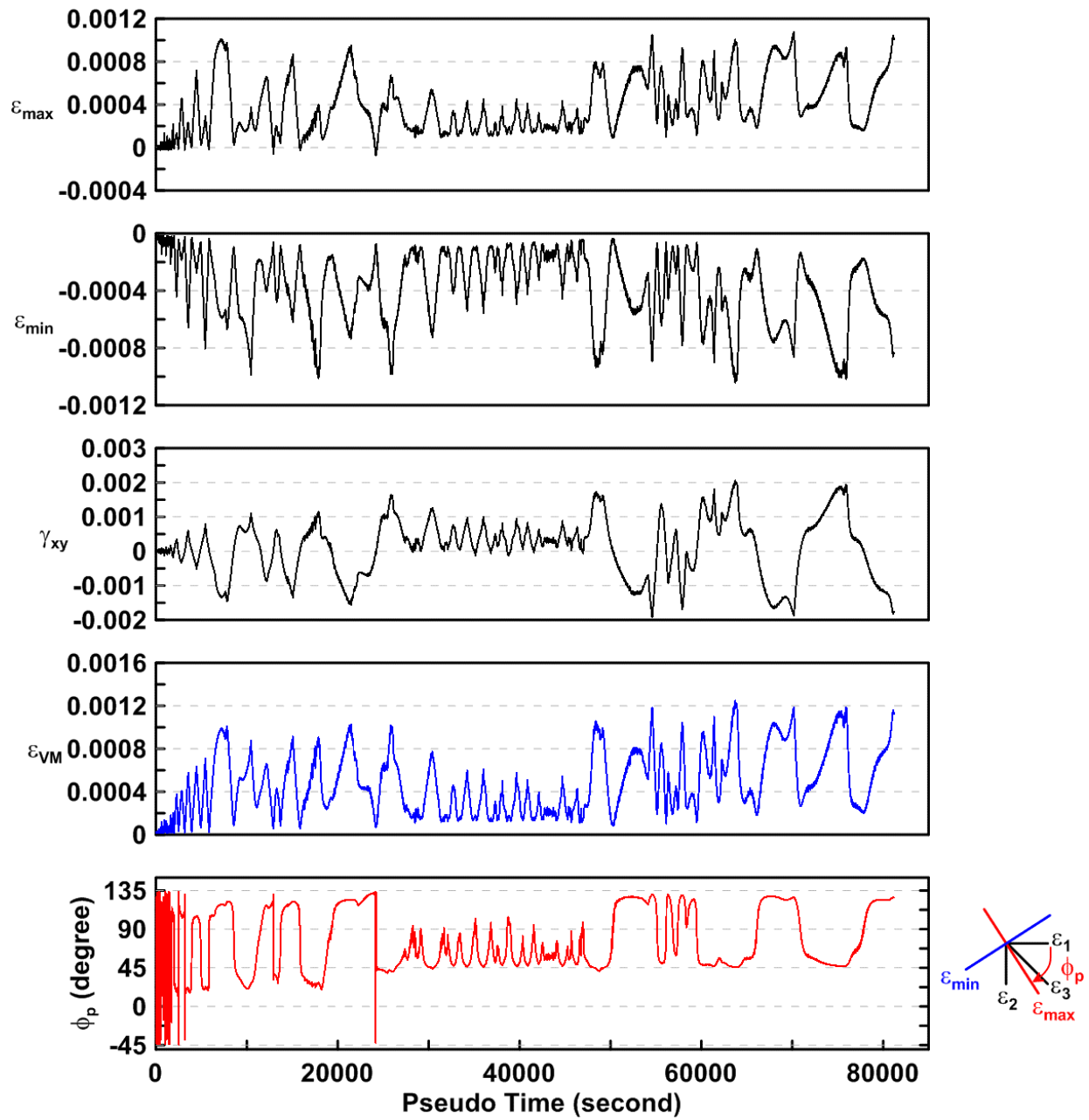


Figure 4.345 Time history of rosette type strain gauge readings in the first story column web of TCBF-B-4 specimen (location: R1)

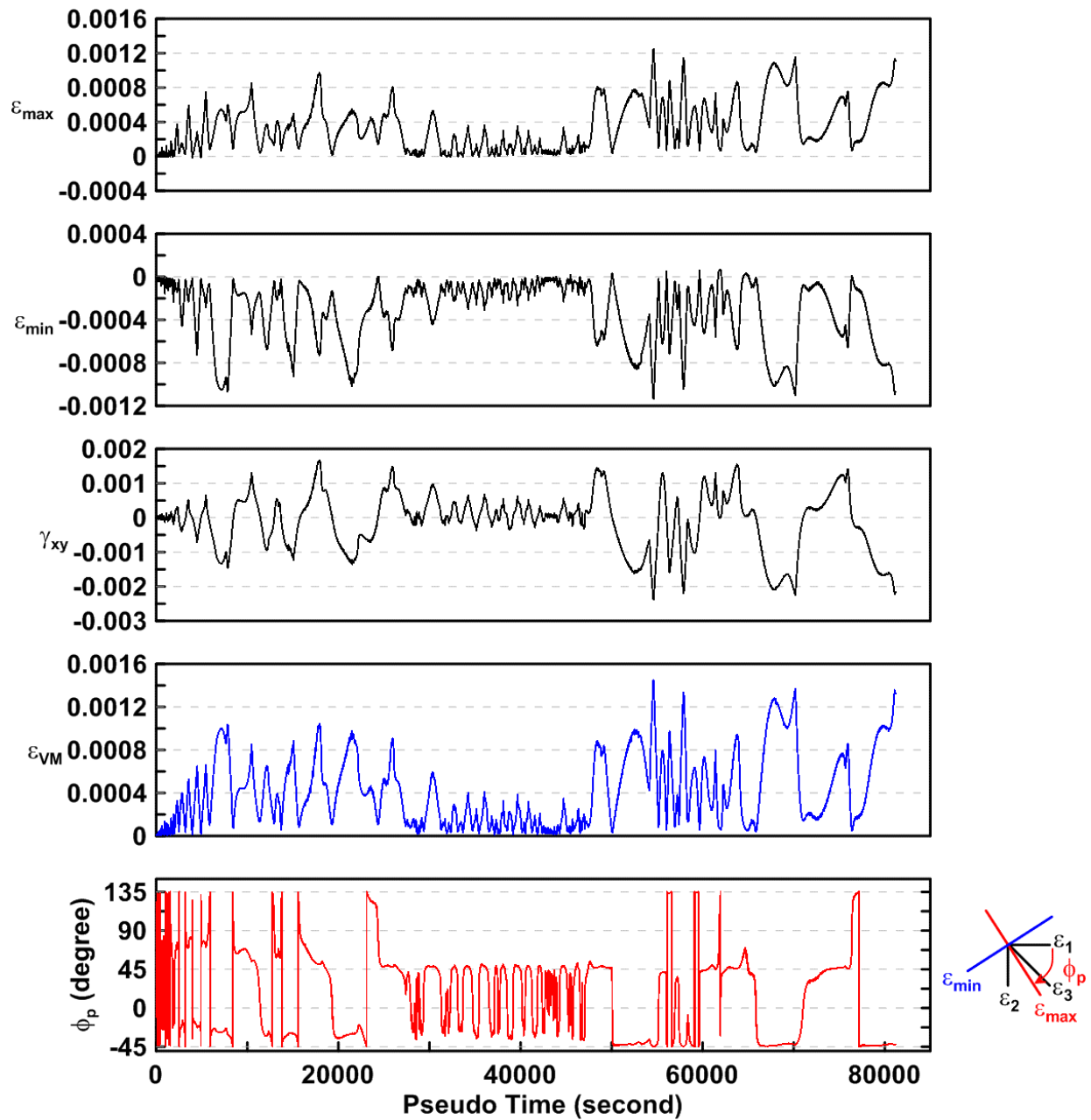


Figure 4.346 Time history of rosette type strain gauge readings in the first story column web of TCBF-B-4 specimen (location: R5)



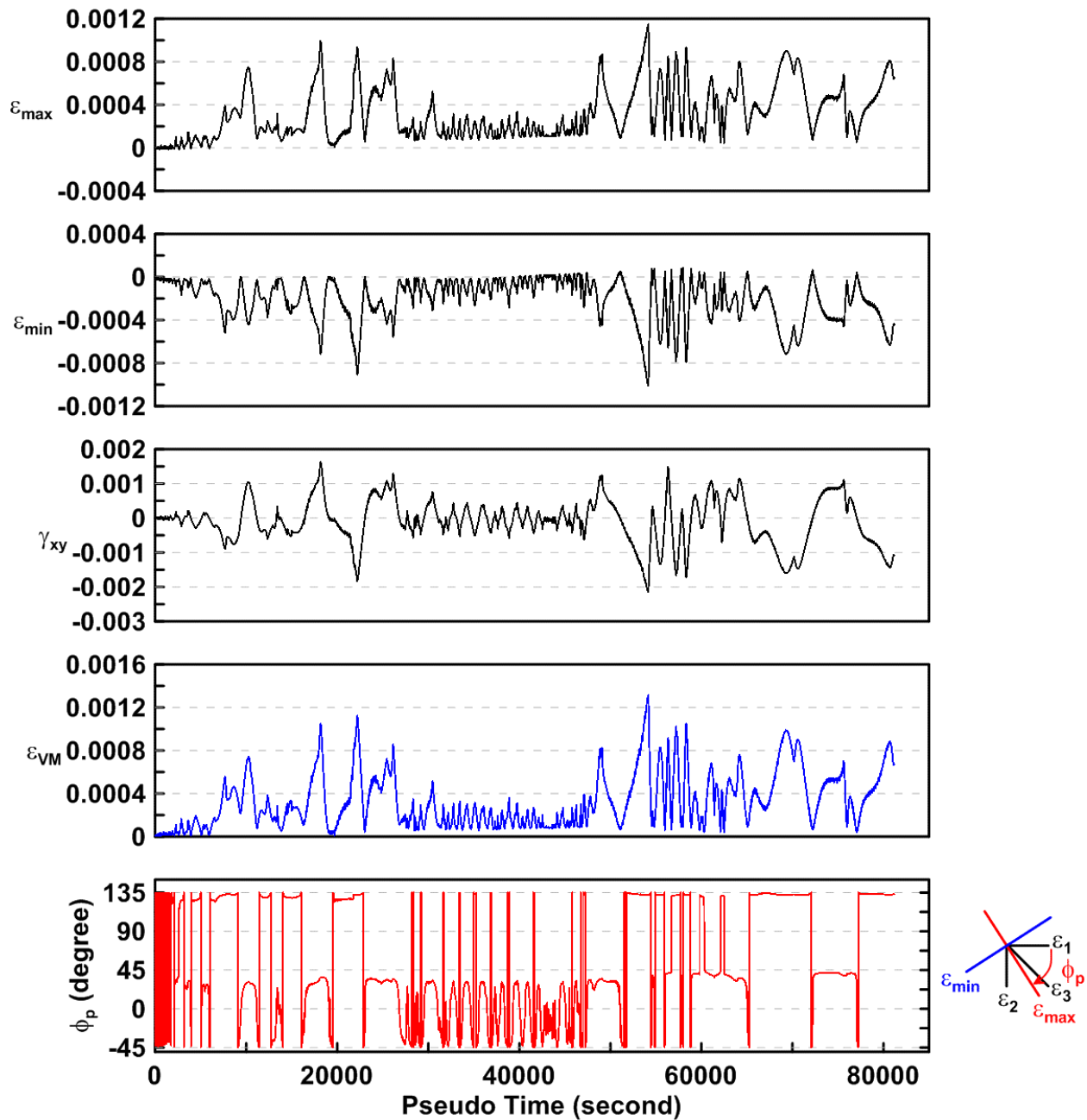


Figure 4.347 Time history of rosette type strain gauge readings in the first story column web of TCBF-B-4 specimen (location: R3)

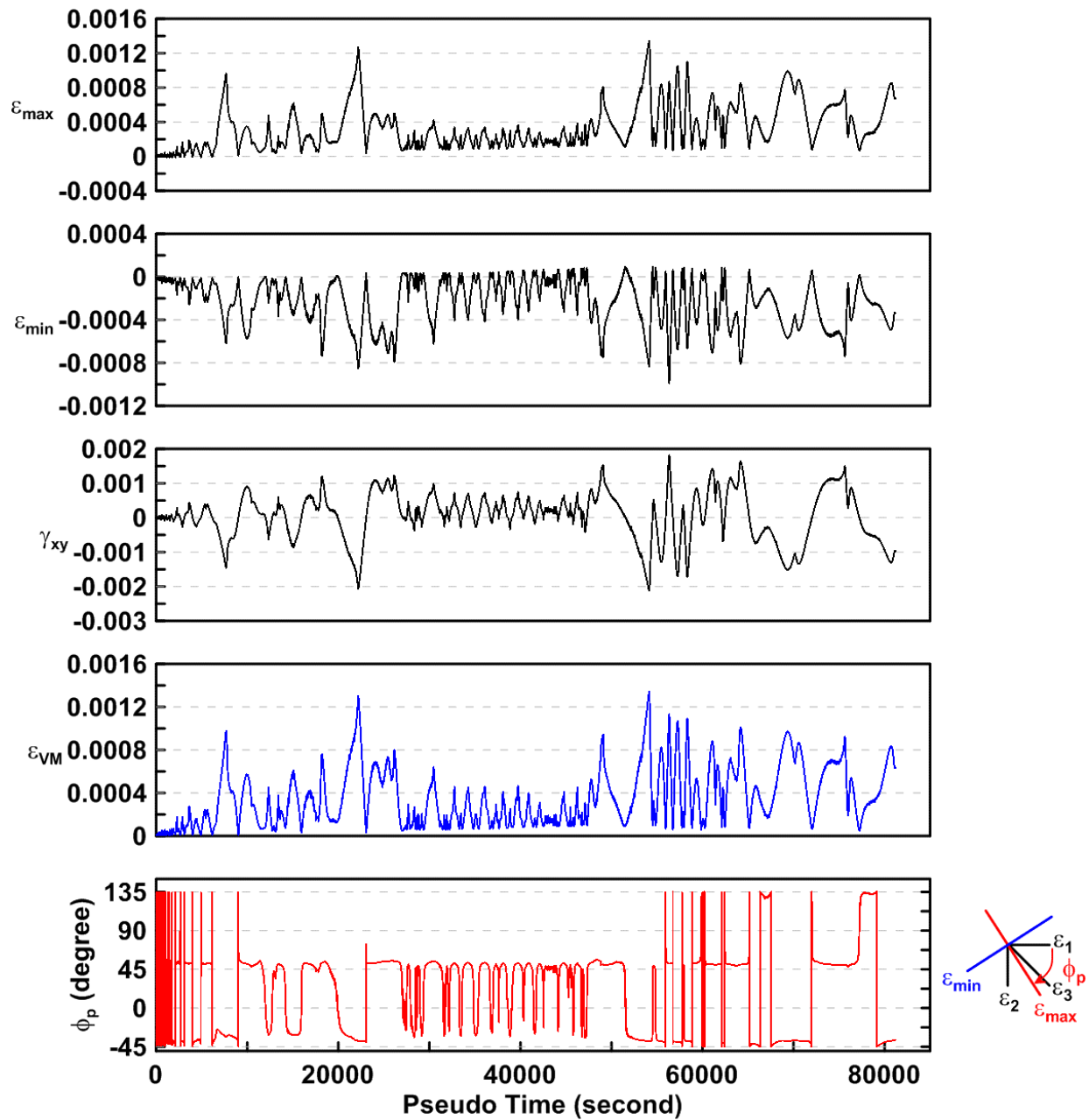


Figure 4.348 Time history of rosette type strain gauge readings in the first story column web of TCBF-B-4 specimen (location: R7)

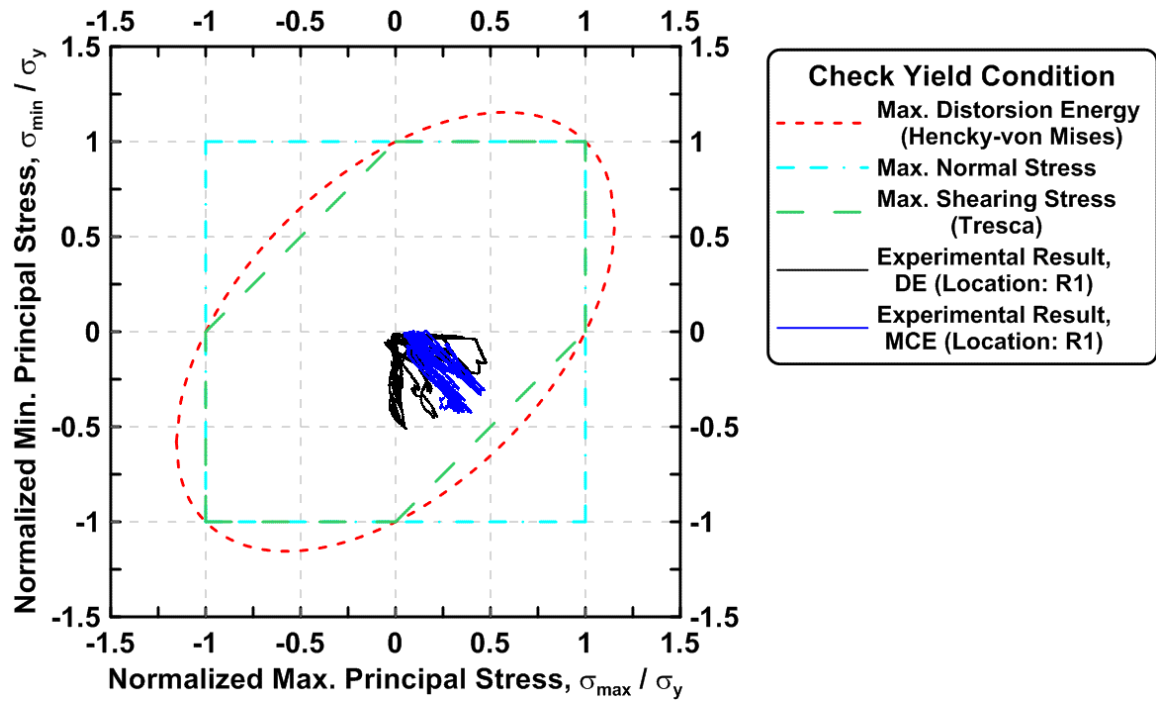


Figure 4.349 Maximum principal stress vs. minimum principal stress in the first story column of TCBF-B-4 specimen (location: R1)

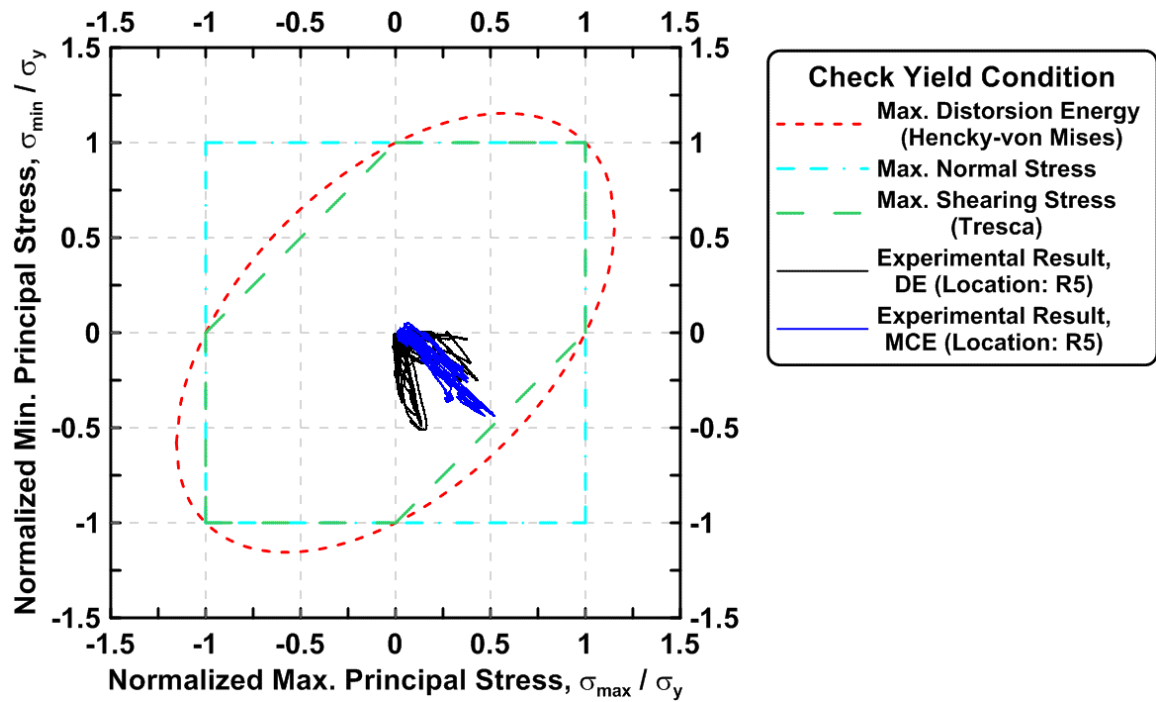


Figure 4.350 Maximum principal stress vs. minimum principal stress in the first story column of TCBF-B-4 specimen (location: R5)

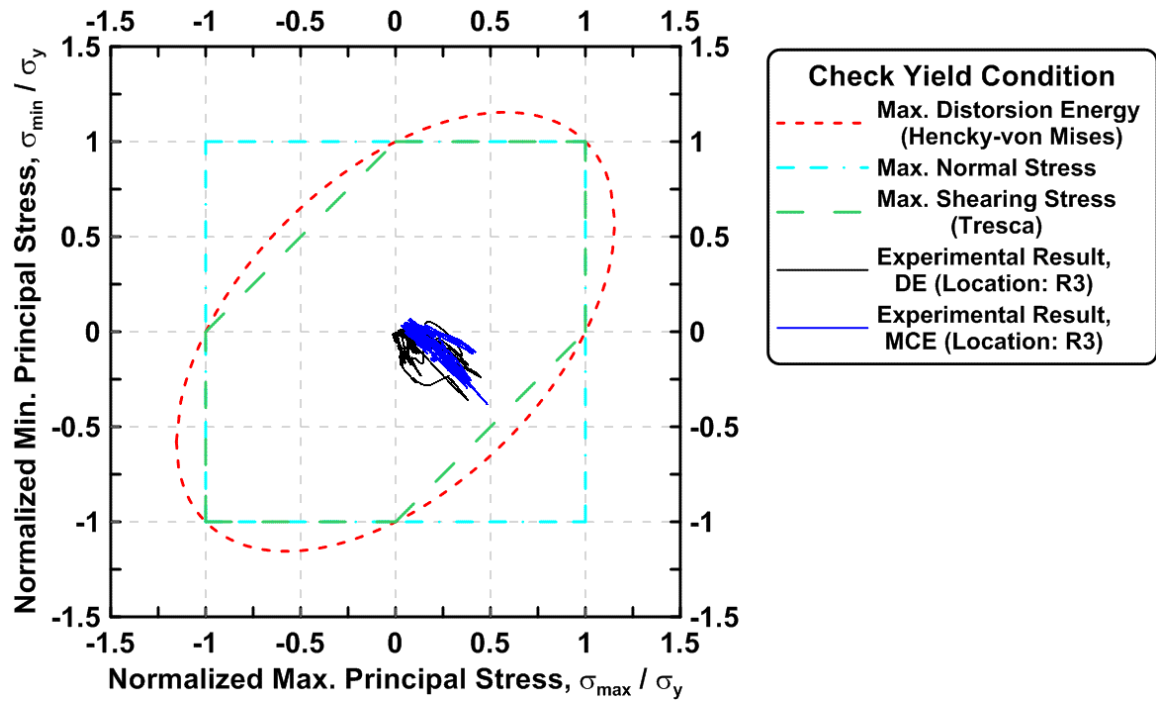


Figure 4.351 Maximum principal stress vs. minimum principal stress in the first story column of TCBF-B-4 specimen (location: R3)

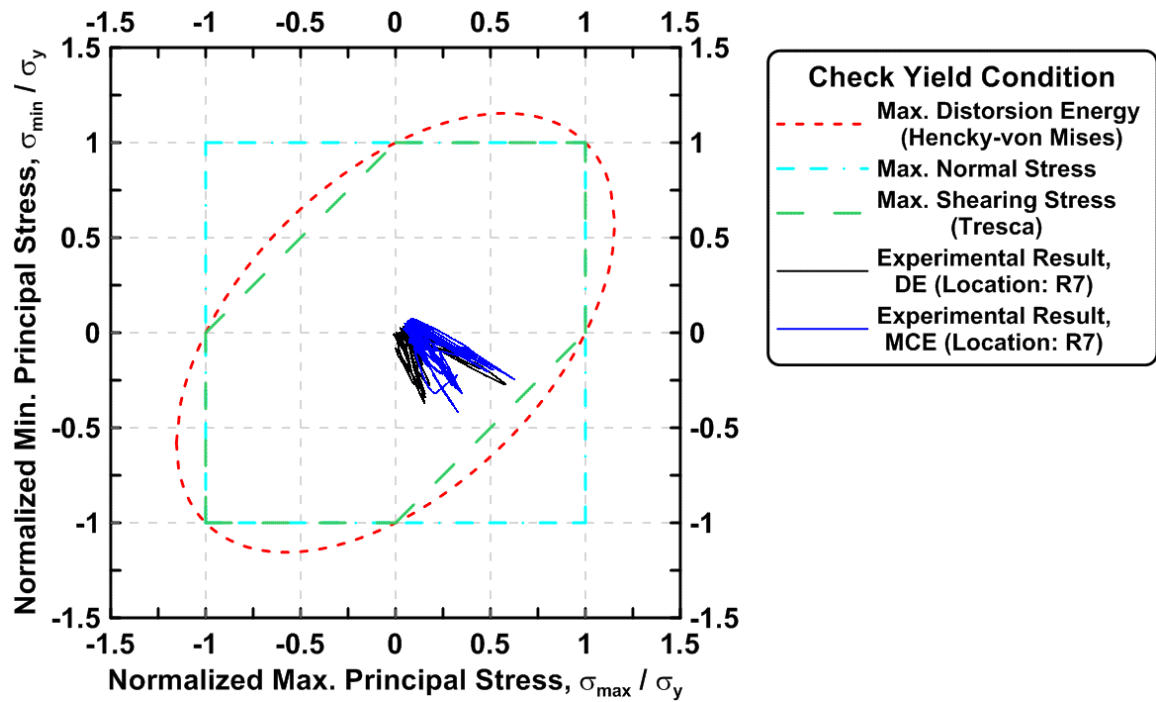


Figure 4.352 Maximum principal stress vs. minimum principal stress in the first story column of TCBF-B-4 specimen (location: R7)

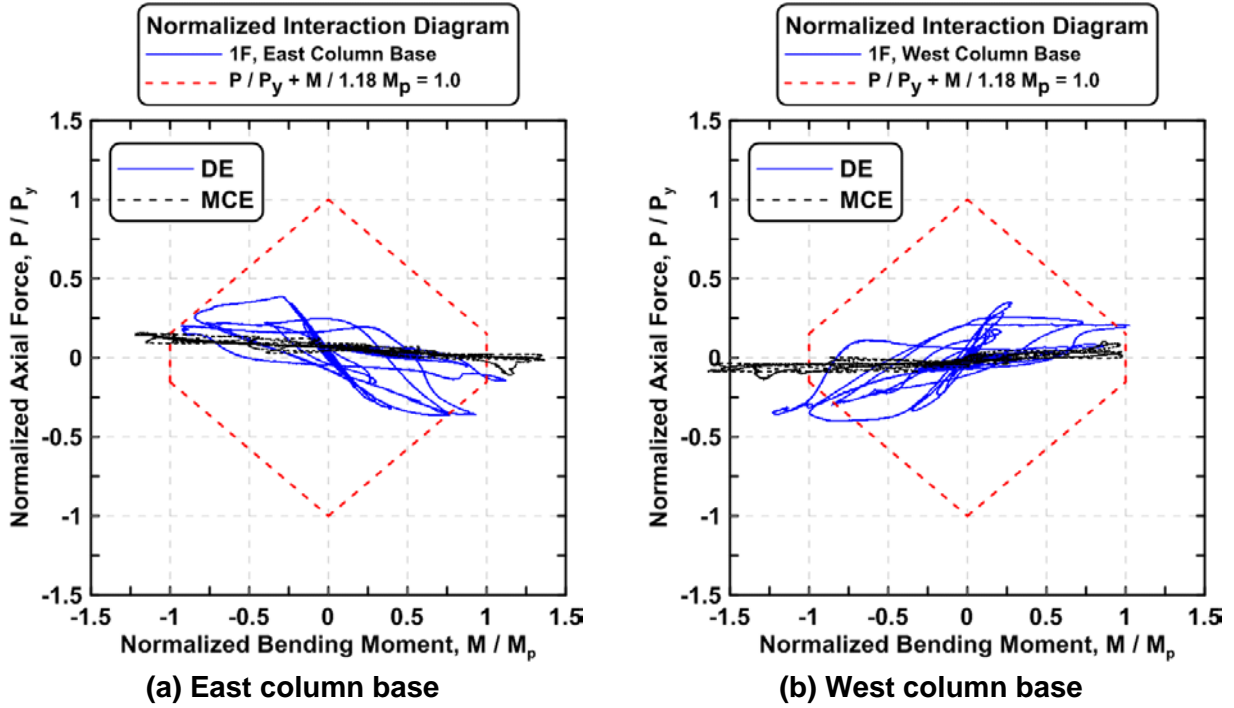


Figure 4.353 Normalized P-M interaction diagrams of the first story columns of TCBF-B-4 specimen

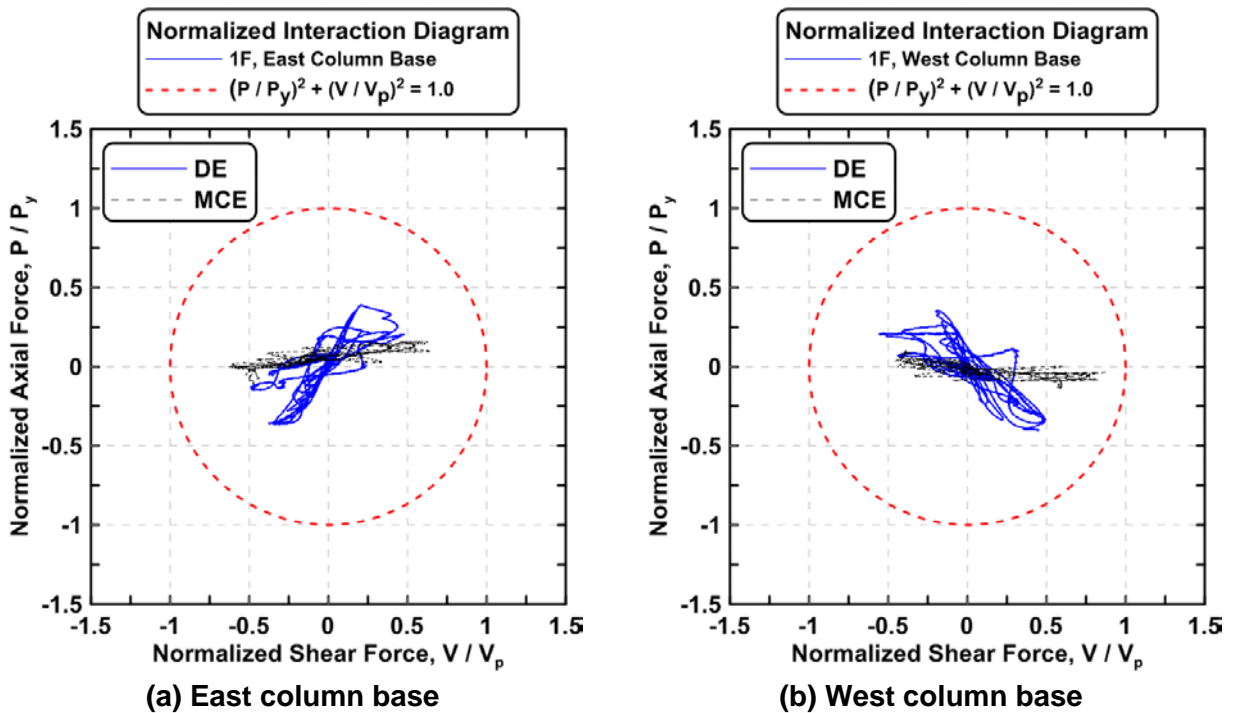


Figure 4.354 Normalized P-V interaction diagrams of the first story columns of TCBF-B-4 specimen

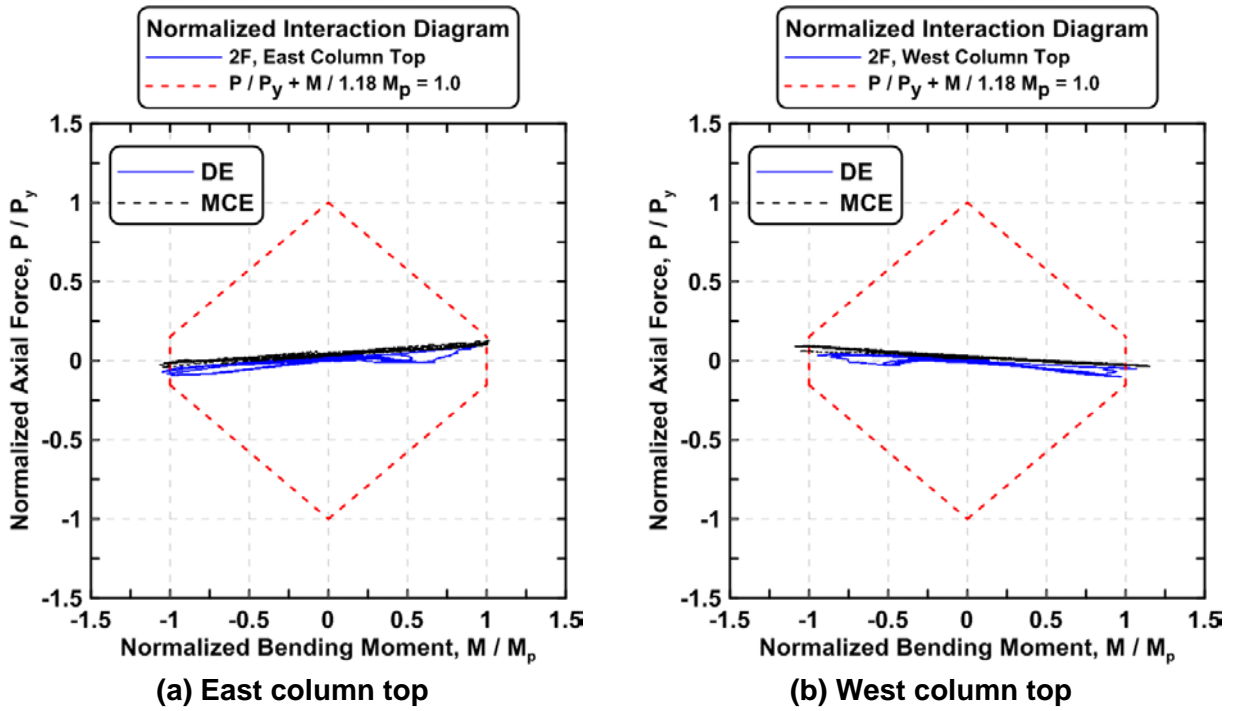


Figure 4.355 Normalized P-M interaction diagrams of the second story columns of TCBF-B-4 specimen

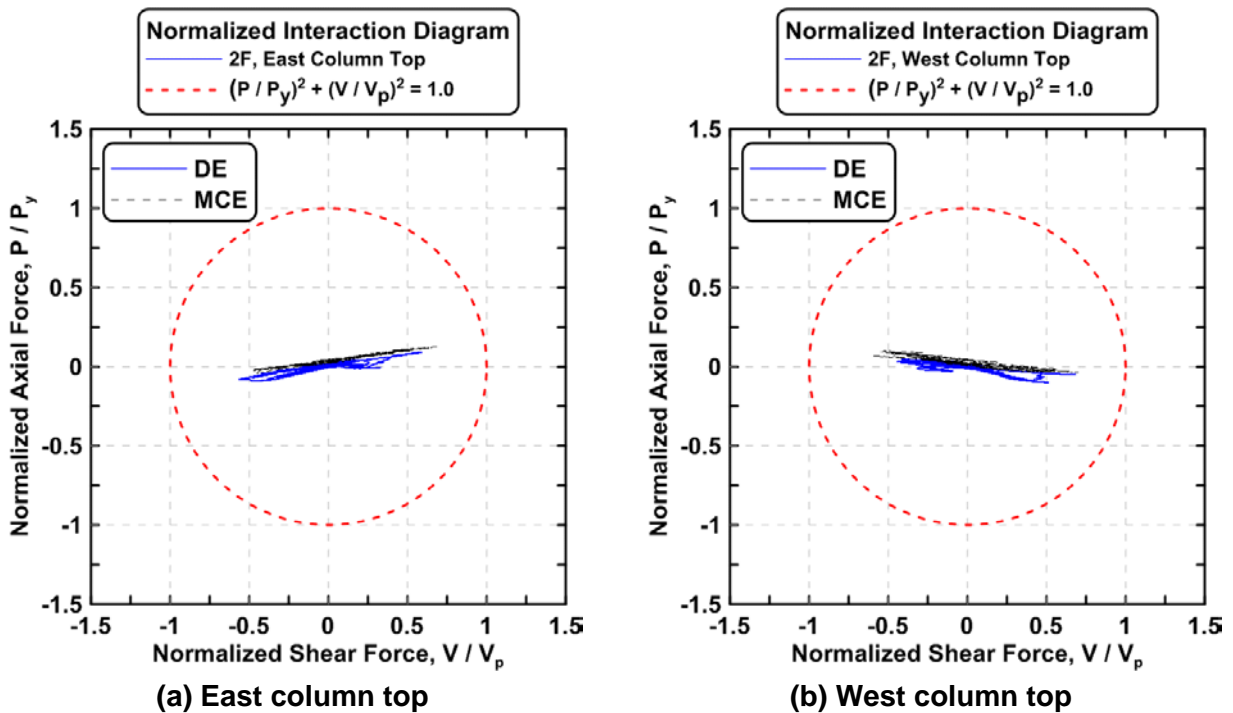


Figure 4.356 Normalized P-V interaction diagrams of the second story columns of TCBF-B-4 specimen

### 4.3.1.3 Beam Response

The vertical deflection time history at the center of W24 × 117 roof beam and W24 × 68 lower beam is plotted in Fig. 4.357. Figures 4.358 and 4.359 show the time history of strain readings at both ends of roof beam and lower beam, respectively. Both beam axial force time histories derived from linear type strain gauges at different locations of the beams are plotted in Figs. 4.360 and 4.361. The bending moment time histories of both beams are shown in Figs. 4.362 and 4.363. Estimated beam shear force time histories are illustrated in Figs. 4.364 and 4.365. The unbalanced force in the roof beam center is plotted in Fig. 4.366.

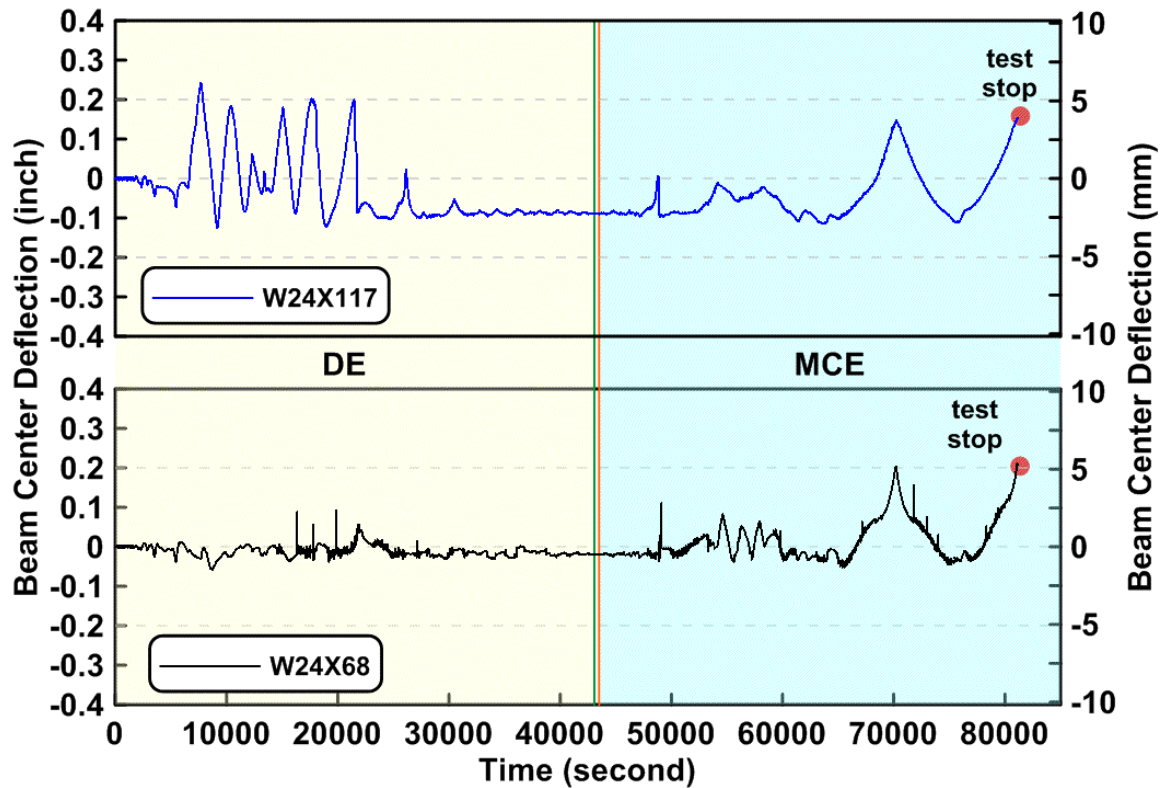
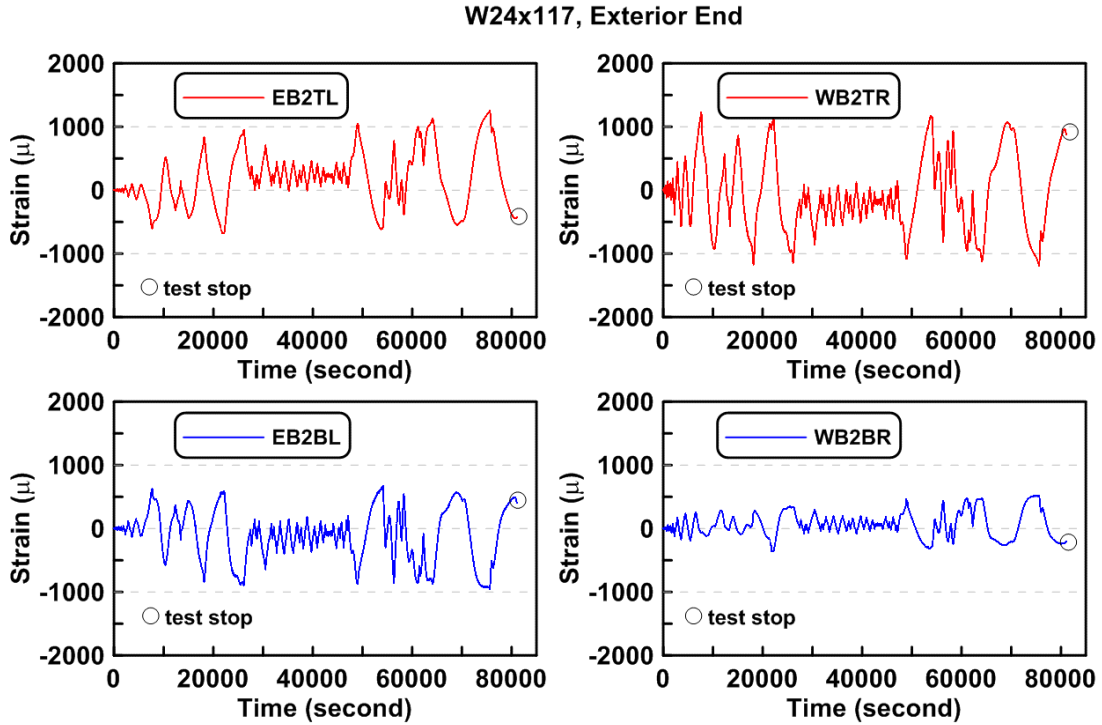
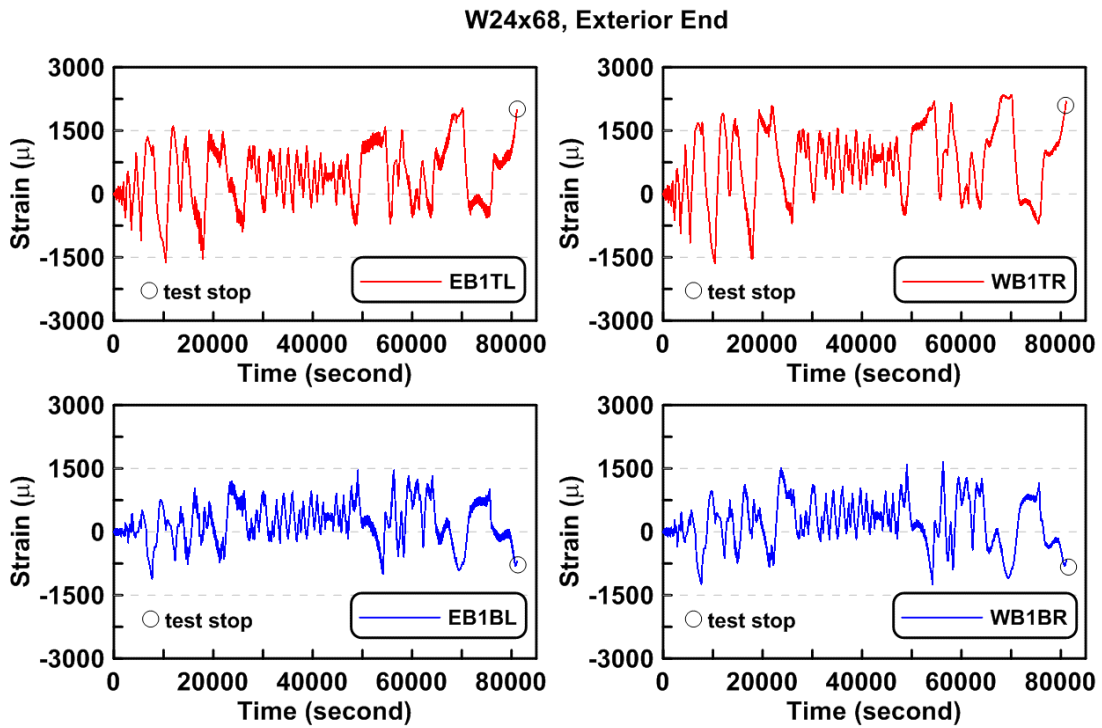


Figure 4.357 The deflection time history at the center of beam span of TCBF-B-4 specimen (roof beam: W24 × 117, lower beam: W24 × 68)



**Figure. 4.358** Time history of strain readings at both exterior ends of W24 × 117 roof beam of TCBF-B-4 specimen



**Figure. 4.359** Time history of strain readings at both exterior ends of W24 × 68 lower beam of TCBF-B-4 specimen



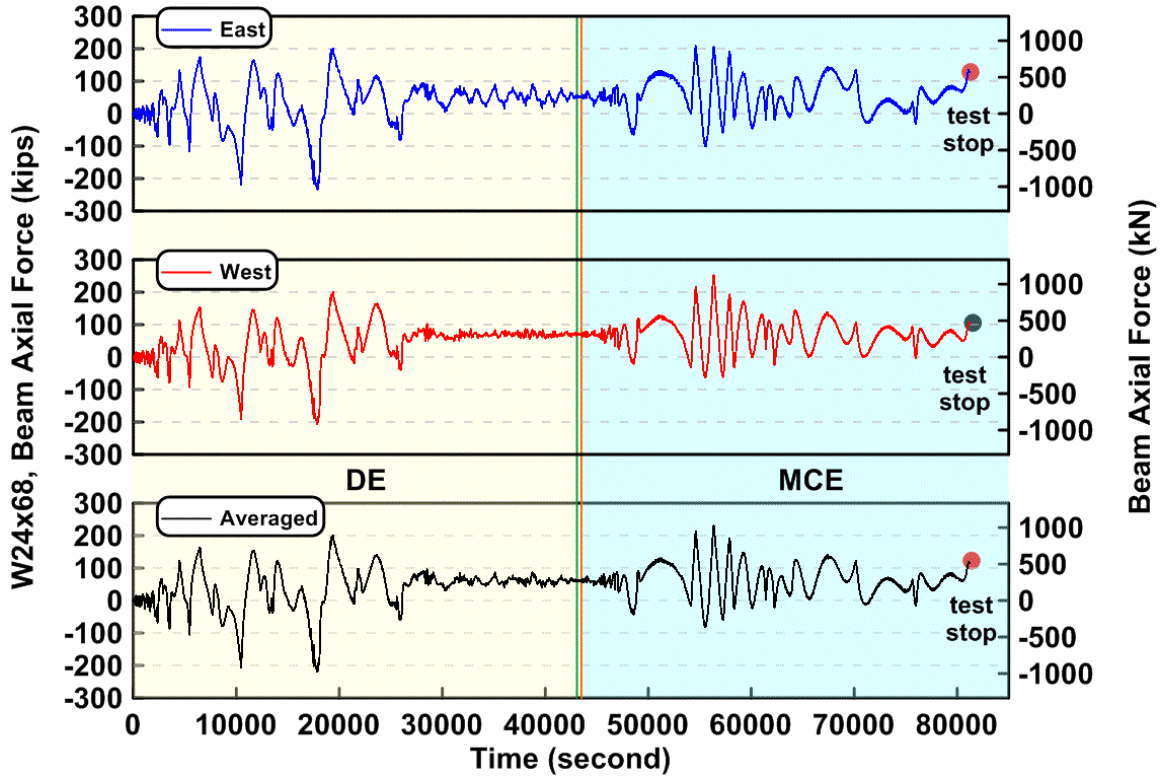


Figure 4.360 Time history of lower beam axial forces of TCBF-B-4 specimen

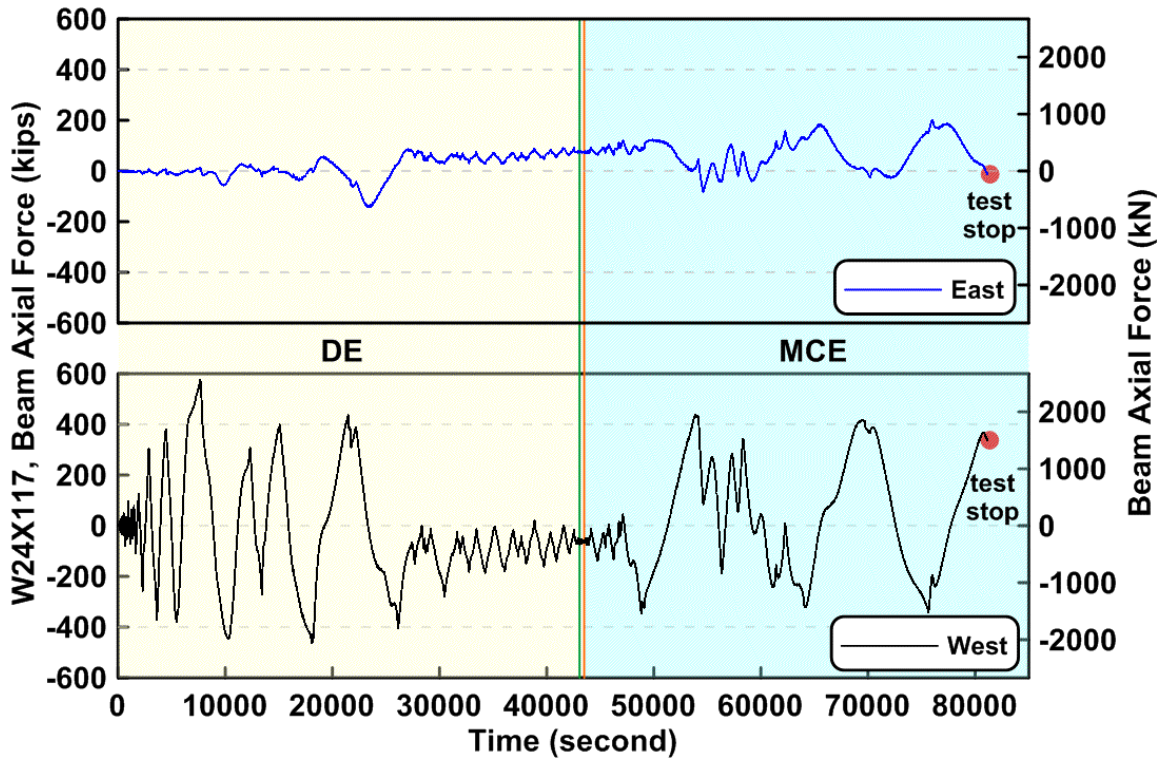


Figure 4.361 Time history of the roof beam axial forces of TCBF-B-4 specimen

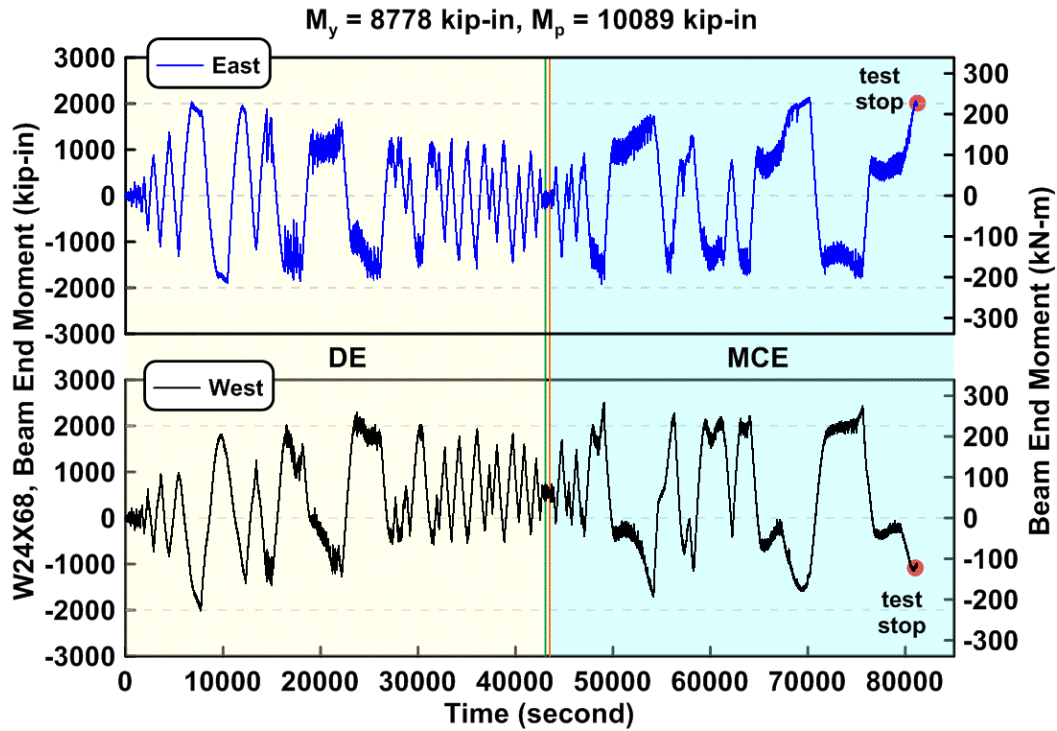


Figure 4.362 Time history of the lower beam end bending moment of TCBF-B-4 specimen

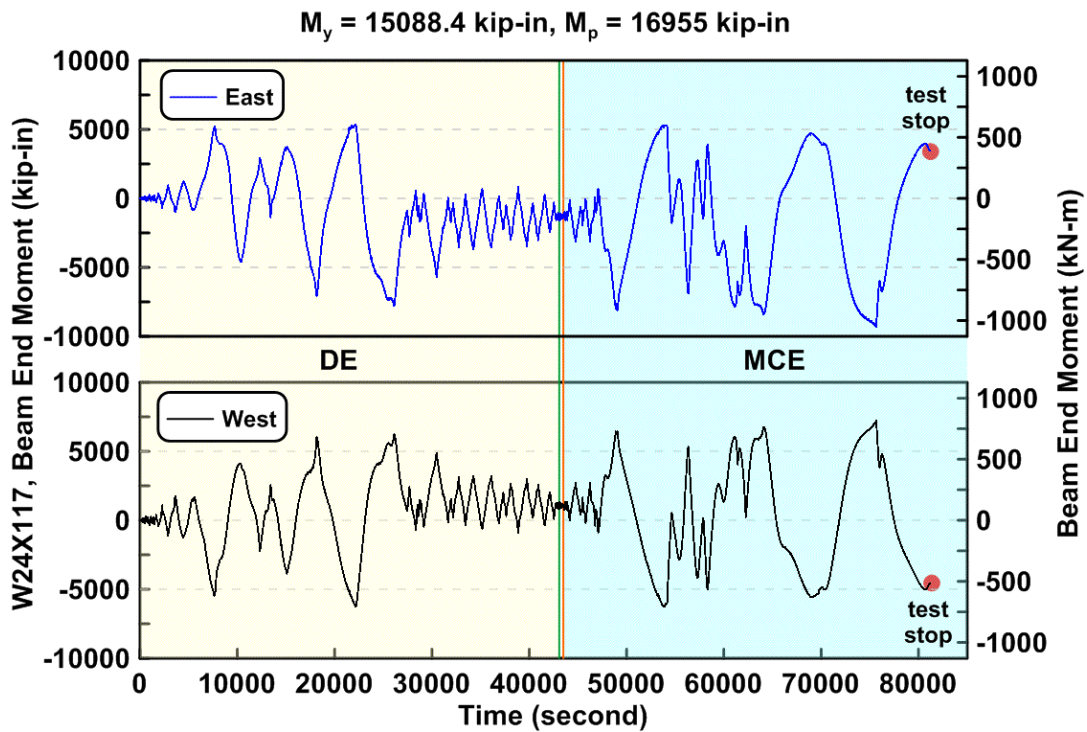


Figure 4.363 Time history of the roof beam end bending moment of TCBF-B-4 specimen

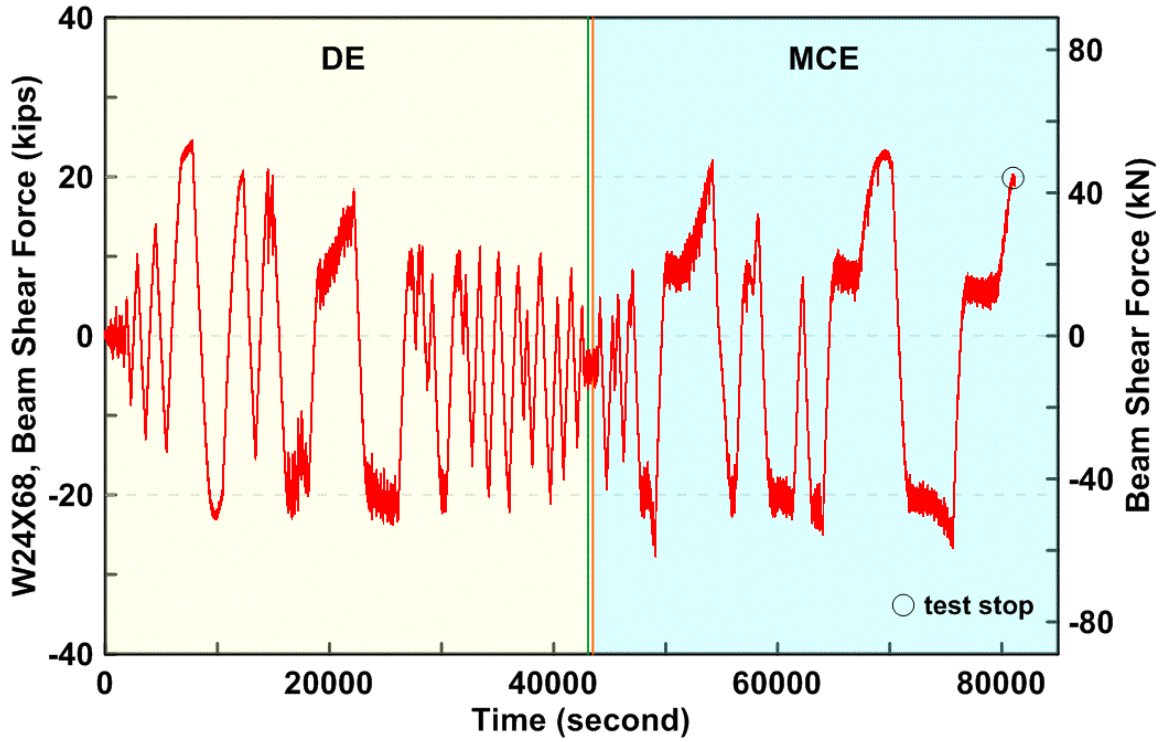


Figure 4.364 Lower beam estimated shear force time history of TCBF-B-4 specimen

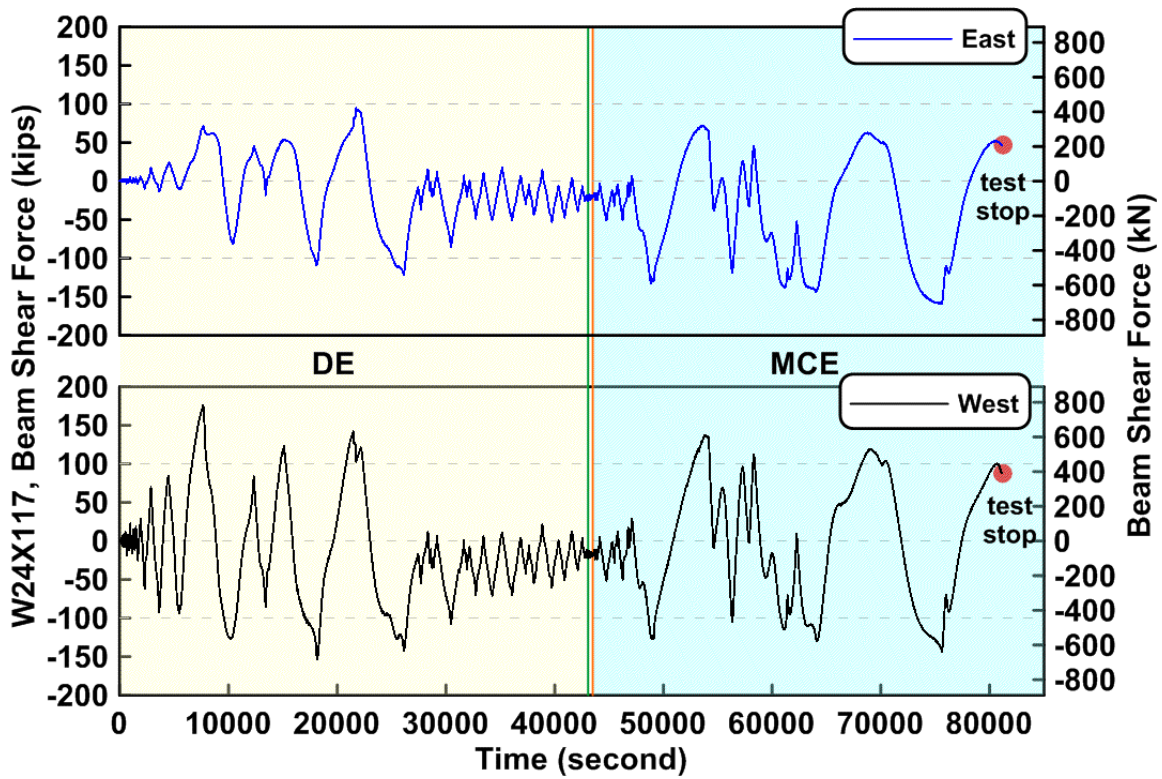


Figure 4.365 Roof beam estimated shear force time history of TCBF-B-4 specimen

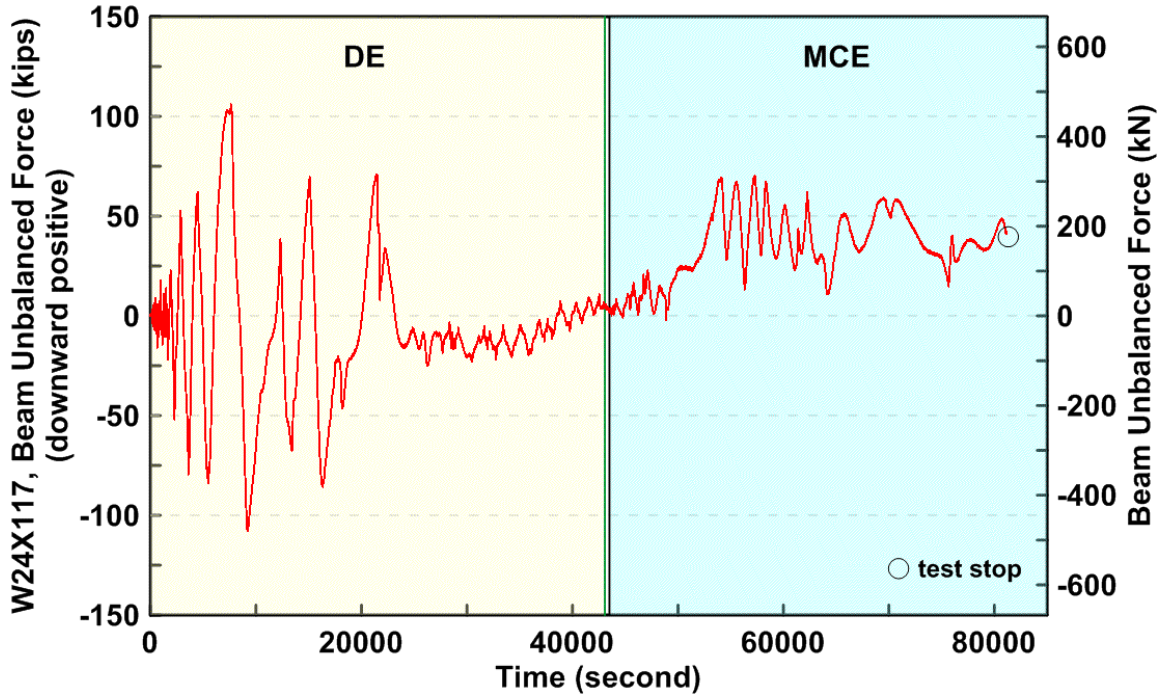


Figure 4.366 Estimated unbalanced force time history of TCBF-B-4 specimen roof beam

#### 4.3.1.4 Brace Response

The estimated brace axial forces versus brace axial deformations for each square HSS brace are shown in Fig. 4.367. The estimated brace axial forces versus measured brace out-of-plane displacements at the brace center point for each square HSS brace are shown in Fig. 4.368. Combined brace axial force, axial deformation, and out-of-plane displacement relationships are shown in Fig. 4.369. The decomposed strain (axial strain, in-plane bending strain, out-of-plane bending strain, and warping strain; definition of strain components are shown in Fig. 4.47(b)) time histories of each brace are plotted in Figs. 4.370 to 4.373.

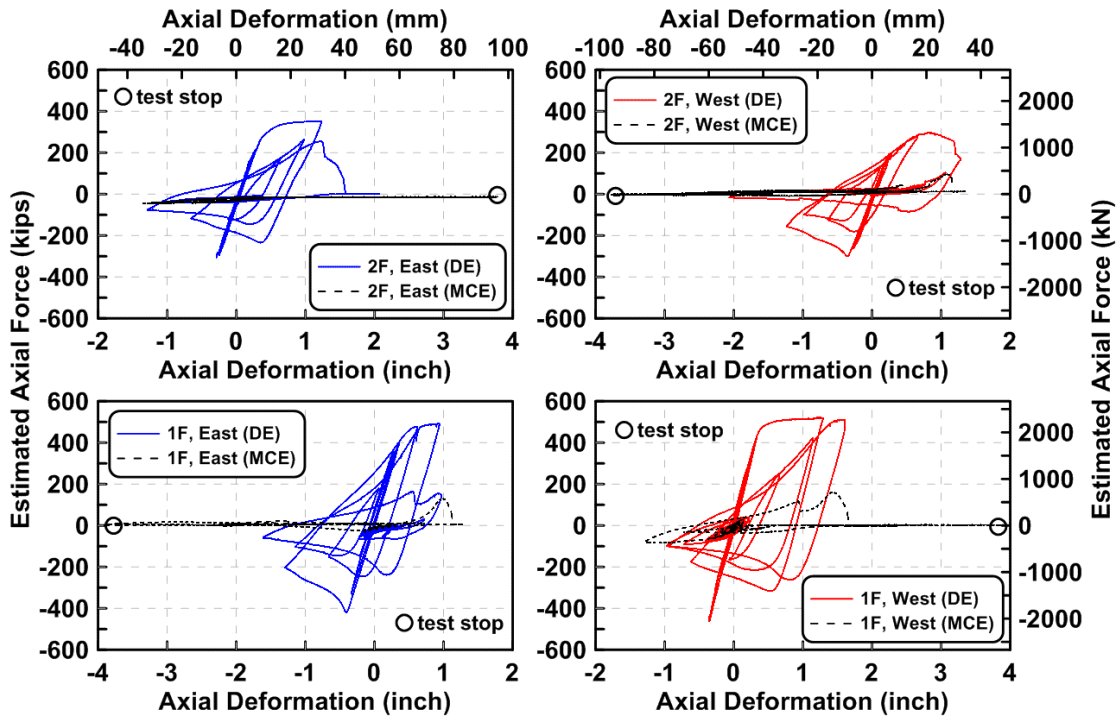


Figure 4.367 Estimated brace axial forces versus brace axial deformations of TCBF-B-4 specimen

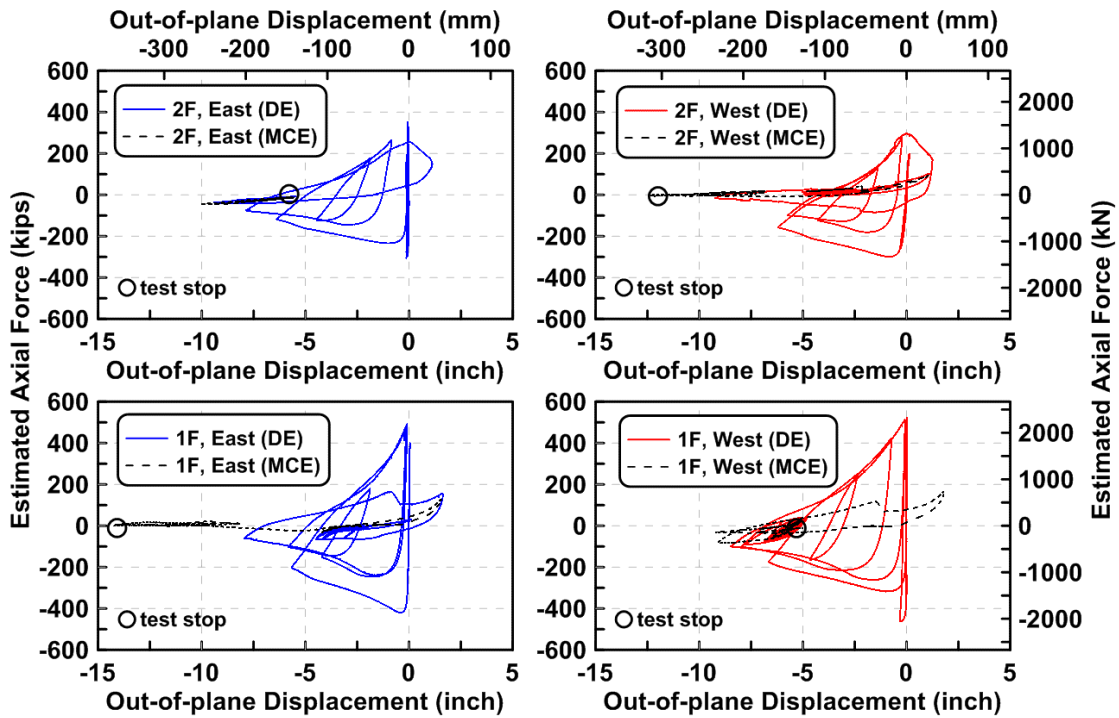


Figure 4.368 Estimated brace axial forces versus measured brace out-of-plane displacements at the brace center point of each HSS brace of TCBF-B-4 specimen

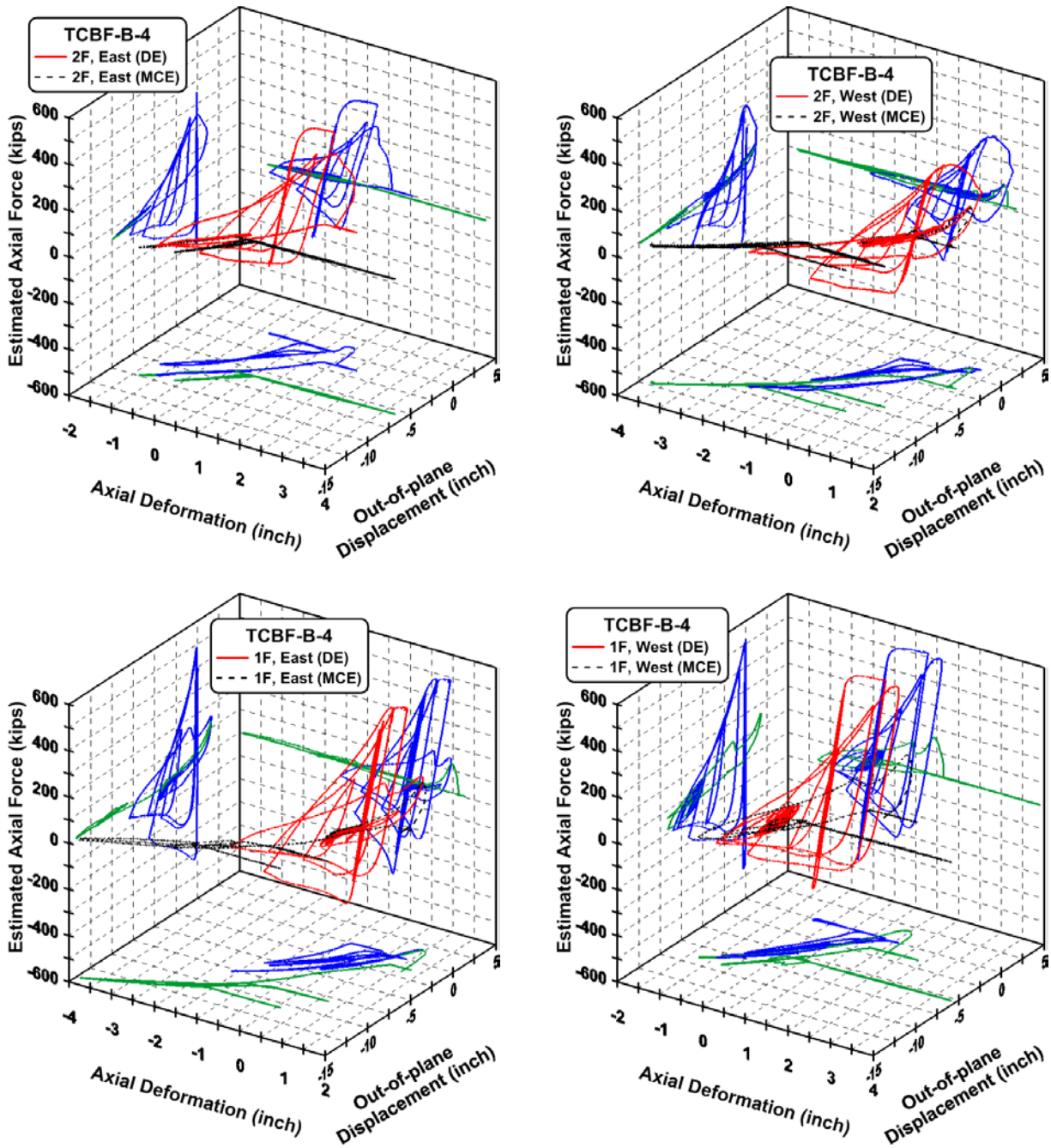


Figure 4.369 Estimated brace axial force, brace axial deformation and measured brace out-of-plane displacement relationships of TCBF-B-4 specimen

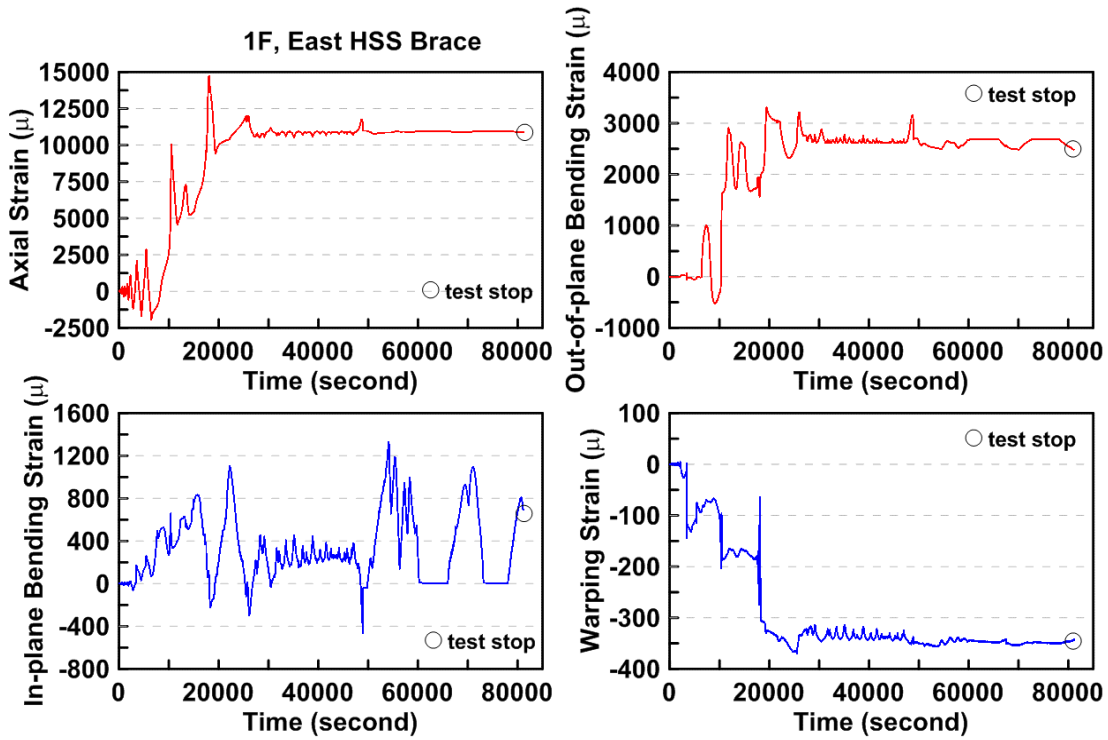


Figure 4.370 Time history of the decomposed strain components of eastern side HSS brace in the first story of TCBF-B-4 specimen

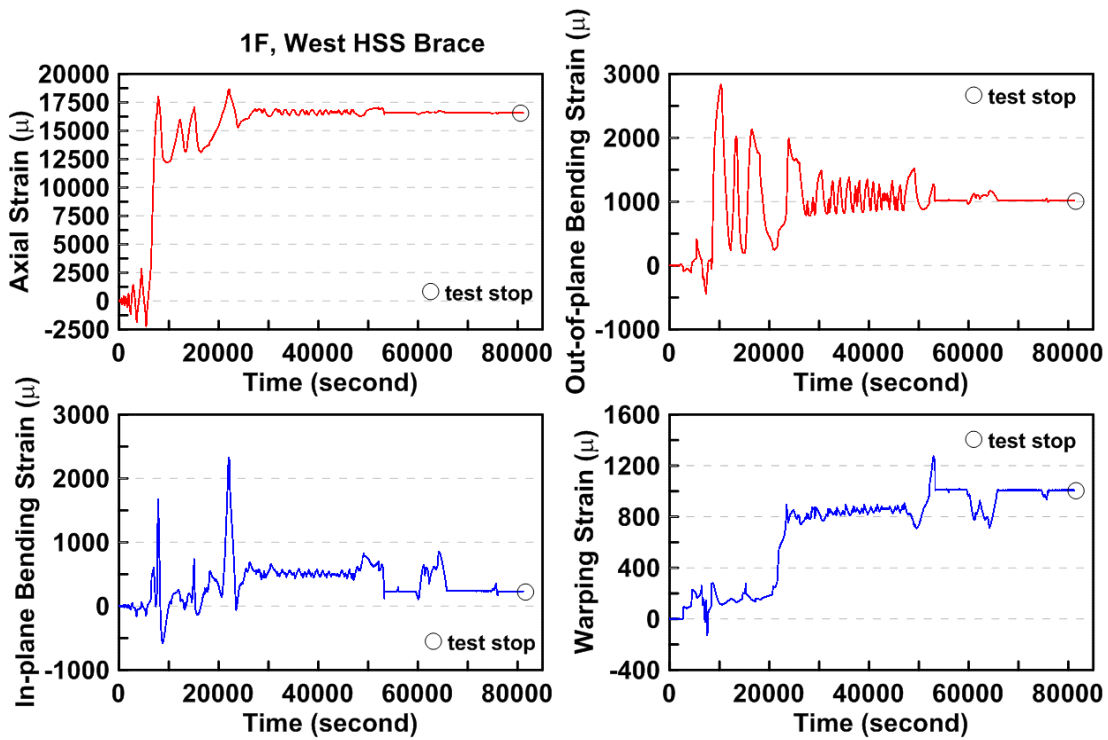


Figure 4.371 Time history of the decomposed strain components of western side HSS brace in the first story of TCBF-B-4 specimen

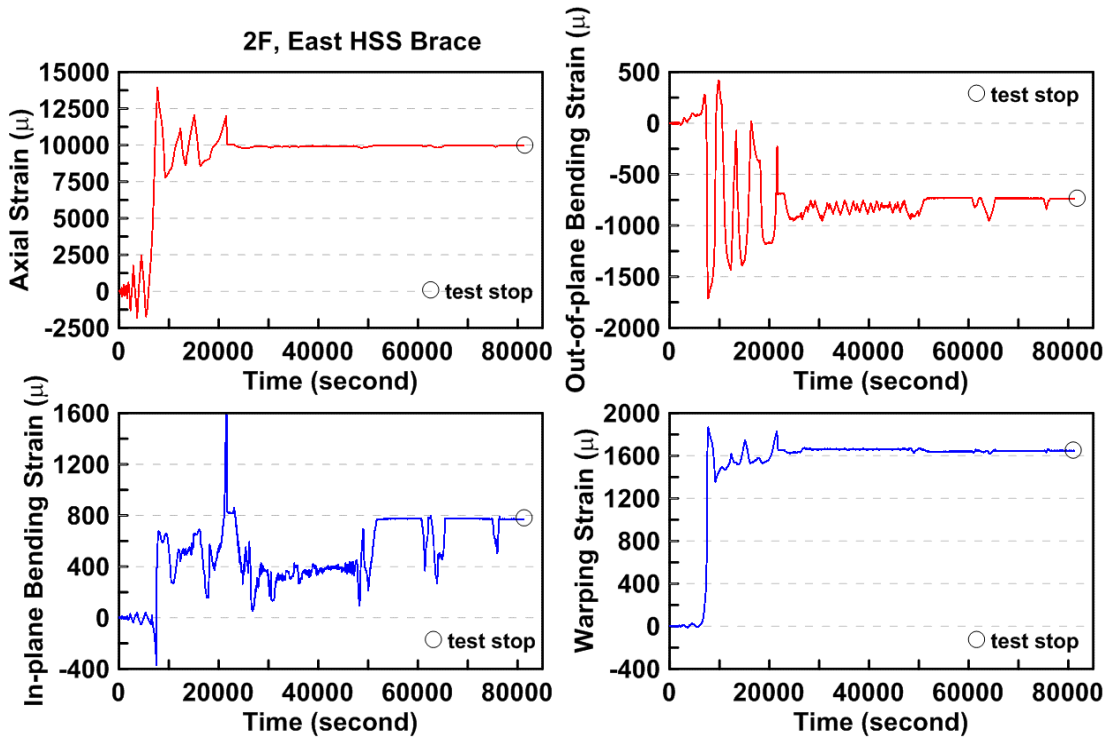


Figure 4.372 Time history of the decomposed strain components of eastern side HSS brace in the second story of TCBF-B-4 specimen

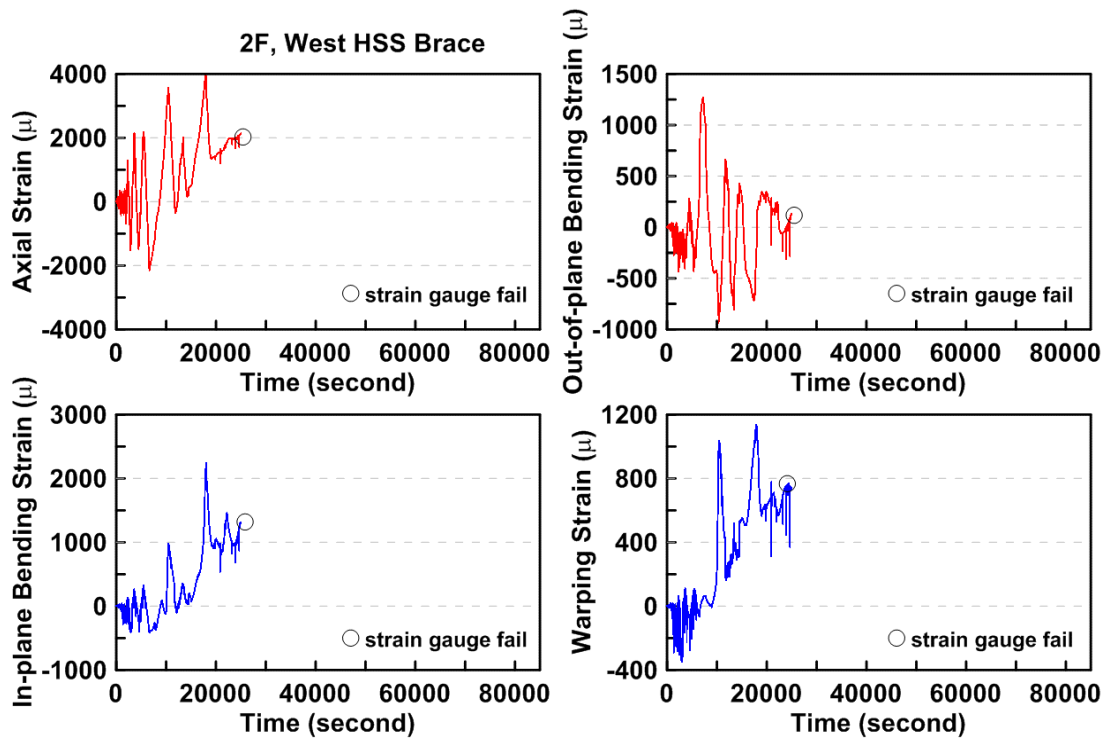


Figure 4.373 Time history of the decomposed strain components of western side HSS brace in the second story of TCBF-B-4 specimen



### 4.3.1.5 Panel Zone Response

Estimated panel zone shear stress versus measured panel zone shear strain relationship for four locations is plotted in Figs. 4.374. The time history of derived rosette-type strain gauge readings in the panel zone area at each story is shown in Figs. 4.375 to 4.378. Normalized maximum and minimum principal stress relationships along with different yield criteria for the panel zone regions are plotted in Figs. 4.379 to 4.382.

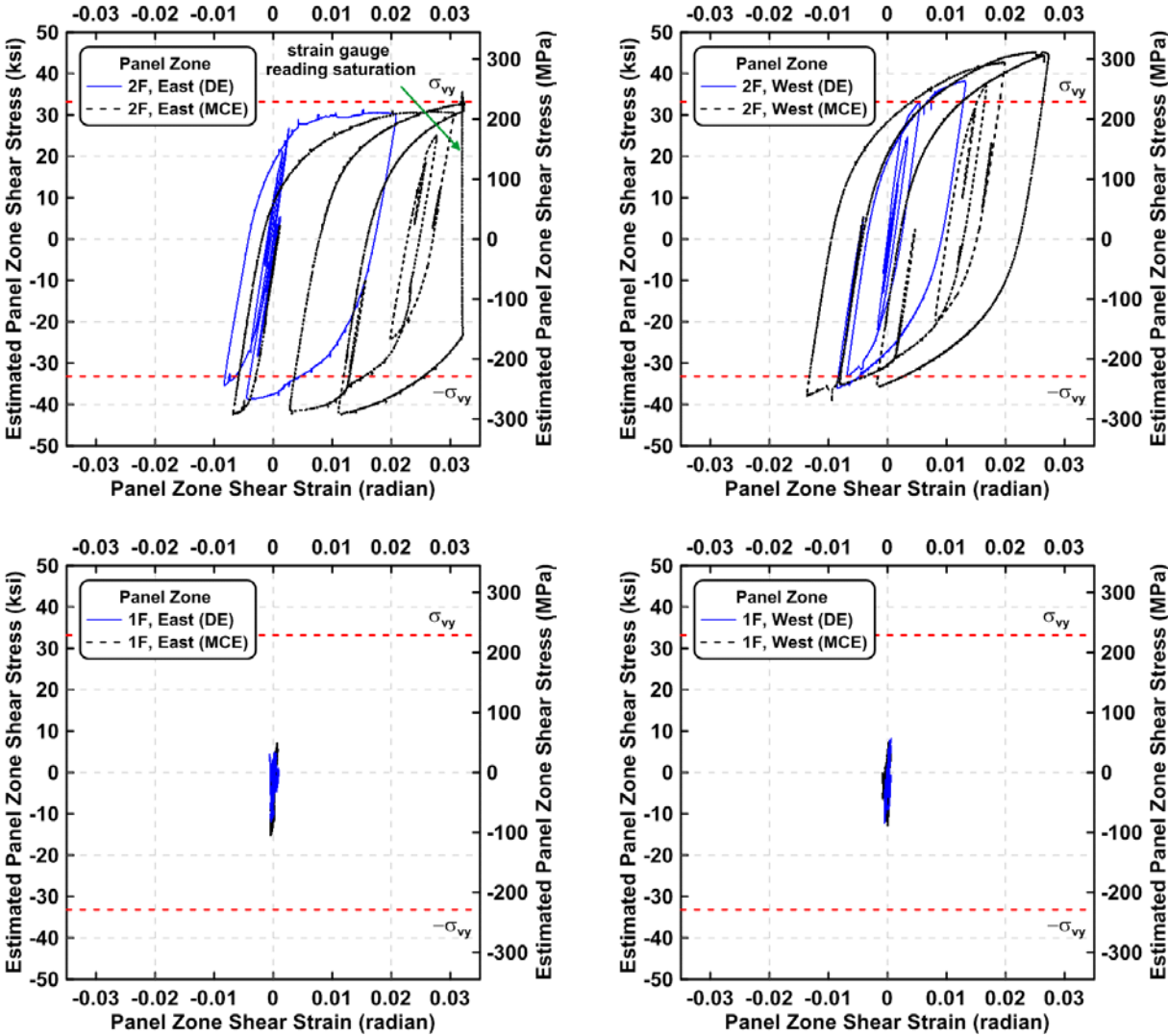


Figure 4.374 Estimated panel zone shear stress vs. shear strain relationships of TCBF-B-4 specimen

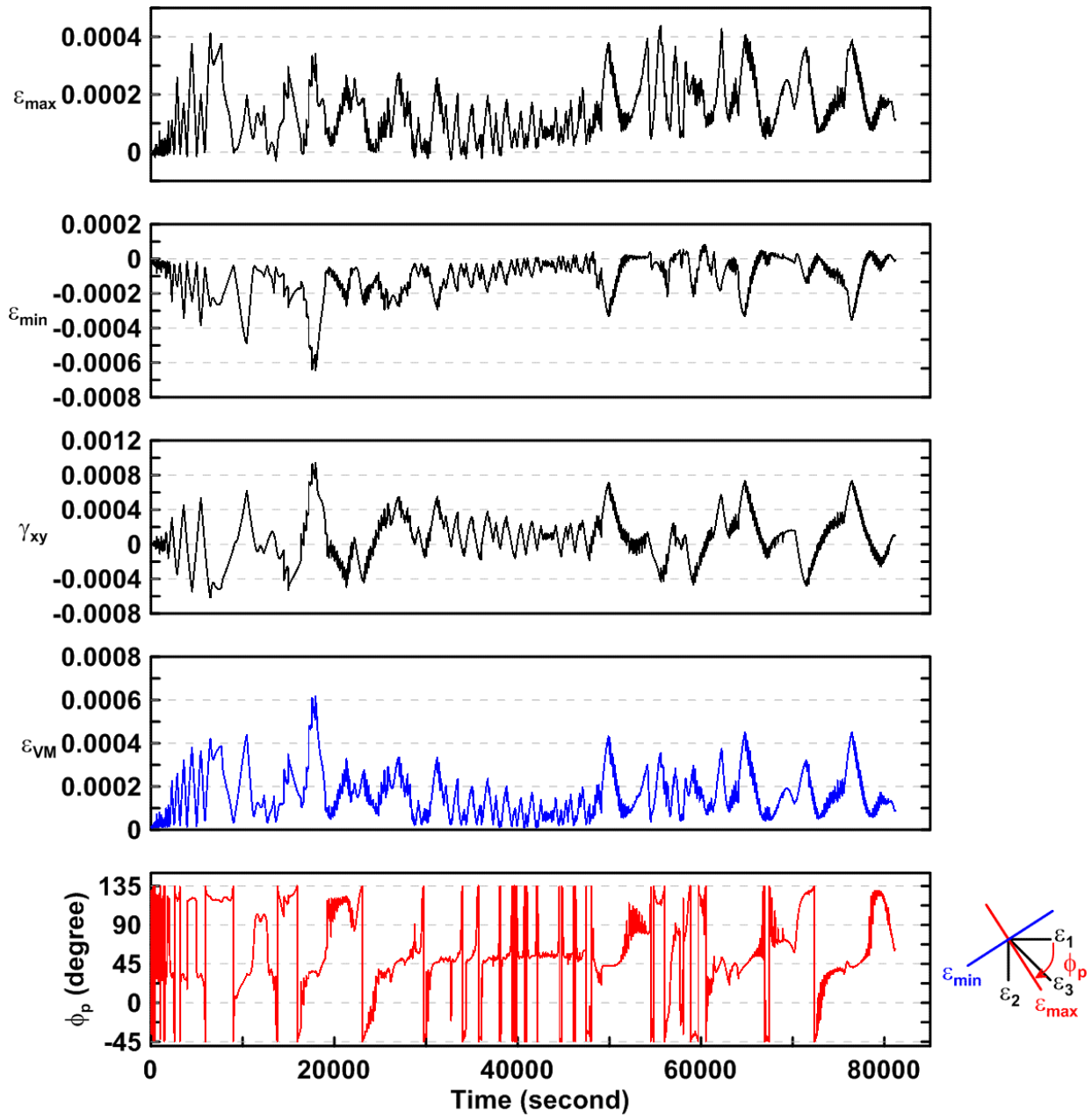


Figure 4.375 Time history of rosette type strain gauge readings in the lower panel zone of TCBF-B-4 specimen (location: R2)

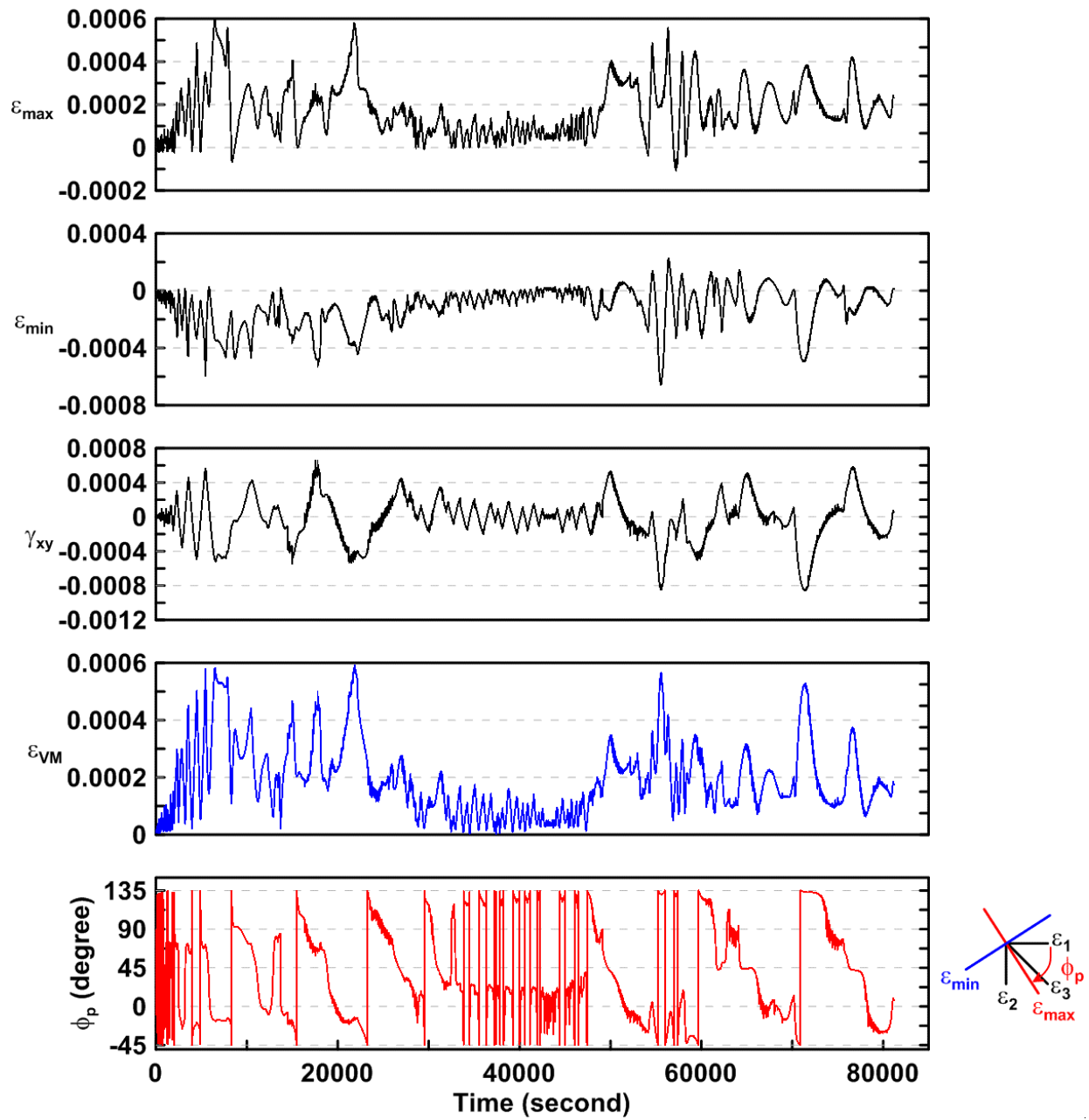


Figure 4.376 Time history of rosette type strain gauge readings in the lower panel zone of TCBF-B-4 specimen (location: R6)

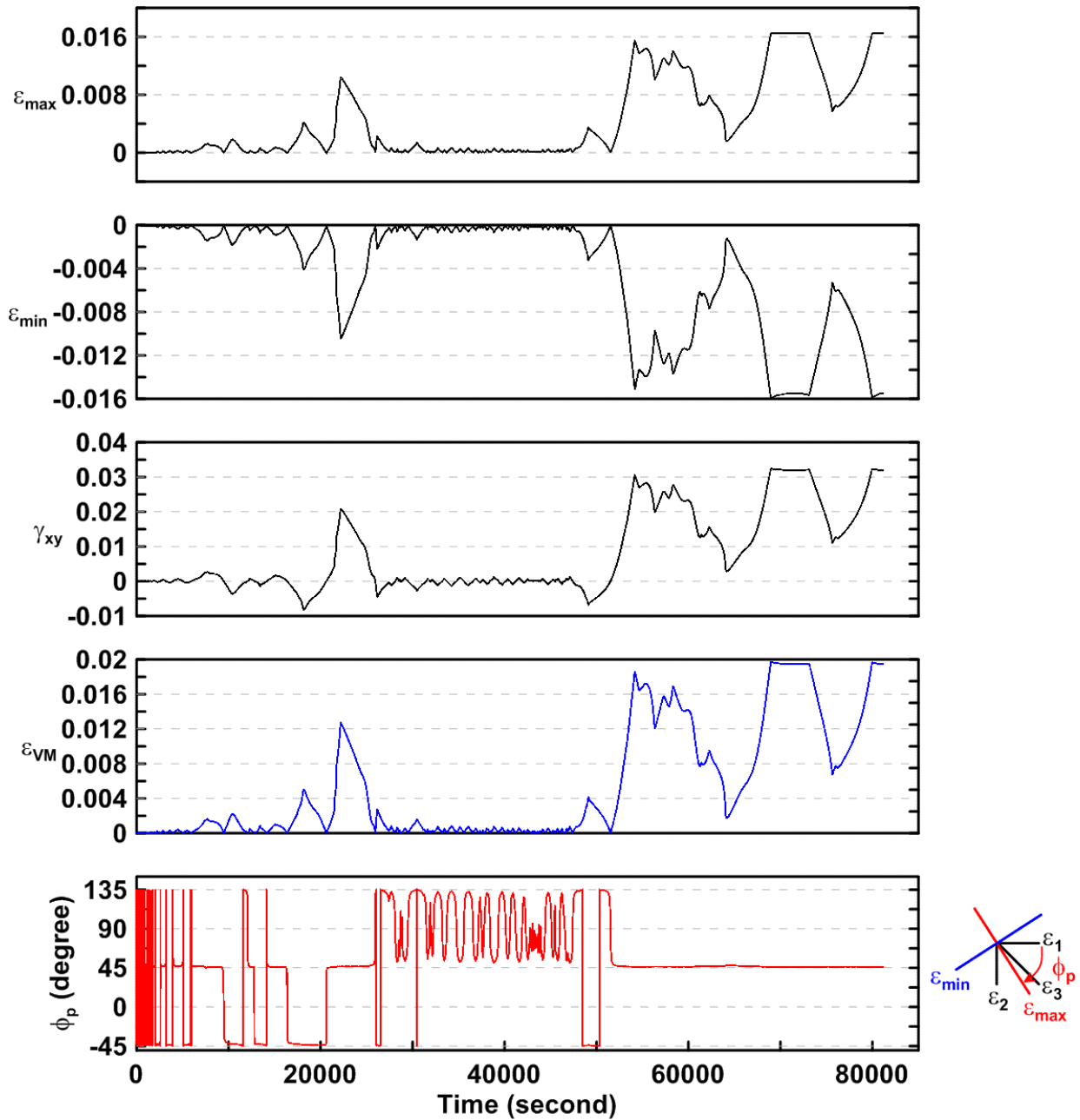


Figure 4.377 Time history of rosette type strain gauge readings in the lower panel zone of TCBF-B-4 specimen (location: R4)

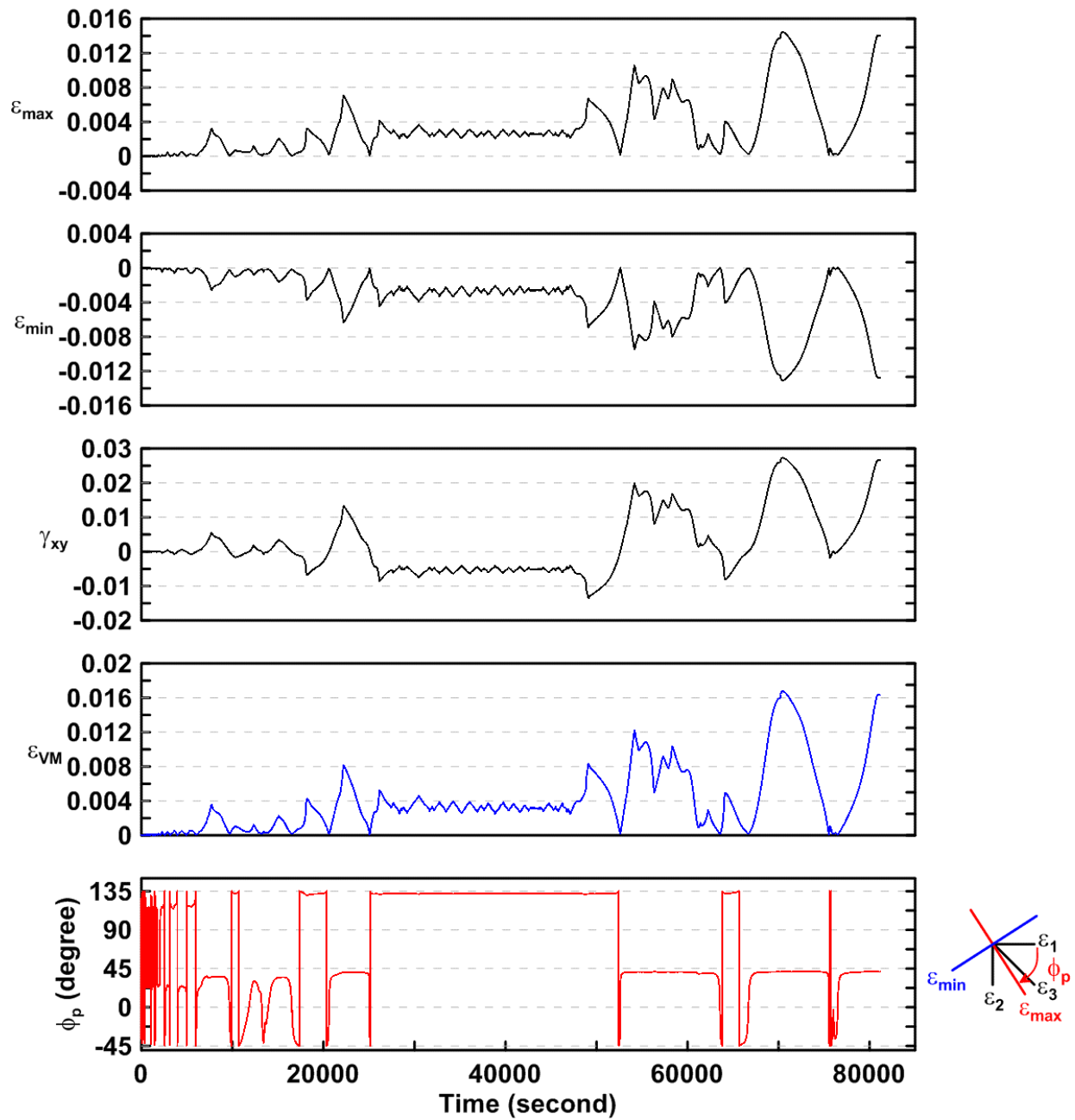


Figure 4.378 Time history of rosette type strain gauge readings in the lower panel zone of TCBF-B-4 specimen (location: R8)

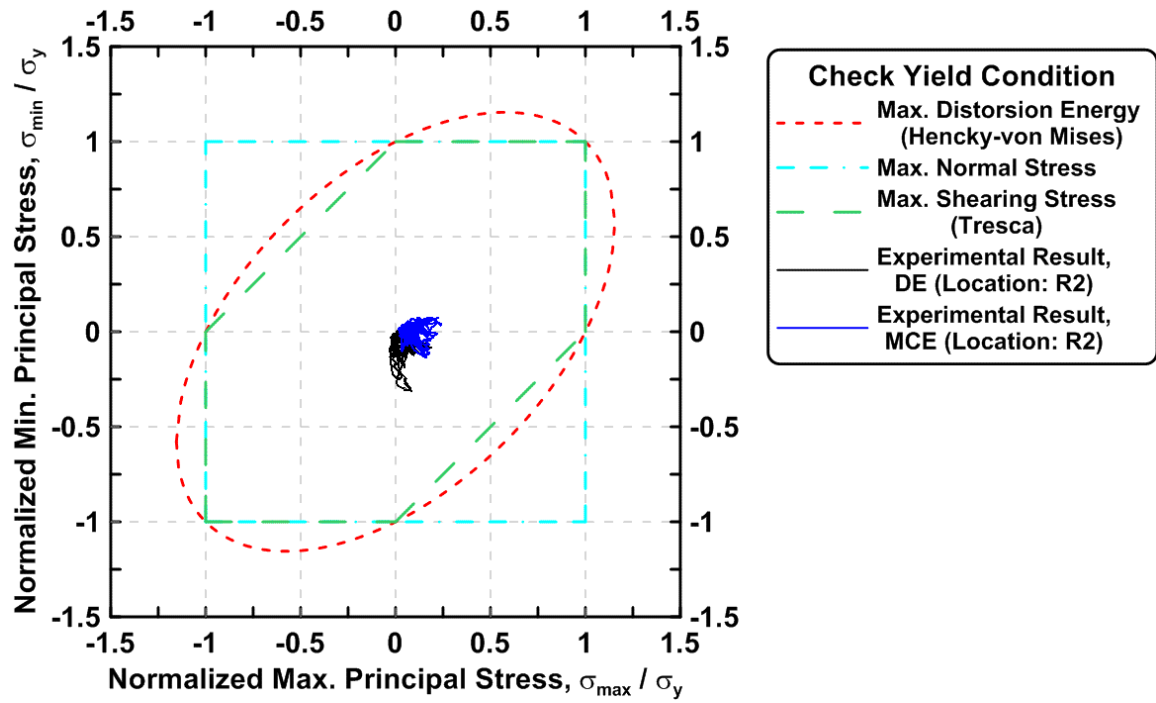


Figure 4.379 Normalized maximum principal stress vs. normalized minimum principal stress in the lower panel zone of TCBF-B-4 specimen (location: R2)

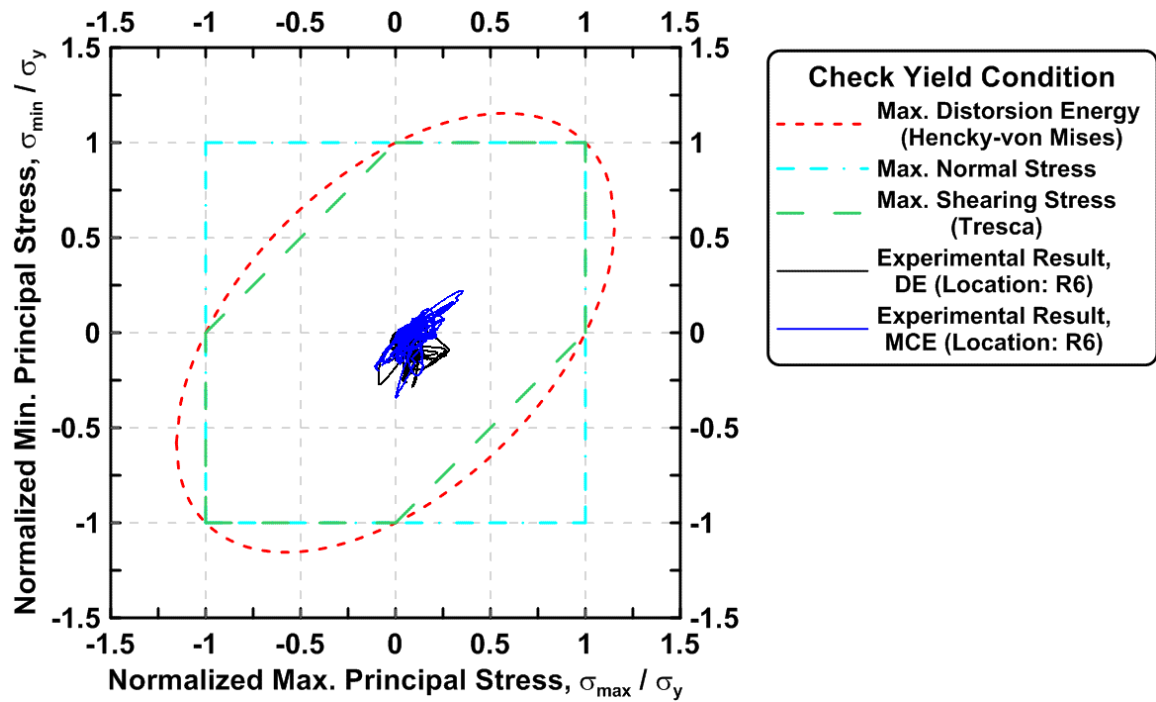


Figure 4.380 Normalized maximum principal stress vs. normalized minimum principal stress in the lower panel zone of TCBF-B-4 specimen (location: R6)

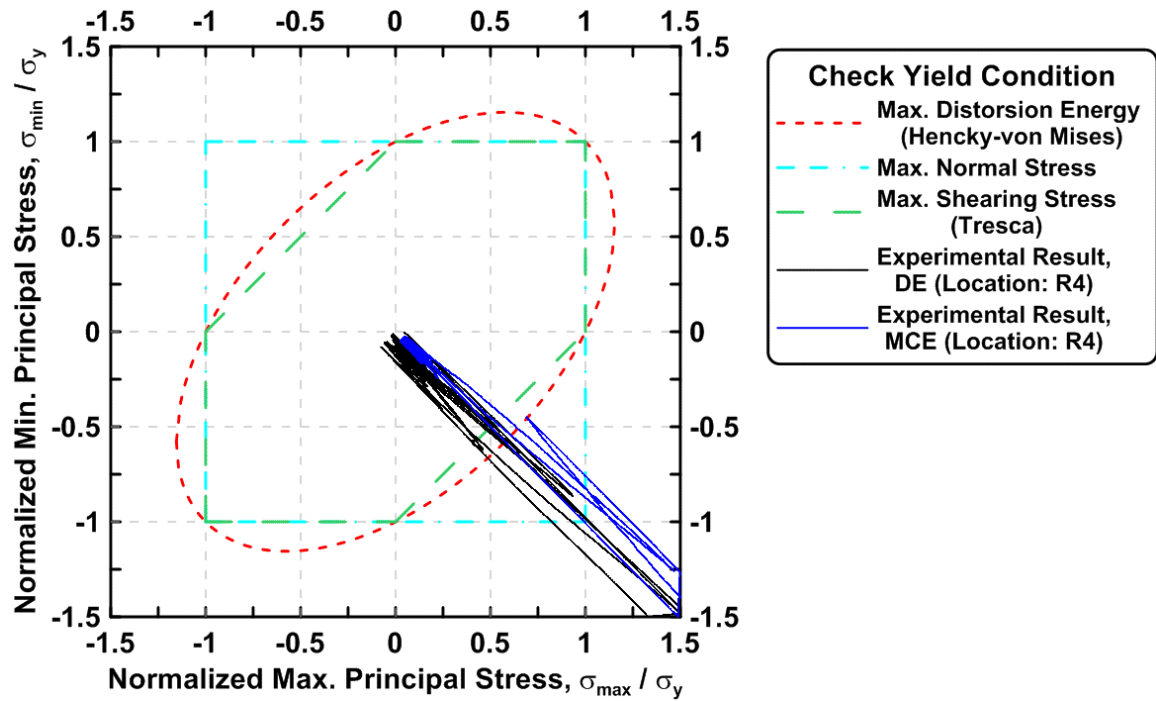


Figure 4.381 Normalized maximum principal stress vs. normalized minimum principal stress in the lower panel zone of TCBF-B-4 specimen (location: R4)

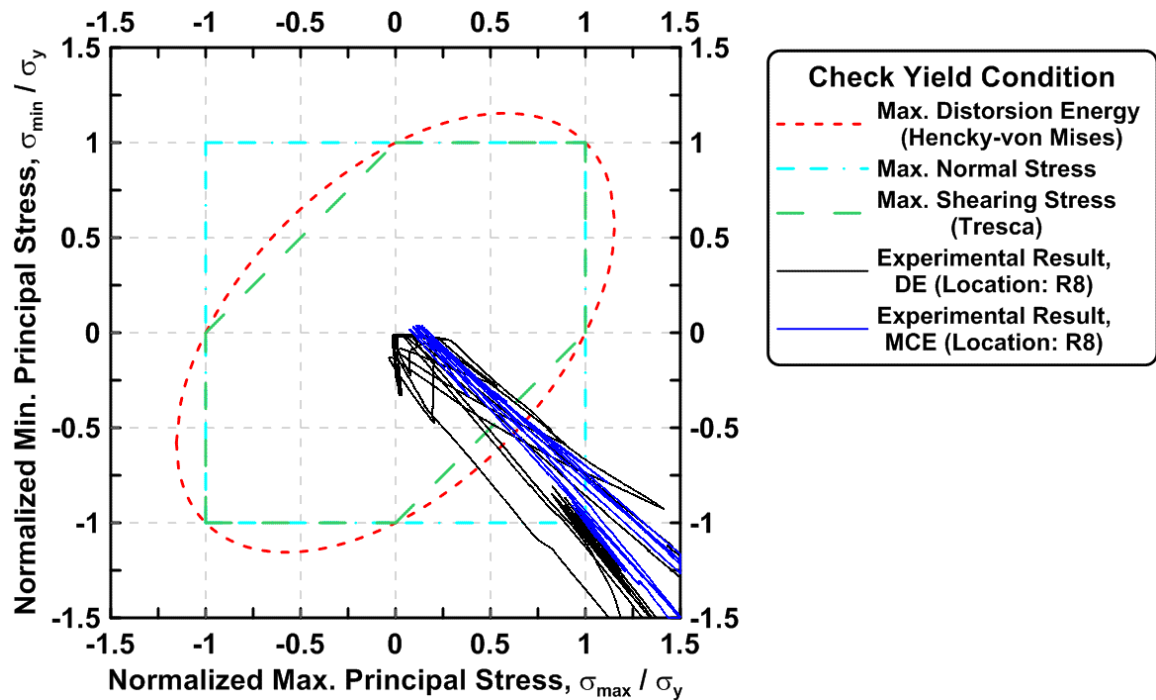


Figure 4.382 Normalized maximum principal stress vs. normalized minimum principal stress in the lower panel zone of TCBF-B-4 specimen (location: R8)

### 4.3.1.6 Gusset Plate Response

The time history derived from rosette-type strain gauge readings in the 3/4-in.-thick one-piece gusset plate is shown in Figs. 4.383 to 4.394. Normalized maximum and minimum principal stress relationships along with different yield criteria for the rosettes on the gusset plate are plotted in Figs. 4.395 to 4.406.

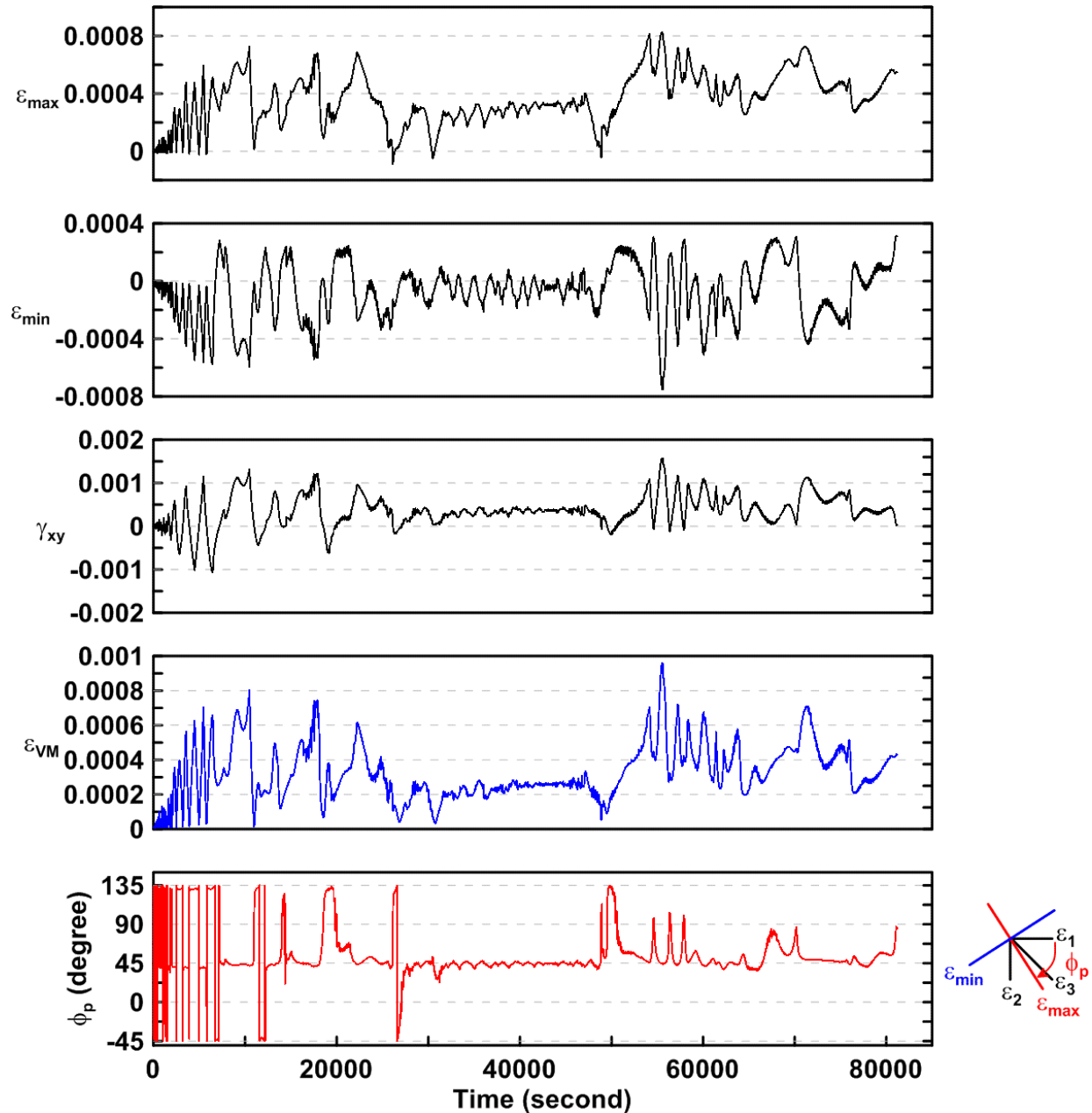


Figure 4.383 Time history of rosette type strain gauge readings in the one-piece gusset plate of TCBF-B-4 specimen (location: R9)



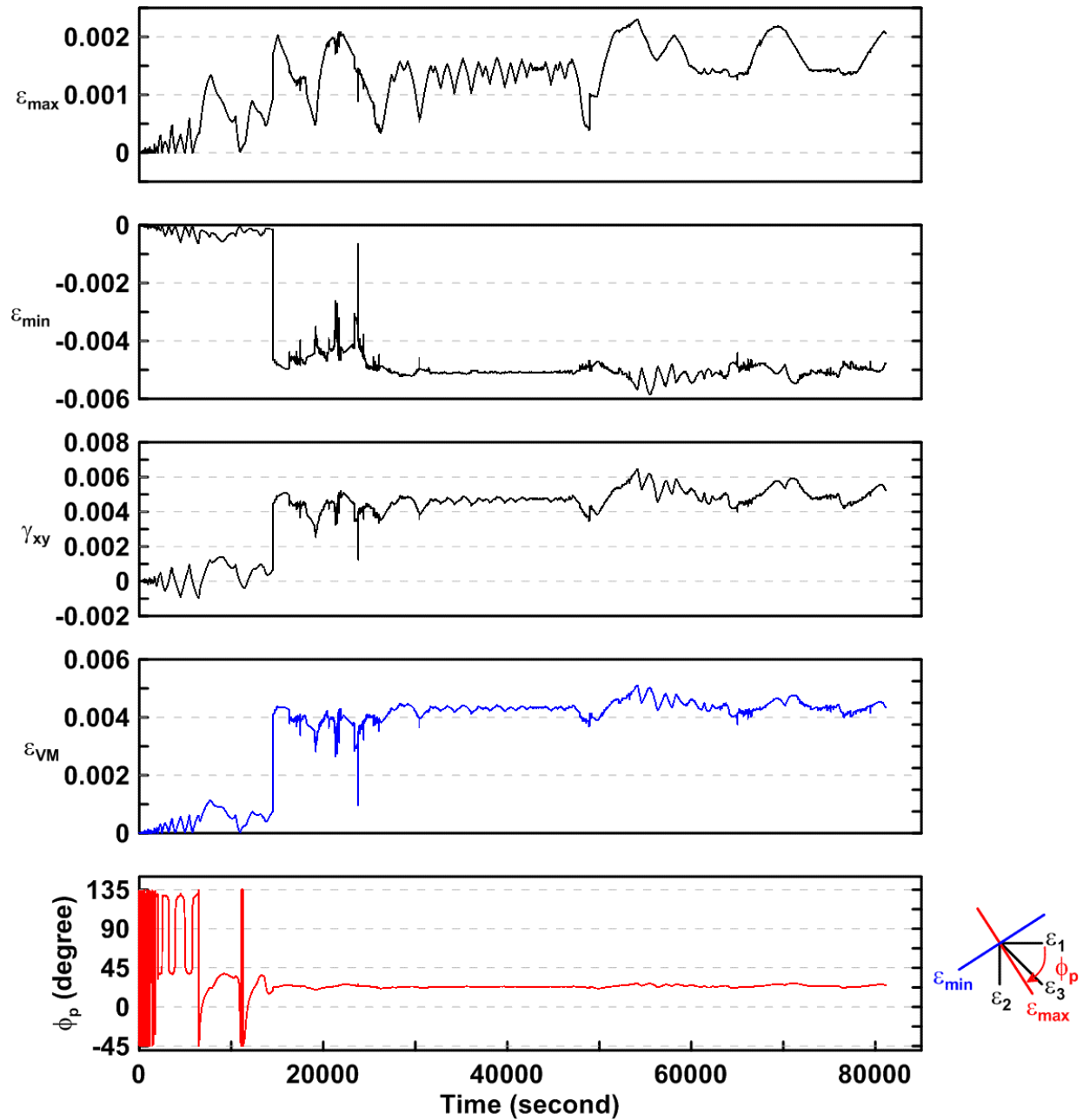


Figure 4.384 Time history of rosette type strain gauge readings in the one-piece gusset plate of TCBF-B-4 specimen (location: R10)

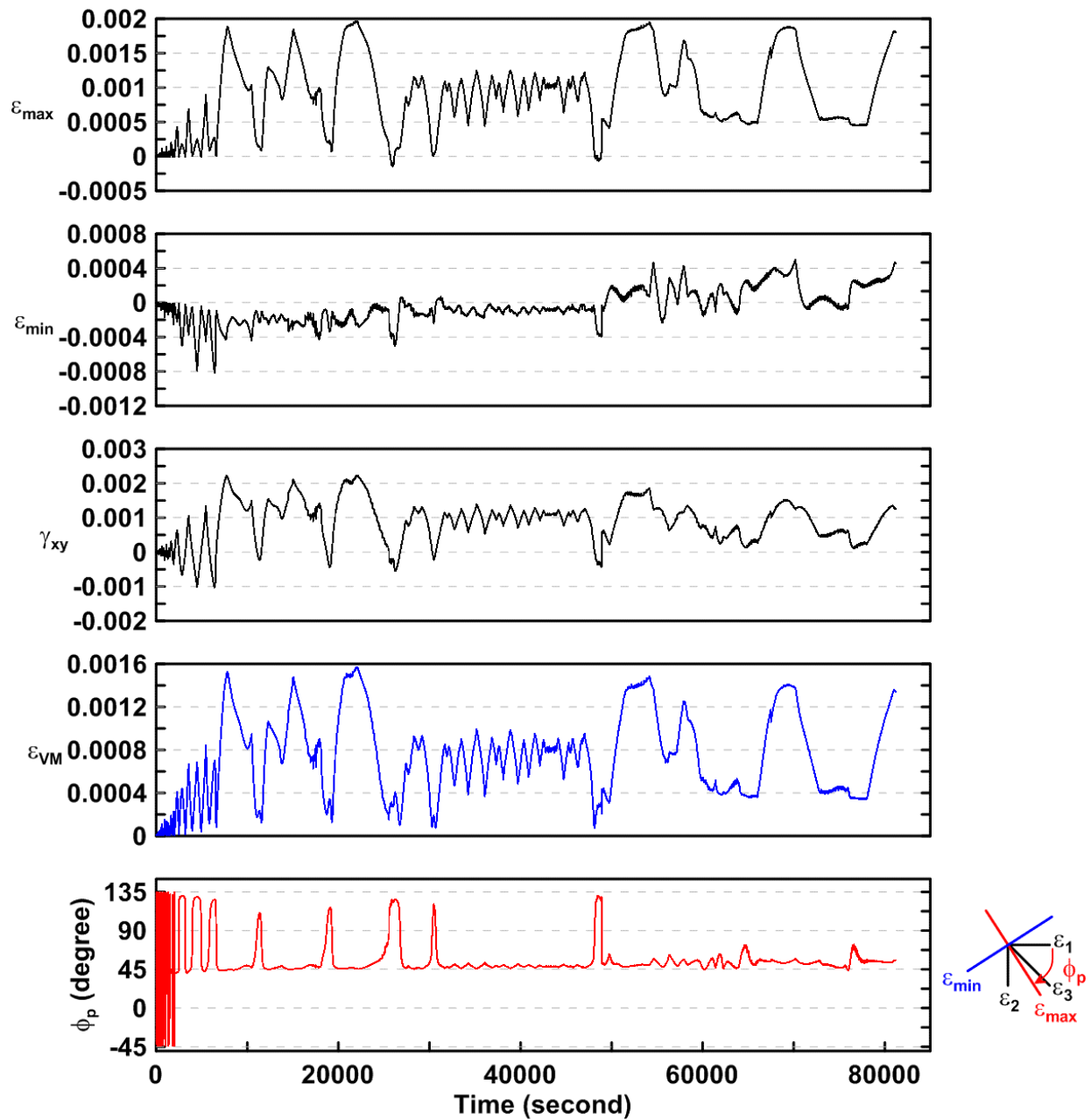


Figure 4.385 Time history of rosette type strain gauge readings in the one-piece gusset plate of TCBF-B-4 specimen (location: R11)

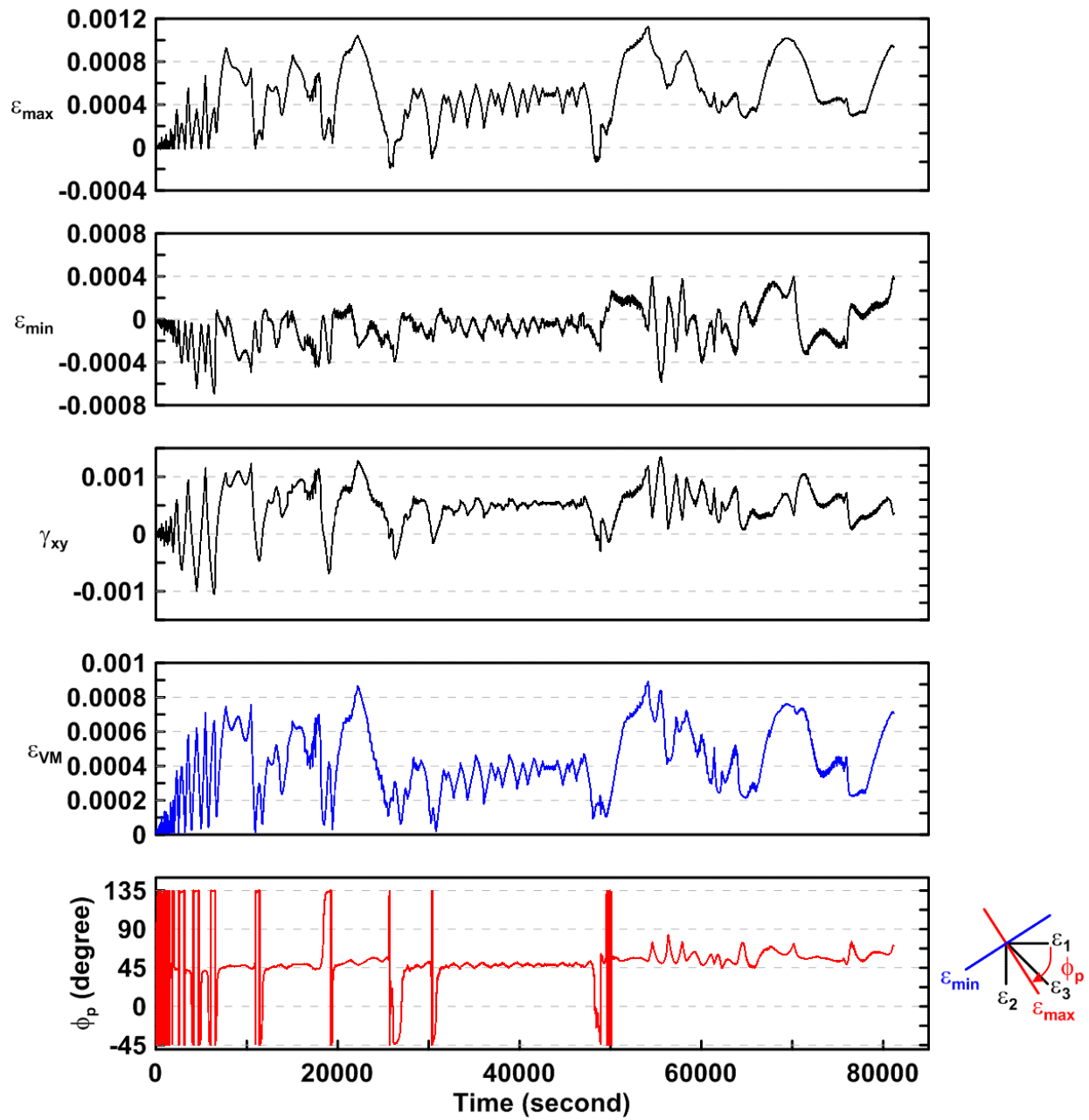


Figure 4.386 Time history of rosette type strain gauge readings in the one-piece gusset plate of TCBF-B-4 specimen (location: R12)

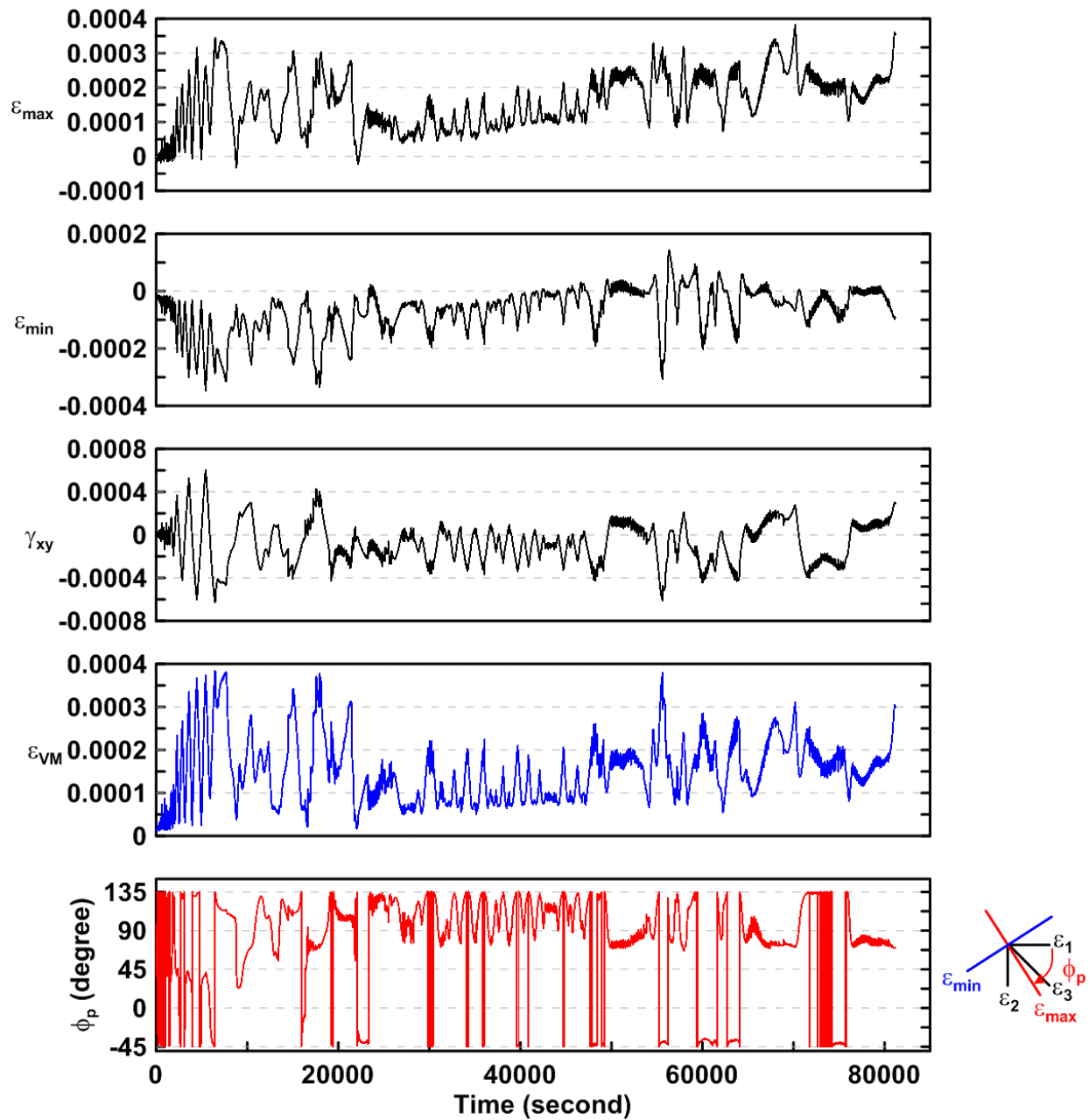


Figure 4.387 Time history of rosette type strain gauge readings in the one-piece gusset plate of TCBF-B-4 specimen (location: R13)

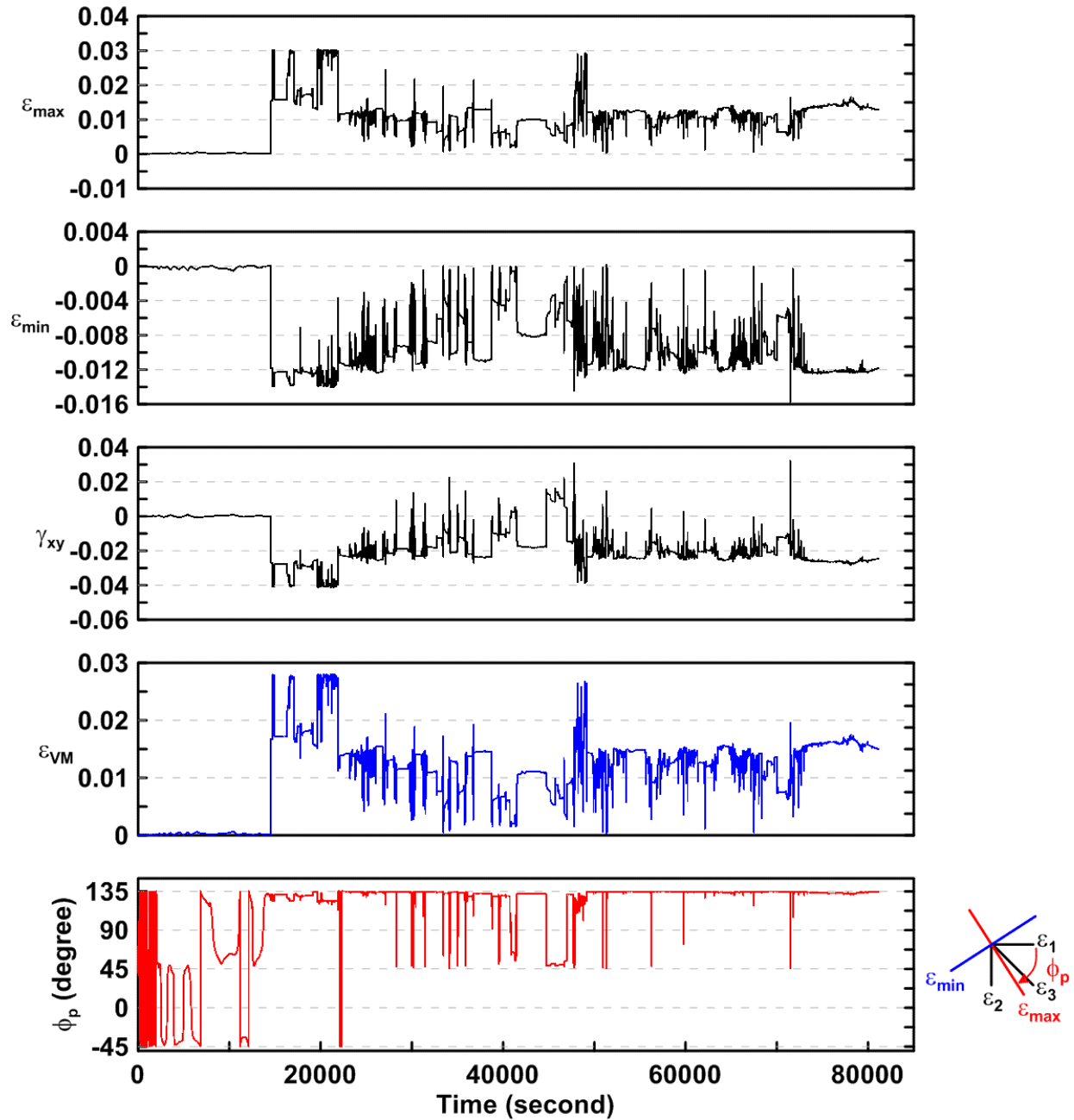


Figure 4.388 Time history of rosette type strain gauge readings in the one-piece gusset plate of TCBF-B-4 specimen (location: R14)

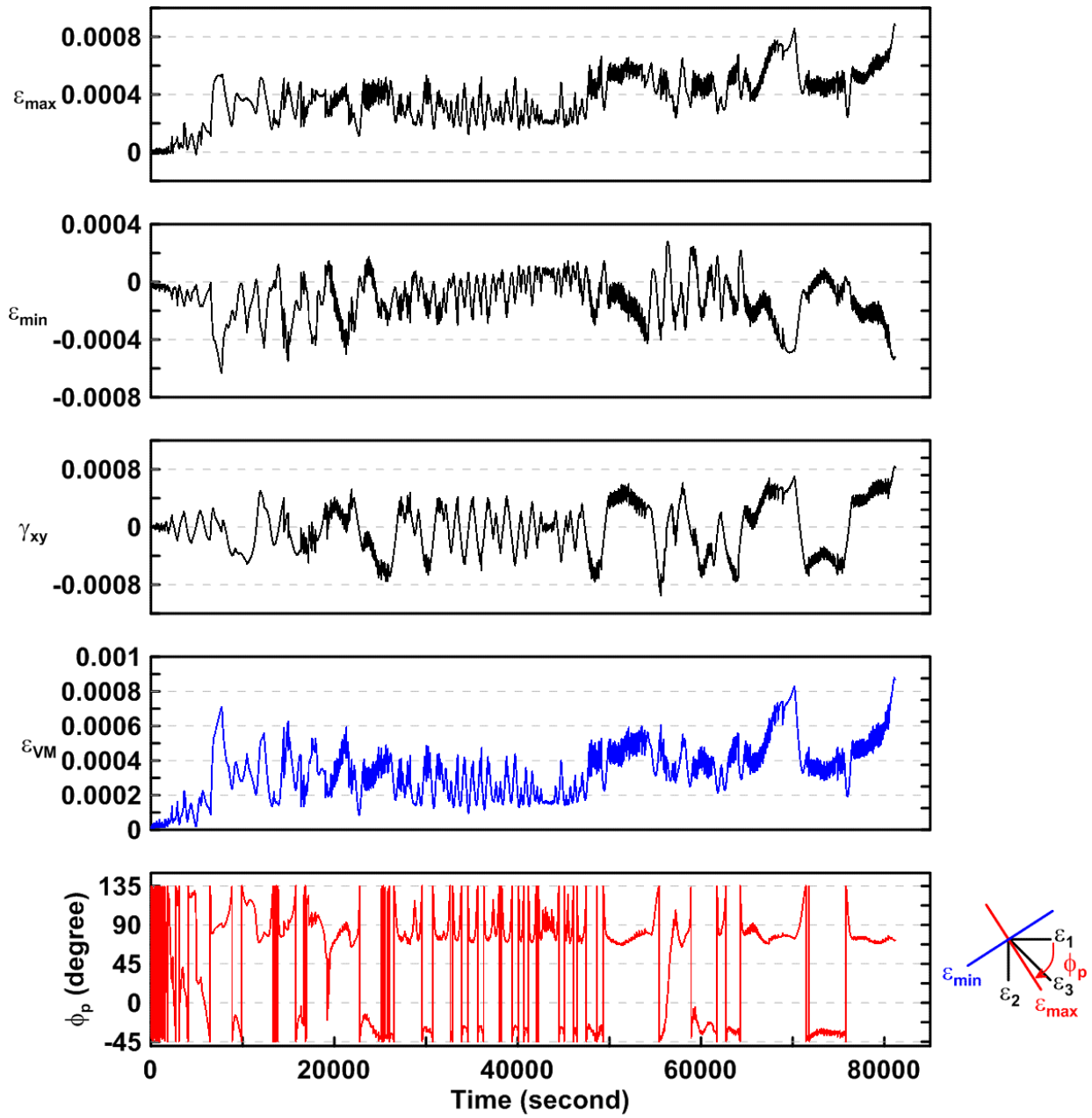


Figure 4.389 Time history of rosette type strain gauge readings in the one-piece gusset plate of TCBF-B-4 specimen (location: R15)

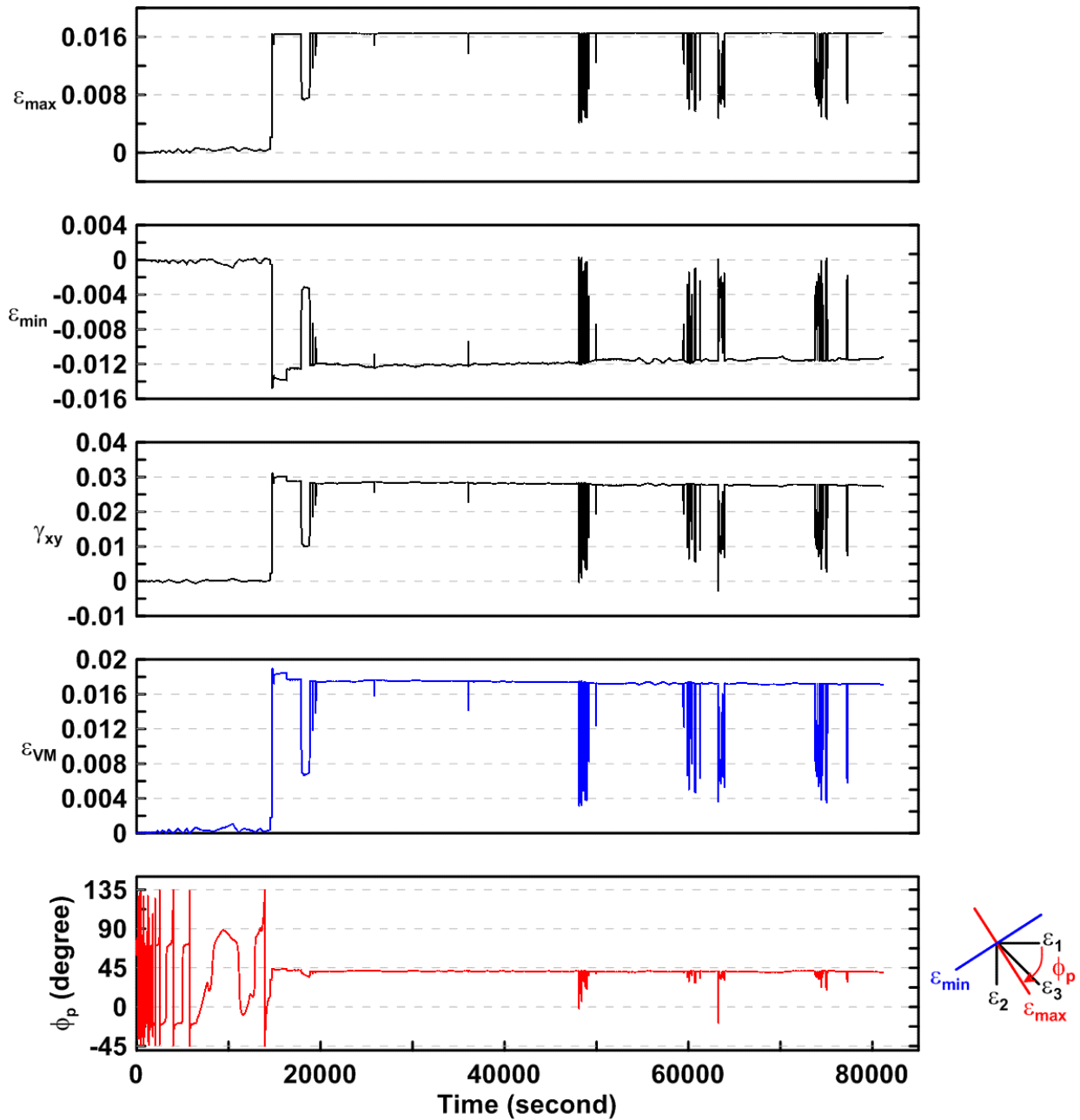


Figure 4.390 Time history of rosette type strain gauge readings in the one-piece gusset plate of TCBF-B-4 specimen (location: R16)

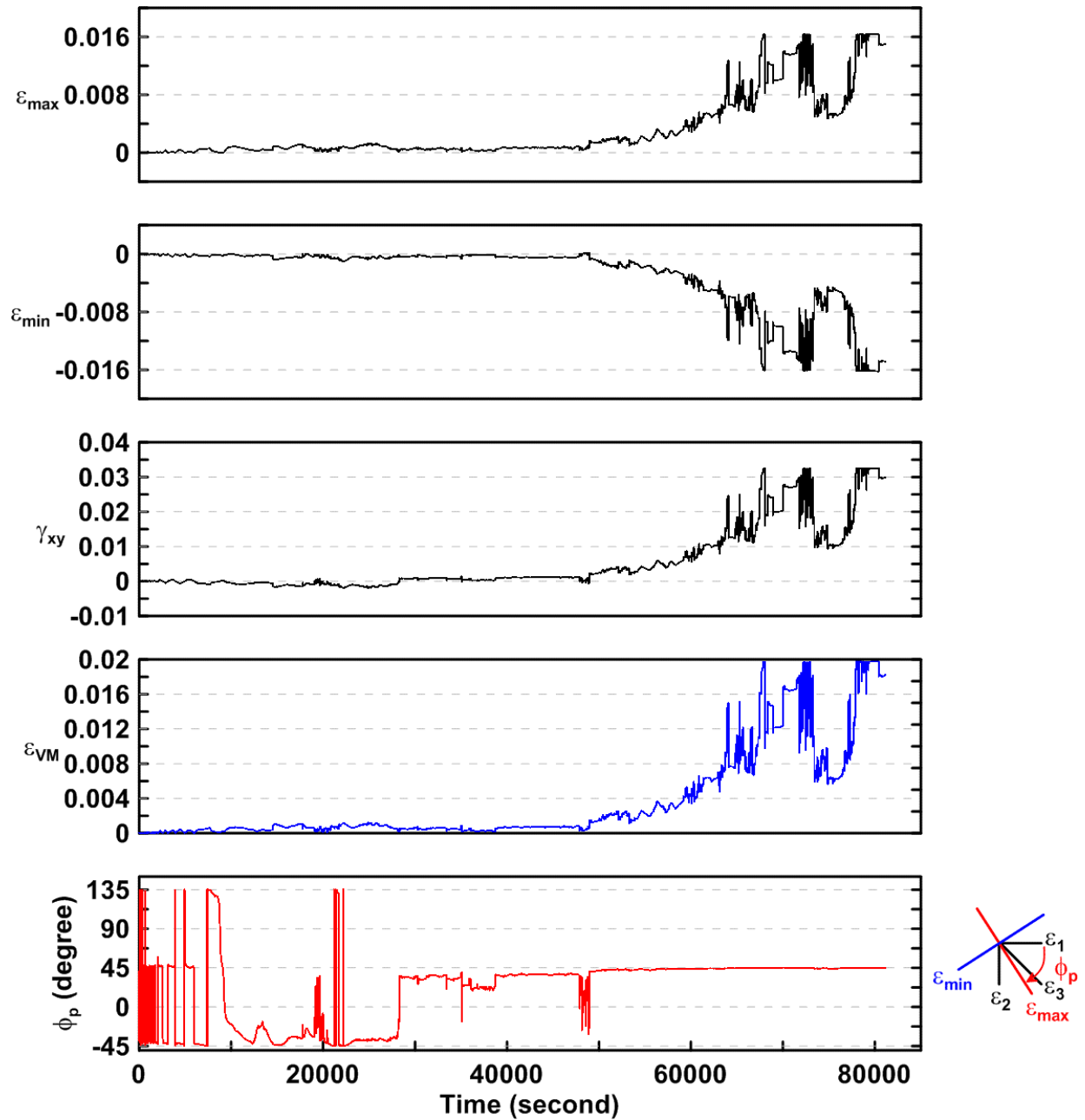


Figure 4.391 Time history of rosette type strain gauge readings in the one-piece gusset plate of TCBF-B-4 specimen (location: R17)



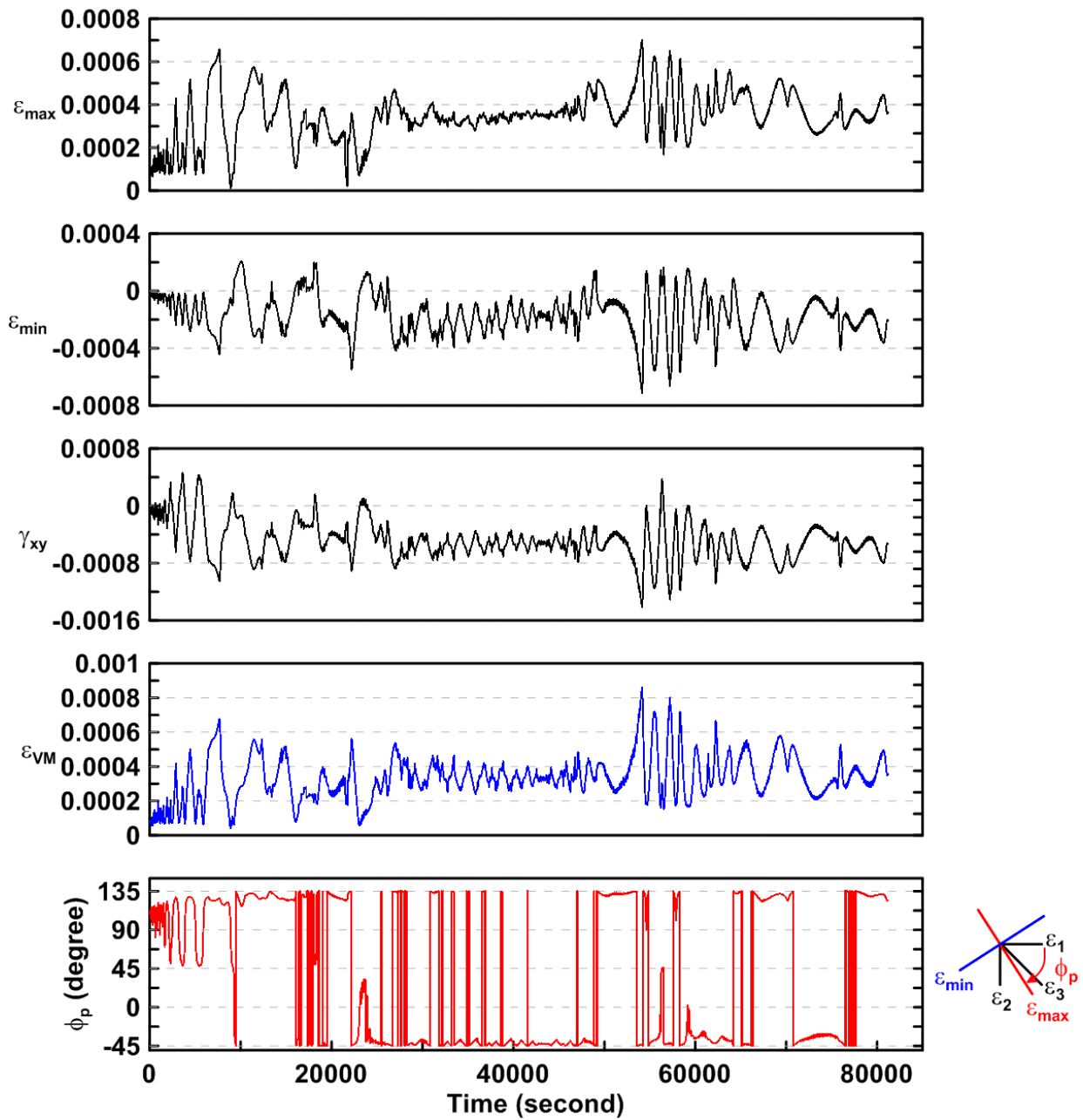


Figure 4.392 Time history of rosette type strain gauge readings in the one-piece gusset plate of TCBF-B-4 specimen (location: R18)

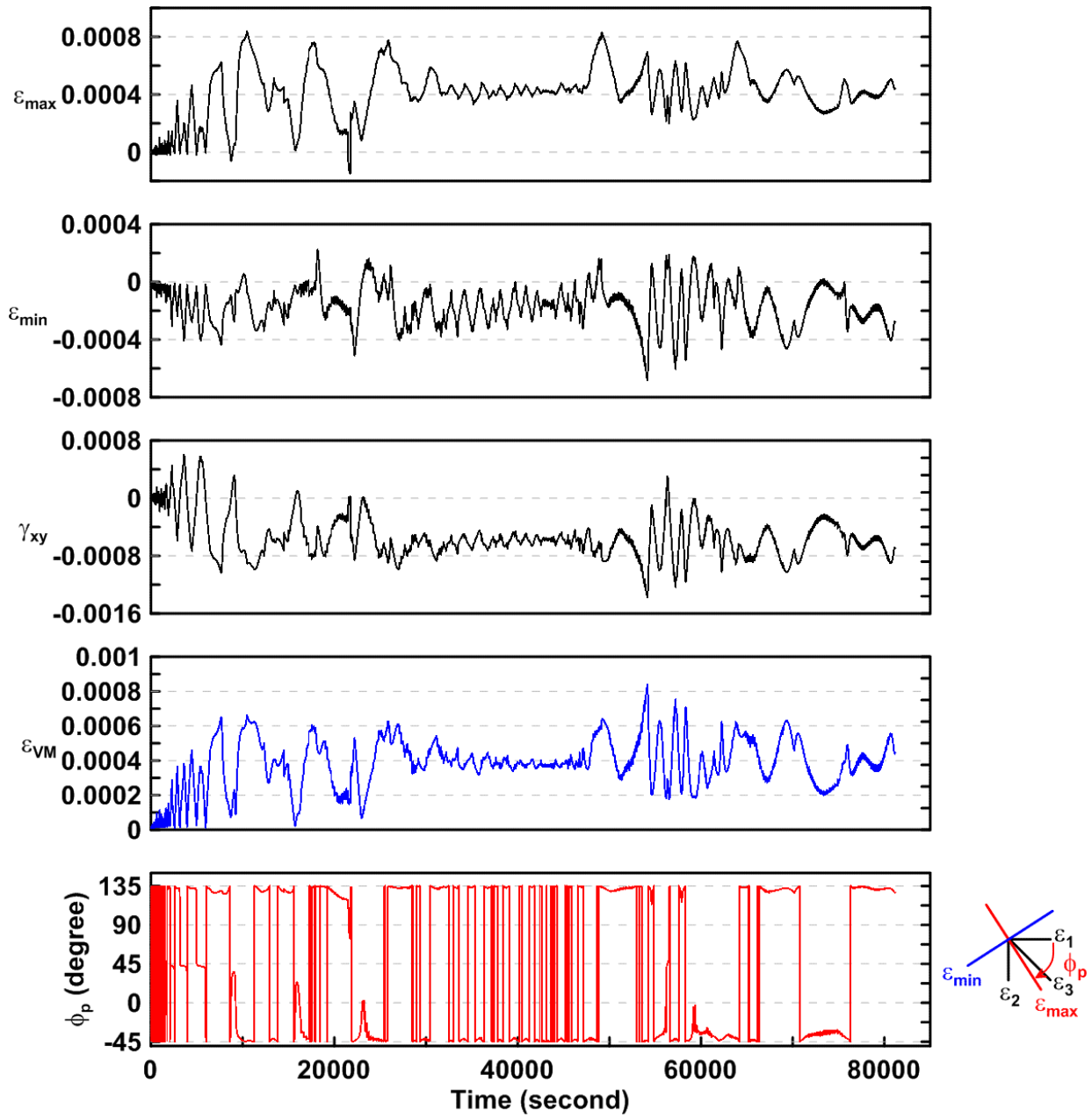


Figure 4.393 Time history of rosette type strain gauge readings in the one-piece gusset plate of TCBF-B-4 specimen (location: R19)

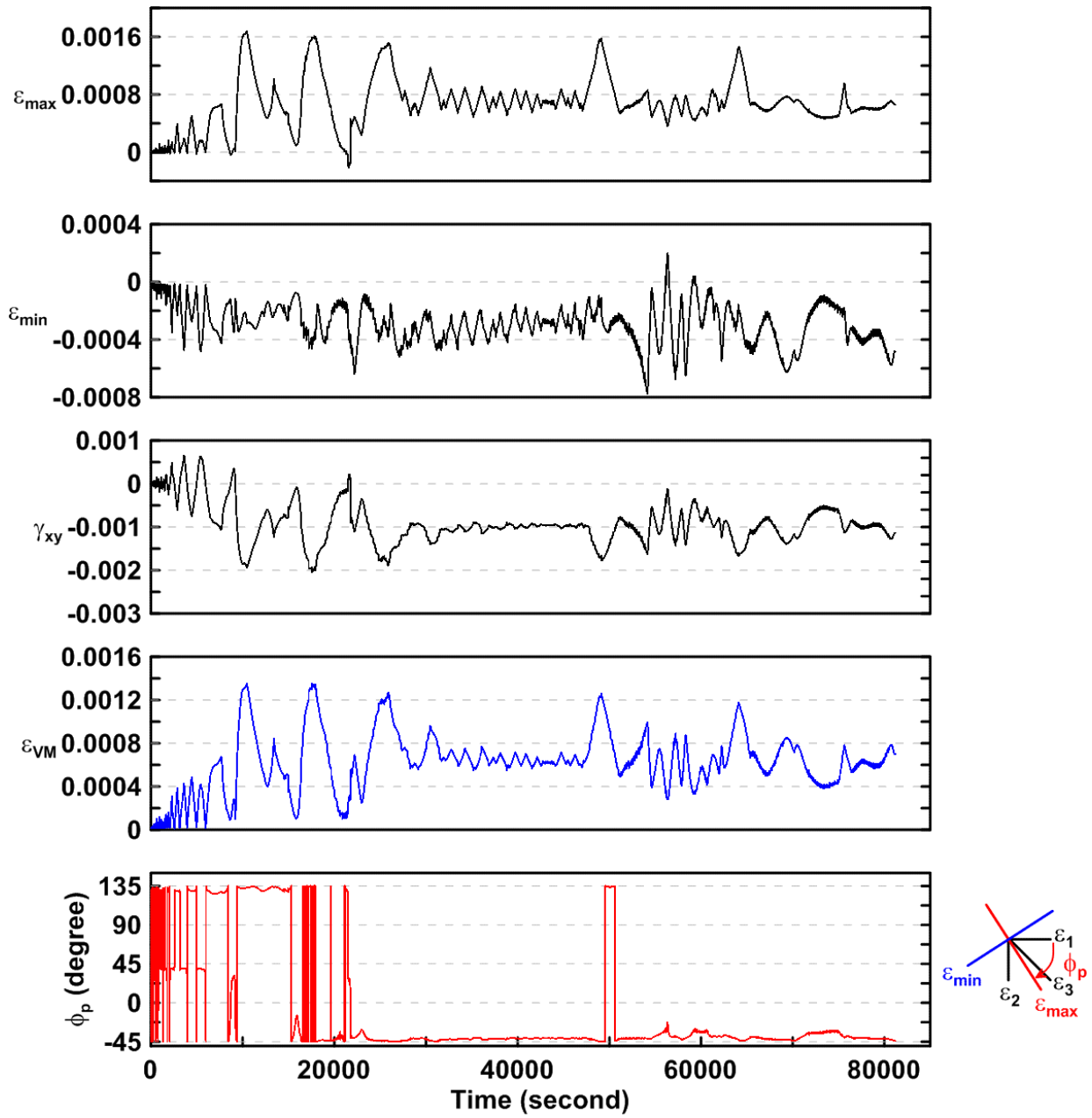


Figure 4.394 Time history of rosette type strain gauge readings in the one-piece gusset plate of TCBF-B-4 specimen (location: R20)

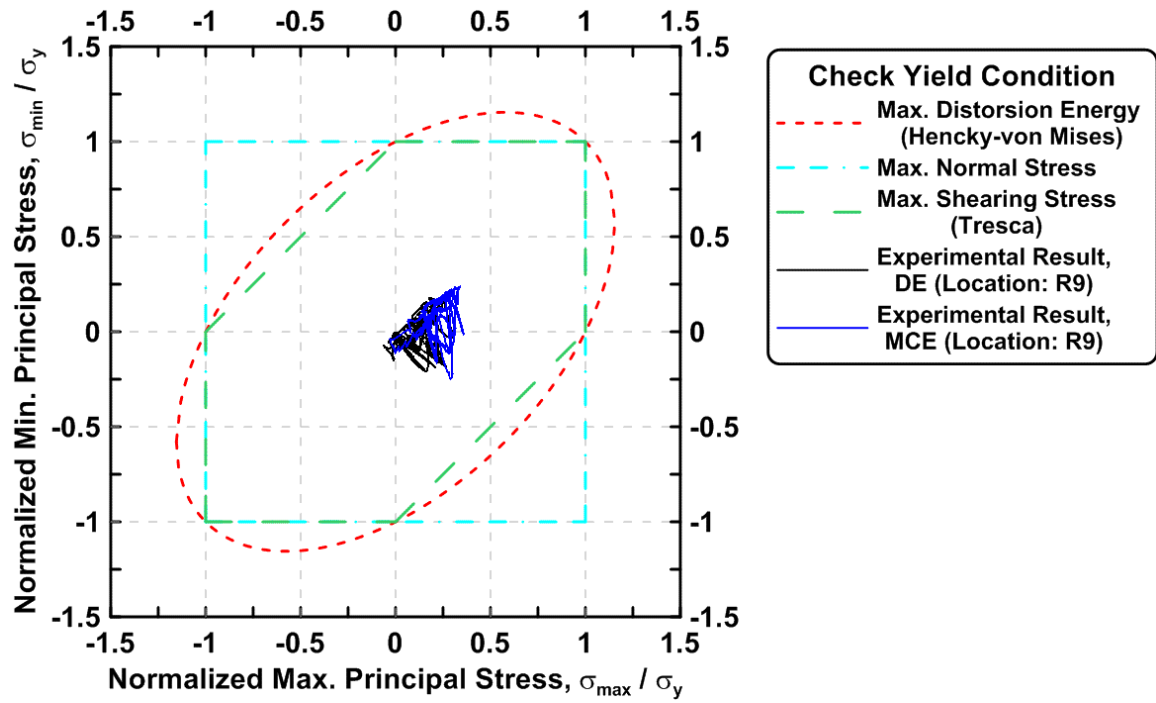


Figure 4.395 Normalized maximum principal stress vs. normalized minimum principal stress in the one-piece gusset plate of TCBF-B-4 specimen (location: R9)

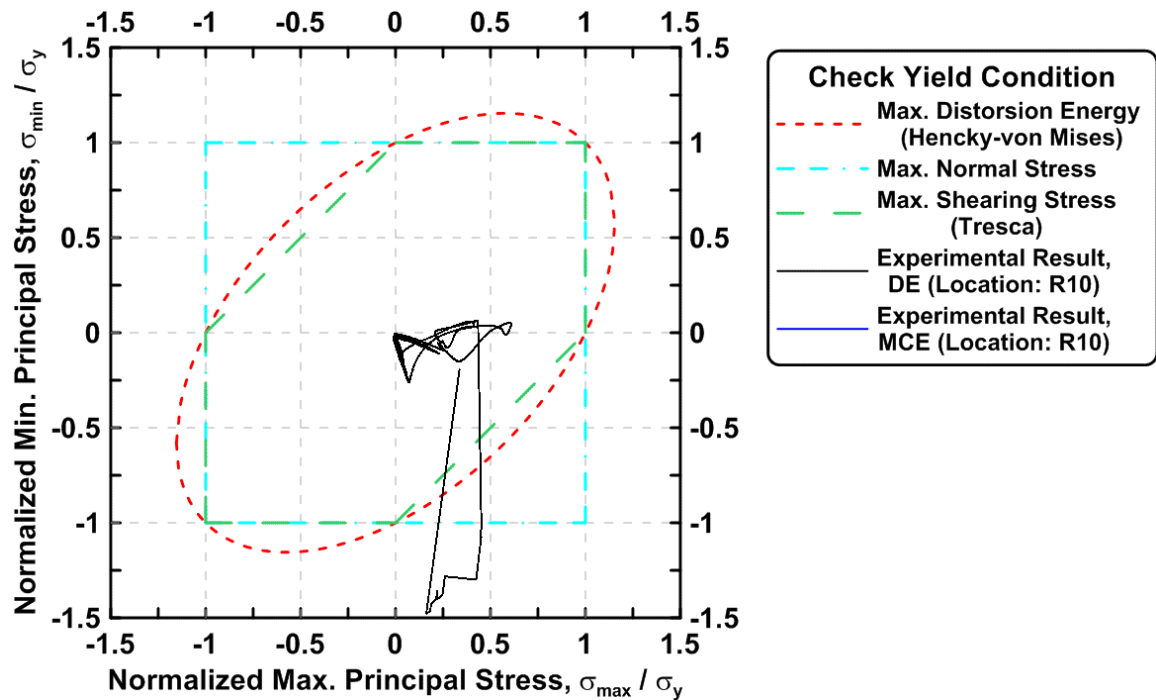


Figure 4.396 Normalized maximum principal stress vs. normalized minimum principal stress in the one-piece gusset plate of TCBF-B-4 specimen (location: R10)

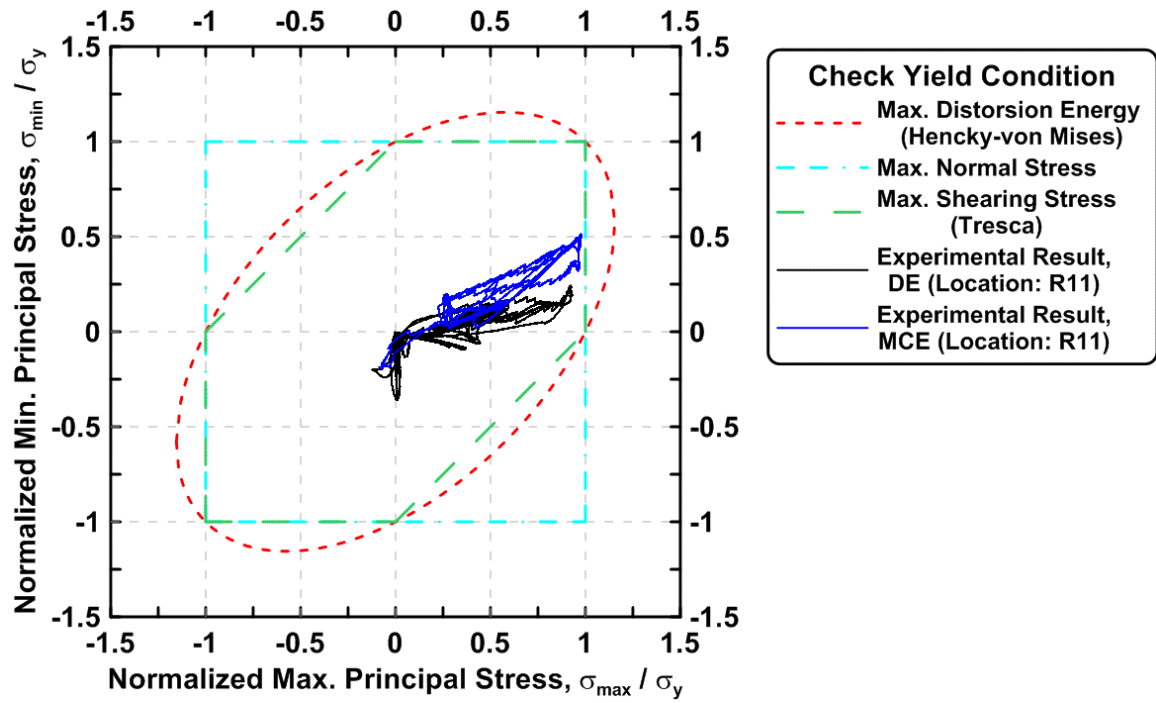


Figure 4.397 Normalized maximum principal stress vs. normalized minimum principal stress in the one-piece gusset plate of TCBF-B-4 specimen (location: R11)

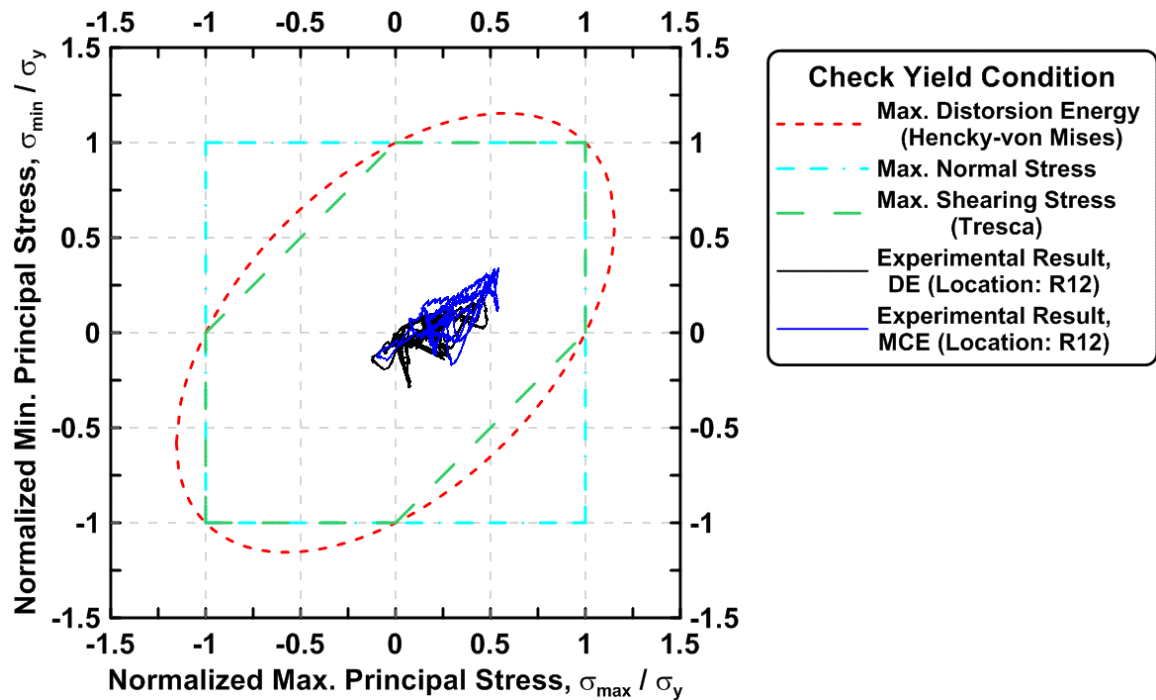


Figure 4.398 Normalized maximum principal stress vs. normalized minimum principal stress in the one-piece gusset plate of TCBF-B-4 specimen (location: R12)

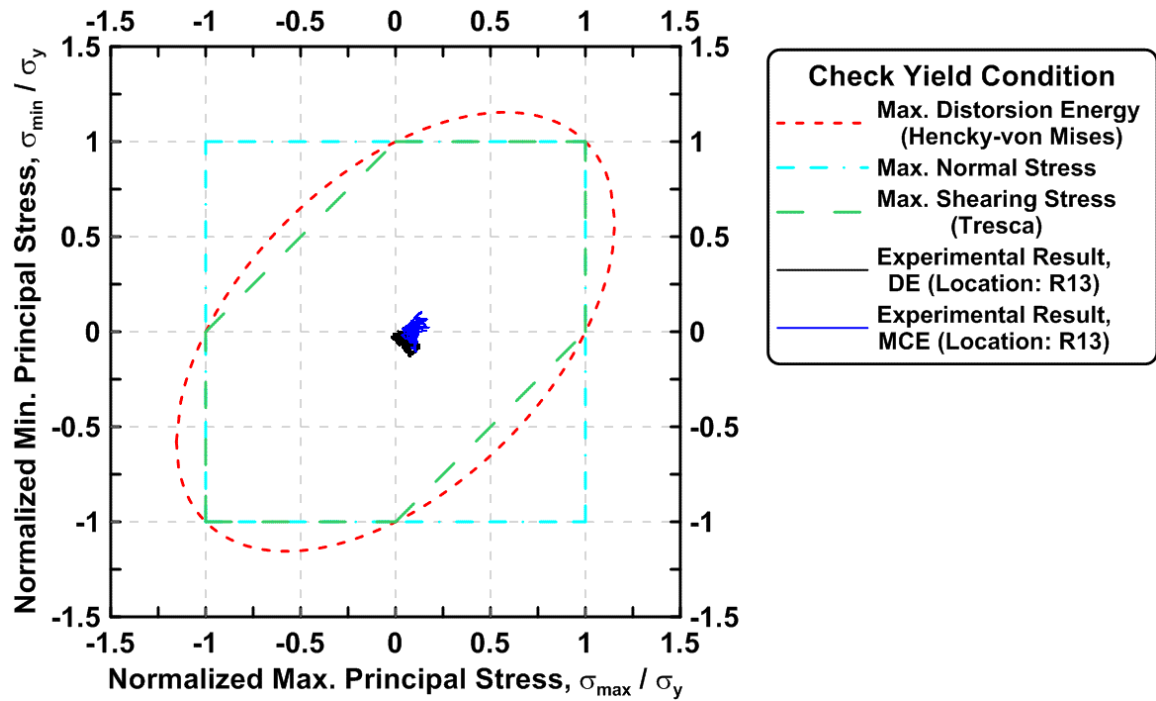


Figure 4.399 Normalized maximum principal stress vs. normalized minimum principal stress in the one-piece gusset plate of TCBF-B-4 specimen (location: R13)

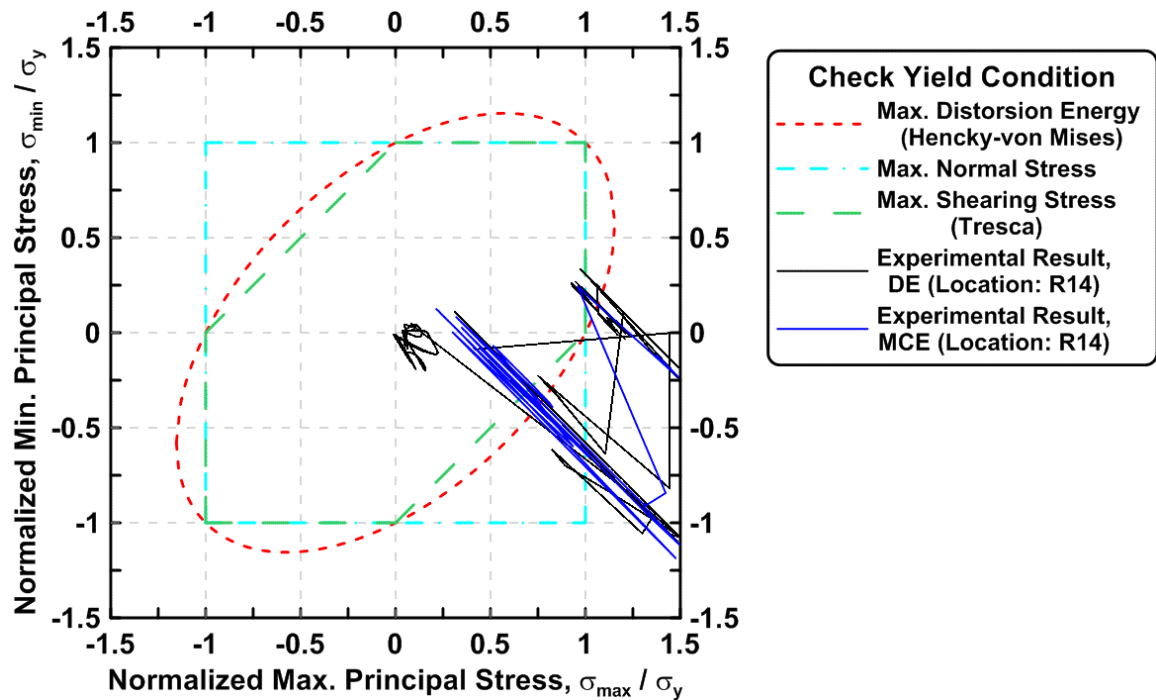


Figure 4.400 Normalized maximum principal stress vs. normalized minimum principal stress in the one-piece gusset plate of TCBF-B-4 specimen (location: R14)

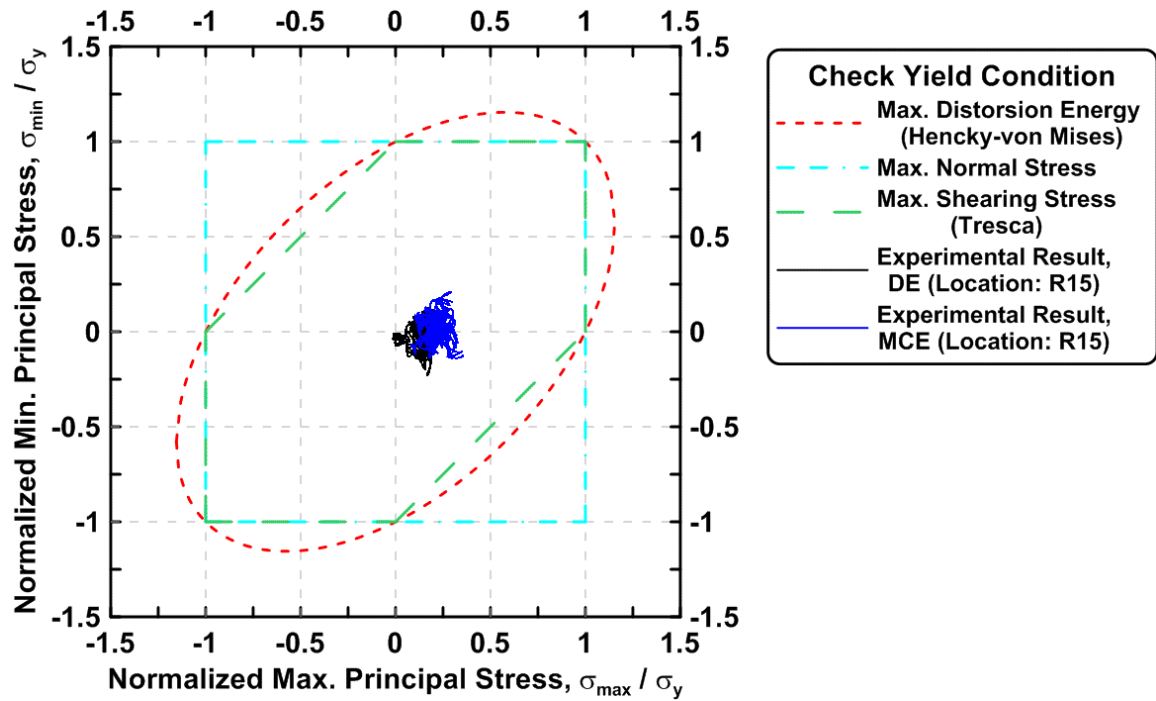


Figure 4.401 Normalized maximum principal stress vs. normalized minimum principal stress in the one-piece gusset plate of TCBF-B-4 specimen (location: R15)

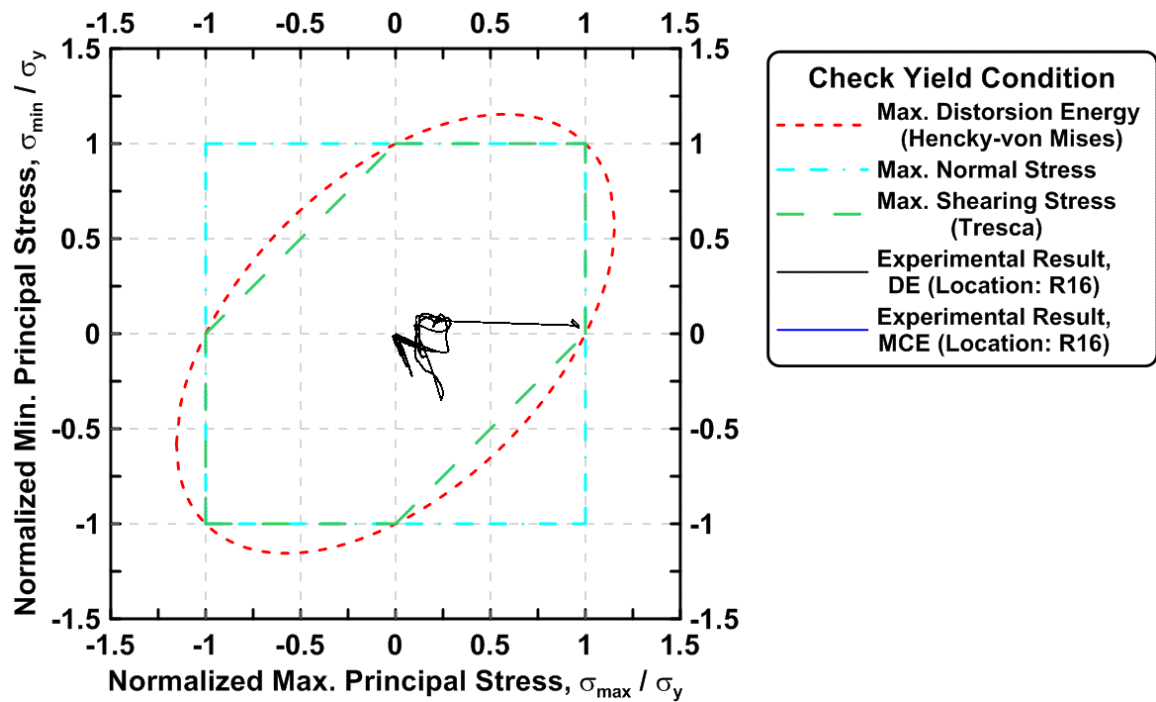


Figure 4.402 Normalized maximum principal stress vs. normalized minimum principal stress in the one-piece gusset plate of TCBF-B-4 specimen (location: R16)

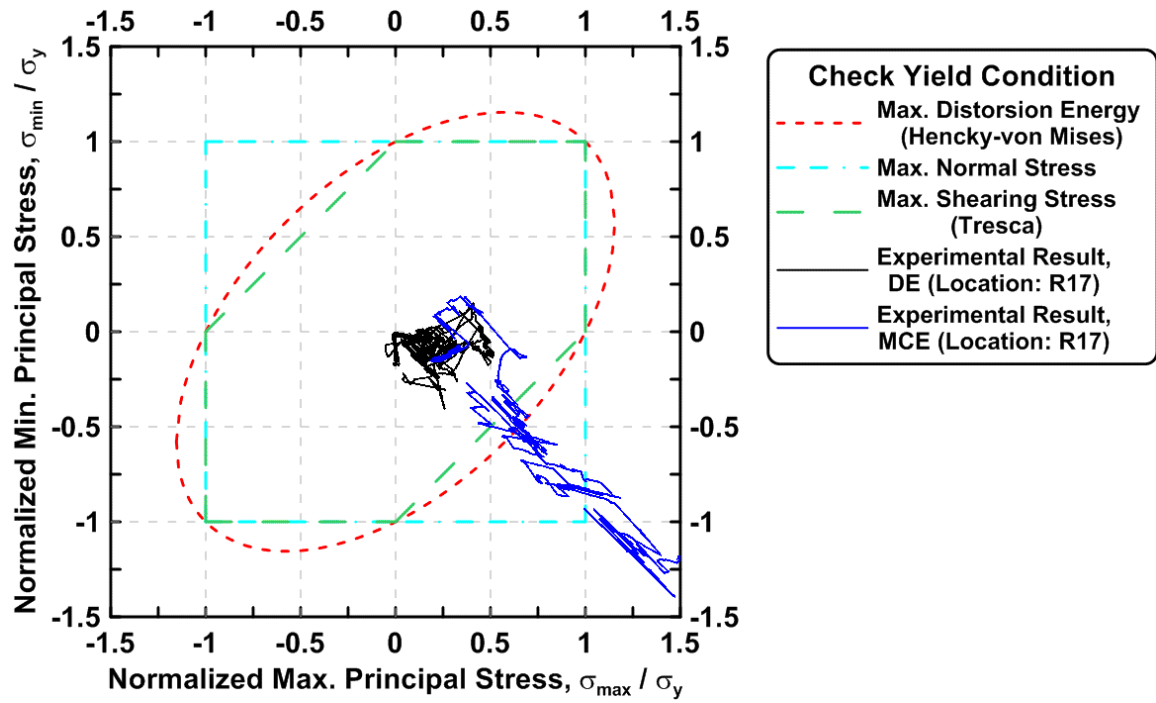


Figure 4.403 Normalized maximum principal stress vs. normalized minimum principal stress in the one-piece gusset plate of TCBF-B-4 specimen (location: R17)

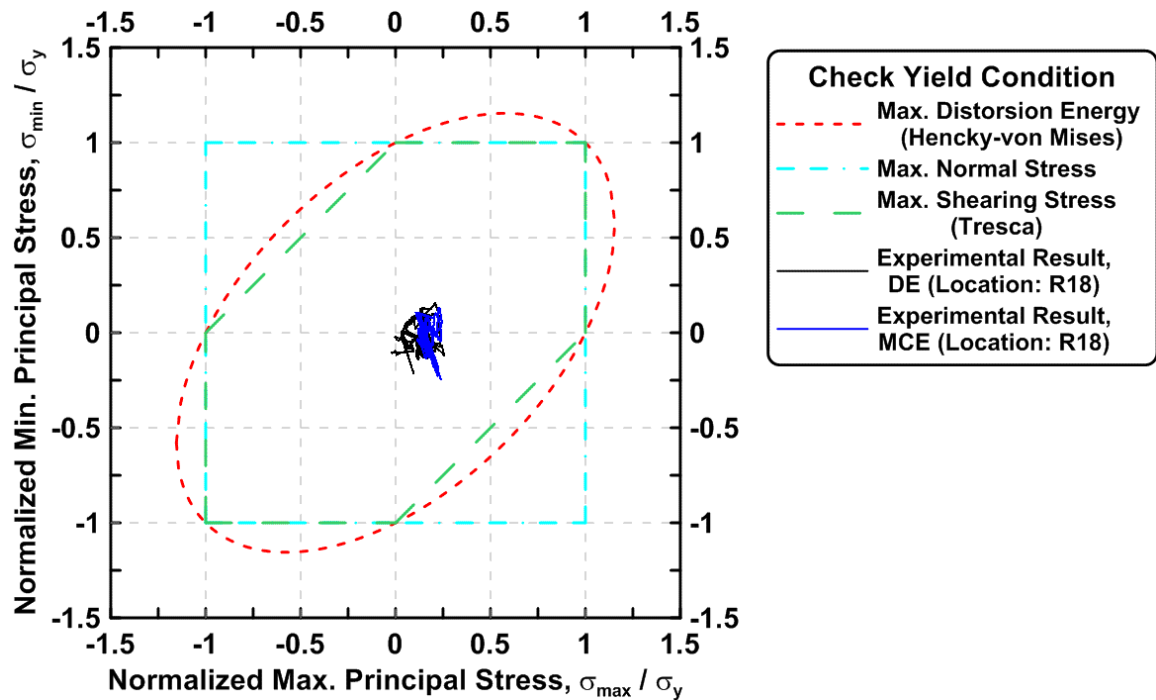


Figure 4.404 Normalized maximum principal stress vs. normalized minimum principal stress in the one-piece gusset plate of TCBF-B-4 specimen (location: R18)



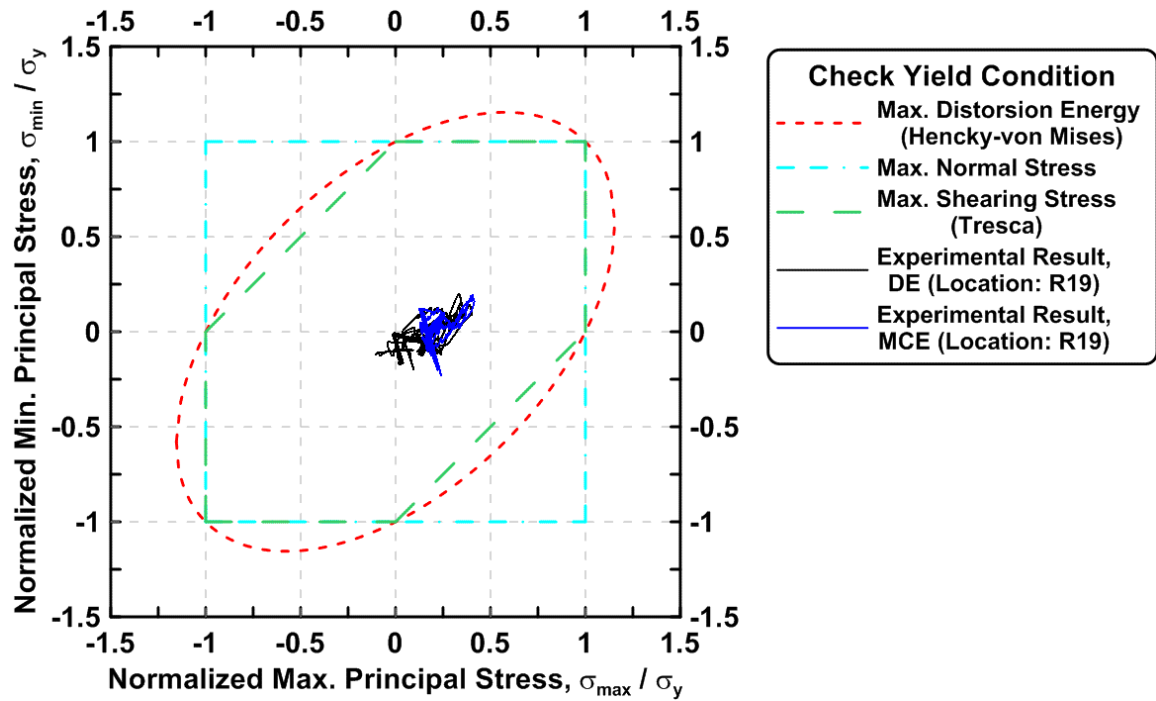


Figure 4.405 Normalized maximum principal stress vs. normalized minimum principal stress in the one-piece gusset plate of TCBF-B-4 specimen (location: R19)

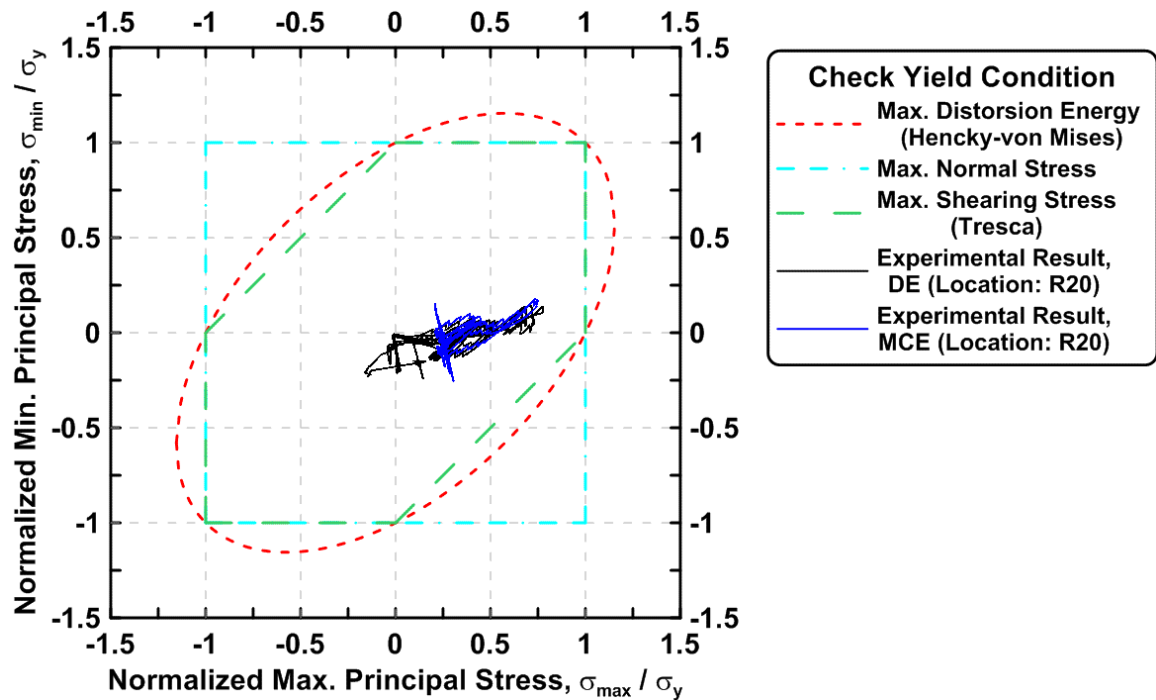


Figure 4.406 Normalized maximum principal stress vs. normalized minimum principal stress in the one-piece gusset plate of TCBF-B-4 specimen (location: R20)

### 4.3.1.7 Test Setup Response

The actuator bracket deformations versus actuator forces are plotted in Fig. 4.407. The relative displacement time history between the base plates of the specimen and the floor beam, relative displacement time history between floor beam and strong floor, and relative displacement time history between integrated reconfigurable reaction wall and strong floor at northern and southern sides are shown in Fig. 4.408. The out-of-plane deformation time history of the lateral supporting frame with respect to the wall of the building at different locations is plotted in Fig. 4.409. The reconfigurable reaction wall (RRW) tip deformation time histories during the test are shown in Fig. 4.410.

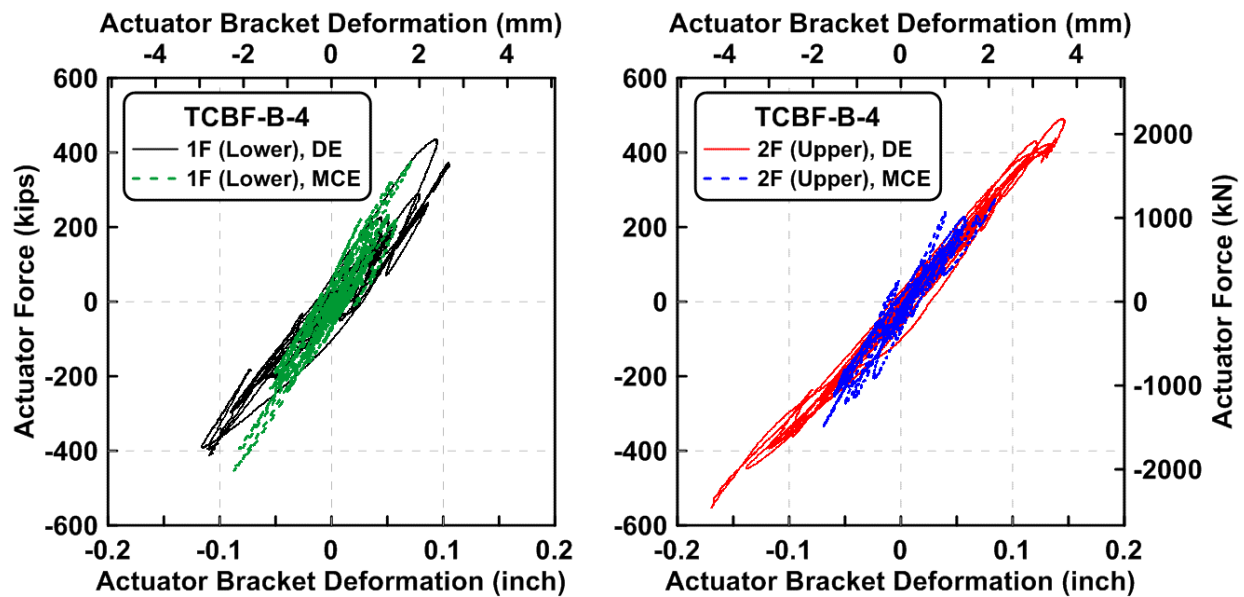


Figure 4.407 The actuator force vs. bracket deformation relationship at both floor levels during hybrid simulation

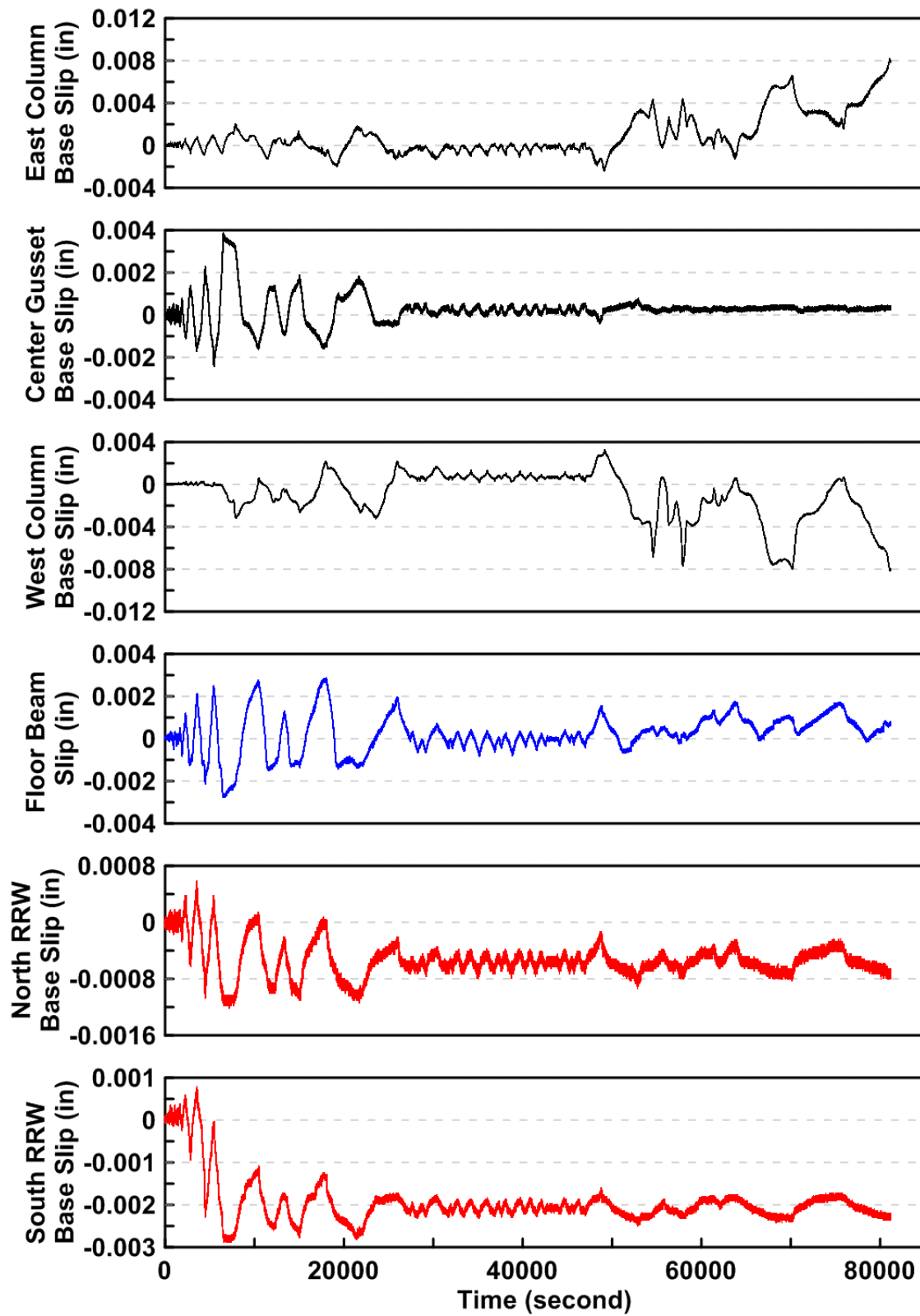


Figure 4.408 Slippage time history between specimen and test setup boundaries during hybrid simulation

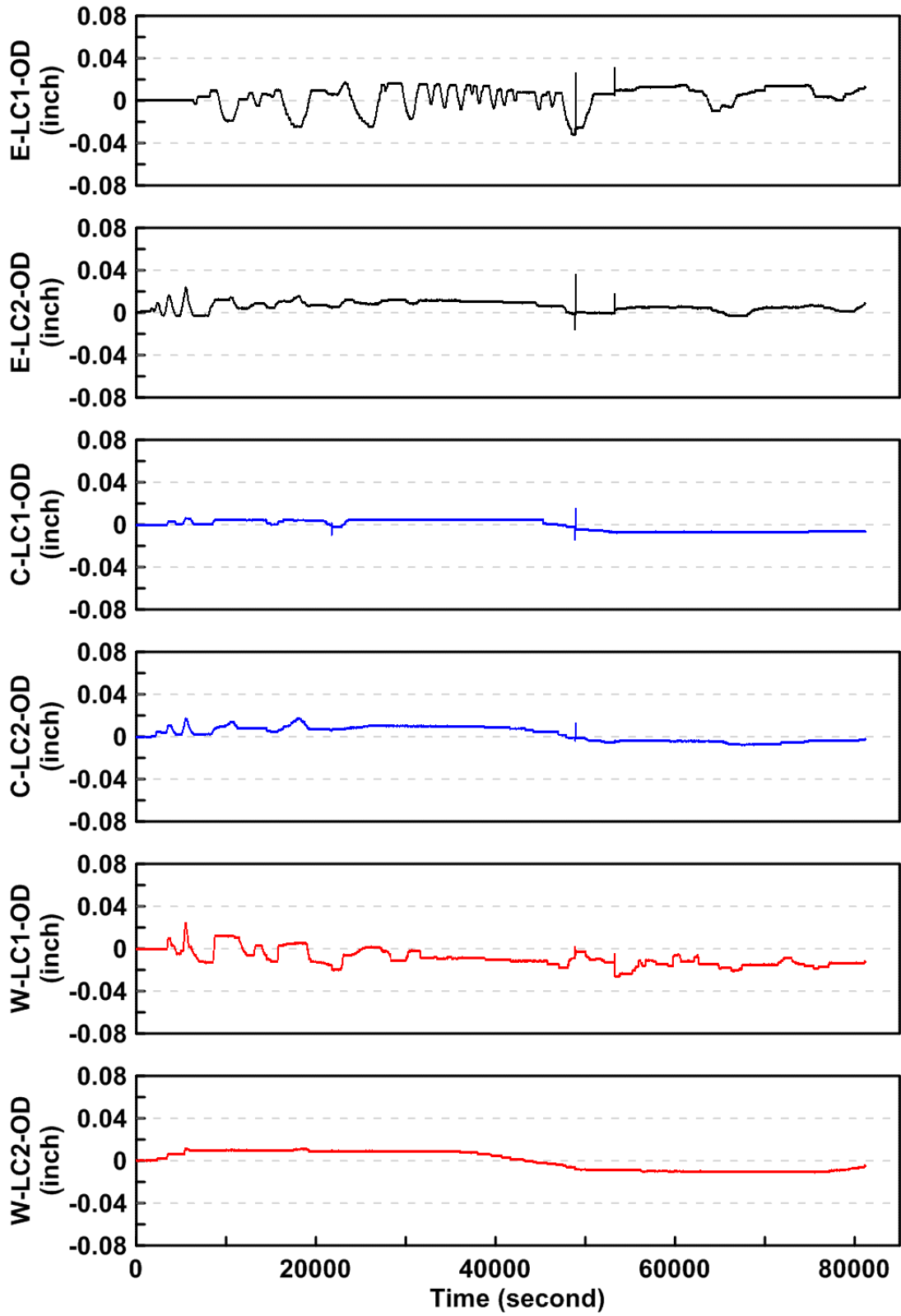


Figure 4.409 The out-of-plane deformation time history of lateral supporting frame at different monitoring points during hybrid simulation

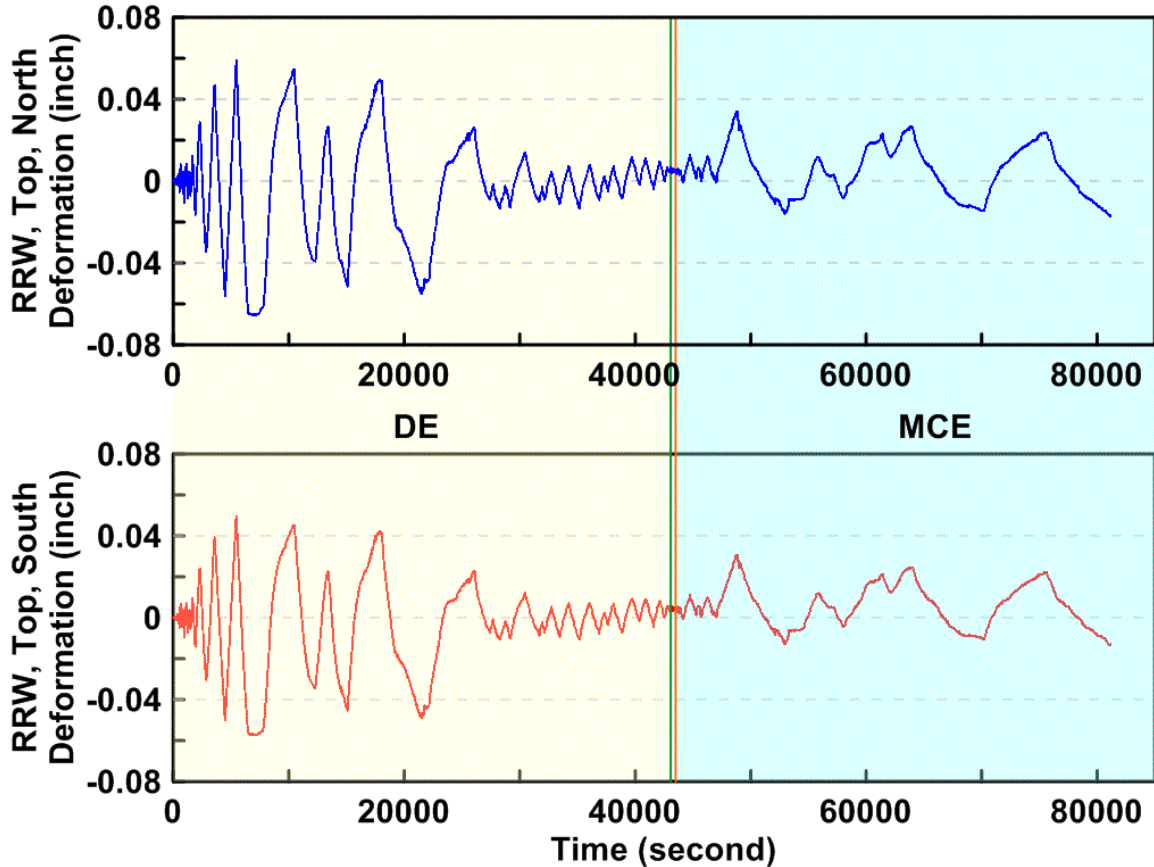


Figure 4.410 The reconfigurable reaction wall (RRW) tip deformation time histories during hybrid simulation

### 4.3.2 Main Observations

The hybrid test started at 10:54 PM on Saturday, March 26, 2011 after two small elastic range tests were completed and instrument readings were carefully checked. The input ground motions for the hybrid simulation are shown in Fig. 3.77. The hybrid test was divided into three major phases: a 20-second long design earthquake (DE) level ground motion, a 3-second silence and followed by a 20-second maximum credible (MCE) level ground motion. The damage condition of the specimen at the end of the MCE event did not permit assessment of the effects of aftershocks.

Some key observations at specific time steps are briefly described below.

**Time step 460 (4.60 second) at 12:11 AM**

Some whitewash flaking (Fig. 4.411) occurred at the northern face of column web in the first story eastern side column.

**Time step 507 (5.07 second) at 12:45 AM**

The east side HSS brace in the lower story began to buckle out-of-plane towards the south side of the lab (Fig. 4.412). The bottom story drift at this time was about 0.79%.

**Time step 510 (5.10 second) at 12:52 AM**

The west side HSS brace in the second story also buckled out-of-plane towards the south side of the lab (Fig. 4.413). The top story drift at this time was about 0.85%.

**Time step 515 (5.15 second) at 1:00 AM**

Local buckling of the square HSS section near the middle part of entire bracing member was observed at both eastern side brace in the bottom story and western side brace in the top story (Figs. 4.414 and 4.415). The bottom story drift at this time was 1.45%.

**Time step 537 (5.37 second) at 1:19 AM**

Minor whitewash flaking occurred at the west bottom side of the lower beam-to-gusset plate splice (Fig. 4.416).

**Time step 540 (5.40 second) at 1:26 AM**

The west side HSS brace in the lower story buckled out-of-plane towards the south side of the lab. The bottom story drift at this time was 0.30%.

**Time step 541 (5.41 second) at 1:30 AM**

The east side HSS brace in the second story also buckled out-of-plane to the south side of the lab. The top story drift at this time was 0.42%.

**Time step 559 (5.59 second) at 1:50 AM**

Local buckling of the square HSS section near the middle part of entire bracing member was observed at both eastern side brace in the second story and western side brace in the first story. Additional flaking of whitewash occurred near the lower beam-to-gusset plate splice at the western beam end (Fig. 4.417). Minor flaking of whitewash also occurred near the west column base in the first story.

**Time step 656 (6.56 second) at 3:04 AM**

Several loud popping noises were heard at the time steps equaled to 648, 652, and 656 when the roof actuator displacement corresponding to -2.4 in., -2.5 in. and -2.9 in. At the same time, panel zones (both east and west sides) in the second story began to yield (detected visually via whitewash flaking, see Fig. 4.418).

**Time step 676 (6.76 second) at 3:30 AM**

Cracks initiated at the corner of the square HSS section in the first-story eastern side brace (Fig. 4.419). The bottom story drift at this time was 0.11%.

**Time step 682(6.82 second) at 3:40 AM**

Cracks initiated at the corner of the square HSS section in the second-story western side brace (Fig. 4.420).

**Time step 701 (7.01 second) at 4:00 AM**

Cracks propagated from the corner of the square HSS section to the center of cross section in the second-story western side brace (Fig. 4.421).

**Time step 726 (7.26 second) at 4:30 AM**

Cracks initiated at the corner of the square HSS section in the first-story western side brace and the second-story eastern side brace (Fig. 4.422).

**Time step 734 (7.34 second) at 4:47 AM**

Cracks propagated from the corner of the square HSS section to the center of the cross section in the second-story east side brace (Fig. 4.423).

**Time step 740 (7.40 second) at 4:57 AM**

The top story eastern side brace completely fractured when the roof actuator was around -4.2 in. (Fig. 4.424). No damage was found in the repaired column base in the first-story east side.

**Time step 1019 (10.19 second) at 7:24 AM**

No special findings observed.

**Time step 2000 (20.00 second) at 10:52 AM**

The design earthquake (DE) level ground motion for the hybrid simulation finished. At this point, one brace completely fractured (top story, east side) and the other three braces partially fractured. No severe column plastic hinging was observed. Fig. 4.329(c) shows the entire specimen after design earthquake level ground motion.

The maximum credible earthquake (MCE) level ground motion for the hybrid simulation continued at time step 2300 after 3-second silence of input ground motion. This period of time without input ground motion was sufficient to stop vibration of the test specimen.

**Time step 2765 (27.65 second) at 12:29 PM**

The second-story western side brace completely fractured (Fig. 4.425).

**Time step 2766 (27.66 second) at 12:30 PM**

The first-story eastern side brace completely fractured (Fig. 4.426).

**Time step 2799 (27.99 second) at 1:42 PM**

The first-story western side brace completely fractured (Fig. 4.427).

**Time step 3023 (30.23 second) at 6:27 PM**

Both column flanges experienced localized buckling near the first-story column base when the roof actuator displacement was about -10.44 in. (Fig. 4.428).

**Time step 3124 (31.24 second) at 9:26 PM**

The roof actuator hit the displacement interlock at about -10.5 inches. This interlock setting was smaller than the ideal capacity of the actuator (12 inches) because the actuator was not exactly at its mid-position at the beginning of the tests. The simulation terminated automatically.

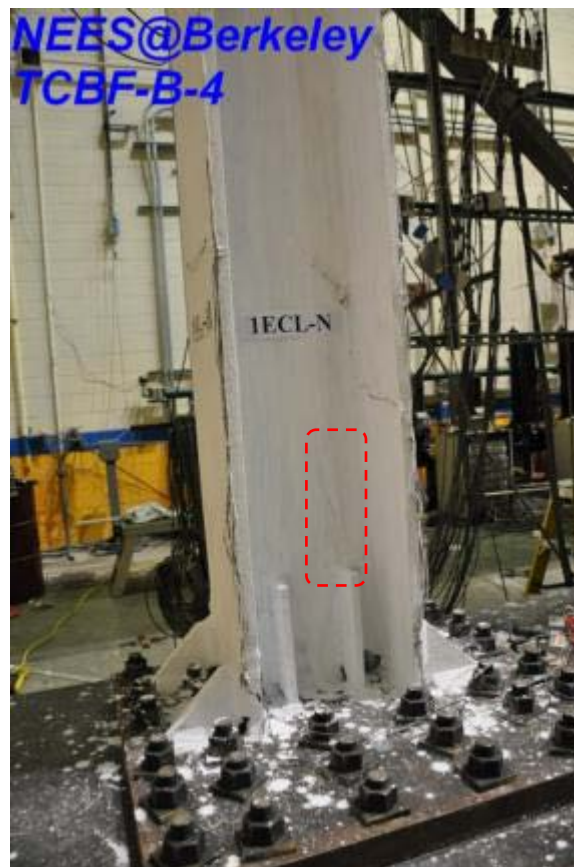


**Figure 4.411 The whitewash flaking near the repaired column base**



Figure 4.412 Global buckling of eastern side brace in the first story



Figure 4.413 Global buckling of western side brace in the second story



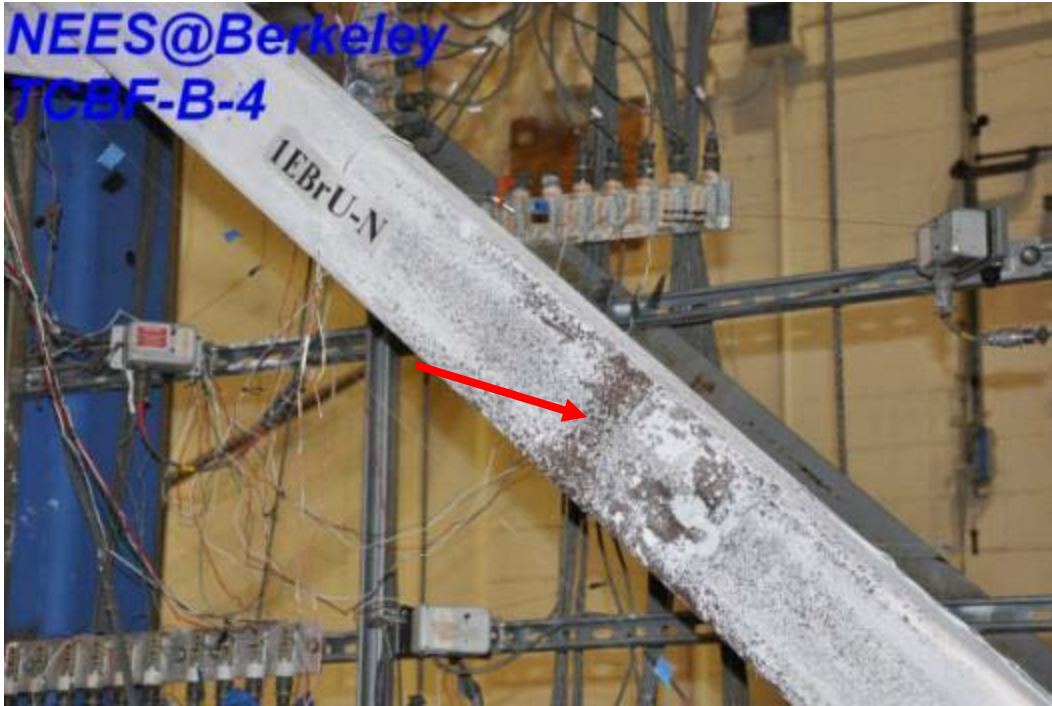


Figure 4.414 Local buckling of eastern side brace in the first story



Figure 4.415 Local buckling of western side brace in the second story



Figure 4.416 Local yielding in the beam-to-gusset plate splice



Figure 4.417 Additional flaking of whitewash near the lower beam splice plate



Figure 4.418 Panel zone yielding in the roof beam to column connection region



Figure 4.419 Cracks in the first story eastern side brace



Figure 4.420 Cracks in the second story western side brace



Figure 4.421 Crack propagation in the second story western side brace



Figure 4.422 Cracks developed in the first story western side brace



Figure 4.423 Cracks opening in the second story eastern brace



Figure 4.424 Completely fracture of the second story eastern side brace



Figure 4.425 Completely fracture of the second story western side brace



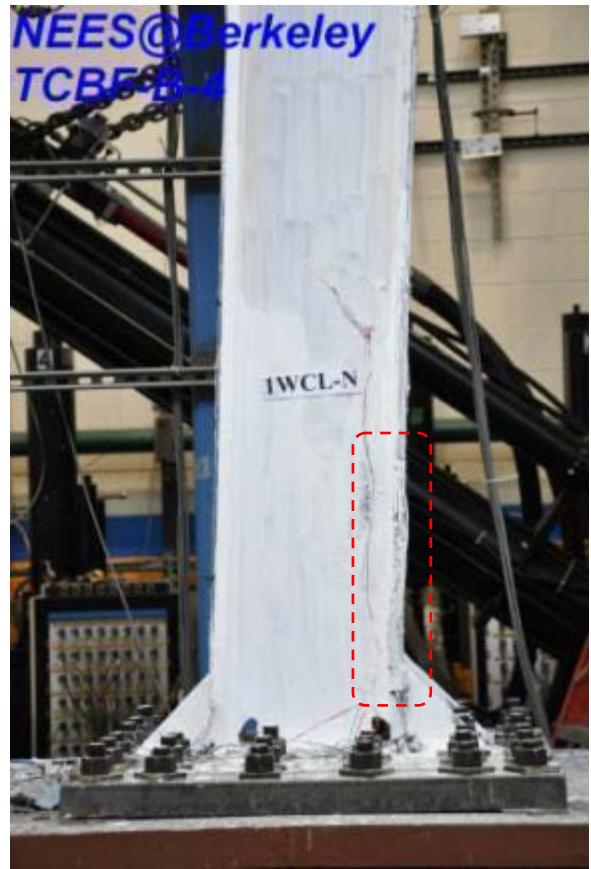
Figure 4.426 Completely fracture of the first story eastern side brace



Figure 4.427 Completely fracture of the first story western side brace



(a) East side



(b) West side

Figure 4.428 Local buckling of column flanges in the first story columns



## 5 Discussion of Experimental Results

In this chapter, the results from tests on four concentric braced frame specimens having the same basic configuration but with different bracing elements and details are examined, compared and discussed. Three of the specimens were tested using the same prescribed cyclic quasi-static displacement history, and one was tested using hybrid simulation. The following sections describe the key response and behavioral characteristics investigated in this study. Test results are compared to numerical simulations in Chapter 6.

### 5.1 QUASI-STATIC TEST RESULTS

The three quasi-statically tested braced frame specimens are discussed in this section. To facilitate further discussion, the cyclic loading protocol shown in Fig. 3.28 is reformatted in Table 5.1. Loading protocol is grouped into several stages (having the same displacement amplitude). The minimum number of cycles for each stage (amplitude) is two (2007, FEMA 461). The design parameter  $D_{be}$  in Table 5.1 is defined as elastic story drift and was determined from the elastic analysis of model building under seismic forces given in Table 3.5 without introducing any amplification factors. Elastic structural analysis indicated a 0.46-in. roof displacement under this distribution of seismic forces. A nominal value of  $D_{be}$  that equals 0.40 in. was selected here. Under the same loading condition, the maximum stress ratio ( $P/\phi_c P_n = 183/270$ ) in the braces was about 0.678. By extrapolation,  $D_{by}$ , the displacement at which a brace would reach its critical compression strength is estimated as:

$$D_{by} = \frac{D_{be}}{0.678} = 0.59 \quad (5.1)$$

and a nominal value of  $D_{by}$  equals to 0.60 in. was selected. The  $D_{bm}$  was selected based on the following formula:

$$D_{bm} = C_d \times D_{be} = 5.0 \times 0.4 = 2.0 \quad (5.2)$$

where  $C_d$  is the deflection amplification factor as defined in AISC Seismic Provisions (AISC 341-05, 2005).

Roof drift ratios are computed as the targeted roof displacement (measured at the centerline of roof beam) divided by roof height times 100, and expressed as percent (%) radians. The excursion numbers in Table 5.1 are the cycle numbers from the very beginning of cyclic test. Note that the table lists all target roof displacements that are reachable based on the stroke of the actuators. The cyclic tests typically stop before reaching the limit of the actuator stroke.

**Table 5.1 Loading Protocol Details of TCBF-B Specimens**

Load Stage Number	Number of Cycles	Target Roof Displacements (inch)	Roof Displacements (design parameters)	Roof Drift Ratio (%)	Excursion Number
1	6	0.2	$0.5 D_{be}$	0.09	1 ~ 6
2	2	0.4	$D_{be}$	0.19	7 ~ 8
3	2	0.6	$D_{by}$	0.28	9 ~ 10
4	2	1.0	$0.5 D_{bm}$	0.46	11 ~ 12
5	2	2.0	$1.0 D_{bm}$	0.93	13 ~ 14
6	2	3.0	$1.5 D_{bm}$	1.39	15 ~ 16
7	2	4.0	$2.0 D_{bm}$	1.85	17 ~ 18
8	2	5.0	$2.5 D_{bm}$	2.31	19 ~ 20
9	2	6.0	$3.0 D_{bm}$	2.78	21 ~ 22
10	2	7.0	$3.5 D_{bm}$	3.24	23 ~ 24
11	2	8.0	$4.0 D_{bm}$	3.70	25 ~ 26
12	2	9.0	$4.5 D_{bm}$	4.17	27 ~ 28
13	2	10.0	$5.0 D_{bm}$	4.63	29 ~ 30
14	2	11.0	$5.5 D_{bm}$	5.09	31 ~ 32
15	2	12.0	$6.0 D_{bm}$	5.56	33 ~ 34

(Note: loading is stopped when both braces completely fracture in the first story)

(Actuator displacement rate is 0.01 in/sec in each load stage)

### 5.1.1 Specimen Global Behavior

Tables 5.2, 5.3 and 5.4 summarize the base shear and roof displacement data in each excursion for the first three specimens. The excursion number column in the aforementioned tables is the cycle number from the very beginning of each cyclic test and the sign that follows the number indicates the positive or negative roof displacement of the excursion. As defined previously, a positive roof displacement means the specimen is pushed towards the east side of the laboratory and a negative roof displacement means the specimen is pulled towards the west. Looking at the target roof displacements and the peak roof displacements in each excursion, we can clearly see that the peak roof displacements in each excursion essentially follow the commands with only minor differences. The exception to this is for Specimen TCBF-B-2, during which an offset of around 0.15 inch was necessitated after excursion 16<sup>+</sup> due to shifting of the specimen during the column base repairs.

There are a number of ways to characterize the deformation capacity of a braced frame. AISC Seismic Provisions for cyclic qualification tests of buckling restrained braces suggests that the capacity would be defined at the onset of rupture, brace instability or connection failures.

This definition will be used here. However, others have recognized the ability of a structural system to deform plastically beyond the first rupture of components. In the case of braced frames, the beams, columns and remaining braces may continue to provide substantial lateral stiffness and lateral load capacity. As such, some guidelines consider the deformation capacity of the structure to be reached when the strength of the system reduces from its peak value by 20% (or other such criteria).

Using the first complete fracture of a brace as the displacement capacity, the first brace completely fractures in Specimen TCBF-B-1 during the excursion number 17<sup>-</sup> (at a 1.85% roof drift ratio). While in the TCBF-B-2 and TCBF-B-3 specimens, the excursion numbers at complete brace fracture correspond to 21<sup>-</sup> (2.78% roof drift ratio) and 19<sup>-</sup> (2.31% roof drift ratio), respectively (see key observations “CF” in Tables 5.2, 5.3 and 5.4). It is clear that the specimen TCBF-B-2 using round hollow structural section as bracing members has the best system deformation capacity among the three specimens tested. The displacement capacity of the specimen with round HSS braces is about 50% greater than that for the specimen with square HSS braces. This also can be seen from the specimen base shear versus roof displacement relationships for all three quasi-static tested specimens (see Figs. 4.8, 4.110 and 4.231).

The maximum base shears during these cyclic loading tests are all less than 900 kips as intended from the specimen design phase (see Fig. 5.1 backbone curves). Maximum base shears for Specimens TCBF-B-1, TCBF-B-2 and TCBF-B-3 are 789.1 kips (13<sup>+</sup>, 0.93%), -845.6 kips (15<sup>-</sup>, 1.39%) and 666.5 (11<sup>+</sup>, 0.46%), respectively, where the values in the parentheses indicates the excursion number, loading direction and target roof drift ratio.

For the TCBF-B-1 and TCBF-B-2 specimens, the peak base shear occurs after the onset of brace global buckling but before local buckling in the braces occurs. However, the peak base shear occurs in the excursion during the TCBF-B-3 test where a wide flange brace begins to buckle globally. While this difference may be associated with the shape of the brace cross section, it plausible to suppose it is due to the difference in the lower beam-to-gusset plate connection rigidity. In the first two specimens, rigid connections (CJP welds at the top and bottom flanges and also at the beam web) are used at both ends of the W24 × 68 lower beam, while pin connections are used in TCBF-B-3 specimen. The lower beam end moment connections substantially contribute to the story shear through the frame action once the braces begin to buckle in the first two specimens. This behavior can also be discovered in the specimen base shear versus roof displacement relationships plotted for these specimens in Figs. 4.8, 4.110 and 4.231.

The peak base shears in each loading excursion degrade faster once local buckling at the middle length of braces occurs, as can be seen in Tables 5.2, 5.3 and 5.4. From those tables, it is found that the specimen TCBF-B-3 has the smallest peak shear degradation rate among the three braced frame specimens. By comparing the specimen base shear versus roof displacement relationships for these specimens (Figs. 4.8, 4.110 and 4.231) at around a positive 4-inch (excursion 17<sup>+</sup>) roof displacement, we find that the peak base shears in this excursion are about the same for all three specimens. At this point in this excursion, based on the test observations, the lower beam-to-gusset plate connections for Specimens TCBF-B-1 and TCBF-B-2 are substantially damaged. Thus, at this point, they are not completely rigid and in both cases only one beam flange remains connected at both ends of the beam to the gusset plates. Thus, moment connections at the ends of the gusset plates partially fracture and deteriorate to act like “pin connections.” As such, it is not believed that the end fixity of the beam to gusset plate has a significant effect on the displacement capacity. With those evidences, it is inference to say that

the peak shear degradations between different load stages in TCBF-B-1 and TCBF-B-2 specimens mainly come from the deteriorations of rigidity of lower beam-to-gusset plate connections while the peak shear degradations within the same load stage come from the deteriorations of buckled braces.

If we look at the total energy dissipation prior to the complete fracture of the first brace, the three specimens individually dissipate 13,698 kip-in, 30,294 kip-in and 15,111 kip-in. It is evident that Specimen TCBF-B-2 dissipates the most energy before the first brace fracture; more than twice that dissipated by either of the other two specimens. Figure 5.2 compares the cumulative energy dissipation of each specimen in a bar chart format. From this figure, one can discover that the total energy dissipation increases substantially after excursion number 11<sup>+</sup> for all three specimens, which is the same excursion where brace global buckling (GB) is observed. Before the first brace completely fractures (CF) in Specimen TCBF-B-1, Specimens TCBF-B-1 and TCBF-B-2 dissipate similar quantities of energy. However, Specimen TCBF-B-3 only dissipates about 80% of the energy dissipated by either of the first two specimens. This may mean that about 20% of the system energy dissipation is contributed by the formation of plastic hinges at the lower beam-to-gusset plate moment connections. This will be examined below.

Examining the energy dissipation in each load excursion (Figs. 5.3, 5.4 and 5.5), it is interesting to note that the energy dissipation typically increases as the excursion number increases (i.e. target displacement increases), but the system energy dissipation per excursion drops after brace fracturing. Also, the energy dissipation decreases in the second cycle of each load stage by comparing the energy dissipation for subsequent pairs of excursions to the same target displacement.

Similar results are found by comparing the cumulative roof plastic deformation (Fig. 5.6) or the normalized energy dissipation (Fig.5.7). The cumulative roof plastic deformation and the normalized energy dissipation are defined in the title row of Tables 5.2, 5.3 and 5.4. The  $P_y$  value used in these equations for each specimen is averaged from four base shear forces corresponding to roof displacements equal to  $\pm 0.6$  inch during the tests. Specimen TCBF-B-2 again has the largest cumulative roof plastic deformation (51.4 inch) and cumulative normalized energy dissipation (85.7) among three specimens before the first brace fractures. The specimens TCBF-B-1 and TCBF-B-3 have cumulative roof plastic deformations, 24.6 inch and 25.8 inch, about half the value for Specimen TCBF-B-2. For the normalized energy dissipation, they have 41.0 and 43.1 respectively, also about half the value for Specimen TCBF-B-2.

A key aspect of behavior of interest to engineers and researchers alike is whether soft story mechanisms form in the specimens as inelastic displacement amplitudes increase. Story deformations or story drifts are taken herein as the difference between the lateral displacements at the top and lower beam for the top story, and the lower beam and the base for the ground story. Looking at the story shear versus story deformation relationships shown in Figs. 4.9, 4.111 and 4.232, we clearly see that in Specimen TCBF-B-1, the story deformation has a tendency to concentrate at the first story during the test. The ratios of story deformation to total roof displacement at each story are shown in Figs. 5.8, 5.9 and 5.10. We see in Fig. 5.8 that story drift ratios during early cycles in Specimen TCBF-B-1 for top and bottom story are around 30% and 70% of the total roof displacement, respectively. It is noted that there is an asymmetry in the data after the first few cycles, with the first story taking a higher percentage of the roof displacement during displacement cycles in the negative direction than when loaded in the positive direction. For Specimens TCBF-B-2 and TCBF-B-3 the displacements were more equally distributed between the two stories during the initial cycles (Figs. 5.9 and 5.10).

It should be pointed out that in Specimen TCBF-B-1, the bottom story deformation was measured using the position transducers located at the west side of the specimen (next to the actuators, see Appendix D for details). This was not the true specimen displacement since the position transducers also measure the gaps between clevis pin, actuator rod head and the specimen end plate. This also results in unsymmetrical readings during the test. It is believed that the unsymmetrical readings cause the story deformation ratios deviate from 50 % in that test. For Specimens TCBF-B-2 and TCBF-B-3 tests, an additional position transducer is installed and directly measures the first story deformation to rule out this effect.

For TCBF-B-2 specimen, the first story contribution to the roof displacements increase once buckling of the braces begin. However, in excursion 17, a significant asymmetry of deformations occurs, with the first floor contributing more than half of the roof displacement in cycles with negative displacement, and less than 50% for positive displacement excursions. This change in behavior occurs when the lower level beams fracture. Suggesting that the asymmetry is associated with the width of the specimen changing during the test. In this case the horizontal displacements are different at the west and east edges of the specimen. The redistribution of axial forces between the braces once buckling occurs results in axial forces in the beam that will change its length, and more significant changes in beam length might be expected with the formation of plastic hinges at the ends of the lower beam, and with the formation of local buckles and especially flange fractures. For specimen TCBF-B-3, the displacement ratios (Fig. 5.10) are essentially close to 50% throughout the test. This specimen had considerable brace yielding in tension and buckling at both levels, and the bolted connections at the face of the gusset plates at the lower floor level prevented the formation of plastic hinges.

The energy dissipation ratios for each story shown in Figs. 5.11, 5.12 and 5.13 indicate that for all three specimens, more than 60% of total energy dissipates in the first story.

**Table 5.2 Base shear and roof displacement data of TCBF-B-1**

**( $P_y = 556.4$  kips from experiment, corresponding to  $D_{by} = 0.6$  inch at roof)**

Excursion $i^+, i^-$	Target Roof Displacement (inch)	Peak Roof Displacement in Excursion (inch)	Base Shear at Peak Roof Displacement (kips)	Max. Base Shear in Excursion (kips)	Cumulative Hysteretic Area (Energy Dissipation) E (kip-in)	Cumulative Plastic Roof Displacement $E / (P_y)$ (inch)	Normalized Energy Dissipation $E / (P_y * D_{by})$	Key Observations
1 <sup>+</sup>	0.2	0.196	194.4	202.3	16	0.0	0.0	
1 <sup>-</sup>	-0.2	-0.198	-198.3	-215.7	21	0.0	0.1	
2 <sup>+</sup>	0.2	0.201	203.9	203.9	23	0.0	0.1	
2 <sup>-</sup>	-0.2	-0.199	-208.7	-215.2	27	0.0	0.1	
3 <sup>+</sup>	0.2	0.199	183.1	202.9	25	0.0	0.1	
3 <sup>-</sup>	-0.2	-0.203	-211.4	-217.6	31	0.1	0.1	
4 <sup>+</sup>	0.2	0.201	183.0	202.2	30	0.1	0.1	
4 <sup>-</sup>	-0.2	-0.197	-216.4	-216.4	38	0.1	0.1	
5 <sup>+</sup>	0.2	0.201	193.5	200.3	35	0.1	0.1	
5 <sup>-</sup>	-0.2	-0.197	-199.8	-216.5	40	0.1	0.1	
6 <sup>+</sup>	0.2	0.199	182.0	200.7	39	0.1	0.1	
6 <sup>-</sup>	-0.2	-0.197	-213.0	-218.8	46	0.1	0.1	
7 <sup>+</sup>	0.4	0.400	359.7	380.2	93	0.2	0.3	
7 <sup>-</sup>	-0.4	-0.403	-411.4	-418.1	124	0.2	0.4	

Excursion $i^+, i^-$	Target Roof Displacement (inch)	Peak Roof Displacement in Excursion (inch)	Base Shear at Peak Roof Displacement (kips)	Max. Base Shear in Excursion (kips)	Cumulative Hysteretic Area (Energy Dissipation) E (kip-in)	Cumulative Plastic Roof Displacement $E / (P_y)$ (inch)	Normalized Energy Dissipation $E / (P_y * D_{by})$	Key Observations
8 <sup>+</sup>	0.4	0.398	366.8	386.4	118	0.2	0.4	
8 <sup>-</sup>	-0.4	-0.400	-410.8	-415.5	140	0.3	0.4	
9 <sup>+</sup>	0.6	0.596	532.3	532.3	219	0.4	0.7	
9 <sup>-</sup>	-0.6	-0.602	-575.5	-580.8	286	0.5	0.9	
10 <sup>+</sup>	0.6	0.599	542.7	550.0	288	0.5	0.9	
10 <sup>-</sup>	-0.6	-0.599	-575.1	-579.7	335	0.6	1.0	
11 <sup>+</sup>	1.0	0.997	723.9	731.4	561	1.0	1.7	GB*
11 <sup>-</sup>	-1.0	-1.001	-735.7	-736.9	819	1.5	2.5	
12 <sup>+</sup>	1.0	0.997	687.7	709.1	991	1.8	3.0	
12 <sup>-</sup>	-1.0	-1.001	-691.3	-711.7	1211	2.2	3.6	
13 <sup>+</sup>	2.0	1.999	779.1	<b>789.1</b>	2057	3.7	6.2	
13 <sup>-</sup>	-2.0	-1.999	-772.8	-778.9	3062	5.5	9.2	
14 <sup>+</sup>	2.0	1.998	737.7	755.7	3844	6.9	11.5	
14 <sup>-</sup>	-2.0	-2.002	-754.3	-760.2	4610	8.3	13.8	
15 <sup>+</sup>	3.0	2.998	725.4	756.9	5993	10.8	18.0	LB*
15 <sup>-</sup>	-3.0	-2.999	-750.7	-761.3	7652	13.8	22.9	
16 <sup>+</sup>	3.0	2.997	656.3	662.4	8964	16.1	26.9	
16 <sup>-</sup>	-3.0	-2.999	-670.1	-685.6	10215	18.4	30.6	
17 <sup>+</sup>	4.0	4.000	651.2	667.1	11915	21.4	35.7	CI*

Excursion $i^+$ , $i^-$	Target Roof Displacement (inch)	Peak Roof Displacement in Excursion (inch)	Base Shear at Peak Roof Displacement (kips)	Max. Base Shear in Excursion (kips)	Cumulative Hysteretic Area (Energy Dissipation) $E$ (kip-in)	Cumulative Plastic Roof Displacement $E / (P_y)$ (inch)	Normalized Energy Dissipation $E / (P_y * D_{by})$	Key Observations
17 <sup>-</sup>	-4.0	-4.019	-443.6	-560.1	<b>13698</b>	<b>24.6</b>	<b>41.0</b>	PF*, CF*
18 <sup>+</sup>	4.0	3.998	484.5	497.5	15103	27.1	45.2	
18 <sup>-</sup>	-4.0	-3.998	-364.6	-375.7	16130	29.0	48.3	BF*
19 <sup>+</sup>	5.0	4.998	353.5	422.3	17419	31.3	52.2	
19 <sup>-</sup>	-5.0	-2.232	-258.3	-258.3	17620	31.7	52.8	

\*Note: GB (global buckling), LB (local buckling), PF (partial fracture), CF (complete fracture), CI (crack initial), BF (lower beam-to-gusset plate fracture)



**Table 5.3 Base shear and roof displacement data of TCBF-B-2**

**( $P_y = 589.0$  kips from experiment, corresponding to  $D_{by} = 0.6$  inch at roof)**

Excursion $i^+, i^-$	Target Roof Displacement (inch)	Peak Roof Displacement in Excursion (inch)	Base Shear at Peak Roof Displacement (kips)	Max. Base Shear in Excursion (kips)	Cumulative Hysteretic Area (Energy Dissipation) E (kip-in)	Cumulative Plastic Roof Displacement $E / (P_y)$ (inch)	Normalized Energy Dissipation $E / (P_y * D_{by})$	Key Observations
1 <sup>+</sup>	0.2	0.204	217.6	217.8	19	0.0	0.1	
1 <sup>-</sup>	-0.2	-0.199	-226.7	-226.9	23	0.0	0.1	
2 <sup>+</sup>	0.2	0.205	218.4	220.7	25	0.0	0.1	
2 <sup>-</sup>	-0.2	-0.199	-224.8	-224.8	28	0.0	0.1	
3 <sup>+</sup>	0.2	0.206	205.6	216.9	29	0.0	0.1	
3 <sup>-</sup>	-0.2	-0.198	-225.3	-225.9	33	0.1	0.1	
4 <sup>+</sup>	0.2	0.204	219.1	219.6	34	0.1	0.1	
4 <sup>-</sup>	-0.2	-0.199	-221.9	-225.5	38	0.1	0.1	
5 <sup>+</sup>	0.2	0.204	211.0	218.6	40	0.1	0.1	
5 <sup>-</sup>	-0.2	-0.199	-222.7	-223.7	43	0.1	0.1	
6 <sup>+</sup>	0.2	0.205	216.9	219.0	45	0.1	0.1	
6 <sup>-</sup>	-0.2	-0.198	-224.6	-224.8	48	0.1	0.1	
7 <sup>+</sup>	0.4	0.405	405.4	405.7	104	0.2	0.3	
7 <sup>-</sup>	-0.4	-0.394	-408.2	-427.5	116	0.2	0.3	
8 <sup>+</sup>	0.4	0.403	394.1	414.2	122	0.2	0.3	
8 <sup>-</sup>	-0.4	-0.396	-408.5	-427.6	133	0.2	0.4	
9 <sup>+</sup>	0.6	0.606	558.7	579.1	220	0.4	0.6	

Excursion $i^+, i^-$	Target Roof Displacement (inch)	Peak Roof Displacement in Excursion (inch)	Base Shear at Peak Roof Displacement (kips)	Max. Base Shear in Excursion (kips)	Cumulative Hysteretic Area (Energy Dissipation) E (kip-in)	Cumulative Plastic Roof Displacement $E / (P_y)$ (inch)	Normalized Energy Dissipation $E / (P_y * D_{by})$	Key Observations
9 <sup>-</sup>	-0.6	-0.595	-603.5	-610.3	265	0.4	0.7	
10 <sup>+</sup>	0.6	0.602	592.9	592.9	286	0.5	0.8	
10 <sup>-</sup>	-0.6	-0.595	-600.9	-607.9	307	0.5	0.9	
11 <sup>+</sup>	1.0	1.005	725.7	748.8	577	1.0	1.6	GB*
11 <sup>-</sup>	-1.0	-0.996	-720.5	-741.1	850	1.4	2.4	
12 <sup>+</sup>	1.0	1.001	704.9	725.6	1073	1.8	3.0	
12 <sup>-</sup>	-1.0	-0.996	-709.0	-728.5	1293	2.2	3.7	
13 <sup>+</sup>	2.0	2.004	817.0	828.1	2227	3.8	6.3	
13 <sup>-</sup>	-2.0	-1.995	-829.8	-839.1	3274	5.6	9.3	
14 <sup>+</sup>	2.0	2.004	771.4	782.3	4023	6.8	11.4	
14 <sup>-</sup>	-2.0	-1.997	-774.4	-791.3	4760	8.1	13.5	
15 <sup>+</sup>	3.0	3.002	777.4	798.7	6111	10.4	17.3	
15 <sup>-</sup>	-3.0	-2.996	-836.9	<b>-845.6</b>	7796	13.2	22.1	
16 <sup>+</sup>	3.0	2.842	695.6	695.6	8988	15.3	25.4	
16 <sup>-</sup>	-3.0	-3.150	-835.3	-845.0	10936	18.6	30.9	
17 <sup>+</sup>	4.0	3.847	661.9	664.2	12598	21.4	35.6	BF*
17 <sup>-</sup>	-4.0	-4.152	-834.2	-839.0	14993	25.5	42.4	
18 <sup>+</sup>	4.0	3.845	587.5	591.8	16338	27.7	46.2	
18 <sup>-</sup>	-4.0	-4.152	-753.0	-756.9	18143	30.8	51.3	

Excursion $i^+$ , $i^-$	Target Roof Displacement (inch)	Peak Roof Displacement in Excursion (inch)	Base Shear at Peak Roof Displacement (kips)	Max. Base Shear in Excursion (kips)	Cumulative Hysteretic Area (Energy Dissipation) E (kip-in)	Cumulative Plastic Roof Displacement $E / (P_y)$ (inch)	Normalized Energy Dissipation $E / (P_y * D_{by})$	Key Observations
19 <sup>+</sup>	5.0	4.843	599.5	604.5	19708	33.5	55.8	LB*
19 <sup>-</sup>	-5.0	-5.152	-797.5	-811.1	22259	37.8	63.0	
20 <sup>+</sup>	5.0	4.845	541.6	554.0	23750	40.3	67.2	
20 <sup>-</sup>	-5.0	-5.148	-727.8	-731.7	25917	44.0	73.3	CI*
21 <sup>+</sup>	6.0	5.843	572.1	575.5	27675	47.0	78.3	
21 <sup>-</sup>	-6.0	-6.152	-545.1	-601.3	<b>30294</b>	<b>51.4</b>	<b>85.7</b>	PF*, CF*
22 <sup>+</sup>	6.0	5.845	506.8	517.1	31790	54.0	90.0	
22 <sup>-</sup>	-6.0	-6.148	-515.3	-521.5	33953	57.6	96.1	
23 <sup>+</sup>	7.0	6.843	385.7	445.2	35500	60.3	100.5	
23 <sup>-</sup>	-7.0	-1.373	-311.8	-311.8	36045	61.2	102.0	

\*Note: GB (global buckling), LB (local buckling), PF (partial fracture), CF (complete fracture), CI (crack initial), BF (lower beam-to-gusset plate fracture)

**Table 5.4 Base shear and roof displacement data of TCBF-B-3**

**( $P_y = 584.8$  kips from experiment, corresponding to  $D_{by} = 0.6$  inch at roof)**

Excursion $i^+, i^-$	Target Roof Displacement (inch)	Peak Roof Displacement in Excursion (inch)	Base Shear at Peak Roof Displacement (kips)	Max. Base Shear in Excursion (kips)	Cumulative Hysteretic Area (Energy Dissipation) E (kip-in)	Cumulative Plastic Roof Displacement $E / (P_y)$ (inch)	Normalized Energy Dissipation $E / (P_y * D_{by})$	Key Observations
1 <sup>+</sup>	0.2	0.202	214.0	214.0	18	0.0	0.1	
1 <sup>-</sup>	-0.2	-0.198	-201.0	-208.4	16	0.0	0.0	
2 <sup>+</sup>	0.2	0.203	212.9	215.0	20	0.0	0.1	
2 <sup>-</sup>	-0.2	-0.197	-200.4	-207.4	18	0.0	0.1	
3 <sup>+</sup>	0.2	0.206	212.8	214.4	22	0.0	0.1	
3 <sup>-</sup>	-0.2	-0.199	-204.9	-206.7	20	0.0	0.1	
4 <sup>+</sup>	0.2	0.203	213.0	215.4	23	0.0	0.1	
4 <sup>-</sup>	-0.2	-0.195	-199.8	-206.2	20	0.0	0.1	
5 <sup>+</sup>	0.2	0.202	213.1	215.2	24	0.0	0.1	
5 <sup>-</sup>	-0.2	-0.199	-203.5	-205.6	23	0.0	0.1	
6 <sup>+</sup>	0.2	0.204	208.3	215.3	24	0.0	0.1	
6 <sup>-</sup>	-0.2	-0.196	-204.4	-206.0	24	0.0	0.1	
7 <sup>+</sup>	0.4	0.404	403.3	404.5	80	0.1	0.2	
7 <sup>-</sup>	-0.4	-0.401	-408.7	-409.4	83	0.1	0.2	
8 <sup>+</sup>	0.4	0.401	402.5	409.0	88	0.2	0.3	
8 <sup>-</sup>	-0.4	-0.399	-407.0	-407.8	90	0.2	0.3	
9 <sup>+</sup>	0.6	0.602	580.4	582.5	180	0.3	0.5	

Excursion $i^+, i^-$	Target Roof Displacement (inch)	Peak Roof Displacement in Excursion (inch)	Base Shear at Peak Roof Displacement (kips)	Max. Base Shear in Excursion (kips)	Cumulative Hysteretic Area (Energy Dissipation) E (kip-in)	Cumulative Plastic Roof Displacement $E / (P_y)$ (inch)	Normalized Energy Dissipation $E / (P_y * D_{by})$	Key Observations
9 <sup>-</sup>	-0.6	-0.595	-587.8	-595.4	196	0.3	0.6	
10 <sup>+</sup>	0.6	0.603	588.7	590.1	210	0.4	0.6	
10 <sup>-</sup>	-0.6	-0.592	-582.3	-594.0	211	0.4	0.6	
11 <sup>+</sup>	1.0	1.006	622.4	<b>666.5</b>	428	0.7	1.2	GB*
11 <sup>-</sup>	-1.0	-0.996	-636.6	-649.8	635	1.1	1.8	
12 <sup>+</sup>	1.0	1.005	611.4	614.7	794	1.4	2.3	
12 <sup>-</sup>	-1.0	-0.998	-620.3	-622.8	934	1.6	2.7	
13 <sup>+</sup>	2.0	2.001	638.4	638.4	1607	2.7	4.6	
13 <sup>-</sup>	-2.0	-1.993	-625.0	-632.8	2373	4.1	6.8	
14 <sup>+</sup>	2.0	2.001	567.0	570.0	2930	5.0	8.3	
14 <sup>-</sup>	-2.0	-1.992	-568.8	-570.8	3450	5.9	9.8	
15 <sup>+</sup>	3.0	2.998	632.0	634.8	4414	7.5	12.6	LB*
15 <sup>-</sup>	-3.0	-2.993	-642.4	-649.8	5519	9.4	15.7	
16 <sup>+</sup>	3.0	2.996	568.1	570.0	6373	10.9	18.2	
16 <sup>-</sup>	-3.0	-2.993	-588.7	-595.1	7235	12.4	20.6	
17 <sup>+</sup>	4.0	4.002	630.5	632.8	8488	14.5	24.2	
17 <sup>-</sup>	-4.0	-3.989	-660.0	-661.0	9984	17.1	28.5	
18 <sup>+</sup>	4.0	3.997	570.6	575.0	11204	19.2	31.9	
18 <sup>-</sup>	-4.0	-3.996	-445.0	-448.1	12206	20.9	34.8	CI*, PF*

Excursion $i^+$ , $i^-$	Target Roof Displacement (inch)	Peak Roof Displacement in Excursion (inch)	Base Shear at Peak Roof Displacement (kips)	Max. Base Shear in Excursion (kips)	Cumulative Hysteretic Area (Energy Dissipation) E (kip-in)	Cumulative Plastic Roof Displacement $E / (P_y)$ (inch)	Normalized Energy Dissipation $E / (P_y * D_{by})$	Key Observations
19 <sup>+</sup>	5.0	4.998	619.6	627.3	13794	23.6	39.3	
19 <sup>-</sup>	-5.0	-4.997	-335.4	-414.7	<b>15111</b>	<b>25.8</b>	<b>43.1</b>	CF*
20 <sup>+</sup>	5.0	1.654	234.8	234.8	15337	26.2	43.7	

\*Note: GB (global buckling), LB (local buckling), PF (partial fracture), CF (complete fracture), CI (crack initial)

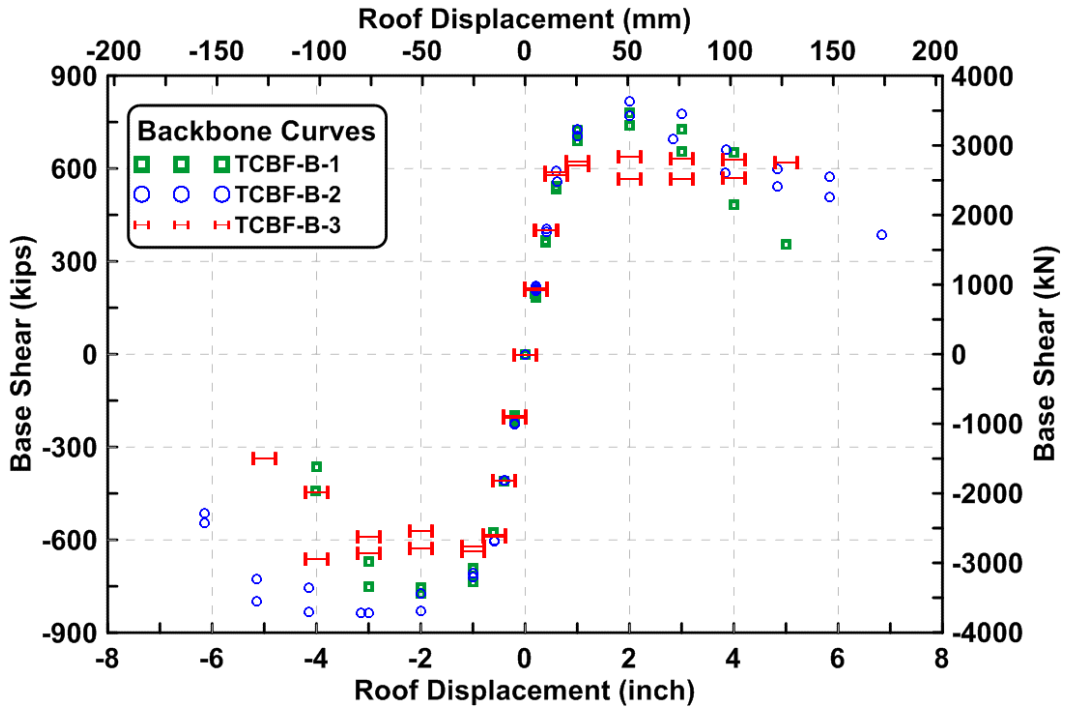


Figure 5.1 Backbone curves of each specimen (both cycle one and cycle two in each load stage)

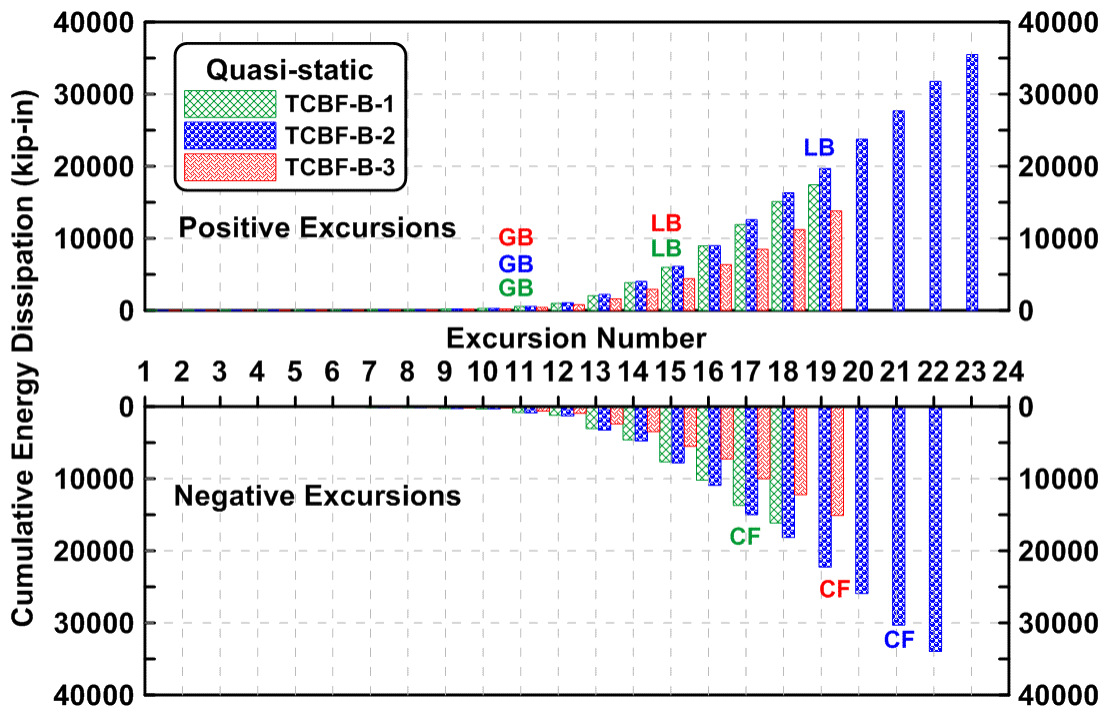


Figure 5.2 Total cumulative energy dissipation of each specimen (GB: global buckling, LB: local buckling, CF: first brace completely fracture)

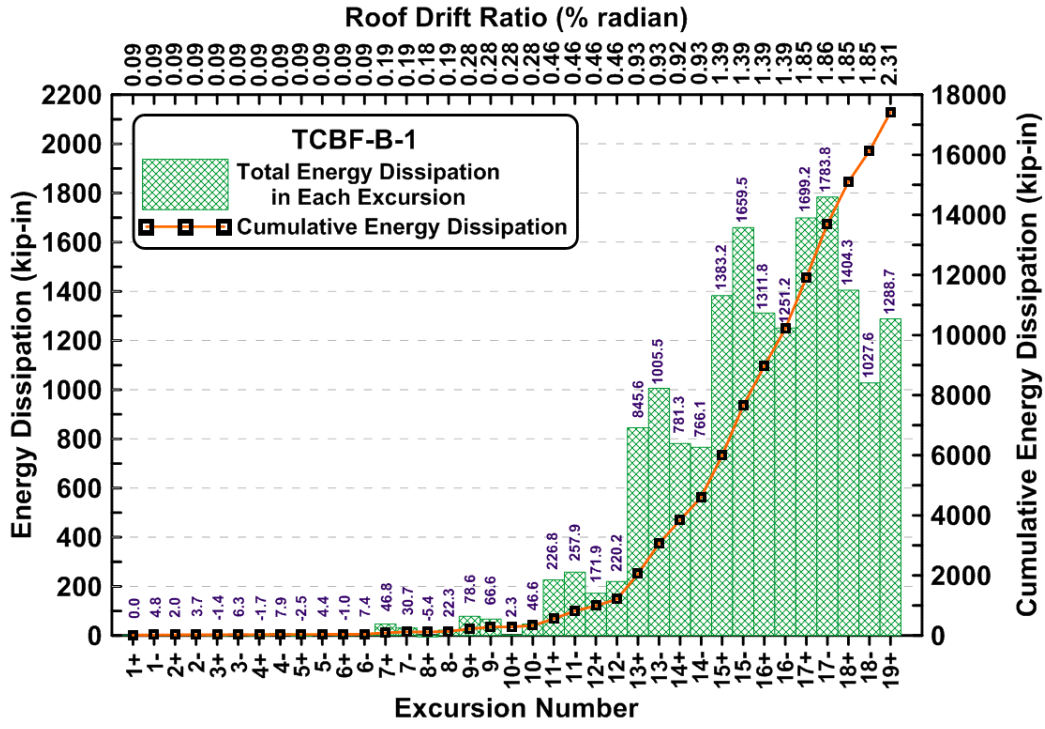


Figure 5.3 Total energy dissipation in each excursion and total cumulative energy dissipation of TCBF-B-1 specimen

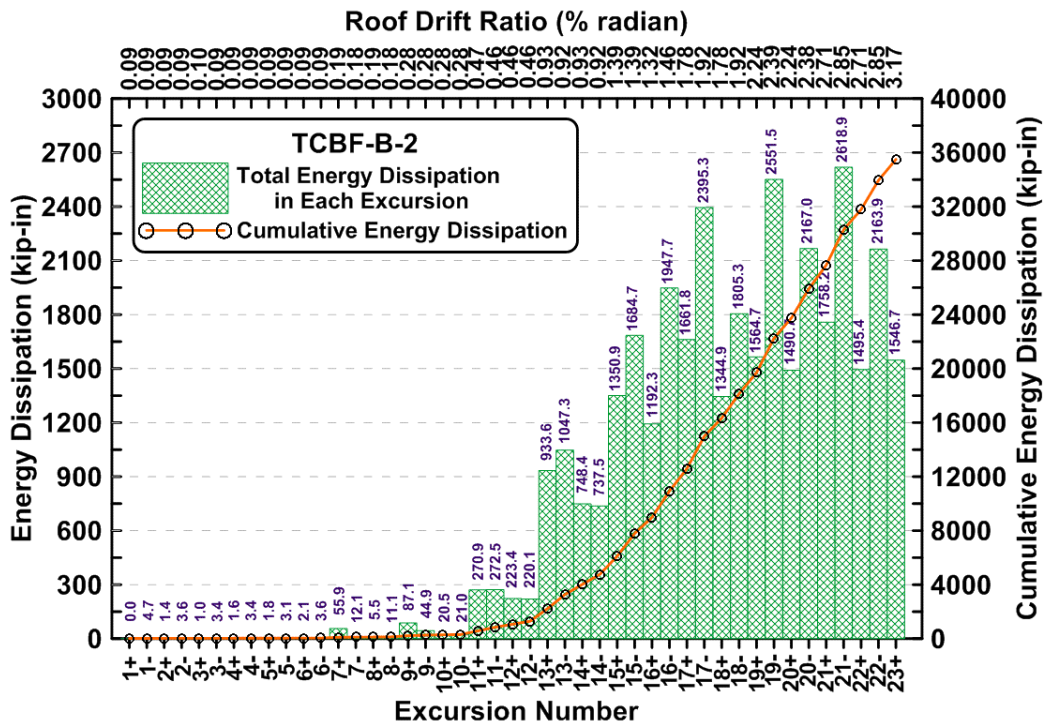


Figure 5.4 Total energy dissipation in each excursion and total cumulative energy dissipation of TCBF-B-2 specimen



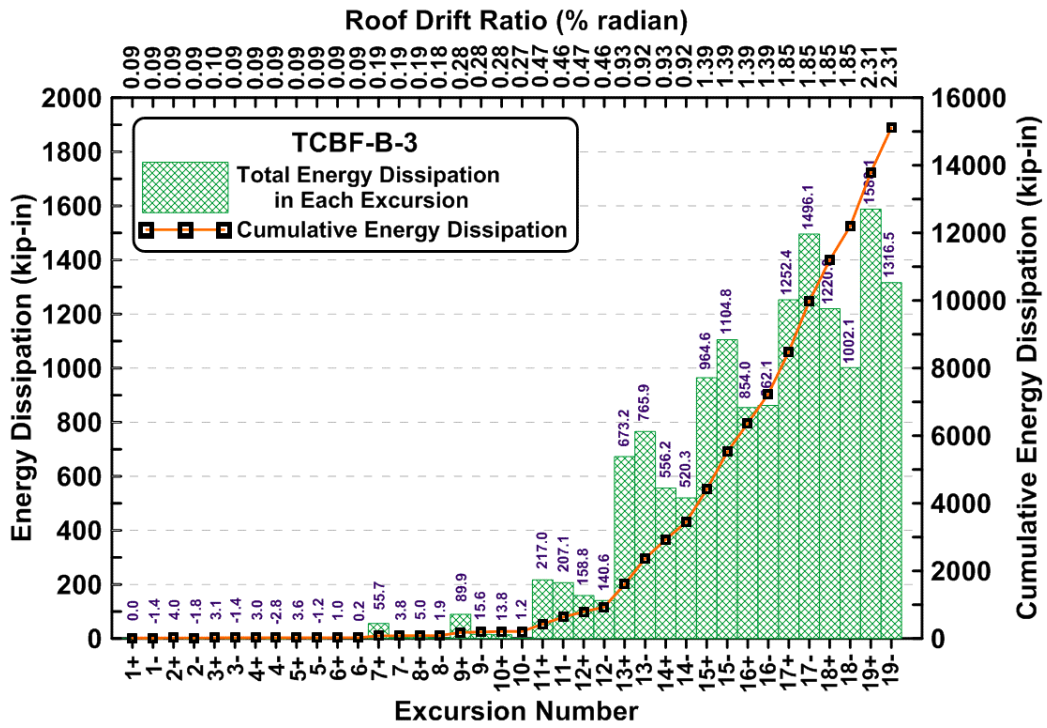
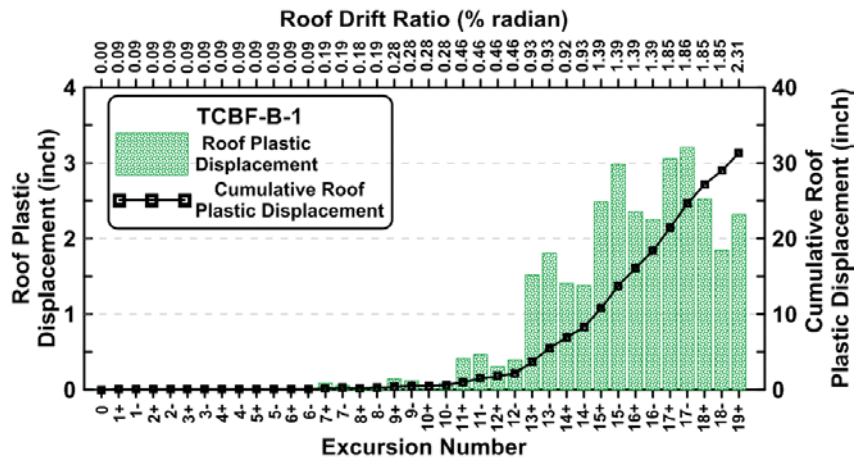
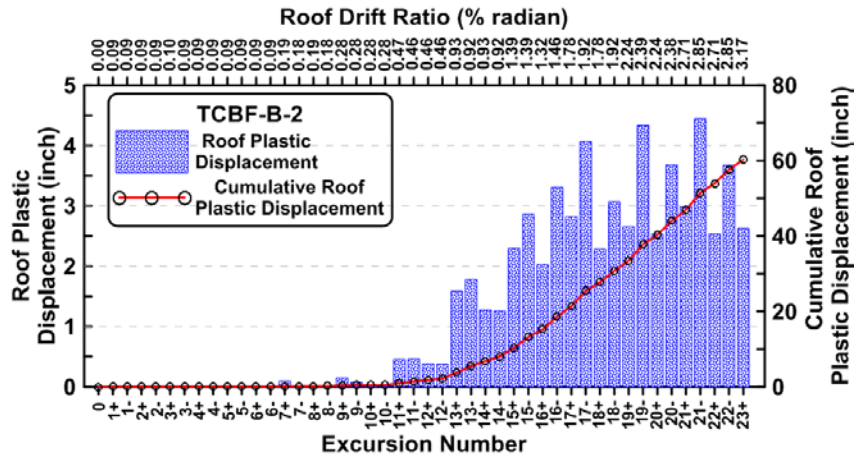


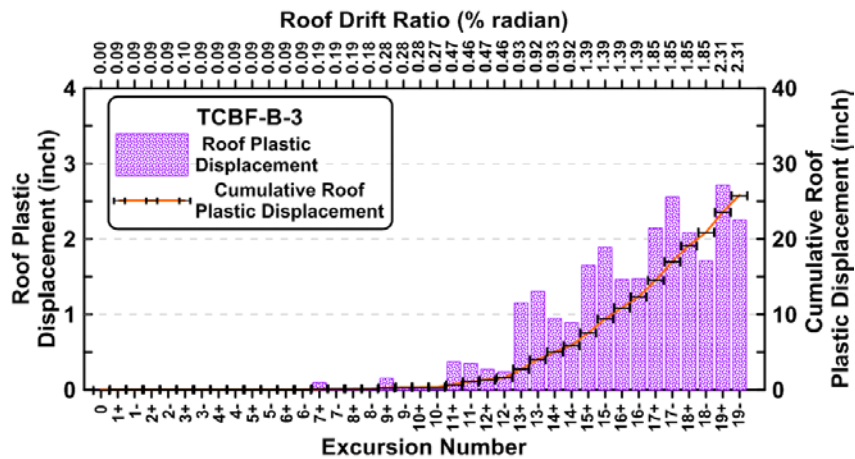
Figure 5.5 Total energy dissipation in each excursion and total cumulative energy dissipation of TCBF-B-3 specimen



(a) TCBF-B-1 specimen

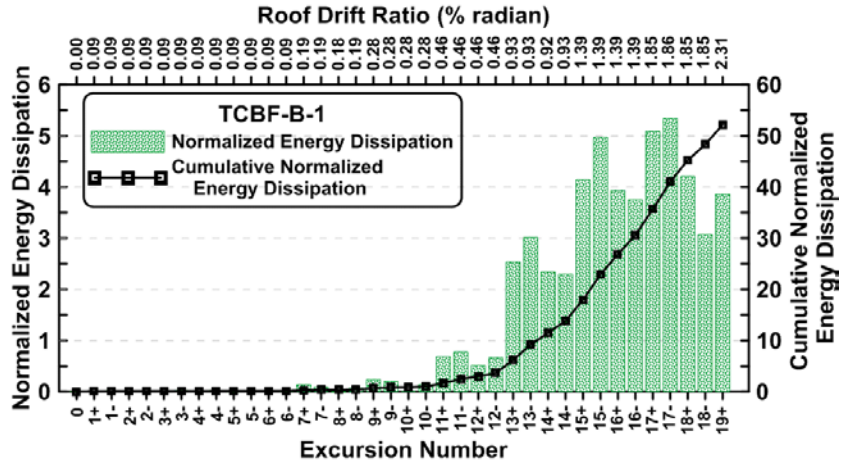


(b) TCBF-B-2 specimen

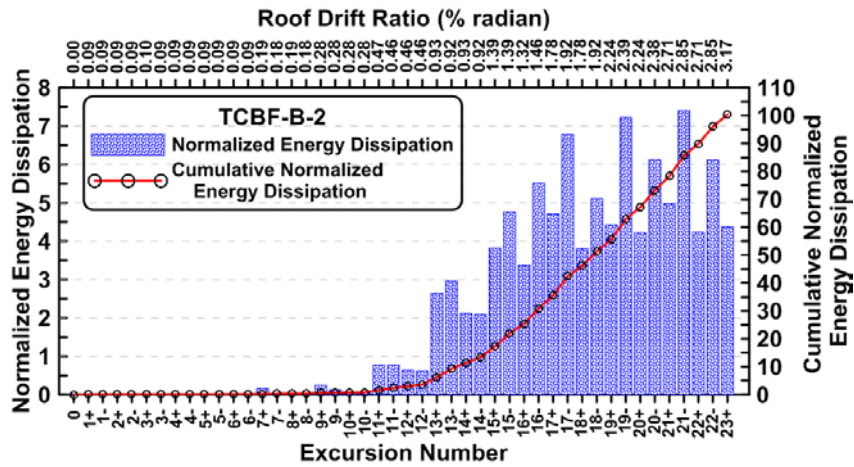


(c) TCBF-B-3 specimen

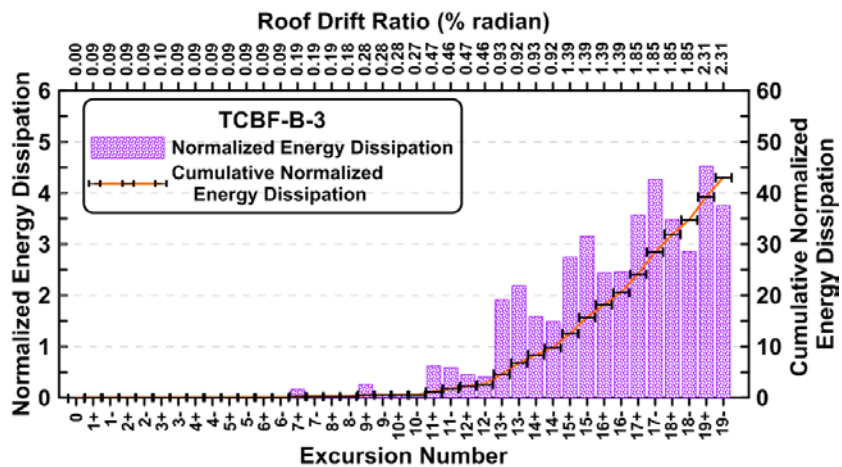
Figure 5.6 Total roof plastic displacement in each excursion and total cumulative roof plastic displacement of three specimens



(a) TCBF-B-1 specimen



(b) TCBF-B-2 specimen



(c) TCBF-B-3 specimen

Figure 5.7 Normalized energy dissipation in each excursion and cumulative normalized energy dissipation of three specimens

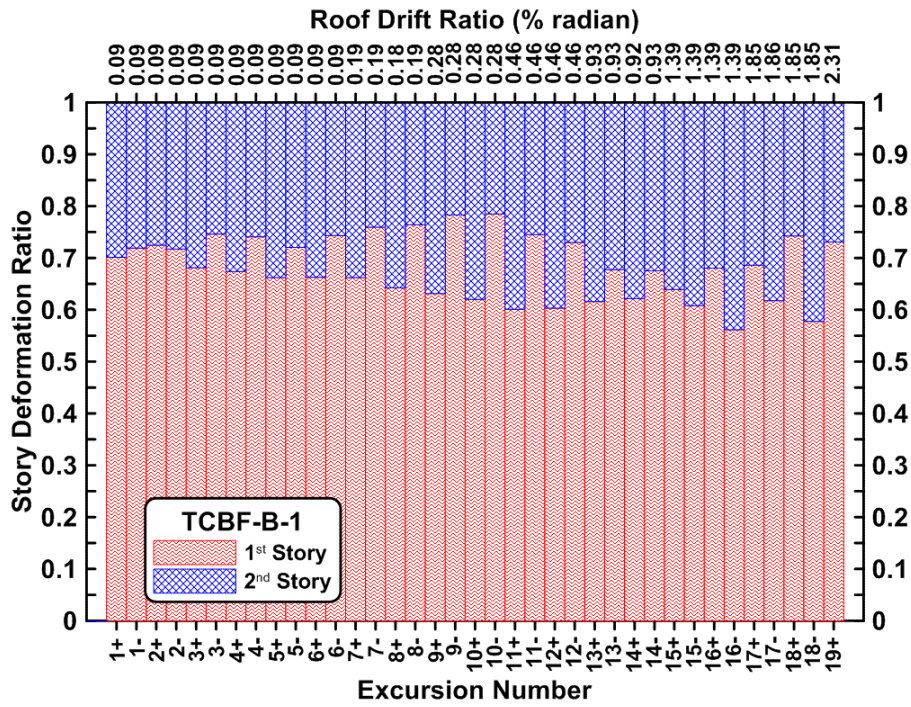


Figure 5.8 Story deformation ratio of TCBF-B-1 specimen

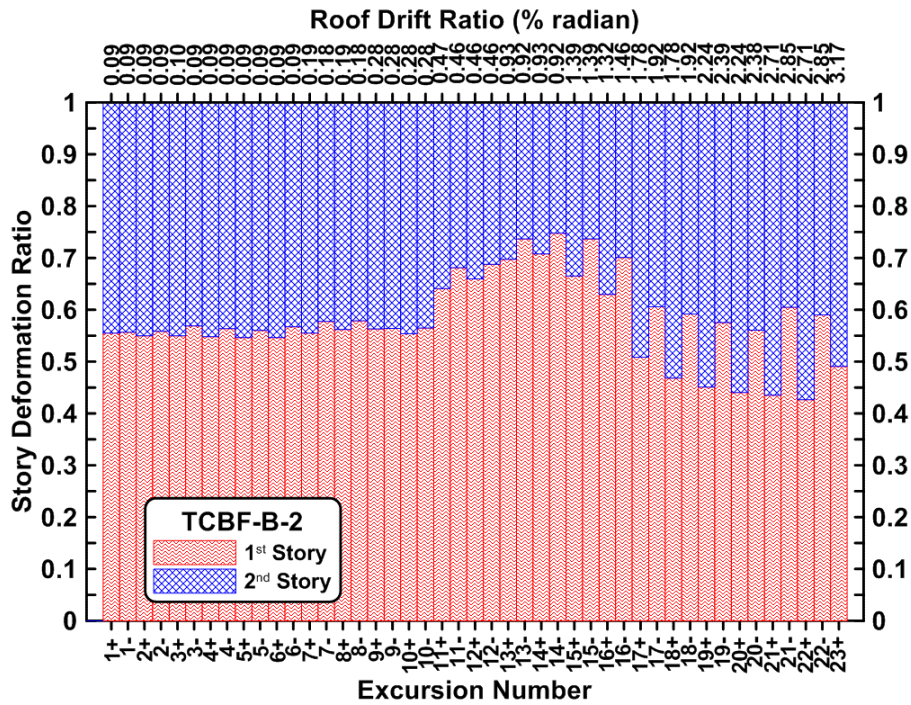


Figure 5.9 Story deformation ratio of TCBF-B-2 specimen

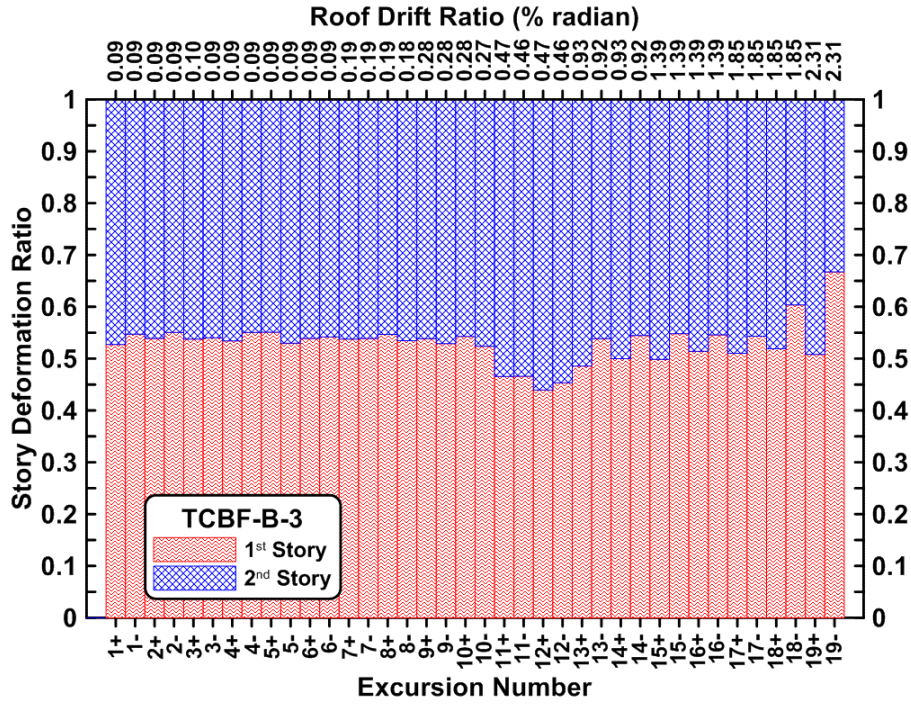


Figure 5.10 Story deformation ratio of TCBF-B-3 specimen

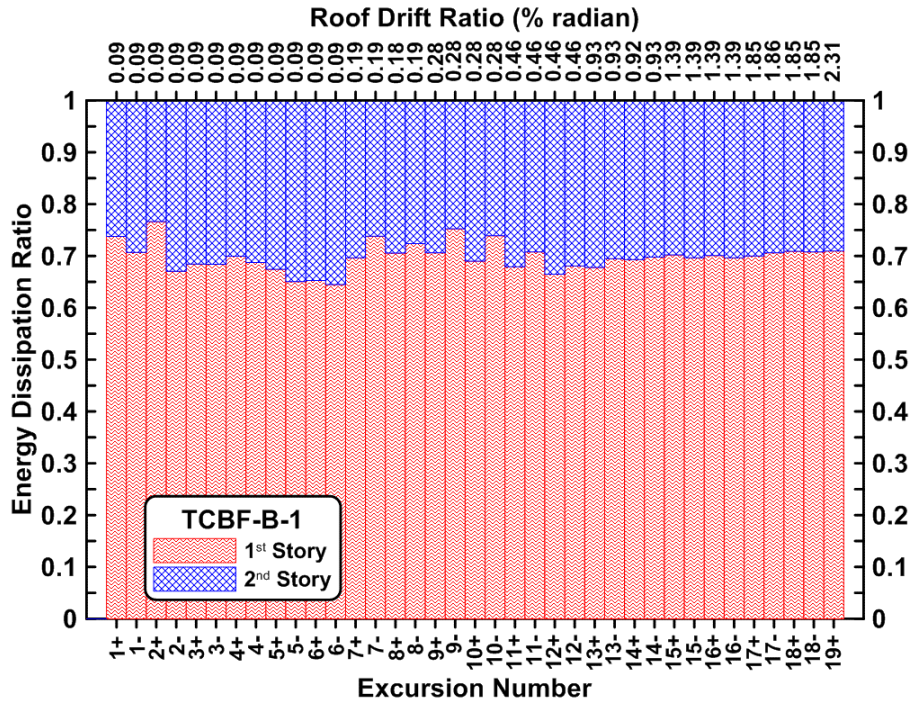


Figure 5.11 Story energy dissipation ratio of TCBF-B-1 specimen

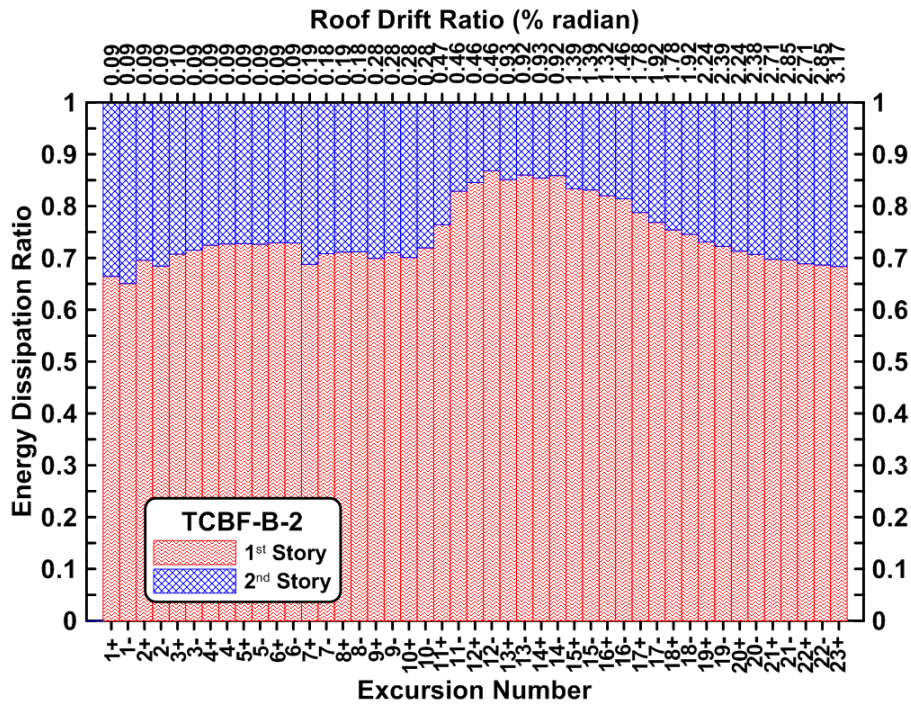


Figure 5.12 Story energy dissipation ratio of TCBF-B-2 specimen

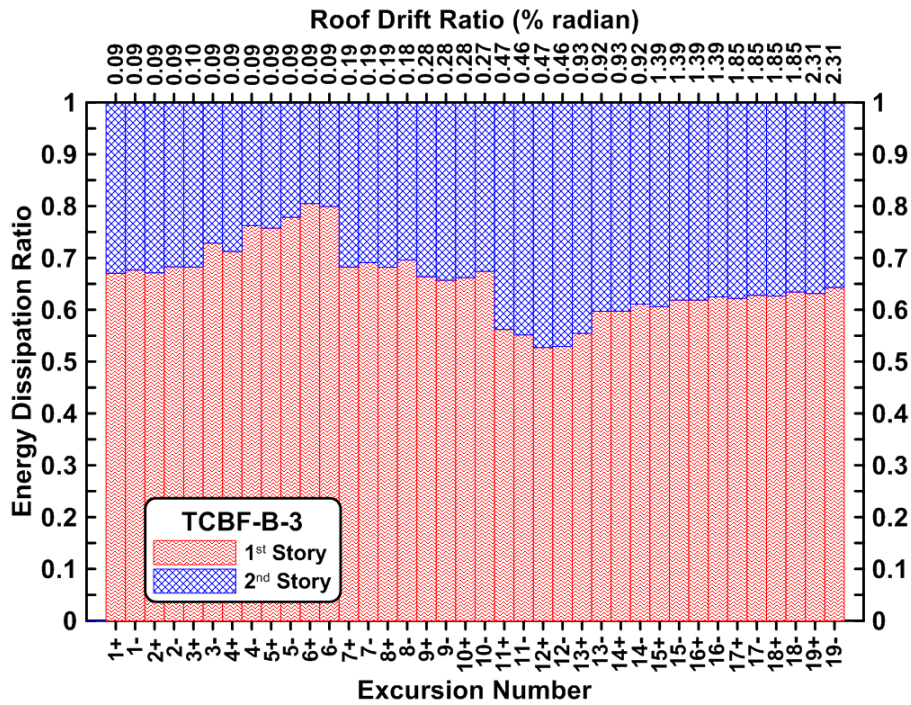


Figure 5.13 Story energy dissipation ratio of TCBF-B-3 specimen

### 5.1.2 Brace Behavior

As expected from the design, all braces buckle out-of-plane during the quasi-static cyclic loading tests. Measured eccentricities (out-of-plane misalignments at gusset plate to brace connections) of bracing members at both top and bottom brace-to-gusset plate connections are shown in Table 5.5. Comparing with the actual direction of out-of-plane buckling during the tests, it is interesting to note that only the TCBF-B-1 specimen has consistent results. The braces connected to the same one-piece gusset plate tend to buckle in the same direction, as shown in Table 5.5 and in test photos in Chapter 4.

From Figs. 4.43, 4.145 and 4.266, the out-of-plane displacement at the middle length of braces can be as much as ten times the axial deformation of the braces. The non-structural component around the braced bay such as partition walls, windows or façade could be severely damaged due to this out-of-plane displacement. It is interesting to note that the brace out-of-plane displacements tend to change sign (see Figs. 4.42 and 4.144) after a crack begins to propagate across a cross section of the brace since the neutral axis of the cracked brace shifts toward the uncracked side of the cross section. This eventually creates an eccentricity that displaces the center of the brace in the opposite direction from which it buckles, when the brace is loaded in tension. This phenomenon is only observed in the cracked square or round HSS braces (as the cracking pattern is different for the wide flange section (Fig. 4.323)).

The brace out-of-plane deformed shapes of each specimen are plotted in Figs. 5.14 to 5.25. Once local buckling of bracing members occurs, the out-of-plane deformed shape concentrates plastic deformations at the middle of the braces. This reduces the member curvature outside the midspan region. This can be seen by comparing the deformed shape in the compression excursions as shown in the upper part of Figs. 5.14 through 5.25. Looking at the initial “elastic range” deformed shapes of braces (see lower part of Figs. 5.14 to 5.25), it is interesting to note that the maximum deflection point is not always at the middle length of brace when the brace deformed elastically.

Strain decomposition plots shown in Chapter 4 illustrate the sources of brace strain readings during the tests. The strain gauge locations are at the quarter length points along the brace close to the gusset plate where two braces meet at the beam side (for more detail on sensor locations, see Appendices D, E and F). Permanent residual strains typically develop for each component (i.e. axial, out-of-plane, in-plane and warping strains) by the end of test. Maximum axial strains in the braces range from 3 to 7 times the yield strain of steel and residual tension strains range from 2 to 4 times the yield strain (Figs. 4.44 to 4.47, 4.146 to 4.149 and 4.267 to 4.279). Axial strains at the monitored locations tend to be tensile because the compression strains during compression phases of a cycle basically concentrate at the central plastic hinge at the middle of the brace. Spread of strain hardening is observed locally via the spreading of Luder’s bands (or whitewash flakings) along the length of braces as shown in the test photos, especially in the wide flange braces (that experienced larger than 0.01 axial strain). Brace cross-section necking (shrinking of shape or thinning of thickness) is observed before brace fracture. Contact bearing of fractured braces is also observed in these three tests when a fractured brace is shortened due to frame movement.

Most of in-plane bending strain readings are close to or less than the yield strain (between  $1600\mu$  to  $2350\mu$  in this study) while out-of-plane stains could be as large as 2 to 4 times the yield strain ( $4000\mu$  to  $8000\mu$ ). Deviation of out-of-plane bending strain also indicates the buckling direction of the brace. For example, all braces buckle to the north side during the TCBF-B-1 test,

which consistent with the deviation of out-of-plane bending strains as shown in Figs. 4.44, 4.45, 4.46 and 4.47 top right corner (deviate to negative side). Note that the sensor locations and sign conventions are different for TCBF-B-2 specimen compare to the TCBF-B-1 and TCBF-B-3 specimens. Effect of frame action on braces can clearly observe through comparing the sign of axial strain and in-plane bending strain of each brace. For instance, the in-plane bending strains always have the same sign as the axial strains of the first story braces while they have opposite sign for the second story braces. In general, the wide flange braces (opened section) do have larger (briefly around 5 times) warping strain compared with square HSS braces (closed section) as expected. Note that no warping strains are assumed to develop in the round HSS braces.

Brace end-to-end cumulative plastic deformations, cumulative ductility ratios, plastic deformations and ductility ratios in each excursion of each specimen are shown in Figs. 5.26 to 5.31. For all three specimens, both the cumulative ductility ratios and cumulative plastic deformations of first story braces have larger values at the end of tests. In the Specimen TCBF-B-1 test, plastic deformations and ductility ratios of both story braces start to accumulate at about the same excursion, but the first story braces accumulate plastic deformations faster than the second story braces consistently throughout the test. The situation is different for Specimen TCBF-B-2 where plastic deformations and ductility ratios of the first story braces begin to cumulate earlier than in the second story. But later the second story braces accumulate faster than the first story braces and catch up by the end of test. Specimen TCBF-B-3 behaves similar to Specimen TCBF-B-1, with plastic deformations and ductility ratios of both story braces starting to accumulate at about the same excursion, but with the first story braces (especially the eastern side brace) accumulating faster than the second story braces later in the test.

The components contributing to the total energy dissipation of the three specimens are identified in Figs. 5.32, 5.33 and 5.34. Braces in each specimen basically contribute significantly more than 50% of total energy dissipated during the tests until the brace fractures. The braces dissipate more energy when they are in tension as indicated in the stacked bar charts of each specimen. Energy dissipation by other components, such as beams, columns and panel zones, increases as the target roof displacement increases.

Table 5.6 summarizes conditions in the specimens at the time the first tow braces completely fracture. It is notable that the cumulative ductility capacities for braces having square HSS, round HSS and wide flange sectional shapes are all within the range from 42 to 55. Clearly the round HSS braces cumulate more plastic deformations than the other two before brace fracture. Looking back to the test observations describe in Chapter 4 and examining the values show in this table, it is presumable that the formation of local buckling of braces could have significant effect on the cumulative plastic deformation capacity under cyclic loading.



**Table 5.5 Measured eccentricities of brace before test and buckling direction during the test**

Location	1F, East Brace		1F, West Brace		2F, East Brace		2F, West Brace	
	Top	Bottom	Top	Bottom	Top	Bottom	Top	Bottom
TCBF-B-1	$\frac{1}{16}$ " N	$\frac{1}{16}$ " N	$\frac{1}{16}$ " N	$\frac{1}{8}$ " S	$\frac{1}{32}$ " N	$\frac{1}{16}$ " N	$\frac{1}{32}$ " N	$\frac{1}{16}$ " N
	N		N		N		N	
TCBF-B-2	$\frac{1}{8}$ " S	$\frac{1}{16}$ " N	$\frac{1}{16}$ " N	$\frac{1}{16}$ " S	$\frac{1}{16}$ " S	$\frac{1}{16}$ " S	$\frac{1}{16}$ " N	$\frac{1}{8}$ " S
	N		S		N		S	
TCBF-B-3	$\frac{1}{16}$ " N	$\frac{1}{16}$ " S	$\frac{1}{16}$ " S	0	0	$\frac{1}{8}$ " N	$\frac{1}{16}$ " S	$\frac{1}{8}$ " N
	S		N		N		N	

(Note: N stands for north, S stands for south and the number before indicates the eccentricity from the centerline of gusset plate)

**Table 5.6 Specimen failure characteristics (brace completely fractures)**

Specimen Name	TCBF-B-1		TCBF-B-2		TCBF-B-3	
	1 <sup>st</sup>	2 <sup>nd</sup>	1 <sup>st</sup>	2 <sup>nd</sup>	1 <sup>st</sup>	2 <sup>nd</sup>
Fracture Sequence						
Location	1F-West	1F-East	1F-West	1F-East	1F-West	N.A.
Load Stage Number	7	8	9	10	8	N.A.
Excursion Number	17 <sup>-</sup>	19 <sup>+</sup>	21 <sup>-</sup>	23 <sup>+</sup>	19 <sup>-</sup>	N.A.
Roof Displacement at Fracture (inch)	-3.8	4.7	-5.3	7.0	-4.3	N.A.
Roof Drift Ratio at Fracture (% radian)	-1.76	2.16	-2.45	3.24	-1.99	N.A.
Brace Cumulative Plastic Deformation at Fracture (inch)	7.7	9.5	11.5	11.9	7.2	N.A.
Brace Cumulative Ductility Ratio at Fracture	44.4	55.0	46.1	47.7	42.3	N.A.

(Note: in TCBF-B-3 specimen, test is stopped before the second brace fracture)

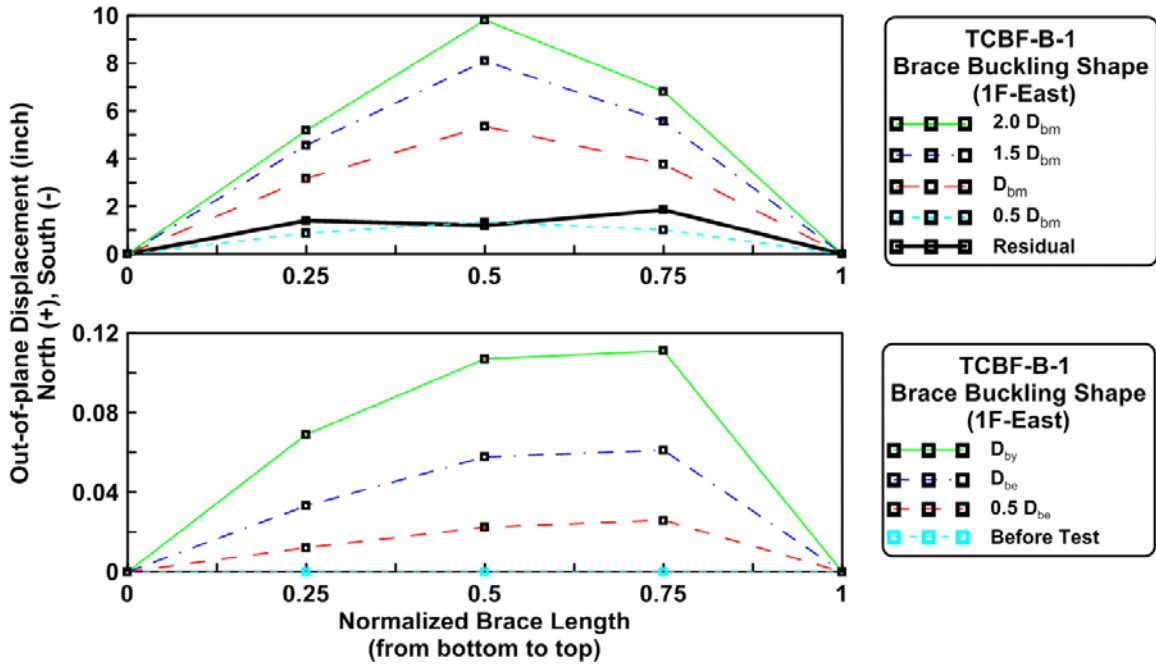


Figure 5.14 Buckling shape of the first story eastern side brace of TCBF-B-1 specimen in compression excursions

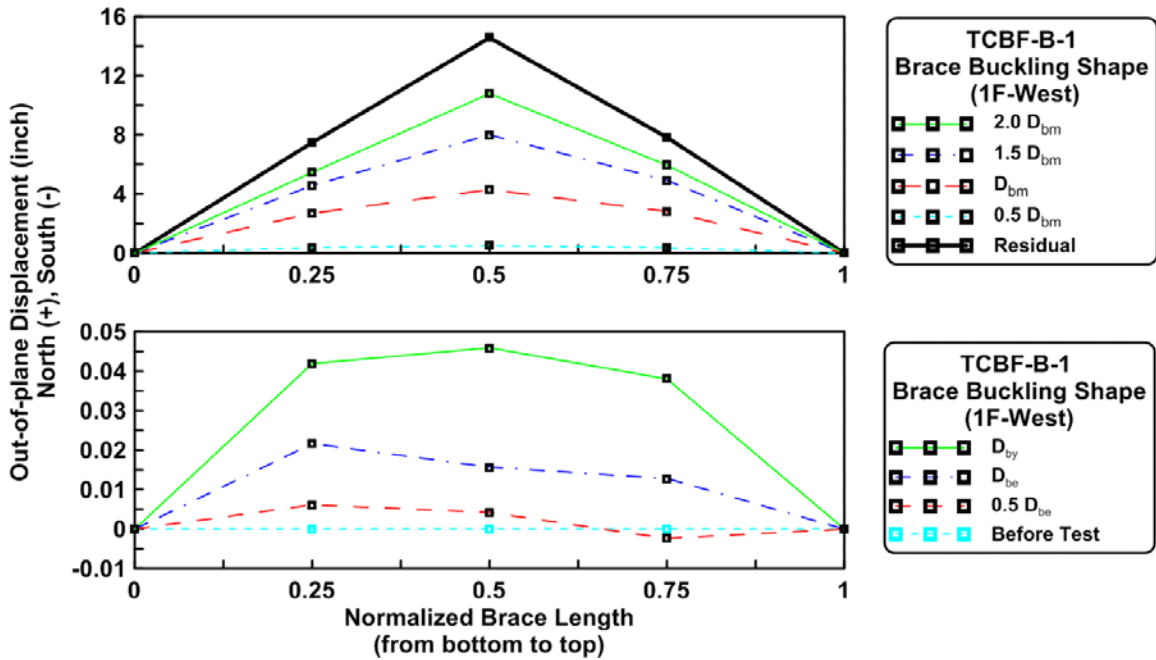


Figure 5.15 Buckling shape of the first story western side brace of TCBF-B-1 specimen in compression excursions

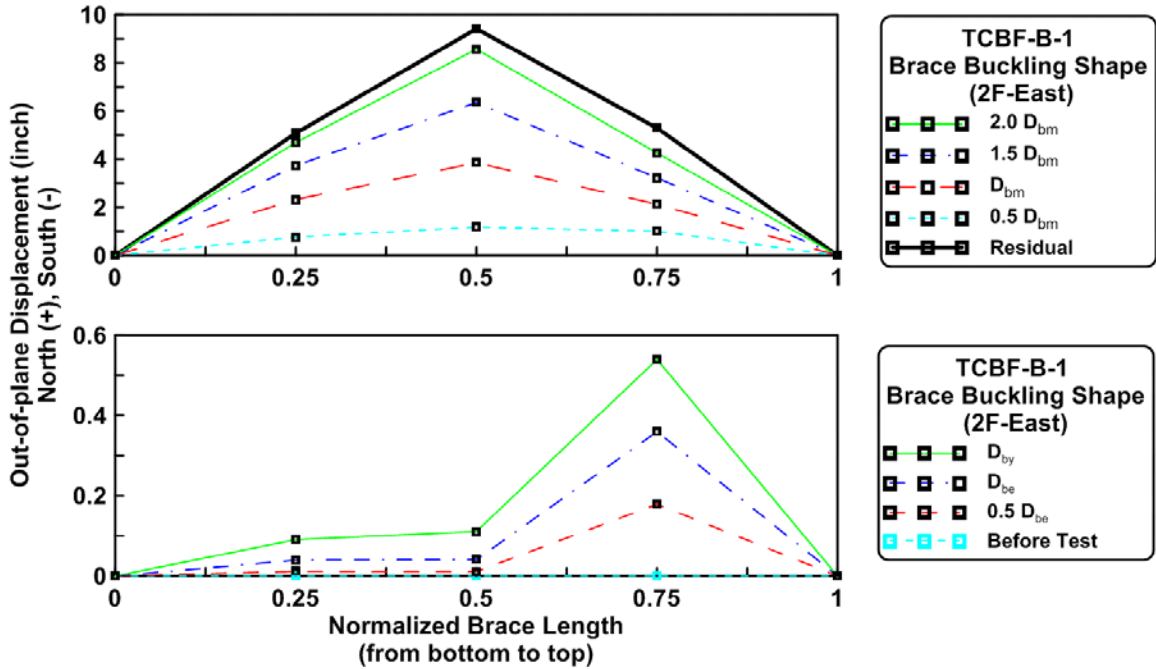


Figure 5.16 Buckling shape of the second story eastern side brace of TCBF-B-1 specimen in compression excursions

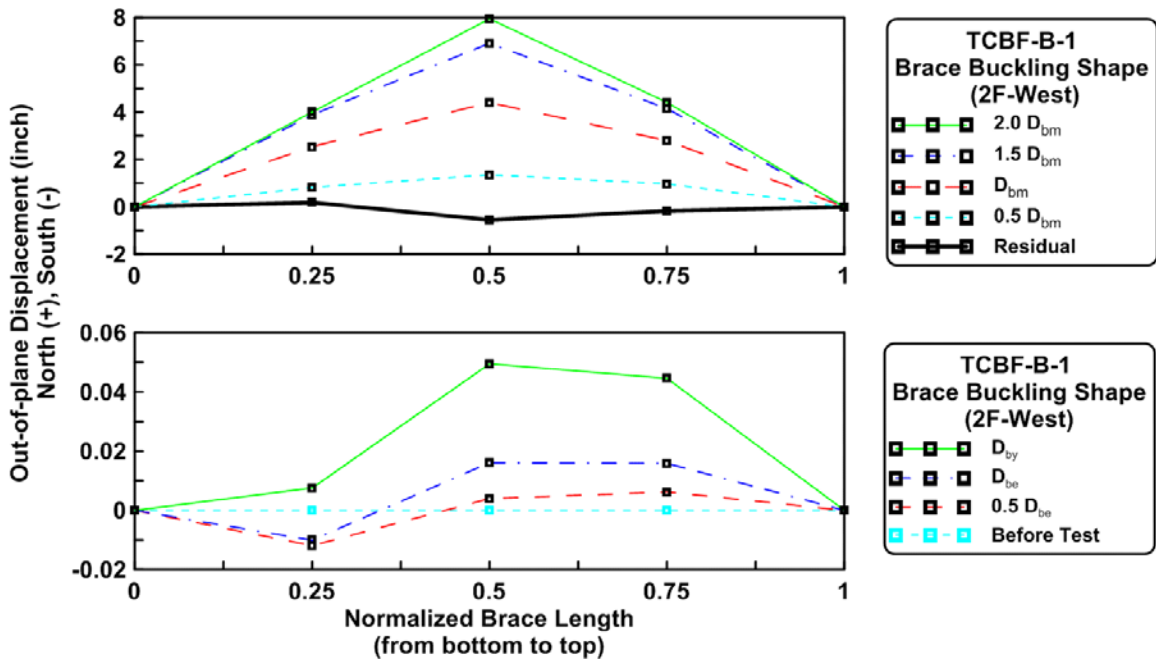


Figure 5.17 Buckling shape of the second story western side brace of TCBF-B-1 specimen in compression excursions

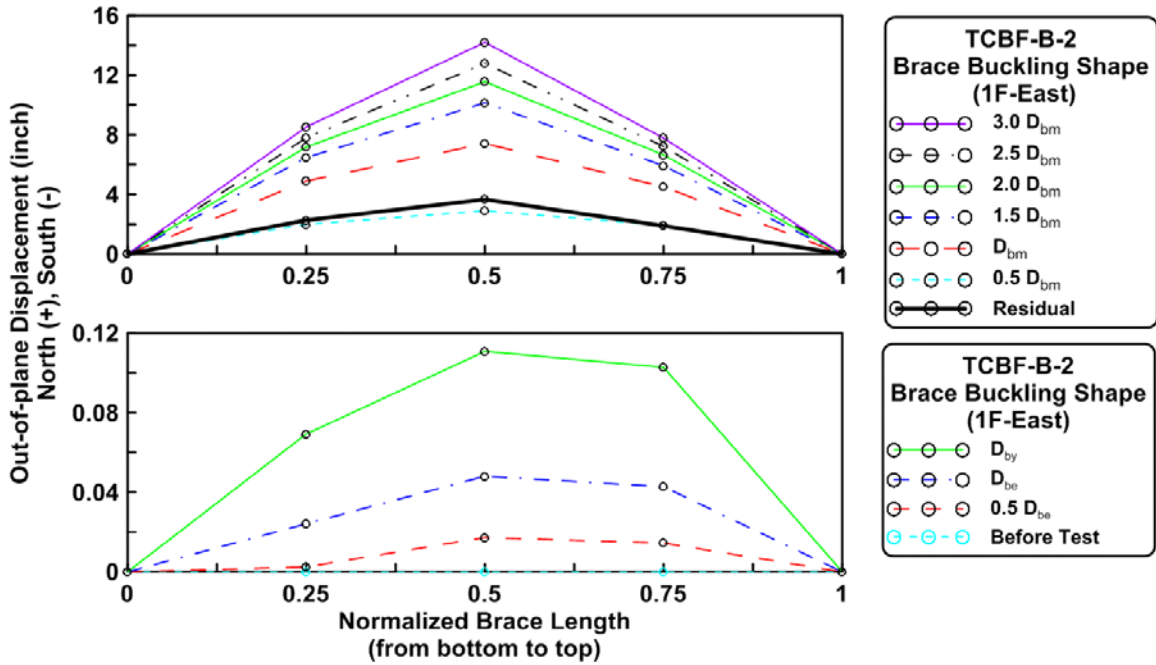


Figure 5.18 Buckling shape of the first story eastern side brace of TCBF-B-2 specimen in compression excursions

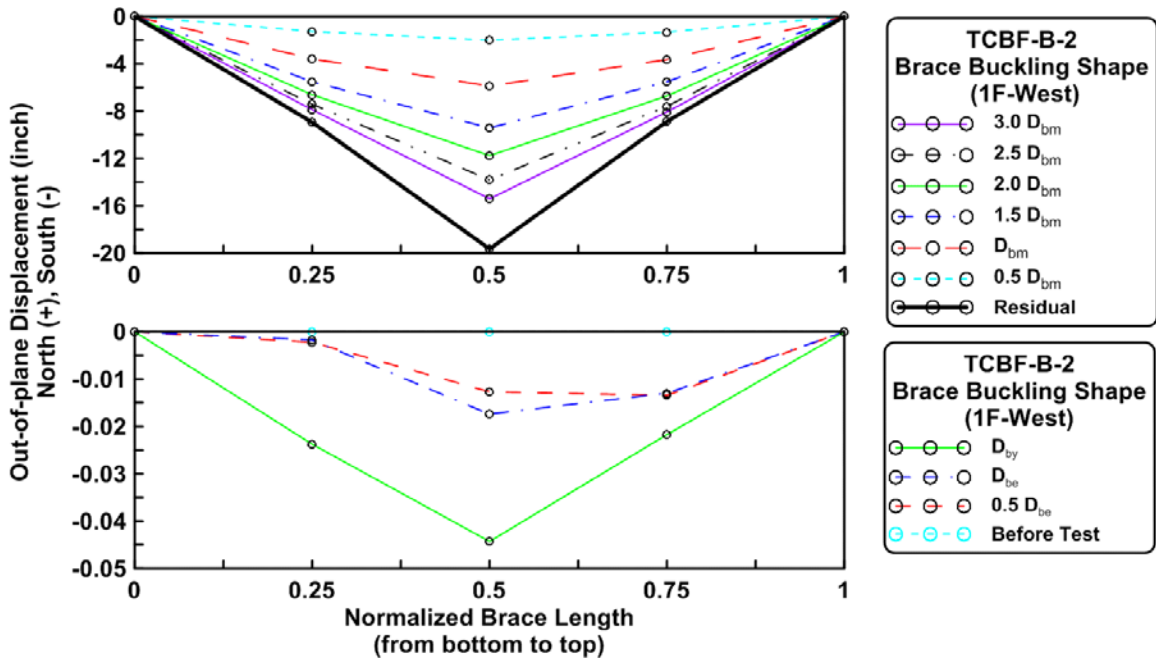


Figure 5.19 Buckling shape of the first story western side brace of TCBF-B-2 specimen in compression excursions

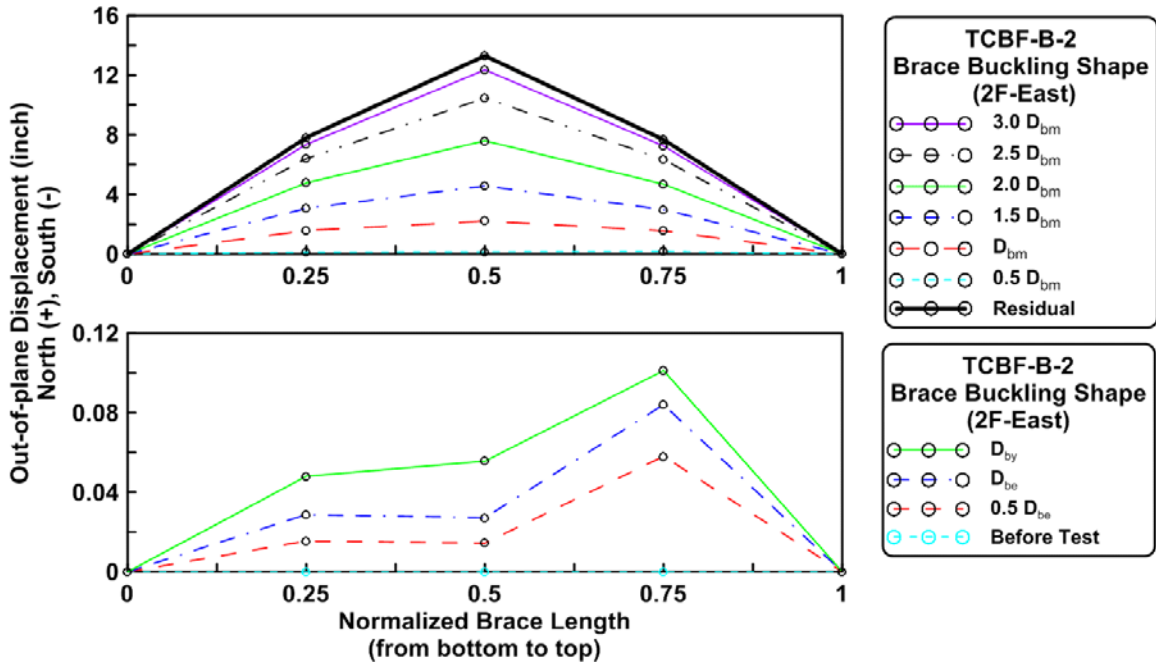


Figure 5.20 Buckling shape of the second story eastern side brace of TCBF-B-2 specimen in compression excursions

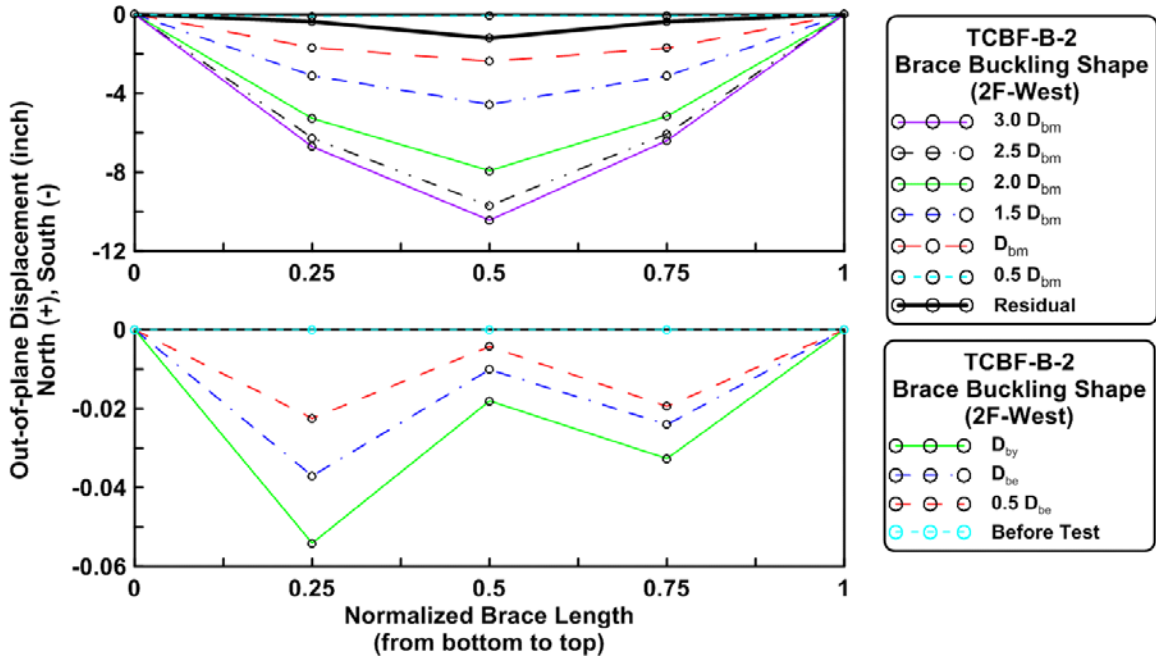


Figure 5.21 Buckling shape of the second story western side brace of TCBF-B-2 specimen in compression excursions

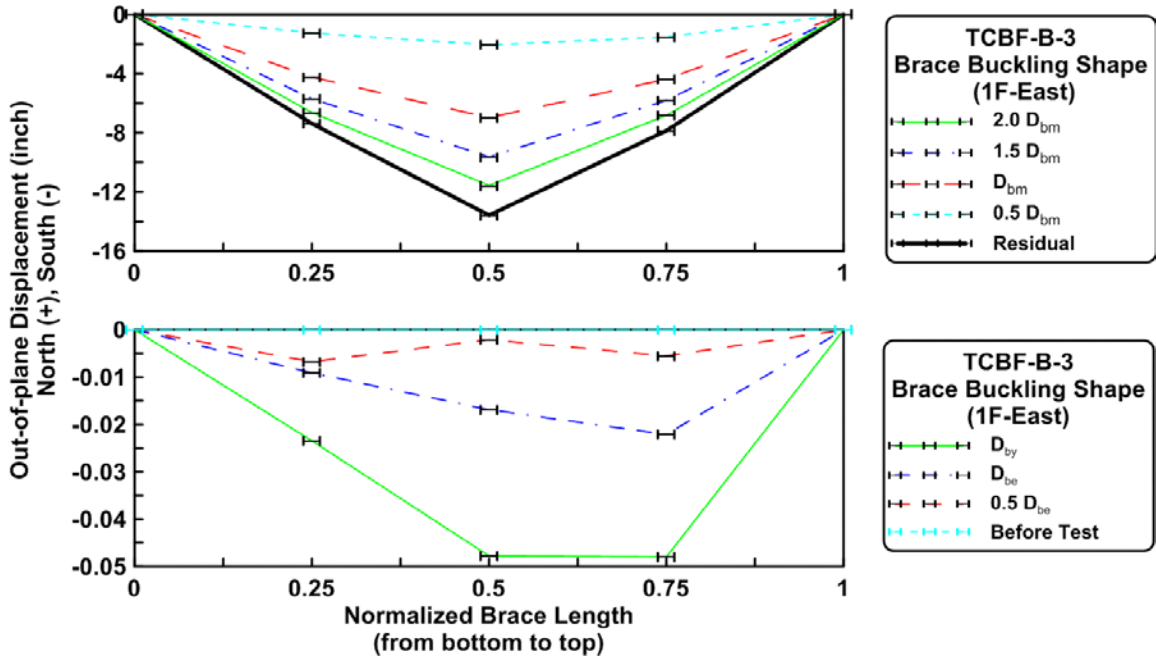


Figure 5.22 Buckling shape of the first story eastern side brace of TCBF-B-3 specimen in compression excursions

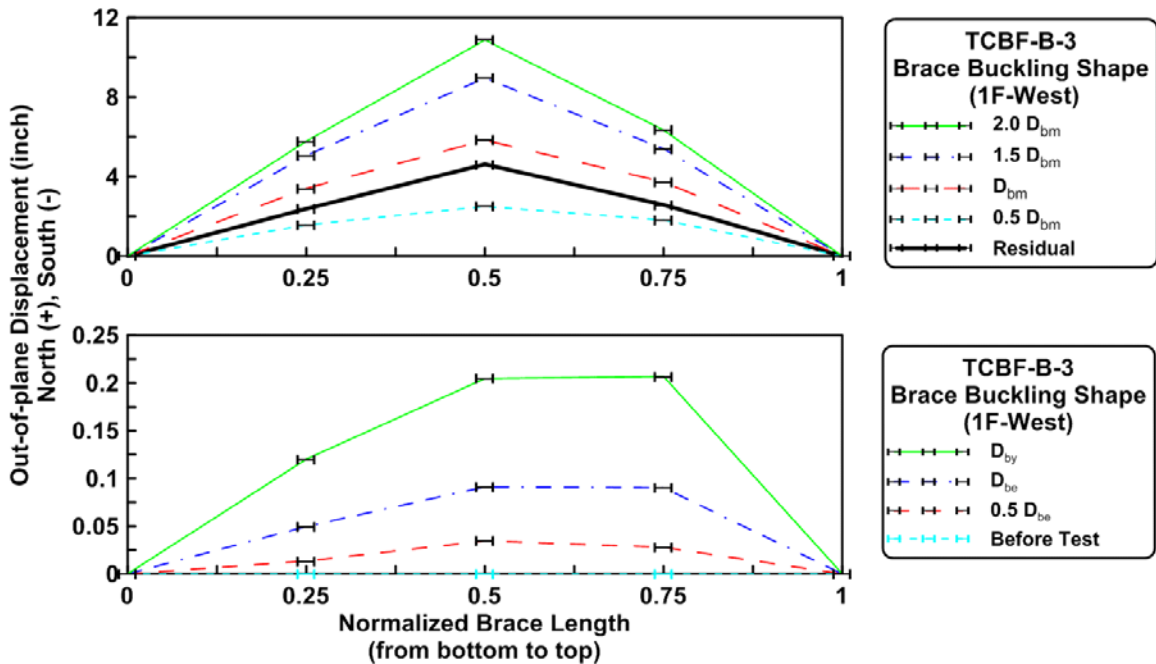


Figure 5.23 Buckling shape of the first story western side brace of TCBF-B-3 specimen in compression excursions

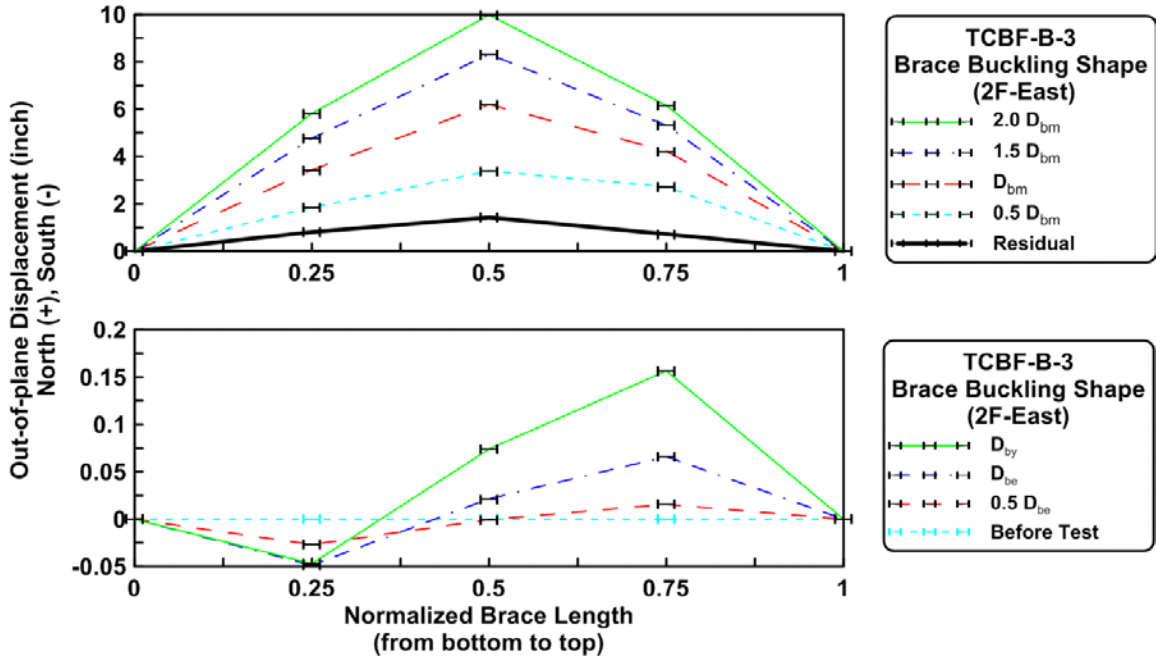


Figure 5.24 Buckling shape of the second story eastern side brace of TCBF-B-3 specimen in compression excursions

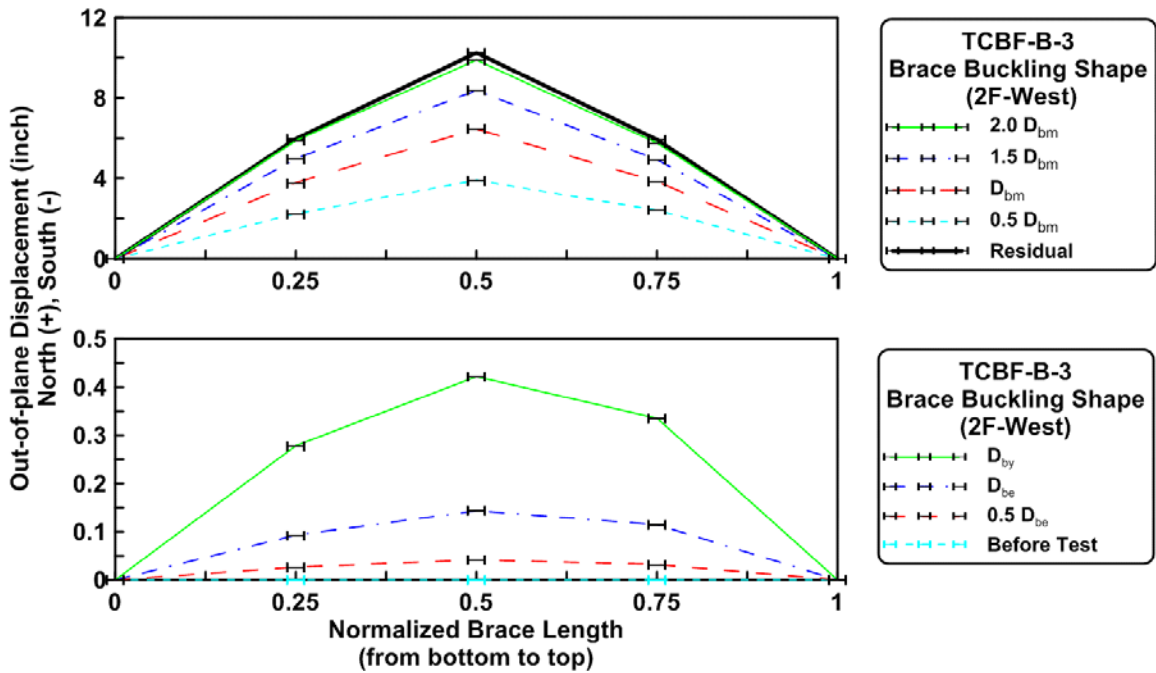


Figure 5.25 Buckling shape of the second story western side brace of TCBF-B-3 specimen in compression excursions

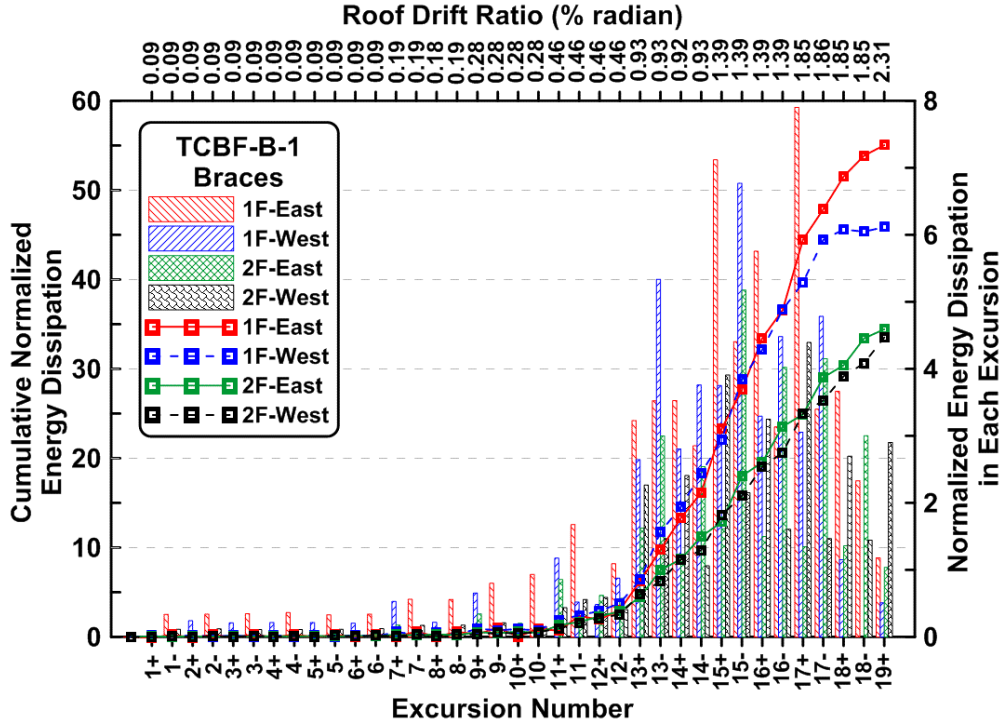


Figure 5.26 Brace cumulative normalized energy dissipation and normalized energy dissipation of TCBF-B-1 specimen in each excursion

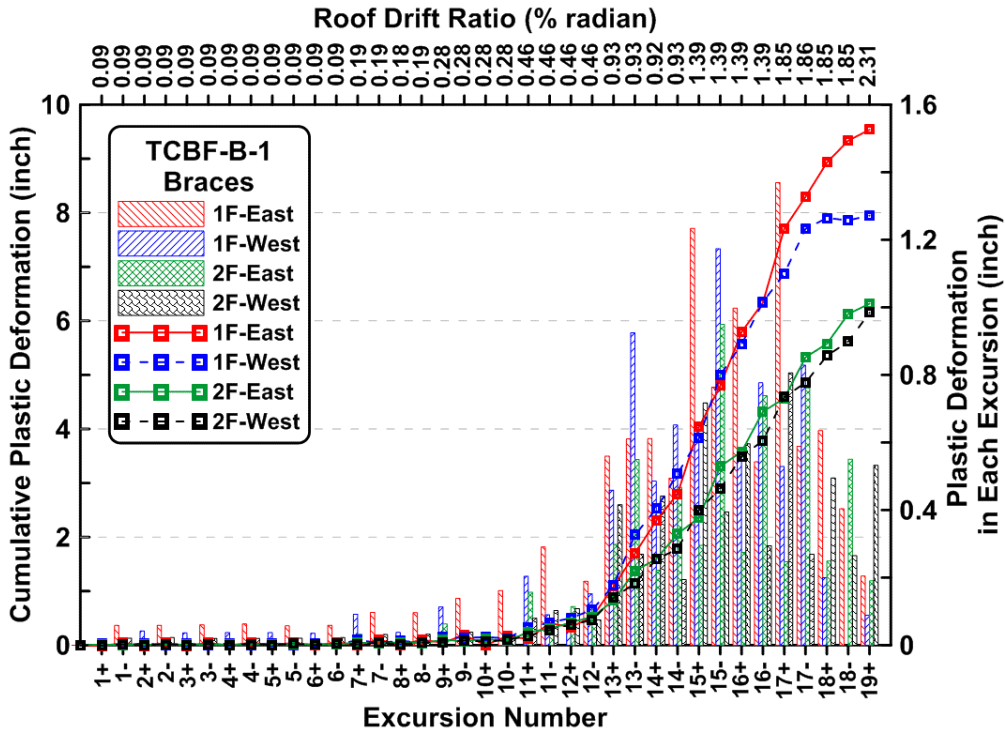


Figure 5.27 Brace cumulative plastic deformations and plastic deformations of TCBF-B-1 specimen in each excursion



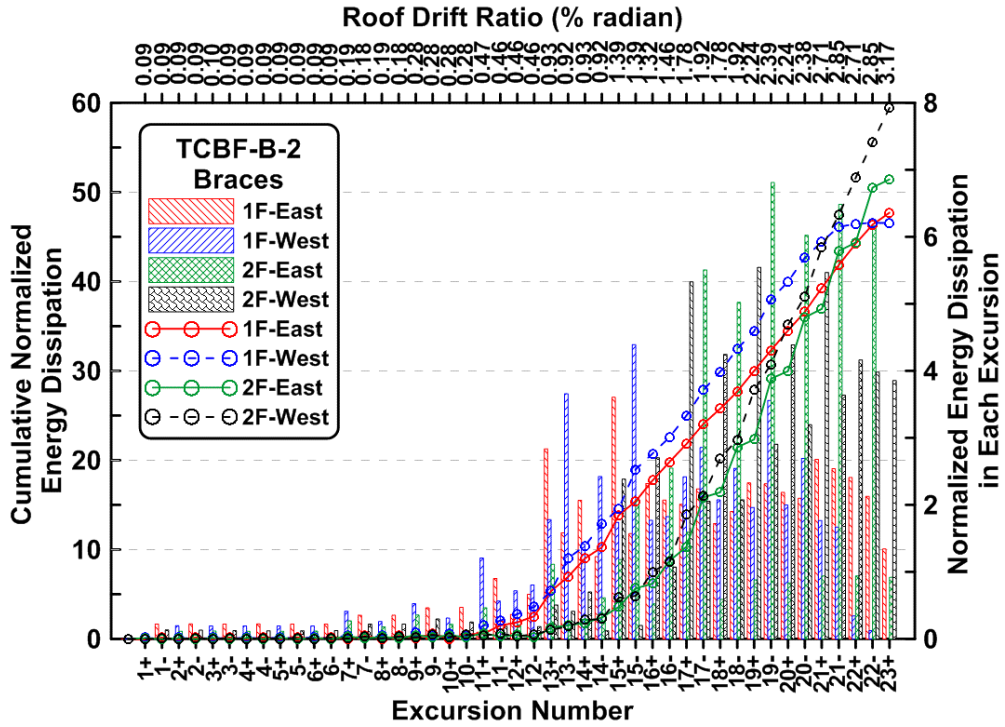


Figure 5.28 Brace cumulative normalized energy dissipation and normalized energy dissipation of TCBF-B-2 specimen in each excursion

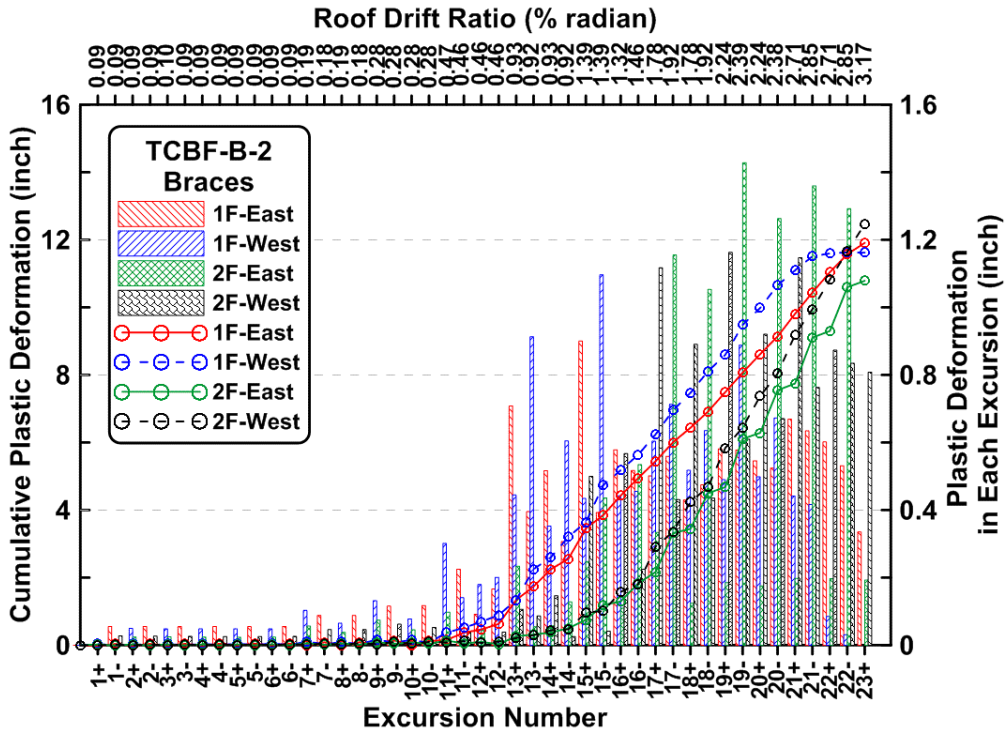


Figure 5.29 Brace cumulative plastic deformations and plastic deformations of TCBF-B-2 specimen in each excursion

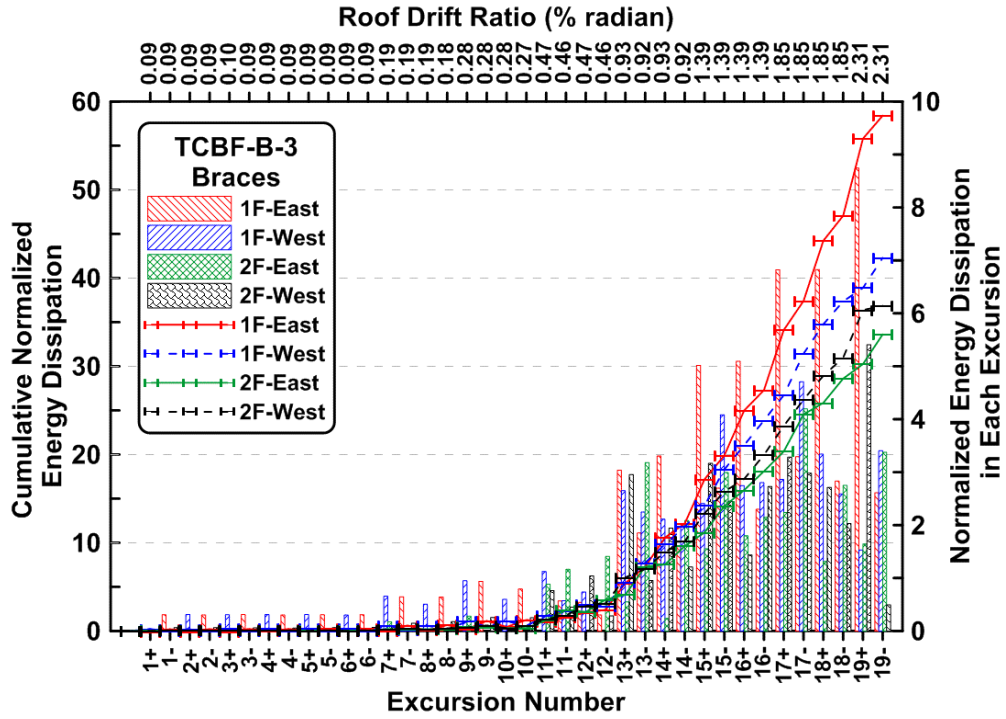


Figure 5.30 Brace cumulative normalized energy dissipation and normalized energy dissipation of TCBF-B-3 specimen in each excursion

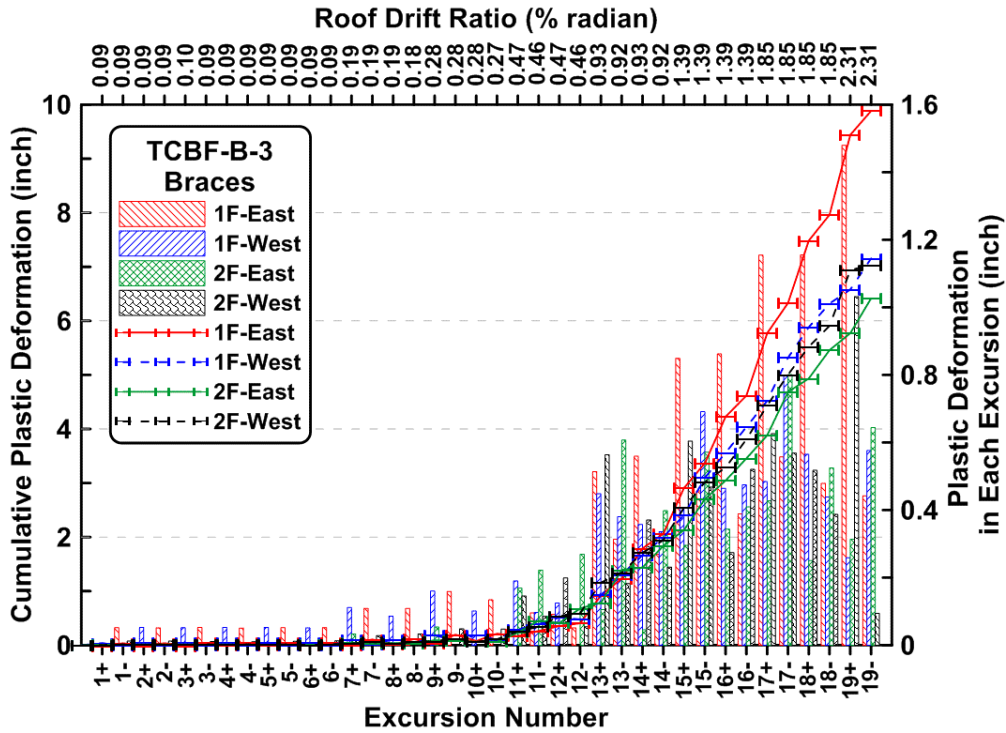


Figure 5.31 Brace cumulative plastic deformations and plastic deformations of TCBF-B-3 specimen in each excursion

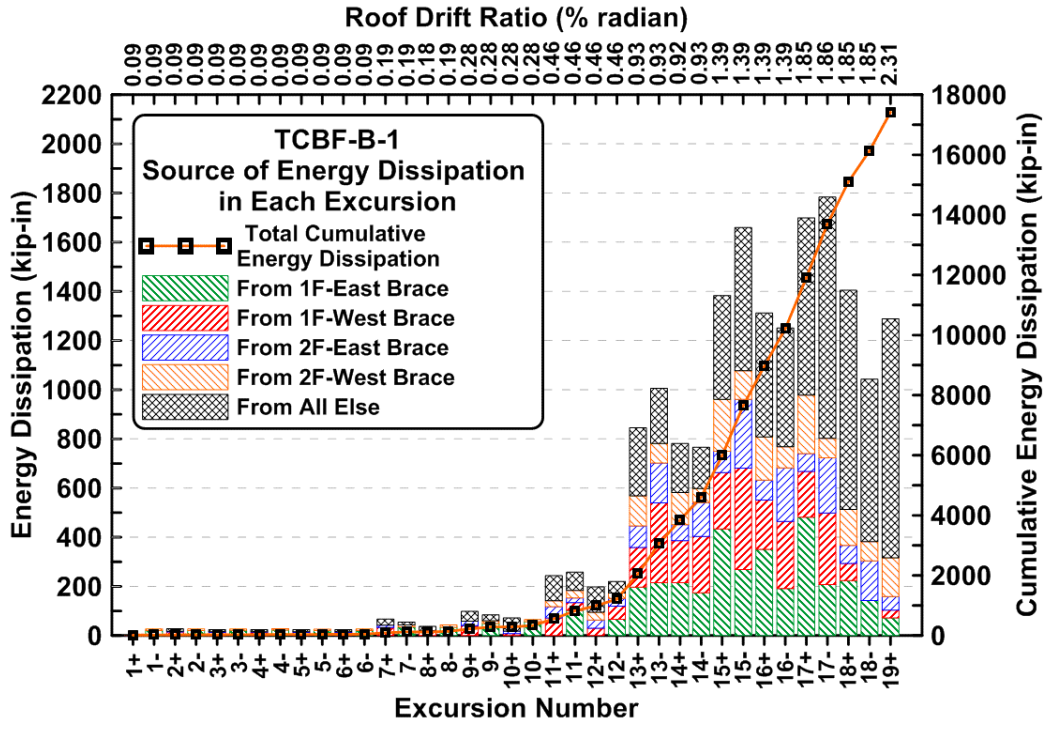


Figure 5.32 Source of total energy dissipation in each excursion and total cumulative energy dissipation of TCBF-B-1 specimen

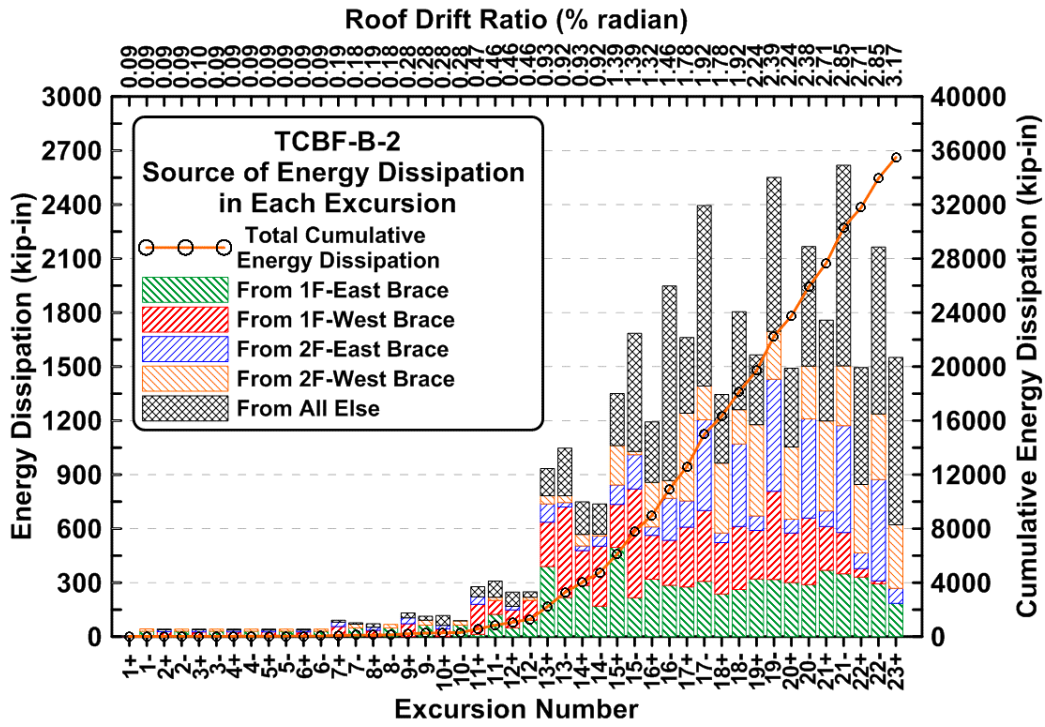


Figure 5.33 Source of total energy dissipation in each excursion and total cumulative energy dissipation of TCBF-B-2 specimen

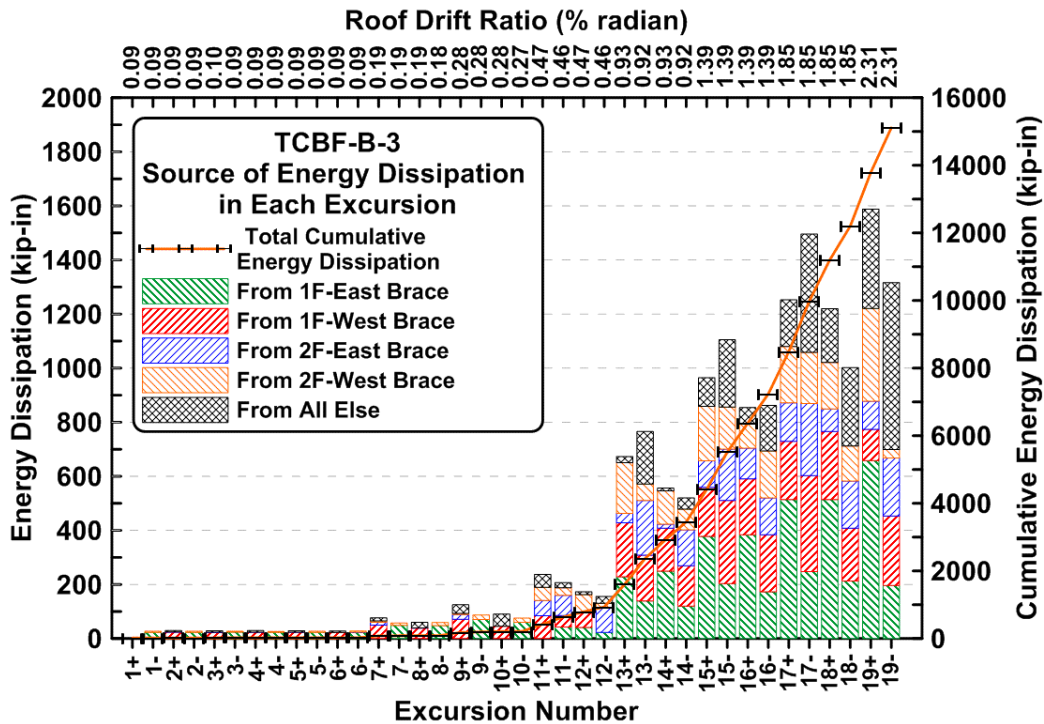


Figure 5.34 Source of total energy dissipation in each excursion and total cumulative energy dissipation of TCBF-B-3 specimen

### 5.1.3 Column Behavior

For all three tests, the column axial forces typically range between 500 kips tension force to 600 kips compression force (see Figs. 4.10, 4.112 and 4.233), except for Specimen TCBF-B-2. For specimen TCBF-B-2, the first story east side column axial forces rise up as shown in Fig. 4.112 to 700 kips (tension) in the excursion just before the weld fractured at the western side of the east column's base plate. The peak axial forces drop as the target roof displacement increases and the peak tension force in the column usually is less than the peak compression force in each test, as shown in Figs. 4.11, 4.113 and 4.234. The column axial forces also drop after the fracture of the braces.

Column bending moments away from the probable plastic hinge zones are derived from the strain gauge readings (typically readings from two locations, near the top and bottom of each column) and then extrapolated to find the bending moment at a specific location in the column. Shear forces in the columns are also derived from the column bending moment diagrams. From the column bending moment time history plots shown in Figs. 4.12, 4.13, 4.114, 4.115, 4.235 and 4.236, the bending moment values are typically within the elastic range, except in the TCBF-B-2 test, where the column base repair details shift the probable plastic hinge zones upward during the second trial. Also, larger target roof displacements were imposed on this specimen since the braces fractured at larger lateral displacements.

Derived column web shear time histories, shown in Figs. 4.14 4.15, 4.16, 4.116, 4.117, 4.118, 4.237, 4.238 and 4.239, indicate significant column web shear yielding in the first story columns and the second story western column of Specimen TCBF-B-2, while the column webs in Specimens TCBF-B-1 and TCBF-B-3 basically remained elastic. Further examination of the

rosette readings on the column webs in 4.17, 4.119 and 4.240 shows different column shear behavior for the three specimens. The eastern side column web in the first story of Specimen TCBF-B-1 has a 2% peak shear strain after the fracture of the braces. Both the west and east side column webs in the first story of Specimen TCBF-B-2 have about 3% peak shear strain after the failure of braces. Column webs remain essentially elastic in TCBF-B-3 specimen, as shown in Fig. 4.240.

Rosette readings also express the primary behaviors of the columns during cyclic tests. Figures 4.19 to 4.26 show that the column axial forces and shear forces obviously interact in the column webs in the first story of Specimen TCBF-B-1 while shear forces dominate the behavior in the column webs in the second story (detected via the time histories of principal strain directions and the slopes in the normalized maximum principal stress vs. normalized minimum principal stress relationships). In Specimen TCBF-B-2, column axial forces and shear forces interact in the column webs in both stories as shown in Figs. 4.121 to 4.128. In Specimen TCBF-B-3, the column axial forces and shear forces interact in the column webs in the first story while in the column webs in the second story, interaction occurs but the axial forces govern the behavior more as shown in Figs. 4.242 to 4.249.

Columns in the first story of each specimen take 10% to 16% of the total story shear at the beginning of tests and eventually take 75% to 100% of the total story shear at the end of tests (braces fracture in the first story). However, columns in the second story of each specimen take 9% to 16% of total story shear at the beginning of tests and eventually take only 33% to 75% of total story shear at the end of tests. These ratios can be estimated from the slopes of the plots shown in Figs. 4.18, 4.120 and 4.241.

Normalized P-M and P-V interaction diagrams at the first story column bases of each specimen illustrate the plastic hinges are formed at the column bases during the cyclic tests (see Figs. 4.27, 4.28, 4.129, 4.130, 4.250 and 4.251). Typically, flexural plastic hinges are formed at the column bases of the three specimens. In Specimen TCBF-B-2 plastic shear deformations also occur at the bases. The interaction diagrams at the second story column top end (the roof beam and column centerlines intersection) of the three specimens (Figs. 4.29, 4.30, 4.131, 4.132, 4.252 and 4.253) show that the cross sections are essentially elastic at those locations.

In the Specimen TCBF-B-2 test, fracture of the column-to-base plate welds is observed during the test. It should be mentioned that the columns were reused after the Specimen TCBF-B-1 test and repair of welds were performed in some locations where cracks were detected.

Because of the fractures that occurred during the Specimen TCBF-B-2 test, reinforcing plates were added at the column to base plate connection in the entirely new TCBF-B-3 specimen. This detailed also suffered an unexpected brittle fracture of column flange at the ends of the welds of the stiffeners.

#### **5.1.4 Beam Behavior**

The roof beam in each specimen basically remains elastic during the tests. No significant damage or flaking of whitewash was observed near the roof beam-to-column connections at either end of the roof level beam. Moreover, elastic behavior is indicated by the time histories of beam flange strain, beam axial force, shear force, and beam end bending moment, as shown in Figs. 4.33, 4.35, 4.37, 4.39, 4.135, 4.137, 4.139, 4.141, 4.256, 4.258, 4.260 and 4.262.

The corresponding time history plots for the lower level beam (see Figs. 4.32, 4.34, 4.36, 4.38, 4.134, 4.136, 4.138, 4.140, 4.257, 4.257, 4.259 and 4.261) indicate significant inelastic

behavior occurs locally. Severe flexural plastic hinges (and fractures in the ensuing local buckles) were observed at both ends of lower beam in the Specimen TCBF-B-1 and TCBF-B-2 tests. The bolted pin connection detail for Specimen TCBF-B-3 was able to avoid this behavior. For Specimen TCBF-B-3, no significant plastic deformations were observed in the lower beam, but small amounts of whitewash flaking was observed in the connection splice plate region.

The maximum average axial forces developed in the lower beam of Specimens TCBF-B-1 and TCBF-B-2 was about 200 kips (in both tension and compression). In the Specimen TCBF-B-3 test, the maximum average axial force in the lower beam is about 200 kips in compression, but only about 50 kips in tension. Very small shear forces are estimated for this beam during all three tests.

Due to a geometric amplification effect caused by the stiff gusset plate details at both ends of the lower beam as illustrated in Fig. 5.35, the lower beam tends to have larger rotational demands than the upper beam (or compared to the overall drift angle). Plastic hinges form at both ends of lower beam between 1% to 2% roof displacement ratio during tests of Specimens TCBF-B-1 and TCBF-B-2. Based on the equation shown in Fig. 5.35, the theoretical amplification factor between beam end plastic rotation and plastic drift of the structure is 1.36 considering the actual dimensions of the specimen. From Fig. 5.36, the slope of plots of lower beam end rotation versus first story drift responses follow the theoretical prediction for Specimen TCBF-B-3. For this specimen, pin connections at this location make the theoretical equation applicable throughout the entire range of testing. For Specimens TCBF-B-1 and TCBF-B-2, elastic behavior preceded the formation of plastic hinges and the relation does not initially match the experimental results. However, test results for Specimen TCBF-B-2 the slopes increase and approach the theoretical slope until sensors fail. Unfortunately, the readings from the tilt-meters used in Specimen TCBF-B-1 stopped giving accurate readings as soon as the beam yielded. The reference targets were moved to give better reading in subsequent tests. It is clear that deterioration of the plastic hinge region due to local buckling and rupture may be exacerbated by the geometric amplification of plastic rotations due to the physical size of the two gusset plates at this level.

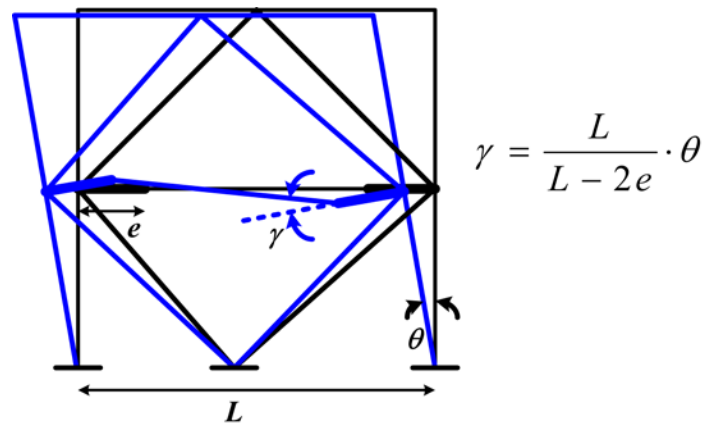


**Figure 5.35 Demonstration of geometry amplification effect at the lower beam to gusset plate connections**

From the beam center deflection time histories of each specimen (see Figs. 4.31, 4.133 and 4.254), larger deflections are found and expected as the result of unbalanced loads developed

in the roof beam of each specimen. Estimated unbalanced loads were as high as 150 kips, 200 kips and 100 kips for the roof beam in Specimens TCBF-B-1, TCBF-B-2 and TCBF-B-3, as shown in Figs. 4.40, 4.142 and 4.263.

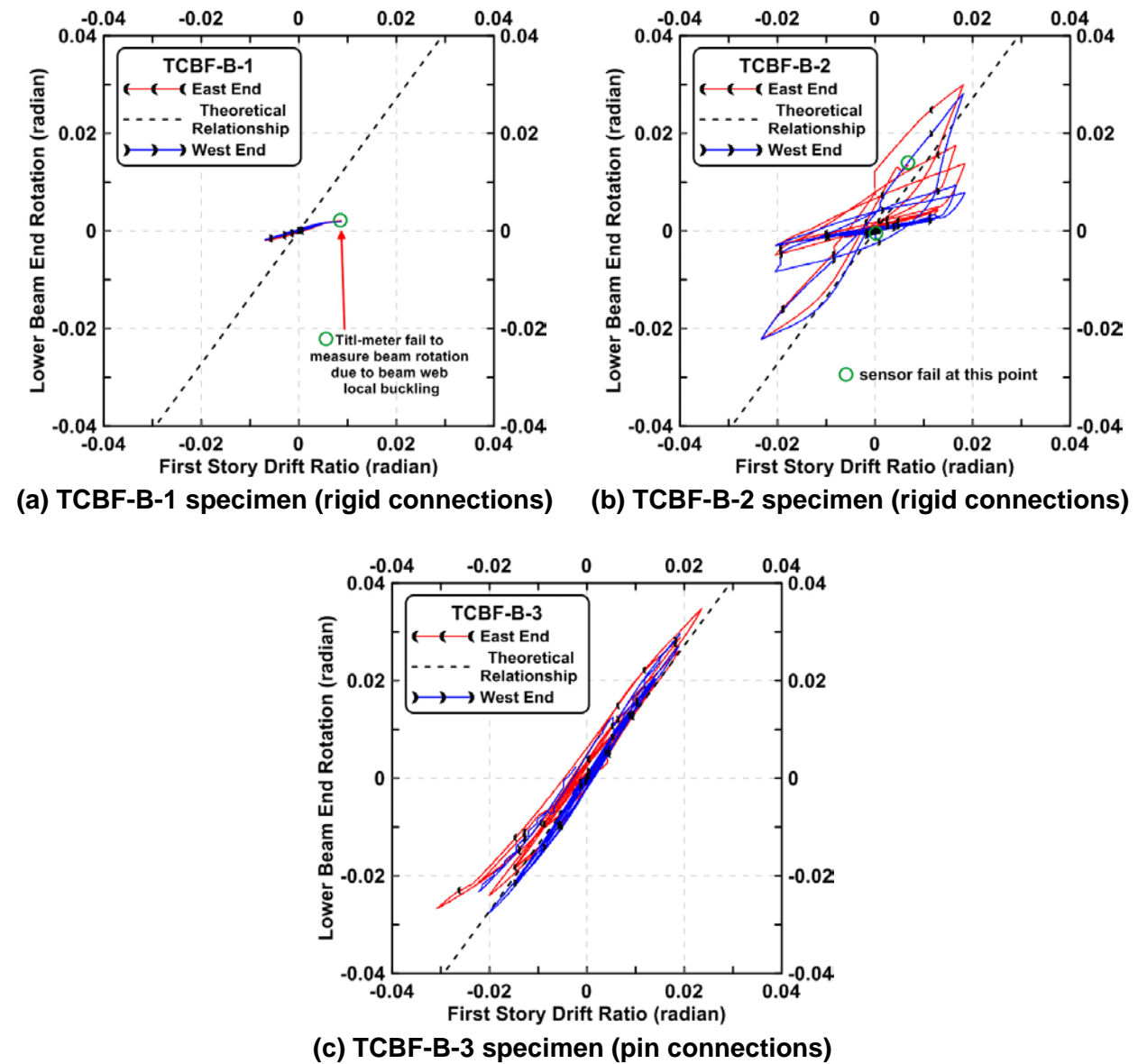


Figure 5.36 The lower beam end rotation versus first story drift ratio relationships of each specimen

### 5.1.5 Panel Zone Behavior

Shear yielding occurred in panel zones adjacent to the roof beam, as shown in Figs. 4.48, 4.150 and 4.271. Panel zones next to the one-piece gusset plate remained elastic throughout the test of each specimen. No doubler plates are used in any of the three specimens to reinforce the panel zones.

At the roof level, maximum panel zones shear strains range from 1.2% to 2.7% as shown in the time histories of rosette readings and the normalized principal stress relationships (Figs. 4.49 to 4.56, 4.151 to 4.158 and 4.272 to 4.279). From the normalized principal stress relationship plots, it is clear that shear strains are the principal deformations in the panel zones (inferred from the slopes in the plots). This also can be seen from the time histories of principal strain directions.

### 5.1.6 Gusset Plate Behavior

The gusset plate fold lines are formed as expected in the  $2t$ -gap region for all four specimens. Significant yielding occurred in the fold line region, detected through flaking of whitewash, time histories of rosette readings and derived strain time histories, as plotted in Figs. 4.57 to 4.60, 4.65 to 4.72, 4.77 to 4.80, 4.159 to 4.162, 4.167 to 4.174, 4.180 to 4.182, 4.280 to 4.283, 4.288 to 4.295 and 4.300 to 4.303. Rosette gauges not located within the fold line regions remain elastic.

The middle portions of one-piece gusset plates of each specimen that connect to the lower beam essentially remain elastic during the test as illustrated by the rosette readings (Figs. 4.61 to 4.64, 4.73 to 4.76, 4.163 to 4.166, 4.175 to 4.178, 4.284 to 4.287 and 4.296 to 4.299). But in Specimen TCBF-B-3, local yields of middle portion of one-piece gusset plate near the splice plate edge are detected via the rosette readings shown in Fig. 4.299 (location R16).

Additional linear strain gauges are used to monitor the strain distributions on one face of the tapered region of the gusset plate at the upper end of the brace on the east side of the first story in the Specimen TCBF-B-2 and TCBF-B-3 tests. It is interesting to observe that both averaged axial strains and in-plane bending strains are higher at sensor locations further from the brace-to-gusset weld lines and higher close to the fold lines (Figs. 4.183, 4.184, 4.304 and 4.305).

### 5.1.7 Test Setup Behavior

Actuator brackets deform elastically during these three tests as shown in Figs. 4.81, 4.185 and 4.306. The derived stiffness of the bracket from those plots is around 3000 kip/inch for both brackets. From Figs. 4.82, 4.186 and 4.307, no significant slippage is observed during these three tests. For the lateral stability frame, maximum out-of-plane deformation is less than 0.1 inch and typically the measured locations that are away from the reconfigurable reaction wall have larger deformations as shown in the time histories in Figs. 4.83, 4.187 and 4.308. The maximum deformations (relative to the 4 M-lb universal test machine, east-west direction) at the tip of reconfigurable reaction wall are also less than 0.08 inch in TCBF-B-2 and TCBF-B-3 tests as illustrated in Figs. 4.188 and 4.309. It is believed that these relatively small reaction wall deformations (less than 2% of the specimen maximum roof displacements) will not significantly affect the experimental control and test results.

## 5.2 HYBRID SIMULATION RESULTS

Specimen TCBF-B-4 results are discussed in this section. The small level elastic test results used to check the operation of the hybrid simulation are not discussed in since the behavior is entirely elastic and observed behavior is similar to that for the cyclically loaded specimens. Thus, results are presented for the 20-second design level earthquake ground motion and the 20-second



maximum credible earthquake level ground motion. Ground motion parameters for the hybrid simulations are briefly summarized here in Table 5.7, detail parameters are listed in Table 3.6 of Chapter 3. The combined ground motion input time history for the hybrid simulation is shown in Fig. 5.37. The OpenFresco time step numbers are also shown in the same plot.

**Table 5.7 Input ground motion parameters**

Ground Motion	Scale Factor	PGA (g)
Elastic Earthquake Level (EE)	0.13	0.063
Design Earthquake Level (DE)	1.30	0.627
Maximum Credible Earthquake Level (MCE)	1.95	0.940

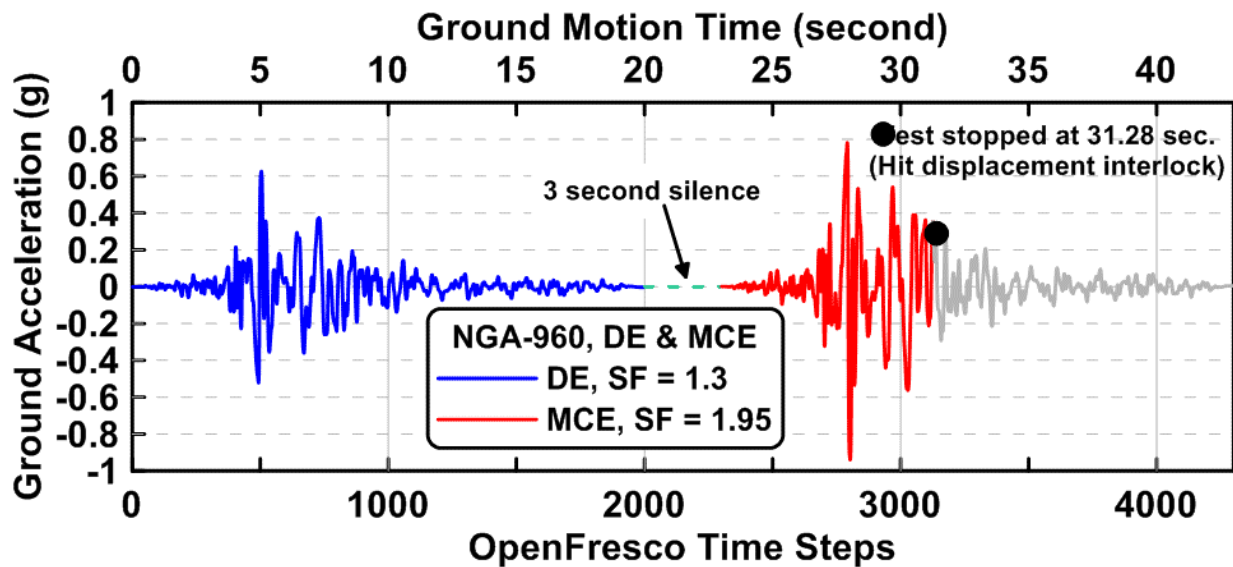


**Figure 5.37 Ground motion time history for the hybrid simulation**

While the dynamic analysis that controlled the hybrid simulation was carried out using a constant time step to integrate the governing equations of motion (see Section 3.10.2), the computed command displacements were imposed by commanding the actuator having the largest incremental displacement for a particular step to move at a constant velocity (0.002 in/sec) until it reached end of the step. The second actuator was commanded to move at an appropriately lower velocity so that it reached its target displacement at the same instant in time as did the faster moving actuator. In this way, the test was completed as quickly as possible. This implementation method for the hybrid simulation can be seen in the actuator displacement time histories shown in Fig. 4.330, where the actuators appear to be moving at nearly a constant velocity. Some actuator velocity variations occur, especially in the lower actuator.

The test was conducted very slowly compared to real time. Thus, the distortion of velocities due to this use of a variable time over which the displacements computed for each integration step is not believed to introduce additional inaccuracies.

The test was continued until the end of the stipulate records or the actuators reaching their displacement limit. Accordingly, the test was stopped at about 11.28 seconds into the 20-second long MCE motion when the upper actuator reached its stroke limit. It can be seen in Fig. 3.330 that both actuator displacements are imposing oscillations in the structure with increasingly negative values towards the end of the simulation.

### 5.2.1 Specimen Global Behavior

From the actuator force time histories plotted in Fig. 4.331, peak actuator forces for upper and lower actuators are 551 kips and 457 kips, respectively. The peak base shear is 761.1 kips, which compares to the maximum value of 789.1 kips for the similar Specimen TCBF-B-1 (note the connections of the lower beam to gusset plates and column base conditions differed).

It is notable that the upper actuator force to lower actuator force ratios typically range from one to six and most of the time maintain a ratio of two during the hybrid test as illustrated in Fig. 4.334. From the same plot, we can see that the upper actuator forces and lower actuator forces may have opposite signs (especially during MCE level ground motion, see the red curves in the plot) during the hybrid test, which indicates a significant story shear redistribution or higher mode effects in the specimen. The actuator force ratios that are closed to a value of two provides a strong support that the lateral force distribution assumption in the quasi-static tests is reasonable. But the observed higher mode effects in the hybrid tests may not be adequately represent in the quasi-static tests.

From the actuator displacement relationships between upper and lower actuators shown Fig. 4.335, some instantaneous local concentrations of deformation in the first story or second story are illustrated via the slope deviating from the 45° orientation. Significant deviation of actuator displacements during the MCE ground motion are also shown in this plot. It should be recalled that the hybrid simulation numerical model incorporates the gravity-only columns and these may help avoid soft story tendencies.

Based on observations from the similar TCBF-B-1 specimen, it is surprising that a HSS brace in the second story fractures near the end of the design earthquake ground motion (see Fig. 4.332). After fracturing of this brace at around 2% roof drift ratio, the second story tends to deform more than the first story, as shown in Fig. 4.333. While no other fractures occurred after the DE motion, there was considerable lateral and local buckling of all of the other braces (see photo in Fig. 4.329(c), and distributed yielding throughout the structure as described in Section 4.3.2. The residual displacement of the frame after the DE level shaking is modest, being about 0.08 inches at the roof and 0.04 inches at the lower level. However, the residual out of plane deformations of the braces were significant, ranging from 6.2-inches near the midspan of the E-2F brace to 3.5-inches near the midspan of the E-1F brace.

The initial stiffness of the entire specimen drops to about 20% of that for the initial undamaged specimen at the end of the design earthquake (via slopes in Fig. 4.332). Story stiffness of both stories has similar reduction after design earthquake (Fig. 4.333).

During the subsequent response to the MCE level ground motion, two braces (2F-West and 1F-East) completely fractured at nearly the same time while in tension at around 1.5% roof drift ratio (Fig. 4.332). Note that the peak base shear drops from around 600 kips to 300 kips

after fracturing these braces. The last remaining brace fractures at about a roof drift ratio of 4.2%.

A total of thirty-six time points during the hybrid simulation are selected to examine local peak responses. Table 5.8 summarizes the local peak story shear and floor level displacement data of the TCBF-B-4 specimen at these points during the hybrid simulation.

Time histories of floor level displacement and the story force are plotted in Figs. 5.38 and 5.39. The vertical light gray grid lines indicate the 36 time points where the local peak responses are further investigated. In these plots, and subsequent discussion, times refer to the times in the computations used to carry out the hybrid simulations (not the actual time in the lab). From Table 5.8, it is noted that the peak base shear is 761.1 kips before the braces begin to buckle globally. Lateral buckling of the first square HSS brace is noted at about 5.22 sec., and local buckling is observed 0.34 sec. later. Cracks initiate at the corner of the cross section about 1.43 sec. later. About 0.5 second (ground motion time) later the first brace fractured at the second story eastern side. Thus, about 2.27 transpired from the first lateral buckling until complete fracture of a brace. Thereafter, no other braces fractured during the rest of the DE ground motion. As noted above, no significant floor level residual displacements are observed after 20 second DE ground motion (see Table 5.8 and Fig. 5.38).

Looking at the total energy dissipations until the first brace completely fractured, the specimen dissipates only 7,799 kip-in and at the end of DE ground motion, the total energy accumulated to 8,832 kip-in. This is only about 60% of energy dissipated in TCBF-B-1 specimen until the first brace fractured. At the instant where all four braces are fractured during the MCE event, the total energy dissipation from the beginning of the test is 10,552 kip-in, also around 60% of energy dissipated in TCBF-B-1 specimen until quasi-static test is stopped. It is believed that the characteristic of the input ground motion during the ground motions used for the hybrid tests introduce several large pulse-liked cyclic displacement excursions (see Fig. 5.38) without developing a series of earlier incremental displacement cycles which causes the brace behavior deteriorates faster.

The total energy dissipated between each of the 36 key points in the ground motion time history is shown in Fig. 5.40. It is notable that the energy dissipation occurs during a few relatively short portions of the ground motion time histories. Much of the energy is dissipated between time 5 and 8 seconds. For example, between the short interval, 6.99 to 7.49 second, more than 20% of the total energy dissipated during the DE ground motion is dissipated. Between these intervals with major energy dissipation, little significant energy dissipation occurs. Similar observations are found during the MCE ground motion.

Comparing the cumulative roof plastic deformation or the normalized energy dissipation, it is not surprising that similar results are observed. Detail roof plastic deformation and the normalized energy dissipation in each ground motion time segment are plotted and compared in Figs. 5.41 and 5.42. Note that the cumulative roof plastic deformation and the normalized energy dissipation are defined in the title row of Table 5.8. The  $P_y$  value for the specimen in the hybrid test is obtained from the initial base shear-roof displacement plot corresponds to a roof displacement of 0.6 inch.

In terms of the story deformation, the ratio of the individual story deformation to total roof displacement at each story is plotted in Fig. 5.43. The story deformation ratios for top and bottom story are around 50% and 50% at the beginning of ground motion. As the intensity of ground shaking increases, especially after local buckling observed in the braces, the second story tends to deform more than the lower story. But the upper story deformation ratio does not exceed

75% most of the time. However, at 20.77 and 29.15 seconds into the ground motion, the story drifts are of opposite sign and the drifts are relatively small (the actuator displacements as listed in Table 5.8 are less than 0.25 inch). Deformation concentration at the second story does happen during the hybrid simulation specifically when the structure deforms to the negative direction (to the west).

The energy dissipation ratios for each story are shown in Fig. 5.44. Although the drifts are larger in the second story, this figure indicates that more than 60% of total energy dissipation comes from the first story, similar to the observations from the quasi-static tests.

**Table 5.8 Story shear and floor level displacement data of TCBF-B-4**

**( $P_y = 589.3$  kips from hybrid simulation, corresponding to  $D_{by} = 0.6$  inch at roof)**

Ground Motion Time (second)	Roof Level Displacement (inch)	Lower Level Displacement (inch)	Base Shear (kips)	Second Story Shear (kips)	Cumulative Hysteretic Area (Energy Dissipation) E (kip-in)	Cumulative Plastic Roof Displacement $E / (P_y)$ (inch)	Normalized Energy Dissipation $E / (P_y * D_{by})$	Key Observations
3.93	0.44	0.22	366.3	299.3	86	0.1	0.2	
4.15	-0.52	-0.27	-414.7	-360.1	128	0.2	0.4	
4.34	0.71	0.37	569.2	420.3	232	0.4	0.7	
4.54	-0.82	-0.45	-735.5	-444.4	353	0.6	1.0	
4.94	0.86	0.48	758.4	433.3	434	0.7	1.2	
5.22	-3.35	-1.71	<b>-761.1</b>	-486.1	2162	3.7	6.1	GB*
5.56	1.71	0.83	692.4	434.5	3383	5.7	9.6	LB*
5.91	-1.75	-0.89	-456.5	-344.8	3705	6.3	10.5	
6.22	0.24	0.08	315.4	306.4	3753	6.4	10.6	
6.61	-2.87	-1.55	-637.4	-390.1	4518	7.7	12.8	
6.99	2.92	1.21	524.6	396.8	5930	10.1	16.8	CI*
7.49	-4.96	-2.17	-540.3	-321.7	<b>7799</b>	<b>13.2</b>	<b>22.1</b>	PF*, CF1*
8.07	2.70	1.28	305.5	300.2	8603	14.6	24.3	
8.78	-0.55	-0.20	-133.4	-74.3	8511	14.4	24.1	
10.11	1.99	0.96	207.7	180.9	8704	14.8	24.6	

Ground Motion Time (second)	Roof Level Displacement (inch)	Lower Level Displacement (inch)	Base Shear (kips)	Second Story Shear (kips)	Cumulative Hysteretic Area (Energy Dissipation) E (kip-in)	Cumulative Plastic Roof Displacement $E / (P_y)$ (inch)	Normalized Energy Dissipation $E / (P_y * D_{by})$	Key Observations
12.97	-0.75	-0.30	-159.6	-75.0	8730	14.8	24.7	
13.45	1.03	0.53	126.4	100.1	8777	14.9	24.8	
15.49	-0.76	-0.27	-144.4	-88.2	8815	15.0	24.9	
15.98	0.86	0.45	118.3	95.6	8838	15.0	25.0	
17.44	-0.59	-0.21	-123.9	-63.3	8845	15.0	25.0	
<b>20.77</b>	<b>-0.06</b>	<b>0.03</b>	<b>-22.4</b>	<b>1.8</b>	<b>8832</b>	<b>15.0</b>	<b>25.0</b>	<b>DE finished</b>
25.31	-0.39	-0.11	-76.0	-49.9	8844	15.0	25.0	
25.68	0.77	0.41	109.1	83.0	8876	15.1	25.1	
26.63	-0.37	-0.11	-63.8	-50.9	8860	15.0	25.1	
26.84	0.58	0.26	52.7	94.0	8874	15.1	25.1	
27.32	-0.56	-0.19	-83.1	-77.8	8885	15.1	25.1	
27.73	3.50	1.70	226.6	208.0	<b>9453</b>	<b>16.0</b>	<b>26.7</b>	CF2*, CF3*
28.07	-6.45	-2.72	-126.4	-323.5	<b>10552</b>	<b>17.9</b>	<b>29.8</b>	CF4*
28.38	-3.23	-1.87	-201.7	233.2	10520	17.9	29.8	
28.71	-6.04	-2.79	-92.8	-234.9	10707	18.2	30.3	
29.15	-0.22	0.03	189.1	103.0	10884	18.5	30.8	
29.4	-1.75	-0.58	110.4	-95.4	10802	18.3	30.6	
29.67	1.77	0.93	164.3	210.0	11247	19.1	31.8	
30.19	-10.39	-5.29	-305.9	-190.0	12752	21.6	36.1	

Ground Motion Time (second)	Roof Level Displacement (inch)	Lower Level Displacement (inch)	Base Shear (kips)	Second Story Shear (kips)	Cumulative Hysteretic Area (Energy Dissipation) E (kip-in)	Cumulative Plastic Roof Displacement E / (P <sub>y</sub> ) (inch)	Normalized Energy Dissipation E / (P <sub>y</sub> *D <sub>by</sub> )	Key Observations
30.6	0.28	0.12	182.7	204.9	13291	22.6	37.6	
<b>31.28</b>	<b>-10.44</b>	<b>-5.31</b>	<b>-316.3</b>	<b>-174.7</b>	<b>14216</b>	<b>24.1</b>	<b>40.2</b>	<b>test stop</b>

\*Note: GB (global buckling), LB (local buckling), PF (partial fracture), CF1 (first brace complete fracture), CI (crack initial)

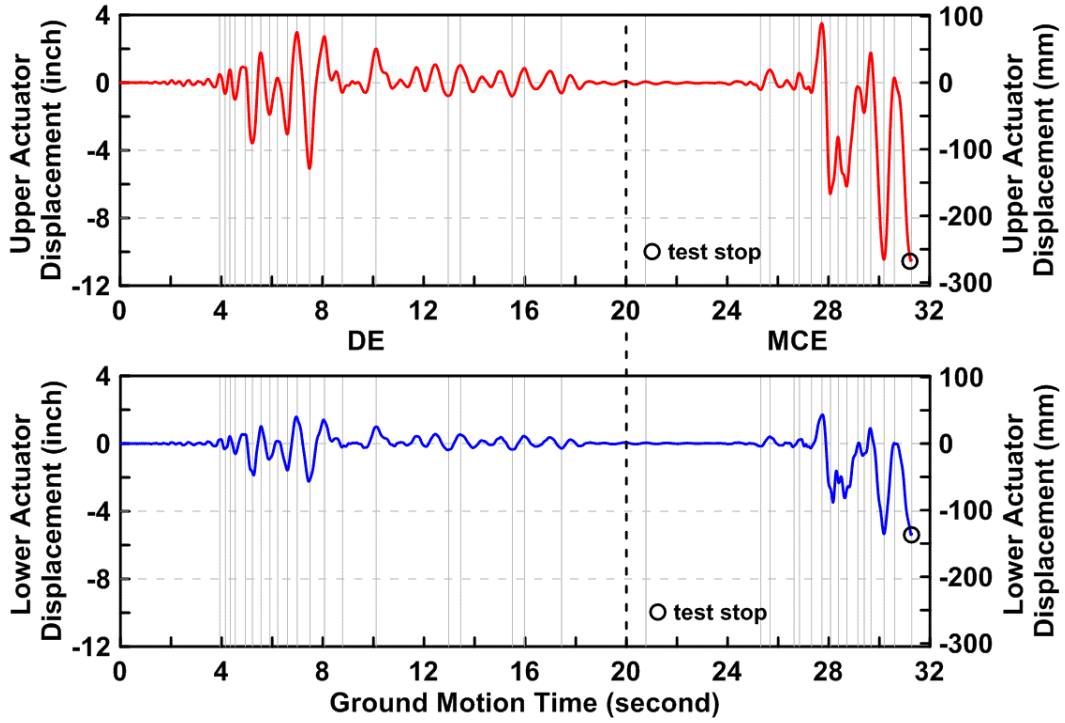


Figure 5.38 Floor level displacement time histories of TCBF-B-4 specimen

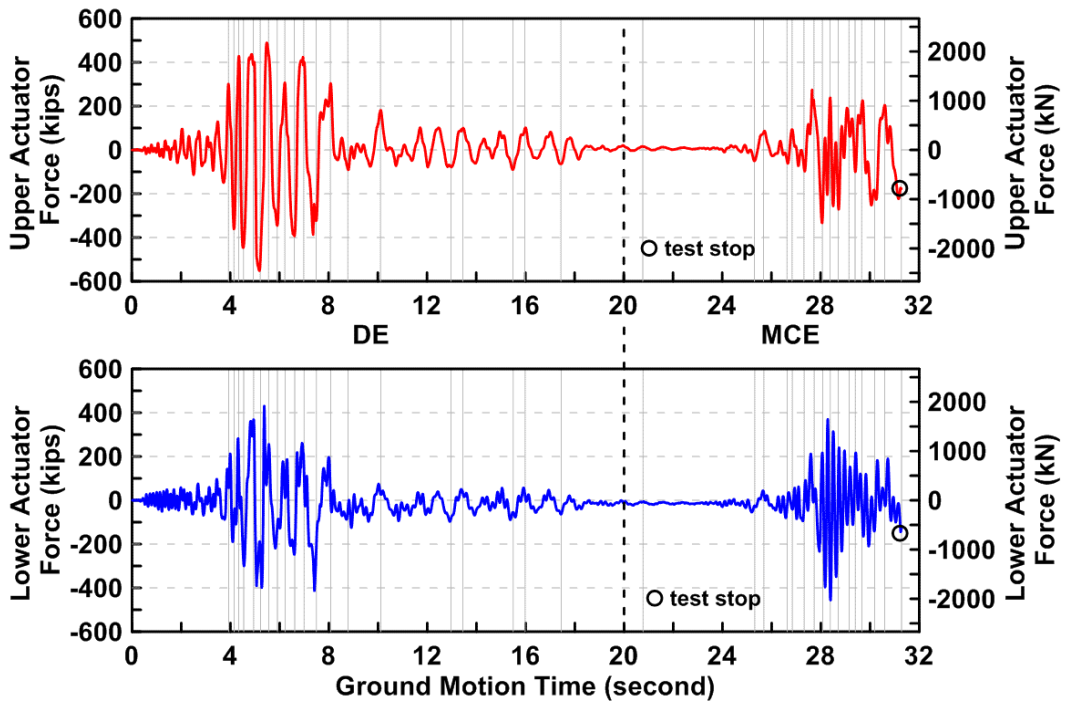


Figure 5.39 Story force time histories of TCBF-B-4 specimen



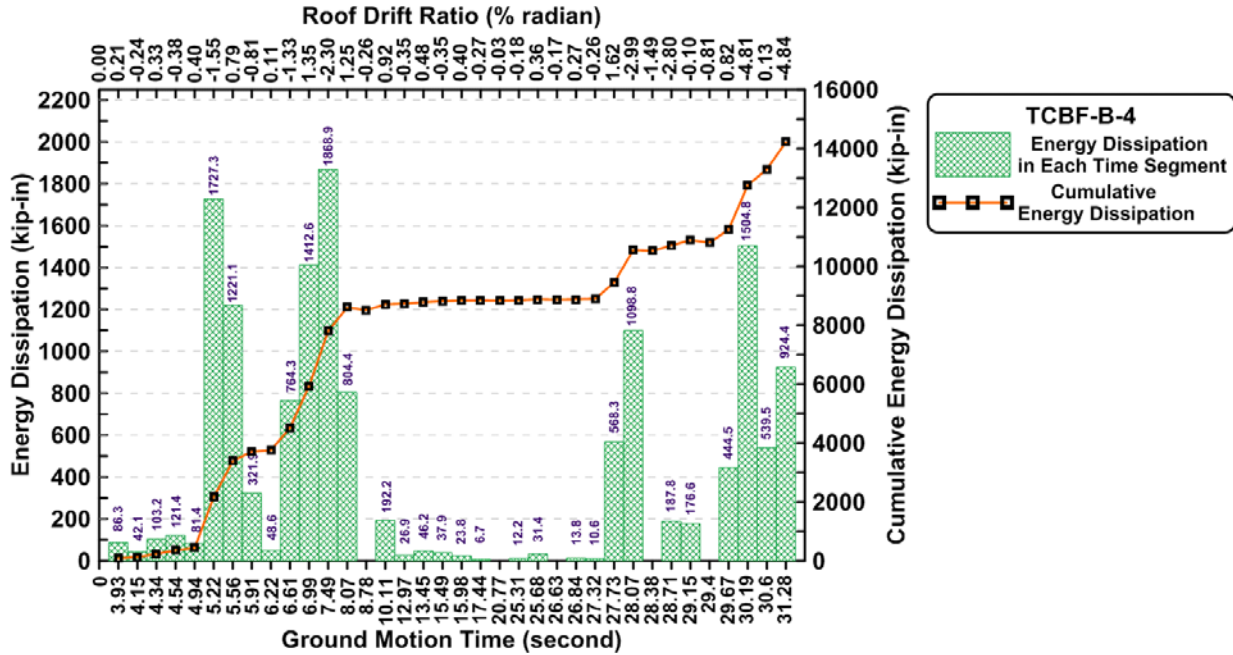


Figure 5.40 Total energy dissipation in each time segment and total cumulative energy dissipation of TCBF-B-4 specimen

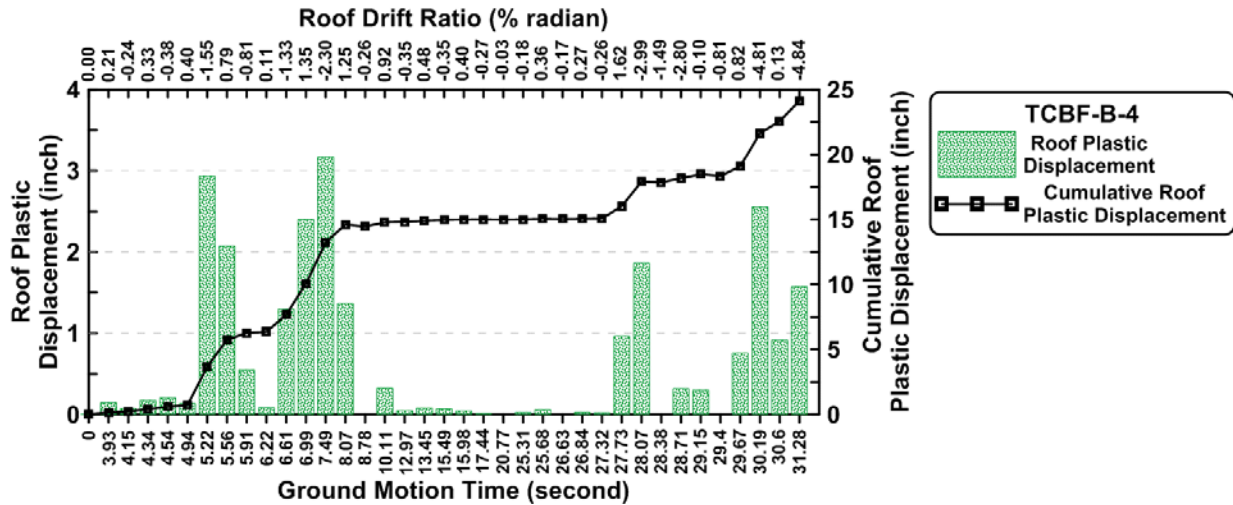


Figure 5.41 Total roof plastic displacement in each time segment and total cumulative roof plastic displacement of TCBF-B-4 specimen

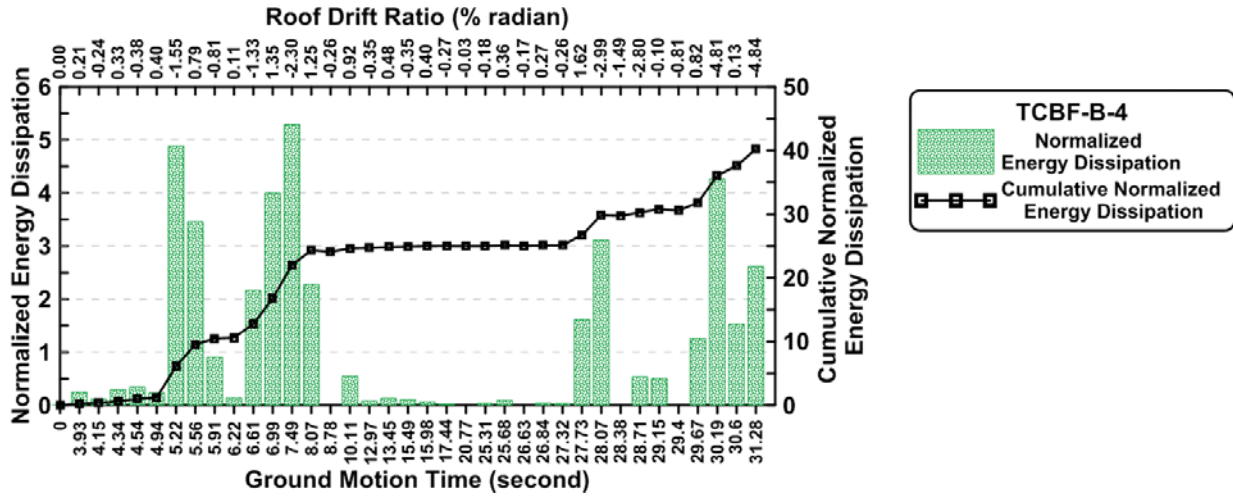


Figure 5.42 Normalized energy dissipation in each time segment and cumulative normalized energy dissipation of TCBF-B-4 specimen

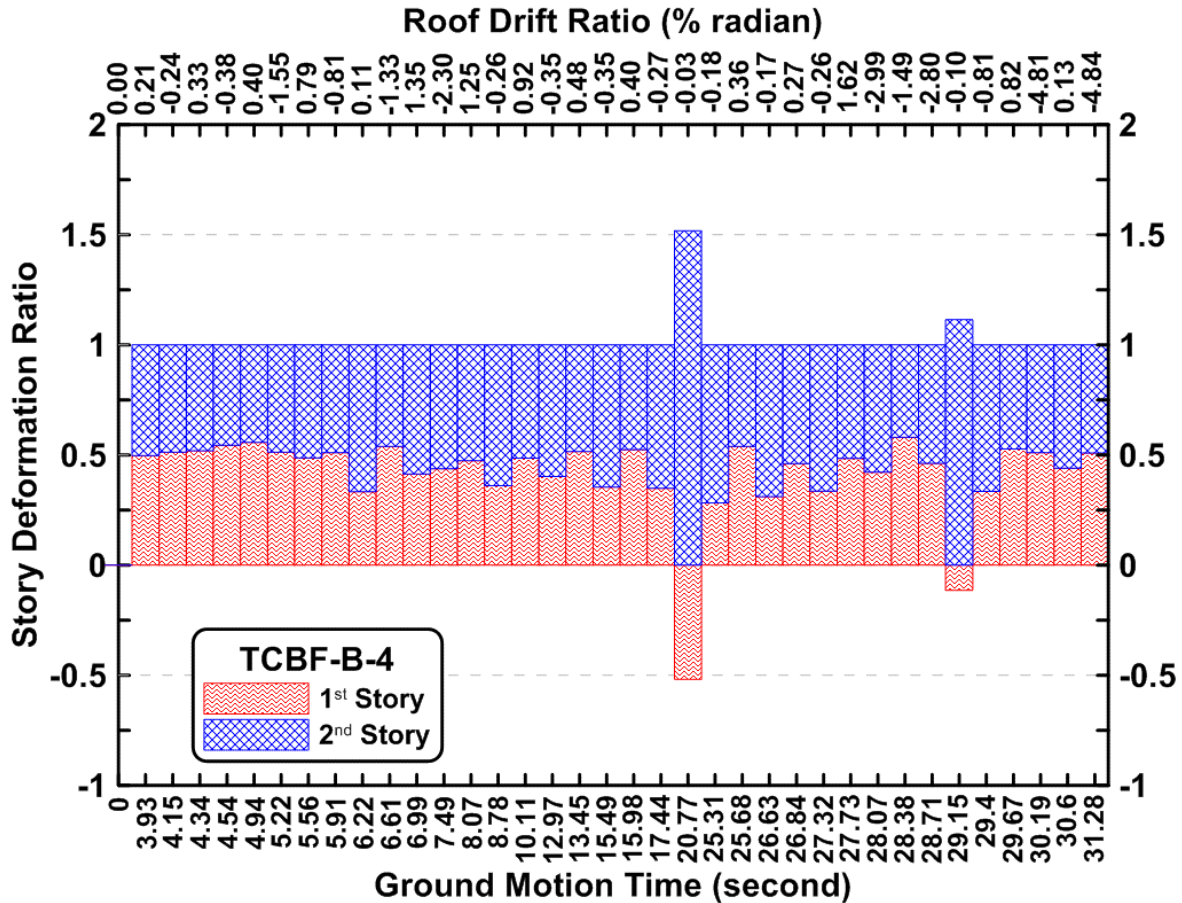


Figure 5.43 Story deformation ratio of TCBF-B-4 specimen

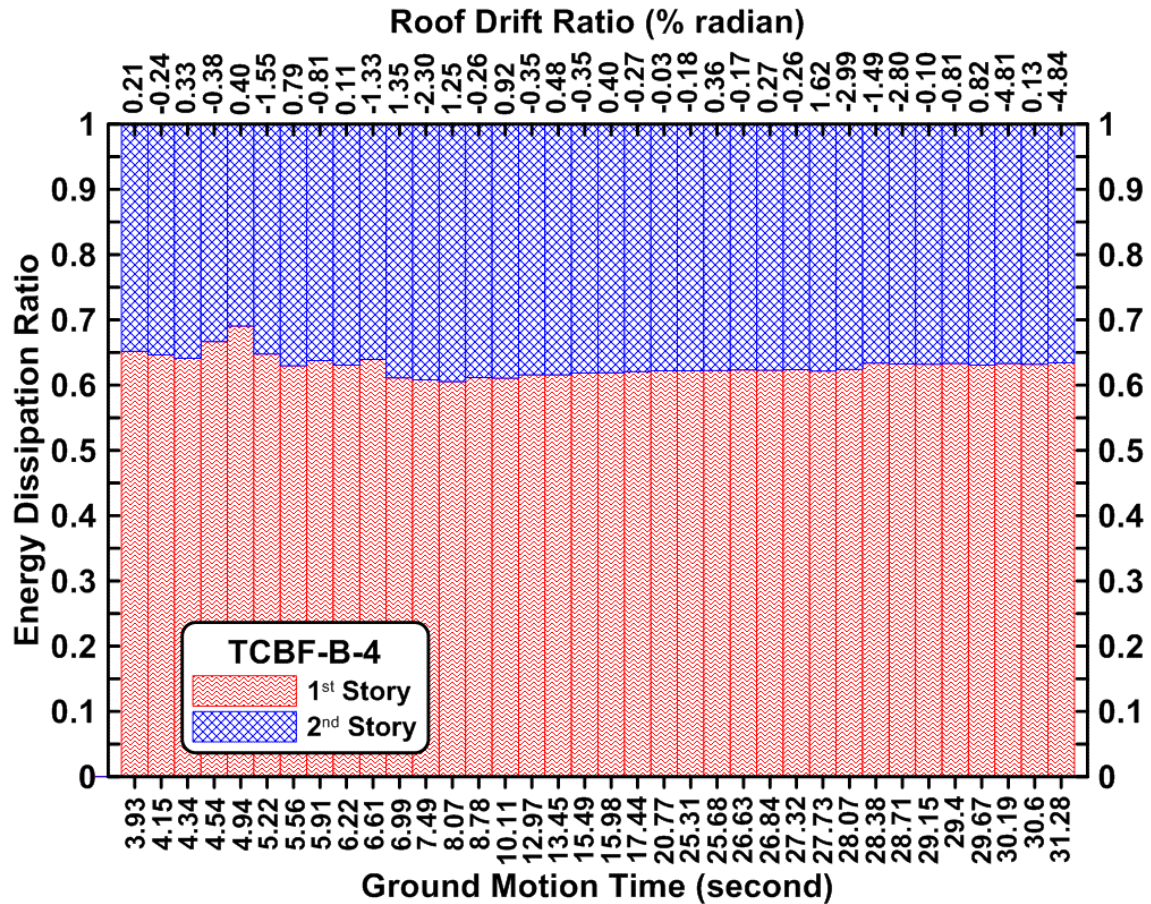


Figure 5.44 Story energy dissipation ratio of TCBF-B-4 specimen

## 5.2.2 Brace Behavior

All four braces buckle out-of-plane to the southern side during the hybrid simulations. Similar to quasi-static tests, the braces connecting to the same one-piece gusset plate tend to buckle to the same direction, as shown in Fig. 4.329.

From Fig. 4.369, the out-of-plane displacement at the middle length of braces can be as much as ten times the axial deformation of the braces. As with the quasi-static tests, the brace out-of-plane displacements tend to change sign during a cycle (see Fig. 4.368) after a crack propagates partially through the cross section since the neutral axis of the cracked braces shifts toward the un-cracked side of the cross section. As mentioned previously, this eventually creates an eccentricity when the braces reload in tension.

Strain decomposition plots for the braces shown in Figs. 4.370 to 4.373 illustrate the sources of strain readings during the hybrid tests. Note that the strain gauge locations are at the quarter length of brace close to the gusset plate where two braces meet at the beam side (see Appendix G sensor locations for detail). Permanent residual strains typically develop for each component by the end of simulation. Maximum axial strains in the braces range from 5 to 9 times the yield strain of steel and residual tension strains range from 5 to 8 times the yield strain. Axial strains shift to tension side because the compression strains basically concentrate around the middle length of braces under compression.

Most of the brace in-plane bending strain readings are close to or less than the yield strain of steel (between  $1200\mu$  to  $2200\mu$ ) and the maximum out-of-plane bending strains are typically larger than in-plane bending strains, ranging from  $1250\mu$  to  $3100\mu$ . Deviation of out-of-plane bending strain also indicates the buckling direction of the brace. Effect of frame action on braces can be clearly observed by comparing the sign of axial strain and in-plane bending strain of each brace.

The brace cumulative plastic deformations, cumulative normalized energy dissipation, plastic deformations and normalized energy dissipation in each ground motion time segment are shown in Figs. 5.45 and 5.46.

Similar to the quasi-static test results, the cumulative normalized energy dissipation and cumulative plastic deformations of first story braces typically have larger values at the end of test. But the normalized energy dissipation and plastic deformations accumulate during the ground motion time segment shows something different; braces in the second story sometimes accumulate more energy or plastic deformations, as can be seen in Figs. 5.45 and 5.46. During the DE level ground motion, plastic deformations and normalized energy dissipation of both story braces start to accumulate at about the same time, but the first story west brace and the second story east brace accumulate faster than the other two remained braces until the second story east brace fractures. Relatively small amount of energy is accumulated by the braces during the MCE ground motion.

The total energy dissipation components during the hybrid test are illustrated in Fig. 5.47. Braces basically contribute more than 50% of total energy dissipated during the DE level ground motion as shown in the stacked bar charts. The total energy dissipated by other components such as beams, columns and panel zones increases as the displacement demand increases. A significant amount of energy is dissipated (50% to 100%) by structure members other than braces during the MCE level ground motion.

Table 5.9 summarizes the specimen failure characteristics regarding to the brace completely fracture during the hybrid simulation. Note that the plastic deformation capacities of the first story braces are about a half of the capacities observed from the TCBF-B-1 quasi-static test results. This is likely due to the different history of deformations associated with the earthquake response simulations.

**Table 5.9 Specimen TCBF-B-4 brace failure characteristics (brace completely fractures)**

<b>Specimen Name</b>	<b>TCBF-B-4</b>			
Fracture Sequence	1 <sup>st</sup>	2 <sup>nd</sup>	3 <sup>rd</sup>	4 <sup>th</sup>
Location	2F-East	2F-West	1F-East	1F-West
Ground Motion Time (sec.)	7.49	27.72	27.73	28.07
Roof Displacement at Fracture (inch)	-4.96	3.49	3.50	-6.45
Roof Drift Ratio at Fracture (% radian)	-2.30	1.62	1.62	-2.99
Brace Cumulative Plastic Deformation at Fracture (inch)	3.2	3.1	3.7	5.4
Brace Cumulative Normalized Energy Dissipation at Fracture	14.4	15.9	17.1	25.0

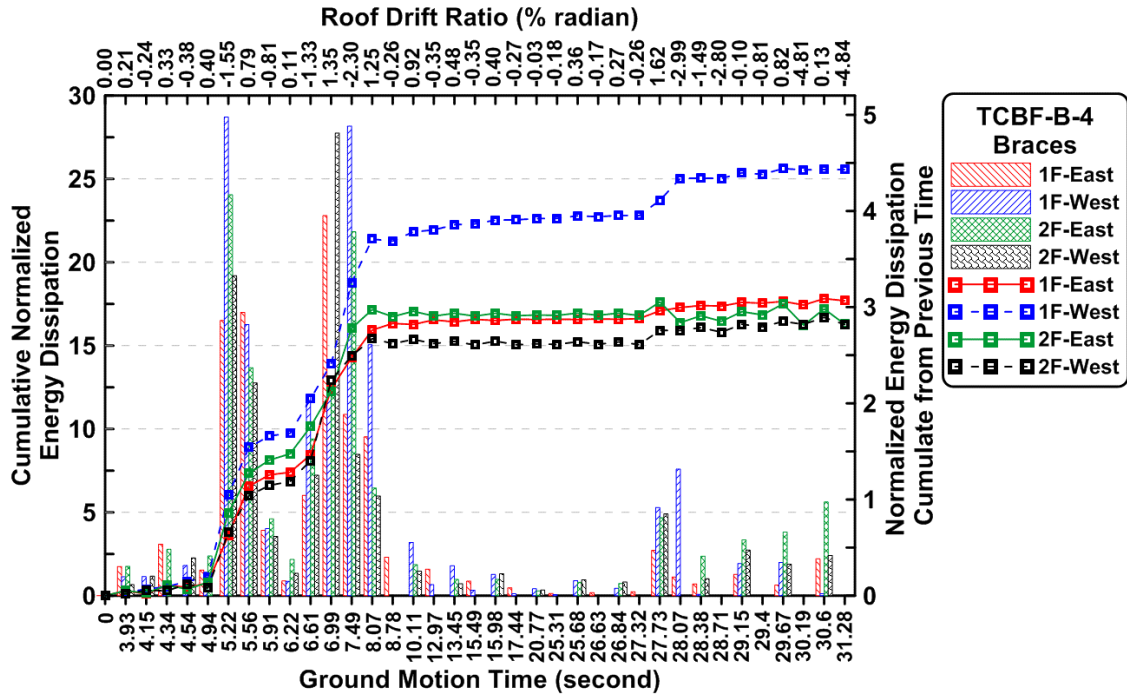


Figure 5.45 Brace cumulative normalized energy dissipation and normalized energy dissipation of TCBF-B-4 specimen in each time segment

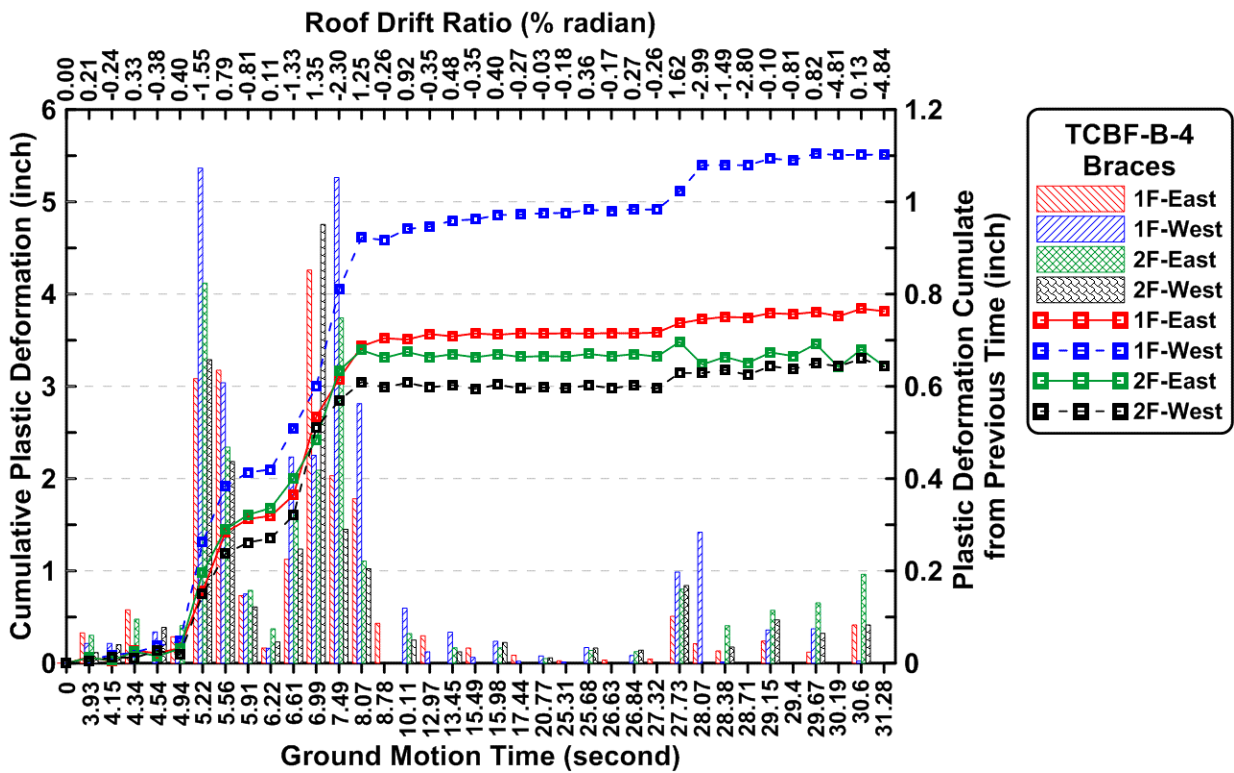


Figure 5.46 Brace cumulative plastic deformations and plastic deformations of TCBF-B-4 specimen in each time segment

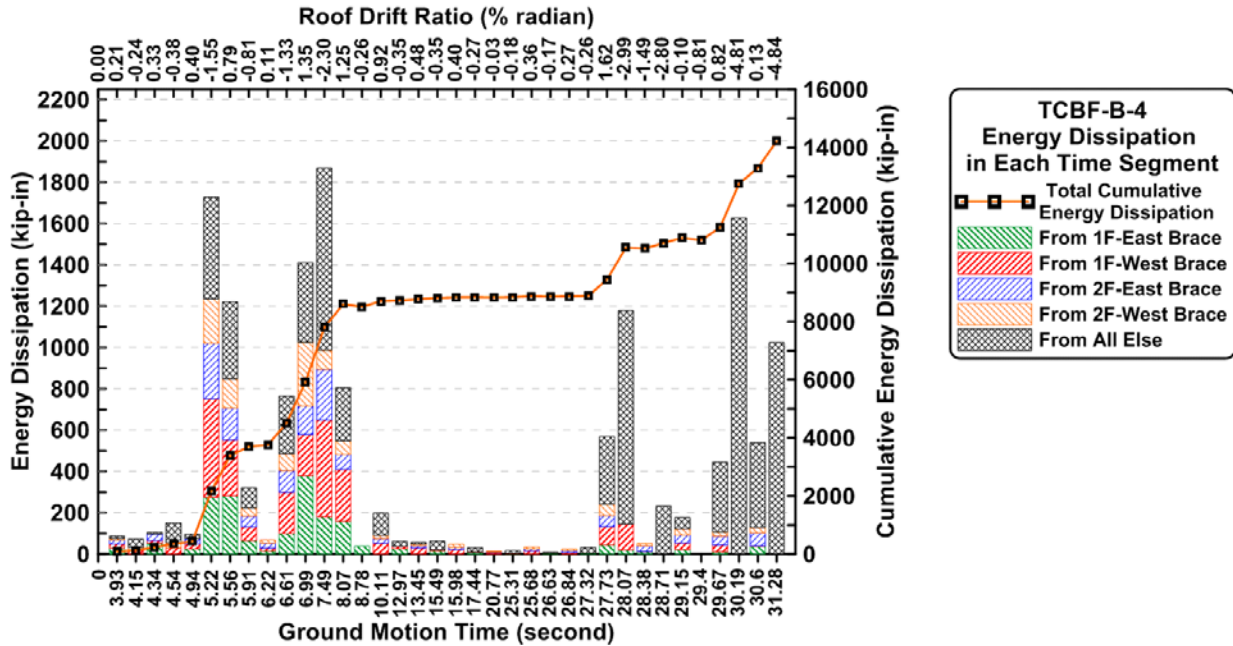


Figure 5.47 Source of energy dissipation in each time segment and total cumulative energy dissipation of TCBF-B-4 specimen

### 5.2.3 Column Behavior

Column axial forces are significantly reduced as a result of the brace fractures that occur in the MCE event. During the MCE ground motion, the column force demands were only about 30 % or less of those developed during the DE level ground motion (see Figs. 4.336 and 4.337). Bending moments in the W12 × 96 columns at both floor levels typically are less than the yield moment except at the column bases (Figs. 4.338 and 4.339). Derived column shear forces in the webs are also less than the yield shear value as shown in Figs. 4.340, 4.341 and 4.342. The column webs essentially remain elastic throughout the hybrid simulations (see Fig. 4.343).

From the column shear versus story shear relationships plotted in Fig. 4.344, columns take about 16% story shear at the beginning of design earthquake ground motion and then gradually contribute more to the story shear during the hybrid simulation. At the end of the DE, the first-story columns resist about 42% of the total story shear while the second-story columns resist the entire story shear in the second-story. Eventually the entire story shear force is taken by the columns after all four braces fracture during the MCE ground motion.

The time histories of rosette readings shown in Figs. 4.345 to 4.348 also demonstrate that the column webs remain elastic. It is notable that the normalized principal stress states at the first-story rosette sensor locations are different during DE (normal stress dominated) and MCE (shear stress dominated) level ground motions. These are presented in Figs. 4.349 and 4.350. Similar to the results from quasi-static tests, column webs stress states dominate more by shear stresses after failure of braces. There are no significant changes of stress states in the second story column webs during the hybrid tests (see Figs. 4.351 and 4.352).

Interaction diagrams shown in Figs. 4.353 and 4.354 reveal that substantial P-M or P-V interaction at the column bases occur during the DE ground motion, while in MCE ground motion, the flexural behavior essentially governs the column base responses. The interaction diagrams for the second story column top end (the roof beam and column centerlines intersection) of this specimen (Figs. 4.355 and 4.356) indicate that the cross sections remain essentially elastic for the hybrid tests.

#### **5.2.4 Beam Behavior**

As with the quasi-static tests, the roof level beam remains elastic during the hybrid tests in spite of the greater distress to the braces in the second story. This behavior can be seen by examining the strain gauge time histories in the beam flanges, axial force time histories, estimated shear force time histories and beam end bending moment time histories in Figs. 4.358, 4.361, 4.363 and 4.365. No significant local yielding was observed near any of the roof beam to column flange welds.

The response of the W24 × 68 lower beam is shown in Figs. 4.359, 4.360, 4.362 and 4.364). Pin connection details are used for TCBF-B-4, rather than the fixed connection used in Specimen TCBF-B-2. Like Specimen TCBF-B-3 no significant plastic deformations are observed in the lower beam, but some local yielding in the connection splice plate was observed via white was flaking. Maximum average axial forces about 200 kips (both tension and compression) are developed in the lower beam of this specimen which are similar to the maximum axial forces observed in lower beam of the Specimen TCBF-B-1 during quasi-static test. Very small shear forces are recorded during hybrid test of the beam with pin connections to the gusset plates.

As with the quasi-static tests, similar rotational amplification effects occur during hybrid simulations in the lower beam ends. From Figs. 5.48, the slopes of responses of TCBF-B-4 specimen essentially follow the theoretical prediction until sensors fail.

From the beam center deflection time histories plotted in Fig. 4.357, higher deflections (compared with Specimen TCBF-B-1) are found and expected as the result of unbalanced loads developed in the roof beam. Estimated peak unbalanced loads is about 100 kips as shown in Figs. 4.366.



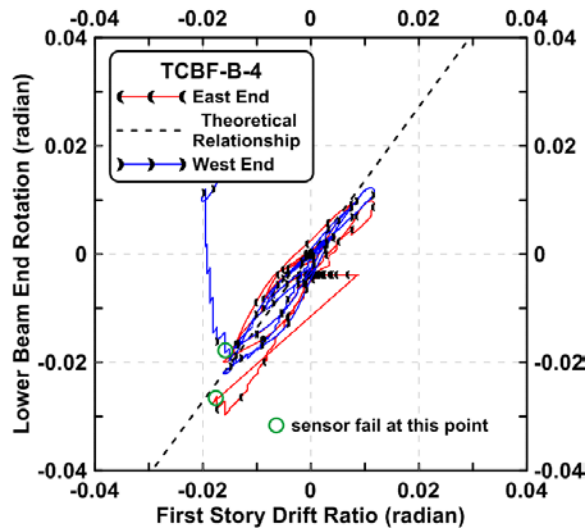


**Figure 5.48 The lower beam end rotation versus first story drift ratio relationships of TCBF-B-4 specimen**

### 5.2.5 Panel Zone Behavior

Shear yielding also occurs in the panel zones that are next to the roof beam during the hybrid simulations, as shown in Figs. 4.374. Maximum panel zones shear strains range from 1.2% to 2% during the DE ground motion and are more than 3% during the MCE ground motion as shown in the time histories of rosette readings and the normalized principal stress relationships in Figs. 4.375 to 4.382. Signal saturation happens in the rosette readings when the shear strains approach to 3.2% in the second story eastern side panel zone. Unlike the upper beam to column connection, the panel zones on the lower floor next to the one-piece gusset plate remain elastic throughout the hybrid tests.

From the normalized principal stress relationship plots, it is clear that the shear strains are the principal deformations in the panel zones (via slopes in the plots). This also can be seen from the time histories of principal strain directions.

### 5.2.6 Gusset Plate Behavior

Similar to quasi-static test results, the gusset plate fold lines are formed as expected in the  $2t$ -gap region for this specimen. Significant yields are found after formation of fold lines through flaking of the whitewash, the time history of rosette readings and the derived strain time histories as plotted in Figs. 4.383 to 4.386, 4.391 to 4.394, 4.395 to 4.398 and 4.403 to 4.406. Again, rosettes at locations not within the fold line regions remain elastic.

The middle portions of one-piece gusset plates of this specimen that connect to the lower beam essentially remain elastic during the test as illustrated by the rosette readings (Figs. 4.387 to 4.390 and 4.399 to 4.402). But local yields of middle portion of one-piece gusset plate near the splice plate edge are detected via the rosette readings shown in Figs. 4.388 and 4.390 (locations R14 and R16).

It is interesting to point out that from the normalized principal stress state plots shown in Figs. 4.397, 4.398 and 4.405 (locations R11, R12 and R19 as illustrated in Appendix G), bi-axial tension stresses occur in the one-piece gusset plate during the hybrid tests (via the trends of plots), especially during the MCE ground motion. Further investigation using finite element models are suggested to examine this observation.

### **5.2.7 Test Setup Behavior**

Like in quasi-static tests, actuator brackets deform elastically during these three tests as shown in Fig. 4.407. The measured stiffness of the bracket is around 3000 kip/inch from both brackets during DE ground motion. Direct measured stiffness is about 30% higher during the MCE ground motion (not corrected with the reaction wall deformations). It is believed that the difference might come from the interaction between test setup and the reference frame used to measure the bracket deformations.

From Fig. 4.408, no significant slippage of the test setup is observed during hybrid simulations. For the lateral stability frame, maximum deformation is less than 0.04 inch and typically the measured locations that are away from the reconfigurable reaction wall have larger deformations as shown in the time histories in Fig. 4.409. The maximum deformations at the tip of reconfigurable reaction wall are less than 0.07 inch in hybrid tests (smaller than 0.04 inch during MCE ground motion test) as illustrated in Fig. 4.410. The maximum deformation of the reaction wall is less than 0.7% of the maximum deformation of the braced specimen. Also should be noted that two position transducers used for external control during the hybrid simulation were mounted on an independent instrument reference frame welded to the laboratory structure. It is believed that the deformations of the reaction wall, strong floor and actuator brackets will not affect the hybrid simulation results.

### **5.2.8 Performance of Servo-Hydraulic Control System**

The performance of servo-hydraulic control system can be evaluated through examining the differences between command and feedback of displacement and force. The differences (or errors) also represent how accurate the hybrid simulation is. From the response histories recorded in the MTS-STS software during the hybrid test, the maximum displacement error for top and bottom actuators were equal to 0.021 in. and 0.0313 in., respectively. These errors corresponded to about 0.2% and 0.58% of the maximum actuator displacement at that floor level. This implies that the servo-control system can accurately push or pull the specimen to the command displacements.

Synchronization subspace plots (Mercan, 2007; Schellenberg et al., 2009) of both actuators are plotted in Figs. 5.49 and 5.50 to help indentifying the source of errors during the hybrid simulation. Displacement errors come from actuator lag, actuator lead, actuator undershoot and actuator overshoot can be indentified if the plot is not a perfect 45° straight line. Note that the top actuator identification number was set to 3 (actID = 3) and the bottom actuator was set to 4 (actID = 4) in the STS software during the hybrid simulation. From the plots shown in Figs. 5.49 and 5.50, it is clear that the displacement errors were very small.

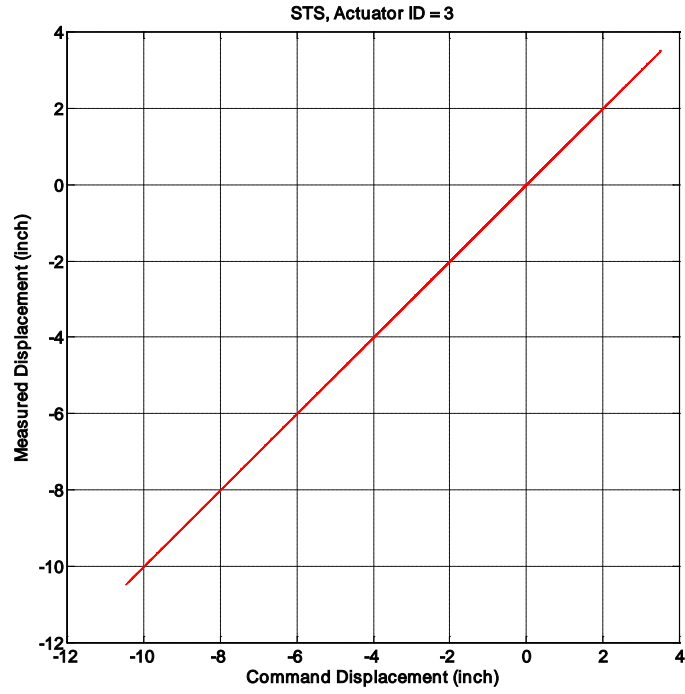


Figure 5.49 Synchronization subspace plot of top actuator during hybrid test

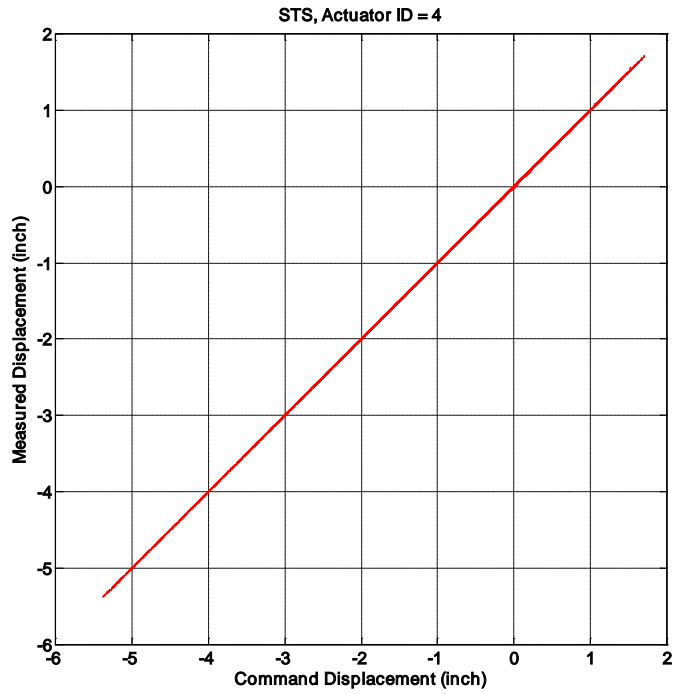


Figure 5.50 Synchronization subspace plot of bottom actuator during hybrid test

### 5.3 CONCLUDING REMARKS

From the experimental results discussed, several conclusions can be summarized:

1. Specimen TCBF-B-2 (round HSS braces) has the largest deformation capacity among the three quasi-static test specimens under the same predefined loading protocol. It also has larger total energy dissipated and cumulative roof plastic deformations among the three specimens.
2. Specimen TCBF-B-3 (wide flange braces) has the smallest peak base shear degradation among the three quasi-static test specimens under the same predefined loading protocol.
3. Two braces connecting to the same one-piece gusset plate tended to buckle in the same out-of-plane direction. Without the floor slab (diaphragm) acting as a restraint, the column that is closest to the single-piece gusset plate may be subject to torsion. Further investigation seems warranted on evaluating the demand of the bi-axial bending or torsion in the column induced by out-of-plane buckling of the braces, and how much this affects the behavior of column when severe buckling occurred in the braced frame.
4. Brace deformation tended to concentrate at the middle length of the brace where the local buckling of section wall occurred, and the brace out-of-plane deformation could be as large as ten times the axial deformation under compression. This indicates that significant damage of nonstructural components near the deformed braced frame could occur.
5. Significant fractures initiated near the complete joint penetration welds at the column bases occurred. Brittle failure mode in the column flange near column base stiffeners also observed during the tests, suggesting need for further research on the cyclic behavior of column bases using standard connection details and common weld procedures.
6. Reinforcing details at the brace-to-gusset plate connections for each specimen performed well during both quasi-static tests and hybrid simulation. Adding reinforcing plates at the net section region to develop sufficient effective net section area was successful.
7. The brace and one-piece gusset plate configuration of the braced frame specimen tended to amplify the rotational demand at both ends of lower beam-to-gusset splices, which is similar to the rotational amplification (due to geometry) in the link beam of an eccentrically brace frame (EBF) system. For specimens TCBF-B-3 and TCBF-B-4, pinned beam-to-gusset details were used to avoid local damage such as flange or web buckling and fracture at these regions. From the observations during these two tests, the pinned connection details effectively avoided any undesired failure mode at beam-to-gusset plate connection regions. However, the entire braced frame lateral capacity was reduced as a result of the moment release at lower beam end connections.
8. During the hybrid simulation, brace fracturing occurred closest to the end of design-level ground motion. And the fractured brace was located in the second story not in the ground story, as was expected. Since only one ground motion record was used during the simulation, the braced frame responses may change as input ground motion changes. This result does not represent the general responses of steel braced frames. Further investigation on the effect of ground motions upon the seismic responses of braced frame systems is suggested before more solid conclusions can be made.
9. Story deformation concentration was observed in the second-story, especially after the second-story brace began localized buckling locally during the hybrid simulation. This deformation concentration was easily identified, especially when entire hybrid test specimen moved toward the negative direction (to the west side of the laboratory).

10. Lateral force distribution during the hybrid simulation demonstrated that the distribution varied with time, but most of the time the shape was close to an inverted triangle. This observation supports the force distribution assumption used in quasi-static tests.
11. From the synchronization subspace plots, it is clear that the errors between command displacement and measured displacement were very small during the hybrid simulation. The servo-control system could reach the target displacement accurately mainly because of the testing was running at a very slow rate.

## 6 Analytical Modelling using OpenSees and LS-DYNA

This chapter focuses on the numerical simulation of the behavior of the four test specimens described in Chapters 3, 4 and 5. Two computer programs were utilized to assess the ability of modern computer software to simulate the observed experimental responses. In the research-oriented program, OpenSees (McKenna, 1997) simplified fiber-based line elements were used, while in the commercial software program LS-DYNA (Hallquist, 1990; LSTC, 2007) more refined finite discretization based on shell elements. Both programs incorporated features to model yielding, lateral buckling and the deterioration and rupture of members due to low cycle fatigue. Other modeling capabilities differed, as described subsequently.

Modeling efforts initially began by comparing the predicted and measured behavior of with individual struts. This was done to insure that the element, material and fatigue models used could simulate actual strut behavior with reasonable accuracy. Next, braced frame models were formulated to model the test specimens, incorporating on the modeling parameters calibrated from the strut studies. Specimen global responses recorded during the quasi-static tests and hybrid simulations were then compared with responses simulated using OpenSees and LS-DYNA. The following sections describe the responses obtained with the analytical models and compare these to experimental results. Results are presented initially for OpenSees, followed by results obtained using LS-DYNA. Simulated responses are typically plotted over the measured responses for discussion convenience.

### 6.1 CALIBRATION USING DATA DERIVED FROM PREVIOUS STRUT TESTS

In order to identify optimal material modeling parameters in OpenSees, calibration was done using existing test data. Simple strut tests had been previously conducted in UC Berkeley's Structural Laboratory located in Davis Hall (Yang and Mahin, 2005). A test set up photo and a specimen shop drawing are shown in Fig. 6.1. A total of five square HSS struts and one round HSS strut were subjected to different loading protocols (see Fig. 6.2). The test data collected from Specimens #4 and #5 were used herein for calibration, since the specimen connection details are most similar to those used for Specimen TCBF-B-1 (with reinforcing plates located on both sides of net section of the brace-to-gusset-plate connections). These two struts were subjected to a near-fault (tension dominated) loading protocol and a symmetrically applied cyclic loading protocol having incrementally increasing displacement amplitudes from cycle to cycle. By using the same material modeling parameters in the OpenSees, comparison of results for these two different protocols can show how sensitive response is to loading protocol.

A total of four line elements were used to model each strut. The number of integration points along each element was set to five. At each integration point, the section was represented by a series of fibers. Four fiber layers across and along the walls of the square HSS struts was used, as shown in Fig. 6.3. For subsequent analyses a similar discretization was used for wide flange strut models, and four fiber layers were used across the round HSS section, but 16 fibers were used around the perimeter. To help initiate lateral buckling, a small initial offset of the midpoint of the brace was assumed, equal to the 1/1000 of the total length of the strut. Each fiber

was represented by a Giuffr -Menegotto-Pinto material model (Steel02 in OpenSees) having the following properties,  $F_y$  (yield strength of steel),  $E = 29000$  ksi (Young's Modulus of steel),  $b = 0.003$  (strain-hardening ratio) and  $R_o = 25$ . The yield strength of steel is based on the mill certificate report provided by the steel fabricator. The factors  $b$  and  $R_o$  are obtained based on trial and error.

The low cycle fatigue wrapper developed by Uriz and Mahin (2008) was also used to simulate rupture of the critical sections. The algorithm uses a modified rain flow cycle counting method to determine the number and amplitude of individual inelastic deformations occurring in each fiber during an analysis. A Coffin-Manson low cycle damage model is used to compute the damage inflicted by each cycle and Miner's rule is used to accumulate the damaging effects of each cycle. The properties of the fiber can be degraded with increasing damage. In this study, individual fibers are removed from the model when the damage model indicates that the low cycle fatigue limit has been reached. Equation 6.1 represents the Coffin-Manson relationship where  $\varepsilon_i$  is the strain amplitude,  $N_f$  is the number of cycles to failure,  $\varepsilon_o$  and  $m$  are material parameters determined from experiments. The low cycle fatigue parameters determined previously (Uriz and Mahin, 2008) for these and other specimens were  $m = -0.458$  (default value) and  $\varepsilon_o = 0.099$ . These were found to be adequate for this study.

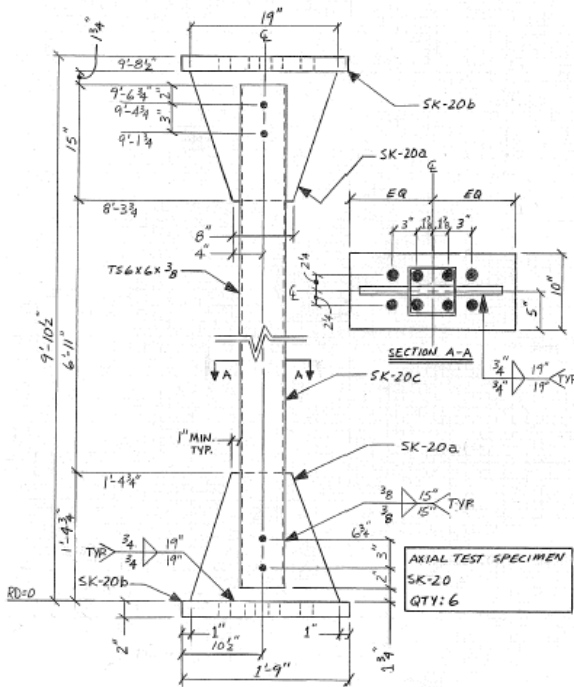
$$\varepsilon_i = \varepsilon_o (N_f)^m \quad (6.1)$$

From the plots of axial force versus axial displacement and axial force versus out-of-plane displacement shown in Figs. 6.4 to 6.7, it is clear that OpenSees results overall match the actual test results with an acceptable degree of accuracy. Suspicious readings from the experiments are pointed out in the plots. Since the fiber-section models in OpenSees assume a constant cross-sectional geometry and that plane sections before deformations remain plane afterwards, they cannot simulate the local buckling observed for the walls of the HSS section near the midpoint (Uriz, 2005). For example, in Figs. 6.4 and 6.6, the OpenSees results tend to over predict the post buckling strength of the struts in compression. Moreover, the Uriz-Mahin damage model is based solely on low cycle considerations, and the effects of fracture mechanics once the section begins to rupture are not considered. As such, the numerical results predict total fracture of the brace with reasonable precision, but the nature of the deterioration prior to complete rupture differs for the two specimens. As noted by Uriz (2005), cyclic test results may differ from analytical results and the behavior of the same specimen tested under the different loading protocols may differ as well.

**Table 6.1 Input parameter details in OpenSees 2D model**

Specimen	Section Name	$F_y$ (ksi)	Young's Modulus $E$ (ksi)	$m$	$\epsilon_0$	Number of Element and Fiber Layers		$\delta_{ecc}$ (inch)
#4	HSS 6 × 6 × 3/8 (near-fault loading protocol)	60.6	29,000	-0.458	0.099	4	4	0.113
#5	HSS 6 × 6 × 3/8 (symmetric-cyclic loading protocol)	60.6	29,000	-0.458	0.099	4	4	0.113

(Note:  $\delta_{ecc} = L/1000$ , is the assumed initial crookedness at the middle length of the strut model)



**(a) Shop drawing**



**(b) Test setup and specimen overview**

**Figure 6.1 Simple strut tests at University of California, Berkeley (Yang and Mahin, 2005)**



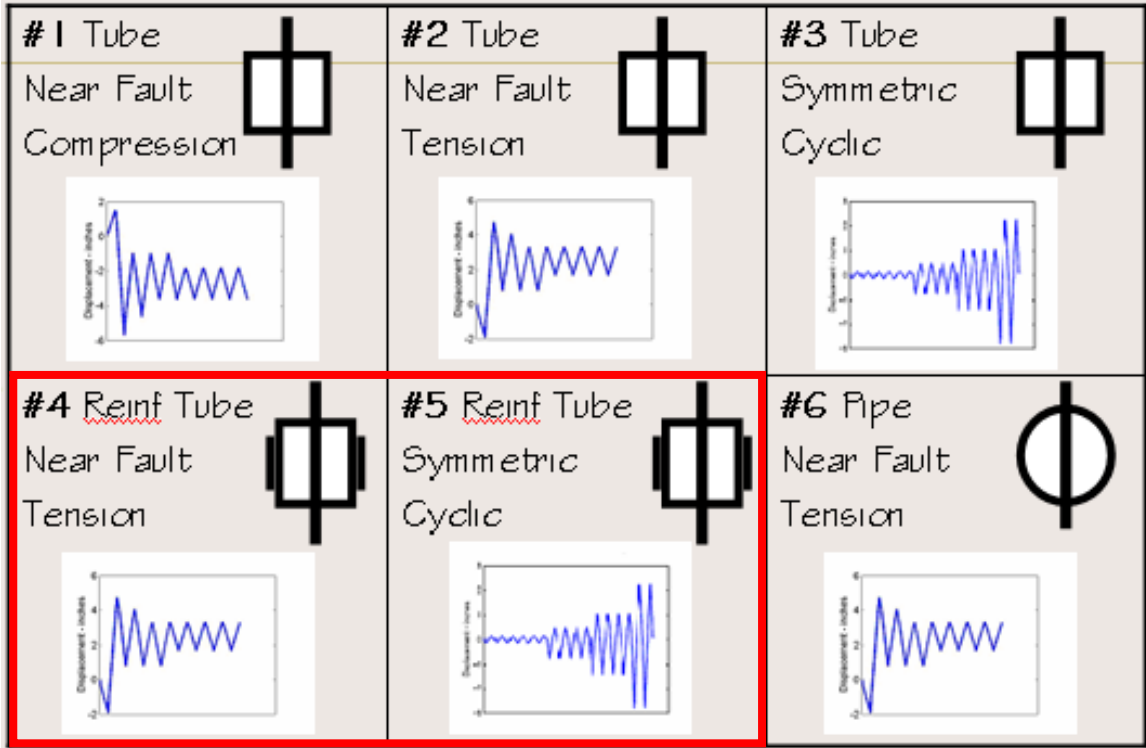


Figure 6.2 Loading protocols of simple strut tests (Yang and Mahin, 2005)

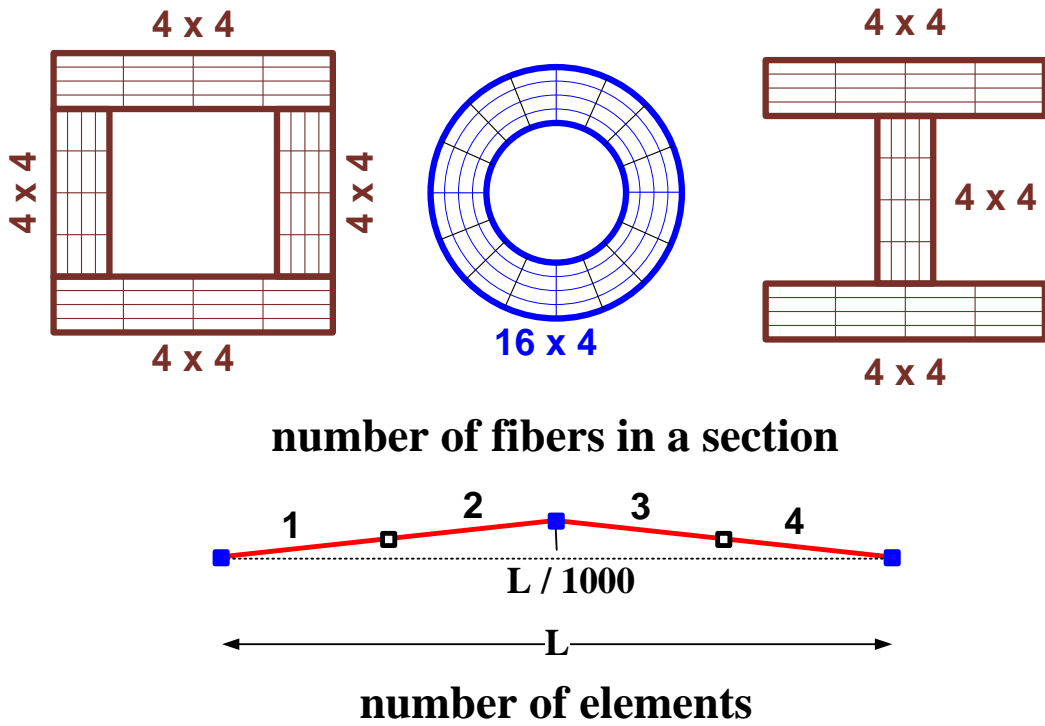


Figure 6.3 Demonstration of the fiber sections and element numbers used in OpenSees strut models

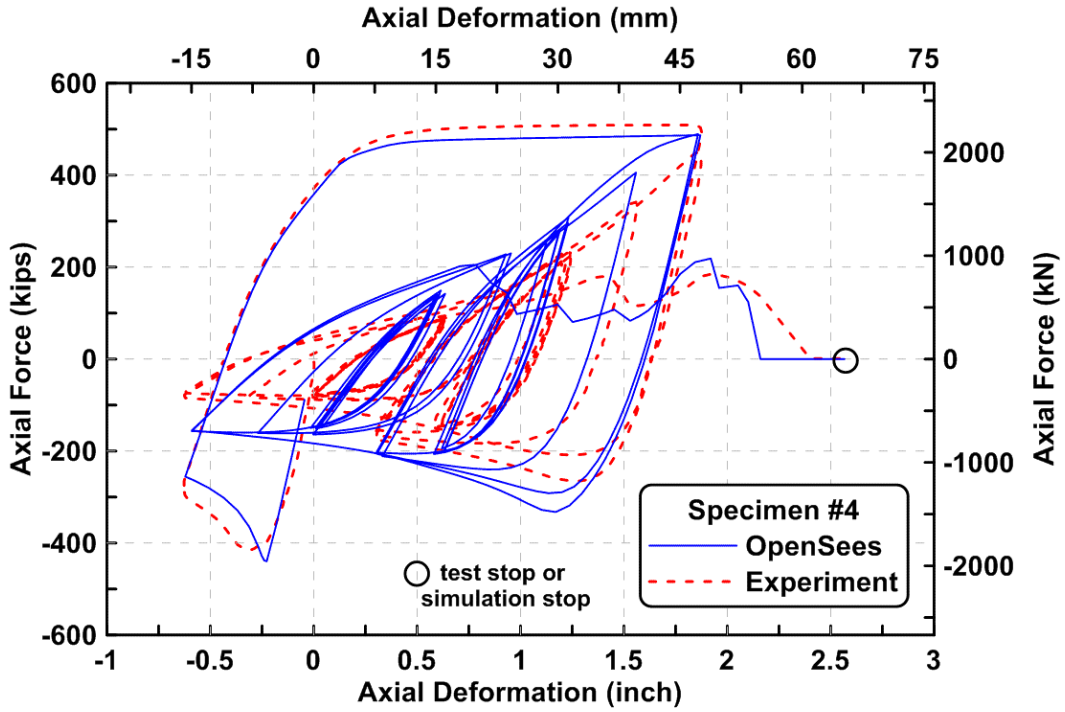


Figure 6.4 Axial force versus axial deformation relationship of specimen #4 from experiment and OpenSees simulation

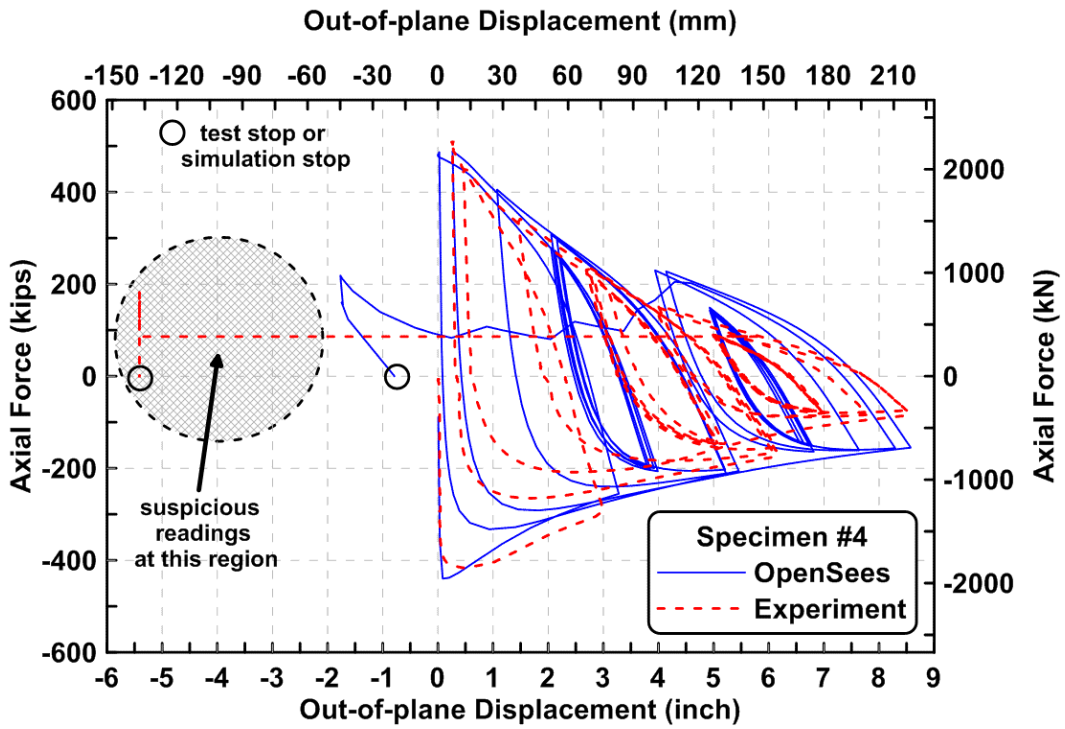


Figure 6.5 Axial force versus out-of-plane displacement relationship of specimen #4 from experiment and OpenSees simulation

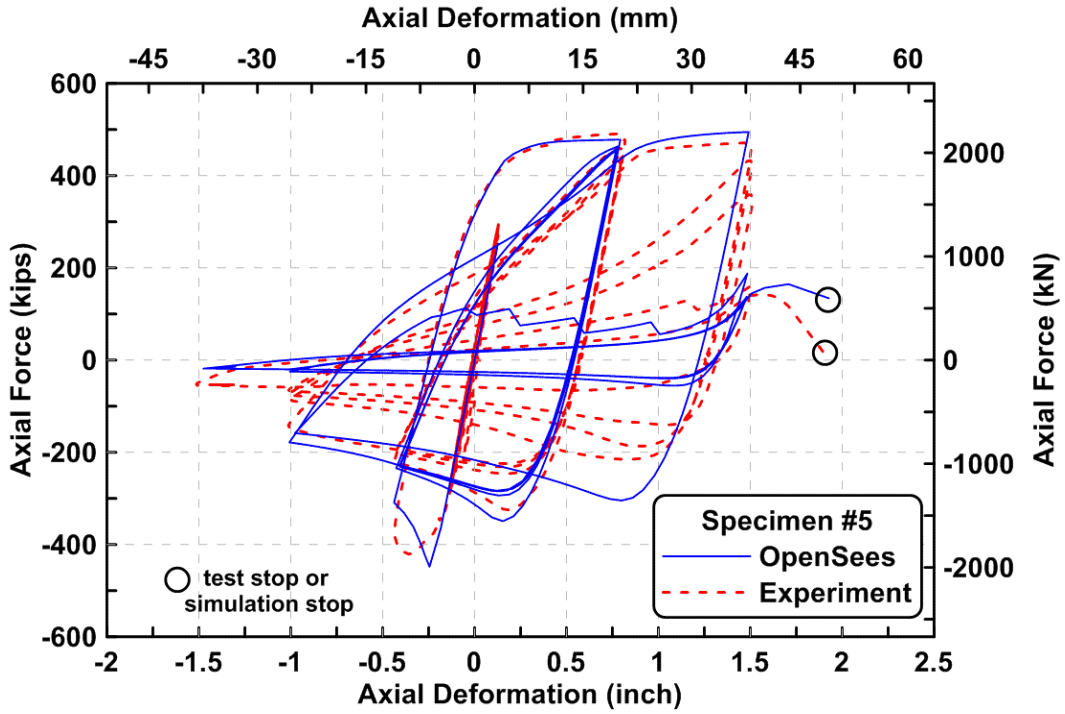


Figure 6.6 Axial force versus axial deformation relationship of specimen #5 from experiment and OpenSees simulation

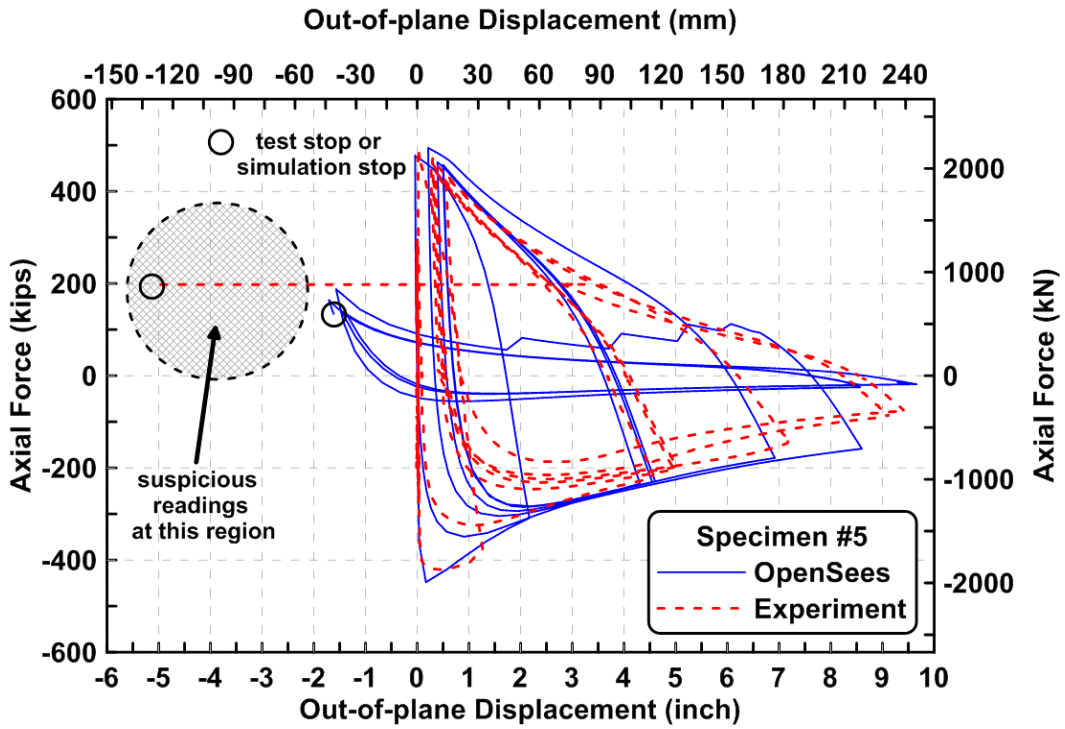


Figure 6.7 Axial force versus out-of-plane displacement relationship of specimen #5 from experiment and OpenSees simulation

## 6.2 PREDICTION OF QUASI-STATIC TEST RESULTS

Two-dimensional models were developed in OpenSees to represent Specimens TCBF-B-1, TCBF-B-2, and TCBF-B-3. Figure 6.8 shows an overview of the nodal distributions, displacement (or load) control nodes, and rigid end zones used for the OpenSees braced frame models. To simplify the model, the braces were assumed to be pin ended at the location of the  $2t_g$  fold line in the gusset plate, and buckling in the analytical model was induced in-plane rather than out-of-plane as observed in the test specimens. This was found to be a reasonable assumption in earlier tests by Uriz (Uriz and Mahin, 2008). As with the previously described models of individual struts, a small initial offset was introduced at the center of each brace to initiate lateral buckling. The beam-to-column connections and the gusset plates were assumed to be perfectly rigid. While some deformations are associated with these regions, the effect is believed to be small once brace buckling commences. Material models were similar to those described in the previous tests. Material strengths were based on mill test reports, along with the modulus of elasticity. The low cycle fatigue damage parameters for fibers were initially set to be the same as used as previously based on past square HSS brace tests.

Cyclic analyses were performed using the same loading protocol as used for the actual specimens. That is, the same lateral displacements were imposed on the top level of the specimen, and a force equal to half of the force needed to impose the specified displacement on the roof was applied to the lower floor level. This was done for the first three specimens that were tested quasi-statically.

From the base shear versus roof displacement relationships shown in Fig. 6.9 for Specimen TCBF-B-1, the initial behavior of the specimen is well predicted. The stiffness and ultimate strength are reasonably predicted. However, it is clear that the simulated base shear from the OpenSees fiber model degrades earlier than in the actual tests results. Additional investigation of the simulation results revealed that the braces in the model fracture earlier than in the test, which causes degradation of the base shear capacity to occur sooner. As shown in Fig. 6.10, modification of the fatigue material input parameter  $\epsilon_0$  from 0.099 to 0.148 and leaving the  $m$  value unchanged resulted in a better match. It is clear that modeling of the complete behavior of the braced frame requires accurate modeling of the deterioration and rupture of the individual braces.

A comparison between the individual brace responses for the trial two fatigue model with the actual test data (Fig. 6.11) shows that the hysteretic brace axial force-axial deformation characteristics are predicted well overall by the numerical model. However, there are substantial discrepancies between the maximum measured and simulated displacements in individual braces, and the behavior as fracture is approached and the sequence of individual brace fractures is not well predicted. For instance, the brace axial deformations derived from the tests in the first story were larger than those from the OpenSees simulations, while the situation in the second story was reversed. The derived brace axial deformations were calculated from story deformations by geometry. As noted previously, for the test of TCBF-B-1, the first-story deformation was calculated from the position transducers that were found not to be ideally positioned. This error in experimental results might explain some of the deviation of peak experimental and numerical axial deformations.

OpenSees results for Specimen TCBF-B-2 are shown in Figs. 6.12 and 6.13. To achieve a reasonable match, the low cycle fatigue parameter  $\epsilon_0$  used for the circular HSS section was again modified, in this case to  $\epsilon_0 = 0.270$ . Although the resulting simulation matches the overall system

behavior well, the brace fracture sequences and the deterioration of base shear with cycling during larger displacement cycles were not the same as the test results. As can be seen in Fig. 6.13, simulated brace peak axial forces were less than the estimated brace peak axial forces obtained from the test. Again, the distribution of axial deformations in the braced during the final few cycles is not well simulated by the fiber based model.

In Specimen TCBF-B-3, the lower beam-to-gusset plate splices were bolted and designed to accommodate significant rotations at the connection. The connections in the numerical model were initially defined as fully pinned connections, but the simulation results did not match the experimental results well. As a result, zero length elements were used instead to simulate semi-rigid connection behavior. More specific information on the method used to model the semi-rigid nature of these connections is provided in Section 6.3. To accommodate the in-plane buckling required using the 2D model implemented in OpenSees, the wide flange braces used in this specimen were pin ended as with the other specimens and rotated 90° about their longitudinal axes to be able to represent weak axis buckling behavior.

Plots of the quasi-static cyclic base shear versus roof displacement results for Specimen TCBF-B-3 are plotted in Figs. 6.14. The simulation matches the overall system test behavior quite well until the final cycle. However, as seen in Fig. 6.15, the simulated response of individual brace differs significantly from those derived from the test results. In particular, the numerically predicted brace peak tensile axial forces are larger in the lower story than derived from the test results. The opposite is true for the upper story, where the numerically simulated peak brace axial forces are larger in compression and smaller in compression than estimated from test results. The numerically predicted brace fracture sequences were not the same as the test results. For this test, the optimum value of the low cycle fatigue parameter  $\epsilon_0$  was found by trial and error to be 0.220; this is between the values determined for the square and round HSS braces.

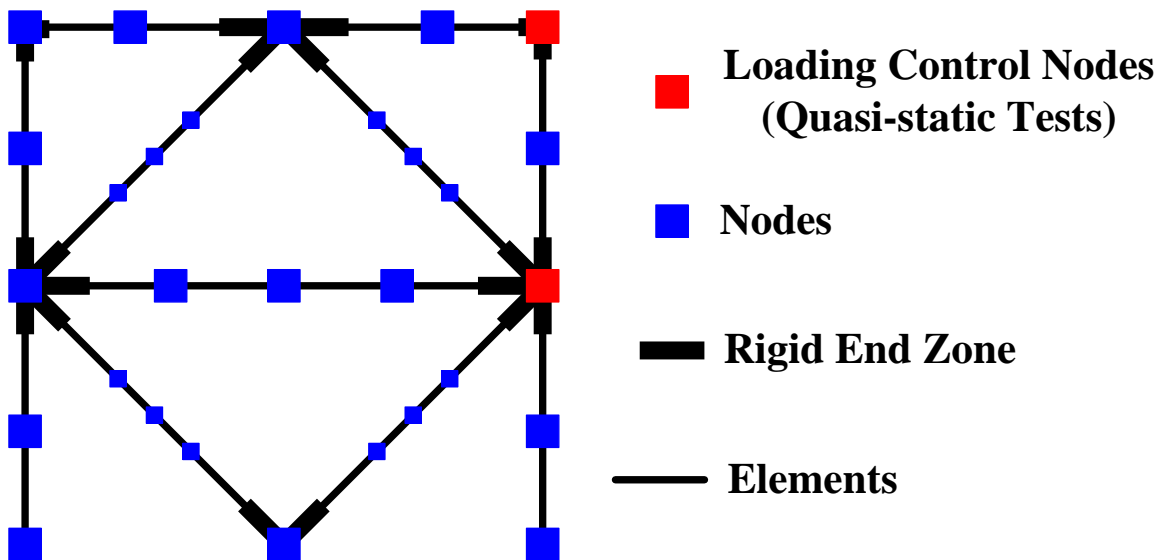


Figure 6.8 Demonstration of a braced frame model in OpenSees

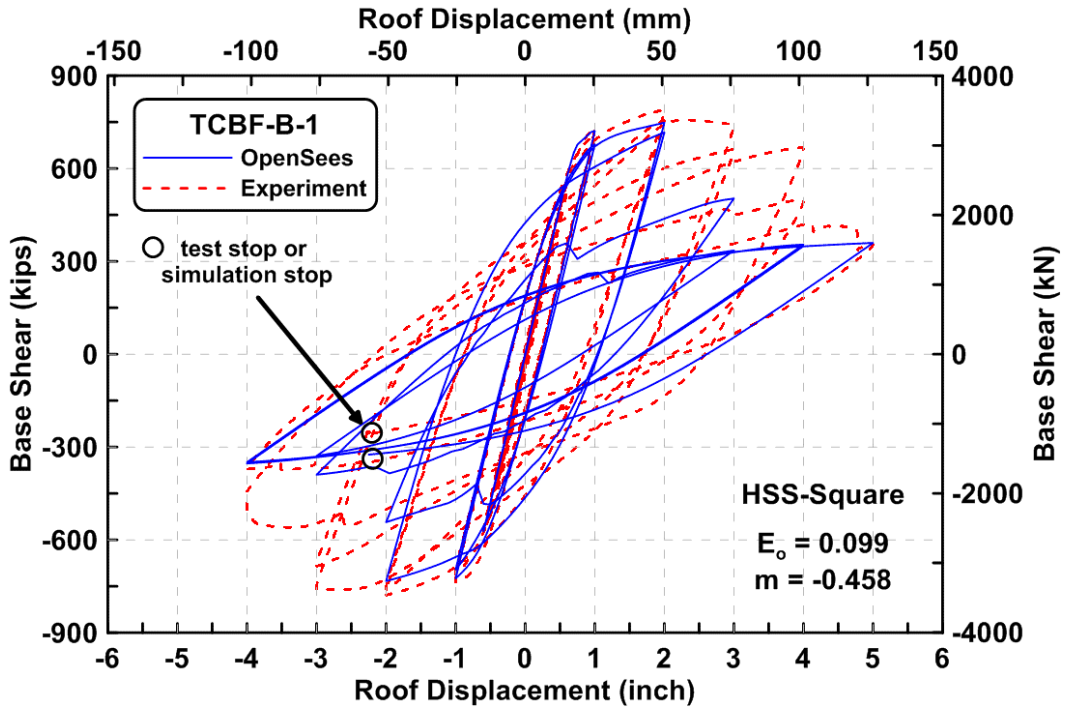


Figure 6.9 Base shear versus roof displacement relationship of TCBF-B-1 specimen from experiment and OpenSees simulation (trial one)

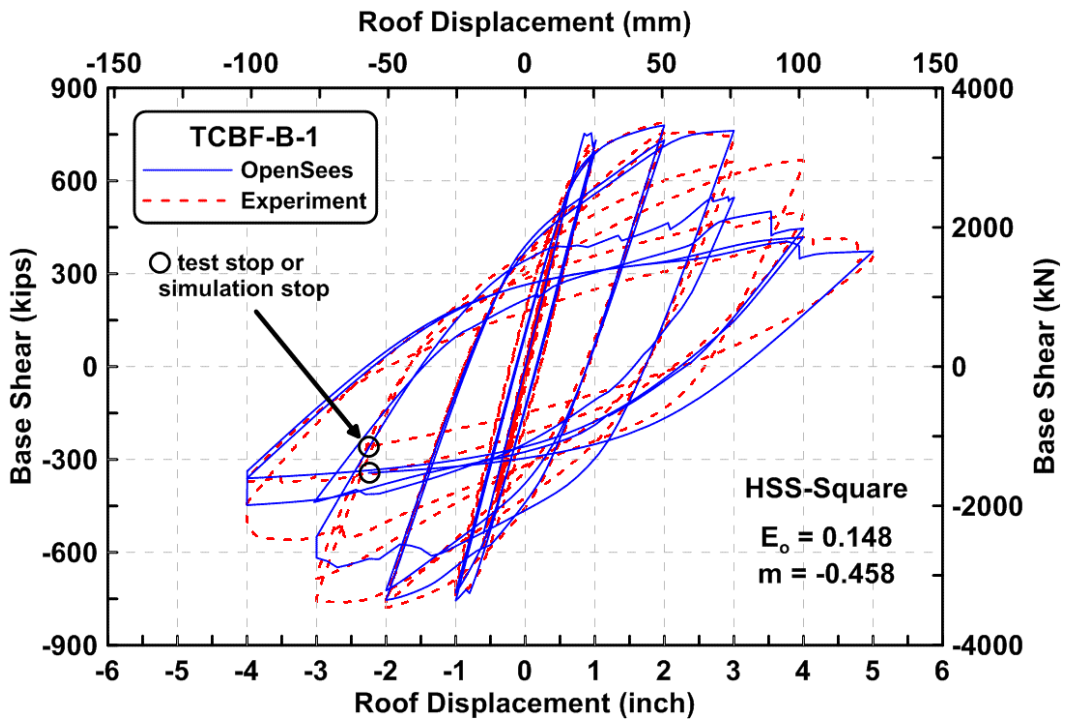


Figure 6.10 Base shear versus roof displacement relationship of TCBF-B-1 specimen from experiment and OpenSees simulation (trial two)

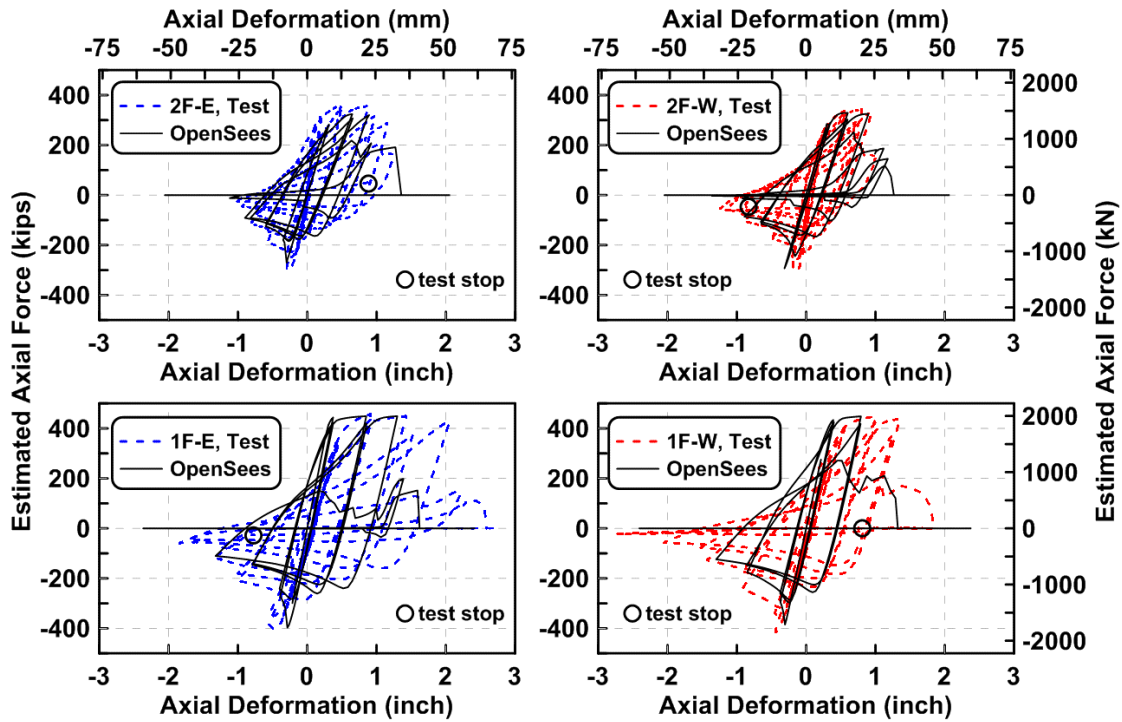


Figure 6.11 Brace Axial Force versus axial deformation relationships of TCBF-B-1 specimen from experiment and OpenSees simulation (trial two)

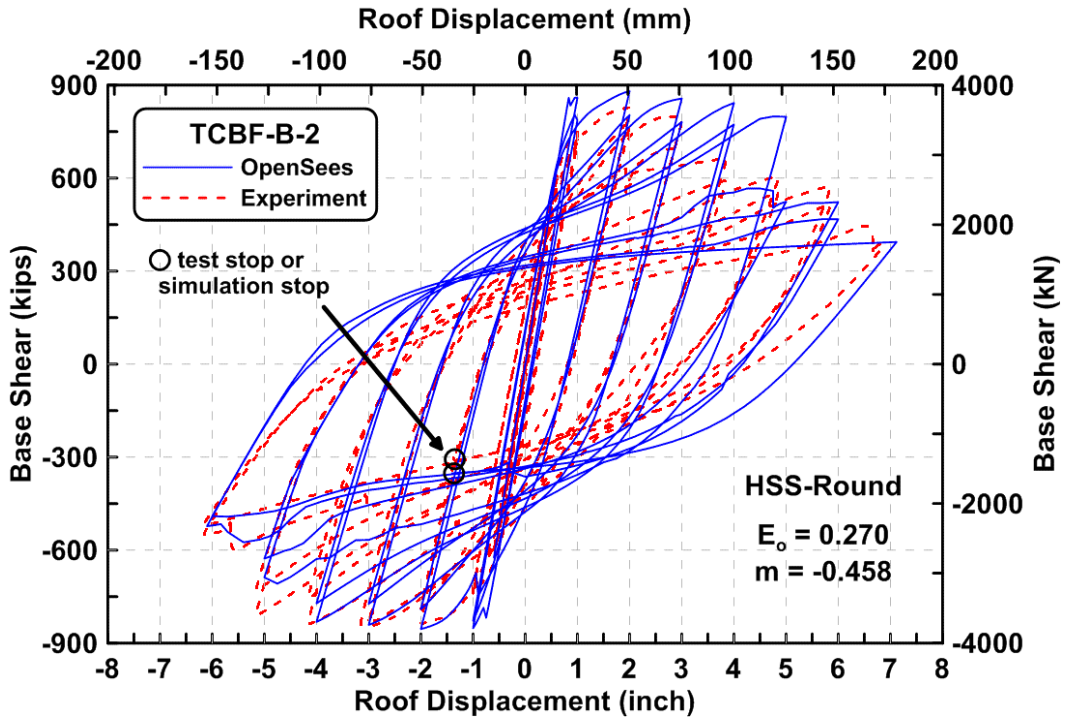


Figure 6.12 Base shear versus roof displacement relationship of TCBF-B-2 specimen from experiment and OpenSees simulation

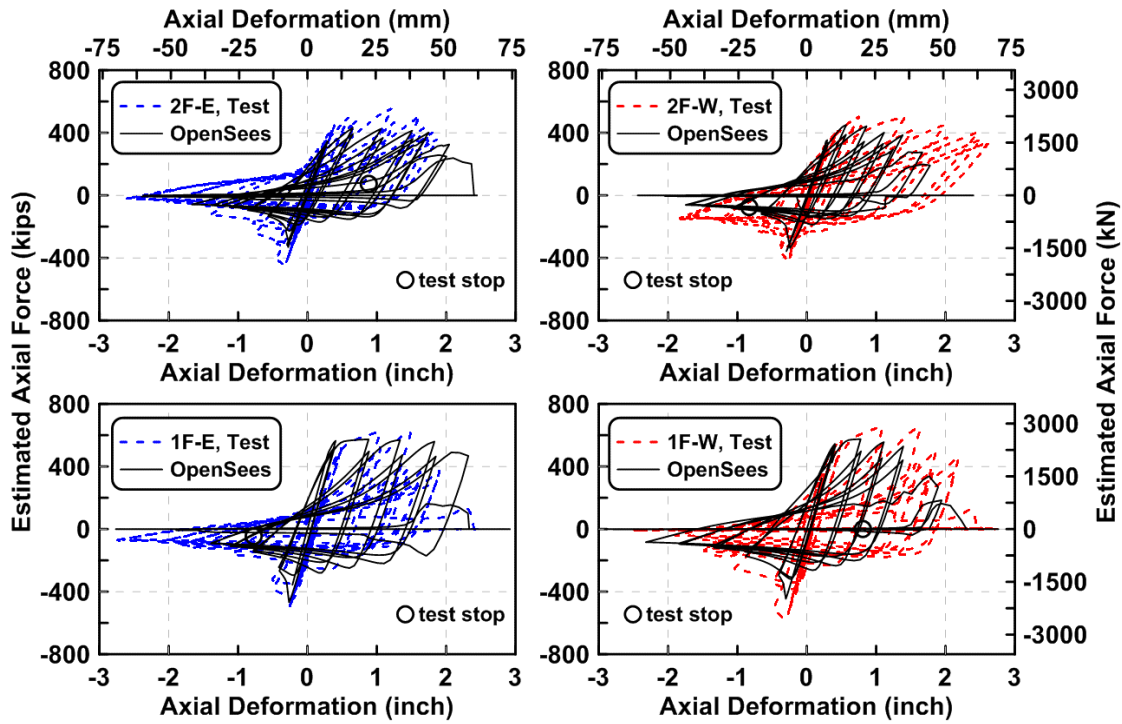


Figure 6.13 Brace Axial Force versus axial deformation relationships of TCBF-B-2 specimen from experiment and OpenSees simulation

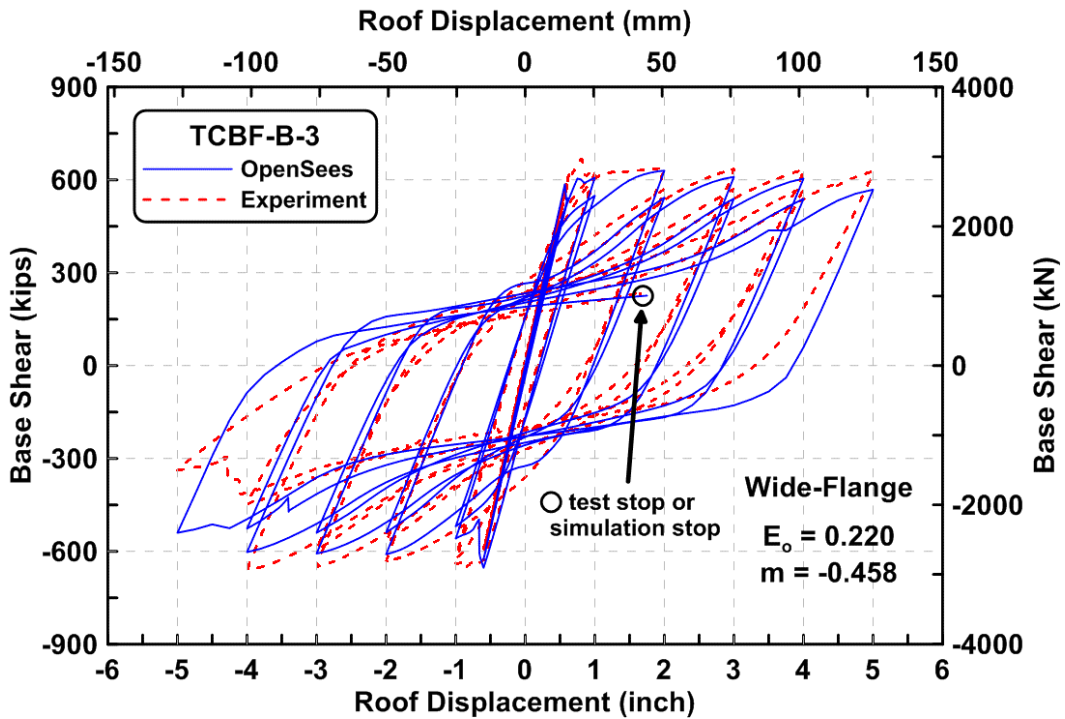


Figure 6.14 Base shear versus roof displacement relationship of TCBF-B-3 specimen from experiment and OpenSees simulation



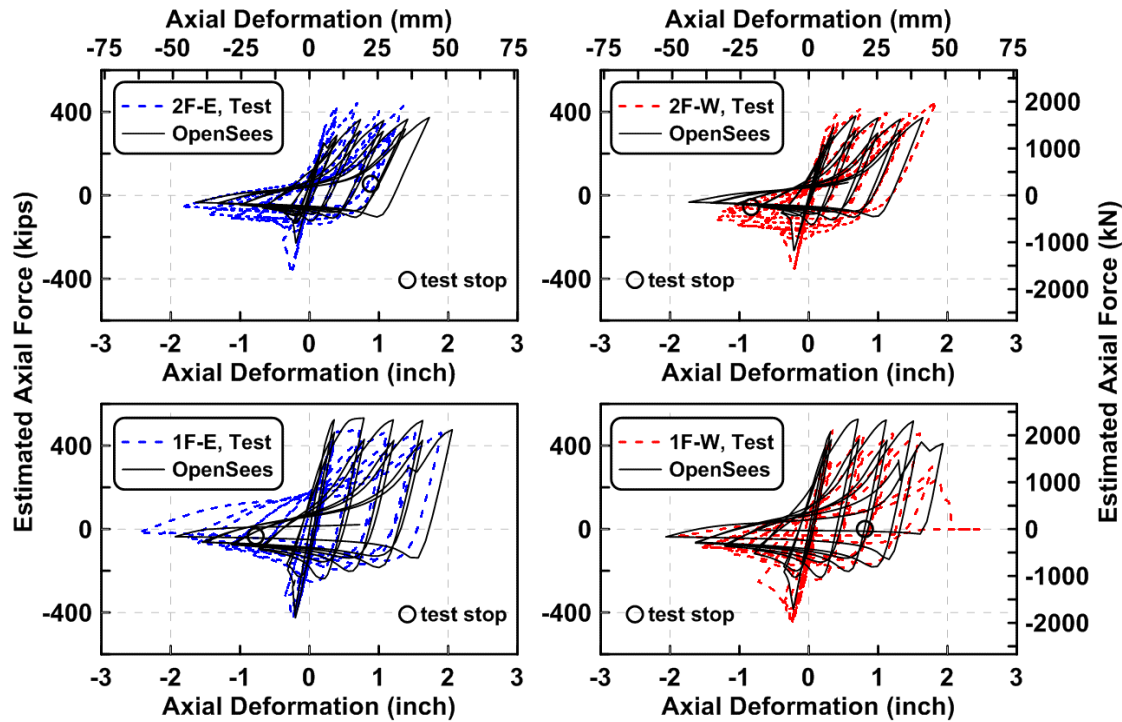


Figure 6.15 Brace Axial Force versus axial deformation relationships of TCBF-B-3 specimen from experiment and OpenSees simulation

### 6.3 PREDICTING THE HYBRID SIMULATION RESULTS

The OpenSees model developed to simulate Specimens TCBF-B-3 and TCBF-B-4 was initially calibrated using the hybrid test results of specimen TCBF-B-4. Specimen TCBF-B-4 utilized identically sized square HSS bracing members as used in Specimen TCBF-B-1. Thus, the basic model and modeling parameters for Specimen TCBF-B-4 were the same as used in Trial 2 for Specimen TCBF-B-1; in particular,  $\varepsilon_0 = 0.148$ ,  $m = -0.458$ . However, the lower beam-to-gusset plate connections were bolted (rather than being continuous) and initially modeled as being fully pinned connections. But the test results in the elastic range show significant discrepancies between measured and computed frame stiffnesses and, for the hybrid test of Specimen TCBF-B-4, in dynamic response. For example, as can be seen in Fig. 6.16, the fundamental period of the specimen from the hybrid simulation and from the OpenSees model do not match when a pin connection is assumed in the numerical model.

To simulate the semi-rigid behavior of the connections, zero-length elements were introduced into the model at these locations, having elastic-perfectly plastic behavior. An estimated moment capacity ( $M_y$ ) of the bolted connections was derived from the equation below (see Fig. 6.18 for a simplified physical interpretation).

$$M_y = P \times L = 1852.2 \text{ kip} - \text{in} \quad (6.2)$$

$$L = 9 \text{ inch}$$

$$P = n_s \cdot n_b \cdot \mu_s \cdot N_b = 2 \cdot 6 \cdot 0.35 \cdot 49 = 208.8 \text{ kip} \quad (6.3)$$

where  $P$  is the resultant friction resistant force of bolts,  $L$  is the moment arm between the resistant forces at the top and bottom side,  $n_s$  is the number of friction surface,  $n_b$  is the number of bolts used to calculate the friction force,  $\mu_s$  is the friction coefficient between steel plates, and  $N_b$  is the minimum code specified pretention force of the tension controlled bolt.

A calibrated rotation limit ( $\theta_y$ ) was used as the input parameters of the uniaxial material properties; the rotation limit is:

$$\theta_y = 0.003 \text{ radians} \quad (6.4)$$

This adjustment improved the fit between the numerical simulation results and the test results (see Fig. 6.17).

A three second long free vibration test was conducted before the main hybrid simulations to identify the fundamental period of the specimen and the inherent damping characteristics of the specimen and the test set up. To perform the hybrid free vibration test, displacements of 0.1 in. and 0.061 in. were imposed on the upper and lower floor levels, respectively, using the computer electro-hydraulic control system. These displacements are proportional to the computed first mode shape of the specimen. The hybrid test control software then simulated the free vibration response of the specimen as it was released from this initial condition (initial deformed shape). The numerical model used in the hybrid model included modest amounts of Rayleigh viscous damping (with mass proportional and constant initial stiffness) corresponding to 1.5% and 2.5% for mode one and mode two, respectively. For this free vibration simulation, the leaning column described in Chapter 3 was included. Figure 6.19 shows the floor level displacement time histories during the hybrid free vibration test. The average period for the first four complete cycles of the free vibration were 0.3799 sec and 0.3740 sec from upper and lower floor level displacement time histories. Using a log decrement approach, the viscous damping ratios were estimated to be 2.65% and 4.06%. Thus, it can be seen that the test specimen and test set up introduce some additional damping effects.

The fundamental period of the OpenSees model of Specimen TCBF-B-4 was 0.3925 sec when pinned lower beam end connections were included in the model. It is apparent that the model with pinned lower beam ends was too soft. However, when semi-rigid lower beam end conditions were included in the model the computed fundamental became 0.3798 sec, which is very close to that measured. Rayleigh damping parameters 2% and 3% for mode one and mode two, respectively, were used in both simulated models (pinned and semi-rigid lower beam end models). Note that in the OpenSees model used for hybrid simulation, the Rayleigh damping parameters 1% and 2% for mode one and mode two, respectively, were used to simply accommodate the damping effects from the test set up.

The displacement time histories of each floor level under the DE ground motion and MCE ground motion during the hybrid test and the OpenSees simulation are plotted in Fig. 6.20. The OpenSees roof displacement predictions were fairly accurate until the first brace fractures (second-story east side brace) at a ground motion time of around 7.49 sec. After that, the numerically predicted roof displacements deviated to the negative side and ended the DE with a 0.65 in. residual roof displacement. The hybrid test results showed a very small residual roof displacement (less than 0.08 in.) after the DE ground motion.

During the MCE level excitation, there are greater discrepancies between the numerically simulated and test results. Nonetheless, the same trend in having the structure go through large inelastic excursions can be seen. While the tests were stopped before the end of the record since the lateral displacements exceeded the stroke capacity of the actuators (about 5% roof drift), the OpenSees results indicate that the structure does not completely collapse due to the diminishing of the excitation. However, the frame has a permanent roof drift of about 16 inches (about 6.6% overall drift).

A comparison the base shear (only the base shear of braced frame, not including the leaning column shear forces) versus roof displacement relationships for the hybrid simulation and OpenSees simulation can be seen in Figs. 6.21(a), 6.21(b) and 6.21(c). During the DE ground motions, the OpenSees model underestimates the peak base shear, especially in the negative roof displacement direction. It can also be seen that the period of the structure has significantly deteriorated by the end of the test (as seen from the slope of the hysteretic loops at the end of the DE portion of the results). However, the OpenSees model is considerably stiffer than observed in the tests.

During the MCE portion of the response, the structure is only able to develop about half of the strength exhibited during the DE phase of the response. The prior damage during the earlier DE portion of the response may have adversely impacted the ability of the frame to withstand subsequent large events (or aftershocks). The OpenSees numerical model is able to develop much greater base shear forces than was seen in the test. The test was stopped due to the stroke capacity of the actuators being reached. The lateral resistance of the frame at the end of the OpenSees simulation was only about 15% of that predicted at first yield.

For the individual brace response, Fig. 6.22 shows a comparison of axial force versus axial deformation relationships for the hybrid test and the OpenSees simulation. Although overall brace behavior was captured by the OpenSees simulation model, the prediction of brace fracturing was not accurate.

As noted above, the DE level event may have adversely affected the ability of the frame to withstand the MCE level event. Thus, the OpenSees simulation was repeated, with the sequence of excitations reversed. Thus, the ground motion input sequence was altered from DE + 3-second silence + MCE to MCE + 3-second silence + DE. In this case, the DE event might represent a strong aftershock following a very rare MCE level seismic event. The predicted response of Specimen TCBF-B-4 for this case is shown in Fig. 6.23. The peak roof drift ratio for during the MCE portion of the response is about 7 inches (2.9% drift ratio), and the residual roof displacements are in the positive direction. These measure 2.60 in. at roof level and 1.35 in. at the lower level (instead of being in the negative direction as shown in Fig. 6.20). The permanent story drift ratio is about 1.1%, which would likely be difficult and costly to repair. The effect of the DE aftershock is to continue motion of the structure in the positive direction with the peak displacement being about 10 inches and a residual displacement being about 7.5 inches (3.1% drift ratio). This indicates a potential adverse problem with low-rise SCBF systems with strong aftershocks.

The base shear versus roof displacement relationships of simulated specimen TCBF-B-4 is plotted in Fig. 6.24. This shows that the MCE level event fractures all of the braces resulting in a much more flexible and weaker structure. The response during the DE aftershock is basically that of the moment frame provided by the semi-rigid lower beam connections and the upper beam. Figure 6.25 shows the axial force versus axial deformation relationships of the simulated specimen under different ground motion series.

From the above comparisons between the results obtained from the OpenSees simulation and those from actual test results, it is safe to say that OpenSees can be used to simulate the overall global behavior of the braced frame structures with reasonable accuracy. However, the localized brace and other member behavior predicted by OpenSees is less accurately predicted. The elements used to model buckling braces cannot simulate localized buckling and fracture of the braces to a high degree of confidence. This behavior is likely to occur during the response of low rise braced frames to DE level and especially MCE level excitations. This is one of intrinsic difficulties of the fiber models used herein in the OpenSees simulations. Using the finite element analysis program to simulate localized brace buckling behavior is one way to overcome this drawback.

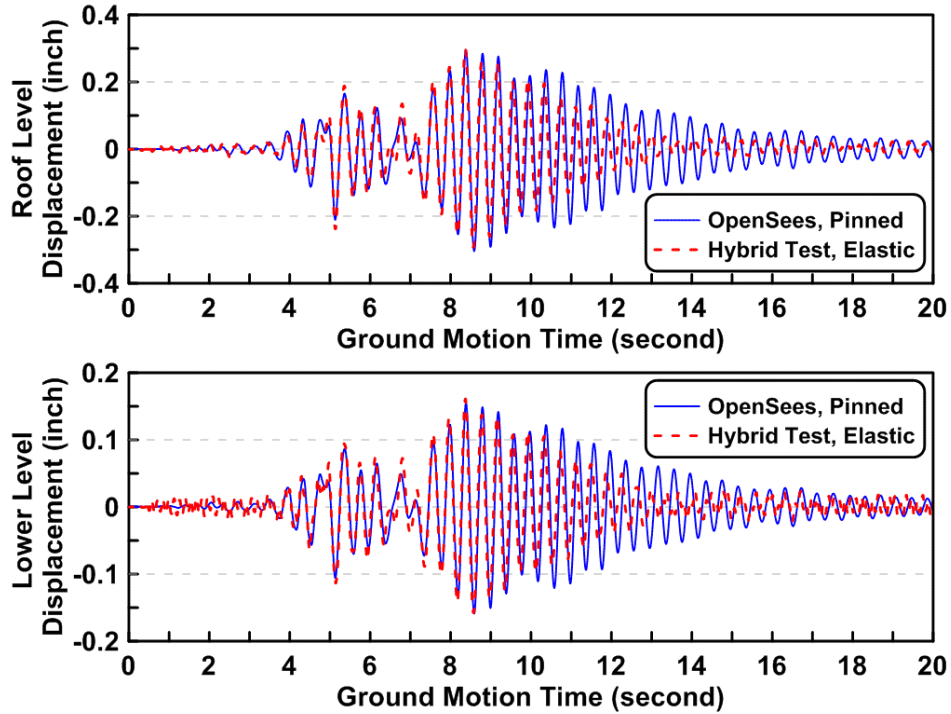


Figure 6.16 Displacement time histories of TCBF-B-4 specimen from elastic hybrid test and OpenSees simulation (pinned lower beam ends)

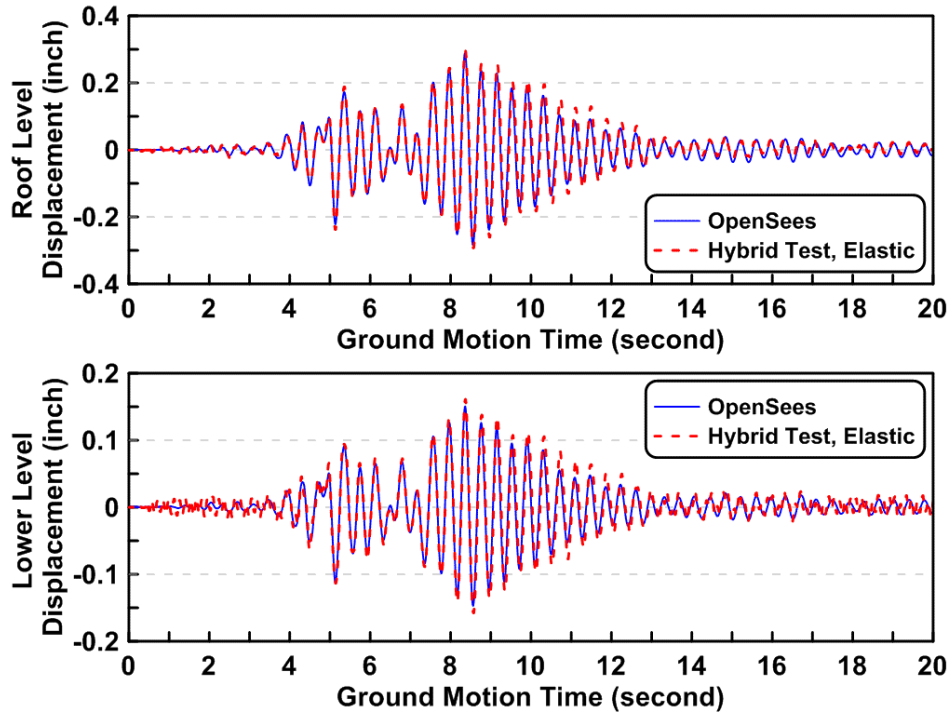


Figure 6.17 Displacement time histories of TCBF-B-4 specimen from elastic hybrid test and OpenSees simulation (semi-rigid lower beam ends)

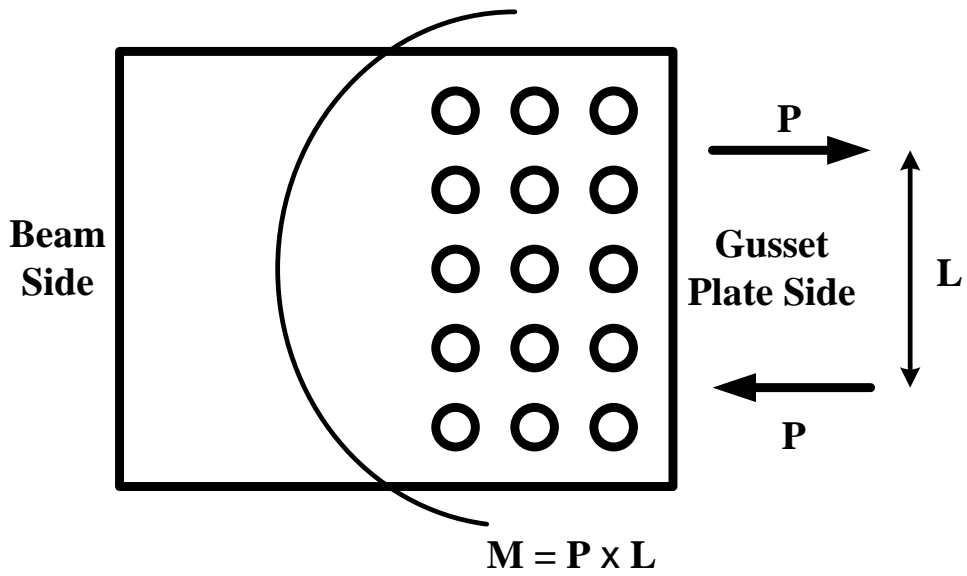


Figure 6.18 Demonstration of semi-rigid lower beam ends in TCBF-B-4 specimen

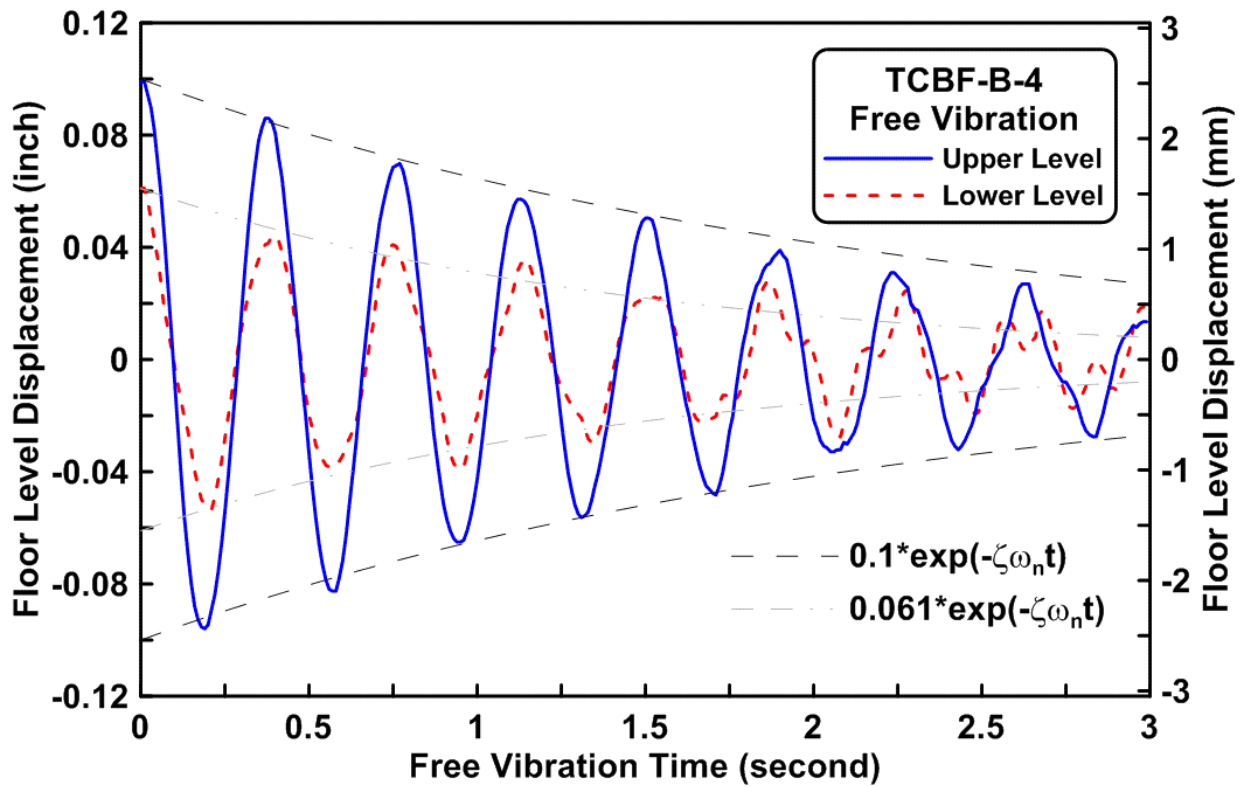


Figure 6.19 Free vibration test results of TCBF-B-4 specimen

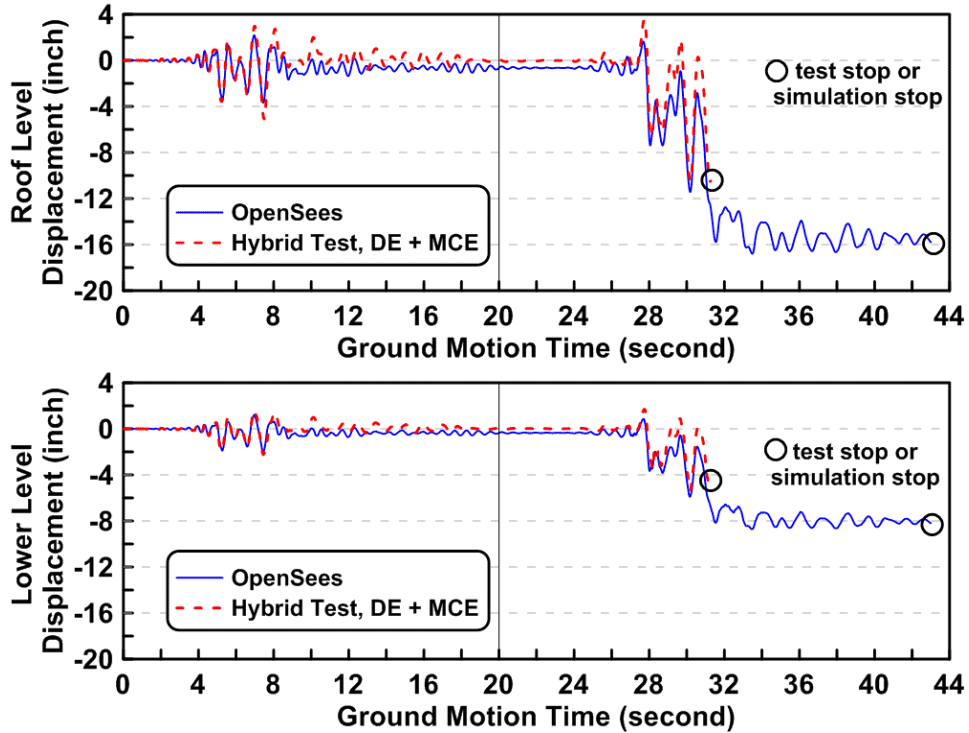


Figure 6.20 Displacement time histories of TCBF-B-4 specimen from DE and MCE hybrid test and OpenSees simulation (semi-rigid lower beam ends)

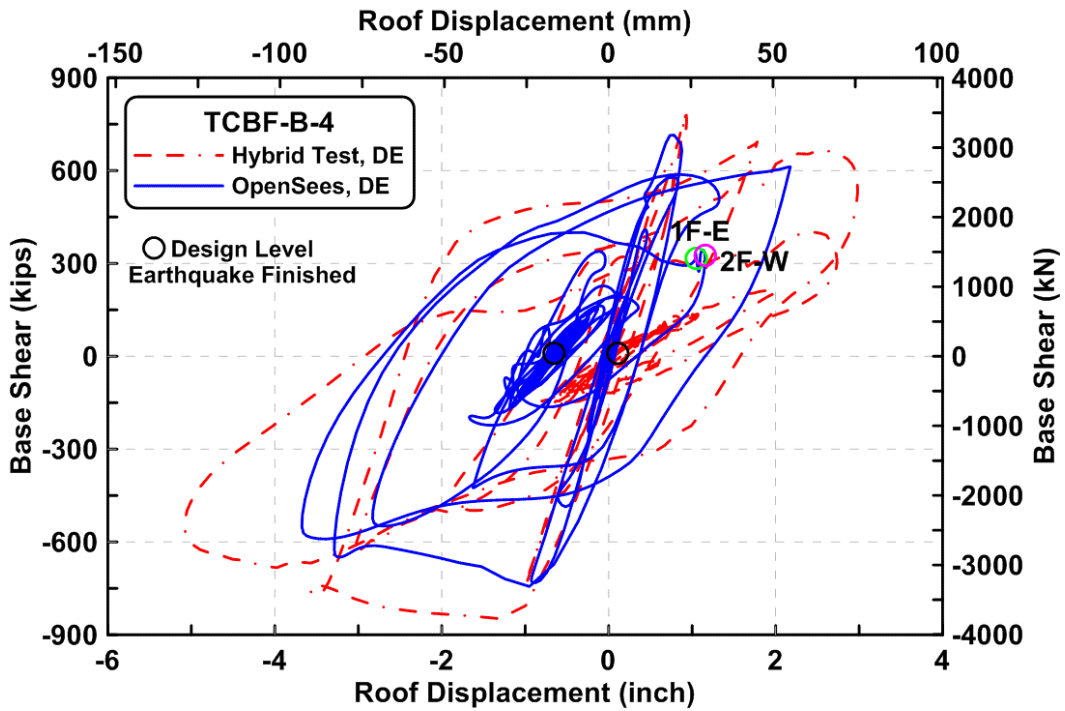


Figure 6.21(a) Base shear versus roof displacement relationships of TCBF-B-4 specimen from DE hybrid test and OpenSees simulation (semi-rigid lower beam ends)

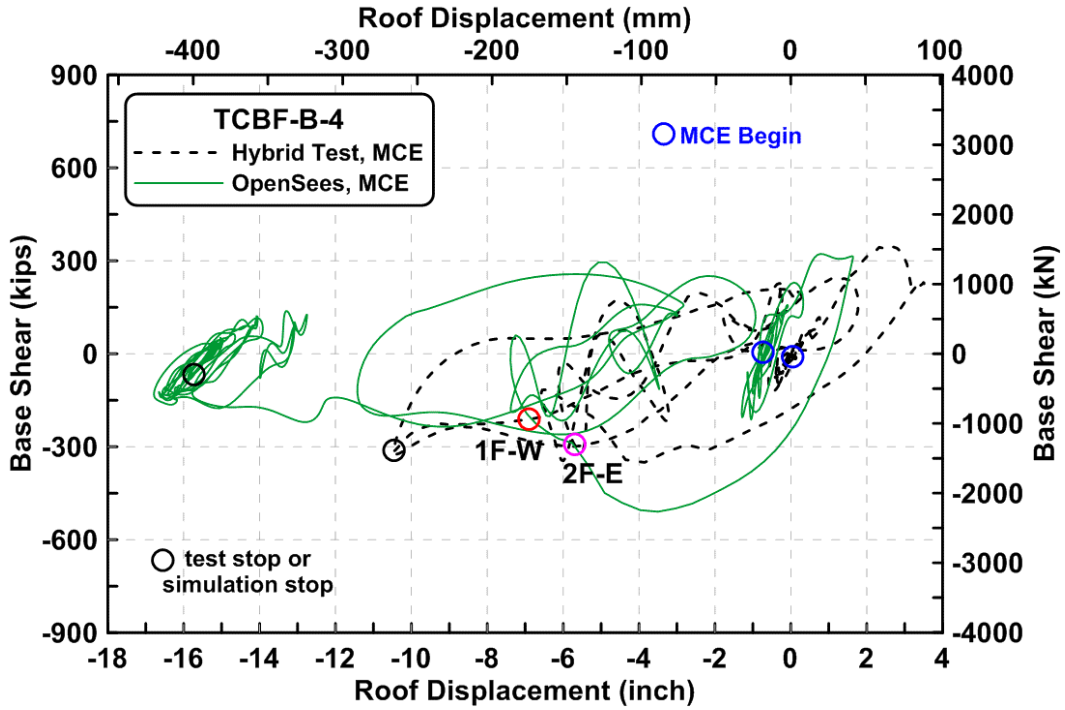


Figure 6.21(b) Base shear versus roof displacement relationships of TCBF-B-4 specimen from MCE hybrid test and OpenSees simulation (semi-rigid lower beam ends)

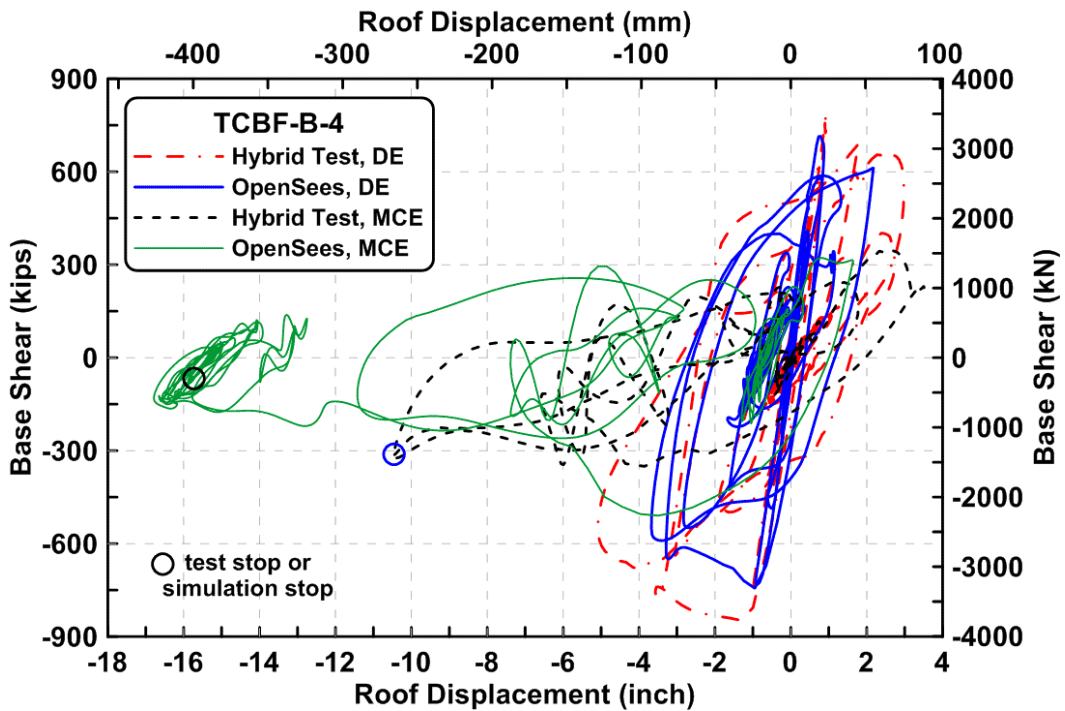


Figure 6.21(c) Base shear versus roof displacement relationships of TCBF-B-4 specimen from DE and MCE hybrid test and OpenSees simulation (semi-rigid lower beam ends)



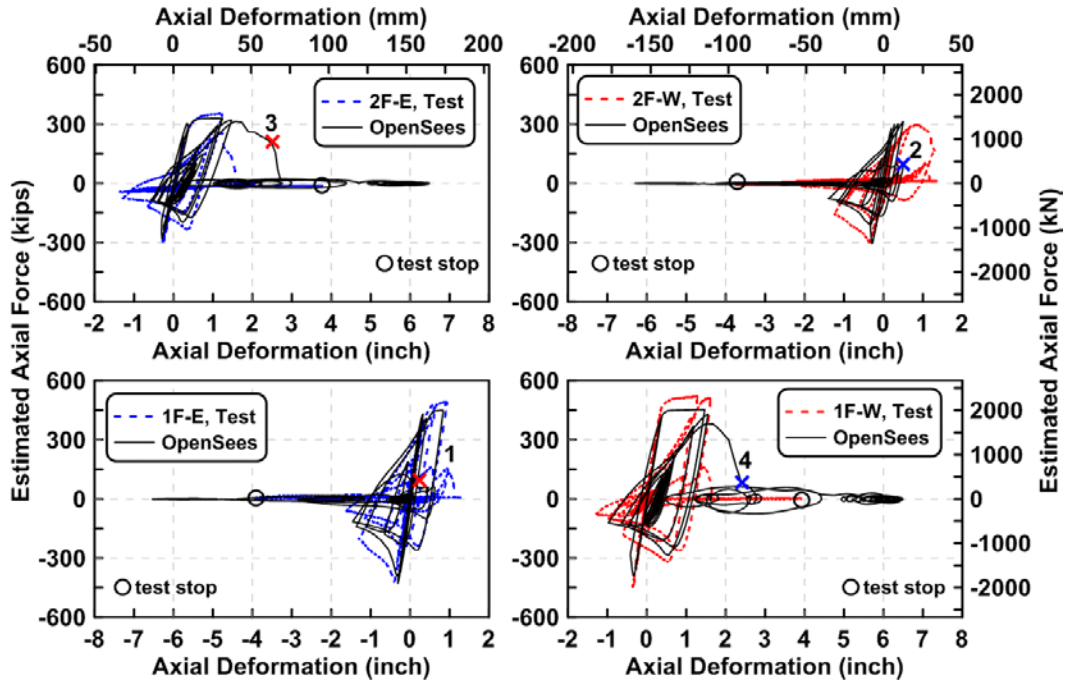


Figure 6.22 Brace axial force versus axial deformation relationships of TCBF-B-4 specimen from DE and MCE hybrid test and OpenSees simulation (semi-rigid lower beam ends)

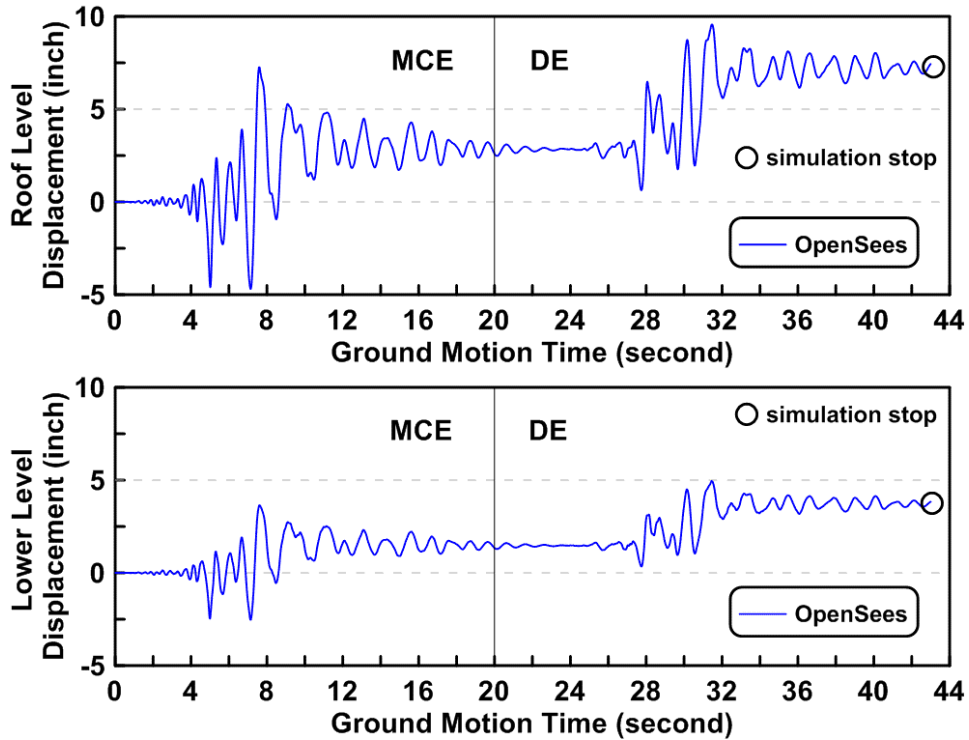


Figure 6.23 Displacement time histories of simulated TCBF-B-4 specimen subjected to MCE ground motion and then DE ground motion (semi-rigid lower beam ends)

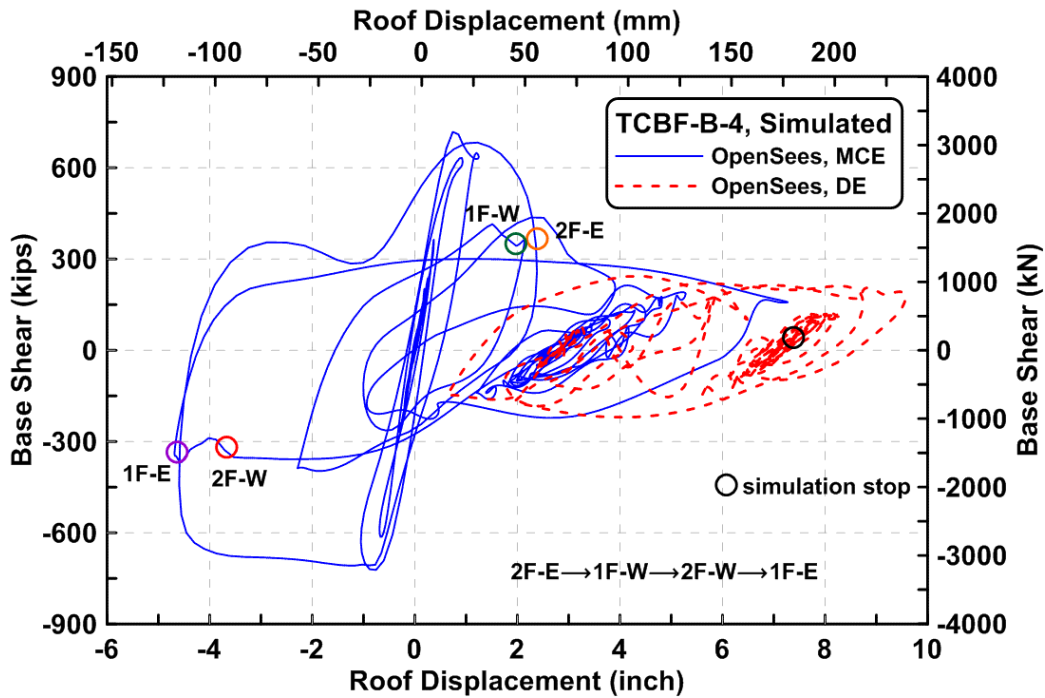


Figure 6.24 Base shear versus roof displacement relationships of simulated TCBF-B-4 specimen subjected to MCE ground motion and then DE ground motion (semi-rigid lower beam ends)

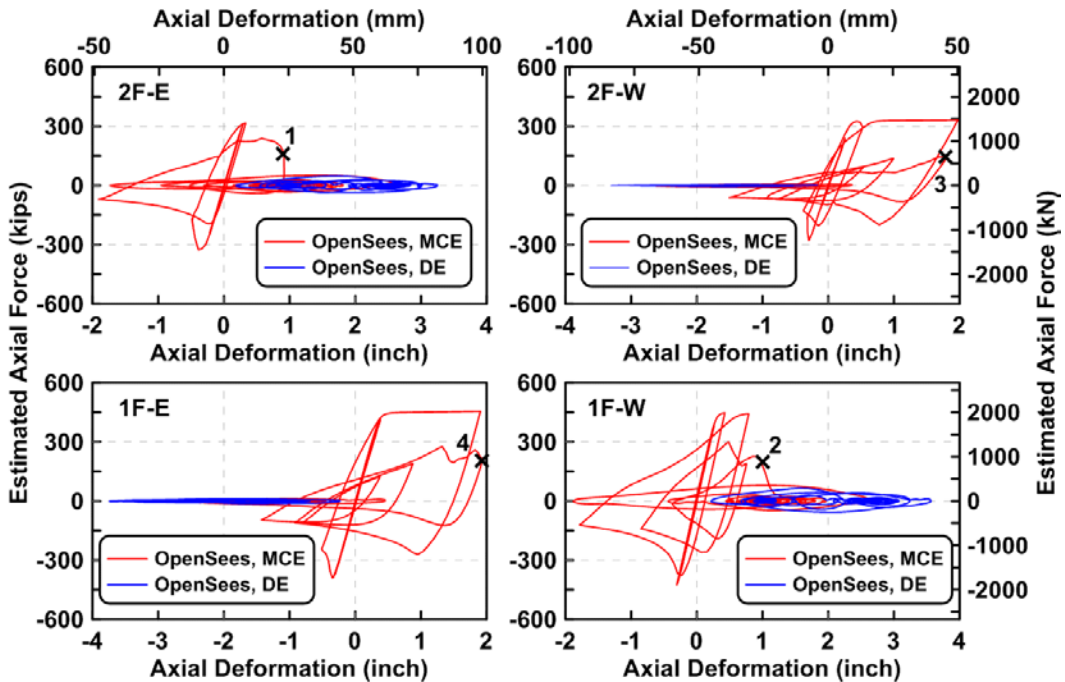


Figure 6.25 Brace axial force versus axial deformation relationships of simulated TCBF-B-4 specimen subjected to MCE ground motion and then DE ground motion (semi-rigid lower beam ends)

## 6.4 COMPARISON OF SQUARE HSS BRACE CYCLIC BEHAVIORS USING OPENSEES

Square hollow structural sections are the most popular section shape used in braced frame structures. They are structurally efficient, economical, and easy to handle at construction sites. Currently, about 88 available square HSS standard dimensions are listed in the AISC Manual of Steel Construction (AISC, 2001). The width of available sections range from 1-1/4 in. (HSS 1-1/4) to 16 in. (HSS 16); the width-to-wall thickness ratios ( $b/t$ ) range from 5.58 to 54.5. There are also larger hollow structural sections (from HSS 18 to HSS 24—also called jumbo square HSS) available by special request from HSS manufacturers. For HSS widths larger than 3 in. but smaller than 18 in., there are 61 available sections and only 40 of these are compact sections. The dimensions of these compact sections are listed in Table 6.2.

Because of the expense in conducting tests on full-scale specimens, a simplified investigation of the effect of  $b/t$  ratio and  $kL/r$  slenderness ratio on brace energy dissipation capacity under cyclic loadings was conducted using OpenSees. The 40 compact sections in Table 6.2 were modeled in OpenSees using fiber sections. The modeling used for these parametric studies is the similar to that described in Section 6.1. However, the yield strength was set equal to 46 ksi for all of the models. The number of elements along the brace length was increased from 4 to 20. The low cycle fatigue material parameters recommended by Uriz and Mahin ( $\epsilon_0 = 0.099$ ,  $m = -0.458$ ) were used for all if the brace models (Uriz and Mahin, 2008). This assumption may not be valid, due to the different degree that strain may localize in braces having different  $kL/r$  and  $b/t$  values. All of the other input parameters, except the cross section geometries and longitudinal dimensions were the same as previously used. As done previously, net reduced section failures or brace-to-gusset plate connection failures were not considered.

The brace models were subjected to symmetric incremental cyclic loadings. The cross sectional properties ( $b/t$  ratio and radius of gyration) of each section were fixed, and the length of the brace was varied to obtain  $kL/r$  ratios of 40, 60, 80, 100, 150, and 200). Note that  $kL/r = 200$  is the AISC maximum limit permitted for compression members. Loading protocols were based on the lateral displacement protocol established for the two story test frames. This is displacement drift protocol is defined in Table 5.1. To convert the protocol from story drifts to brace axial displacements it was assumed that the braces were installed in a 45° angle configuration, as illustrated in Fig. 6.26. The axial deformation protocols were determined using the equation shown in the left-hand corner of Fig. 6.26. As a result, there were a total of 240 cyclic analyses conducted, considering 40 different cross sections and six different  $kL/r$  ratios. In some cases, unrealistically short or long brace lengths may result by having small braces with small sections and  $kL/r$  ratios, or large sections and  $kL/r$  ratios. Because of the limitation of OpenSees in predicting local buckling and brace fracture, this investigation is not able to determine the exact fatigue life or energy dissipation capacity of the selected braces, but helps provide understanding the overall influence of  $b/t$  and  $kL/r$  on brace cyclic behavior.

Strut axial force versus axial deformation relationship, axial force versus out-of-plane deformation relationship, and cumulative energy dissipation were the main responses of interest. Outputs from the simulations were normalized for easy comparison. For example, axial forces were normalized by axial tension yield forces ( $P_y$ ), axial deformations were normalized by yield deformations ( $\delta_y$ ) under tensile loading, brace out-of-plane deformations were also normalized by  $\delta_y$ , and the cumulative energy dissipations were normalized by  $P_y \cdot \delta_y$ .

Response plots for two specific HSS braces with different  $kL/r$  ratios are shown in Figs. 6.27 and 6.28. Plots for all 240 cases are shown in Appendix J. Table 6.3 summarizes the normalized cumulative energy dissipation of selected square hollow structural sections for different  $kL/r$  ratios. Figure 6.29 to 6.34 summarize the normalized cumulative energy dissipation ratios for each  $kL/r$  ratio in bar chart format, and Fig. 6.35 combined those results in a single plot.

In general, the normalized cumulative energy dissipation ratio is a minimum for sections with  $kL/r$  ratios between 60 and 100. The energy dissipation capacity does not change that much for the square HSS with slenderness ratios equal to 60, 80, or 100. This range is typical for braces used in practice. When the  $kL/r$  ratio increases in the range from 80 to 200, the normalized cumulative energy dissipation increases (due to the increasing contribution of tension yielding). Similarly, the normalized cumulative energy dissipation ratio increase as the  $kL/r$  ratio decreases from 60 to 40 (stocky braces with limited deterioration of compression capacity during buckling). In most cases, the normalized cumulative energy dissipation was larger for very stocky braces than for very slender braces (Fig. 6.35 and Table 6.3).

For the braces used in special concentric braced frames, the AISC code specifies an upper bound limit on  $kL/r$ :

$$\frac{kL}{r} \leq 4 \sqrt{\frac{E}{F_y}} = 4 \sqrt{\frac{29000}{46}} = 100.4 \quad (6.5)$$

where  $E$  is the Young's modulus of steel, and  $F_y$  is the yield strength of the steel. As seen, for the conditions assumed in these analyses, the slenderness ratio limit is equal to 100.4.

Table 6.4 groups the  $b/t$  ratios into three ranges to help understand how  $b/t$  ratio effects the energy dissipation. Group 1 contains the square HSS sections that satisfy the seismic compactness requirements of the 2010 AISC Seismic Provisions for structural steel buildings. Group 2 contains the square HSS sections that satisfy the seismic compactness per the 2005 AISC Seismic Provisions, but that do not satisfy the 2010 AISC Seismic Provisions. Group 3 contains sections that are not seismically compact. From Fig. 6.36, it appears that  $b/t$  ratios have limited impact on normalized energy dissipation. In particular, the 14% reduction of the limit on  $b/t$  ratio imposed by the 2010 AISC Seismic Provisions has little effect in these fiber model analyses. There is some difference when  $b/t$  exceeds 16.1, but it is not too great. Limit actually does not improve the energy dissipation capacity of the braces significantly. However, these results related to the effect of  $b/t$  ratio should be viewed with skepticism. The fiber models do not account for the effect of section distortion (which reduces brace compression capacity) due to local buckling, and the tremendous effect of local buckling on the fatigue life of materials in critical regions of the brace. These results show some interesting dependencies with  $kL/r$ , but the inability to account for sensitivity of response to  $b/t$  raises some interesting questions about the veracity of fiber based models, and suggests the need for additional full-scale experiments and numerical analyses using more sophisticated finite element models that can account for local buckling of sections and the initiation and propagation of cracks due to low cycle fatigue.

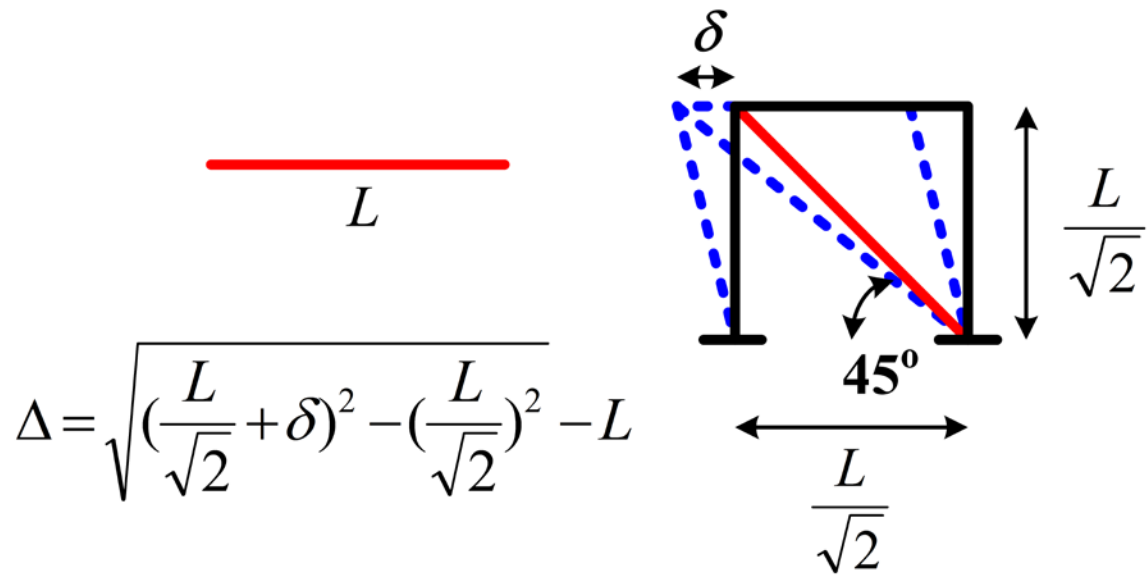


Figure 6.26 Assumed braced bay for the square HSS struts and the relationship between brace axial deformation and story drift

**Table 6.2 The dimensions of selected square hollow structural sections**

Section Name	$r_x$ (in)	b/t	$A_s$ (in <sup>2</sup> )	Section Name	$r_x$ (in)	b/t	$A_s$ (in <sup>2</sup> )
HSS 16 × 16 × 5/8	6.25	24.5	35	HSS 6 × 6 × 5/16	2.31	17.6	6.43
HSS 14 × 14 × 5/8	5.44	21.1	30.3	HSS 6 × 6 × 1/4	2.34	22.8	5.24
HSS 14 × 14 × 1/2	5.49	27.1	24.6	HSS 5-1/2 × 5-1/2 × 3/8	2.08	12.8	6.88
HSS 12 × 12 × 5/8	4.62	17.7	25.7	HSS 5-1/2 × 5-1/2 × 5/16	2.11	15.9	5.85
HSS 12 × 12 × 1/2	4.68	22.8	20.9	HSS 5-1/2 × 5-1/2 × 1/4	2.13	20.6	4.77
HSS 10 × 10 × 5/8	3.8	14.2	21	HSS 5 × 5 × 1/2	1.82	7.75	7.88
HSS 10 × 10 × 1/2	3.86	18.5	17.2	HSS 5 × 5 × 3/8	1.87	11.3	6.18
HSS 10 × 10 × 3/8	3.92	25.7	13.2	HSS 5 × 5 × 5/16	1.9	14.2	5.26
HSS 8 × 8 × 5/8	2.99	10.8	16.4	HSS 5 × 5 × 1/4	1.93	18.5	4.3
HSS 8 × 8 × 1/2	3.04	14.2	13.5	HSS 5 × 5 × 3/16	1.96	25.7	3.28
HSS 8 × 8 × 3/8	3.1	19.9	10.4	HSS 4-1/2 × 4-1/2 × 1/2	1.61	6.68	6.95
HSS 8 × 8 × 5/16	3.13	24.5	8.76	HSS 4-1/2 × 4-1/2 × 3/8	1.67	9.89	5.48
HSS 7 × 7 × 5/8	2.58	9.05	14	HSS 4-1/2 × 4-1/2 × 5/16	1.7	12.5	4.68
HSS 7 × 7 × 1/2	2.63	12.1	11.6	HSS 4-1/2 × 4-1/2 × 1/4	1.73	16.3	3.84
HSS 7 × 7 × 3/8	2.69	17.1	8.97	HSS 4-1/2 × 4-1/2 × 3/16	1.75	22.9	2.93
HSS 7 × 7 × 5/16	2.72	21.1	7.59	HSS 4 × 4 × 1/2	1.41	5.6	6.02
HSS 7 × 7 × 1/4	2.75	27	6.17	HSS 4 × 4 × 3/8	1.47	8.46	4.78
HSS 6 × 6 × 5/8	2.17	7.33	11.7	HSS 4 × 4 × 5/16	1.49	10.7	4.1
HSS 6 × 6 × 1/2	2.23	9.9	9.74	HSS 4 × 4 × 1/4	1.52	14.2	3.37
HSS 6 × 6 × 3/8	2.28	14.2	7.58	HSS 4 × 4 × 3/16	1.55	20	2.58

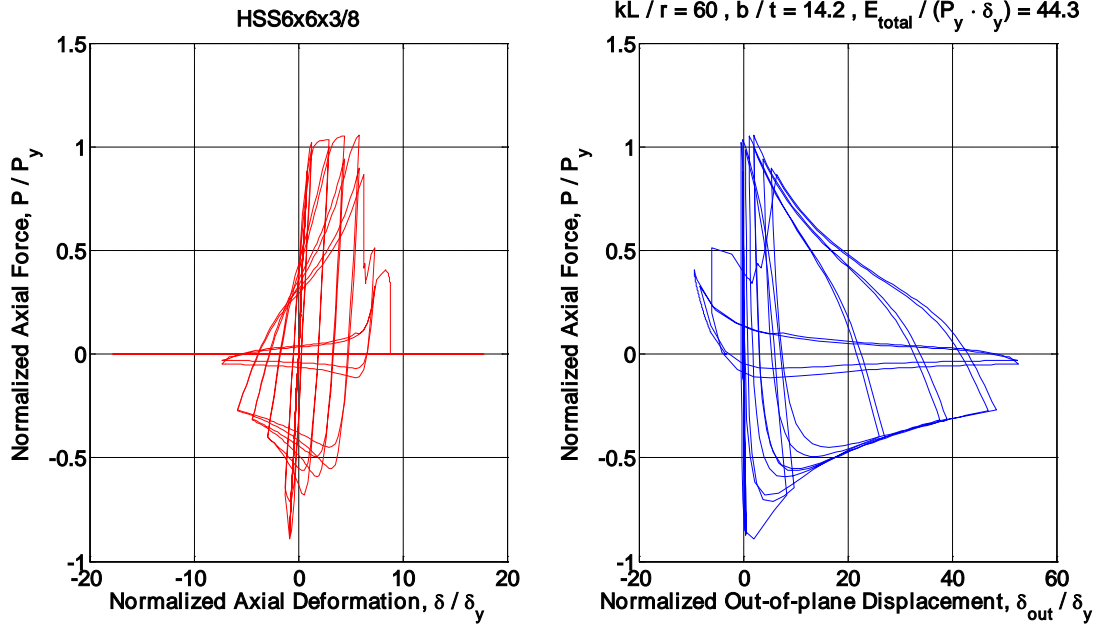


Figure 6.27 Normalized axial force versus normalized axial deformation and normalized out-of-plane deformation relationships of square HSS  $6 \times 6 \times 3/8$  with  $kL/r = 60$

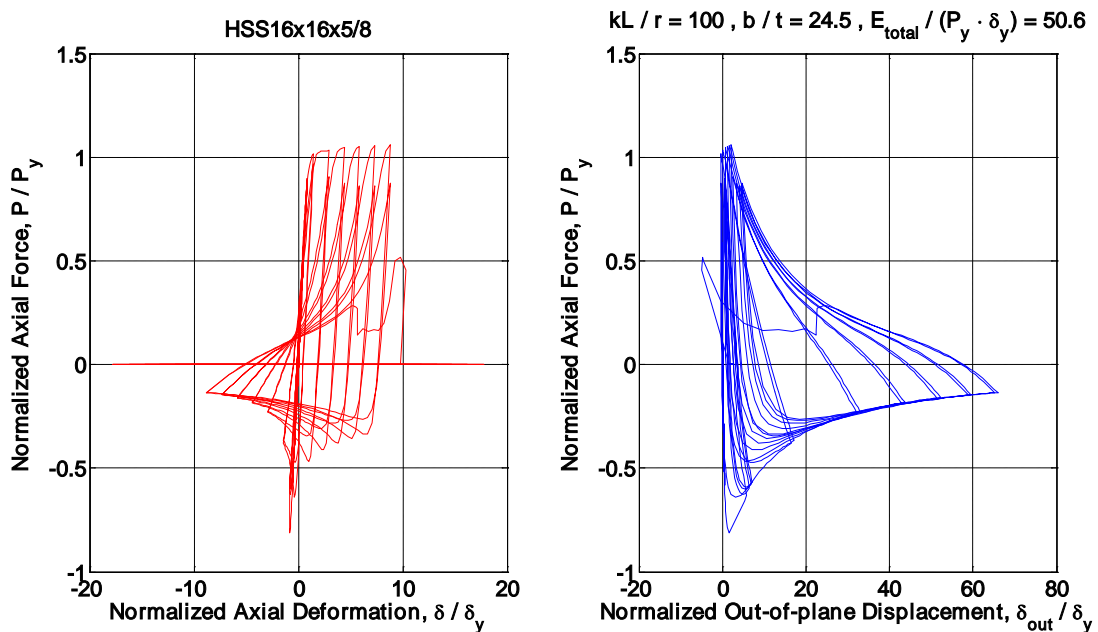


Figure 6.28 Normalized axial force versus normalized axial deformation and normalized out-of-plane deformation relationships of square HSS  $16 \times 16 \times 5/8$  with  $kL/r = 100$

**Table 6.3 Normalized cumulative energy dissipation of selected square hollow structural sections under different  $kL/r$  ratios**

ID	Section Name	$b/t$	$E_{total} / (P_y \cdot \delta_y)$					
			$kL/r$					
			40	60	80	100	150	200
1	HSS 16 × 16 × 5/8	24.5	102.0	52.4	48.7	50.6	65.3	76.3
2	HSS 14 × 14 × 5/8	21.1	72.2	52.5	50.2	50.6	62.9	75.3
3	HSS 14 × 14 × 1/2	27.1	58.6	52.4	45.3	49.3	63.3	75.1
4	HSS 12 × 12 × 5/8	17.7	74.5	52.9	50.0	49.9	63.8	76.1
5	HSS 12 × 12 × 1/2	22.8	71.1	53.5	49.6	50.4	64.6	75.2
6	HSS 10 × 10 × 5/8	14.2	74.8	50.3	51.0	49.7	59.4	75.7
7	HSS 10 × 10 × 1/2	18.5	80.2	52.2	49.9	50.6	64.4	75.9
8	HSS 10 × 10 × 3/8	25.7	69.5	52.8	45.5	50.8	63.9	70.8
9	HSS 8 × 8 × 5/8	10.8	94.1	52.6	46.7	51.7	61.0	74.9
10	HSS 8 × 8 × 1/2	14.2	100.3	49.8	48.8	49.4	58.2	73.1
11	HSS 8 × 8 × 3/8	19.9	95.7	46.5	49.9	50.8	62.9	76.3
12	HSS 8 × 8 × 5/16	24.5	71.9	52.0	47.8	51.4	62.8	53.2
13	HSS 7 × 7 × 5/8	9.05	64.6	49.3	46.1	49.9	60.1	73.5
14	HSS 7 × 7 × 1/2	12.1	74.3	49.8	46.2	50.4	60.2	72.8
15	HSS 7 × 7 × 3/8	17.1	76.5	43.6	50.3	47.4	65.2	72.7
16	HSS 7 × 7 × 5/16	21.1	65.8	47.0	48.7	49.5	63.2	74.3
17	HSS 7 × 7 × 1/4	27	62.6	49.9	47.9	51.2	63.1	76.7
18	HSS 6 × 6 × 5/8	7.33	69.8	48.5	47.9	47.5	59.9	69.3
19	HSS 6 × 6 × 1/2	9.9	89.0	51.2	47.7	48.1	59.5	68.8
20	HSS 6 × 6 × 3/8	14.2	60.2	44.3	47.0	48.9	62.0	51.9
21	HSS 6 × 6 × 5/16	17.6	65.4	47.3	49.8	48.6	63.8	76.4
22	HSS 6 × 6 × 1/4	22.8	64.2	46.4	49.3	49.7	64.7	54.7
23	HSS 5-1/2 × 5-1/2 × 3/8	12.8	70.1	48.6	44.9	48.8	58.4	72.6
24	HSS 5-1/2 × 5-1/2 × 5/16	15.9	65.2	47.6	45.3	47.9	63.6	71.5
25	HSS 5-1/2 × 5-1/2 × 1/4	20.6	67.0	46.9	48.8	47.4	63.2	75.0



ID	Section Name	b/t	$E_{total} / (P_y \cdot \delta_y)$					
			kL/r					
			40	60	80	100	150	200
26	HSS 5 × 5 × 1/2	7.75	79.5	51.2	49.4	47.5	54.5	69.5
27	HSS 5 × 5 × 3/8	11.3	68.9	50.7	45.5	50.3	59.5	71.6
28	HSS 5 × 5 × 5/16	14.2	74.1	49.2	44.9	49.4	58.4	73.4
29	HSS 5 × 5 × 1/4	18.5	67.9	47.7	47.0	48.0	63.6	71.4
30	HSS 5 × 5 × 3/16	25.7	55.3	48.1	47.5	51.8	59.9	65.7
31	HSS 4-1/2 × 4-1/2 × 1/2	6.68	64.0	48.7	46.7	47.6	59.2	68.3
32	HSS 4-1/2 × 4-1/2 × 3/8	9.89	76.5	49.2	46.6	51.4	61.2	74.3
33	HSS 4-1/2 × 4-1/2 × 5/16	12.5	103.7	50.6	46.0	50.9	59.7	74.4
34	HSS 4-1/2 × 4-1/2 × 1/4	16.3	61.3	46.6	49.4	51.1	63.7	74.1
35	HSS 4-1/2 × 4-1/2 × 3/16	22.9	59.3	41.9	47.7	50.6	61.9	54.2
36	HSS 4 × 4 × 1/2	5.6	77.1	49.1	46.1	46.7	53.1	69.0
37	HSS 4 × 4 × 3/8	8.46	79.1	49.8	47.7	48.5	60.3	69.5
38	HSS 4 × 4 × 5/16	10.7	77.2	52.0	46.9	51.1	61.6	74.6
39	HSS 4 × 4 × 1/4	14.2	104.4	51.2	46.2	51.0	59.9	74.8
40	HSS 4 × 4 × 3/16	20	58.0	46.4	44.9	52.4	63.3	73.1
-	<b>Mean</b>	<b>16.3</b>	<b>74.1</b>	<b>49.3</b>	<b>47.6</b>	<b>49.7</b>	<b>61.5</b>	<b>71.1</b>
-	<b>Median</b>	<b>16.1</b>	<b>71.5</b>	<b>49.5</b>	<b>47.7</b>	<b>49.9</b>	<b>61.9</b>	<b>73.2</b>
-	<b>Standard Deviation</b>	<b>6.2</b>	<b>13.1</b>	<b>2.7</b>	<b>1.8</b>	<b>1.5</b>	<b>2.73</b>	<b>6.5</b>
-	<b>Maximum</b>	<b>27.1</b>	<b>104.4</b>	<b>53.5</b>	<b>51</b>	<b>52.4</b>	<b>65.3</b>	<b>76.7</b>
-	<b>Minimum</b>	<b>5.6</b>	<b>55.3</b>	<b>41.9</b>	<b>44.9</b>	<b>46.7</b>	<b>53.1</b>	<b>51.9</b>
-	<b>Range</b>	<b>21.5</b>	<b>49.1</b>	<b>11.6</b>	<b>6.1</b>	<b>5.8</b>	<b>12.2</b>	<b>24.8</b>

**Table 6.4 Normalized cumulative energy dissipation of selected group of square hollow structural sections under different  $kL/r$  ratios**

Group ID	$b/t$ Range (number of sections in the group)	$E_{total} / (P_y \cdot \delta_y)$						
		Statistical Value	$kL/r$					
			40	60	80	100	150	200
1	$b/t < 13.8$ (14)	Mean	77.7	50.1	46.7	49.3	59.2	71.6
		Median	76.7	49.8	46.6	49.4	59.8	72.1
		Standard Deviation	11.3	1.3	1.1	1.7	2.4	2.5
		Maximum	103.7	52.6	49.4	51.7	61.6	74.9
		Minimum	64	48.5	44.9	46.7	53.1	68.3
		Range	39.7	4.1	4.5	5.0	8.5	6.7
2	$13.8 \leq b/t \leq 16.1$ (6)	Mean	79.8	48.8	47.2	49.4	60.2	70.0
		Median	74.5	49.5	46.6	49.4	59.7	73.2
		Standard Deviation	18.3	2.5	2.3	1.0	2.1	9.0
		Maximum	104.4	51.3	51	51.0	63.6	75.7
		Minimum	60.2	44.3	44.9	47.9	58.2	51.9
		Range	44.2	6.9	6.1	3.2	5.4	23.8
3	$b/t > 16.1$ (20)	Mean	69.9	48.9	48.4	50.1	63.5	71.1
		Median	67.4	47.9	48.7	50.6	63.5	74.6
		Standard Deviation	11.9	3.4	1.7	1.4	1.2	7.8
		Maximum	102.1	53.4	50.3	52.4	65.3	76.7
		Minimum	55.3	41.8	44.9	47.4	59.9	53.2
		Range	46.7	11.6	5.4	5.1	5.4	23.5

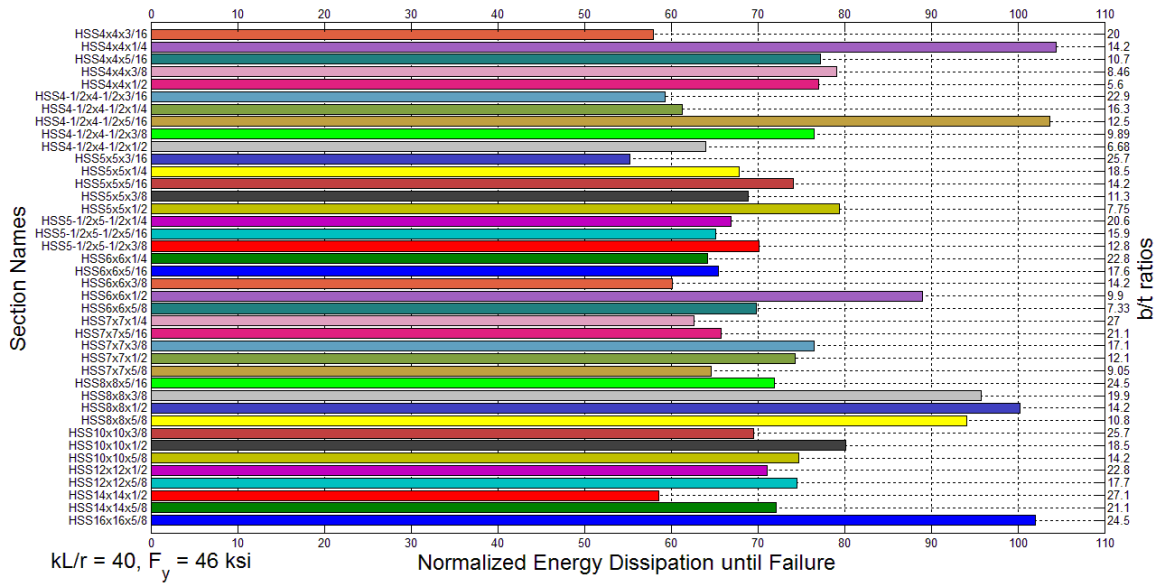


Figure 6.29 Normalized energy dissipation of selected square hollow structural sections until brace failure ( $kL/r = 40$ )

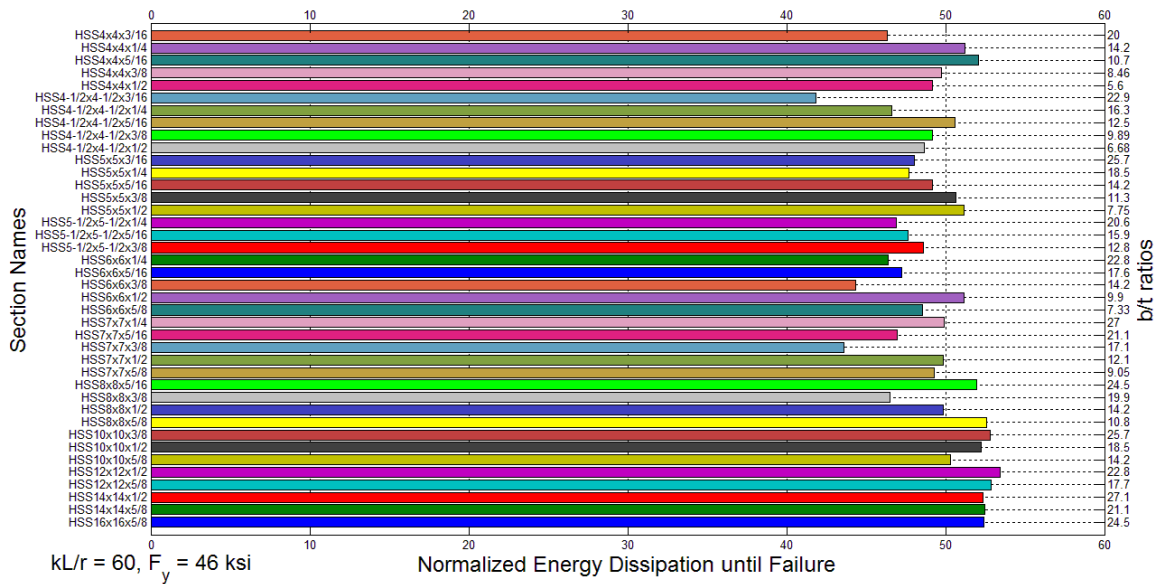


Figure 6.30 Normalized energy dissipation of selected square hollow structural sections until brace failure ( $kL/r = 60$ )

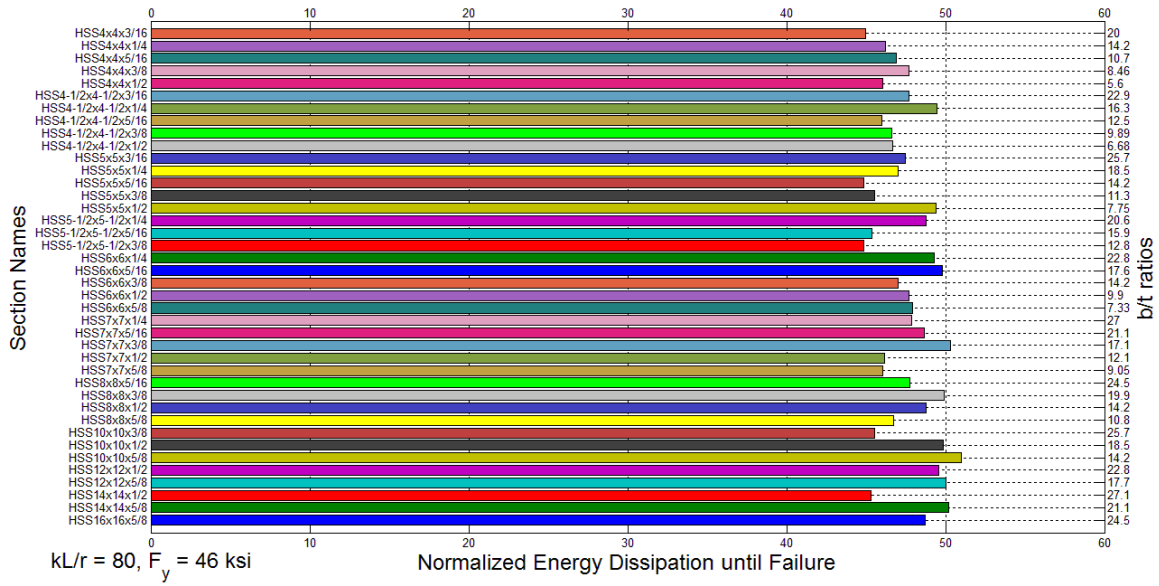


Figure 6.31 Normalized energy dissipation of selected square hollow structural sections until brace failure ( $kL/r = 80$ )

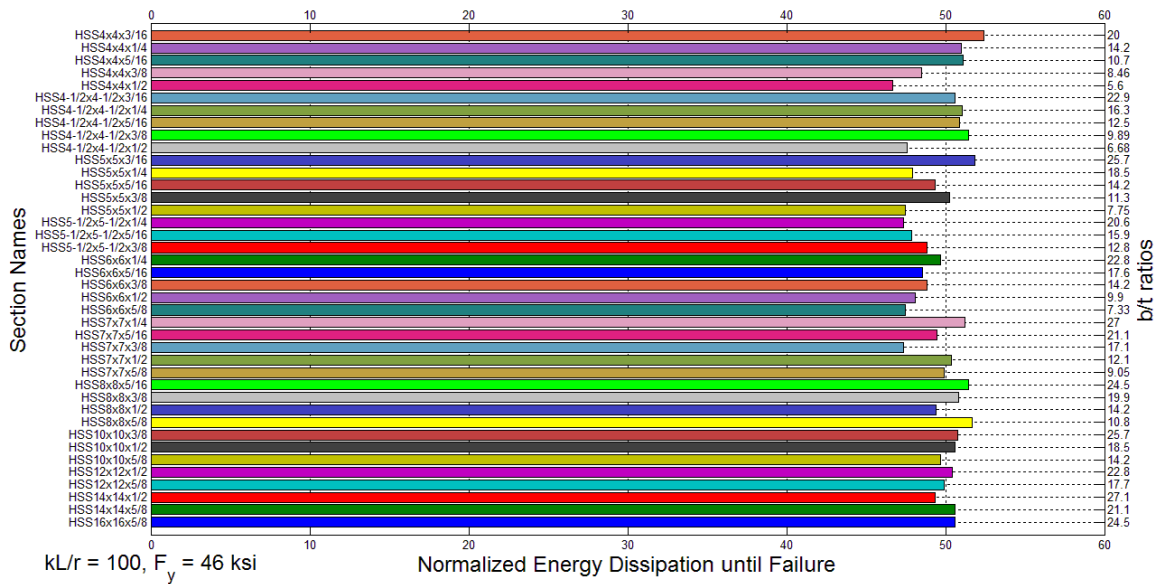
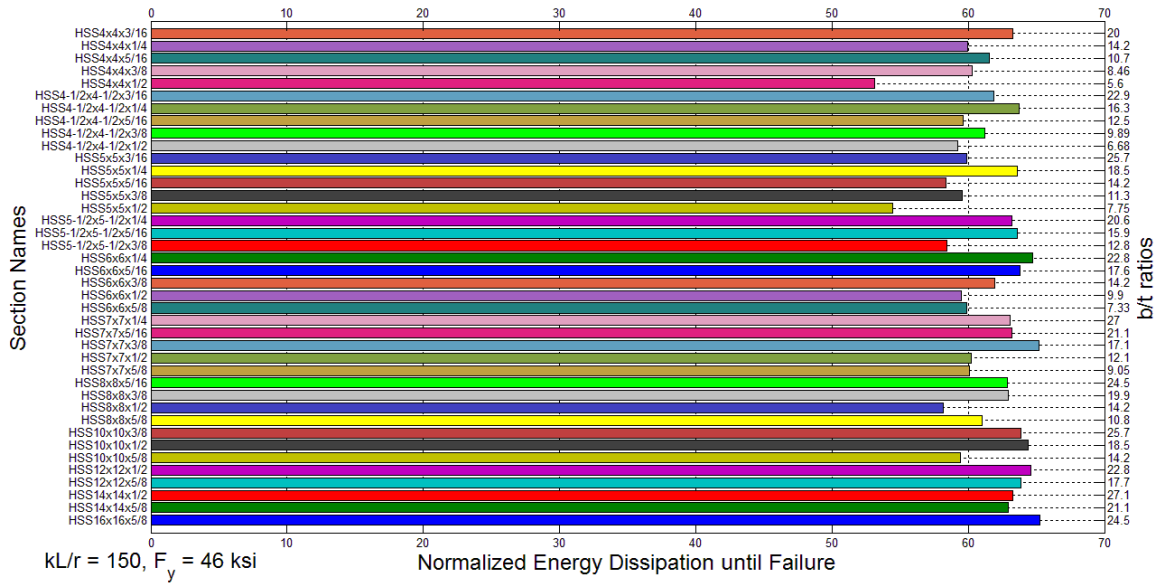
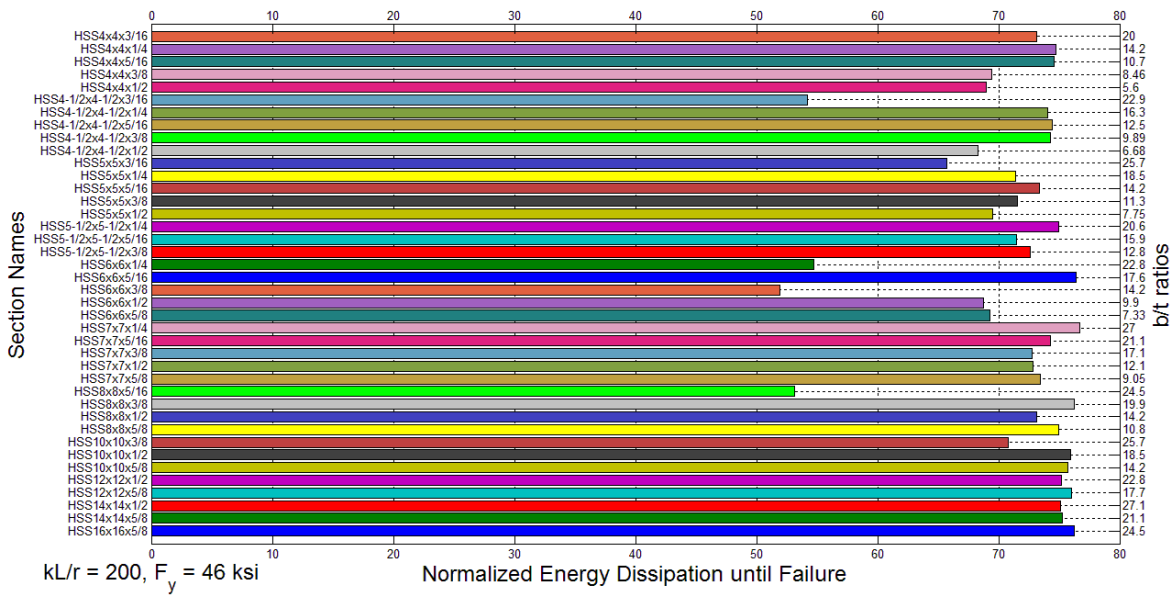


Figure 6.32 Normalized energy dissipation of selected square hollow structural sections until brace failure ( $kL/r = 100$ )



**Figure 6.33** Normalized energy dissipation of selected square hollow structural sections until brace failure ( $kL/r = 150$ )



**Figure 6.34** Normalized energy dissipation of selected square hollow structural sections until brace failure ( $kL/r = 200$ )

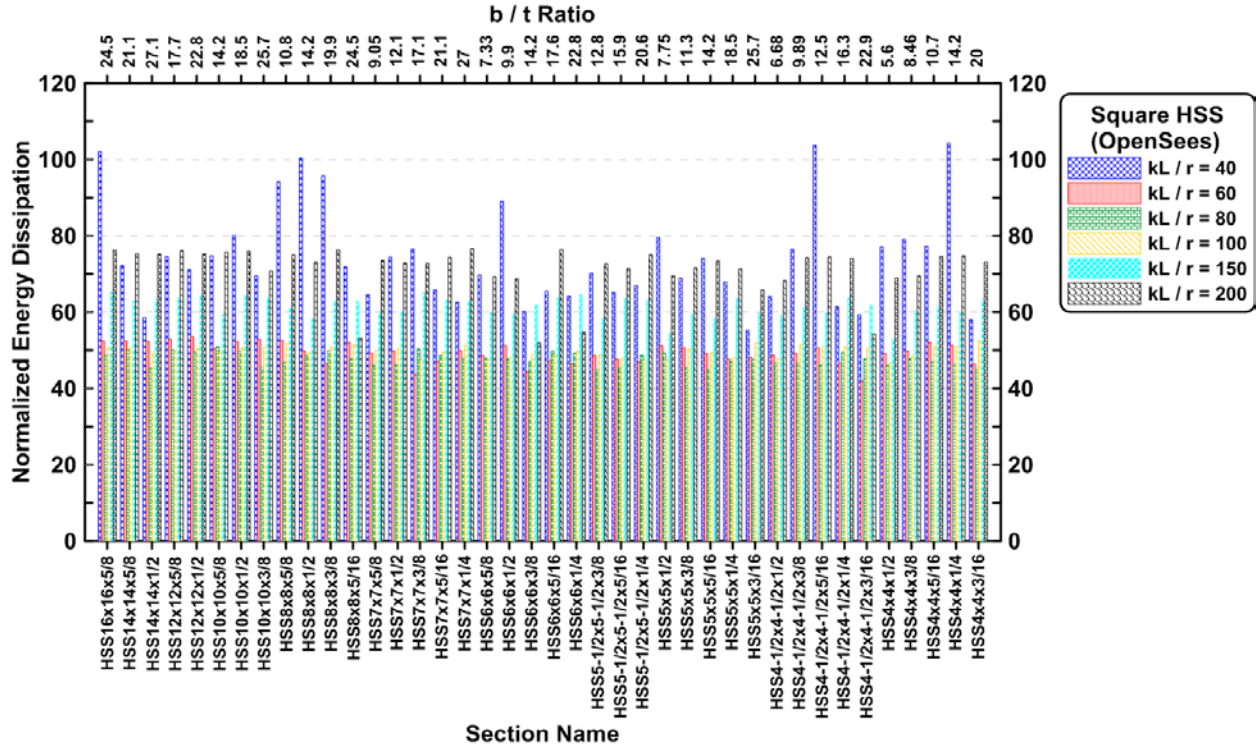


Figure 6.35 Normalized energy dissipation until brace failure of selected square hollow structural sections with different  $kL/r$  ratios

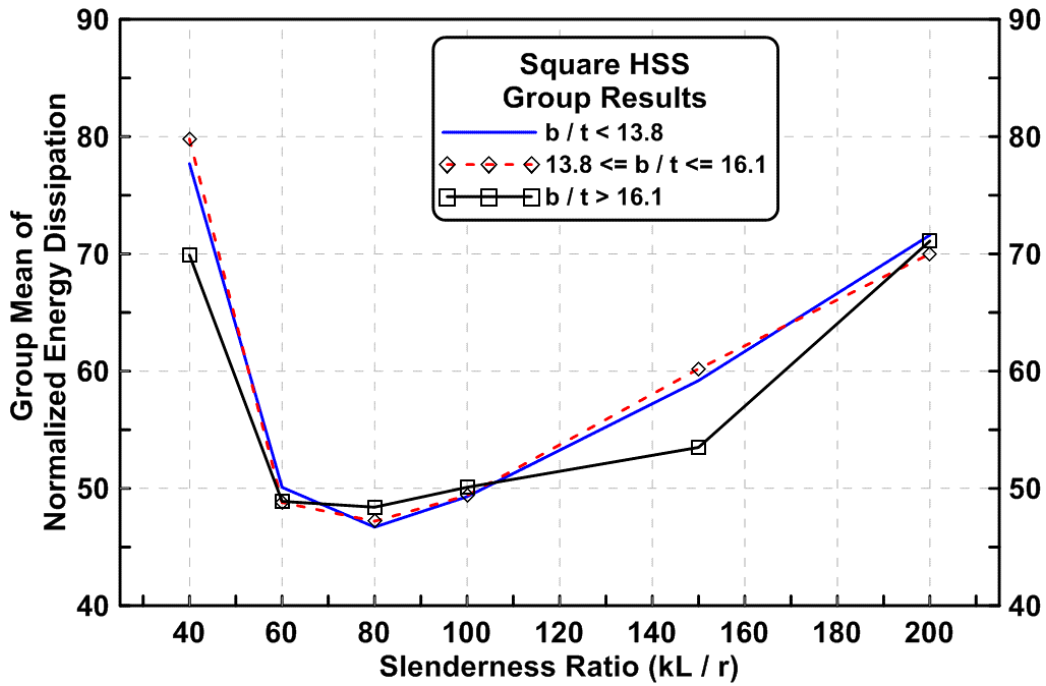


Figure 6.36 Group comparisons of normalized energy dissipation of selected square hollow structural sections with different  $kL/r$  ratios

## 6.5 PREDICTION OF STRUT AND BRACED FRAME SPECIMEN BEHAVIORS USING LS-DYNA

More detailed three-dimensional finite element models of individual struts and of the braced frame test specimens were developed using shell elements available in the software package LS-DYNA (LSTC, 2007). These models permitted consideration of material yielding, deterioration and rupture of materials due to low cycle fatigue, local buckling of critical local regions, global buckling of elements and geometric nonlinearities. The models were not formulated to account for issues related to fracture mechanics. Numerous shell elements were used to model elements and connection regions. Material models including plasticity and damage mechanics were utilized.

Shell elements with Belytschko-Tsay formulation were assigned in the model. The material type named Damage\_3 (MAT 153) developed by Huang and Mahin (2010) in LS-DYNA was selected to model the low cycle fatigue deterioration behavior of the steel. This model incorporates a low cycle fatigue damage index and the member properties can deteriorate (erode) and the local element removed from the model when the low cycle fatigue life of the material is exceeded. Material properties used here were calibrated from existing cyclic test results extracted from the existing study (Fujimoto et al., 1985) and properly scaled to match the yield strength as reported in the mill certificates for each specimen.

Adaptive meshing (LSTC, 2007) with hourglass control was selected in the model was to account for local deformation concentration along bracing members (also used in the two-story braced frame simulations) during the simulation. The minimum element size to be adapted was set equal to the thickness of HSS section wall. Explicit analysis with time scaling was used to simulate the specimens under quasi-static cyclic loading. No initial member imperfections were introduced in the finite element model, since the three dimensional frame models are likely to have in-plane and other deformations to trigger global buckling of the braces, or buckling can be triggered by numerical round-off errors during the analysis.

### 6.5.1 LS-DYNA Analysis of Individual Struts

The same specimens analyzed in Section 6.1 using OpenSees fiber-based elements are again analyzed using shell elements in LS-DYNA. Figure 6.37 shows the mesh pattern of a simple brace modeled as a complete strut, including gusset plates. Several ways can be used to simplify this model and speed execution of the analysis of the strut in LS-DYNA; for example, a reduced model and reduced half model are shown in Fig. 6.38. The experimental results of square HSS simple struts (Yang and Mahin, 2005) tested under different loading histories were utilized to compare with the simulation outputs from LS-DYNA. Figure 6.37 shows the mesh pattern of a simple strut model used here (the full model).

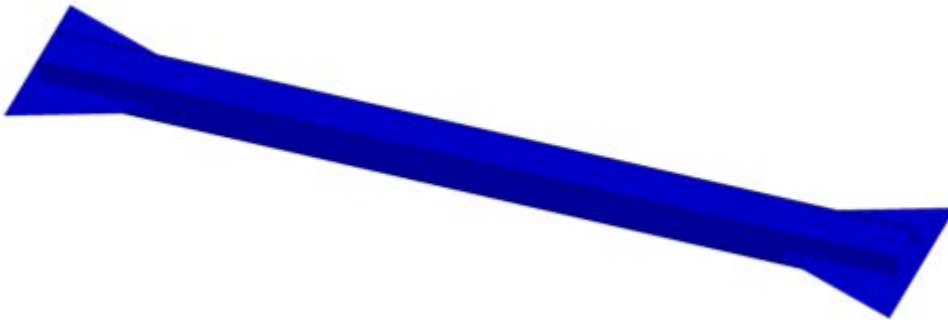
Figures 6.39 to 6.47 illustrate the LS-DYNA simulation results compared with the test data and photos taken during the cyclic testing. The analyses are able to match the tests quite well, including the nature and time of brace rupture. The discrepancy of the model is most likely due to the material constitutive model not exactly matching the materials used in the test specimen. Moreover, initial imperfections and residual fabrication stresses were not included in the model. It is clear that localized buckling of HSS section walls can be simulated using shell elements, and that the finite element model properly mimics the brace rupture behavior that occurs due to damage accumulation due to low cycle fatigue.



(a) Top view

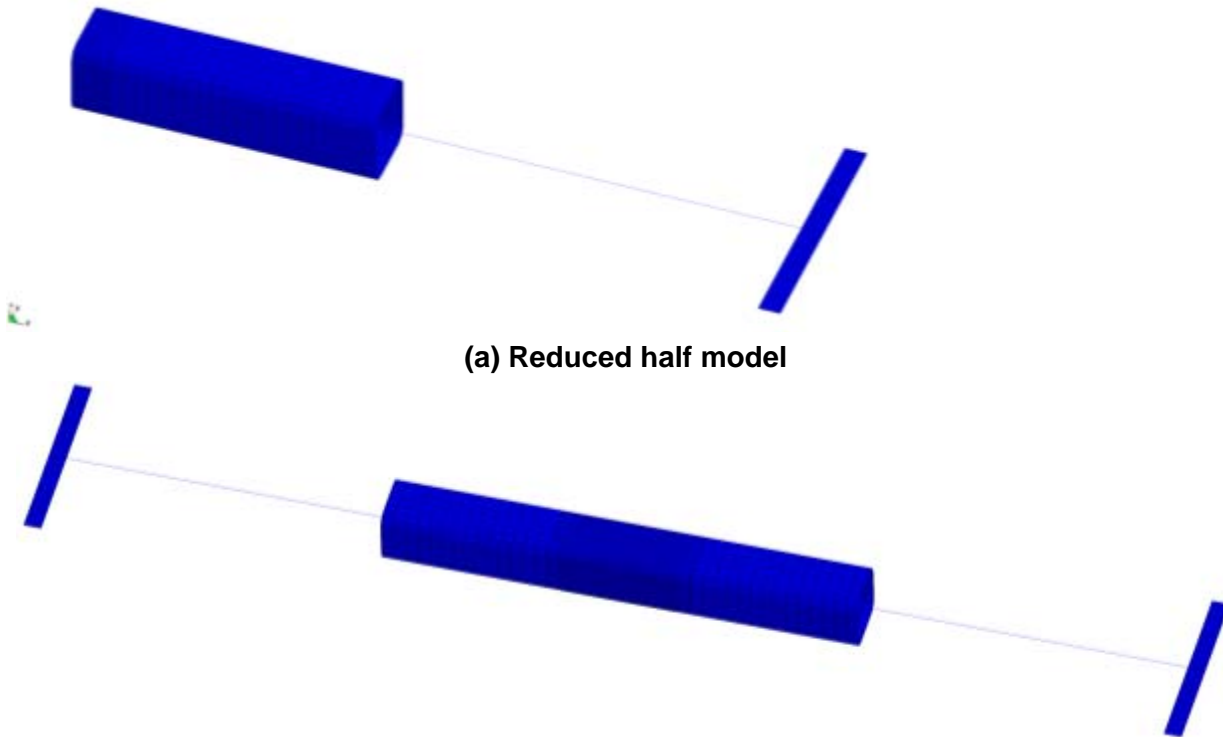
Square F55 8 x 8 x 30, Length = 112"

Title = 6 Model104, Rev0010



(b) Perspective view

Figure 6.37 Mesh pattern for the simple strut modelling in LS-DYNA



(a) Reduced half model

(b) Reduced model

Figure 6.38 Illustration of simplified models for the simple strut modeling in LS-DYNA



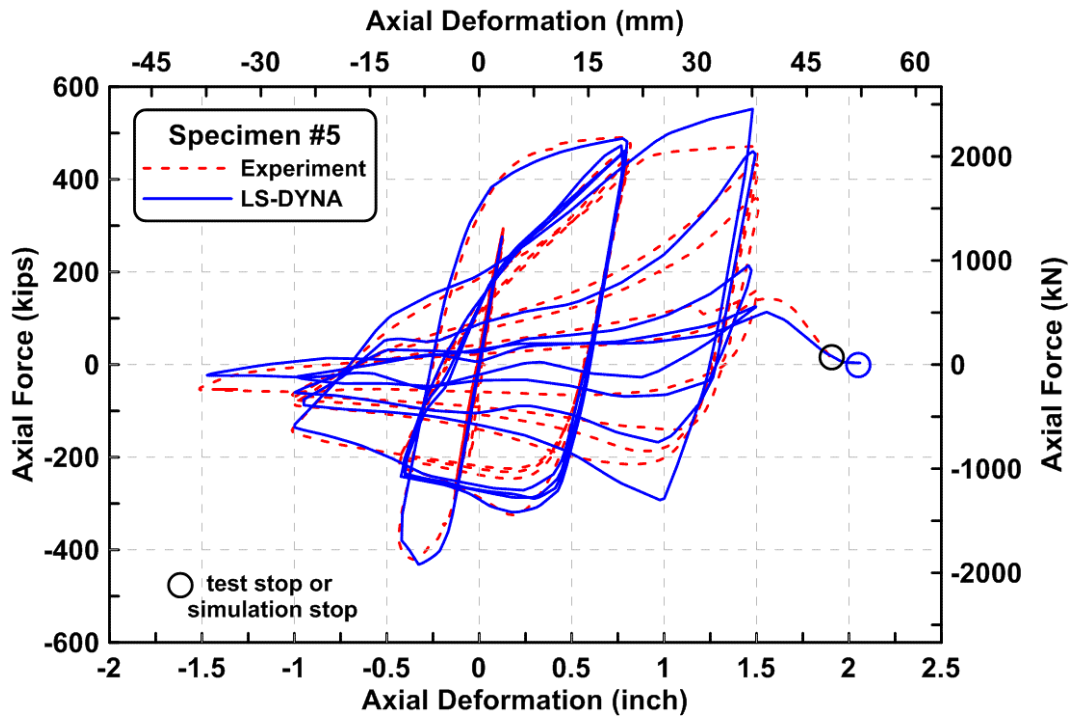


Figure 6.39 Axial force versus axial deformation relationship of specimen #5 from experiment and LS-DYNA simulation

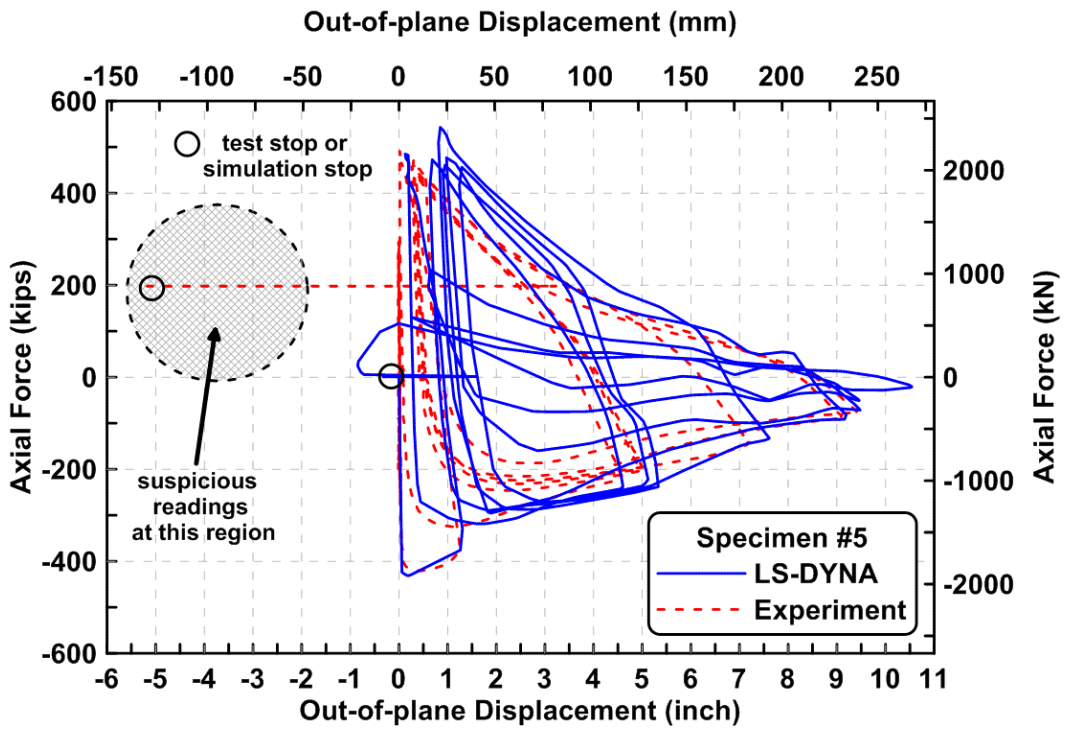
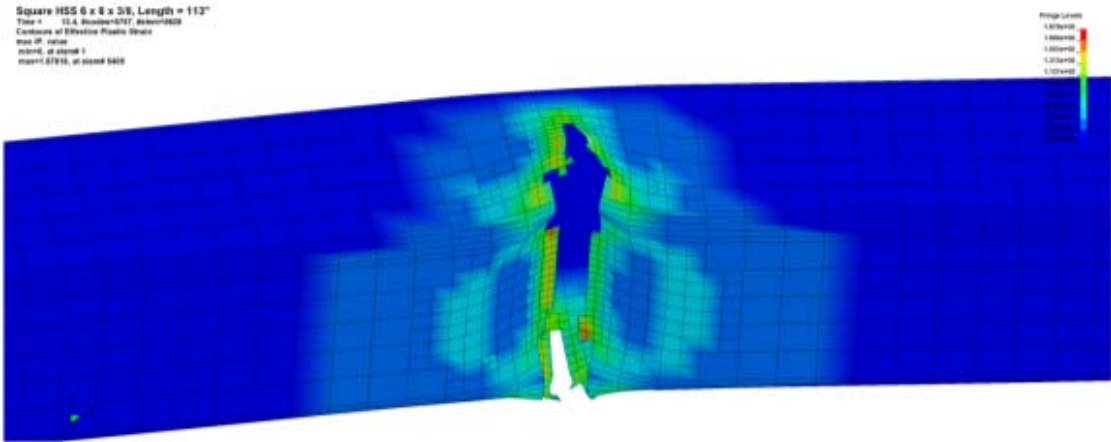
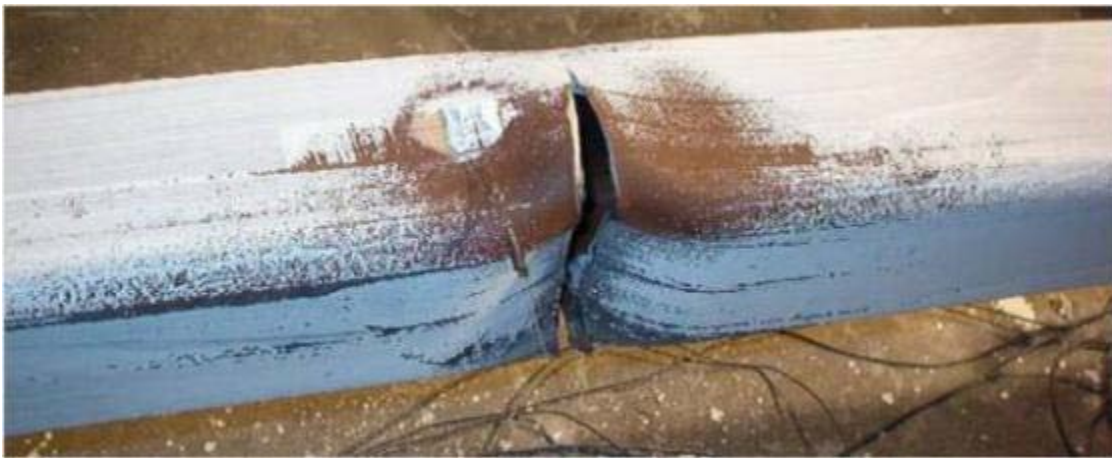


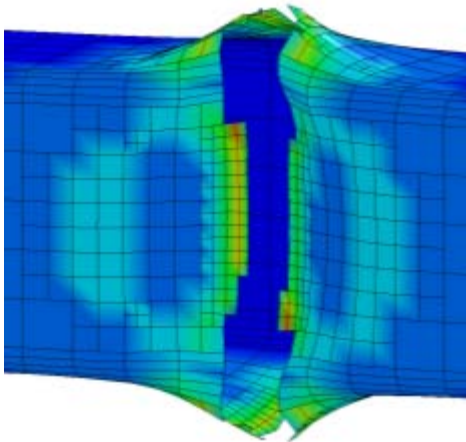
Figure 6.40 Axial force versus out-of-plane displacement relationship of specimen #5 from experiment and LS-DYNA simulation



(a) Effective plastic strain distribution contour from LS-DYNA simulation



(b) Crack propagated at the middle length of brace (extracted from Fig.6 in Yang and Mahin, 2005)



(c) Effective plastic strain distribution contour from LS-DYNA simulation (closed view)



(d) Closed view at middle of brace (extracted from Fig.6 in Yang and Mahin, 2005)

Figure 6.41 Comparison between actual test and LS-DYNA simulation results at the final cycle

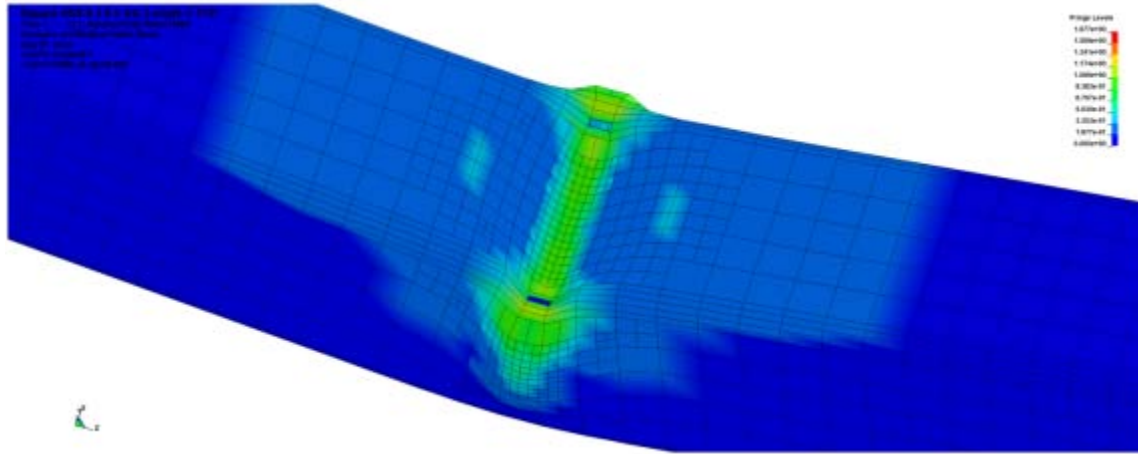
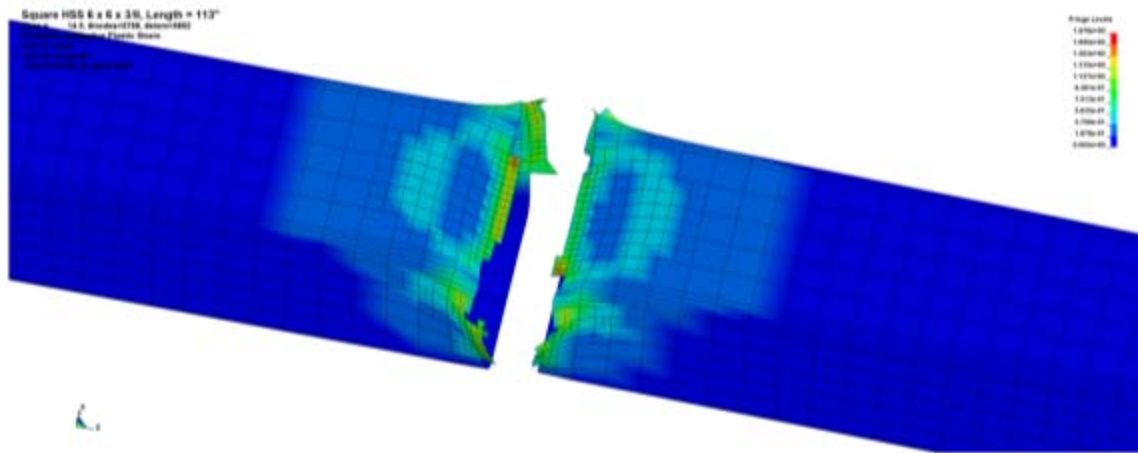
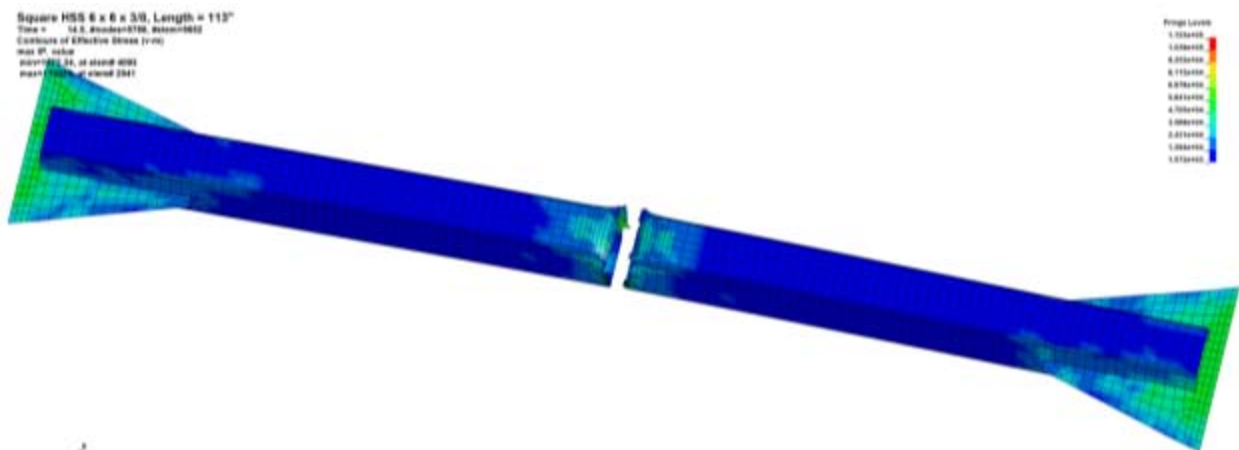


Figure 6.42 Crack initiation in HSS brace section wall simulated by LS-DYNA model



(a) Closed view of the strut after rupture



(b) Overview of the strut after rupture

Figure 6.43 Complete fracture in the LS-DYNA strut model

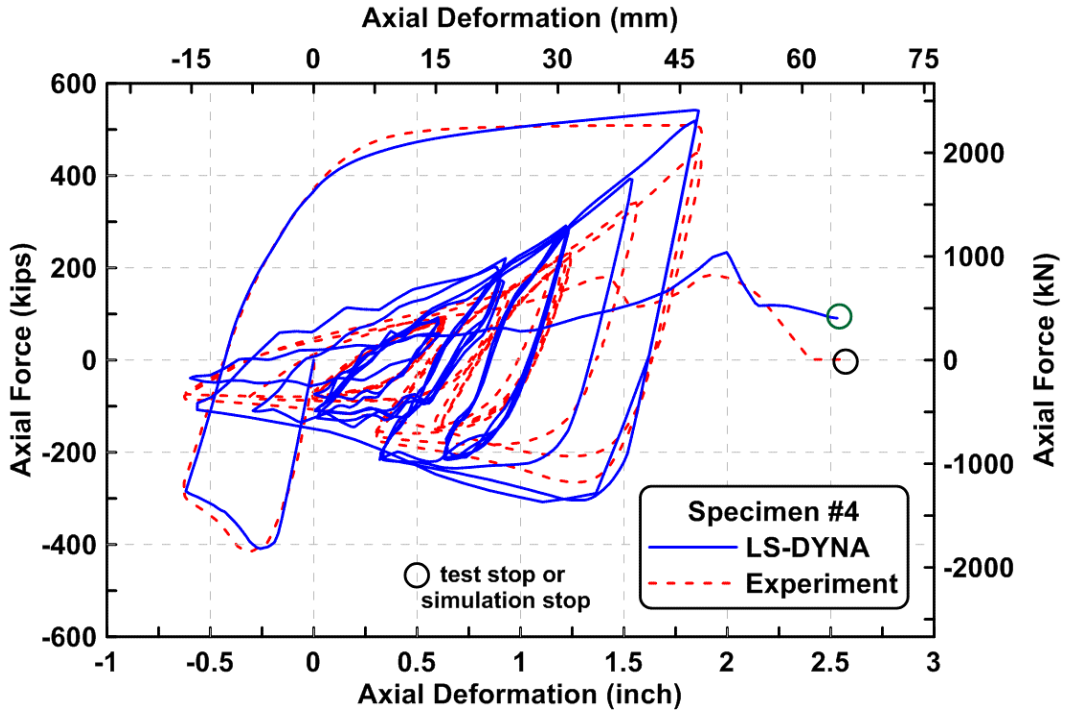


Figure 6.44 Axial force versus axial deformation relationship of specimen #4 from experiment and LS-DYNA simulation

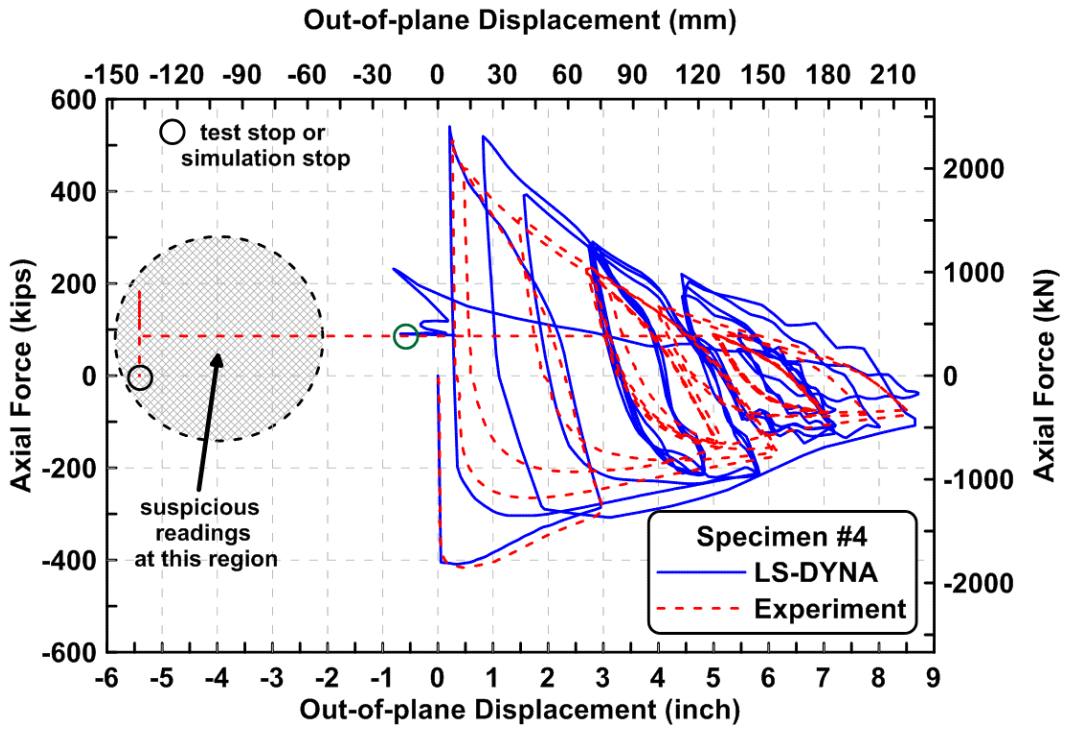
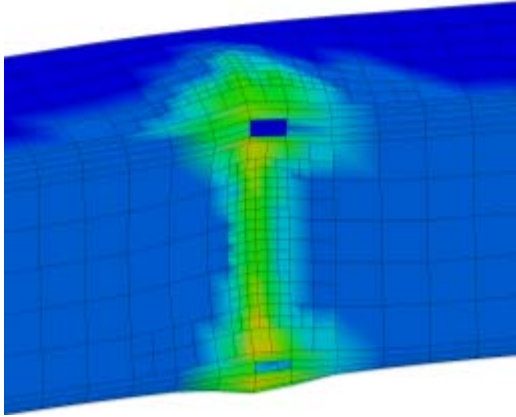
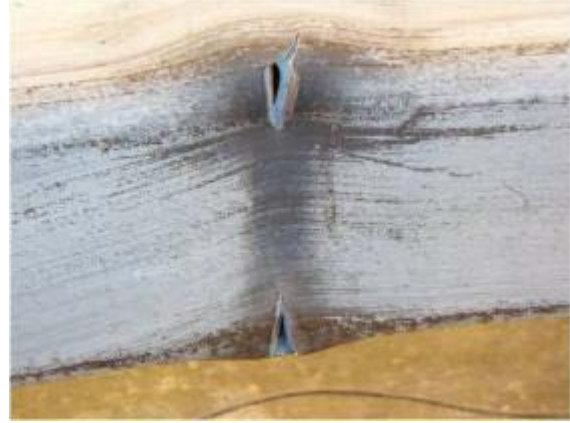


Figure 6.45 Axial force versus out-of-plane displacement relationship of specimen #4 from experiment and LS-DYNA simulation

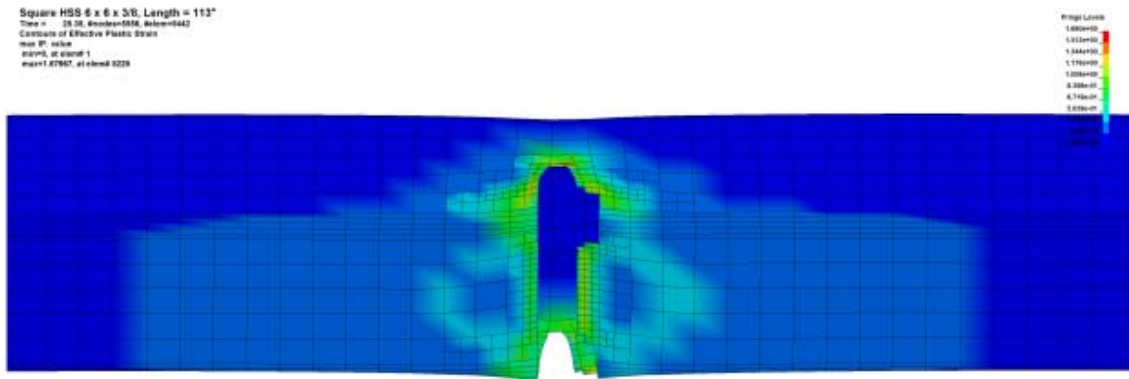


(a) Crack initiation in HSS section walls (LS-DYNA model)



(b) Crack initiation at center region of brace (extracted from Fig. 12 in Yang and Mahin, 2005)

Figure 6.46 Comparison between actual test and FE model under near-fault loading protocol



(a) LS-DYNA model



(b) Test photo at middle length of HSS brace (extracted from Fig. 12 in Yang and Mahin, 2005)

Figure 6.47 Comparison between actual test and FE model at the final stage of testing

## 6.5.2 LS-DYNA Analysis of Quasi-static TCBF Test Specimens

The two-story quasi-static tests were also simulated using LS-DYNA. Figure 6.48 shows the entire model and the mesh layout for specimen TCBF-B-1. To save simulation time, prescribed displacement histories for both floor levels were specified, based on the measured test results. This is not the same as the method used during the test, where half of the force applied at the roof level was imposed at the lower floor level. LS-DYNA does not have load functions that are similar to actual test conditions. However, the whiffletree (Harris and Sabins, 1999) concept can be applied in the LS-DYNA model to represent the actual load pattern. Other possible numerical constraint schemes (Huang and Mahin, 2010) can also be applied in LS-DYNA. This is an area for further investigation.

Figure 6.49 shows the LS-DYNA simulated base shear versus roof displacement relationship superimposed on the actual experimental results obtained from Specimen TCBF-B-1. The simulation results match the quasi-static test results quite well. The hysteretic loops from the finite element simulation show a bit more rapid initial deterioration in the positive direction than the experiment, and dissipate more energy than the test specimen in the final few cycles. Localized buckling of brace section walls and beam-to-gusset plate connection regions were simulated (see Figs. 6.50 and 6.51). Crack initiation and partial propagation are also shown.

Simulation results of specimens TCBF-B-2 and TCBF-B-3 are shown in Fig. 6.52 to Fig. 6.57. The results for Specimen TCBF-B-2, with round HSS braces, were particularly well modeled throughout its response. The initial simulation of Specimen TCBF-B-3 is good, but poorer than the other simulations in later cycles. This may be associated with the modeling of the bolted lower beam to gusset plate connections, which were simplified for these analyses.

The explicit analysis in LS-DYNA took a significantly greater amount of computer time to finish the quasi-static loading histories than for the simpler fiber based models in OpenSees.

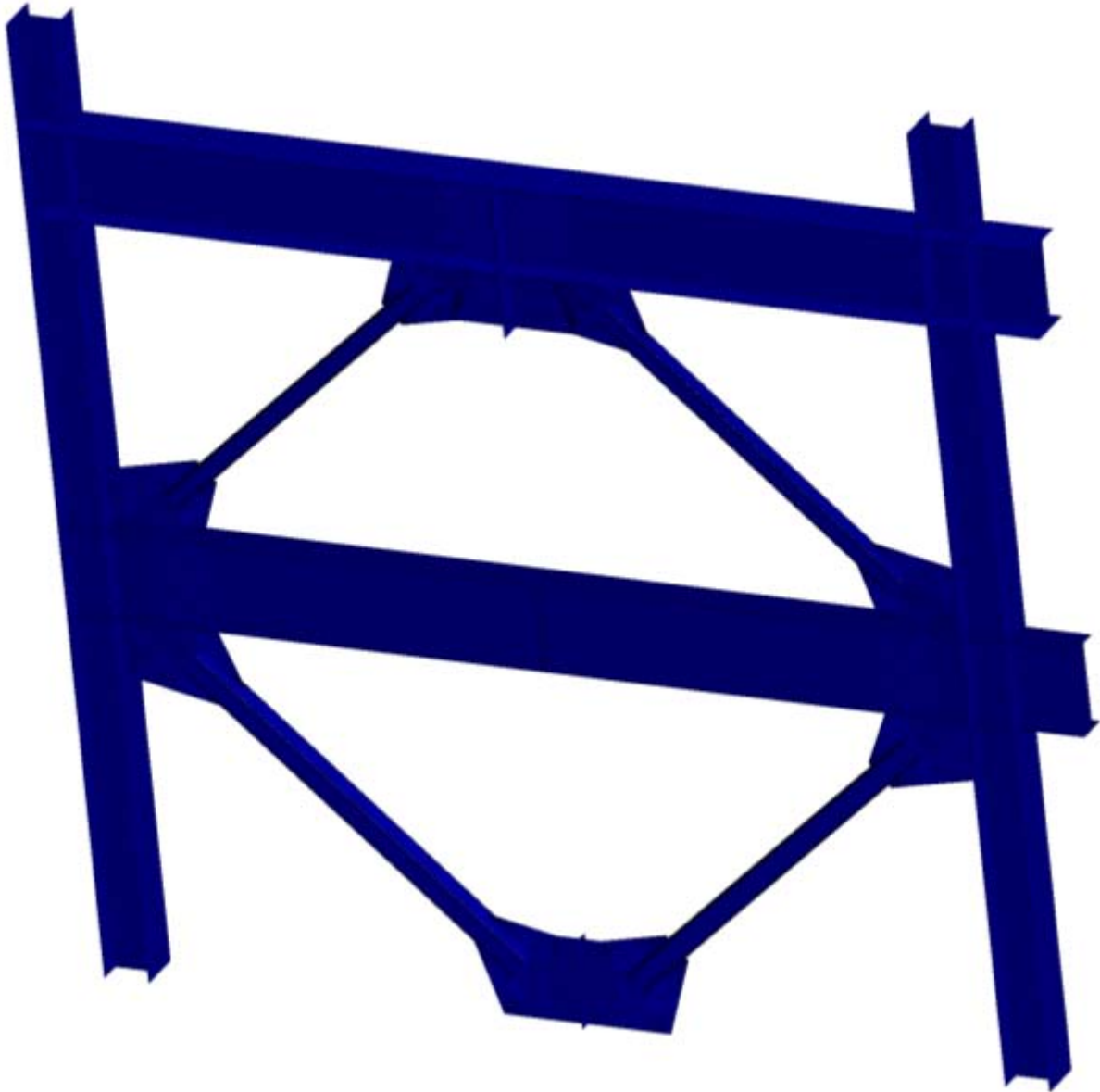


**Figure 6.48** Mesh layout in the LS-DYNA simulation for TCBF-B-1 specimen

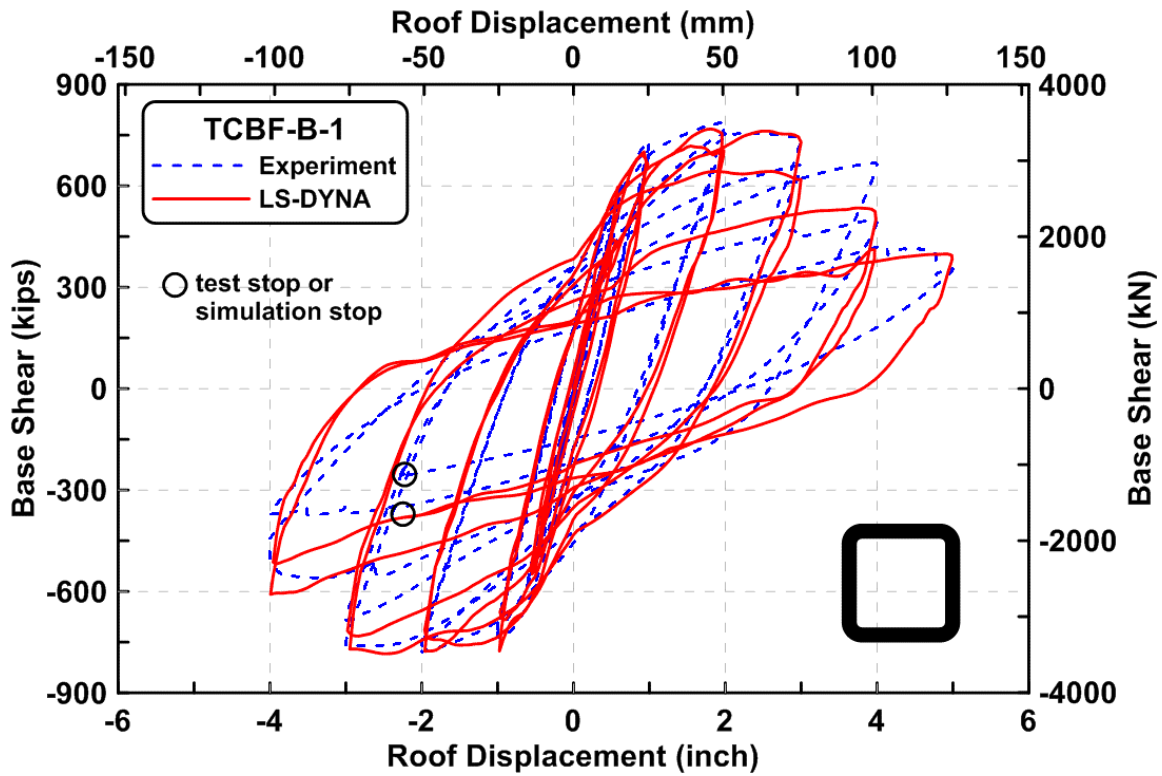


Figure 6.49 Base shear versus roof displacement from LS-DYNA simulation for TCBF-B-1 specimen

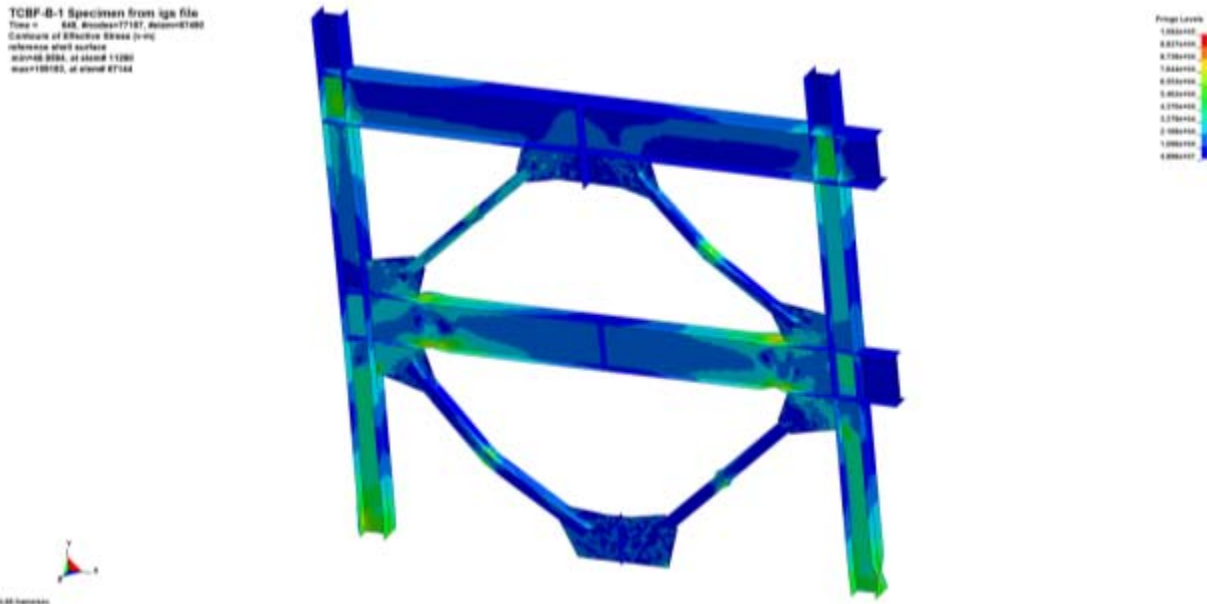
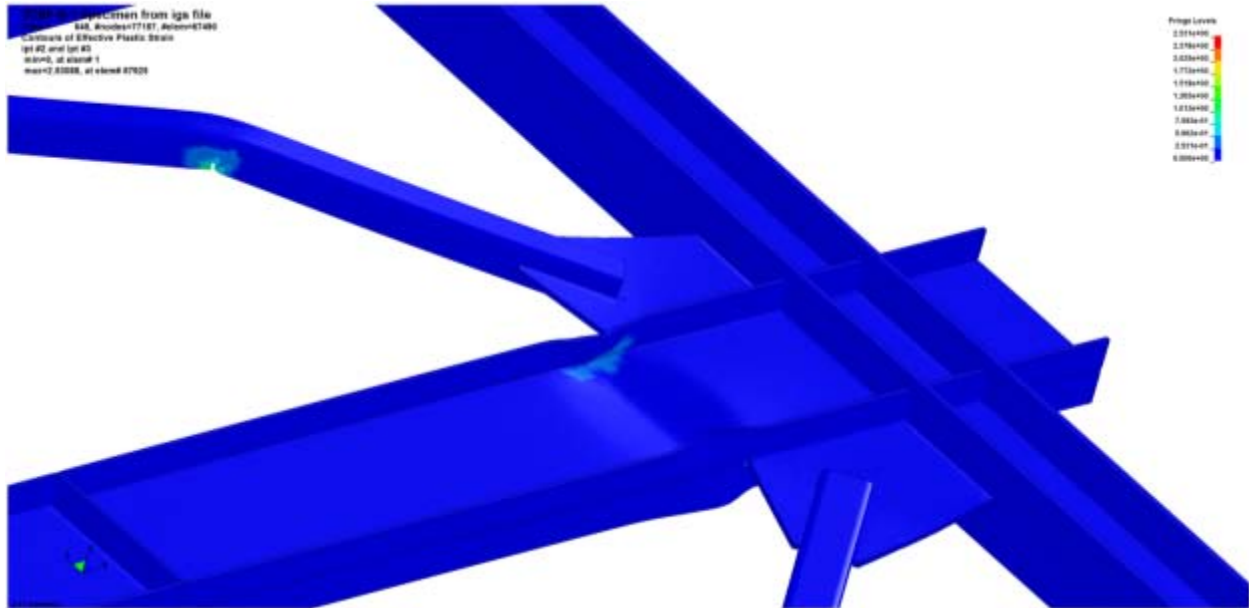
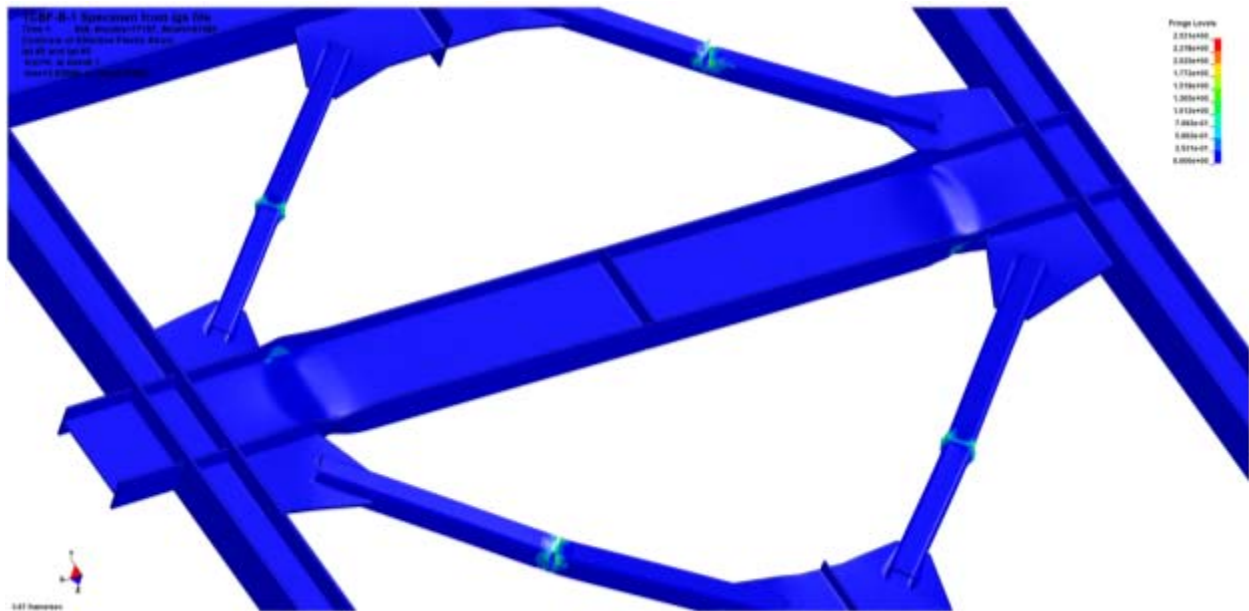


Figure 6.50 Von Mises stress distribution of TCBF-B-1 specimen at the end of LS-DYNA simulation





(a) Western side beam-to-gusset plate connection region  
(local buckling of beam web, top and bottom flanges)



(b) Overview of specimen from south-west side (crack initiated and partially propagated in all four braces, lower beam end plastic hinges are also shown)

Figure 6.51 Plastic strain distribution of TCBF-B-1 specimen at the end of LS-DYNA simulation

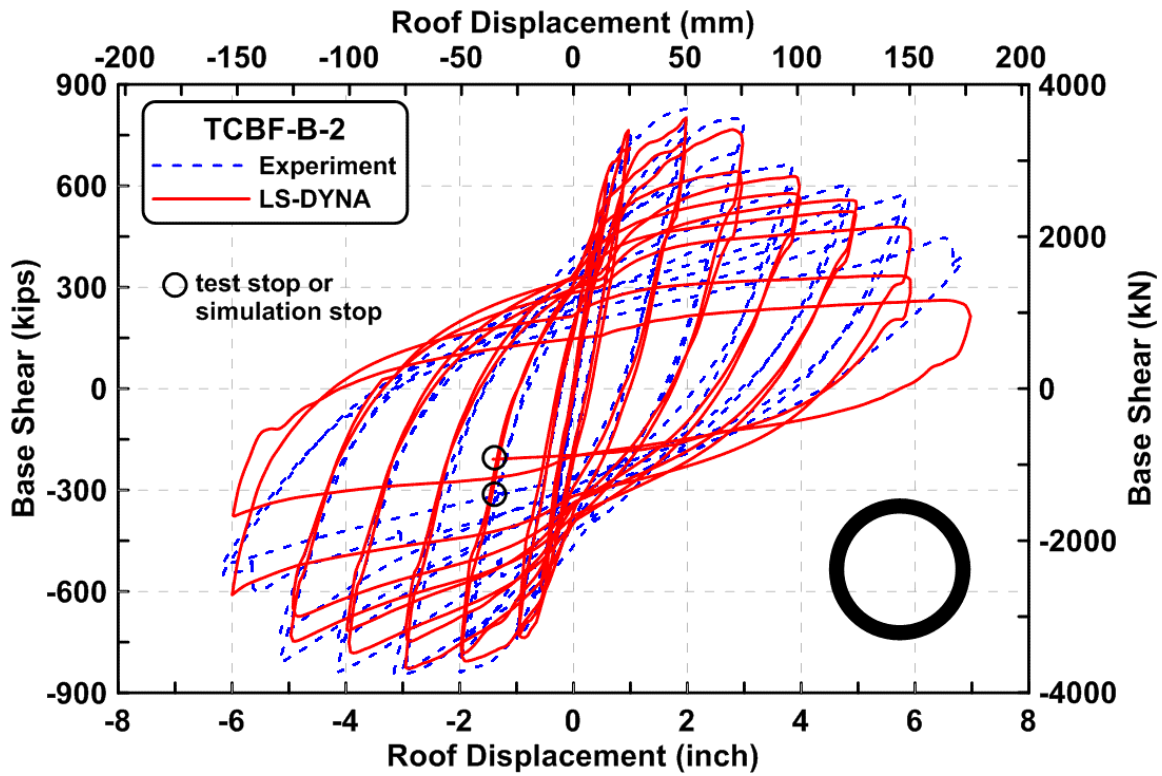


Figure 6.52 Base shear versus roof displacement from LS-DYNA simulation for TCBF-B-2 specimen

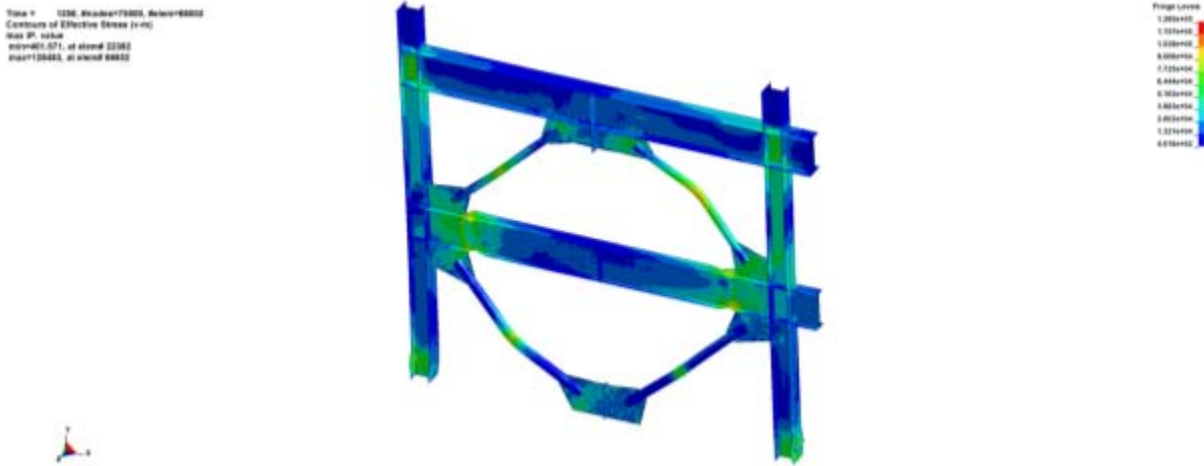
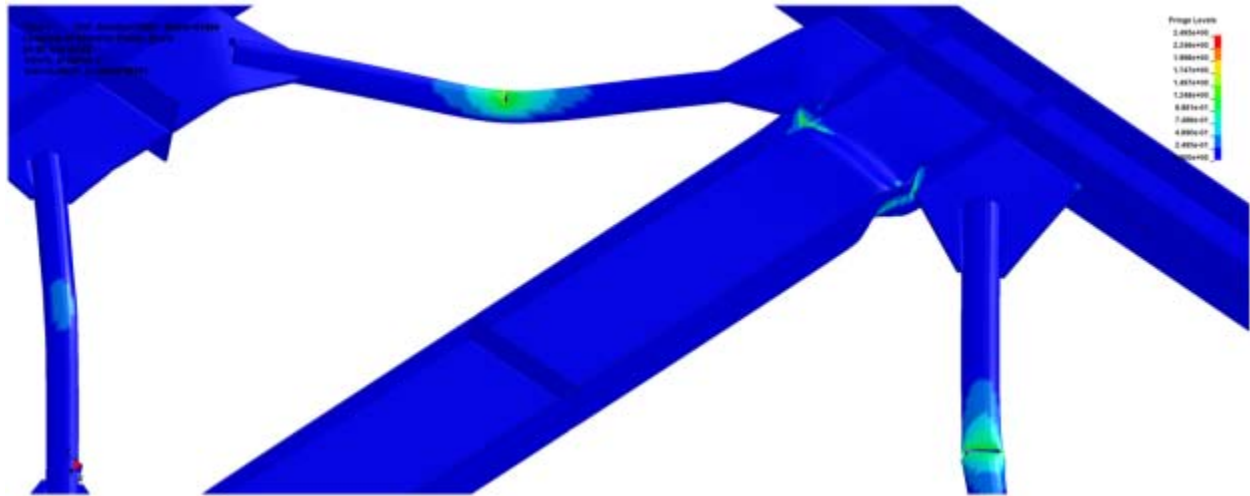
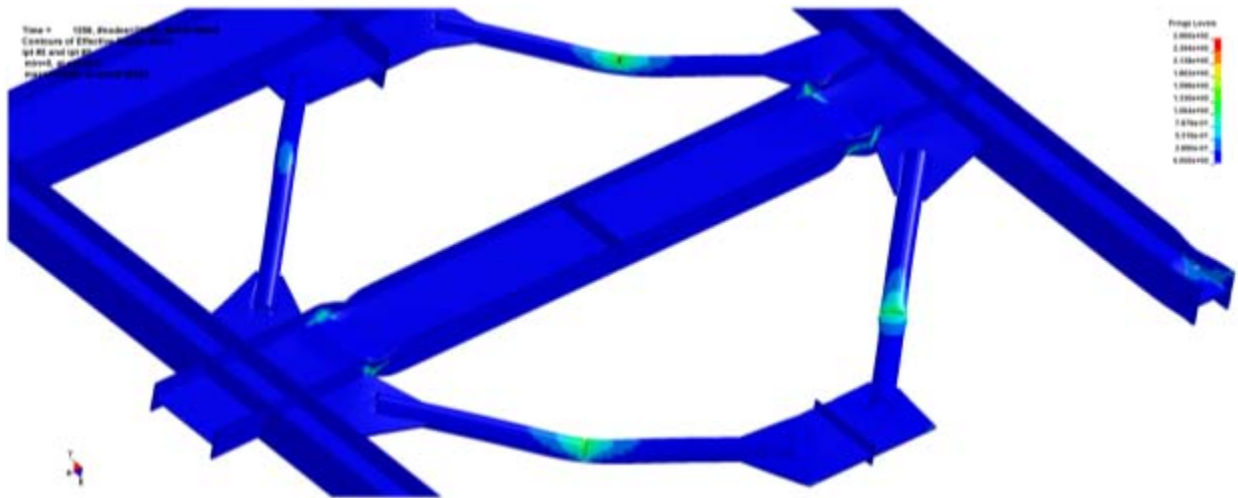


Figure 6.53 Von Mises stress distribution of TCBF-B-2 specimen at the end of LS-DYNA simulation



(a) Eastern side beam-to-gusset plate connection region  
(local buckling of beam web, top and bottom flanges)



(b) Overview of specimen from south-west side (crack initiated and partially propagated in three braces, lower beam end plastic hinges are also shown)

Figure 6.54 Plastic strain distribution of TCBF-B-2 specimen at the end of LS-DYNA simulation

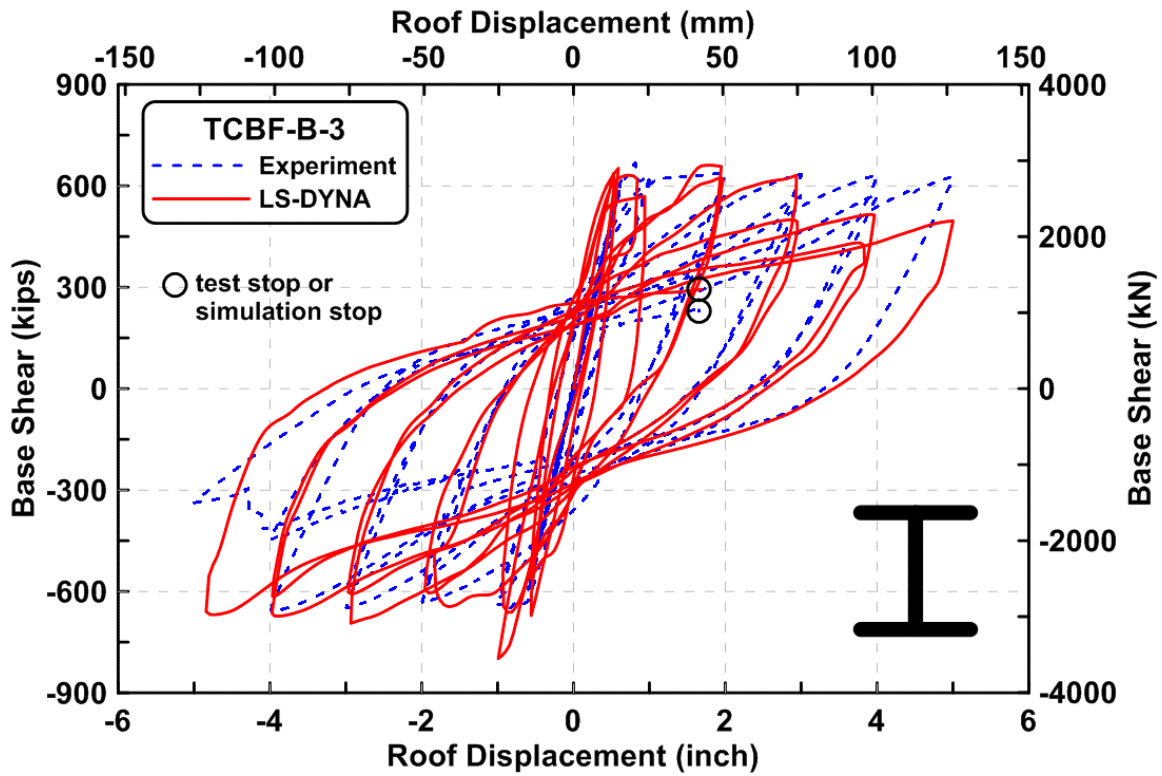


Figure 6.55 Base shear versus roof displacement from LS-DYNA simulation for TCBF-B-3 specimen

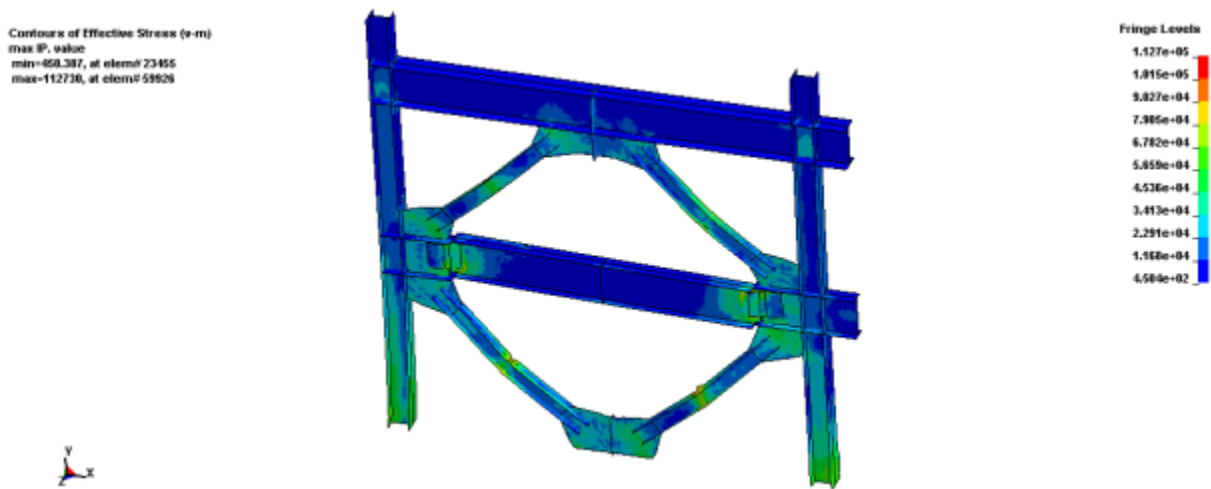
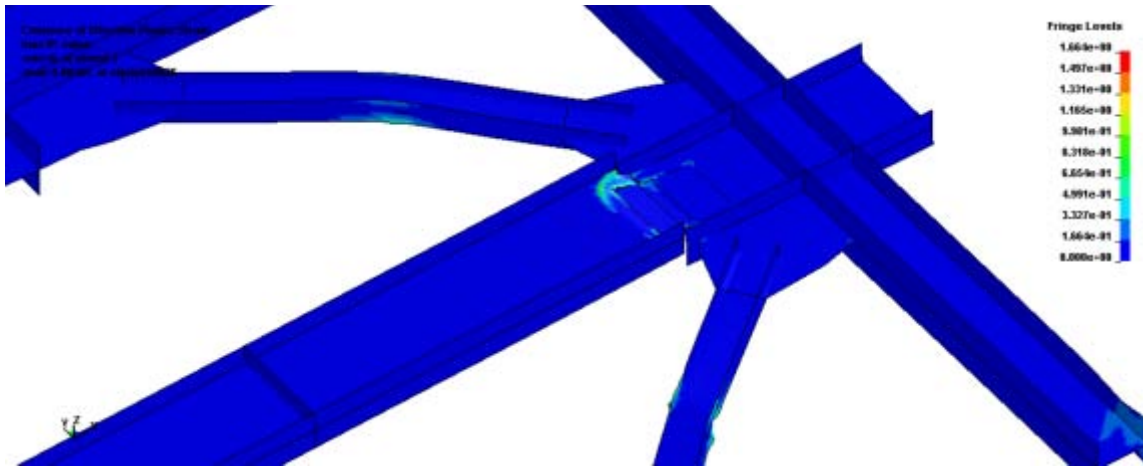
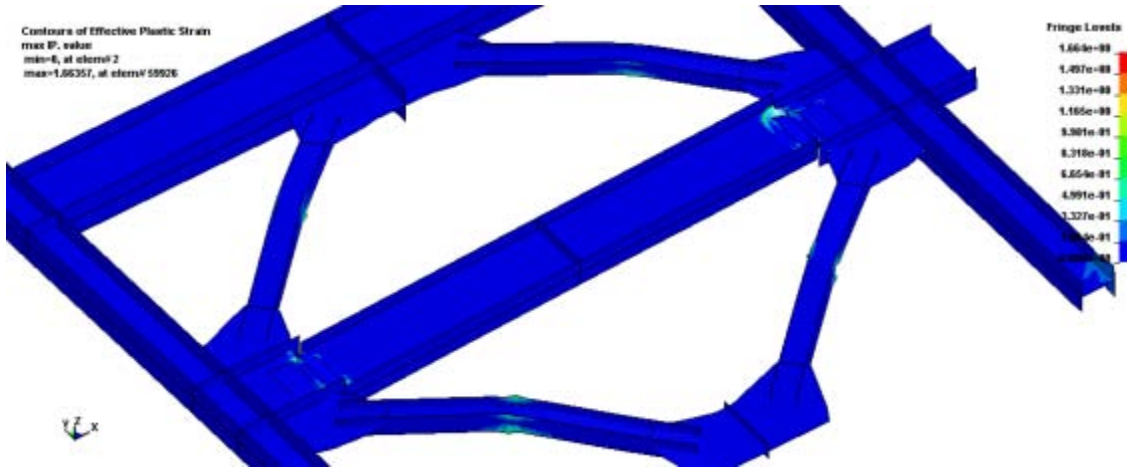


Figure 6.56 Von Mises stress distribution of TCBF-B-3 specimen at the end of LS-DYNA simulation



(a) Eastern side beam-to-gusset plate connection region  
(twisting of beam web)



(b) Overview of specimen from north-east side

**Figure 6.57 Plastic strain distribution of TCBF-B-3 specimen at the end of LS-DYNA simulation**

## 6.6 CONCLUDING REMARKS

From the specimen response comparisons discussed above, it is clear that both OpenSees and LS-DYNA can simulate global test responses with reasonable accuracy. The simulation of deterioration details and local behavior such as local buckling and member rupture is generally far better when shell models are used rather than fiber-based element models. However, the simulation time required for the OpenSees fiber based models is typically considerably shorter than that needed for the LS-DYNA model. Nonetheless, in practice, the OpenSees model seems to be a more efficient choice for predicting the global response of for large and complicated structures.

# 7 Hybrid Braced Frames: The Strong-back System

In previous chapters, the tendency of braced frames to form weak story mechanisms was identified, both in past literature and in the current test program. This limits the overall ability of concentrically braced frames to resist earthquakes safely, but making their overall safety dependent on the most severely damaged story. This chapter examines a newly developed seismic force-resisting system, the Strong-Back System (SBS). This is a hybrid system, combining the features of two types of lateral load resisting systems to achieve improved behavior, not easily achievable using either system alone. In this case, a traditional braced frame is combined with a rocking or leaning braced frame or mast. The mast acts like a “strong back” that acts to resist the formation of soft or weak story mechanisms. Its aim is to promote more or less uniform story drifts over the height of the structure, consistent with the stiffness of the mast and dynamic characteristics of the overall structure.

In this chapter, relevant literature is first reviewed to show how the hybrid concept evolved. Based on the ideas presented, three prototypes of SBSs (SB6-3, SB6-3B and SB6-3L) were designed and analyzed considering a variety of earthquake excitations. Computed responses are compared with responses for three other concentric braced frame systems. The systems used for comparison include two conventional symmetric, concentric braced frames (V6 and X6) as well as a novel asymmetric concentric double-story X braced frame (X6-3) that has similar geometry to the hybrid systems studied. Quasi-static inelastic analyses, both monotonic and cyclic, were initially conducted on these six braced frame systems to enable comparison of the fundamental hysteretic behavior of the systems under simplified loading. A series of nonlinear dynamic time-history analyses were then performed on each system to compare the system’s dynamic responses, both globally and locally.

## 7.1 INTRODUCTION

It is well-known that during strong earthquake ground shaking, conventional steel concentrically braced frames are prone to form a weak-story mechanism (Khatib et al., 1988). This concentration of deformations in one or a few stories intensifies damage to braces at these levels, leading to greater nonstructural and structural damage at these levels, and premature rupture of the braces, compared to systems with more uniform distribution of damage over height. Weak stories are also likely to have significant residual displacements, which can be costly or infeasible to repair.

Over the years, researchers and engineers have explored many ideas in an attempt to improve the behavior of braced frame systems. An obvious example is the development of buckling-restrained braces (Watanabe et al., 1988). This kind of brace significantly improves the hysteresis behavior and the energy dissipation capacity at the component level (Watanabe et al., 1988; Kalyanamaran et al., 1998 and 2003; Chen et al., 2001; Mahin et al., 2004; Lai et al., 2004). Although the entire system behavior benefits from the higher brace ductility capacity, the deformation concentration and the system’s permanent deformations are not generally

ameliorated and may be even larger than that observed in conventional concentric braced frames (Sabelli et al., 2003; Uriz and Mahin, 2008; Kiggins and Uang, 2006; Chen and Mahin, 2010).

Another component-focused strategy is that of engineered self-centering brace elements (Aiken, Nims and Kelly, 1992; McCormick et al., 2007; Christopoulos et al., 2008; Tremblay et al., 2008; Yang, DesRoches and Leon, 2010). These devices exhibit “flag pole” shaped hysteretic loops that have significant, but reduced, energy dissipation capabilities compared to buckling restrained braces with similar strength and deformation capabilities. These pinched hysteretic loops give the braces substantial re-centering characteristics that minimize the permanent deformations in the overall system. While such devices are able when properly designed to reduce residual displacements of the structural system within which they are placed, the systems are still likely to concentrate structural and nonstructural damage in one or a few stories. Moreover, many current designs for self-centering braces have a limited displacement range over which self-centering is realized, and they may not be able to fully re-center if larger displacements concentrate at one story.

As such, it is desirable to provide concentric braced frames with improved capabilities to avoid the concentration of deformations and damage in a few stories. If a system is able to mitigate soft or weak story behavior, the peak deformation demands on individual braces and maximum residual displacements might be reduced. Several approaches have been followed to modify the system behavior of braced frames to develop large deformation capacity, reduce damage concentration, and achieve smaller residual displacement. These systems include: (1) dual systems, where a moment frame is used in addition to the braced frame, (2) zipper or vertical tie bar systems, (3) rocking/uplifting systems and (4) masted or strong-back hybrid systems.

## 7.2 PREVIOUS STUDY

Building codes in the US have for many years encouraged the use of dual systems, where one system with limited ductility is provided with a backup system. In early design approaches, the primary system and the combined systems were designed to resist 100% of the lateral load required by the code, and in addition, the secondary system alone was required to carry 25% of the design seismic lateral load. Such dual systems were allowed to be used in taller structures, and in some cases designed for lower overall lateral seismic loads. With the advent of buckling restrained braces, additional interest in dual systems was raised by the possible benefit of the backup system helping reduce soft story behavior and reducing residual displacements. In these cases, independent moment-resisting frames were introduced into structural systems and combined with the existing BRB frames. Often, the moment frame employed was the columns and beams providing framing for the buckling restrained braced bays. The addition of flexible moment-resisting frames was intended to provide a partial re-centering mechanism to return the entire structure to its original position after strong earthquakes. In the studies by Kiggins and Uang (2006), it was found that using dual BRB/moment frames reduced the ductility demand slightly, and the maximum story drift was reduced about 10% to 12%. Analytical studies demonstrated significant reduction in residual drift when the dual system was used. However, when large inter-story drifts occur and both the BRB and moment frame yield, the re-centering tendencies are expected to be significantly reduced.

Previous research on reducing weak story behavior in braced frame systems was conducted at University of California, Berkeley (Khatib et al., 1988). In that study, zipper braced

frame systems and tie-bar-to-ground braced frame systems were designed to help prevent weak story mechanisms. The responses of these systems were compared with other basic braced frame systems (see Fig. 7.1). In the zipper or tie bar to ground systems, the vertical struts at the center of the bays were intended promote the formation of the same mechanism at each level. In the case of the zipper system, the unbalanced force at the center of a chevron brace pattern would normally tend to displace the beam intersected by the braces in the vertical direction. With the addition of the vertical strut, this vertical movement would be transferred to the floors above and below. In these zipper/tie-bar systems, the braces on both sides of the central strut were expected to yield, one by tensile yielding and the other through buckling. The authors showed that this approach was effective, but did not indicate how to size or proportion the vertical struts. In the tie bar to ground, they found that the unbalanced forces simply accumulated and that the vertical tie bar was required to carry large forces and its size increased so that it simply became another column in the system; that is, the system became a two bay frame with a single diagonal brace in each bay. The analytical studies found that both these systems performed better than the chevron braced frame system preferred in practice at that time.

The results of the analytical studies by Khatib et al. (1988) also demonstrated that the steel braced frame behavior was extremely sensitive to the ground motion records selected and the distribution of lateral forces used in design. It was demonstrated that behavior could be improved by using more realistic distributions of lateral force over the height of the structure, rather than simplified distributions that are a part of equivalent static lateral force design methods. Further research, such as shaking table or pseudo-dynamic tests, and more advanced analytical studies, were suggested to validate the feasibility and the superiority of these two alternative braced frame systems.

Additional zipper frame system studies have been carried out to improve the performance of this system and to develop design recommendations (e.g., Sabelli, 2001; Tirca and Tremblay, 2004; Yang, Leon and DesRoches, 2008 and 2010). In most of these studies, it was demonstrated that the vertical struts in zipper braced frames incorporating conventional buckling braces needed to be very large to prevent yielding. While elastic behavior was not a condition for the design of these vertical struts in the original work by Khatib et al., development of simple and effective design guidance for cases where these struts yielded proved difficult to formulate. Yielding of the vertical struts and higher mode effects made it difficult to achieve the desired uniform distributed story drifts. It was noted by several investigators that the zipper frame system might not be suitable for structures located in near-fault seismicity zones and in structures over four stories in height (e.g., Tirca and Tremblay, 2004).

Another approach was suggested by MacRae, Kimura and Roeder (2004). They noted that in most concentric braced frames there were a large number of gravity load-resisting columns. While these columns were often pinned at their base, they were generally spliced in such a way that they might be considered continuous for the height of the structure. Since there were many such columns, their combined stiffness and strength might be effective in minimizing soft or weak story effects. They developed equations for two-story and general multistory concentric braced frame buildings to predict moment amplifications in the columns and the increase in displacements relative to a uniform distribution over the height. They found that these elements were indeed able to reduce the soft story tendency. However, there was significant variability in the response and the number and size of columns needed to be large in some cases to provide adequate control of the formation of weak stories.



Researchers have also looked at the effectiveness of allowing concentric braced frames to rock during seismic response (Uriz and Mahin 2008; Midorikawa et al., 2010). In these cases the braced frame remained essentially elastic and energy dissipation was provided by impact or energy dissipation devices installed in the direction of the uplift. These systems were found to be effective in reducing soft story behavior and re-centering behavior was achieved. Design procedures to proportion members and to select appropriate amounts of supplemental damping are still active areas of research.

Building on the ideas related to the continuous leaning columns by MacRae, Kimura and Roeder, and uplifting/rocking braced frames, Canadian researchers proposed a modified zipper bracing configuration where a vertical strut was provided along the center of a braced bay, and framing in one half of the bay along with the vertical strut remained elastic and inelastic action in conventional braces or buckling restrained braces was permitted in the other half of the bay (Tremblay, 2003; Tremblay and Merzouq, 2004). Thus, the half of the braced bay that remains elastic and deforms like a very strong column or mast. The structural deformation shape looks essentially like a single-degree of freedom system that occurs for braced frames that uplift or rock. Incremental dynamic analyses performed by Tremblay on an eight-story building showed that although the hybrid bracing system uniformly distributed the deformation, the elastic bracing member force demands varied from two to at least fifteen times the brace force demands corresponding to the design level lateral load calculated from elastic analysis. The half of the braced bay that remains essentially elastic acts like a vertical elastic truss or strong back that attempts to achieve a uniform distribution of drifts over the height of the building. Engineers have recently applied this concept in both new constructions and retrofit projects (Mar, 2010). They found that such “trussed mast frames” or strong-back braced frames provided better performance compared to traditional braced frames and are also cost effective.

In this chapter, the trussed mast frame or strong-back system is examined in more detail. The SBS concept as described herein does not specifically incorporate a self-centering component, but self-centering braces can be used in conjunction with the system by incorporating self-centering braces, various forms of prestress, or providing additional frames that uplift. This simpler approach is pursued here to see if the avoidance of a weak story is sufficient to reduce residual displacements to tolerable levels.

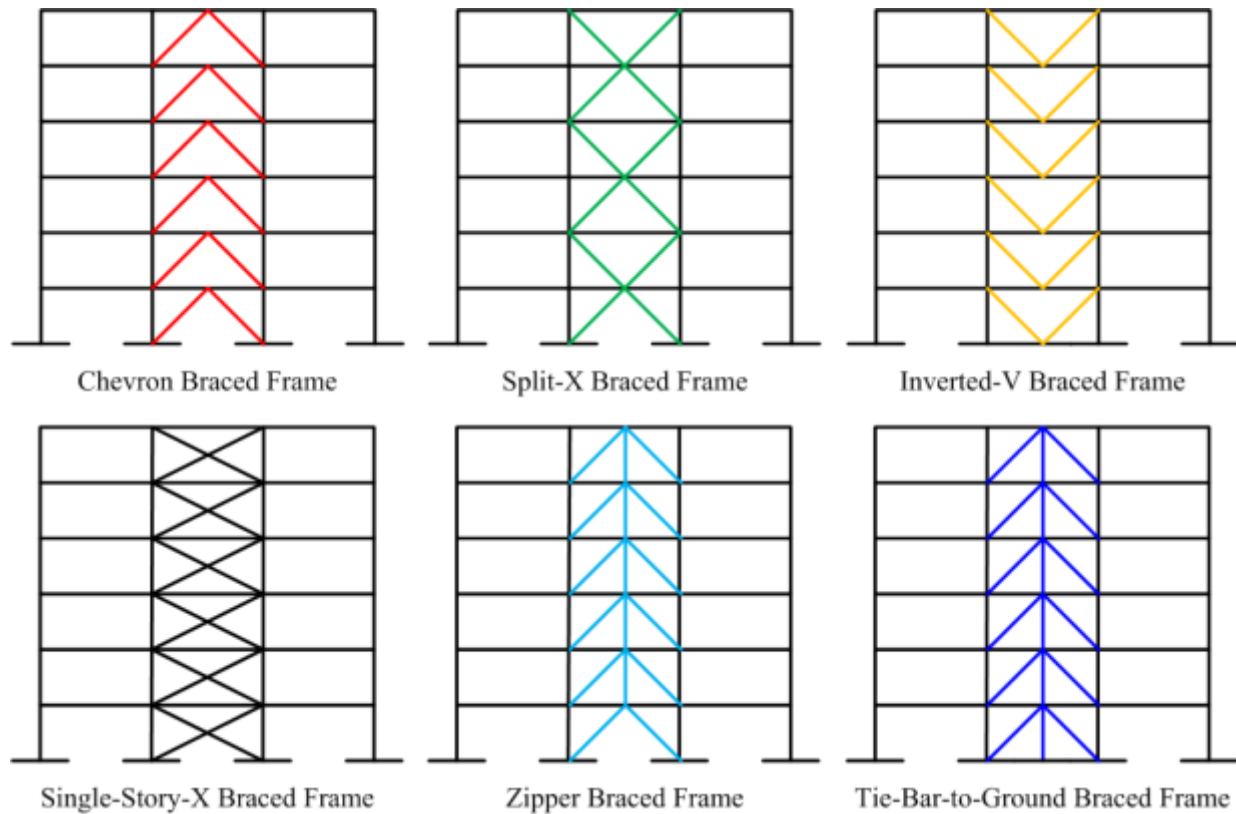


**Figure 7.1 Illustration of different braced frame systems (Khatib, Mahin and Pister, 1988)**

### 7.3 THE PROPOSED HYBRID BRACED FRAME SYSTEM

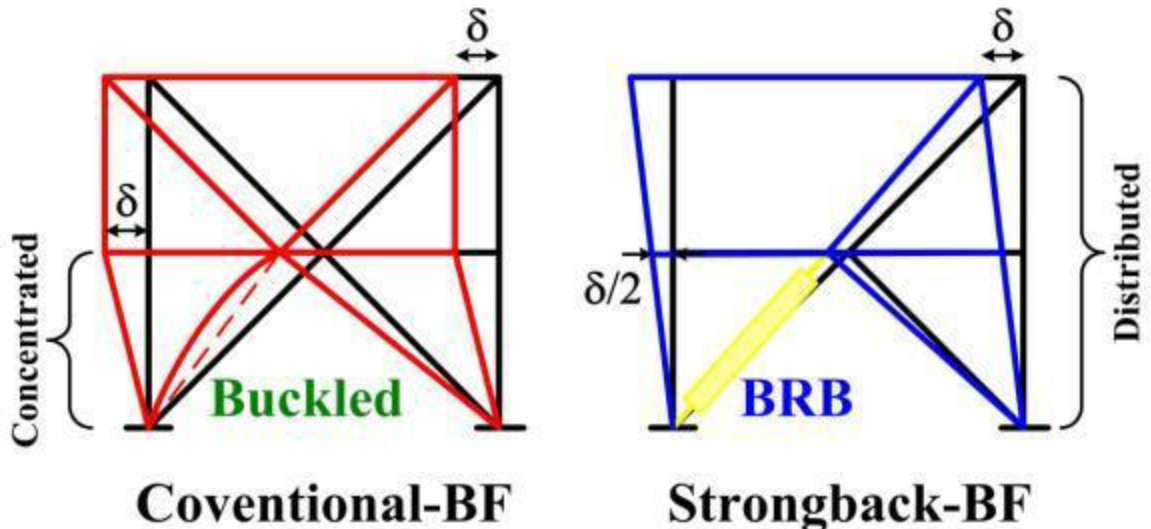
In the remainder of this chapter, the concept of a hybrid system based on the strong-back truss system (Mahin and Lai, 2008) is extended. The intent is to incorporate a vertical truss that remains elastic within a braced bay or system. The vertical elastic truss provides a strong back or mast that imposes a nearly uniform story deformation over the height of the structures (see Fig. 7.2). Other possible bracing configurations and strong-back spines are shown in Figs. 7.3 and 7.4. The braces used in the system could be either conventional, buckling restrained or self-centering braces (see Figs. 7.3 and 7.4).

For cases with chevron, inverted V or dual-story X bracing systems, the intersection of the braces at the floor beams can be shifted from the center of the beam. This can help in proportioning the load to the various members in the SBS. In the cases considered herein, vertical elastic truss portion of the bay is narrower than half the bay width. This makes the inelastic elements longer so that they have greater length over which to yield, but the sizes in the spine may need to become larger than customary. However, by reducing the inclination of the inelastic braces, they can be smaller to resist the same load. Moreover, for large lateral displacements of the frame, the increased length of the beam in the inelastic portion of the bay will be longer, reducing its shear and the plastic hinge rotations that might form at the ends of the beams.

In one of the cases examined below, low-yield strength steel is used in the buckling restrained bracing members. It has been noted that frames with buckling restrained braces are

often larger than those for SCBF systems since the area of steel in the braces is less, resulting in a more flexible (longer period) and weaker system. By using lower strength steel, more steel is required for the same strength, and the flexibility and period are reduced. Depending on the period range, this may increase the amount of steel needed even more. The intent of using the low strength steel is to increase the stiffness and decrease the displacement of the system without increasing the strength by a large amount. High strength steel could be considered for portions of the structure not expected to yield. Low-yield strength steel is available in current market and usually has lower yield-to-tensile ratio compared with other grades of steel. The lower yield-to-tensile ratio typically implies the material has higher potential to deform between first significant yielding and material tensile failure. This provides a buffer, redistributing the member forces to other members without failure. Members made of low-yield strength steels usually have larger cross-sectional areas compared to those made of normal strength steels (assuming the force demands are similar). This is also an advantage when proportioning member sizes and tuning the stiffness ratios within the structural system.

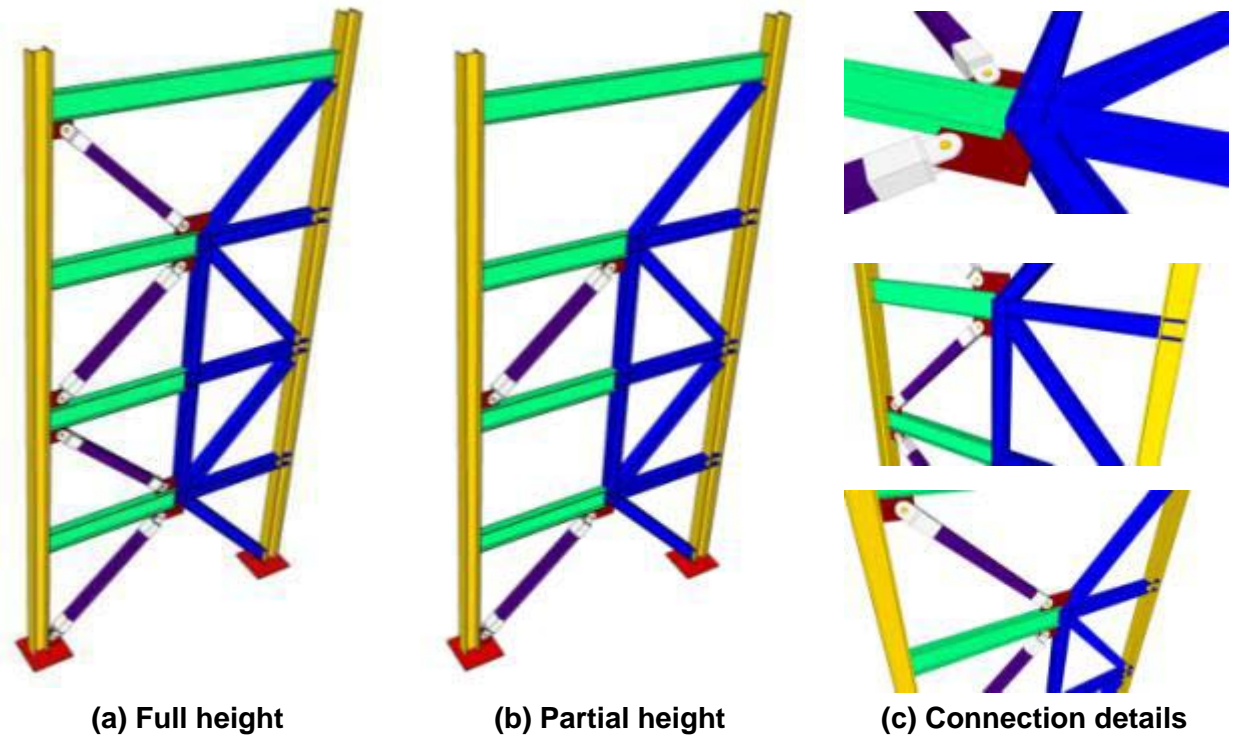
The following sections assess the SBS's performance by comparing their dynamic responses with several more conventional braced frame systems subjected to different hazard level ground motions. Quasi-static monotonic and cyclic analysis results are also presented.



(a) Concentrated drift in conventional braced frame system

(b) More uniform drift in braced frame with strong-back system

Figure 7.2 Comparison of concentrically braced frame drifts with and without strong-back concept

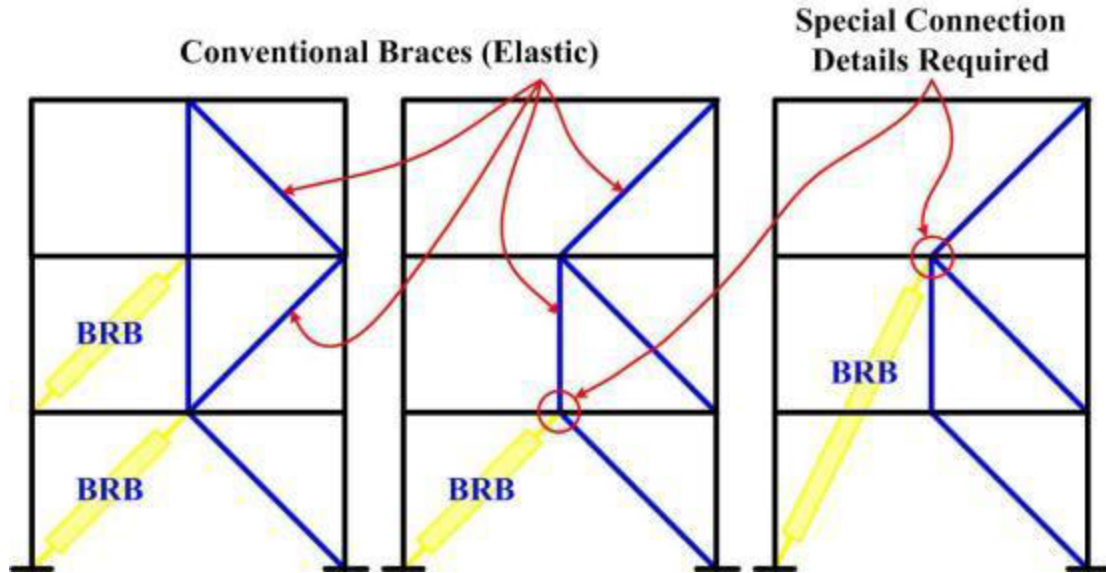


(a) Full height

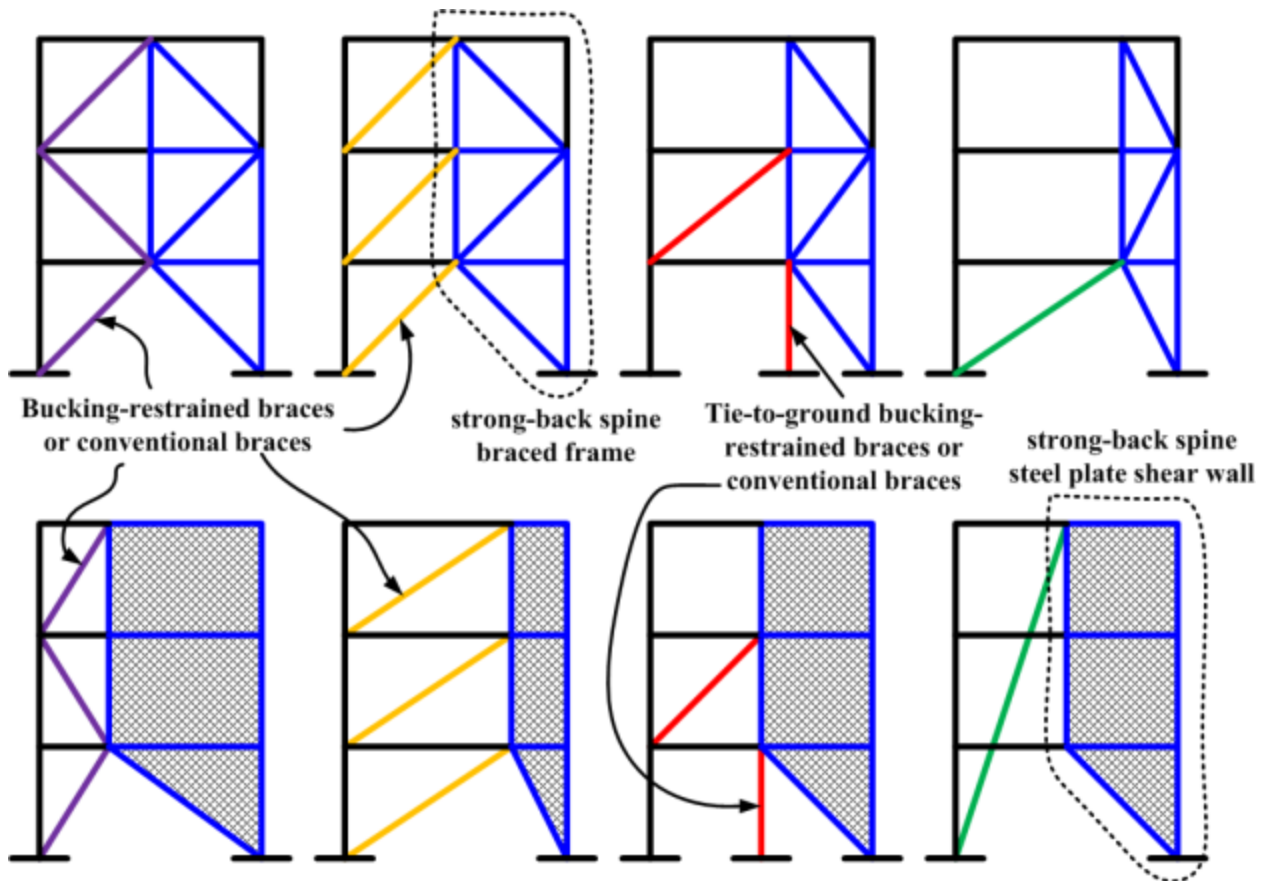
(b) Partial height

(c) Connection details

Figure 7.3 Possible strong-back configuration details with buckling-restrained braces along the entire or partial height of the building



(a) Different strong-back system configurations with buckling-restrained braces



(b) Different strong-back spine configurations with conventional braces or buckling-restrained braces

Figure 7.4 More possible strong-back configurations with different spine systems

## 7.4 ANALYTICAL STUDY OF THE STRONG-BACK SYSTEM

In this section, a comparison is made of the inelastic responses of the proposed hybrid SBS with those for more common braced frame systems. The example building, seismic force-resisting systems, and some basic assumptions will be introduced, the quasi-static monotonic and cyclic analyses results presented, and finally nonlinear response history analyses of each system will be compared for different hazard level ground motions.

### 7.4.1 Example Building

The six-story model building used in these studies is shown in Fig. 7.5. Its seismic force-resisting systems in both directions are indicated. Each direction had five beam spans. Bay widths are equal to 30 ft. Each story is 13 ft high, except the ground story, which is 18 ft high. The same site location and site conditions were used as described in Chapter 3. The following criteria applied:

Governing Code: ASCE-7-2005

Occupancy: Typical Office Building

Location: Downtown Berkeley, zip code 94720

Site Class: D

Floor Height: Ground Story = 18-ft; all other stories = 13-ft

Typical Bay Size: 30-ft by 30-ft

Dead Load: 100 psf

Live Load: 50 psf

And the seismic design coefficients are briefly summarized below:

Importance Factor,  $I$ : 1.0

Seismic Design Category: D

Site Class: D

Response Modification Factor,  $R$ : 6

System Overstrength Factor,  $\Omega_o$ : 2.0

Deflection Amplification Factor,  $C_d$ : 5.0

$S_1$ : 0.787

$S_S$ : 2.014

$F_a$ : 1.0

$F_v$ : 1.5

$S_{D1}$ : 0.787

$S_{DS}$ : 1.343

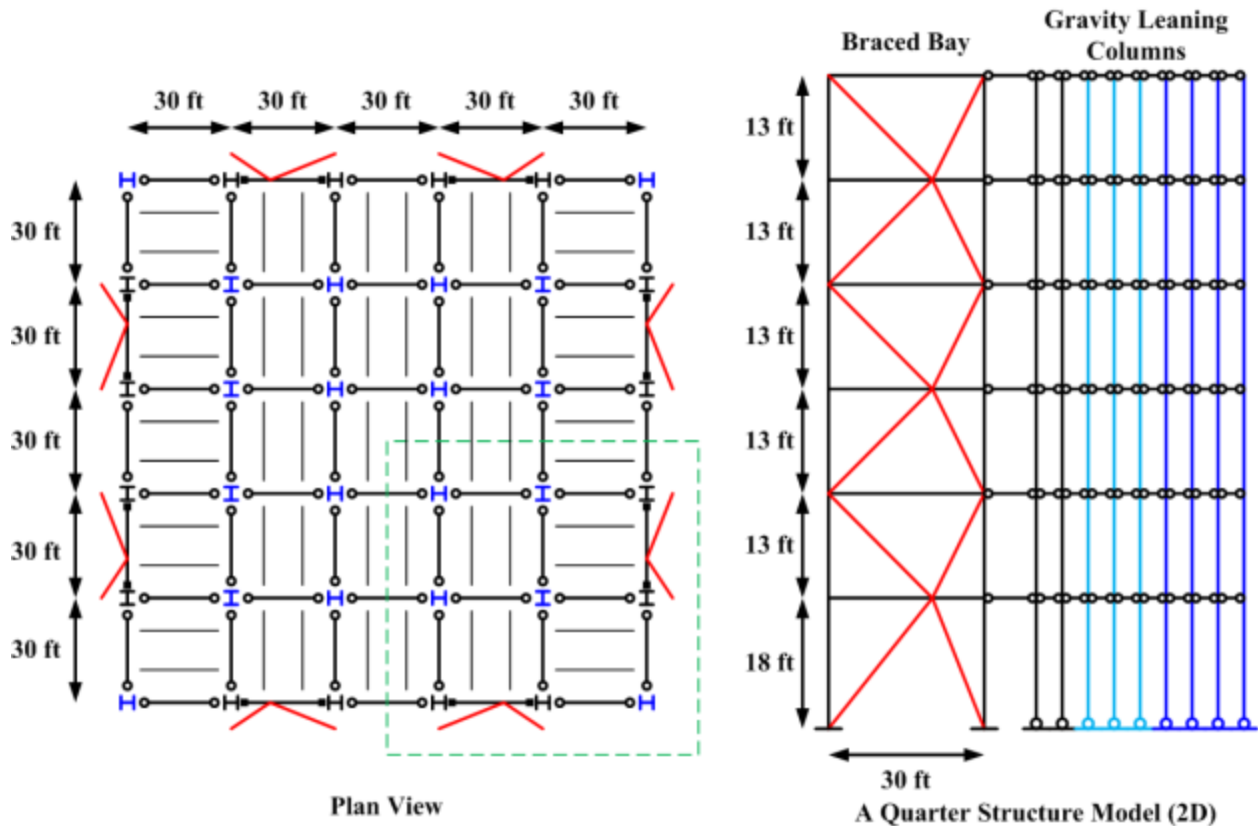


Figure 7.5 Plan view of the example building and the two-dimensional model elevation

### 7.4.2 Seismic Force-Resisting Systems and Design Strategies

A total six different configurations of seismic force-resisting systems were selected for this study (see Fig. 7.6). Table 7.1 summarizes the braced frame systems considered. The V6 model—a typical stacked chevron bracing configuration—was used as the benchmark. The two-story split-X bracing configuration (model X6) was selected as representative of another typical configuration. A transformed model (model X6-3) is basically the same as Model X6, but the meeting points of braces are shifted from the beam middle points to the one-third points. Each direction of the prototype building has four braced bays (two at each perimeter face). To ensure a symmetric lateral force-resisting system, the shifted points are aligned about the centerline of the elevation. That is, if one bay has a yielding/buckling braced inclined to the left, the other bay has the corresponding brace inclined to the right. Design of these three braced frame systems basically follows the ASCE-07 and the AISC Seismic Provisions.

System X6-3 was transformed to SBS SB6-3 by incorporating a vertical tie-column along the height of the braced bay from the second story to the fifth story. This completes the vertical spine. In addition to the basic design requirements stipulated in ASCE-07 and the AISC Seismic Provisions, the members in the vertical elastic truss were designed to remain essentially elastic under the design level seismic forces. The simple concept used here for design is based on the system code specified over-strength factor, which is 2.0 for this case. Member stress checks were performed in SAP2000 using the load combinations listed in ASCE-07. Stress ratios in members within the vertical spine were specified to be less than 0.5, which is the reciprocal of

the system overstrength factor for special concentrically braced frames. All tie-columns use the same member size for their full height. Although the vertical spine was designed to essentially remain elastic, it was expected that under severe ground shaking some members in the vertical spine would be subjected to inelastic demands. One of the reasons behind using this simple design strategy is to design a system that achieves the goal of preventing deformation concentration in the system at little increased cost. It is acknowledged that design optimization based on the performance goals is possible, but is not within the scope of this study.

The bracing members in Models V6, X6, X6-3, and SB6-3 were all conventional buckling braces. Hysteresis behaviors of buckling braces are typically non-symmetric and severe degradations of compression strengths are usually observed under cyclic loadings. As mentioned above, BRBs have nearly symmetric hysteresis loops and stable energy dissipation characteristics. As a result, BRBs are used in the SBS outside the vertical spine, as shown in model SB6-3B of Fig. 7.6 ( $F_{y, \text{brb}} = 42$  ksi). Model SB6-3L is essentially the same as model SB6-3B, except the materials used in the steel cores of BRBs were composed of low-yield strength steels ( $F_{y, \text{brb}} = 15$  ksi). The design strategy of the vertical spine in these two models was the same as for model SB6-3. The selection procedures for the steel cores of the BRBs followed the Steel Tips report by Lopez and Sabelli (2004). Note that the stiffness modification factors were taken as 1.3 for the first-story BRB and 1.4 for all other stories. These were applied in the structural analysis phase to account for the variation in steel core area from the yielding core to the enlarged attachment regions at the brace ends. Tables 7.2 to 7.7 list the member size for each model.



**Table 7.1 Six-story model building with different seismic force-resisting systems**

Model Number	Structural System Descriptions	ID	Note
1	six-story Chevron brace configuration	V6	Benchmark
2	six-story double story split-X brace configuration	X6	
3	six-story double story split-X brace configuration meeting at one-third point of beam span	X6-3	
4	six-story strong-back brace configuration meeting at one-third point of beam span	SB6-3	
5	six-story strong-back brace configuration meeting at one-third point of beam span with buckling-restrained braces using normal yield strength steel cores	SB6-3B	$F_{y, brb} = 42 \text{ ksi}^*$ $F_{u, brb} = 58 \text{ ksi}$
6	six-story strong-back brace configuration meeting at one-third point of beam span with buckling-restrained braces using low-yield strength steel cores	SB6-3L	$F_{y, brb} = 15 \text{ ksi}$ $F_{u, brb} = 38 \text{ ksi}$

(\*Note: the  $F_{y, brb} = 42 \text{ ksi}$  is calculated from the average of upper bound and lower bound BRB steel core yield strength typically used in practice, where  $38 \text{ ksi} \leq F_{y, brb} \leq 46 \text{ ksi}$ )

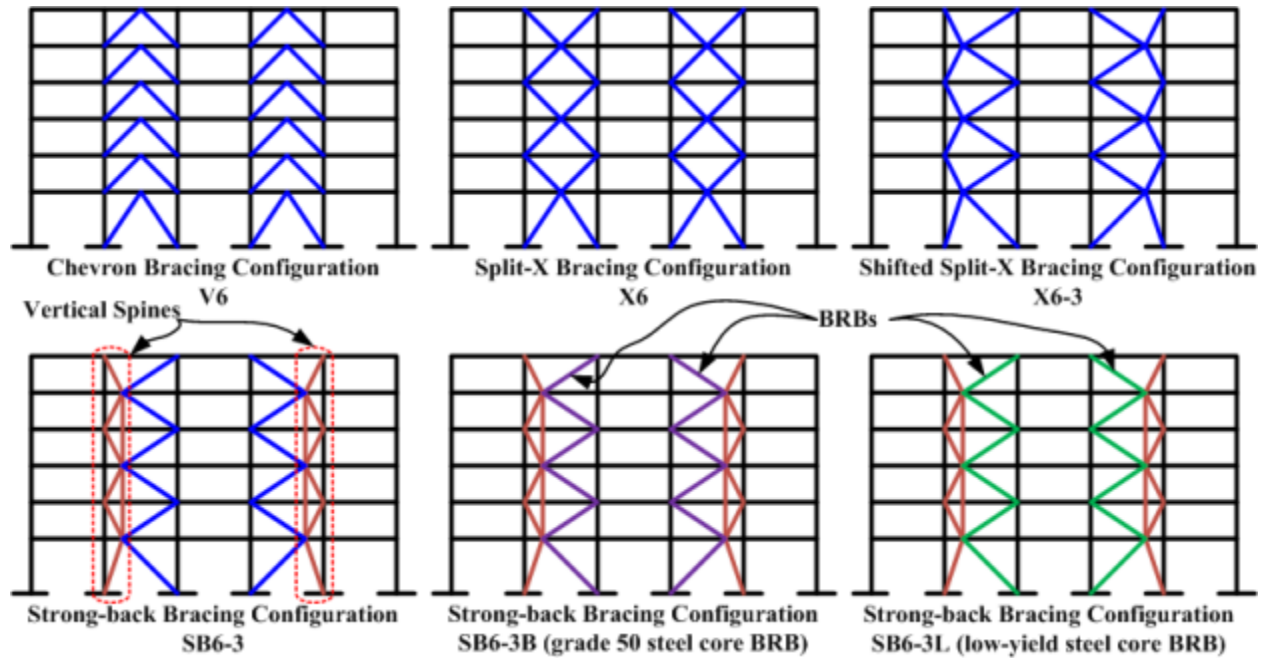


**Figure 7.6 Elevation views of six different bracing configurations**

**Table 7.2 Model V6 Member Size Information**

Story	Braced Bay Column	Braced Bay Beam	Brace	Gravity Column (corner)	Gravity Column (interior)	Gravity Beam
1	W14x342	W36x282	HSS10x10x5/8	W14x68	W14x68	W18x71
2	W14x342	W30x261	HSS9x9x5/8	W14x68	W14x68	W18x71
3	W14x342	W30x261	HSS8x8x1/2	W14x68	W14x132	W18x71
4	W14x132	W27x217	HSS8x8x1/2	W14x68	W14x132	W18x71
5	W14x132	W27x217	HSS7x7x1/2	W14x68	W14x132	W18x71
6	W14x132	W27x161	HSS6x6x1/2	W14x68	W14x132	W18x71

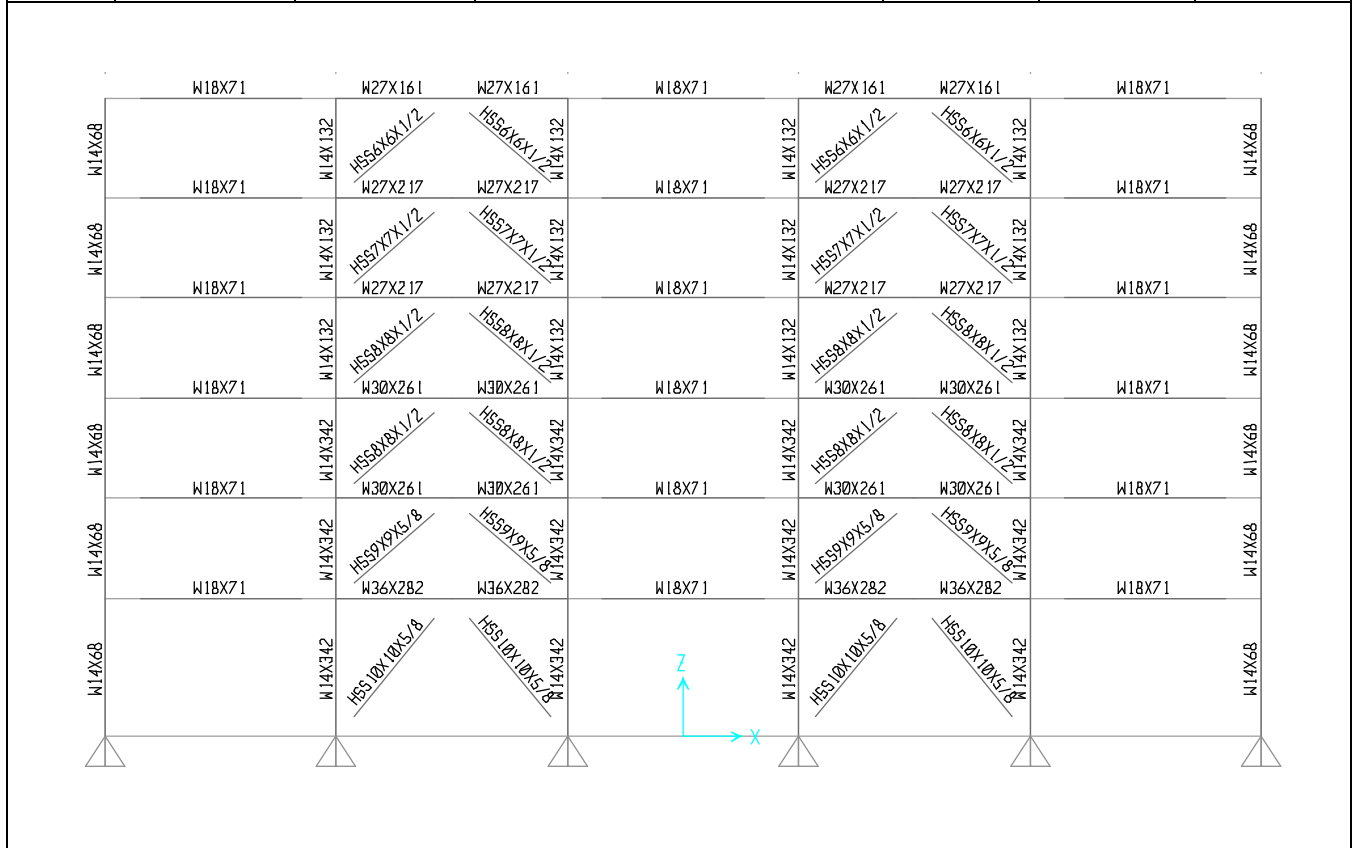


**Table 7.3 Model X6 Member Size Information**

Story	Braced Bay Column	Braced Bay Beam	Brace	Gravity Column (corner)	Gravity Column (interior)	Gravity Beam
1	W14x342	W18x86	HSS10x10x5/8	W14x68	W14x68	W18x71
2	W14x342	W18x86	HSS9x9x5/8	W14x68	W14x68	W18x71
3	W14x342	W18x86	HSS8x8x1/2	W14x68	W14x132	W18x71
4	W14x132	W18x86	HSS8x8x1/2	W14x68	W14x132	W18x71
5	W14x132	W18x86	HSS7x7x1/2	W14x68	W14x132	W18x71
6	W14x132	W18x86	HSS6x6x1/2	W14x68	W14x132	W18x71

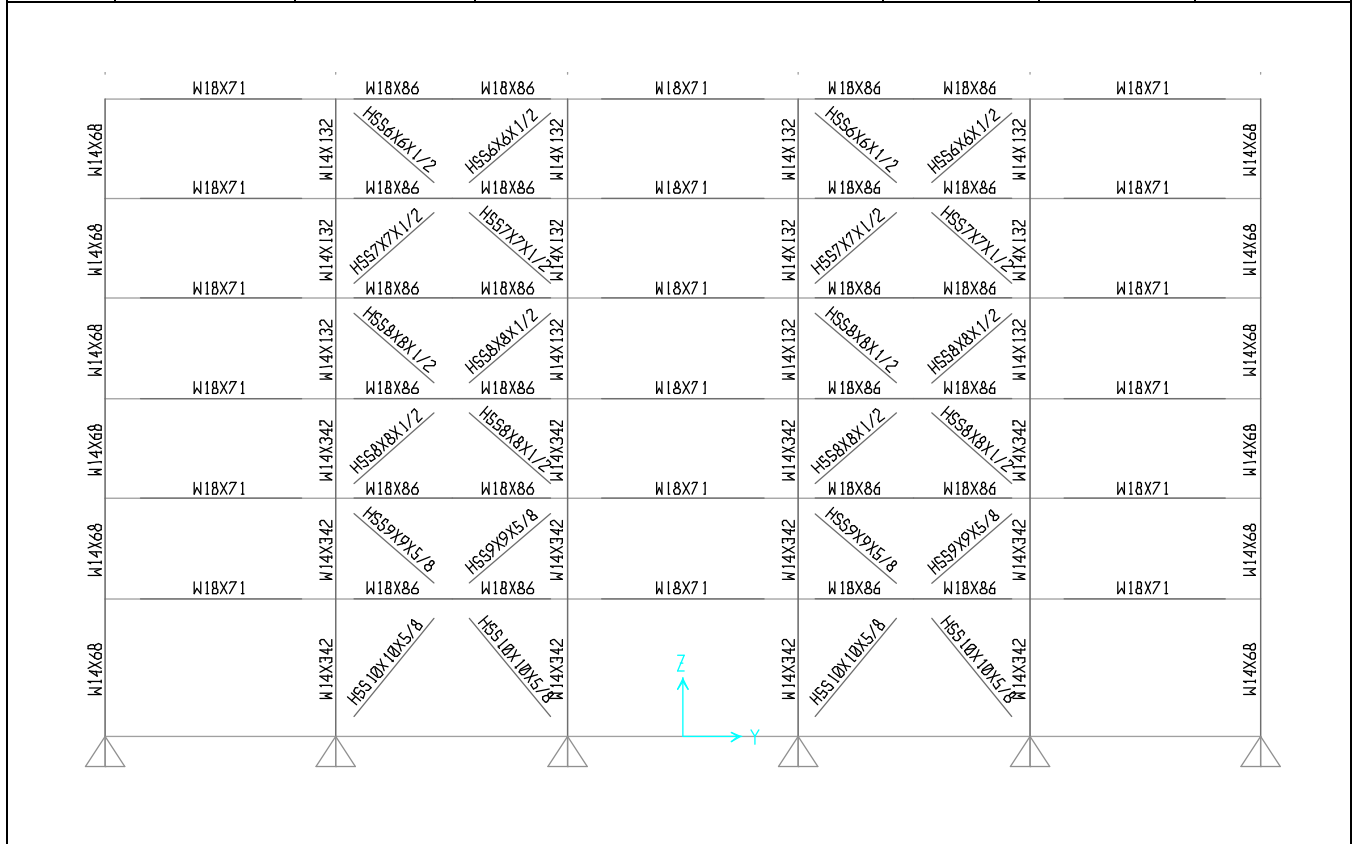


**Table 7.4 Model X6-3 Member Size Information**

Story	Braced Bay Column	Braced Bay Beam	Brace		Gravity Column (corner)	Gravity Column (interior)	Gravity Beam
1	W14x342	W18x86	HSS12x12x5/8	HSS9x9x5/8	W14x68	W14x68	W18x71
2	W14x342	W18x86	HSS10x10x5/8	HSS9x9x5/8	W14x68	W14x68	W18x71
3	W14x342	W18x86	HSS9x9x5/8	HSS8x8x1/2	W14x68	W14x132	W18x71
4	W14x132	W18x86	HSS9x9x5/8	HSS8x8x1/2	W14x68	W14x132	W18x71
5	W14x132	W18x86	HSS8x8x1/2	HSS6x6x1/2	W14x68	W14x132	W18x71
6	W14x132	W18x86	HSS7x7x1/2	HSS5x5x1/2	W14x68	W14x132	W18x71

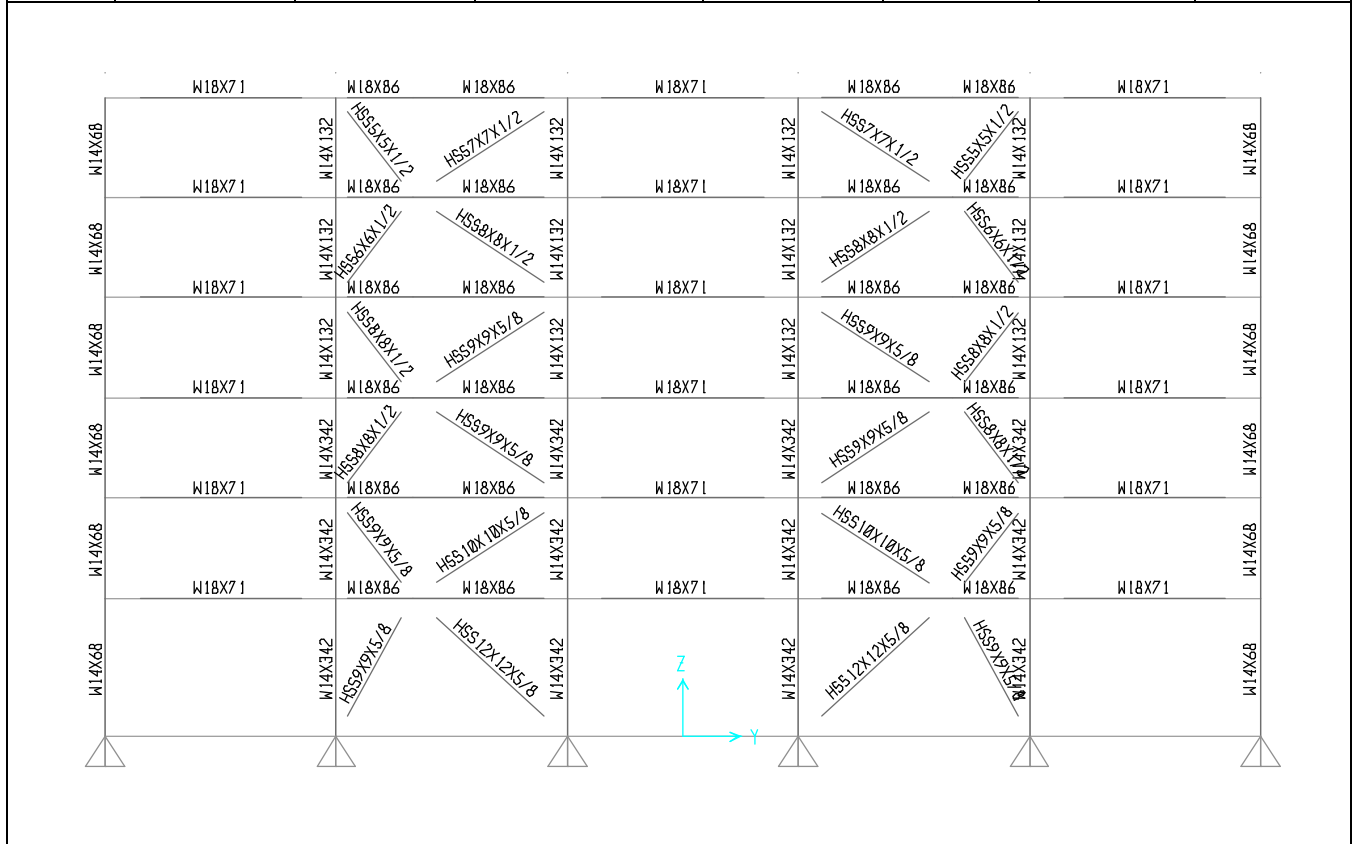


**Table 7.5 Model SB6-3 Member Size Information**

Story	Braced Bay Column	Braced Bay Beam	Brace and Tie-Column			Gravity Column (corner)	Gravity Column (interior)	Gravity Beam
1	W14x342	W18x86	HSS 12x12x5/8	-	W14x132	W14x68	W14x68	W18x71
2	W14x342	W18x86	HSS 10x10x5/8	HSS 5x5x1/2	HSS 12x12x5/8	W14x68	W14x68	W18x71
3	W14x342	W18x86	HSS 9x9x5/8	HSS 5x5x1/2	HSS 12x12x5/8	W14x68	W14x132	W18x71
4	W14x132	W18x86	HSS 9x9x5/8	HSS 5x5x1/2	HSS 10x10x1/2	W14x68	W14x132	W18x71
5	W14x132	W18x86	HSS 8x8x1/2	HSS 5x5x1/2	HSS 10x10x1/2	W14x68	W14x132	W18x71
6	W14x132	W18x86	HSS 7x7x1/2	-	HSS 5x5x1/2	W14x68	W14x132	W18x71

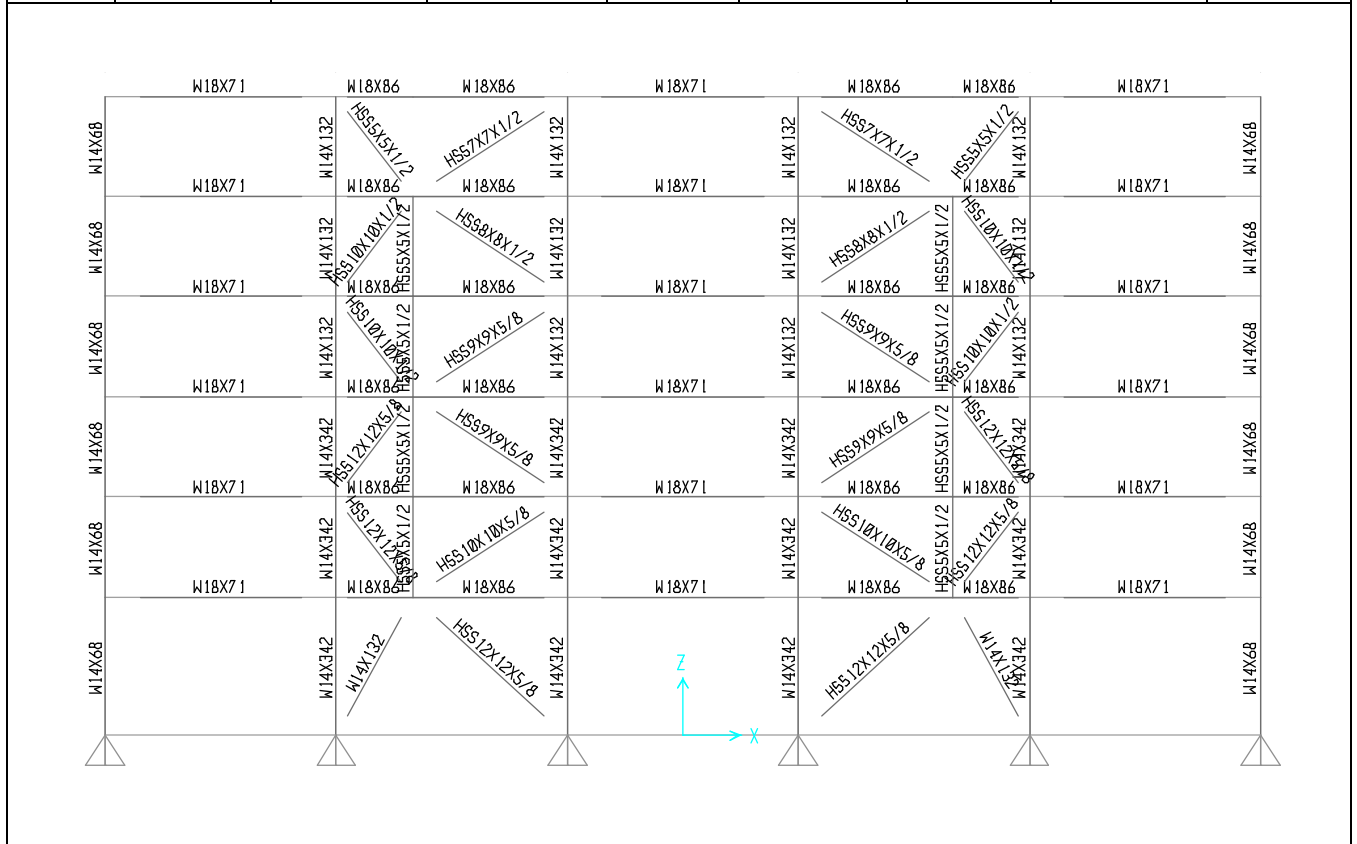


**Table 7.6 Model SB6-3B Member Size Information**

Story	Braced Bay Column	Braced Bay Beam	Brace and Tie-Column			Gravity Column (corner)	Gravity Column (interior)	Gravity Beam
			BRB	HSS	HSS			
1	W14x342	W18x86	BRB 18 in <sup>2</sup>	-	W14x132	W14x68	W14x68	W18x71
2	W14x342	W18x86	BRB 16 in <sup>2</sup>	HSS 5x5x1/2	HSS 12x12x5/8	W14x68	W14x68	W18x71
3	W14x342	W18x86	BRB 14 in <sup>2</sup>	HSS 5x5x1/2	HSS 12x12x5/8	W14x68	W14x132	W18x71
4	W14x132	W18x86	BRB 12 in <sup>2</sup>	HSS 5x5x1/2	HSS 10x10x1/2	W14x68	W14x132	W18x71
5	W14x132	W18x86	BRB 8 in <sup>2</sup>	HSS 5x5x1/2	HSS 10x10x1/2	W14x68	W14x132	W18x71
6	W14x132	W18x86	BRB 4 in <sup>2</sup>	-	HSS 5x5x1/2	W14x68	W14x132	W18x71

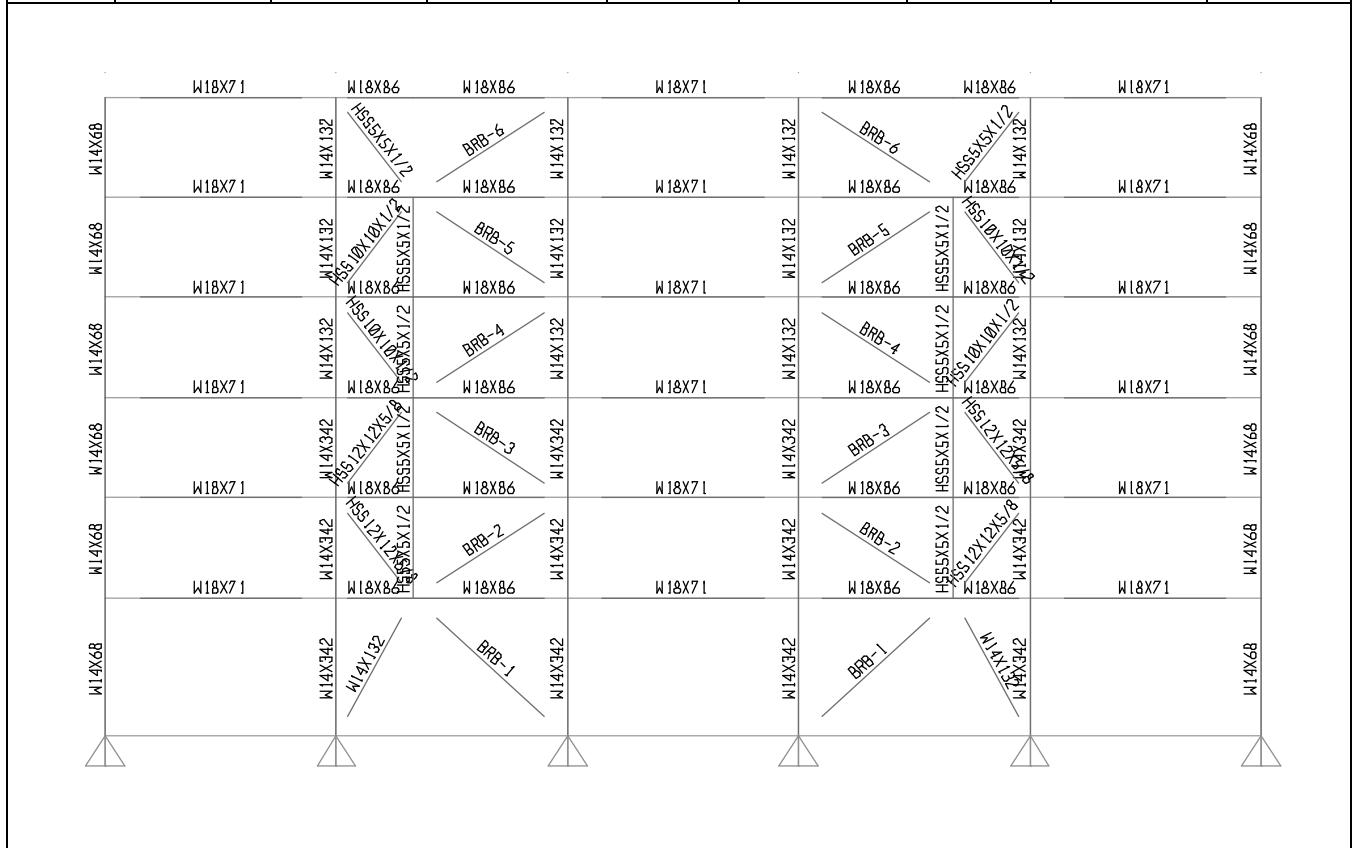
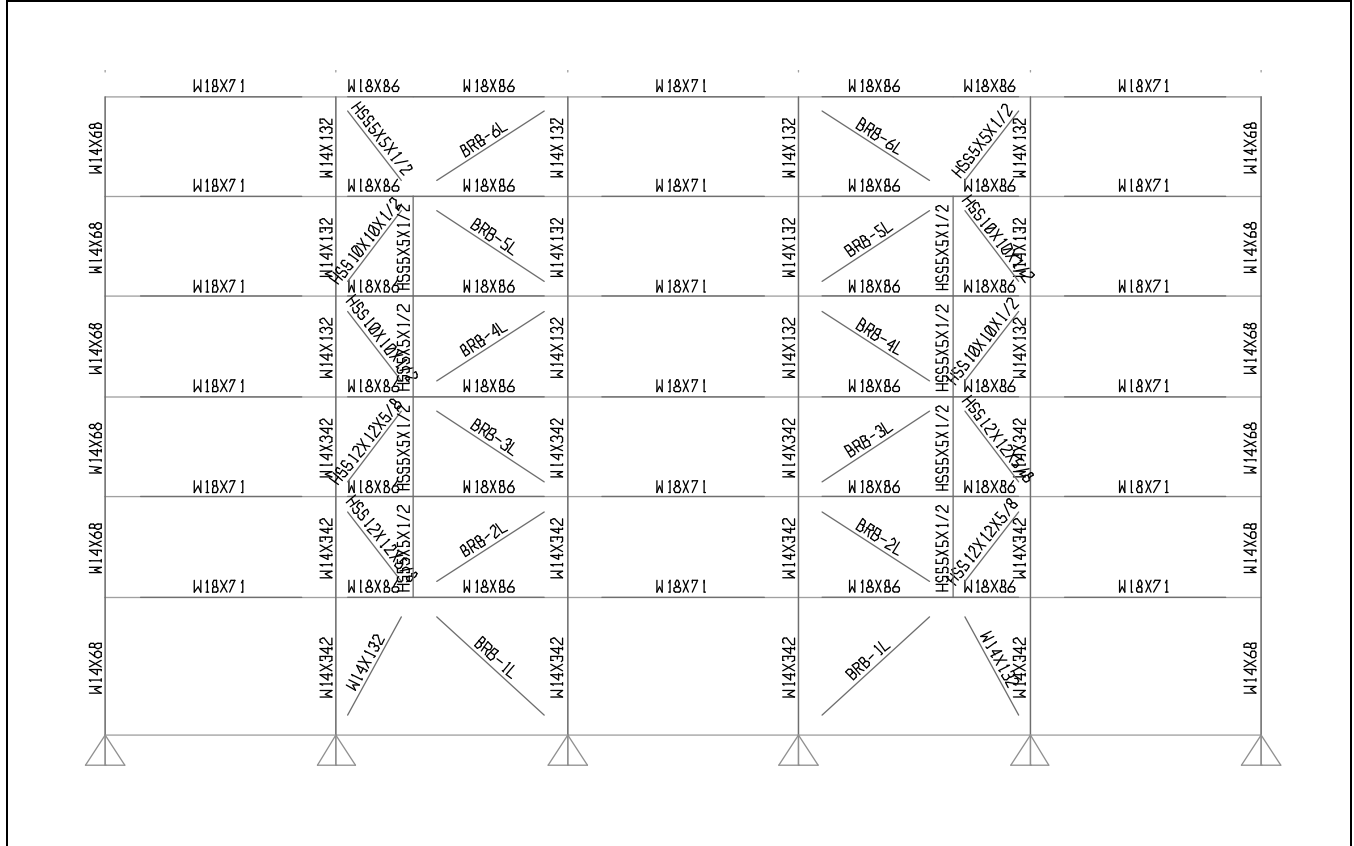


**Table 7.7 Model SB6-3L Member Size Information**

Story	Braced Bay Column	Braced Bay Beam	Brace and Tie-Column			Gravity Column (corner)	Gravity Column (interior)	Gravity Beam
1	W14x342	W18x86	BRB-LYS* 70 in <sup>2</sup>	-	W14x132	W14x68	W14x68	W18x71
2	W14x342	W18x86	BRB-LYS 62 in <sup>2</sup>	HSS 5x5x1/2	HSS 12x12x5/8	W14x68	W14x68	W18x71
3	W14x342	W18x86	BRB-LYS 50 in <sup>2</sup>	HSS 5x5x1/2	HSS 12x12x5/8	W14x68	W14x132	W18x71
4	W14x132	W18x86	BRB-LYS 46 in <sup>2</sup>	HSS 5x5x1/2	HSS 10x10x1/2	W14x68	W14x132	W18x71
5	W14x132	W18x86	BRB-LYS 30 in <sup>2</sup>	HSS 5x5x1/2	HSS 10x10x1/2	W14x68	W14x132	W18x71
6	W14x132	W18x86	BRB-LYS 16 in <sup>2</sup>	-	HSS 5x5x1/2	W14x68	W14x132	W18x71



(\*Note: LYS stands for low-yield strength steel)

### 7.4.3 Modeling

Two-dimensional computer models were developed in OpenSees using the same modeling concepts described in Section 6.2. Because of symmetry, only a quarter of the building was included in the analytical model. The braced bay was modeled and the gravity columns modeled as leaning columns aside the braced bay, as illustrated in Fig. 7.5 right. The leaning columns were pinned at the base and individually modeled for each gravity column line in OpenSees. All leaning columns were connected at each floor level using rigid links. Tributary gravity forces at each floor level were added for the corresponding nodal points of leaning columns. Monotonic and, cyclic quasi-static analyses, and nonlinear time history analyses were performed for each structural system (Models V6, X6, X6-3, SB6-3, SB6-3B, and SB6-3L). A Rayleigh damping parameter of 2% was used for both first and second mode for all six analyses. Initial imperfections equal to 1/1000 of brace entire length was used in the models for all conventional buckling braces. Rigid end zones were applied at member ends based on the actual member sizes in the models. Pinned connections were assumed at every brace end.

### 7.4.4 Ground Motions

Ground motions for dynamic analysis were selected from the PEER Ground Motion Database (Beta version, [http://peer.berkeley.edu/peer\\_ground\\_motion\\_database/](http://peer.berkeley.edu/peer_ground_motion_database/)). Two different hazard levels were considered: design level ground motion (10% probability of exceedance in 50 years) and maximum consider level ground motion (2% probability of exceedance in 50 years). Each hazard level contained five pairs of ground motions, representing the fault normal and fault parallel components. This results in ten excitations being considered for the 2D model analyzed. Vertical components of ground motions were not included in this study.

Each ground motion pair is selected using the online ground motion database searching tool with predefined record acceptance criteria. The scale factors of the ground motions are limited to be less than three. Table 7.8 summarizes the criteria used in the search engine. Each pair of ground motions is summarized in Table 7.9. Scaled average spectral acceleration of selected ground motion records are plotted in Fig. 7.7 with the target spectrum (for design level ground motions). The scale factors for the maximum consider level ground motions are simply 1.5 times the scale factors for the design level ground motions.



**Table 7.8 Predefined ground motion search criteria**

Criteria	Magnitude (min.)	Magnitude (max.)	$V_{S30}$ (m/sec)	Fault Type	Weighted Period Range (min. ~ max.)	Scale Factor
Values	5.0	7.5	182 ~ 366	Strike Slip (SS)	0.2T ~ 1.5T	< 3.0

(Note: T is the fundamental period of the structure, T = 0.6 sec. is used for six-story structures in this case)

**Table 7.9 Selected ground motion pairs for nonlinear dynamic response history analysis**

NGA No.	Event	Year	Magnitude	Mechanism	$V_{S30}$ (m/sec)	$R_{rup}$ (km)	Scale Factor
160	Imperial Valley-06	1979	6.53	Strike-Slip	223	2.7	0.8848
1119	Kobe- Japan	1995	6.9	Strike-Slip	312	0.3	0.9566
558	Chalfant Valley-02	1986	6.19	Strike-Slip	271.4	7.6	1.2984
1853	Yountville	2000	5.0	Strike-Slip	271.4	11.4*	1.5067
1602	Duzce- Turkey	1999	7.14	Strike-Slip	326	12	1.0469

(Note:  $R_{rup}$  with asterisk is estimated value)

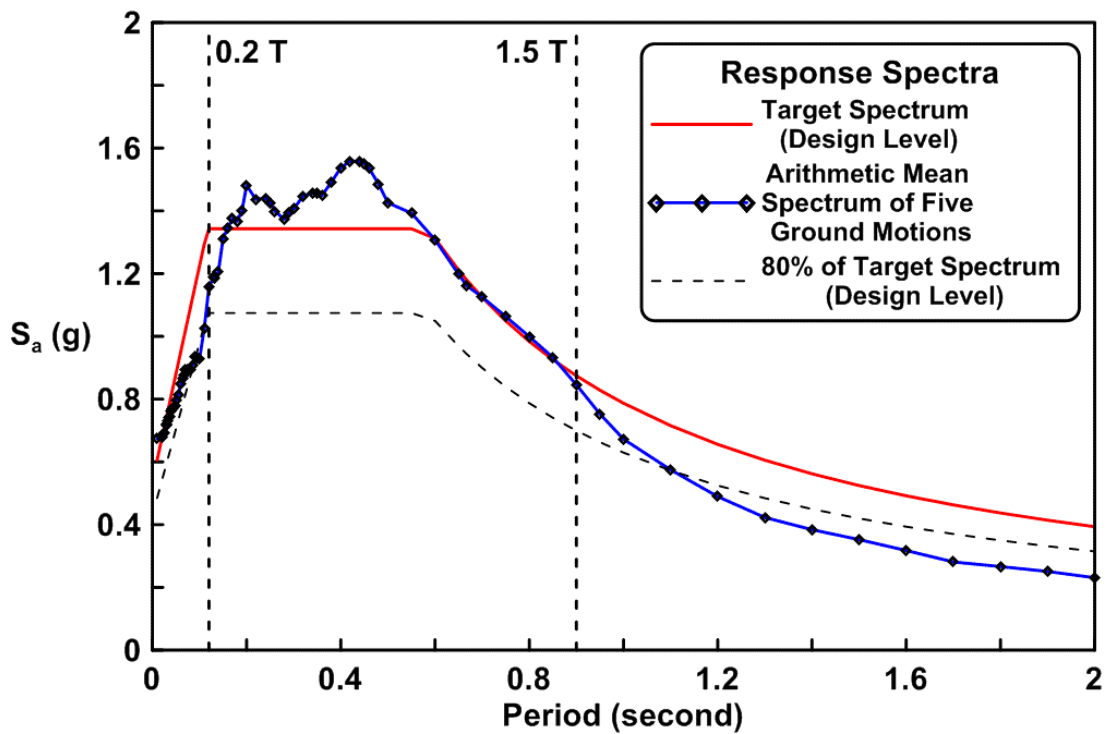


**Figure 7.7 Averaged spectrum of selected ground motion records**

## 7.5 RESPONSE OF HYBRID STRONG-BACK SYSTEM

### 7.5.1 Monotonic Pushover Results

Static pushover analyses were performed on the six models using OpenSees with a control node at the roof level of the example building. The target displacement was set to be equal to 5% roof drift, which in this case corresponds to 49.8 in. An inverted triangle lateral force distribution was maintained during the pushover analyses. Monotonic pushover curves are shown in Fig. 7.8. Note that all models were pushed in the positive direction. And the gravity forces were included in the analytical models.

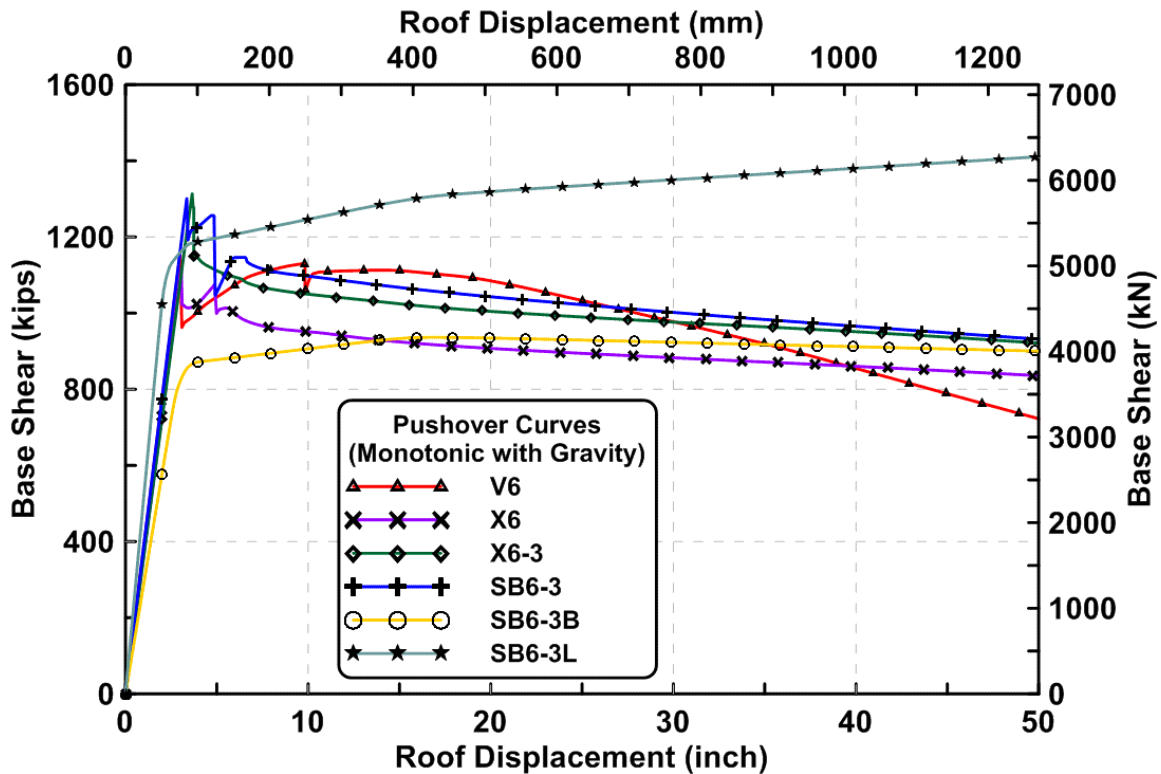


Figure 7.8 Base shear versus roof displacement relationships of six models

### 7.5.2 Quasi-static Cyclic Results

In addition, cyclic analyses were performed in OpenSees for all six models. The pre-defined cyclic target roof displacements are listed in Table 7.10 for all six models. Similar to monotonic pushover analyses, an inverted triangle lateral force distribution was applied during the cyclic loading. Hysteretic curves with including gravity effects are shown in Fig. 7.9 for each model.

**Table 7.10 Prescribed roof displacements for cyclic pushover analyses**

<b>Sequence Number</b>	<b>Number of Cycle</b>	<b>Target Roof Displacement (inch)</b>	<b>Corresponding Roof Drift Ratio (%)</b>
1	2	±2.99	±0.3
2	2	±4.98	±0.5
3	2	±9.96	±1.0
4	2	±19.92	±2.0
5	2	±29.88	±3.0
6	2	±39.84	±4.0
7	2	±49.8	±5.0

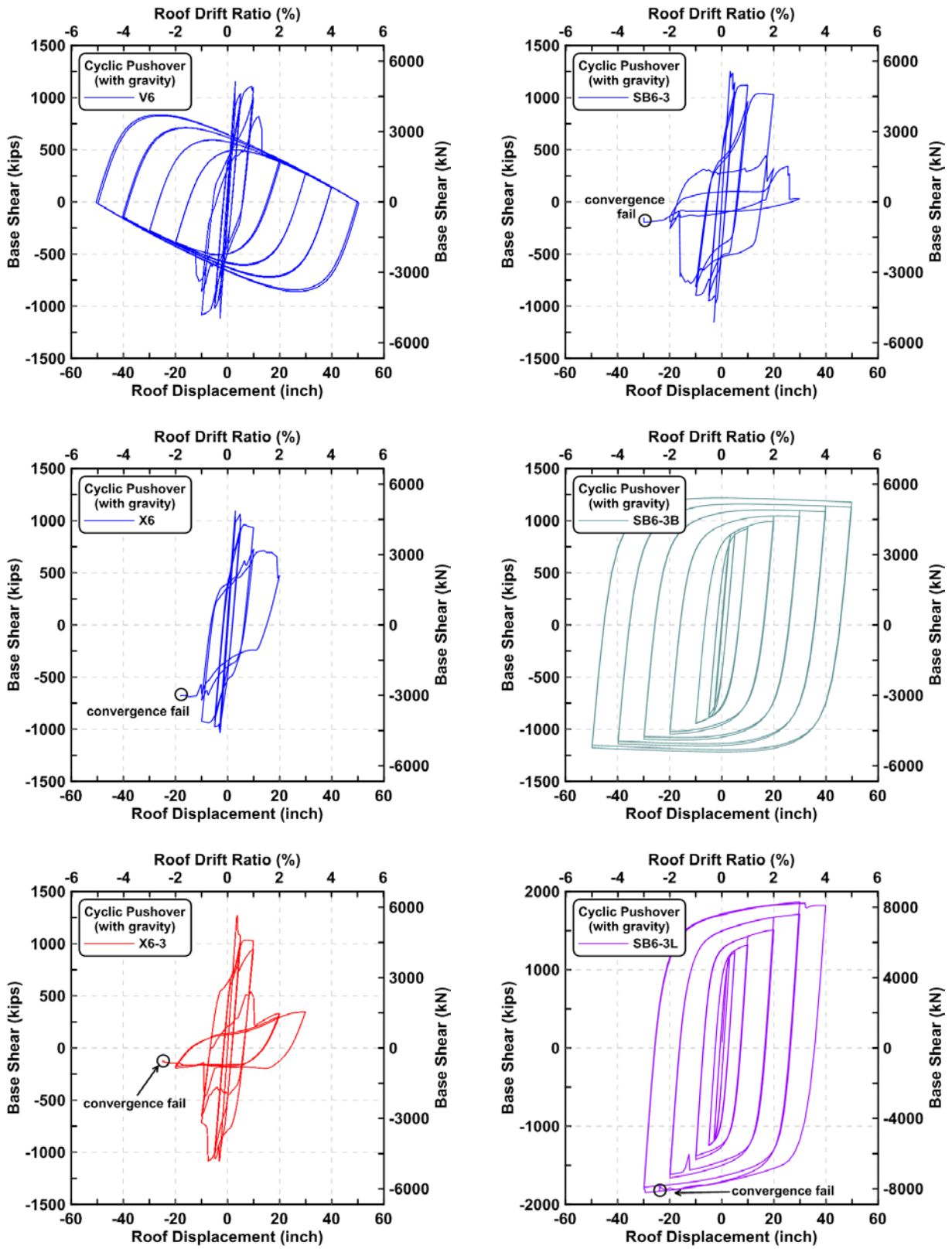


Figure 7.9 Base shear versus roof displacement relationships of each model under cyclic pushover

### 7.5.3 Nonlinear Response History Analysis Results

A total of 10 ground motions (two components from 5 records) were used in the dynamic analysis. These were rotated to the fault normal and fault parallel directions. As mentioned earlier, ground motions were scaled to match two hazard levels. For simulation convenience, all ground motions were assigned an identification number as listed in Table 7.11. Several dynamic response quantities were examined and summarized for each model. Table 7.12 shows the first two highest periods for each model. The fundamental period of each model is close to the empirical value of 0.6 sec and larger than the code empirical period of 0.55 sec ( $T = 0.02 \times 83^{0.75} = 0.55$ ). Tables 7.13 to 7.16 list the mean responses of each model under selected ground motion pairs.

**Table 7.11 Identification number list for all ground motions**

<b>ID</b>	<b>NGA Number</b>	<b>Component</b>	<b>Scale Factor</b>	<b><math>\Delta t</math> (second)</b>	<b>Duration (second)</b>
01	NGA-160	fault-normal	0.8848	0.005	37.61
02	NGA-558	fault-normal	1.2984	0.005	39.98
03	NGA-1119	fault-normal	0.9566	0.01	40.96
04	NGA-1602	fault-normal	1.0469	0.01	55.90
05	NGA-1853	fault-normal	1.5067	0.005	72.00
06	NGA-160	fault-parallel	0.8848	0.005	37.61
07	NGA-558	fault-parallel	1.2984	0.005	39.98
08	NGA-1119	fault-parallel	0.9566	0.01	40.96
09	NGA-1602	fault-parallel	1.0469	0.01	55.90
10	NGA-1853	fault-parallel	1.5067	0.005	72.00
11	NGA-160	fault-normal	1.3272	0.005	37.61
12	NGA-558	fault-normal	1.9476	0.005	39.98
13	NGA-1119	fault-normal	1.4349	0.01	40.96
14	NGA-1602	fault-normal	1.5704	0.01	55.90
15	NGA-1853	fault-normal	2.2601	0.005	72.00
16	NGA-160	fault-parallel	1.3272	0.005	37.61
17	NGA-558	fault-parallel	1.9476	0.005	39.98
18	NGA-1119	fault-parallel	1.4349	0.01	40.96
19	NGA-1602	fault-parallel	1.5704	0.01	55.90
20	NGA-1853	fault-parallel	2.2601	0.005	72.00

**Table 7.12 Fundamental and second mode periods of each model**

<b>Model Name</b>	<b>1<sup>st</sup> Mode (second)</b>	<b>2<sup>nd</sup> Mode (second)</b>
V6	0.688	0.245
X6	0.701	0.244
X6-3	0.701	0.248
SB6-3	0.671	0.237
SB6-3B	0.774	0.290
SB6-3L	0.569	0.197

**Table 7.13 Mean responses of each model under selected ground motions  
(10% probability of exceedance in 50-years events, fault-normal component)**

<b>Mean Response</b>	<b>V6</b>	<b>X6</b>	<b>X6-3</b>	<b>SB6-3</b>	<b>SB6-3B</b>	<b>SB6-3L</b>
Max. Base Shear (kips)	1199.7	1272.6	1354.7	1436.3	1016.1	1381.7
Max. Roof Displacement (inch)	5.10	5.14	5.70	5.64	6.27	5.12
Max. 1 <sup>st</sup> Story Drift Ratio (%)	1.208	0.634	0.658	0.653	0.527	0.353
Max. 2 <sup>nd</sup> Story Drift Ratio (%)	0.305	0.514	0.662	0.655	0.536	0.380
Max. 3 <sup>rd</sup> Story Drift Ratio (%)	0.406	0.980	0.852	0.688	0.566	0.486
Max. 4 <sup>th</sup> Story Drift Ratio (%)	0.565	0.857	0.793	0.751	0.668	0.578
Max. 5 <sup>th</sup> Story Drift Ratio (%)	0.487	0.540	0.819	0.761	0.922	0.765
Max. 6 <sup>th</sup> Story Drift Ratio (%)	0.376	0.382	0.444	0.810	1.403	0.913
Residual Roof Displacement (inch)	0.322	0.498	0.286	0.216	0.597	0.630
Residual 1 <sup>st</sup> Story Drift Ratio (%)	0.092	0.150	0.110	0.054	0.087	0.048
Residual 2 <sup>nd</sup> Story Drift Ratio (%)	0.010	0.091	0.078	0.033	0.065	0.047
Residual 3 <sup>rd</sup> Story Drift Ratio (%)	0.029	0.060	0.081	0.051	0.057	0.066
Residual 4 <sup>th</sup> Story Drift Ratio (%)	0.037	0.080	0.068	0.046	0.056	0.084
Residual 5 <sup>th</sup> Story Drift Ratio (%)	0.034	0.057	0.049	0.048	0.074	0.083
Residual 6 <sup>th</sup> Story Drift Ratio (%)	0.006	0.013	0.028	0.054	0.116	0.101
Max. Column Uplift Force, LHS (kips)	2122.7	2022.3	2364.7	2323.8	1522.4	2266.8
Max. Column Uplift Force, RHS (kips)	2104.9	1994.1	2132.2	2263.7	1554.8	2209.9
Max. 2 <sup>nd</sup> Floor Acceleration (g)	1.17	1.05	1.15	1.26	1.08	1.15
Max. 3 <sup>rd</sup> Floor Acceleration (g)	1.08	1.10	1.14	1.07	1.02	0.98
Max. 4 <sup>th</sup> Floor Acceleration (g)	0.98	1.00	1.06	0.96	0.86	0.87
Max. 5 <sup>th</sup> Floor Acceleration (g)	0.92	0.81	0.90	0.84	0.77	0.69
Max. 6 <sup>th</sup> Floor Acceleration (g)	0.84	0.66	0.72	0.66	0.57	0.49
Max. Roof Acceleration (g)	1.24	1.30	1.38	1.31	1.12	1.39

(Note: LHS stands for left hand side, RHS stands for right hand side)

**Table 7.14 Mean responses of each model under selected ground motions  
(10% probability of exceedance in 50-years events, fault-parallel component)**

<b>Mean Response</b>	<b>V6</b>	<b>X6</b>	<b>X6-3</b>	<b>SB6-3</b>	<b>SB6-3B</b>	<b>SB6-3L</b>
Max. Base Shear (kips)	1186.3	1237.2	1349.6	1412.1	1036.7	1335.3
Max. Roof Displacement (inch)	6.23	6.52	6.68	6.46	7.99	5.56
Max. 1 <sup>st</sup> Story Drift Ratio (%)	1.627	0.971	0.994	0.778	0.596	0.367
Max. 2 <sup>nd</sup> Story Drift Ratio (%)	0.324	0.703	0.720	0.763	0.655	0.433
Max. 3 <sup>rd</sup> Story Drift Ratio (%)	0.422	1.017	0.865	0.773	0.740	0.525
Max. 4 <sup>th</sup> Story Drift Ratio (%)	0.620	0.909	0.765	0.859	0.851	0.579
Max. 5 <sup>th</sup> Story Drift Ratio (%)	0.480	0.548	0.866	0.703	1.038	0.762
Max. 6 <sup>th</sup> Story Drift Ratio (%)	0.363	0.362	0.400	0.610	1.423	1.027
Residual Roof Displacement (inch)	0.351	0.899	0.588	0.531	1.037	0.984
Residual 1 <sup>st</sup> Story Drift Ratio (%)	0.103	0.161	0.110	0.081	0.089	0.093
Residual 2 <sup>nd</sup> Story Drift Ratio (%)	0.012	0.124	0.092	0.076	0.099	0.088
Residual 3 <sup>rd</sup> Story Drift Ratio (%)	0.022	0.098	0.073	0.049	0.107	0.093
Residual 4 <sup>th</sup> Story Drift Ratio (%)	0.062	0.085	0.081	0.057	0.116	0.091
Residual 5 <sup>th</sup> Story Drift Ratio (%)	0.031	0.048	0.115	0.041	0.119	0.094
Residual 6 <sup>th</sup> Story Drift Ratio (%)	0.008	0.010	0.015	0.063	0.147	0.151
Max. Column Uplift Force, LHS (kips)	2191.2	2106.9	2460.3	2388.8	1592.2	2225.1
Max. Column Uplift Force, RHS (kips)	2155.6	1937.3	2108.1	2215.6	1556.1	2237.6
Max. 2 <sup>nd</sup> Floor Acceleration (g)	1.08	0.98	0.96	1.03	0.86	1.00
Max. 3 <sup>rd</sup> Floor Acceleration (g)	0.84	0.91	0.87	0.90	0.79	0.87
Max. 4 <sup>th</sup> Floor Acceleration (g)	0.83	0.84	0.88	0.85	0.69	0.72
Max. 5 <sup>th</sup> Floor Acceleration (g)	0.80	0.78	0.70	0.67	0.58	0.55
Max. 6 <sup>th</sup> Floor Acceleration (g)	0.72	0.56	0.60	0.62	0.46	0.38
Max. Roof Acceleration (g)	1.21	1.17	1.26	1.22	1.15	1.16

(Note: LHS stands for left hand side, RHS stands for right hand side)



**Table 7.15 Mean responses of each model under selected ground motions  
(2% probability of exceedance in 50-years events, fault-normal component)**

<b>Mean Response</b>	<b>V6</b>	<b>X6</b>	<b>X6-3</b>	<b>SB6-3</b>	<b>SB6-3B</b>	<b>SB6-3L</b>
Max. Base Shear (kips)	1212.6	1288.9	1341.9	1465.5	1098.7	1536.0
Max. Roof Displacement (inch)	7.90	8.12	8.12	8.98	8.94	6.73
Max. 1 <sup>st</sup> Story Drift Ratio (%)	2.206	1.368	1.725	1.075	0.829	0.662
Max. 2 <sup>nd</sup> Story Drift Ratio (%)	0.427	0.977	0.971	0.997	0.854	0.695
Max. 3 <sup>rd</sup> Story Drift Ratio (%)	0.484	1.156	0.923	0.959	0.858	0.699
Max. 4 <sup>th</sup> Story Drift Ratio (%)	0.727	0.896	0.753	1.044	0.958	0.732
Max. 5 <sup>th</sup> Story Drift Ratio (%)	0.601	0.627	0.956	1.136	1.214	0.910
Max. 6 <sup>th</sup> Story Drift Ratio (%)	0.408	0.401	0.428	1.289	1.993	1.203
Residual Roof Displacement (inch)	0.728	1.767	1.583	1.484	1.423	0.884
Residual 1 <sup>st</sup> Story Drift Ratio (%)	0.202	0.298	0.248	0.151	0.168	0.139
Residual 2 <sup>nd</sup> Story Drift Ratio (%)	0.048	0.298	0.215	0.158	0.160	0.121
Residual 3 <sup>rd</sup> Story Drift Ratio (%)	0.050	0.254	0.208	0.144	0.147	0.084
Residual 4 <sup>th</sup> Story Drift Ratio (%)	0.091	0.129	0.139	0.148	0.140	0.091
Residual 5 <sup>th</sup> Story Drift Ratio (%)	0.046	0.052	0.101	0.142	0.136	0.115
Residual 6 <sup>th</sup> Story Drift Ratio (%)	0.022	0.012	0.033	0.156	0.182	0.163
Max. Column Uplift Force, LHS (kips)	2104.1	1984.5	2198.4	2099.7	1543.7	2370.8
Max. Column Uplift Force, RHS (kips)	2232.5	2057.7	2175.2	2271.6	1634.2	2340.1
Max. 2 <sup>nd</sup> Floor Acceleration (g)	1.58	1.44	1.47	1.71	1.48	1.54
Max. 3 <sup>rd</sup> Floor Acceleration (g)	1.31	1.37	1.37	1.36	1.40	1.37
Max. 4 <sup>th</sup> Floor Acceleration (g)	1.29	1.32	1.39	1.34	1.33	1.23
Max. 5 <sup>th</sup> Floor Acceleration (g)	1.22	1.21	1.18	1.18	1.11	0.97
Max. 6 <sup>th</sup> Floor Acceleration (g)	1.10	1.04	0.95	0.90	0.89	0.71
Max. Roof Acceleration (g)	1.64	1.56	1.63	1.67	1.48	1.78

(Note: LHS stands for left hand side, RHS stands for right hand side)

**Table 7.16 Mean responses of each model under selected ground motions  
(2% probability of exceedance in 50-years events, fault-parallel component)**

<b>Mean Response</b>	<b>V6</b>	<b>X6</b>	<b>X6-3</b>	<b>SB6-3</b>	<b>SB6-3B</b>	<b>SB6-3L</b>
Max. Base Shear (kips)	1197.2	1265.0	1344.5	1405.7	1095.0	1486.3
Max. Roof Displacement (inch)	11.19	11.06	11.30	12.37	11.53	9.37
Max. 1 <sup>st</sup> Story Drift Ratio (%)	3.291	1.862	1.876	1.426	0.962	0.768
Max. 2 <sup>nd</sup> Story Drift Ratio (%)	0.593	1.426	1.292	1.450	1.004	0.820
Max. 3 <sup>rd</sup> Story Drift Ratio (%)	0.535	1.530	1.315	1.378	1.062	0.903
Max. 4 <sup>th</sup> Story Drift Ratio (%)	0.812	1.157	1.387	1.409	1.170	0.930
Max. 5 <sup>th</sup> Story Drift Ratio (%)	0.662	0.719	1.052	1.187	1.412	1.097
Max. 6 <sup>th</sup> Story Drift Ratio (%)	0.426	0.414	0.509	1.367	2.042	1.600
Residual Roof Displacement (inch)	2.030	2.607	1.541	2.136	2.157	2.033
Residual 1 <sup>st</sup> Story Drift Ratio (%)	0.689	0.495	0.342	0.272	0.202	0.222
Residual 2 <sup>nd</sup> Story Drift Ratio (%)	0.113	0.400	0.227	0.253	0.209	0.222
Residual 3 <sup>rd</sup> Story Drift Ratio (%)	0.060	0.322	0.173	0.220	0.223	0.215
Residual 4 <sup>th</sup> Story Drift Ratio (%)	0.071	0.182	0.100	0.193	0.235	0.214
Residual 5 <sup>th</sup> Story Drift Ratio (%)	0.060	0.074	0.036	0.173	0.237	0.186
Residual 6 <sup>th</sup> Story Drift Ratio (%)	0.046	0.016	0.040	0.159	0.208	0.212
Max. Column Uplift Force, LHS (kips)	2302.5	1987.4	2326.8	2305.5	1663.3	2339.4
Max. Column Uplift Force, RHS (kips)	2233.2	2076.1	2199.6	2282.0	1606.2	2426.9
Max. 2 <sup>nd</sup> Floor Acceleration (g)	1.41	1.37	1.38	1.33	1.23	1.34
Max. 3 <sup>rd</sup> Floor Acceleration (g)	1.14	1.31	1.23	1.36	1.13	1.08
Max. 4 <sup>th</sup> Floor Acceleration (g)	1.13	1.21	1.12	1.20	1.02	0.97
Max. 5 <sup>th</sup> Floor Acceleration (g)	1.06	1.00	0.99	0.91	0.81	0.79
Max. 6 <sup>th</sup> Floor Acceleration (g)	0.95	0.86	0.80	0.86	0.62	0.57
Max. Roof Acceleration (g)	1.53	1.53	1.52	1.58	1.54	1.61

(Note: LHS stands for left hand side, RHS stands for right hand side)

## 7.6 DISCUSSION

### 7.6.1 Pushover Analysis

The monotonic pushover curves shown in Fig. 7.8 show that the first four models (V6, X6, X6-3 and SB6-3) had similar initial stiffnesses. Models V6 and X6 had similar peak base shear capacity. Models X6-3 and SB6-3 had similar peak base shear capacity and were about 10% higher than that found for models V6 and X6. Once the brace at a certain floor level began to buckle, the base shear began to drop. The base shear of model V6 dropped after the brace at first story buckled, but later increased. With continued lateral displacement of Model V6, the unbalanced forces in the first story pulled down the center of the beam and plastic hinges formed in the beam ends (beam-to-column connections were rigid connections). Later, plastic hinges formed in the columns, and the entire model developed a negative tangent stiffness at around 17.5-in. roof displacement. The beam-to-column connections were pinned in Models X6, X6-3, and SB6-3; once the story mechanism formed in these models, the base shear decreased gradually. Note that the negative slopes were smaller than for Model V6. The pushover curve of Model SB6-3 had several local peaks, indicating that braces other than first story buckled or yielded.

Pushover curves of Models SB6-3B and SB6-3L both exhibited a tri-linear shape. Model SB6-3L had a higher initial stiffness (due to larger brace areas) while model SB6-3B had lower initial stiffness compared to the other four models (due to its smaller brace areas). The slope of the pushover curve of model SB6-3L never became negative. Model SB6-3B did exhibit a slightly negative slope when the roof displacement exceeded 18 in.

Quasi-static cyclic analyses show that the cyclic base shear capacity of model V6 degraded more rapidly compared to the monotonic pushover analysis; the braces at the first story fractured at about 1.5% roof drift ratio, and the base shear capacity dropped to about zero at roof drift ratio corresponding to 5% (see Fig. 7.9). Models X6, X6-3, and SB6-3 failed to complete the entire cyclic analysis protocol due to numerical convergence issues. Brace fracturing in these three models was observed, as can be deduced from Fig. 7.9. Substantial cyclic hardening was observed in Models SB6-3B and SB6-3L. Note that the base shear capacity kept increasing in model SB6-3L, while in model SB6-3B the base shear capacity very gradually decreased at larger roof displacements. Brace fracturing of part of the vertical spine of the six-story conventional brace (Model SB6-3) was observed in the cyclic analyses; see the noticeable small spike Fig. 7.9. The material modeling used for buckling-restrained braces did not include low-cycle fatigue features.

Clearly, the SBS with conventional braces or BRBs out-performed the braced frames with traditional bracing configurations. Using low-yield strength BRBs in the strong-back hybrid system had a greater post-yield deformation hardening characteristic than did the conventional BRBF.

### 7.6.2 Dynamic Analysis

As listed in Tables 7.13 to 7.16, peak base shear forces were all between 1000 kips to 1500 kips. The order of peak base shear forces from dynamic analysis basically followed the order of the fundamental periods of six models: the lower the fundamental period, the higher the peak shear force.

Maximum roof displacements under fault-parallel ground motions were all larger than the maximum roof displacements under fault-normal ground motions. The strong-back system with low-yield strength BRBs tended to have small roof displacements. Because of using a larger cross-section area of steel cores, the SB6-3L model was stiffer and stronger. As such, it tended to have smaller maximum roof displacements.

From Fig. 7.10, it is clear that a weak-ground-story formed in Model V6. Under the MCE-level event, this model exhibited a mean drift ratio of more than 3% that was concentrated at first story. Model X6 tended to form a soft two-story-panel mechanism. It is interesting to note that larger story drift ratios tend to happen in the upper stories of the SBS's especially in Model SB6-3B. The distribution of story drift ratios of model SB6-3 was close to a uniform pattern. The story drift ratios of models SB6-3B and SB6-3L had quite a uniform distribution at the lower stories. All residual story drift ratios were less than 0.7%, as shown in Fig. 7.11.

For the column base force demands, Model SB6-3B had the smallest column uplift forces among all six models for the two hazard levels (about 25% smaller). The other five models had similar column uplift force demands.

Distributions of floor accelerations exhibited a sickle-shaped pattern for all six models, as shown in Fig. 7.12. For example, maximum floor acceleration under 2% probability of exceedance in 50 years varied from around 1.5g at the top of the first story to about 1.0g at the top of the fifth story, and the jumped to about 1.5g at roof level.

Base shear versus roof displacement loop diagrams, story drift ratio histories of each floor level, and axial force-deformation relationships of all twelve braces for each model are shown from Fig. 7.13 to Fig. 7.60. Only the responses selected from two ground motions, NGA-1119 fault-normal component (GM #03) and NGA-1602 fault-parallel component (GM #19) are shown in this section. Each figure represents one hazard level and one ground motion component, with larger responses out of five ground motions in the analysis group.

From Figs. 7.14 to 7.16, it is clear that for Model V6, as the ground shaking intensity increased, the deformation began to concentrate at the first story, the concentration still occurred at the ground story, as shown in Figs. 7.18 to 7.20. Localized concentration of deformation improved slightly in model X6, but the lower stories tended to have higher story drift ratios (Fig. 7.22 and Fig. 7.26). Model X6-3 responded similarly, but successfully preventing localized concentration of the deformation.

Model SB6-3 successfully prevented localized concentration of story deformation (Figs. 7.42 and 7.38). All braces in the vertical spine remained elastic during the dynamic analyses, and all braces outside the spine were triggered to buckle (Figs. 7.39 and 7.40; Figs. 7.43 and 7.44).

Similar system responses were observed in models SB6-3B and SB6-3L. All BRBs deformed into the nonlinear range and exhibited stable hysteresis loops. Significant strain hardening in the BRBs was observed. Most of the bracing members in the vertical spine remained elastic during the ground shakings, except the six-story braces exhibited nonlinear demands, as shown in Figs. 7.47, 7.51, and 7.55. Buckling of tie-columns in the strong-back vertical spine was also observed in some events.

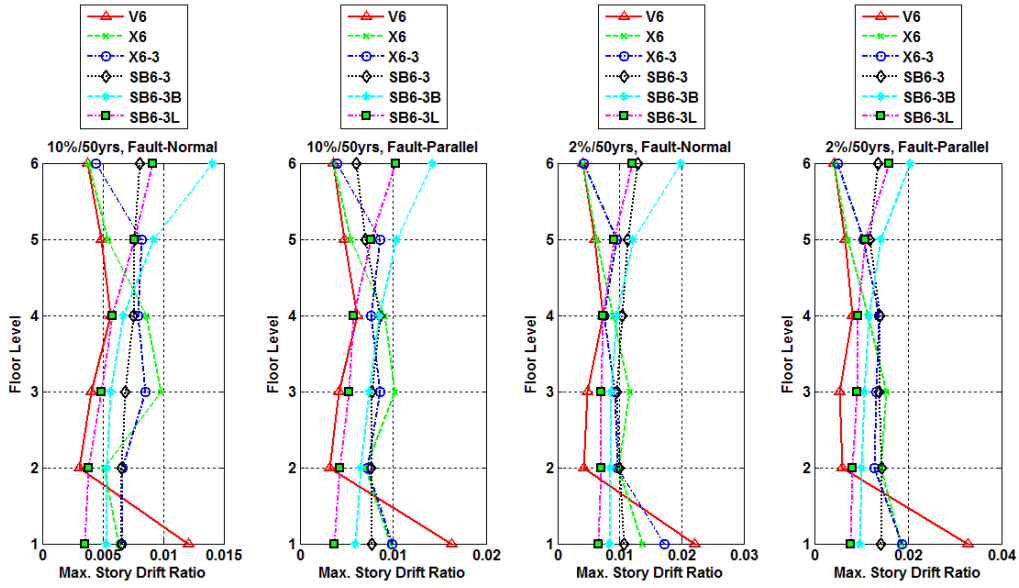


Figure 7.10 Maximum story drift ratios for each model under different hazard level ground motions

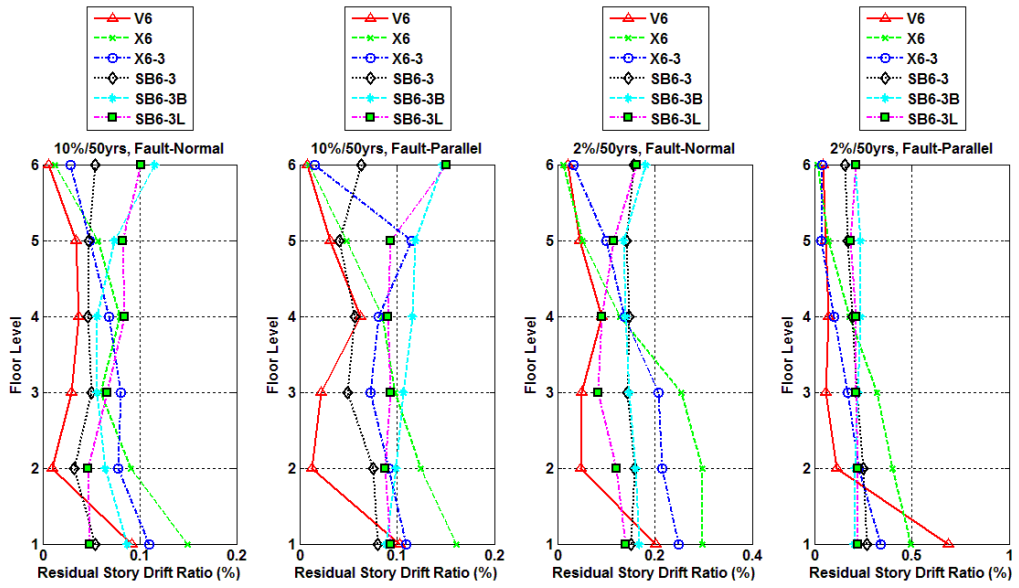
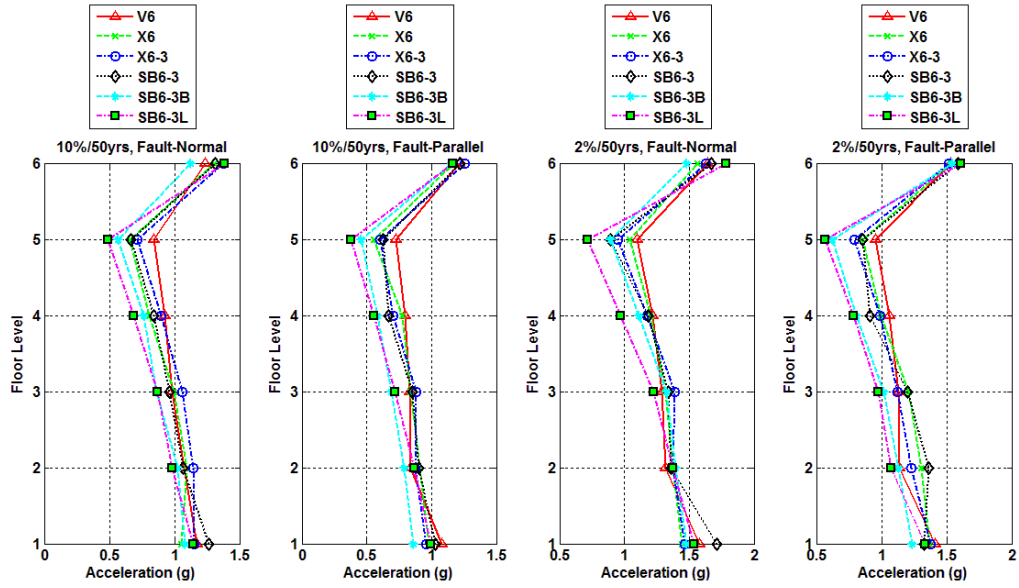
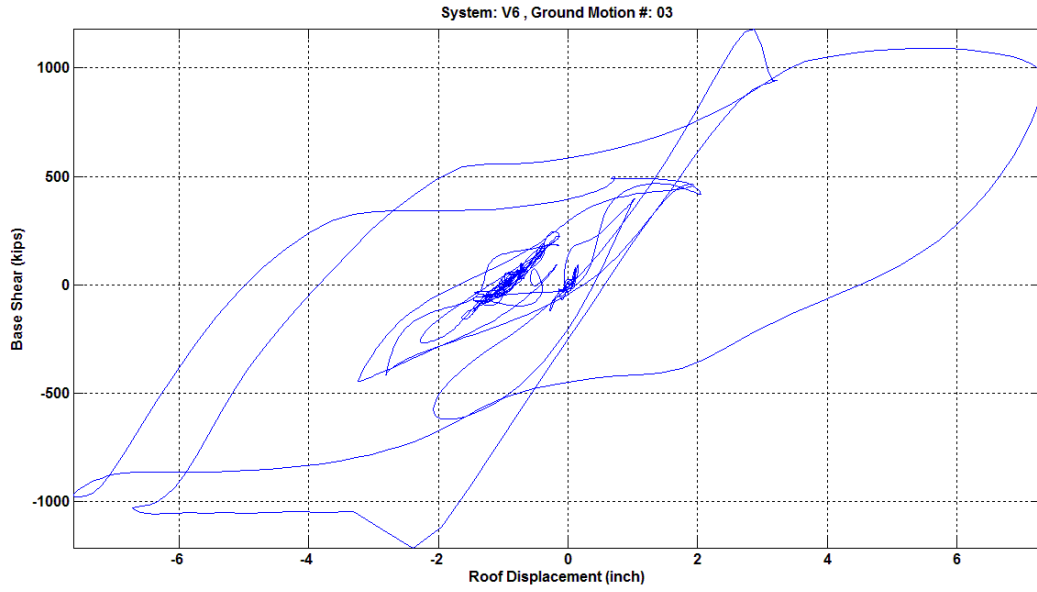


Figure 7.11 Residual story drift ratios for each model after different hazard level ground excitations



**Figure 7.12 Maximum floor level accelerations for each model under different hazard level ground motions**



**Figure 7.13 Base shear versus roof displacement relationship of model V6 under NGA 1119 fault-normal component ground motion**

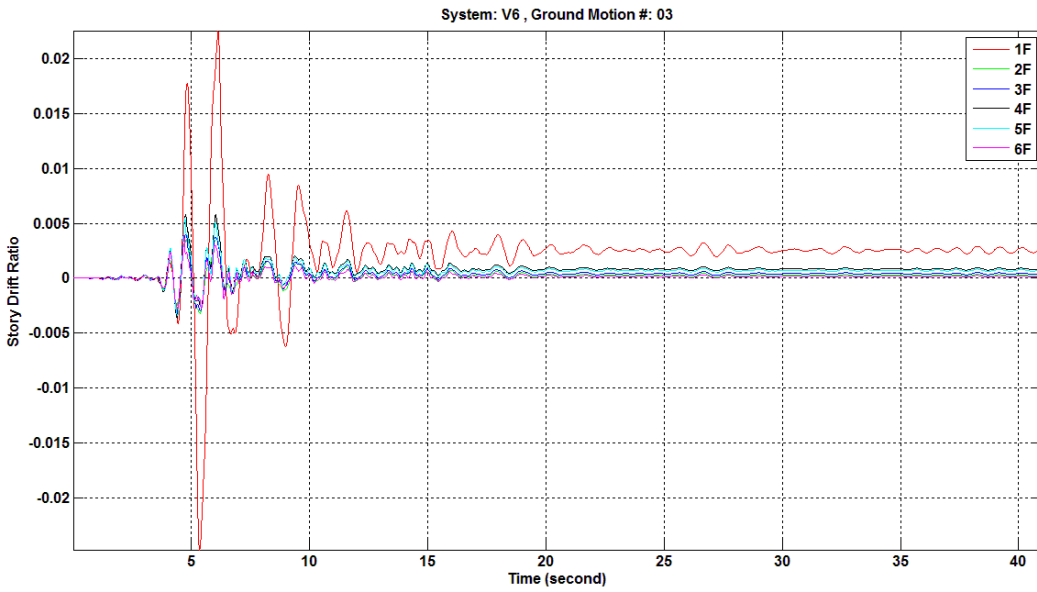


**Figure 7.14 Story drift ratio histories of model V6 under NGA 1119 fault-normal component ground motion**

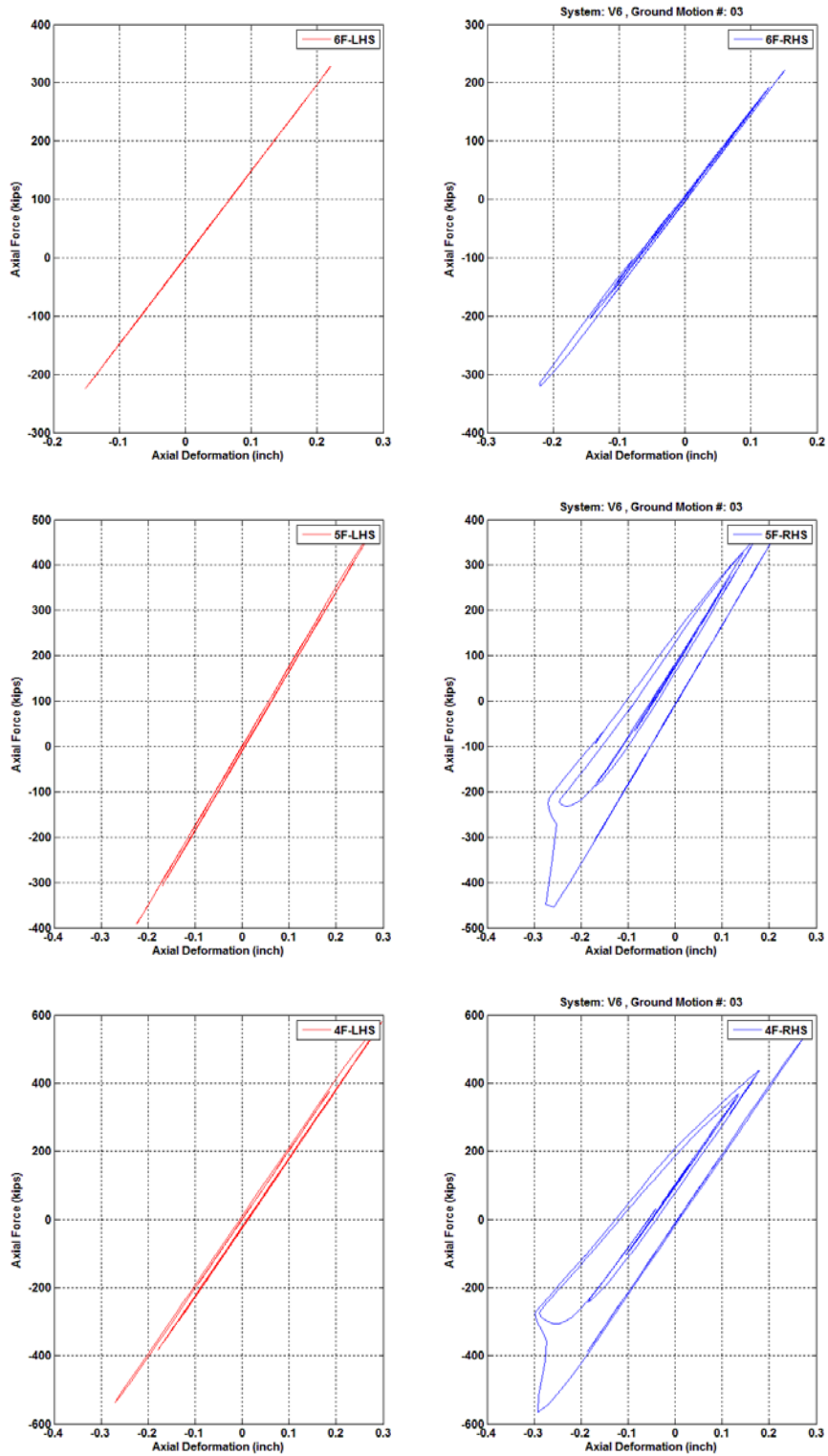
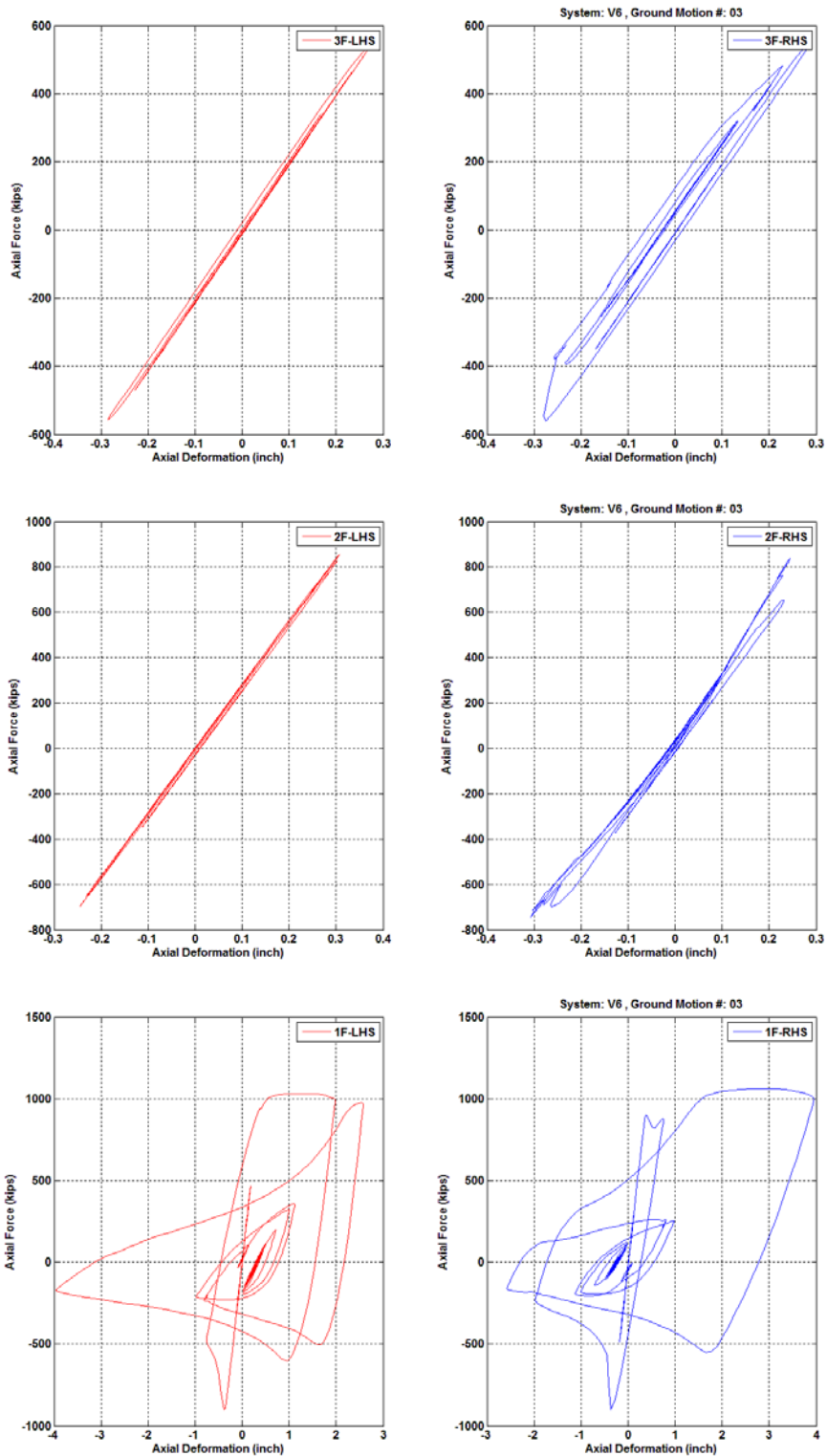
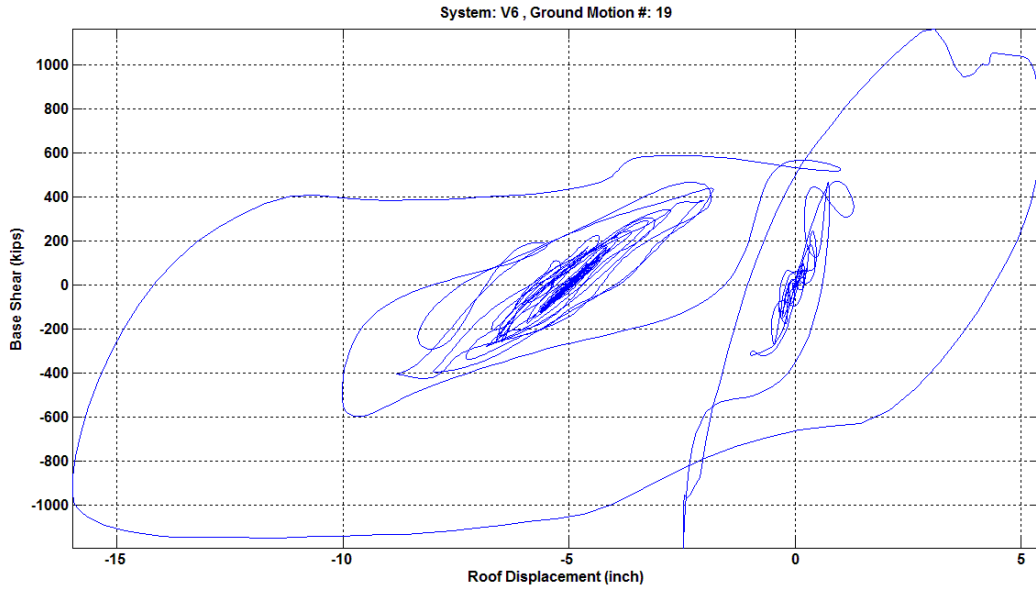


Figure 7.15 Fourth story to sixth story brace axial force versus axial deformation relationships of model V6 under NGA 1119 fault-normal component ground motion





**Figure 7.16 First story to third story brace axial force versus axial deformation relationships of model V6 under NGA 1119 fault-normal component ground motion**



**Figure 7.17 Base shear versus roof displacement relationship of model V6 under NGA 1602 fault-parallel component ground motion**

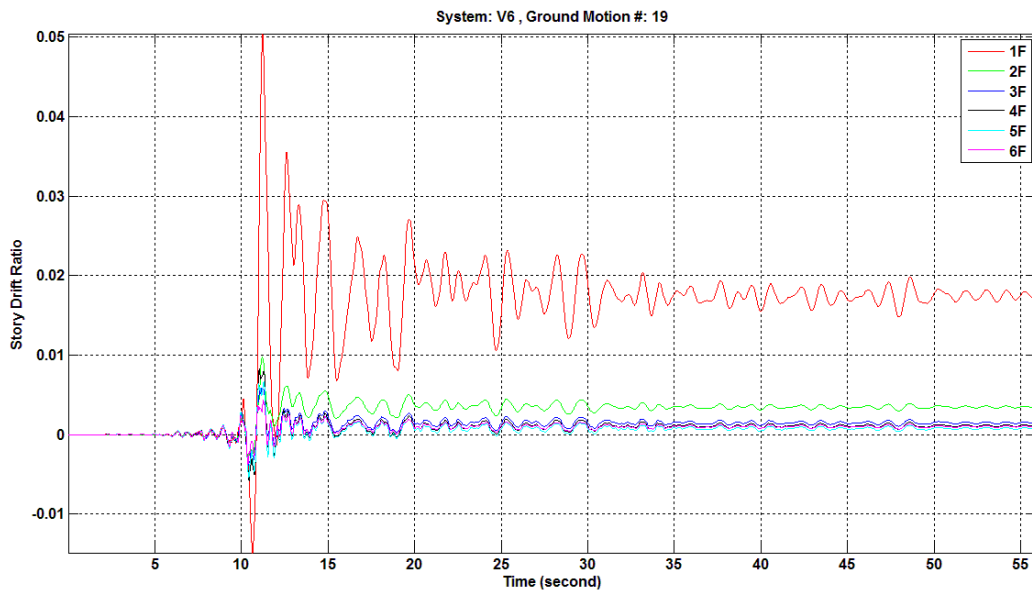


**Figure 7.18 Story drift ratio histories of model V6 under NGA 1602 fault-parallel component ground motion**

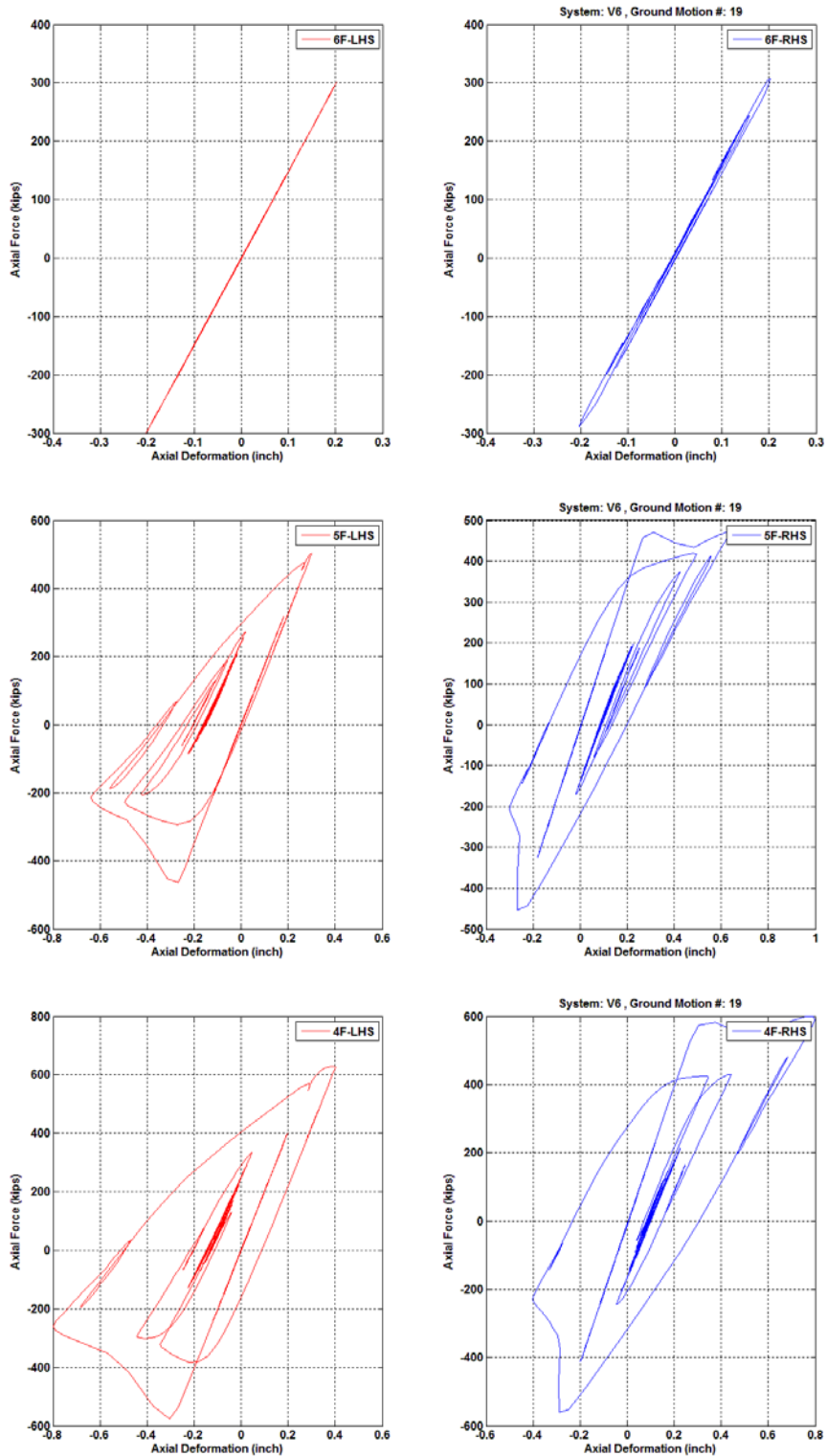


**Figure 7.19 Fourth story to sixth story brace axial force versus axial deformation relationships of model V6 under NGA 1602 fault-parallel component ground motion**

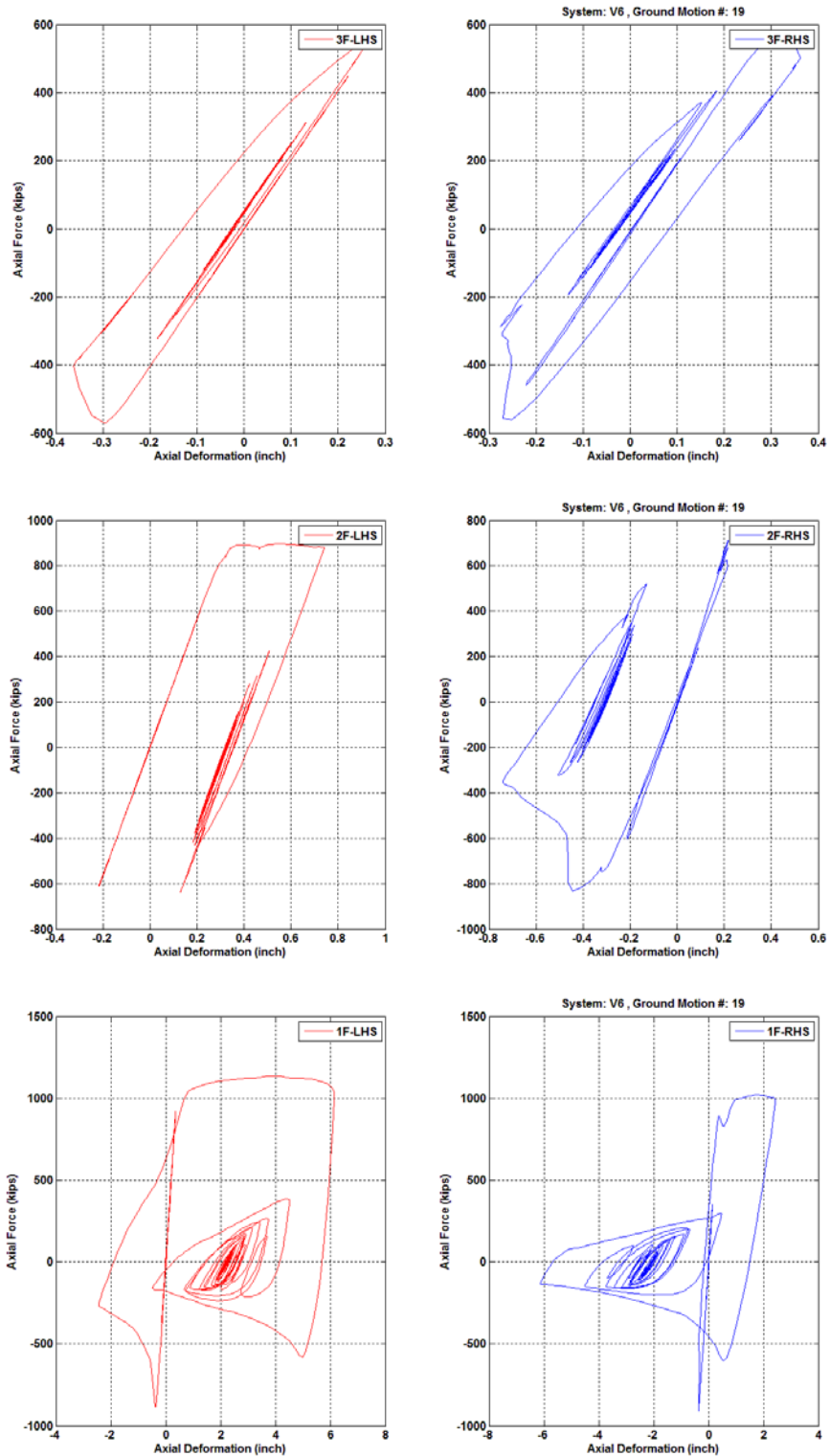


**Figure 7.20** First story to third story brace axial force versus axial deformation relationships of model V6 under NGA 1602 fault-parallel component ground motion

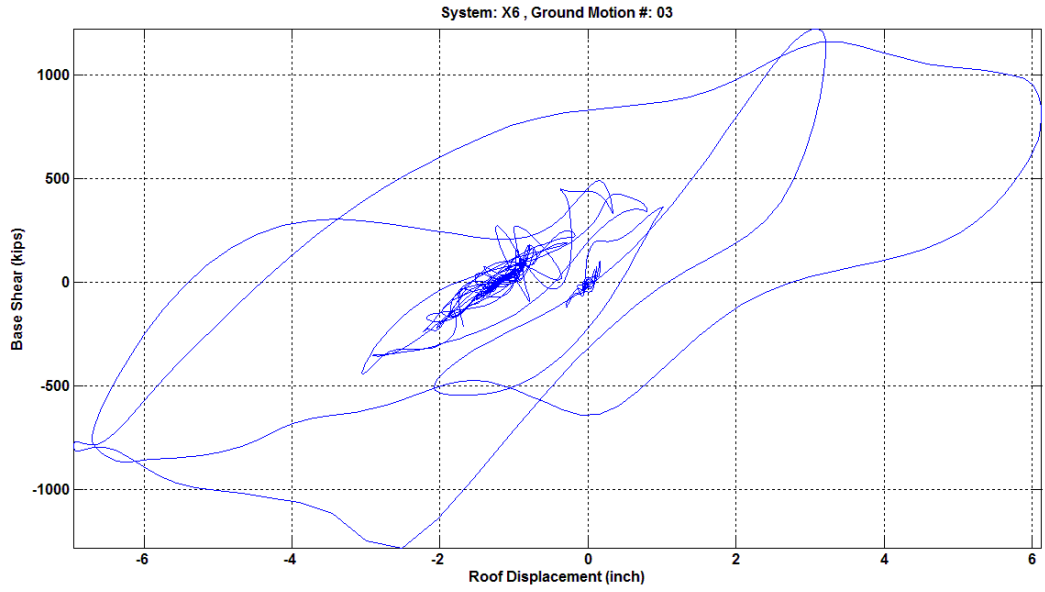


**Figure 7.21 Base shear versus roof displacement relationship of model X6 under NGA 1119 fault-normal component ground motion**

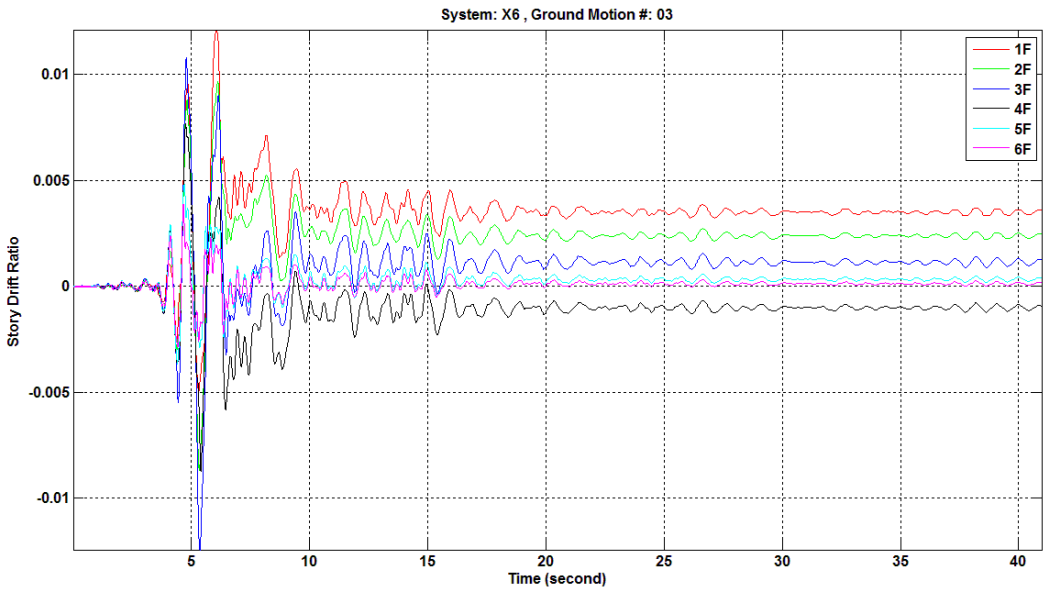


**Figure 7.22 Story drift ratio histories of model X6 under NGA 1119 fault-normal component ground motion**

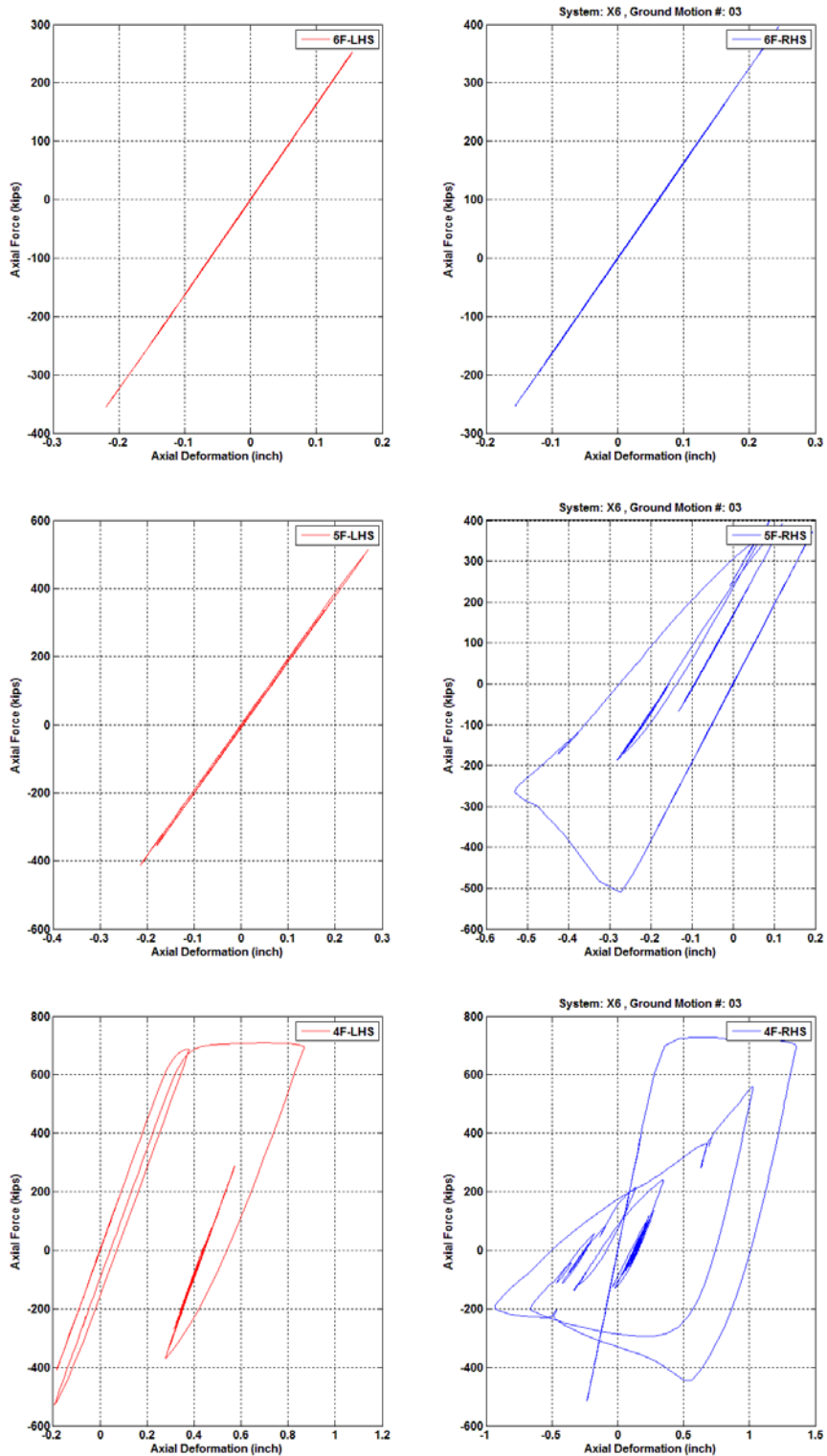
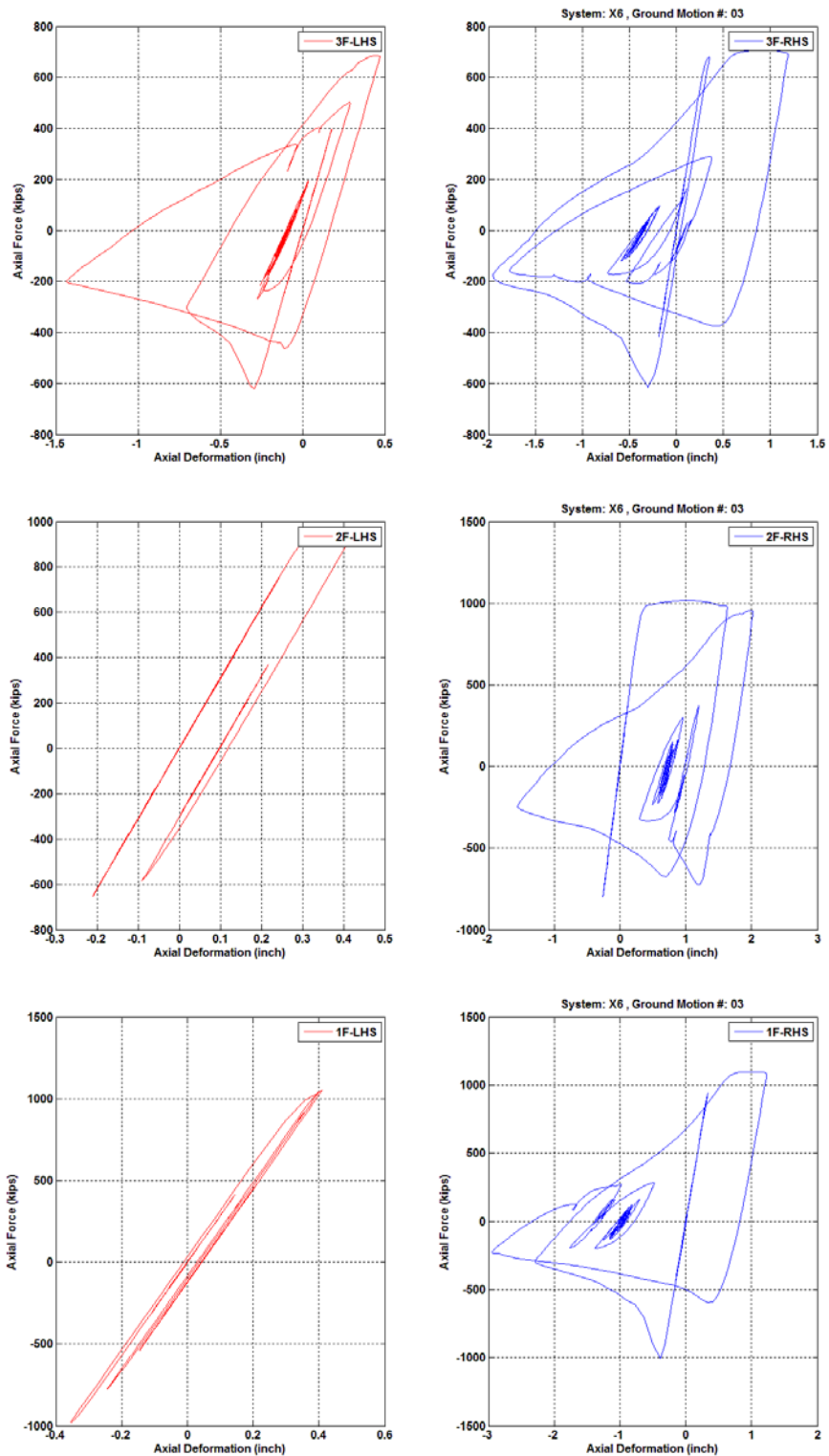
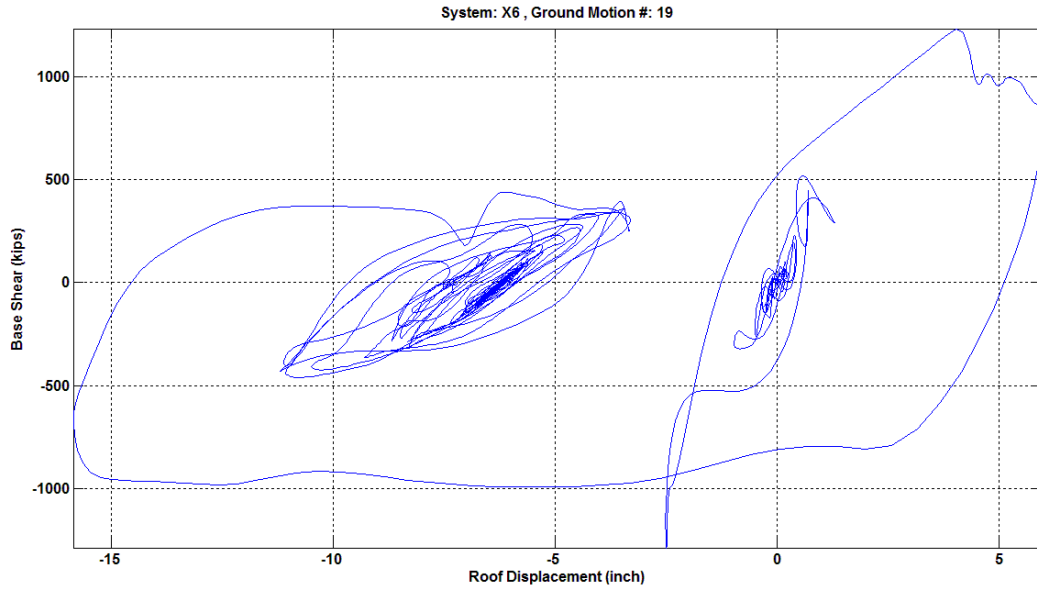


Figure 7.23 Fourth story to sixth story brace axial force versus axial deformation relationships of model X6 under NGA 1119 fault-normal component ground motion



**Figure 7.24** First story to third story brace axial force versus axial deformation relationships of model X6 under NGA 1119 fault-normal component ground motion



**Figure 7.25 Base shear versus roof displacement relationship of model X6 under NGA 1602 fault-parallel component ground motion**

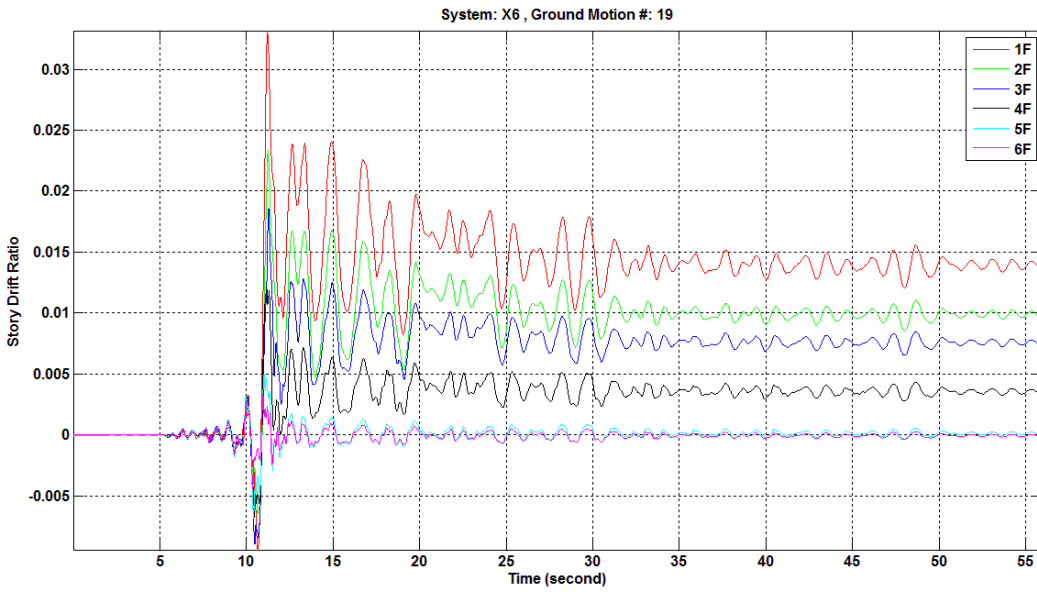


**Figure 7.26 Story drift ratio histories of model X6 under NGA 1602 fault-parallel component ground motion**



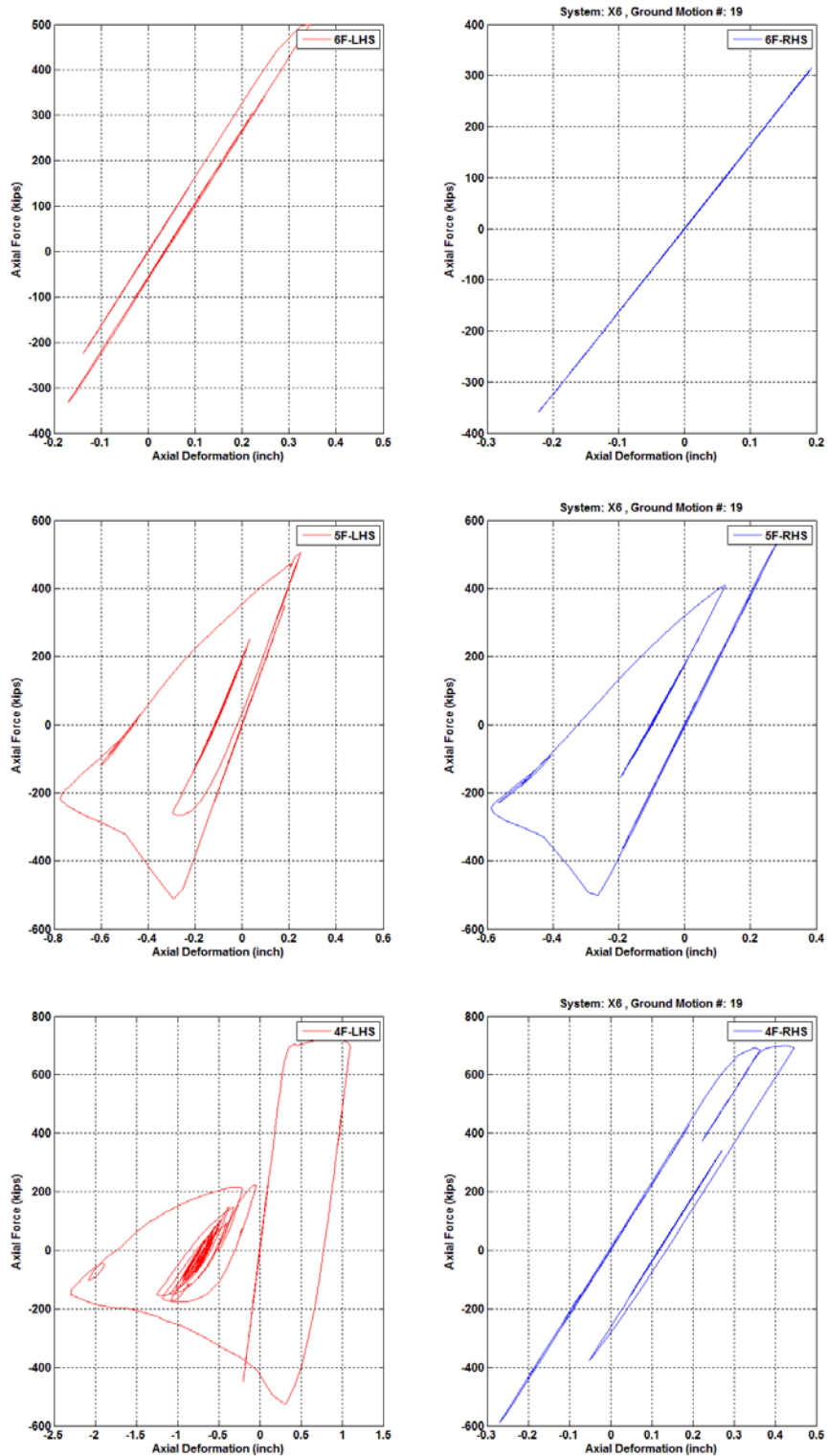
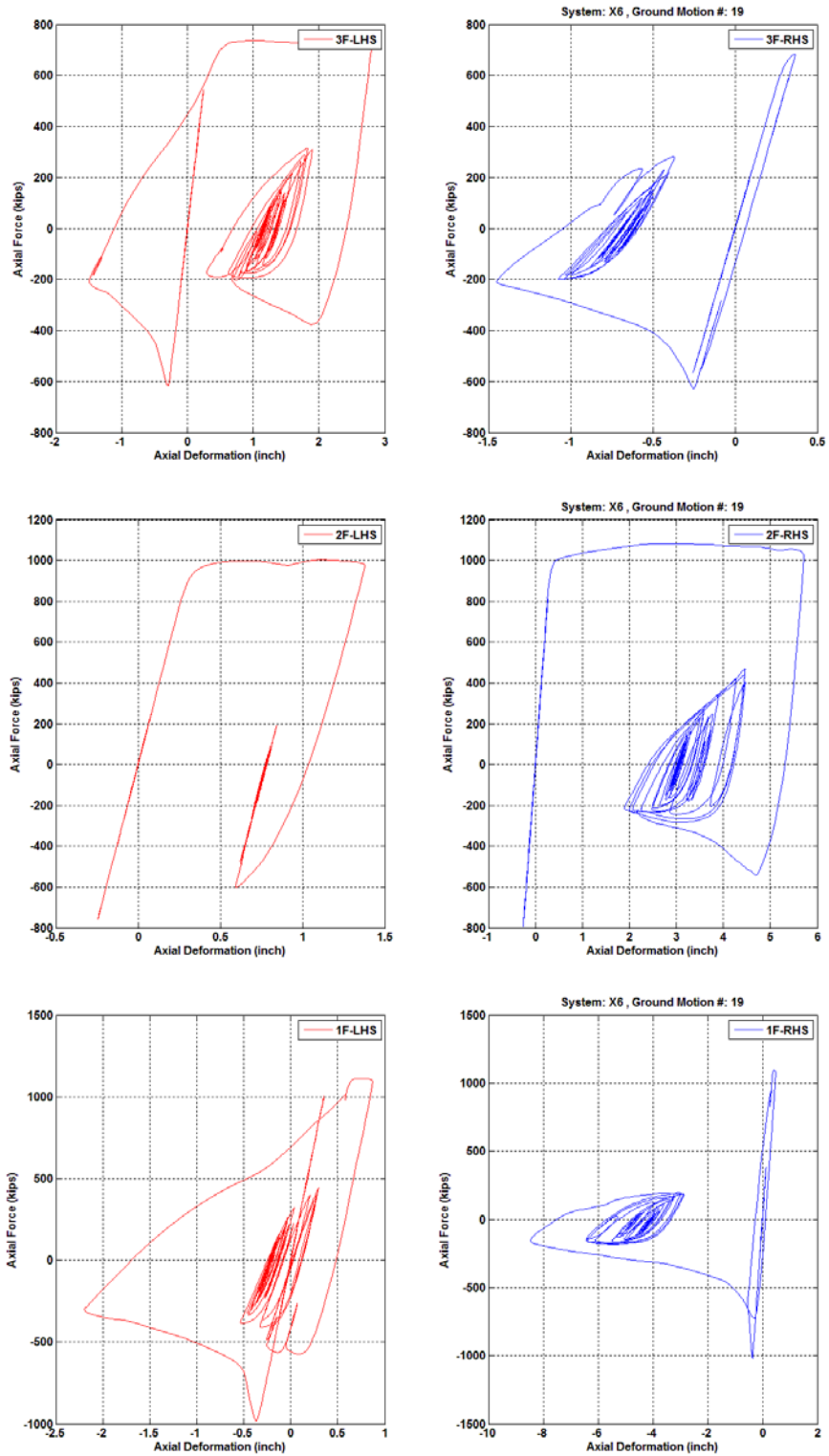
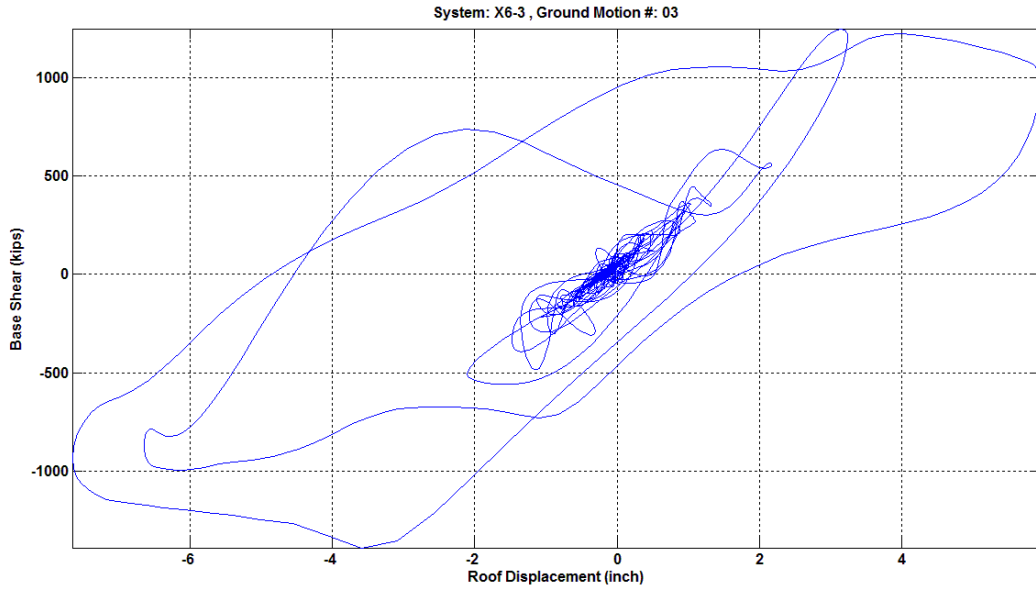


Figure 7.27 Fourth story to sixth story brace axial force versus axial deformation relationships of model X6 under NGA 1602 fault-parallel component ground motion



**Figure 7.28** First story to third story brace axial force versus axial deformation relationships of model X6 under NGA 1602 fault-parallel component ground motion



**Figure 7.29** Base shear versus roof displacement relationship of model X6-3 under NGA 1119 fault-normal component ground motion

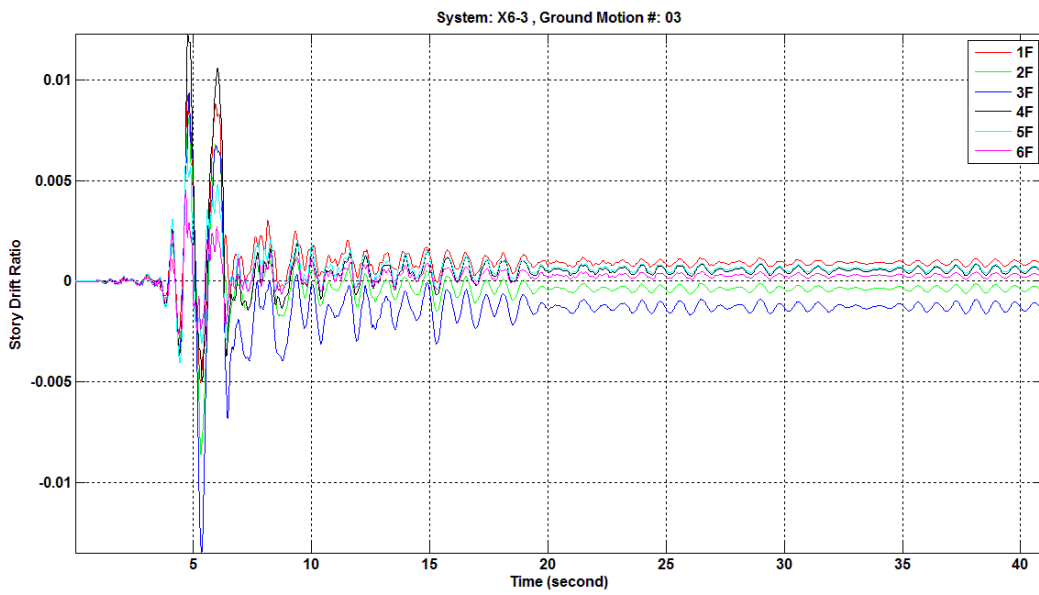


**Figure 7.30** Story drift ratio histories of model X6-3 under NGA 1119 fault-normal component ground motion

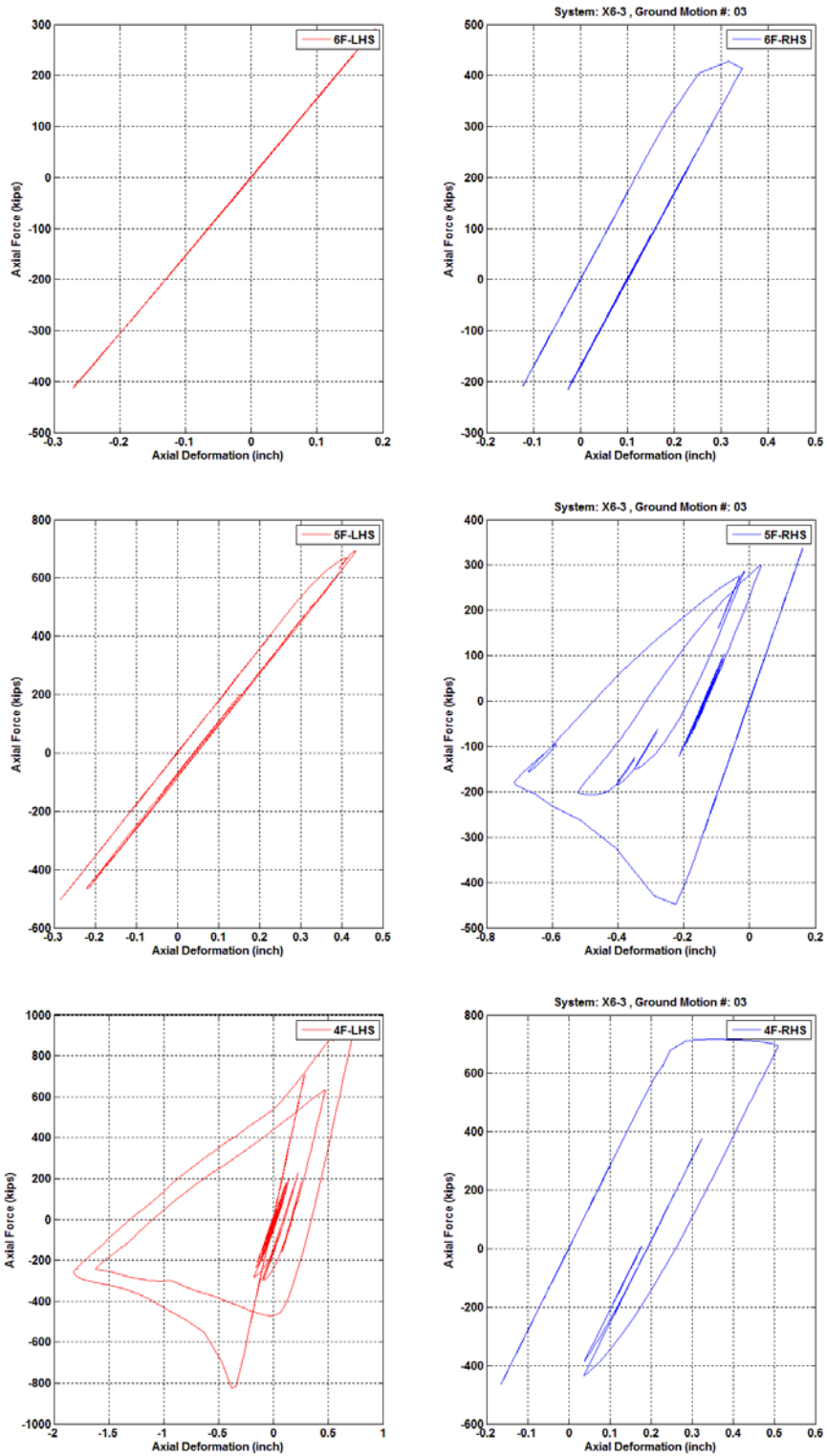
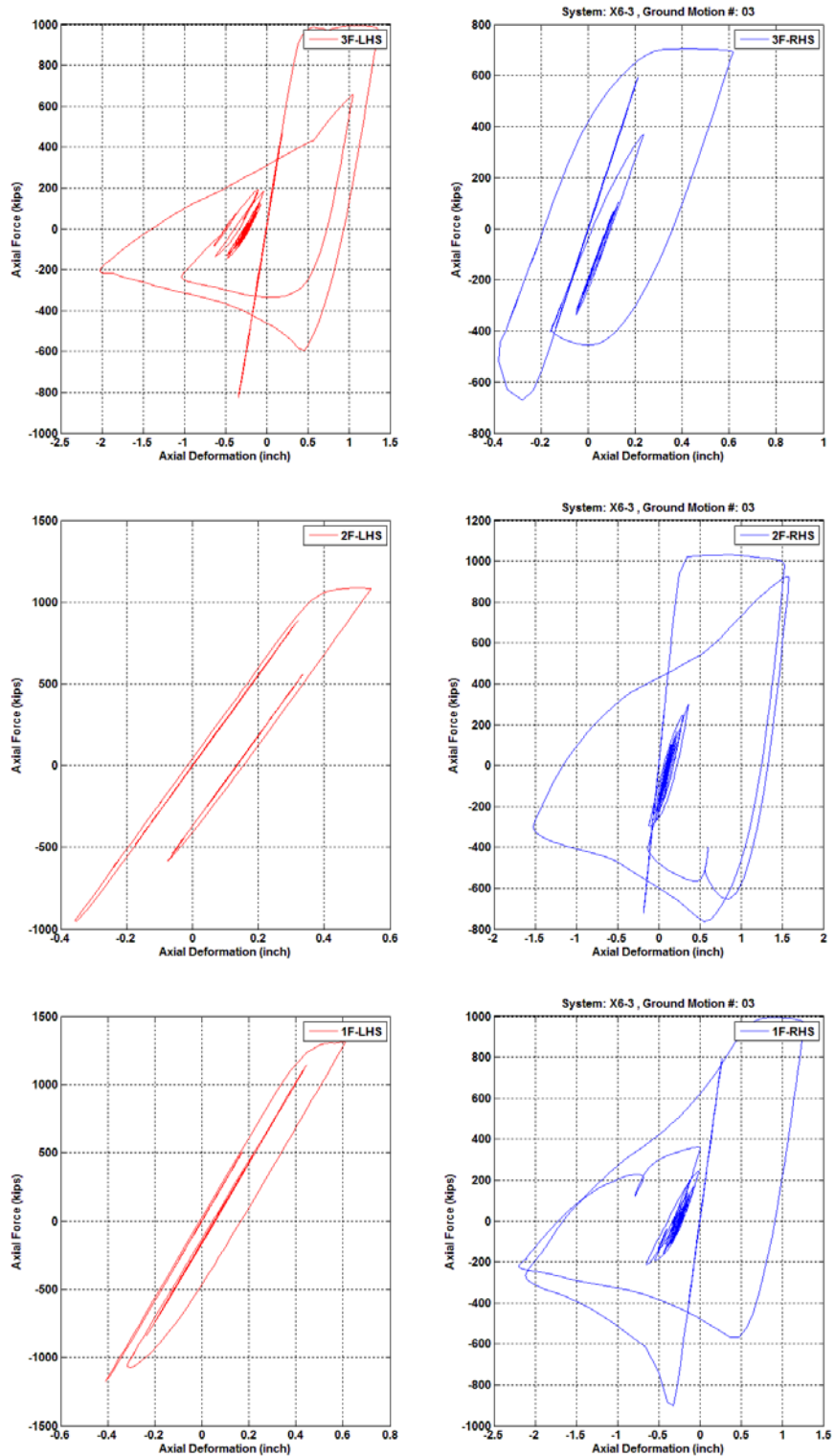
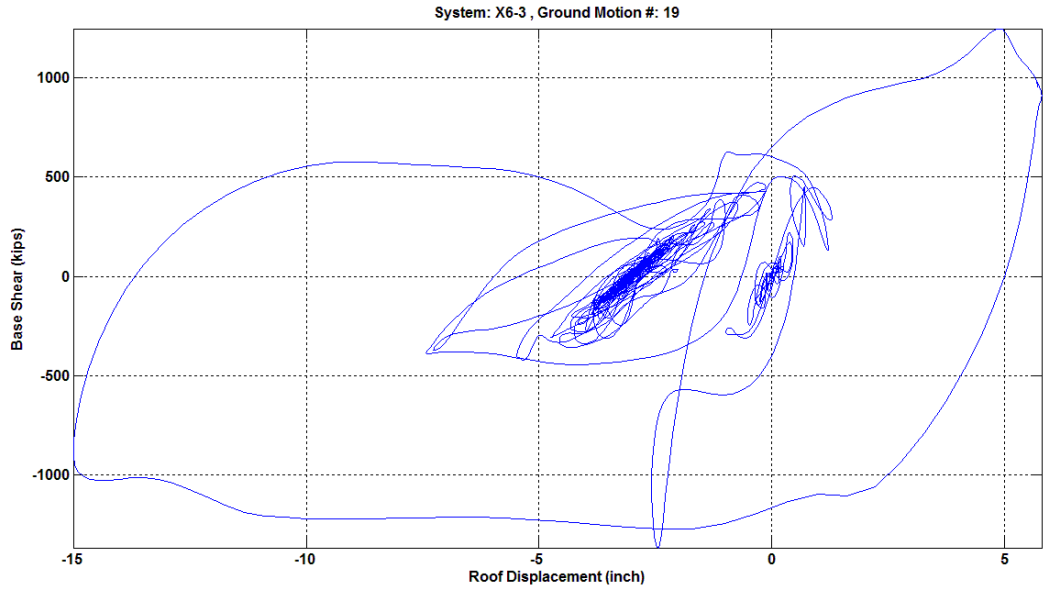


Figure 7.31 Fourth story to sixth story brace axial force versus axial deformation relationships of model X6-3 under NGA 1119 fault-normal component ground motion



**Figure 7.32** First story to third story brace axial force versus axial deformation relationships of model X6-3 under NGA 1119 fault-normal component ground motion



**Figure 7.33 Base shear versus roof displacement relationship of model X6-3 under NGA 1602 fault-parallel component ground motion**

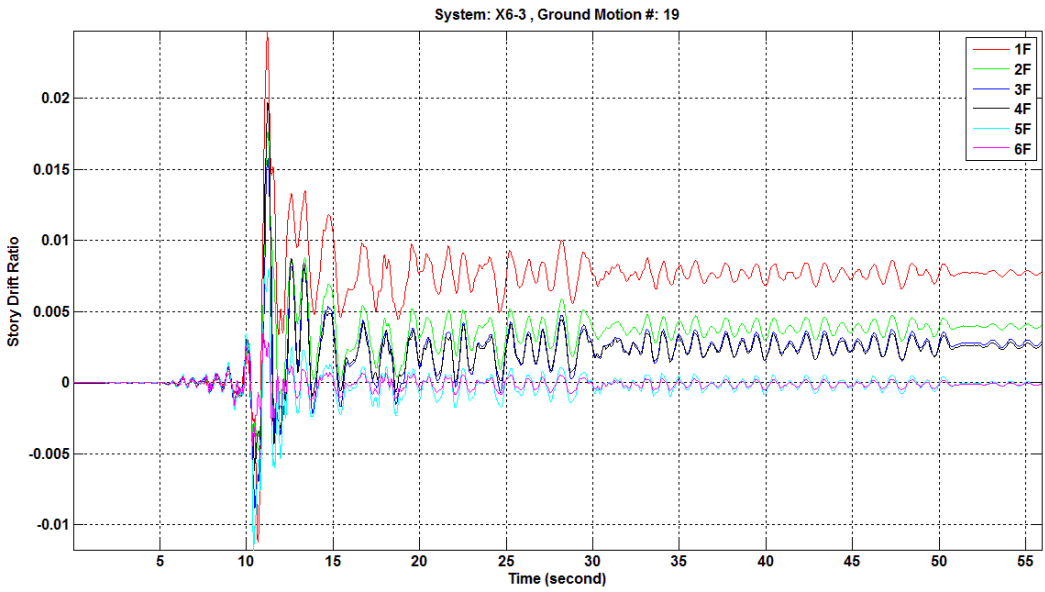


**Figure 7.34 Story drift ratio histories of model X6-3 under NGA 1602 fault-parallel component ground motion**

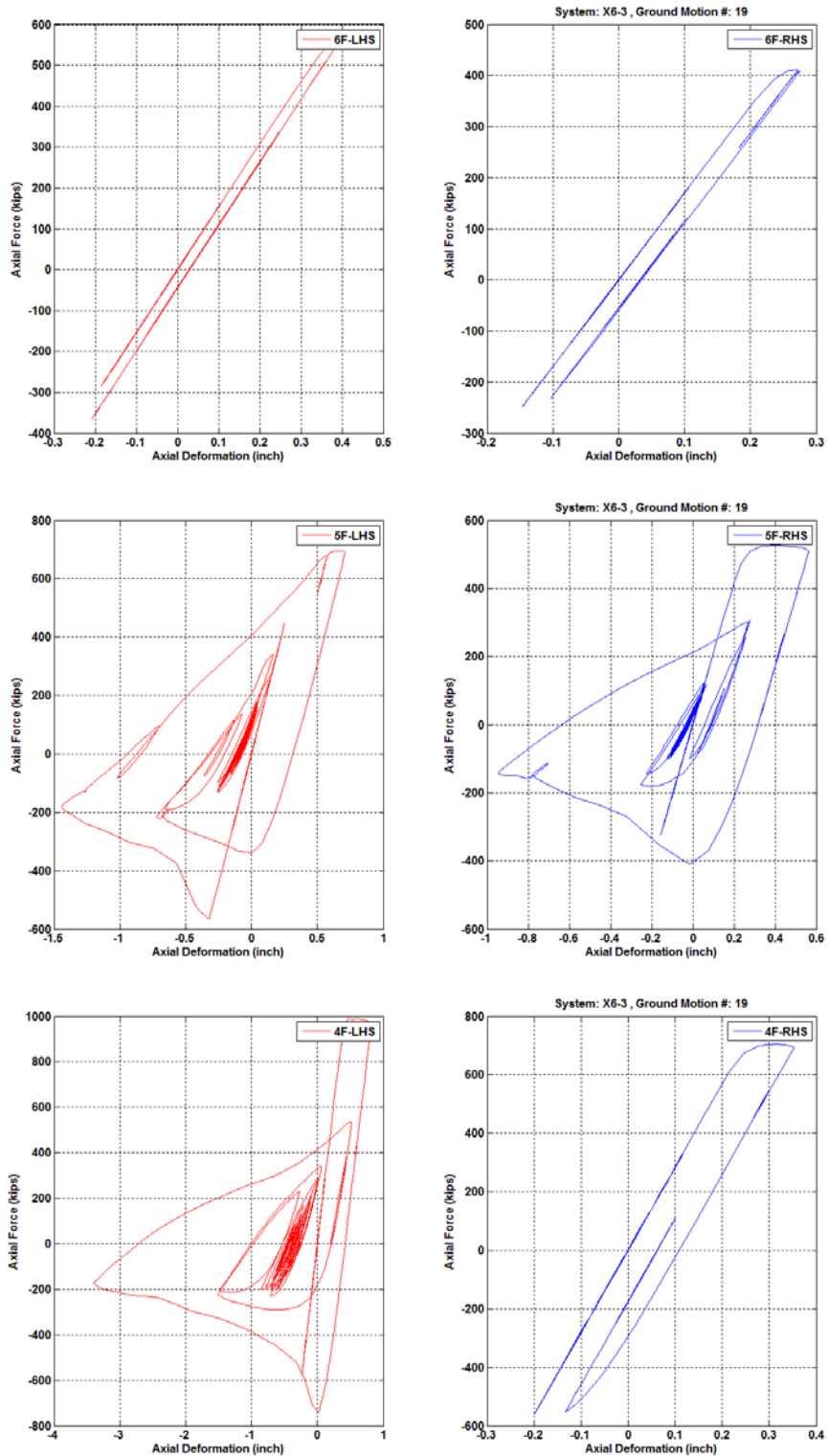
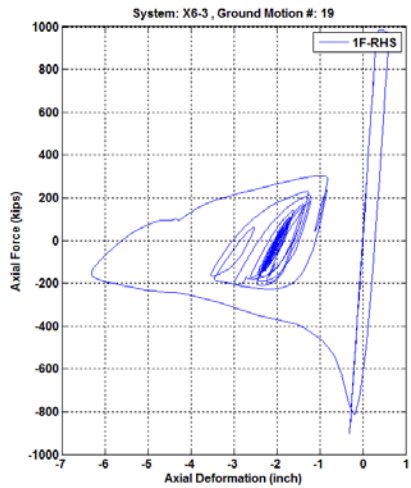
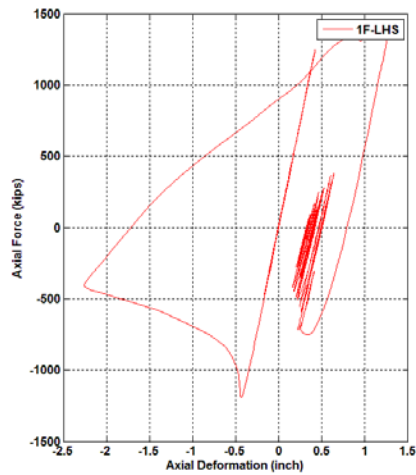
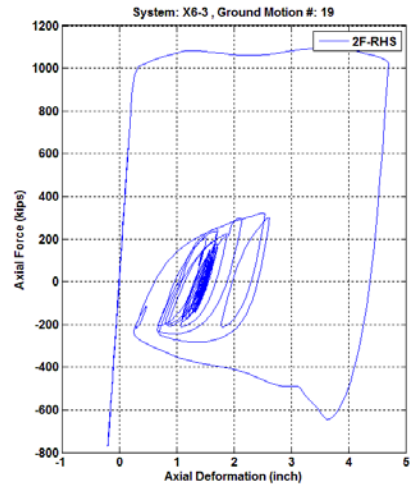
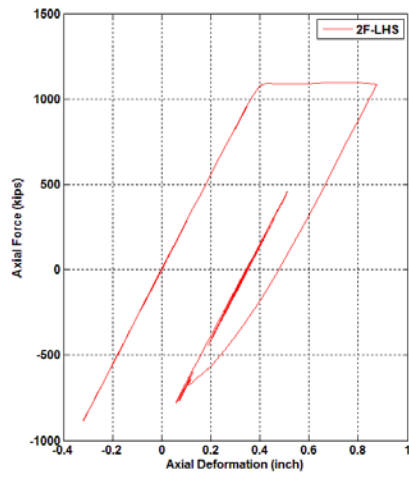
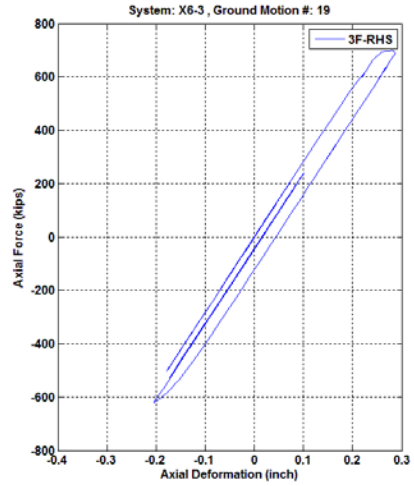
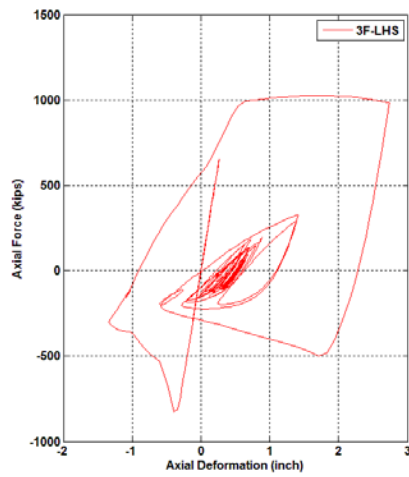
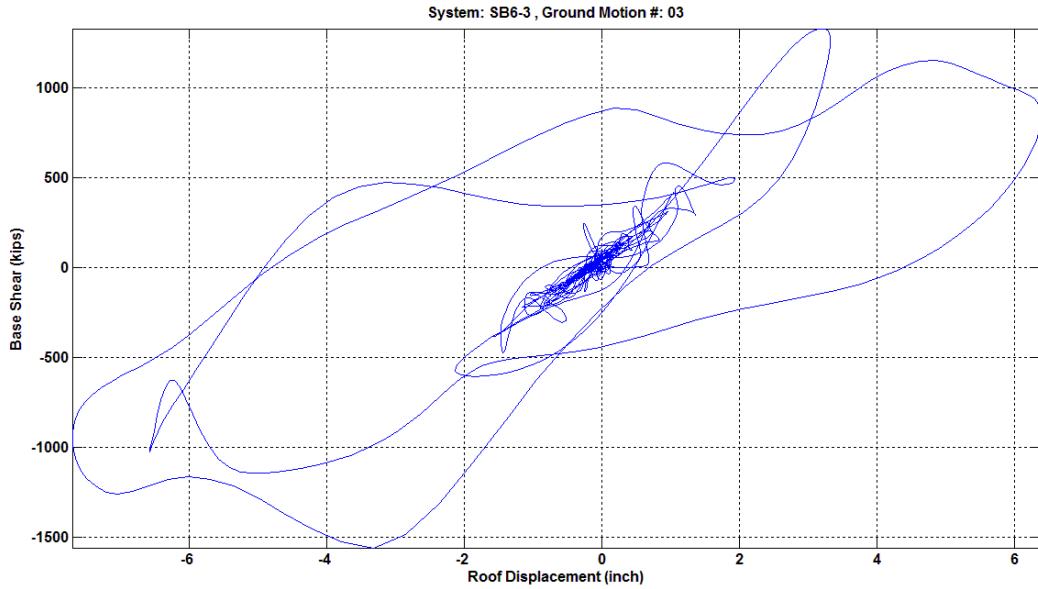


Figure 7.35 Fourth story to sixth story brace axial force versus axial deformation relationships of model X6-3 under NGA 1602 fault-parallel component ground motion



**Figure 7.36** First story to third story brace axial force versus axial deformation relationships of model X6-3 under NGA 1602 fault-parallel component ground motion





**Figure 7.37** Base shear versus roof displacement relationship of model SB6-3 under NGA 1119 fault-normal component ground motion

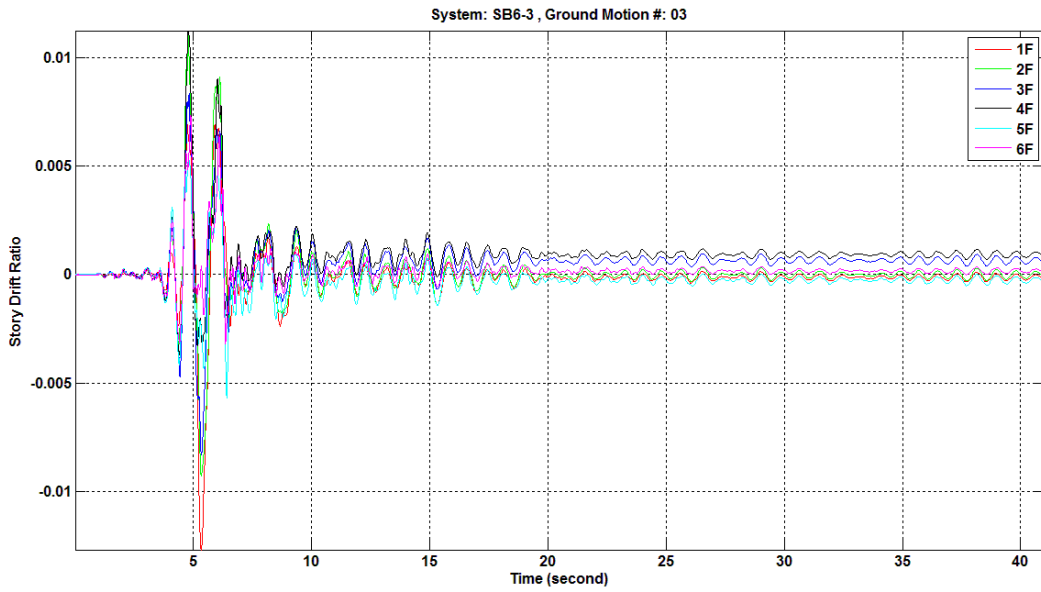


**Figure 7.38** Story drift ratio histories of model SB6-3 under NGA 1119 fault-normal component ground motion

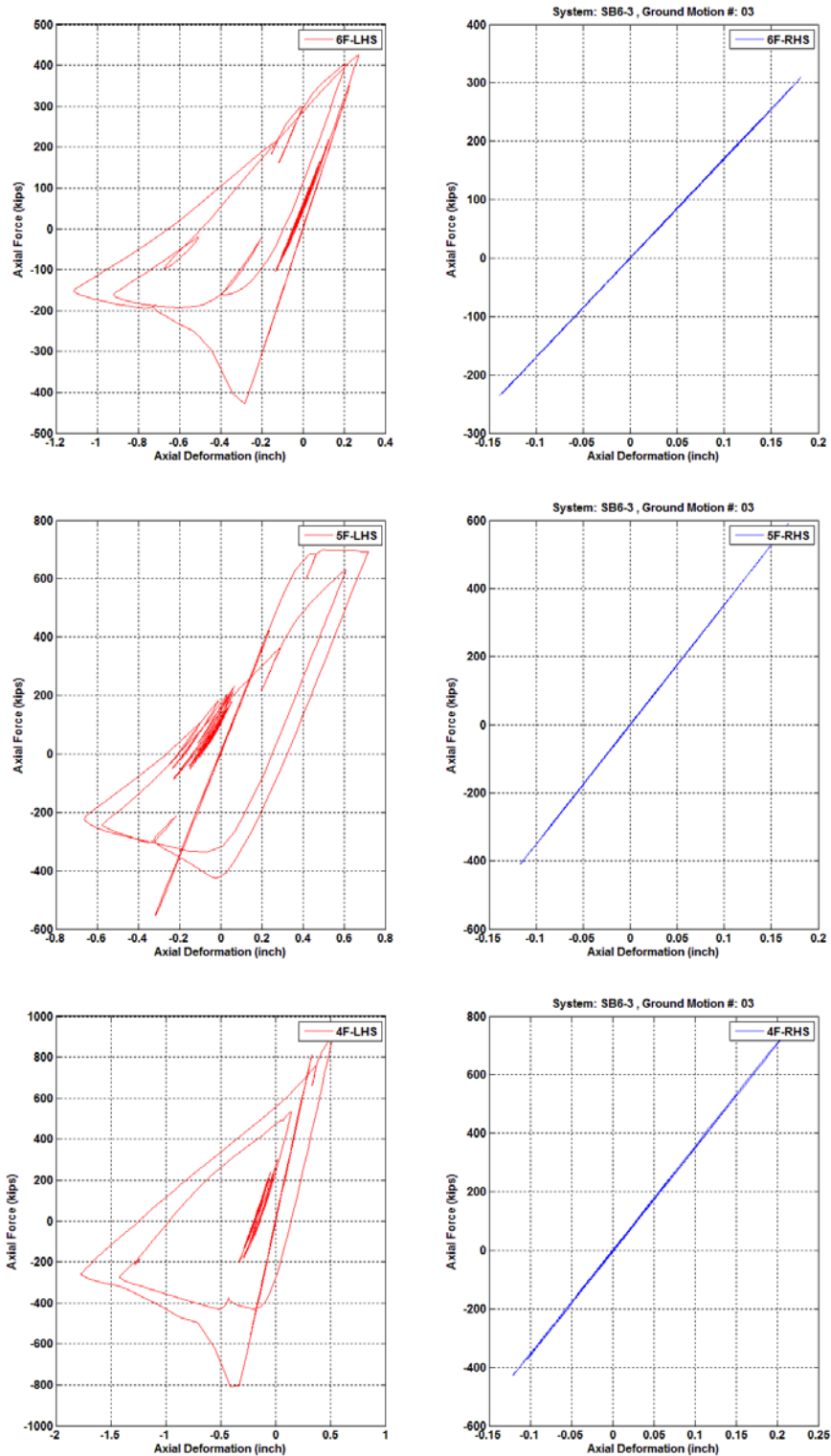


**Figure 7.39 Fourth story to sixth story brace axial force versus axial deformation relationships of model SB6-3 under NGA 1119 fault-normal component ground motion**

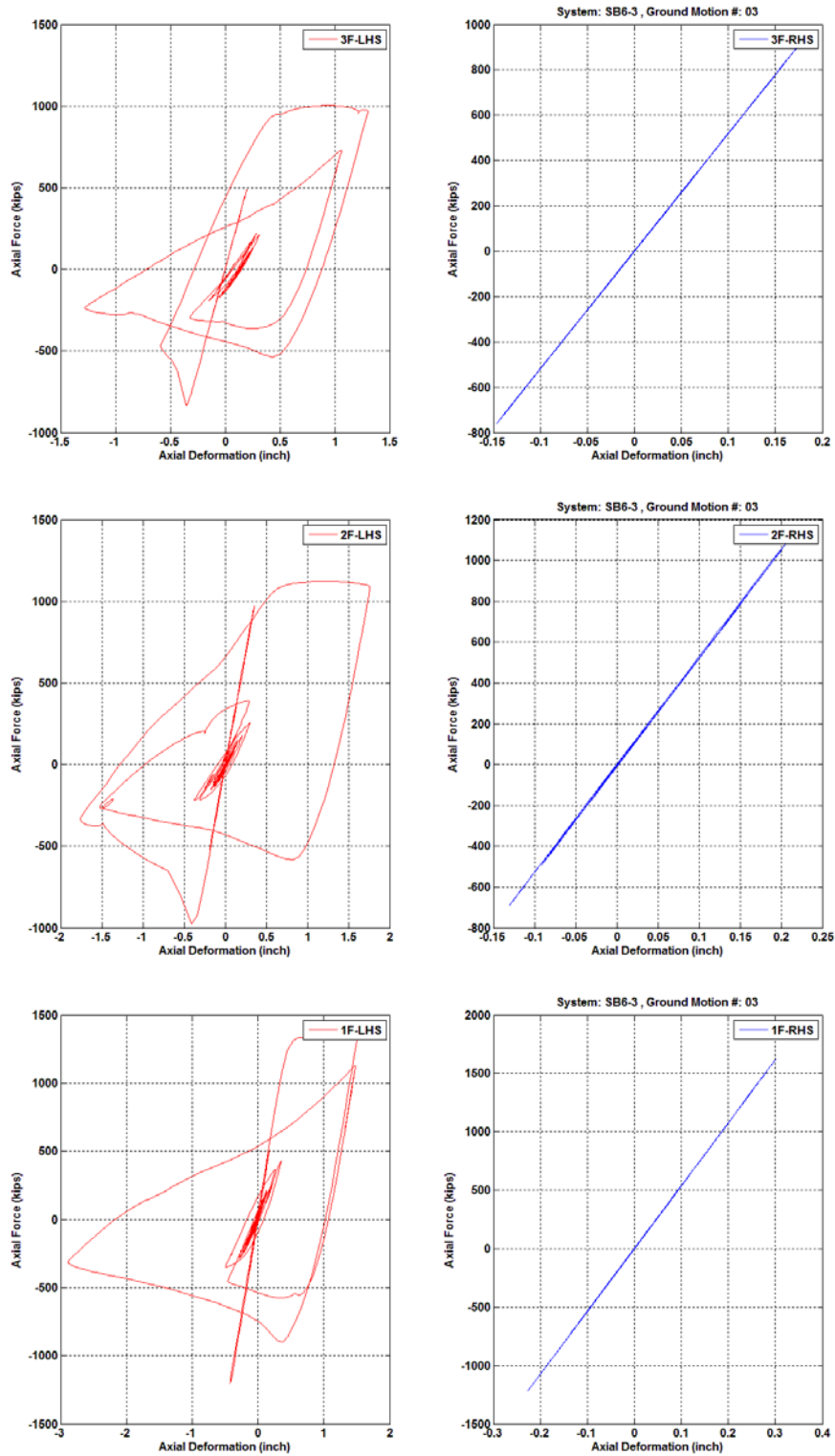


**Figure 7.40** First story to third story brace axial force versus axial deformation relationships of model SB6-3 under NGA 1119 fault-normal component ground motion

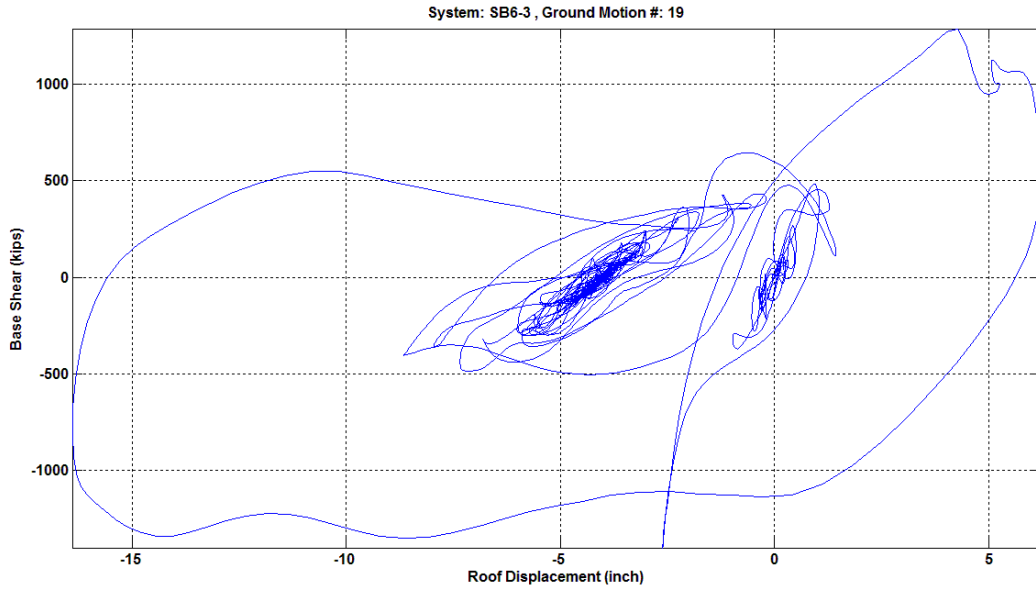


**Figure 7.41 Base shear versus roof displacement relationship of model SB6-3 under NGA 1602 fault-parallel component ground motion**

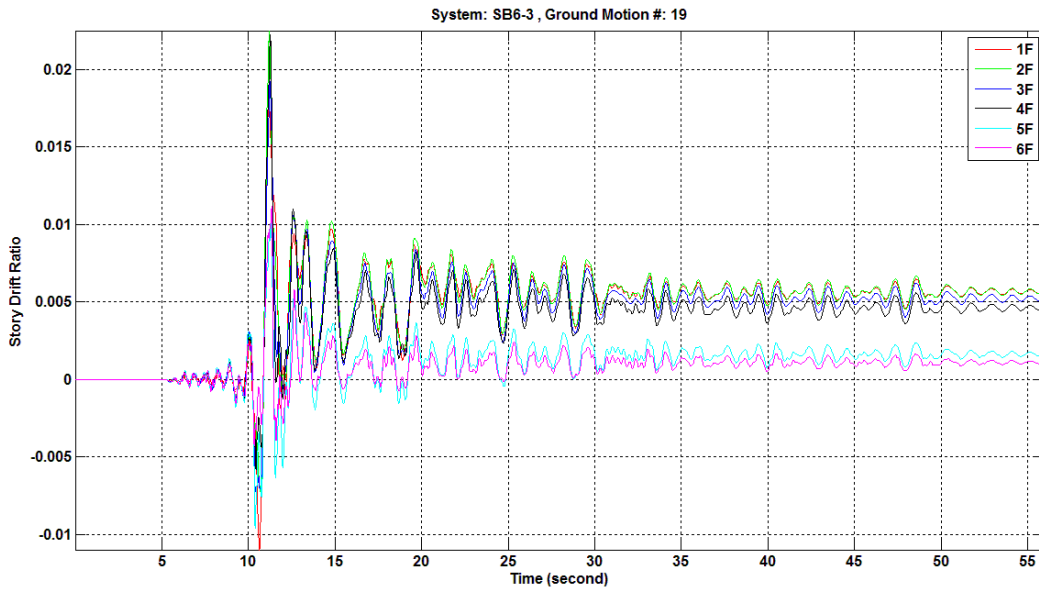


**Figure 7.42 Story drift ratio histories of model SB6-3 under NGA 1602 fault-parallel component ground motion**

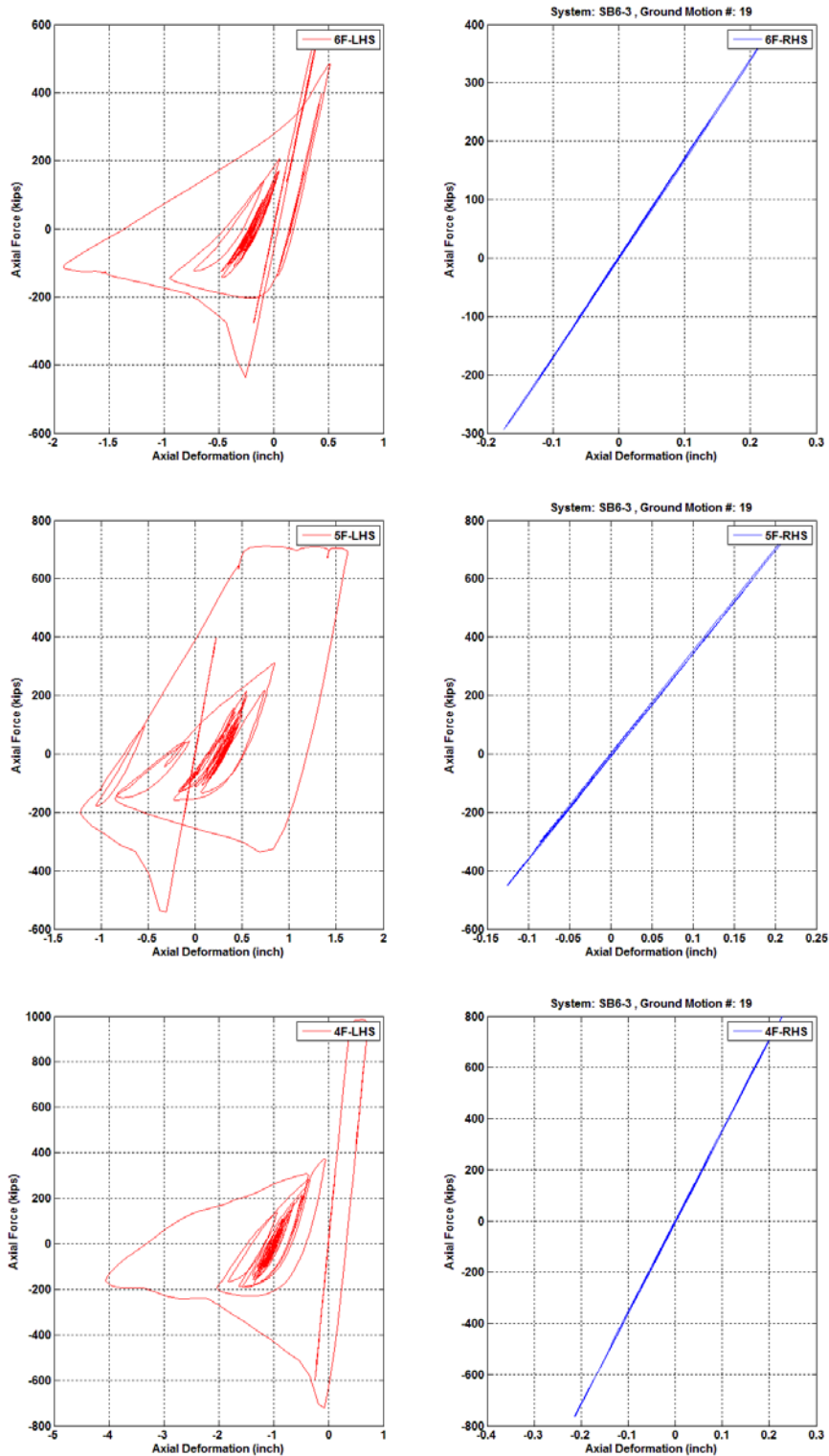
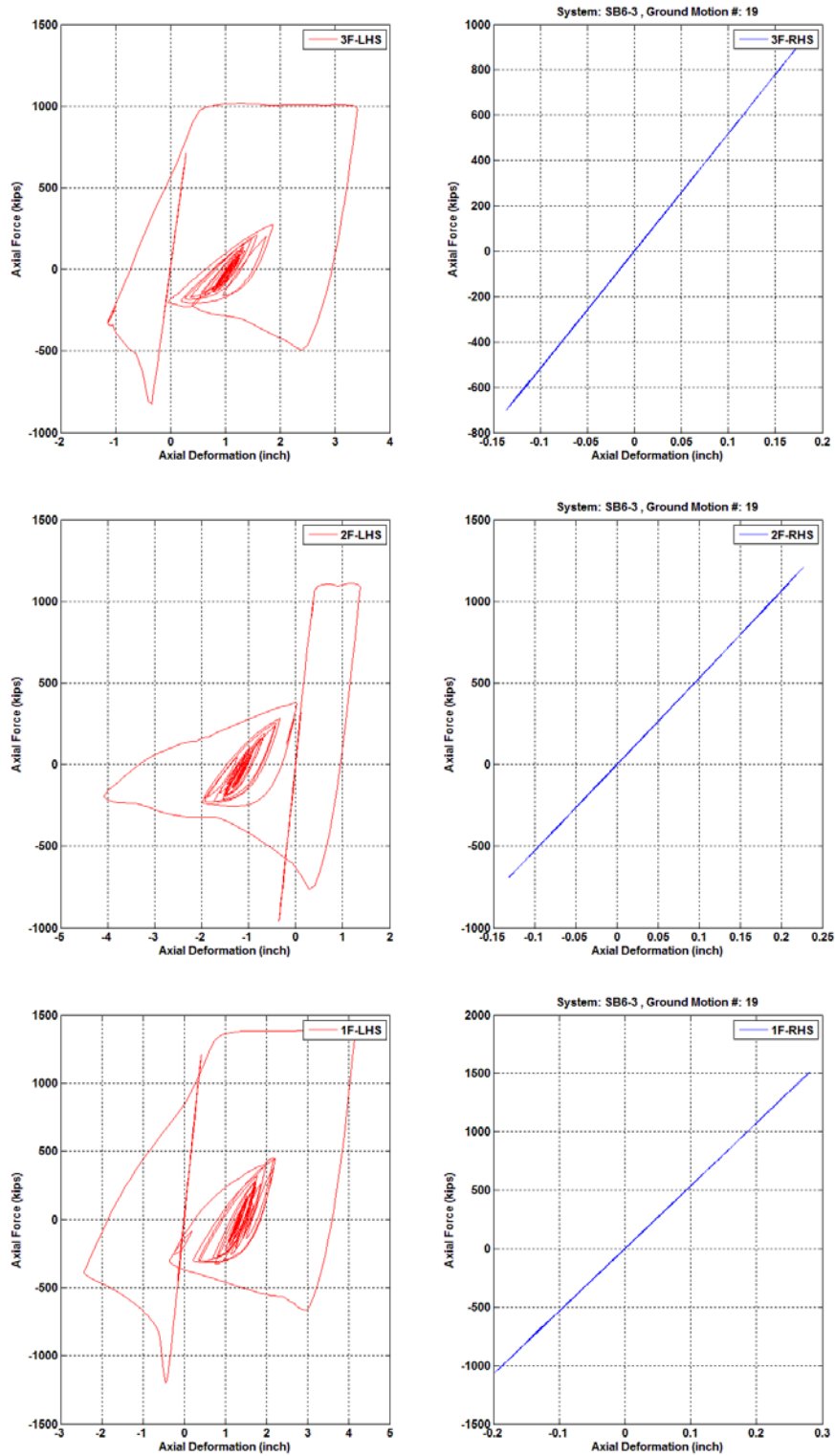
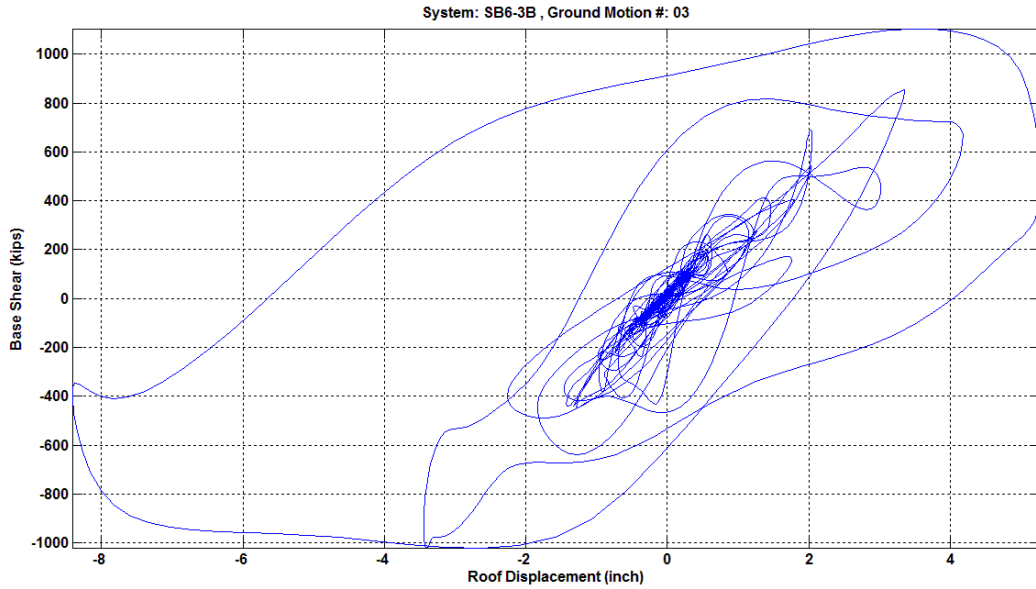


Figure 7.43 Fourth story to sixth story brace axial force versus axial deformation relationships of model SB6-3 under NGA 1602 fault-parallel component ground motion



**Figure 7.44** First story to third story brace axial force versus axial deformation relationships of model SB6-3 under NGA 1602 fault-parallel component ground motion



**Figure 7.45 Base shear versus roof displacement relationship of model SB6-3B under NGA 119 fault-normal component ground motion**

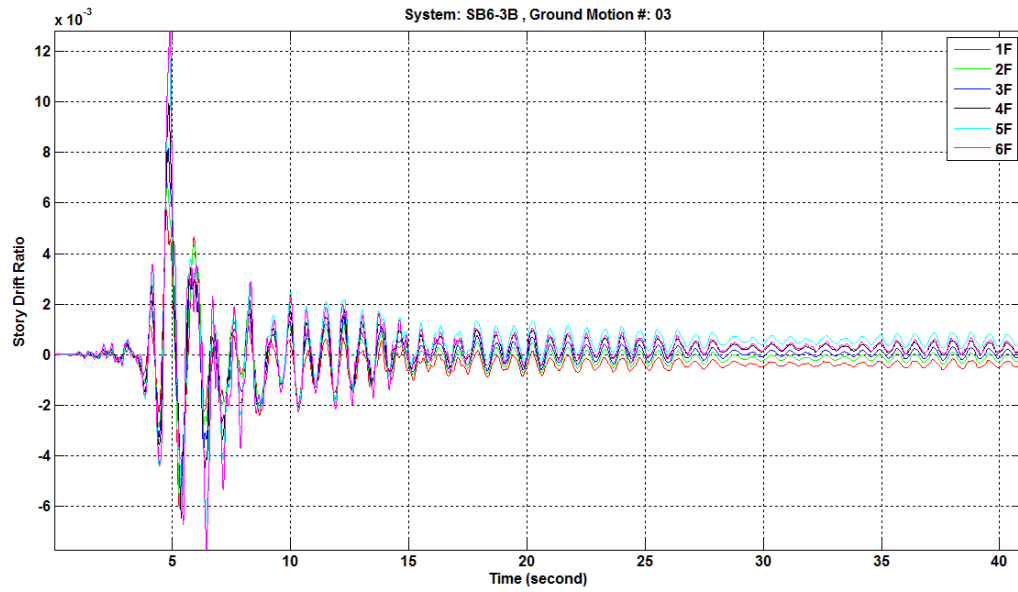


**Figure 7.46 Story drift ratio histories of model SB6-3B under NGA 119 fault-normal component ground motion**

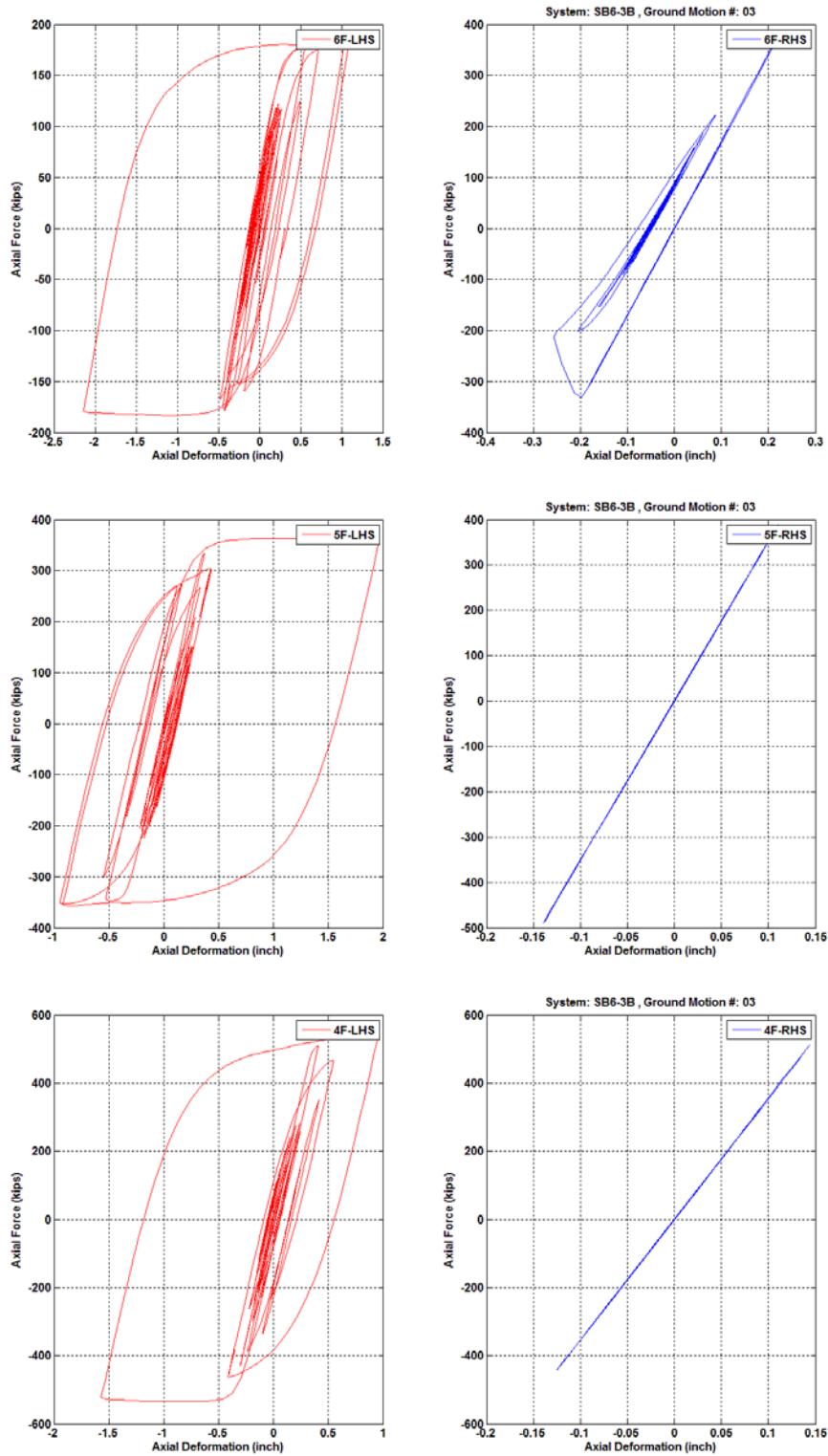
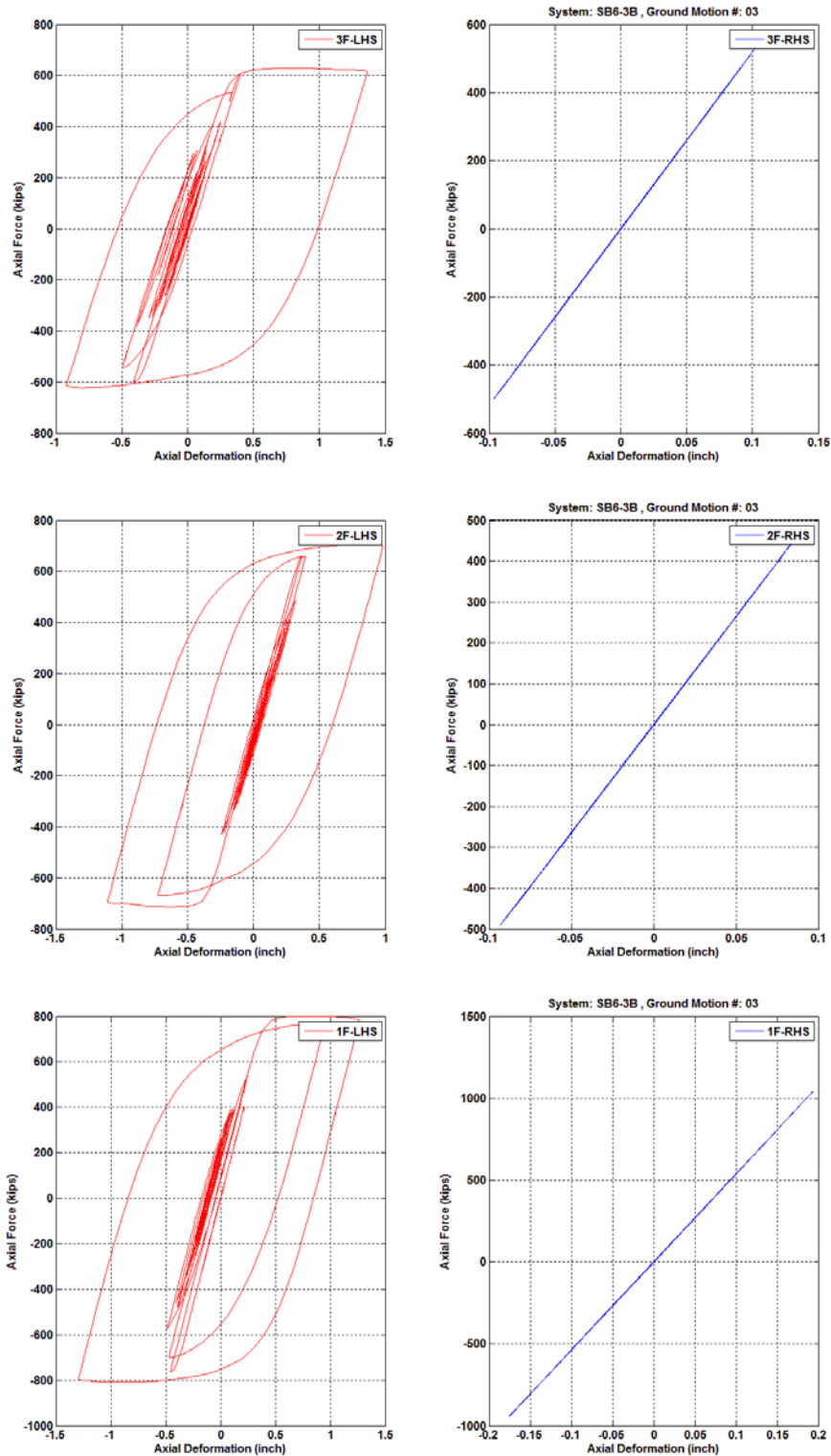
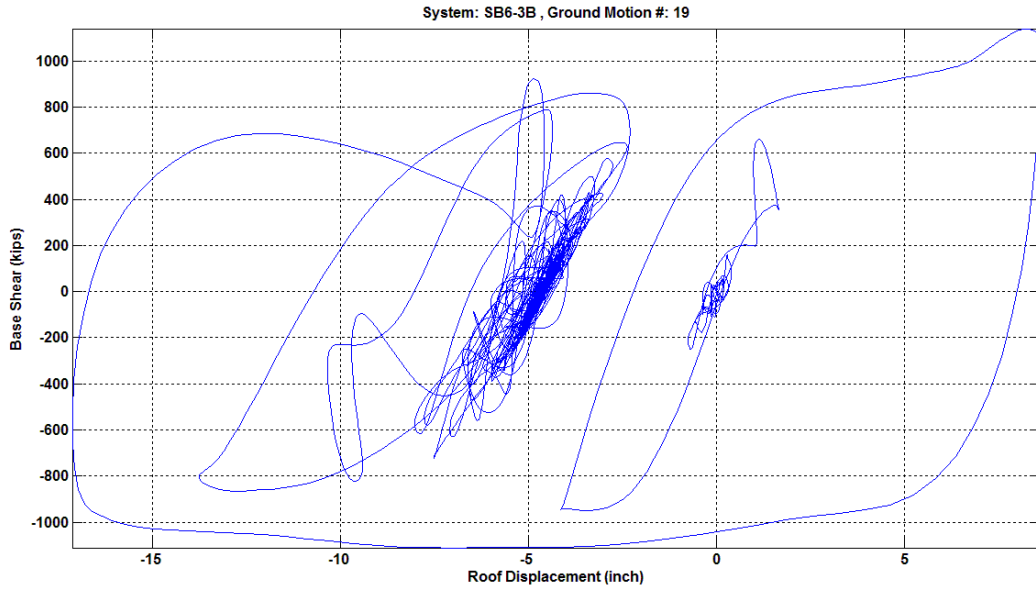


Figure 7.47 Fourth story to sixth story brace axial force versus axial deformation relationships of model SB6-3B under NGA 1119 fault-normal component ground motion





**Figure 7.48 First story to third story brace axial force versus axial deformation relationships of model SB6-3B under NGA 1119 fault-normal component ground motion**



**Figure 7.49** Base shear versus roof displacement relationship of model SB6-3B under NGA 1602 fault-parallel component ground motion

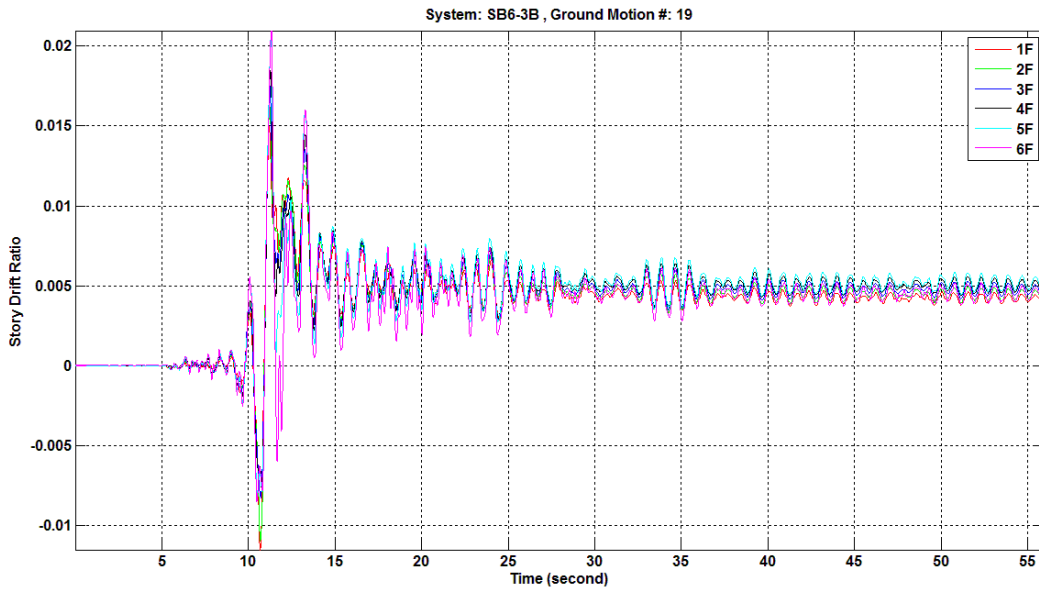


**Figure 7.50** Story drift ratio histories of model SB6-3B under NGA 1602 fault-parallel component ground motion

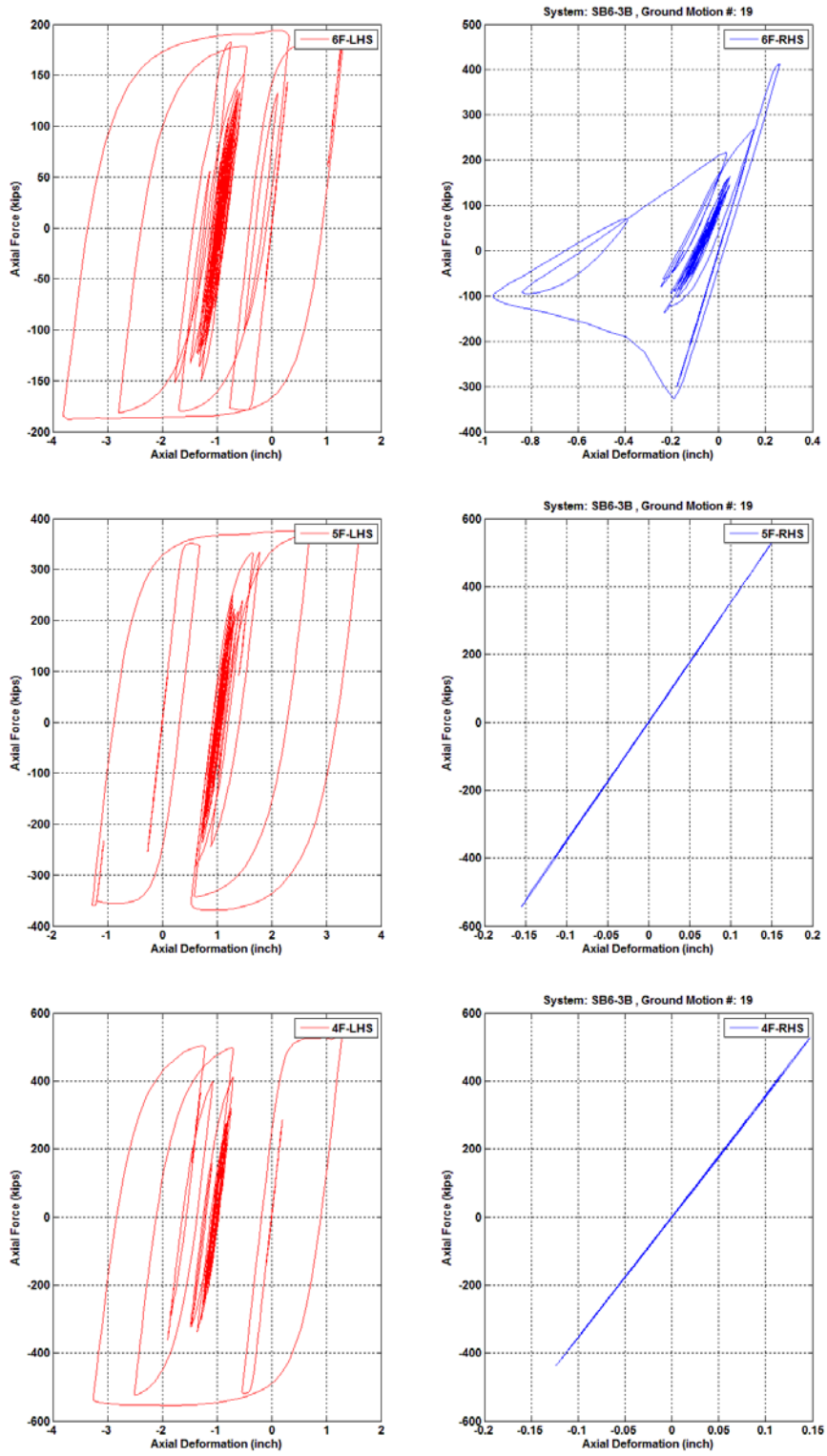
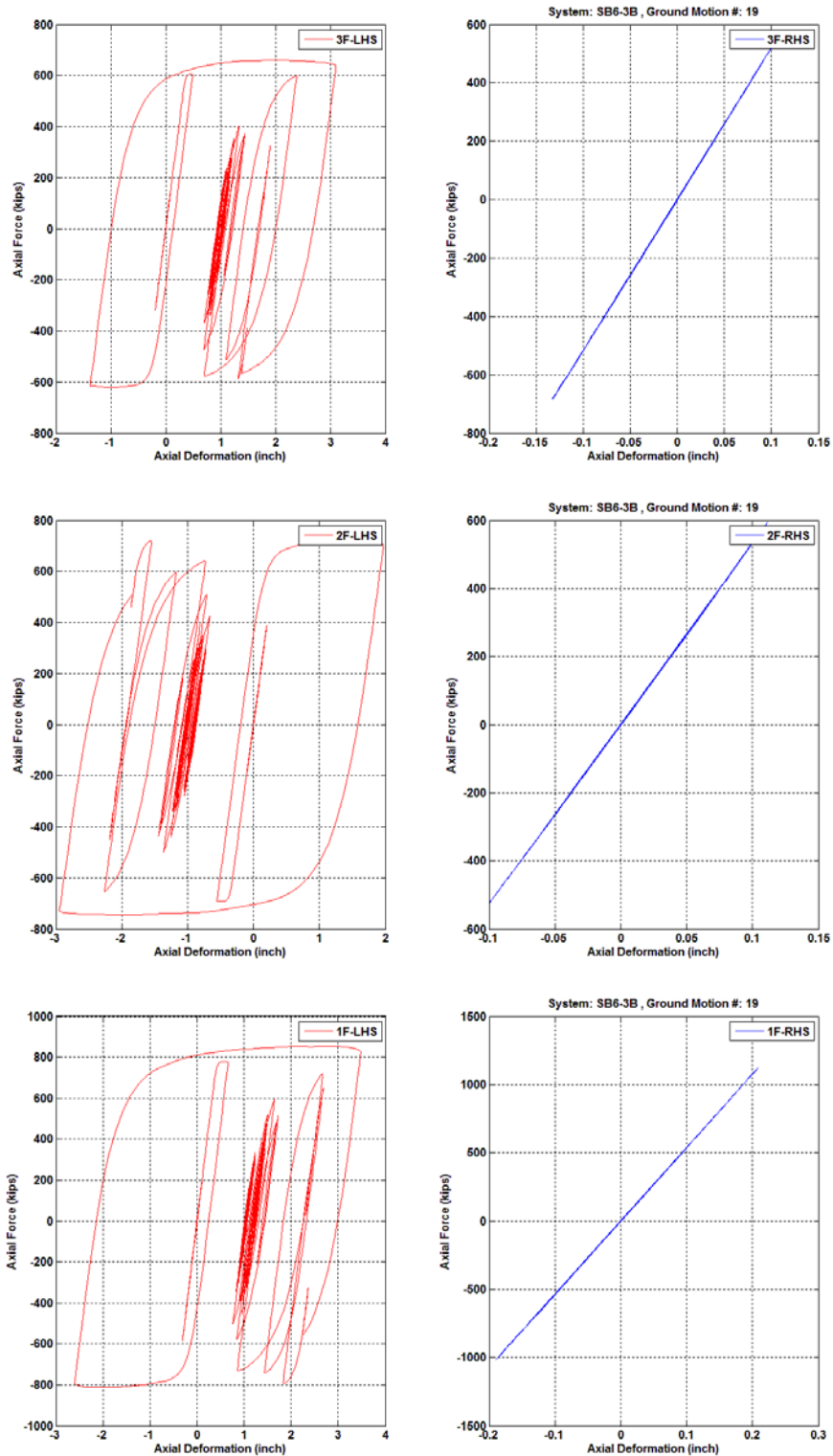
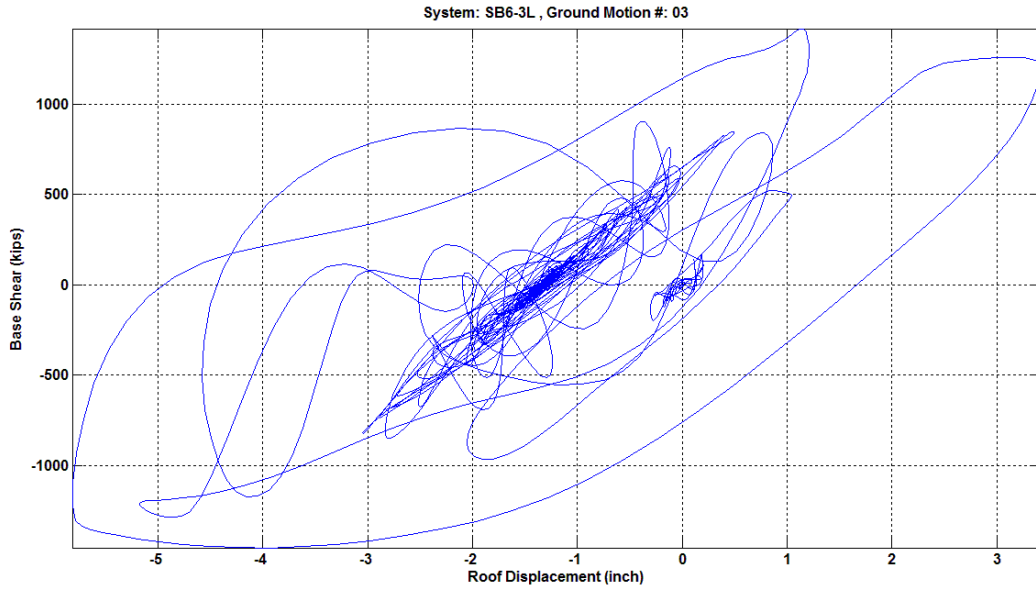


Figure 7.51 Fourth story to sixth story brace axial force versus axial deformation relationships of model SB6-3B under NGA 1602 fault-parallel component ground motion



**Figure 7.52** First story to third story brace axial force versus axial deformation relationships of model SB6-3B under NGA 1602 fault-parallel component ground motion



**Figure 7.53 Base shear versus roof displacement relationship of model SB6-3L under NGA 119 fault-normal component ground motion**

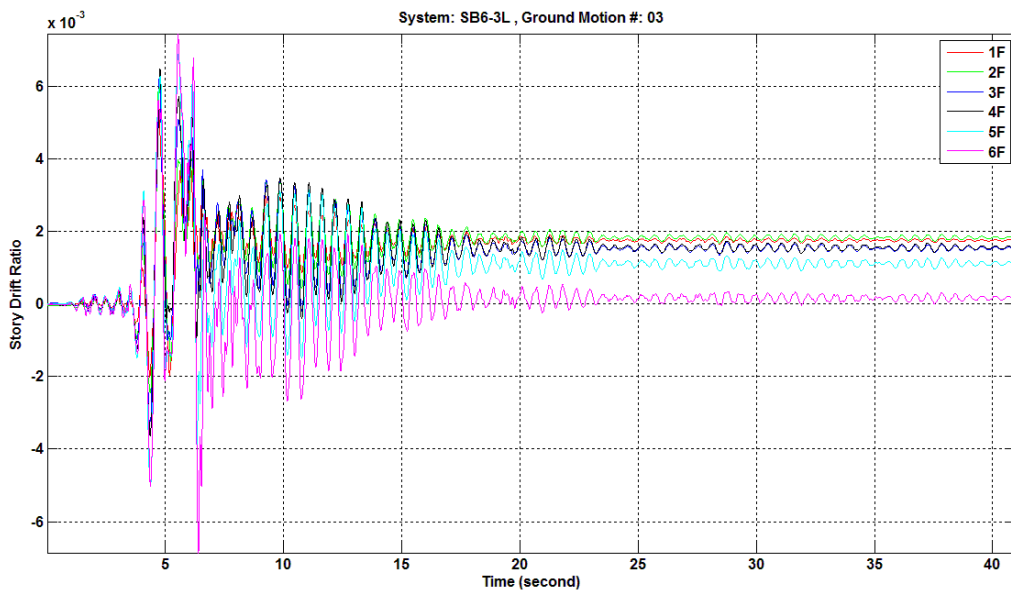


**Figure 7.54 Story drift ratio histories of model SB6-3L under NGA 119 fault-normal component ground motion**

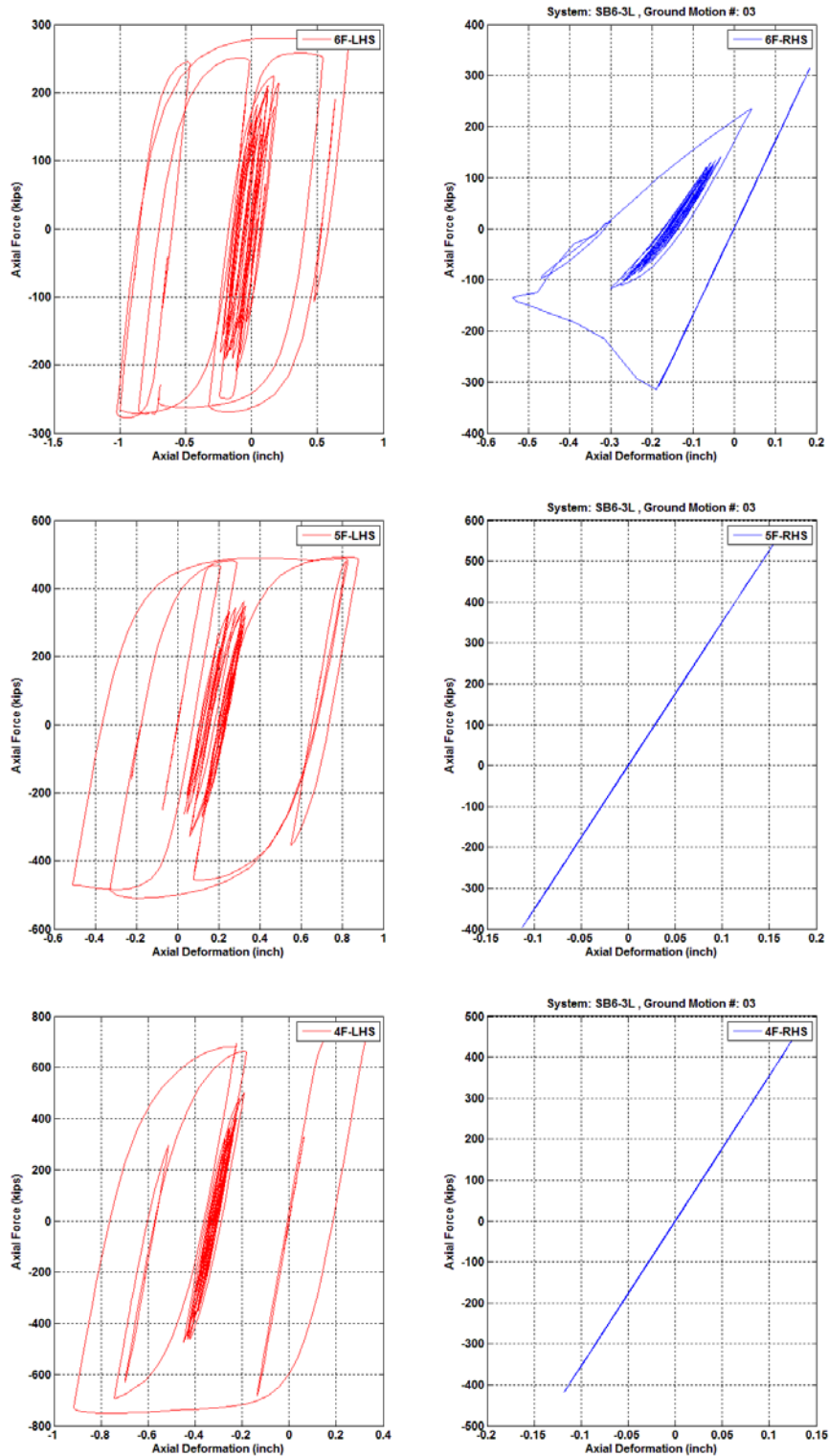
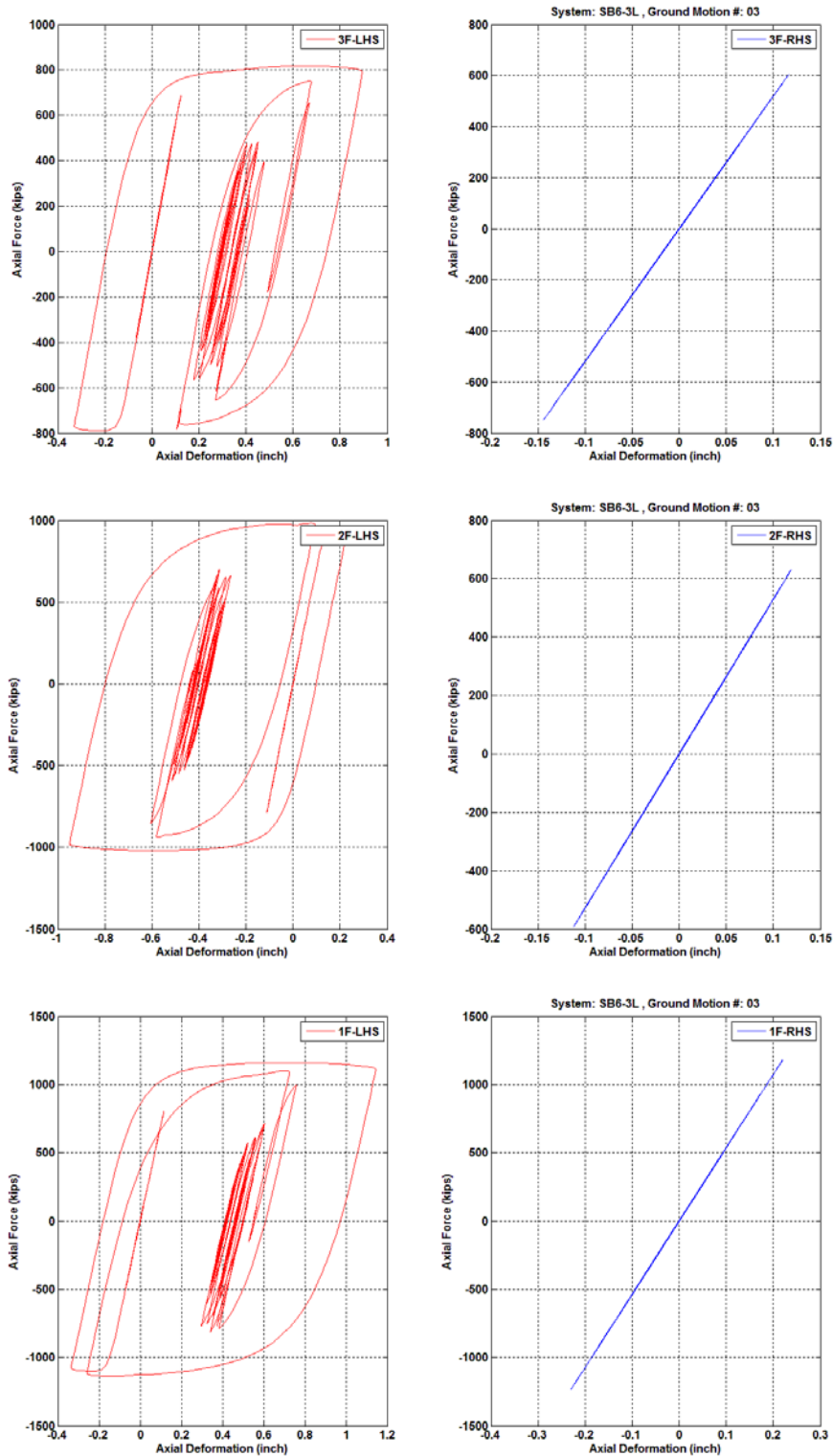
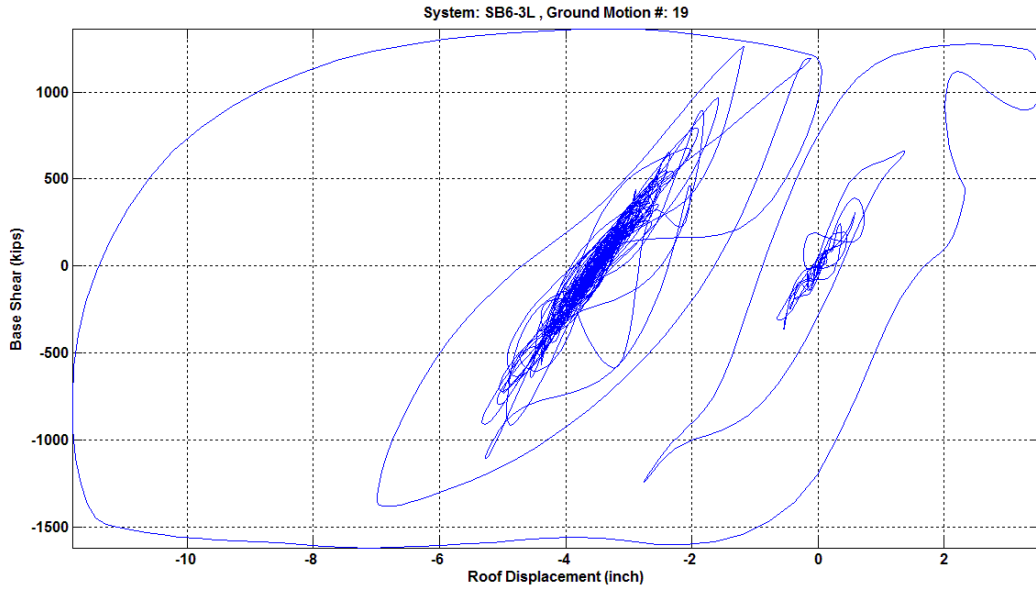


Figure 7.55 Fourth story to sixth story brace axial force versus axial deformation relationships of model SB6-3L under NGA 1119 fault-normal component ground motion



**Figure 7.56 First story to third story brace axial force versus axial deformation relationships of model SB6-3L under NGA 1119 fault-normal component ground motion**



**Figure 7.57** Base shear versus roof displacement relationship of model SB6-3L under NGA 1602 fault-parallel component ground motion

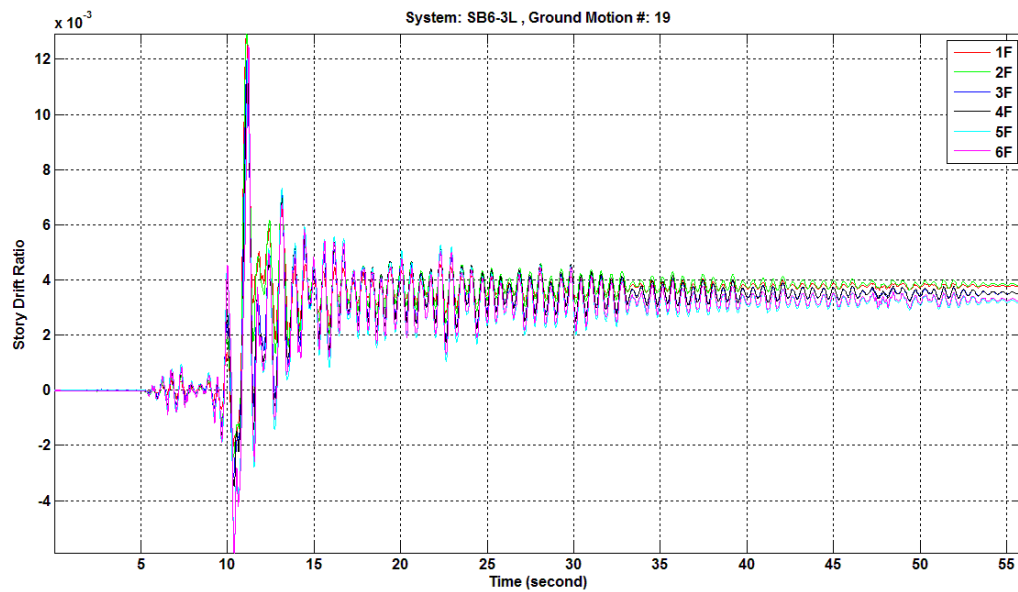


**Figure 7.58** Story drift ratio histories of model SB6-3L under NGA 1602 fault-parallel component ground motion



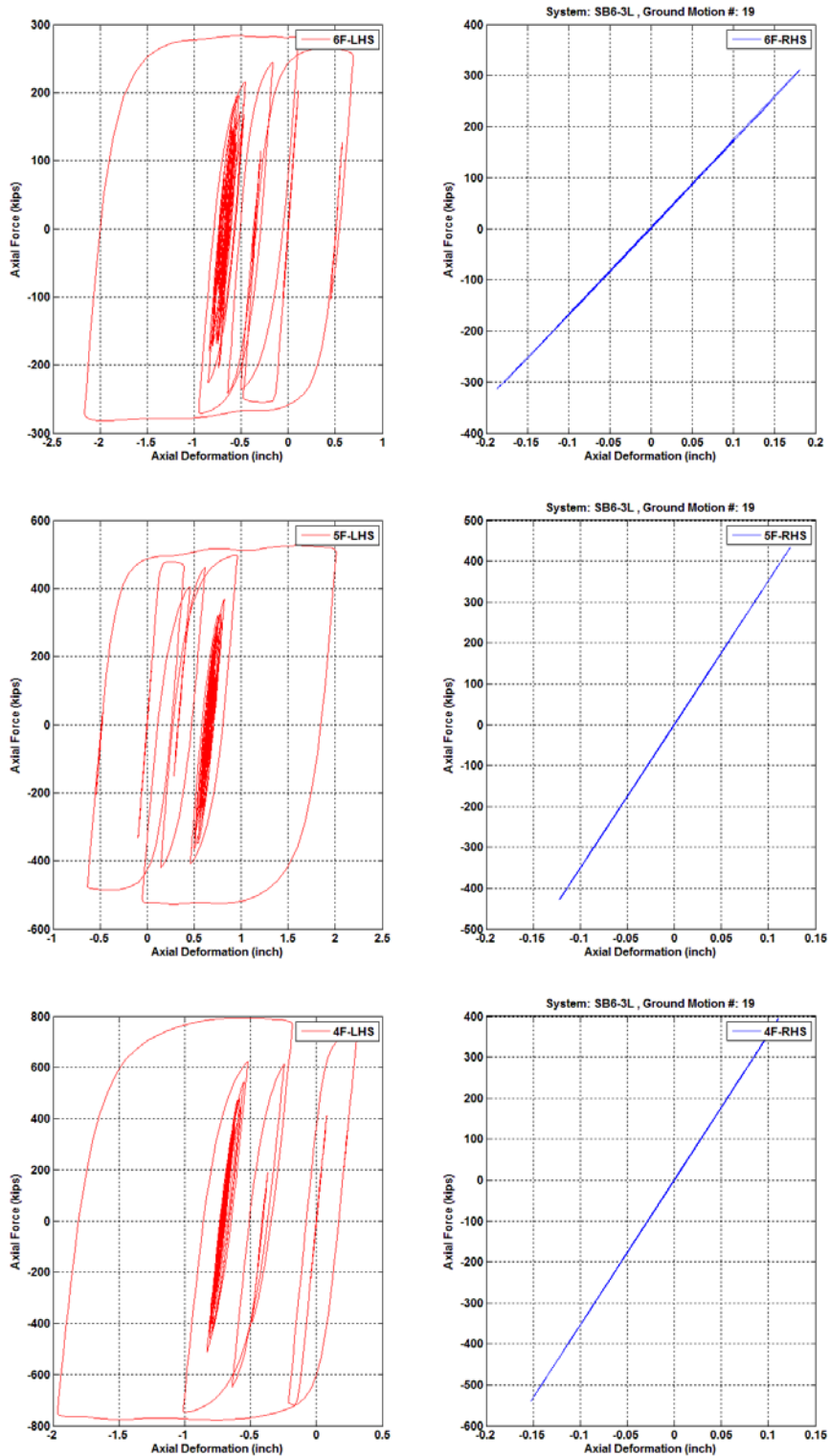
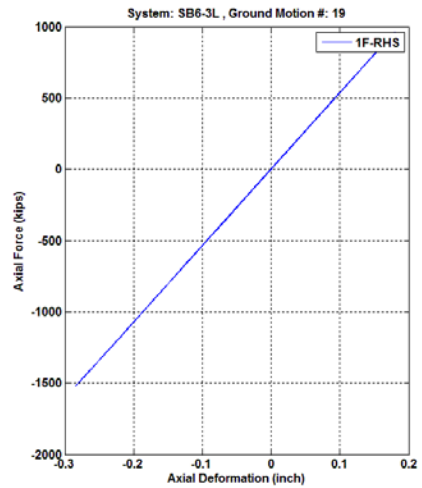
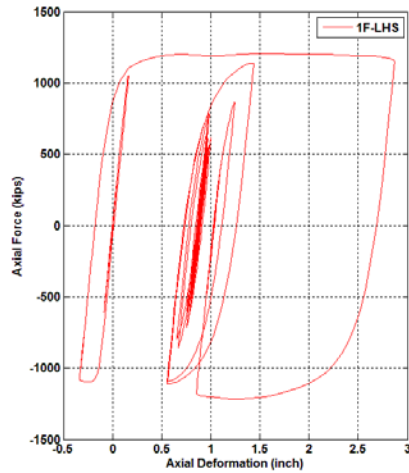
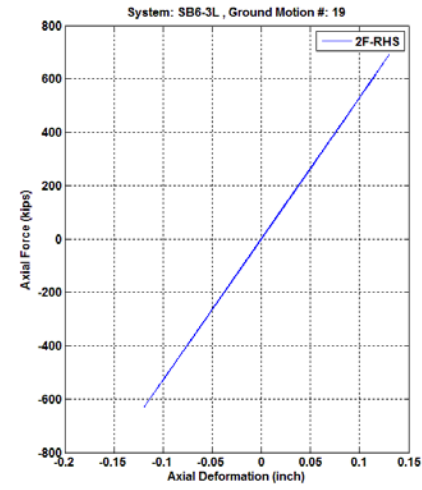
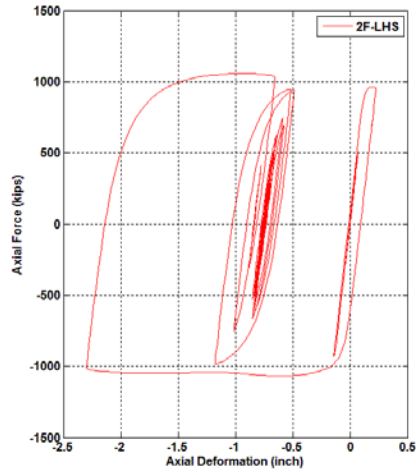
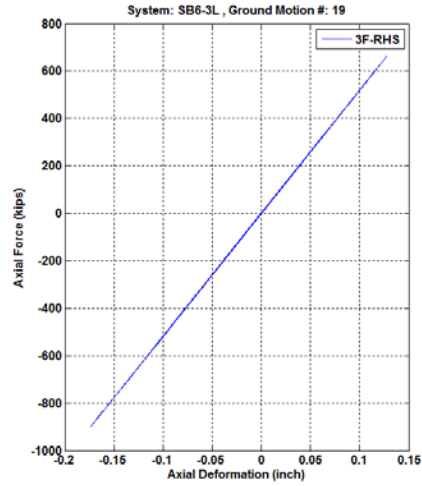
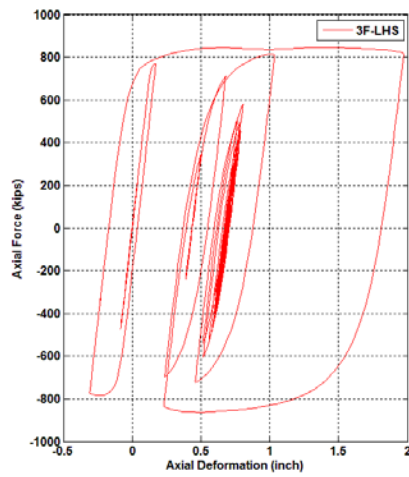


Figure 7.59 Fourth story to sixth story brace axial force versus axial deformation relationships of model SB6-3L under NGA 1602 fault-parallel component ground motion



**Figure 7.60 First story to third story brace axial force versus axial deformation relationships of model SB6-3L under NGA 1602 fault-parallel component ground motion**

## 7.7 CONCLUDING REMARKS

Based on the static pushover analysis and nonlinear dynamic response history analysis results, the following conclusions can be drawn:

1. The proposed hybrid strong-back system effectively prevented the soft-story mechanism in the braced frame system.
2. The simplified design strategy that proportioned vertical spine member sizes in the hybrid strong-back system appeared to achieve a key performance goal: uniform story deformation. Design optimization of this simple strategy should be studied further.
3. Although using high-performance braces such as BRBs in the strong-back system can further improve the deformation capacity of the entire system, larger residual deformations are expected to occur in such hybrid braced frame systems. Using the devices with self-centering mechanism can further reduce the residual deformation.
4. The current analytical study demonstrated that the shape-tailing concept used in the strong-back system tended to impose higher deformation demands at higher floor levels, especially at the roof floor level. Such a fling effect needs to further investigation.

## 8 Conclusions and Recommendations

This study focused on determining through experimental and analytical means a better understanding of the seismic behavior of concentrically steel braced frame systems, and using that understanding to improve response. A literature review was initially carried out to identify gaps in knowledge and trends in research so that specific high priority experimental and analytical research objectives would be addressed. Relatively few studies of complete concentric braced frame systems had been completed at the beginning of this research, so priority was placed on obtaining experimental data on the behavior of complete large-scale braced frame systems. A total of four full-scale, one-bay, two-story concentrically steel braced frame specimens were tested using both quasi-static and hybrid simulation techniques. These frames a number of details intended to facilitate construction and improve seismic performance. Three different bracing member sectional shapes were considered to be able to relate the behavior of individual braces to system behavior. To examine the sensitivity of observed behavior on test method and loading history, a standard quasi-statically applied test protocol was used as well as a more realistic hybrid test that simulated the response of the frame to an actual earthquake. Various changes in the specimen designs were made during the test program to take advantage of knowledge learned in earlier tests.

Analytical models of the test specimens were developed using line elements with fiber-based section representations (in OpenSees) and using shell elements (in LS-DYNA). In both cases, modeling of the rupture of braces and other key elements was evaluated using available low-cycle fatigue damage models incorporated into the software. The relative benefits and deficiencies of these modeling approaches were identified. The validated numerical modeling approach developed for OpenSees was then used to examine the performance of “vertical truss masted” or “strong-back” braced frame systems with different configurations, and to compare computed responses with those for more the conventional braced frames.

Each chapter presents conclusions and discussions with regard to that phase of this study. The following sections summarize the overall conclusions with some recommendations for future research.

### 8.1 EXPERIMENTAL PHASE

**General behavior of braces.** – The braces buckles as expected in all specimens, and at relatively low levels of story drift compared to first yielding of moment resisting frames. The tapered gusset plates with  $2t_g$  inelastic yield lines performed well in all of the tests. The brace out-of-plane displacement could be as large as ten times the axial displacement under compression. This indicates that significant damage of nearby nonstructural components could occur. Brace inelastic deformations tended to concentrate at the middle length of the braces. Local buckling of section occurred at these locations and braces tended to rupture due to low-cycle fatigue in the region where local buckles occur around 1.9% inter-story drift. The remaining braces and frame are called upon to resist subsequent loading.

**Effect of brace cross-sectional shape.** – From the three experiments having the same quasi-static cyclic loading protocol, it is clear that braced frames using round hollow structural sections as bracing members (i.e., specimen TCBF-B-2) exhibited greater lateral deformation capacity before the onset of significant strength deterioration than specimens using square hollow structural sections (TCBF-B-1) or wide flange sections (TCBF-B-3) for the braces. However, among these three specimens, the peak base shear forces degraded more slowly in specimen TCBF-B-3 with wide flange braces. Local buckling of the bracing members and large loss of specimen lateral capacity occurred later in Specimen TCBF-B-2 specimen. Typically, available round hollow structural sections in the current design manual have width-to-thickness ratios ( $D/t$ ) that are far below the code limit, whereas square and wide flange members used are often at or near the corresponding code limits. Consequently, round hollow structural sections as brace components will usually be more resistant to local buckling than these other sections, thereby improving the performance of the system. This is consistent with component test results seen in previous studies by others.

**Adequacy of reinforcement provided at the net reduced areas regions of brace to gusset plate connections.** – Reinforcing details at the brace-to-gusset plate connections for each specimen performed well during both quasi-static and pseudo-dynamic tests. The details provided satisfy current AISC Seismic Provisions.

**Formation of weak or soft stories.** – Once buckling initiated, the story drifts at each story in Specimens TCBF-B-2 and TCBF-B-3 tended to be more uniform than in Specimen TCBF-B-1. This may be a result of the more severe deterioration of the hysteretic characteristics of square HSS sections (based on the observations). The three quasi-statically tested specimens were subjected to the same loading protocol where identical roof displacements were imposed and the forces applied to the lower floor were half of the force applied at the roof. For the case where hybrid simulation was used, damage was more uniformly distributed over the height of the structure. Thus, the effects of higher modes, and other characteristics of the response (local deterioration), that would change the distribution of dynamic loads over the height may be important (and potentially beneficial) effects to consider in future tests.

**Frame action.** – The brace and gusset plate configuration at the lower floor resulted in large, stiff “haunches” at the ends of the beam. During lateral deformation of the frame, the gusset plate geometry tends to amplify the rotational demand at both ends of lower beam-to-gusset splices. This is similar to the rotational amplification (due to geometry) in the link beam of an eccentrically brace frame system. For Specimens TCBF-B-3 and TCBF-B-4, pinned beam-to-gusset details were used to avoid local damage such as flange or web buckling and fracture at these regions. From the observations during these two tests, the pinned connection details effectively avoided any undesired failure mode at beam-to-gusset plate connection regions. However, the entire braced frame lateral capacity was reduced as a result of the moment release at lower beam end connections.

**Effectiveness of one-piece gusset plates.** – No adverse effects were detected with use of one-piece gusset plates rather than two separate gusset plates, one located above and another below a beam where two braces intersect at a column. As noted above, and in other research (Uriz and Mahin, 2008), yielding of the beam at the end of the gusset plate can fracture to due stress

concentrations in the beam at the end of the gusset plates. These details are complicated especially where the one piece gusset plate and its stiffeners are welded to the beam to mimic a continuous beam that extends all of the way to the column. The weld access holes and other details at this location may have exacerbated, but not caused the fractures identified in Specimens TCBF-B-1 and TCBF-B-2. The pinned connection used in Specimens TCBF-B-3 and TCBF-B-4 performed as intended. It is not clear that the single piece gusset plates improve constructability or reduce construction costs.

**Effects of brace lateral buckling on frame behavior.** – Local eccentricities at the both ends of each bracing member measured after the fabrication were not always consistent with the actual direction of out-of-plane buckling, and other source of eccentricities at gusset plate-to-beam and gusset plate-to-column interfaces can also effect the buckling direction. For example, two braces connecting to the same one-piece gusset plate tended to buckle in the same out-of-plane direction. Without the floor slab acting as a restraint, the column that is adjacent to the single-piece gusset plate may be subject to torsion due to the eccentricities of the buckled braces. Further investigation seems warranted on evaluating the demand of the bi-axial bending or torsion in the column induced by out-of-plane buckling of the braces, and how much this affects the behavior of column when severe buckling occurred in the braced frame.

**Concern for column base plate behavior.** – In all of the tests, significant fractures initiated in the complete joint penetration welds at the column bases or near the ends of stiffeners provided at this location. Because of the diamond shape configuration of the braces in the specimens tested, gusset plates were not present at the base of the columns. Thus, these connections resemble situations where thick base plates are provided at the base of columns in moment resisting frames. This suggests the need for further research on the cyclic inelastic behavior of column bases where high variations of axial load are expected.

**Effect of loading protocol.** – As noted previously, the quasi-static tests tended to form weak or soft stories to varying degrees. For the hybrid simulation, damage at the end of the two earthquake records imposed was more equally distributed between the two stories. During the hybrid simulation one brace fractured near the end of design-level ground motion. The fractured brace was located in the second story not in the ground story, as was expected based on the quasi-static tests. Story deformation concentration was observed in the second story, especially after the second-story brace began localized buckling locally during the hybrid test. This deformation concentration was easily identified, especially when entire hybrid test specimen moved toward the negative direction (to the west side of the lab). No significant residual roof level displacements were found after the 20 sec. at the design-level ground motion.

Since only one ground motion record was used during the simulation, the braced frame responses may change as input ground motion changes. It was also noted in subsequent analysis that the behavior of the braced frame depends on the earthquake histories used. In particular, the hybrid simulation indicated that the specimen would not be able to withstand a design level event followed by a larger MCE level aftershock, but it could withstand the MCE level event had the earlier event not occurred. Thus, this result suggests that behavior is sensitive to the characteristics, intensity and duration of main shocks and aftershocks. Further investigation on the effect of ground motions upon the seismic responses of braced frame systems is suggested

before more solid conclusions can be made. The interested reader is referred to Chen and Mahin (2010).

Lateral force distribution during the hybrid testing demonstrated that the distribution varied with time, but most of the time the shape was close to an inverted triangle. This observation supports the force distribution assumption used in quasi-static tests.

**Recommendations for future experiments.** – The experimental results of four braced framed specimens described in this dissertation focused on a specific bracing configuration, several common braces with different cross-section shapes, and typical details in the field. A specific set of geometric parameters were used in the specimen in response to the limitations of the test set up, laboratory space, the laboratory facility, and research funding. A more comprehensive test program covering a wide spectrum of the brace sections, particularly those commonly used in the field, is needed.

## 8.2 ANALYTICAL PHASE

**Adequacy of fiber-based models.** – The fiber based section models used in conjunction with line elements in OpenSees were able in this study to capture the overall behavior of the braced frame specimens. It was found that due to the early deterioration and fracture of the braces and other elements modeling of the degradation and rupture of elements due to low-cycle fatigue is essential. With the low-cycle fatigue model enabled in OpenSees, the cyclic degradation of bracing and frame members was possible to track approximately. Fatigue material parameters used in OpenSees for three different brace section shapes were slightly different, based on calibration of the numerical model with the actual test results. Although the global behaviors of the braced frame specimens matched the fiber model results within an acceptable range, the match of behaviors of individual brace were not as accurate. As noted previously, the fiber model used in OpenSees cannot simulate local buckling in braces or other elements.

Based on the calibrated fiber models, a parametric analysis was carried out on braces with square hollow structural sections. These braces had different dimensions and lengths and were subjected to the same normalized cyclic deformations (Chapter 6.4). The group mean of normalized energy dissipation is highly related to the member slenderness ratios and is also affected by the width-to-thickness ratios of the braces. It is noteworthy that the width-to-thickness ratio of the braces has only minor effect on the simulated brace energy dissipation capacity. This is because fiber models as implemented in OpenSees models do not simulate local buckling effects. Because of the limitations of fiber models, more complete data from full-scale experiments or from sophisticated finite element analyses are required before the successful modeling of localized buckling of braces and the propagation of cracks can occur.

**Adequacy of shell based models.** – Finite element models using the shell elements implemented in LS-DYNA were able to simulate yielding, lateral buckling and local buckling as well as deterioration of individual shell elements due to low-cycle fatigue. As a result, they were able to predict braced frame global behavior and member response with higher fidelity than the fiber based models. Existing mechanics-based damage material models with element erosion were able to simulate initiation and propagation of section rupturing due to low-cycle fatigue. Adaptive meshing technique used in the finite element model provides an efficient way to refine the mesh layout only at the regions where the deformations were relatively larger. Input

parameters used in LS-DYNA model were also calibrated from the available test data. Additional material testing is suggested to develop a database of material and low-cycle fatigue input parameters for the steel material types that are commonly used in braced frame systems.

**Relative advantages of fiber and shell element modeling approaches.** – Compared to the fiber based elements in OpenSees, the shell element models implemented in LS-DYNA require significantly more execution time. For larger and more complicated structures, it is impractical to run an analysis in LS-DYNA. Thus, a multistep approach may be needed where refined models of members and/or connections are based on realistic shell elements, and these results are used to calibrate more efficient and simpler fiber based models in programs like OpenSees. Alternatively, different levels of refinement may be used in programs like LS-DYNA, where critical regions are identified and these are modeled in a refined manner, but other regions are modeled using simpler elements.

**Improving the behavior of concentric braced frames.** – As noted previously, concentric braced frames constructed using conventional or buckling restrained braces tend to concentrate damage in one or a few stories. The proposed hybrid vertical elastic truss or strong-back braced frame system was suggested as a method for avoiding weak story behavior. A simplified design method was proposed. This was applied on systems utilizing conventional as well as buckling restrained braces. These systems were quite effective in mitigating the formation of a weak story mechanism. Monotonic and cyclic inelastic analyses demonstrated the benefits of the strong-back system. These systems out perform traditional braced frame systems in terms of system deformation capacity, shape of hysteresis loops, energy dissipation, and story drift distributions. The strong-back systems studied here typically had higher base shear capacities than conventional braced frames since all of the braces over the height of the structure contributed to the lateral load resistance. For, the strong-back system that used conventional buckling restrained braces (SB6-3B) the strength was not as high as some systems with conventional braces because of the overstrength in tension associated with conventional braces. The strong back system with low yield strength steel buckling restrained braces was found to have lower drifts than a similar system with normal strength bracing, since its flexibility and period decreased and its design strength increased accordingly due the larger area of steel provided in the braces.

Dynamic analysis results show that the peak base shear forces were inversely proportional to the fundamental periods of the six models studied: the lower the fundamental period, the higher the peak shear force. Compared with the conventional chevron brace configuration design (i.e. model V6), the peak story drifts were greater in the strong-back systems, but the story drift distributions were more uniform in the strong-back systems. The tendency for the story drift in the strong-back frames to increase substantially in the upper few stories was noted. Such behavior needs further investigation. Peak floor accelerations at the roof level for all six models were typically higher than the floor levels below roof. Although using high-performance braces such as buckling-restrained braces in the strong-back system can improve the deformation capacity of the entire system, larger residual deformations were predicted for this case. The use of devices with self-centering mechanism may be a topic for future study.

The simplified design strategy for proportioning vertical spine member sizes in the hybrid strong-back system appeared to achieve the performance goal: nearly uniform story



deformation. No soft-story mechanisms (neither single- nor multi- story mechanisms) were found in the strong-back systems. The optimization of design strategy needs to be further studied to improve the system performance.

### 8.3 RECOMMENDATIONS FOR FUTURE RESEARCH

As noted, there were some issues found during this study and many other related topics were not covered here that still need to be further studied including:

1. The cyclic behavior of the column bases using current design details and weld procedures.
2. The demand of the bi-axial bending and torsion in the braced frame columns due to the out-of-plane buckling of the braces.
3. A brace component test program covering a wider range of sizes and shapes especially those commonly used in the field. Standard loading protocol also needs to be developed for the test program.
4. The effect of ground motion characteristics on the response of conventional braced frame systems and also the strong-back systems.
5. A material testing program to develop a database of material and low-cycle fatigue input parameters for the steel materials that are commonly used in the braced frame systems.
6. The use of self-centering devices in the strong-back systems to minimize the residual deformations after earthquake.
7. Optimization of the design strategy for the strong-back system.
8. The relative cost comparisons of different types of braced frame systems and the strong-back systems.
9. Quantification of the seismic performance factors (SPFs) of the strong-back systems using the FEMA P-695 (ATC-63) methodology (FEMA, 2009).

## REFERENCES

- AIJ, (1995) "Reconnaissance Report on Damage to Steel Building Structures Observed from the 1995 Hyogoken-Nanbu (Hanshin/Awaji) Earthquake", Steel Committee of Kinki Branch, Architectural Institute of Japan.
- Aiken, I.D, Nims, D.K., and Kelly, J.M., (1992) "Comparative Study of Four Passive Energy Dissipation Systems", Bulletin of the New Zealand National Society for Earthquake Engineering, Vol. 25, No. 3, pp.175-192.
- AISC, (1978) "Specification for the Design, Fabrication and Erection of Structural Steel for Buildings", American Institutes of Steel Construction, Inc. Chicago, IL.
- AISC, (1992) "Seismic Provisions for Structural Steel Buildings", American Institutes of Steel Construction, Inc. Chicago, IL.
- AISC, (1997) "Seismic Provisions for Structural Steel Buildings", American Institutes of Steel Construction, Inc. Chicago, IL.
- AISC, (2001) "Manual of Steel Construction: Load and Resistance Factor Design", the 3<sup>rd</sup> Edition, November 15, American Institute of Steel Construction, Inc. Chicago, IL.
- AISC 341-02, (2002) "Seismic Provisions for Structural Steel Buildings", American Institutes of Steel Construction, Inc. Chicago, IL.
- AISC, (2005), "Steel Construction Manual", the 13<sup>th</sup> Edition, American Institutes of Steel Construction, Inc. Chicago, IL.
- AISC 341-05, (2005) "Seismic Provisions for Structural Steel Buildings", American Institutes of Steel Construction, Inc. Chicago, IL.
- AISC 341-10, (2010) "Seismic Provisions for Structural Steel Buildings", American Institutes of Steel Construction, Inc. Chicago, IL.
- AISC 360-10, (2010) "Specification for Structural Steel Buildings", American Institutes of Steel Construction, Inc. Chicago, IL.
- Aktan A.E. and Bertero, V.V., (1981) "The Seismic Resistant Design of R/C Coupled Structural Walls", UCB/EERC-81/07 Report, Earthquake Engineering Research Center, University of California, Berkeley, California.
- ASCE, (2005) "ASCE 7-05: Minimum Design Loads for Buildings and Other Structures", American Society of Civil Engineers, Washington, D.C., ISBN: 9780784408094.
- Astaneh-Asl, A., Goel, S.C., and Hanson, R.D., (1981) "Behavior of Steel Diagonal Bracing." ASCE Conference, October 26-31, St. Louis, Missouri.
- Astaneh-Asl, A., (1982) "Cyclic Behavior of Double Angle Bracing Members with End Gusset Plates", Ph.D. Dissertation, the University of Michigan.
- Astaneh-Asl, A., Goel, S.C., and Hanson, R. D. (1982) "Cyclic Behavior of Double Angle Bracing Members with End Gusset Plates", UMEE 82R7 Report, University of Michigan, Ann Arbor.
- Astaneh-Asl, A., Goel, S.C., and Hanson, R.D., (1985) "Cyclic Out-of-plane Buckling of Double-Angle Bracing", Journal of Structural Engineering, Vol. 111, No.5, pp.1135-1153.
- Astaneh-Asl, A., Goel, S.C., and Hanson, R.D., (1986) "Earthquake-Resistant Design of Double Angle Bracing," the AISC Engineering Journal, Vol. 23, No. 4, 4<sup>th</sup> Quarter, Chicago, IL.
- Astaneh-Asl, A, (1989) "Simple Methods for Design of Gusset Plates", Proceedings of ASCE Structures Congress, San Francisco, CA, May 1-5, pp.345-354.
- Astaneh-Asl, A, (1998) "Seismic Behavior and Design of Gusset Plates", Structural Steel Education Council, Steel Tips, December, 1998, Moraga, CA.

- Becker, R., (1995) "Seismic Design of Special Concentrically Braced Steel Frames," Structural Steel Education Council, Steel Tips, November, 1995, Moraga, CA.
- Bertero, V.V., Uang, C.M., Llopiz, C.R. and Igarashi, K., (1989) "Earthquake Simulator Testing of Concentric Braced Dual System", Journal of Structural Engineering, Vol.115, No.8, pp.1877-1894.
- Birkemoe, P.C., (1966) "Distribution of Stress and Partition of Loads in Gusseted Connections", Ph.D. Dissertation, the University of Illinois, Urbana.
- Black, R.G., Bill Wenger, W.A. and Popov, E.P., (1980) "Inelastic Buckling of Steel Struts under Cyclic Load Reversals", UCB/EERC-80/40 Report, University of California, Berkeley.
- Bonneville, D., and Bartoletti, S., (1996) "Case Study 2.3: Concentric Braced Frame, Lankershim Boulevard, North Hollywood", 1994 Northridge Earthquake Building Case Studies Project, Proposition 122: Product 3.2, SSC 94-06, Seismic Safety Commission State of California.
- Chambers, J.J. and Ernst, C.J., (2005) "Brace Frame Gusset Plate Research - Phase 1 Literature Review, Volumes 1 and 2", Department of Civil Engineering, University of Utah, Salt Lake City, UT.
- Chamber, J.J. and Bartley, T.C., (2007) "Geometric Formulas for Gusset Plate Design", the AISC Engineering Journal, 3<sup>rd</sup> Quarter, pp.255-207.
- Chen, C.C., Chen, S.Y. and Liaw, J.J., (2001) "Application of Low Yield Strength Steel on Controlled Plasticification Ductile Concentrically Braced Frames", Canadian Journal of Civil Engineering, Vol.28, No.5, pp.823-836.
- Chen, C.H. and Mahin, S.A., (2010) "Seismic Collapse Performance of Concentrically Steel Braced Frames", NASCC the Steel Conference and the Structures Congress, May 12-15, Orlando, FL.
- Cheng, J.J.R., Kulak, G.L. and Khoo, H.A., (1998) "Strength of Slotted Tubular Tension Members", Canadian Journal of Civil Engineering, Vol.25, No.6, pp.982-991.
- Christopoulos, C., Tremblay, R., Kim, H.J. and Lacerte M., (2008) "Self-Centering Energy Dissipative Bracing System for the Seismic Resistance of Structures: Development and Validation", Journal of Structural Engineering, Vol. 134, No.1, pp.96-107.
- Cochran, M.L., (2000) "Design and Detailing of Steel SCBF Connections", SEAOC Seminar Series, Structural Engineers Association of California, Sacramento, California.
- Cochran, M.L., (2003) "Seismic Design and Steel Connection Detailing", Proceedings of the 2003 North American Structural Steel Construction Conference, Baltimore, MD, April 2-5.
- Computers and Structures, Inc., (2009) "SAP2000, Integrated Software for Structural Analysis and Design", Version 14.0, Berkeley, CA.
- Daugherty, D., Hanley, J. and Rodgers, G.P., (2011) "Real-Time Data Viewer 2.2.3", <http://nees.org/resources/rdv>.
- Ding, X., Foutch, D. and Han, S.W., (2008) "Fracture Modeling of Rectangular Hollow Section Steel Braces", the AISC Engineering Journal, 3<sup>rd</sup> Quarter, pp.171-186.
- Dowswell, B., (2006) "Effective Length Factors for Gusset Plate Buckling", the AISC Engineering Journal, 2<sup>nd</sup> Quarter, pp.91-101.
- EERI, (1978) "Reconnaissance Report Miyagi-Ken-Oki, Japan Earthquake, June 12, 1978", December, Earthquake Engineering Research Institute, Berkeley, CA.
- Fell, B.V., (2008) "Large-Scale Testing and Simulation of Earthquake-Induced Ultra Low Cycle Fatigue in Bracing Members Subjected to Cyclic Inelastic Buckling", Ph.D. Dissertation, University of California, Davis.
- Fell, B.V. and Kanvinde, A.M., (2010) "Tensile Forces for Seismic Design of Braced Frame Connections – Experimental Results", Journal of Constructional Steel Research, Vol.66, Issue 4, pp.496-503.
- FEMA, (2009) "Quantification of Building Seismic Performance Factors", FEMA P-695, Federal Emergency Management Agency, Washington, D.C.
- Field, C., (2003) "Simulation of Full-Scale Seismic-Resistant Structural Frame Tests using LS-DYNA 960 Implicit Solver", the 4<sup>th</sup> European LS-DYNA Users Conference, May 22-23, Ulm, Germany.

- Foutch, D.A., Goel, S.C. and Roeder, C.W., (1986) "Preliminary Report on Seismic Testing of a Full-Scale Six-Story Steel Building", University of Illinois at Urbana-Champaign, Urbana, Illinois.
- Foutch, D.A., Goel, S.C. and Roeder, C.W., (1987) "Seismic Testing on Full-Scale Steel Building-Part I", Journal of Structural Engineering, Vol.113, No.11, pp.2111-2129.
- Fujimoto, M., Aoyagi, T., Ukai, K., Wada, A. and Saito, K., (1972) "Structural Characteristics of Eccentric K-Braced Frames", Transactions of the Architectural Institute of Japan, Vol. 195, pp.39-49.
- Fujimoto, M., Hashimoto, A., Nakagomi, T. and Yamada, T., (1985) "Study on Fracture of Welded Connections in Steel Structures under Cyclic Loads Based on Nonlinear Fracture Mechanics", Journal of Structural and Construction Engineering, Transactions of Architecture Institute of Japan, Vol. 365, pp. 93-102.
- Fukuta, T., Nishiyama, I., Yamanouchi, H. and Kato, B., (1989) "Seismic Performance of Steel Frames with Inverted V Braces", Journal of Structural Engineering, Vol. 115, No.8, pp.2016-2028.
- Ghannaat, Y., (1980) "Study of X-Braced Steel Frame Structures under Earthquake Simulation", UCB/EERC-80/08 Report, Earthquake Engineering Research Center, University of California, Berkeley.
- Ghannaat, Y. and Clough, R.W., (1982) "Shaking Table Tests of a Tubular Steel Frame Model", UCB/EERC-82/02 Report, Earthquake Engineering Research Center, University of California, Berkeley.
- Goel, S.C. and Liu, Z., (1987) "Cyclic Behavior of Concrete-Filled Tubes", Proceedings of the sessions at Structures Congress '87 related to Dynamics of Structures, August 17-20, New York, NY, pp.427-440.
- Gugerli, H. and Goel, S.C., (1982) "Inelastic Cyclic Behavior of Steel Bracing Members", UMEE 82R1 Report, the University of Michigan, Ann Arbor.
- Hallquist, J.O., (1990) "LS-DYNA User's Manual (Nonlinear Dynamic Analysis of Solids in Three Dimensions)", Report 1007, Livermore Software Technology Corporation, CA.
- Han, S.W., Kim, W.T. and Foutch, D.A., (2007) "Seismic Behavior of HSS Bracing Members according to Width-Thickness Ratio under Symmetric Cyclic Loading", Journal of Structural Engineering, Vol.133, No.2, pp.264-273.
- Harris, H.G. and Sabins, G.M., (1999) "Structural Modeling and Experimental Techniques", 2<sup>nd</sup> Edition, CRC Press, ISBN-13: 978-0849324697.
- Higginbotham, A.B., (1973) "The Inelastic Cyclic Behavior of Axially-Loaded Steel Members", Ph.D. Dissertation, the University of Michigan.
- Huang, Y. and Mahin, S.A., (2007) "Simulating the Behavior of Steel Members subjected to Deterioration", Kajima-CUREE Joint Research Program Report, University of California, Berkeley.
- Huang, Y. and Mahin, S.A., (2010) "Simulating the Inelastic Seismic Behavior of Steel Braced Frames including the Effects of Low-Cycle Fatigue", PEER-2010/104 Report, Pacific Earthquake Engineering Research Center, University of California, Berkeley.
- Ikeda, K., Mahin, S.A. and Dermitzakis, S.N., (1984) "Phenomenological Modeling of Steel Braces under Cyclic Loading", UCB/EERC-84/09 Report, Earthquake Engineering Research Center, University of California, Berkeley.
- Ikeda, K. and Mahin, S.A., (1984) "A Refined Physical Theory Model for Predicting the Seismic Behavior of Braced Steel Frames", UCB/EERC-84/12 Report, Earthquake Engineering Research Center, University of California, Berkeley.
- Ikeda, K. and Mahin, S.A., (1986) "Cyclic Response of Steel Braces", Journal of Structural Engineering, Vol.112, No.2, pp.342-361.
- Jain, A.K., Goel, S.C. and Hanson, R.D., (1977) "Static & Dynamic Hysteresis Behavior of Steel Tubular Members with Welded Gusset Plates", UMEE 77R3 Report, the University of Michigan, Ann Arbor.
- Jain, A.K., Goel, S.C. and Hanson, R.D., (1978a) "Hysteresis Behavior of Bracing Members and Seismic Response of Braced Frames with Different Proportions", UMEE 78R3 Report, the University of Michigan, Ann Arbor.

- Jain, A.K. and Goel, S.C., (1978b) "Hysteresis Models for Steel Members subjected to Cyclic Buckling or Cyclic End Moments and Buckling", UMEE 78R6 Report, the University of Michigan, Ann Arbor.
- Kahn, L.F. and Hanson, R.D., (1976) "Inelastic Cycles of Axially Loaded Steel Members", Journal of the Structural Division, Vol.102, No.5, May 1976, pp.947-959.
- Kalyanaraman, V., Mahadevan, K. and Thairani, V., (1998) "Core Loaded Earthquake Resistant Bracing System", Journal of Constructional Steel Research, Vol. 46, Issue 1-3, pp.437-439.
- Kalyanaraman, V., Ramachandran B., Prasad, B.K. and Sridhara, B.N., (2003) "Analytical Study of 'Sleeved Column' Buckling Restrained Braced System", Proceedings of SEAOC 72<sup>nd</sup> Annual Convention, Squaw Creek, California, USA.
- Kanaan, A.E. and Powell, G.H., (1973) "General Purpose Computer Program for Inelastic Dynamic Response of Plane Structures", UCB/EERC-73/6 Report, Earthquake Engineering Research Center, University of California, Berkeley.
- Katib, I.F., Mahin, S.A. and Pister, K.S., (1988) "Seismic Behavior of Concentrically Braced Frames", UCB/EERC-88/01 Report, Earthquake Engineering Research Center, University of California, Berkeley, CA.
- Kiggins, S. and Uang, C.M., (2006) "Reducing residual drift of buckling-restrained braced frames as a dual system", Engineering Structures, Vol.28, pp.1525-1532.
- Korol, R. M., (1996) "Shear Lag in Slotted HSS Tension Members", Canadian Journal of Civil Engineering, Vol.23, No.6, pp.1350-1354.
- Lai, J.W., Tsai, K.C., Lin, S.L. and Hsiao, P.C. (2004), "Large Scale Buckling Restrained Brace Research in Taiwan", 1<sup>st</sup> Asia Conference on Earthquake Engineering, March 5-6, Manila, Philippine.
- Lai, J.W., Chen, C.H. and Mahin, S.A. (2010). "Experimental and Analytical Performance of Concentrically Braced Steel Frames", NASCC the Steel Conference and the Structures Congress, May 12-15, Orlando, FL.
- Lee, S. and Goel, S.C., (1987) "Seismic Behavior of Hollow and Concrete-Filled Square Tubular Bracing Members", UMCE 87-11 Report, the University of Michigan, Ann Arbor.
- Lehman, D., Roeder, C., Yoo, J.H. and Johnson, S., (2004) "Seismic Response of Braced Frame Connections", the 13<sup>th</sup> World Conference on Earthquake Engineering, August 1-6, Vancouver, B.C., Canada, paper no. 1459.
- Liu, Z. and Goel, S.C., (1987) "Investigation of Concrete-Filled Steel Tubes under Cyclic Bending and Buckling", UMCE 87-3 Report, the University of Michigan, Ann Arbor.
- Liu, Z. and Goel, S.C., (1988) "Cyclic Load Behavior of Concrete-Filled Tubular Braces", Journal of Structural Engineering, Vol.114, No.7, pp.1488-1506.
- Lopez, W.A. and Sabelli, R., (2004) "Seismic Design of Buckling-Restrained Braced Frames", Steel Tips, Structural Steel Education Council.
- MacRae, G.A., Kimura, Y. and Roeder, C., (2004) "Effect of Column Stiffness on Braced Frame Seismic Behavior", Journal of Structural Engineering, Vol. 130, No. 3, pp.381-391.
- Mahin, S. and Lai, J.W., (2008) "An Innovative Approach to Improving the Seismic Behavior of Steel Concentric Braced Frames", Proposal for SEAONC Special Projects Initiative.
- Mahin, S.A. and Shing, B.P., (1985) "Pseudodynamic Method for Seismic Testing", Journal of Structural Engineering, Vol.111, No.7, pp.1482-1503.
- Mahin, S.A., Uriz, P., Aiken, I, Field, C. and Ko, E., (2004) "Seismic Performance of Buckling Restrained Braced Frame Systems", the 13<sup>th</sup> World Conference on Earthquake Engineering, August 1-6, Vancouver, B.C., Canada, Paper No. 1681.
- Maison, B. and Popov, E.P., (1980) "Cyclic Response Prediction for Braced Steel Frames", Journal of the Structural Division, Vol.106, No.7, pp.1401-1416.
- Mangat, P.S., (1969) "Influence of the Slenderness and b/t Ratios on the Inelastic Local Buckling of Angles", Master of Applied Science Thesis, University of Windsor, Ontario, Canada.

- Mar, D., (2010) "Design Examples using Mode Shaping Spines for Frame and Wall Buildings", Proceedings of the 9<sup>th</sup> U.S. National and 10<sup>th</sup> Canadian Conference on Earthquake Engineering, July 25-29, Toronto, Ontario, Canada, Paper No. 1400.
- Marshall, P.W., (1978) "Design Considerations for Offshore Structures Having Nonlinear Response to Earthquakes", ASCE Annual Convention and Exposition, October, Chicago, USA.
- Martinez-Saucedo, G., Packer, J. A. and Christopoulos, C., (2008) "Gusset Plate Connections to Circular Hollow Section Braces under Inelastic Cyclic Loading", Journal of Structure Engineering, Vol.134, No.7, pp.1252-1258.
- Martinez-Saucedo, G., Tremblay R. and Packer, J. A., (2008) "Seismic Response of Circular Hollow Section Braces with Slotted End Connections", Proceedings of the 12<sup>th</sup> International Symposium on Tubular Structures, Shanghai, China, October 8-10, pp.227-233.
- McCormick, J., DesRoches, R., Fugazza, D. and Auricchio, F., (2007) "Seismic Assessment of Concentrically Braced Steel Frames with Shape Memory Alloy Braces", Journal of Structural Engineering, Vol. 133, No. 6, pp.862-870.
- McKenna, F., (1997) "Object Oriented Finite Element Programming Frameworks for Analysis, Algorithms and Parallel Computing", Ph.D. Dissertation, University of California, Berkeley.
- Midorikawa, M., Takeuchi, T., Hikino, T., Kasai, K., Deierlein, G., Ohbayashi, M., Yamazaki, R. and Kishiki, S., (2010) "Seismic Performance of Controlled Rocking Frames with Shear Fuse and PT Wire Anchorage- Shaking Table Tests on Controlled Rocking Steel Frames using Multipurpose Inertial Mass System: Part I", Journal of Structural and Construction Engineering, Architectural Institute of Japan, Vol. 75, No. 654, pp.1547-1556 (in Japanese).
- Midorikawa, M., (2011) "Seismic and Tsunami Damage on Building Structures Caused by the 2011 Tohoku Japan Earthquake", IISEE-UNESCO Lecture Notes Archive, <http://iisee.kenken.go.jp>.
- Mitsui, Y. and Kurobane, Y., (1981) "Experimental Study on Tube-to-Through-Gusset Plate Joints", Summaries of Technical Papers of Annual Meeting, Architectural Institute of Japan, Structural Systems, Vol. 56, pp.1829-1830.
- Mitsui, Y. and Maeda, N., (1986) "Experimental Study on Ultimate Tensile Strength of Welded Tube-to-Through Gusset Plate Joints : Examination of Methods for Repairing and Excessive Opening at the tip of the Gusset Plate", Proceedings of Annual Research Meeting, Kyushu Chapter, Architectural Institute of Japan, Structural Systems, Vol. 29, pp.317-320.
- Muir, L.S., (2008) "Designing Compact Gussets with Uniform Force Method", the AISC Engineering Journal, 1<sup>st</sup> Quarter, pp.13-19.
- Naito, T., (1926) "Damages to the steel frame buildings in Tokyo", Investigation Report for Earthquake Disaster Prevention Committee, October 13<sup>th</sup>, the University of Tokyo (in Japanese).
- Nast, T.E., (1999) "Cyclic Behavior of Stiffened Gusset Plate-Brace Member Assemblies", Master of Science Thesis, University of Alberta, Canada.
- Nilforoushan, R., (1973) "Seismic Behavior of Multi-Story K-Braced Frame Structures", UMEE 73R9 Report, the University of Michigan, Ann Arbor.
- Packer, J.A., (2006) "Tubular Brace Member Connections in Braced Steel Frames", Proceedings of 11<sup>th</sup> International Symposium on Tubular Structures, Quebec, Canada, pp.3-14.
- Palmer, K., Roeder, C.W., Okazaki, T., Shield, C. and Lehman, D.E., (2011) "Three-Dimensional Tests of Two-Story, One-Bay by One-Bay, Steel Concentric Braced Frames", the ASCE Structures Congress, pp.3057-3067.
- Phipps, M.T., Jirsa, J.O., Picado, M. and Karp, R., (1992) "Performance of High Technology Industries in the Loma Prieta Earthquake", Proceedings of the 10<sup>th</sup> World Conference on Earthquake Engineering, July 19-24, Madrid, Spain.

- Phipps, M.T., (1997) "Reducing Earthquake Damage through Quality Construction", Earthquake Engineering Research Institute, Oakland, CA.
- Pons, H.F., (1997) "Dynamic Behavior of Tubular Bracing Members with Single Plate Concentric Connections", Master of Applied Science Thesis, University of Toronto, Canada.
- Popov, E.P., Takahashi, K. and Roeder, C.W., (1976) "Structural Steel Bracing Systems: Behavior under Cyclic Loading", UCB/EERC-76/17 Report, Earthquake Engineering Research Center, University of California, Berkeley.
- Powell, G.H., (1973) "DRAIN-2D User's Guide", UCB/EERC-73/22 Report, Earthquake Engineering Research Center, University of California, Berkeley.
- Powell, J., Clark, K., Tsai, K.C., Roeder, C.W., Lehman, D., (2008) "Test of a Full Scale Concentrically Braced Frame with Multi-story X-bracing", the ASCE Structures Congress.
- Rabinovitch, J.S., (1993) "Cyclic Behavior of Steel Gusset Plate Connections", Master of Science Thesis, University of Alberta, Canada.
- Roeder, C.W. and Popov, E.P., (1977) "Inelastic Behavior of Eccentrically Braced Frames under Cyclic Loading", UCB/EERC-77/18 Report, Earthquake Engineering Research Center, University of California, Berkeley.
- Roeder, C.W., (1989) "Seismic Behavior of Concentrically Braced Frame", Journal of Structural Engineering, Vol.115, No.8, pp.1837-1856.
- Roeder, C.W. and Lehman D.E., (2007) "SCBF Gusset Plate Connection Design", Proceedings of the 2007 North American Structural Steel Construction Conference, New Orleans, LA, pp.266-282.
- Roeder, C.W., Lumpkin, E.J. and Lehman D.E., (2011) "A Balanced Design Procedure for Special Concentrically Braced Frame Connections", Journal of Constructional Steel Research, Vol.67, Issue 11, pp.1760-1772.
- Roeder, C.W., Lehman, D.E., Clark, K., Powell, J., Yoo, J.H., Tsai, K.C., Lin, C.H. and Wei, C.Y., (2011) "Influence of Gusset Plate Connections and Braces on the Seismic Performance of X-braced Frames", Earthquake Engineering and Structural Dynamics, Vol.40, pp.355-374.
- Sabelli, R., (2001) "Research on Improving the Design and Analysis of Earthquake-Resistant Steel-Braced Frames", Earthquake Engineering Research Institute, the 2000 NEHRP Professional Fellowship Report, PF2000-9.
- Sabelli, R., Mahin, S.A. and Chang, C., (2003) "Seismic Demands on Steel Braced Frame Buildings with Buckling Restrained Braces", Engineering Structures, Vol.25, pp.655-666.
- Schellenberg, A.H., Mahin, S.A. and Fenves, G.L., (2009) "Advanced Implementation of Hybrid Simulation", PEER-2009/104, Pacific Earthquake Engineering Research Center (PEER), University of California, Berkeley.
- SEAOC, (1991) "Reflections on the Loma Prieta Earthquake October 17, 1989", Ad Hoc Earthquake Reconnaissance Committee, Structural Engineers Association of California, Sacramento, CA.
- Shaback, J.B., (2001) "Behavior of Square HSS Braces with End Connections under Reversed Cyclic Axial Loading", Master of Applied Science Thesis, University of Calgary, Canada.
- Shaback, B. and Brown, T., (2003) "Behavior of Square Hollow Structural Steel Braces with End Connections under Reversed Cyclic Axial Loading", Canadian Journal of Civil Engineering, Vol.30, No.4, pp.745-753.
- Shibata, M., Nakamura, T., Yoshida, N., Morino, S., Nonaka, T. and Wakabayashi, M., (1973) "Elastic-Plastic Behavior of Steel Braces under Repeated Axial Loading", the 5<sup>th</sup> World Conference on Earthquake Engineering, June 25-29, Rome, Italy, Vol. 1, Paper No. 845.
- Singh, P., (1977) "Seismic Behavior of Braces and Braced Steel Frames", UMEE 77R1 Report, the University of Michigan, Ann Arbor.
- Skidmore, Owings & Merrill, (1963) "Test Slabs Design Calculations for the University of California Richmond Field Station Structural Research Laboratory", Skidmore, Owings & Merrill LLP, One Maritime Plaza, San Francisco, CA 94111, USA.

- Skidmore, Owings & Merrill, (1964) "Test Slab Details for the University of California Richmond Field Station Structural Research Laboratory", Drawing Number S7 & S7-SUP-1, Skidmore, Owings & Merrill LLP, One Maritime Plaza, San Francisco, CA 94111, USA.
- Steinbrugge, K.V., Schader, E.E., Bigglestone, H.C. and Weers, C.A., (1971) "San Fernando Earthquake February 9, 1971", Pacific Fire Rating Bureau, San Francisco, CA.
- Tanabashi, R., Kaneta, K. and Ishiba, T., (1973) "On the Rigidity and Ductility of Steel Bracing Assemblage", the 5<sup>th</sup> World Conference on Earthquake Engineering, June 25-29, Rome, Italy.
- Tang, X. and Goel, S.C., (1987) "Seismic Analysis and Design Considerations of Braced Steel Structures", UMCE 87-4 Report, University of Michigan, Ann Arbor, MI.
- Thornton, W.A. (1984), "Bracing Connections for Heavy Construction", the AISC Engineering Journal, AISC, Vol. 21, No. 3, pp.139-148.
- Thornton, W.A. (1991), "On the Analysis and Design of Bracing Connections", National Steel Construction Conference Proceedings, American Institutes of Steel Construction, Inc. Chicago, IL.
- Thornton, W.A. (1992), "Designing for Cost Efficient Fabrication", Structural Steel Education Council, Steel Tips, April, 1992.
- Thornton, W.A. and Muir, L.S., (2009) "Design of Vertical Bracing Connections for High-Seismic Drift", Modern Steel Construction, March.
- Tirca, L. and Tremblay, R., (2004) "Influence of Building Height and Ground Motion Type on the Seismic Behavior of Zipper Concentrically Braced Steel Frames", the 13<sup>th</sup> World Conference on Earthquake Engineering, August 1-6, Vancouver, B.C., Canada, Paper No. 2894.
- Trembaly, R., (2003) "Achieving a Stable Inelastic Seismic Response for Multi-Story Concentrically Braced Steel Frames", the AISC Engineering Journal, 2<sup>nd</sup> Quarter, pp.111-129.
- Tremblay, R. and Merzouq, S., (2004) "Dual Buckling Restrained Braced Steel Frames for Enhanced Seismic Response", Passive Control Symposium 2004, November 15-16, Yokohama, Japan.
- Tremblay, R., Haddad, M., Martinez, G., Richard, J. and Moffatt, K., (2008) "Inelastic Cyclic Testing of Large Size Steel Bracing Members", the 14<sup>th</sup> World Conference on Earthquake Engineering, October 12-17, Beijing, China.
- Tremblay, R., Lacerte, M. and Christopoulos, C., (2008) "Seismic Response of Multistory Buildings with Self-Centering Energy Dissipative Steel Braces", Journal of Structural Engineering, Vol.134, No.1, pp.108-120.
- Tsai, K.C., Hsiao, P.C., Wang, K.J., Weng, Y.T., Lin, M.L., Lin, K.C., Chen, C.H., Lai, J.W. and Lin, S.L., (2008) "Pseudo-Dynamic Tests of a Full-Scale CFT/BRB Frame - Part I: Specimen Design, Experiment and Analysis", Earthquake Engineering and Structural Dynamics, Vol.37, pp.1081-1098.
- Uang, C.M. and Bertero, V.V., (1986) "Earthquake Simulation Tests and Associated Studies of a 0.3-Scale Model of a Six-Story Concentrically Braced Steel Structure", UCB/EERC-86/10 Report, Earthquake Engineering Research Center, University of California, Berkeley, CA.
- Uriz, P. and Mahin, S.A., (2004) "Seismic Performance Assessment of Concentrically Braced Steel Frames", Proceedings of 13<sup>th</sup> World Conference on Earthquake Engineering, Vancouver, British Columbia, Canada, August 1-6.
- Uriz, P., (2005) "Toward Earthquake-Resistant Design of Concentrically Braced Steel-Frame Structures", Ph.D. Dissertation, University of California, Berkeley.
- Uriz, P., Filippou, F.C. and Mahin, S.A., (2008) "Model for Cyclic Inelastic Buckling of Steel Braces", Journal of Structural Engineering, Vol.134, No.4, pp.619-628.
- Uriz, P. and Mahin, S.A., (2008) "Toward Earthquake-Resistant Design of Concentrically Braced Steel-Frame Structures", PEER-2008/08 Report, Pacific Earthquake Engineering Research Center, University of California, Berkeley.



- Wakabayashi et al., (1972) “Experimental Elastic-Plastic Behavior of Steel Bars under Repeated Axial Loading, Part 1”, Summaries of Technical Papers of Annual Meeting, Vol.47 (Structural System), Architectural Institute of Japan, pp.1315-1316 (in Japanese).
- Wakabayashi et al., (1973) “Experimental Elastic-Plastic Behavior of Steel Bars under Repeated Axial Loading, Part 2”, Summaries of Technical Papers of Annual Meeting, Vol.48 (Structural System), Architectural Institute of Japan, pp.971-972 (in Japanese).
- Wakabayashi, M., (1973) “Experimental Elastic-Plastic Behavior of Steel Braces under Repeated Axial Loading”, of Journal of Architecture and Building Science, Vol.72, Architectural Institute of Japan, pp.441-443 (in Japanese).
- Wakabayashi, M., Matsui, C., Minami, K. and Mitani, I., (1974) “Inelastic Behavior of Full-Scale Steel Frames with and without Bracings”, Bulletin of the Disaster Prevention Research Institute, Vol.24, No.1, pp.1-23.
- Wakabayashi et al., (1976) “Experimental Elastic-Plastic Behavior of End Rotational Restrained Steel Members under Repeated Axial Loading”, Summaries of Technical Papers of Annual Meeting, Vol.51 (Structural System), Architectural Institute of Japan, pp.1037-1038 (in Japanese).
- Wakabayashi, M., Matsui, C. and Mitani, I., (1977) “Cyclic Behavior of a Restrained Steel Brace under Axial Loading”, the 6<sup>th</sup> World Conference on Earthquake Engineering, January 10-14, New Delhi, India, Vol. 3, Paper No. 3181.
- Walbridge, S., Grondin, G.Y. and Cheng, J.J.R., (1998) “An Analysis of the Cyclic Behaviour of Steel Gusset Plate Connections”, Structural Engineering Report No. 225, University of Alberta, Edmonton, Alberta, Canada.
- Watanabe, A., Hitomi, Y., Saeki, E., Wada, A., and Fujimoto, M. (1988). “Properties of Brace Encased in Buckling-Restraining Concrete and Steel Tube”, Proceedings of Ninth World Conference on Earthquake Engineering, Tokyo-Kyoto, Japan, Paper No. 6-7-4, pp. 719–724.
- Whitmore, R.E. (1952), “Experimental Investigation of Stresses in Gusset Plates”, The University of Tennessee, Engineering Experiment Station, Bulletin No.16.
- Willibald, S., Packer, J.A. and Martinez-Saucedo, G., (2006) “Behavior of Gusset Plate Connections to Ends of Round and Elliptical Hollow Structural Section Members”, Canadian Journal of Civil Engineering, Vol.33, No.4, pp.373-383.
- Wyss, Theophil, (1923) “Beitrag zur Spannungsuntersuchung an Knotenblechen eiserner Fachwerke”, Swiss Federal Institute of Technology Zurich, Doctoral Dissertation (in German).
- Yam, M.C.H., (1994) “Compressive Behavior and Strength of Steel Gusset Plate Connections”, Doctoral Dissertation, University of Alberta, Canada.
- Yam, M.C.H. and Cheng, J.J.R., (2002) “Behavior and Design of Gusset Plate Connections in Compression”, Journal of Constructional Steel Research, Vol.58, Issue 5-8, pp.1143-1159.
- Yamanouchi, H., Midorikawa, M., Nishiyama, I. and Watabe, M., (1989) “Seismic Behavior of Full-Scale Concentrically Braced Steel Building Structure”, Journal of Structural Engineering, Vol.115, No.8, pp.1917-1929.
- Yang, C.S., DesRoches, R. and Leon, R.T., (2010) “Design and Analysis of Braced Frames with Shape Memory Alloy and Energy-Absorbing Hybrid Devices”, Engineering Structures, Vol. 32, pp.498-507.
- Yang, C.S., Leon, R.T. and DesRoches, R., (2008) “Pushover Response of a Braced Frame with Suspended Zipper Struts”, Journal of Structural Engineering, Vol.134, No.10, pp.1619-1626.
- Yang, C.S., Leon, R.T. and DesRoches, R., (2010) “Cyclic Behavior of Zipper-Braced Frames”, Earthquake Spectra, Vol.26, Issue 2, pp.561-582.
- Yang, F. and Mahin, S. A., (2005) “Limiting Net Section Fracture in Slotted Tube Braces”, Structural Steel Education Council, Steel Tips, April, 2005.
- Yoo, J.H., (2006) “Analytical investigation on the seismic performance of special concentrically braced frames”, Doctoral Dissertation, University of Washington, Seattle.

- Yoo, J.H., Lehman, D.E. and Roeder, C.W., (2008) "Influence of Connection Design Parameters on the Seismic Performance of Braced Frames", *Journal of Constructional Steel Research*, Vol.64, Issue 6, pp.607-623.
- Yoo, J.H., Roeder, C.W. and Lehman, D.E., (2009) "Simulated Behavior of Multi-Story X-Braced Frames", *Engineering Structures*, Vol.31, pp.182-197.
- Zayas, V.A., Popov, E.P. and Mahin, S.A., (1980a) "Cyclic Inelastic Buckling of Tubular Steel Braces", UCB/EERC-80/16 Report, Earthquake Engineering Research Center, University of California, Berkeley.
- Zayas, V.A., Mahin, S.A. and Popov, E.P., (1980b) "Cyclic Inelastic Behavior of Steel Offshore Structures", UCB/EERC-80/27 Report, Earthquake Engineering Research Center, University of California, Berkeley.
- Zayas, V.A., Shing, B.P., Mahin, S.A. and Popov, E.P., (1981) "Inelastic Structural Modeling of Braced Offshore Platforms for Seismic Loading", UCB/EERC-81/04 Report, Earthquake Engineering Research Center, University of California, Berkeley.

## APPENDICES

---

## Appendix A

### Test Setup Design Calculations

---

#### A.1 General Assumption

Assume the target (maximum) story shear distribution is 600 kips at roof level and 300 kips at the top of the first story. Thus, the total shear is 900 kips at base. The friction coefficient between reconfigurable reaction blocks is assumed equal to 0.5 under the condition that the blocks were properly grouted (Mosalam and Elkhoraibi, 2004). While the friction coefficient between steel plate and concrete surface is assumed equal to 0.33 without grouting and equal to 0.5 with properly grouting between them. Assume the eccentricity of the actuator measured from the concrete block surface to the center line of the actuator is 36 inch in this case. The total eccentricity from the center of gravity of concrete block sections to the center line of actuator is  $36 + (10 \text{ ft} \times 12 \text{ in/ft} / 2) = 96 \text{ inch}$ .

#### A.2 Materials:

##### Concrete:

Strong floor:  $f'_c = 4500 \text{ psi}$  (Skidmore, Owings & Merrill 1963 and 1964)

Reconfigurable reaction wall (RRW):  $f'_c = 8000 \text{ psi}$  (Arici and Mosalam, 2001; Mosalam and Elkhoraibi, 2004; Clyde, 2001)

##### Steel plate and rebar:

ASTM A36 steel plate:  $f_y = 36 \text{ ksi}$ ,  $f_u = 58 \text{ ksi}$  (ASTM, 2004)

ASTM A572 Grade 50 steel plate:  $f_y = 50 \text{ ksi}$ ,  $f_u = 65 \text{ ksi}$  (ASTM, 2003)

ASTM A706 rebar:  $f_y = 60 \text{ ksi}$  (ASTM, 2004)

##### Pre-stress rod (all-thread-bar):

Williams Form 150 ksi all-thread-bar:  $f_y = 127.7 \text{ ksi}$ ,  $f_u = 150 \text{ ksi}$  (Williams Form Eng. Corp., 2008].

The appearance of a typical all-thread-bar is shown in Fig. A.1 and Table A.1 shows the typical dimension and material properties of 150 ksi all-thread-bar used in the NEES Berkeley lab.

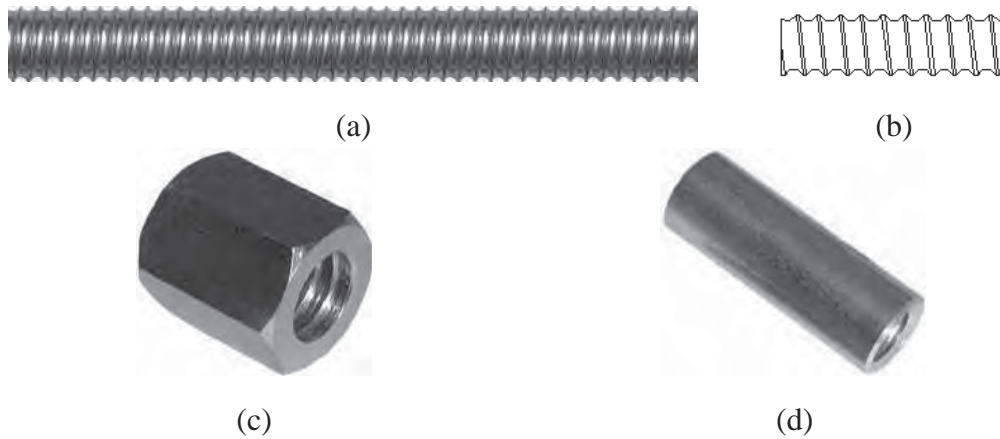


Figure A.1 Appearance of a typical all-thread-bar, nut and coupler  
(adopted from Williams Form Eng. Corp. website)

Table A.1 Typical dimension and material properties of 150 ksi all-thread-bar

Outside Diameter (in)	Nominal Diameter (in)	Net Area (in <sup>2</sup> )	$P_y$ (kips)	$P_u$ (kips)	70% $P_u$ (kips)
1-9/16	1-3/8	1.48	189	222	155

(Note: the strong floor has 2.5 in inside diameter holes 3 ft on center each direction)

Consider the outside diameter of coupling is normally 7/8 inch larger than the nominal diameter of the all-thread-bar. For a 2.5 inch hole and the all-thread-bar with 1-3/8 inch nominal diameter,  $1.375 + 7/8 = 2.25 < 2.5$  inch, the holes in the strong floor are large enough for using the all-thread-bar with couplers. Table A.2 and A.3 show the available all-thread-bars in the lab and the required quantities for the test setup.

Table A.2 Number of all-thread-bars available in RFS lab

Outside Diameter (in)	Nominal Diameter (in)	Length (ft)	Quantity	Note
1-9/16	1-3/8	13	> 90	8 ft length also available

(Need to check the quantities we have in RFS)

Table A.3 Number of required all-thread-bars and accessories for three stacks of RRW

Post-tension Direction	Grip Length (ft)	All-thread-bars Length		Couplers, Nuts and End Plates
		13 ft	8 ft	
Vertical	27	30	60	60 each
Horizontal	27	20	40	40 each
Horizontal (inside RRW)	4	0	60	120 (nuts and plates)
Total		50	160	220 (nuts and plates)

(Note: Assume at least 2 ft working length for pre-stressing)

### A.3 Design Checks and Calculations

#### A.3.1. Check the possible failure modes of test setup

The calculation checks basically follow the load path from the upper level of the RRW (Reconfigurable Reaction Wall) to the bottom level of the RRW and then to the lab strong floor. The following paragraphs describe the design check sequences.

(1) Check the actuator bracket capacity:

The two existing brackets in the lab were originally designed for the Caltrans research project (Astaneh-Asl and Ravat, 1998). The capacity of combined brackets (back-to-back) was 1500 kips to fit in with the 1.5 million pound actuators available in the lab. Therefore, the capacity of each bracket is initially estimated to be at least 750 kips. Here we conservatively check the critical stress in the back plate of a bracket under 600 kips loading and assume the steel brackets were made by ASTM A572 Grade 50 steel. Fig. A.2 shows the simple beam model to calculate the stress distribution in the back plate. From the formula listed in the structural design manual (Kiyota and Tamagawa, 2004), we can calculate the stresses at three critical points (middle and both ends of the beam) in the beam model:

$$a = 13"; b = 34"; l = 2a + b = 60"; t = 4"$$

$$I = \frac{1}{12} \cdot 44" \cdot (4")^3 = 235 \text{ in}^4$$

$$w = \frac{600 \text{ kips}}{34"} = 17.6 \text{ kip/in}$$

$$M_A = M_B = \frac{wb}{24l} \left( 3l^2 - \frac{b^2}{2} \right) = 4248 \text{ kip-in}$$

$$\sigma_A = \sigma_B = \frac{M_A \cdot t}{2 \cdot I} = 36.2 \text{ ksi} < 50 \text{ ksi}$$

$$M_C = \frac{wb}{24l} (3l^2 + \frac{b^2}{2} - 3bl) = 2185 \text{ kip-in}$$

$$\sigma_C = \frac{M_C \cdot t}{2 \cdot I} = 18.6 \text{ ksi} < 50 \text{ ksi}$$

$$\delta_C = \frac{wb}{216EI} (l^3 - \frac{b^2 l}{2} + \frac{b^3}{2}) = 0.082''$$

The stresses in the beam model are less than the minimum yield strength of the back plates assumed in the calculation.

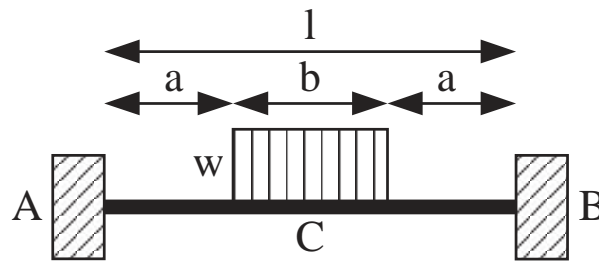


Figure A.2 The simple beam model for stress check

- (2) Check the upper level bracket base plate to concrete block surface friction: (assume 100 kips and 50 kips pretension forces in the all-thread-bars)

$$\mu = 0.33$$

$$R = (100 \text{ kips} \cdot 21 + 50 \text{ kips} \cdot 18) \cdot 0.33 = 990 \text{ kips} > 600 \text{ kips (OK)}$$

- (3) Check the strain in the base plate of upper level bracket to prevent cracks in the RRW blocks:

$$f_t = 0.1 \cdot f_c' = 0.1 \cdot 8000 \text{ psi} = 800 \text{ psi}$$

$$E_c = w_c^{1.5} \cdot 33 \sqrt{f_c'} = 145^{1.5} \cdot 33 \cdot \sqrt{8000} = 5153.6 \text{ ksi}$$

$$\varepsilon_{cr} = \frac{f_t}{E_c} = 1.55 \times 10^{-4}$$

$$\text{check } \varepsilon_{\text{plate}} < \varepsilon_{cr} \text{ (under 600 kips)}$$

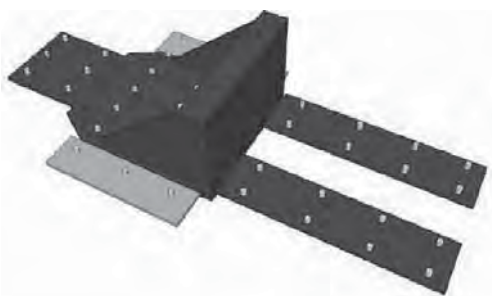
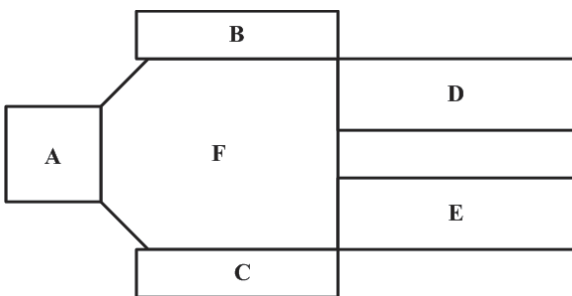
$$\sigma_{\text{plate}} = E_S \cdot \varepsilon_{\text{plate}} < E_S \cdot \varepsilon_{cr} = 4.5 \text{ ksi}$$

$$\text{check } \frac{P}{A_S} < 4.5 \text{ ksi}$$

From Table A.4, we can clearly see that stresses in all plate extensions are less than the estimated allowable stress.

Table A.4 Stress distribution in each base plate extensions

Zone	Force Ratio	Force P (kips)	A <sub>s</sub> (in <sup>2</sup> )	Stress (ksi)	Safety Factor (S.F.)
A	0.15	90	84	1.07	4.2
B	0.083	49.8	36	1.38	3.3
C	0.083	49.8	36	1.38	3.3
D	0.2	120	48	2.5	1.8
E	0.2	120	48	2.5	1.8
F	0.284	170.4	210	0.81	5.6

(4) Check local shear in RRW block:

Refer to Fig. A.3 below. One can check the shear force transferred in the concrete blocks.

Shear force in the typical profile in each concrete block:

$$\frac{600 \text{ kips}}{6 \cdot 2} = 50 \text{ kips}$$

$$V_n = V_c + V_s$$

$$V_c = 2 \cdot \sqrt{8000} \cdot 30'' \cdot (23.5 - 1.5 \times 2 - 0.5 \times 2) = 104.6 \text{ kips}$$

$$V_s = \frac{A_v f_y d}{s} = \frac{2 \cdot 0.20 \cdot 60 \text{ ksi} \cdot 19.5}{4} = 117 \text{ kips}$$

$$\phi V_n = 0.85 \cdot 221.6 = 188.4 > 50 \text{ kips (OK)}$$



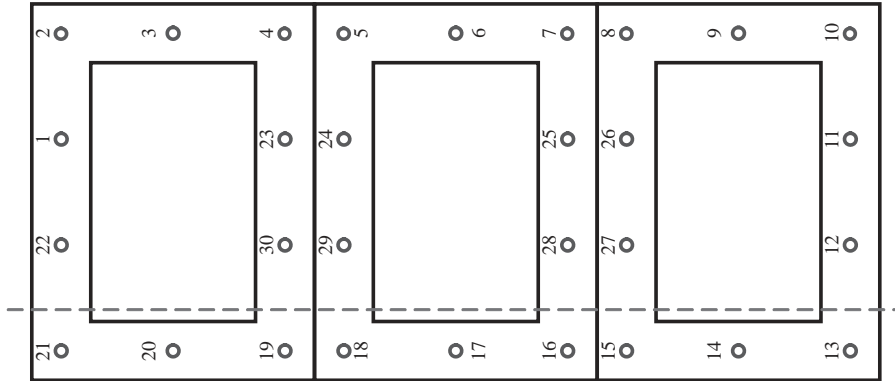


Figure A.3 Local shear force profile for the concrete blocks

- (5) Check the torsional resistance between the concrete blocks: (assume 100 kips pretension for all-thread-bars)

Using the traditional elastic (vector) analysis method (Salmon and Johnson, 1996) to calculate the torsional resistance of the concrete blocks. Fig. A.4 demonstrates the concept of this method.

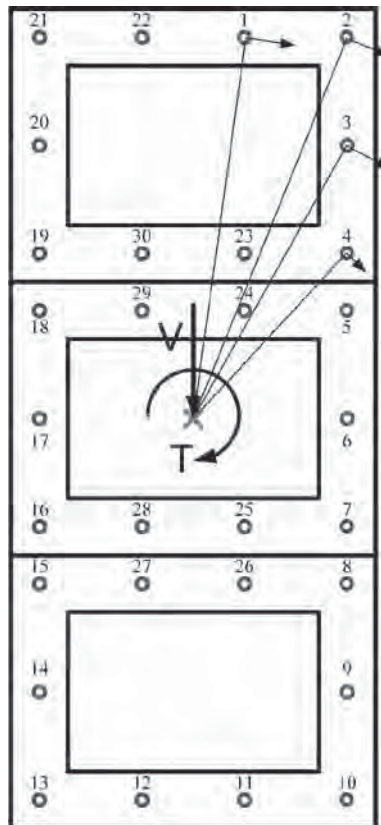


Figure A.4 Torsional force profile for the RRW concrete blocks

In Fig. A.4,

$$T = 600 \text{ kips} \cdot 96 \text{ in} = 57600 \text{ kip-in}$$

$$V = 600 \text{ kips}$$

$$F = \mu N = 0.5 \cdot 100 = 50 \text{ kips}$$

The screenshot from the excel calculation sheet is shown in Fig. A.5.

PT#	$x_i$	$y_i$	$r_i$	$r_i^2$	$r_i / r_i^2$	$F_x$	$F_y$	$F_z$	Vector Sum	Check	
Clockwise	in	in	in	$\text{in}^2$	$1 / \text{in}$	kips	kips	kips	kips	50	
1	18	144	145.12	21060.00	0.000452	26.06	25.86	3.23	20	34.76	Okay
2	54	144	153.79	23652.00	0.000479	27.62	25.86	9.70	20	39.38	Okay
3	54	108	120.75	14580.00	0.000376	21.68	19.39	9.70	20	35.47	Okay
4	54	72	90.00	8100.00	0.000281	16.16	12.93	9.70	20	32.39	Okay
5	54	36	64.90	4212.00	0.000202	11.65	6.46	9.70	20	30.39	Okay
6	54	0	54.00	2916.00	0.000168	9.70	0.00	9.70	20	29.70	Okay
7	54	-36	64.90	4212.00	0.000202	11.65	-6.46	9.70	20	30.39	Okay
8	54	-72	90.00	8100.00	0.000281	16.16	-12.93	9.70	20	32.39	Okay
9	54	-108	120.75	14580.00	0.000376	21.68	-19.39	9.70	20	35.47	Okay
10	54	-144	153.79	23652.00	0.000479	27.62	-25.86	9.70	20	39.38	Okay
11	18	-144	145.12	21060.00	0.000452	26.06	-25.86	3.23	20	34.76	Okay
12	-18	-144	145.12	21060.00	0.000452	26.06	-25.86	-3.23	20	30.82	Okay
13	-54	-144	153.79	23652.00	0.000479	27.62	-25.86	-9.70	20	27.84	Okay
14	-54	-108	120.75	14580.00	0.000376	21.68	-19.39	-9.70	20	21.96	Okay
15	-54	-72	90.00	8100.00	0.000281	16.16	-12.93	-9.70	20	16.53	Okay
16	-54	-36	64.90	4212.00	0.000202	11.65	-6.46	-9.70	20	12.16	Okay
17	-54	0	54.00	2916.00	0.000168	9.70	0.00	-9.70	20	10.30	Okay
18	-54	36	64.90	4212.00	0.000202	11.65	6.46	-9.70	20	12.16	Okay
19	-54	72	90.00	8100.00	0.000281	16.16	12.93	-9.70	20	16.53	Okay
20	-54	108	120.75	14580.00	0.000376	21.68	19.39	-9.70	20	21.96	Okay
21	-54	144	153.79	23652.00	0.000479	27.62	25.86	-9.70	20	27.84	Okay
22	-18	144	145.12	21060.00	0.000452	26.06	25.86	-3.23	20	30.82	Okay
23	18	72	74.22	5508.00	0.000231	13.33	12.93	3.23	20	26.59	Okay
24	18	36	40.25	1620.00	0.000125	7.23	6.46	3.23	20	24.11	Okay
25	18	-36	40.25	1620.00	0.000125	7.23	-6.46	3.23	20	24.11	Okay
26	18	-72	74.22	5508.00	0.000231	13.33	-12.93	3.23	20	26.59	Okay
27	-18	-72	74.22	5508.00	0.000231	13.33	-12.93	-3.23	20	21.17	Okay
28	-18	-36	40.25	1620.00	0.000125	7.23	-6.46	-3.23	20	17.97	Okay
29	-18	36	40.25	1620.00	0.000125	7.23	6.46	-3.23	20	17.97	Okay
30	-18	72	74.22	5508.00	0.000231	13.33	12.93	-3.23	20	21.17	Okay
320760.00											

T	57600	kip-in	(clockwise)		Pretension	100	kips
V	600	kips	(downward)		$\mu$	0.5	
ecc	96	in					

Figure A.5 A screenshot from the excel calculation sheet

(6) Check the torsion in the concrete blocks:

Assume three RRW blocks behave together as a cell at upper level:

$$A_{cp} = (10 \times 12)(27 \times 12) = 38880 \text{ in}^2$$

$$p_{cp} = 2 \cdot [(10 \times 12) + (27 \times 12)] = 888 \text{ in}$$

$$t = \frac{A_{cp}}{p_{cp}} = 43.8 \text{ in}$$

$$T_{\min} = \phi \sqrt{f_c} \frac{A_{cp}^2}{p_{cp}} = 1.3 \times 10^8 \text{ lb-in} = 129421 \text{ kip-in} > 57600 \text{ kip-in} \quad (\text{Meyer, 1996})$$

Thus, we can neglect the torsional effect in the RRW block, this failure mode will not govern.

(7) Check shear force in the entire concrete blocks:

Assume three RRW blocks behave together at upper level: (Fig. A.6)

$$V_u = 600 \text{ kips}$$

$$V_n = V_c + V_s$$

$$V_c = 2 \cdot \sqrt{8000} \cdot (18.75 \times 2) \cdot (27 \times 12 - 1.5 \times 2 - 0.5 \times 2) = 2146.6 \text{ kips}$$

$$\phi V_c = 0.85 \cdot 2146.6 = 1824.6 > 600 \text{ kips} \quad (\text{OK})$$

From the calculation shown above (neglect contribution of shear reinforcements), this failure mode will not control.

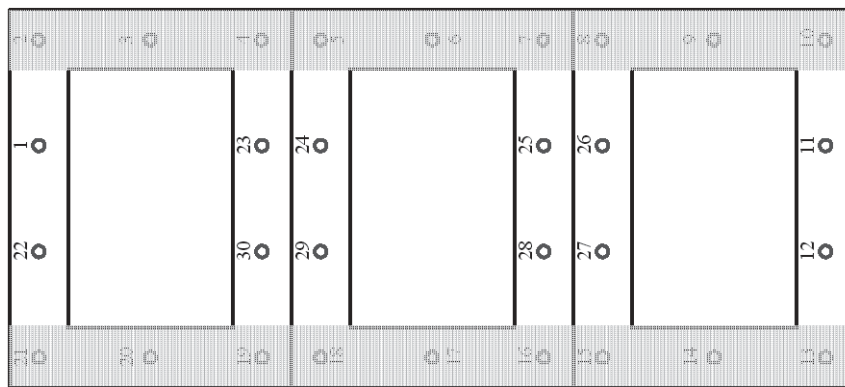


Figure A.6 Assumed shear force profile for the concrete blocks

(8) Check the (shear) friction between concrete blocks:

$$\mu = 0.5$$

$$(10 \times 3) \times 100 \text{ kips} \times \mu = 1500 \text{ kips} > 600 \text{ kips} \quad (\text{OK})$$

(9) Check the overturning moment for upper level (10 ft height):

From the excel calculation file (Schellenberg, 2004) downloaded from NEES@berkeley website. One can calculate the moment capacity for the two-stack RRW:

$$600 \text{ kips} \times 10 \text{ ft} = 6000 \text{ k-ft} < 7210 \text{ k-ft} \text{ (OK)}$$

Note that this is the two-stack RRW result. It is reasonable to assume that the three-stack RRW will have larger moment capacity. Fig. A.7 shows screen shots of the excel calculation results.

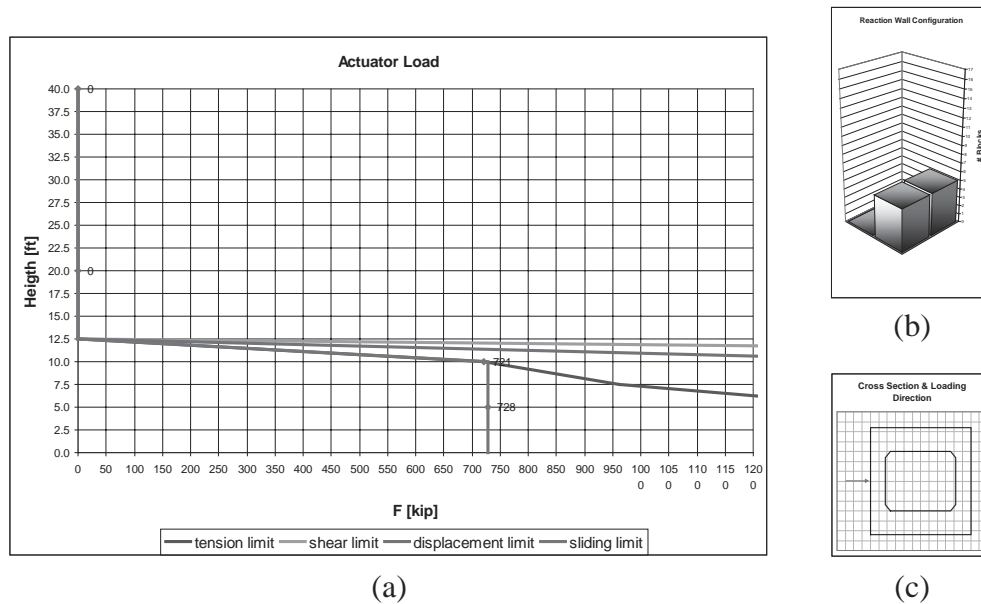


Figure A.7 The screenshots of the excel calculation results

(10) Check the lower level bracket base plate to concrete block surface friction: (assume 100 kips and 50 kips pretension forces in the all-thread-bars)

$$\mu = 0.33$$

$$R = (100 \text{ kips} \cdot 23 + 50 \text{ kips} \cdot 17) \cdot 0.33 = 1040 \text{ kips} > 300 \text{ kips} \text{ (OK)}$$

(11) Check the strain in the base plate of lower level bracket to prevent cracks in the RRW concrete blocks:

$$f_t = 0.1 \cdot f'_c = 0.1 \cdot 8000 \text{ psi} = 800 \text{ psi}$$

$$E_c = w_c^{1.5} \cdot 33 \sqrt{f'_c} = 145^{1.5} \cdot 33 \cdot \sqrt{8000} = 5153.6 \text{ ksi}$$

$$\varepsilon_{cr} = \frac{f_t}{E_c} = 1.55 \times 10^{-4}$$

check  $\varepsilon_{plate} < \varepsilon_{cr}$  (under 300 kips)

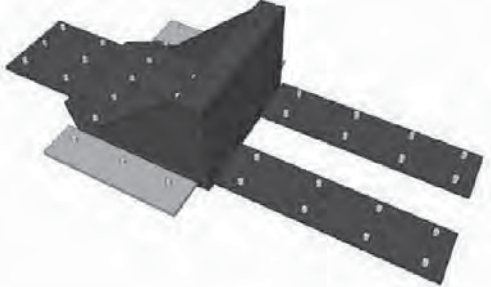
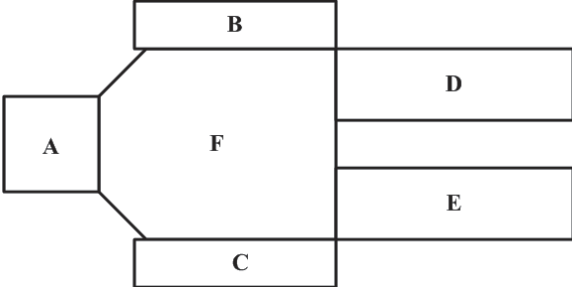
$$\sigma_{plate} = E_s \cdot \varepsilon_{plate} < E_s \cdot \varepsilon_{cr} = 4.5 \text{ ksi}$$

$$\text{check } \frac{P}{A_s} < 4.5 \text{ ksi}$$

From Table A.5, we can clearly see that stresses in all plate extensions are less than the estimated allowable stress.

Table A.5 Stress distribution in each base plate extensions

Zone	Force Ratio	Force P (kips)	$A_s$ (in <sup>2</sup> )	Stress (ksi)	Safety Factor (S.F.)
A	0.143	42.9	84	0.51	8.8
B	0.08	24	36	0.67	6.7
C	0.08	24	36	0.67	6.7
D	0.19	57	48	1.19	3.8
E	0.19	57	48	1.19	3.8
F	0.317	95.1	210	0.45	10.0

(12) Check local shear in RRW concrete block:

Refer to Fig. A.8 below. One can check the shear force transferred in the concrete blocks. Shear force in the typical profile in each concrete block:

$$\frac{600 \text{ kips} + 300 \text{ kips}}{6 \cdot 2} = 75 \text{ kips}$$

$$V_n = V_c + V_s$$

$$V_c = 2 \cdot \sqrt{8000} \cdot 30'' \cdot (23.5 - 1.5 \times 2 - 0.5 \times 2) = 104.6 \text{ kips}$$

$$V_s = \frac{A_v f_y d}{s} = \frac{2 \cdot 0.20 \cdot 60 \text{ ksi} \cdot 19.5}{4} = 117 \text{ kips}$$

$$\phi V_n = 0.85 \cdot 221.6 = 188.4 > 75 \text{ kips (OK)}$$

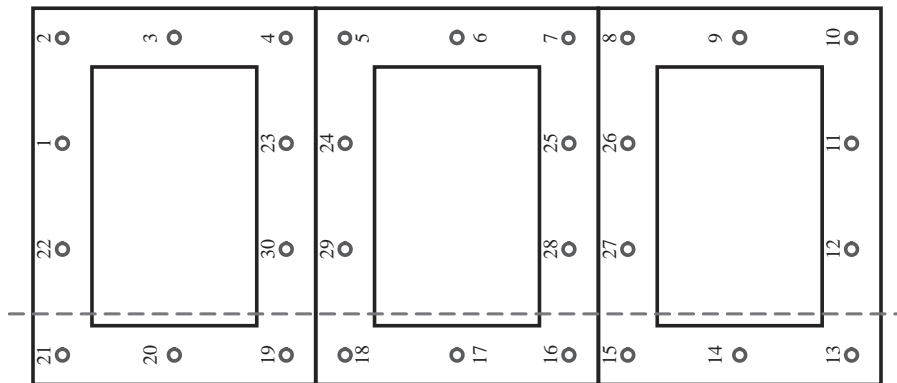


Figure A.8 Local shear force profile in the RRW concrete blocks

- (13) Check the torsional resistance between the concrete blocks: (assume 100 kips pretension for all-thread-bars)

Using the traditional elastic (vector) analysis method (Salmon and Johnson, 1996) to calculate the torsional resistance of the concrete blocks. Fig. A.9 demonstrates the concept of this method.

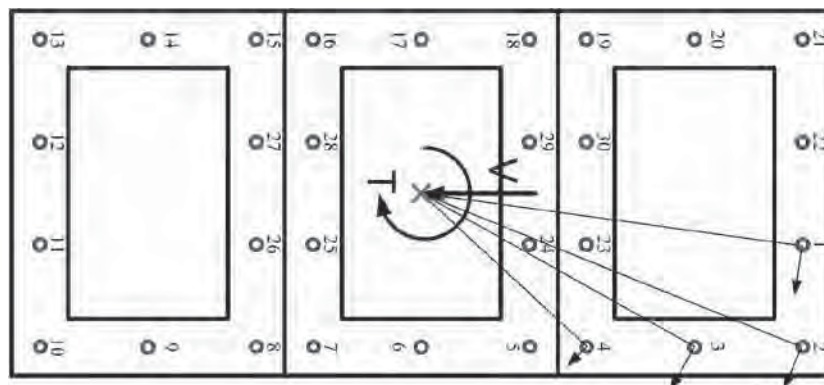


Figure A.9 Torsional force profile for the concrete blocks

In Fig. A.9,

$$T = 900 \text{ kips} \cdot 96 \text{ in} = 86400 \text{ kip-in}$$

$$V = 900 \text{ kips}$$

$$F = \mu N = 0.5 \cdot 100 = 50 \text{ kips}$$

The screenshot of the detail calculation sheet is shown in Fig. A.10 below.

PT#	x <sub>i</sub>	y <sub>i</sub>	r <sub>i</sub>	r <sub>i</sub> <sup>2</sup>	r <sub>i</sub> / r <sub>i</sub> <sup>3</sup>	F <sub>i</sub>	F <sub>ix</sub>	F <sub>iy</sub>	F <sub>v</sub>	Vector Sum	Check	
Clockwise	in	in	in	in <sup>2</sup>	1 / in	kips	kips	kips	kips	kips	50	
1	18	144	145.12	21060.00	0.000452	39.09	38.79	4.85	30	52.14	NG	
2	54	144	153.79	23652.00	0.000479	41.43	38.79	14.55	30	59.07	NG	
3	54	108	120.75	14580.00	0.000376	32.52	29.09	14.55	30	53.20	NG	
4	54	72	90.00	8100.00	0.000281	24.24	19.39	14.55	30	48.58	Okay	
5	54	36	64.90	4212.00	0.000202	17.48	9.70	14.55	30	45.59	Okay	
6	54	0	54.00	2916.00	0.000168	14.55	0.00	14.55	30	44.55	Okay	
7	54	-36	64.90	4212.00	0.000202	17.48	-9.70	14.55	30	45.59	Okay	
8	54	-72	90.00	8100.00	0.000281	24.24	-19.39	14.55	30	48.58	Okay	
9	54	-108	120.75	14580.00	0.000376	32.52	-29.09	14.55	30	53.20	NG	
10	54	-144	153.79	23652.00	0.000479	41.43	-38.79	14.55	30	59.07	NG	
11	18	-144	145.12	21060.00	0.000452	39.09	-38.79	4.85	30	52.14	NG	
12	-18	-144	145.12	21060.00	0.000452	39.09	-38.79	-4.85	30	46.23	Okay	
13	-54	-144	153.79	23652.00	0.000479	41.43	-38.79	-14.55	30	41.75	Okay	
14	-54	-108	120.75	14580.00	0.000376	32.52	-29.09	-14.55	30	32.94	Okay	
15	-54	-72	90.00	8100.00	0.000281	24.24	-19.39	-14.55	30	24.80	Okay	
16	-54	-36	64.90	4212.00	0.000202	17.48	-9.70	-14.55	30	18.24	Okay	
17	-54	0	54.00	2916.00	0.000168	14.55	0.00	-14.55	30	15.45	Okay	
18	-54	36	64.90	4212.00	0.000202	17.48	9.70	-14.55	30	18.24	Okay	
19	-54	72	90.00	8100.00	0.000281	24.24	19.39	-14.55	30	24.80	Okay	
20	-54	108	120.75	14580.00	0.000376	32.52	29.09	-14.55	30	32.94	Okay	
21	-54	144	153.79	23652.00	0.000479	41.43	38.79	-14.55	30	41.75	Okay	
22	-18	144	145.12	21060.00	0.000452	39.09	38.79	-4.85	30	46.23	Okay	
23	18	72	74.22	5508.00	0.000231	19.99	19.39	4.85	30	39.88	Okay	
24	18	36	40.25	1620.00	0.000125	10.84	9.70	4.85	30	36.17	Okay	
25	18	-36	40.25	1620.00	0.000125	10.84	-9.70	4.85	30	36.17	Okay	
26	18	-72	74.22	5508.00	0.000231	19.99	-19.39	4.85	30	39.88	Okay	
27	-18	-72	74.22	5508.00	0.000231	19.99	-19.39	-4.85	30	31.76	Okay	
28	-18	-36	40.25	1620.00	0.000125	10.84	-9.70	-4.85	30	26.96	Okay	
29	-18	36	40.25	1620.00	0.000125	10.84	9.70	-4.85	30	26.96	Okay	
30	-18	72	74.22	5508.00	0.000231	19.99	19.39	-4.85	30	31.76	Okay	
					320760.00							

T	86400	kip-in	(clockwise)	Pretension	100	kips
V	900	kips	(downward)	μ	0.5	
ecc	96	in				

Figure A.10 The screenshot of the excel calculation sheet

The required pretension forces for each post-tension rod to resist the torsion force are shown in Fig. A.11 below.

PT#	x <sub>i</sub>	y <sub>i</sub>	r <sub>i</sub>	r <sub>i</sub> <sup>2</sup>	r <sub>i</sub> / r <sub>i</sub> <sup>2</sup>	F <sub>ix</sub>	F <sub>ix</sub>	F <sub>iy</sub>	F <sub>v</sub>	Vector Sum	Check
Clockwise	in	in	in	in <sup>2</sup>	1 / in	kip	kip	kip	kip	kip	
1	18	144	145.12	21060.00	0.000452	39.09	38.79	4.85	30	52.14	Okay
2	54	144	153.79	23652.00	0.000479	41.43	38.79	14.55	30	59.07	Okay
3	54	108	120.75	14580.00	0.000376	32.52	29.09	14.55	30	53.20	Okay
4	54	72	90.00	8100.00	0.000281	24.24	19.39	14.55	30	48.58	Okay
5	54	36	64.90	4212.00	0.000202	17.48	9.70	14.55	30	45.59	Okay
6	54	0	54.00	2916.00	0.000168	14.55	0.00	14.55	30	44.55	Okay
7	54	-36	64.90	4212.00	0.000202	17.48	-9.70	14.55	30	45.59	Okay
8	54	-72	90.00	8100.00	0.000281	24.24	-19.39	14.55	30	48.58	Okay
9	54	-108	120.75	14580.00	0.000376	32.52	-29.09	14.55	30	53.20	Okay
10	54	-144	153.79	23652.00	0.000479	41.43	-38.79	14.55	30	59.07	Okay
11	18	-144	145.12	21060.00	0.000452	39.09	-38.79	4.85	30	52.14	Okay
12	-18	-144	145.12	21060.00	0.000452	39.09	-38.79	-4.85	30	46.23	Okay
13	-54	-144	153.79	23652.00	0.000479	41.43	-38.79	-14.55	30	41.75	Okay
14	-54	-108	120.75	14580.00	0.000376	32.52	-29.09	-14.55	30	32.94	Okay
15	-54	-72	90.00	8100.00	0.000281	24.24	-19.39	-14.55	30	24.80	Okay
16	-54	-36	64.90	4212.00	0.000202	17.48	-9.70	-14.55	30	18.24	Okay
17	-54	0	54.00	2916.00	0.000168	14.55	0.00	-14.55	30	15.45	Okay
18	-54	36	64.90	4212.00	0.000202	17.48	9.70	-14.55	30	18.24	Okay
19	-54	72	90.00	8100.00	0.000281	24.24	19.39	-14.55	30	24.80	Okay
20	-54	108	120.75	14580.00	0.000376	32.52	29.09	-14.55	30	32.94	Okay
21	-54	144	153.79	23652.00	0.000479	41.43	38.79	-14.55	30	41.75	Okay
22	-18	144	145.12	21060.00	0.000452	39.09	38.79	-4.85	30	46.23	Okay
23	18	72	74.22	5508.00	0.000231	19.99	19.39	4.85	30	39.88	Okay
24	18	36	40.25	1620.00	0.000125	10.84	9.70	4.85	30	36.17	Okay
25	18	-36	40.25	1620.00	0.000125	10.84	-9.70	4.85	30	36.17	Okay
26	18	-72	74.22	5508.00	0.000231	19.99	-19.39	4.85	30	39.88	Okay
27	-18	-72	74.22	5508.00	0.000231	19.99	-19.39	-4.85	30	31.76	Okay
28	-18	-36	40.25	1620.00	0.000125	10.84	-9.70	-4.85	30	26.96	Okay
29	-18	36	40.25	1620.00	0.000125	10.84	9.70	-4.85	30	26.96	Okay
30	-18	72	74.22	5508.00	0.000231	19.99	19.39	-4.85	30	31.76	Okay

320760.00

T	86400	kip-in	(clockwise)
V	900	kip	(downward)
ecc	96	in	

Pretension	119	kip
μ	0.5	

Figure A.11 The screenshot of the required post-tension forces from the excel calculation sheet

Thus, it is suggested to increase the post-tension force from 100 kips to 120 kips per all-thread-bar.

(14) Check the torsion in the concrete blocks:

Assume three RRW blocks behave together as a cell at lower level:

$$A_{cp} = (10 \times 12)(27 \times 12) = 38880 \text{ in}^2$$

$$P_{cp} = 2 \cdot [(10 \times 12) + (27 \times 12)] = 888 \text{ in}$$

$$t = \frac{A_{cp}}{P_{cp}} = 43.8 \text{ in}$$



$$T_{\min} = \phi \sqrt{f'_c} \frac{A_{cp}^2}{P_{cp}} = 1.3 \times 10^8 \text{ lb-in} = 129421 \text{ kip-in} > 86400 \text{ kip-in} \quad (\text{Meyer, 1996})$$

Thus, we can neglect the torsional effect in the RRW concrete blocks, this failure mode will not govern.

(15) Check shear force in the entire concrete blocks:

Assume three RRW blocks behave together at lower level: (Fig. A.12)

$$V_u = 900 \text{ kips}$$

$$V_n = V_c + V_s$$

$$V_c = 2 \cdot \sqrt{8000} \cdot (18.75 \times 2) \cdot (27 \times 12 - 1.5 \times 2 - 0.5 \times 2) = 2146.6 \text{ kips}$$

$$\phi V_c = 0.85 \cdot 2146.6 = 1824.6 > 900 \text{ kips} \quad (OK)$$

From the calculation shown above (neglect contribution of shear reinforcements), this mode will not control.

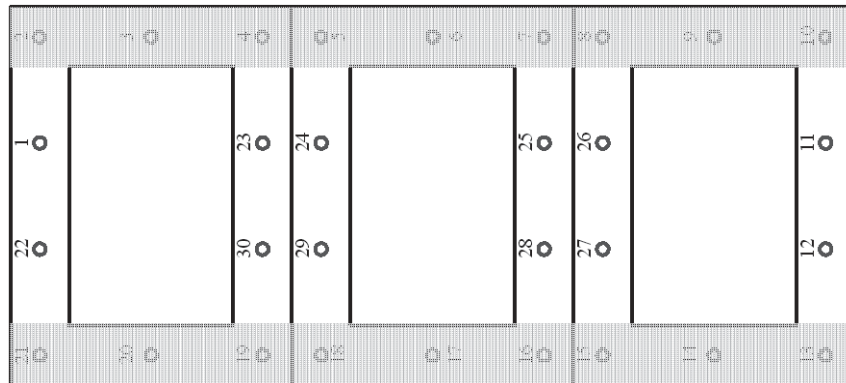


Figure A.12 Shear force profile for the concrete blocks

(16) Check the friction between concrete blocks: (Fig. A.13)

$$\mu = 0.5$$

$$(10 \times 3) \times 100 \text{ kips} \times \mu = 1500 \text{ kips} > 900 \text{ kips} \quad (OK)$$

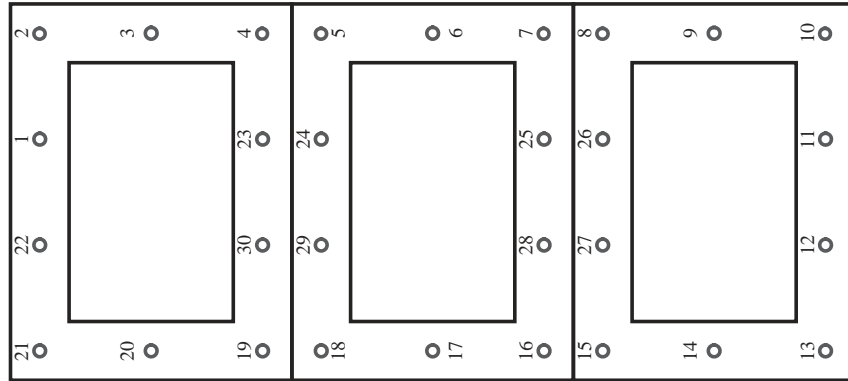


Figure A.13 Friction profile for the concrete blocks

(17) Check the overturning moment at RRW base for overall RRW (20 ft height):

Using the similar concept (Fig. A.14) in the original excel file (Schellenberg, 2004) on NEES@berkeley website, from the modified excel file we found (Fig. A.15):

$$16992 k - ft > (600 \cdot 20 + 300 \cdot 10) = 15000 k - ft$$

$$15000 k - ft < 20000 k - ft \text{ (OK)}$$

Also note that the design flexural capacity of strong floor, two-cell box girder, is 20000 kip-ft and the shear capacity is 1500 kips, distributed equally to three webs, which are adopted from the UCB/EERC-81/07 report (Aktan and Bertero, 1981, page 130 and 131). From the calculation sheet shows in Fig. A.16, the maximum all-thread-bar tension force after applying moment is 142.3 kip, less than 70%  $P_u$  (155 kips) of all-thread-bar (Shigley, 1972).

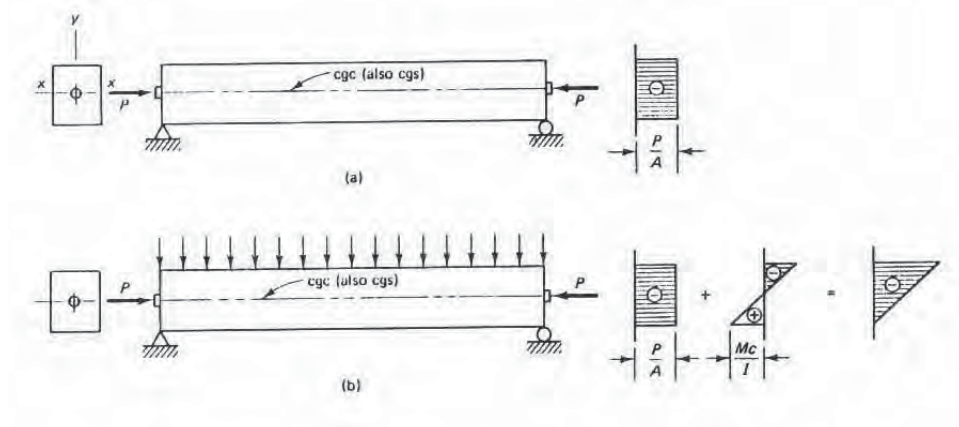


Figure A.14 Concepts of prestressing (Nawy, 1996)

Load Direction	weak	strong	axis
b	10.0	9.0	ft
d	9.0	10.0	ft
bt	2.0	1.5	ft
dt	1.5	2.0	ft
I	534.58	607.08	ft <sup>4</sup>
(per block)	1.11E+07	1.26E+07	in <sup>4</sup>
A	55.00	55.00	ft <sup>2</sup>
(per block)	7920.00	7920.00	in <sup>2</sup>
RRW weight / block	20.0	20.0	kip
PT per rod	100	100	kip
# of PT rods per RRW	10	10	rods
# of RRW per stack	10	10	blocks
# of stacks	3	3	stacks
Normal Stress	151.5	151.5	psi
y	162	180	in
I <sub>overall</sub>	2.18E+08	2.66E+08	in <sup>4</sup>
M <sub>allow</sub>	16992	18649	kip-ft

Figure A.15 Detail calculation of the allowable overturning moment

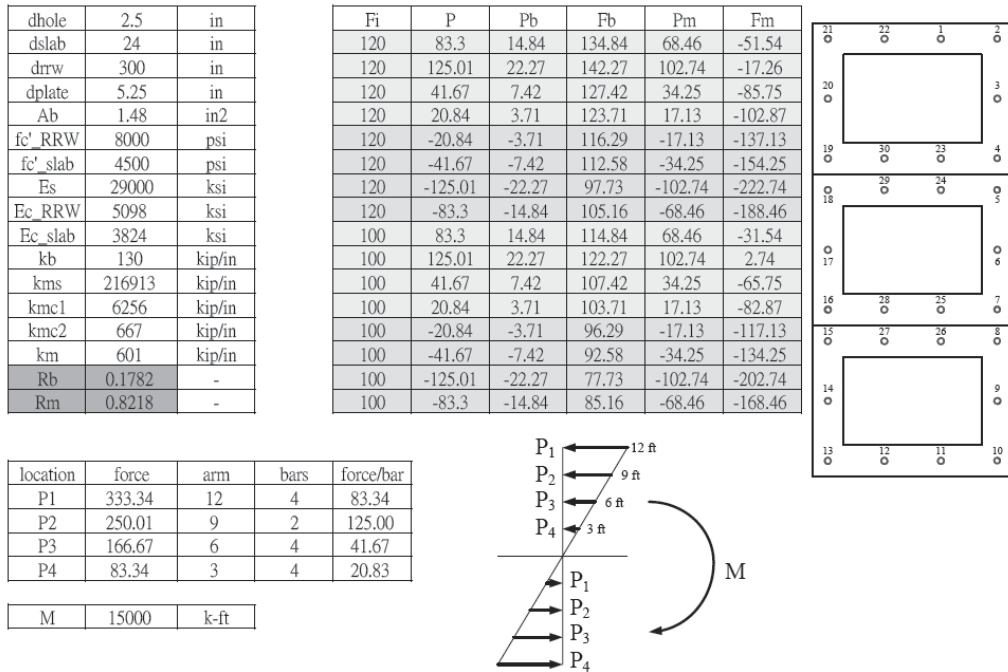


Figure A.16 Detail calculations of the pre-stressing forces in the post-tension rods

(18) Check the overturning moment that the strong floor can take (check the moment transfer through shear, see Fig. A.17):

From the formula adopted from Meyer's book (Meyer, 1996):

$$h = 24 \text{ in}, d = h - 1.5 = 22.5 \text{ in}$$

$$b_1 = a + d = 9 \cdot 3 \cdot 12 + 22.5 = 346.5 \text{ in}, b_2 = b + d = 10 \cdot 12 + 22.5 = 142.5 \text{ in}$$

$$c = \frac{b_1}{2} = 173.3 \text{ in}$$

$$J = 2\left(\frac{b_1^3 d}{12} + \frac{b_1 d^3}{12}\right) + 2b_2 d \cdot \left(\frac{b_1}{2}\right)^2 = 3.5 \times 10^8 \text{ in}^4, \gamma_v = 1 - \frac{1}{1 + \frac{2}{3} \sqrt{\frac{b_1}{b_2}}} = 0.51$$

$$M_v = \gamma_v \cdot M_u = 0.51 \cdot (600 \cdot 20 + 300 \cdot 10) = 7650 \text{ k} - \text{ft}$$

$$v_u = \frac{V_u}{b_o d} + \frac{\gamma_v \cdot M_u \cdot c}{J} = \left( \frac{20 \text{ kips} \cdot 30 \text{ blocks}}{978 \cdot 22.5} + \frac{(7650 \text{ k} - \text{ft}) \cdot 12 \cdot 173.3}{3.5 \times 10^8} \right) \cdot 1000$$

$$v_u = 27.3 + 45.5 = 72.8 \text{ psi}$$

$$v_c = \frac{V_c}{b_o d} = \min \left[ \left(2 + \frac{4}{\beta_c}\right) \sqrt{f'_c}, \left(2 + \frac{\alpha_s d}{b_o}\right) \sqrt{f'_c}, 4 \sqrt{f'_c} \right]$$

$$\text{where } \beta_c = \frac{346.5}{142.5} = 2.4, \alpha_s = 40, b_o = (b_1 + b_2) \times 2 = 978 \text{ in}$$

$$v_c = \min [ 3.7 \sqrt{f'_c}, 2.9 \sqrt{f'_c}, 4 \sqrt{f'_c} ] = 2.9 \sqrt{f'_c} = 2.9 \sqrt{4500} = 194.5 \text{ psi}$$

$$\phi = 0.85 \Rightarrow v_u = 0.85 \times 194.5 = 165.4 \text{ psi} > 72.8 \text{ psi (OK)}$$

This failure mode will not control.

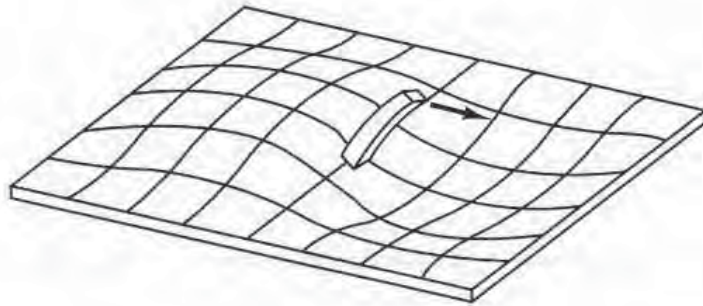


Figure A.17 Demonstration of the moment transfer through shear to the slab  
(Meyer, 1996)

(19) Check the required horizontal post-tension forces:

The horizontal shear force between RRW blocks is about 900 kip at lower level. Using the formula in mechanics of material textbook (Gere and Timoshenko, 1990) to check the vertical shear flow between RRW blocks:

$$f = \frac{VQ}{I} = \frac{900 \text{ kip} \cdot (10 \times 9 - 7 \times 5) \times 144 \text{ in}^2 \cdot 108 \text{ in}}{220195713 \text{ in}^4} = 3.5 \text{ kip/in}$$

$$F = f \cdot l = 3.5 \text{ kip/in} \cdot 120 \text{ in} = 420 \text{ kips (vertical)}$$

Assume  $\mu = 0.5$ , then we need at least 840 kips pre-stress force for lower four blocks. Provide two horizontal pre-stress rods per block and 120 kips pre-stress load for each rod:

$$R = 0.5 \times 4 \times 2 \times 120 \text{ kips} = 480 \text{ kips} > 420 \text{ kips} \text{ (OK)}$$

(20) Check the vertical shear in the RRW concrete block assembly:

$$f = \frac{VQ}{I} = \frac{900 \text{ kip} \cdot (10 \times 9 - 7 \times 5) \times 144 \text{ in}^2 (108 \text{ in} + 0.5 \cdot 34.6 \text{ in})}{220195713 \text{ in}^4} = 4.1 \text{ kip/in}$$

$$F = f \cdot l = 4.1 \text{ kip/in} \cdot 120 \text{ in} = 492 \text{ kips (vertical)}$$

$$V_c = (2 \cdot \sqrt{8000}) \cdot [4 \text{ blocks} \cdot (2.5 \cdot 12) \cdot (17.5 - 1.5 \cdot 2 - 0.5 \cdot 2)] \times 2 \text{ sides} = 579.6 \text{ kips}$$

$$\phi V_c = 0.85 \cdot 579.6 = 492.7 > 492 \text{ kips (OK)}$$

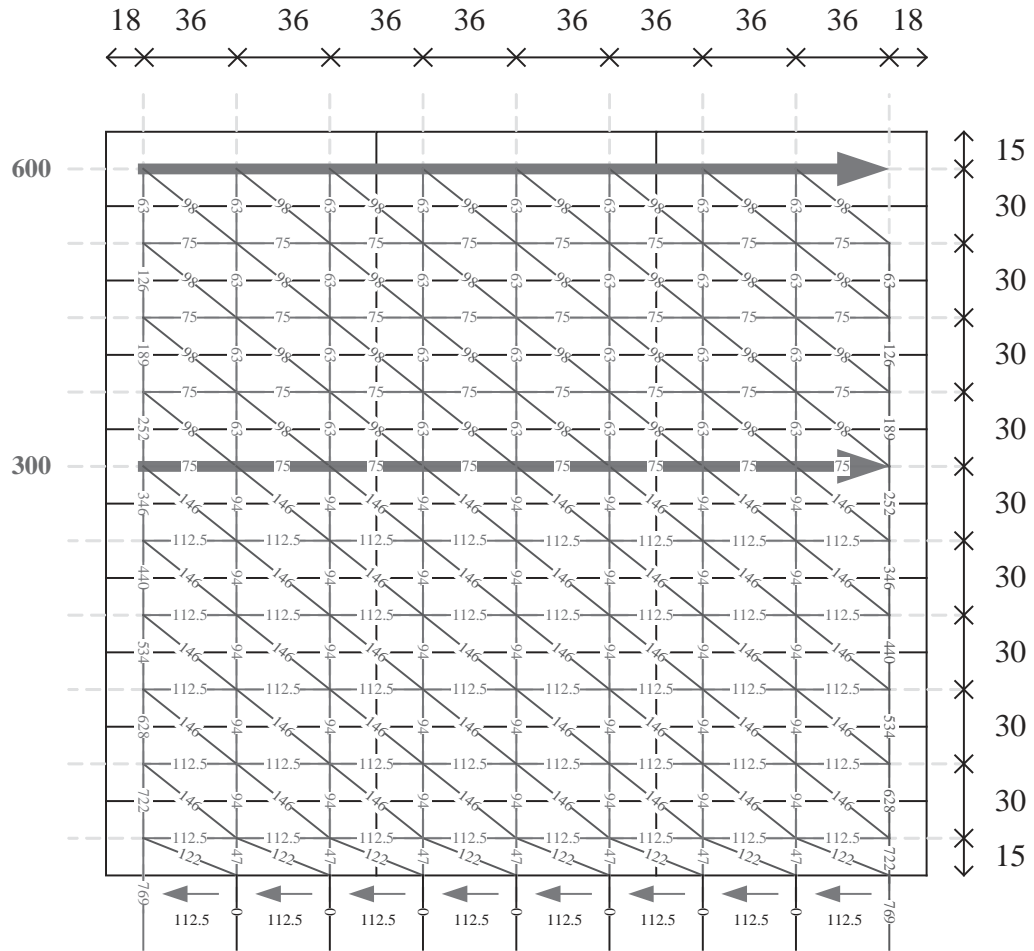
(21) Check the RRW using strut and tie models:

Assume the strut angle  $25^\circ < \theta < 65^\circ$  (ACI 318-05), and three stacks of blocks work as a single block together. Then we can calculate  $\theta = \tan^{-1}(30/36) = 40^\circ$ . The width of compression strut is:  $30 \cdot \cos(\tan^{-1}(30/36)) = 23.1''$  and the thickness of the RRW is about 18 inch. Then:

$$23.1'' \cdot 18'' \cdot 0.85 f'_c = 2827 \text{ kip (CCC node)}$$

$$23.1'' \cdot 18'' \cdot 0.65 f'_c = 2162 \text{ kip (CTT node)}$$

From Fig. A.18, all the node forces are less than 800 kips. This RRW wall can sustain the applied forces.



(Check equilibrium, OK!)

Figure A.18 The RRW strut and tie model

(22) Check the strong floor punching shear per hole: (Meyer, 1996)

Refer to Fig. A.19, without considering the contribution of shear reinforcement in the floor and assume three different possible cases.

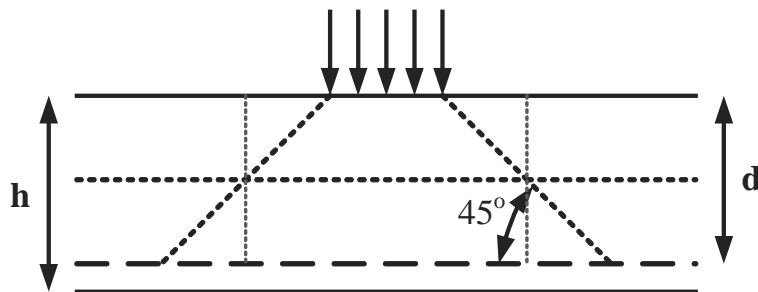


Figure A.19 The sketch of punching shear mechanism

(a) Assume 9 in by 9 in square plate as a washer:

$$h = 24 \text{ in}; d = h - 1.5 = 22.5 \text{ in}$$

$$V_c = \min \left[ \left(2 + \frac{4}{\beta_c}\right) \sqrt{f'_c b_o d}, \left(2 + \frac{\alpha_s d}{b_o}\right) \sqrt{f'_c b_o d}, 4 \sqrt{f'_c b_o d} \right]$$

$$\text{where } \beta_c = \frac{9}{9} = 1, \alpha_s = 40, b_o = (9 + 22.5) \times 4 = 126 \text{ in}$$

$$f'_c = 4500 \text{ psi}$$

$$V_c = \min [ 6 \sqrt{f'_c b_o d}, 9.14 \sqrt{f'_c b_o d}, 4 \sqrt{f'_c b_o d} ]$$

$$= 4 \sqrt{f'_c b_o d} = 4 \sqrt{4500 \times 126 \times 22.5} = 760.7 \text{ kips}$$

$$\phi = 0.85 \Rightarrow V_u = 0.85 \times 760.7 = 646.6 \text{ kips}$$

(b) Assume 7 in by 5 in square plate as a washer:

$$h = 24 \text{ in}; d = h - 1.5 = 22.5 \text{ in}$$

$$V_c = \min \left[ \left(2 + \frac{4}{\beta_c}\right) \sqrt{f'_c b_o d}, \left(2 + \frac{\alpha_s d}{b_o}\right) \sqrt{f'_c b_o d}, 4 \sqrt{f'_c b_o d} \right]$$

$$\text{where } \beta_c = \frac{7}{5} = 1.4, \alpha_s = 40, b_o = (7 + 5 + 22.5 \times 2) \times 2 = 114 \text{ in}$$

$$f'_c = 4500 \text{ psi}$$

$$V_c = \min [ 4.8 \sqrt{f'_c b_o d}, 9.9 \sqrt{f'_c b_o d}, 4 \sqrt{f'_c b_o d} ]$$

$$= 4 \sqrt{f'_c b_o d} = 4 \sqrt{4500 \times 114 \times 22.5} = 688.3 \text{ kips}$$

$$\phi = 0.85 \Rightarrow V_u = 0.85 \times 688.3 = 585.1 \text{ kips}$$

(c) Assume no washer: (Note: the strong floor has 2.5 in inside diameter holes 3 ft on center each direction)

$$h = 24 \text{ in}; d = h - 1.5 = 22.5 \text{ in}$$

$$r = \frac{2.5}{2} = 1.2 \text{ in}$$

$$V_c = \min \left[ \left(2 + \frac{4}{\beta_c}\right) \sqrt{f'_c b_o d}, \left(2 + \frac{\alpha_s d}{b_o}\right) \sqrt{f'_c b_o d}, 4 \sqrt{f'_c b_o d} \right]$$

$$\text{where } \beta_c = 1, \alpha_s = 40, b_o = 2 \cdot \pi \cdot \left(r + \frac{d}{2}\right) = 78.2 \text{ in}$$

$$f'_c = 4500 \text{ psi}$$

$$V_c = \min [ 6 \sqrt{f'_c b_o d}, 13.5 \sqrt{f'_c b_o d}, 4 \sqrt{f'_c b_o d} ]$$

$$= 4 \sqrt{f'_c b_o d} = 4 \sqrt{4500 \times 78.2 \times 22.5} = 472.1 \text{ kips}$$

$$\phi = 0.85 \Rightarrow V_u = 0.85 \times 472.1 = 401.3 \text{ kips}$$

From the calculations shown above, the punching shear will not govern in this case.

(23) Check the local moment and shear in the two-cell box girder:

Using SAP2000 (Computers and Structures, Inc., 2005) to analysis a 2-D frame cutting transversely from the two-cell box girder. Fig. A.20 shows the 2-D model, bending moment diagram and element forces for loading condition seven in SAP2000. For checking purpose, total ten loading conditions are selected and demonstrated in Fig. A.22. Note that each loading point has 100 kips concentrate force. Notations for Member and Joint End Forces are shown in Fig. A.21. For a 3-ft-wide strip (using concept of tributary area), under ten different loading conditions on the slab, the maximum member forces and joint end forces are summarized in Table A.6.

The bending moment and shear capacity at several locations in the frame model are calculated and briefly described below:

For tension capacity:

$$T_n = (0.1 \cdot 4500) \cdot (3 \cdot 12) \cdot 16'' = 259.2 \text{ kips}$$

(did not consider the contribution of reinforcements in the rib)

For shear capacity:

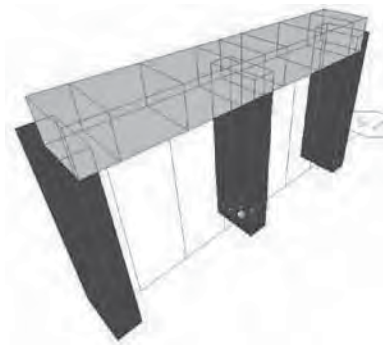
$$V_n = (3 \cdot \sqrt{4500}) \cdot (3 \cdot 12) \cdot 24'' = 173.9 \text{ kips}$$

(the shear strength of concrete is somewhere between  $1.9\sqrt{f'_c}$  and  $3.5\sqrt{f'_c}$ , did not consider the contribution of shear reinforcements in the slab)

For joint moment capacity (derived from joint shear capacity):

$$M_n = [(3 \cdot \sqrt{4500}) \cdot (3 \cdot 12) \cdot 16''] \times (24'' - 3'' - \frac{24''}{3}) = 177.1 \text{ kip-ft}$$

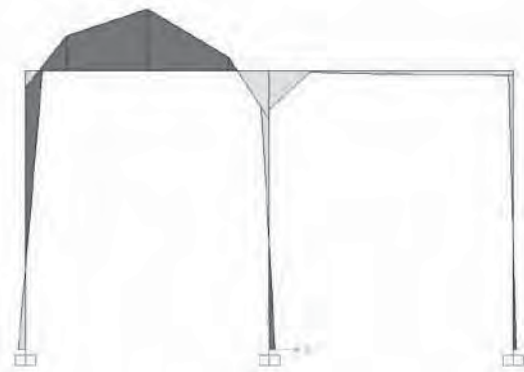




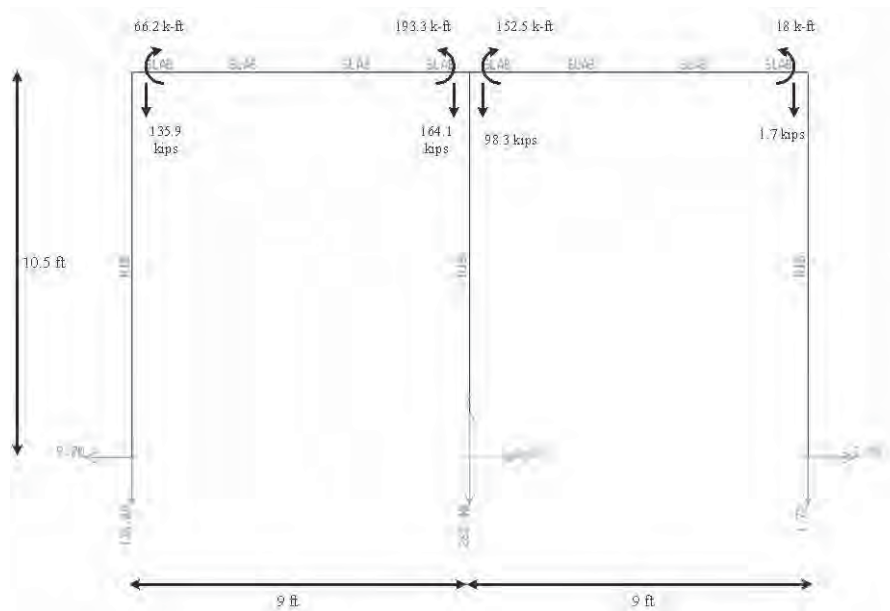
(a) 2-D model



(b) Joint external loads



(c) Bending moment diagram on tension side



(d) Element forces

Figure A.20 Analytical model in SAP2000

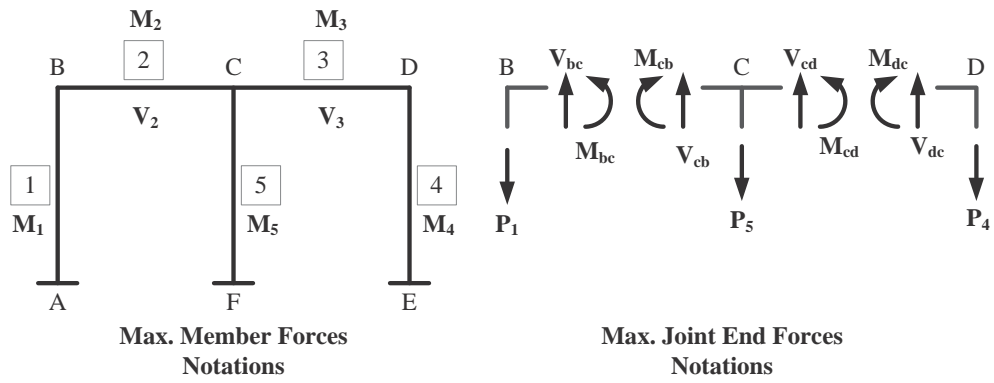


Figure A.21 Notations for member and joint end forces

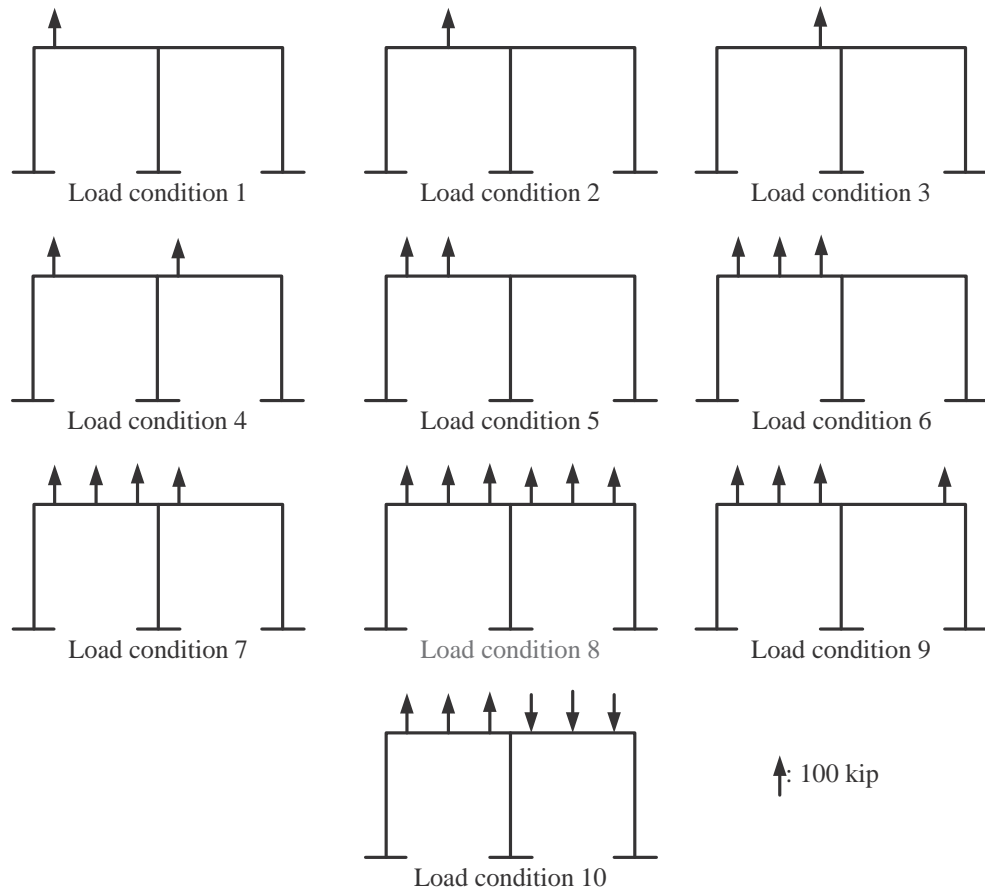


Figure A.22 Load conditions and load patterns  
(note that each loading point has 100 kips concentrate force)

Table A.6 Maximum member forces and joint end forces

Load Conditions	1	2	3	4	5	6	7	8	9	10
M <sub>1</sub>	18.3	30.3	16.6	19.3	48.7	65.2	66.2	66.6	65.7	63.8
M <sub>2</sub>	102.9	169.7	85.8	97.3	215	259.8	245.3	273.9	246.0	314.9
V <sub>2</sub>	80.8	55.5	86.4	77.8	125.3	161.1	164.1	173.0	164.0	150.8
M <sub>3</sub>	26.9	53.7	28.1	70.7	80.6	108.8	152.2	273.9	150.0	314.9
V <sub>3</sub>	2.9	6.0	3.0	89.3	8.9	11.9	98.3	173.0	68.9	150.8
M <sub>4</sub>	2.0	1.9	1.0	17.1	3.8	4.3	18.0	66.6	19.7	63.8
M <sub>5</sub>	14.2	26.5	15.6	1.3	40.8	56.3	40.8	0	42.1	112.7
M <sub>bc</sub>	18.3	30.3	16.6	19.3	48.7	65.2	66.2	66.6	65.7	63.8
M <sub>cb</sub>	41.2	80.2	43.7	69.3	121.4	165.1	193.3	273.9	192.1	56.3
M <sub>cd</sub>	26.9	53.7	28.1	70.7	80.6	108.8	152.5	273.9	150.0	-56.3
M <sub>dc</sub>	0.5	-0.2	1.0	17.1	0.4	1.4	18.0	66.6	19.7	-63.8
V <sub>bc</sub>	80.8	44.5	13.7	77.8	125.3	138.9	135.9	127.0	136.0	150.8
V <sub>cb</sub>	19.2	55.5	86.4	22.2	74.8	161.1	164.1	173.0	164.0	149.2
V <sub>cd</sub>	2.9	6.0	3.0	89.3	80.6	11.9	98.3	173.0	31.1	-149.2
V <sub>dc</sub>	-2.9	-6.0	-3.0	10.7	-8.9	-11.9	1.7	127.0	68.9	-150.8
P <sub>1</sub>	80.8	44.5	13.7	77.8	125.3	138.9	135.9	127.0	136.0	150.8
P <sub>5</sub>	22.2	61.5	89.4	111.5	83.7	173.3	262.4	346.0	195.2	0
P <sub>4</sub>	-2.9	-6.0	-3.0	10.7	-8.9	-11.9	1.7	127.0	68.9	-150.8

(unit: kip-ft and kip)

For moment capacity:

A moment-curvature relationship for the section is developed and the moment corresponds to the extreme concrete compression strain equal to 0.05% is selected as the elastic limit. From Mander's concrete model (Mander et. al, 1988), the 0.05% strain in concrete corresponds to 1892 psi, which is  $0.42f'_c$  in this case. This means the section behaves essentially elastic (see Figs. A.23 and A.24) although the bending moment exceed cracking moment. Figs. A.25 and A.26 show the moment curvature relationships for slab strip section and rib strip section, respectively. Table A.7 summaries the safety factors of the sections under different loading conditions in

different stage of behaviors. Table A.8 shows the safety factors of the sections correspond to sectional elastic limit under different loading conditions.

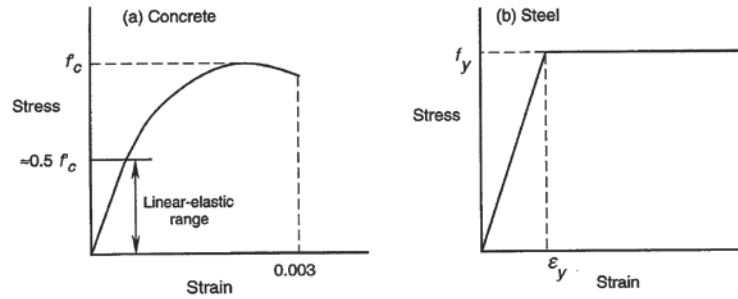


Figure A.23 Stress-strain relations for concrete and steel rebar (Meyer, 1996)

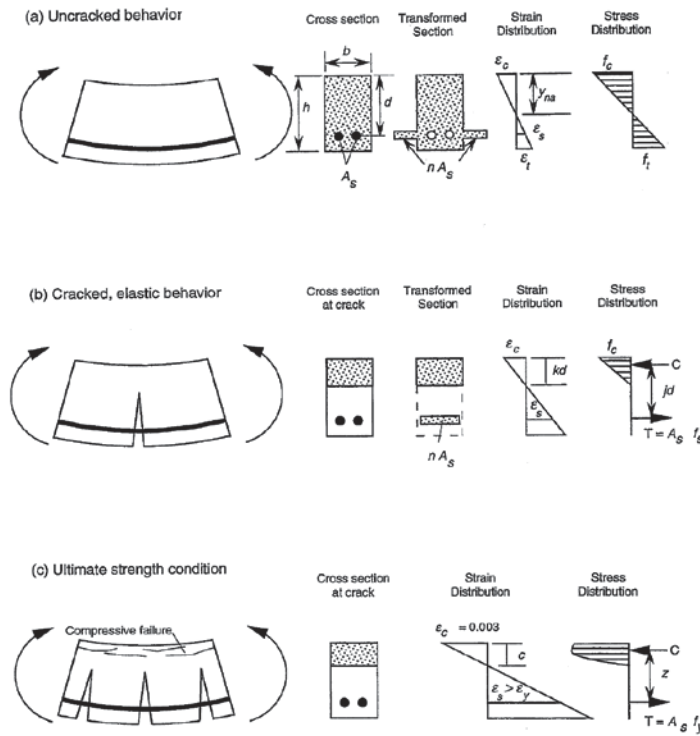


Figure A.24 Reinforced concrete beam behavior in different stages (Meyer, 1996)

### Moment - Curvature Relationships for Slab Strip

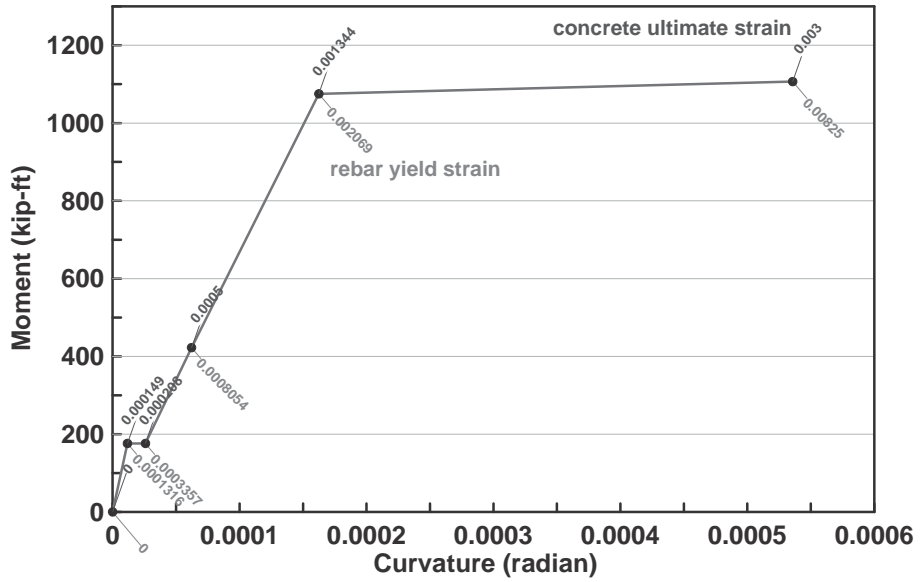


Figure A.25 Moment-curvature relationships for slab strip

### Moment - Curvature Relationships for Rib Strip

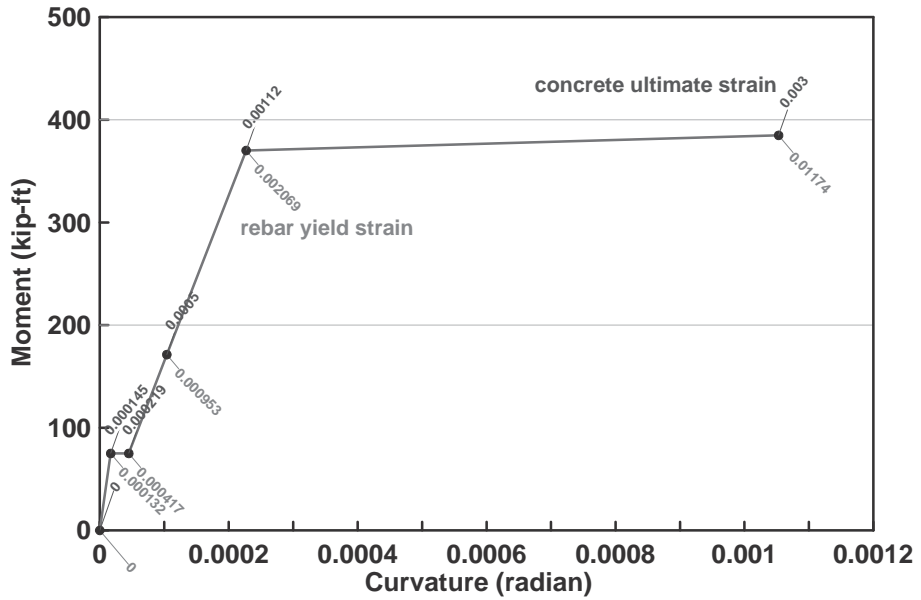


Figure A.26 Moment-curvature relationships for rib strip

Table A.7 Element and joint capacity vs. safety factors under different load conditions

Load Conditions		1	2	3	4	5	6	7	8	9	10
Capacity		Safety Factors (SF)									
M <sub>1</sub>	74.9 (cracking)	4.09	2.47	4.51	3.88	1.54	1.15	1.13	1.12	1.14	1.17
	171.2 (elastic limit)	9.36	5.65	10.3	8.87	3.52	2.63	2.59	2.57	2.61	2.68
	384.8 (ultimate)	21.0	12.7	23.2	19.9	7.90	5.90	5.81	5.78	5.86	6.03
M <sub>2</sub>	176.1 (cracking)	1.71	1.04	2.05	1.81	0.82	0.68	0.72	0.64	0.72	0.56
	422.5 (elastic limit)	4.11	2.49	4.92	4.34	1.97	1.63	1.72	1.54	1.72	1.34
	1106.6 (ultimate)	10.8	6.52	12.9	11.4	5.15	4.26	4.51	4.04	4.50	3.51
V <sub>2</sub>	173.9	2.15	3.13	2.01	2.24	1.39	1.08	1.06	1.01	1.06	1.15
M <sub>3</sub>	176.1 (cracking)	6.55	3.28	6.27	2.49	2.18	1.62	1.16	0.64	1.17	0.56
	422.5 (elastic limit)	15.7	7.87	15.0	5.98	5.24	3.88	2.78	1.54	2.82	1.34
	1106.6 (ultimate)	41.1	20.6	39.4	15.7	13.7	10.2	7.27	4.04	7.38	3.51
V <sub>3</sub>	173.9	60.0	29.0	58.0	1.95	19.5	14.6	1.77	1.01	2.52	1.15
M <sub>4</sub>	74.9 (cracking)	37.5	39.4	74.9	4.38	19.7	17.4	4.16	1.12	3.80	1.17
	171.2 (elastic limit)	85.6	90.1	171	10.0	45.1	39.8	9.51	2.57	8.69	2.68
	384.8 (ultimate)	192	203	385	22.5	101	89.5	21.4	5.78	19.5	6.03
M <sub>5</sub>	74.9 (cracking)	5.27	2.83	4.80	57.6	1.84	1.33	1.84	-	1.78	0.66
	171.2 (elastic limit)	12.1	6.46	11.0	132	4.20	3.04	4.20	-	4.07	1.52
	384.8 (ultimate)	27.1	14.5	24.7	296	9.43	6.83	9.43	-	9.14	3.41
M <sub>bc</sub>	177.1	9.68	5.84	10.7	9.18	3.64	2.72	2.68	2.66	2.70	2.78
M <sub>cb</sub> (unbalanced)	177.1	12.4	6.70	11.4	127	4.30	3.10	4.30	-	4.20	1.57
M <sub>cd</sub> (unbalanced)	177.1	12.4	6.70	11.4	126.5	4.30	3.10	4.30	-	4.20	1.57
M <sub>dc</sub>	177.1	354	886	177	10.4	443	126	9.84	2.66	8.99	2.78
V <sub>bc</sub>	173.9	2.15	3.91	12.7	2.24	1.39	1.25	1.28	1.37	1.28	1.15
V <sub>cb</sub>	173.9	9.06	3.13	2.01	7.83	2.32	1.08	1.06	1.01	1.06	1.17
V <sub>cd</sub>	173.9	59.9	28.9	57.9	1.95	2.16	14.6	1.77	1.01	5.59	1.17
V <sub>dc</sub>	173.9	59.9	28.9	57.9	16.3	19.5	14.6	102	1.37	2.52	1.15
P <sub>1</sub>	259.2	3.21	5.82	18.9	3.33	2.07	1.87	1.91	2.04	1.91	1.72

P <sub>5</sub>	259.2	11.7	4.21	2.90	2.32	3.10	1.50	1.0	0.75	1.33	-
P <sub>4</sub>	259.2	89.4	43.2	86.4	24.2	29.1	21.8	153	2.04	3.76	1.72
<b>Min. (SF)</b>	-	<b>1.71</b>	<b>1.04</b>	<b>2.01</b>	<b>1.81</b>	<b>0.82</b>	<b>0.68</b>	<b>0.72</b>	<b>0.64</b>	<b>0.72</b>	<b>0.56</b>

(unit: kip-ft and kip)

Table A.8 Minimum Safety Factors for each Load Conditions

Load Conditions	1	2	3	4	5	6	7	8	9	10
	Safety Factors (SF)									
<b>Min. (SF)*</b>	2.15	2.49	2.01	1.95	1.39	1.08	1.06	<b>0.75</b>	1.06	1.15
<b>Critical Location</b>	V <sub>2</sub>	M <sub>2</sub>	V <sub>2</sub>	V <sub>3</sub>	V <sub>2</sub>	V <sub>2</sub>	V <sub>2</sub>	P <sub>5</sub>	V <sub>2</sub>	V <sub>2</sub>

\*Note: the safety factors correspond to the cross section elastic limit.

From the tables show above, loading condition 8 will govern under these ten loading conditions.

(24) Check the load conditions for different RRW configurations under applied overturning moment on the slab:

Assume the applied overturning moment is 600 kip x 20 ft + 300 kip x 10 ft = 15000 k-ft. From previous results we can derive the load combinations acting on the frame model as shown in Fig. A.27. Note that some reaction forces are extracted from SAP2000 analysis results under 800 kips uplifting force at one end of floor beam and made an assumption of providing four stiff load transfer beam below the floor slab longitudinally at both ends of floor beam. Thus:

$$\frac{1}{3}(118.3 + 266.1 + 80.2) = 155 \text{ kips}$$

$$\frac{1}{3}(73.5 + 178.5 + 39.6) = 97.2 \text{ kips}$$

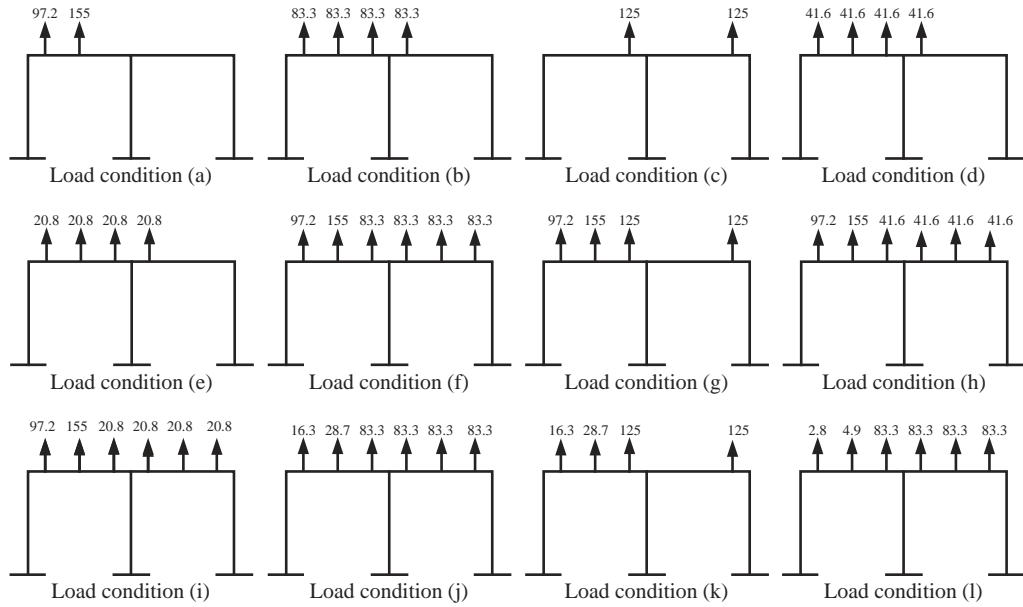


Figure A.27 Possible loading combinations (unit: kip)

From the results shown in Table A.9 and Table A.10, the option (i) is selected as the final configuration. In actual case, the concentrated uplifting force acting on the floor slab will lower than 800 kips and more close to 675 kips:

$$P_{uplift} = (600 \text{ kips} \cdot 18 \text{ ft} + 300 \text{ kips} \cdot 9 \text{ ft}) / 20 \text{ ft} = 675 \text{ kips}$$

$$S.F. = 1.06 \times \frac{800}{675} = 1.26$$

The actual safety factor for option (i) will be at least 1.26, conservatively.

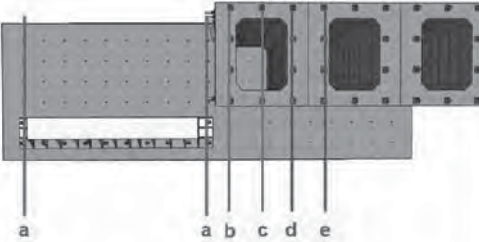
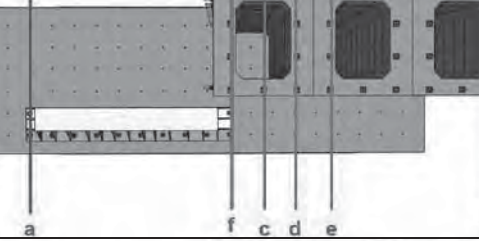
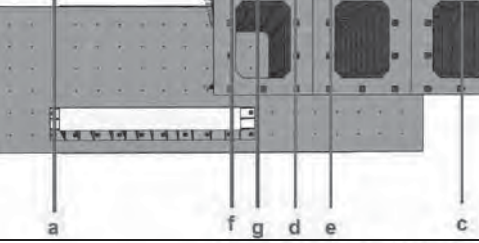
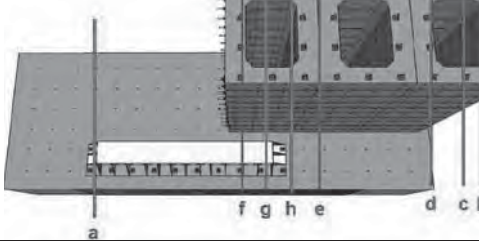
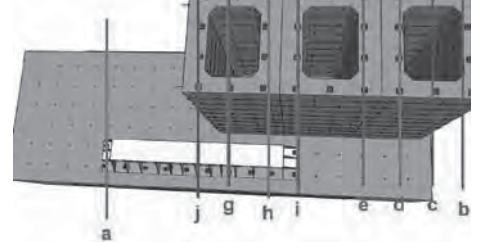
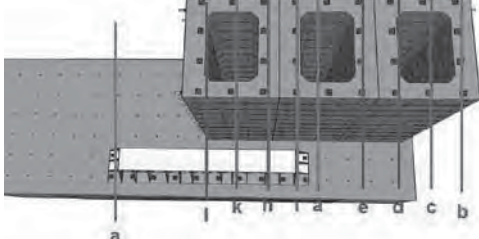
Table A.9 Safety factors for possible loading combinations

Load Conditions	a	b	c	d	e	f	g	h	i	j	k	l
	Safety Factors (SF)											
<b>Min. (SF)*</b>	1.06	1.19	1.56	2.34	4.74	0.77	0.8	0.97	1.01	1.08	1.33	1.17
<b>Critical Location</b>	V <sub>2</sub>	P <sub>5</sub>	V <sub>3</sub>	P <sub>5</sub>	P <sub>5</sub>	P <sub>5</sub>	V <sub>cb</sub>	V <sub>2</sub>	V <sub>2</sub>	P <sub>5</sub>	V <sub>cb</sub>	P <sub>5</sub>

\*Note: the safety factors correspond to the cross section elastic limit.



Table A.10 Critical safety factors for different configurations

Configuration	Plan view & Load Conditions	Min. SF & Critical Loaction		
(i) Shift 6 ft outward		<b>a</b>	<b>1.06</b>	<b>V<sub>2</sub></b>
(ii) Shift 3 ft outward		<b>f</b>	<b>0.77</b>	<b>P<sub>5</sub></b>
(iii) Current position		<b>f</b>	<b>0.77</b>	<b>P<sub>5</sub></b>
(iv) Shift 3 ft toward		<b>f</b>	<b>0.77</b>	<b>P<sub>5</sub></b>
(v) Shift 6 ft toward		<b>g</b>	<b>0.80</b>	<b>V<sub>cb</sub></b>
(vi) Shift 9 ft toward		<b>h</b>	<b>0.97</b>	<b>V<sub>2</sub></b>

### A.3.2. Check the floor beam above the test slab

The floor beam is selected to be modified from the existing floor beam in Davis Hall laboratory. Total twenty anchor holes are available to mount to the strong floor in the lab.

$$R = 0.5 \times (20 \times 100 \text{ kips}) = 1000 \text{ kips} > 900 \text{ kips}$$

Thus, it is suggested to prestress the all-thread-bars to at least 100 kips. Simple calculation of the uplifting force per side:

$$P_{uplift} = (18 \text{ ft} \times 600 \text{ kips} + 9 \text{ ft} \times 300 \text{ kips}) / 20 \text{ ft} = 675 \text{ kips}$$

The entire floor beam is modeled using shell elements in SAP2000, Figs. A.28 and A.29 illustrate the mesh distribution and the boundary condition settings in the model. Conservatively using 800 kips as the uplift force transfers to the floor beam in SAP model. The von Mises stress distribution in the floor beam under 800 kips uplift force is shown in Figs. A.30 and A.31. The maximum von Mises stress is about 27 ksi. The distribution of reaction forces under 800 kips uplift force is superimposed on the stress distribution as shown in Fig. A.32. Maximum reaction force is 135 kips. If using hinge supports in the SAP model, which represents the extreme case, the maximum reaction force is 266 kips as shown in Fig. A.33.

Note that the existing floor beam in Davis Hall is weight about 22.5 kip. After welding the stiffeners and plates aside the flange, the estimated weight is about 30.3 kip. The overhead traveling crane in the Richmond Field Station structural lab (i.e. NEES Berkeley lab) has about 26270 lb (117 kN, 12 US-ton) capacity.

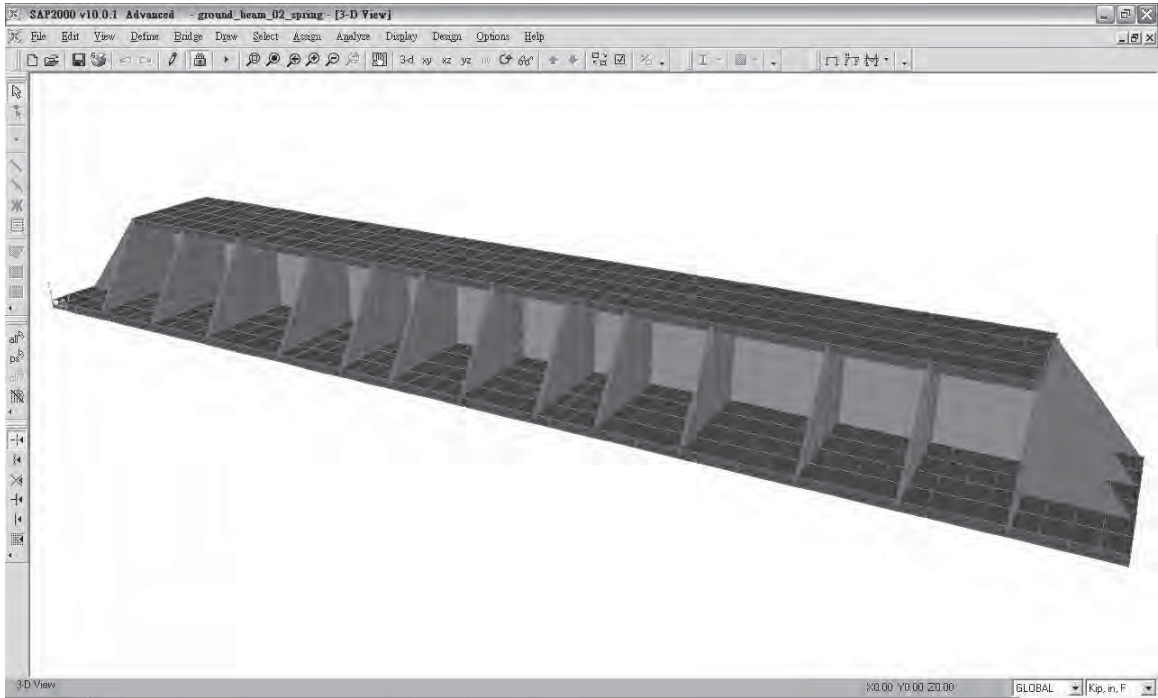


Figure A.28 The SAP2000 shell elements model for floor beam

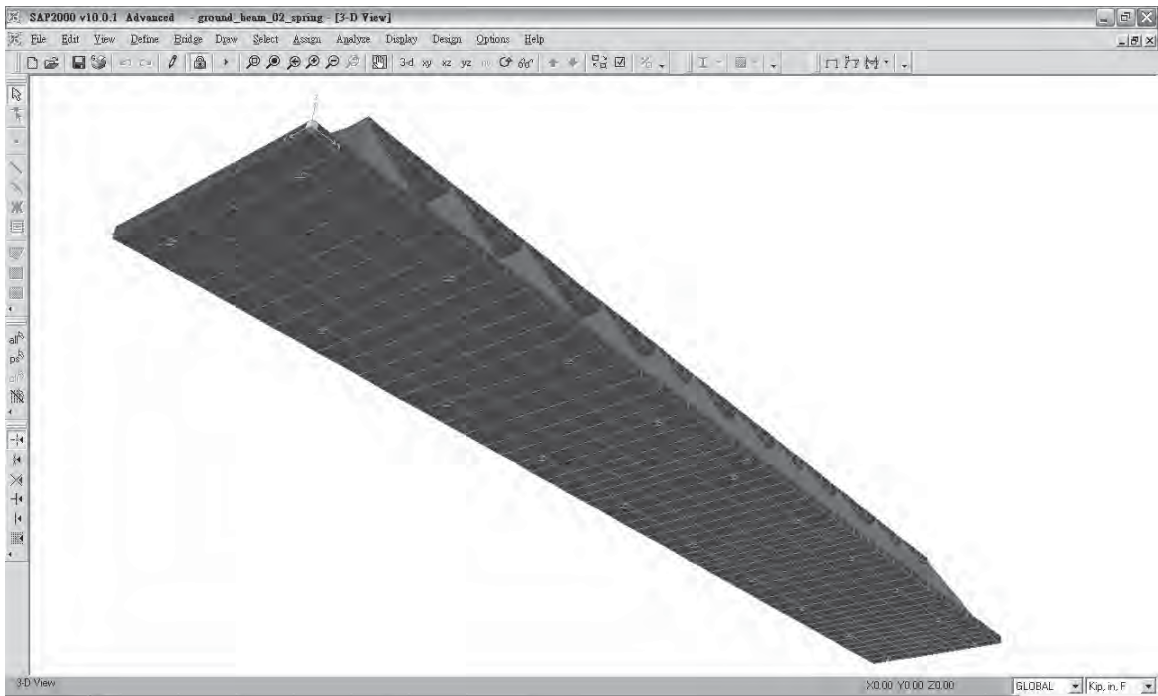


Figure A.29 Spring boundary condition used in the SAP2000 model

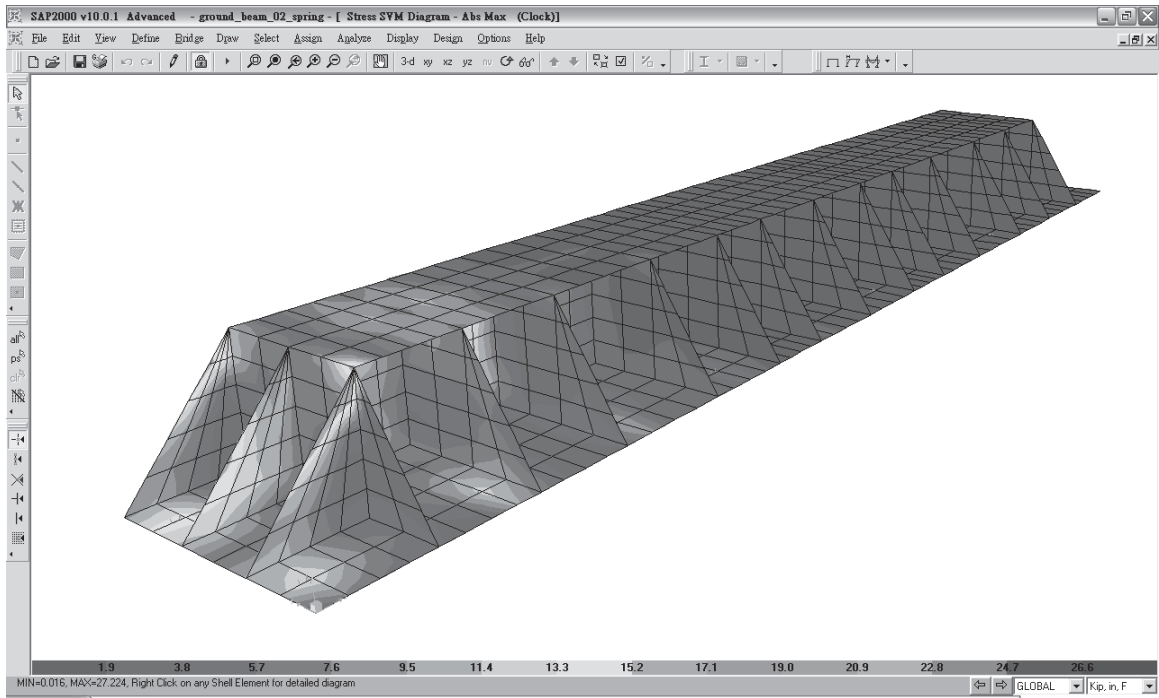


Figure A.30 The von Mises stress distribution in the floor beam under 800 kips uplift force (averaged stress, view from top)

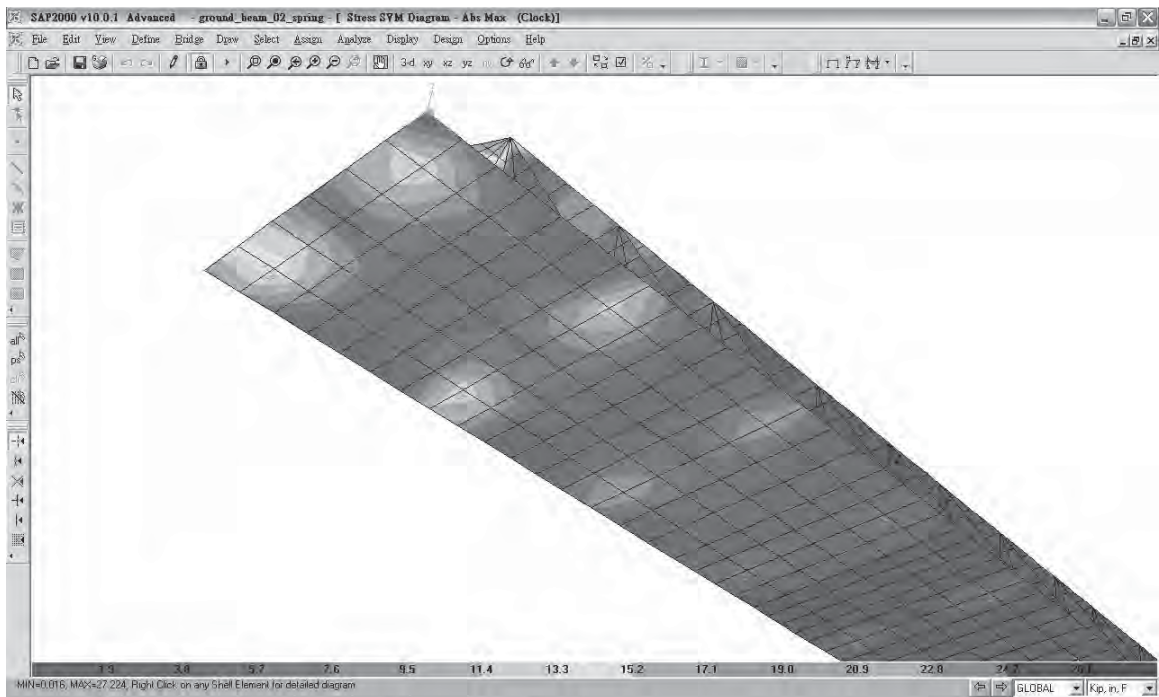


Figure A.31 The von Mises stress distribution in the floor beam under 800 kips uplift force (averaged stress, view from bottom)

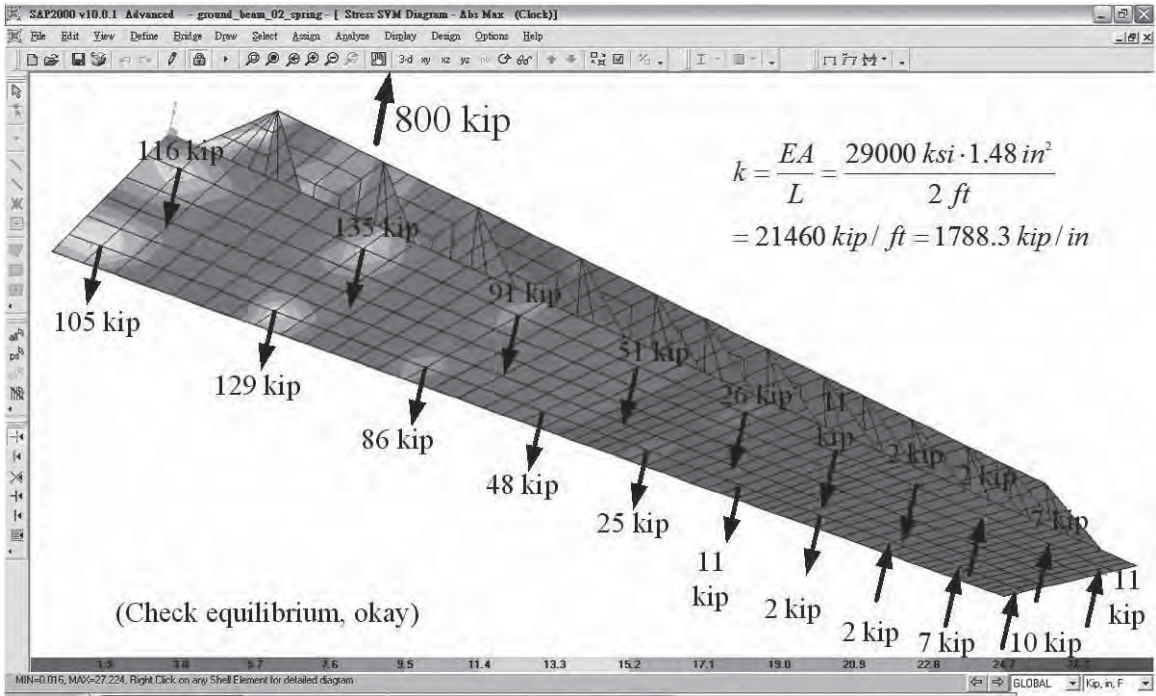


Figure A.32 The distribution of reaction forces under 800 kips uplift force (spring supports)

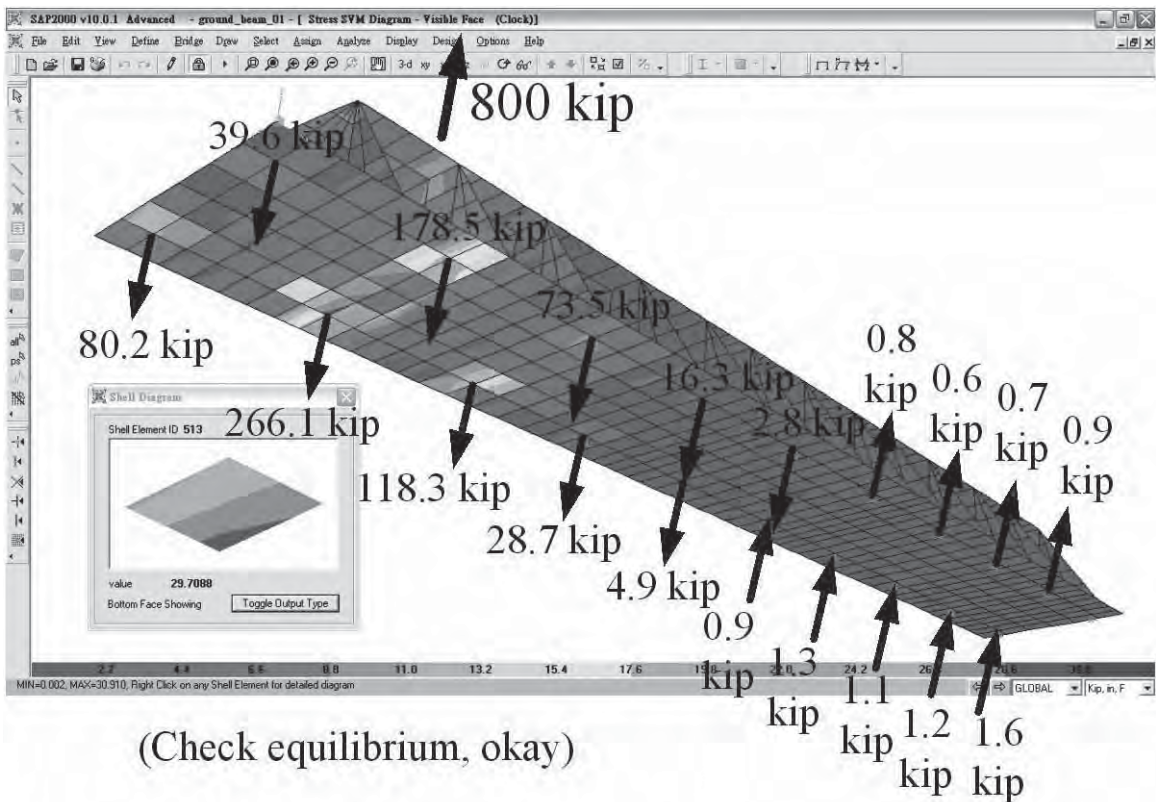


Figure A.33 The distribution of reaction forces under 800 kips uplift force (hinge supports)

Now we consider all-thread-bar, floor beam base plate, under-floor beam and concrete slab in series since they are gripped together. Based on the assumption in mechanical design handbook (Shigley, 1972; Norton 2006), the portion of total external load on post tensioned assembly taken by all-thread-bar and members (i.e. ground beam base plate, under-floor beam and concrete slab) as well as the resultant loads in all-thread-bar and the resultant loads on members can be calculated. Table A.11 shows the safety factors for yielding and separation in the assembly under different external loads and different all-thread-bar diameters.

Table A.11 Safety factors for yielding and separation in the assembly

Nominal Diameter (in)	1-3/8	1-3/8	1-3/4	1-3/4
Minimum Yield Strength (kips)	190	190	320	320
Pretention Load (kips)	140	140	200	200
External Load (kips)	131	224	131	224
$P_b$ (kips)	29	50	44	75
$P_m$ (kips)	102	174	87	149
Safety Factor for Yielding	1.12	0.99	1.31	1.16
Safety Factor for Separation	1.38	0.80	2.31	1.34

Note: (from Fig. A.33)

$$\frac{1}{3}(118.3 + 266.1 + 80.2) = 155 \text{ kips} \Rightarrow 155 \cdot \frac{675}{800} = 131 \text{ kips}$$

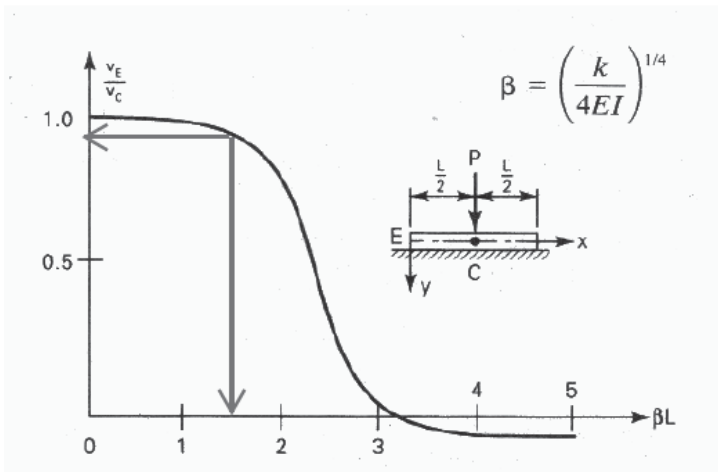
$$266.1 \cdot \frac{675}{800} = 224 \text{ kips}$$

From the calculation results shown above, using larger rod diameter with higher pretension load (i.e. 1-3/4" rod with 200 kips pretension load) can prevent separation of the assembly and reduce the probability to yield the post tension rods. This also increase the shear resistant on the floor beam to at least 1320 kips if the friction coefficient is taken as 0.33 for all 20 rods. Again, this is under a very conservative loading and analysis condition.

### A.3.3. Design the floor beam below the test slab (the under-floor beam)

Now we need to find the required flexural stiffness of the beam under the floor slab to spread out the uplift force. From Ugural and Fenster "Advanced Strength and Applied Elasticity" Chapter 9 (Ugural and Fenster, 2004), we can find theoretical solutions for a finite beam sitting on an elastic foundation. In order to spread out uplift force to adjacent anchor points, we need a

relatively rigid beam to achieve this goal. By comparing the center and end deflection (theoretically) of a finite beam on an elastic foundation subjected to a centrally concentrated load, the required flexural stiffness of the beam under the floor slab can be determined using the formula and figure provided in the book. Choose  $\beta L = 1.5$  (see the left of Fig. A.34) and the beam length is equal to 72 inch (6 ft), and then we can determine the required moment of inertia of the beam which is  $7564.5 \text{ in}^4$ . This is closed to the moment of inertia of the AISC W24 x 229 section ( $I = 7650 \text{ in}^4$ ). The required moment of inertia for different beam length is listed on the right in Fig. A.34.



$\beta L$	1.5	$\text{in}^2$
E	29000	ksi
k	165.3	ksi
L	72	in
I	7564.5	$\text{in}^4$

L	I
in	$\text{in}^4$
36	472.8
48	1494.2
60	3648.0
72	7564.5
84	14014.2
96	23907.5
108	38295.2
120	58368.0

(a) Comparison of the center and end deformations of a finite length beam on an elastic support under a concentrated load at center (Ugural and Fenster, 2004)

(b) Calculation results

Figure A.34 Required moment of inertia for the under-floor beam

The selected W24 x 229 beam, both web and flange are compact and the material type is ASTM A572 Grade 50 steel. The following failure modes are checked:

- (1) Web shear yielding: (no tension field action)

$$V_n = 0.6 \cdot F_y \cdot A_w \cdot C_v = 0.6 \cdot 50 \cdot (26" \cdot 0.96") \cdot 1.0 = 749 \text{ kips}$$

$$\phi V_n = 0.9 \cdot 749 = 674 \text{ kips} > 320 \text{ kips}$$

- (2) Web local yielding:

$$\text{Assume } N = 6"; k = 2.23" \Rightarrow N + 5k = 17.2" \Rightarrow \frac{N + 5k}{2} = 8.6" > 12"$$

$$d = 26" > 12"$$

$$R_n = (2.5k + N) \cdot F_{yw} \cdot t_w = 556 \text{ kips} \Rightarrow \phi R_n = 1.0 \cdot 556 = 556 \text{ kips} > 320 \text{ kips}$$

(3) Web crippling:

$$\frac{d}{2} = 13" > 12"; \frac{N}{d} = \frac{6}{26} = 0.23 > 0.2$$

$$\Rightarrow R_n = 0.4 \cdot t_w^2 \left[ 1 + \left( \frac{4N}{d} - 0.2 \right) \left( \frac{t_w}{t_f} \right)^{1.5} \right] \sqrt{\frac{E \cdot F_{yw} \cdot t_f}{t_w}} = 774 \text{ kips}$$

$$\Rightarrow \phi R_n = 0.75 \cdot 774 = 581 \text{ kips} > 320 \text{ kips}$$

(4) Buckling capacity of the  $\phi = 3"$  extra-strong pipe welded to beam web:

$$P_{cr} = \frac{\pi^2 E \cdot I}{(kL)^2} = \frac{\pi^2 (29000 \text{ ksi}) \cdot 3.89 \text{ in}^4}{(1.0 \cdot 26")^2} = 1647 \text{ kips} > 320 \text{ kips}$$

(5) Buckling of stiffeners: (four stiffeners around each hole)

$$I = \frac{1}{12} \cdot \left( 6 \frac{1}{16} " \right) \cdot 1^3 = 0.5 \text{ in}^4; L = 26"$$

$$P_{cr} = 4 \cdot \frac{\pi^2 E \cdot I}{(kL)^2} = 4 \cdot \frac{\pi^2 (29000 \text{ ksi}) \cdot 0.5 \text{ in}^4}{(1.0 \cdot 26")^2} = 847 \text{ kips} > 320 \text{ kips}$$

(6) Yielding of compression strut: (pipe plus four stiffeners around each hole)

$$A_{\text{pipe}} = 3.02 \text{ in}^2; A_{\text{stiffeners}} = 4 \cdot \left( 6 \frac{1}{16} " \cdot 1" \right) = 24.25 \text{ in}^2$$

$$R_n = 50 \text{ ksi} \cdot (3.02 + 24.25) = 1364 \text{ kips} > 320 \text{ kips}$$

### A.3.4. Check the lateral supporting frame

The SAP2000 model for the lateral supporting frame is shown in Fig. A.35. It is assumed that 5% of maximum actuator forces (for each floor level) acting on six supporting points.

$$F_1 = 300 \cdot 0.05 = 15 \text{ kips}$$

$$F_2 = 600 \cdot 0.05 = 30 \text{ kips}$$

Check the stress ratios directly in the SAP2000 model:  $SR_{\max} = 0.72 < 1.0$

From static analysis, check the stress at the root of cantilever beam:



$V = 123 \text{ kips}; M = 21900 \text{ kip-in}; T = 43.8 \text{ kip-in}$

$f_n = 26.2 \text{ ksi (bending)} + 3.34 \text{ ksi (wrapping)} = 29.54 \text{ ksi} < 0.9 \cdot 36 = 32.4 \text{ ksi}$

$f_{v-web} = 4.94 \text{ ksi (shear)} + 0.15 \text{ ksi (wrapping)} = 5.09 \text{ ksi} < 0.9 \cdot 0.6 \cdot 36 = 19.4 \text{ ksi}$

$f_{v-flange} = 1.1 \text{ ksi (shear)} + 0.09 \text{ ksi (wrapping)} = 1.19 \text{ ksi} < 0.9 \cdot 0.6 \cdot 36 = 19.4 \text{ ksi}$

Check the maximum lateral displacement:

$$\delta_{max} = 1.36'' \Rightarrow \frac{1.36''}{(312 + 2 - 16 - 3.25)} = \frac{4.6}{1000} < \frac{5}{1000}$$

Providing a HSS 8 x 8 x 0.5 brace at the middle of cantilever beam, the maximum deflection will be much lower than this value. The stresses in the Tee sections, guider plate assemblies (saddles) and kickers are also checked briefly by hand.

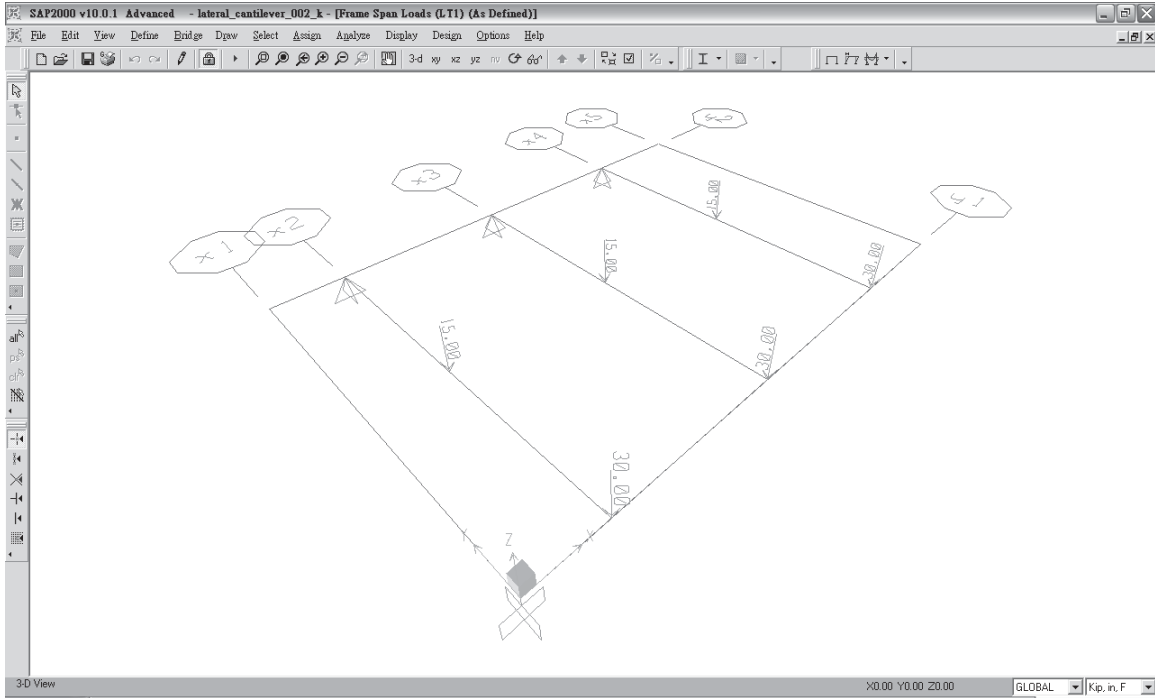


Figure A.35 The SAP2000 model for lateral supporting frame

**A.3.5. Check the weight of 1.5 M-lb actuators**

The total weight of a 1.5 M-lb actuator should be less than the capacity of bridge crane in NEES lab for setup installation. The overhead bridge crane capacity in the lab is about 26270 lb (117 kN, 12 US-ton). From Table A.12 and Fig. A.36, the total weight of 1.5 M-lb actuator is less than the crane capacity. Two W8 x 40 cantilever beams with 48 inches in length are provided to temporarily support the actuators during the specimen fabrication stage.

Table A.12 Detail lists of the 1.5 M-lb actuator parts

Actuator parts	Qty.	Weight (lb) (from drawings)	Weight (lb) (Approx. calculation)	Weight (lb) (from photos)
① Assembly	1	N.A.	< 12,000	14600 (①+③+⑥)
② Cap end mounting bracket	1	4,045	4,136	4100 (②)
③ Rod eye	1	1,100	1,153	-
④ Rod end mounting bracket	1	4,860	4,970	4860 (④)
⑤ Pin	2	672	673	1450 (⑤+⑦)
⑥ Load cell	1	175	207	-
⑦ Pin retainer plate	2	N.A.	6.8	-
<b>Sum</b>			<b>&lt; 23,825 lb</b>	<b>25,010 lb</b>

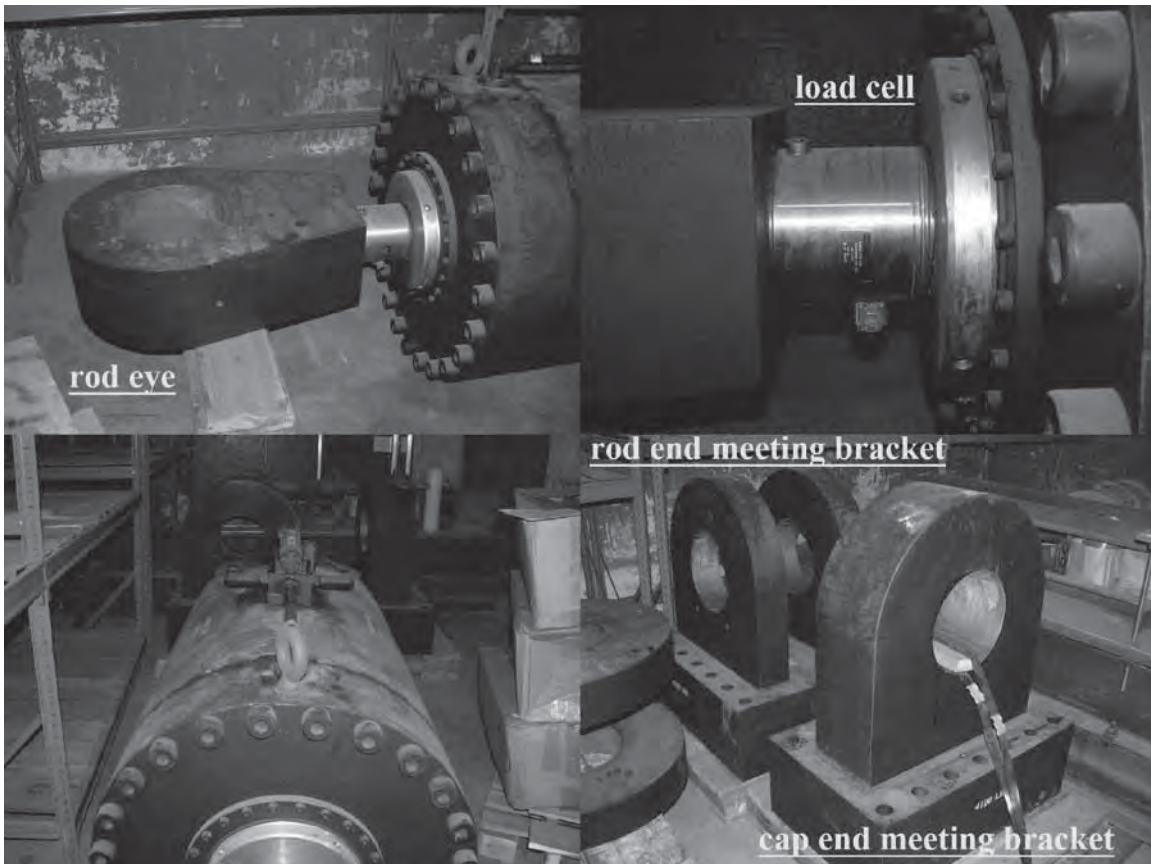


Figure A.36 The 1.5 M-lb actuator assemblies in Richmond Field Station structural lab

## Reference Lists for Appendix A

1. Aktan A.E. and Bertero, V.V. (1981), "The Seismic Resistant Design of R/C Coupled Structural Walls", UCB/EERC-81/07 Report, Earthquake Engineering Research Center, University of California, Berkeley, California.
2. Astaneh-Asl A. and Ravat S. (1998), "Cyclic Behavior and Seismic Design of Steel H-piles", UCB/CEE-Steel-98/01, Final Report to the California Department of Transportation, May 20, 1998.
3. Arici Y. and Mosalam, K.M. (2001), "NEES-UCB Reconfigurable Reaction Wall Design", UCB/SEMM-2001, In-house Report, Structural Engineering, Mechanics and Materials (SEMM), Department of Civil and Environmental Engineering, University of California, Berkeley, Summer 2001.
4. ASTM Standard A572/A572M-03 (2003), "Standard Specification for High-Strength Low-Alloy Columbium-Vanadium Structural Steel", ASTM International, West Conshohocken, PA, <http://www.astm.org>.
5. ASTM Standard A36/A36M-04 (2004), "Standard Specification for Carbon Structural Steel", ASTM International, West Conshohocken, PA, <http://www.astm.org>.
6. ASTM Standard A706/A706M-04 (2004), "Standard Specification for Low-Alloy Steel Deformed and Plain Bars for Concrete Reinforcement", ASTM International, West Conshohocken, PA, <http://www.astm.org>.
7. ACI Committee 318 (2005), "Building Code Requirements for Structural Concrete (ACI 318-05) and Commentary (ACI 318R-05)", American Concrete Institute, Farmington Hills, MI, U.S.A.
8. Clyde, D. (2001), "Reaction Blocks Design Drawings", AutoCAD file.
9. Computers and Structures, Inc. (2005), "SAP2000 Linear and Nonlinear Static and Dynamic Analysis and Design of Three-Dimensional Structures: Basic Analysis Reference Manual", Computers and Structures, Inc. Berkeley, California, USA, <http://www.csiberkeley.com>.
10. Gere, J.M. and Timoshenko, S.P. (1990), "Mechanics of Materials", 3<sup>rd</sup> edition, PWS-KENT Publishing Company, Boston, ISBN: 0-534-92174-4.
11. Mander, J. B., Priestley, M. J. N. and Park, R. (1988), "Theoretical Stress-Strain Model for Confined Concrete", Journal of Structural Engineering, Vol. 114, Issue 8, pp.1804-1826.
12. Meyer, C. (1996), "Design of Concrete Structures", Upper Saddle River, N.J., Prentice Hall, ISBN: 0-13-203654-1.
13. Mosalam, K.M. and Elkhoraibi, T. (2004), "RRW System: Specifications, Usage and Training Example", Structural Engineering, Mechanics and Materials (SEMM), Department

of Civil and Environmental Engineering, University of California, Berkeley, September 15, 2004.

14. Mosalam, K.M. and Elkhoraibi, T. (2004), "RRW System: Appendices", Structural Engineering, Mechanics and Materials (SEMM), Department of Civil and Environmental Engineering, University of California, Berkeley, September 15, 2004.
15. Nawy, E.G. (1996), "Reinforced Concrete: A Fundamental Approach", 3<sup>rd</sup> edition, Upper Saddle River, N.J., Prentice Hall, ISBN: 0-13-123498-6.
16. Norton, R.L. (2006), "Machine Design: An Integrated Approach", 3<sup>rd</sup> edition, Upper Saddle River, N.J., Prentice Hall, ISBN: 0-13-148-190-8.
17. Skidmore, Owings & Merrill (1963), "Test Slabs Design Calculations for the University of California Richmond Field Station Structural Research Laboratory", Skidmore, Owings & Merrill LLP, One Maritime Plaza, San Francisco, CA 94111, USA.
18. Skidmore, Owings & Merrill (1964), "Test Slab Details for the University of California Richmond Field Station Structural Research Laboratory", Drawing Number S7 & S7-SUP-1, Skidmore, Owings & Merrill LLP, One Maritime Plaza, San Francisco, CA 94111, USA.
19. Shigley, J. E. (1972), "Mechanical engineering design", Chapter 7, p.305, 2<sup>nd</sup> edition, McGraw-Hill, New York.
20. Salmon, C.G. and Johnson, J.E. (1996), "Steel Structures: Design and Behavior, Emphasizing Load and Resistance Factor Design", Chapter 4, p.139, 4<sup>th</sup> edition, HarperCollins Publishers Inc., ISBN: 0-673-99786-3.
21. Seaburg, P.A. and Carter, C.J. (1997), "Torsional Analysis of Structural Steel Members", Steel Design Guide Series 9, American Institute of Steel Construction, Chicago, IL.
22. Schellenberg, A. (2004), "Reaction Wall Design Spreadsheet", Excel file.
23. Ugural, A.C. and Fenster, S.K. (2004), "Advanced Strength and Applied Elasticity", Chapter 9, p.358, 4<sup>th</sup> edition, Pearson Education Taiwan Ltd., ISBN: 986-7491-92-0.
24. Williams Form Engineering Corp. (2008), "Threaded Bars with Fasteners: 150 ksi all-thread-bar", Online Catalog, <http://www.williamsform.com>.
25. Kiyota, S. and Tamagawa, H. (2004), "New Construction Manual for Civil Engineering Structures", Society of Science and Technology, Tokyo, ISBN:4-8445-3315-0 (in Japanese).

---

## **Appendix B**

### **Test Setup Shop Drawings**

---



REV	REVISION	DATE

revisions

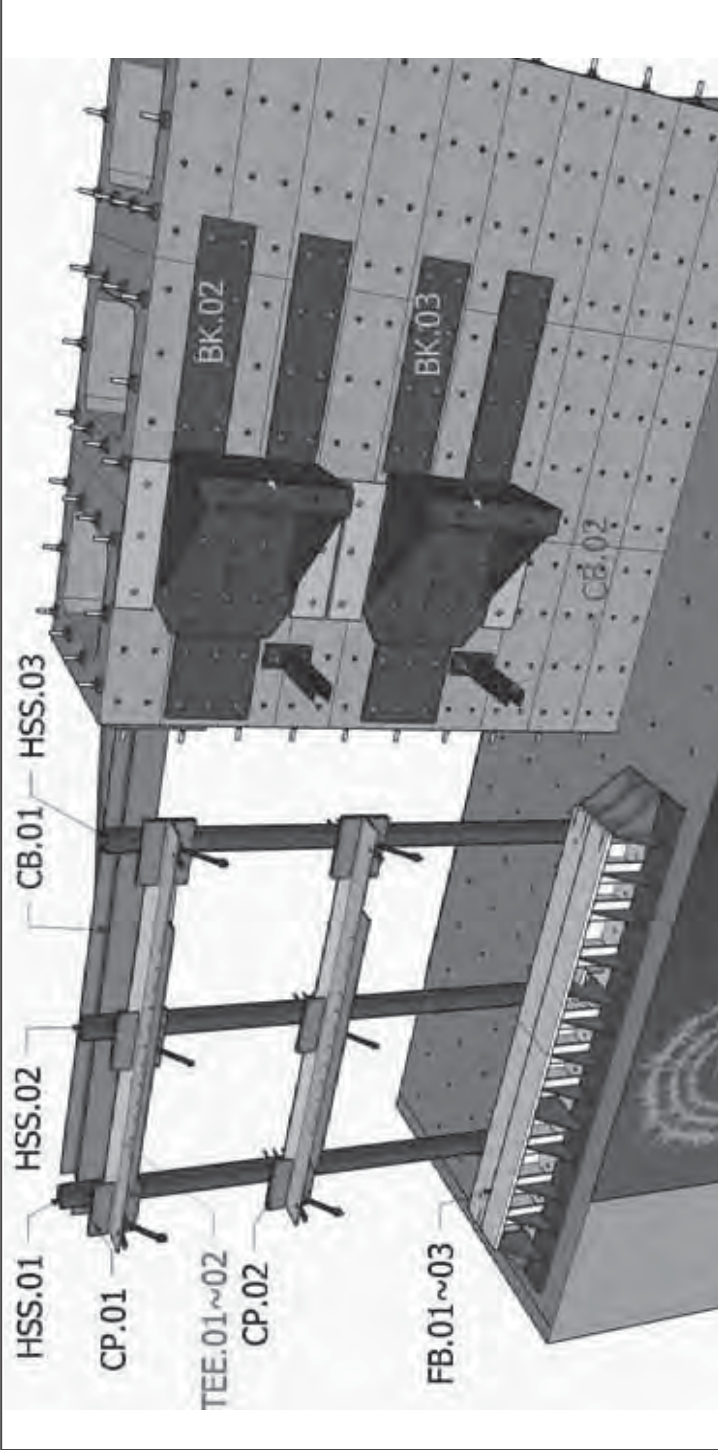
**project**  
SCBF  
Phase-01  
1301 South 48th Street  
Richmond, California, 94804

**Address**  
UC Berkeley  
Richmond Field Station  
Building 464, Structural Research Lab

**content**  
Test Rig  
3D Overview

**drawn by:** Jim-Wen Lai (Jwlai)  
**checked by:** Jim-Wen Lai (Jwlai)  
**date:** Aug. 2008

**drawing no.**  
TR.01



- Material:**
- (1) ASTM A572 GR.50 steel plates and sections.
  - (2) ASTM A36 steel plates.
  - (3) ASTM A490 bolts and bolt rods.
  - (4) E70XX electrode.
  - (5) ASTM A500B for HSS sections.

- General Notes:**
- (1) Tolerance:  $\pm \frac{1}{16}$ ".
  - (2) Anything unclear please see TR.01 for reference.
  - (3) Other questions please email to: [adrian.jwlai@berkeley.edu](mailto:adrian.jwlai@berkeley.edu).



**International Hybrid  
Simulation of  
Tomorrow's Braced  
Steel Frame Structures**

REV	REVISION	DATE

**revisions**

**project**

SCBF  
Phase-01  
1301 South 46th Street  
Richmond, California, 94804

**Address**

UC Berkeley  
Richmond Field Station  
Building 464, Structural Research Lab

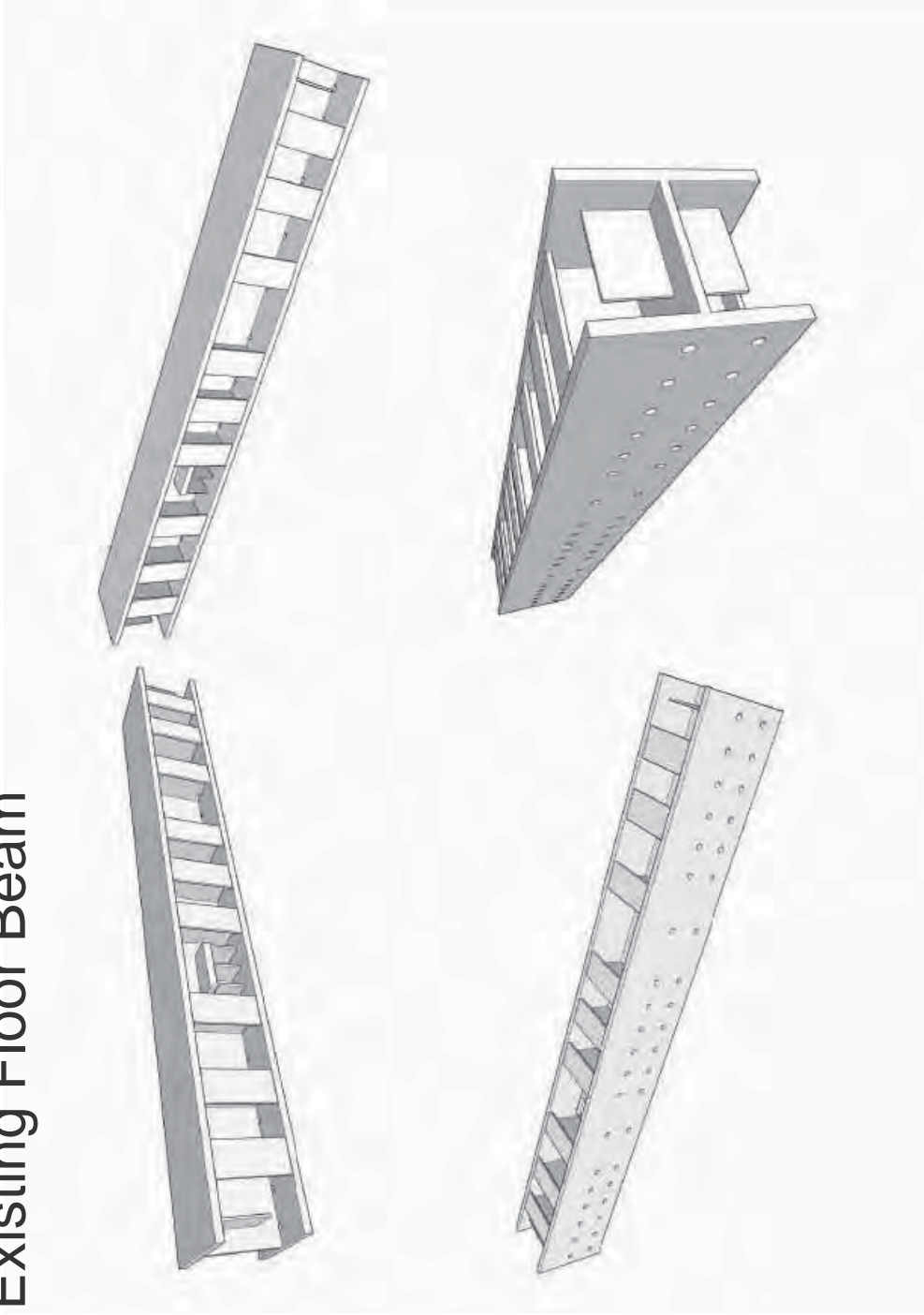
**content**

Test Rig  
3D Overview

**drawn by:** Jun-Wai Lai (Adeem)  
**checked by:** Jun-Wai Lai (Adeem)  
**date:** Aug, 2008

**drawing no.** TR.01

**Existing Floor Beam**





REV.	REVISION	DATE

revisions

project

SCBF  
Phase-01  
1301 South 46th Street  
Richmond, California, 94804

Address

UC Berkeley  
Richmond Field Station  
Building 464, Structural Research Lab

content

Test Rig  
3D Overview

drawn by: Jun-Wai Lai (Jwlai)

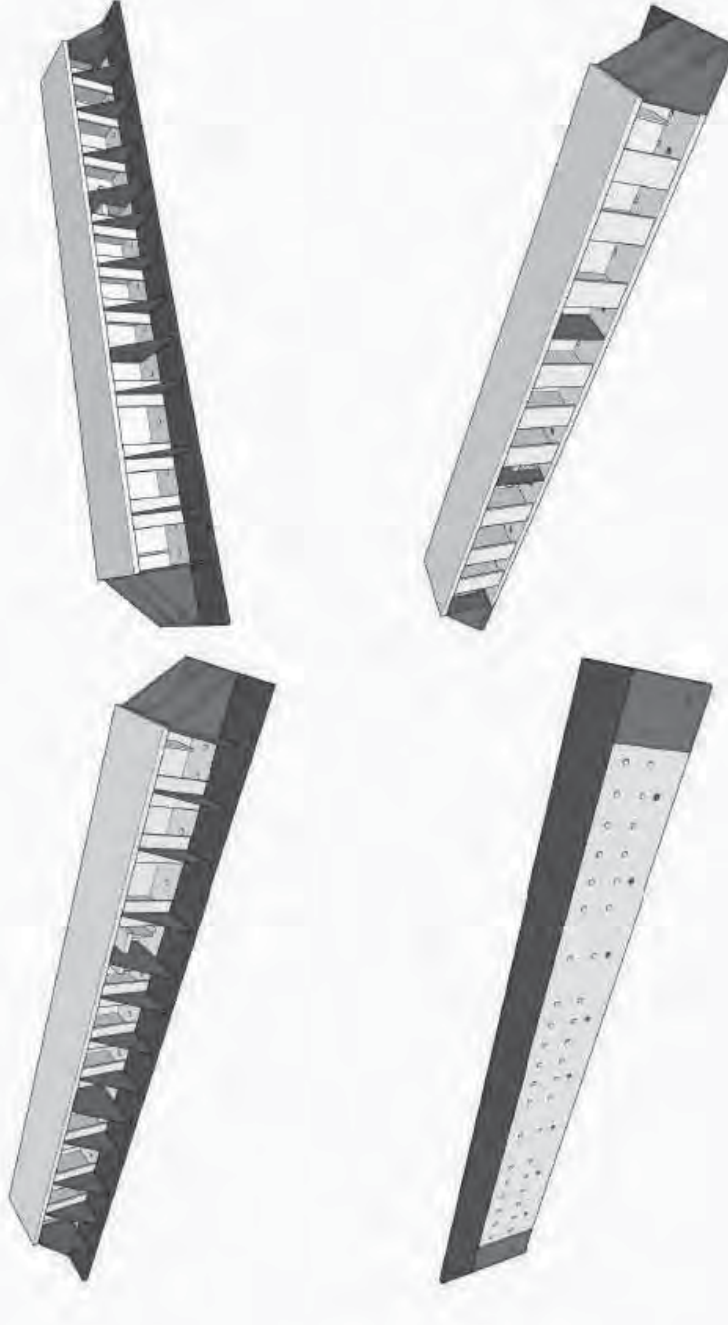
checked by: Jun-Wai Lai (Jwlai)

date: Aug, 2008

drawing no.

TR.01

# Modified Floor Beam







REV	REVISION	DATE

revisions

project

SCBF  
Phase-01  
1301 South 46th Street  
Richmond, California, 94804

Address

UC Berkeley  
Richmond Field Station  
Building 464, Structural Research Lab

content

Test Rig  
3D Overview

drawn by:

Jin-Wai Lai (Adeim)

checked by:

Jin-Wai Lai (Adeim)

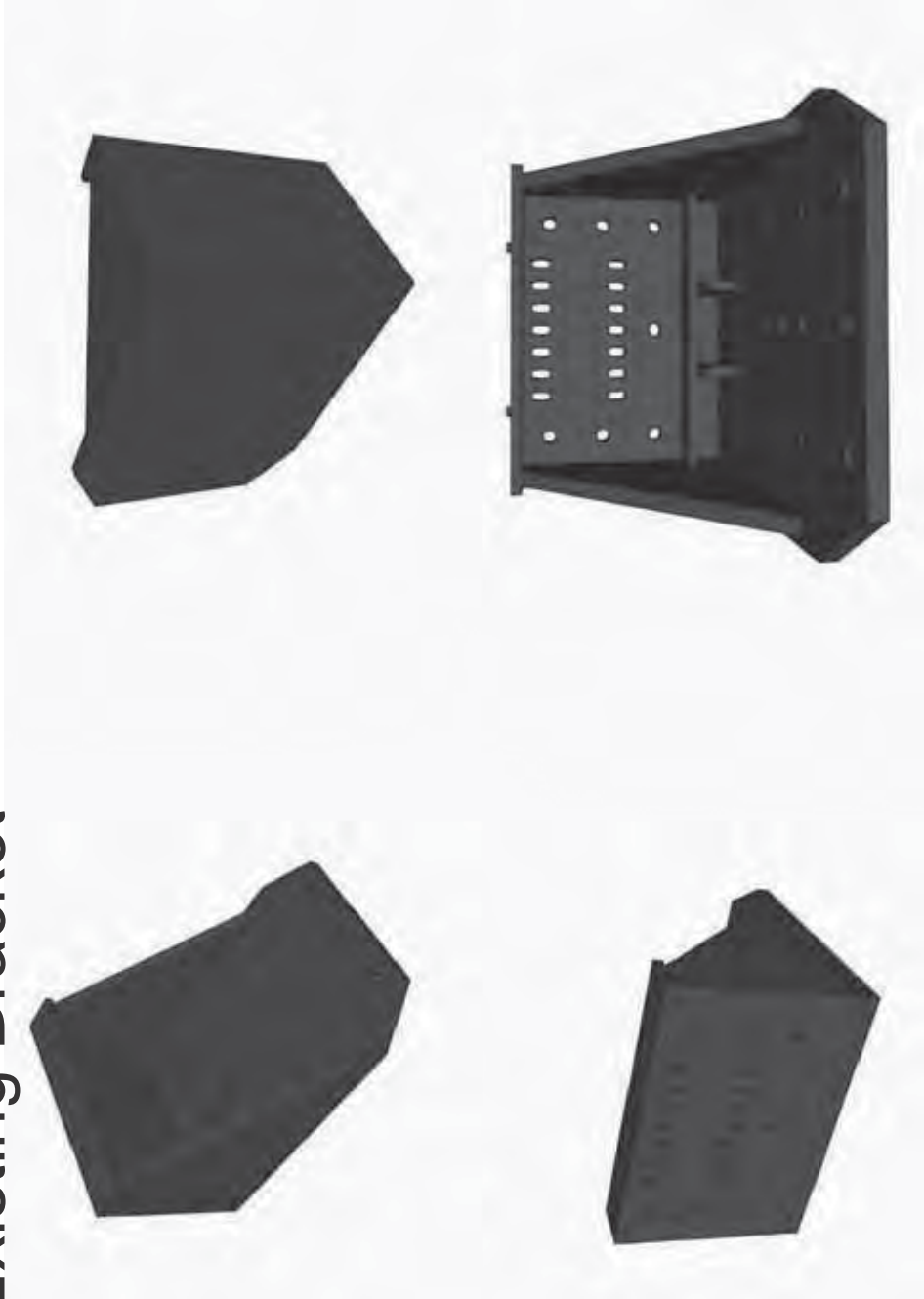
date:

Aug. 2008

drawing no.

TR.01

# Existing Bracket





REV	REVISION	DATE

revisions

project

SCBF  
Phase-01  
1301 South 46th Street  
Richmond, California, 94804

Address

UC Berkeley  
Richmond Field Station  
Building 464, Structural Research Lab

content

Test Rig  
3D Overview

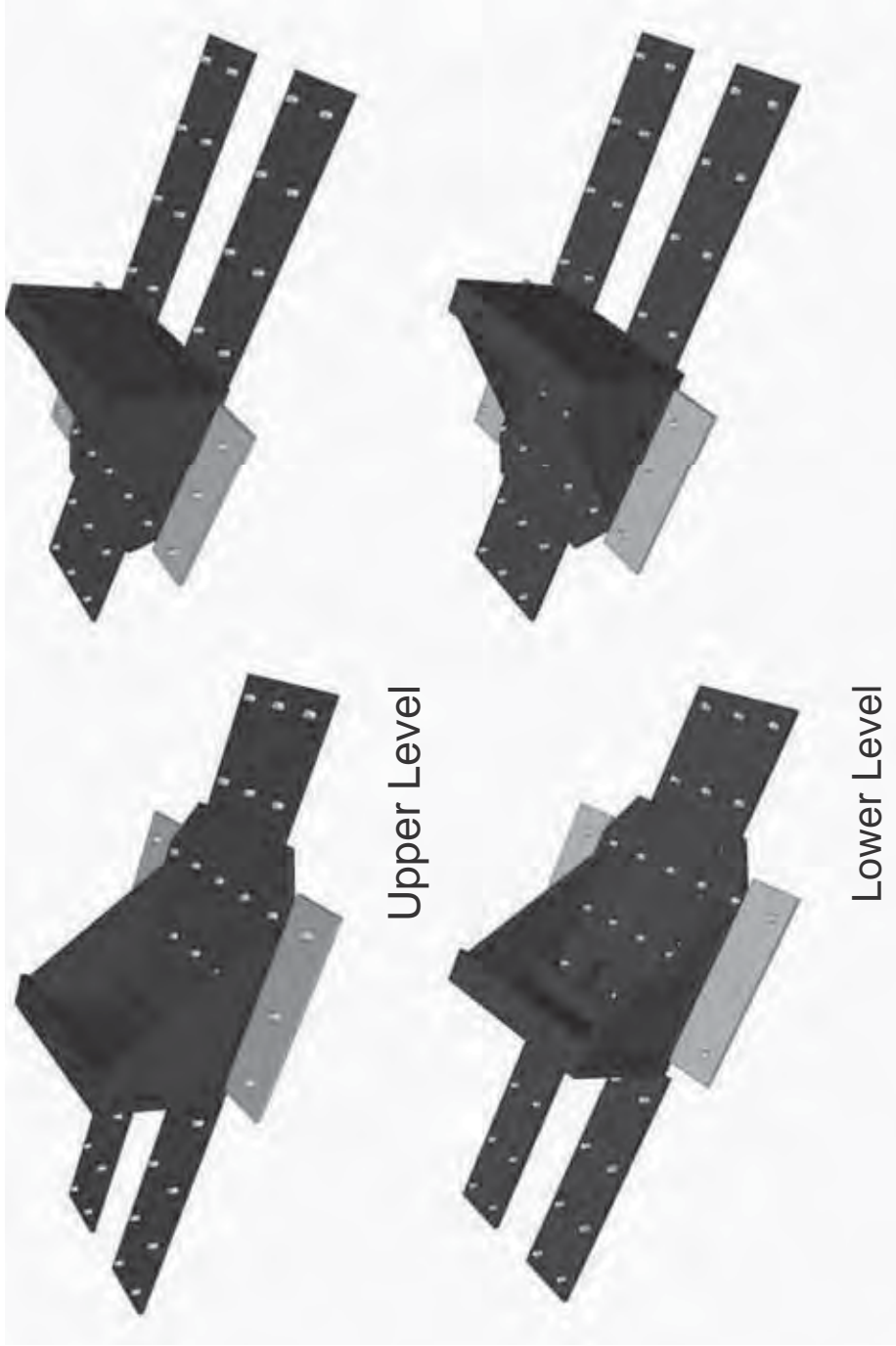
drawn by: Jun-Wai Lai (Adam)

checked by: Jun-Wai Lai (Adam)

date: Aug. 2008

drawing no. TR.01

Modified Bracket



Upper Level

Lower Level



REV.	REVISION	DRAWN

revisions

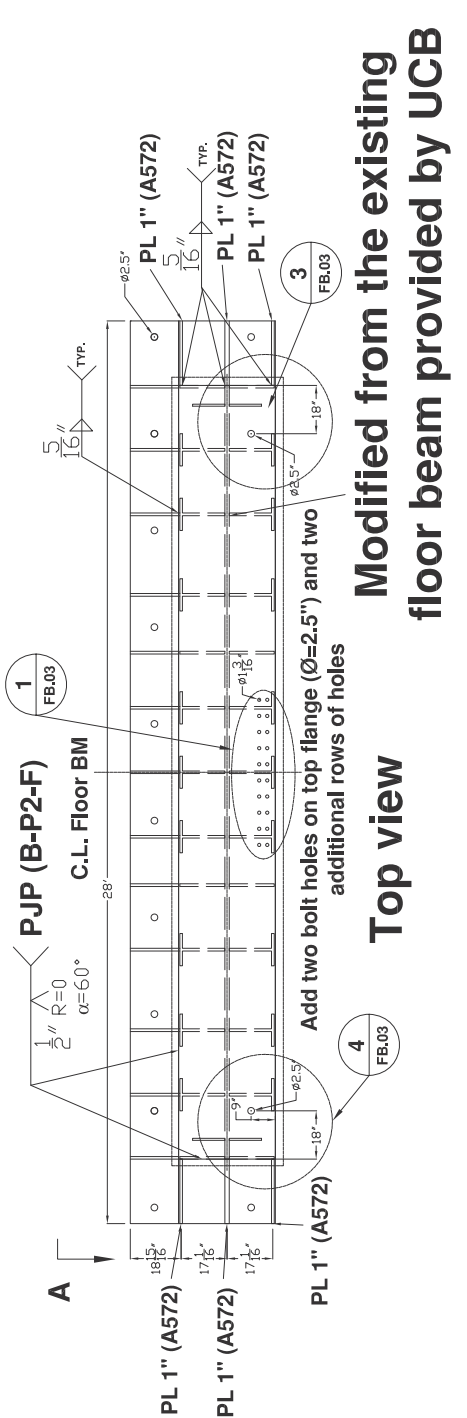
**project**  
SCBF  
Phase-01  
1301 South 46th Street  
Richmond, California, 94804

**Address**  
UC Berkeley  
Richmond Field Station  
Building 464, Structural Research Lab

**content**  
Test Rig  
Floor Beam

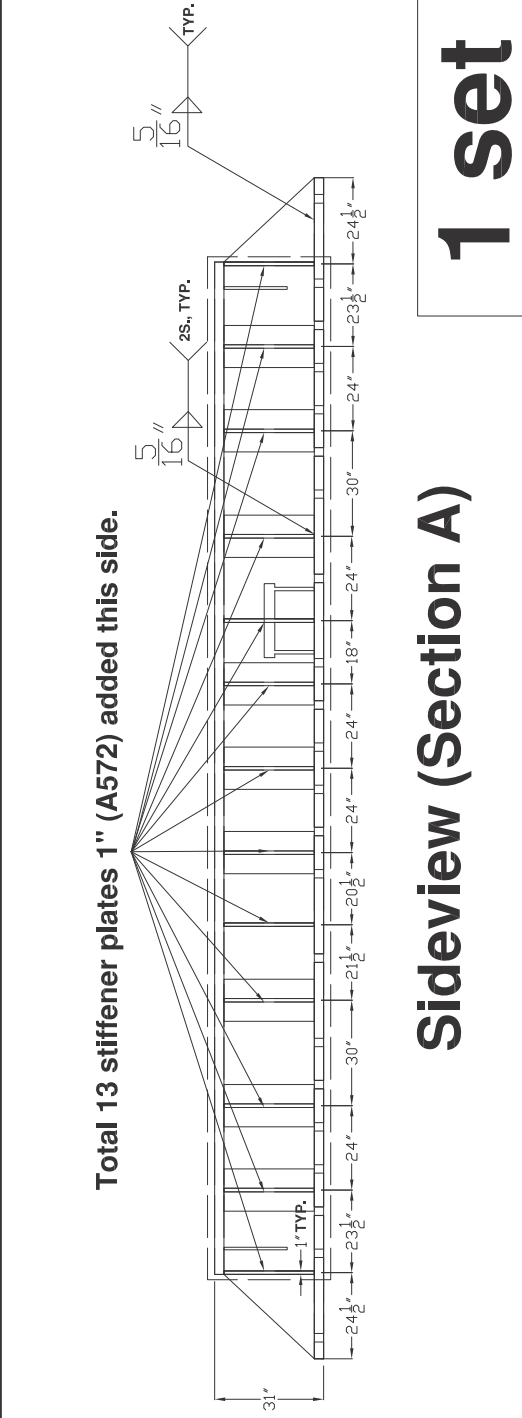
**drawn by:** Jim-Wei Lai (Admin)  
**checked by:** Jim-Wei Lai (Admin)  
**date:** Aug. 2008

**drawing no.**  
FB.01



**Modified from the existing  
floor beam provided by UCB**

**Top view**



**Sideview (Section A)**

**1 set**



REV.	REVISION	DATE

revisions

project

SCBF  
Phase-01  
1301 South 46th Street  
Richmond, California, 94804

Address

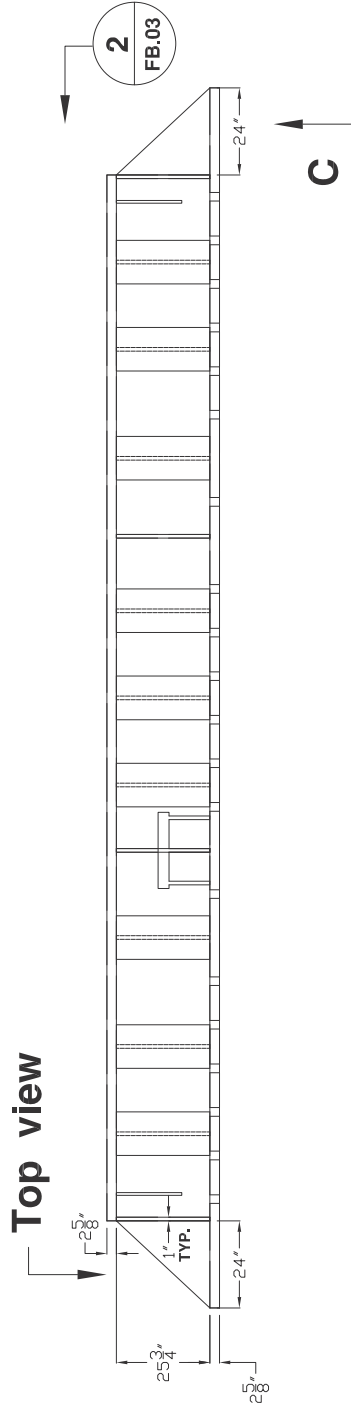
UC Berkeley  
Richmond Field Station  
Building 464, Structural Research Lab

content

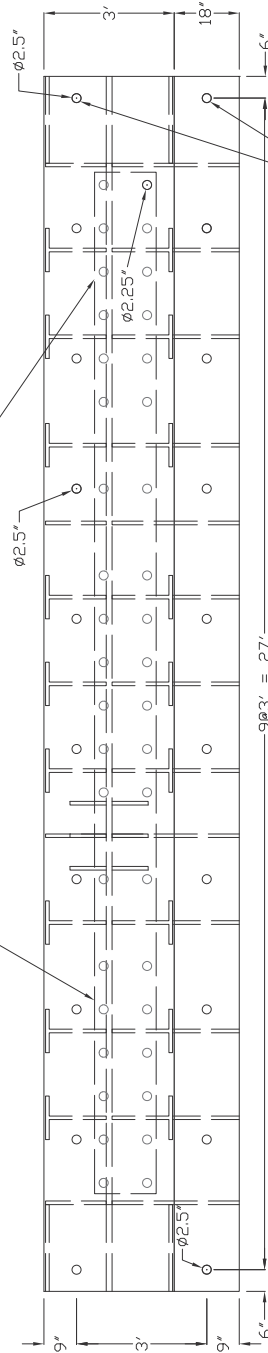
Test Rig  
Floor Beam

drawn by: Jim-Wai Lai (Jwlai)  
checked by: Jim-Wai Lai (Jwlai)  
date: Aug. 2008

drawing no. **FB.02**



**Existing Bolt Holes (Ø=2.25")**



**Bottom view (Section C)**

Add two rows of bolt holes on bottom flange (Ø=2.5")



REV.	REVISION	DATE

revisions

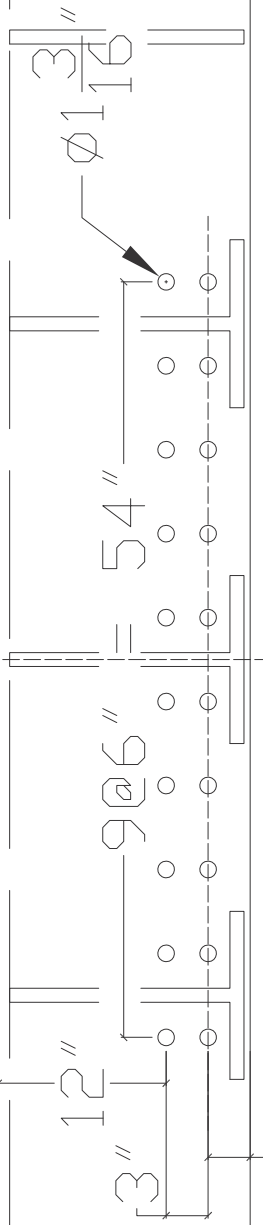
**project**  
SCBF  
Phase-01  
1301 South 48th Street  
Richmond, California, 94804

**Address**  
UC Berkeley  
Richmond Field Station  
Building 464, Structural Research Lab

**content**  
Test Rig  
Floor Beam

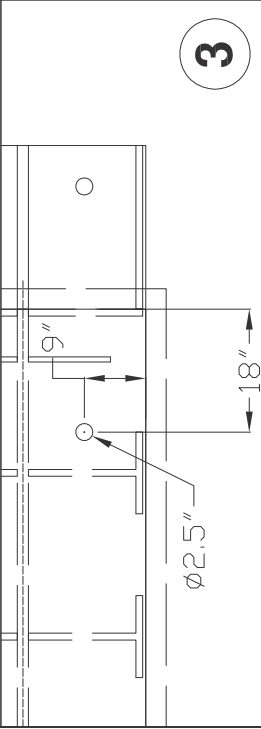
**drawn by:** Jim-Wai Lai (Adeim)  
**checked by:** Jim-Wai Lai (Adeim)  
**date:** Aug. 2008  
**drawing no.** FB.03

**Add two and two additional rows of holes**

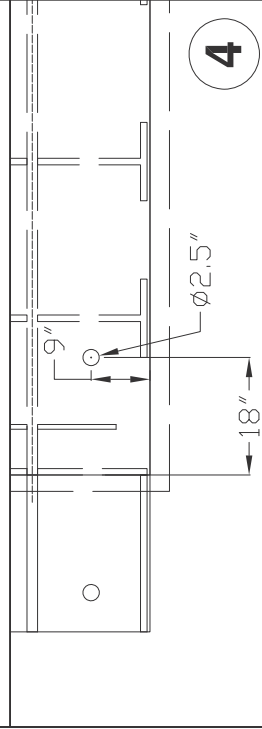


**C.L. Floor BM**

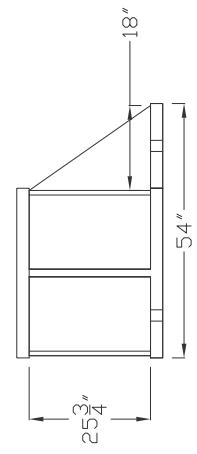
1



3



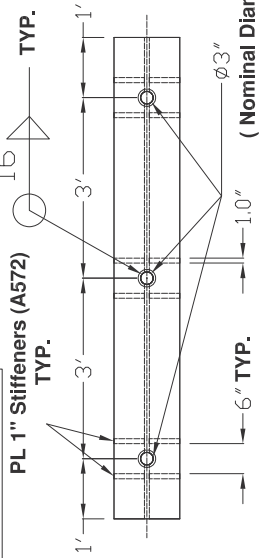
4



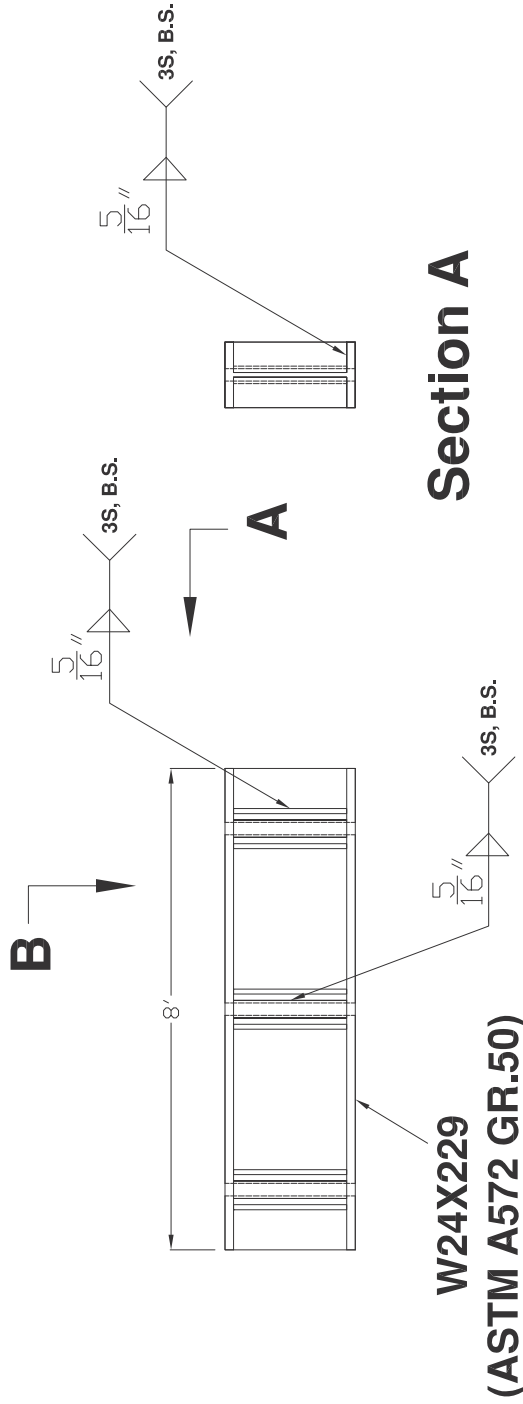
**Section B**

2

# 4 sets



## Section B



## Section A

University of California  
at Berkeley



International Hybrid  
Simulation of  
Tomorrow's Braced  
Steel Frame Structures

REV.	REVISION	DATE

### revisions

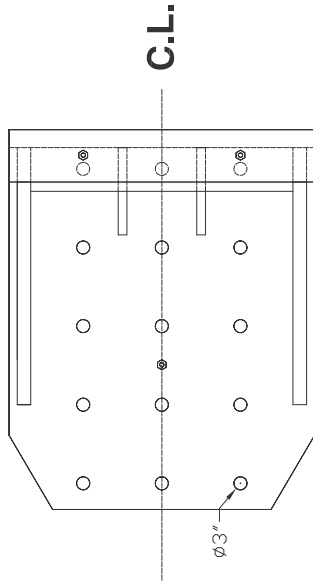
**project**  
SCRF  
Phase-01  
1301 South 48th Street  
Richmond, California, 94804

**Address**  
UC Berkeley  
Richmond Field Station  
Building 484, Structural Research Lab

**content**  
Test Rig  
Under Floor Beams

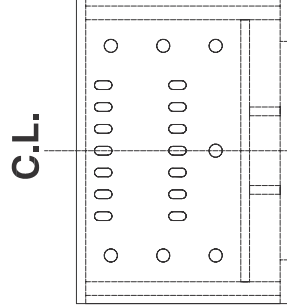
**drawn by:** Jim-Wai Lai (Aster)  
**checked by:** Jim-Wai Lai (Aster)  
**date:** Aug. 2008  
**drawing no.** UB.01

**2 sets**



**Top view**

# Existing Brackets in UCB Lab



**Side view**

University of California  
at Berkeley



**International Hybrid  
Simulation of  
Tomorrow's Braced  
Steel Frame Structures**

REV.	REVISION	DATE

**revisions**

**project**  
SCBF  
Phase-01  
1301 South 46th Street  
Richmond, California, 94804

**Address**  
UC Berkeley  
Richmond Field Station  
Building 464, Structural Research Lab

**content**  
Test Rig  
Existing Brackets (Provided by UCB)

**drawn by:** Jim-Wai Lai (Adeim)  
**checked by:** Jim-Wai Lai (Adeim)  
**date:** Aug. 2008

**drawing no.** BK.01



REV.	REVISION	DATE

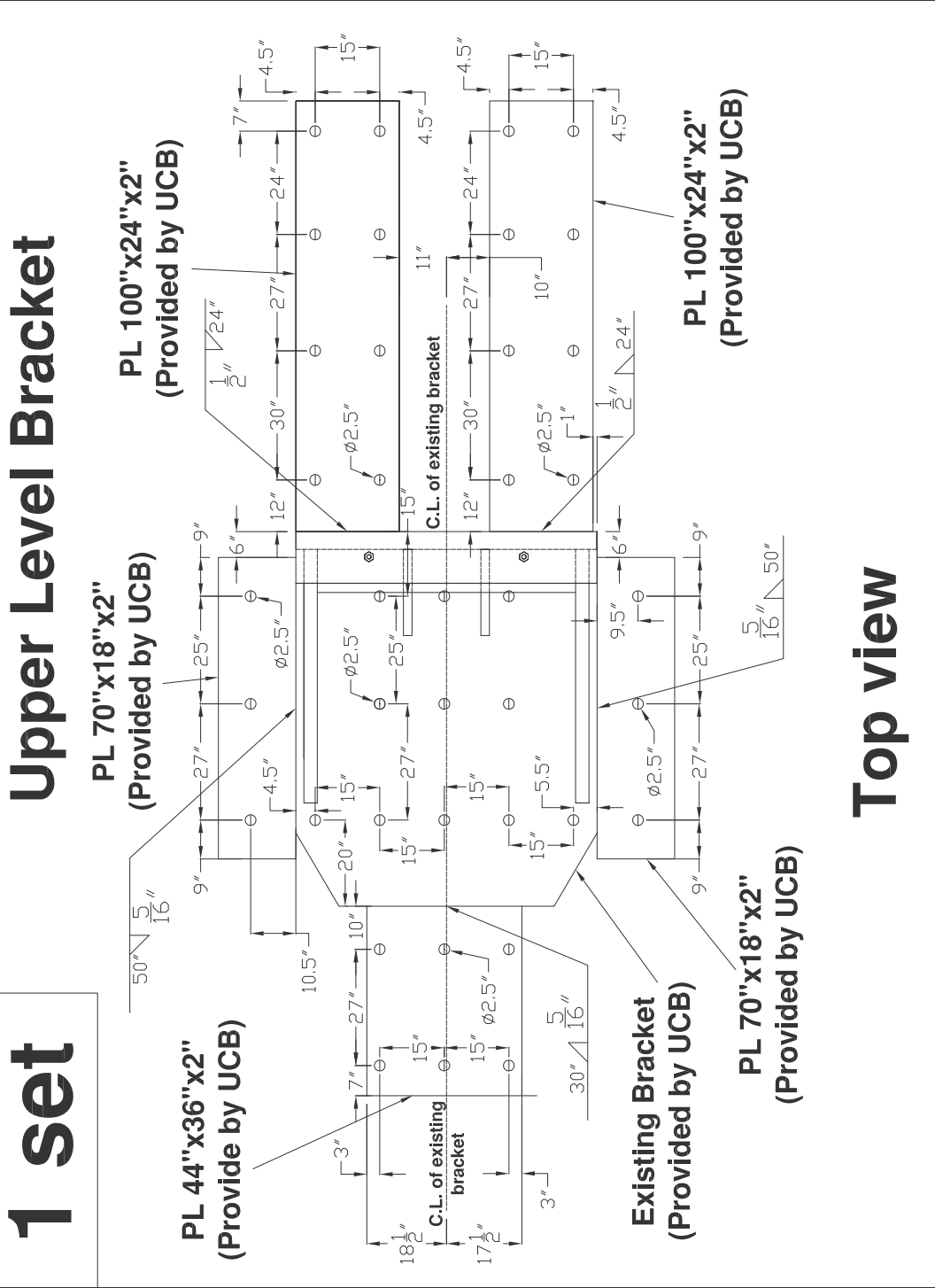
revisions

**project**  
SCBF  
Phase-01  
1301 South 48th Street  
Richmond, California, 94804

**Address**  
UC Berkeley  
Richmond Field Station  
Building 464, Structural Research Lab

**content**  
Test Rig  
Upper Level Bracket

**drawn by:** Jim-Wai Lai (Jwlai)  
**checked by:** Jim-Wai Lai (Jwlai)  
**date:** Aug. 2008  
**drawing no.** BK.02







REV.	REVISION	DATE

**revisions**

**project**

SCBF  
Phase-01  
1301 South 48th Street  
Richmond, California, 94804

**Address**

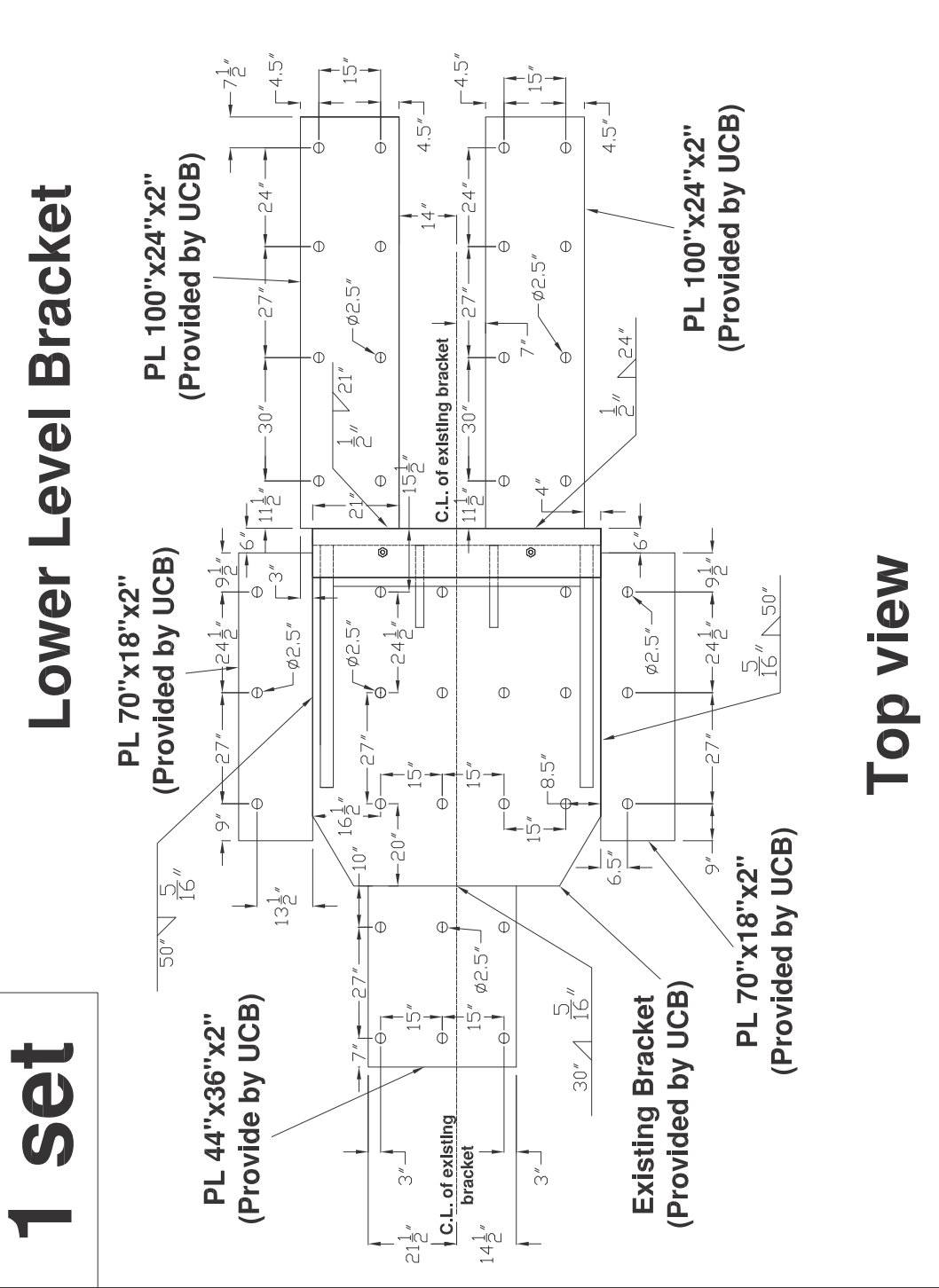
UC Berkeley  
Richmond Field Station  
Building 464, Structural Research Lab

**content**

Test Rig  
Lower Level Bracket

**drawn by:** Jim-Wai Lai (Jwlai)  
**checked by:** Jim-Wai Lai (Jwlai)  
**date:** Aug. 2008

**drawing no.** BK.03





REV.	REVISION	DATE

revisions

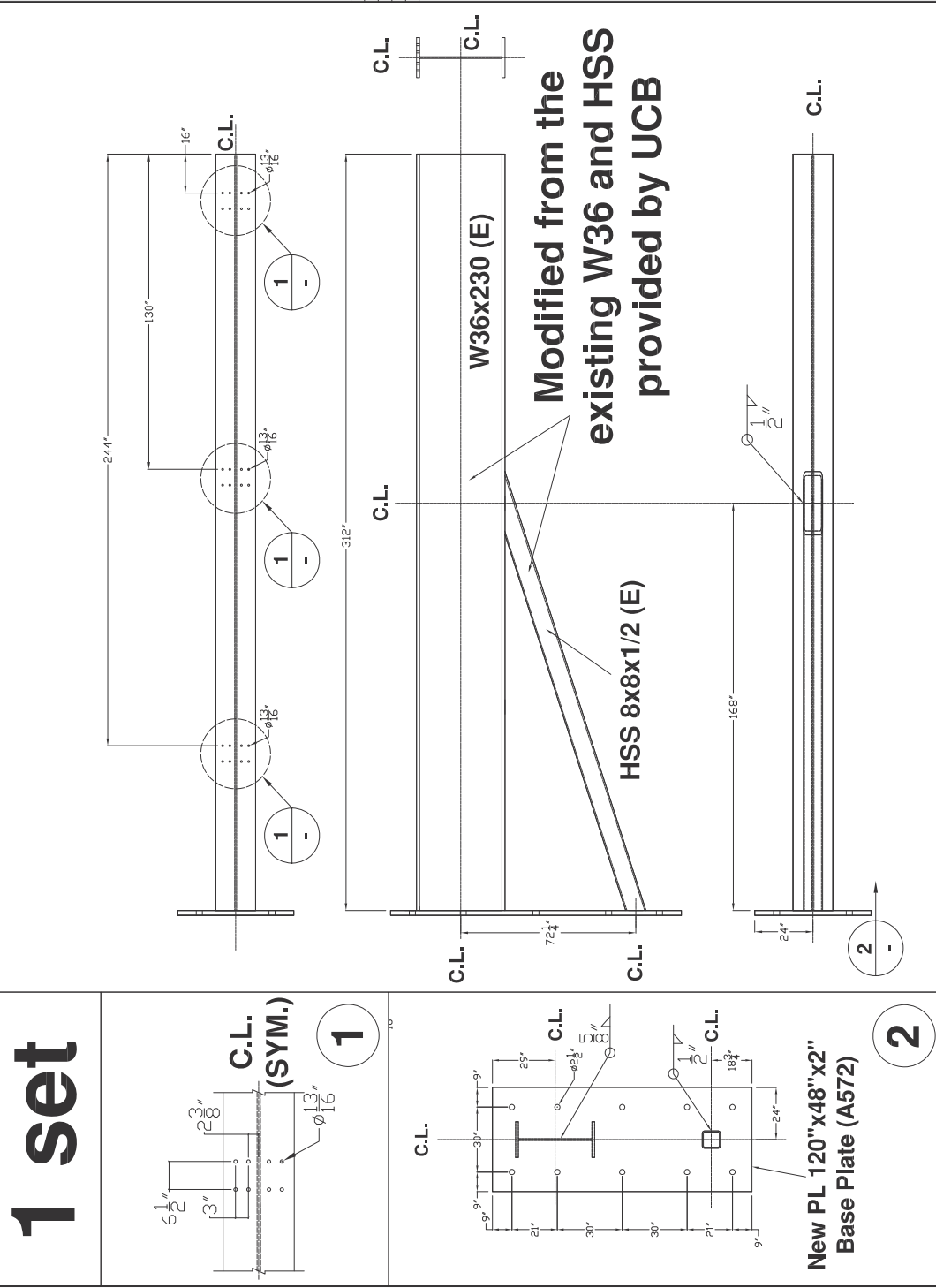
**project**  
SCBF  
Phase-01  
1301 South 48th Street  
Richmond, California, 94804

**Address**  
UC Berkeley  
Richmond Field Station  
Building 464, Structural Research Lab

**content**  
Test Rig  
Cantilever Beam

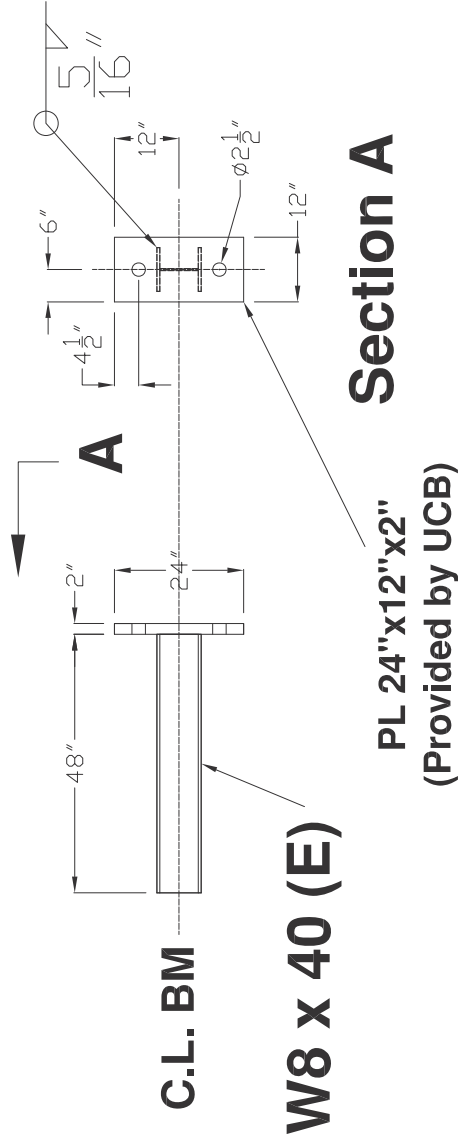
**drawn by:** Jim-Wai Lai (Adeim)  
**checked by:** Jim-Wai Lai (Adeim)  
**date:** Aug. 2008

**drawing no.** CB.01



**2 sets**

**Modified from the existing sections and  
2" plates provide by UCB**



University of California  
at Berkeley



International Hybrid  
Simulation of  
Tomorrow's Braced  
Steel Frame Structures

REV.	REVISION	DATE

**revisions**

**project**  
SCBF  
Phase-01  
1301 South 48th Street  
Richmond, California, 94804

**Address**  
UC Berkeley  
Richmond Field Station  
Building 464, Structural Research Lab

**content**  
Test Rig  
Cantilever Beams

**drawn by:** Jim-Wai Lai (Adeim)  
**checked by:** Jim-Wai Lai (Adeim)  
**date:** Aug. 2008

**drawing no.** CB.02



REV.	REVISION	DATE

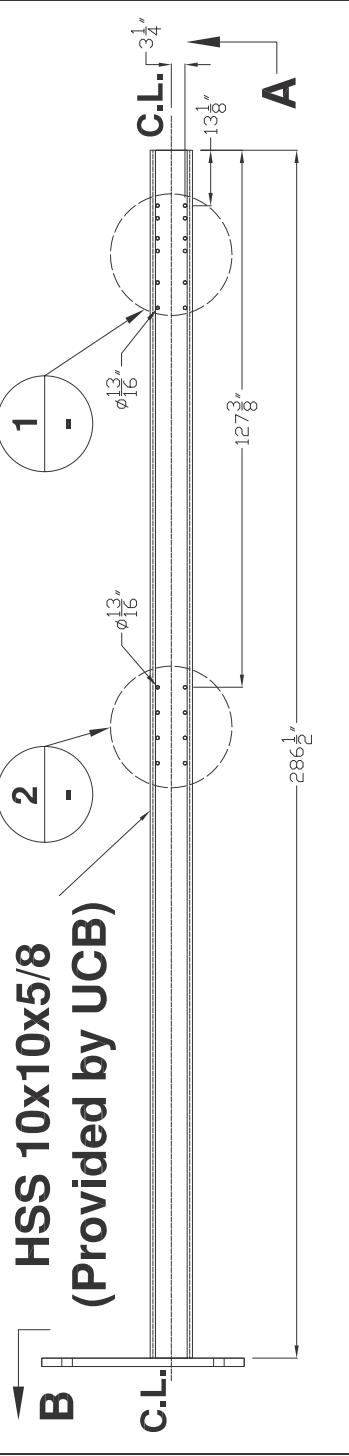
revisions

project  
SCBF  
Phase-01  
1301 South 46th Street  
Richmond, California, 94804

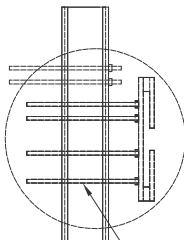
Address  
UC Berkeley  
Richmond Field Station  
Building 464, Structural Research Lab

content  
Test Rig  
HSS Columns

drawn by: Jim-Wai Lai (Jwlai)  
checked by: Jim-Wai Lai (Jwlai)  
date: Aug. 2008  
drawing no. HSS.01

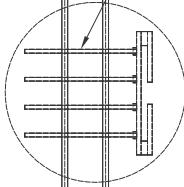


**CP.01**



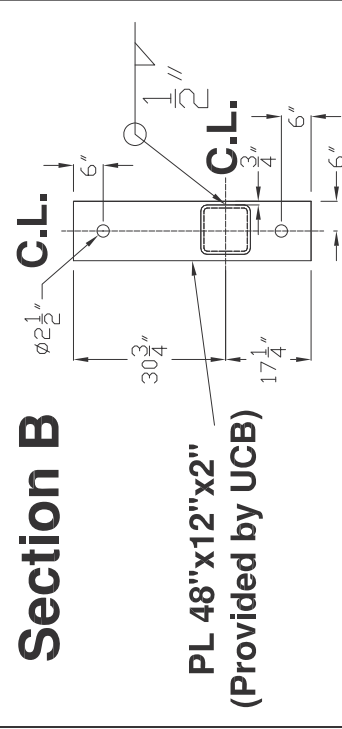
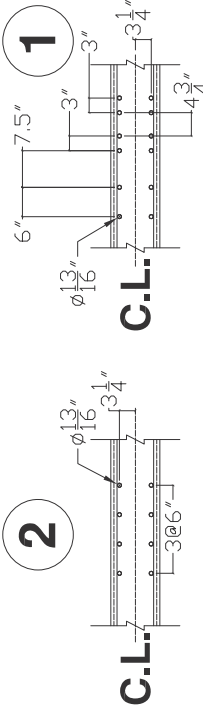
**ASTM A490  
all-threaded bolt rods  
with  $\phi = 3/4$ " ( L = 24" )**

**CP.02**



**PL 48"x12"x2"  
(Provided by UCB)**

**Section A**



**1 set**



REV.	REVISION	DATE

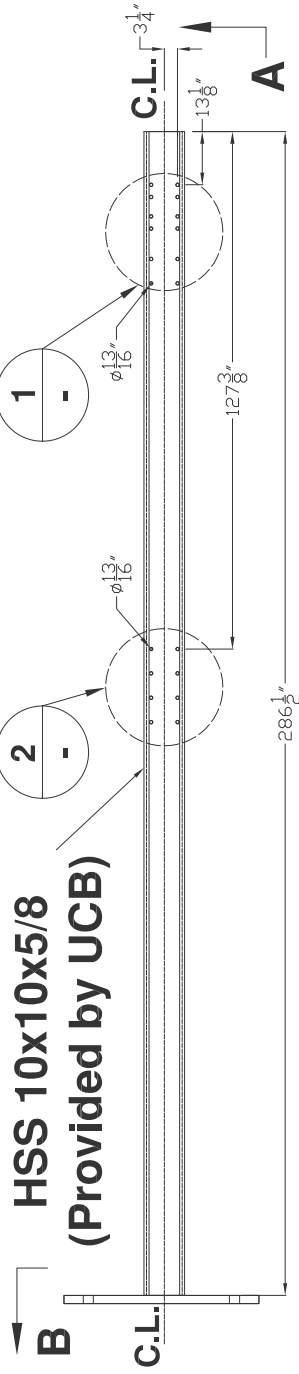
revisions

project  
SCBF  
Phase-01  
1301 South 48th Street  
Richmond, California, 94804

Address  
UC Berkeley  
Richmond Field Station  
Building 464, Structural Research Lab

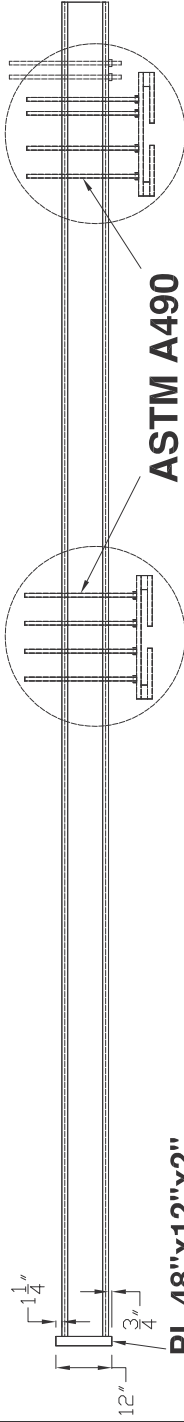
content  
Test Rig  
HSS Columns

drawn by: Jim-Wai Lai (Astm)  
checked by: Jim-Wai Lai (Astm)  
date: Aug. 2008  
drawing no. HSS.02

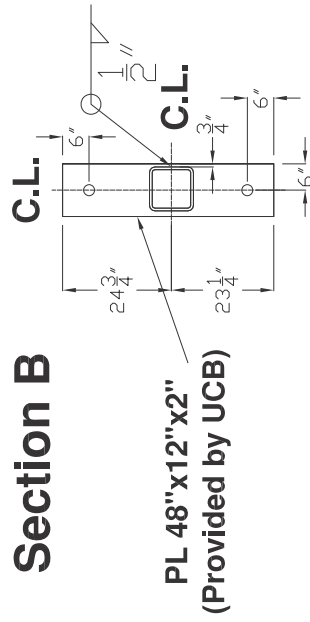
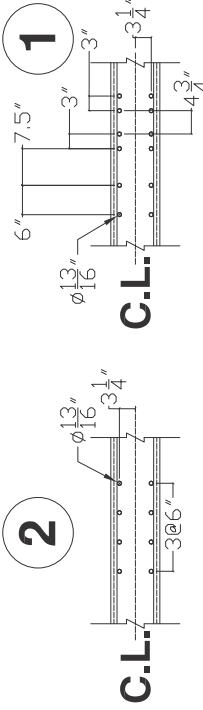


**CP.01**

**CP.02**



**Section A**



**1 set**



REV.	REVISION	DATE

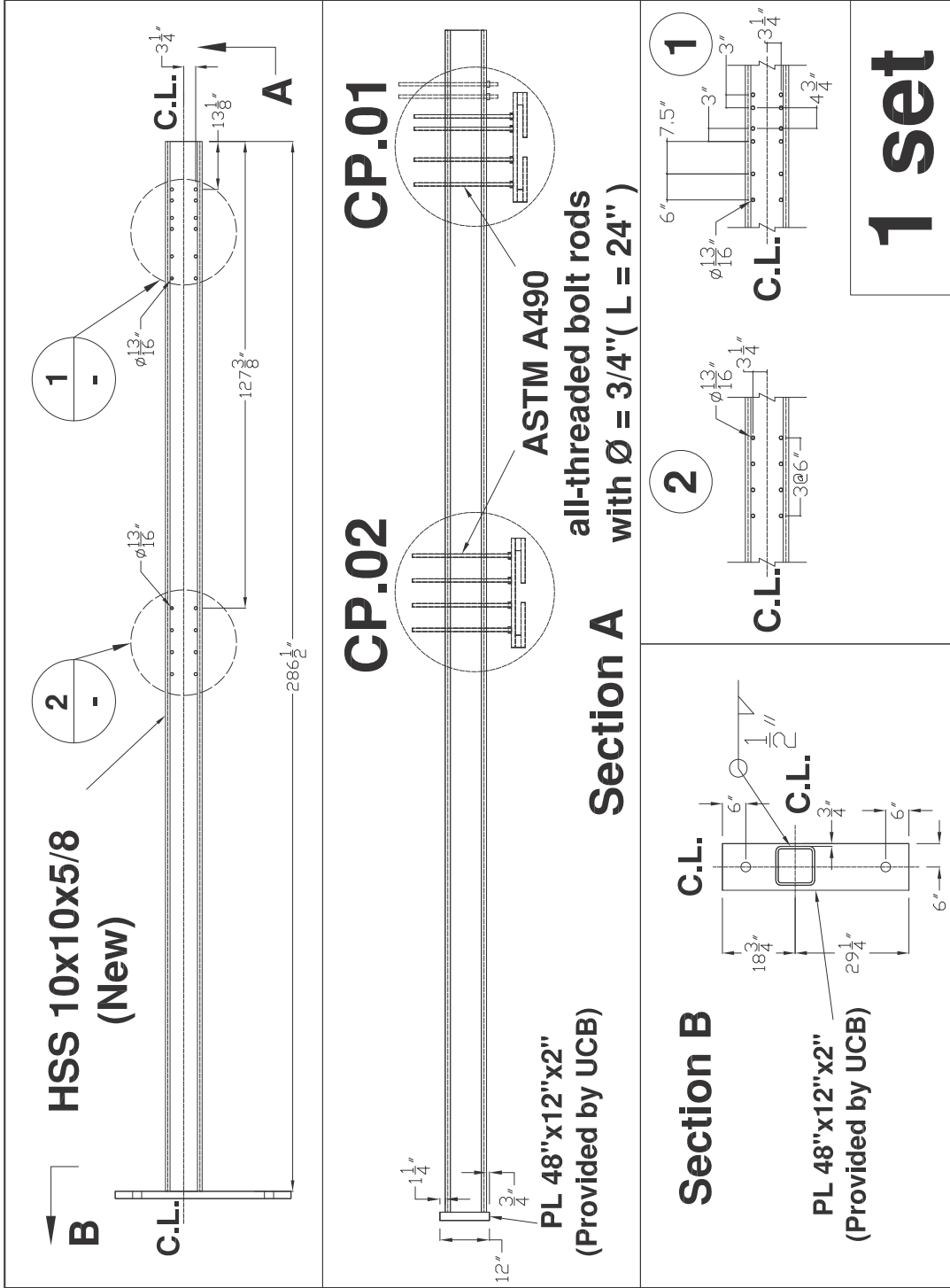
revisions

project  
SCBF  
Phase-01  
1301 South 48th Street  
Richmond, California, 94804

Address  
UC Berkeley  
Richmond Field Station  
Building 464, Structural Research Lab

content  
Test Rig  
HSS Columns

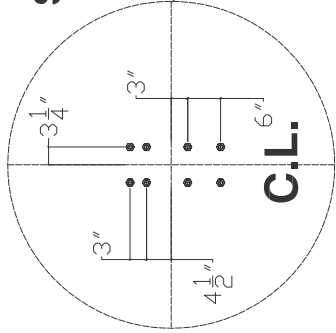
drawn by: Jim-Wai Lai (Aster)  
checked by: Jim-Wai Lai (Aster)  
date: Aug. 2008  
drawing no. HSS.03



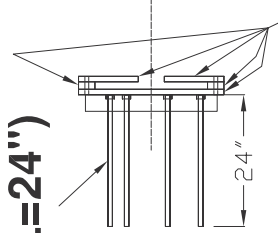
# 3 sets

Note: Each all-threaded bolt rod need three bolt nuts and two washers. (one of bolt nuts welded to PL 36"x26.5"x1")

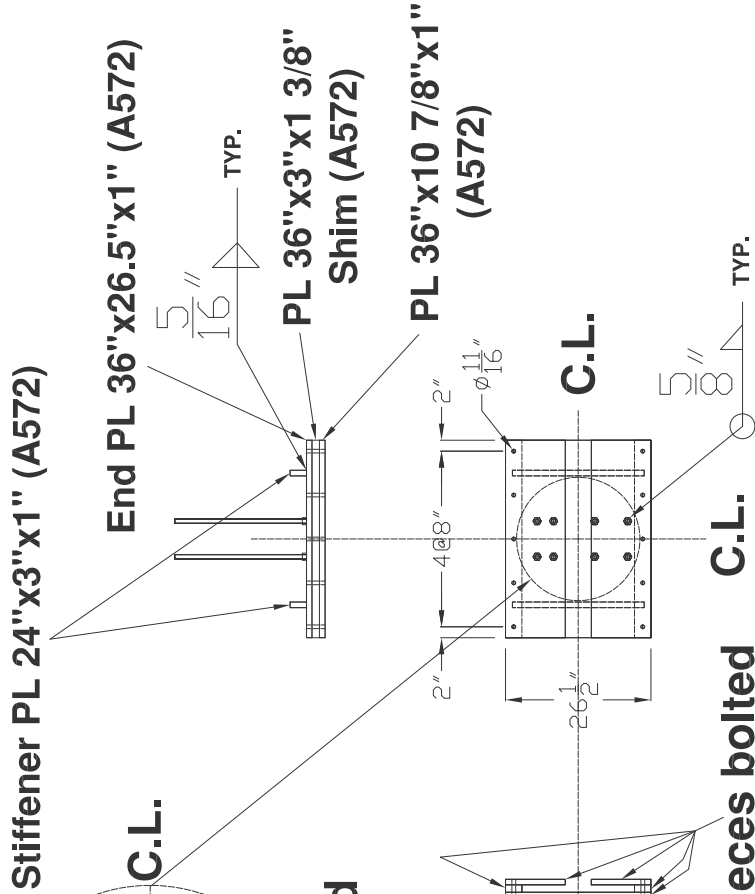
## Bolt Group Details



A490 all-threaded bolt rods with  $\text{Ø}=3/4"$  (L=24")



5 pieces bolted together



REV.	REVISION	DATE

revisions

project SCBF Phase-01 1301 South 48th Street Richmond, California, 94804

Address

UC Berkeley Richmond Field Station Building 464, Structural Research Lab

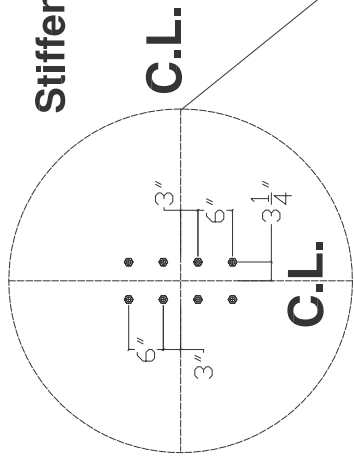
content

Test Rig Clamp Plates (Upper Level)

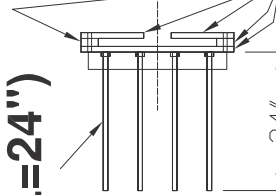
drawn by: Jim-Wai Lai (Aster) checked by: Jim-Wai Lai (Aster) date: Aug. 2008 drawing no. CP.01

# 3 sets

## Bolt Group Details



**A490 all-threaded  
bolt rods with  
Ø=3/4" (L=24")**



**5 pieces bolted  
together**

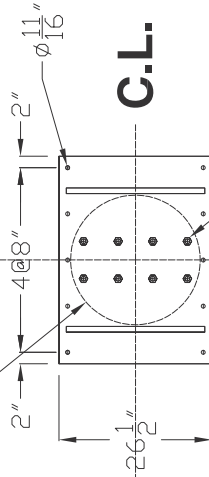
**Note: Each all-threaded bolt rod need three bolt nuts and two washers. (one of bolt nuts welded to PL 36"x26.5"x1")**

**Stiffener PL 24"x3"x1" (A572)**

**End PL 36"x26.5"x1" (A572)**

**PL 36"x3"x1 3/8"  
Shim (A572)**

**PL 36"x10 7/8"x1"  
(A572)**



REV.	REVISION	DATE

**revisions**

**project**  
SCBF  
Phase-01  
1301 South 48th Street  
Richmond, California, 94804

**Address**  
UC Berkeley  
Richmond Field Station  
Building 464, Structural Research Lab

**content**  
Test Rig  
Clamp Plates (Lower Level)

**drawn by:** Jim-Wai Lai (Jwlai)  
**checked by:** Jim-Wai Lai (Jwlai)  
**date:** Aug. 2008

**drawing no.** CP.02





REV.	REVISION	DATE

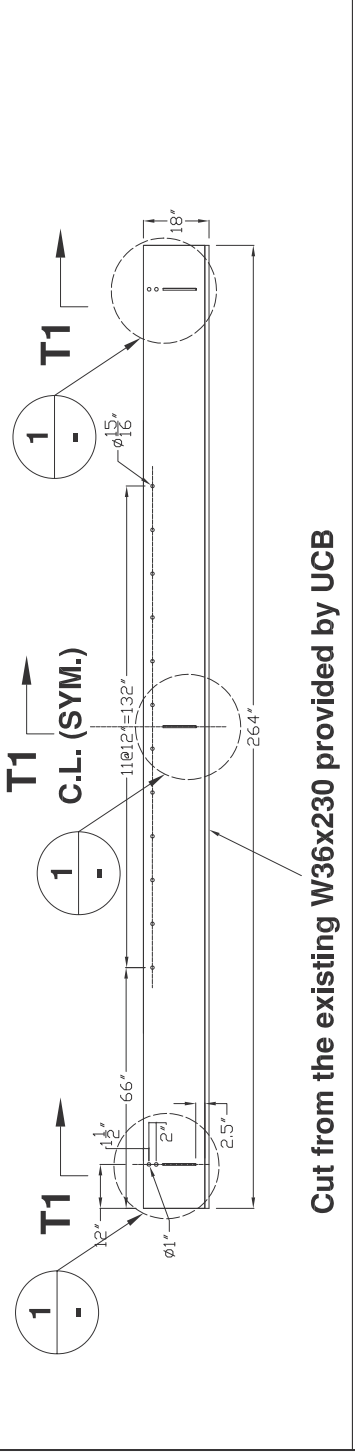
revisions

**project**  
SCBF  
Phase-01  
1301 South 48th Street  
Richmond, California, 94804

**Address**  
UC Berkeley  
Richmond Field Station  
Building 484, Structural Research Lab

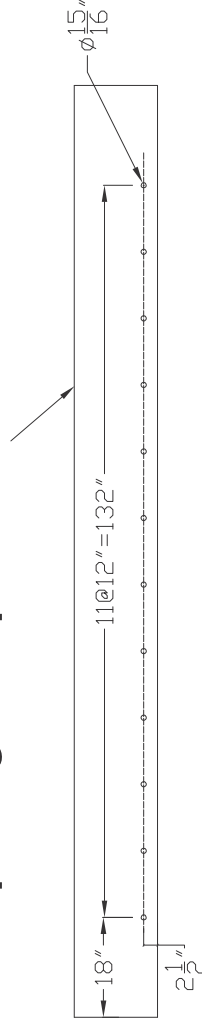
**content**  
Test Rig  
Lateral Tee Sections

**drawn by:** Jim-Wai Lai (Aster)  
**checked by:** Jim-Wai Lai (Aster)  
**date:** Aug. 2008  
**drawing no.** TEE.01

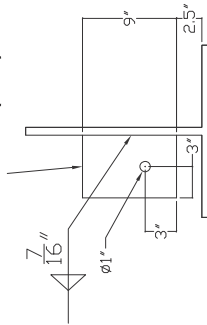


Cut from the existing W36x230 provided by UCB

**PL 168"x15"x3/4" (A36), field fillet weld (1/8")  
to top flange of specimen beam sections**



**PL 9"x6"x1/2" (A36)**



**Section T1**

**1**

**2 sets**



REV.	REVISION	DATE

revisions

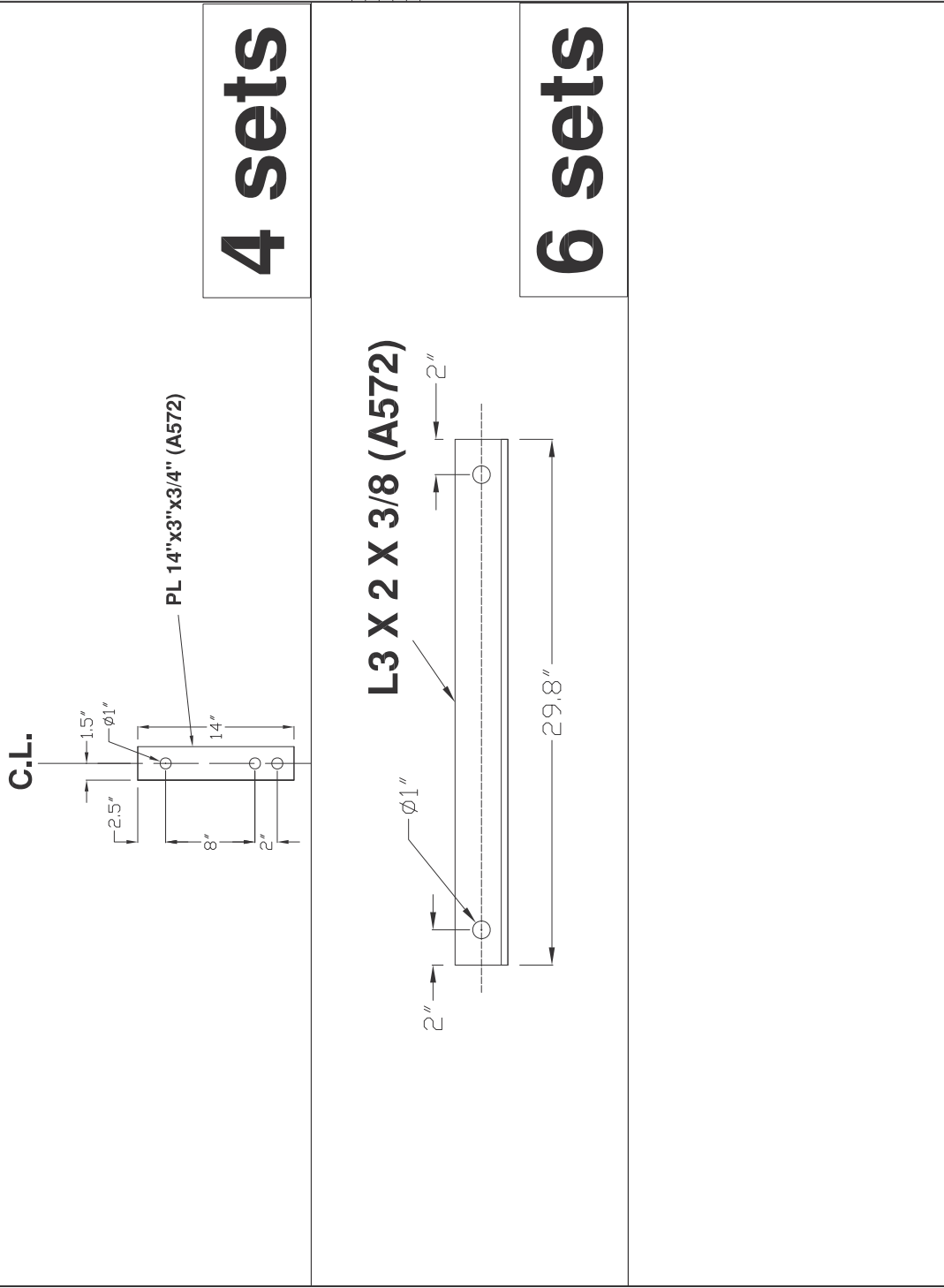
**project**  
SCBF  
Phase-01  
1301 South 48th Street  
Richmond, California, 94804

**Address**  
UC Berkeley  
Richmond Field Station  
Building 484, Structural Research Lab

**content**  
Test Rig  
Lateral Tee Sections

**drawn by:** Jim=Wei Lai (Aster)  
**checked by:** Jim=Wei Lai (Aster)  
**date:** Aug, 2008

**drawing no.**  
TEE.02



**4 sets**

**6 sets**

---

## **Appendix C**

### **Specimen Shop Drawings (TCBF-B-1 to TCBF-B-4)**

---

**TCBF-B-1 Shop Drawings  
(UC Berkeley)**



**International Hybrid  
Simulation of  
Tomorrow's Braced  
Steel Frame Structures**

REV.	REVISION	DATE

**revisions**

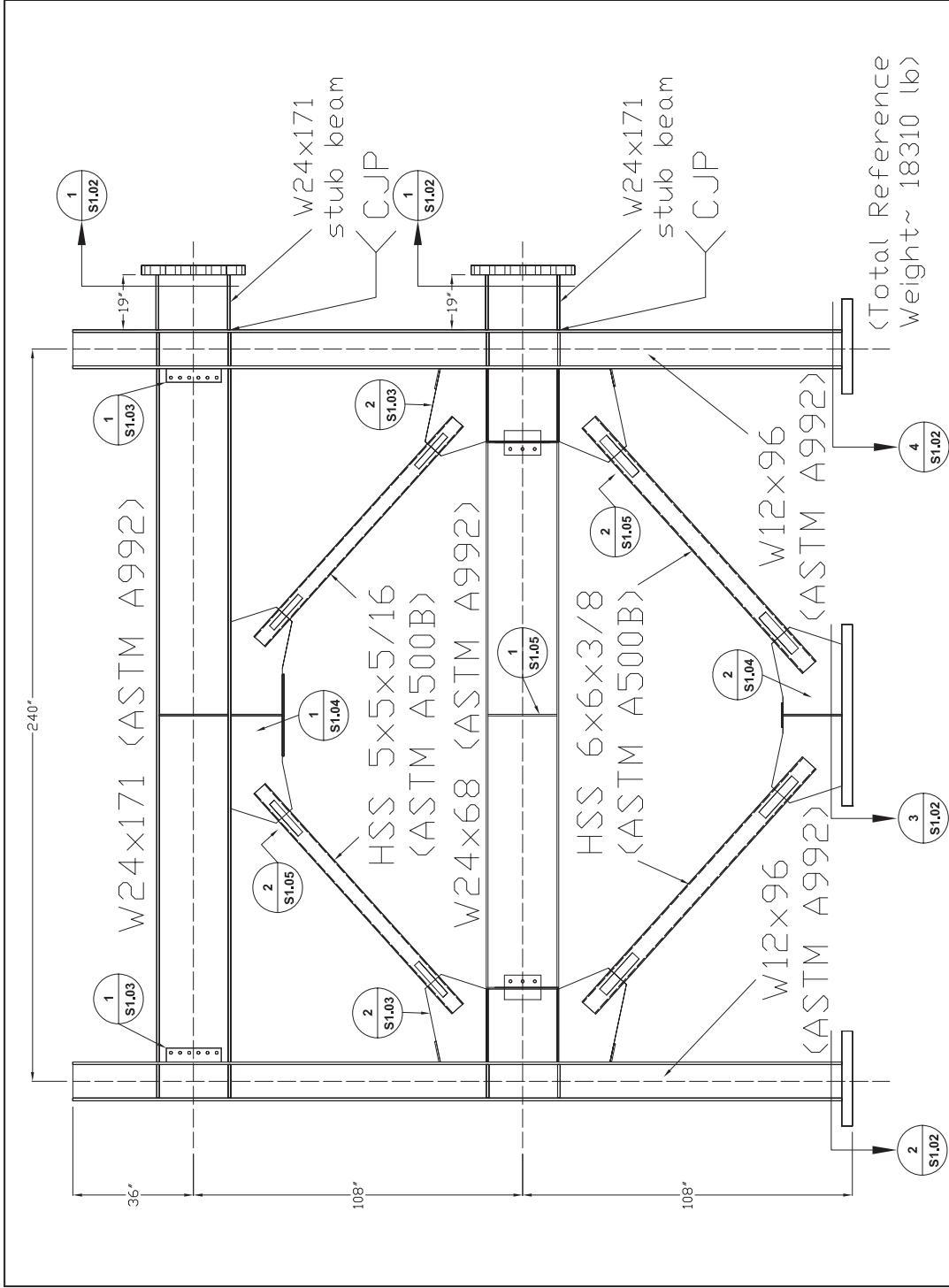
**project**  
SCBF  
Phase-01  
1301 South 48th Street  
Richmond, California, 94804

**Address**  
UC Berkeley  
Richmond Field Station  
Building 464, Structural Research Lab

**content**  
Specimen Detail  
Framing Elevations

**drawn by:** Jim-Wai Lai (Aster)  
**checked by:** Jim-Wai Lai (Aster)  
**date:** Aug. 2008

**drawing no.** S1.01



Filename: SCBF\_20080823\_Specimen-Only.dwg Plotted: 8/25/2008 9:34:59 AM Plot Device: Adobe PDF Page Setup: -- Plotted by: jwli



REV.	REVISION	DATE

revisions

project

SCBF  
Phase-01  
1301 South 48th Street  
Richmond, California, 94804

Address

UC Berkeley  
Richmond Field Station  
Building 464, Structural Research Lab

content

Specimen Detail  
Base Plates & End Plates

drawn by: Jin-Wai Lai (Admin)

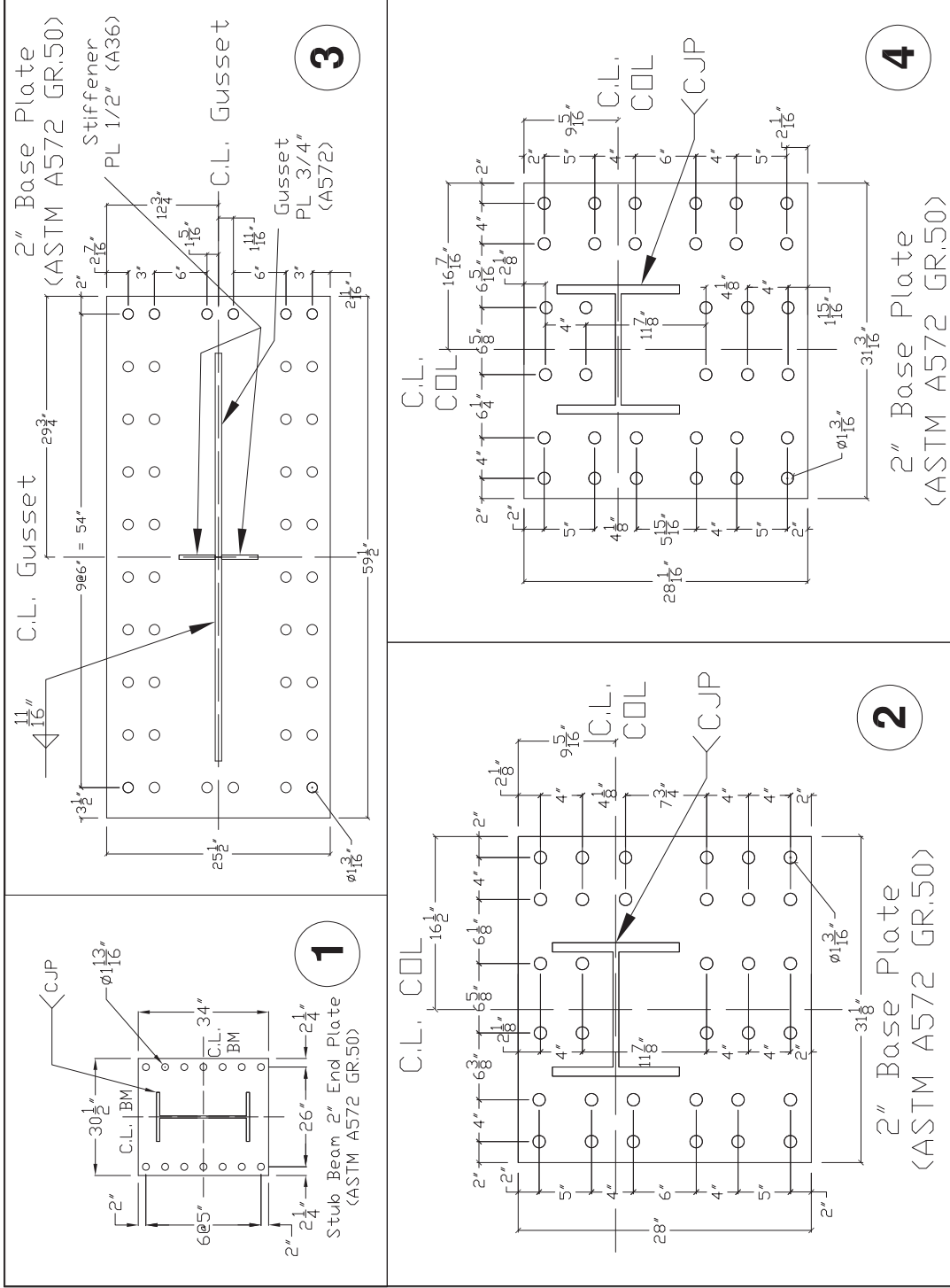
Jin-Wai Lai (Admin)

Aug. 2008

checked by: Jin-Wai Lai (Admin)

date: Aug. 2008

drawing no. **S1.02**





**International Hybrid  
Simulation of  
Tomorrow's Braced  
Steel Frame Structures**

REV.	REVISION	DATE

**revisions**

**project**

SCBF  
Phase-01  
1301 South 48th Street  
Richmond, California, 94804

**Address**

UC Berkeley  
Richmond Field Station  
Building 464, Structural Research Lab

**content**

Specimen Detail  
Connections

**drawn by:**

Jin-Wen Lai (Aster)

**checked by:**

Jin-Wen Lai (Aster)

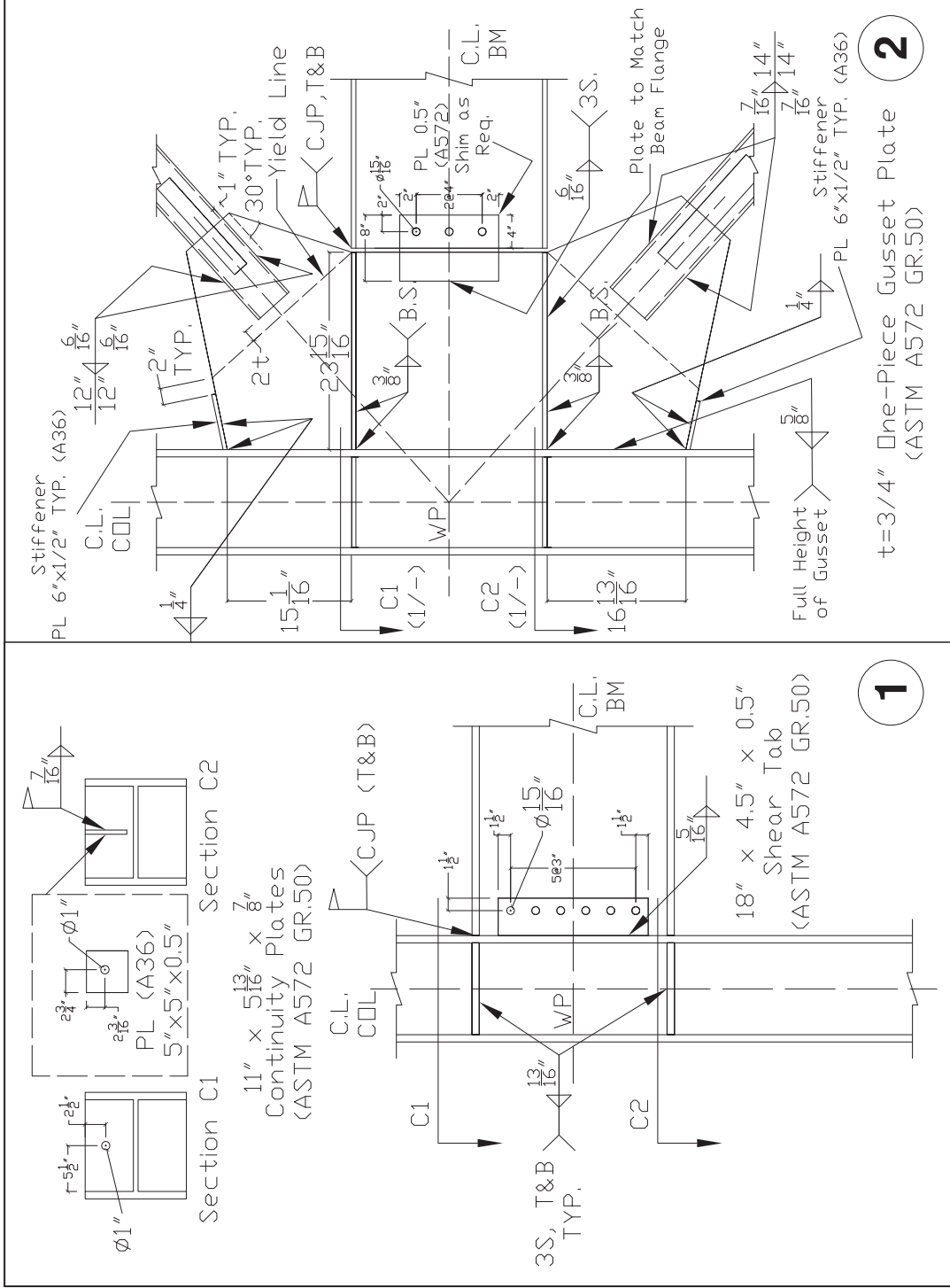
Aug. 2008

**date:**

Aug. 2008

**drawing no.**

**S1.03**





**International Hybrid  
Simulation of  
Tomorrow's Braced  
Steel Frame Structures**

REV.	REVISION	DATE

revisions

**project**

SCBF  
Phase-01  
1301 South 48th Street  
Richmond, California, 94804

**Address**

UC Berkeley  
Richmond Field Station  
Building 464, Structural Research Lab

**content**

Specimen Detail  
Gusset Plates

**drawn by:**

Jin-Jin Lai (Aster)

**checked by:**

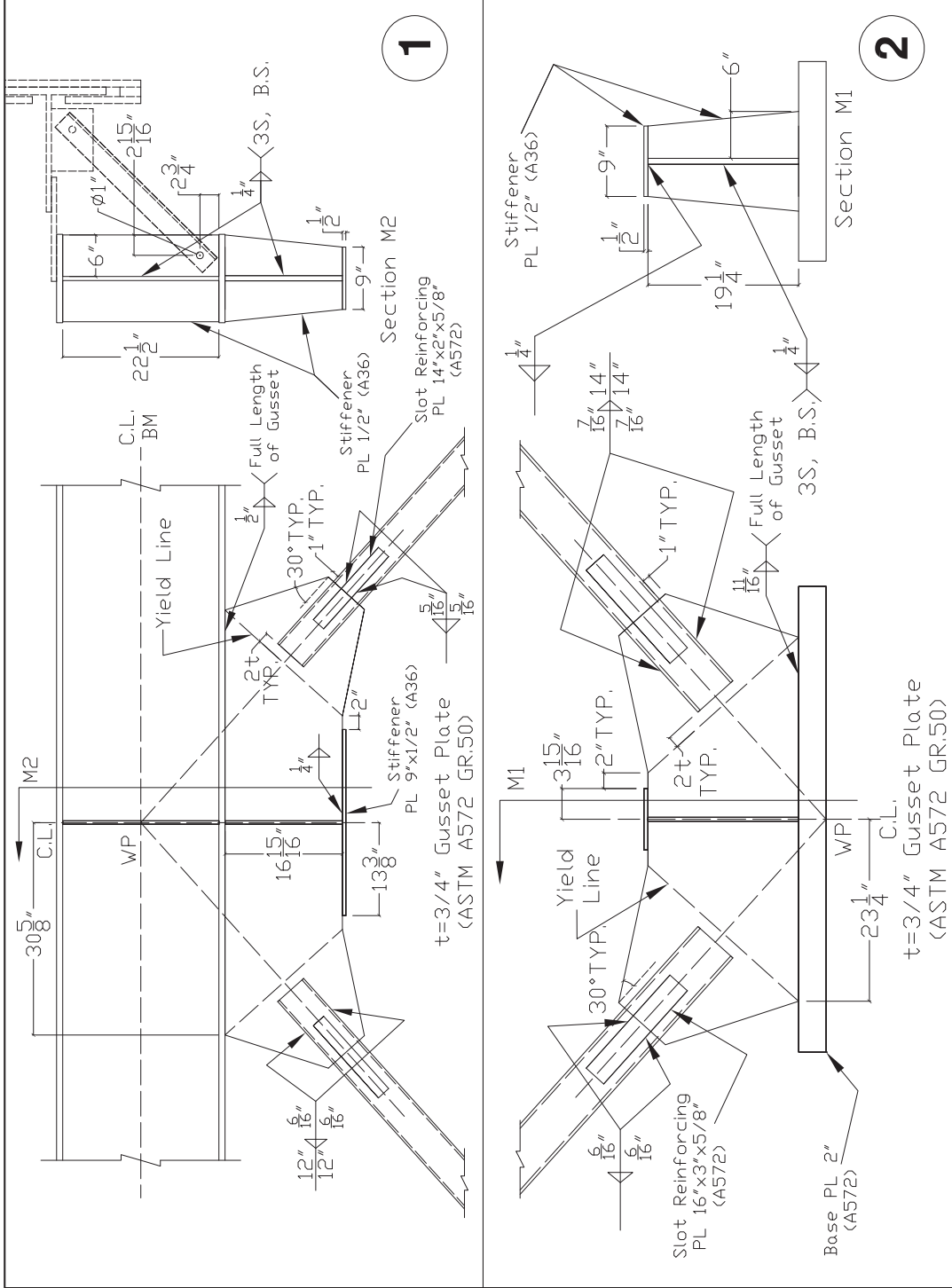
Jin-Jin Lai (Aster)

**date:**

Aug. 2008

**drawing no.**

**S1.04**



Filename: SCBF\_20080823\_Specimen-Only.dwg Plotted: 8/25/2008 9:29:12 Plot Device: Adobe PDF Page Setup: -- Plotted by: Jwlai





International Hybrid  
Simulation of  
Tomorrow's Braced  
Steel Frame Structures

REV.	REVISION	DATE

revisions

project

SCBF  
Phase-01  
1301 South 48th Street  
Richmond, California, 94804

Address

UC Berkeley  
Richmond Field Station  
Building 484, Structural Research Lab

content

Specimen Detail  
MISC Details

drawn by:

Jin-Wen Lai (Aster)

checked by:

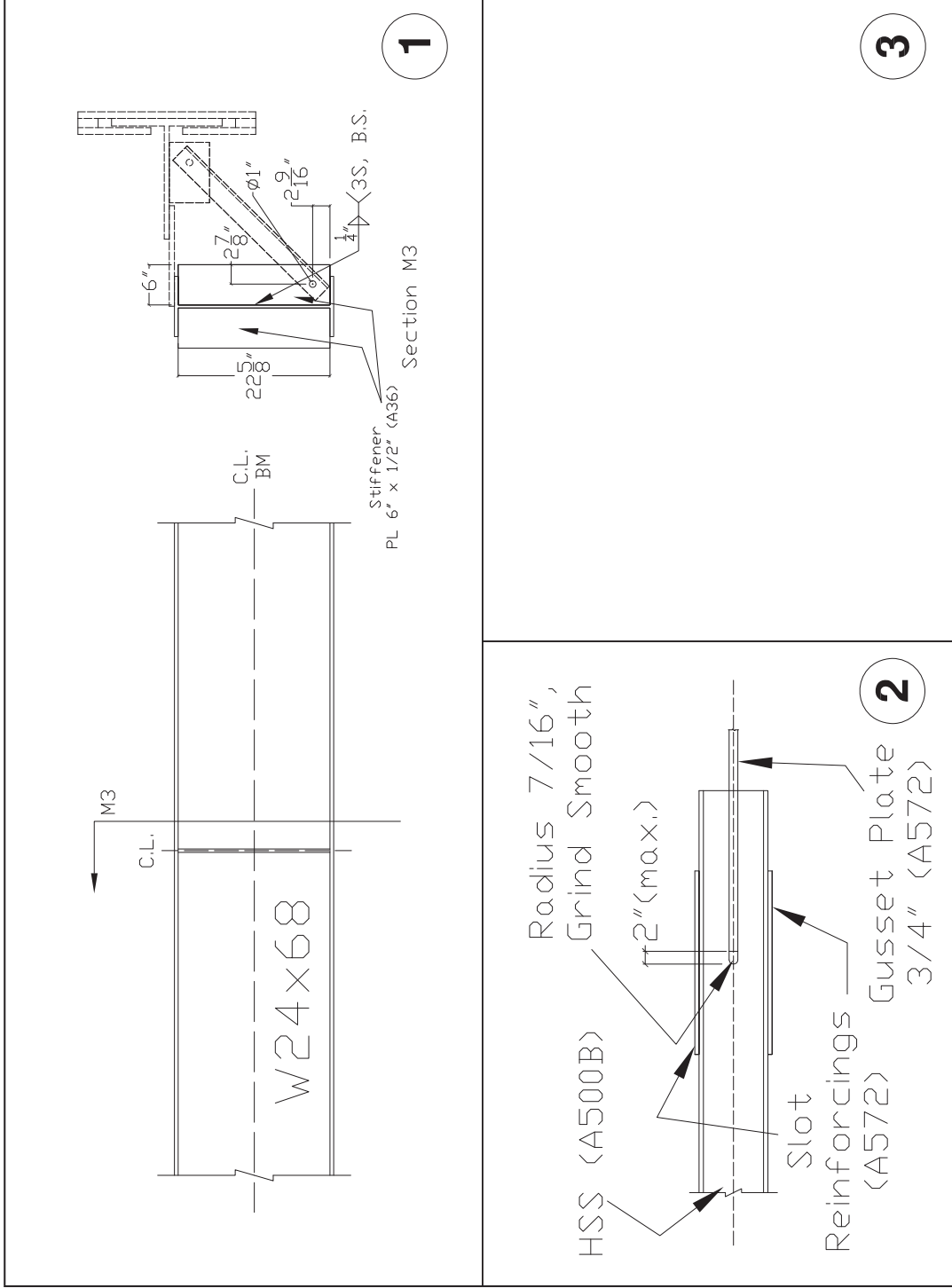
Jin-Wen Lai (Aster)

date:

Aug. 2008

drawing no.

S1.05

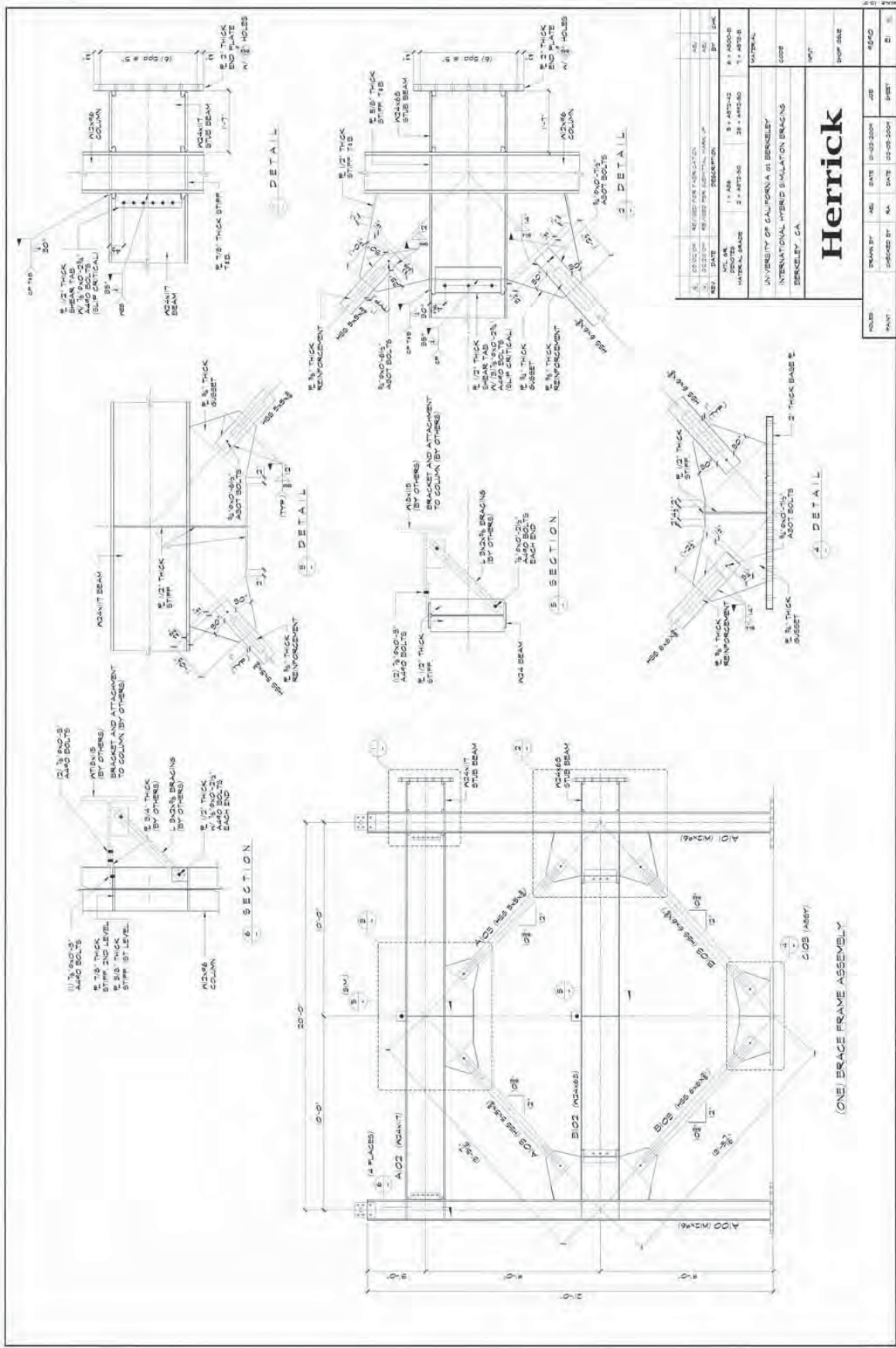


1

3

2

**TCBF-B-1 Shop Drawings  
(Herrick Steel)**

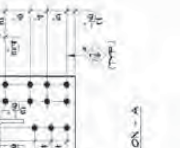
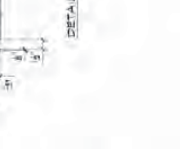
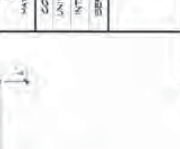
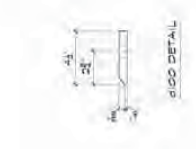
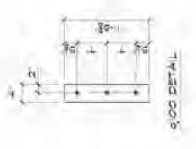
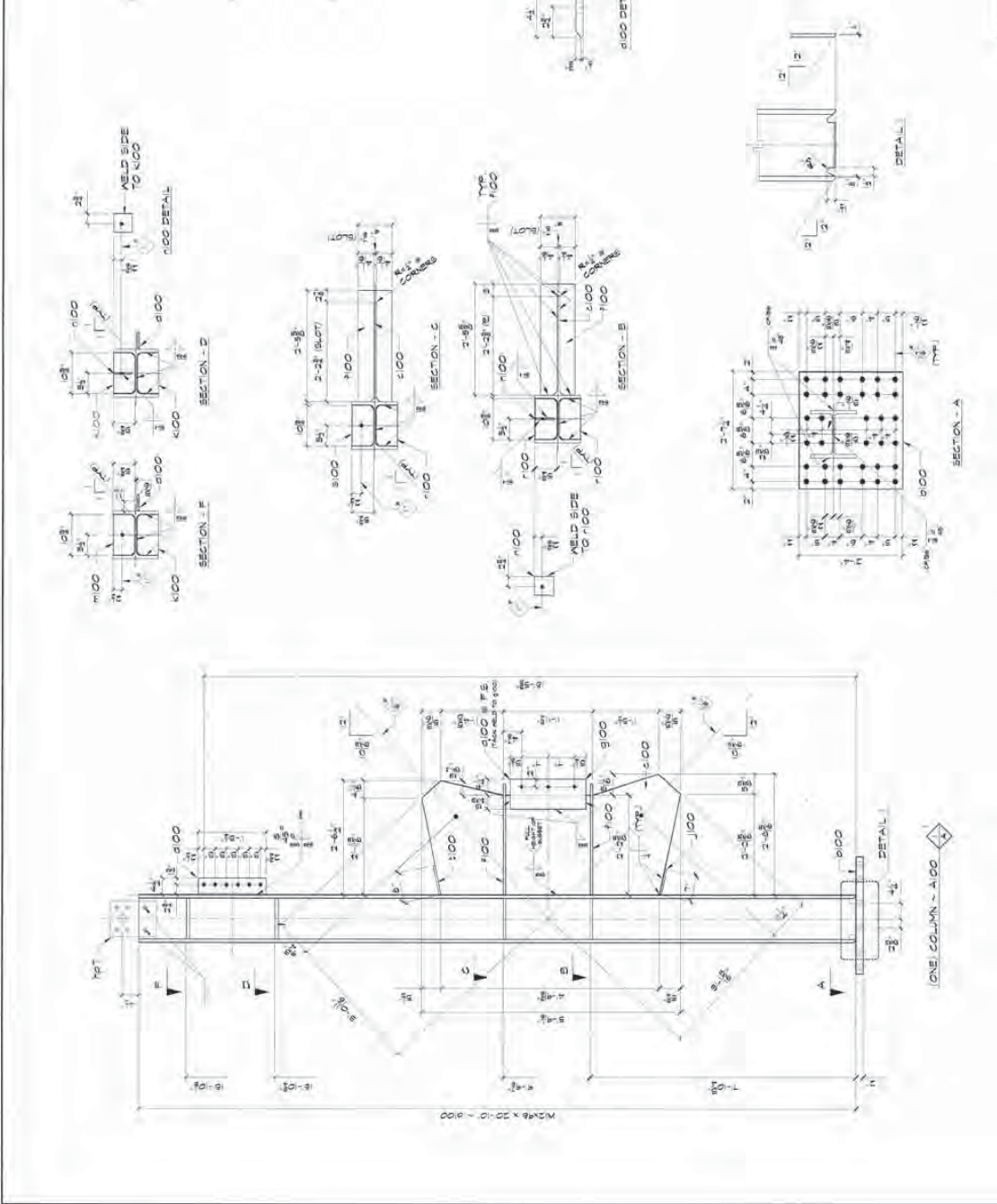


NO.	DESCRIPTION	QTY	UNIT
1	STEEL	1	TON
2	REINFORCEMENT	1	TON
3	WELDS	1	TON
4	PAINT	1	TON
5	BRACE	1	TON
6	BRACE	1	TON
7	BRACE	1	TON
8	BRACE	1	TON
9	BRACE	1	TON
10	BRACE	1	TON
11	BRACE	1	TON
12	BRACE	1	TON
13	BRACE	1	TON
14	BRACE	1	TON
15	BRACE	1	TON
16	BRACE	1	TON
17	BRACE	1	TON
18	BRACE	1	TON
19	BRACE	1	TON
20	BRACE	1	TON
21	BRACE	1	TON
22	BRACE	1	TON
23	BRACE	1	TON
24	BRACE	1	TON
25	BRACE	1	TON
26	BRACE	1	TON
27	BRACE	1	TON
28	BRACE	1	TON
29	BRACE	1	TON
30	BRACE	1	TON
31	BRACE	1	TON
32	BRACE	1	TON
33	BRACE	1	TON
34	BRACE	1	TON
35	BRACE	1	TON
36	BRACE	1	TON
37	BRACE	1	TON
38	BRACE	1	TON
39	BRACE	1	TON
40	BRACE	1	TON
41	BRACE	1	TON
42	BRACE	1	TON
43	BRACE	1	TON
44	BRACE	1	TON
45	BRACE	1	TON
46	BRACE	1	TON
47	BRACE	1	TON
48	BRACE	1	TON
49	BRACE	1	TON
50	BRACE	1	TON
51	BRACE	1	TON
52	BRACE	1	TON
53	BRACE	1	TON
54	BRACE	1	TON
55	BRACE	1	TON
56	BRACE	1	TON
57	BRACE	1	TON
58	BRACE	1	TON
59	BRACE	1	TON
60	BRACE	1	TON
61	BRACE	1	TON
62	BRACE	1	TON
63	BRACE	1	TON
64	BRACE	1	TON
65	BRACE	1	TON
66	BRACE	1	TON
67	BRACE	1	TON
68	BRACE	1	TON
69	BRACE	1	TON
70	BRACE	1	TON
71	BRACE	1	TON
72	BRACE	1	TON
73	BRACE	1	TON
74	BRACE	1	TON
75	BRACE	1	TON
76	BRACE	1	TON
77	BRACE	1	TON
78	BRACE	1	TON
79	BRACE	1	TON
80	BRACE	1	TON
81	BRACE	1	TON
82	BRACE	1	TON
83	BRACE	1	TON
84	BRACE	1	TON
85	BRACE	1	TON
86	BRACE	1	TON
87	BRACE	1	TON
88	BRACE	1	TON
89	BRACE	1	TON
90	BRACE	1	TON
91	BRACE	1	TON
92	BRACE	1	TON
93	BRACE	1	TON
94	BRACE	1	TON
95	BRACE	1	TON
96	BRACE	1	TON
97	BRACE	1	TON
98	BRACE	1	TON
99	BRACE	1	TON
100	BRACE	1	TON

UNIVERSITY OF CALIFORNIA AT BERKELEY	DATE	BY	CHKD
INTERNATIONAL HYBRID SIMULATION BRACING	11/15/00	11/15/00	11/15/00
BERKELEY, CA	11/15/00	11/15/00	11/15/00
<b>Herrick</b>			
DESIGNED BY	DATE	JOB	SCALE
11/15/00	11/15/00	11/15/00	11/15/00
CHECKED BY	DATE	SHEET	NO.
11/15/00	11/15/00	11/15/00	11/15/00

BILL OF MATERIALS

QTY.	DESCRIPTION	SIZE	MARK.	US	REMARKS	CODE
ONE	COLUMN		A100	*		
ONE	A100	20	10	600	20	PER FE 48
ONE	A100	2	7 1/2	600	2	D 7
ONE	A100	5	5/8	600	2	D 14
ONE	A100	1	8 1/2	600	2	D 15
ONE	A100	2	5/8	600	2	D 16
ONE	A100	1	3/4	600	2	D 17
ONE	A100	1	3/4	600	2	D 18
ONE	A100	1	3/4	600	2	D 19
ONE	A100	1	3/4	600	2	D 20
ONE	A100	1	3/4	600	2	D 21
ONE	A100	1	3/4	600	2	D 22
ONE	A100	1	3/4	600	2	D 23
ONE	A100	1	3/4	600	2	D 24
ONE	A100	1	3/4	600	2	D 25
ONE	A100	1	3/4	600	2	D 26
ONE	A100	1	3/4	600	2	D 27
ONE	A100	1	3/4	600	2	D 28
ONE	A100	1	3/4	600	2	D 29
ONE	A100	1	3/4	600	2	D 30
ONE	A100	1	3/4	600	2	D 31
ONE	A100	1	3/4	600	2	D 32
ONE	A100	1	3/4	600	2	D 33
ONE	A100	1	3/4	600	2	D 34
ONE	A100	1	3/4	600	2	D 35
ONE	A100	1	3/4	600	2	D 36
ONE	A100	1	3/4	600	2	D 37
ONE	A100	1	3/4	600	2	D 38
ONE	A100	1	3/4	600	2	D 39
ONE	A100	1	3/4	600	2	D 40
ONE	A100	1	3/4	600	2	D 41
ONE	A100	1	3/4	600	2	D 42
ONE	A100	1	3/4	600	2	D 43
ONE	A100	1	3/4	600	2	D 44
ONE	A100	1	3/4	600	2	D 45
ONE	A100	1	3/4	600	2	D 46
ONE	A100	1	3/4	600	2	D 47
ONE	A100	1	3/4	600	2	D 48
ONE	A100	1	3/4	600	2	D 49
ONE	A100	1	3/4	600	2	D 50



REVISIONS

NO.	DATE	BY	DESCRIPTION
1			
2			
3			
4			
5			
6			
7			
8			
9			
10			

TITLE: COLUMN  
 DRAWN BY: [NAME]  
 CHECKED BY: [NAME]  
 DATE: [DATE]  
 PROJECT: [PROJECT]  
 SHEET: [SHEET] OF [TOTAL]

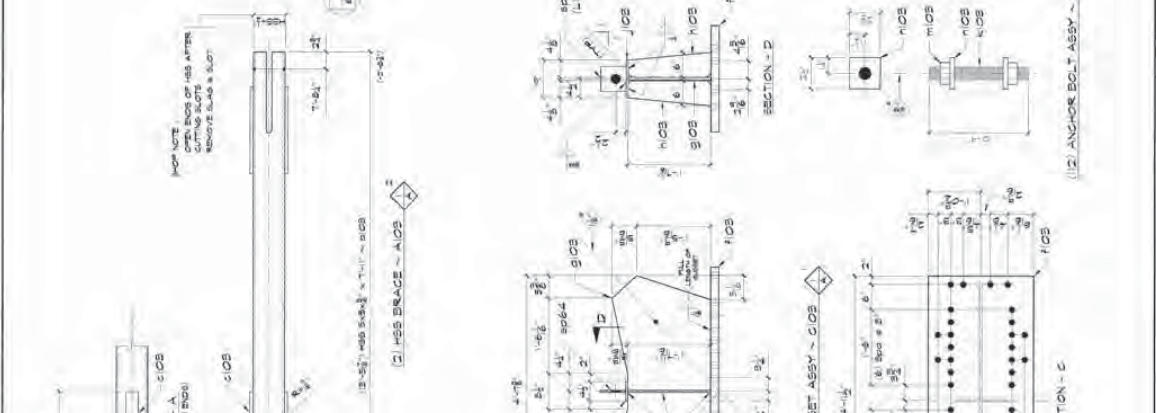
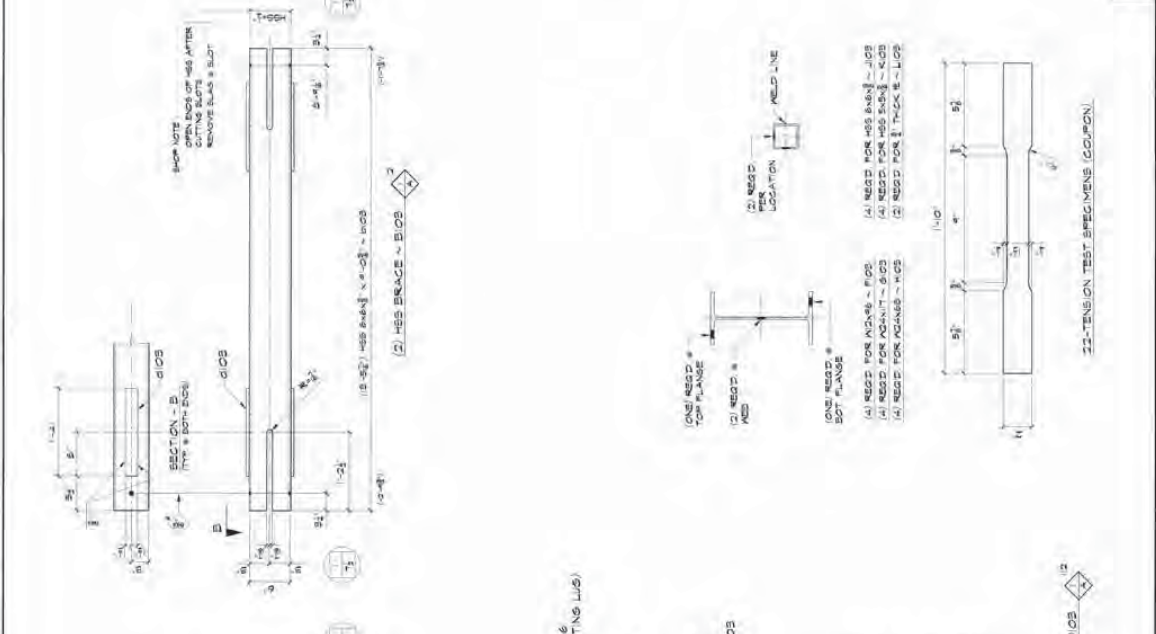
MATERIAL:  
 REINFORCEMENT: 10 M, 15 M, 20 M, 25 M, 30 M, 35 M, 40 M, 45 M, 50 M, 55 M, 60 M, 65 M, 70 M, 75 M, 80 M, 85 M, 90 M, 95 M, 100 M  
 CONCRETE: 3000 PSI  
 WELD: E70XX  
 FINISH: S1, S2, S3, S4, S5, S6, S7, S8, S9, S10, S11, S12, S13, S14, S15, S16, S17, S18, S19, S20, S21, S22, S23, S24, S25, S26, S27, S28, S29, S30, S31, S32, S33, S34, S35, S36, S37, S38, S39, S40, S41, S42, S43, S44, S45, S46, S47, S48, S49, S50, S51, S52, S53, S54, S55, S56, S57, S58, S59, S60, S61, S62, S63, S64, S65, S66, S67, S68, S69, S70, S71, S72, S73, S74, S75, S76, S77, S78, S79, S80, S81, S82, S83, S84, S85, S86, S87, S88, S89, S90, S91, S92, S93, S94, S95, S96, S97, S98, S99, S100

**Herrick**  
 INTERNATIONAL HYBRID ISOLATION BRACING  
 BERKELEY, CA





BILL OF MATERIALS									
QTY	DESCRIPTION	UNIFORM MARK	MAK	IN REMAINS	QTY	REMARKS	QTY	UNIT	WGT
2	HSS BRACE		A102		2				
4	HSS 2x2x1/4	1	D102	6	4				
4	HSS 2x2x3/8	2	D102	2	4				
4	1/2 A307	0	615	10482					
2	HSS BRACE		B102		2				
2	HSS 2x2x1/4	8	D14	D102	6				
4	1/2 A307	0	715	10472					
ONE	ASSEMBLY		C102		1				
ONE	2x2x1/4	4	115	102	2				
ONE	2x2x3/8	4	115	B102	2				
2	2x2x1/4	0	8	H102	1				
ONE	2x2x1/4	0	8	J102	1				
ONE	2x2x1/4	0	8	666					
12	ANCHOR BOLT ASSY		D102		12				
12	1/2" X 6"	0	4	N102	12				
224	2" X 1/2"	0	21	N102	2				
224	1 1/2" X 1/4"	0	21	N102	2				
4	COUPONS	1	10	F102	24				
4	COUPONS	1	10	S102	24				
4	COUPONS	1	10	H102	24				
4	COUPONS	1	10	J102	24				
2	COUPONS	1	10	K102	6				
1	COUPONS	1	10	L102	2				
ONE	HSS 2x2x1/4	40	0	M102	8				
ONE	HSS 2x2x1/4	40	0	N102	8				



1	COUPON	REFLECT FOR FABRICATION	1 1/2" X 6"	24	1	1	1	1	1	1
1	COUPON	REFLECT FOR FABRICATION	2" X 1/2"	2	1	1	1	1	1	1
1	COUPON	REFLECT FOR FABRICATION	1 1/2" X 1/4"	2	1	1	1	1	1	1
1	COUPON	REFLECT FOR FABRICATION	2" X 1/4"	2	1	1	1	1	1	1
1	COUPON	REFLECT FOR FABRICATION	1" X 1/2"	24	1	1	1	1	1	1
1	COUPON	REFLECT FOR FABRICATION	1" X 1/4"	24	1	1	1	1	1	1
1	COUPON	REFLECT FOR FABRICATION	1" X 1/4"	6	1	1	1	1	1	1
1	COUPON	REFLECT FOR FABRICATION	1" X 1/4"	2	1	1	1	1	1	1
1	COUPON	REFLECT FOR FABRICATION	1" X 1/4"	8	1	1	1	1	1	1
1	COUPON	REFLECT FOR FABRICATION	1" X 1/4"	8	1	1	1	1	1	1

**Herrick**

UNIVERSITY OF CALIFORNIA AT BERKELEY  
 INTERNATIONAL HYPERID SIMULATION BRACING  
 DENVER, CO.

REVISION: 1/25/20  
 DRAWN BY: JEF  
 DATE: 01-20-2008  
 PART: ONE  
 CHECKED BY: N/A  
 DATE: 02-05-2008  
 SHEET: 13 OF 13

**TCBF-B-2, TCBF-B-3 and TCBF-B-4 Shop Drawings  
(UC Berkeley)**





REV.	REVISION	DATE

revisions

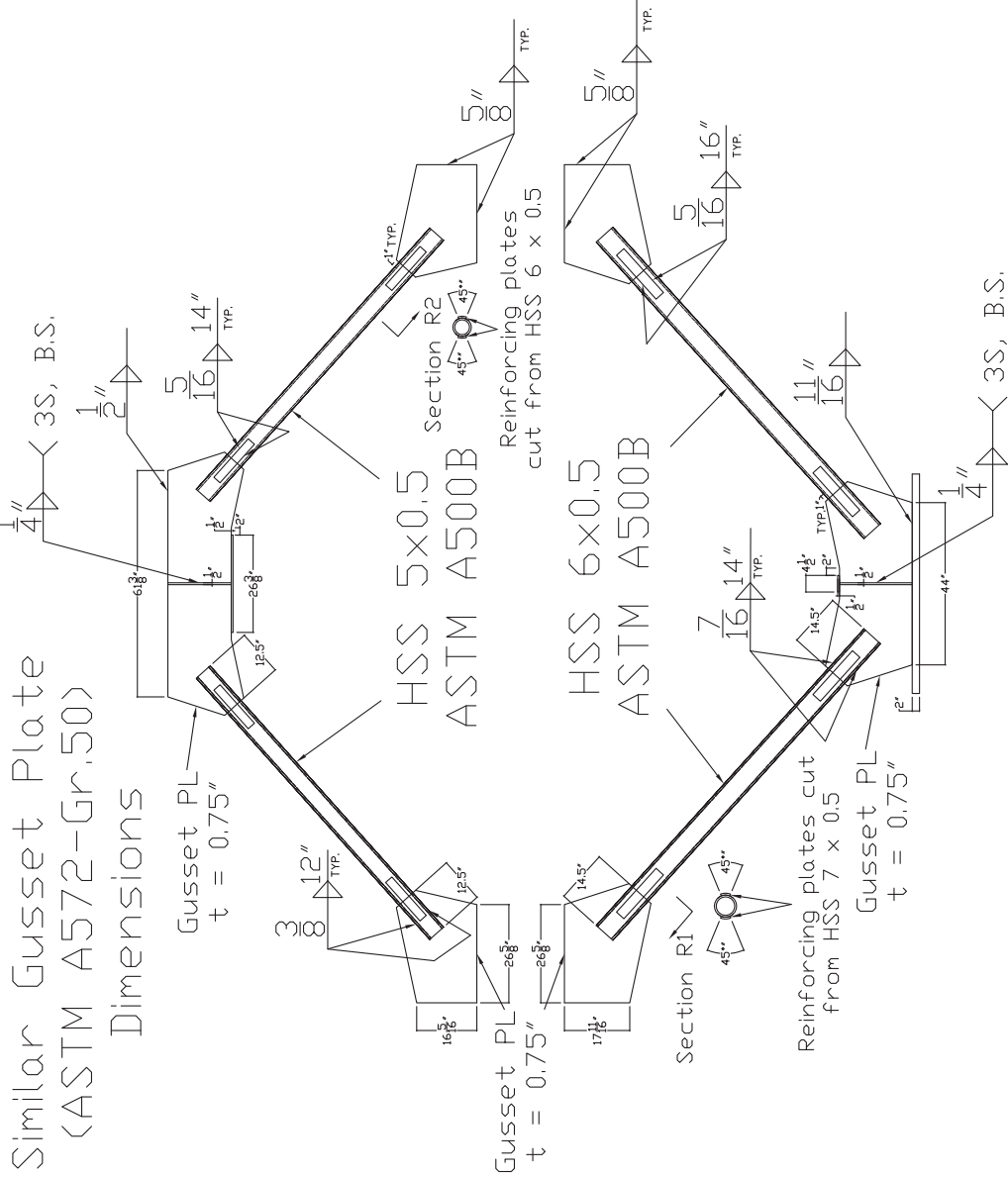
**project**  
SCRF (HSS-Round)  
Phase-01  
1301 South 48th Street  
Richmond, California, 94804

**Address**  
UC Berkeley  
Rathbone Hall Station  
Building 464, Structural Research Lab

**content**  
Specimen Detail  
Framing Elevations

**drawn by:** Jim-Wai Lai (Astin)  
**checked by:** Jim-Wai Lai (Astin)  
**date:** May, 2009

**drawing no.** R1.01





**International Hybrid  
Simulation of  
Tomorrow's Braced  
Steel Frame Structures**

REV.	REVISION	DATE

**revisions**

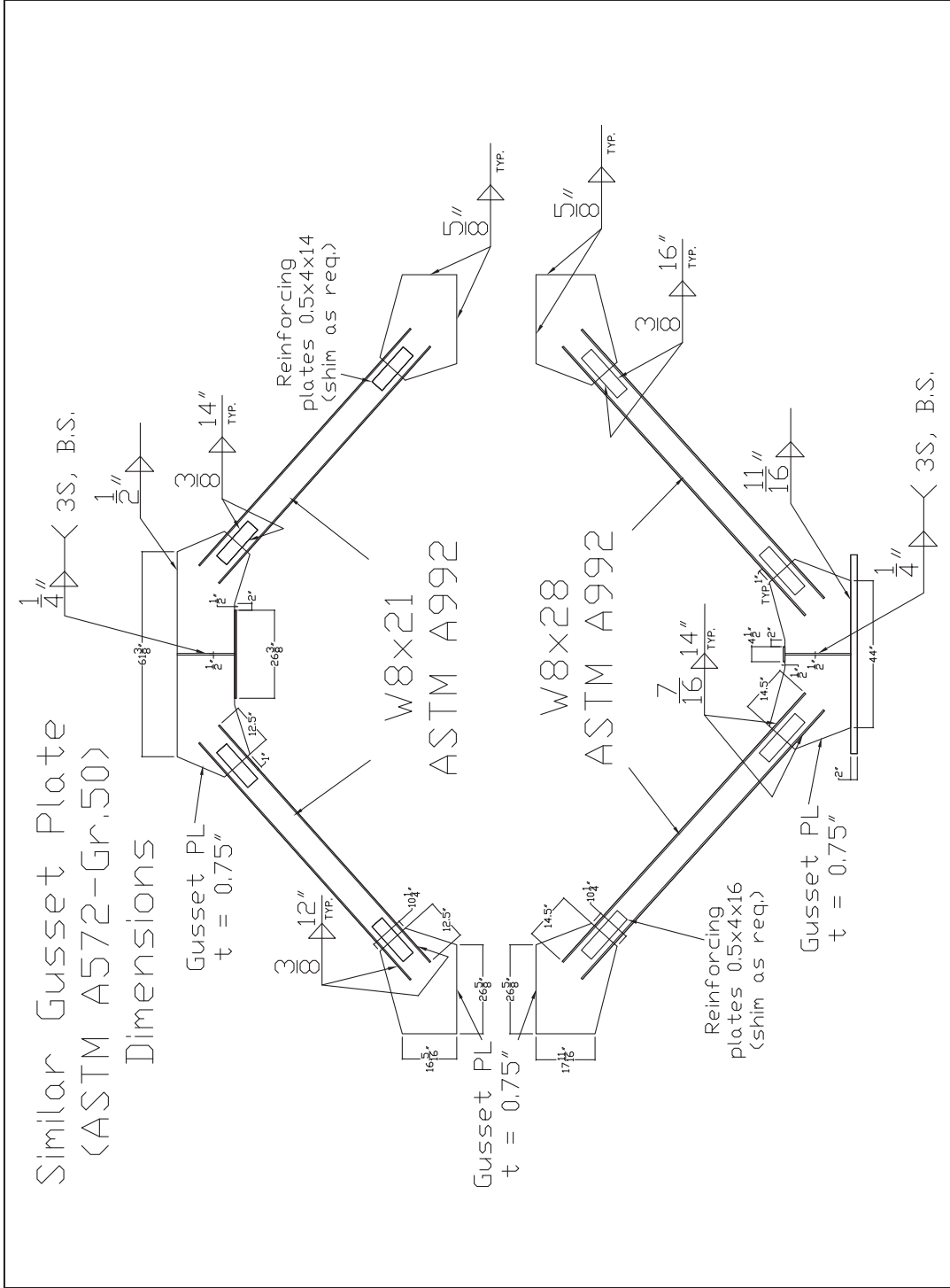
**project**  
SCRF (WF)  
Phase-01  
1301 South 48th Street  
Richmond, California, 94804

**Address**  
UC Berkeley  
Ragland Hall Station  
Building 464, Structural Research Lab

**content**  
Specimen Detail  
Framing Elevations

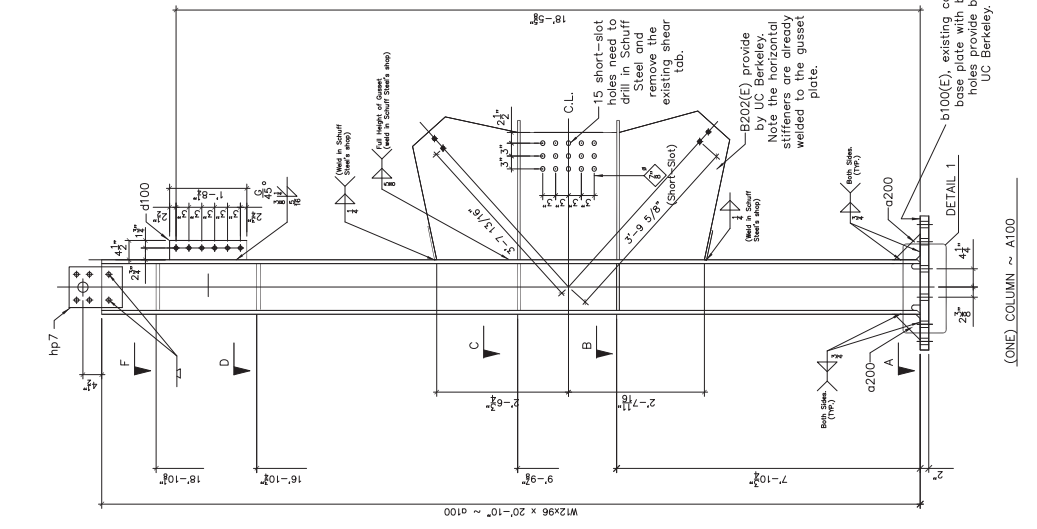
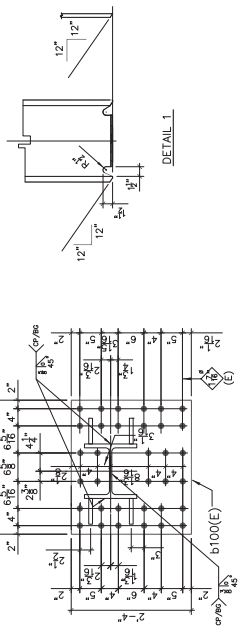
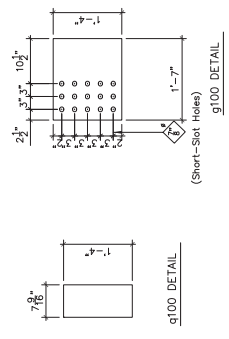
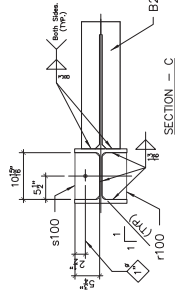
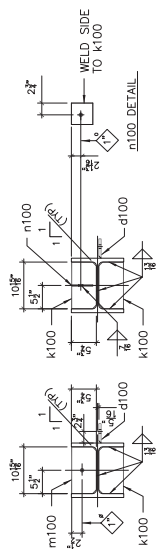
**drawn by:** Jun-Wei Lai (Astin)  
**checked by:** Jun-Wei Lai (Astin)  
**date:** May, 2009

**drawing no.** **W1.01**



Similar Gusset Plate  
(ASTM A572-Gr.50)  
Dimensions

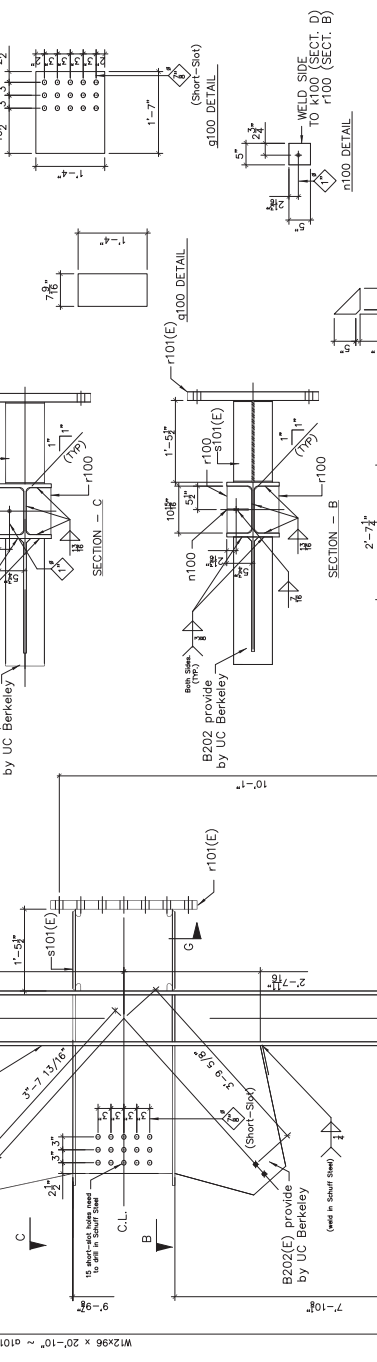
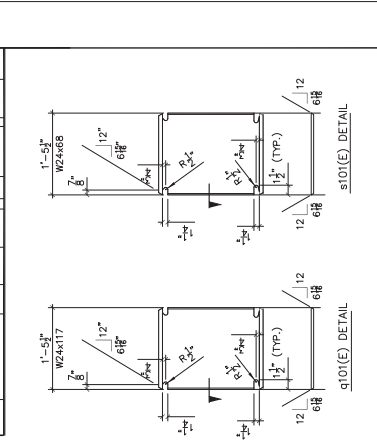
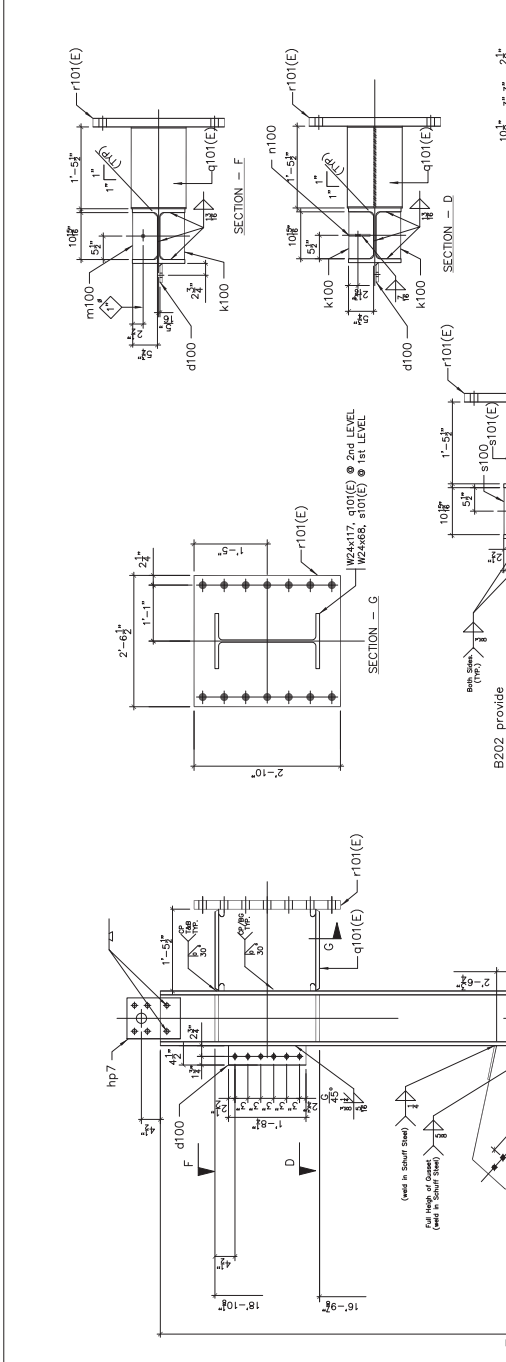
BILL OF MATERIALS							
QTY.	DESCRIPTION	LENGTH FT INCHES	MARK	MTL GR	REMARKS	CODE	MO WTD
ONE	COLUMN		A100	0			
ONE	W12x96	20	1100	28		PLATE (96x1)	
ONE	PL 2x8x6	2	714	0100	2	Provide by UC Berkeley	
ONE	PL 7/8x4	0	5200	0		PL 7/8x4	
ONE	PL 1/2x4.1/2	1	514	0100	2	PL 1/2x4.1/2	
4	PL 1/2x1/2	1	7	5100	1	PL 1/2x1/2	
ONE	PL 3/8x5/2	1	2.84	197	2	PL 3/8x5/2	
ONE	PL 7/8x5.3/4	0	101516	0100	2	PL 7/8x5.3/4	
ONE	PL 7/8x5.3/4	0	101516	0100	2	PL 7/8x5.3/4	
2	PL 1/2x5	1	5100	1	514	PL 1/2x5	
4	PL 1/2x7/8x1/8	1	4	5100	1	514	PL 1/2x7/8x1/8
ONE	PL 5/8x5.3/4	0	101516	0100	2	PL 5/8x5.3/4	
ONE	PL 5/8x5.3/4	0	101516	0100	2	PL 5/8x5.3/4	
ONE	Gusset Plate Assembly		B202			Provide by UC Berkeley	
30	Ø 7/8" - A490 SC	0	314				
2	Ø 1/2" - A490 SC	0	212				
2	Ø 1/2" - A490 SC	0	3				



REV.	DATE	DESCRIPTION	BY	CHK
1	ASB	1 = ASB	5 = A572-50	6 = A500-B
2	ASB	2 = A572-50	7 = A572-50	7 = A572-50
3	ASB	3 = A572-50	8 = A572-50	8 = A572-50
4	ASB	4 = A572-50	9 = A572-50	9 = A572-50
5	ASB	5 = A572-50	10 = A572-50	10 = A572-50
6	ASB	6 = A572-50	11 = A572-50	11 = A572-50
7	ASB	7 = A572-50	12 = A572-50	12 = A572-50
8	ASB	8 = A572-50	13 = A572-50	13 = A572-50
9	ASB	9 = A572-50	14 = A572-50	14 = A572-50
10	ASB	10 = A572-50	15 = A572-50	15 = A572-50
11	ASB	11 = A572-50	16 = A572-50	16 = A572-50
12	ASB	12 = A572-50	17 = A572-50	17 = A572-50
13	ASB	13 = A572-50	18 = A572-50	18 = A572-50
14	ASB	14 = A572-50	19 = A572-50	19 = A572-50
15	ASB	15 = A572-50	20 = A572-50	20 = A572-50
16	ASB	16 = A572-50	21 = A572-50	21 = A572-50
17	ASB	17 = A572-50	22 = A572-50	22 = A572-50
18	ASB	18 = A572-50	23 = A572-50	23 = A572-50
19	ASB	19 = A572-50	24 = A572-50	24 = A572-50
20	ASB	20 = A572-50	25 = A572-50	25 = A572-50
21	ASB	21 = A572-50	26 = A572-50	26 = A572-50
22	ASB	22 = A572-50	27 = A572-50	27 = A572-50
23	ASB	23 = A572-50	28 = A572-50	28 = A572-50
24	ASB	24 = A572-50	29 = A572-50	29 = A572-50
25	ASB	25 = A572-50	30 = A572-50	30 = A572-50

HOLD:	DATE	DRAWN BY	DATE	JOB
18 JUN 09	09-21-2010		09-21-2010	TG8F-B
PART: NONE	CHECKED BY	DATE	SHEET	100

BILL OF MATERIALS				
QTY.	DESCRIPTION	LENGTH FT	MARK	REMARKS
ONE	COLUMN		A101	
ONE	W24x48	20	q101	2B
ONE	PL 2x20	2	10101	2
ONE	PL 1/2x41/2	1	q100	2
ONE	PL 1/2x48	1	q100	1
ONE	Steel Plate Assembly		B202	Provide by UC
3	PL 7/8x5/8	0	10100	2
ONE	PL 7/8x5/8	0	10100	2
ONE	PL 1/2x5/8	1	10100	2
ONE	PL 3/8x5/8	1	10100	2
ONE	W24x117	2	q101	2B
ONE	W24x301/2	2	q101	2B
ONE	W24x88	1	q101	2B
ONE	PL 1/2x7/8	1	q101	2B
ONE	PL 5/8x3/4	0	10100	2
ONE	PL 7/8x5/8	0	10100	2
30	W7/8x485/8	0	3104	2
2	W7/8x485/8	0	2102	2
2	W7/8x485/8	0	3	2

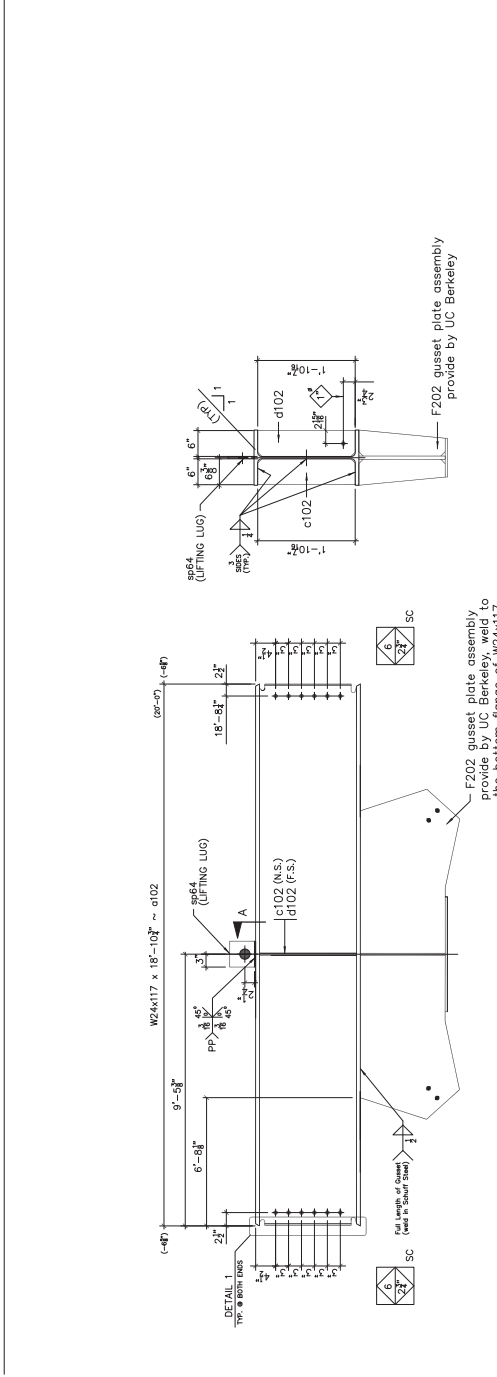


REV.	DATE	DESCRIPTION	BY	CHK
1	10/1/00	1 = ASB	5 = A272-42	6 = A500-B
2	10/1/00	2 = A572-50	7 = A572-50	8 = A572-50

WEST SIDE COLUMN  
UNIVERSITY OF CALIFORNIA, BERKELEY  
INT'L HYBRID SIMULATION OF TCBF  
BERKELEY, CA.

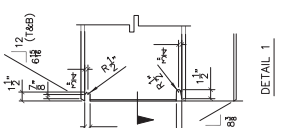
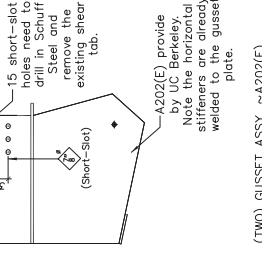
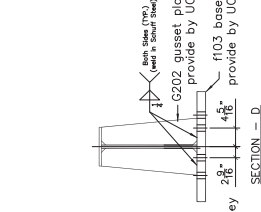
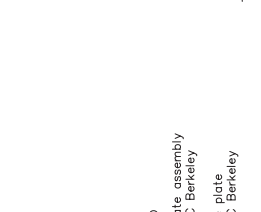
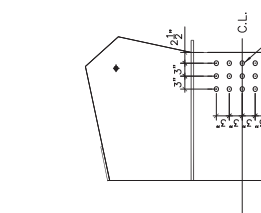
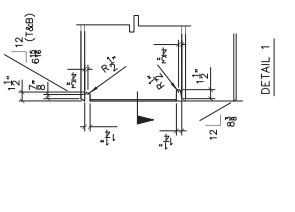
INDEX	UNO	DRAWN BY	DATE	99-21-2010	JOB	TCBF-B
PANT	NONE	CHECKED BY	DATE	99-21-2010	SHEET	101

QTY.	DESCRIPTION	MATERIAL	MARK	MIL. OR.	REMARKS	CODE	NO. INFO
ONE	BEAM		A102				
ONE	W24 X 117	18	10 7/16	A102	2B		W14.3
ONE	PL 1/2 X 6	1	10 7/16	A102	1		PA 300.44
ONE	PL 1/2 X 6	1	10 7/16	A102	1		PA 300.44
ONE	PL 1/2 X 6	0	6	A102	1		
2	#1/2" x 4-00 SC	0	2.04				
2	#1/2" x 4-00 SC	0	2.12				
ONE	Gusset Plate		F202		Provide by UC		
ONE	" Gusset Plate		F103		Provide by UC		
ONE	Gusset Plate		G202		Provide by UC		
TWO	Gusset Plate		A202		Provide by UC		
ONE	W24 X 117 (Flange)	1	11	CP24F	2B		Per Coupon
ONE	W24 X 117 (Web)	1	11	CP24F	2B		Per Coupon
ONE	W24 X 86 (Flange)	1	11	CP24F	2B		Per Coupon
ONE	W24 X 86 (Web)	1	11	CP24F	2B		Per Coupon



SECTION - A

(ONE) GUSSET ASSY ~ G103



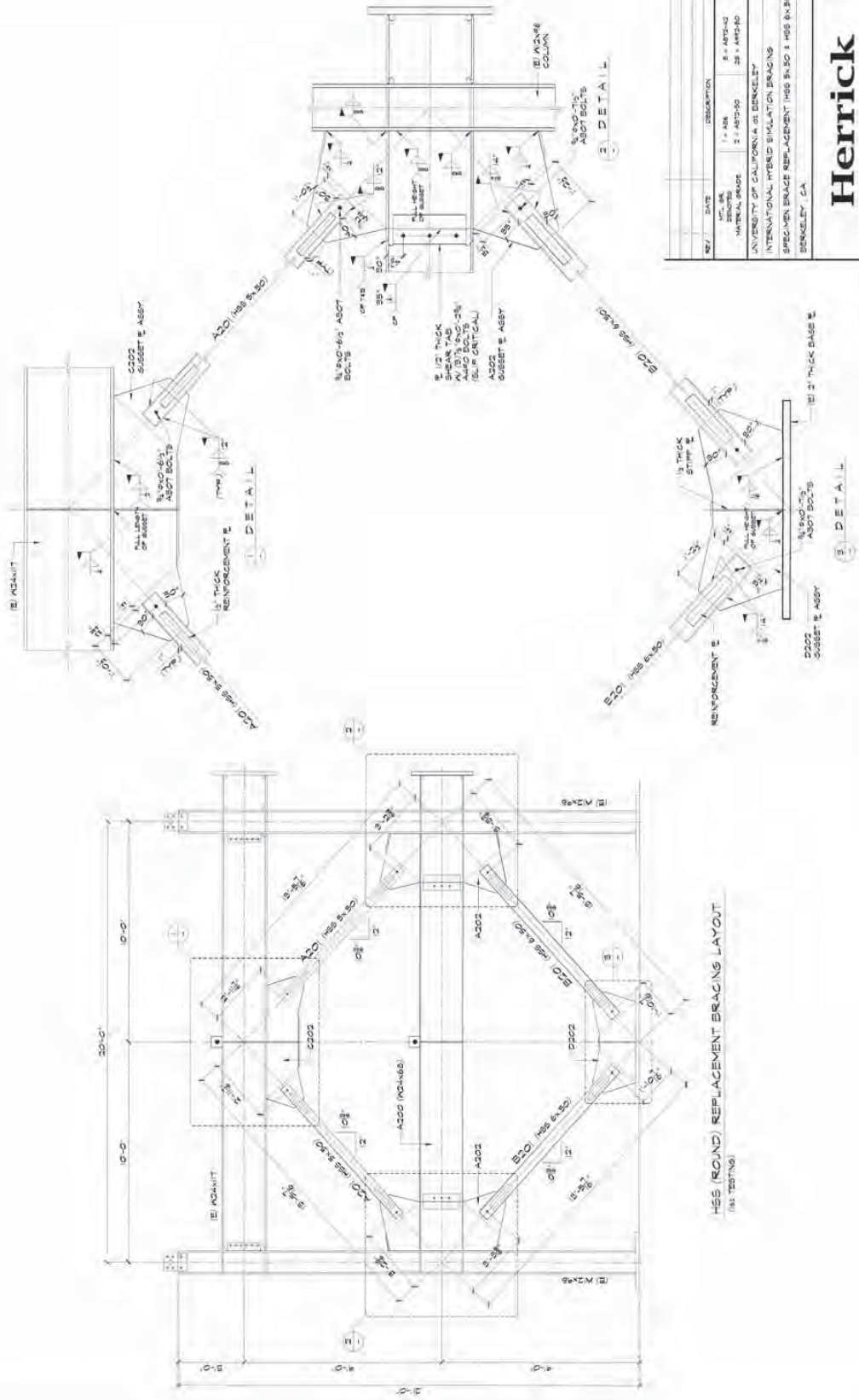
REV.	DATE	DESCRIPTION	BY	CHK
1	08	1 = 08		
2	08	2 = 08		
3	08	3 = 08		
4	08	4 = 08		
5	08	5 = 08		
6	08	6 = 08		
7	08	7 = 08		

UNIVERSITY OF CALIFORNIA, BERKELEY  
INT'L HYBRID SIMULATION OF TCBF  
BERKELEY, CA

SHIP ISSUE

DATE: 08-21-2010  
JOB: TCBF-B  
SHEET: 102

**TCBF-B-2, TCBF-B-3 and TCBF-B-4 Shop Drawings  
(Herrick Steel)**



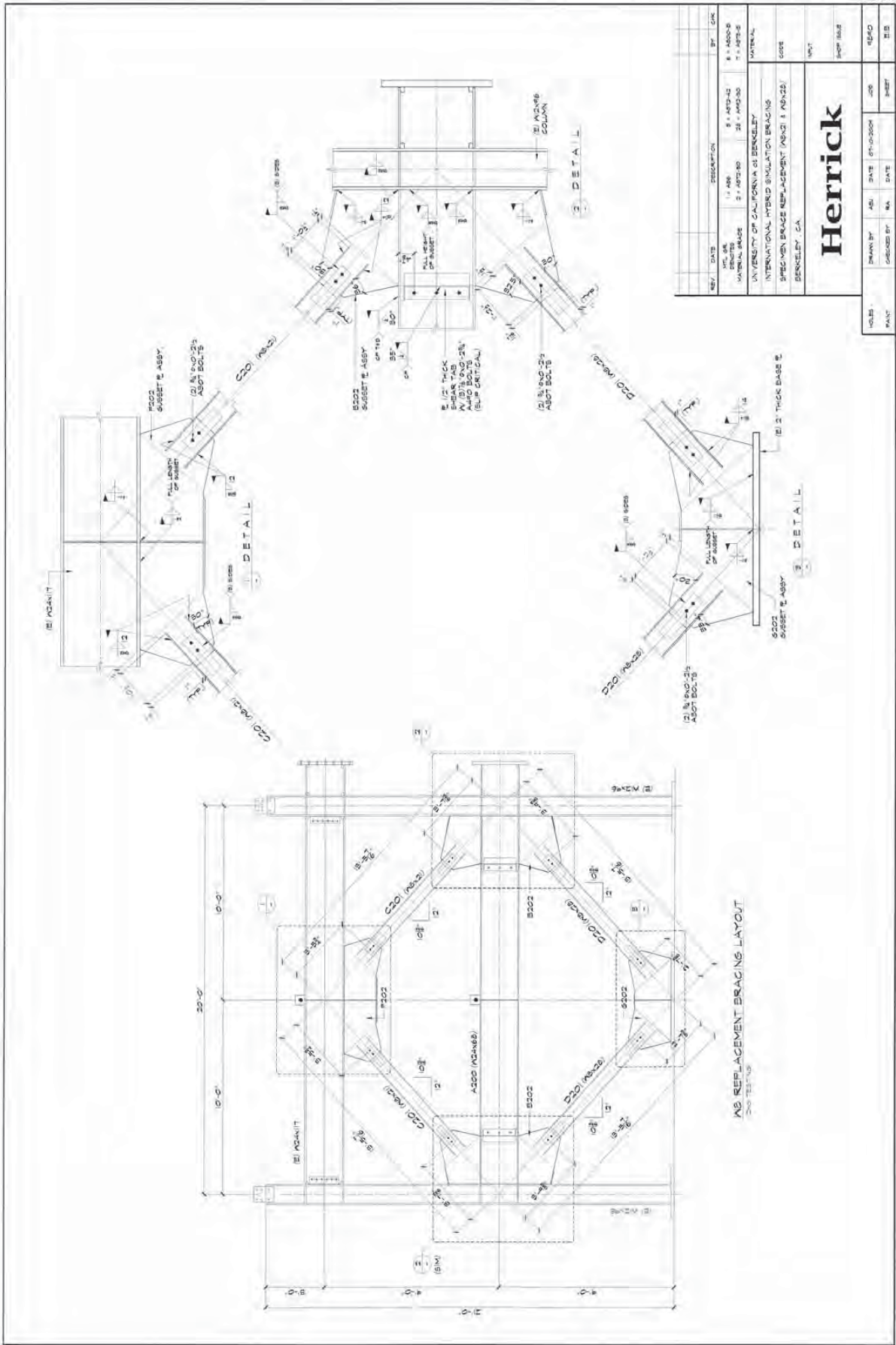
HSS (ROUND) REPLACEMENT BRACING LAYOUT  
(1/8" TESTING)

REV	DATE	DESCRIPTION	BY	CHK
1	08-20-2008	1 - ASB	ASB	ASB
2	08-20-2008	2 - AMB	AMB	AMB
3	08-20-2008	3 - AMB	AMB	AMB
4	08-20-2008	4 - AMB	AMB	AMB
5	08-20-2008	5 - AMB	AMB	AMB
6	08-20-2008	6 - AMB	AMB	AMB
7	08-20-2008	7 - AMB	AMB	AMB
8	08-20-2008	8 - AMB	AMB	AMB
9	08-20-2008	9 - AMB	AMB	AMB
10	08-20-2008	10 - AMB	AMB	AMB
11	08-20-2008	11 - AMB	AMB	AMB
12	08-20-2008	12 - AMB	AMB	AMB
13	08-20-2008	13 - AMB	AMB	AMB
14	08-20-2008	14 - AMB	AMB	AMB
15	08-20-2008	15 - AMB	AMB	AMB
16	08-20-2008	16 - AMB	AMB	AMB
17	08-20-2008	17 - AMB	AMB	AMB
18	08-20-2008	18 - AMB	AMB	AMB
19	08-20-2008	19 - AMB	AMB	AMB
20	08-20-2008	20 - AMB	AMB	AMB
21	08-20-2008	21 - AMB	AMB	AMB
22	08-20-2008	22 - AMB	AMB	AMB
23	08-20-2008	23 - AMB	AMB	AMB
24	08-20-2008	24 - AMB	AMB	AMB
25	08-20-2008	25 - AMB	AMB	AMB
26	08-20-2008	26 - AMB	AMB	AMB
27	08-20-2008	27 - AMB	AMB	AMB
28	08-20-2008	28 - AMB	AMB	AMB
29	08-20-2008	29 - AMB	AMB	AMB
30	08-20-2008	30 - AMB	AMB	AMB
31	08-20-2008	31 - AMB	AMB	AMB
32	08-20-2008	32 - AMB	AMB	AMB
33	08-20-2008	33 - AMB	AMB	AMB
34	08-20-2008	34 - AMB	AMB	AMB
35	08-20-2008	35 - AMB	AMB	AMB
36	08-20-2008	36 - AMB	AMB	AMB
37	08-20-2008	37 - AMB	AMB	AMB
38	08-20-2008	38 - AMB	AMB	AMB
39	08-20-2008	39 - AMB	AMB	AMB
40	08-20-2008	40 - AMB	AMB	AMB
41	08-20-2008	41 - AMB	AMB	AMB
42	08-20-2008	42 - AMB	AMB	AMB
43	08-20-2008	43 - AMB	AMB	AMB
44	08-20-2008	44 - AMB	AMB	AMB
45	08-20-2008	45 - AMB	AMB	AMB
46	08-20-2008	46 - AMB	AMB	AMB
47	08-20-2008	47 - AMB	AMB	AMB
48	08-20-2008	48 - AMB	AMB	AMB
49	08-20-2008	49 - AMB	AMB	AMB
50	08-20-2008	50 - AMB	AMB	AMB
51	08-20-2008	51 - AMB	AMB	AMB
52	08-20-2008	52 - AMB	AMB	AMB
53	08-20-2008	53 - AMB	AMB	AMB
54	08-20-2008	54 - AMB	AMB	AMB
55	08-20-2008	55 - AMB	AMB	AMB
56	08-20-2008	56 - AMB	AMB	AMB
57	08-20-2008	57 - AMB	AMB	AMB
58	08-20-2008	58 - AMB	AMB	AMB
59	08-20-2008	59 - AMB	AMB	AMB
60	08-20-2008	60 - AMB	AMB	AMB
61	08-20-2008	61 - AMB	AMB	AMB
62	08-20-2008	62 - AMB	AMB	AMB
63	08-20-2008	63 - AMB	AMB	AMB
64	08-20-2008	64 - AMB	AMB	AMB
65	08-20-2008	65 - AMB	AMB	AMB
66	08-20-2008	66 - AMB	AMB	AMB
67	08-20-2008	67 - AMB	AMB	AMB
68	08-20-2008	68 - AMB	AMB	AMB
69	08-20-2008	69 - AMB	AMB	AMB
70	08-20-2008	70 - AMB	AMB	AMB
71	08-20-2008	71 - AMB	AMB	AMB
72	08-20-2008	72 - AMB	AMB	AMB
73	08-20-2008	73 - AMB	AMB	AMB
74	08-20-2008	74 - AMB	AMB	AMB
75	08-20-2008	75 - AMB	AMB	AMB
76	08-20-2008	76 - AMB	AMB	AMB
77	08-20-2008	77 - AMB	AMB	AMB
78	08-20-2008	78 - AMB	AMB	AMB
79	08-20-2008	79 - AMB	AMB	AMB
80	08-20-2008	80 - AMB	AMB	AMB
81	08-20-2008	81 - AMB	AMB	AMB
82	08-20-2008	82 - AMB	AMB	AMB
83	08-20-2008	83 - AMB	AMB	AMB
84	08-20-2008	84 - AMB	AMB	AMB
85	08-20-2008	85 - AMB	AMB	AMB
86	08-20-2008	86 - AMB	AMB	AMB
87	08-20-2008	87 - AMB	AMB	AMB
88	08-20-2008	88 - AMB	AMB	AMB
89	08-20-2008	89 - AMB	AMB	AMB
90	08-20-2008	90 - AMB	AMB	AMB
91	08-20-2008	91 - AMB	AMB	AMB
92	08-20-2008	92 - AMB	AMB	AMB
93	08-20-2008	93 - AMB	AMB	AMB
94	08-20-2008	94 - AMB	AMB	AMB
95	08-20-2008	95 - AMB	AMB	AMB
96	08-20-2008	96 - AMB	AMB	AMB
97	08-20-2008	97 - AMB	AMB	AMB
98	08-20-2008	98 - AMB	AMB	AMB
99	08-20-2008	99 - AMB	AMB	AMB
100	08-20-2008	100 - AMB	AMB	AMB

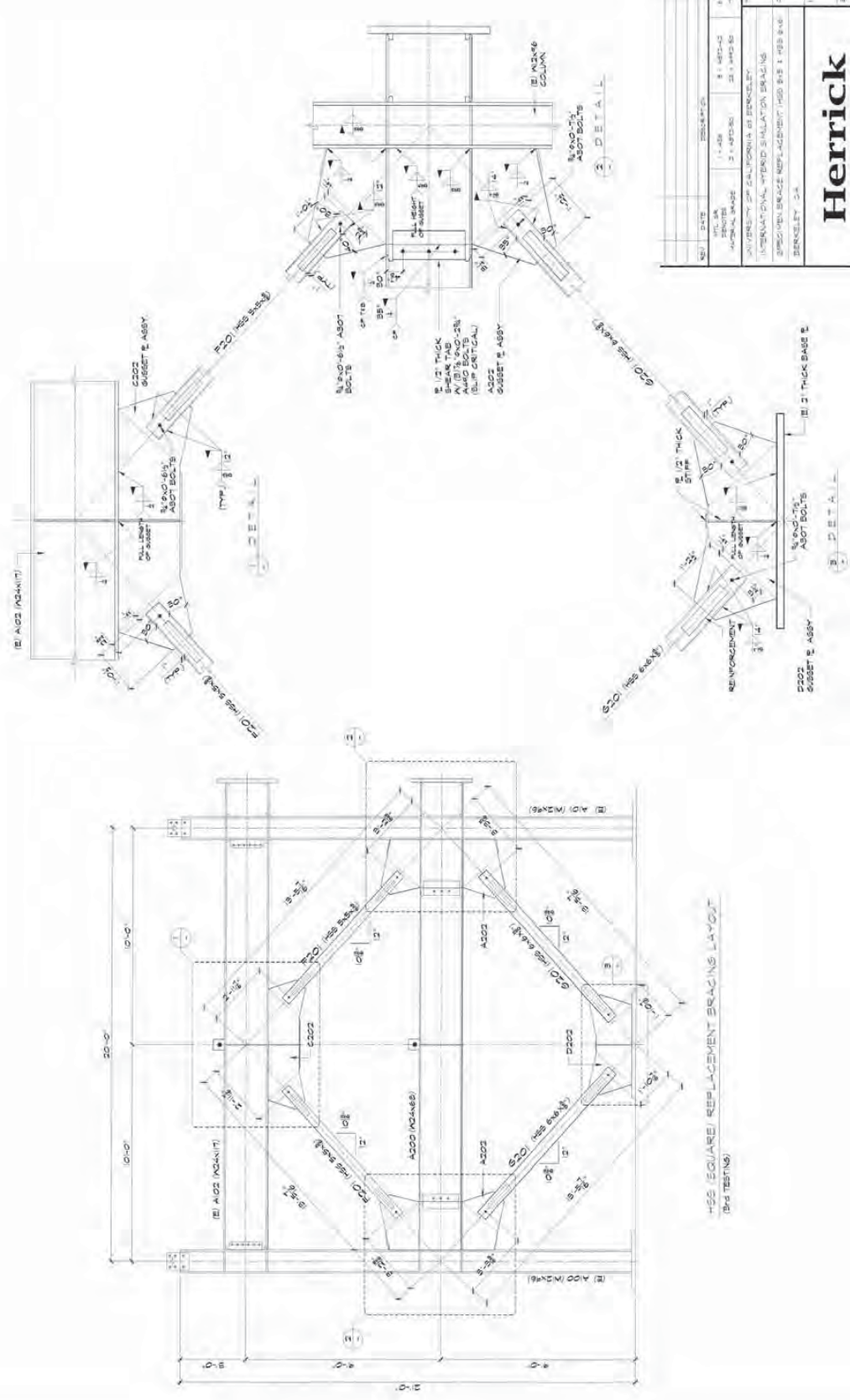
UNIVERSITY OF CALIFORNIA, BERKELEY  
INTERNATIONAL HYBRID SIMILATION BRACING  
SPECIMEN BRACE REPLACEMENT (HSS 6x30 & HSS 8x30)  
BERKELEY, CA

**Herrick**

NO. 15  
DATE: 08-20-2008  
DRAWN BY: ASB  
CHECKED BY: ASB  
DATE: 08-20-2008  
JOB: 08-20-2008  
SHEET: 11  
EIA







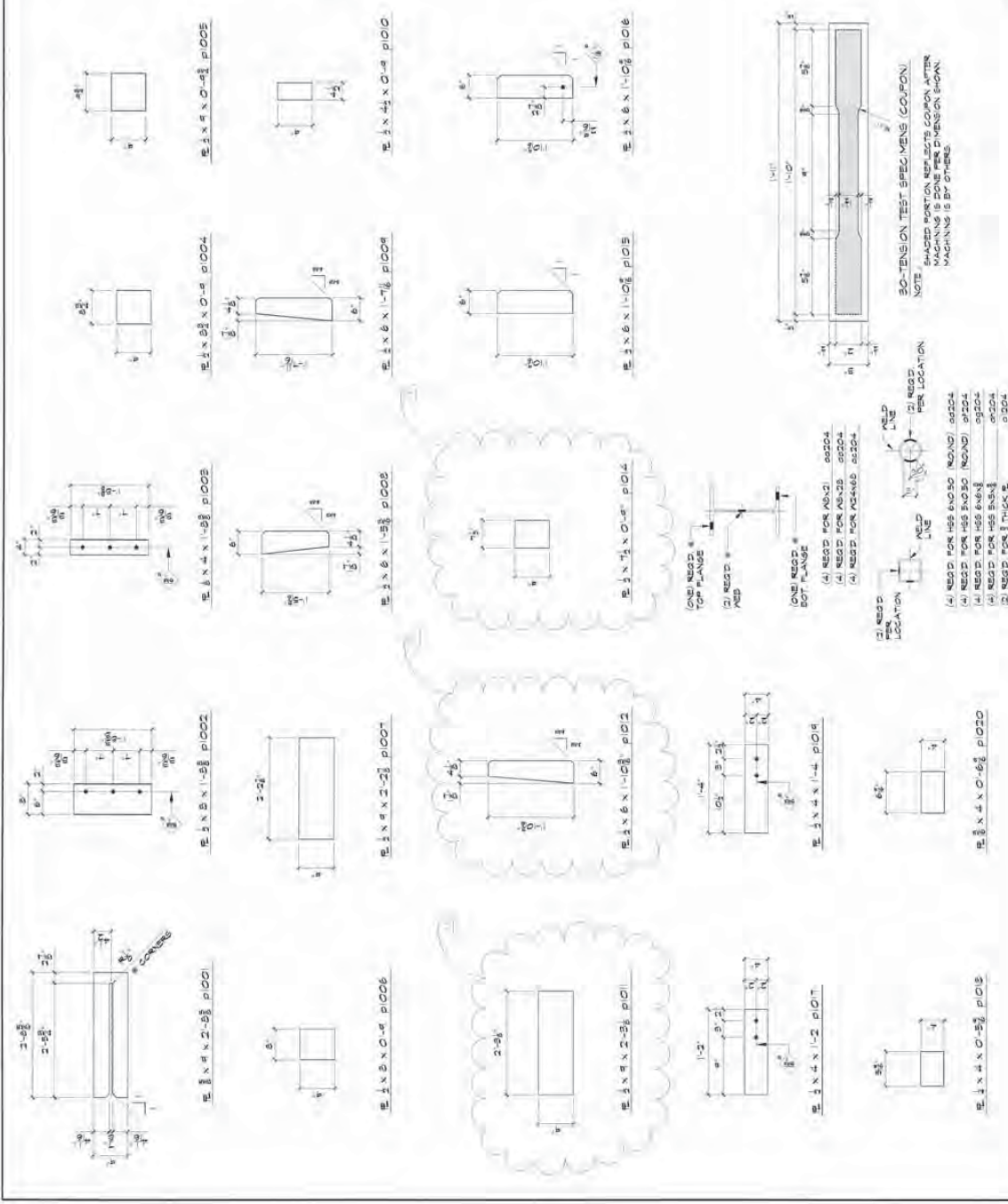
HSS SQUARE REPLACEMENT BRACING LAYOUT  
(BUS TESTING)

NO.	DATE	DESCRIPTION	BY	CHK
1	11-20-03	ISSUE FOR PERMIT	W. J. HERRICK	W. J. HERRICK
2	11-20-03	REVISED FOR PERMIT	W. J. HERRICK	W. J. HERRICK
3	11-20-03	REVISED FOR PERMIT	W. J. HERRICK	W. J. HERRICK
4	11-20-03	REVISED FOR PERMIT	W. J. HERRICK	W. J. HERRICK
5	11-20-03	REVISED FOR PERMIT	W. J. HERRICK	W. J. HERRICK
6	11-20-03	REVISED FOR PERMIT	W. J. HERRICK	W. J. HERRICK
7	11-20-03	REVISED FOR PERMIT	W. J. HERRICK	W. J. HERRICK
8	11-20-03	REVISED FOR PERMIT	W. J. HERRICK	W. J. HERRICK
9	11-20-03	REVISED FOR PERMIT	W. J. HERRICK	W. J. HERRICK
10	11-20-03	REVISED FOR PERMIT	W. J. HERRICK	W. J. HERRICK

# Herrick

DESIGNED BY	DATE	PROJECT	NO.	DATE	PROJECT	NO.
W. J. HERRICK	11-20-03	UNIVERSITY OF CALIFORNIA AT BERKELEY	1	11-20-03	UNIVERSITY OF CALIFORNIA AT BERKELEY	1
W. J. HERRICK	11-20-03	UNIVERSITY OF CALIFORNIA AT BERKELEY	2	11-20-03	UNIVERSITY OF CALIFORNIA AT BERKELEY	2
W. J. HERRICK	11-20-03	UNIVERSITY OF CALIFORNIA AT BERKELEY	3	11-20-03	UNIVERSITY OF CALIFORNIA AT BERKELEY	3
W. J. HERRICK	11-20-03	UNIVERSITY OF CALIFORNIA AT BERKELEY	4	11-20-03	UNIVERSITY OF CALIFORNIA AT BERKELEY	4
W. J. HERRICK	11-20-03	UNIVERSITY OF CALIFORNIA AT BERKELEY	5	11-20-03	UNIVERSITY OF CALIFORNIA AT BERKELEY	5
W. J. HERRICK	11-20-03	UNIVERSITY OF CALIFORNIA AT BERKELEY	6	11-20-03	UNIVERSITY OF CALIFORNIA AT BERKELEY	6
W. J. HERRICK	11-20-03	UNIVERSITY OF CALIFORNIA AT BERKELEY	7	11-20-03	UNIVERSITY OF CALIFORNIA AT BERKELEY	7
W. J. HERRICK	11-20-03	UNIVERSITY OF CALIFORNIA AT BERKELEY	8	11-20-03	UNIVERSITY OF CALIFORNIA AT BERKELEY	8
W. J. HERRICK	11-20-03	UNIVERSITY OF CALIFORNIA AT BERKELEY	9	11-20-03	UNIVERSITY OF CALIFORNIA AT BERKELEY	9
W. J. HERRICK	11-20-03	UNIVERSITY OF CALIFORNIA AT BERKELEY	10	11-20-03	UNIVERSITY OF CALIFORNIA AT BERKELEY	10

ITEM	DESCRIPTION	QTY	UNIT	STANDARD	REMARKS	DATE	BY
1	PLATE	1	PC	A36			
2	PLATE	1	PC	A36			
3	PLATE	1	PC	A36			
4	PLATE	1	PC	A36			
5	PLATE	1	PC	A36			
6	PLATE	1	PC	A36			
7	PLATE	1	PC	A36			
8	PLATE	1	PC	A36			
9	PLATE	1	PC	A36			
10	PLATE	1	PC	A36			
11	PLATE	1	PC	A36			
12	PLATE	1	PC	A36			
13	PLATE	1	PC	A36			
14	PLATE	1	PC	A36			
15	PLATE	1	PC	A36			
16	PLATE	1	PC	A36			
17	PLATE	1	PC	A36			
18	PLATE	1	PC	A36			
19	PLATE	1	PC	A36			
20	PLATE	1	PC	A36			
21	PLATE	1	PC	A36			
22	PLATE	1	PC	A36			
23	PLATE	1	PC	A36			
24	PLATE	1	PC	A36			
25	PLATE	1	PC	A36			
26	PLATE	1	PC	A36			
27	PLATE	1	PC	A36			
28	PLATE	1	PC	A36			
29	PLATE	1	PC	A36			
30	PLATE	1	PC	A36			
31	PLATE	1	PC	A36			
32	PLATE	1	PC	A36			
33	PLATE	1	PC	A36			
34	PLATE	1	PC	A36			
35	PLATE	1	PC	A36			
36	PLATE	1	PC	A36			
37	PLATE	1	PC	A36			
38	PLATE	1	PC	A36			
39	PLATE	1	PC	A36			
40	PLATE	1	PC	A36			
41	PLATE	1	PC	A36			
42	PLATE	1	PC	A36			
43	PLATE	1	PC	A36			
44	PLATE	1	PC	A36			
45	PLATE	1	PC	A36			
46	PLATE	1	PC	A36			
47	PLATE	1	PC	A36			
48	PLATE	1	PC	A36			
49	PLATE	1	PC	A36			
50	PLATE	1	PC	A36			



1	PLATE	1	PC	A36			
2	PLATE	1	PC	A36			
3	PLATE	1	PC	A36			
4	PLATE	1	PC	A36			
5	PLATE	1	PC	A36			
6	PLATE	1	PC	A36			
7	PLATE	1	PC	A36			
8	PLATE	1	PC	A36			
9	PLATE	1	PC	A36			
10	PLATE	1	PC	A36			
11	PLATE	1	PC	A36			
12	PLATE	1	PC	A36			
13	PLATE	1	PC	A36			
14	PLATE	1	PC	A36			
15	PLATE	1	PC	A36			
16	PLATE	1	PC	A36			
17	PLATE	1	PC	A36			
18	PLATE	1	PC	A36			
19	PLATE	1	PC	A36			
20	PLATE	1	PC	A36			
21	PLATE	1	PC	A36			
22	PLATE	1	PC	A36			
23	PLATE	1	PC	A36			
24	PLATE	1	PC	A36			
25	PLATE	1	PC	A36			
26	PLATE	1	PC	A36			
27	PLATE	1	PC	A36			
28	PLATE	1	PC	A36			
29	PLATE	1	PC	A36			
30	PLATE	1	PC	A36			
31	PLATE	1	PC	A36			
32	PLATE	1	PC	A36			
33	PLATE	1	PC	A36			
34	PLATE	1	PC	A36			
35	PLATE	1	PC	A36			
36	PLATE	1	PC	A36			
37	PLATE	1	PC	A36			
38	PLATE	1	PC	A36			
39	PLATE	1	PC	A36			
40	PLATE	1	PC	A36			
41	PLATE	1	PC	A36			
42	PLATE	1	PC	A36			
43	PLATE	1	PC	A36			
44	PLATE	1	PC	A36			
45	PLATE	1	PC	A36			
46	PLATE	1	PC	A36			
47	PLATE	1	PC	A36			
48	PLATE	1	PC	A36			
49	PLATE	1	PC	A36			
50	PLATE	1	PC	A36			

**Herrick**

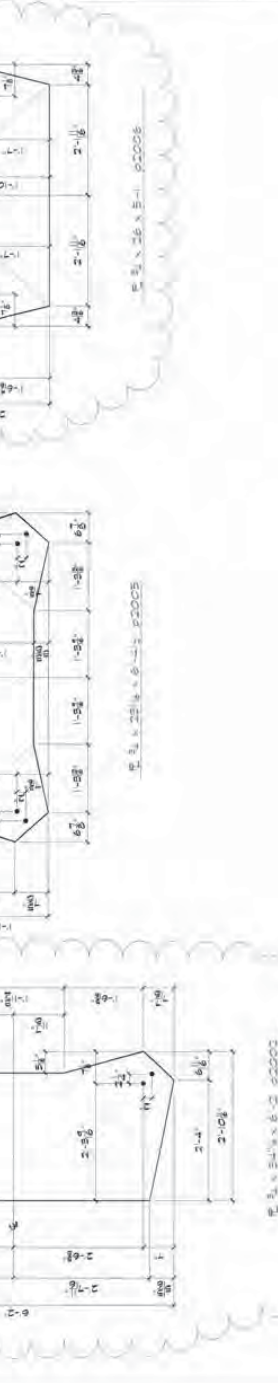
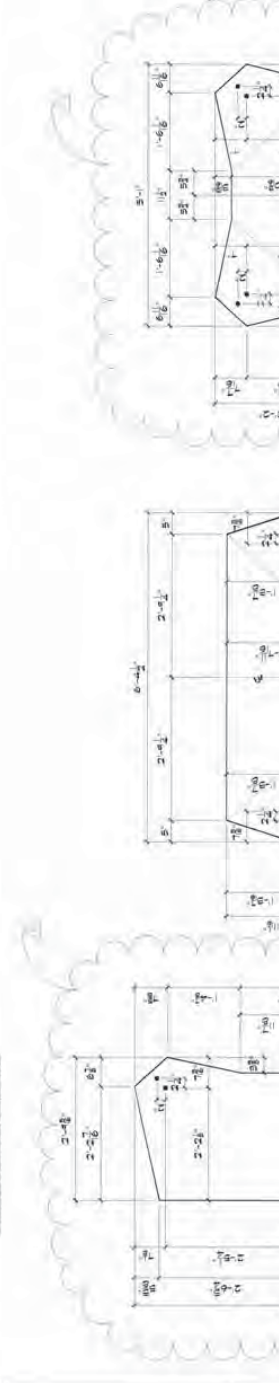
UNIVERSITY OF CALIFORNIA AT BERKELEY  
 SPECIMEN DRAGGING REPLACEMENT  
 BERKELEY, CA

DATE: 10/10/2014  
 DRAWN BY: AE  
 CHECKED BY: AE  
 PART: 08-10-1004  
 SHEET: 1 OF 1

30-TENSION TEST SPECIMENS (COUPON)  
 NOTE: MACHINED PORTION REFLECTS COMMON PRACTICE MACHINING IS DONE PER DIMENSION SHOWN

LEGEND:  
 (1) REQD FOR A36  
 (2) REQD FOR A36S  
 (3) REQD FOR A36SS  
 (4) REQD FOR A36SS (ROUND)  
 (5) REQD FOR A36SS (ROUND)  
 (6) REQD FOR A36SS (ROUND)  
 (7) REQD FOR A36SS (ROUND)  
 (8) REQD FOR A36SS (ROUND)  
 (9) REQD FOR A36SS (ROUND)  
 (10) REQD FOR A36SS (ROUND)

SUM OF MATERIALS			
QTY	DESCRIPTION	UNIT	REMARKS
3	E 1/2" x 1/2"	PC2001	3 1/2"
2	E 1/2" x 1/2"	PC2002	2 1/2"
2	E 1/2" x 1/2"	PC2003	2 1/2"
2	E 1/2" x 1/2"	PC2004	2 1/2"
ONE	E 1/2" x 1/2"	PC2005	2 1/2"
ONE	E 1/2" x 1/2"	PC2006	2 1/2"



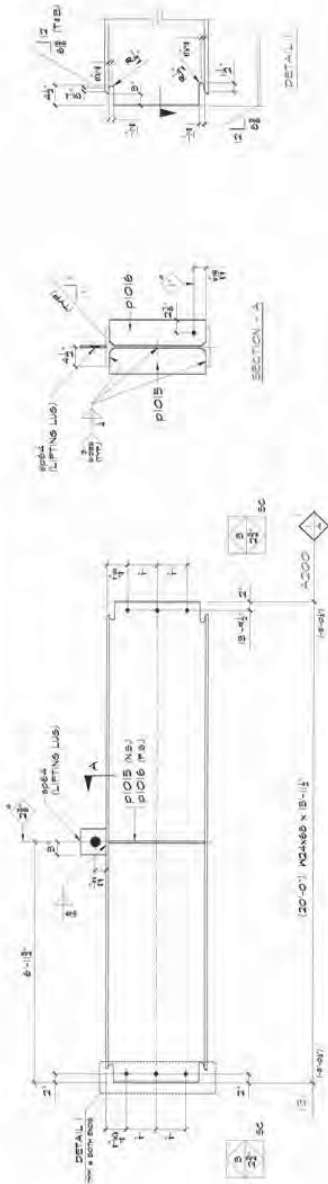
REV	DATE	DESCRIPTION	BY	CHK
1	10/10/00	REVISED	...	...
2	10/10/00	REVISED	...	...
3	10/10/00	REVISED	...	...

SHEET PLATES  
 UNIVERSITY OF CALIFORNIA AT BERKELEY  
 SOEP SPECIMEN BRACING REPLACEMENT  
 BERKELEY, CA

**Herrick**  
 1000 16th St  
 Berkeley, CA 94710

Bill of Materials

QTY	DESCRIPTION	UNIT	MARK	REV.	REMARKS	DATE
1	BEAM	1	1000	1		
1	FLANGE	1	1000	1		
1	W/	1	1000	1		
1	W/	1	1000	1		
1	W/	1	1000	1		
1	W/	1	1000	1		



REV.	DATE	DESCRIPTION	BY	CHK.
1		1. ADD	B. M	
2		2. CHANGE	B. M	
3		3. ADD	B. M	
4		4. CHANGE	B. M	
5		5. ADD	B. M	
6		6. CHANGE	B. M	

DRAWN BY: B. M  
 CHECKED BY: A. M  
 DATE: 09-20-00  
 PROJECT: 05-01-000

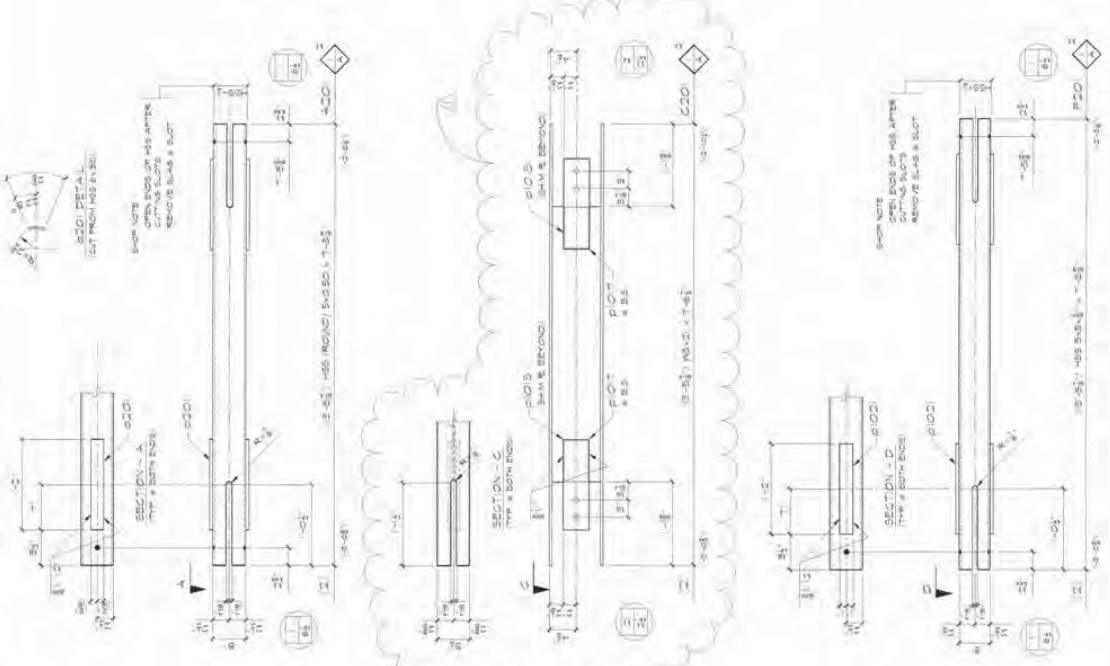
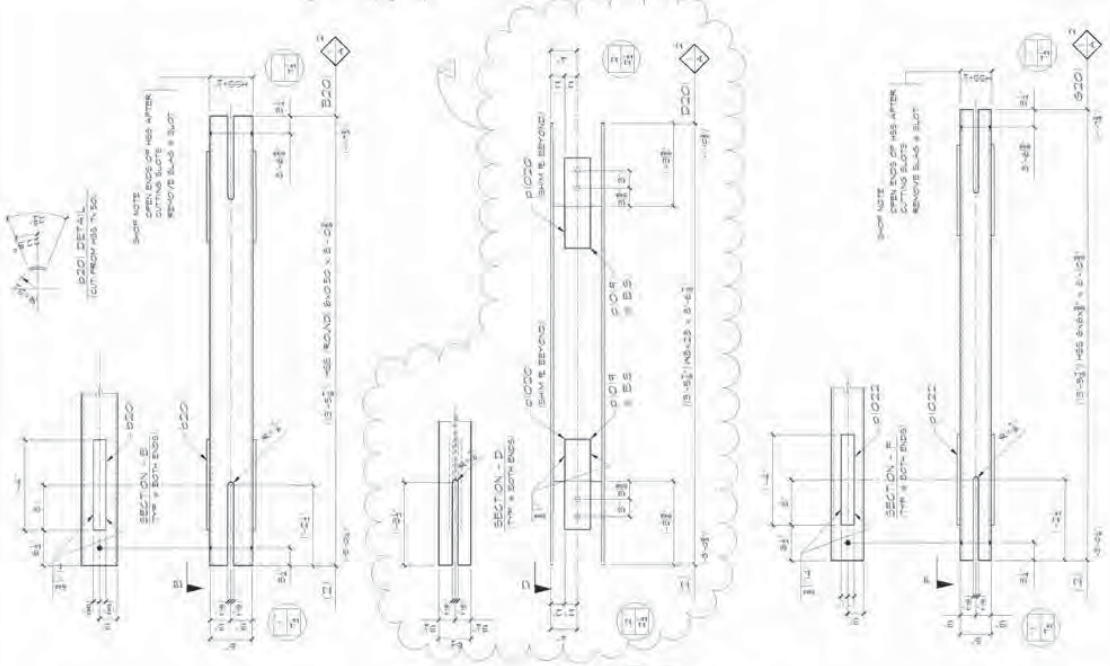
UNIVERSITY OF CALIFORNIA AT BERKELEY  
 SOOP SPECIFIC BRACING REPLACEMENT  
 BERKELEY, CA.

HERRICK  
 ORIGINAL  
 HERRICK

DATE: 08-04-00  
 SCALE: AS SHOWN  
 SHEET: 10 OF 10

**BILL OF MATERIALS**

QTY	DESCRIPTION	ENVIRONMENTAL MARK	PK	REMARKS	CODE
3	MS BRACE	5 1/4" AS20	6		MS-0
3	MS END BRACE	10 5/8" AS20	6		MS-0
3	MS 1/8" BRACKET	10 5/8" AS20	6		MS-0
3	MS 1/8" BRACKET	10 5/8" AS20	6		MS-0
3	MS BRACE	5 1/4" AS20	6		MS-0
3	MS END BRACE	10 5/8" AS20	6		MS-0
3	MS 1/8" BRACKET	10 5/8" AS20	6		MS-0
3	MS 1/8" BRACKET	10 5/8" AS20	6		MS-0
3	MS BRACE	5 1/4" AS20	6		MS-0
3	MS END BRACE	10 5/8" AS20	6		MS-0
3	MS 1/8" BRACKET	10 5/8" AS20	6		MS-0
3	MS 1/8" BRACKET	10 5/8" AS20	6		MS-0
3	MS BRACE	5 1/4" AS20	6		MS-0
3	MS END BRACE	10 5/8" AS20	6		MS-0
3	MS 1/8" BRACKET	10 5/8" AS20	6		MS-0
3	MS 1/8" BRACKET	10 5/8" AS20	6		MS-0
3	MS BRACE	5 1/4" AS20	6		MS-0
3	MS END BRACE	10 5/8" AS20	6		MS-0
3	MS 1/8" BRACKET	10 5/8" AS20	6		MS-0
3	MS 1/8" BRACKET	10 5/8" AS20	6		MS-0
3	MS BRACE	5 1/4" AS20	6		MS-0
3	MS END BRACE	10 5/8" AS20	6		MS-0
3	MS 1/8" BRACKET	10 5/8" AS20	6		MS-0
3	MS 1/8" BRACKET	10 5/8" AS20	6		MS-0
3	MS BRACE	5 1/4" AS20	6		MS-0
3	MS END BRACE	10 5/8" AS20	6		MS-0
3	MS 1/8" BRACKET	10 5/8" AS20	6		MS-0
3	MS 1/8" BRACKET	10 5/8" AS20	6		MS-0



REV.	DATE	BY	DESCRIPTION	NO.	REV.
1	08-20-04	JK	ISSUED FOR FABRICATION	1	1
2	08-20-04	JK	ISSUED FOR FABRICATION	2	2
3	08-20-04	JK	ISSUED FOR FABRICATION	3	3
4	08-20-04	JK	ISSUED FOR FABRICATION	4	4

UNIVERSITY OF CALIFORNIA, BERKELEY  
 SOEP DESIGN BRACING REPLACEMENT  
 BERKELEY, CA

**Herrick**

DESIGNED BY: JK  
 CHECKED BY: JK  
 DATE: 08-20-04

PROJECT NO.: MS-0  
 SHEET NO.: 1

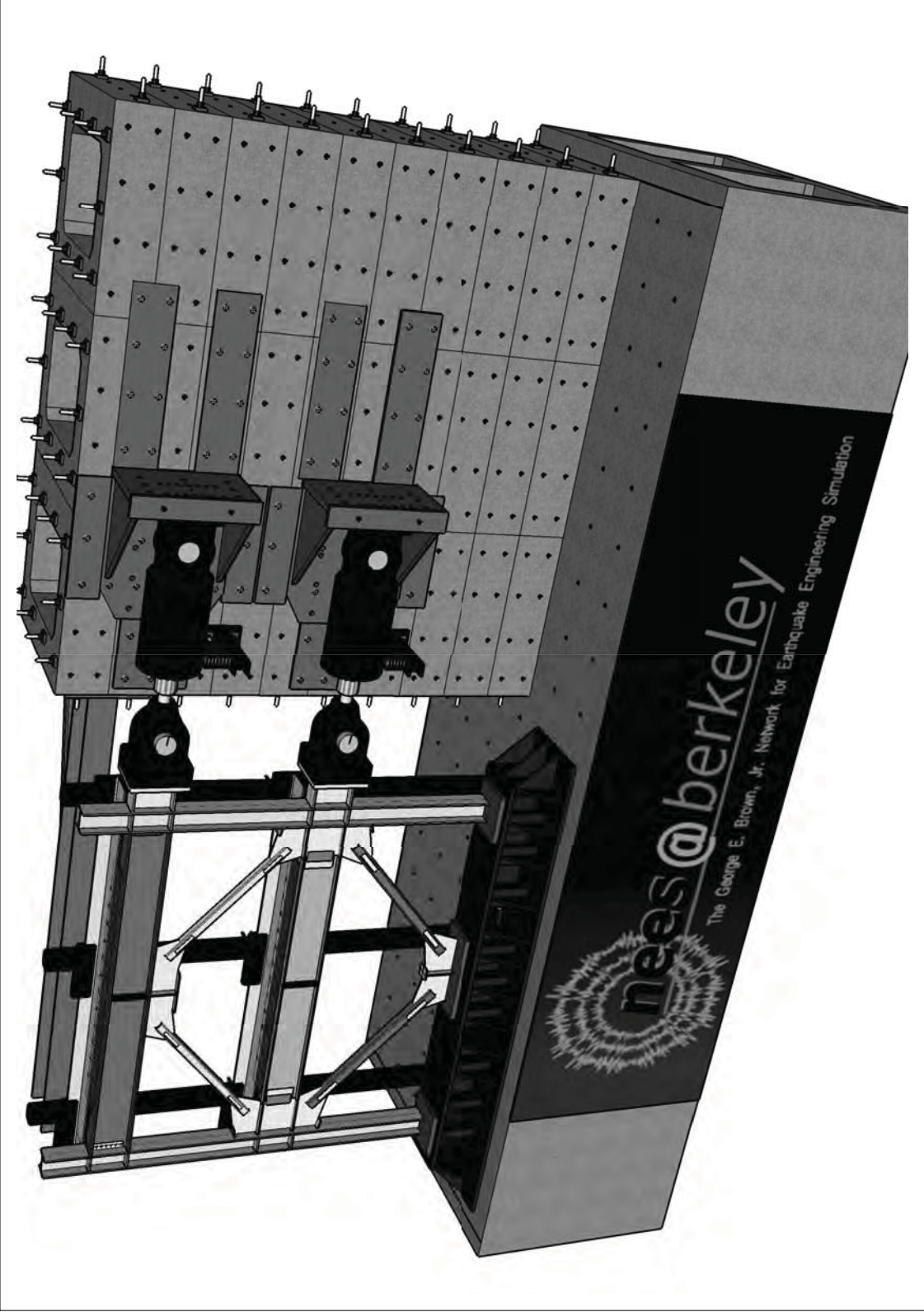


---

## **Appendix D**

### **Channel Locations and Lists for TCBF-B-1 Specimen**

---



**TCBF-B-1, Sensor Locations  
S.00**

**ISSUE**  
Aug 01, 2009

**DRAWN BY**  
Jiun-Wei Lai

**PROJECT NO.**  
TCBF-B-1

**PROJECT**  
TCBF

International Hybrid  
Simulation of  
Tomorrow's Braced  
Steel Frame Structures







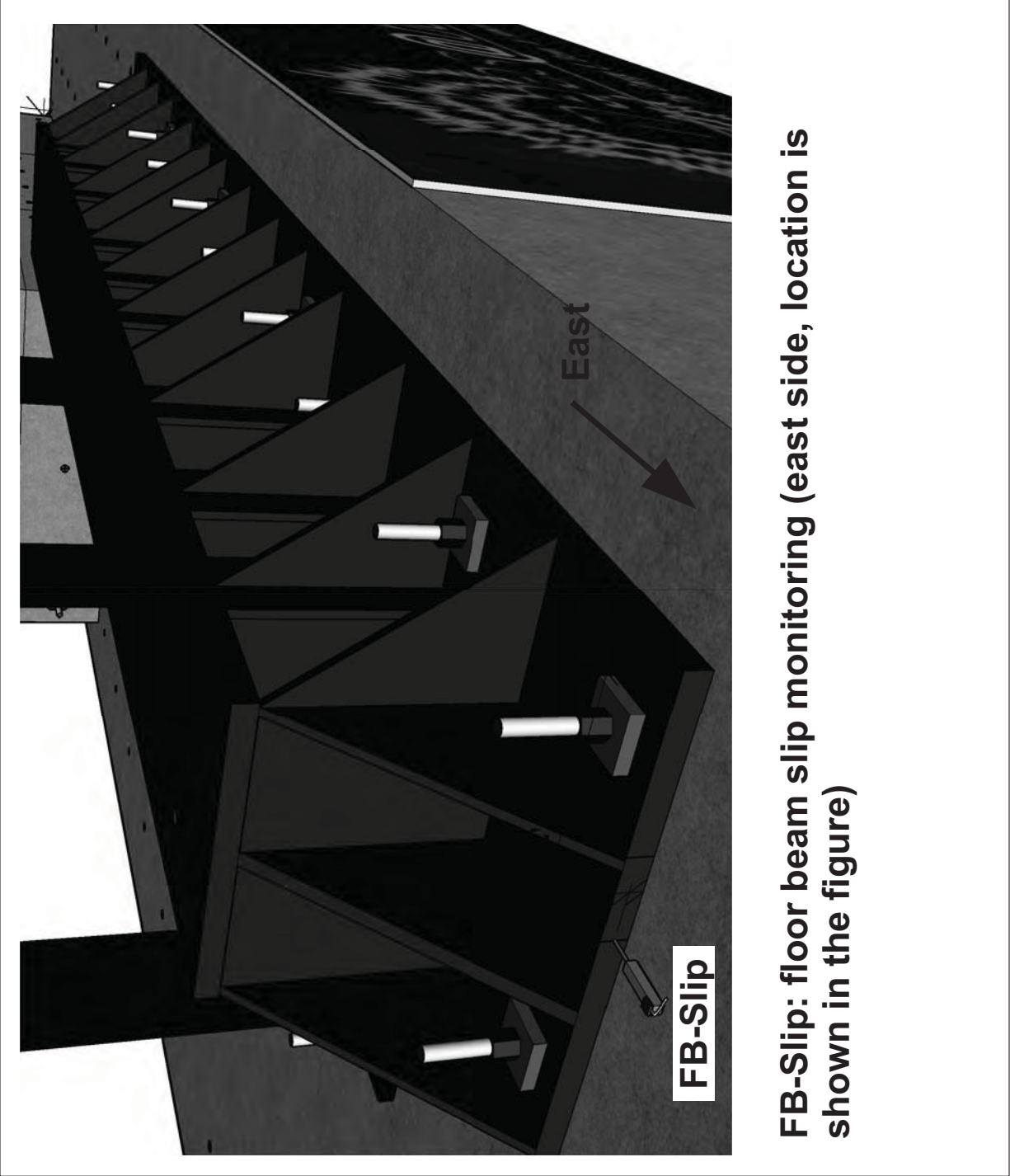
International Hybrid  
Simulation of  
Tomorrow's Braced  
Steel Frame  
Structures

University of California,  
Berkeley  
TCBF-B-1

PROJECT  
TCFB  
Aug 01,  
2009  
DRAWN BY  
J.W. Lai  
PROJECT NO.  
TCBF-B-1

Sensor  
Locations

S.01





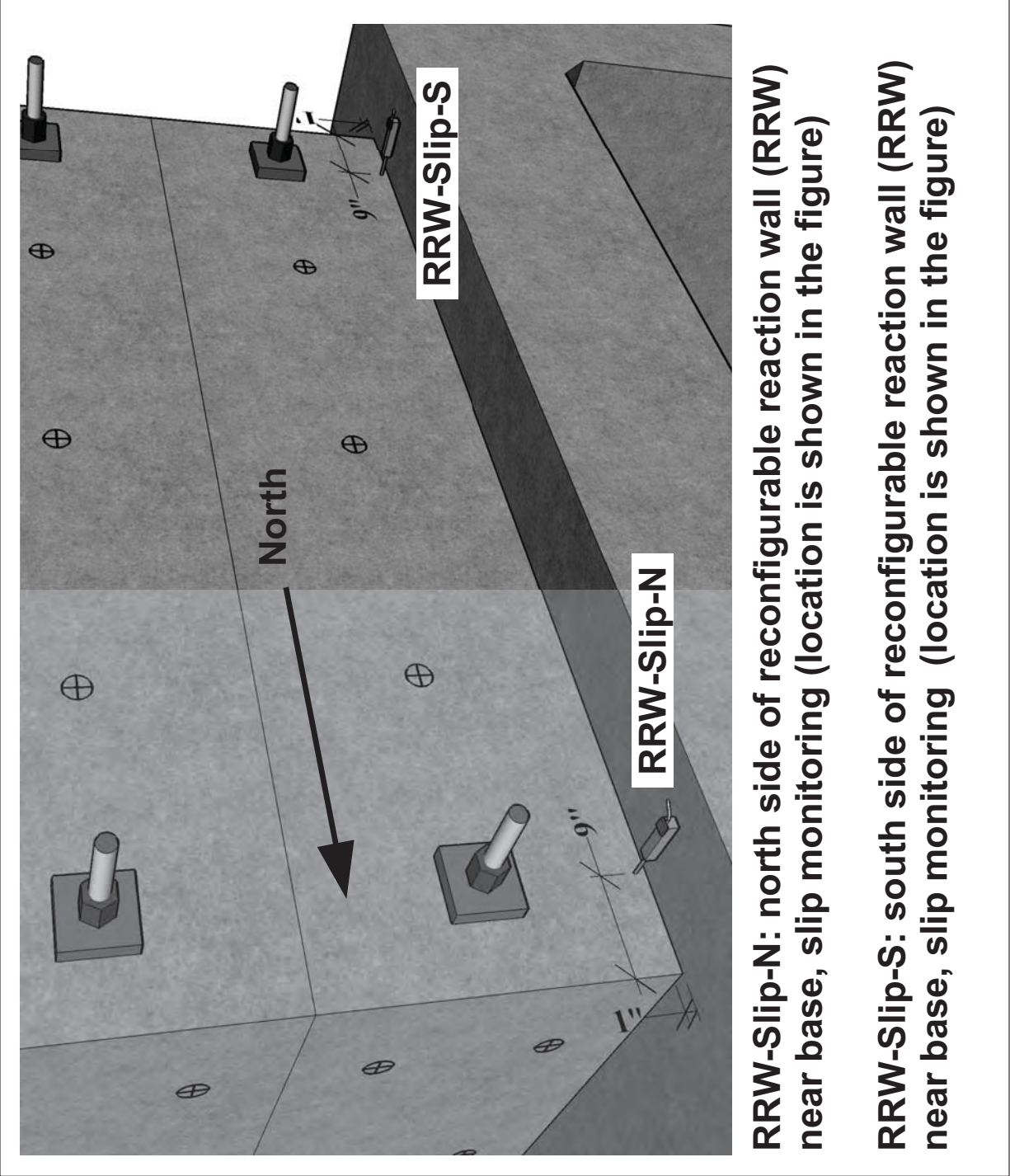
International Hybrid  
Simulation of  
Tomorrow's Braced  
Steel Frame  
Structures

University of California,  
Berkeley  
TCBF-B-1

PROJECT  
TCFB  
Aug 01,  
2009  
ISSUE  
DRAWN BY  
J.W. Lai  
PROJECT NO.  
TCBF-B-1

Sensor  
Locations

**S.02**





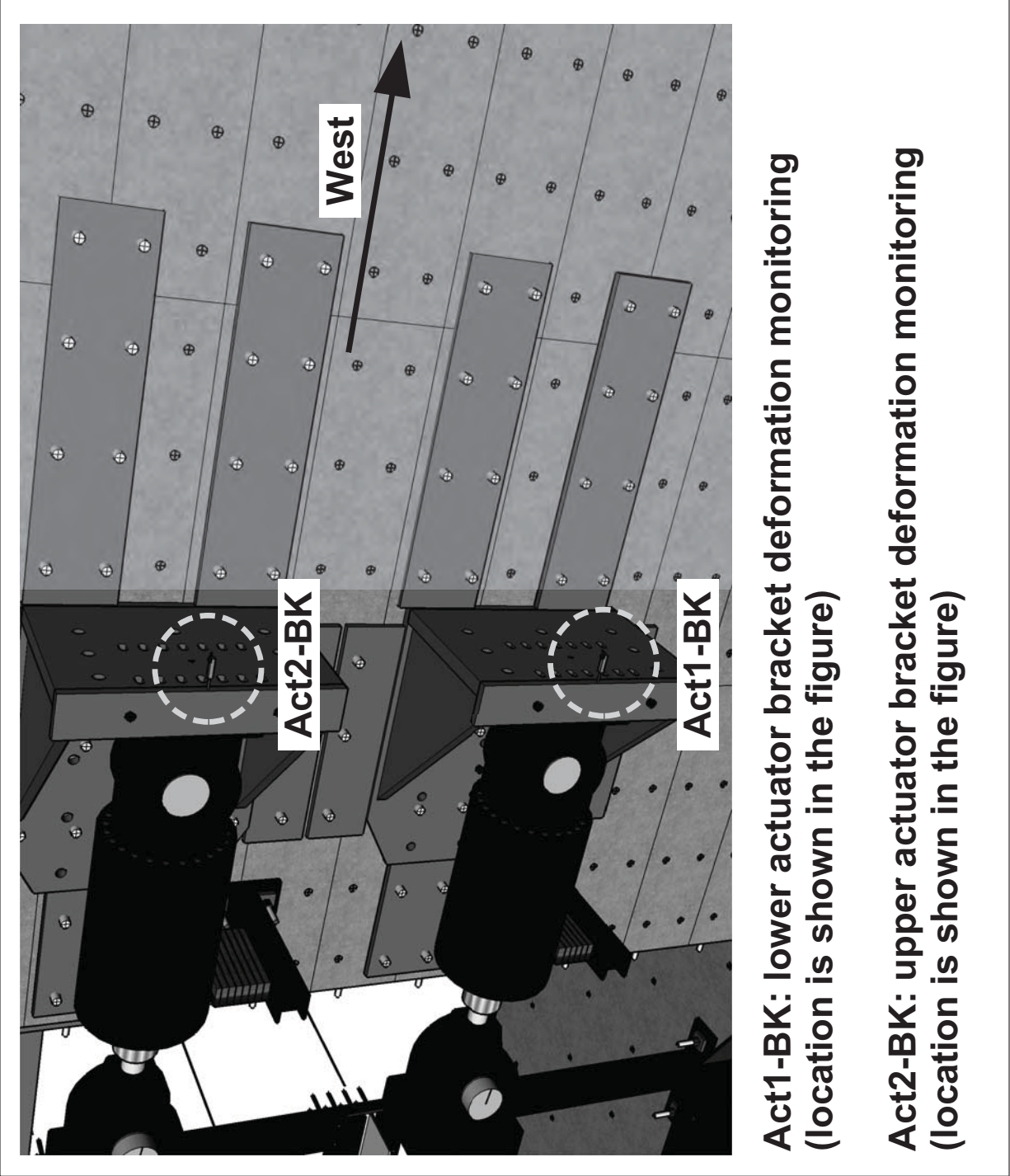
International Hybrid  
Simulation of  
Tomorrow's Braced  
Steel Frame  
Structures

University of California,  
Berkeley  
TCBF-B-1

PROJECT  
TCFB  
Aug 01,  
2009  
ISSUE  
DRAWN BY  
J.W. Lai  
PROJECT NO.  
TCBF-B-1

Sensor  
Locations

S.03



**Act1-BK: lower actuator bracket deformation monitoring  
(location is shown in the figure)**

**Act2-BK: upper actuator bracket deformation monitoring  
(location is shown in the figure)**



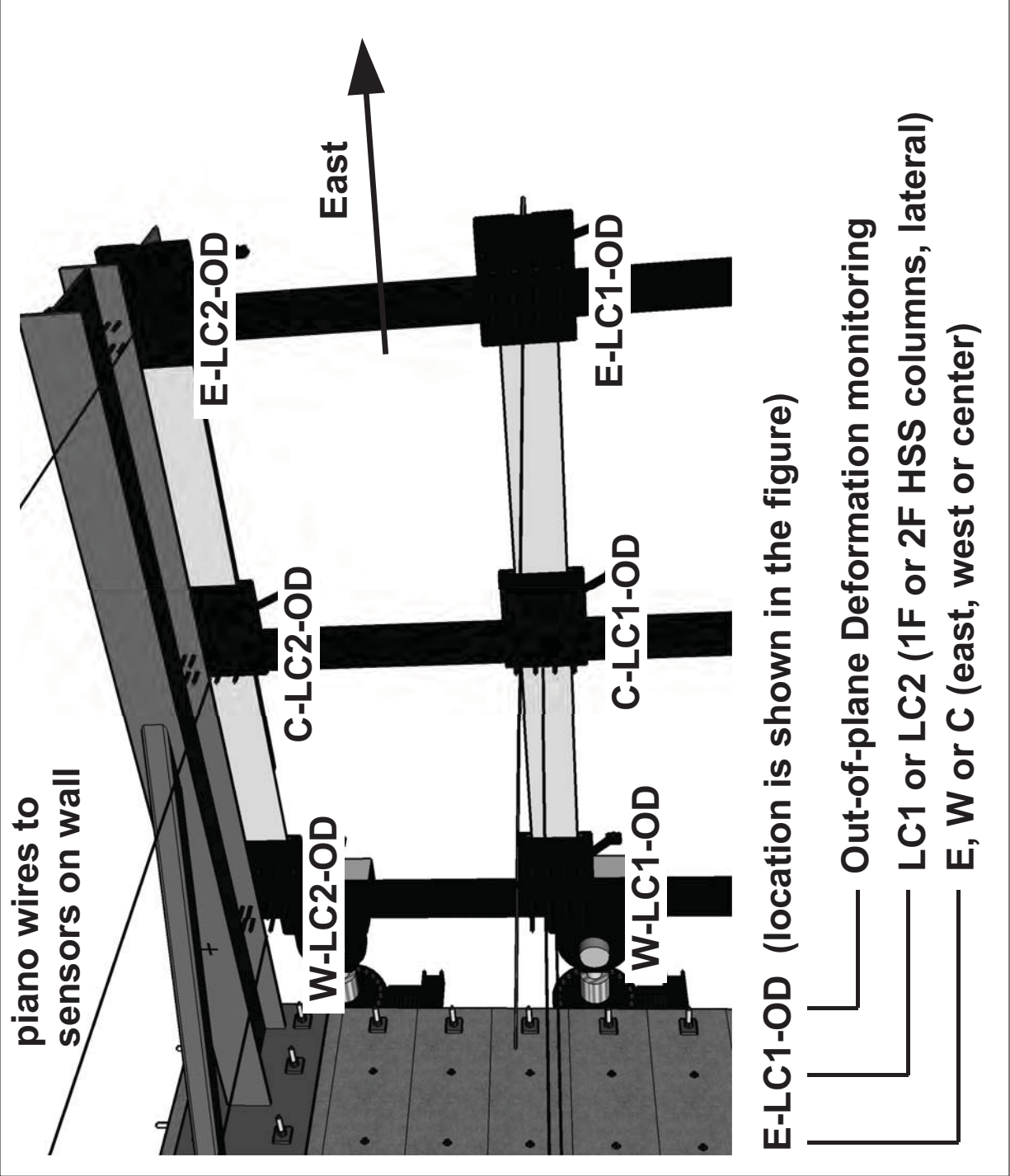
International Hybrid  
Simulation of  
Tomorrow's Braced  
Steel Frame  
Structures

University of California,  
Berkeley  
TCBF-B-1

PROJECT  
TCFB  
Aug 01,  
2009  
DRAWN BY  
J.W. Lai  
TCBF-B-1  
PROJECT NO.

Sensor  
Locations

S.04





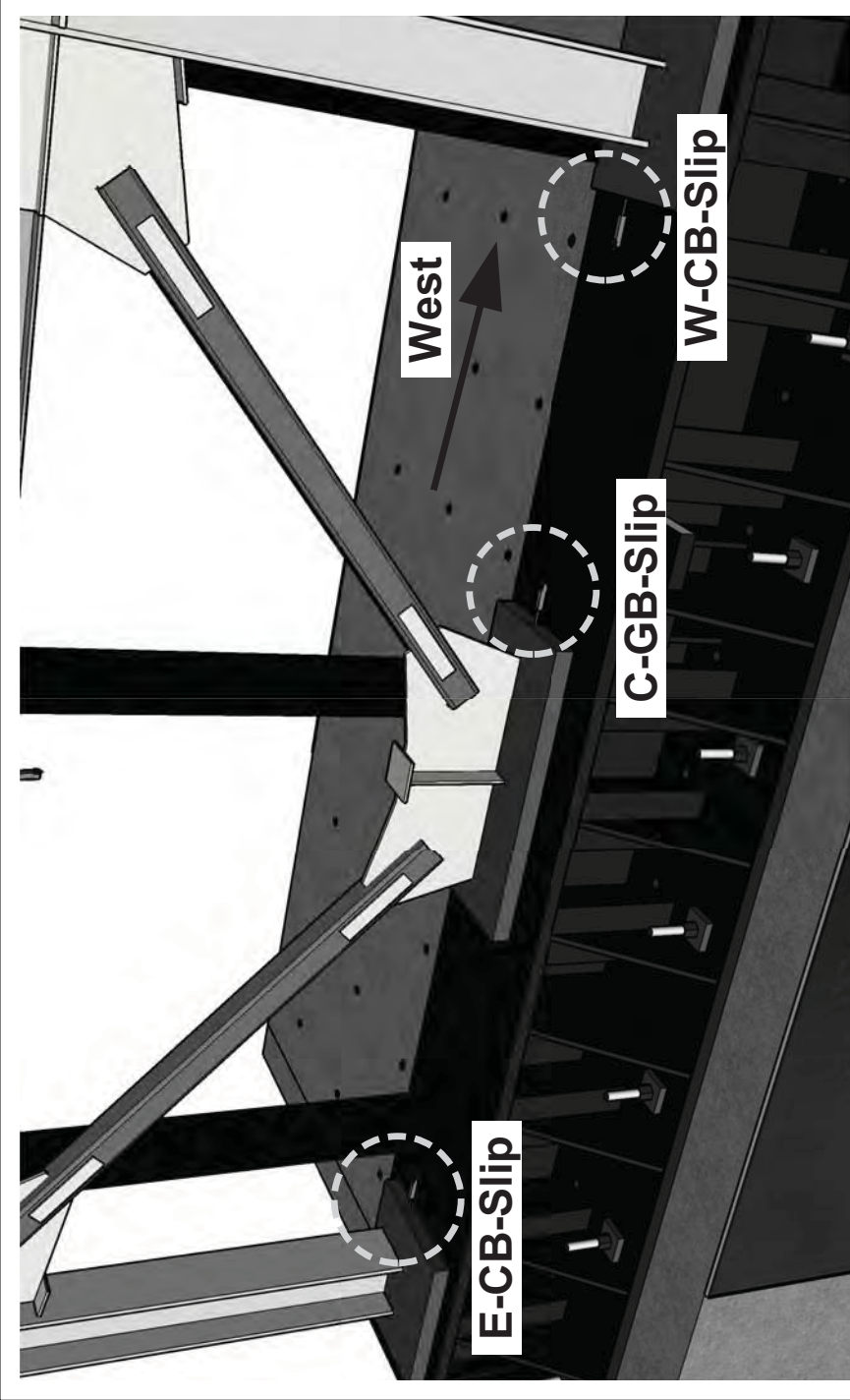
International Hybrid  
Simulation of  
Tomorrow's Braced  
Steel Frame  
Structures

University of California,  
Berkeley  
TCBF-B-1

PROJECT  
TCFB  
Aug 01,  
2009  
DRAWN BY  
J.W. Lai  
PROJECT NO.  
TCBF-B-1

## Sensor Locations

### S.05



**E-CB-Slip: east column base slip monitoring**  
**C-GB-Slip: center gusset plate base slip monitoring**  
**W-CB-Slip: west column base slip monitoring**  
 (locations are shown in the figure, align with the brace  
 frame center plane)



International Hybrid  
Simulation of  
Tomorrow's Braced  
Steel Frame  
Structures

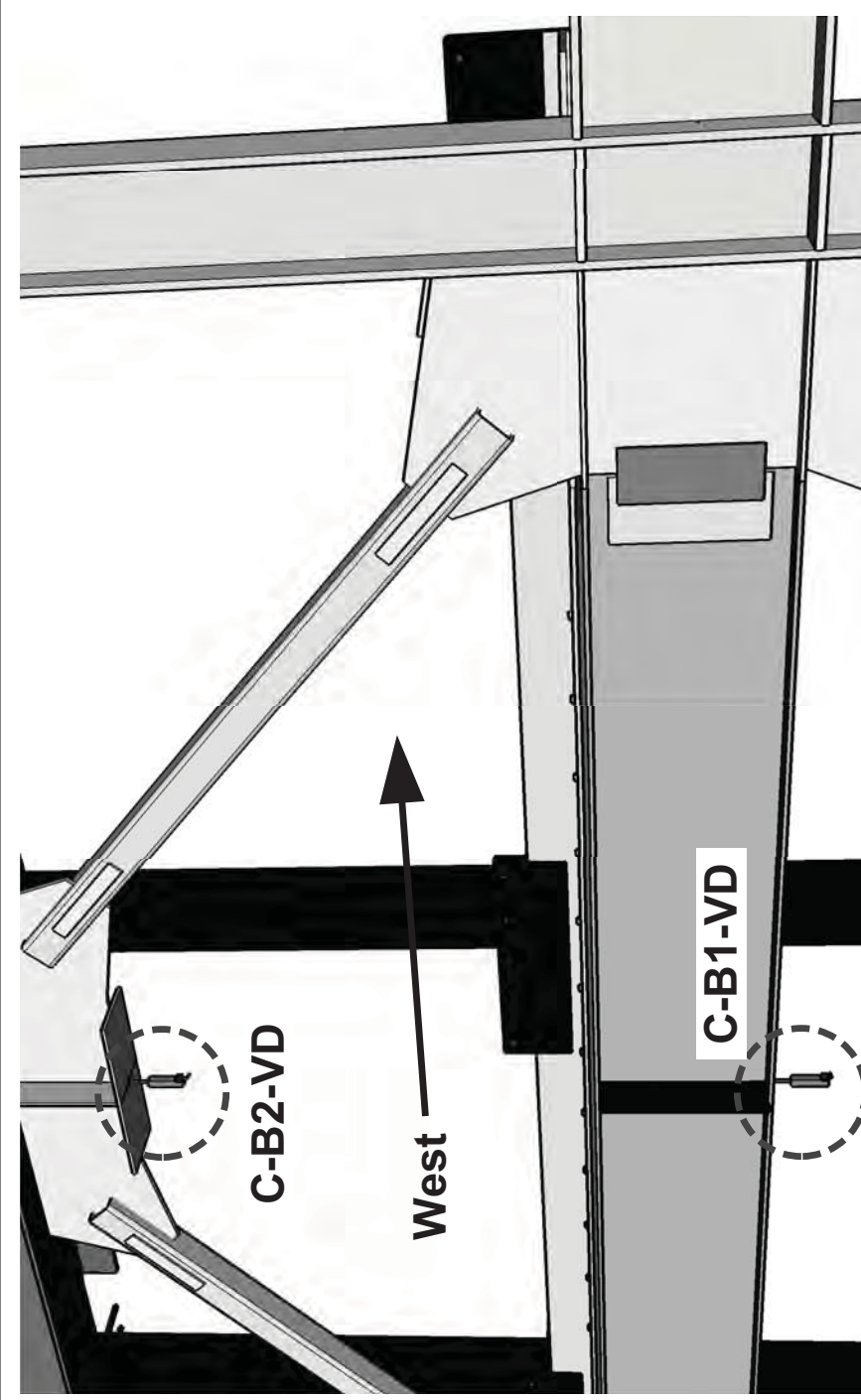
University of California,  
Berkeley  
TCBF-B-1

PROJECT  
TCFB  
TCBF-B-1

ISSUE  
Aug 01,  
2009  
DRAWN BY  
J.W. Lai

Sensor  
Locations

S.06



**C-B2-VD: roof beam (2F) center deflection monitoring**  
**C-B1-VD: lower beam (1F) center deflection monitoring**  
 (locations are shown in the figure, align with the beam bottom flange center line)



International Hybrid  
Simulation of  
Tomorrow's Braced  
Steel Frame  
Structures

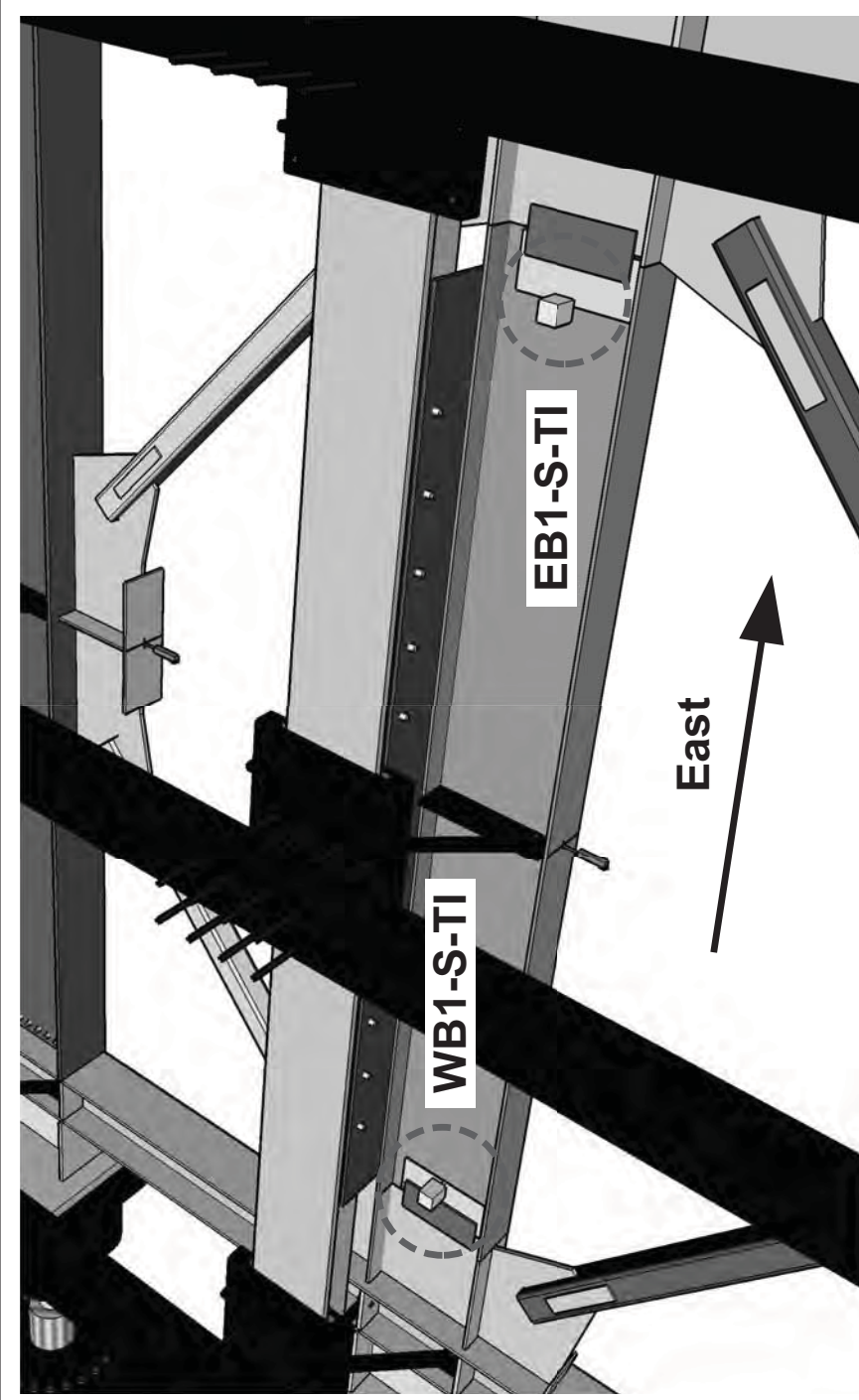
University of California,  
Berkeley  
TCBF-B-1

PROJECT  
TCFB  
Aug 01,  
2009

ISSUE  
Aug 01,  
2009  
DRAWN BY  
J.W. Lai

Sensor  
Locations

S.07



WB1-S-TI: west lower beam (1F) rotation monitoring  
EB1-S-TI: east lower beam (1F) rotation monitoring

(locations are shown in the figure, align with the beam web center line)



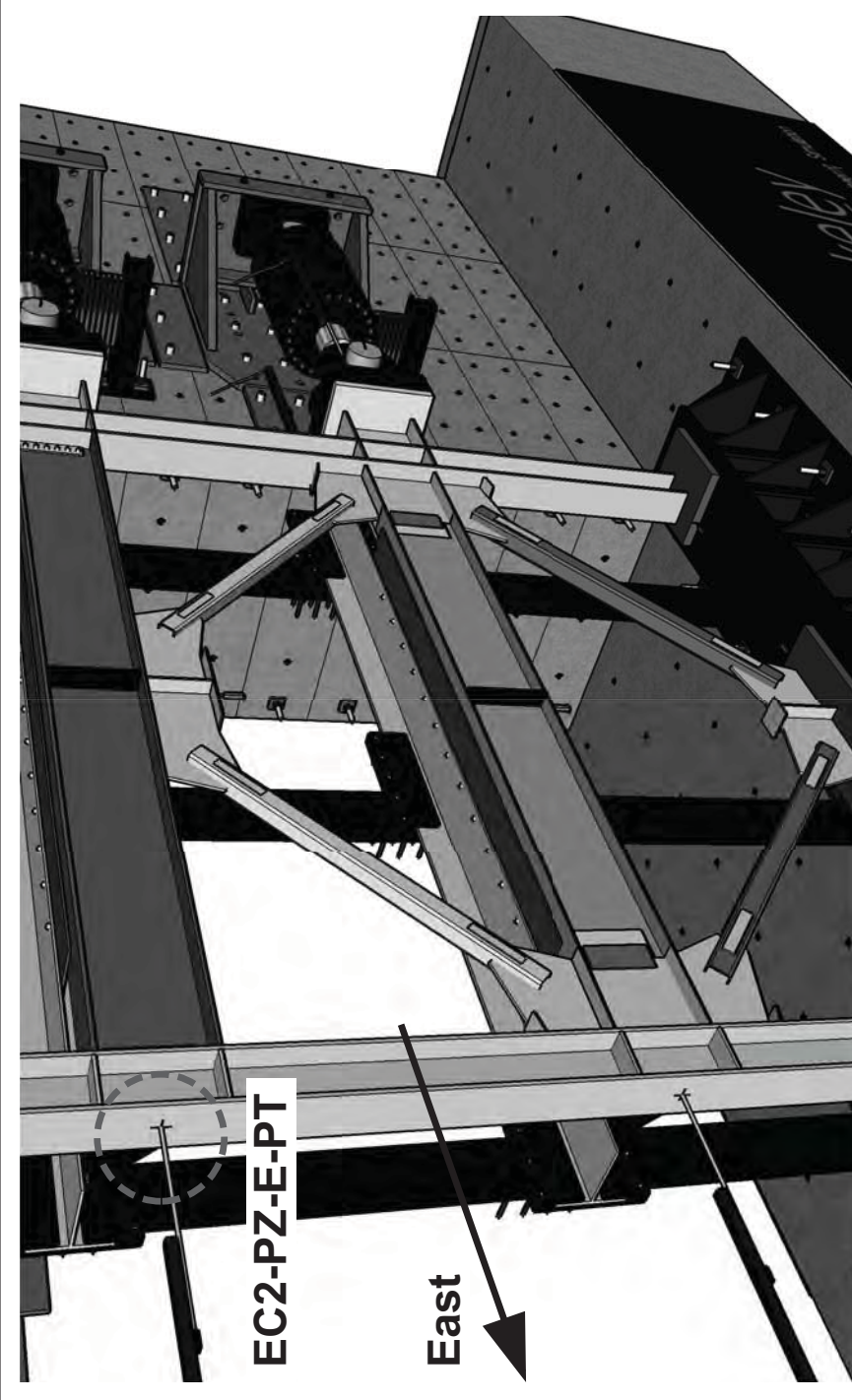
International Hybrid  
Simulation of  
Tomorrow's Braced  
Steel Frame  
Structures

University of California,  
Berkeley  
TCBF-B-1

PROJECT  
TCFB  
Aug 01,  
2009  
ISSUE  
DRAWN BY  
J.W. Lai  
PROJECT NO.  
TCBF-B-1

Sensor  
Locations

S.08



**EC2-PZ-E-PT: roof level (2F) displacement monitoring**

**(locations are shown in the figure, align with the beam center line at each level)**





International Hybrid  
Simulation of  
Tomorrow's Braced  
Steel Frame  
Structures

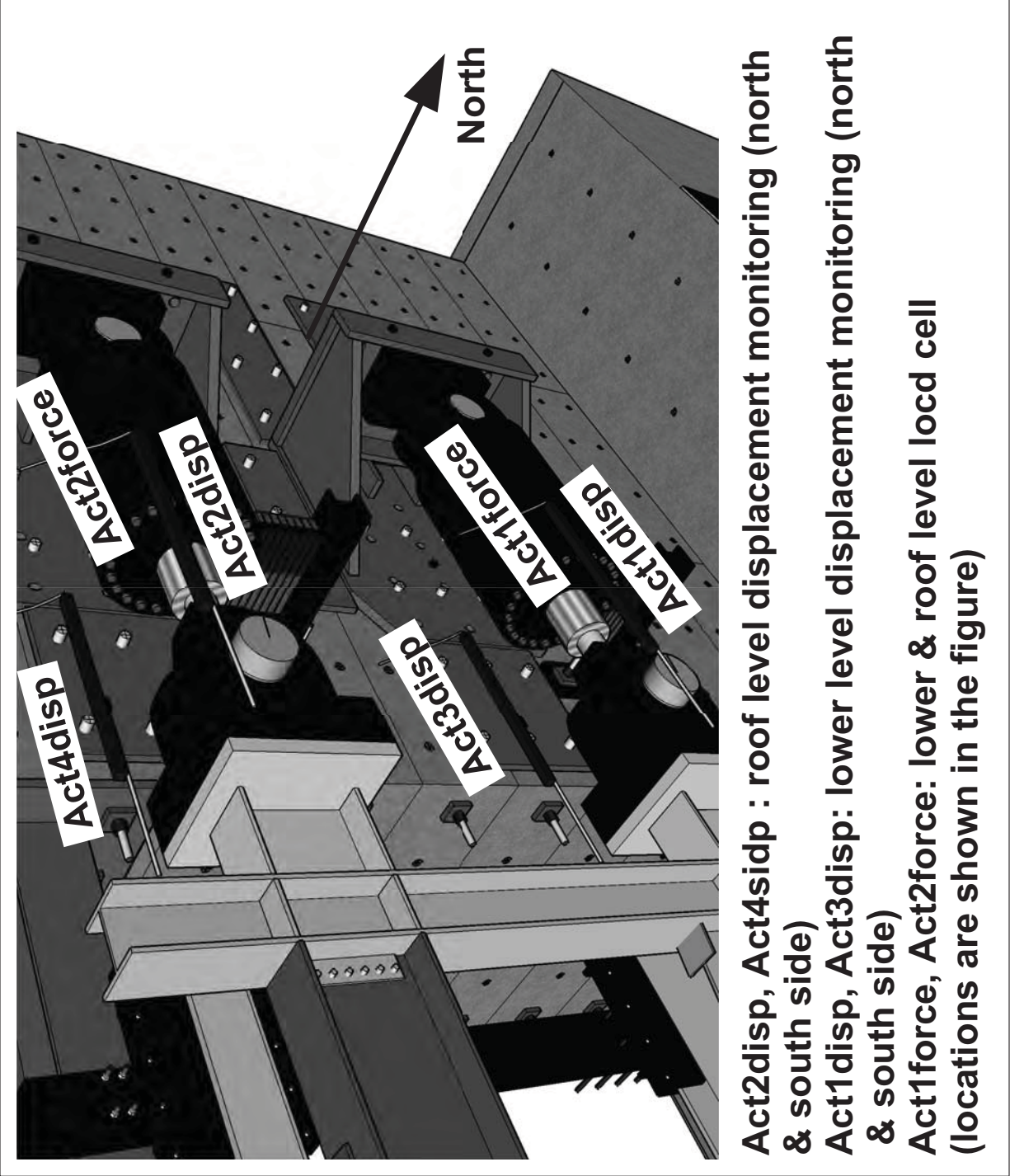
University of California,  
Berkeley  
TCBF-B-1

PROJECT  
TCFB  
Aug 01,  
2009

ISSUE  
Aug 01,  
2009  
DRAWN BY  
J.W. Lai

Sensor  
Locations

S.09





International Hybrid  
Simulation of  
Tomorrow's Braced  
Steel Frame  
Structures

University of California,  
Berkeley  
TCBF-B-1

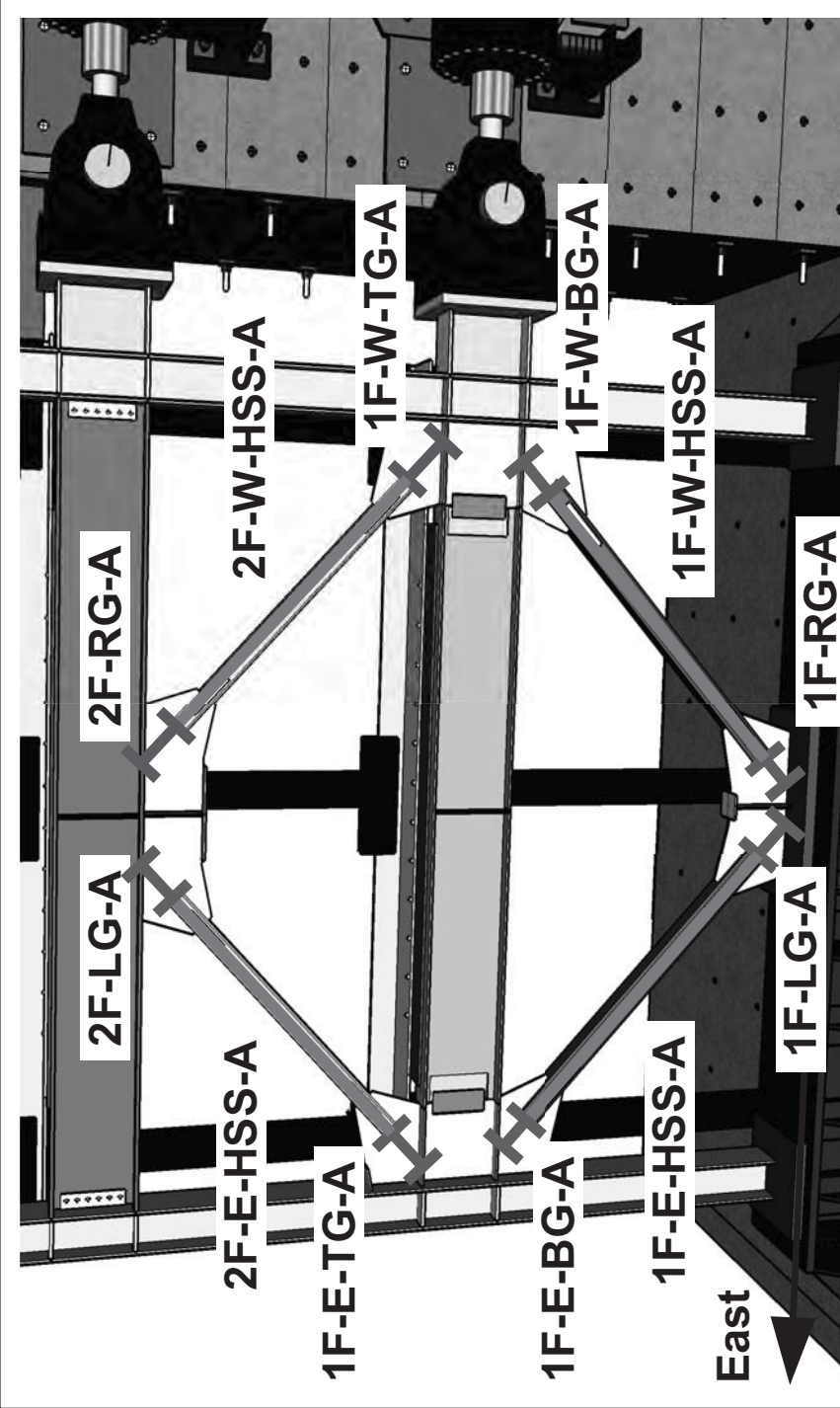
PROJECT  
TCFB  
Aug 01,  
2009

ISSUE  
Aug 01,  
2009  
DRAWN BY  
J.W. Lai

PROJECT NO.  
TCBF-B-1

Sensor  
Locations

S-10



LG: left gusset plate region; RG: right gusset plate region  
TG: top gusset plate region; BG: bottom gusset plate region  
E: east side; W: west side; A: axial

brace axial deformation monitoring along the axis of brace  
(wire pot locations are shown in the figure)



International Hybrid  
Simulation of  
Tomorrow's Braced  
Steel Frame  
Structures

University of California,  
Berkeley  
TCBF-B-1

PROJECT  
TCFB  
2009

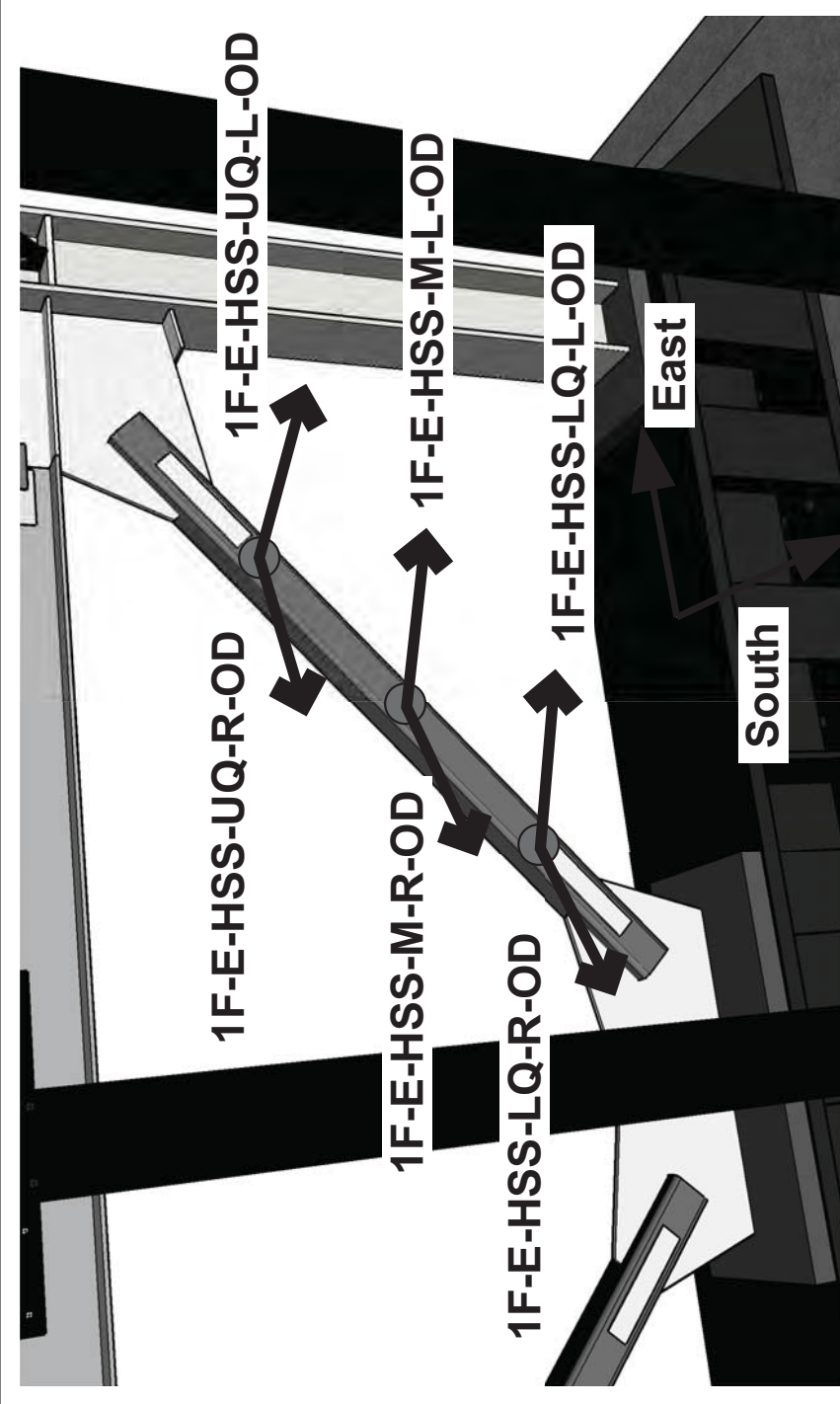
ISSUE  
Aug 01,  
2009

DRAWN BY  
J.W. Lai

PROJECT NO.  
TCBF-B-1

## Sensor Locations

### S.11



Typical brace out-of-plane deformation monitoring (wire pot directions are shown in the figure for one brace, other braces are similar, six wire pots per brace)

1F-E-HSS-UQ-R-OD

- \_\_\_\_\_ lefthand (L) or righthand (R) side when facing to south
- \_\_\_\_\_ upper quarter (UQ), middle (M) or lower quarter point (LQ)
- \_\_\_\_\_ east side brace (E-HSS) or west side brace (W-HSS)
- \_\_\_\_\_ first story (1F) or second story brace (2F)



International Hybrid  
Simulation of  
Tomorrow's Braced  
Steel Frame  
Structures

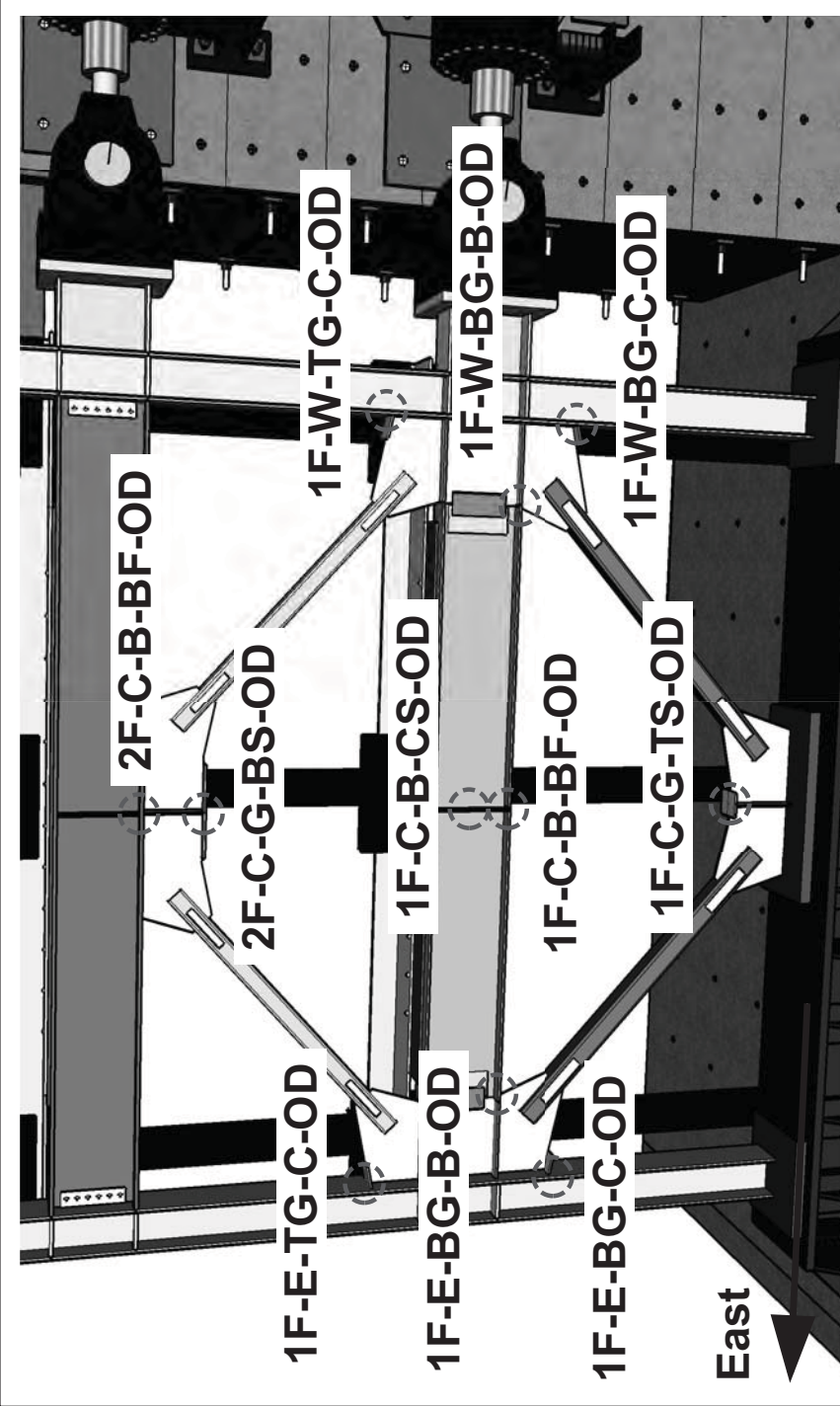
University of California,  
Berkeley  
TCBF-B-1

PROJECT  
TCFB  
PROJECT NO.  
TCBF-B-1

ISSUE  
Aug 01,  
2009  
DRAWN BY  
J.W. Lai

## Sensor Locations

**S-12**



**C:** column side corner; **B:** beam side corner  
**C-B:** beam center point; **BF:** bottom flange corner  
**BS, CS:** bottom stiffener corner, center stiffener corner  
**TG:** top gusset plate region; **BG:** bottom gusset plate region  
**E:** east side; **W:** west side; **A:** axial; **1F, 2F:** 1st & 2nd story  
 (wire pot target locations are shown in the figure)



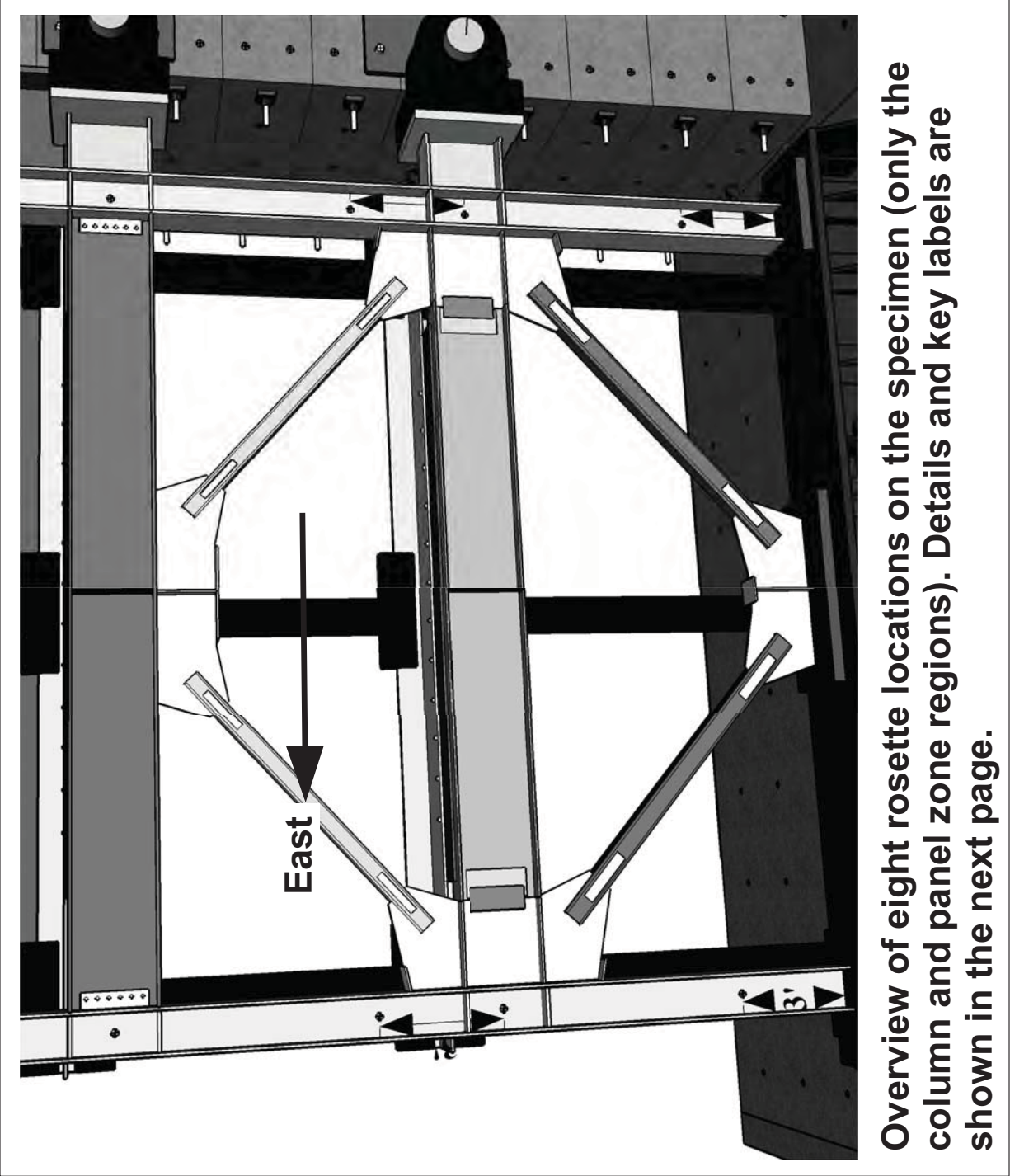
International Hybrid  
Simulation of  
Tomorrow's Braced  
Steel Frame  
Structures

University of California,  
Berkeley  
TCBF-B-1

PROJECT  
TCFB  
Aug 01,  
2009  
ISSUE  
DRAWN BY  
J.W. Lai  
PROJECT NO.  
TCBF-B-1

Sensor  
Locations

S-13



Overview of eight rosette locations on the specimen (only the column and panel zone regions). Details and key labels are shown in the next page.



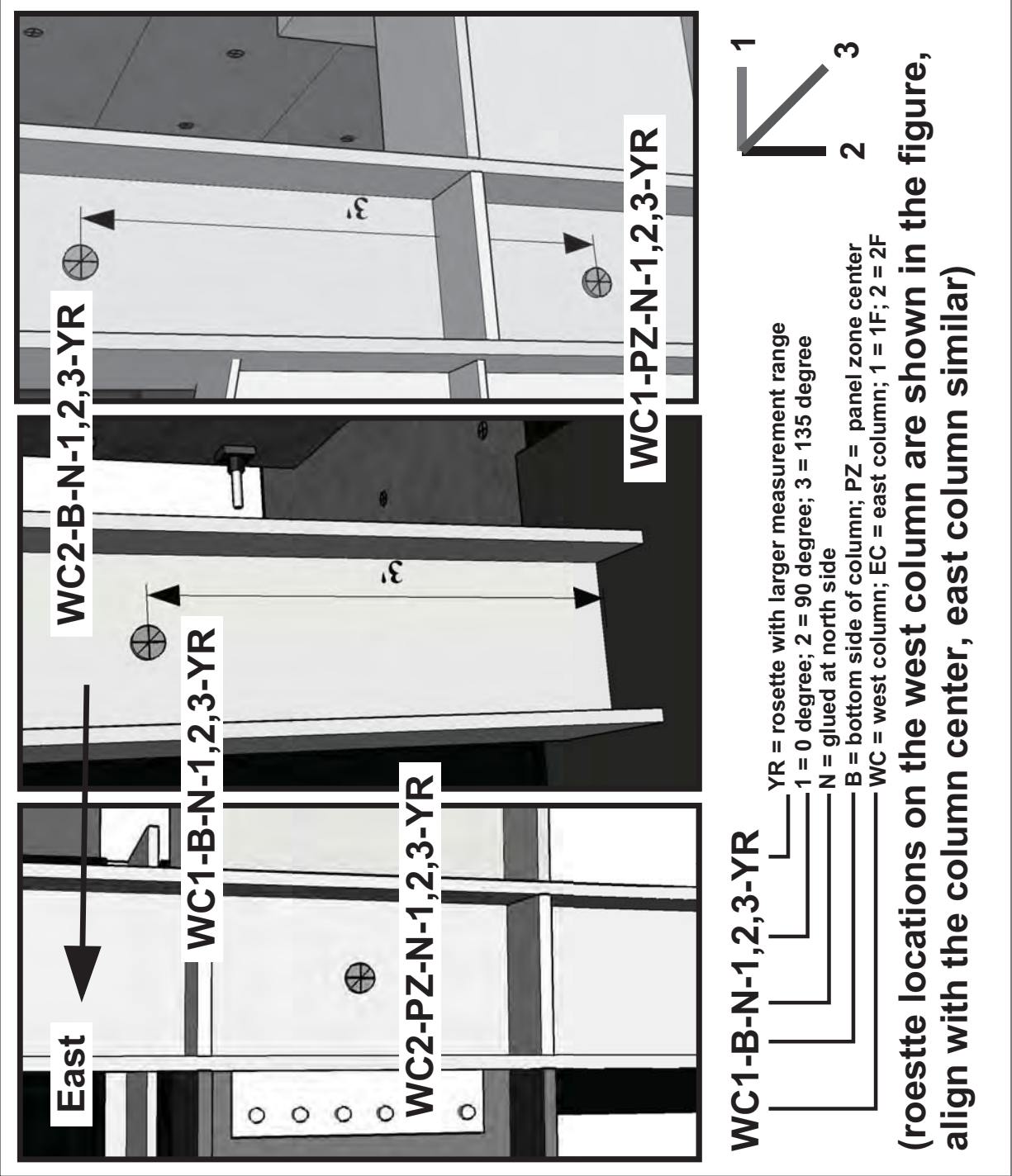
International Hybrid  
Simulation of  
Tomorrow's Braced  
Steel Frame  
Structures

University of California,  
Berkeley  
TCBF-B-1

PROJECT  
TCFB  
Aug 01, 2009  
DRAWN BY  
J.W. Lai  
TCBF-B-1  
PROJECT NO.

Sensor  
Locations

S-14





International Hybrid  
Simulation of  
Tomorrow's Braced  
Steel Frame  
Structures

University of California,  
Berkeley  
TCBF-B-1

PROJECT  
TCFB  
Aug 01, 2009  
ISSUE  
DRAWN BY  
J.W. Lai  
PROJECT NO.  
TCBF-B-1

Sensor  
Locations

S-15

**1F-E-TG-TL-1,2,3-N-YR**

**1F-E = east gusset plate**

**TG = top region**

**MG = middle region**

**BG = bottom region**

**TL = top left side**

**BL = bottom left side**

**TR = top right side**

**BR = bottom right side**

**TC = top center**

**BC = bottom center**

**1 = 0 degree (direction)**

**2 = 90 degree**

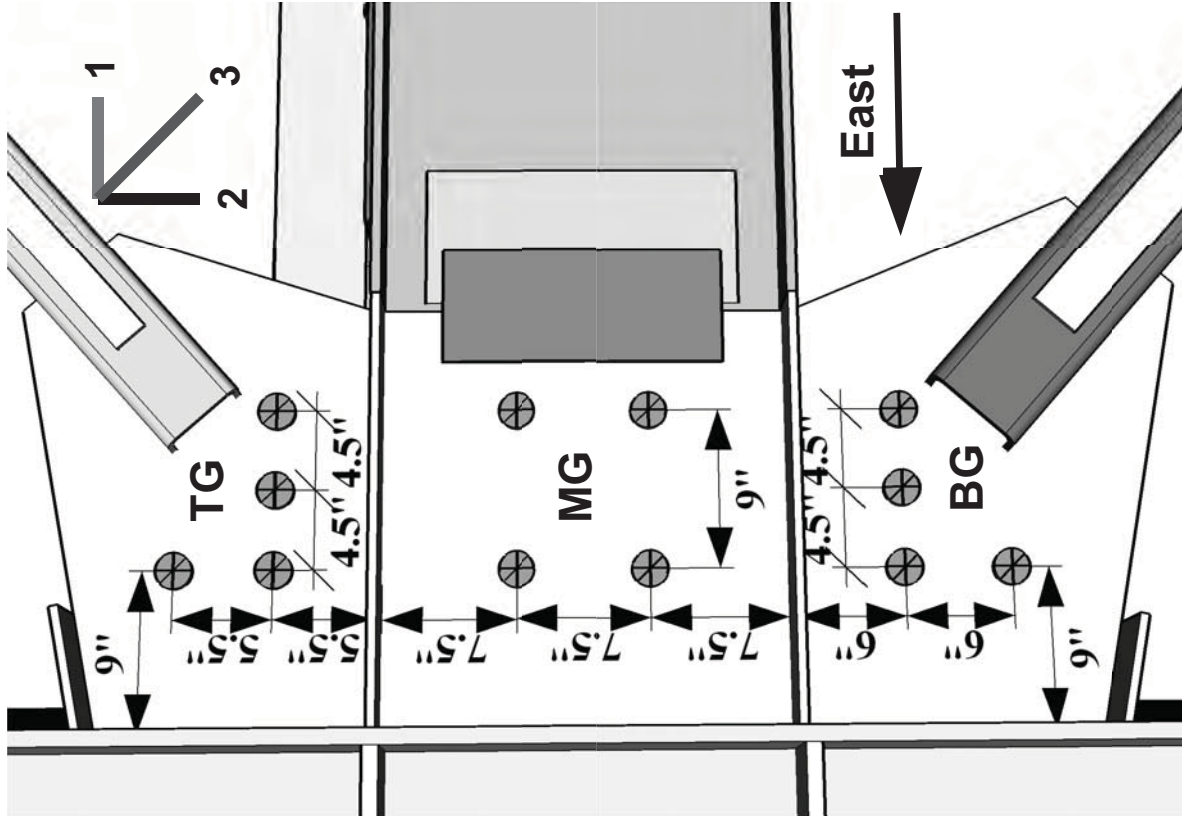
**3 = 135 degree**

**N = glued on north side**

**YR = rosette with larger**

**measurement range**

**(twelve rosette locations on the one-piece gusset plate, key labels are shown above)**





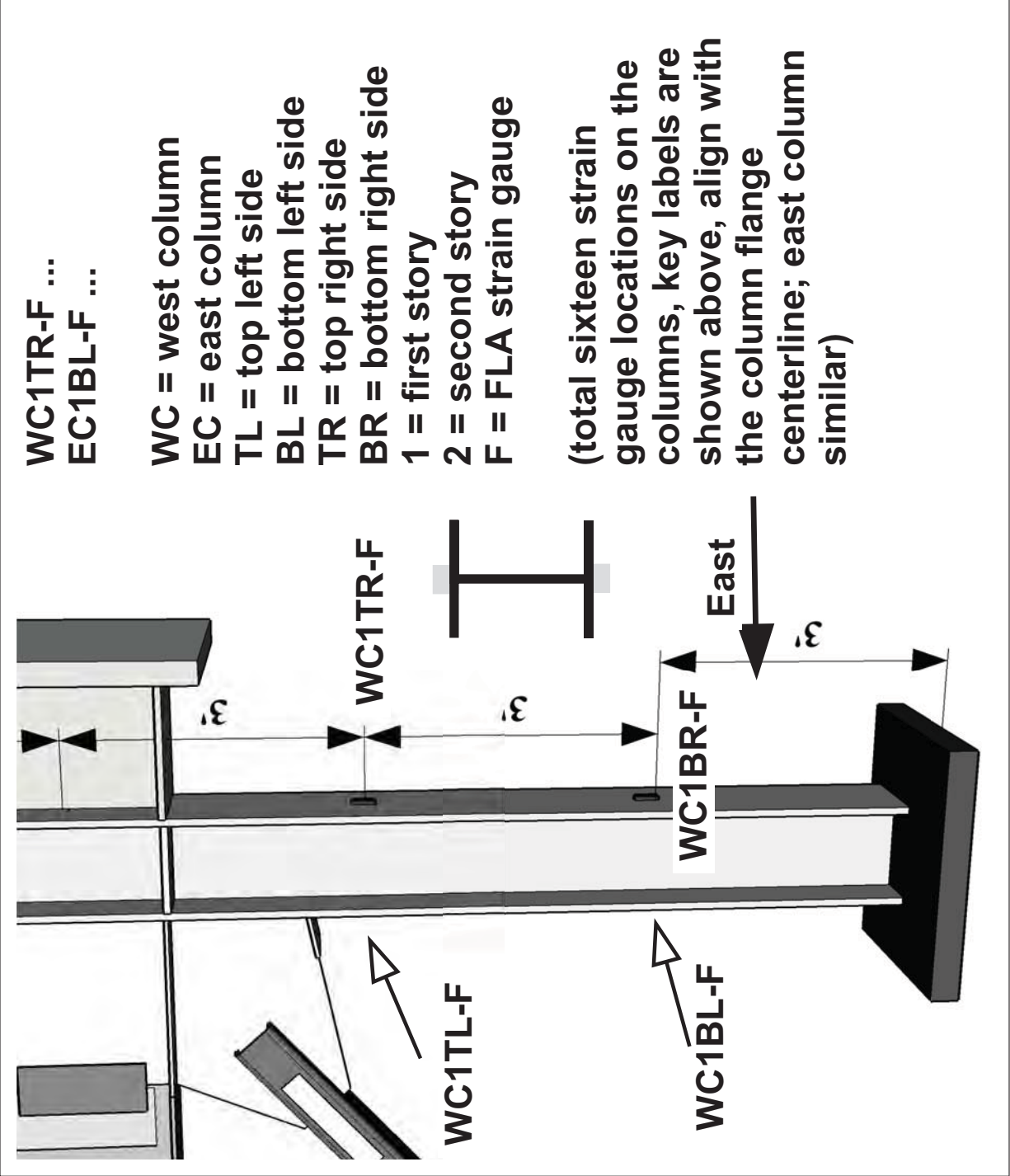
International Hybrid  
Simulation of  
Tomorrow's Braced  
Steel Frame  
Structures

University of California,  
Berkeley  
TCBF-B-1

PROJECT  
TCFB  
Aug 01, 2009  
DRAWN BY  
J.W. Lai  
TCBF-B-1  
PROJECT NO.

## Sensor Locations

S-16



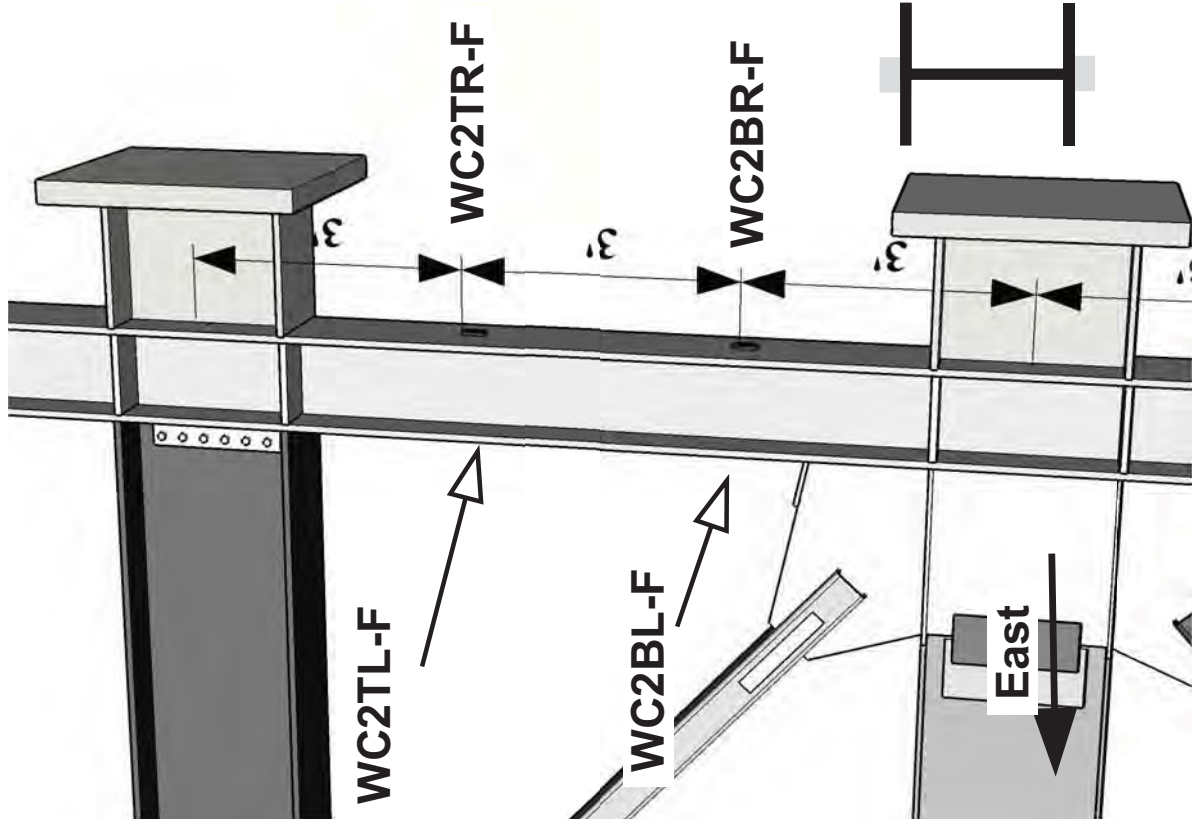




WC2TR-F ...  
EC2BL-F ...

WC = west column  
EC = east column  
TL = top left side  
BL = bottom left side  
TR = top right side  
BR = bottom right side  
1 = first story  
2 = second story  
F = FLA strain gauge

(total sixteen strain  
gauge locations on the  
columns, key labels are  
shown above, align with  
the column flange  
centerline; east column  
similar)





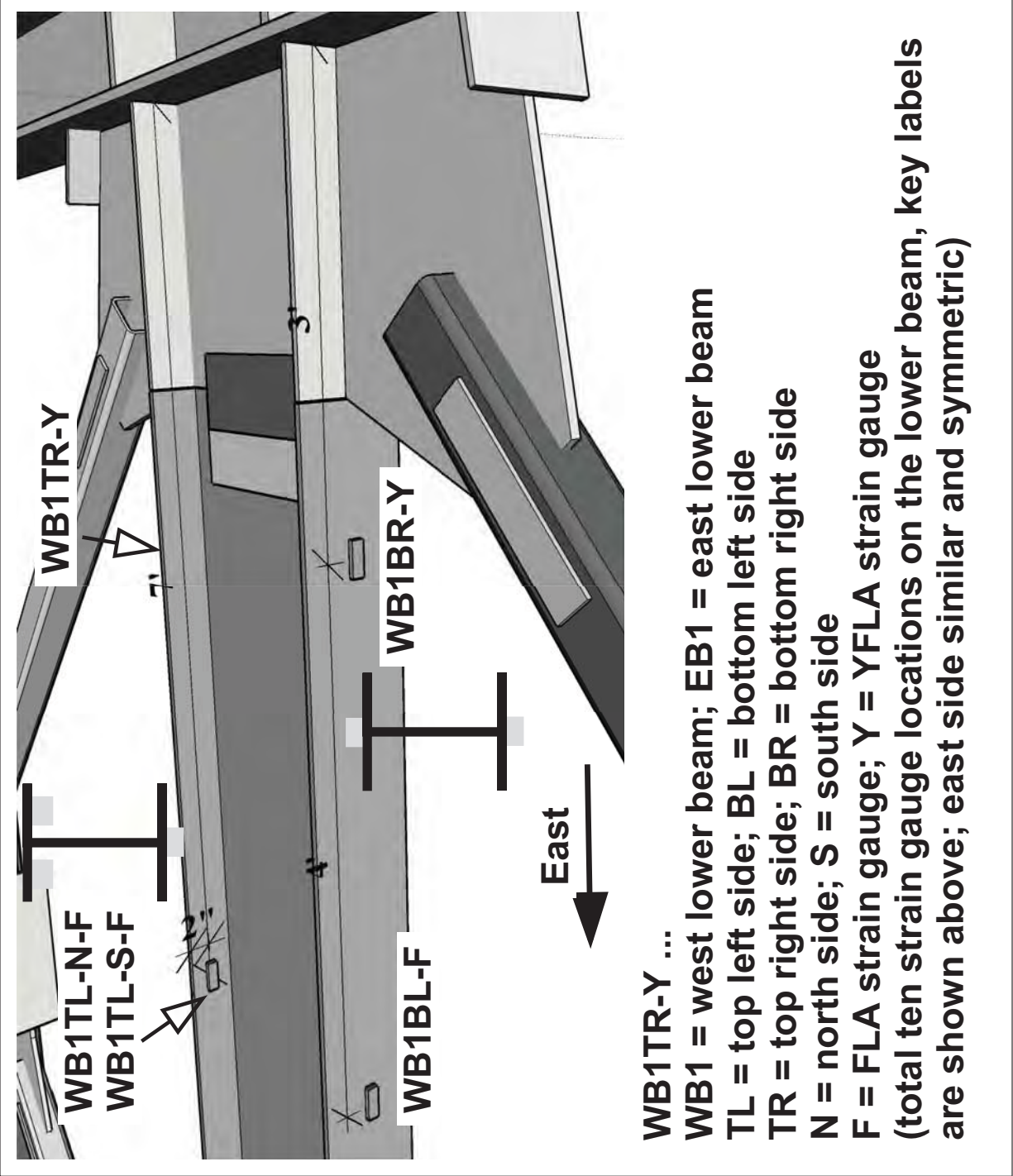
International Hybrid  
Simulation of  
Tomorrow's Braced  
Steel Frame  
Structures

University of California,  
Berkeley  
TCBF-B-1

PROJECT  
TCFB  
Aug 01,  
2009  
DRAWN BY  
J.W. Lai  
PROJECT NO.  
TCBF-B-1

Sensor  
Locations

S-18





International Hybrid  
Simulation of  
Tomorrow's Braced  
Steel Frame  
Structures

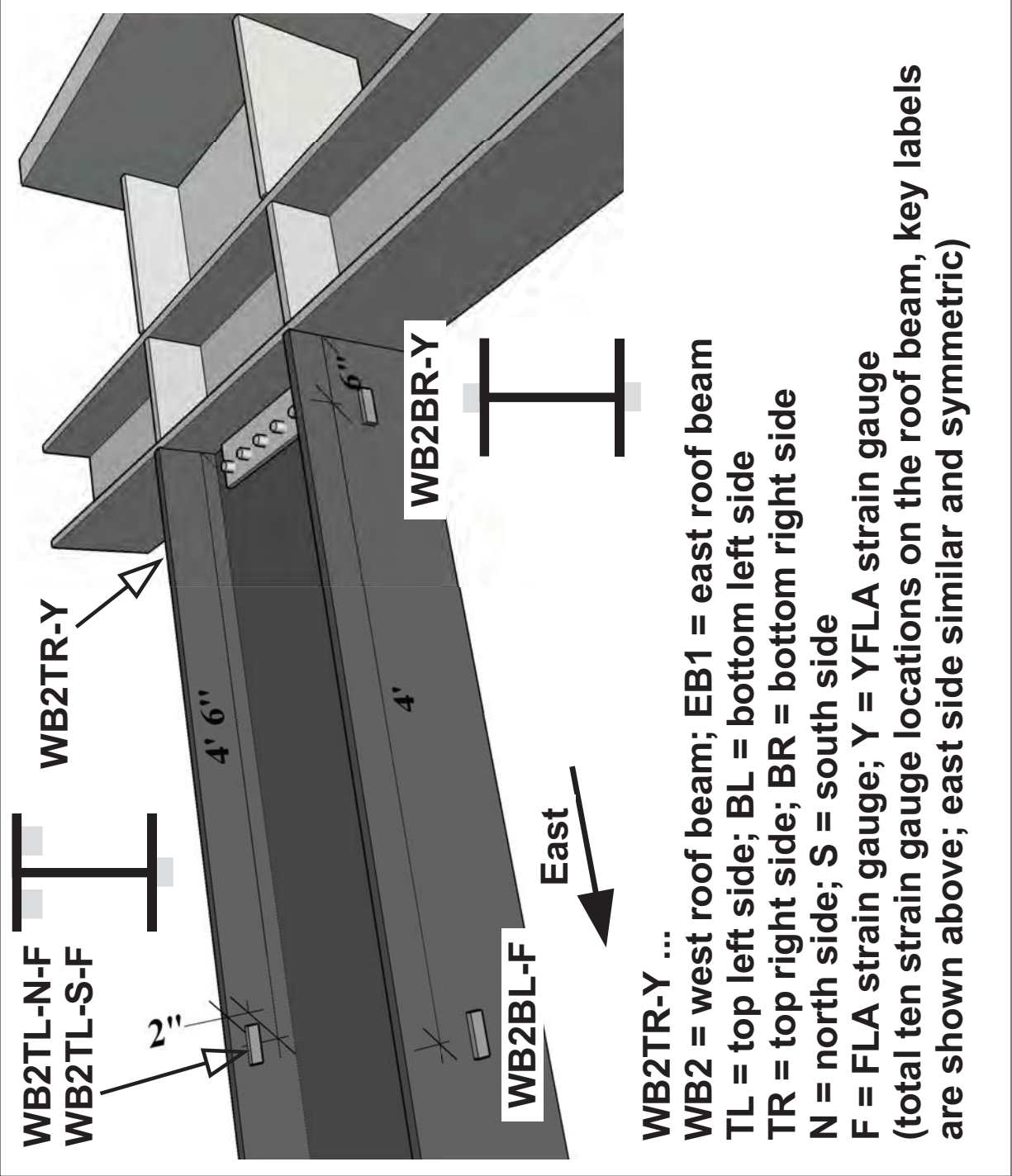
University of California,  
Berkeley  
TCBF-B-1

PROJECT  
TCFB  
Aug 01,  
2009

ISSUE  
Aug 01,  
2009  
DRAWN BY  
J.W. Lai

Sensor  
Locations

S-19





International Hybrid  
Simulation of  
Tomorrow's Braced  
Steel Frame  
Structures

University of California,  
Berkeley  
TCBF-B-1

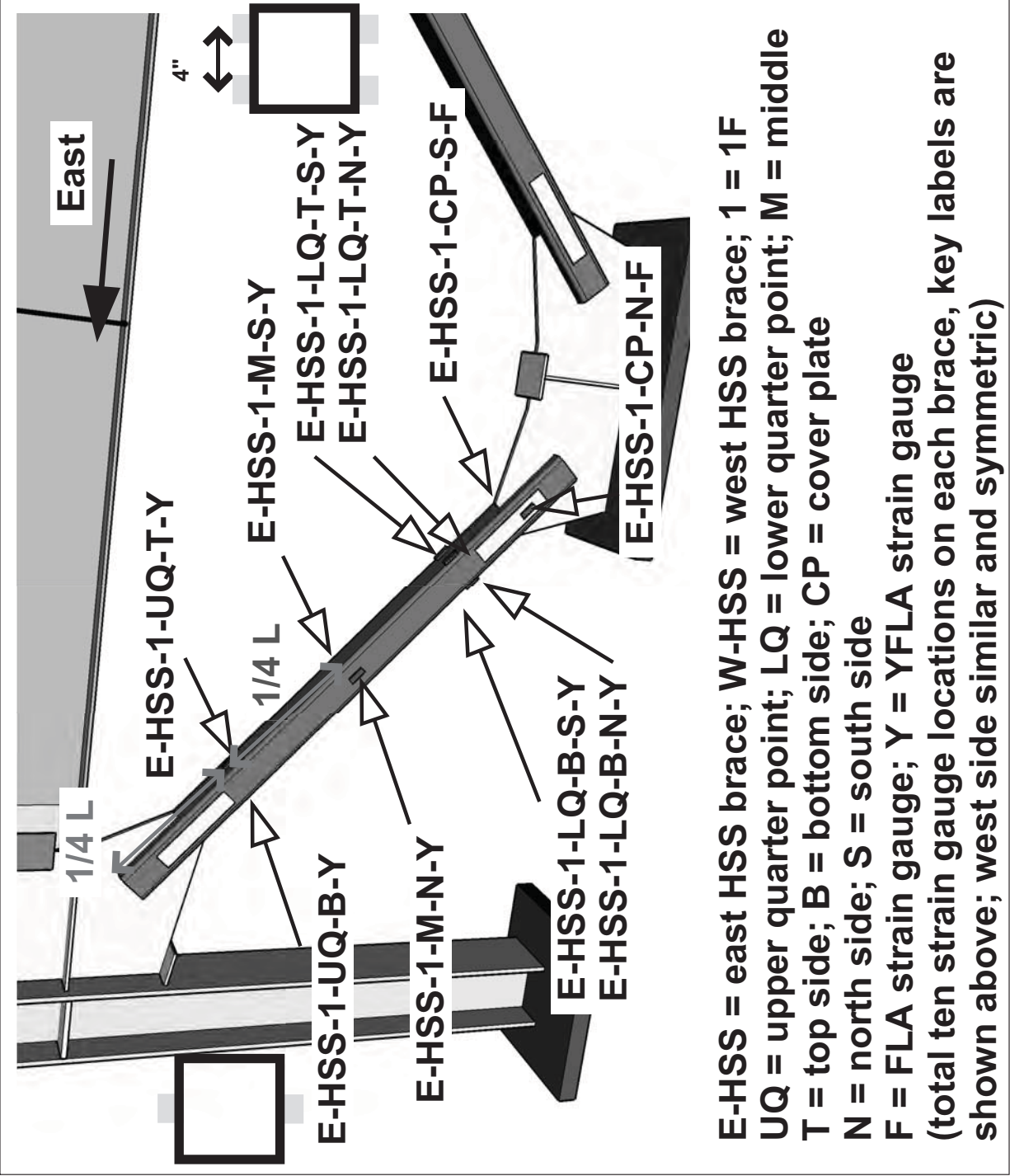
PROJECT  
TCFB  
Aug 01,  
2009

ISSUE  
Aug 01,  
2009  
DRAWN BY  
J.W. Lai

PROJECT NO.  
TCBF-B-1

Sensor  
Locations

S-20





International Hybrid  
Simulation of  
Tomorrow's Braced  
Steel Frame  
Structures

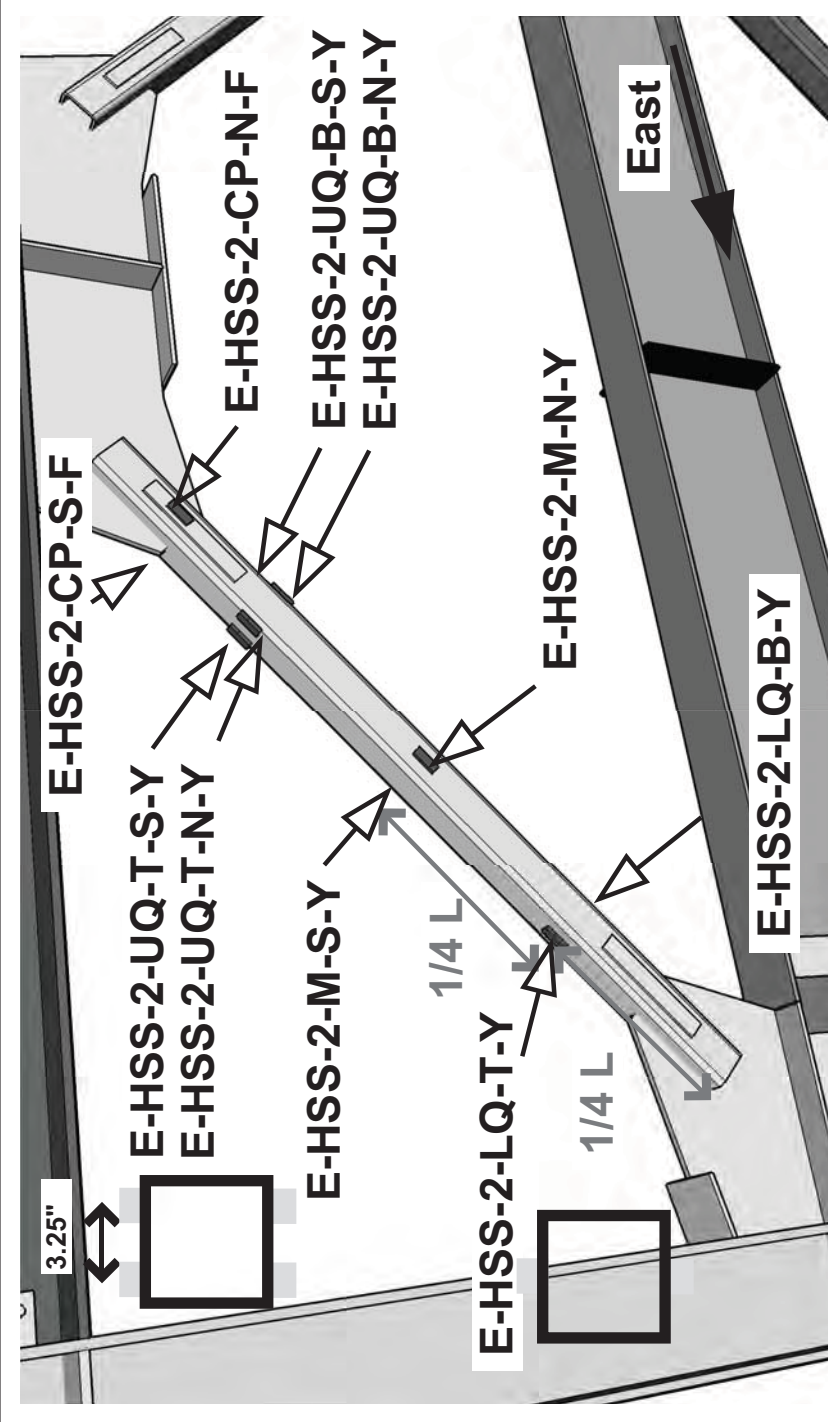
University of California,  
Berkeley  
TCBF-B-1

PROJECT  
TCFB  
Aug 01,  
2009

ISSUE  
Aug 01,  
2009  
DRAWN BY  
J.W. Lai

Sensor  
Locations

S.21



E-HSS = east HSS brace; W-HSS = west HSS brace; 2 = 2F  
 UQ = upper quarter point; LQ = lower quarter point; M = middle  
 T = top side; B = bottom side; CP = cover plate  
 N = north side; S = south side  
 F = FLA strain gauge; Y = YFLA strain gauge  
 (total ten strain gauge locations on each brace, key labels are  
 shown above; west side similar and symmetric)

TCBF-B-1 Channel Lists

Channel	ID	Label	Device	Range	Serial No.	Cable No.	DAQ Box ID	Note	Column #
1	S1	EC1BL-F	strain gauge	-	-	13	0:3:0	1/4 bridge	14
2	S2	EC1BR-F	strain gauge	-	-	14	0:3:1	1/4 bridge	15
3	S3	EC1TL-F	strain gauge	-	-	15	0:3:2	1/4 bridge	16
4	S4	EC1TR-F	strain gauge	-	-	16	0:3:3	1/4 bridge	17
5	S5	E-HSS-1-UQ-T-Y	strain gauge	-	-	5	0:1:0	1/4 bridge	6
6	S6	E-HSS-1-UQ-B-Y	strain gauge	-	-	6	0:1:1	1/4 bridge	7
7	S7	E-HSS-1-M-N-Y	strain gauge	-	-	7	0:1:2	1/4 bridge	8
8	S8	E-HSS-1-M-S-Y	strain gauge	-	-	8	0:1:3	1/4 bridge	9
9	S9	E-HSS-1-LQ-T-N-Y	strain gauge	-	-	9	0:2:0	1/4 bridge	10
10	S10	E-HSS-1-LQ-T-S-Y	strain gauge	-	-	10	0:2:1	1/4 bridge	11
11	S11	E-HSS-1-LQ-B-N-Y	strain gauge	-	-	11	0:2:2	1/4 bridge	12
12	S12	E-HSS-1-LQ-B-S-Y	strain gauge	-	-	12	0:2:3	1/4 bridge	13
13	S13	E-HSS-1-CP-N-F	strain gauge	-	-	3	0:0:2	1/4 bridge	4
14	S14	E-HSS-1-CP-S-F	strain gauge	-	-	4	0:0:3	1/4 bridge	5
15	S15	EB1BL-Y	strain gauge	-	-	45	0:11:0	1/4 bridge	46
16	S16	EB1TL-Y	strain gauge	-	-	44	0:10:3	1/4 bridge	45
17	S17	EB1BR-F	strain gauge	-	-	204/70	1:1:1	1/4 bridge	71
18	S18	EB1TR-N-F	strain gauge	-	-	46	0:11:1	full-bridge	47
19	S19	EB1TR-S-F	strain gauge	-	-	46	0:11:1	full-bridge	47
20	S20	WB1BL-F	strain gauge	-	-	342/68	1:0:3	1/4 bridge	69
21	S21	WB1TL-N-F	strain gauge	-	-	322/69	1:1:0	full-bridge	70
22	S22	WB1TL-S-F	strain gauge	-	-	322/69	1:1:0	full-bridge	70
23	S23	WB1BR-Y	strain gauge	-	-	338/84	1:4:3	1/4 bridge	85
24	S24	WB1TR-Y	strain gauge	-	-	325/57	0:14:0	1/4 bridge	58
25	S25	W-HSS-1-CP-N-F	strain gauge	-	-	1	0:0:0	1/4 bridge	2
26	S26	W-HSS-1-CP-S-F	strain gauge	-	-	2	0:0:1	1/4 bridge	3
27	S27	W-HSS-1-LQ-T-N-Y	strain gauge	-	-	25	0:6:0	1/4 bridge	26
28	S28	W-HSS-1-LQ-T-S-Y	strain gauge	-	-	26	0:6:1	1/4 bridge	27
29	S29	W-HSS-1-LQ-B-N-Y	strain gauge	-	-	27	0:6:2	1/4 bridge	28
30	S30	W-HSS-1-LQ-B-S-Y	strain gauge	-	-	28	0:6:3	1/4 bridge	29
31	S31	W-HSS-1-M-N-Y	strain gauge	-	-	29	0:7:0	1/4 bridge	30
32	S32	W-HSS-1-M-S-Y	strain gauge	-	-	30	0:7:1	1/4 bridge	31
33	S33	W-HSS-1-UQ-T-Y	strain gauge	-	-	31	0:7:2	1/4 bridge	32
34	S34	W-HSS-1-UQ-B-Y	strain gauge	-	-	32	0:7:3	1/4 bridge	33

TCBF-B-1 Channel Lists

Channel	ID	Label	Device	Range	Serial No.	Cable No.	DAQ Box ID	Note	Column #
35	S35	WC1TL-F	strain gauge	-	-	95	1:7:2	1/4 bridge	96
36	S36	WC1TR-F	strain gauge	-	-	93	1:7:0	1/4 bridge	94
37	S37	WC1BL-F	strain gauge	-	-	94	1:7:1	1/4 bridge	95
38	S38	WC1BR-F	strain gauge	-	-	92	1:6:3	1/4 bridge	93
39	S39	EC2BL-F	strain gauge	-	-	39	0:9:2	1/4 bridge	40
40	S40	EC2BR-F	strain gauge	-	-	40	0:9:3	1/4 bridge	41
41	S41	EC2TL-F	strain gauge	-	-	41	0:10:0	1/4 bridge	42
42	S42	EC2TR-F	strain gauge	-	-	42	0:10:1	1/4 bridge	43
43	S43	EB2BL-Y	strain gauge	-	-	43	0:10:2	1/4 bridge	44
44	S44	EB2TL-Y	strain gauge	-	-	200/348	2:4:3	1/4 bridge	149
45	S45	EB2BR-F	strain gauge	-	-	197/145	2:4:0	1/4 bridge	146
46	S46	EB2TR-N-F	strain gauge	-	-	199/147	2:4:2	full-bridge	148
47	S47	EB2TR-S-F	strain gauge	-	-	199/147	2:4:2	full-bridge	148
48	S48	E-HSS-2-LQ-T-Y	strain gauge	-	-	48	0:11:3	1/4 bridge	49
49	S49	E-HSS-2-LQ-B-Y	strain gauge	-	-	49	0:12:0	1/4 bridge	50
50	S50	E-HSS-2-M-N-Y	strain gauge	-	-	50	0:12:1	1/4 bridge	51
51	S51	E-HSS-2-M-S-Y	strain gauge	-	-	51	0:12:2	1/4 bridge	52
52	S52	E-HSS-2-UQ-T-N-Y	strain gauge	-	-	52	0:12:3	1/4 bridge	53
53	S53	E-HSS-2-UQ-T-S-Y	strain gauge	-	-	53	0:13:0	1/4 bridge	54
54	S54	E-HSS-2-UQ-B-N-Y	strain gauge	-	-	54	0:13:1	1/4 bridge	55
55	S55	E-HSS-2-UQ-B-S-Y	strain gauge	-	-	55	0:13:2	1/4 bridge	56
56	S56	E-HSS-2-CP-N-F	strain gauge	-	-	56	0:13:3	1/4 bridge	57
57	S57	E-HSS-2-CP-S-F	strain gauge	-	-	47	0:11:2	1/4 bridge	48
58	S58	W-HSS-2-CP-N-F	strain gauge	-	-	324/58	0:14:1	1/4 bridge	59
59	S59	W-HSS-2-CP-S-F	strain gauge	-	-	326/59	0:14:2	1/4 bridge	60
60	S60	W-HSS-2-UQ-T-N-Y	strain gauge	-	-	333/60	0:14:3	1/4 bridge	61
61	S61	W-HSS-2-UQ-T-S-Y	strain gauge	-	-	327/61	0:15:0	1/4 bridge	62
62	S62	W-HSS-2-UQ-B-N-Y	strain gauge	-	-	320/62	0:15:1	1/4 bridge	63
63	S63	W-HSS-2-UQ-B-S-Y	strain gauge	-	-	321/63	0:15:2	1/4 bridge	64
64	S64	W-HSS-2-M-N-Y	strain gauge	-	-	322/64	0:15:3	1/4 bridge	65
65	S65	W-HSS-2-M-S-Y	strain gauge	-	-	203/65	1:0:0	1/4 bridge	66
66	S66	W-HSS-2-LQ-T-Y	strain gauge	-	-	315/66	1:0:1	1/4 bridge	67
67	S67	W-HSS-2-LQ-B-Y	strain gauge	-	-	343/67	1:0:2	1/4 bridge	68
68	S68	WB2BL-F	strain gauge	-	-	346/137	2:2:0	1/4 bridge	138

TCBF-B-1 Channel Lists

Channel	ID	Label	Device	Range	Serial No.	Cable No.	DAQ Box ID	Note	Column #
69	S69	WB2TL-N-F	strain gauge	-	-	328/138	2:2:1	full-bridge	139
70	S70	WB2TL-S-F	strain gauge	-	-	328/138	2:2:1	full-bridge	139
71	S71	WB2BR-Y	strain gauge	-	-	201/71	1:1:2	1/4 bridge	72
72	S72	WB2TR-Y	strain gauge	-	-	345/140	2:2:3	1/4 bridge	141
73	S73	WC2TL-F	strain gauge	-	-	316/73	1:2:0	1/4 bridge	74
74	S74	WC2TR-F	strain gauge	-	-	349/74	1:2:1	1/4 bridge	75
75	S75	WC2BL-F	strain gauge	-	-	351/75	1:2:2	1/4 bridge	76
76	S76	WC2BR-F	strain gauge	-	-	318/76	1:2:3	1/4 bridge	77
77	R1-1	EC1-B-N-1-YR	rosette	-	-	17	0:4:0	1/4 bridge	18
78	R1-2	EC1-B-N-2-YR	rosette	-	-	18	0:4:1	1/4 bridge	19
79	R1-3	EC1-B-N-3-YR	rosette	-	-	19	0:4:2	1/4 bridge	20
80	R2-1	EC1-PZ-N-1-YR	rosette	-	-	33	0:8:0	1/4 bridge	34
81	R2-2	EC1-PZ-N-2-YR	rosette	-	-	34	0:8:1	1/4 bridge	35
82	R2-3	EC1-PZ-N-3-YR	rosette	-	-	35	0:8:2	1/4 bridge	36
83	R3-1	EC2-B-N-1-YR	rosette	-	-	36	0:8:3	1/4 bridge	37
84	R3-2	EC2-B-N-2-YR	rosette	-	-	37	0:9:0	1/4 bridge	38
85	R3-3	EC2-B-N-3-YR	rosette	-	-	38	0:9:1	1/4 bridge	39
86	R4-1	EC2-PZ-N-1-YR	rosette	-	-	196/149	2:5:0	1/4 bridge	150
87	R4-2	EC2-PZ-N-2-YR	rosette	-	-	198/150	2:5:1	1/4 bridge	151
88	R4-3	EC2-PZ-N-3-YR	rosette	-	-	195/151	2:5:2	1/4 bridge	152
89	R5-1	WC1-B-N-1-YR	rosette	-	-	89	1:6:0	1/4 bridge	90
90	R5-2	WC1-B-N-2-YR	rosette	-	-	90	1:6:1	1/4 bridge	91
91	R5-3	WC1-B-N-3-YR	rosette	-	-	91	1:6:2	1/4 bridge	92
92	R6-1	WC1-PZ-N-1-YR	rosette	-	-	317/77	1:3:0	1/4 bridge	78
93	R6-2	WC1-PZ-N-2-YR	rosette	-	-	350/78	1:3:1	1/4 bridge	79
94	R6-3	WC1-PZ-N-3-YR	rosette	-	-	302/79	1:3:2	1/4 bridge	80
95	R7-1	WC2-B-N-1-YR	rosette	-	-	301/80	1:3:3	1/4 bridge	81
96	R7-2	WC2-B-N-2-YR	rosette	-	-	323/81	1:4:0	1/4 bridge	82
97	R7-3	WC2-B-N-3-YR	rosette	-	-	336/82	1:4:1	1/4 bridge	83
98	R8-1	WC2-PZ-N-1-YR	rosette	-	-	352/141	2:3:0	1/4 bridge	142
99	R8-2	WC2-PZ-N-2-YR	rosette	-	-	319/142	2:3:1	1/4 bridge	143
100	R8-3	WC2-PZ-N-3-YR	rosette	-	-	329/143	2:3:2	1/4 bridge	144
101	R9-1	IF-E-BG-TL-1-N-YR	rosette	-	-	101	1:9:0	1/4 bridge	102
102	R9-2	IF-E-BG-TL-2-N-YR	rosette	-	-	102	1:9:1	1/4 bridge	103



TCBF-B-1 Channel Lists

Channel	ID	Label	Device	Range	Serial No.	Cable No.	DAQ Box ID	Note	Column #
103	R9-3	IF-E-BG-TL-3-N-YR	rosette	-	-	103	1:9:2	1/4 bridge	104
104	R10-1	IF-E-BG-BL-1-N-YR	rosette	-	-	104	1:9:3	1/4 bridge	105
105	R10-2	IF-E-BG-BL-2-N-YR	rosette	-	-	105	1:10:0	1/4 bridge	106
106	R10-3	IF-E-BG-BL-3-N-YR	rosette	-	-	106	1:10:1	1/4 bridge	107
107	R11-1	IF-E-BG-TR-1-N-YR	rosette	-	-	107	1:10:2	1/4 bridge	108
108	R11-2	IF-E-BG-TR-2-N-YR	rosette	-	-	108	1:10:3	1/4 bridge	109
109	R11-3	IF-E-BG-TR-3-N-YR	rosette	-	-	109	1:11:0	1/4 bridge	110
110	R12-1	IF-E-BG-TC-1-N-YR	rosette	-	-	110	1:11:1	1/4 bridge	111
111	R12-2	IF-E-BG-TC-2-N-YR	rosette	-	-	111	1:11:2	1/4 bridge	112
112	R12-3	IF-E-BG-TC-3-N-YR	rosette	-	-	112	1:11:3	1/4 bridge	113
113	R13-1	IF-E-MG-TL-1-N-YR	rosette	-	-	113	1:12:0	1/4 bridge	114
114	R13-2	IF-E-MG-TL-2-N-YR	rosette	-	-	114	1:12:1	1/4 bridge	115
115	R13-3	IF-E-MG-TL-3-N-YR	rosette	-	-	115	1:12:2	1/4 bridge	116
116	R14-1	IF-E-MG-BL-1-N-YR	rosette	-	-	116	1:12:3	1/4 bridge	117
117	R14-2	IF-E-MG-BL-2-N-YR	rosette	-	-	117	1:13:0	1/4 bridge	118
118	R14-3	IF-E-MG-BL-3-N-YR	rosette	-	-	118	1:13:1	1/4 bridge	119
119	R15-1	IF-E-MG-TR-1-N-YR	rosette	-	-	119	1:13:2	1/4 bridge	120
120	R15-2	IF-E-MG-TR-2-N-YR	rosette	-	-	120	1:13:3	1/4 bridge	121
121	R15-3	IF-E-MG-TR-3-N-YR	rosette	-	-	121	1:14:0	1/4 bridge	122
122	R16-1	IF-E-MG-BR-1-N-YR	rosette	-	-	122	1:14:1	1/4 bridge	123
123	R16-2	IF-E-MG-BR-2-N-YR	rosette	-	-	123	1:14:2	1/4 bridge	124
124	R16-3	IF-E-MG-BR-3-N-YR	rosette	-	-	124	1:14:3	1/4 bridge	125
125	R17-1	IF-E-TG-TL-1-N-YR	rosette	-	-	125	1:15:0	1/4 bridge	126
126	R17-2	IF-E-TG-TL-2-N-YR	rosette	-	-	126	1:15:1	1/4 bridge	127
127	R17-3	IF-E-TG-TL-3-N-YR	rosette	-	-	127	1:15:2	1/4 bridge	128
128	R18-1	IF-E-TG-BL-1-N-YR	rosette	-	-	128	1:15:3	1/4 bridge	129
129	R18-2	IF-E-TG-BL-2-N-YR	rosette	-	-	129	2:0:0	1/4 bridge	130
130	R18-3	IF-E-TG-BL-3-N-YR	rosette	-	-	130	2:0:1	1/4 bridge	131
131	R19-1	IF-E-TG-BC-1-N-YR	rosette	-	-	131	2:0:2	1/4 bridge	132
132	R19-2	IF-E-TG-BC-2-N-YR	rosette	-	-	303	2:0:3	1/4 bridge	133
133	R19-3	IF-E-TG-BC-3-N-YR	rosette	-	-	133	2:1:0	1/4 bridge	134
134	R20-1	IF-E-TG-BR-1-N-YR	rosette	-	-	134	2:1:1	1/4 bridge	135
135	R20-2	IF-E-TG-BR-2-N-YR	rosette	-	-	135	2:1:2	1/4 bridge	136
136	R20-3	IF-E-TG-BR-3-N-YR	rosette	-	-	136	2:1:3	1/4 bridge	137

TCBF-B-1 Channel Lists

Channel	ID	Label	Device	Range	Serial No.	Cable No.	DAQ Box ID	Note	Column #
137	WP07	1F-E-HSS-UQ-R-OD	wire pot	30"	2000NC51151	159	2:7:2	-	160
138	WP04	1F-E-HSS-M-R-OD	wire pot	40"	2005NC51006	156	2:6:3	-	157
139	WP02	1F-E-HSS-LQ-R-OD	wire pot	30"	2006NC51015	154	2:6:1	-	155
140	WP03	1F-E-HSS-UQ-L-OD	wire pot	30"	2006NC51012	155	2:6:2	-	156
141	WP05	1F-E-HSS-M-L-OD	wire pot	40"	2005NC01003	157	2:7:0	-	158
142	WP01	1F-E-HSS-LQ-L-OD	wire pot	30"	2006NC51014	153	2:6:0	-	154
143	WP06	1F-W-HSS-LQ-R-OD	wire pot	30"	2000NC51124	158	2:7:1	-	159
144	WP12	1F-W-HSS-M-R-OD	wire pot	40"	2005NC01008	164	2:8:3	-	165
145	WP09	1F-W-HSS-UQ-R-OD	wire pot	30"	2000NC51106	161	2:8:0	-	162
146	WP08	1F-W-HSS-LQ-L-OD	wire pot	30"	2006NC51016	160	2:7:3	-	161
147	WP11	1F-W-HSS-M-L-OD	wire pot	40"	2005NC01006	163	2:8:2	-	164
148	WP10	1F-W-HSS-UQ-L-OD	wire pot	30"	2000NC51116	162	2:8:1	-	163
149	WP14	2F-E-HSS-LQ-R-OD	wire pot	30"	2006NC51013	166/305	2:9:1	-	167
150	WP17	2F-E-HSS-M-R-OD	wire pot	40"	2005NC51002	169/308	2:10:0	-	170
151	WP13	2F-E-HSS-UQ-R-OD	wire pot	30"	2000NC51114	165/304	2:9:0	-	166
152	WP16	2F-E-HSS-LQ-L-OD	wire pot	30"	2000NC51125	168/307	2:9:3	-	169
153	WP18	2F-E-HSS-M-L-OD	wire pot	40"	2005NC51007	170/309	2:10:1	-	171
154	WP15	2F-E-HSS-UQ-L-OD	wire pot	30"	2000NC51105	167/306	2:9:2	-	168
155	WP22	2F-W-HSS-UQ-R-OD	wire pot	40"	2005NC01010	174/313	2:11:1	-	175
156	WP20	2F-W-HSS-M-R-OD	wire pot	40"	2005NC01009	172/311	2:10:3	-	173
157	WP24	2F-W-HSS-LQ-R-OD	wire pot	30"	2000NC51153	176/315	2:11:3	-	177
158	WP21	2F-W-HSS-UQ-L-OD	wire pot	40"	2005NC51010	173/312	2:11:0	-	174
159	WP19	2F-W-HSS-M-L-OD	wire pot	40"	2005NC01007	171/310	2:10:2	-	172
160	WP23	2F-W-HSS-LQ-L-OD	wire pot	30"	2000NC51111	175/314	2:11:2	-	176
161	WP25	1F-E-HSS-A	wire pot	40"	2005NC51009	177	2:12:0	-	178
162	WP26	1F-W-HSS-A	wire pot	40"	2005NC01004	178	2:12:1	-	179
163	WP27	2F-E-HSS-A	wire pot	40"	2005NC01001	300	2:14:0	-	186
164	WP28	2F-W-HSS-A	wire pot	40"	2000NC51131	301	2:14:1	-	187
165	WP34	1F-E-BG-A	wire pot	40"	2005NC51004	97	2:13:0	-	182
166	WP35	1F-LG-A	wire pot	40"	2005NC51008	98	2:13:1	-	183
167	WP37	1F-RG-A	wire pot	40"	2000NC51130	100	2:13:3	-	185
168	WP36	1F-W-BG-A	wire pot	30"	2000NC51149	307	2:13:2	-	184
169	WP38	1F-E-TG-A	wire pot	30"	2000NC51113	183	1:8:0	-	98
170	WP39	2F-LG-A	wire pot	30"	2000NC51109	184	1:8:1	-	99

## TCBF-B-1 Channel Lists

Channel	ID	Label	Device	Range	Serial No.	Cable No.	DAQ Box ID	Note	Column #
171	WP40	2F-RG-A	wire pot	30"	2000NC51156	318	1:8:2	-	100
172	WP41	1F-W-TG-A	wire pot	30"	2000NC51115	319	1:8:3	-	101
173	WP30	1F-C-G-TS-OD	wire pot	40"	2005NC01005	21	0:5:0	-	22
174	WP47	1F-W-TG-C-OD	wire pot	30"	2000NC51150	313	1:5:3	-	89
175	WP33	1F-E-BG-C-OD	wire pot	40"	2005NC51001	24	0:5:3	-	25
176	WP29	1F-W-BG-C-OD	wire pot	40"	2005NC51005	20	0:4:3	-	21
177	WP43	1F-E-BG-B-OD	wire pot	30"	2000NC51098	320	1:4:2	-	84
178	WP31	1F-C-B-BF-OD	wire pot	30"	2000NC51128	22	0:5:1	-	23
179	WP32	1F-C-B-CS-OD	wire pot	40"	2005NC51003	23	0:5:2	-	24
180	WP42	1F-W-BG-B-OD	wire pot	30"	2000NC51117	314	1:1:3	-	73
181	WP46	1F-E-TG-C-OD	wire pot	30"	2000NC51152	312	1:5:2	-	88
182	WP44	2F-C-B-BF-OD	wire pot	30"	2000NC51126	310	1:5:0	-	86
183	WP45	2F-C-G-BS-OD	wire pot	30"	2000NC51129	311	1:5:1	-	87
184	A5	Act2disp	position transducer	40"	2007NC01001	182/363	2:12:3	ST01	181
185	ST2	C-GB-Slip	stick	1"	2004NC01015	181/358	2:12:2	-	180
186	ST3	W-CB-Slip	stick	1"	2004NC01012	96/357	1:7:3	-	97
187	ST4	E-LC1-OD	stick	6"	2007NC01009	179	2:15:2	-	192
188	ST5	E-LC2-OD	stick	6"	2007NC01010	302	2:14:2	-	188
189	ST6	C-LC1-OD	stick	6"	2007NC01011	180	2:15:3	-	193
190	ST7	C-LC2-OD	stick	6"	2007NC51006	303	2:14:3	-	189
191	ST8	W-LC1-OD	stick	6"	2007NC51007	304	2:15:0	-	190
192	ST9	W-LC2-OD	stick	6"	2007NC51010	305	2:15:1	-	191
193	ST10	C-B1-VD	stick	4"	2007NC01006	144	2:3:3	-	145
194	ST11	C-B2-VD	stick	4"	2007NC01003	210	2:5:3	Novo100_02-210	153
195	T11	EB1-S-TI	tiltmeter	10 Deg	2004NC04008	316	2:2:2	Tilt1	140
196	T12	WB1-S-TI	tiltmeter	10 Deg	2004NC04007	323	2:4:1	Tilt2	147
197	PT1	EC1-PZ-E-PT	position transducer	40"	-	-	-	not use	-
198	PT2	EC2-PZ-E-PT	position transducer	40"	-	CS2-disp	3:0:4	Displacement Control	198
199	A1	Act1disp	position transducer	40"	2006NC01002	CS1-disp	3:0:0	-	194
200	A2	Act1force	load cell	-	-	CS1-load	3:0:1	From LC1	195
201	A3	Act1dispCmd	-	-	-	-	3:0:2	From STS (CMD)	196
202	A4	Act1dispAct3	position transducer	40"	2006NC01003	CS3-disp	3:0:3	-	197
203	PT2	EC2-PZ-E-PT	position transducer	40"	-	CS2-disp	3:0:4	Act2disp (A5)	198
204	A6	Act2force	load cell	-	-	CS2-load	3:0:5	From LC2	199

TCBF-B-1 Channel Lists

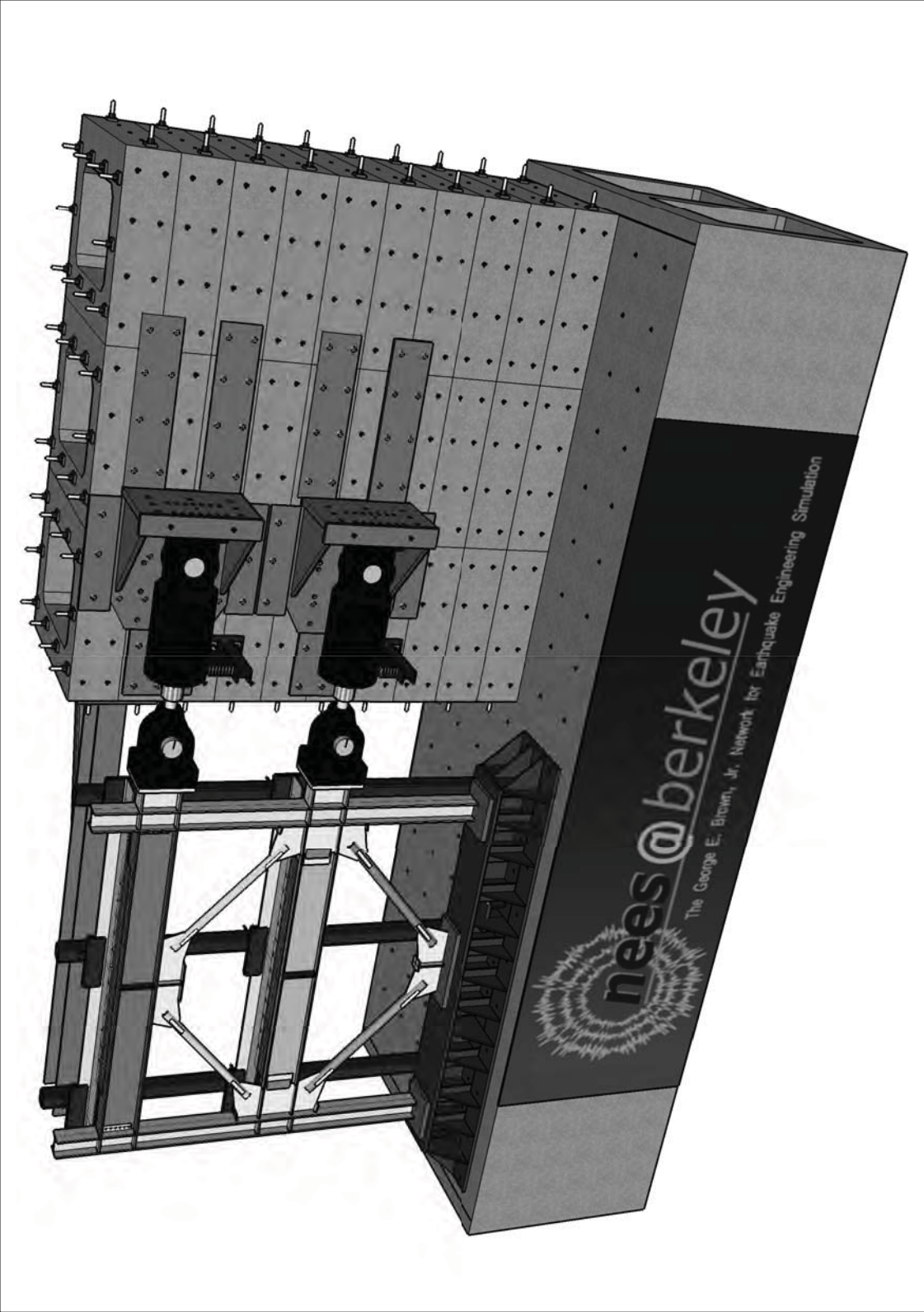
Channel	ID	Label	Device	Range	Serial No.	Cable No.	DAQ Box ID	Note	Column #
205	A7	Act2dispCmd	-	-	-	-	3:0:6	From STS (CMD)	200
206	A8	Act2dispAct4	position transducer	40"	2004NC01061	CS4-disp	3:0:7	-	201
207	ST12	FB-Slip	stick	4"	2004NC01023	308	3:1:0	D-Space (Novo50_DS1)	202
208	ST13	RRW-Slip-N	stick	4"	2004NC01019	309	3:1:1	D-Space (Novo50_DS2)	203
209	ST14	RRW-Slip-S	stick	4"	2004NC01028	306	3:1:2	D-Space (Novo50_DS3)	204
210	ST15	Act1-BK	stick	1"	2004NC01025	361	3:1:3	D-Space (Novo50_DS4)	205
211	ST16	Act2-BK	stick	1"	2004NC01020	355	3:1:4	D-Space (Novo50_DS5)	206
212	TG1	TriggerCanon	-	-	-	207	3:1:5	D-Space	207
213	TG2	TriggerLeica	-	-	-	208	3:1:6	D-Space	208
214	ST1	E-CB-Slip	stick	1"	2004NC01014	379	3:1:7	D-Space	209

---

## **Appendix E**

### **Channel Locations and Lists for TCBF-B-2 Specimen**

---



**TCBF-B-2, Sensor Locations  
S.00**

**ISSUE**  
Oct 12, 2009

**DRAWN BY**  
Jiun-Wei Lai

**PROJECT NO.**  
TCBF-B-2

**PROJECT**  
TCBF

International Hybrid  
Simulation of  
Tomorrow's Braced  
Steel Frame Structures





International Hybrid  
Simulation of  
Tomorrow's Braced  
Steel Frame  
Structures

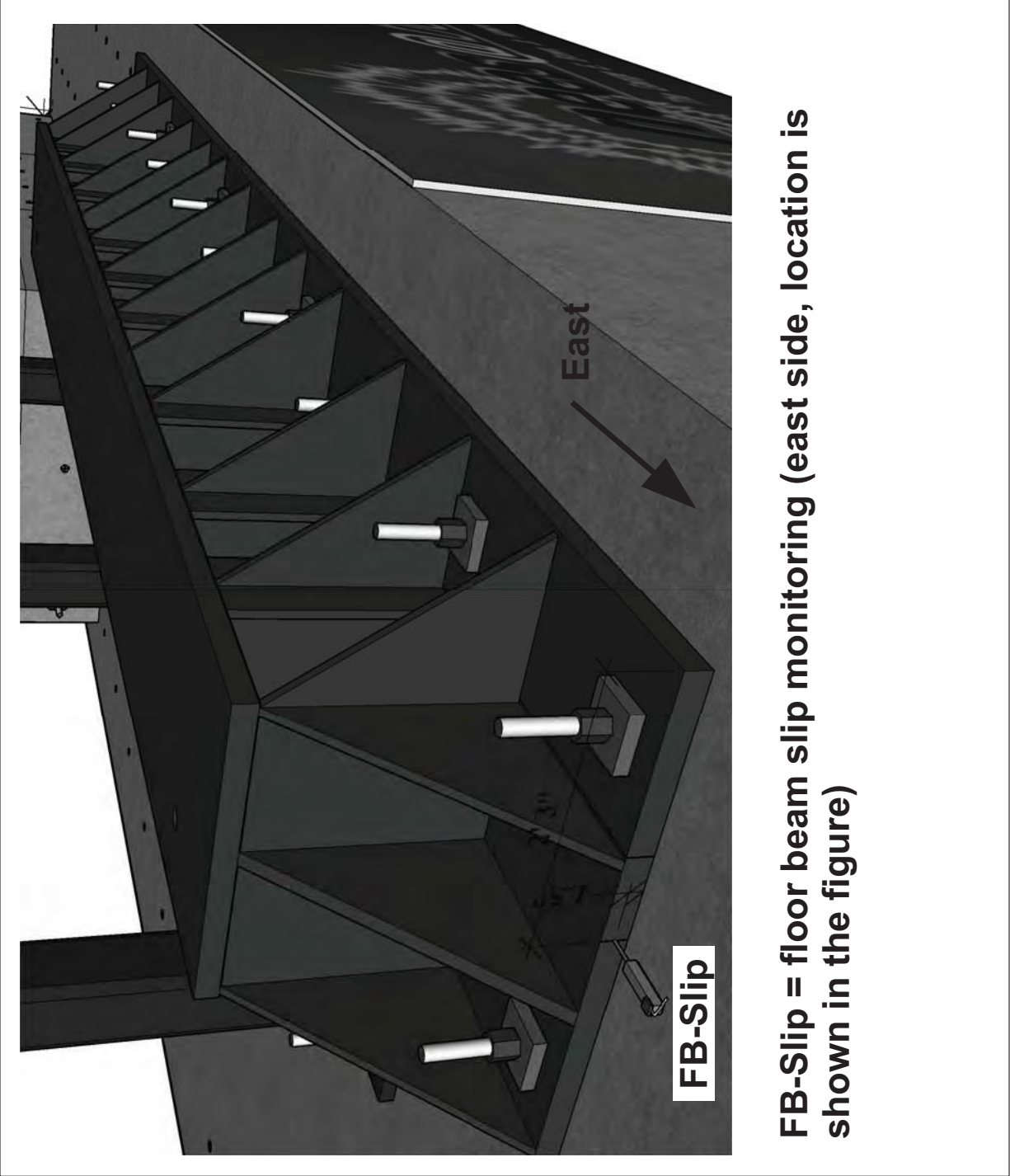
University of California,  
Berkeley  
TCBF-B-2

PROJECT  
TCFB  
PROJECT NO.  
TCBF-B-2  
DRAWN BY  
J.W. Lai

ISSUE  
Oct 12,  
2009

Sensor  
Locations

S.01





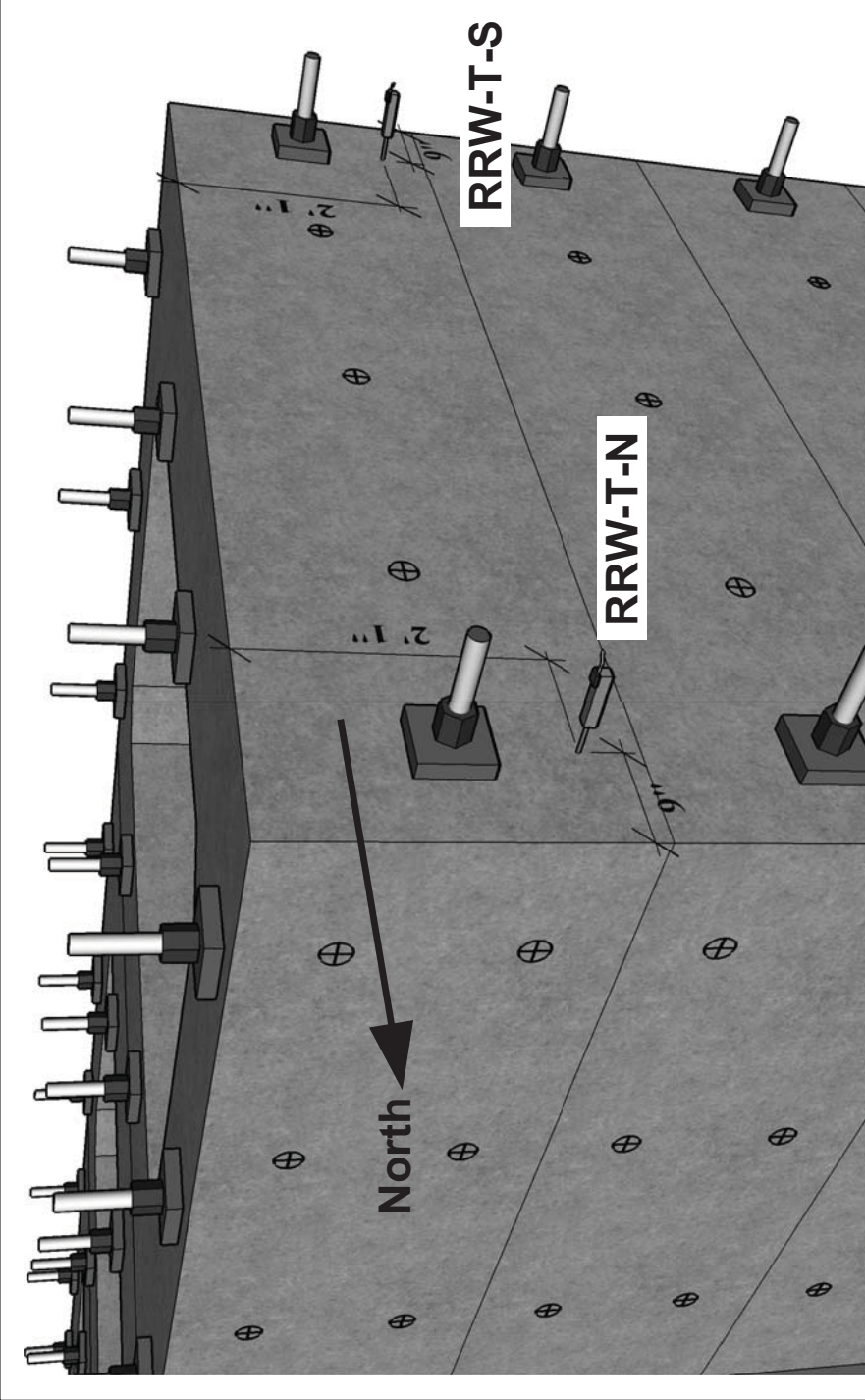
International Hybrid  
Simulation of  
Tomorrow's Braced  
Steel Frame  
Structures

University of California,  
Berkeley  
TCBF-B-2

PROJECT  
TCFB  
2009  
ISSUE  
Oct 12,  
DRAWN BY  
J.W. Lai  
PROJECT NO.  
TCBF-B-2

## Sensor Locations

### S.02



**RRW-T-N = north side of reconfigurable reaction wall (RRW), top deformation monitoring (location is shown in the figure)**

**RRW-T-S = south side of reconfigurable reaction wall (RRW), top deformation monitoring (location is shown in the figure)**





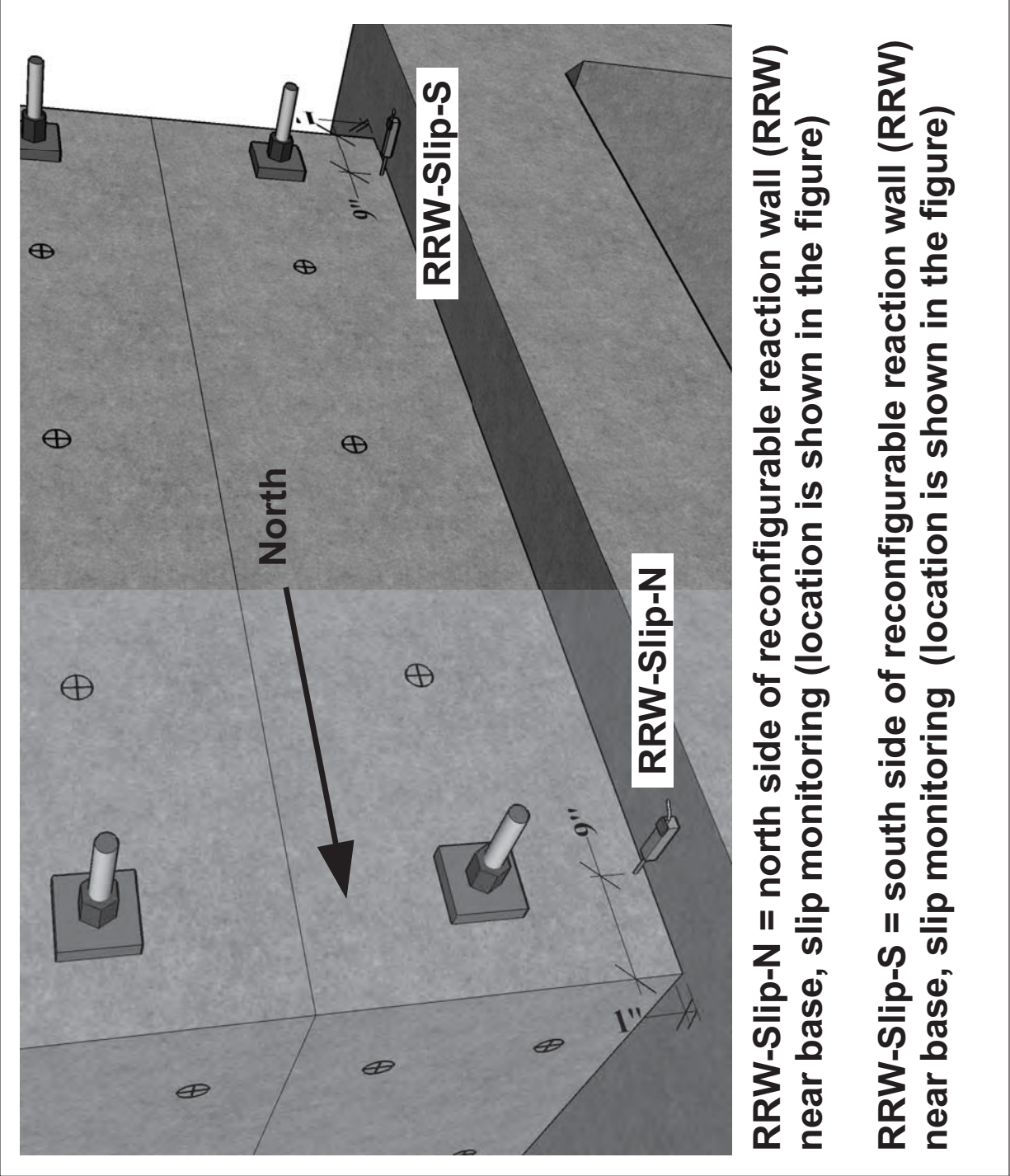
International Hybrid  
Simulation of  
Tomorrow's Braced  
Steel Frame  
Structures

University of California,  
Berkeley  
TCBF-B-2

PROJECT  
TCFB  
2009  
Oct 12,  
ISSUE  
DRAWN BY  
J.W. Lai  
PROJECT NO.  
TCBF-B-2

Sensor  
Locations

S.03





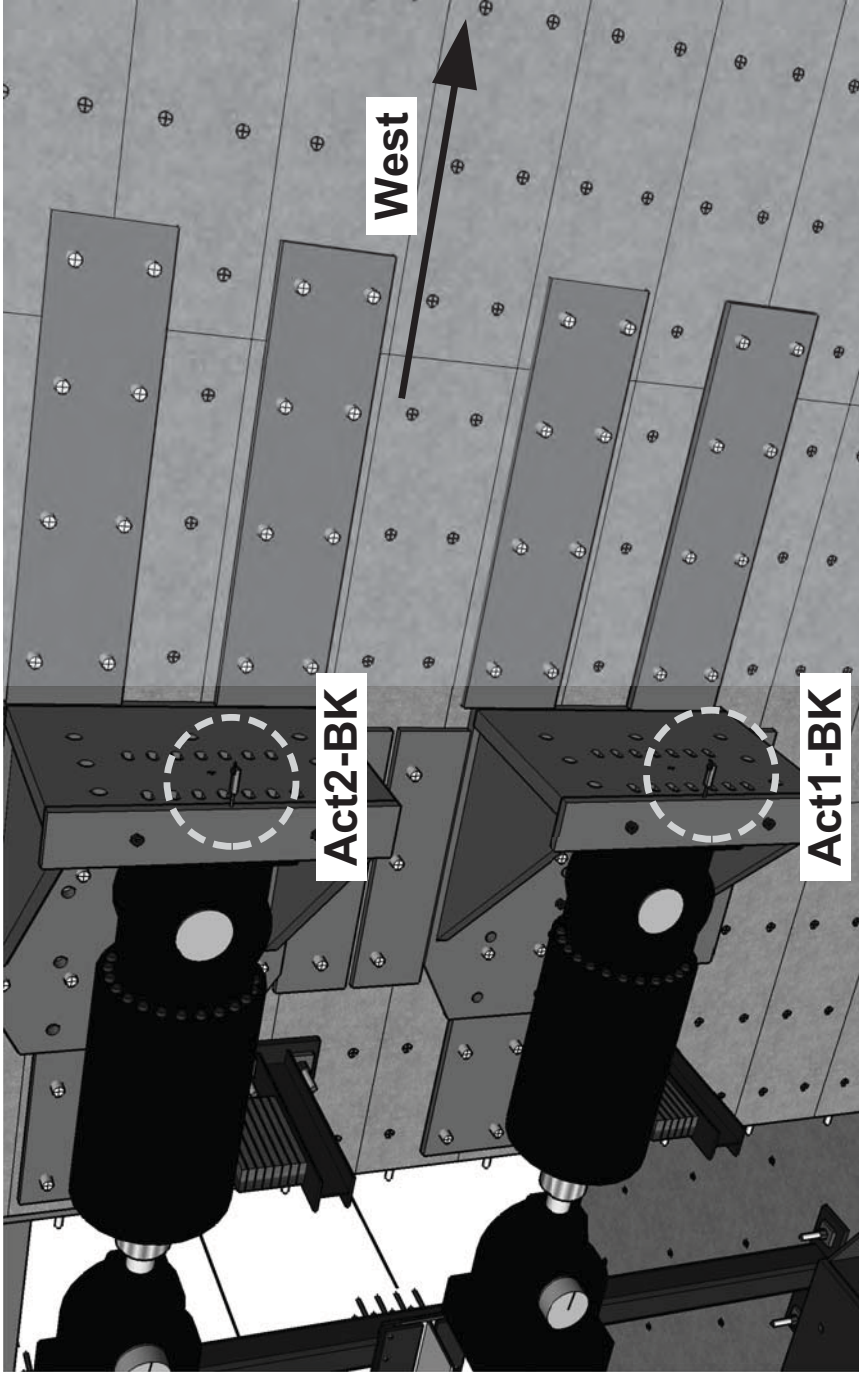
International Hybrid  
Simulation of  
Tomorrow's Braced  
Steel Frame  
Structures

University of California,  
Berkeley  
TCBF-B-2

PROJECT  
TCFB  
Oct 12,  
2009  
ISSUE  
DRAWN BY  
J.W. Lai  
PROJECT NO.  
TCBF-B-2

Sensor  
Locations

S.04



**Act1-BK = lower actuator bracket deformation monitoring  
(location is shown in the figure)**

**Act2-BK = upper actuator bracket deformation monitoring  
(location is shown in the figure)**



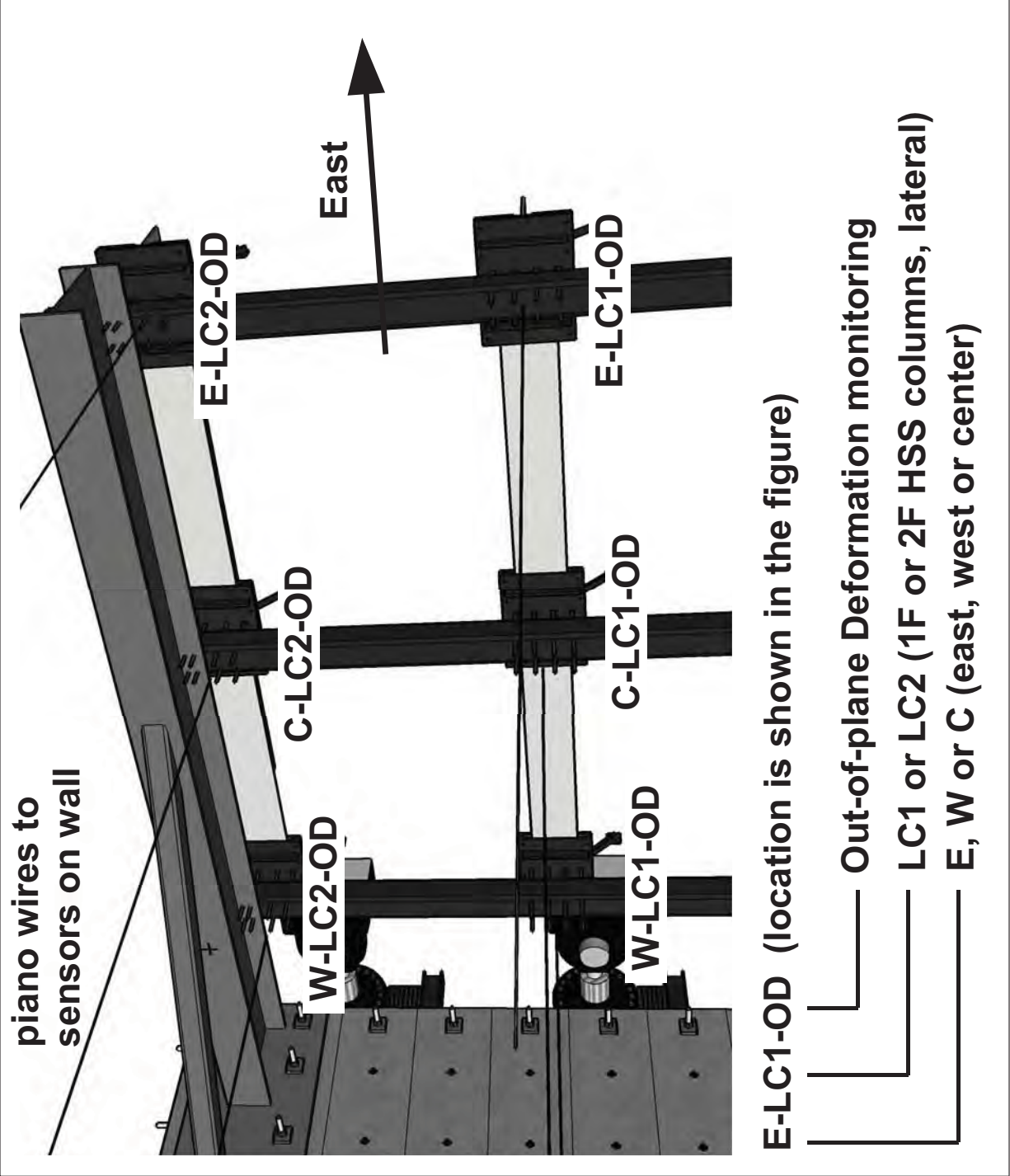
International Hybrid  
Simulation of  
Tomorrow's Braced  
Steel Frame  
Structures

University of California,  
Berkeley  
TCBF-B-2

PROJECT  
TCFB  
Oct 12,  
2009  
DRAWN BY  
J.W. Lai  
TCBF-B-2  
PROJECT NO.

Sensor  
Locations

S.05





International Hybrid  
Simulation of  
Tomorrow's Braced  
Steel Frame  
Structures

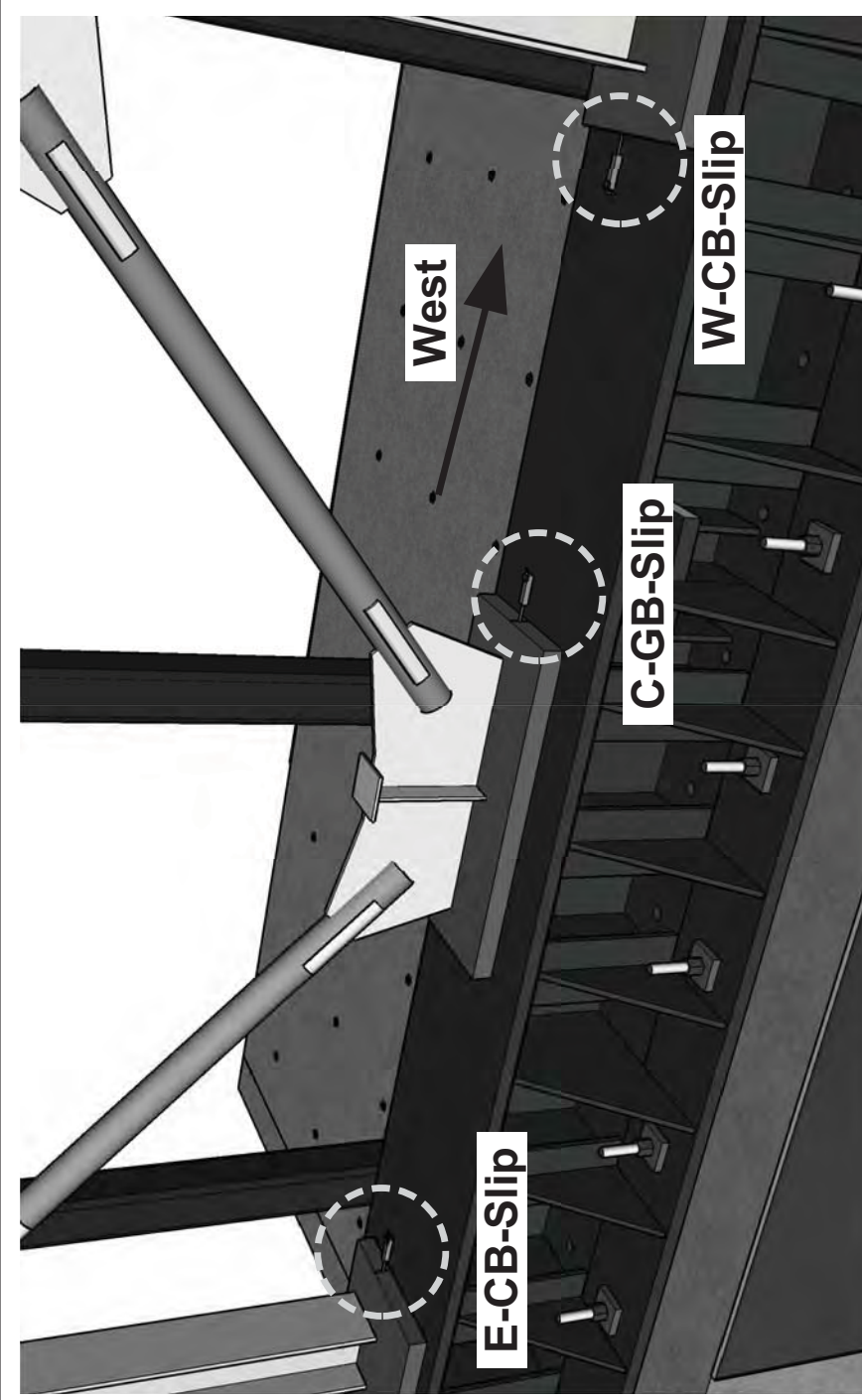
University of California,  
Berkeley  
TCBF-B-2

PROJECT  
TCFB  
PROJECT NO.  
TCBF-B-2

ISSUE  
Oct 12,  
2009  
DRAWN BY  
J.W. Lai

## Sensor Locations

**S.06**



**E-CB-Slip = east column base slip monitoring  
C-GB-Slip = center gusset base slip monitoring  
W-CB-Slip = west column base slip monitoring  
(locations are shown in the figure, align with the braced  
frame center plane)**



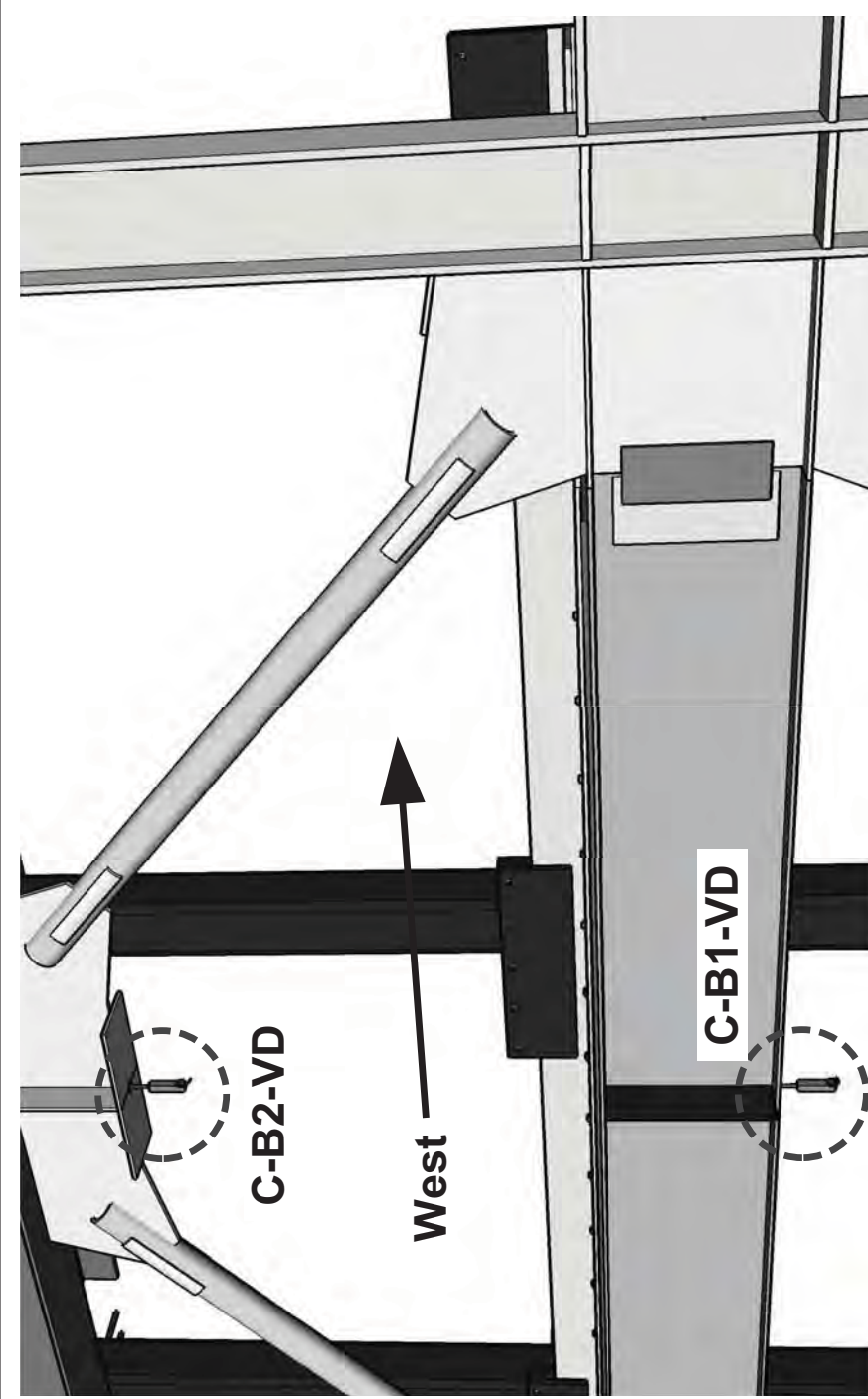
International Hybrid  
Simulation of  
Tomorrow's Braced  
Steel Frame  
Structures

University of California,  
Berkeley  
TCBF-B-2

PROJECT  
TCFB  
2009  
Oct 12,  
ISSUE  
DRAWN BY  
J.W. Lai  
PROJECT NO.  
TCBF-B-2

Sensor  
Locations

S.07



**C-B2-VD = roof beam (2F) center deflection monitoring**  
**C-B1-VD = lower beam (1F) center deflection monitoring**  
 (locations are shown in the figure, align with the beam  
 bottom flange centerline)



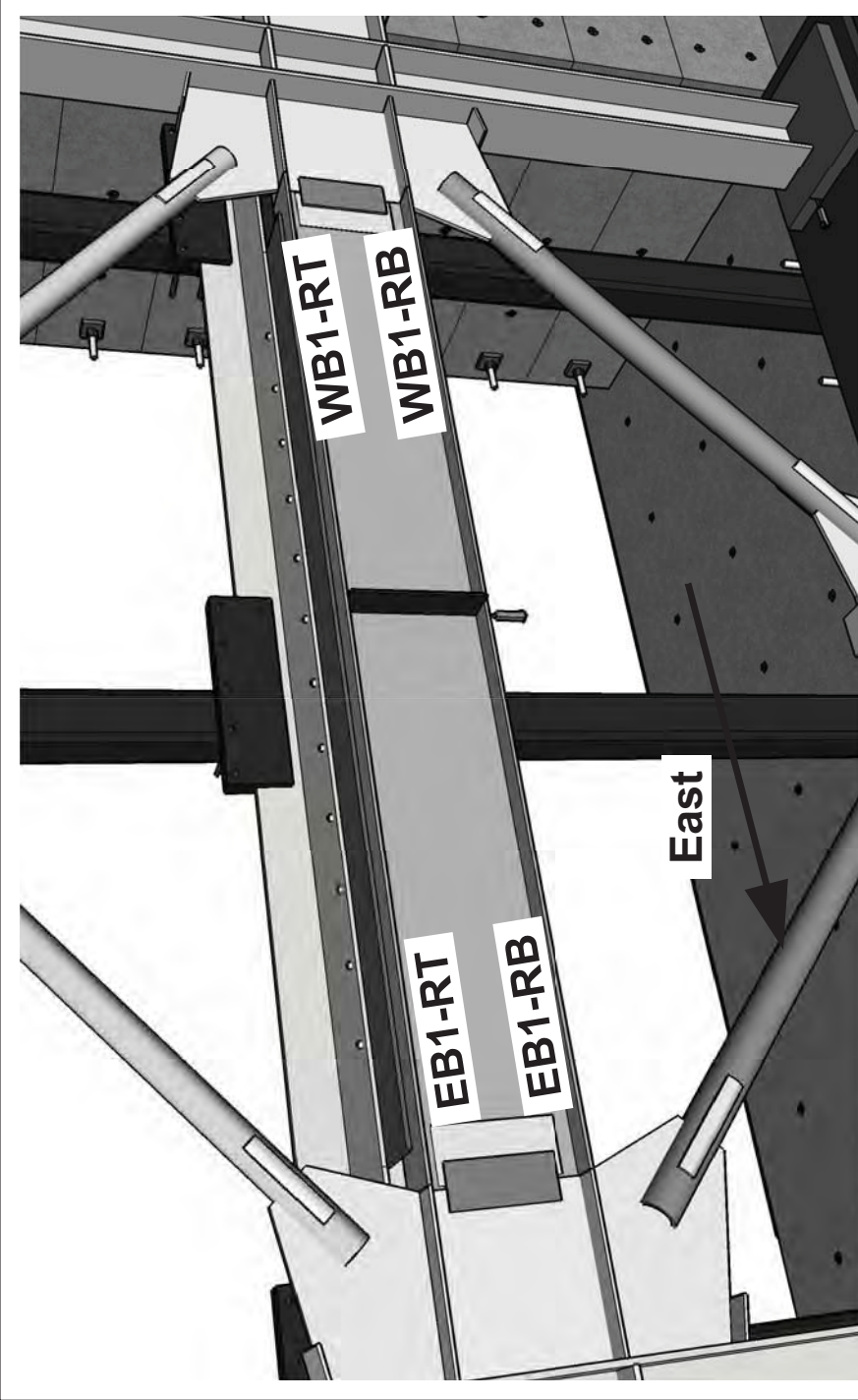
International Hybrid  
Simulation of  
Tomorrow's Braced  
Steel Frame  
Structures

University of California,  
Berkeley  
TCBF-B-2

PROJECT  
TCFB  
Oct 12,  
2009  
DRAWN BY  
J.W. Lai  
PROJECT NO.  
TCBF-B-2

Sensor  
Locations

S.08



**WB1-RT, WB1-RB = west lower beam (1F) rotation monitoring**  
**EB1-RT, EB1-RB = east lower beam (1F) rotation monitoring**  
**RT, RB = top or bottom side**  
**(locations are shown in the figure, distance between two centerlines of top and bottom sticks is 18")**



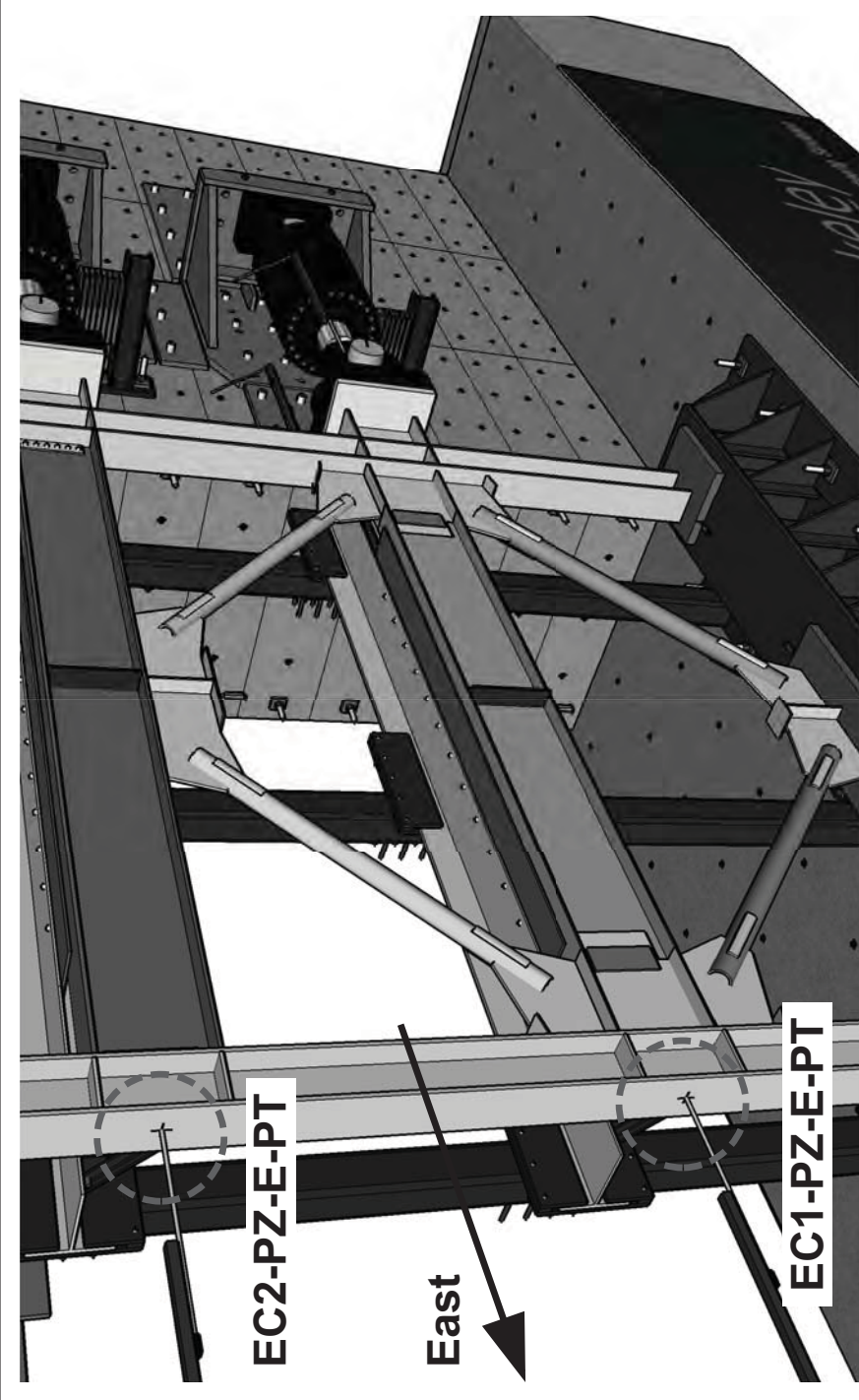
International Hybrid  
Simulation of  
Tomorrow's Braced  
Steel Frame  
Structures

University of California,  
Berkeley  
TCBF-B-2

PROJECT  
TCFB  
Oct 12,  
2009  
DRAWN BY  
J.W. Lai  
TCBF-B-2  
PROJECT NO.

Sensor  
Locations

S.09



EC2-PZ-E-PT = roof level (2F) displacement monitoring  
EC1-PZ-E-PT = lower level (1F) displacement monitoring

(locations are shown in the figure, align with the beam  
centerline at each floor level)



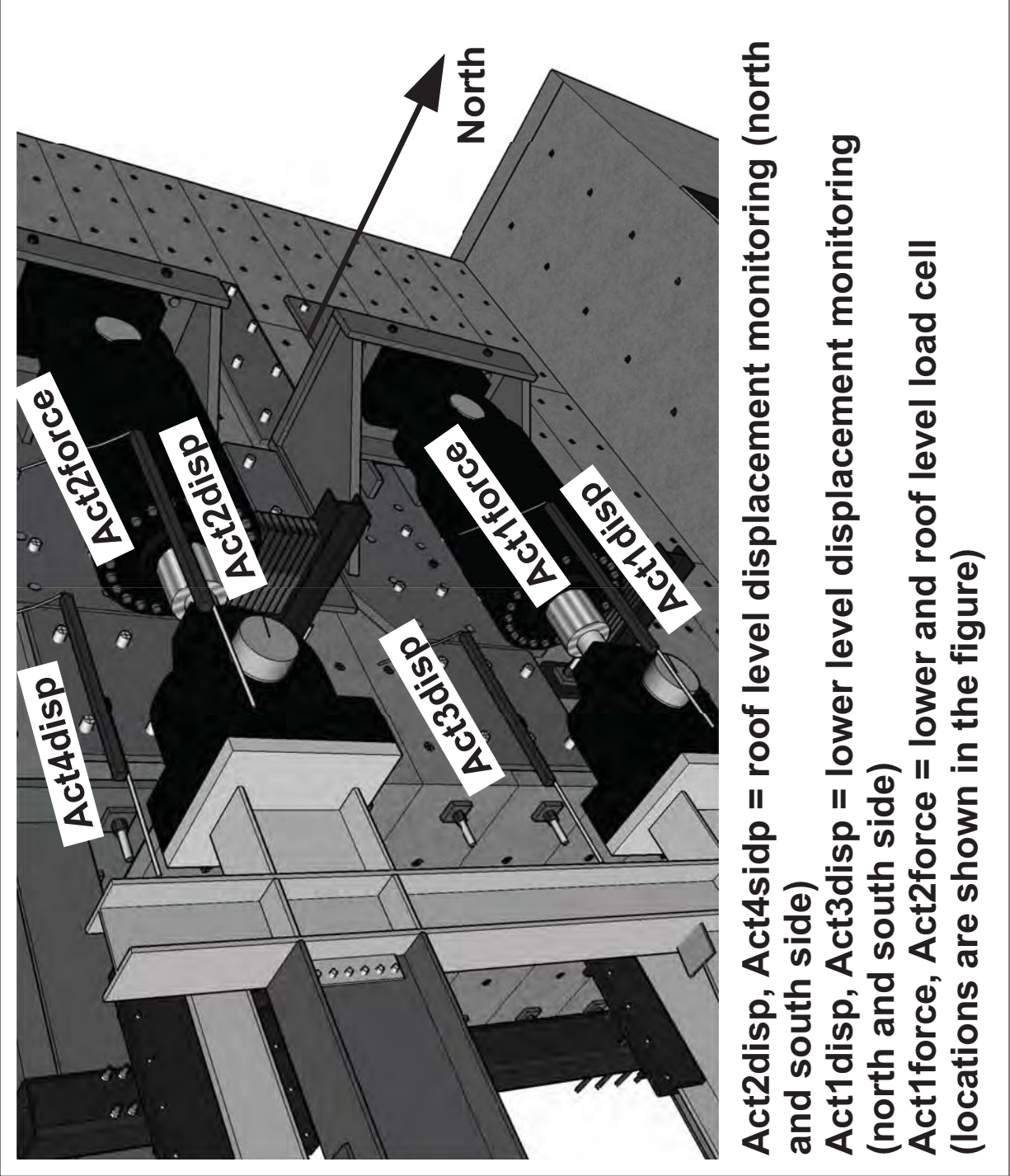
International Hybrid  
Simulation of  
Tomorrow's Braced  
Steel Frame  
Structures

University of California,  
Berkeley  
TCBF-B-2

PROJECT  
TCFB  
Oct 12,  
2009  
DRAWN BY  
J.W. Lai  
PROJECT NO.  
TCBF-B-2

Sensor  
Locations

S-10







International Hybrid  
Simulation of  
Tomorrow's Braced  
Steel Frame  
Structures

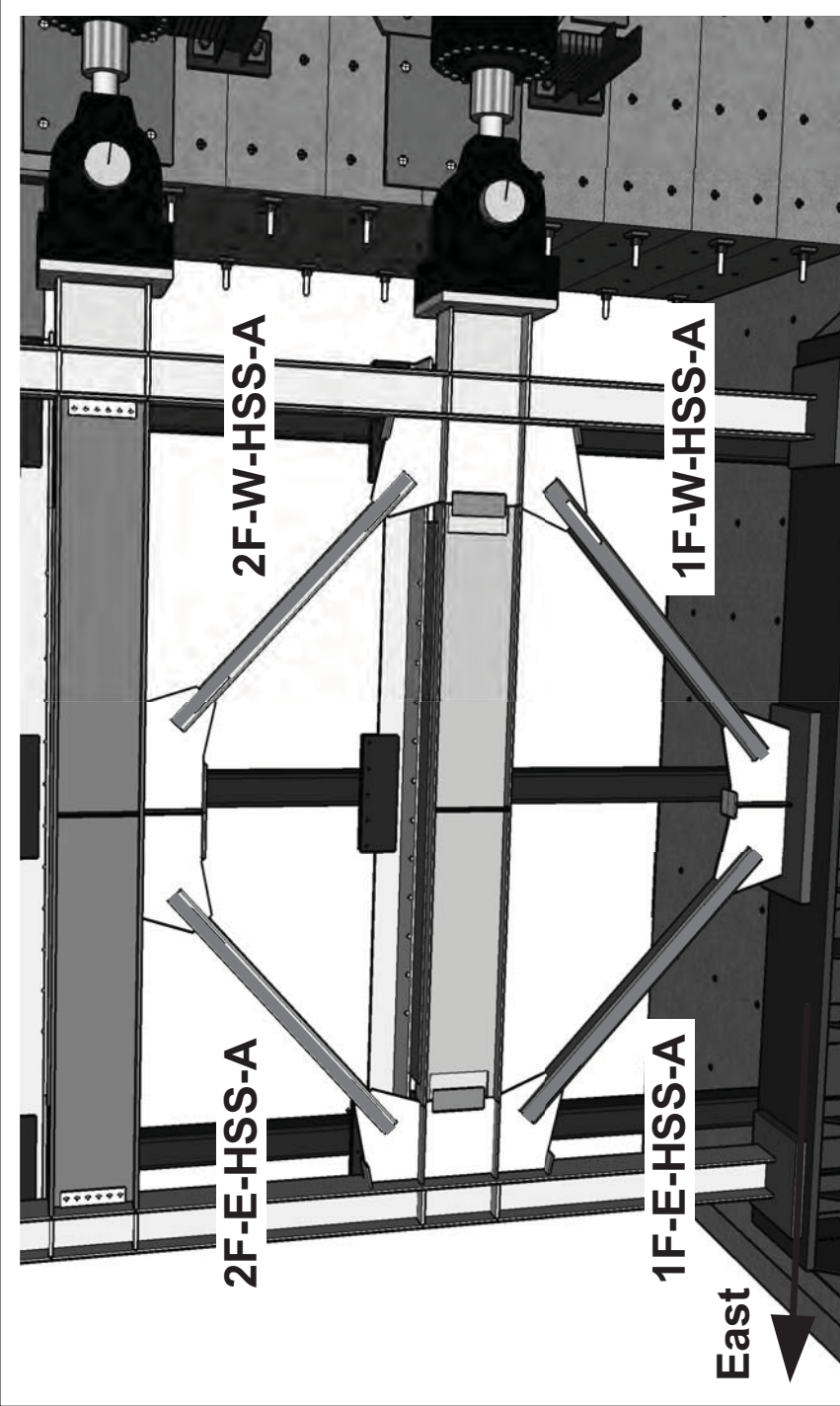
University of California,  
Berkeley  
TCBF-B-2

PROJECT  
TCFB  
PROJECT NO.  
TCBF-B-2

ISSUE  
Oct 12,  
2009  
DRAWN BY  
J.W. Lai

Sensor  
Locations

S.11



1F = first story; 2F = second story

E = east side; W = west side; A = axial direction

Round HSS brace axial deformation monitoring along the axis of brace (wire pot locations are shown in the figure)



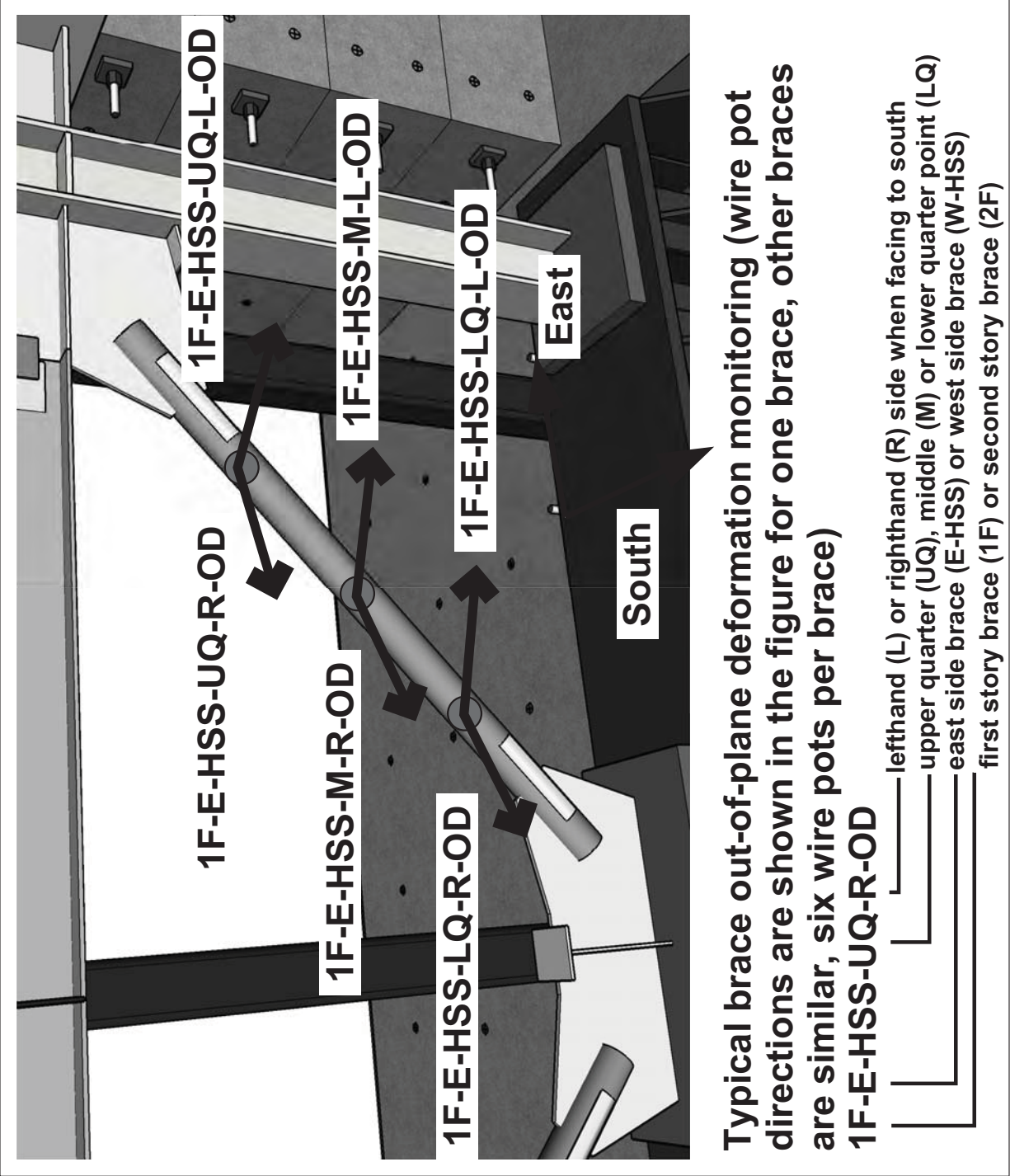
International Hybrid  
Simulation of  
Tomorrow's Braced  
Steel Frame  
Structures

University of California,  
Berkeley  
TCBF-B-2

PROJECT  
TCFB  
Oct 12, 2009  
ISSUE  
DRAWN BY  
J.W. Lai  
PROJECT NO.  
TCBF-B-2

Sensor  
Locations

**S.12**





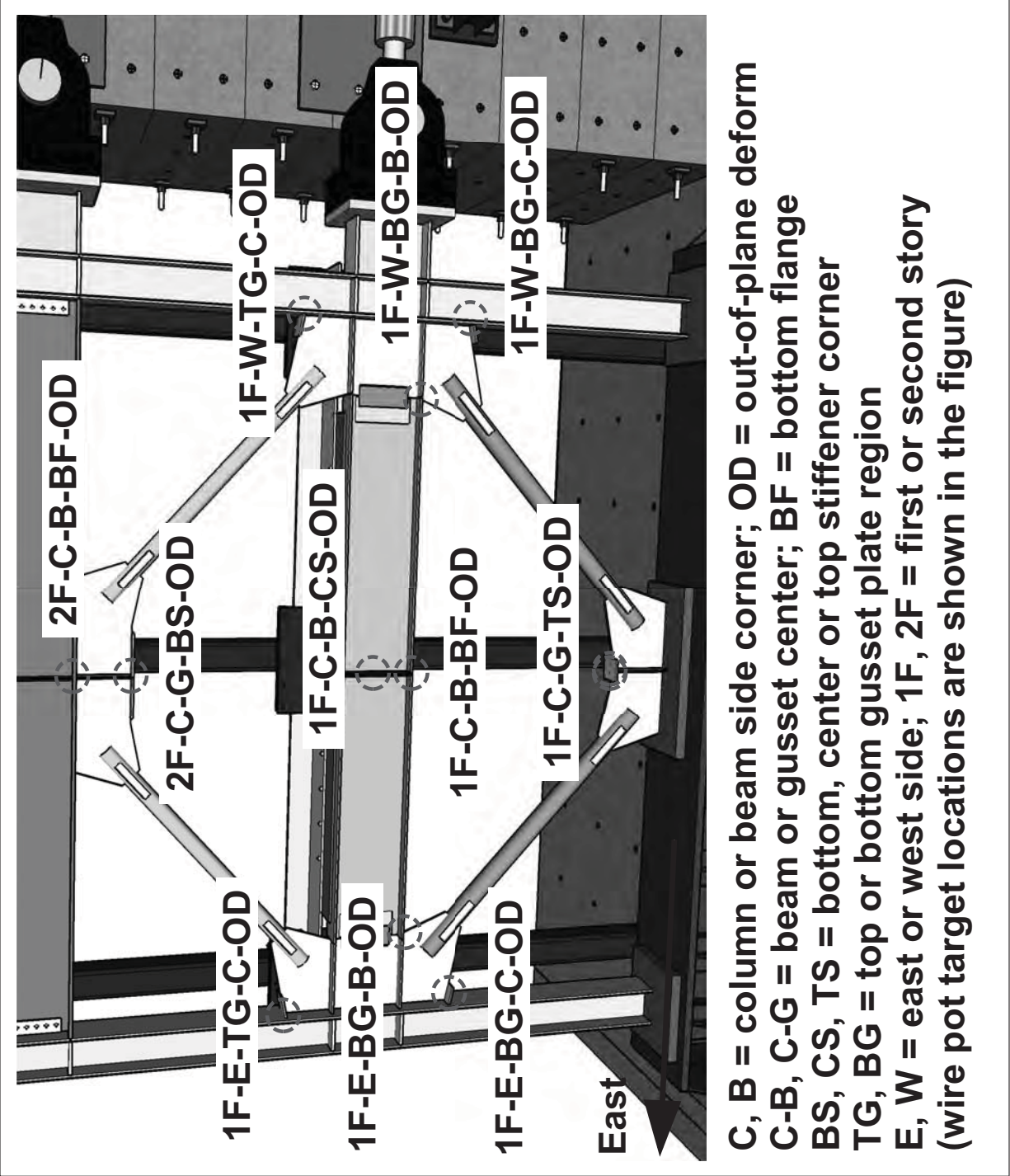
International Hybrid  
Simulation of  
Tomorrow's Braced  
Steel Frame  
Structures

University of California,  
Berkeley  
TCBF-B-2

PROJECT  
TCFB  
Oct 12, 2009  
DRAWN BY  
J.W. Lai  
PROJECT NO.  
TCBF-B-2

Sensor  
Locations

S-13





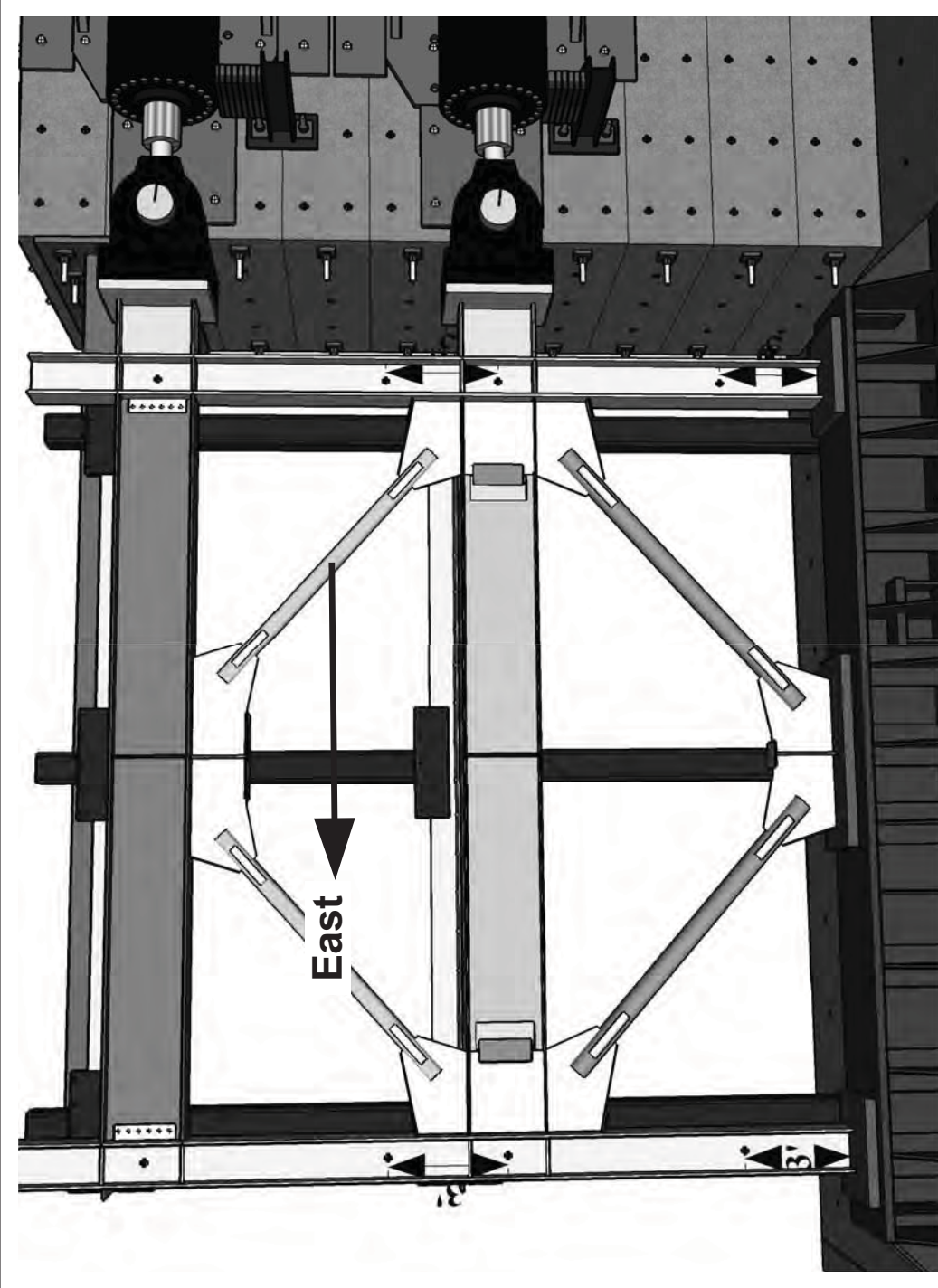
International Hybrid  
Simulation of  
Tomorrow's Braced  
Steel Frame  
Structures

University of California,  
Berkeley  
TCBF-B-2

PROJECT  
TCFB  
Oct 12,  
2009  
ISSUE  
DRAWN BY  
J.W. Lai  
PROJECT NO.  
TCBF-B-2

Sensor  
Locations

S.14



Overview of eight rosette locations on the specimen (only the column and panel zone regions). Details and label keys are shown in the next page.



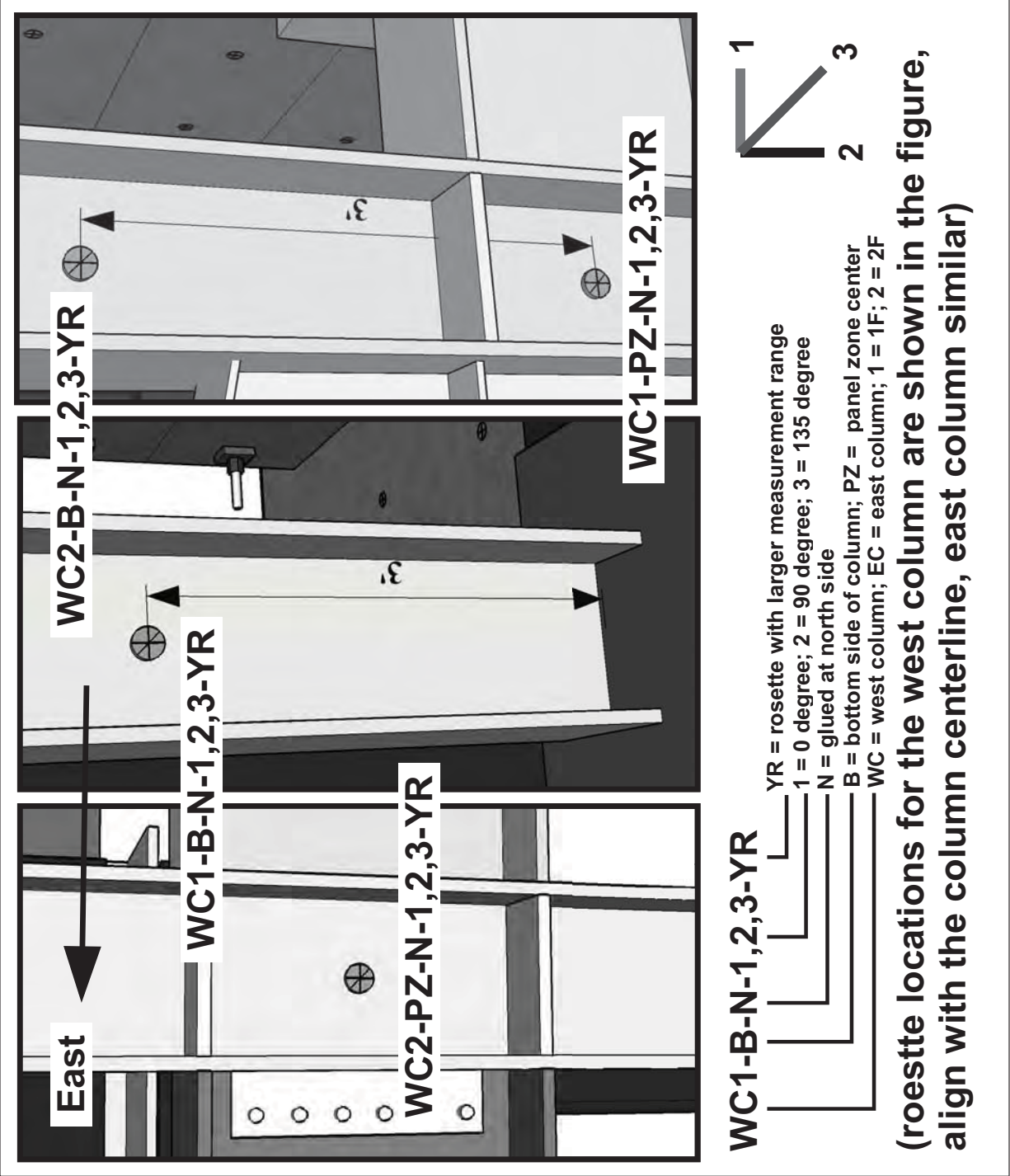
International Hybrid  
Simulation of  
Tomorrow's Braced  
Steel Frame  
Structures

University of California,  
Berkeley  
TCBF-B-2

PROJECT  
TCFB  
Oct 12, 2009  
DRAWN BY  
J.W. Lai  
TCBF-B-2  
PROJECT NO.

Sensor  
Locations

S-15





International Hybrid  
Simulation of  
Tomorrow's Braced  
Steel Frame  
Structures

University of California,  
Berkeley  
TCBF-B-2

PROJECT  
TCFB  
Oct 12, 2009  
ISSUE  
DRAWN BY  
J.W. Lai  
TCBF-B-2  
PROJECT NO.

Sensor  
Locations

S-16

**1F-E-TG-TL-1,2,3-N-YR**

**1F-E = east gusset plate**

**TG = top region**

**MG = middle region**

**BG = bottom region**

**TL = top left side**

**BL = bottom left side**

**TR = top right side**

**BR = bottom right side**

**TC = top center**

**BC = bottom center**

**1 = 0 degree (direction)**

**2 = 90 degree**

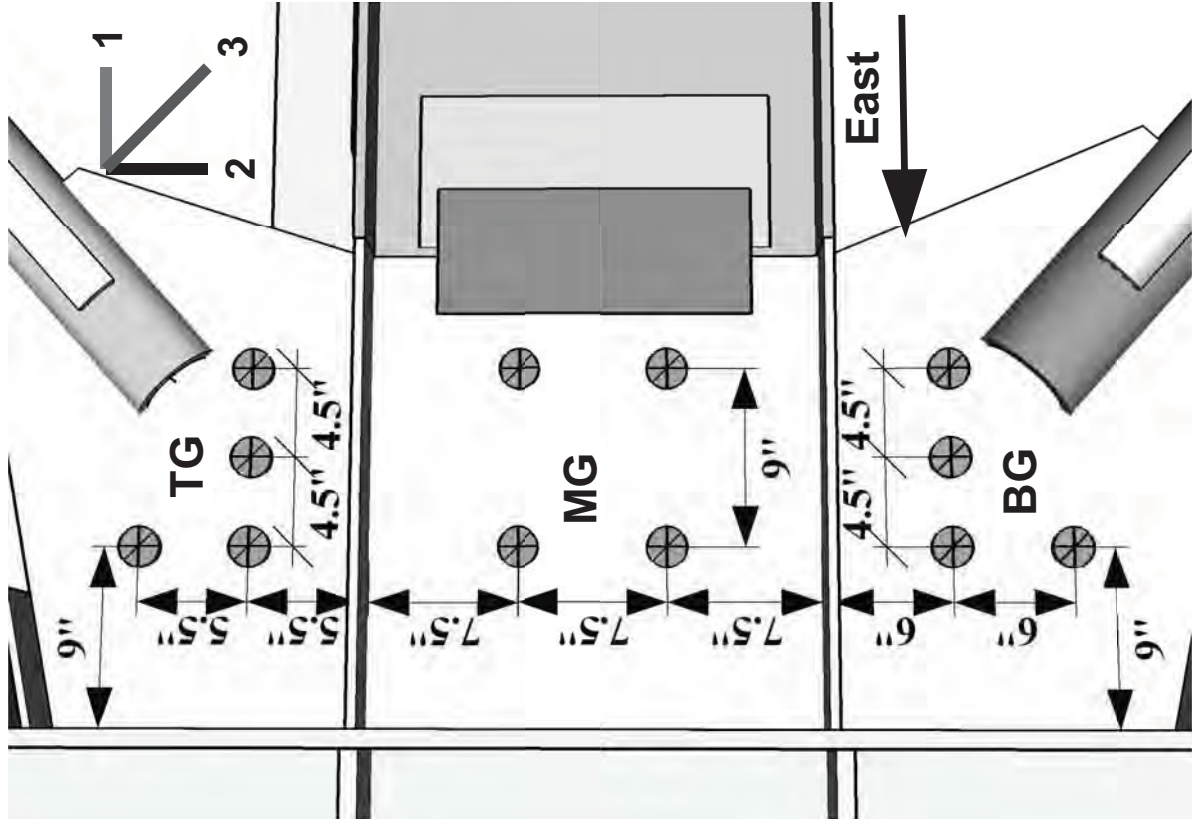
**3 = 135 degree**

**N = glued at north side**

**YR = rosette with larger**

**measurement range**

**(twelve rosette locations for the one-piece gusset plate, label keys are shown above)**

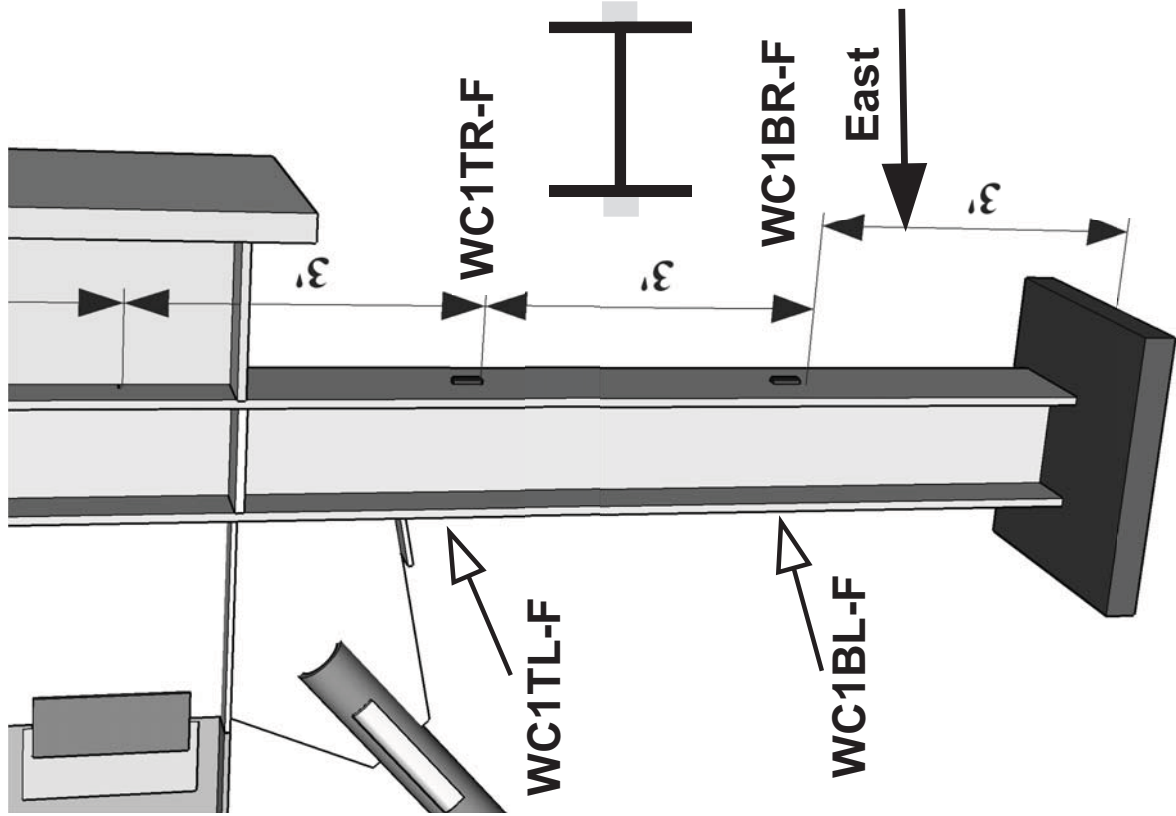


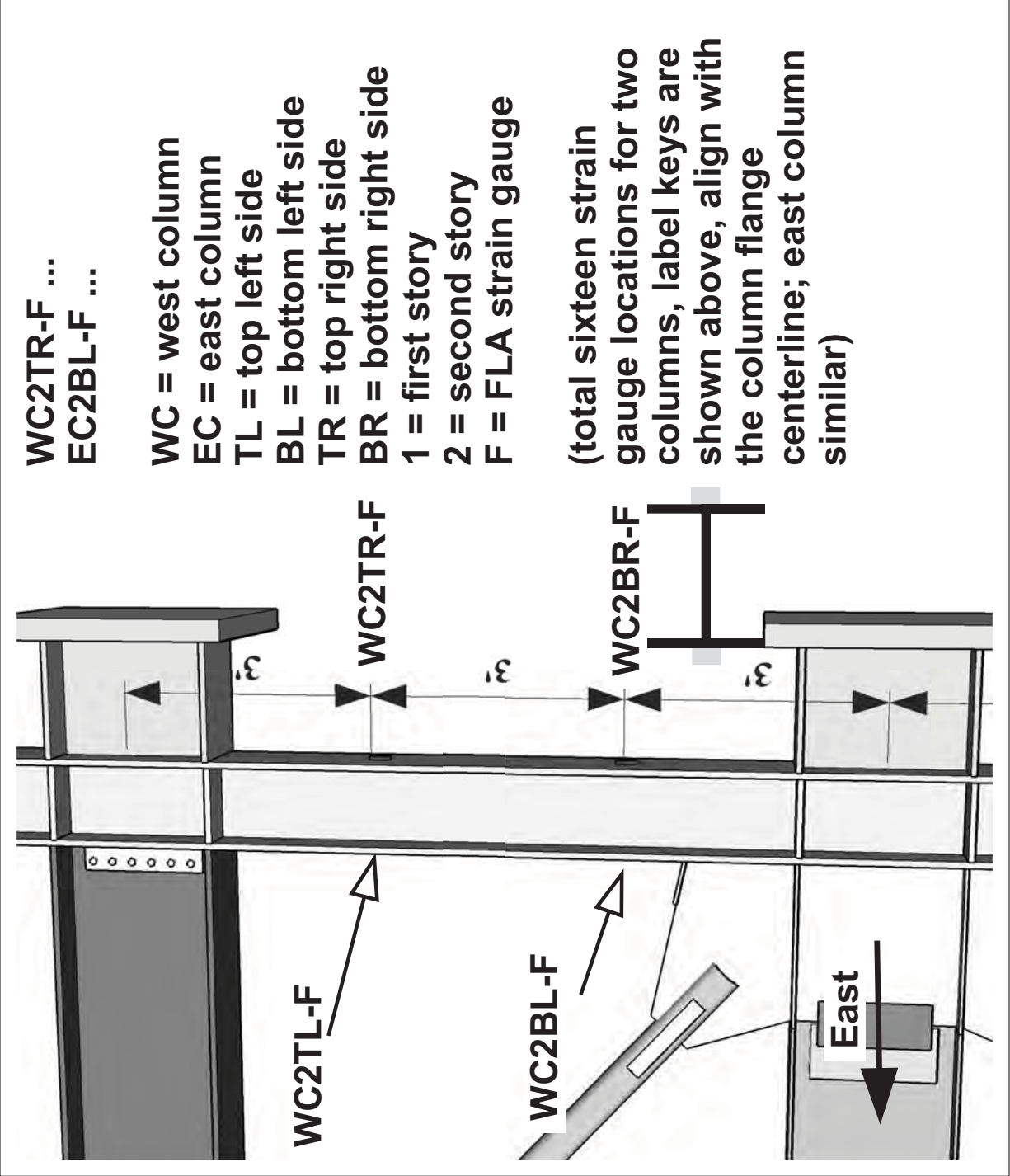


WC1TR-F ...  
EC1BL-F ...

WC = west column  
EC = east column  
TL = top left side  
BL = bottom left side  
TR = top right side  
BR = bottom right side  
1 = first story  
2 = second story  
F = FLA strain gauge

(total sixteen strain gauge locations for two columns, label keys are shown above, align with the column flange centerline; east column similar)









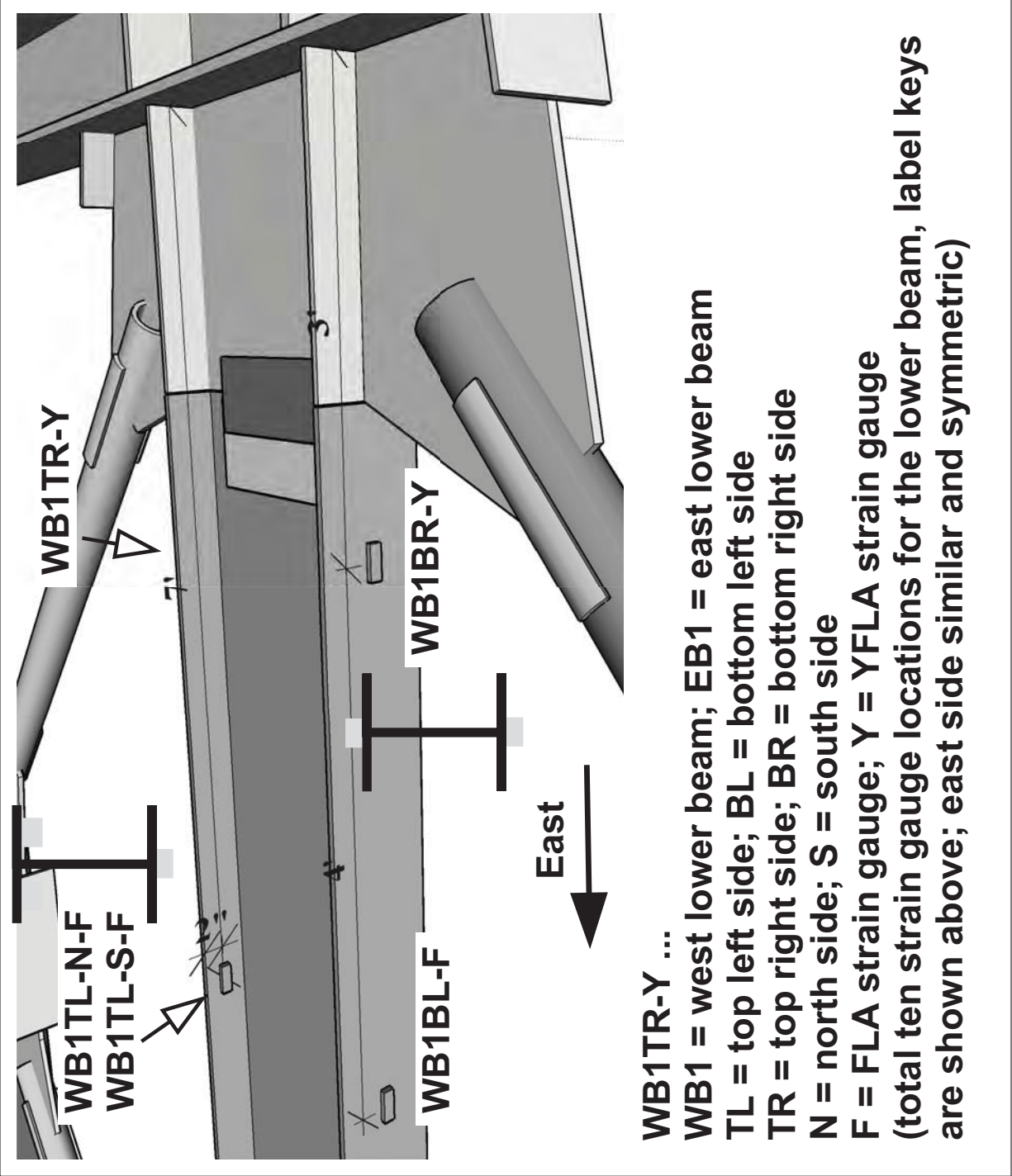
International Hybrid  
Simulation of  
Tomorrow's Braced  
Steel Frame  
Structures

University of California,  
Berkeley  
TCBF-B-2

PROJECT  
TCFB  
Oct 12,  
2009  
DRAWN BY  
J.W. Lai  
PROJECT NO.  
TCBF-B-2

Sensor  
Locations

S-19





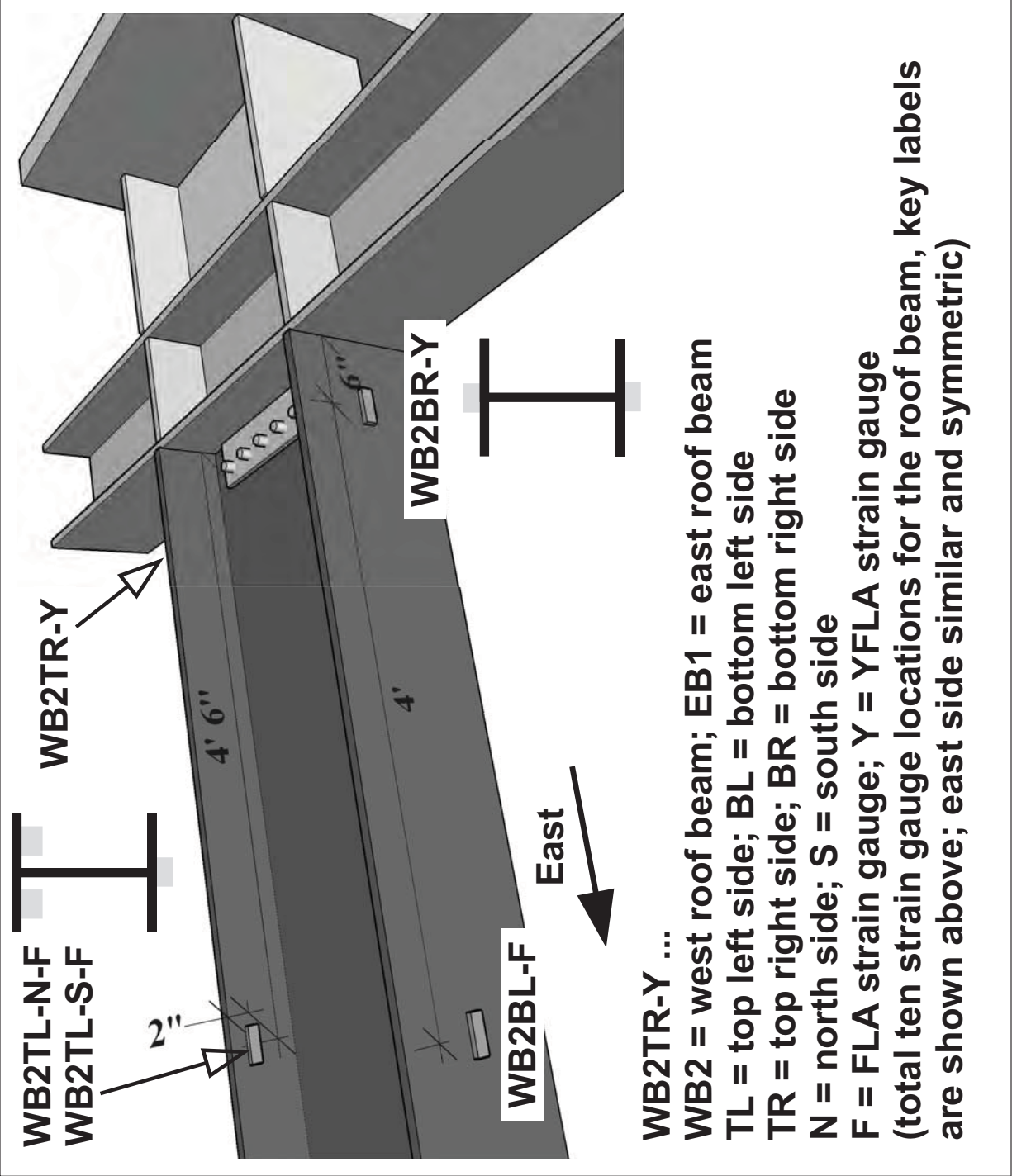
International Hybrid  
Simulation of  
Tomorrow's Braced  
Steel Frame  
Structures

University of California,  
Berkeley  
TCBF-B-2

PROJECT  
TCFB  
Oct 12, 2009  
DRAWN BY  
J.W. Lai  
PROJECT NO.  
TCBF-B-2

Sensor  
Locations

S-20





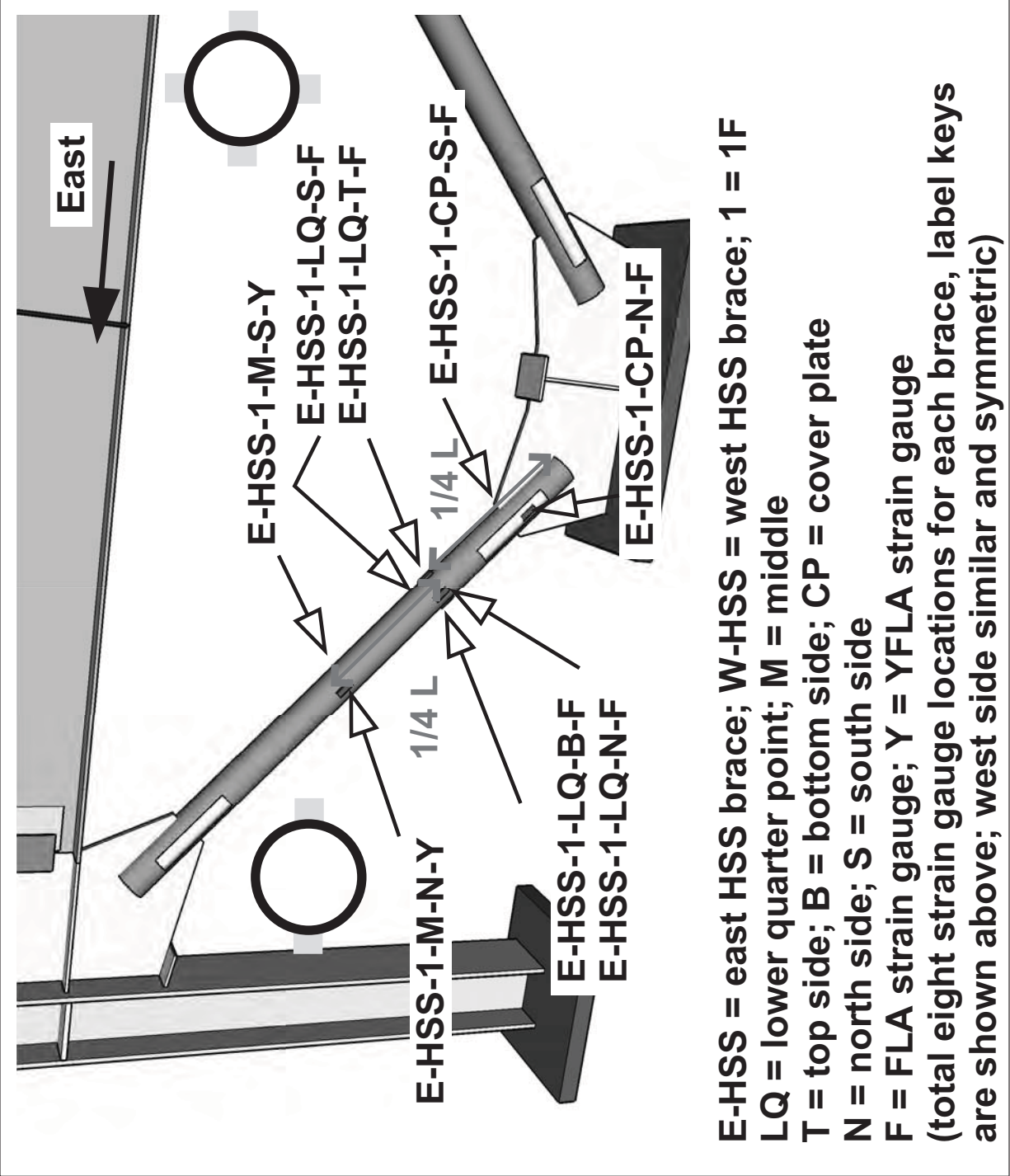
International Hybrid  
Simulation of  
Tomorrow's Braced  
Steel Frame  
Structures

University of California,  
Berkeley  
TCBF-B-2

PROJECT  
TCFB  
2009  
Oct 12,  
ISSUE  
DRAWN BY  
J.W. Lai  
TCBF-B-2  
PROJECT NO.

Sensor  
Locations

S.21





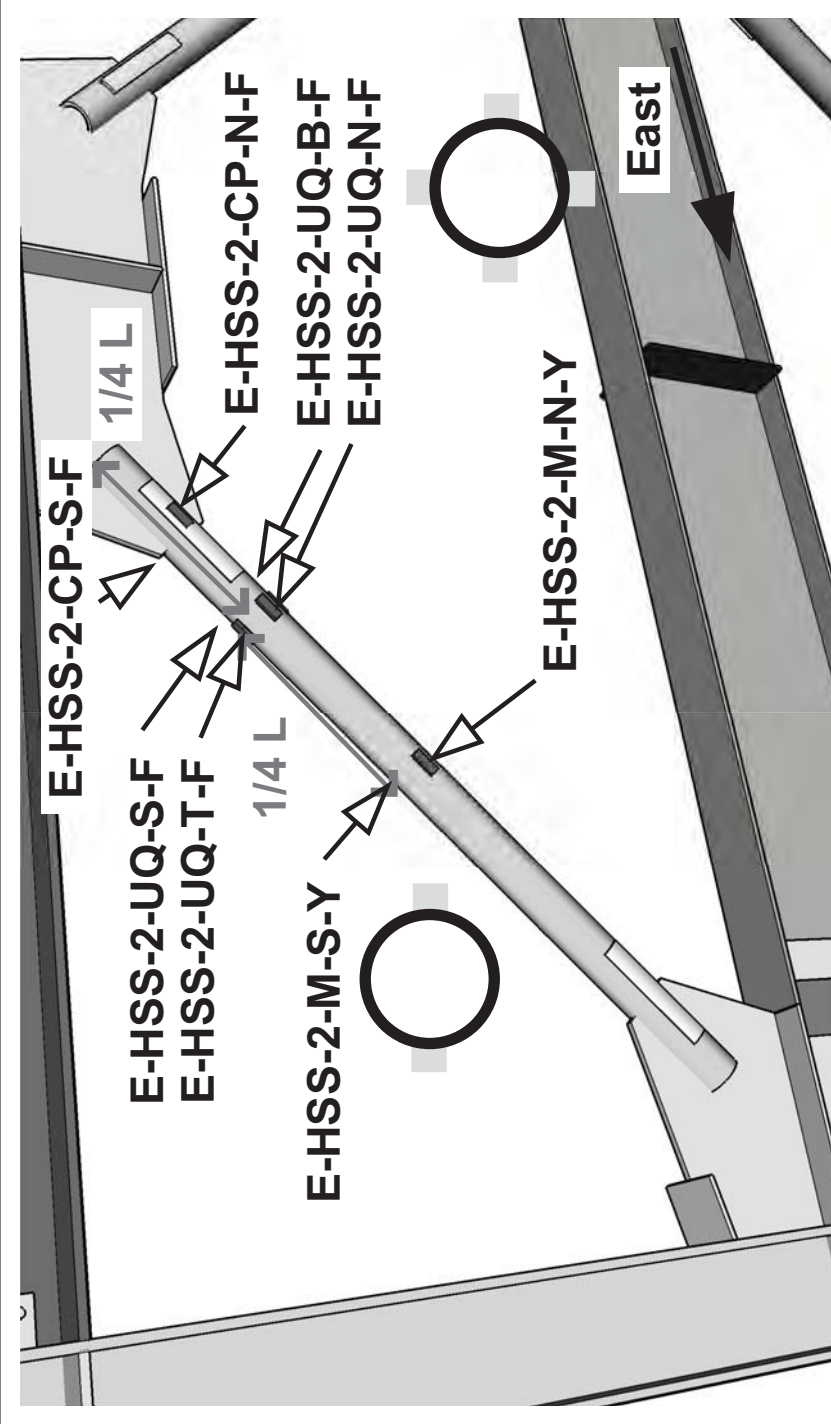
International Hybrid  
Simulation of  
Tomorrow's Braced  
Steel Frame  
Structures

University of California,  
Berkeley  
TCBF-B-2

PROJECT  
TCFB  
Oct 12, 2009  
ISSUE  
DRAWN BY  
J.W. Lai  
TCBF-B-2  
PROJECT NO.

Sensor  
Locations

**S.22**



**E-HSS = east HSS brace; W-HSS = west HSS brace; 2 = 2F**  
**UQ = upper quarter point; M = middle**  
**T = top side; B = bottom side; CP = cover plate**  
**N = north side; S = south side**  
**F = FLA strain gauge; Y = YFLA strain gauge**  
**(total eight strain gauge locations for each brace, label keys are shown above; west side similar and symmetric)**



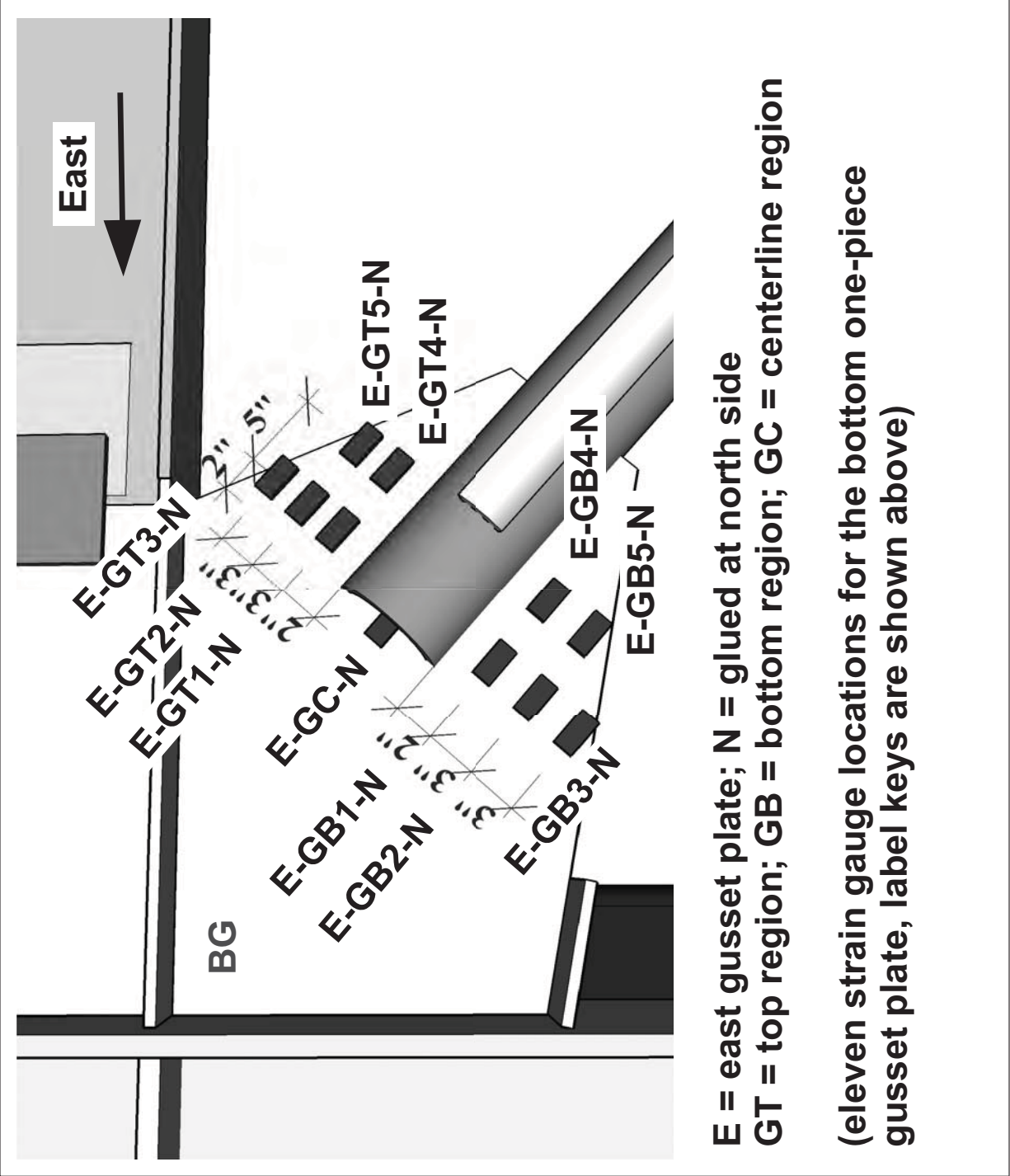
International Hybrid  
Simulation of  
Tomorrow's Braced  
Steel Frame  
Structures

University of California,  
Berkeley  
TCBF-B-2

PROJECT  
TCFB  
2009  
Oct 12,  
ISSUE  
DRAWN BY  
J.W. Lai  
PROJECT NO.  
TCBF-B-2

Sensor  
Locations

S.23



Channel	ID	Label	Device	Range	Serial No.	Cable No.	DAQ Box ID	Note	Column #
1	S1	EC1BL-F	strain gauge	-	-	13	0:3:0	1/4 bridge	14
2	S2	EC1BR-F	strain gauge	-	-	14	0:3:1	1/4 bridge	15
3	S3	EC1TL-F	strain gauge	-	-	15	0:3:2	1/4 bridge	16
4	S4	EC1TR-F	strain gauge	-	-	16	0:3:3	1/4 bridge	17
5	S5	E-GT1-N	strain gauge	-	-	5	0:1:0	1/4 bridge	6
6	S6	E-GT2-N	strain gauge	-	-	6	0:1:1	1/4 bridge	7
7	S7	E-HSS-1-M-N-Y	strain gauge	-	-	7	0:1:2	1/4 bridge	8
8	S8	E-HSS-1-M-S-Y	strain gauge	-	-	8	0:1:3	1/4 bridge	9
9	S9	E-HSS-1-LQ-T-F	strain gauge	-	-	9	0:2:0	1/4 bridge	10
10	S10	E-HSS-1-LQ-S-F	strain gauge	-	-	10	0:2:1	1/4 bridge	11
11	S11	E-HSS-1-LQ-N-F	strain gauge	-	-	11	0:2:2	1/4 bridge	12
12	S12	E-HSS-1-LQ-B-F	strain gauge	-	-	12	0:2:3	1/4 bridge	13
13	S13	E-HSS-1-CP-N-F	strain gauge	-	-	3	0:0:2	1/4 bridge	4
14	S14	E-HSS-1-CP-S-F	strain gauge	-	-	4	0:0:3	1/4 bridge	5
15	S15	EB1BL-Y	strain gauge	-	-	45	0:11:0	1/4 bridge	46
16	S16	EB1TL-Y	strain gauge	-	-	44	0:10:3	1/4 bridge	45
17	S17	EB1BR-F	strain gauge	-	-	204/70	1:1:1	1/4 bridge	71
18	S18	EB1TR-N-F	strain gauge	-	-	46	0:11:1	full-bridge	47
19	S19	EB1TR-S-F	strain gauge	-	-	46	0:11:1	full-bridge	47
20	S20	WB1BL-F	strain gauge	-	-	342/68	1:0:3	1/4 bridge	69
21	S21	WB1TL-N-F	strain gauge	-	-	322/69	1:1:0	full-bridge	70
22	S22	WB1TL-S-F	strain gauge	-	-	322/69	1:1:0	full-bridge	70
23	S23	WB1BR-Y	strain gauge	-	-	338/84	1:4:3	1/4 bridge	85
24	S24	WB1TR-Y	strain gauge	-	-	325/57	0:14:0	1/4 bridge	58
25	S25	W-HSS-1-CP-N-F	strain gauge	-	-	1	0:0:0	1/4 bridge	2
26	S26	W-HSS-1-CP-S-F	strain gauge	-	-	2	0:0:1	1/4 bridge	3
27	S27	W-HSS-1-LQ-T-F	strain gauge	-	-	25	0:6:0	1/4 bridge	26
28	S28	W-HSS-1-LQ-S-F	strain gauge	-	-	26	0:6:1	1/4 bridge	27
29	S29	W-HSS-1-LQ-N-F	strain gauge	-	-	27	0:6:2	1/4 bridge	28
30	S30	W-HSS-1-LQ-B-F	strain gauge	-	-	28	0:6:3	1/4 bridge	29
31	S31	W-HSS-1-M-N-Y	strain gauge	-	-	29	0:7:0	1/4 bridge	30
32	S32	W-HSS-1-M-S-Y	strain gauge	-	-	30	0:7:1	1/4 bridge	31
33	S33	E-GT3-N	strain gauge	-	-	31	0:7:2	1/4 bridge	32
34	S34	E-GT4-N	strain gauge	-	-	32	0:7:3	1/4 bridge	33

Channel	ID	Label	Device	Range	Serial No.	Cable No.	DAQ Box ID	Note	Column #
35	S35	WC1TL-F	strain gauge	-	-	95	1:7:2	1/4 bridge	96
36	S36	WC1TR-F	strain gauge	-	-	93	1:7:0	1/4 bridge	94
37	S37	WC1BL-F	strain gauge	-	-	94	1:7:1	1/4 bridge	95
38	S38	WC1BR-F	strain gauge	-	-	92	1:6:3	1/4 bridge	93
39	S39	EC2BL-F	strain gauge	-	-	39	0:9:2	1/4 bridge	40
40	S40	EC2BR-F	strain gauge	-	-	40	0:9:3	1/4 bridge	41
41	S41	EC2TL-F	strain gauge	-	-	41	0:10:0	1/4 bridge	42
42	S42	EC2TR-F	strain gauge	-	-	42	0:10:1	1/4 bridge	43
43	S43	EB2BL-Y	strain gauge	-	-	43	0:10:2	1/4 bridge	44
44	S44	EB2TL-Y	strain gauge	-	-	200/148	2:4:3	1/4 bridge	149
45	S45	EB2BR-F	strain gauge	-	-	197/145	2:4:0	1/4 bridge	146
46	S46	EB2TR-N-F	strain gauge	-	-	199/147	2:4:2	full-bridge	148
47	S47	EB2TR-S-F	strain gauge	-	-	199/147	2:4:2	full-bridge	148
48	S48	E-GT5-N	strain gauge	-	-	48	0:11:3	1/4 bridge	49
49	S49	E-GB1-N	strain gauge	-	-	49	0:12:0	1/4 bridge	50
50	S50	E-HSS-2-M-N-Y	strain gauge	-	-	50	0:12:1	1/4 bridge	51
51	S51	E-HSS-2-M-S-Y	strain gauge	-	-	51	0:12:2	1/4 bridge	52
52	S52	E-HSS-2-UQ-T-F	strain gauge	-	-	52	0:12:3	1/4 bridge	53
53	S53	E-HSS-2-UQ-S-F	strain gauge	-	-	53	0:13:0	1/4 bridge	54
54	S54	E-HSS-2-UQ-N-F	strain gauge	-	-	54	0:13:1	1/4 bridge	55
55	S55	E-HSS-2-UQ-B-F	strain gauge	-	-	55	0:13:2	1/4 bridge	56
56	S56	E-HSS-2-CP-N-F	strain gauge	-	-	56	0:13:3	1/4 bridge	57
57	S57	E-HSS-2-CP-S-F	strain gauge	-	-	47	0:11:2	1/4 bridge	48
58	S58	W-HSS-2-CP-N-F	strain gauge	-	-	324/58	0:14:1	1/4 bridge	59
59	S59	W-HSS-2-CP-S-F	strain gauge	-	-	326/59	0:14:2	1/4 bridge	60
60	S60	W-HSS-2-UQ-T-F	strain gauge	-	-	333/60	0:14:3	1/4 bridge	61
61	S61	W-HSS-2-UQ-S-F	strain gauge	-	-	327/61	0:15:0	1/4 bridge	62
62	S62	W-HSS-2-UQ-N-F	strain gauge	-	-	320/62	0:15:1	1/4 bridge	63
63	S63	W-HSS-2-UQ-B-F	strain gauge	-	-	321/63	0:15:2	1/4 bridge	64
64	S64	W-HSS-2-M-N-Y	strain gauge	-	-	322/64	0:15:3	1/4 bridge	65
65	S65	W-HSS-2-M-S-Y	strain gauge	-	-	203/65	1:0:0	1/4 bridge	66
66	S66	E-GB2-N	strain gauge	-	-	315/66	1:0:1	1/4 bridge	67
67	S67	E-GB3-N	strain gauge	-	-	343/67	1:0:2	1/4 bridge	68
68	S68	WB2BL-F	strain gauge	-	-	346/137	2:2:0	1/4 bridge	138

Channel	ID	Label	Device	Range	Serial No.	Cable No.	DAQ Box ID	Note	Column #
69	S69	WB2TL-N-F	strain gauge	-	-	328/138	2:2:1	full-bridge	139
70	S70	WB2TL-S-F	strain gauge	-	-	328/138	2:2:1	full-bridge	139
71	S71	WB2BR-Y	strain gauge	-	-	201/71	1:1:2	1/4 bridge	72
72	S72	WB2TR-Y	strain gauge	-	-	345/140	2:2:3	1/4 bridge	141
73	S73	WC2TL-F	strain gauge	-	-	316/73	1:2:0	1/4 bridge	74
74	S74	WC2TR-F	strain gauge	-	-	349/74	1:2:1	1/4 bridge	75
75	S75	WC2BL-F	strain gauge	-	-	351/75	1:2:2	1/4 bridge	76
76	S76	WC2BR-F	strain gauge	-	-	318/76	1:2:3	1/4 bridge	77
77	R1-1	EC1-B-N-1-YR	rosette	-	-	17	0:4:0	1/4 bridge	18
78	R1-2	EC1-B-N-2-YR	rosette	-	-	18	0:4:1	1/4 bridge	19
79	R1-3	EC1-B-N-3-YR	rosette	-	-	19	0:4:2	1/4 bridge	20
80	R2-1	EC1-PZ-N-1-YR	rosette	-	-	33	0:8:0	1/4 bridge	34
81	R2-2	EC1-PZ-N-2-YR	rosette	-	-	34	0:8:1	1/4 bridge	35
82	R2-3	EC1-PZ-N-3-YR	rosette	-	-	35	0:8:2	1/4 bridge	36
83	R3-1	EC2-B-N-1-YR	rosette	-	-	36	0:8:3	1/4 bridge	37
84	R3-2	EC2-B-N-2-YR	rosette	-	-	37	0:9:0	1/4 bridge	38
85	R3-3	EC2-B-N-3-YR	rosette	-	-	38	0:9:1	1/4 bridge	39
86	R4-1	EC2-PZ-N-1-YR	rosette	-	-	196/149	2:5:0	1/4 bridge	150
87	R4-2	EC2-PZ-N-2-YR	rosette	-	-	198/150	2:5:1	1/4 bridge	151
88	R4-3	EC2-PZ-N-3-YR	rosette	-	-	195/151	2:5:2	1/4 bridge	152
89	R5-1	WC1-B-N-1-YR	rosette	-	-	89	1:6:0	1/4 bridge	90
90	R5-2	WC1-B-N-2-YR	rosette	-	-	90	1:6:1	1/4 bridge	91
91	R5-3	WC1-B-N-3-YR	rosette	-	-	91	1:6:2	1/4 bridge	92
92	R6-1	WC1-PZ-N-1-YR	rosette	-	-	317/77	1:3:0	1/4 bridge	78
93	R6-2	WC1-PZ-N-2-YR	rosette	-	-	350/78	1:3:1	1/4 bridge	79
94	R6-3	WC1-PZ-N-3-YR	rosette	-	-	302/79	1:3:2	1/4 bridge	80
95	R7-1	WC2-B-N-1-YR	rosette	-	-	301/80	1:3:3	1/4 bridge	81
96	R7-2	WC2-B-N-2-YR	rosette	-	-	323/81	1:4:0	1/4 bridge	82
97	R7-3	WC2-B-N-3-YR	rosette	-	-	336/82	1:4:1	1/4 bridge	83
98	R8-1	WC2-PZ-N-1-YR	rosette	-	-	352/141	2:3:0	1/4 bridge	142
99	R8-2	WC2-PZ-N-2-YR	rosette	-	-	319/142	2:3:1	1/4 bridge	143
100	R8-3	WC2-PZ-N-3-YR	rosette	-	-	329/143	2:3:2	1/4 bridge	144
101	R9-1	1F-E-BG-TL-1-N-YR	rosette	-	-	101	1:9:0	1/4 bridge	102
102	R9-2	1F-E-BG-TL-2-N-YR	rosette	-	-	102	1:9:1	1/4 bridge	103



Channel	ID	Label	Device	Range	Serial No.	Cable No.	DAQ Box ID	Note	Column #
103	R9-3	IF-E-BG-TL-3-N-YR	rosette	-	-	103	1:9:2	1/4 bridge	104
104	R10-1	IF-E-BG-BL-1-N-YR	rosette	-	-	104	1:9:3	1/4 bridge	105
105	R10-2	IF-E-BG-BL-2-N-YR	rosette	-	-	105	1:10:0	1/4 bridge	106
106	R10-3	IF-E-BG-BL-3-N-YR	rosette	-	-	106	1:10:1	1/4 bridge	107
107	R11-1	IF-E-BG-TR-1-N-YR	rosette	-	-	107	1:10:2	1/4 bridge	108
108	R11-2	IF-E-BG-TR-2-N-YR	rosette	-	-	108	1:10:3	1/4 bridge	109
109	R11-3	IF-E-BG-TR-3-N-YR	rosette	-	-	109	1:11:0	1/4 bridge	110
110	R12-1	IF-E-BG-TC-1-N-YR	rosette	-	-	110	1:11:1	1/4 bridge	111
111	R12-2	IF-E-BG-TC-2-N-YR	rosette	-	-	111	1:11:2	1/4 bridge	112
112	R12-3	IF-E-BG-TC-3-N-YR	rosette	-	-	112	1:11:3	1/4 bridge	113
113	R13-1	IF-E-MG-TL-1-N-YR	rosette	-	-	113	1:12:0	1/4 bridge	114
114	R13-2	IF-E-MG-TL-2-N-YR	rosette	-	-	114	1:12:1	1/4 bridge	115
115	R13-3	IF-E-MG-TL-3-N-YR	rosette	-	-	115	1:12:2	1/4 bridge	116
116	R14-1	IF-E-MG-BL-1-N-YR	rosette	-	-	116	1:12:3	1/4 bridge	117
117	R14-2	IF-E-MG-BL-2-N-YR	rosette	-	-	117	1:13:0	1/4 bridge	118
118	R14-3	IF-E-MG-BL-3-N-YR	rosette	-	-	118	1:13:1	1/4 bridge	119
119	R15-1	IF-E-MG-TR-1-N-YR	rosette	-	-	119	1:13:2	1/4 bridge	120
120	R15-2	IF-E-MG-TR-2-N-YR	rosette	-	-	120	1:13:3	1/4 bridge	121
121	R15-3	IF-E-MG-TR-3-N-YR	rosette	-	-	121	1:14:0	1/4 bridge	122
122	R16-1	IF-E-MG-BR-1-N-YR	rosette	-	-	122	1:14:1	1/4 bridge	123
123	R16-2	IF-E-MG-BR-2-N-YR	rosette	-	-	123	1:14:2	1/4 bridge	124
124	R16-3	IF-E-MG-BR-3-N-YR	rosette	-	-	124	1:14:3	1/4 bridge	125
125	R17-1	IF-E-TG-TL-1-N-YR	rosette	-	-	125	1:15:0	1/4 bridge	126
126	R17-2	IF-E-TG-TL-2-N-YR	rosette	-	-	126	1:15:1	1/4 bridge	127
127	R17-3	IF-E-TG-TL-3-N-YR	rosette	-	-	127	1:15:2	1/4 bridge	128
128	R18-1	IF-E-TG-BL-1-N-YR	rosette	-	-	128	1:15:3	1/4 bridge	129
129	R18-2	IF-E-TG-BL-2-N-YR	rosette	-	-	129	2:0:0	1/4 bridge	130
130	R18-3	IF-E-TG-BL-3-N-YR	rosette	-	-	130	2:0:1	1/4 bridge	131
131	R19-1	IF-E-TG-BC-1-N-YR	rosette	-	-	131	2:0:2	1/4 bridge	132
132	R19-2	IF-E-TG-BC-2-N-YR	rosette	-	-	303	2:0:3	1/4 bridge	133
133	R19-3	IF-E-TG-BC-3-N-YR	rosette	-	-	133	2:1:0	1/4 bridge	134
134	R20-1	IF-E-TG-BR-1-N-YR	rosette	-	-	134	2:1:1	1/4 bridge	135
135	R20-2	IF-E-TG-BR-2-N-YR	rosette	-	-	135	2:1:2	1/4 bridge	136
136	R20-3	IF-E-TG-BR-3-N-YR	rosette	-	-	136	2:1:3	1/4 bridge	137

Channel	ID	Label	Device	Range	Serial No.	Cable No.	DAQ Box ID	Note	Column #
137	WP07	1F-E-HSS-UQ-R-OD	wire pot	30"	2000NC51151	159	2:7:2	-	160
138	WP04	1F-E-HSS-M-R-OD	wire pot	40"	2005NC51006	156	2:6:3	-	157
139	WP02	1F-E-HSS-LQ-R-OD	wire pot	30"	2006NC51015	154	2:6:1	-	155
140	WP03	1F-E-HSS-UQ-L-OD	wire pot	30"	2006NC51012	155	2:6:2	-	156
141	WP05	1F-E-HSS-M-L-OD	wire pot	40"	2005NC01003	157	2:7:0	-	158
142	WP01	1F-E-HSS-LQ-L-OD	wire pot	30"	2006NC51014	153	2:6:0	-	154
143	WP06	1F-W-HSS-LQ-R-OD	wire pot	30"	2000NC51124	158	2:7:1	-	159
144	WP12	1F-W-HSS-M-R-OD	wire pot	40"	2005NC01008	164	2:8:3	-	165
145	WP09	1F-W-HSS-UQ-R-OD	wire pot	30"	2000NC51106	161	2:8:0	-	162
146	WP08	1F-W-HSS-LQ-L-OD	wire pot	30"	2006NC51016	160	2:7:3	-	161
147	WP11	1F-W-HSS-M-L-OD	wire pot	40"	2005NC01006	163	2:8:2	-	164
148	WP10	1F-W-HSS-UQ-L-OD	wire pot	30"	2000NC51116	162	2:8:1	-	163
149	WP14	2F-E-HSS-LQ-R-OD	wire pot	30"	2006NC51013	166/305	2:9:1	-	167
150	WP17	2F-E-HSS-M-R-OD	wire pot	40"	2005NC51002	169/308	2:10:0	-	170
151	WP13	2F-E-HSS-UQ-R-OD	wire pot	40"	2009NC01052	342	2:9:0	-	166
152	WP16	2F-E-HSS-LQ-L-OD	wire pot	30"	2000NC51125	168/307	2:9:3	-	169
153	WP18	2F-E-HSS-M-L-OD	wire pot	40"	2005NC51007	170/309	2:10:1	-	171
154	WP15	2F-E-HSS-UQ-L-OD	wire pot	30"	2000NC51105	167/306	2:9:2	-	168
155	WP22	2F-W-HSS-UQ-R-OD	wire pot	40"	2005NC01010	174/313	2:11:1	-	175
156	WP20	2F-W-HSS-M-R-OD	wire pot	40"	2005NC01009	172/311	2:10:3	-	173
157	WP24	2F-W-HSS-LQ-R-OD	wire pot	30"	2000NC51153	176/315	2:11:3	-	177
158	WP21	2F-W-HSS-UQ-L-OD	wire pot	40"	2005NC51010	173/312	2:11:0	-	174
159	WP19	2F-W-HSS-M-L-OD	wire pot	40"	2009NC01046	394	2:10:2	-	172
160	WP23	2F-W-HSS-LQ-L-OD	wire pot	30"	2000NC51111	175/314	2:11:2	-	176
161	WP25	1F-E-HSS-A	wire pot	40"	2005NC51009	177	2:12:0	-	178
162	WP26	1F-W-HSS-A	wire pot	40"	2005NC01004	178	2:12:1	-	179
163	WP27	2F-E-HSS-A	wire pot	40"	2005NC01001	300	2:14:0	-	186
164	WP28	2F-W-HSS-A	wire pot	40"	2000NC51131	301	2:14:1	-	187
165	S201	E-GB5-N	strain gauge	-	-	97	2:13:0	1/4 bridge	182
166	S202	E-GB4-N	strain gauge	-	-	98	2:13:1	1/4 bridge	183
167	S203	E-GC-N	strain gauge	-	-	100	2:13:3	1/4 bridge	185
168	ST20	WB1-RT	stick	4"	2004NC01031	307	2:13:2	Novo 100	184
169	ST22	EB1-RT	stick	4"	2006NC01024	183	1:8:0	Novo 100	98
170	ST21	EB1-RB	stick	4"	2007NC51005	184	1:8:1	Novo 100	99

Channel	ID	Label	Device	Range	Serial No.	Cable No.	DAQ Box ID	Note	Column #
171	ST17	RRW-T-N	stick	4"	2009NC01008	318/398	1:8:2	Novo100	100
172	ST18	RRW-T-S	stick	4"	2009NC01007	319/393	1:8:3	Novo100	101
173	WP30	IF-C-G-TS-OD	wire pot	40"	2005NC01005	21	0:5:0	-	22
174	WP47	IF-W-TG-C-OD	wire pot	30"	2000NC51150	313	1:5:3	-	89
175	WP33	IF-E-BG-C-OD	wire pot	40"	2005NC51001	24	0:5:3	-	25
176	WP29	IF-W-BG-C-OD	wire pot	40"	2005NC51005	20	0:4:3	-	21
177	WP43	IF-E-BG-B-OD	wire pot	30"	2000NC51098	320	1:4:2	-	84
178	WP31	IF-C-B-BF-OD	wire pot	30"	2000NC51128	22	0:5:1	-	23
179	WP32	IF-C-B-CS-OD	wire pot	40"	2005NC51003	23	0:5:2	-	24
180	WP42	IF-W-BG-B-OD	wire pot	30"	2000NC51117	314	1:1:3	-	73
181	WP46	IF-E-TG-C-OD	wire pot	30"	2000NC51152	312	1:5:2	-	88
182	WP44	2F-C-B-BF-OD	wire pot	30"	2000NC51126	310	1:5:0	-	86
183	WP45	2F-C-G-BS-OD	wire pot	30"	2000NC51129	311	1:5:1	-	87
184	A5	Act2disp	position transducer	40"	2007NC01001	182/363	2:12:3	ST01	181
185	ST2	C-GB-Slip	stick	1"	2004NC01015	181/358	2:12:2	-	180
186	ST3	W-CB-Slip	stick	1"	2004NC01012	96/357	1:7:3	-	97
187	ST4	E-LC1-OD	stick	6"	2007NC01009	179	2:15:2	-	192
188	ST5	E-LC2-OD	stick	6"	2007NC01010	302	2:14:2	-	188
189	ST6	C-LC1-OD	stick	6"	2007NC01011	180	2:15:3	-	193
190	ST7	C-LC2-OD	stick	6"	2007NC51006	303	2:14:3	-	189
191	ST8	W-LC1-OD	stick	6"	2007NC51007	304	2:15:0	-	190
192	ST9	W-LC2-OD	stick	6"	2007NC51010	305	2:15:1	-	191
193	ST10	C-B1-VD	stick	4"	2007NC01006	144	2:3:3	-	145
194	ST11	C-B2-VD	stick	4"	2007NC01003	210	2:5:3	Novo100_02-210	153
195	ST19	WB1-RB	stick	4"	2009NC01004	316	2:2:2	Novo100	140
196	PT1	EC1-PZ-E-PT	position transducer	20"	2004NC01053	323	2:4:1	Novo500	147
197	PT2	EC2-PZ-E-PT	position transducer	40"	-	CS2-disp	3:0:4	Displacement Control	198
198	A1	Act1disp	position transducer	40"	2006NC01002	CS1-disp	3:0:0	-	194
199	A2	Act1force	load cell	-	-	CS1-load	3:0:1	From LC1	195
200	A3	Act1dispCmd	-	-	-	-	3:0:2	From STS (CMD)	196
201	A4	Act1dispAct3	position transducer	40"	2006NC01003	CS3-disp	3:0:3	-	197
202	PT2	EC2-PZ-E-PT	position transducer	40"	-	CS2-disp	3:0:4	Act2disp (A5)	198
203	A6	Act2force	load cell	-	-	CS2-load	3:0:5	From LC2	199
204	A7	Act2dispCmd	-	-	-	-	3:0:6	From STS (CMD)	200

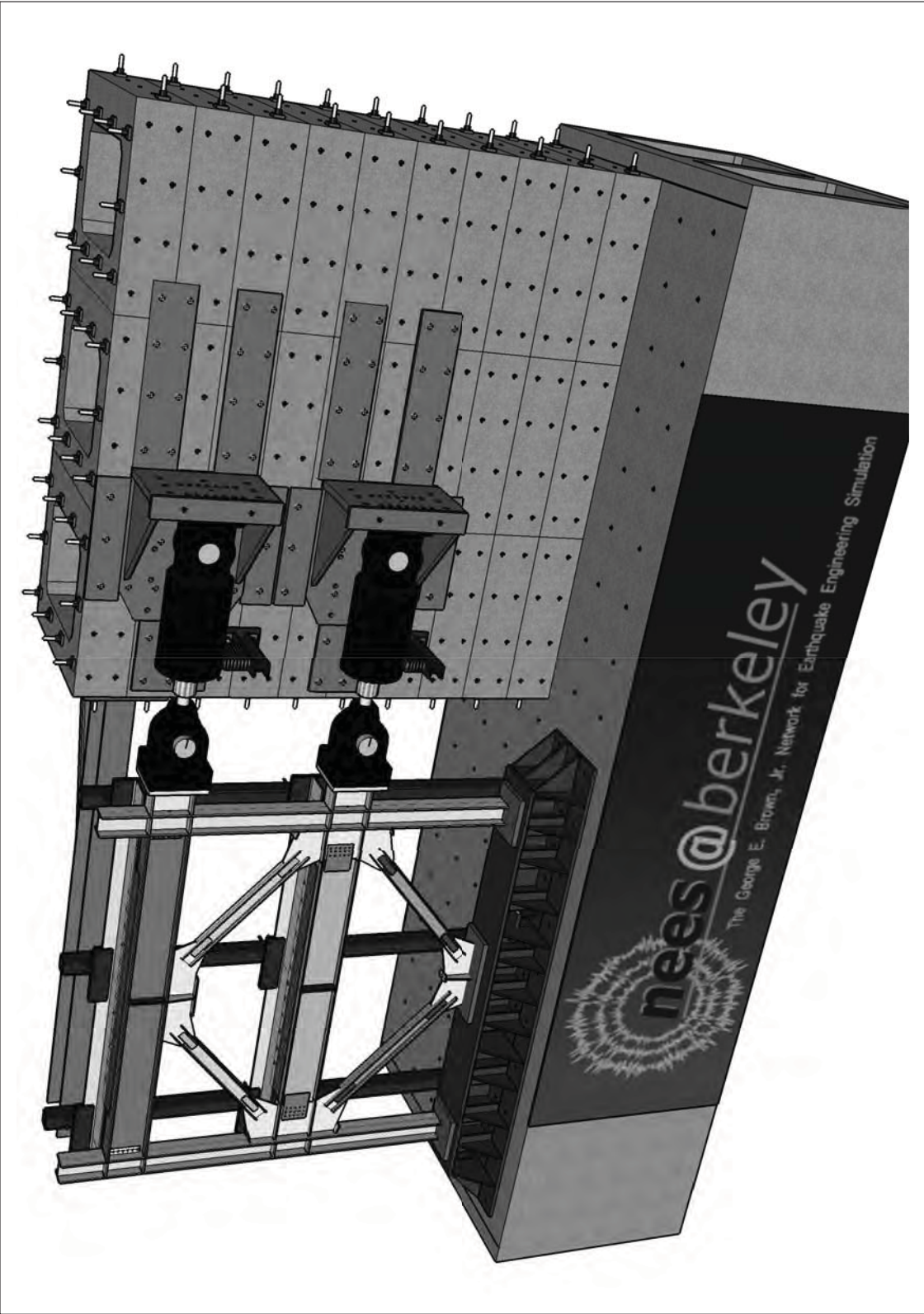
Channel	ID	Label	Device	Range	Serial No.	Cable No.	DAQ Box ID	Note	Column #
205	A8	Act2dispAct4	position transducer	40"	2004NC01061	CS4-disp	3:0:7	-	201
206	ST12	FB-Slip	stick	2"	2004NC01023	308	3:1:0	D-Space (Novo50_DS1)	202
207	ST13	RRW-Slip-N	stick	2"	2004NC01019	309	3:1:1	D-Space (Novo50_DS2)	203
208	ST14	RRW-Slip-S	stick	2"	2004NC01028	306	3:1:2	D-Space (Novo50_DS3)	204
209	ST15	Act1-BK	stick	2"	2004NC01025	361	3:1:3	D-Space (Novo50_DS4)	205
210	ST16	Act2-BK	stick	2"	2004NC01020	355	3:1:4	D-Space (Novo50_DS5)	206
211	TG1	TriggerCanon	-	-	-	207	3:1:5	D-Space	207
212	TG2	TriggerLeica	-	-	-	208	3:1:6	D-Space	208
213	ST1	E-CB-Slip	stick	1"	2004NC01014	379	3:1:7	D-Space	209

---

## **Appendix F**

### **Channel Locations and Lists for TCBF-B-3 Specimen**

---



International Hybrid  
Simulation of  
Tomorrow's Braced  
Steel Frame Structures

**PROJECT**  
TCBF

**PROJECT NO.**  
TCBF-B-3

**DRAWN BY**  
Jiun-Wei Lai

**ISSUE**  
Jan 11, 2011

**TCBF-B-3, Sensor Locations**  
**S.00**



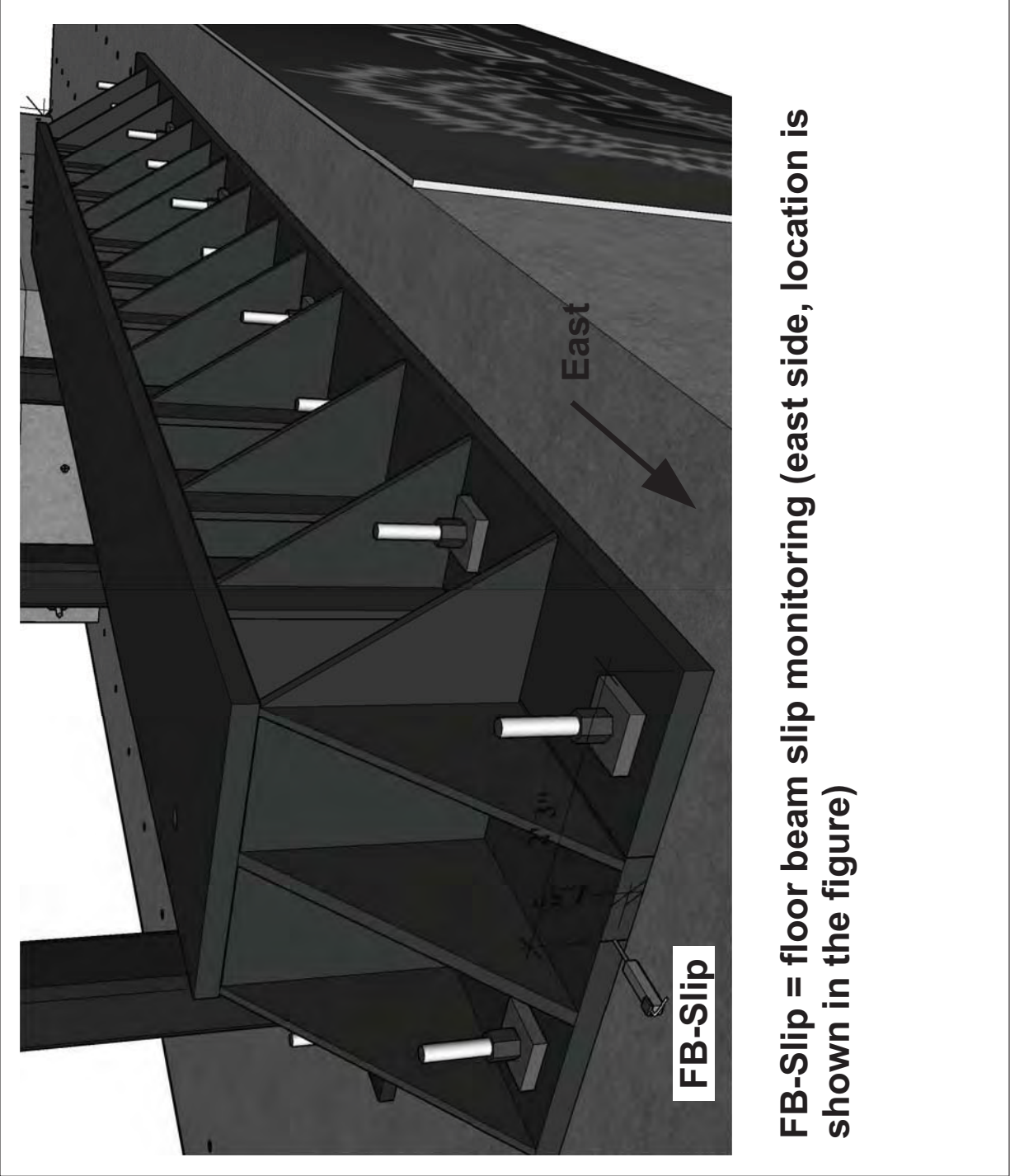
International Hybrid  
Simulation of  
Tomorrow's Braced  
Steel Frame  
Structures

University of California,  
Berkeley  
TCBF-B-3

PROJECT  
TCFB  
Jan 11,  
2011  
ISSUE  
DRAWN BY  
J.W. Lai  
PROJECT NO.  
TCBF-B-3

Sensor  
Locations

S.01





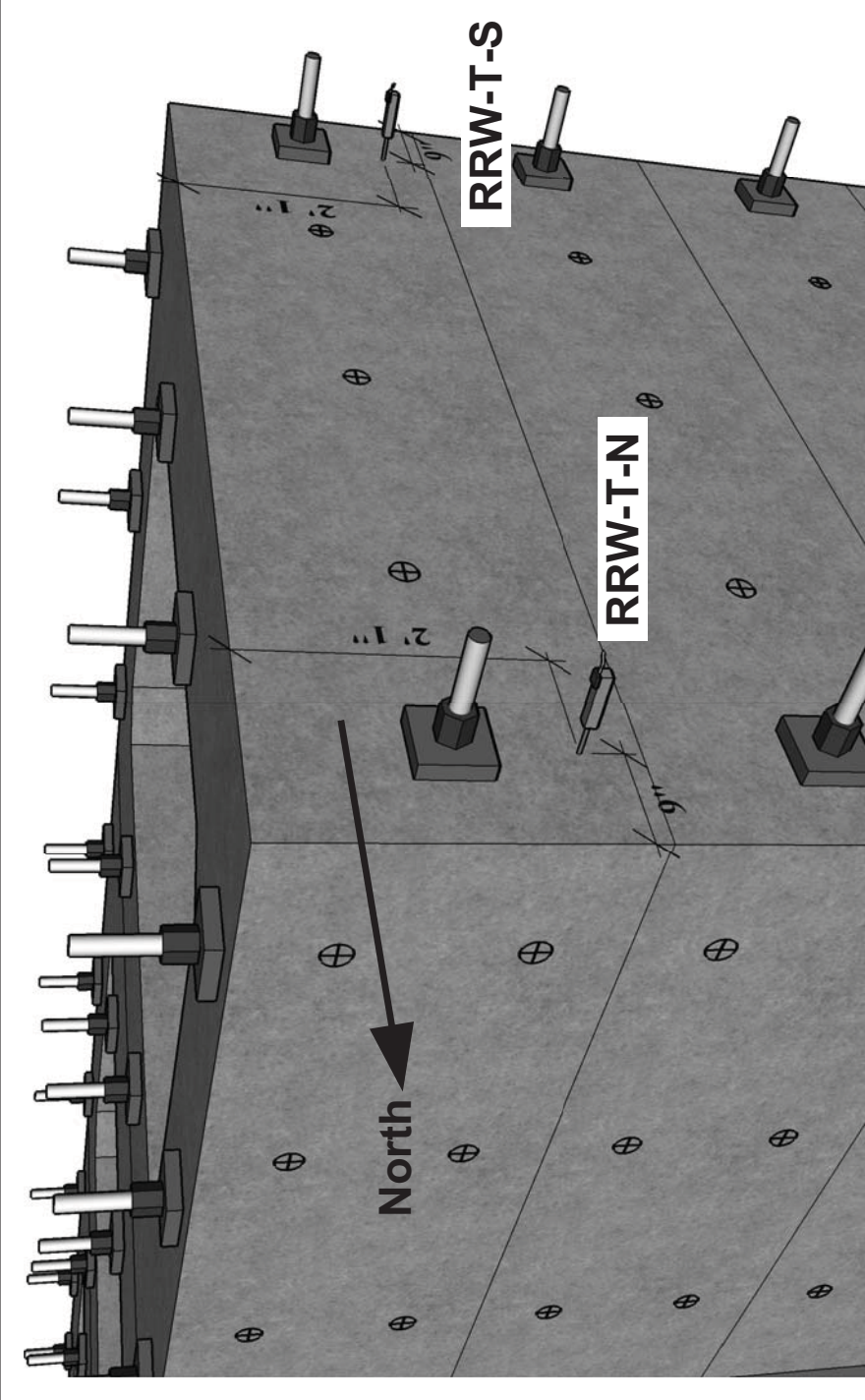
International Hybrid  
Simulation of  
Tomorrow's Braced  
Steel Frame  
Structures

University of California,  
Berkeley  
TCBF-B-3

PROJECT  
TCFB  
2011  
ISSUE  
Jan 11,  
2011  
DRAWN BY  
J.W. Lai  
PROJECT NO.  
TCBF-B-3

Sensor  
Locations

S.02



**RRW-T-N = north side of reconfigurable reaction wall (RRW), top deformation monitoring (location is shown in the figure)**

**RRW-T-S = south side of reconfigurable reaction wall (RRW), top deformation monitoring (location is shown in the figure)**





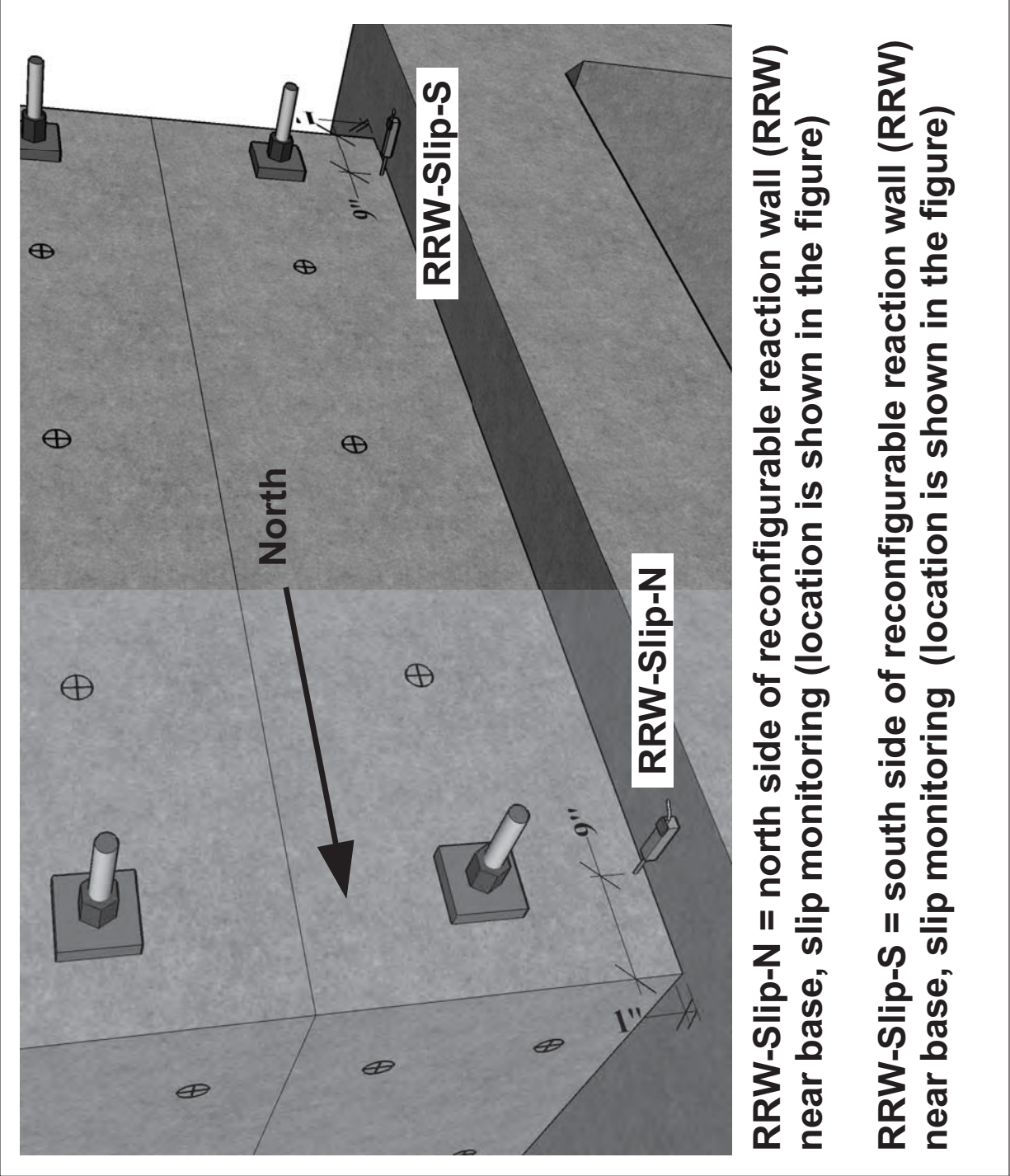
International Hybrid  
Simulation of  
Tomorrow's Braced  
Steel Frame  
Structures

University of California,  
Berkeley  
TCBF-B-3

PROJECT  
TCFB  
Jan 11, 2011  
ISSUE  
DRAWN BY  
J.W. Lai  
PROJECT NO.  
TCBF-B-3

Sensor  
Locations

S.03





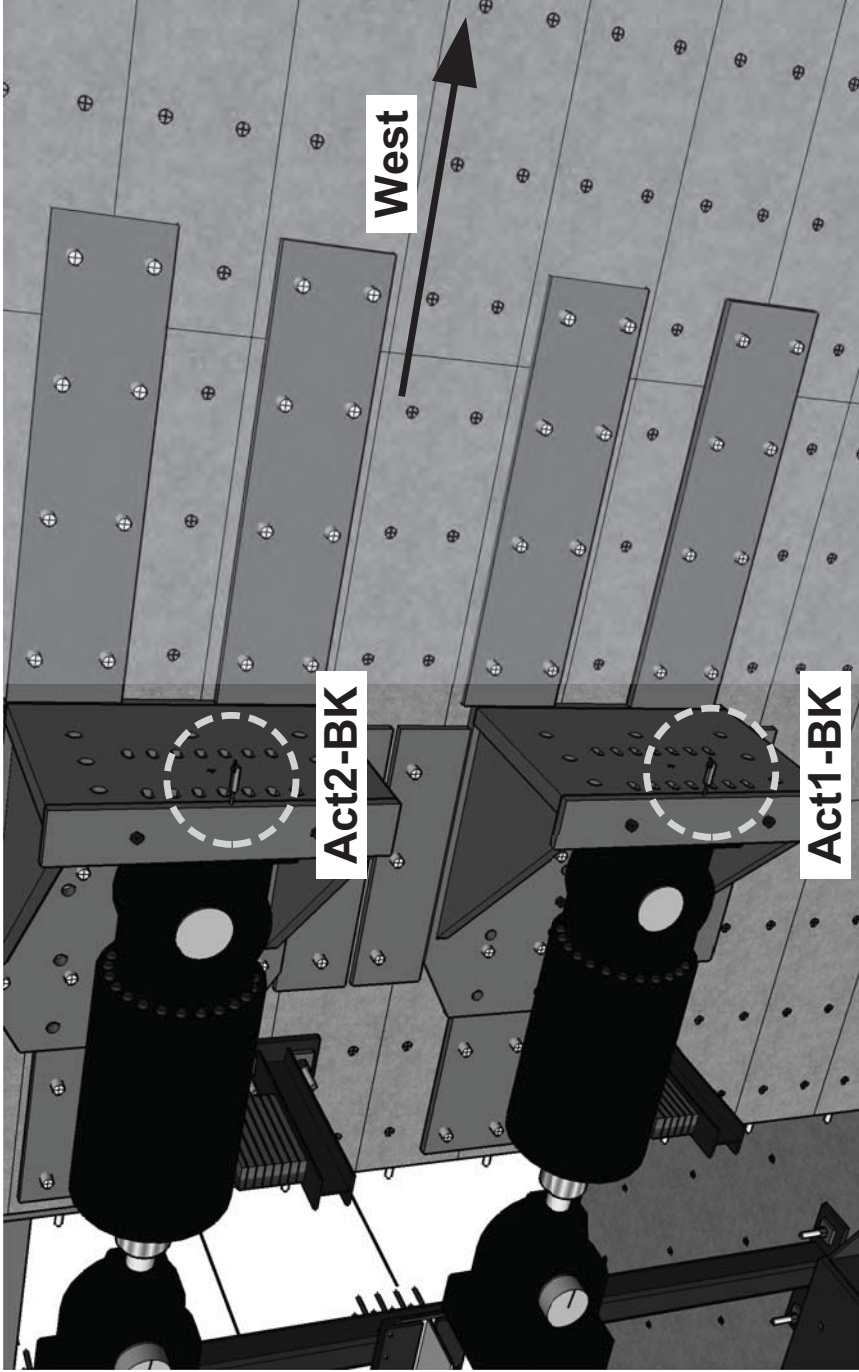
International Hybrid  
Simulation of  
Tomorrow's Braced  
Steel Frame  
Structures

University of California,  
Berkeley  
TCBF-B-3

PROJECT  
TCFB  
Jan 11,  
2011  
ISSUE  
DRAWN BY  
J.W. Lai  
PROJECT NO.  
TCBF-B-3

Sensor  
Locations

S.04



**Act1-BK = lower actuator bracket deformation monitoring  
(location is shown in the figure)**

**Act2-BK = upper actuator bracket deformation monitoring  
(location is shown in the figure)**



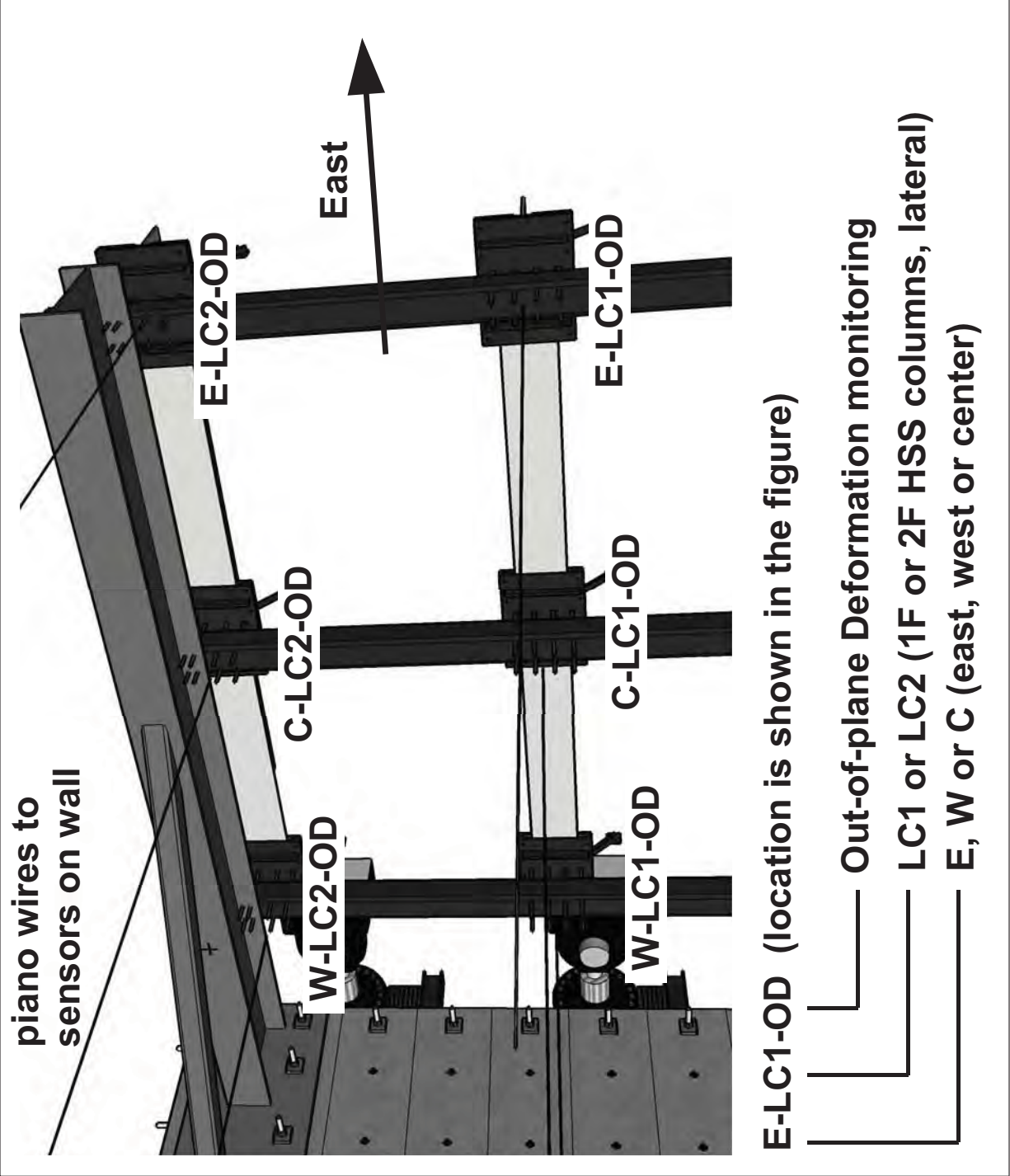
International Hybrid  
Simulation of  
Tomorrow's Braced  
Steel Frame  
Structures

University of California,  
Berkeley  
TCBF-B-3

PROJECT  
TCFB  
Jan 11, 2011  
DRAWN BY  
J.W. Lai  
TCBF-B-3  
PROJECT NO.

Sensor  
Locations

S.05





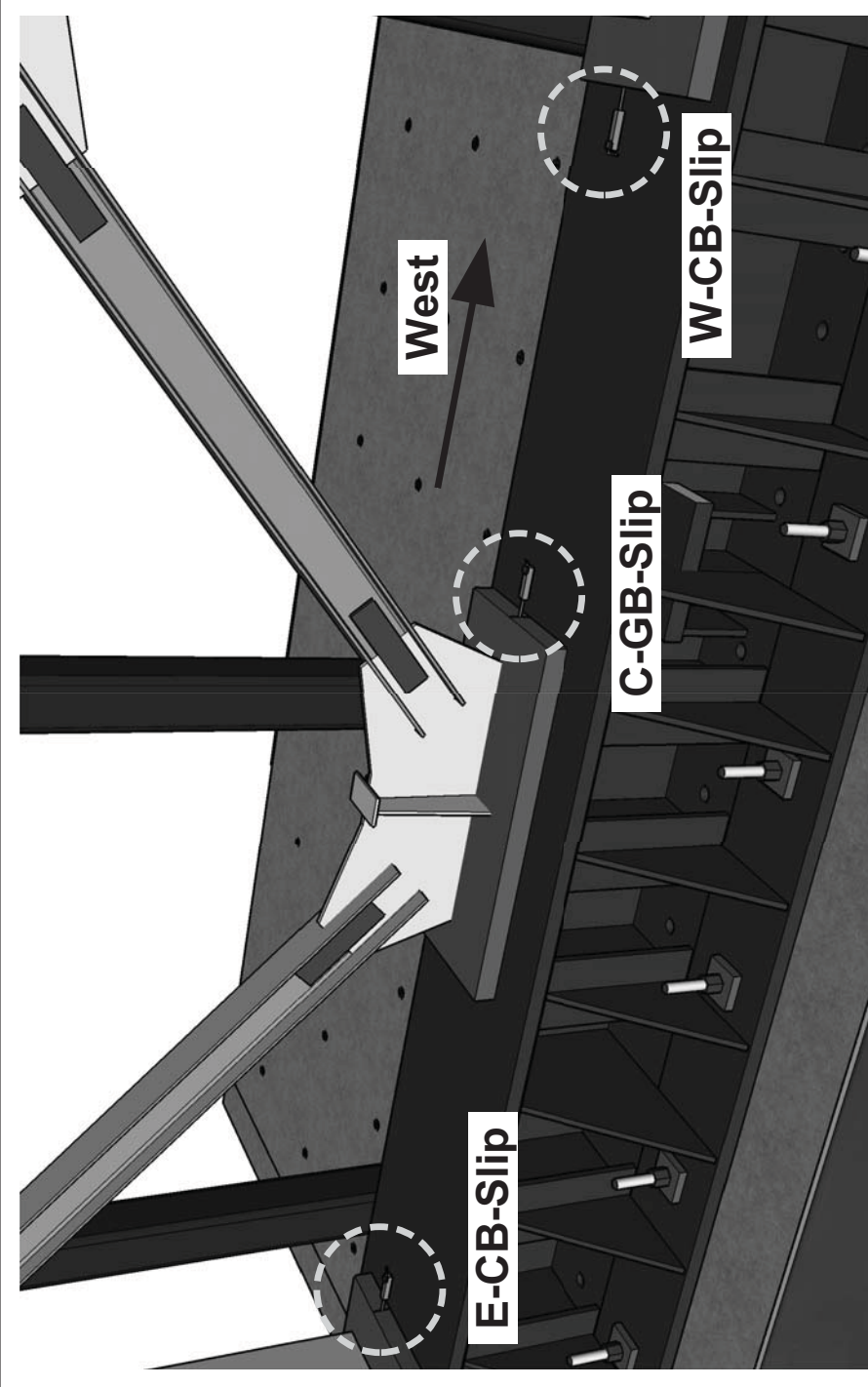
International Hybrid  
Simulation of  
Tomorrow's Braced  
Steel Frame  
Structures

University of California,  
Berkeley  
TCBF-B-3

PROJECT  
TCFB  
Jan 11,  
2011  
ISSUE  
DRAWN BY  
J.W. Lai  
PROJECT NO.  
TCBF-B-3

## Sensor Locations

### S.06



**E-CB-Slip = east column base slip monitoring  
C-GB-Slip = center gusset base slip monitoring  
W-CB-Slip = west column base slip monitoring  
(locations are shown in the figure, align with the braced  
frame center plane)**



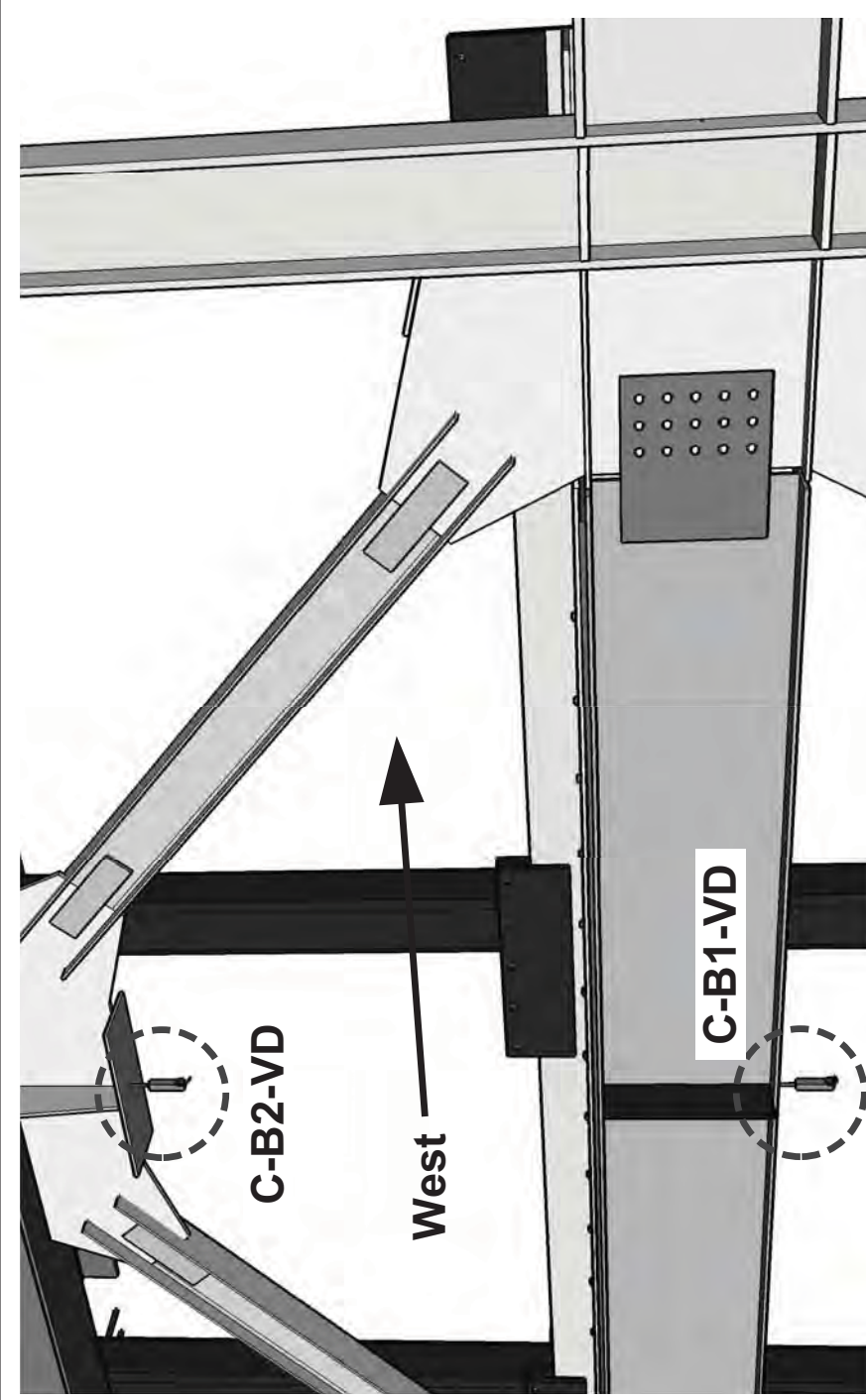
International Hybrid  
Simulation of  
Tomorrow's Braced  
Steel Frame  
Structures

University of California,  
Berkeley  
TCBF-B-3

PROJECT  
TCFB  
2011  
ISSUE  
Jan 11,  
DRAWN BY  
J.W. Lai  
PROJECT NO.  
TCBF-B-3

Sensor  
Locations

S.07



**C-B2-VD = roof beam (2F) center deflection monitoring**  
**C-B1-VD = lower beam (1F) center deflection monitoring**

**(locations are shown in the figure, align with the beam  
 bottom flange centerline)**



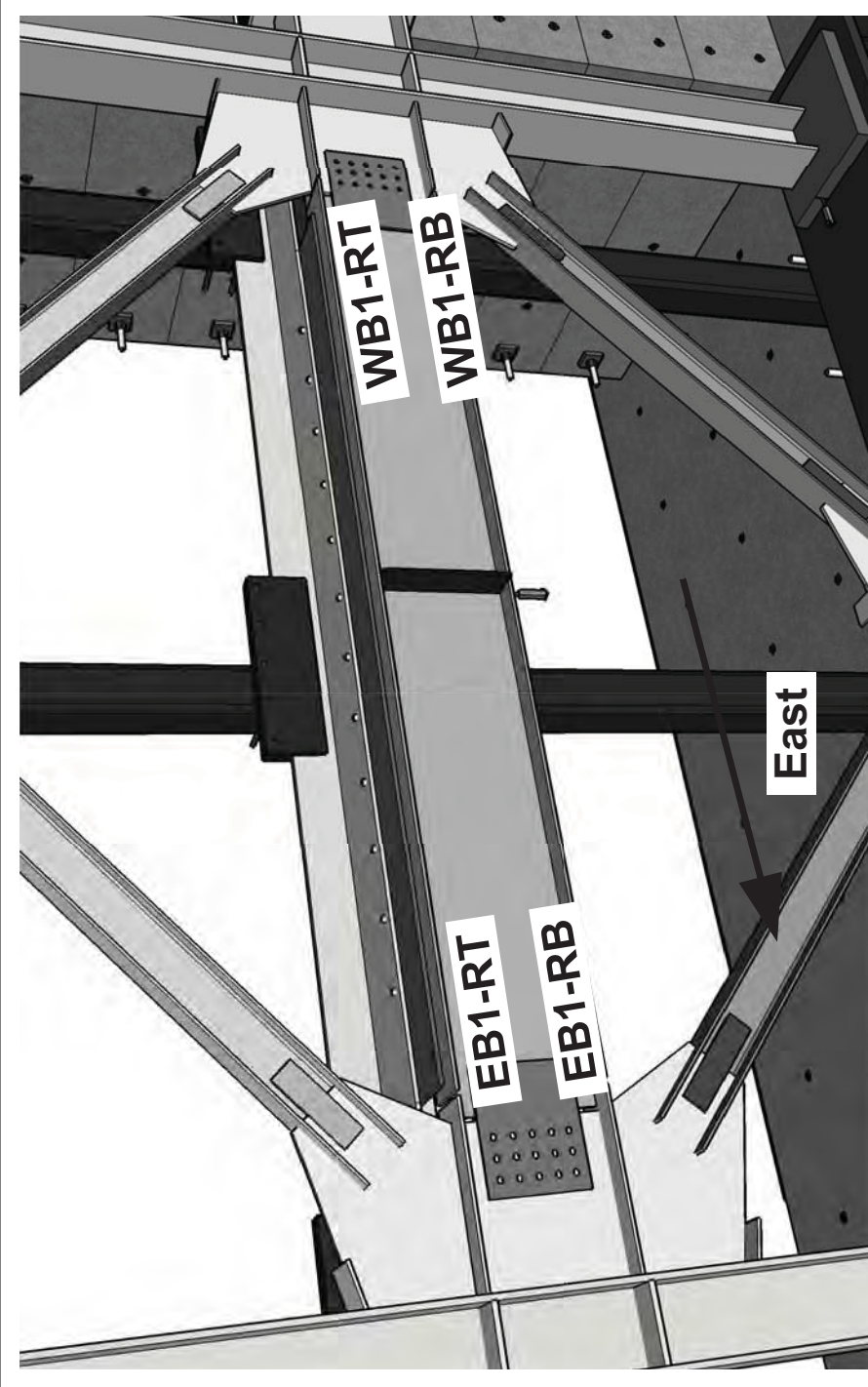
International Hybrid  
Simulation of  
Tomorrow's Braced  
Steel Frame  
Structures

University of California,  
Berkeley  
TCBF-B-3

PROJECT  
TCFB  
Jan 11,  
2011  
ISSUE  
DRAWN BY  
J.W. Lai  
PROJECT NO.  
TCBF-B-3

Sensor  
Locations

S.08



**WB1-RT, WB1-RB = west lower beam (1F) rotation monitoring**  
**EB1-RT, EB1-RB = east lower beam (1F) rotation monitoring**  
**RT, RB = top or bottom side**  
**(locations are shown in the figure, distance between two centerlines of top and bottom sticks is 21")**



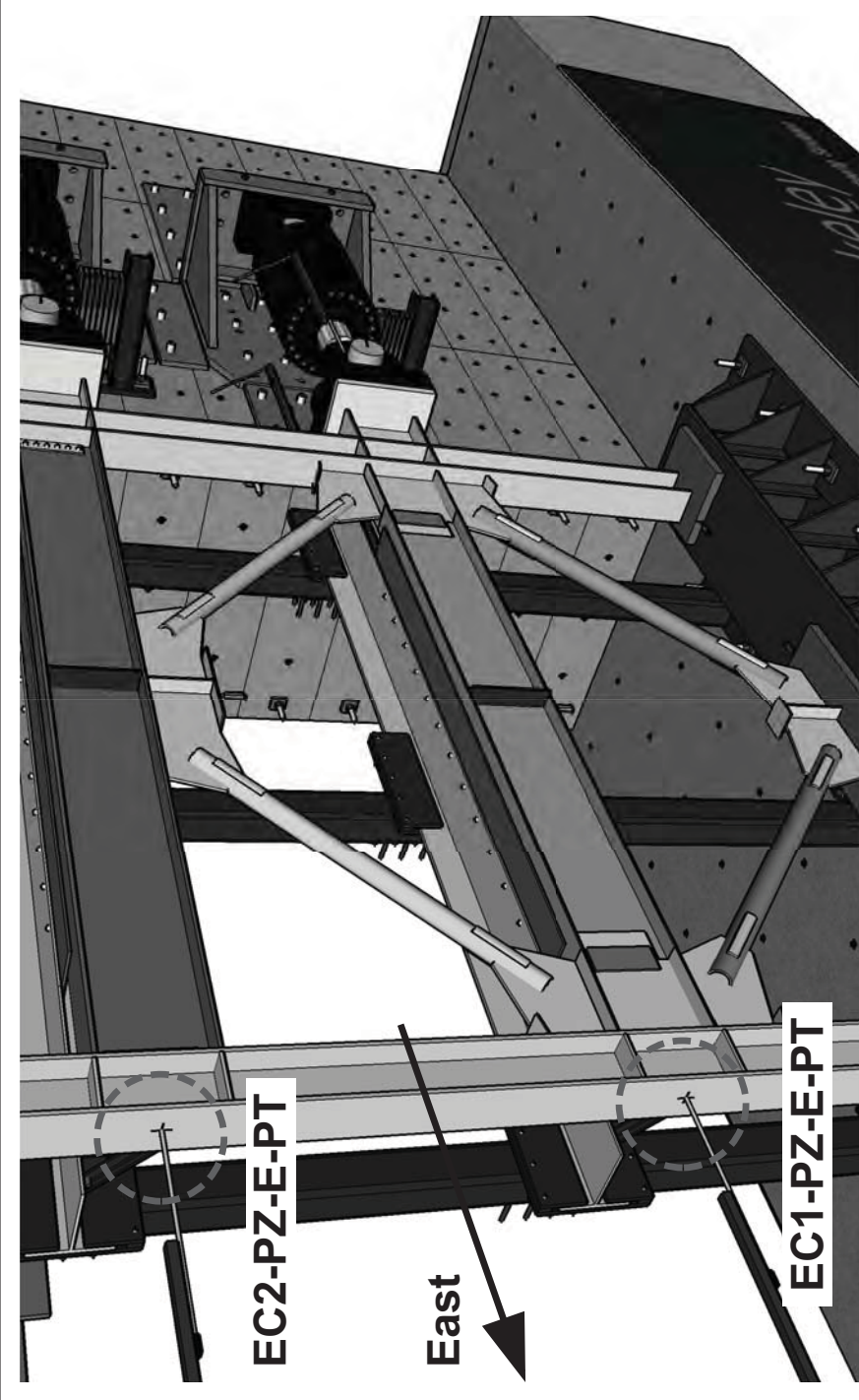
International Hybrid  
Simulation of  
Tomorrow's Braced  
Steel Frame  
Structures

University of California,  
Berkeley  
TCBF-B-3

PROJECT  
TCFB  
Jan 11, 2011  
ISSUE  
DRAWN BY  
J.W. Lai  
PROJECT NO.  
TCBF-B-3

## Sensor Locations

### S.09



**EC2-PZ-E-PT = roof level (2F) displacement monitoring**  
**EC1-PZ-E-PT = lower level (1F) displacement monitoring**

**(locations are shown in the figure, align with the beam  
 centerline at each floor level)**



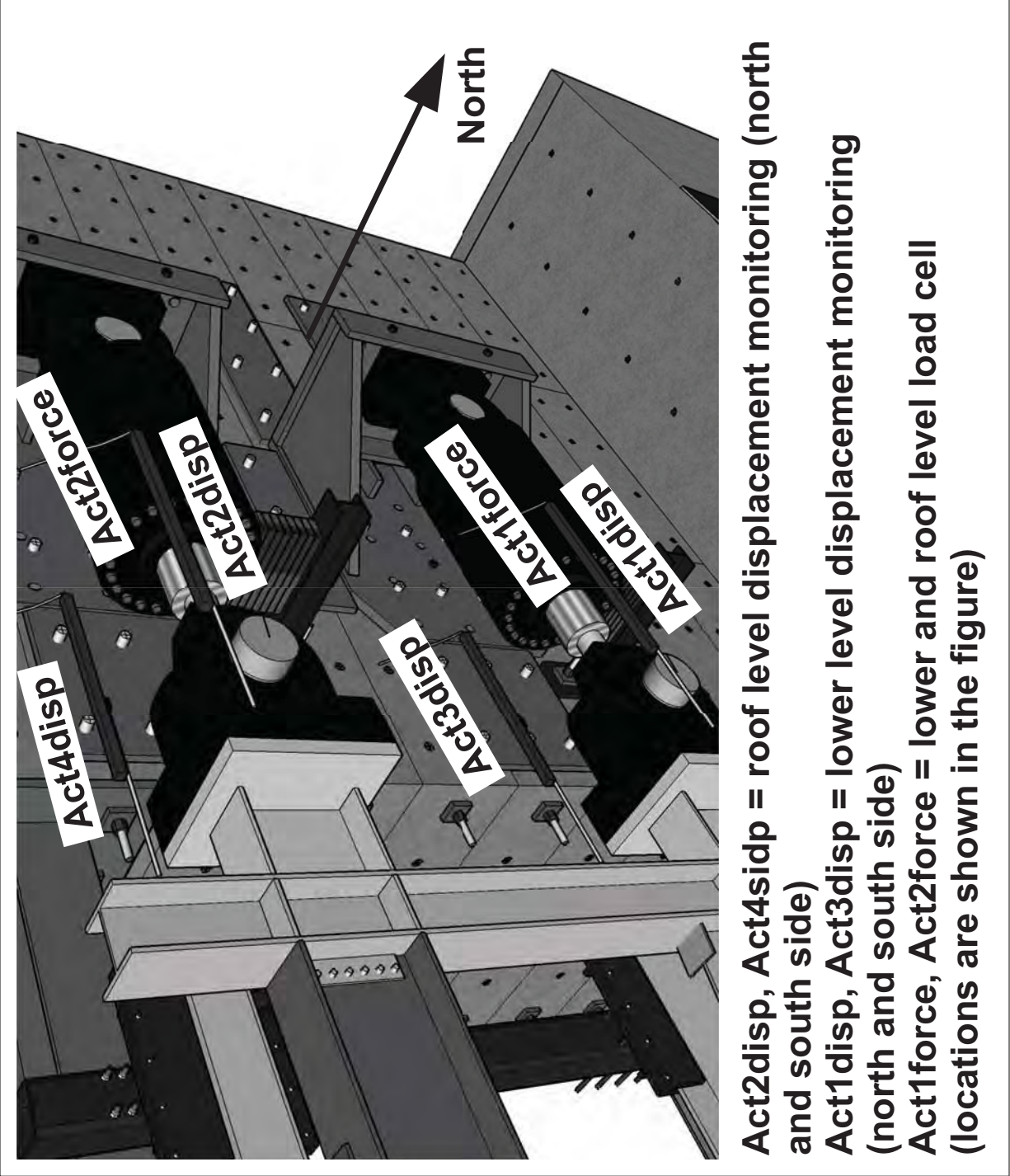
International Hybrid  
Simulation of  
Tomorrow's Braced  
Steel Frame  
Structures

University of California,  
Berkeley  
TCBF-B-3

PROJECT  
TCFB  
Jan 11,  
2011  
DRAWN BY  
J.W. Lai  
TCBF-B-3  
PROJECT NO.

Sensor  
Locations

S-10







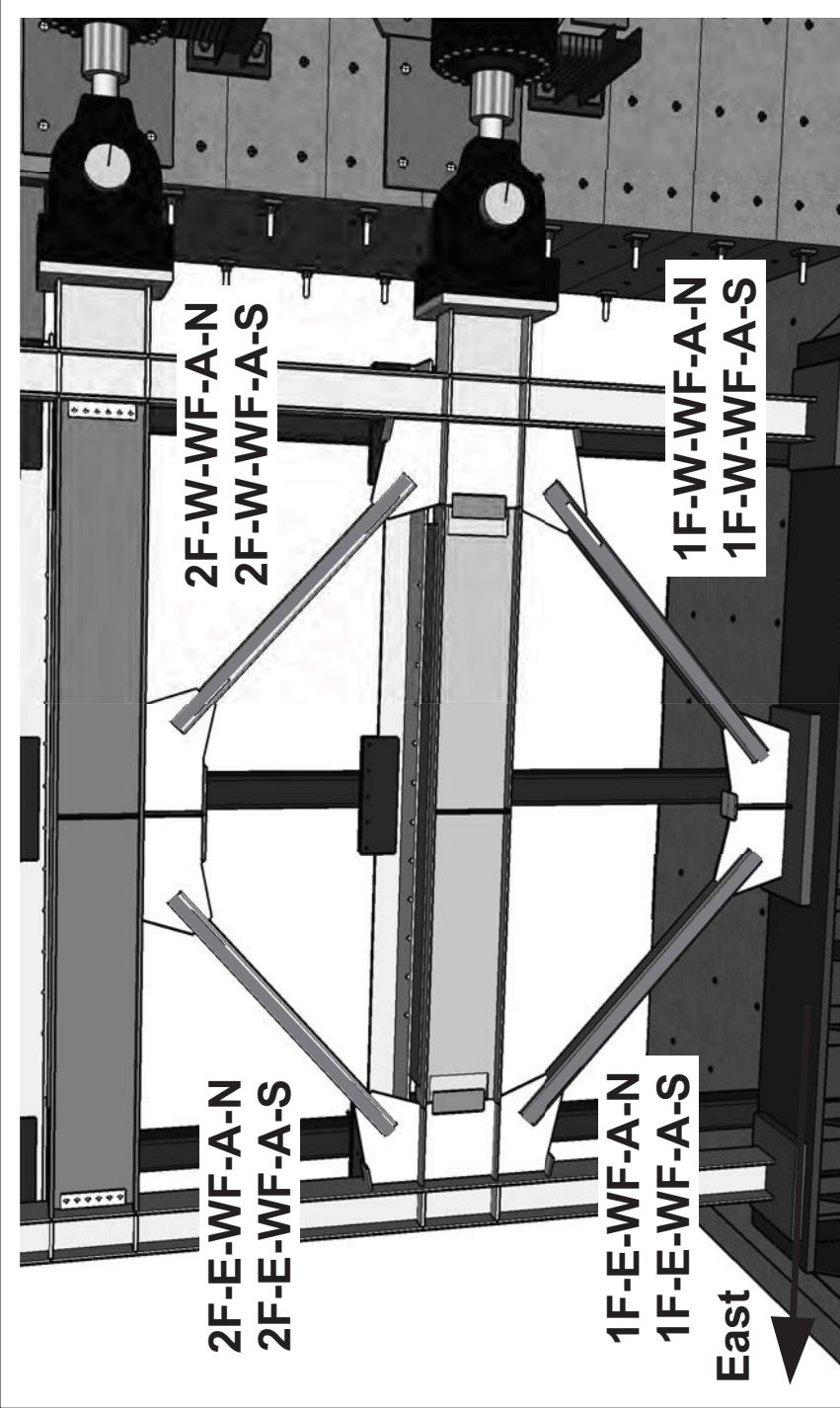
International Hybrid  
Simulation of  
Tomorrow's Braced  
Steel Frame  
Structures

University of California,  
Berkeley  
TCBF-B-3

PROJECT  
TCBF  
Jan 11,  
2011  
ISSUE  
DRAWN BY  
J.W. Lai  
PROJECT NO.  
TCBF-B-3

Sensor  
Locations

S.11



1F = first story; 2F = second story

E = east side; W = west side; A = axial direction

N = north side; S = south side

Wide flange brace axial deformation monitoring along the axis of brace (wire pot locations are shown in the figure)



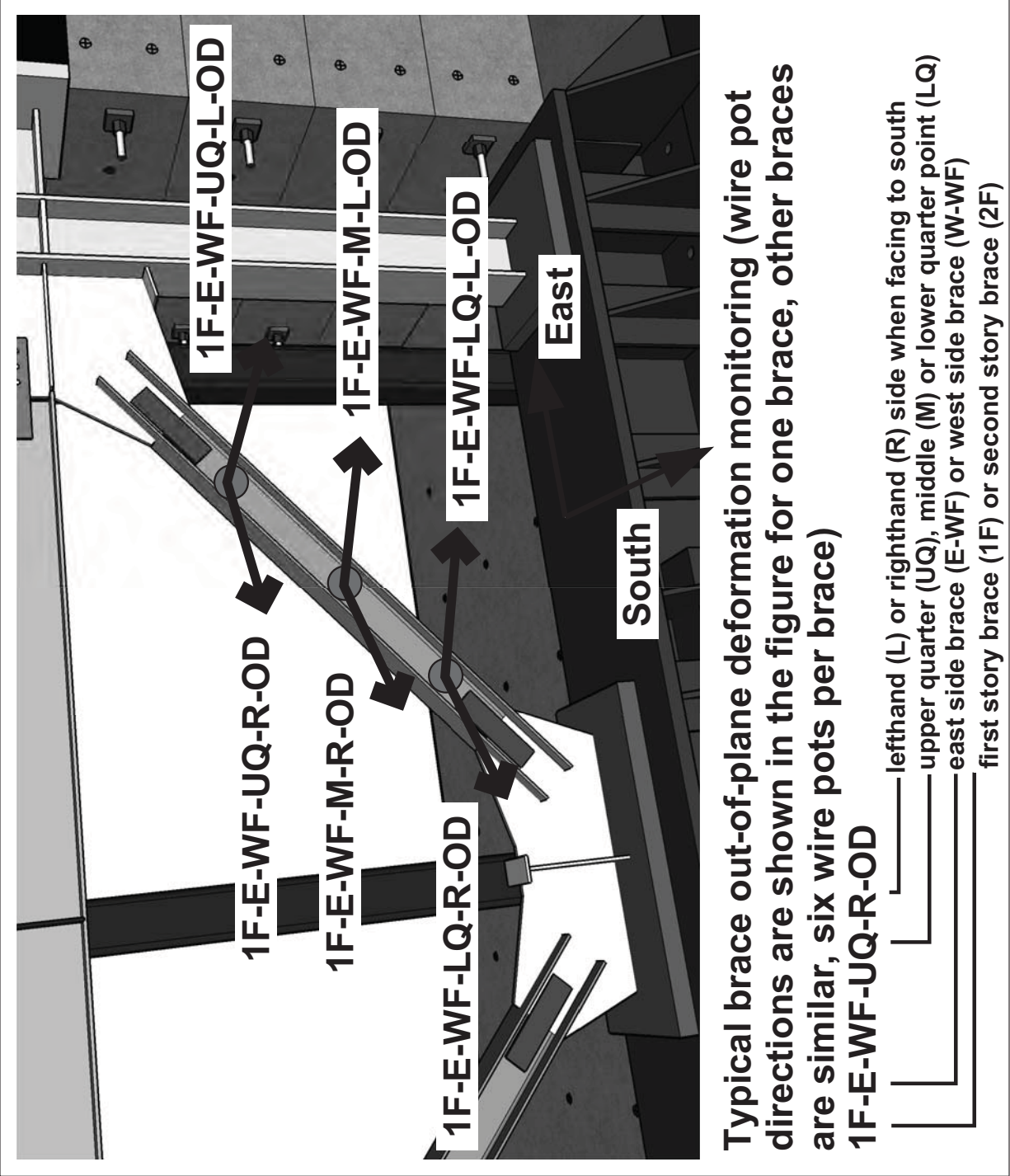
International Hybrid  
Simulation of  
Tomorrow's Braced  
Steel Frame  
Structures

University of California,  
Berkeley  
TCBF-B-3

ISSUE  
Jan 11, 2011  
PROJECT  
TCFB  
DRAWN BY  
J.W. Lai  
PROJECT NO.  
TCBF-B-3

Sensor  
Locations

S.12





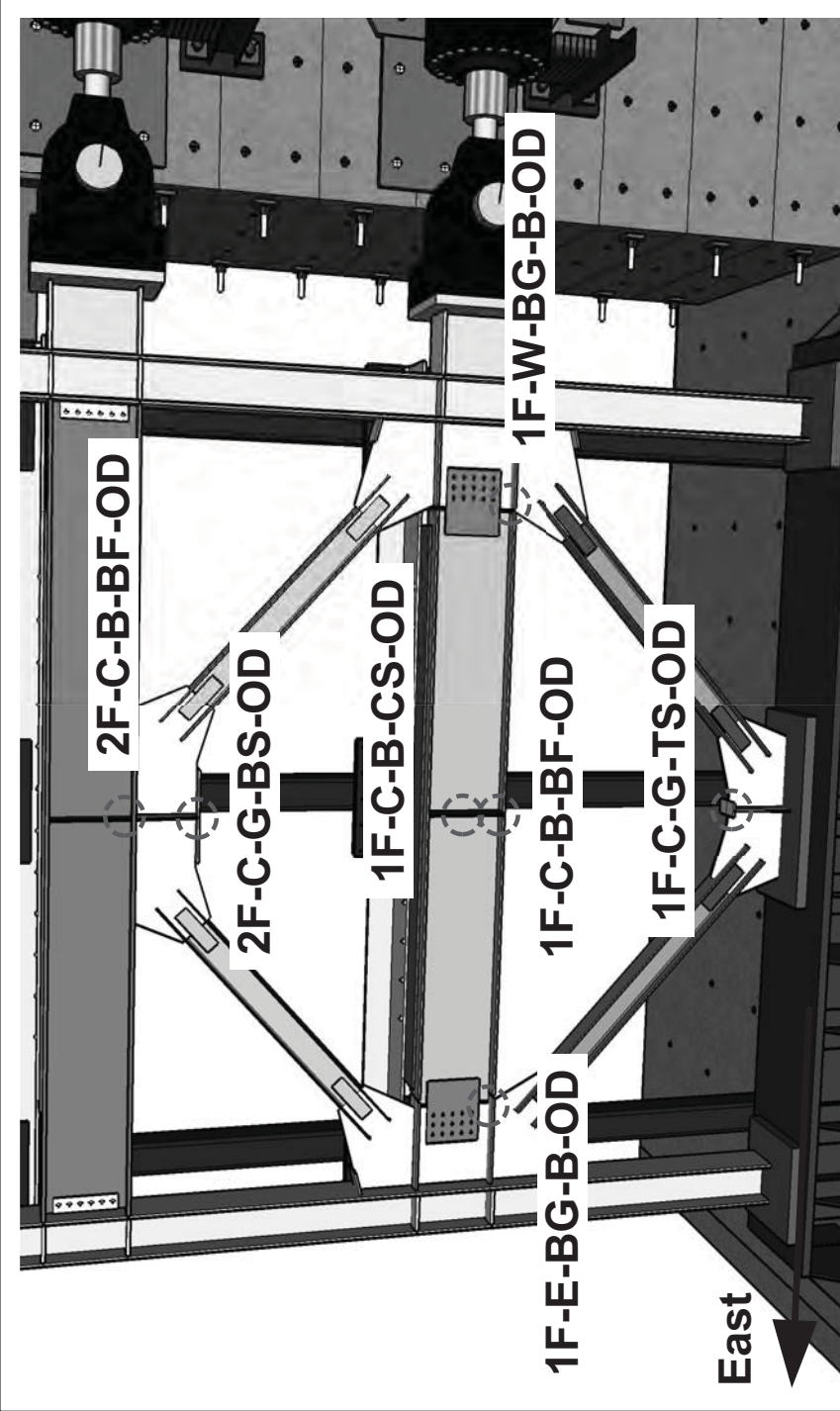
International Hybrid  
Simulation of  
Tomorrow's Braced  
Steel Frame  
Structures

University of California,  
Berkeley  
TCBF-B-3

PROJECT  
TCFB  
Jan 11, 2011  
ISSUE  
DRAWN BY  
J.W. Lai  
PROJECT NO.  
TCBF-B-3

## Sensor Locations

### S-13



**B = beam side corner; OD = out-of-plane deformation  
C-B, C-G = beam or gusset center; BF = bottom flange  
BS, CS, TS = bottom, center or top stiffener corner  
BG = bottom gusset plate region  
E, W = east or west side; 1F, 2F = first or second story  
(wire pot target locations are shown in the figure)**



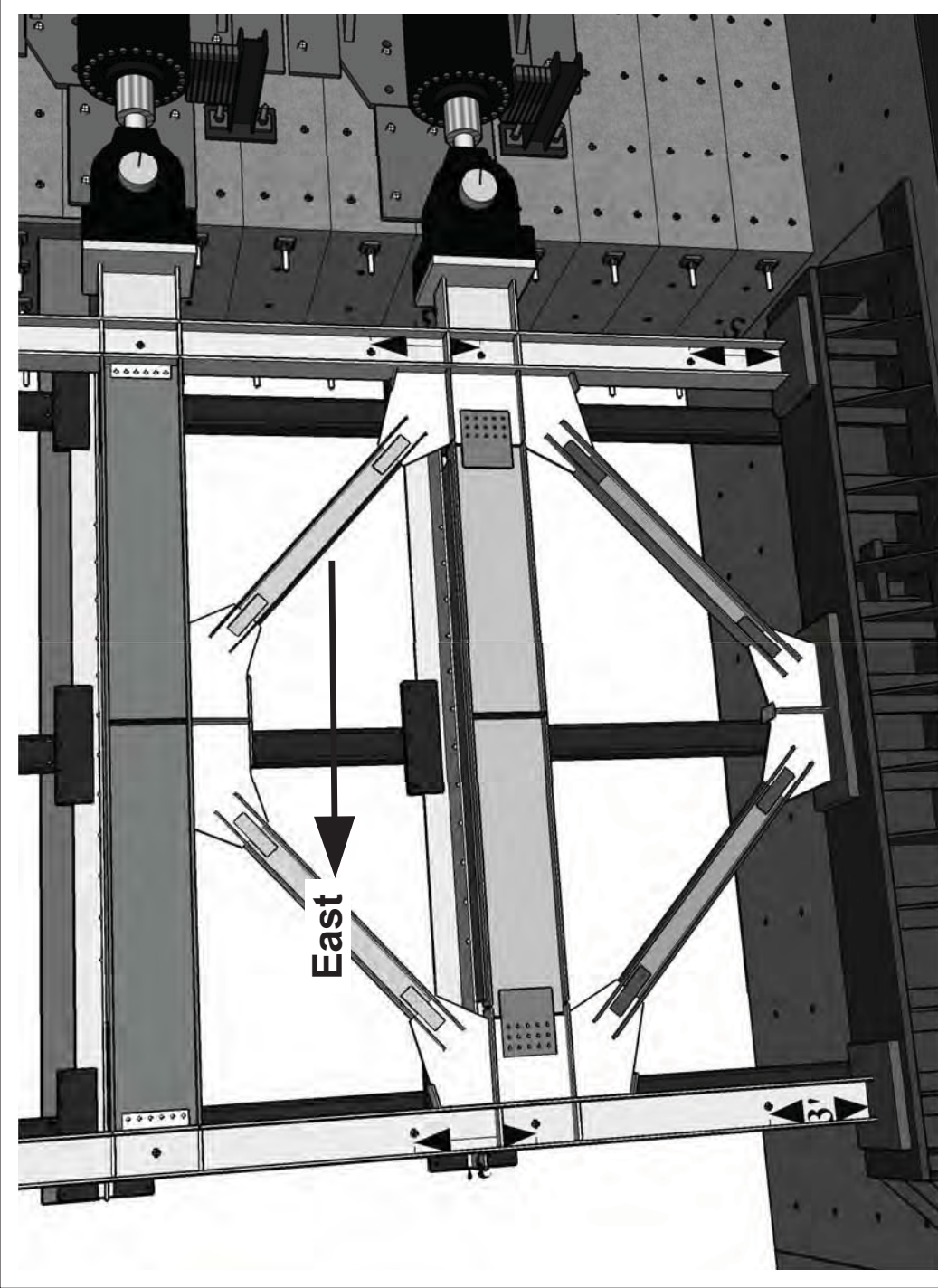
International Hybrid  
Simulation of  
Tomorrow's Braced  
Steel Frame  
Structures

University of California,  
Berkeley  
TCBF-B-3

PROJECT  
TCFB  
Jan 11,  
2011  
ISSUE  
DRAWN BY  
J.W. Lai  
PROJECT NO.  
TCBF-B-3

## Sensor Locations

### S.14



Overview of eight rosette locations on the specimen (only the column and panel zone regions). Details and label keys are shown in the next page.



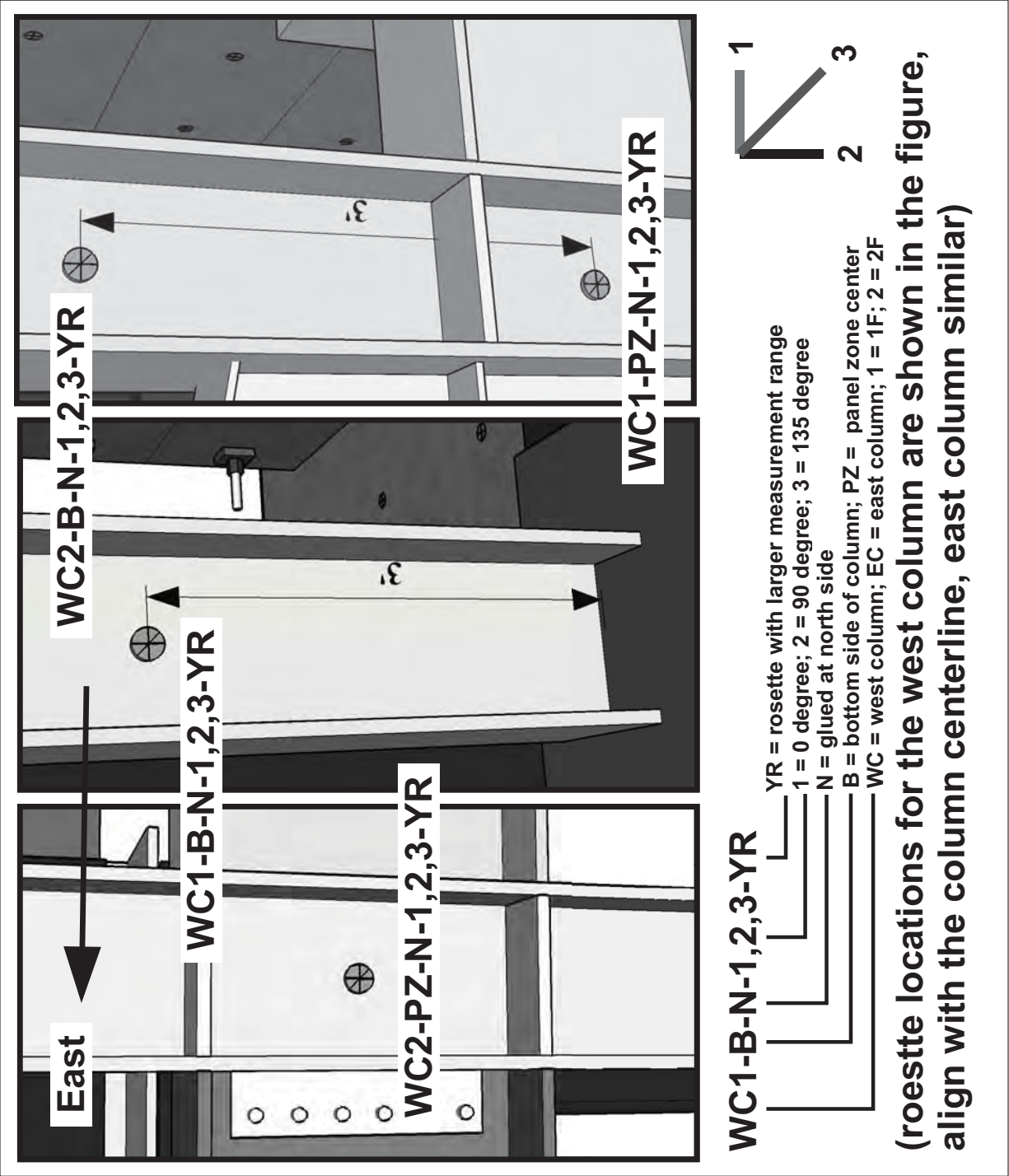
International Hybrid  
Simulation of  
Tomorrow's Braced  
Steel Frame  
Structures

University of California,  
Berkeley  
TCBF-B-3

PROJECT  
TCFB  
Jan 11, 2011  
DRAWN BY  
J.W. Lai  
TCBF-B-3  
PROJECT NO.

Sensor  
Locations

S.15





International Hybrid  
Simulation of  
Tomorrow's Braced  
Steel Frame  
Structures

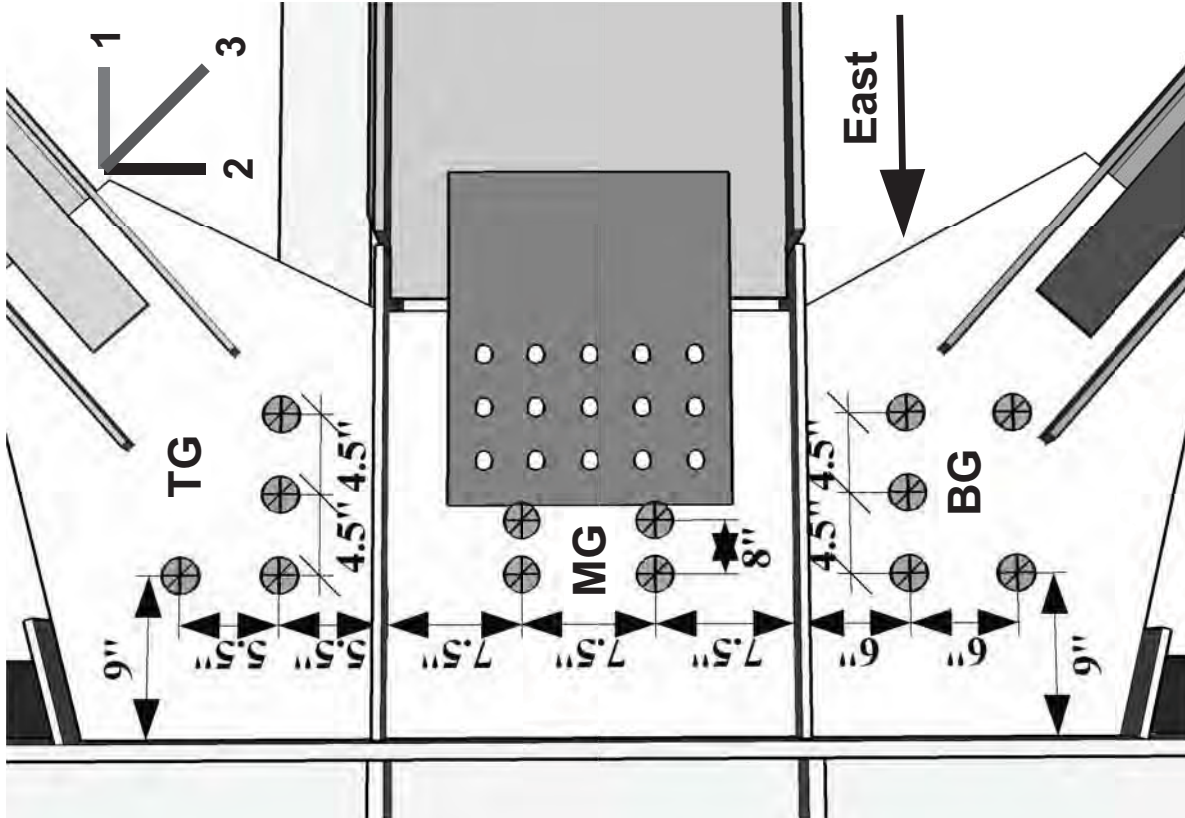
University of California,  
Berkeley  
TCBF-B-3

PROJECT  
TCFB  
Jan 11, 2011  
ISSUE  
DRAWN BY  
J.W. Lai  
PROJECT NO.  
TCBF-B-3

Sensor  
Locations

S-16

- 1F-E-TG-TL-1,2,3-N-YR**
- 1F-E** = east gusset plate
  - TG** = top region
  - MG** = middle region
  - BG** = bottom region
  - TL** = top left side
  - BL** = bottom left side
  - TR** = top right side
  - BR** = bottom right side
  - TC** = top center
  - BC** = bottom center
  - 1** = 0 degree (direction)
  - 2** = 90 degree
  - 3** = 135 degree
  - N** = glued at north side
  - YR** = rosette with larger measurement range
- (thirteen rosette locations for the one-piece gusset plate, label keys are shown above)





International Hybrid  
Simulation of  
Tomorrow's Braced  
Steel Frame  
Structures

University of California,  
Berkeley  
TCBF-B-3

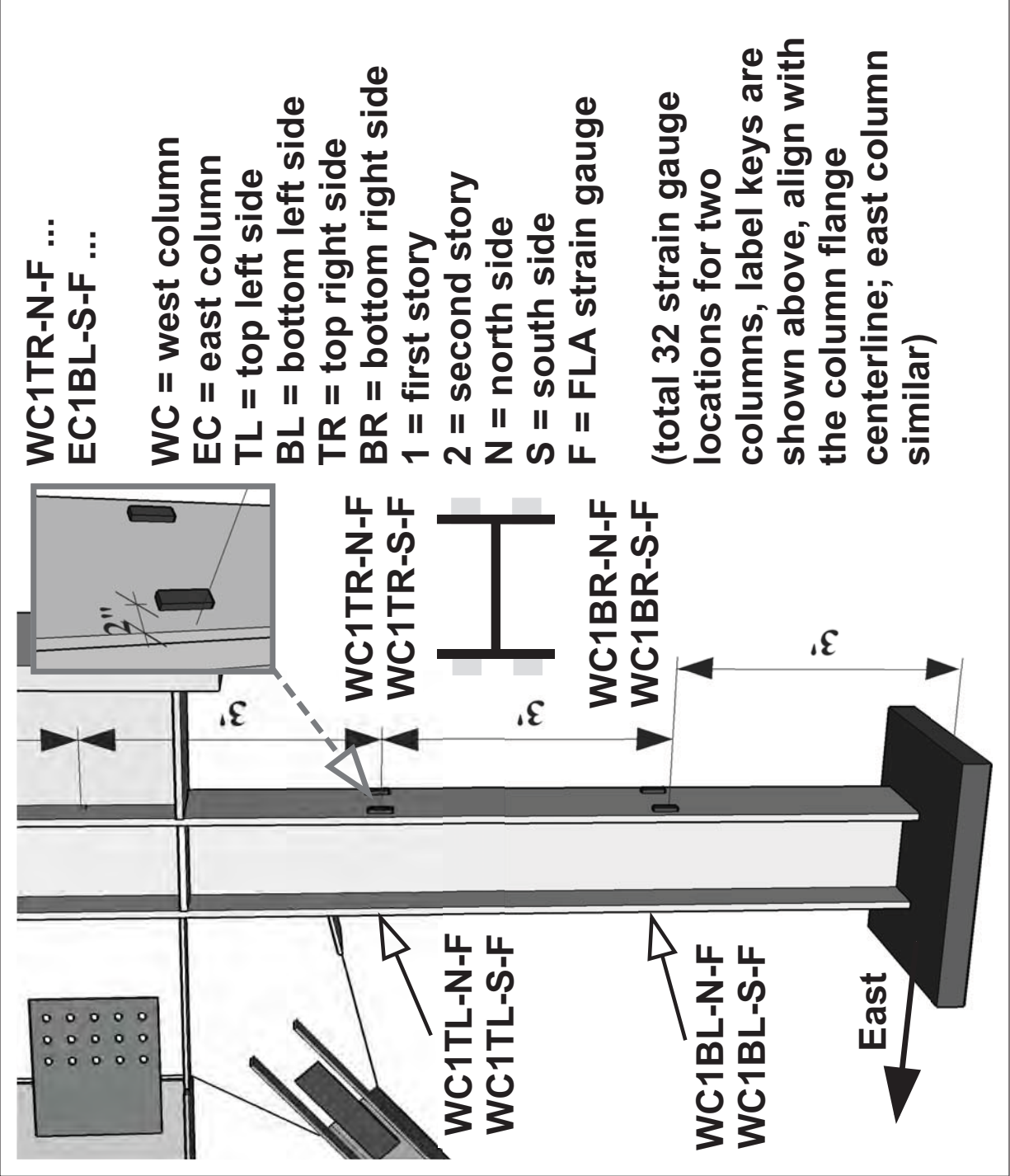
PROJECT  
TCFB  
Jan 11,  
2011

ISSUE  
Jan 11,  
2011  
DRAWN BY  
J.W. Lai

PROJECT NO.  
TCBF-B-3

## Sensor Locations

### S-17





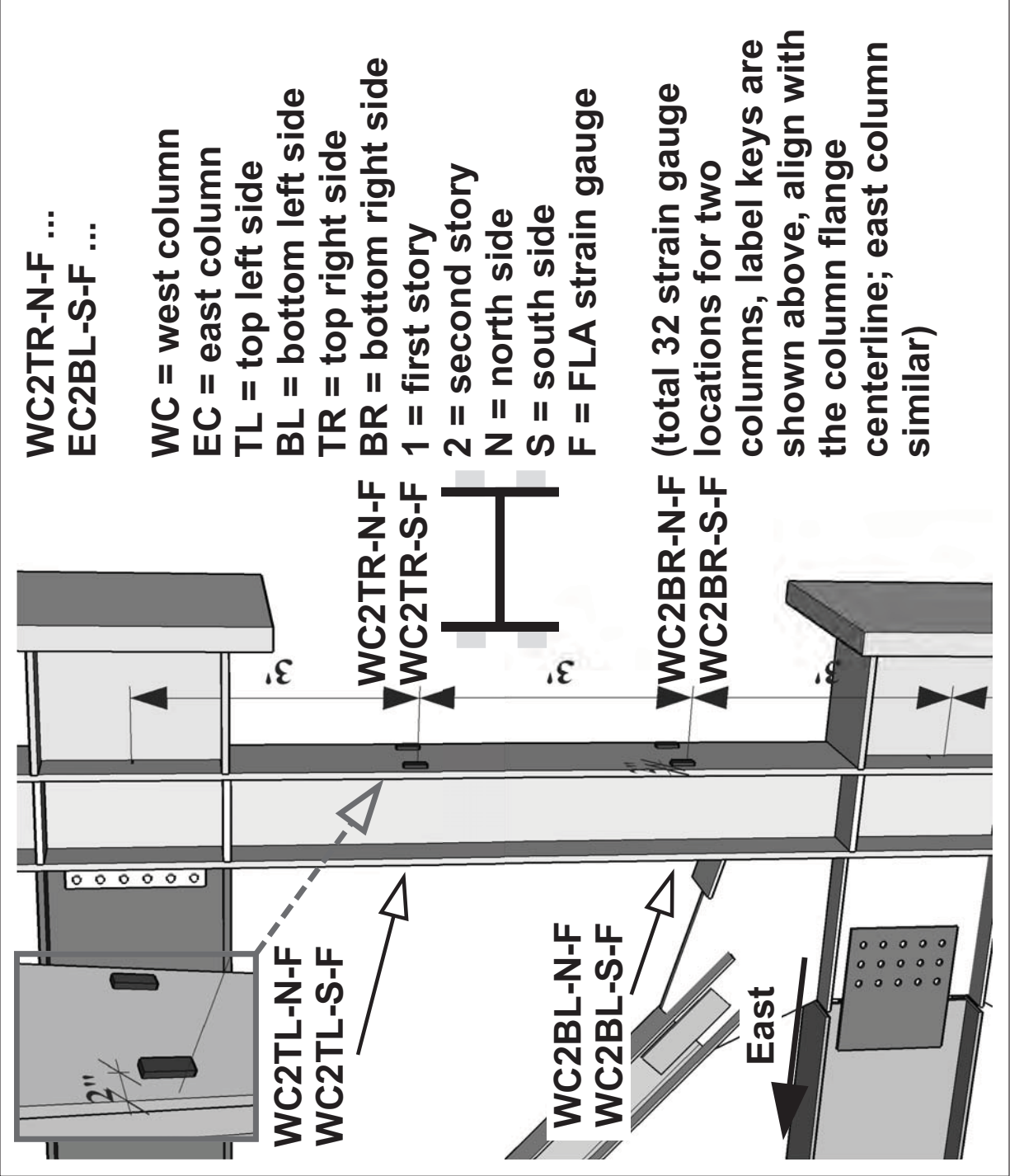
International Hybrid  
Simulation of  
Tomorrow's Braced  
Steel Frame  
Structures

University of California,  
Berkeley  
TCBF-B-3

PROJECT  
TCFB  
Jan 11, 2011  
DRAWN BY  
J.W. Lai  
PROJECT NO.  
TCBF-B-3

Sensor  
Locations

S-18







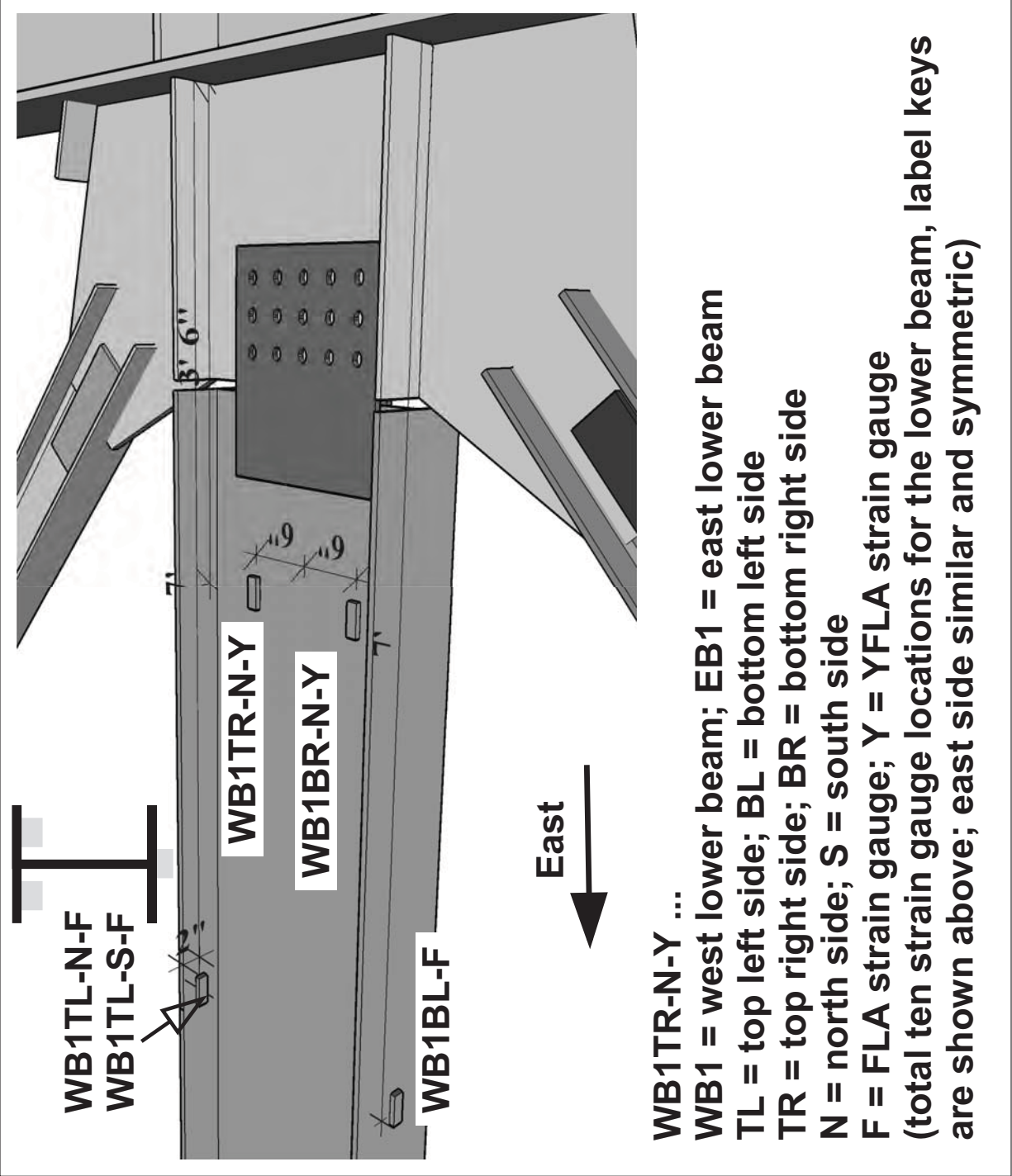
International Hybrid  
Simulation of  
Tomorrow's Braced  
Steel Frame  
Structures

University of California,  
Berkeley  
TCBF-B-3

PROJECT  
TCFB  
Jan 11,  
2011  
ISSUE  
DRAWN BY  
J.W. Lai  
PROJECT NO.  
TCBF-B-3

Sensor  
Locations

S.19





International Hybrid  
Simulation of  
Tomorrow's Braced  
Steel Frame  
Structures

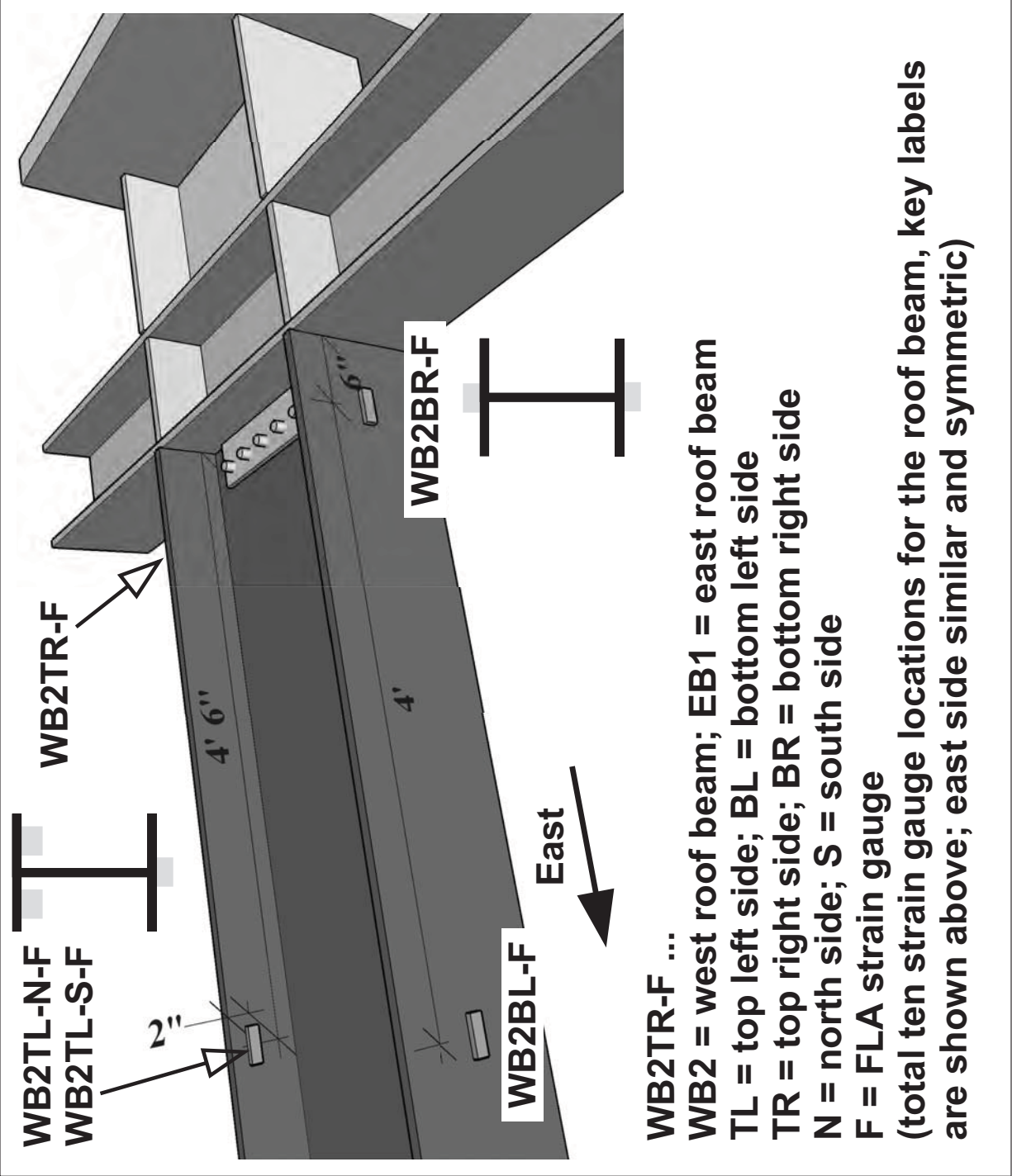
University of California,  
Berkeley  
TCBF-B-3

PROJECT  
TCFB  
Jan 11, 2011

ISSUE  
J.W. Lai  
DRAWN BY  
TCBF-B-3  
PROJECT NO.

Sensor  
Locations

S-20





International Hybrid  
Simulation of  
Tomorrow's Braced  
Steel Frame  
Structures

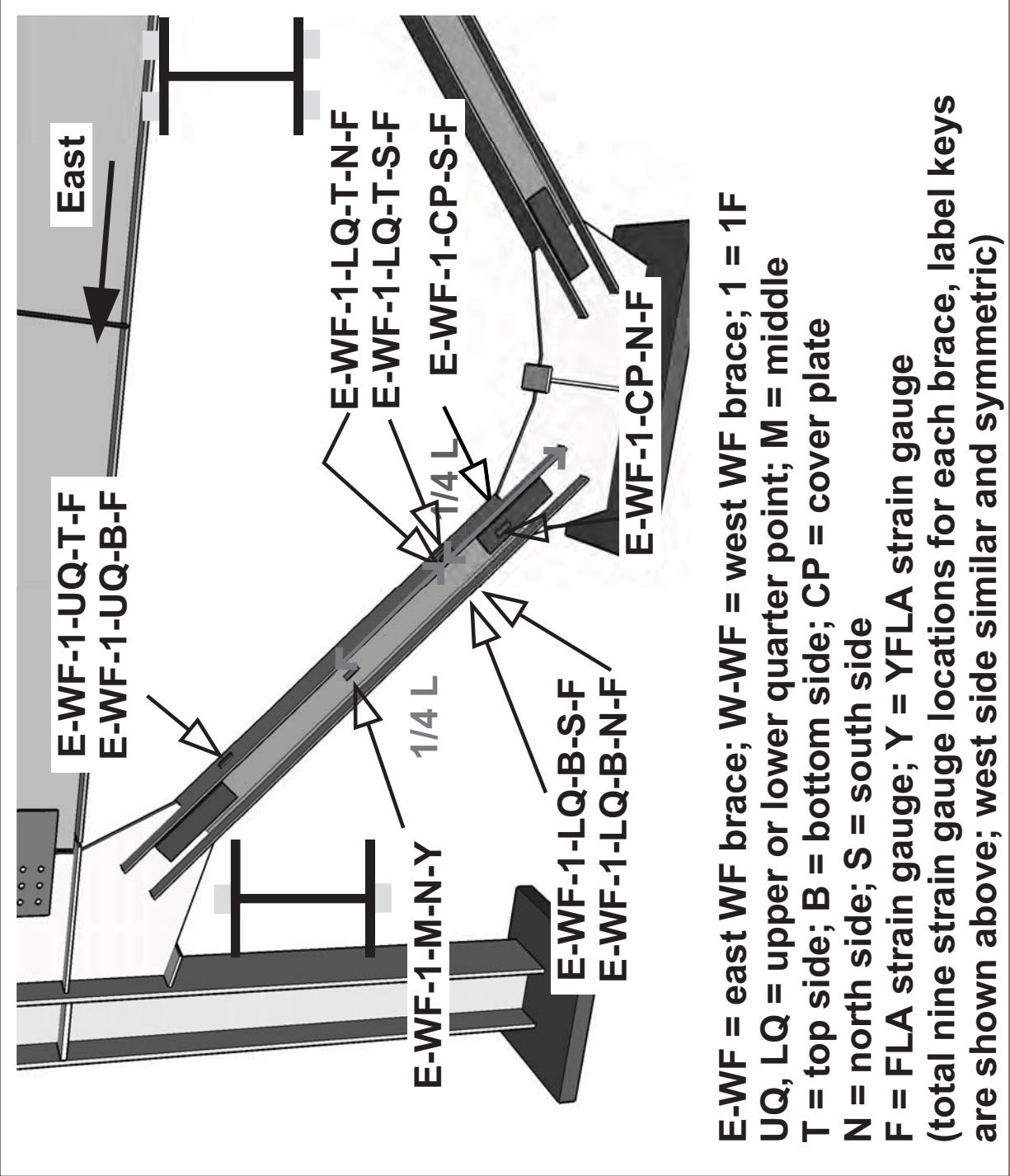
University of California,  
Berkeley  
TCBF-B-3

PROJECT  
TCFB  
2011

ISSUE  
Jan 11,  
2011  
DRAWN BY  
J.W. Lai

Sensor  
Locations

S.21





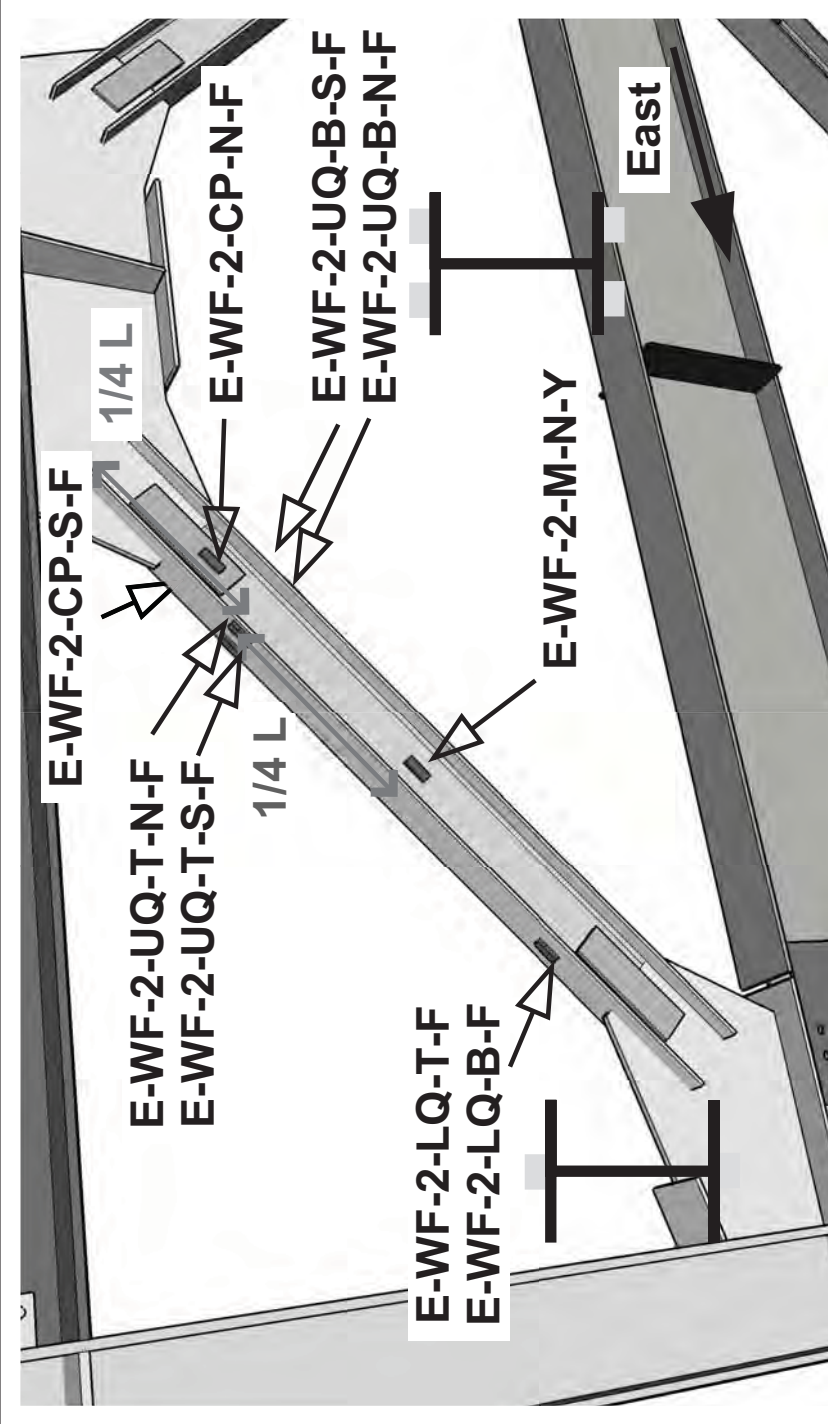
International Hybrid  
Simulation of  
Tomorrow's Braced  
Steel Frame  
Structures

University of California,  
Berkeley  
TCBF-B-3

PROJECT  
TCFB  
Jan 11,  
2011  
ISSUE  
DRAWN BY  
J.W. Lai  
PROJECT NO.  
TCBF-B-3

Sensor  
Locations

**S.22**



**E-WF = east WF brace; W-WF = west WF brace; 2 = 2F  
LQ, UQ = lower or upper quarter point; M = middle  
T = top side; B = bottom side; CP = cover plate  
N = north side; S = south side  
F = FLA strain gauge; Y = YFLA strain gauge  
(total nine strain gauge locations for each brace, label keys  
are shown above; west side similar and symmetric)**



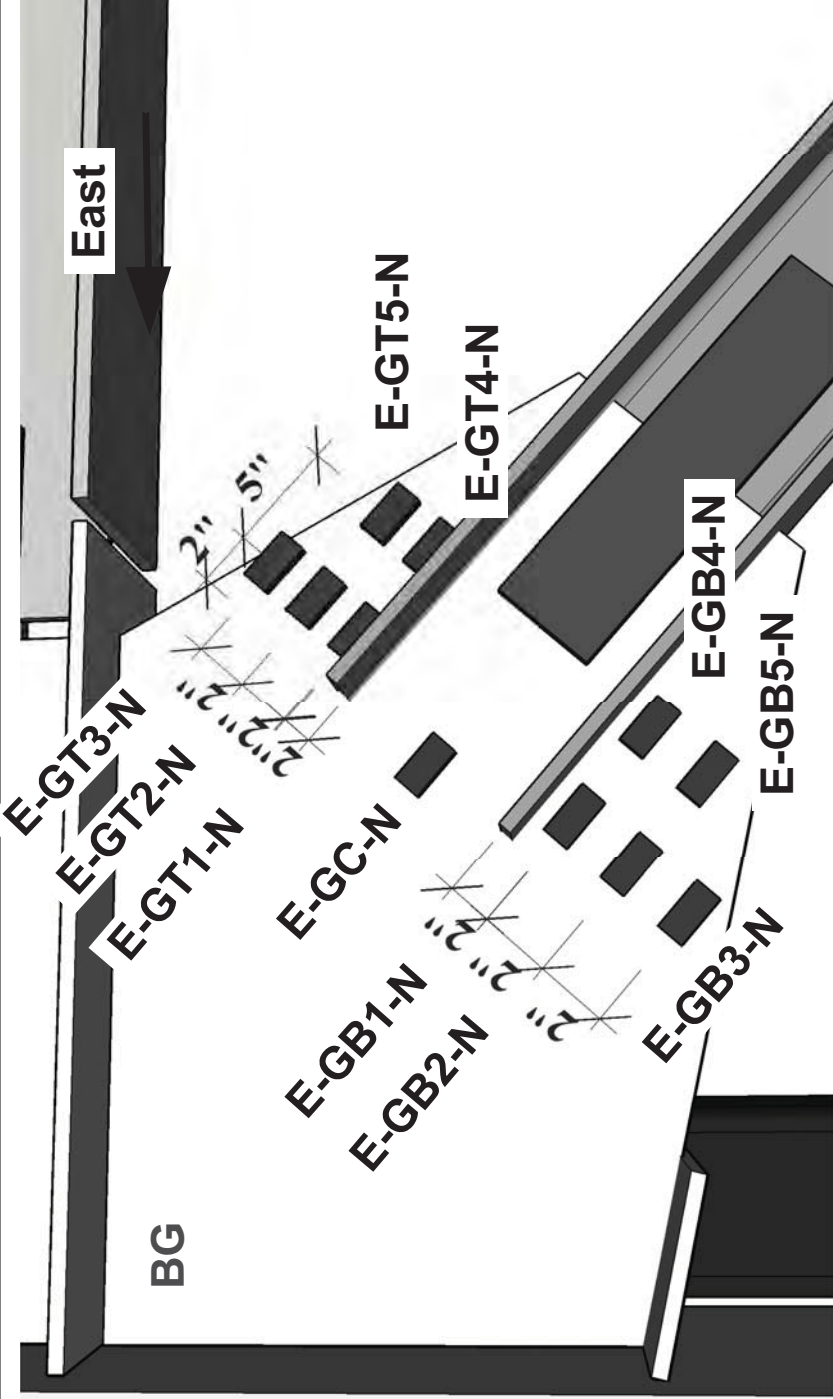
International Hybrid  
Simulation of  
Tomorrow's Braced  
Steel Frame  
Structures

University of California,  
Berkeley  
TCBF-B-3

PROJECT  
TCFB  
Jan 11, 2011  
ISSUE  
DRAWN BY  
J.W. Lai  
PROJECT NO.  
TCBF-B-3

Sensor  
Locations

S.23



E = east gusset plate; N = glued at north side  
GT = top region; GB = bottom region; GC = centerline region  
(eleven strain gauge locations for the bottom one-piece gusset plate, label keys are shown above)



International Hybrid  
Simulation of  
Tomorrow's Braced  
Steel Frame  
Structures

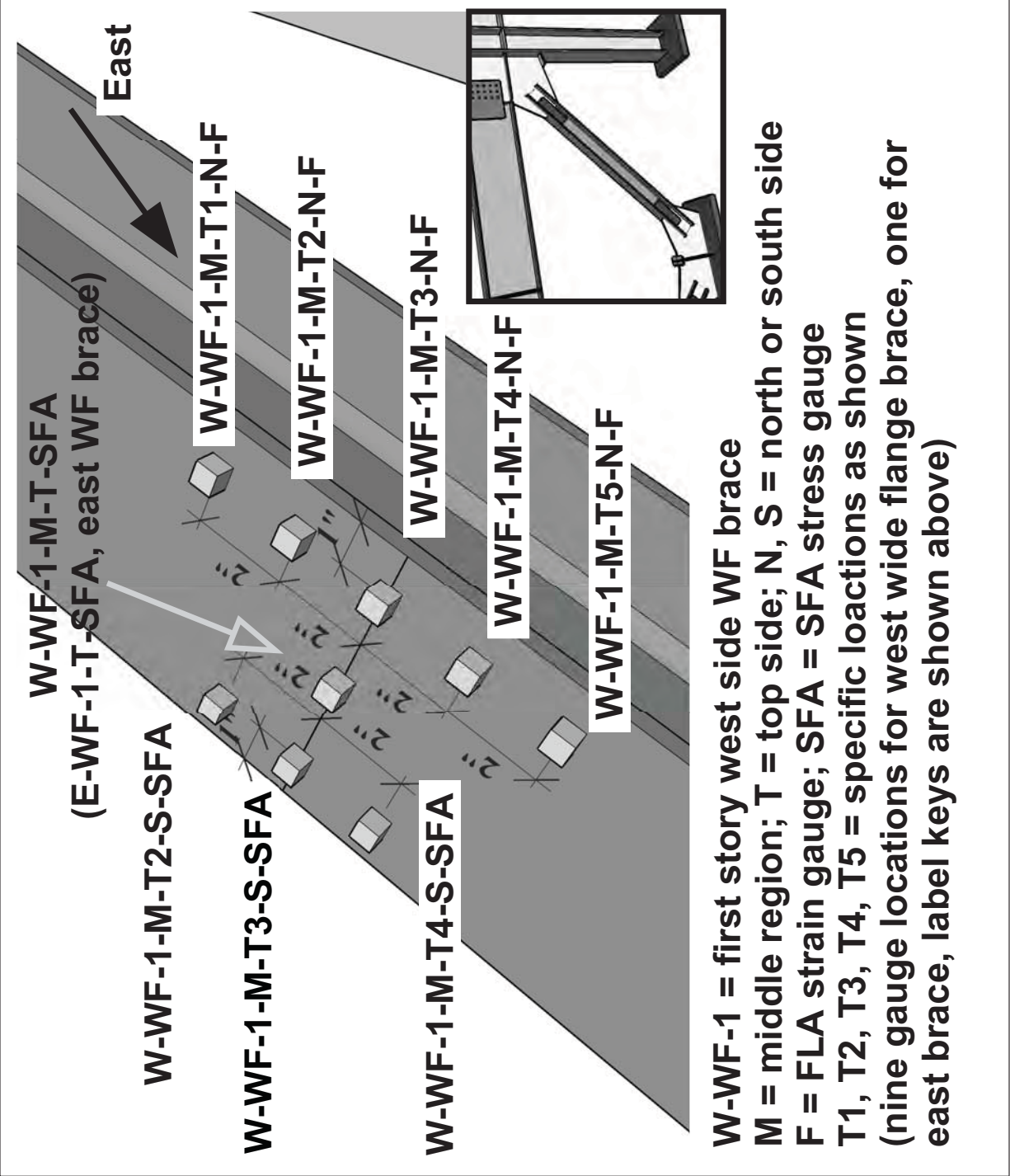
University of California,  
Berkeley  
TCBF-B-3

PROJECT  
TCFB  
2011

ISSUE  
Jan 11,  
2011  
DRAWN BY  
J.W. Lai

Sensor  
Locations

S.24





International Hybrid  
Simulation of  
Tomorrow's Braced  
Steel Frame  
Structures

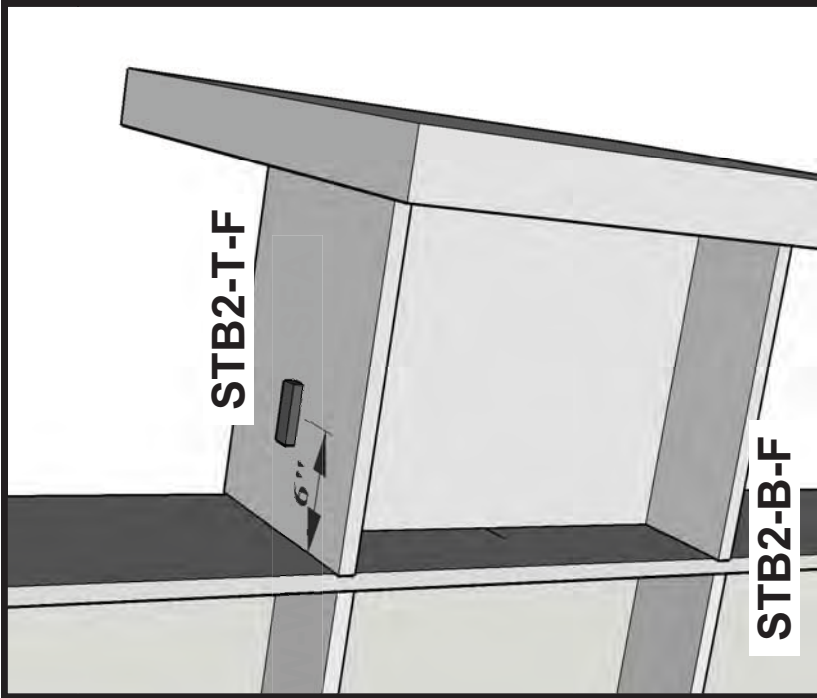
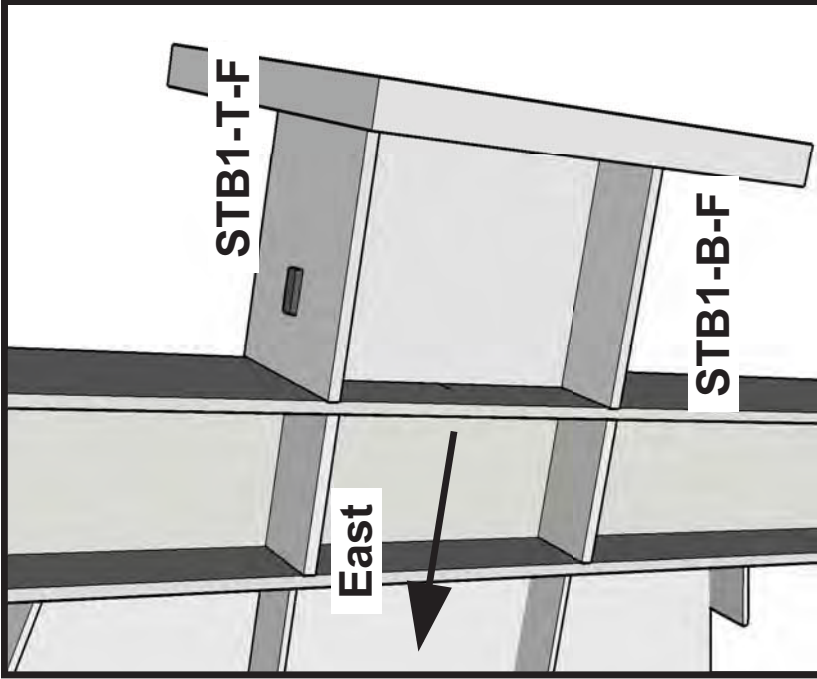
University of California,  
Berkeley  
TCBF-B-3

PROJECT  
TCFB  
PROJECT NO.  
TCBF-B-3

ISSUE  
Jan 11,  
2011  
DRAWN BY  
J.W. Lai

Sensor  
Locations

**S.25**



**STB = stub beam**

**1, 2 = first story or second story**

**T= top flange side; B = bottom flange side**

**F = FLA strain gauge**

**(two strain gauge locations for each stub beam at each floor level, align with flange centerline, label keys are shown above)**

Channel	ID	Label	Device	Range	Serial No.	Cable No.	DAQ Box ID	Note	Column #
1	ST12	FB-Slip	stick	2"	2004NC01023	308	0:3:0	Novo 50 (recalibrated)	14
2	ST13	RRW-Slip-N	stick	2"	2009NC01016	309	0:3:1	Novo 50 (recalibrated)	15
3	ST14	RRW-Slip-S	stick	2"	2009NC01020	306	0:3:2	Novo 50 (recalibrated)	16
4	ST15	Act1-BK	stick	2"	2009NC01011	361	0:3:3	Novo 50 (recalibrated)	17
5	S5	E-WF-1-UQ-T-F	strain gauge	-	-	5	0:1:0	1/4-Bridge	6
6	S6	E-WF-1-UQ-B-F	strain gauge	-	-	6	0:1:1	1/4-Bridge	7
7	S7	E-WF-1-M-N-Y	strain gauge	-	-	7	0:1:2	1/4-Bridge	8
8	S8	E-WF-1-M-T-SFA	strain gauge	-	-	8	0:1:3	Stress Gauge (1/4-Bridge)	9
9	S9	E-WF-1-LQ-TN-F	strain gauge	-	-	9	0:2:0	1/4-Bridge	10
10	S10	E-WF-1-LQ-TS-F	strain gauge	-	-	10	0:2:1	1/4-Bridge	11
11	S11	E-WF-1-LQ-BN-F	strain gauge	-	-	11	0:2:2	1/4-Bridge	12
12	S12	E-WF-1-LQ-BS-F	strain gauge	-	-	12	0:2:3	1/4-Bridge	13
13	S13	E-WF-1-CP-N-F	strain gauge	-	-	3	0:0:2	1/4-Bridge	4
14	S14	E-WF-1-CP-S-F	strain gauge	-	-	4	0:0:3	1/4-Bridge	5
15	S15	EB1BL-N-Y	strain gauge	-	-	381	0:11:0	1/4-Bridge	46
16	S16	EB1TL-N-Y	strain gauge	-	-	380	0:10:3	1/4-Bridge	45
17	S17	EB1BR-F	strain gauge	-	-	204/70	1:1:1	1/4-Bridge	71
18	S18	EB1TR-S-F	strain gauge	-	-	382	0:11:1	1/4-Bridge	47
19	S19	WB1BL-F	strain gauge	-	-	342/68	1:0:3	1/4-Bridge	69
20	S20	WB1TL-S-F	strain gauge	-	-	322/69	1:1:0	1/4-Bridge	70
21	S21	WB1BR-N-Y	strain gauge	-	-	338/84	1:4:3	1/4-Bridge	85
22	S22	WB1TR-N-Y	strain gauge	-	-	325/57	0:14:0	1/4-Bridge	58
23	S23	W-WF-1-CP-N-F	strain gauge	-	-	1	0:0:0	1/4-Bridge	2
24	S24	W-WF-1-CP-S-F	strain gauge	-	-	2	0:0:1	1/4-Bridge	3
25	S25	W-WF-1-LQ-TN-F	strain gauge	-	-	25	0:6:0	1/4-Bridge	26
26	S26	W-WF-1-LQ-TS-F	strain gauge	-	-	26	0:6:1	1/4-Bridge	27
27	S27	W-WF-1-LQ-BN-F	strain gauge	-	-	27	0:6:2	1/4-Bridge	28
28	S28	W-WF-1-LQ-BS-F	strain gauge	-	-	28	0:6:3	1/4-Bridge	29
29	S29	W-WF-1-M-N-Y	strain gauge	-	-	29	0:7:0	1/4-Bridge	30
30	S30	W-WF-1-M-T-SFA	strain gauge	-	-	30	0:7:1	Stress Gauge (1/4-Bridge)	31
31	S31	W-WF-1-UQ-T-F	strain gauge	-	-	31	0:7:2	1/4-Bridge	32
32	S32	W-WF-1-UQ-B-F	strain gauge	-	-	32	0:7:3	1/4-Bridge	33
33	S33	WC1TL-S-F	strain gauge	-	-	95	1:7:2	1/4-Bridge	96
34	S34	WC1TR-S-F	strain gauge	-	-	93	1:7:0	1/4-Bridge	94
35	S35	WC1TL-N-F	strain gauge	-	-	94	1:7:1	1/4-Bridge	95
36	S36	WC1TR-N-F	strain gauge	-	-	92	1:6:3	1/4-Bridge	93



Channel	ID	Label	Device	Range	Serial No.	Cable No.	DAQ Box ID	Note	Column #
37	S37	EC2BL-S-F	strain gauge	-	-	390	0:9:2	1/4-Bridge	40
38	S38	EC2BR-S-F	strain gauge	-	-	391	0:9:3	1/4-Bridge	41
39	S39	EC2BL-N-F	strain gauge	-	-	376	0:10:0	1/4-Bridge	42
40	S40	EC2BR-N-F	strain gauge	-	-	377	0:10:1	1/4-Bridge	43
41	S41	EB2BL-F	strain gauge	-	-	378	0:10:2	1/4-Bridge	44
42	S42	EB2TL-F	strain gauge	-	-	200/348	2:4:3	1/4-Bridge	149
43	S43	EB2BR-F	strain gauge	-	-	197/145	2:4:0	1/4-Bridge	146
44	S44	EB2TR-S-F	strain gauge	-	-	199/147	2:4:2	1/4-Bridge	148
45	S45	E-WF-2-LQ-T-F	strain gauge	-	-	48	0:11:3	1/4-Bridge	49
46	S46	E-WF-2-LQ-B-F	strain gauge	-	-	392	0:12:0	1/4-Bridge	50
47	S47	E-WF-2-M-N-Y	strain gauge	-	-	362	0:12:1	1/4-Bridge	51
48	S48	EB1TR-N-F	strain gauge	-	-	365	0:12:2	1/4-Bridge	52
49	S49	E-WF-2-UQ-TN-F	strain gauge	-	-	366	0:12:3	1/4-Bridge	53
50	S50	E-WF-2-UQ-TS-F	strain gauge	-	-	367	0:13:0	1/4-Bridge	54
51	S51	E-WF-2-UQ-BN-F	strain gauge	-	-	368	0:13:1	1/4-Bridge	55
52	S52	E-WF-2-UQ-BS-F	strain gauge	-	-	369	0:13:2	1/4-Bridge	56
53	S53	E-WF-2-CP-N-F	strain gauge	-	-	370	0:13:3	1/4-Bridge	57
54	S54	E-WF-2-CP-S-F	strain gauge	-	-	383	0:11:2	1/4-Bridge	48
55	S55	W-WF-2-CP-N-F	strain gauge	-	-	324/58	0:14:1	1/4-Bridge	59
56	S56	W-WF-2-CP-S-F	strain gauge	-	-	326/59	0:14:2	1/4-Bridge	60
57	S57	W-WF-2-UQ-TN-F	strain gauge	-	-	333/60	0:14:3	1/4-Bridge	61
58	S58	W-WF-2-UQ-TS-F	strain gauge	-	-	327/61	0:15:0	1/4-Bridge	62
59	S59	W-WF-2-UQ-BN-F	strain gauge	-	-	320/62	0:15:1	1/4-Bridge	63
60	S60	W-WF-2-UQ-BS-F	strain gauge	-	-	321/63	0:15:2	1/4-Bridge	64
61	S61	W-WF-2-M-N-Y	strain gauge	-	-	322/64	0:15:3	1/4-Bridge	65
62	S62	WB1TL-N-F	strain gauge	-	-	203/65	1:0:0	1/4-Bridge	66
63	S63	W-WF-2-LQ-T-F	strain gauge	-	-	315/66	1:0:1	1/4-Bridge	67
64	S64	W-WF-2-LQ-B-F	strain gauge	-	-	343/67	1:0:2	1/4-Bridge	68
65	S65	WB2BL-F	strain gauge	-	-	346/137	2:2:0	1/4-Bridge	138
66	S66	WB2TL-S-F	strain gauge	-	-	328/138	2:2:1	1/4-Bridge	139
67	S67	WB2BR-F	strain gauge	-	-	201/71	1:1:2	1/4-Bridge	72
68	S68	WB2TR-F	strain gauge	-	-	345/140	2:2:3	1/4-Bridge	141
69	S69	WC2BL-N-F	strain gauge	-	-	316/73	1:2:0	1/4-Bridge	74
70	S70	WC2BR-N-F	strain gauge	-	-	349/74	1:2:1	1/4-Bridge	75
71	S71	WC2BL-S-F	strain gauge	-	-	351/75	1:2:2	1/4-Bridge	76
72	S72	WC2BR-S-F	strain gauge	-	-	318/76	1:2:3	1/4-Bridge	77

Channel	ID	Label	Device	Range	Serial No.	Cable No.	DAQ Box ID	Note	Column #
73	ST16	Act2-BK	stick	2"	2009NC01019	355	0:4:0	Novo 50 (recalibrated)	18
74	ST1	E-CB-Slip	stick	1"	2004NC01014	379	0:4:1	Novo 25 (recalibrated)	19
75	R73	STB2-T-F	strain gauge	-	-	396	0:4:2	1/4-Bridge	20
76	R2-1	EC1-PZ-N-1-YR	rosette	-	-	384	0:8:0	1/4-Bridge	34
77	R2-2	EC1-PZ-N-2-YR	rosette	-	-	385	0:8:1	1/4-Bridge	35
78	R2-3	EC1-PZ-N-3-YR	rosette	-	-	386	0:8:2	1/4-Bridge	36
79	R3-1	EC2-B-N-1-YR	rosette	-	-	387	0:8:3	1/4-Bridge	37
80	R3-2	EC2-B-N-2-YR	rosette	-	-	388	0:9:0	1/4-Bridge	38
81	R3-3	EC2-B-N-3-YR	rosette	-	-	389	0:9:1	1/4-Bridge	39
82	R4-1	EC2-PZ-N-1-YR	rosette	-	-	196/149	2:5:0	1/4-Bridge	150
83	R4-2	EC2-PZ-N-2-YR	rosette	-	-	198/150	2:5:1	1/4-Bridge	151
84	R4-3	EC2-PZ-N-3-YR	rosette	-	-	195/151	2:5:2	1/4-Bridge	152
85	R5-1	WC1-B-N-1-YR	rosette	-	-	89	1:6:0	1/4-Bridge	90
86	R5-2	WC1-B-N-2-YR	rosette	-	-	90	1:6:1	1/4-Bridge	91
87	R5-3	WC1-B-N-3-YR	rosette	-	-	91	1:6:2	1/4-Bridge	92
88	R6-1	WC1-PZ-N-1-YR	rosette	-	-	317/77	1:3:0	1/4-Bridge	78
89	R6-2	WC1-PZ-N-2-YR	rosette	-	-	350/78	1:3:1	1/4-Bridge	79
90	R6-3	WC1-PZ-N-3-YR	rosette	-	-	302/79	1:3:2	1/4-Bridge	80
91	R7-1	WC2-B-N-1-YR	rosette	-	-	301/80	1:3:3	1/4-Bridge	81
92	R7-2	WC2-B-N-2-YR	rosette	-	-	323/81	1:4:0	1/4-Bridge	82
93	R7-3	WC2-B-N-3-YR	rosette	-	-	336/82	1:4:1	1/4-Bridge	83
94	R8-1	WC2-PZ-N-1-YR	rosette	-	-	352/141	2:3:0	1/4-Bridge	142
95	R8-2	WC2-PZ-N-2-YR	rosette	-	-	319/142	2:3:1	1/4-Bridge	143
96	R8-3	WC2-PZ-N-3-YR	rosette	-	-	329/143	2:3:2	1/4-Bridge	144
97	R9-1	IF-E-BG-TL-1-N-YR	rosette	-	-	101	1:9:0	1/4-Bridge	102
98	R9-2	IF-E-BG-TL-2-N-YR	rosette	-	-	102	1:9:1	1/4-Bridge	103
99	R9-3	IF-E-BG-TL-3-N-YR	rosette	-	-	103	1:9:2	1/4-Bridge	104
100	R10-1	IF-E-BG-BL-1-N-YR	rosette	-	-	104	1:9:3	1/4-Bridge	105
101	R10-2	IF-E-BG-BL-2-N-YR	rosette	-	-	105	1:10:0	1/4-Bridge	106
102	R10-3	IF-E-BG-BL-3-N-YR	rosette	-	-	106	1:10:1	1/4-Bridge	107
103	R11-1	IF-E-BG-TR-1-N-YR	rosette	-	-	107	1:10:2	1/4-Bridge	108
104	R11-2	IF-E-BG-TR-2-N-YR	rosette	-	-	108	1:10:3	1/4-Bridge	109
105	R11-3	IF-E-BG-TR-3-N-YR	rosette	-	-	109	1:11:0	1/4-Bridge	110
106	R12-1	IF-E-BG-TC-1-N-YR	rosette	-	-	110	1:11:1	1/4-Bridge	111
107	R12-2	IF-E-BG-TC-2-N-YR	rosette	-	-	111	1:11:2	1/4-Bridge	112
108	R12-3	IF-E-BG-TC-3-N-YR	rosette	-	-	112	1:11:3	1/4-Bridge	113

Channel	ID	Label	Device	Range	Serial No.	Cable No.	DAQ Box ID	Note	Column #
109	R13-1	IF-E-MG-TL-1-N-YR	rosette	-	-	113	1:12:0	1/4-Bridge	114
110	R13-2	IF-E-MG-TL-2-N-YR	rosette	-	-	114	1:12:1	1/4-Bridge	115
111	R13-3	IF-E-MG-TL-3-N-YR	rosette	-	-	115	1:12:2	1/4-Bridge	116
112	R14-1	IF-E-MG-BL-1-N-YR	rosette	-	-	116	1:12:3	1/4-Bridge	117
113	R14-2	IF-E-MG-BL-2-N-YR	rosette	-	-	117	1:13:0	1/4-Bridge	118
114	R14-3	IF-E-MG-BL-3-N-YR	rosette	-	-	118	1:13:1	1/4-Bridge	119
115	R15-1	IF-E-MG-TR-1-N-YR	rosette	-	-	119	1:13:2	1/4-Bridge	120
116	R15-2	IF-E-MG-TR-2-N-YR	rosette	-	-	120	1:13:3	1/4-Bridge	121
117	R15-3	IF-E-MG-TR-3-N-YR	rosette	-	-	121	1:14:0	1/4-Bridge	122
118	R16-1	IF-E-MG-BR-1-N-YR	rosette	-	-	122	1:14:1	1/4-Bridge	123
119	R16-2	IF-E-MG-BR-2-N-YR	rosette	-	-	123	1:14:2	1/4-Bridge	124
120	R16-3	IF-E-MG-BR-3-N-YR	rosette	-	-	124	1:14:3	1/4-Bridge	125
121	R17-1	IF-E-TG-TL-1-N-YR	rosette	-	-	125	1:15:0	1/4-Bridge	126
122	R17-2	IF-E-TG-TL-2-N-YR	rosette	-	-	126	1:15:1	1/4-Bridge	127
123	R17-3	IF-E-TG-TL-3-N-YR	rosette	-	-	127	1:15:2	1/4-Bridge	128
124	R18-1	IF-E-TG-BL-1-N-YR	rosette	-	-	128	1:15:3	1/4-Bridge	129
125	R18-2	IF-E-TG-BL-2-N-YR	rosette	-	-	129	2:0:0	1/4-Bridge	130
126	R18-3	IF-E-TG-BL-3-N-YR	rosette	-	-	130	2:0:1	1/4-Bridge	131
127	R19-1	IF-E-TG-BC-1-N-YR	rosette	-	-	131	2:0:2	1/4-Bridge	132
128	R19-2	IF-E-TG-BC-2-N-YR	rosette	-	-	303	2:0:3	1/4-Bridge	133
129	R19-3	IF-E-TG-BC-3-N-YR	rosette	-	-	133	2:1:0	1/4-Bridge	134
130	R20-1	IF-E-TG-BR-1-N-YR	rosette	-	-	134	2:1:1	1/4-Bridge	135
131	R20-2	IF-E-TG-BR-2-N-YR	rosette	-	-	135	2:1:2	1/4-Bridge	136
132	R20-3	IF-E-TG-BR-3-N-YR	rosette	-	-	136	2:1:3	1/4-Bridge	137
133	WP07	IF-E-WF-UQ-R-OD	wire pot	30"	2000NC51151	159	2:7:2	-	160
134	WP04	IF-E-WF-M-R-OD	wire pot	40"	2005NC51006	156	2:6:3	-	157
135	WP02	IF-E-WF-LQ-R-OD	wire pot	30"	2006NC51015	154	2:6:1	-	155
136	WP03	IF-E-WF-UQ-L-OD	wire pot	30"	2006NC51012	155	2:6:2	-	156
137	WP05	IF-E-WF-M-L-OD	wire pot	40"	2005NC01003	157	2:7:0	-	158
138	WP01	IF-E-WF-LQ-L-OD	wire pot	30"	2006NC51014	153	2:6:0	-	154
139	WP06	IF-W-WF-LQ-R-OD	wire pot	30"	2000NC51124	158	2:7:1	-	159
140	WP12	IF-W-WF-M-R-OD	wire pot	40"	2005NC01008	164	2:8:3	-	165
141	WP09	IF-W-WF-UQ-R-OD	wire pot	30"	2000NC51106	161	2:8:0	-	162
142	WP08	IF-W-WF-LQ-L-OD	wire pot	30"	2006NC51016	160	2:7:3	-	161
143	WP11	IF-W-WF-M-L-OD	wire pot	40"	2005NC01006	163	2:8:2	-	164
144	WP10	IF-W-WF-UQ-L-OD	wire pot	40"	2005NC51005	162	2:8:1	(recalibrated)	163

Channel	ID	Label	Device	Range	Serial No.	Cable No.	DAQ Box ID	Note	Column #
145	WP14	2F-E-WF-LQ-R-OD	wire pot	30"	2006NC51013	166/305	2:9:1	-	167
146	WP17	2F-E-WF-M-R-OD	wire pot	40"	2005NC51002	169/308	2:10:0	-	170
147	WP13	2F-E-WF-UQ-R-OD	wire pot	40"	2009NC01052	342	2:9:0	165/304 old cables N.G.	166
148	WP16	2F-E-WF-LQ-L-OD	wire pot	30"	2000NC51125	168/307	2:9:3	-	169
149	WP18	2F-E-WF-M-L-OD	wire pot	40"	2005NC51007	170/309	2:10:1	-	171
150	WP15	2F-E-WF-UQ-L-OD	wire pot	30"	2000NC51105	167/306	2:9:2	-	168
151	WP22	2F-W-WF-UQ-R-OD	wire pot	40"	2005NC01010	174/313	2:11:1	-	175
152	WP20	2F-W-WF-M-R-OD	wire pot	40"	2005NC01009	172/311	2:10:3	-	173
153	WP24	2F-W-WF-LQ-R-OD	wire pot	30"	2000NC51153	176/315	2:11:3	-	177
154	WP21	2F-W-WF-UQ-L-OD	wire pot	40"	2005NC51010	173/312	2:11:0	-	174
155	WP19	2F-W-WF-M-L-OD	wire pot	40"	2005NC01007	171/310	2:10:2	394 (171 N.G.)	172
156	WP23	2F-W-WF-LQ-L-OD	wire pot	30"	2000NC51111	175/314	2:11:2	-	176
157	WP25	1F-E-WF-A-N	wire pot	40"	2005NC51009	177	2:12:0	-	178
158	WP26	1F-W-WF-A-N	wire pot	40"	2005NC01004	178	2:12:1	-	179
159	WP27	2F-E-WF-A-N	wire pot	40"	2005NC01001	300	2:14:0	-	186
160	WP28	2F-W-WF-A-N	wire pot	40"	2000NC51131	399	2:14:1	(checked, not recalibrated)	187
161	-	-	-	-	-	-	2:13:0	not use	182
162	-	-	-	-	-	-	2:13:1	not use	183
163	-	-	-	-	-	-	2:13:3	not use	185
164	ST17	WB1-RT	stick	4"	2009NC01008	307	2:13:2	Novo100 (recalibrated)	184
165	ST18	EB1-RT	stick	4"	2009NC01009	183	1:8:0	Novo100 (recalibrated)	98
166	ST19	EB1-RB	stick	4"	2009NC01001	184	1:8:1	Novo100 (recalibrated)	99
167	ST20	RRW-T-N	stick	4"	2004NC01037	318/86	1:8:2	Novo100 (recalibrated)	100
168	ST21	RRW-T-S	stick	4"	2004NC01038	319/395	1:8:3	Novo100 (recalibrated)	101
169	WP30	1F-C-G-TS-OD	wire pot	40"	2005NC01005	21	0:5:0	-	22
170	WP47	2F-W-WF-A-S	wire pot	30"	2000NC51150	313	1:5:3	-	89
171	WP33	1F-E-WF-A-S	wire pot	40"	2009NC01054	24	0:5:3	(recalibrated)	25
172	WP29	1F-W-WF-A-S	wire pot	40"	2009NC01053	20	0:4:3	(recalibrated)	21
173	WP43	1F-E-BG-B-OD	wire pot	30"	2000NC51098	320	1:4:2	-	84
174	WP31	1F-C-B-BF-OD	wire pot	30"	2000NC51128	22	0:5:1	-	23
175	WP32	1F-C-B-CS-OD	wire pot	40"	2005NC51003	23	0:5:2	(recalibrated)	24
176	WP42	1F-W-BG-B-OD	wire pot	30"	2000NC51117	314	1:1:3	-	73
177	WP46	2F-E-WF-A-S	wire pot	30"	2000NC51152	312	1:5:2	-	88
178	WP44	2F-C-B-BF-OD	wire pot	30"	2000NC51126	310	1:5:0	-	86
179	WP45	2F-C-G-BS-OD	wire pot	30"	2000NC51129	311	1:5:1	-	87
180	-	-	-	-	-	182/363	2:12:3	not use	181

Channel	ID	Label	Device	Range	Serial No.	Cable No.	DAQ Box ID	Note	Column #
181	ST2	C-GB-Slip	stick	1"	2009NC01028	181	2:12:2	Novo 25 (recalibrated)	180
182	ST3	W-CB-Slip	stick	1"	2009NC01026	96	1:7:3	Novo 25 (recalibrated)	97
183	ST4	E-LC1-OD	stick	6"	2007NC01009	179	2:15:2	-	192
184	ST5	E-LC2-OD	stick	6"	2007NC01010	302	2:14:2	-	188
185	ST6	C-LC1-OD	stick	6"	2007NC01011	180	2:15:3	-	193
186	ST7	C-LC2-OD	stick	6"	2007NC51006	303	2:14:3	-	189
187	ST8	W-LC1-OD	stick	6"	2007NC51007	304	2:15:0	-	190
188	ST9	W-LC2-OD	stick	6"	2007NC51010	305	2:15:1	-	191
189	ST10	C-B1-VD	stick	4"	2007NC01006	144	2:3:3	-	145
190	ST11	C-B2-VD	stick	4"	2007NC01003	210	2:5:3	Novo100	153
191	ST22	WB1-RB	stick	4"	2009NC01004	316	2:2:2	Novo100 (recalibrated)	140
192	PT1	EC1-PZ-E-PT	Position Transducer	20"	-	323	2:4:1	Novo500	147
193	PT2	EC2-PZ-E-PT	Position Transducer	40"	-	-	3:0:0	MTS-ST5, Roof Disp. Control	194
194	A1	EC2-PZ-E-PT	Position Transducer	40"	-	-	3:0:0	MTS-ST5 (Act3disp) Control	194
195	A2	Act2force	Load Cell	-	-	-	3:0:1	MTS-ST5 (Act3force)	195
196	A3	-	Position Transducer	40"	-	-	3:0:2	MTS-ST5 (Act1dispFT)	196
197	A4	Act3disp	Position Transducer	40"	-	-	3:0:3	MTS-ST5 (Act2dispFT)	197
198	A5	Act2disp	Position Transducer	40"	-	-	3:0:4	MTS-ST5 (Act3dispFT)	198
199	A6	Act4disp	Position Transducer	40"	-	-	3:0:5	MTS-ST5 (Act4dispFT)	199
200	A7	Act1disp	Position Transducer	40"	-	-	3:0:6	MTS-ST5 (Act4disp)	200
201	A8	Act1force	Load Cell	-	-	-	3:0:7	MTS-ST5 (Act4force)	201
202	TG1	TriggerCanon	TriggerCanon	-	-	207	3:1:5	D-Space	207
203	TG2	TriggerLeica	TriggerLeica	-	-	208	3:1:6	D-Space	208
204	500	IRIGday-500	-	-	-	-	3:15:0	For time sync. (BNC to STS)	210
205	501	IRIGhour-501	-	-	-	-	3:15:1	For time sync. (BNC to STS)	211
206	502	IRIGmin-502	-	-	-	-	3:15:2	For time sync. (BNC to STS)	212
207	503	IRIGsec-503	-	-	-	-	3:15:3	For time sync. (BNC to STS)	213
208	504	IRIGmsec-504	-	-	-	-	3:15:4	For time sync. (BNC to STS)	214
209	505	IRIGusec-505	-	-	-	-	3:15:5	For time sync. (BNC to STS)	215
210	506	IRIGstatus-506	-	-	-	-	3:15:6	For time sync. (BNC to STS)	216

Channel	ID	Label	Device	Range	Serial No.	Cable No.	DAQ Box ID	Note	Column #
1	PS1	EC1BL-S-F	strain gauge	-	-	13	0:0:0	S1	2
2	PS2	EC1BR-S-F	strain gauge	-	-	14	0:0:1	S2	3
3	PS3	EC1TL-S-F	strain gauge	-	-	15	0:0:2	S3	4
4	PS4	EC1TR-S-F	strain gauge	-	-	16	0:0:3	S4	5
5	PS5	EB2TR-N-F	strain gauge	-	-	339/198A	0:0:4	S77	6
6	PS6	WB2TL-N-F	strain gauge	-	-	193	0:0:5	S78	7
7	PS7	EC1-B-N-1-R	rosette	-	-	17	0:0:6	R1-1 (Red)	8
8	PS8	EC1-B-N-2-R	rosette	-	-	18	0:0:7	R1-2 (White)	9
9	PS9	EC1-B-N-3-R	rosette	-	-	19	0:1:0	R1-3 (Green)	10
10	PS10	EC1BL-N-F	strain gauge	-	-	38	0:1:1	S79	11
11	PS11	EC1BR-N-F	strain gauge	-	-	40	0:1:2	S80	12
12	PS12	EC1TL-N-F	strain gauge	-	-	37	0:1:3	S81	13
13	PS13	EC1TR-N-F	strain gauge	-	-	39	0:1:4	S82	14
14	PS14	WC1BL-S-F	strain gauge	-	-	34	0:1:5	S83	15
15	PS15	WC1BR-S-F	strain gauge	-	-	33	0:1:6	S84	16
16	PS16	WC1BL-N-F	strain gauge	-	-	36	0:1:7	S85	17
17	PS17	WC1BR-N-F	strain gauge	-	-	35	0:2:0	S86	18
18	PS18	EC2TL-S-F	strain gauge	-	-	52	0:2:1	S87	19
19	PS19	EC2TR-S-F	strain gauge	-	-	51	0:2:2	S88	20
20	PS20	EC2TL-N-F	strain gauge	-	-	49	0:2:3	S89	21
21	PS21	EC2TR-N-F	strain gauge	-	-	50	0:2:4	S90	22
22	PS22	WC2TL-S-F	strain gauge	-	-	55	0:2:5	S91	23
23	PS23	WC2TR-S-F	strain gauge	-	-	56	0:2:6	S92	24
24	PS24	WC2TL-N-F	strain gauge	-	-	120C	0:2:7	S93	25
25	PS25	WC2TR-N-F	strain gauge	-	-	54	0:3:0	S94	26
26	PS26	E-GT1-N	strain gauge	-	-	402	0:3:1	S95	27
27	PS27	E-GT2-N	strain gauge	-	-	44	0:3:2	S96	28
28	PS28	E-GT3-N	strain gauge	-	-	45	0:3:3	S97	29
29	PS29	E-GT4-N	strain gauge	-	-	46	0:3:4	S98	30
30	PS30	E-GT5-N	strain gauge	-	-	47	0:3:5	S99	31
31	PS31	E-GC-N	strain gauge	-	-	87	0:3:6	S100	32
32	PS32	E-GB1-N	strain gauge	-	-	85	0:3:7	S101	33
33	PS33	E-GB2-N	strain gauge	-	-	88	0:4:0	S102	34
34	PS34	E-GB3-N	strain gauge	-	-	152	0:4:1	S103	35
35	PS35	E-GB4-N	strain gauge	-	-	331	0:4:2	S104	36
36	PS36	E-GB5-N	strain gauge	-	-	401	0:4:3	S105	37

Channel	ID	Label	Device	Range	Serial No.	Cable No.	DAQ Box ID	Note	Column #
37	PS37	IF-E-BG-BR-1-N-R	rosette	-	-	41	0:4:4	R21-1 (Red)	38
38	PS38	IF-E-BG-BR-2-N-R	rosette	-	-	42	0:4:5	R21-2 (White)	39
39	PS39	IF-E-BG-BR-3-N-R	rosette	-	-	43	0:4:6	R21-3 (Green)	40
40	PS40	STB1-T-F	strain gauge	-	-	97	0:4:7	S74	41
41	PS41	STB1-B-F	strain gauge	-	-	98	0:5:0	S75	42
42	PS42	STB2-B-F	strain gauge	-	-	100	0:5:1	S76	43
43	PS43	W-WF-1-M-T1-N-F	strain gauge	-	-	36C	0:5:2	(C for color coded cable)	44
44	PS44	W-WF-1-M-T2-N-F	strain gauge	-	-	37C	0:5:3	-	45
45	PS45	W-WF-1-M-T3-N-F	strain gauge	-	-	38C	0:5:4	-	46
46	PS46	W-WF-1-M-T4-N-F	strain gauge	-	-	341	0:5:5	-	47
47	PS47	W-WF-1-M-T5-N-F	strain gauge	-	-	399	0:5:6	-	48
48	PS48	W-WF-1-M-T2-S-SFA	strain gauge	-	-	33C	0:5:7	Stress Gauge (1/4-Bridge)	49
49	PS49	W-WF-1-M-T3-S-SFA	strain gauge	-	-	34C	0:6:0	Stress Gauge (1/4-Bridge)	50
50	PS50	W-WF-1-M-T4-S-SFA	strain gauge	-	-	35C	0:6:1	Stress Gauge (1/4-Bridge)	51
51	73	IRIGday-73	-	-	-	-	0:9:0	For time sync. (BNC to STS)	52
52	74	IRIGhour-74	-	-	-	-	0:9:1	For time sync. (BNC to STS)	53
53	75	IRIGmin-75	-	-	-	-	0:9:2	For time sync. (BNC to STS)	54
54	76	IRIGsec-76	-	-	-	-	0:9:3	For time sync. (BNC to STS)	55
55	77	IRIGmsec-77	-	-	-	-	0:9:4	For time sync. (BNC to STS)	56
56	78	IRIGusec-78	-	-	-	-	0:9:5	For time sync. (BNC to STS)	57
57	79	IRIGstatus-79	-	-	-	-	0:9:6	For time sync. (BNC to STS)	58

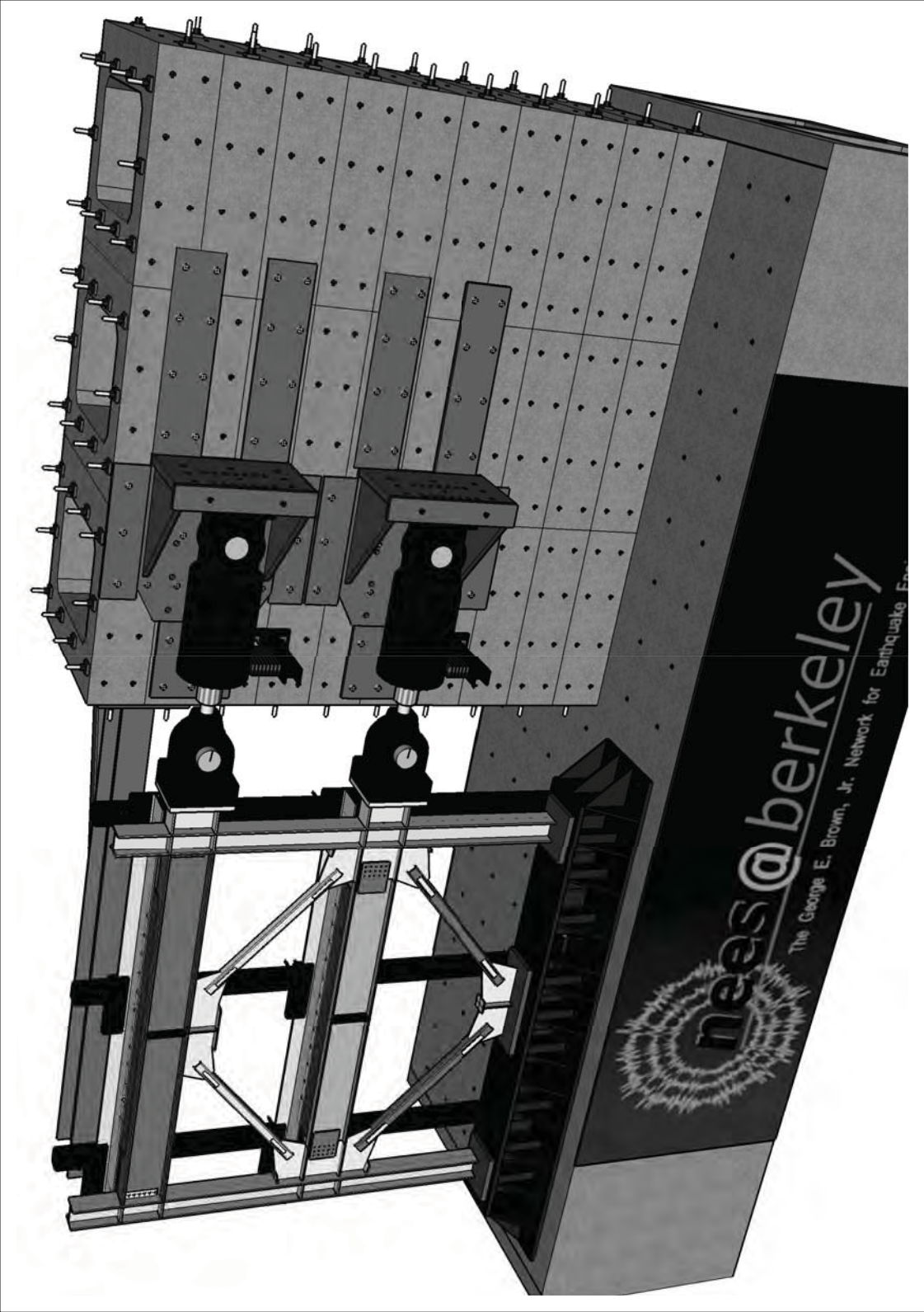
---

## **Appendix G**

### **Channel Locations and Lists for TCBF-B-4 Specimen**

---





**TCBF-B-4, Sensor Locations  
S.00**

**ISSUE**  
Mar 07, 2011

**DRAWN BY**  
Jiun-Wei Lai

**PROJECT NO.**  
TCBF-B-4

**PROJECT**  
TCBF

International Hybrid  
Simulation of  
Tomorrow's Braced  
Steel Frame Structures



**S.01**

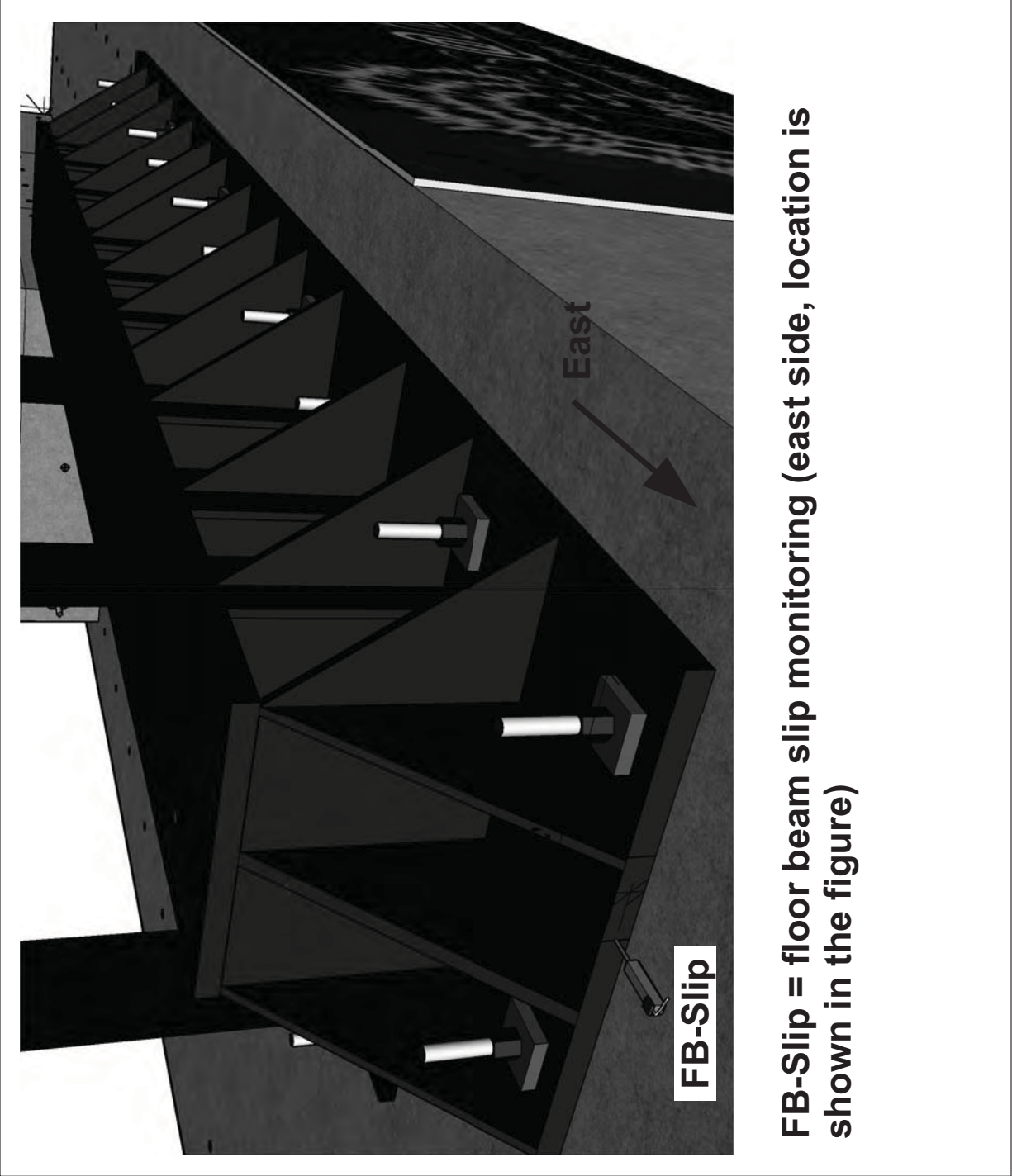
**Sensor Locations**

ISSUE  
Mar 07,  
2011  
DRAWN BY  
J.W. Lai

PROJECT  
TCFB  
TCBF-B-4  
PROJECT NO.  
TCBF-B-4

University of California,  
Berkeley  
TCBF-B-4

International Hybrid  
Simulation of  
Tomorrow's Braced  
Steel Frame  
Structures



**FB-Slip = floor beam slip monitoring (east side, location is shown in the figure)**



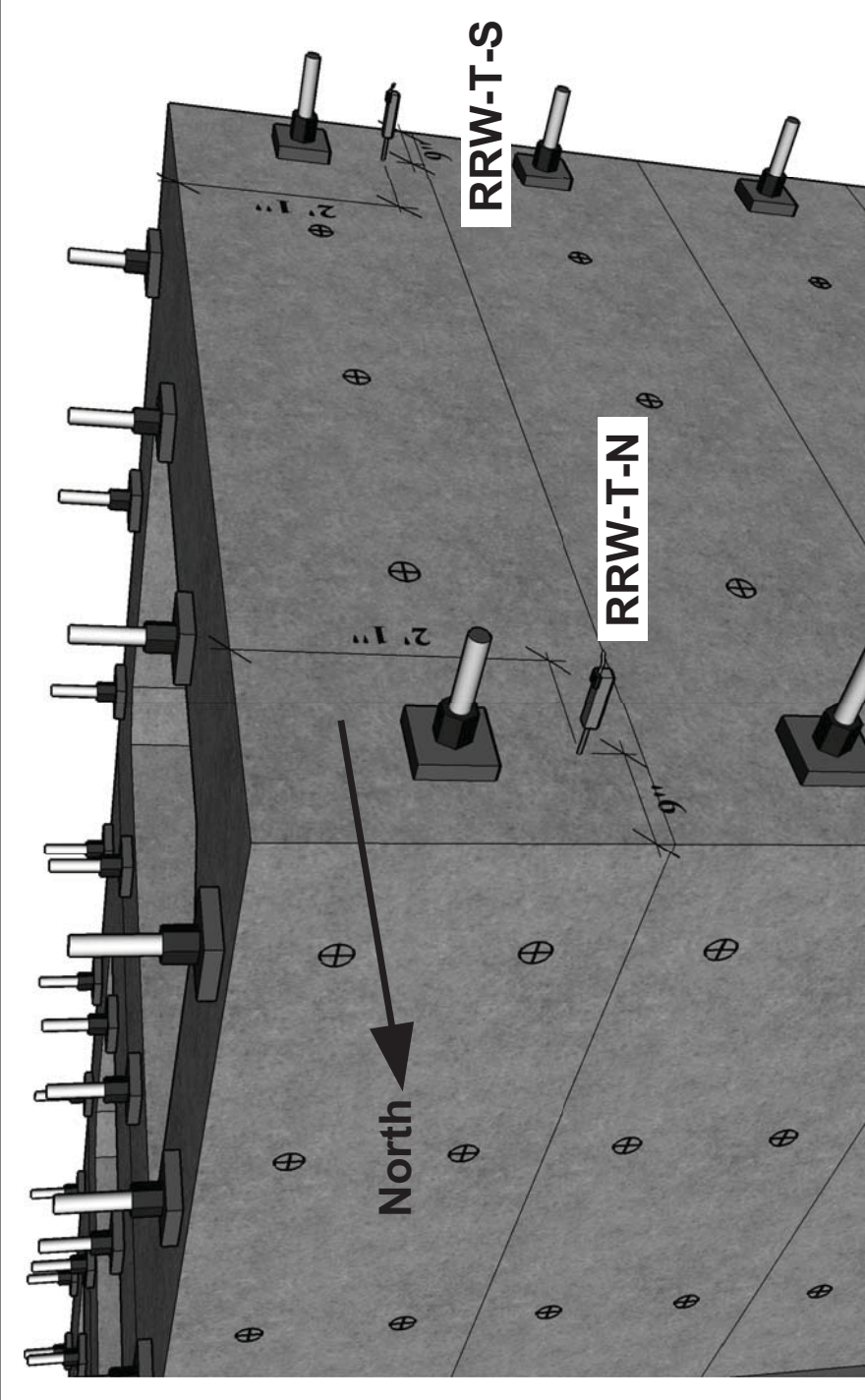
International Hybrid  
Simulation of  
Tomorrow's Braced  
Steel Frame  
Structures

University of California,  
Berkeley  
TCBF-B-4

PROJECT  
TCFB  
2011  
Mar 07,  
ISSUE  
DRAWN BY  
J.W. Lai  
TCBF-B-4  
PROJECT NO.

Sensor  
Locations

S.02



**RRW-T-N = north side of reconfigurable reaction wall (RRW), top deformation monitoring (location is shown in the figure)**

**RRW-T-S = south side of reconfigurable reaction wall (RRW), top deformation monitoring (location is shown in the figure)**



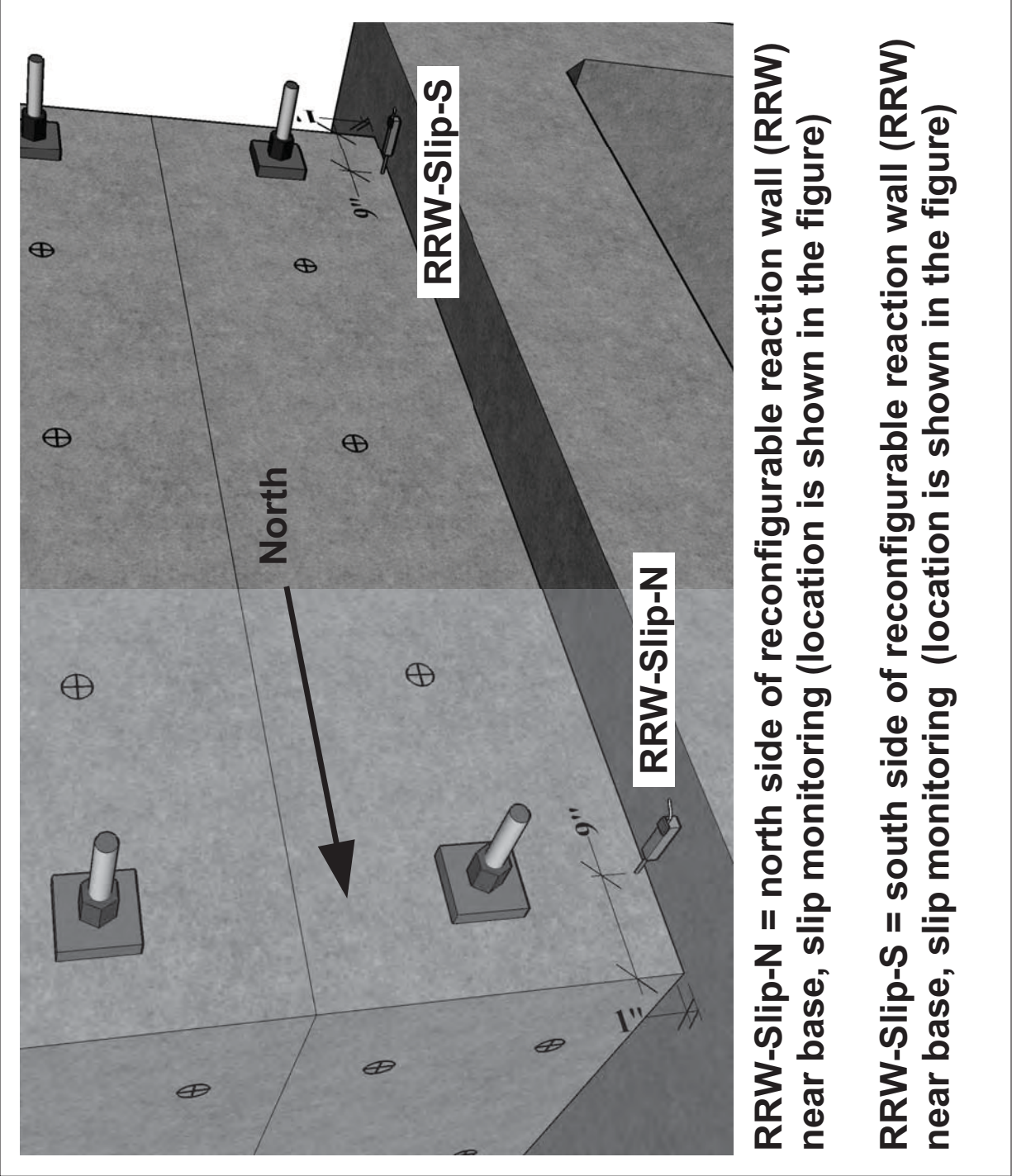
International Hybrid  
Simulation of  
Tomorrow's Braced  
Steel Frame  
Structures

University of California,  
Berkeley  
TCBF-B-4

PROJECT  
TCFB  
Mar 07,  
2011  
ISSUE  
DRAWN BY  
J.W. Lai  
PROJECT NO.  
TCBF-B-4

Sensor  
Locations

S.03





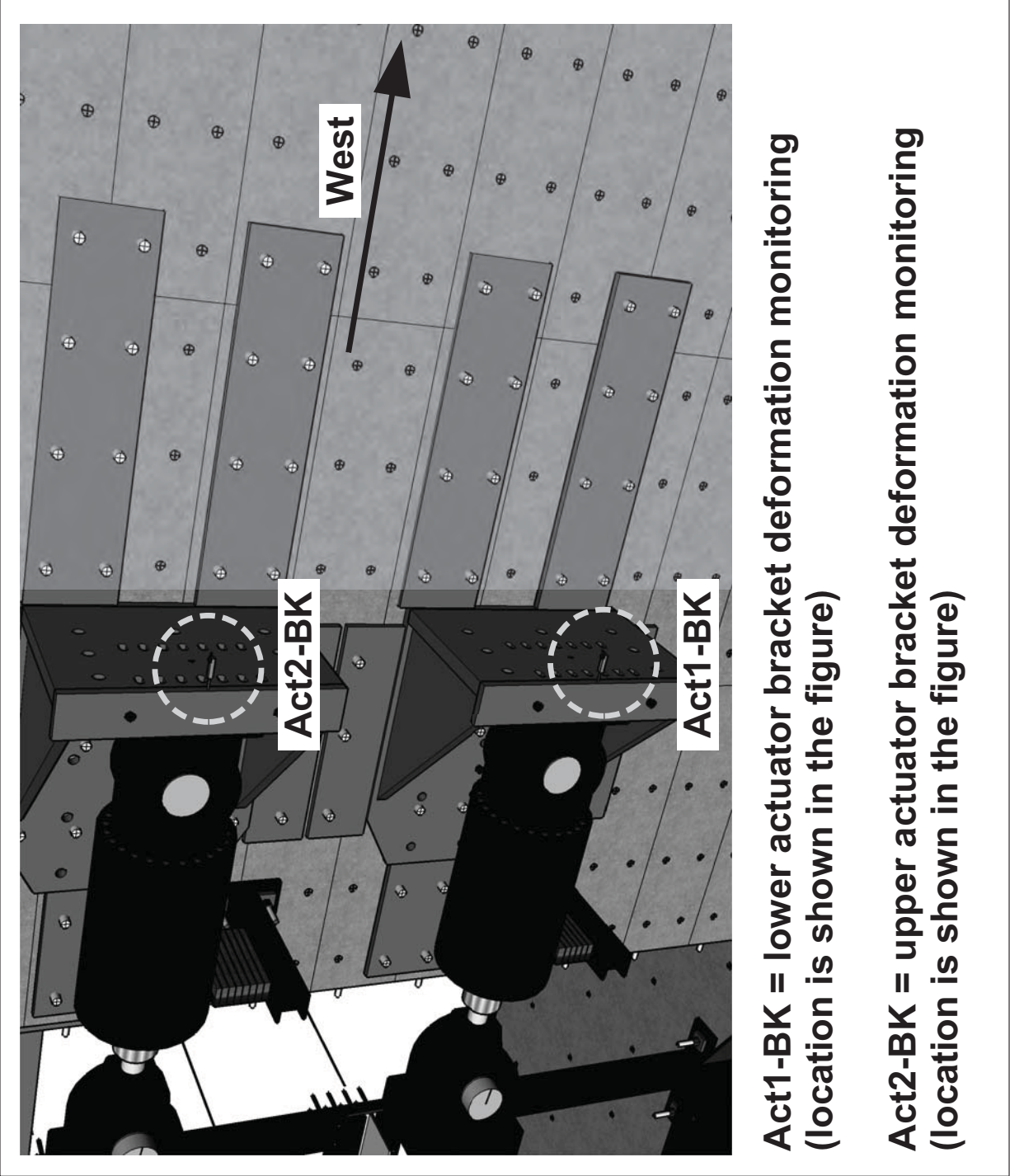
International Hybrid  
Simulation of  
Tomorrow's Braced  
Steel Frame  
Structures

University of California,  
Berkeley  
TCBF-B-4

PROJECT  
TCFB  
Mar 07,  
2011  
ISSUE  
DRAWN BY  
J.W. Lai  
PROJECT NO.  
TCBF-B-4

Sensor  
Locations

S.04



**Act1-BK = lower actuator bracket deformation monitoring  
(location is shown in the figure)**

**Act2-BK = upper actuator bracket deformation monitoring  
(location is shown in the figure)**



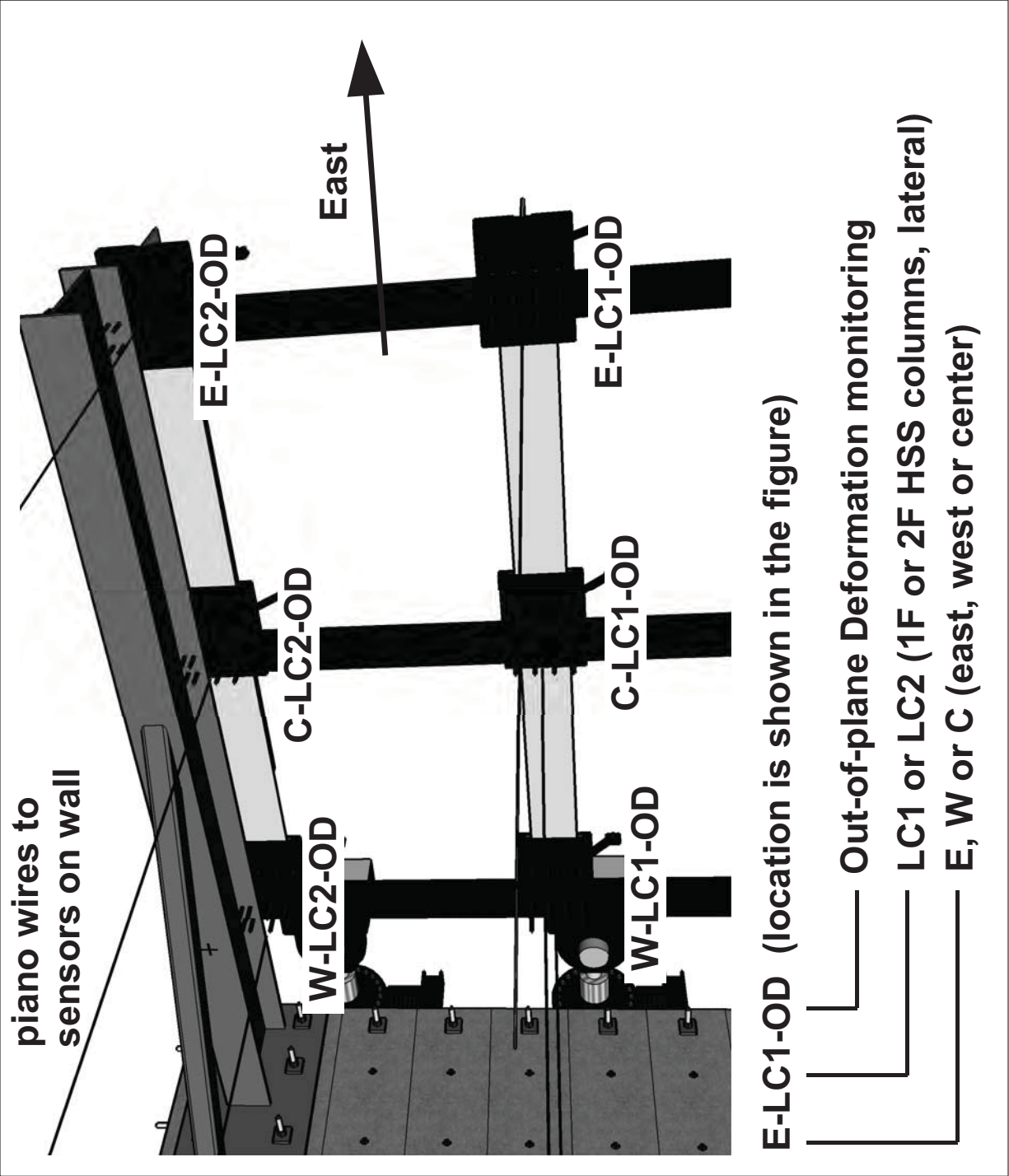
International Hybrid  
Simulation of  
Tomorrow's Braced  
Steel Frame  
Structures

University of California,  
Berkeley  
TCBF-B-4

PROJECT  
TCFB  
Mar 07, 2011  
ISSUE  
DRAWN BY  
J.W. Lai  
TCBF-B-4  
PROJECT NO.

Sensor  
Locations

S.05





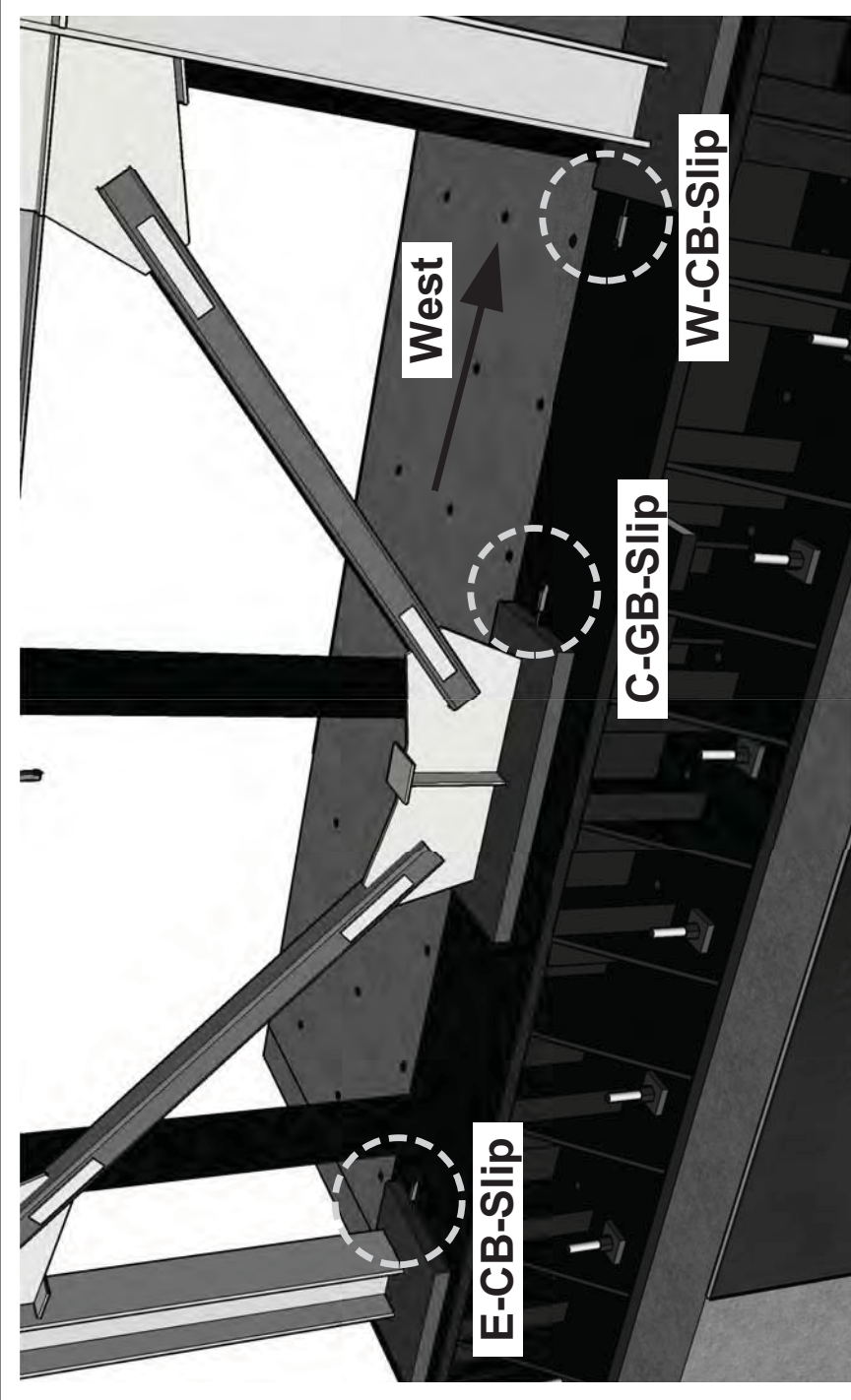
International Hybrid  
Simulation of  
Tomorrow's Braced  
Steel Frame  
Structures

University of California,  
Berkeley  
TCBF-B-4

PROJECT  
TCFB  
Mar 07, 2011  
DRAWN BY  
J.W. Lai  
PROJECT NO.  
TCBF-B-4

## Sensor Locations

### S.06



**E-CB-Slip = east column base slip monitoring**  
**C-GB-Slip = center gusset base slip monitoring**  
**W-CB-Slip = west column base slip monitoring**  
 (locations are shown in the figure, align with the braced frame center plane)



International Hybrid  
Simulation of  
Tomorrow's Braced  
Steel Frame  
Structures

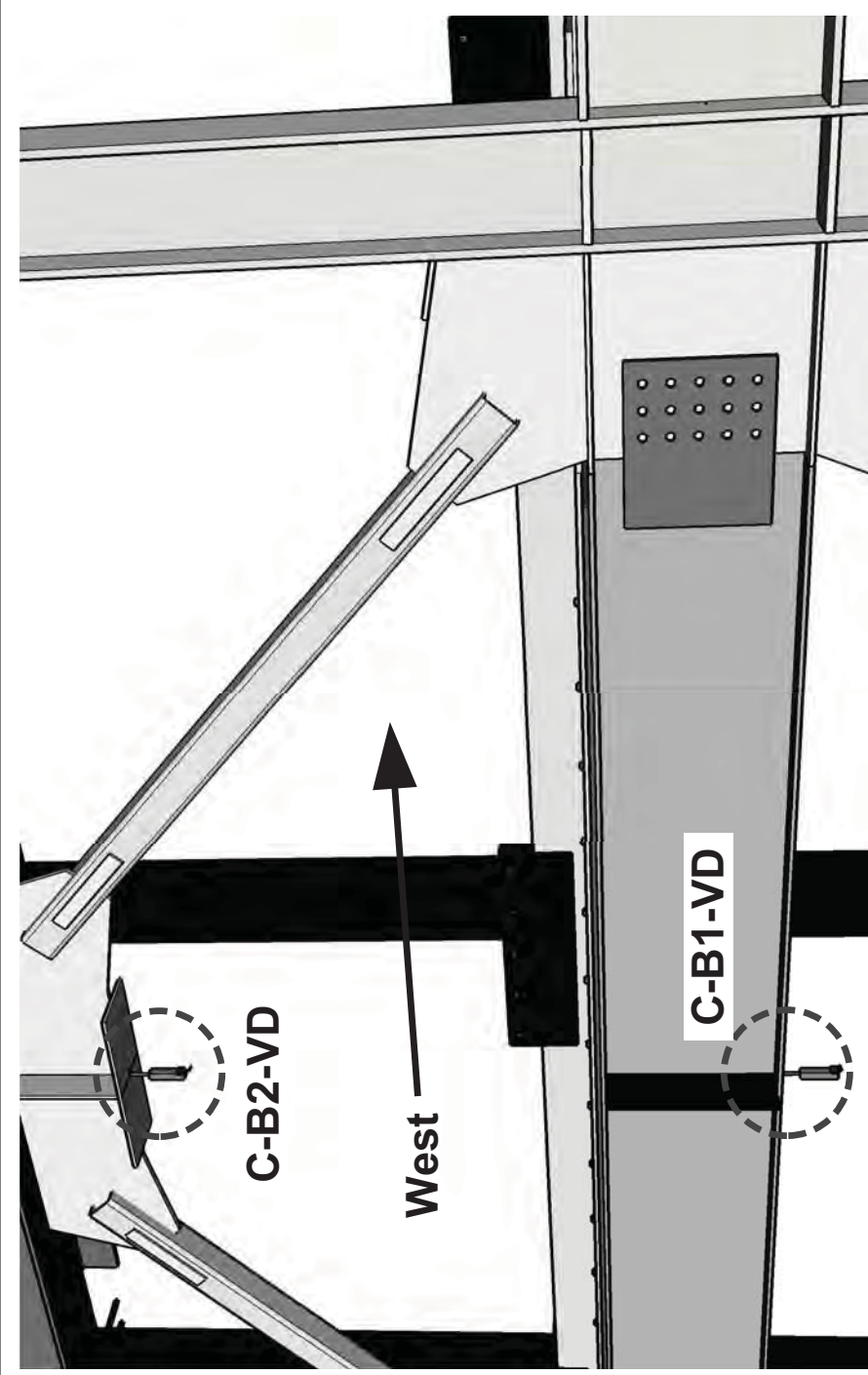
University of California,  
Berkeley  
TCBF-B-4

PROJECT  
TCFB  
TCBF-B-4  
PROJECT NO.

ISSUE  
Mar 07,  
2011  
DRAWN BY  
J.W. Lai

Sensor  
Locations

S.07



C-B2-VD = roof beam (2F) center deflection monitoring  
C-B1-VD = lower beam (1F) center deflection monitoring

(locations are shown in the figure, align with the beam bottom flange centerline)





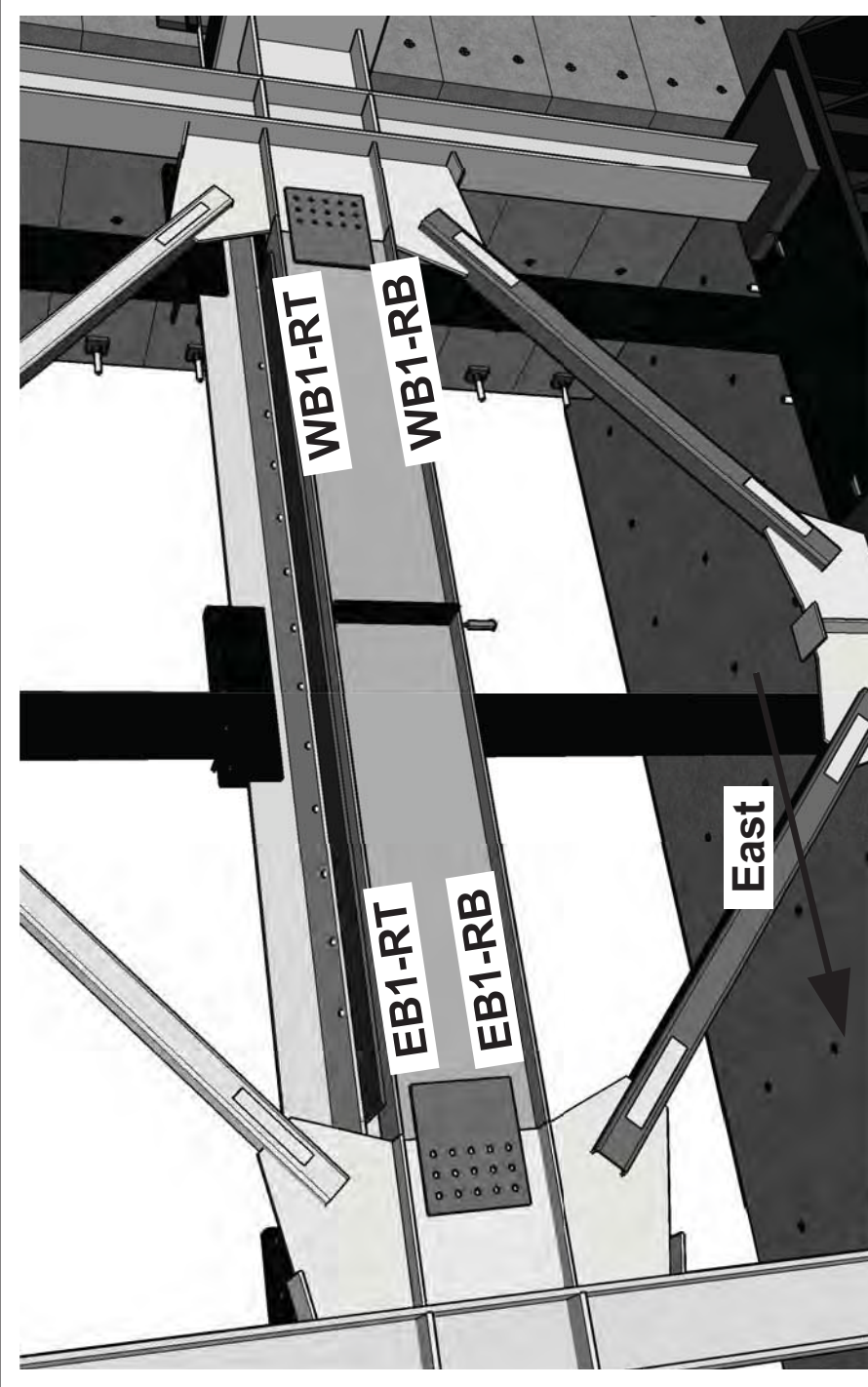
International Hybrid  
Simulation of  
Tomorrow's Braced  
Steel Frame  
Structures

University of California,  
Berkeley  
TCBF-B-4

PROJECT  
TCFB  
Mar 07,  
2011  
ISSUE  
DRAWN BY  
J.W. Lai  
PROJECT NO.  
TCBF-B-4

Sensor  
Locations

S.08



**WB1-RT, WB1-RB = west lower beam (1F) rotation monitoring  
EB1-RT, EB1-RB = east lower beam (1F) rotation monitoring  
RT, RB = top or bottom side  
(locations are shown in the figure, distance between two  
centerlines of top and bottom sticks is 21")**



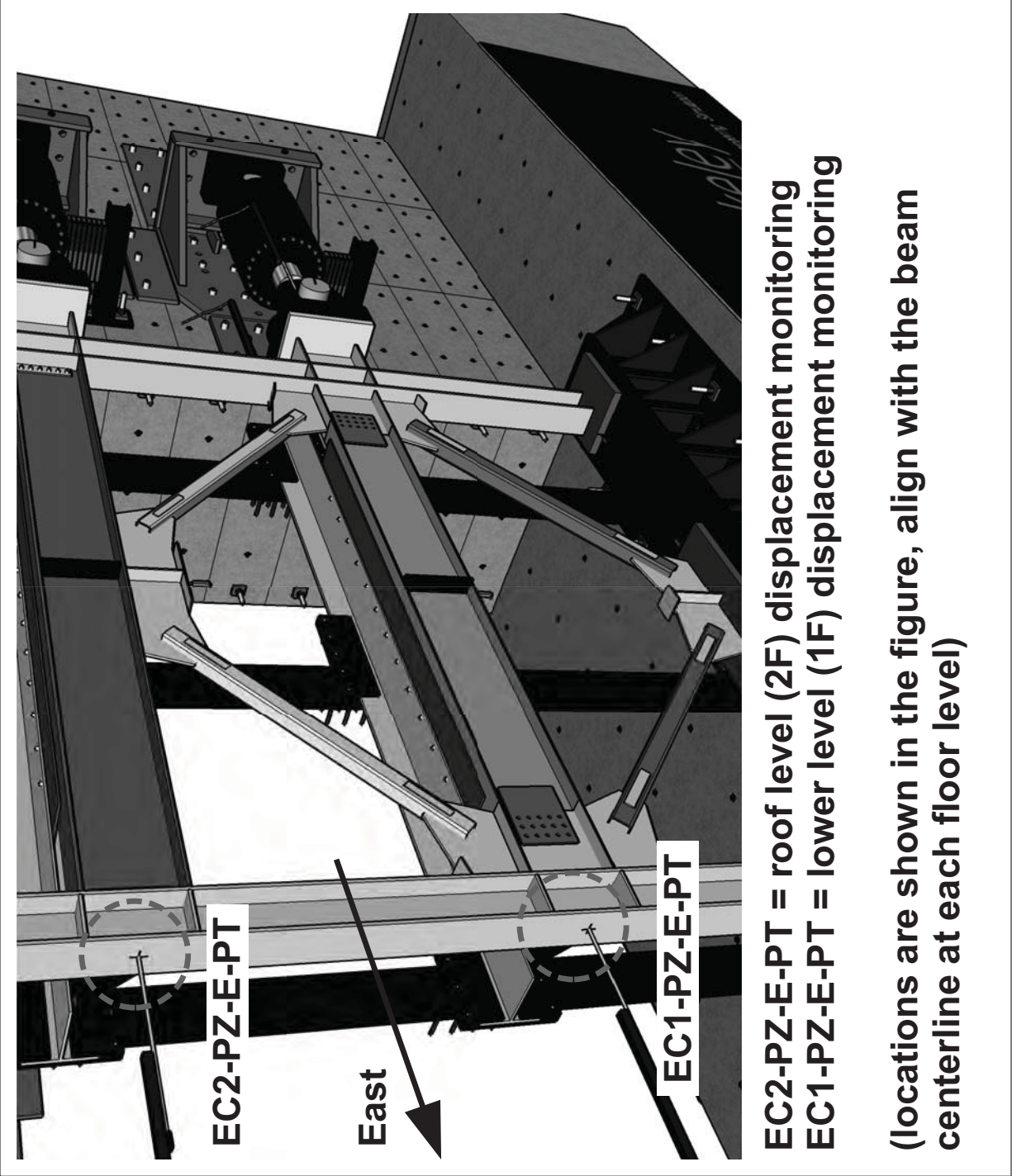
International Hybrid  
Simulation of  
Tomorrow's Braced  
Steel Frame  
Structures

University of California,  
Berkeley  
TCBF-B-4

PROJECT  
TCFB  
Mar 07, 2011  
DRAWN BY  
J.W. Lai  
PROJECT NO.  
TCBF-B-4

## Sensor Locations

### S.09





International Hybrid  
Simulation of  
Tomorrow's Braced  
Steel Frame  
Structures

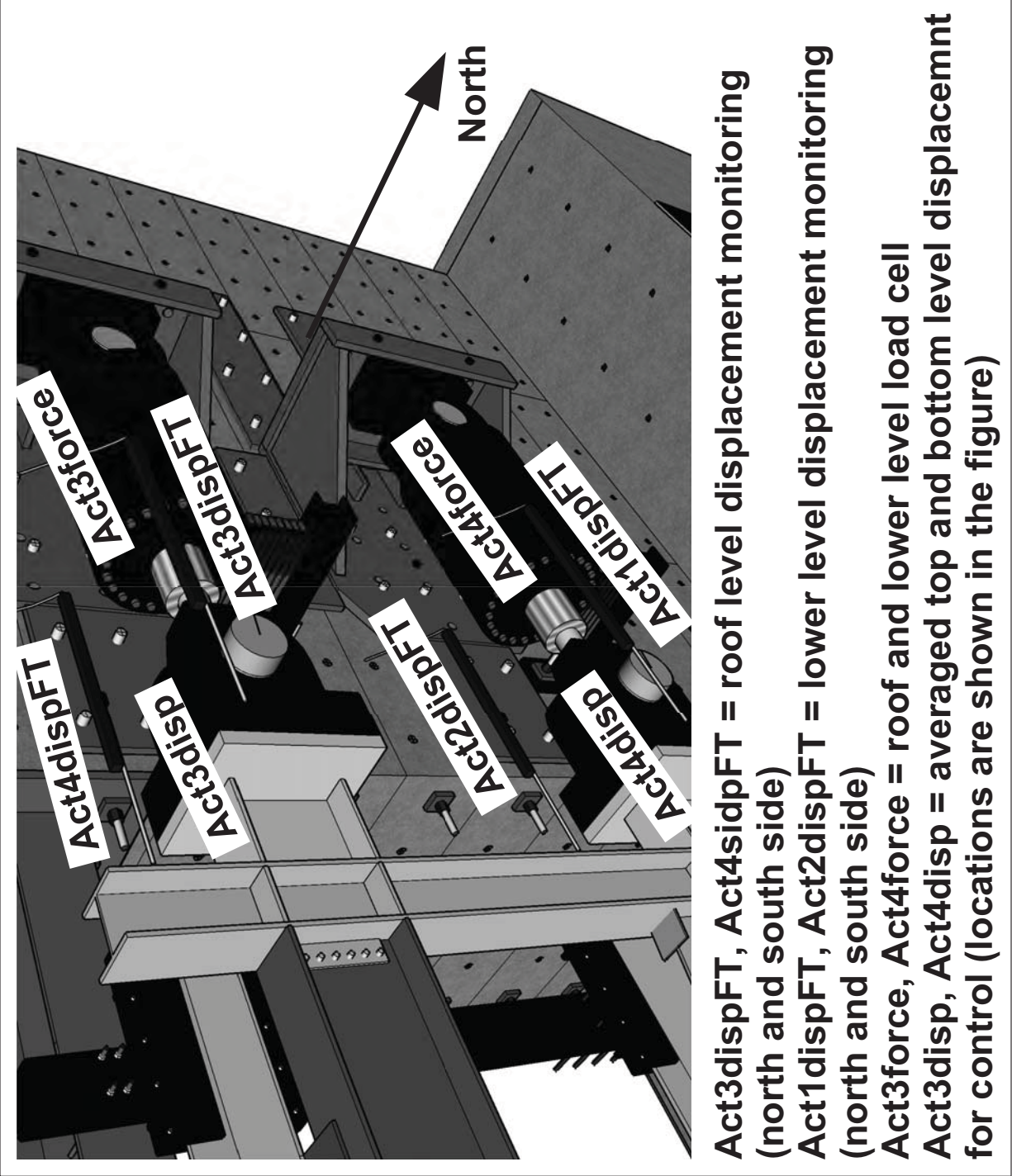
University of California,  
Berkeley  
TCBF-B-4

PROJECT  
TCFB  
Mar 07,  
2011

ISSUE  
Mar 07,  
2011  
DRAWN BY  
J.W. Lai

Sensor  
Locations

S-10





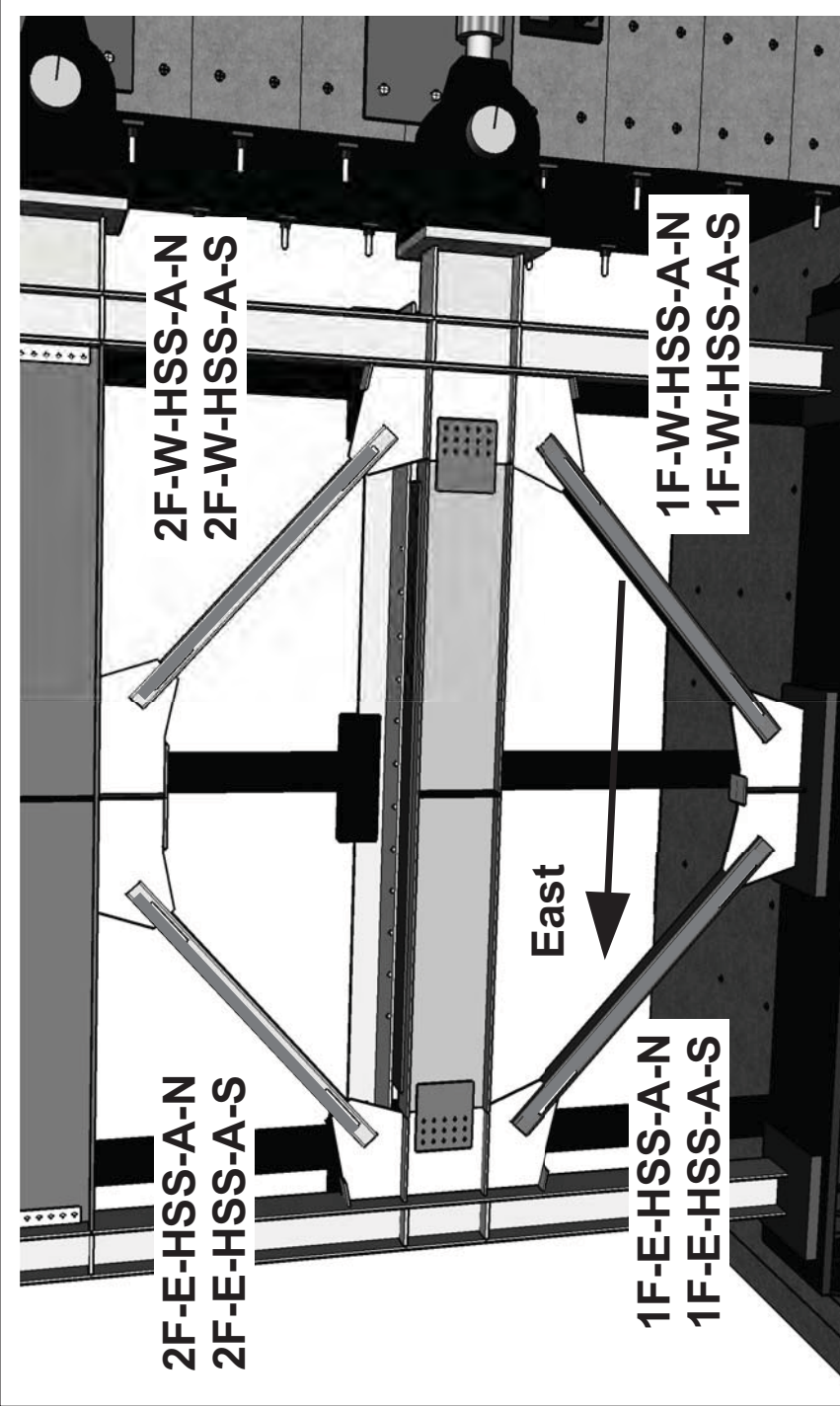
International Hybrid  
Simulation of  
Tomorrow's Braced  
Steel Frame  
Structures

University of California,  
Berkeley  
TCBF-B-4

PROJECT  
TCFB  
Mar 07,  
2011  
ISSUE  
DRAWN BY  
J.W. Lai  
TCBF-B-4  
PROJECT NO.

Sensor  
Locations

S.11



1F = first story; 2F = second story

E = east side; W = west side; A = axial direction

S = south side; N = north side

Square HSS brace axial deformation monitoring along the axis  
of brace (wire pot locations are shown in the figure)



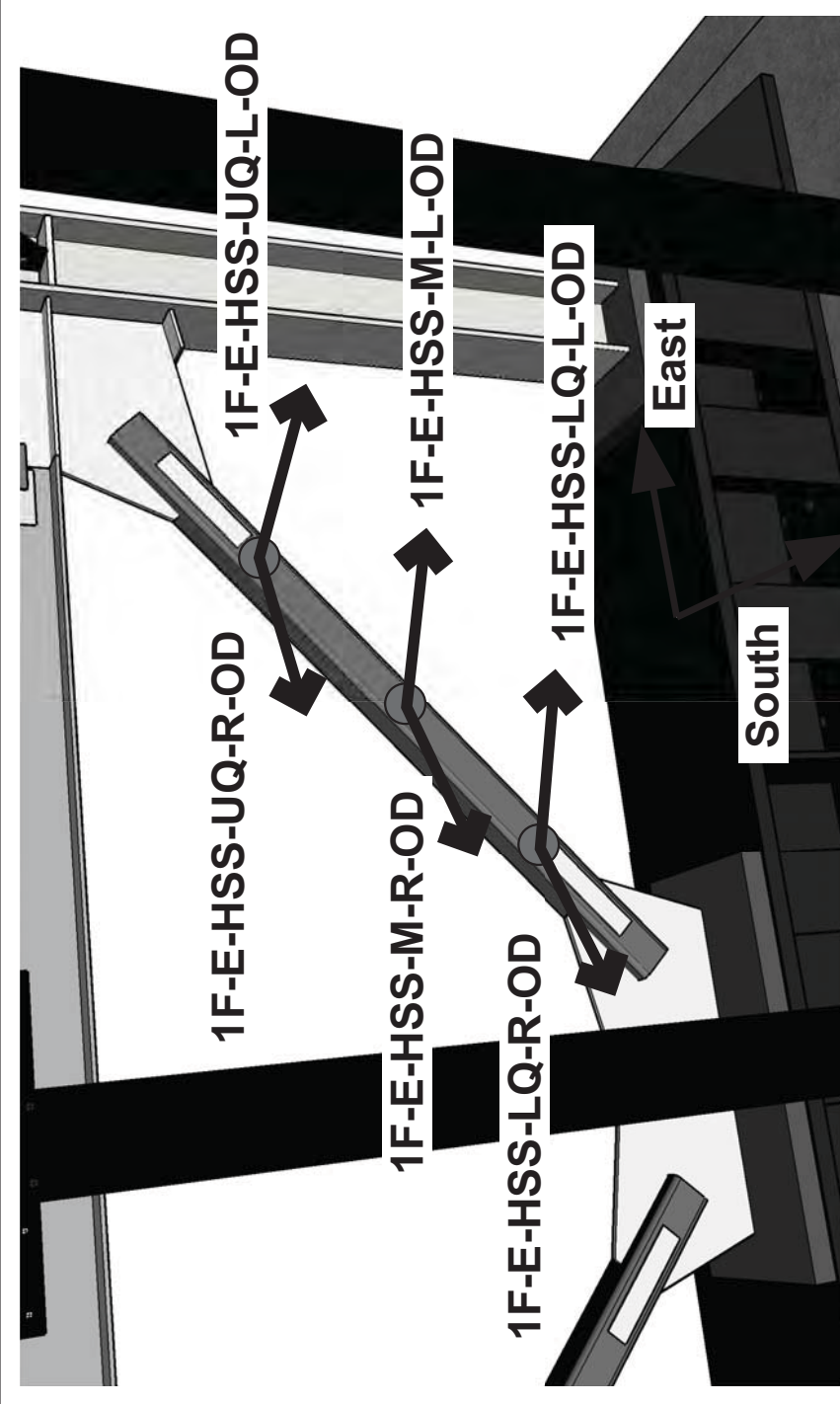
International Hybrid  
Simulation of  
Tomorrow's Braced  
Steel Frame  
Structures

University of California,  
Berkeley  
TCBF-B-4

PROJECT  
TCFB  
Mar 07, 2011  
ISSUE  
DRAWN BY  
J.W. Lai  
TCBF-B-4  
PROJECT NO.

Sensor  
Locations

S.12



Typical brace out-of-plane deformation monitoring (wire pot directions are shown in the figure for one brace, other braces are similar, six wire pots per brace)

1F-E-HSS-UQ-R-OD

- \_\_\_\_\_ lefthand (L) or righthand (R) side when facing to south
- \_\_\_\_\_ upper quarter (UQ), middle (M) or lower quarter point (LQ)
- \_\_\_\_\_ east side brace (E-HSS) or west side brace (W-HSS)
- \_\_\_\_\_ first story brace (1F) or second story brace (2F)



International Hybrid  
Simulation of  
Tomorrow's Braced  
Steel Frame  
Structures

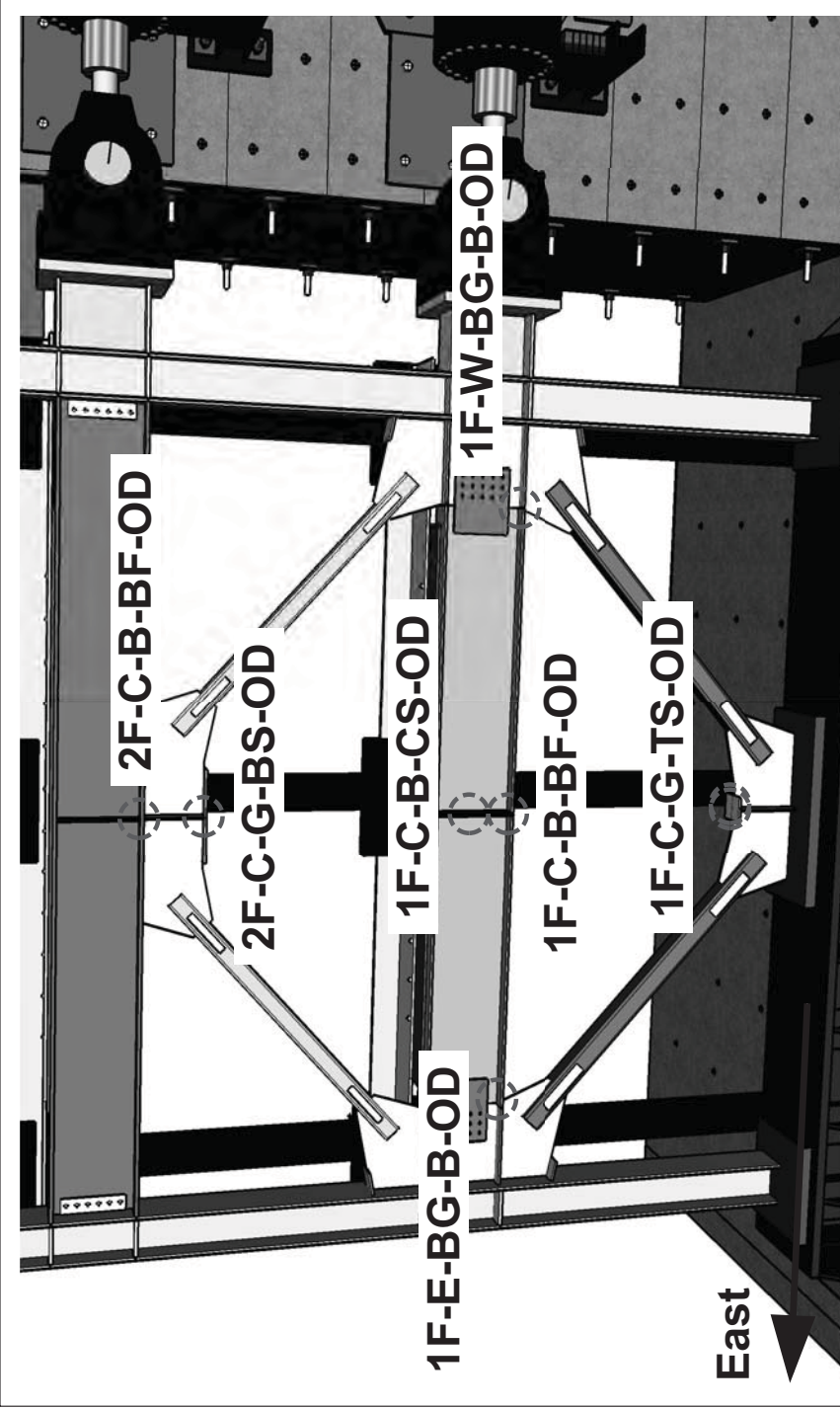
University of California,  
Berkeley  
TCBF-B-4

PROJECT  
TCFB  
Mar 07, 2011

ISSUE  
Mar 07, 2011  
DRAWN BY  
J.W. Lai

Sensor  
Locations

S-13



B = beam side corner; OD = out-of-plane deformation  
 C-B, C-G = beam or gusset center; BF = bottom flange  
 BS, CS, TS = bottom, center or top stiffener corner  
 BG = bottom gusset plate region  
 E = east side; W = west side; 1F, 2F = first or second story  
 (wire pot target locations are shown in the figure)



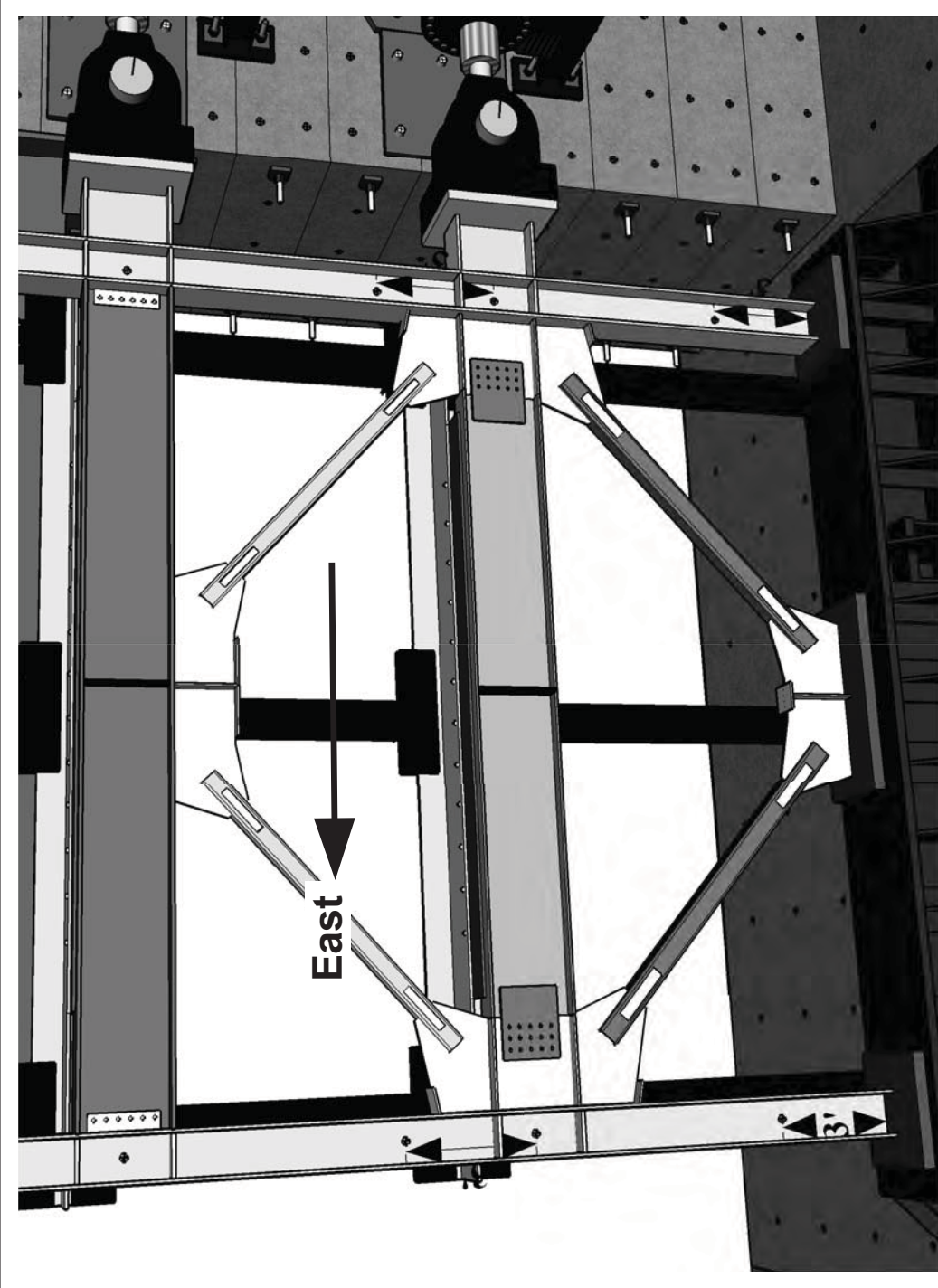
International Hybrid  
Simulation of  
Tomorrow's Braced  
Steel Frame  
Structures

University of California,  
Berkeley  
TCBF-B-4

PROJECT  
TCFB  
Mar 07,  
2011  
ISSUE  
DRAWN BY  
J.W. Lai  
PROJECT NO.  
TCBF-B-4

Sensor  
Locations

S.14



Overview of eight rosette locations on the specimen (only the column and panel zone regions). Details and label keys are shown in the next page.



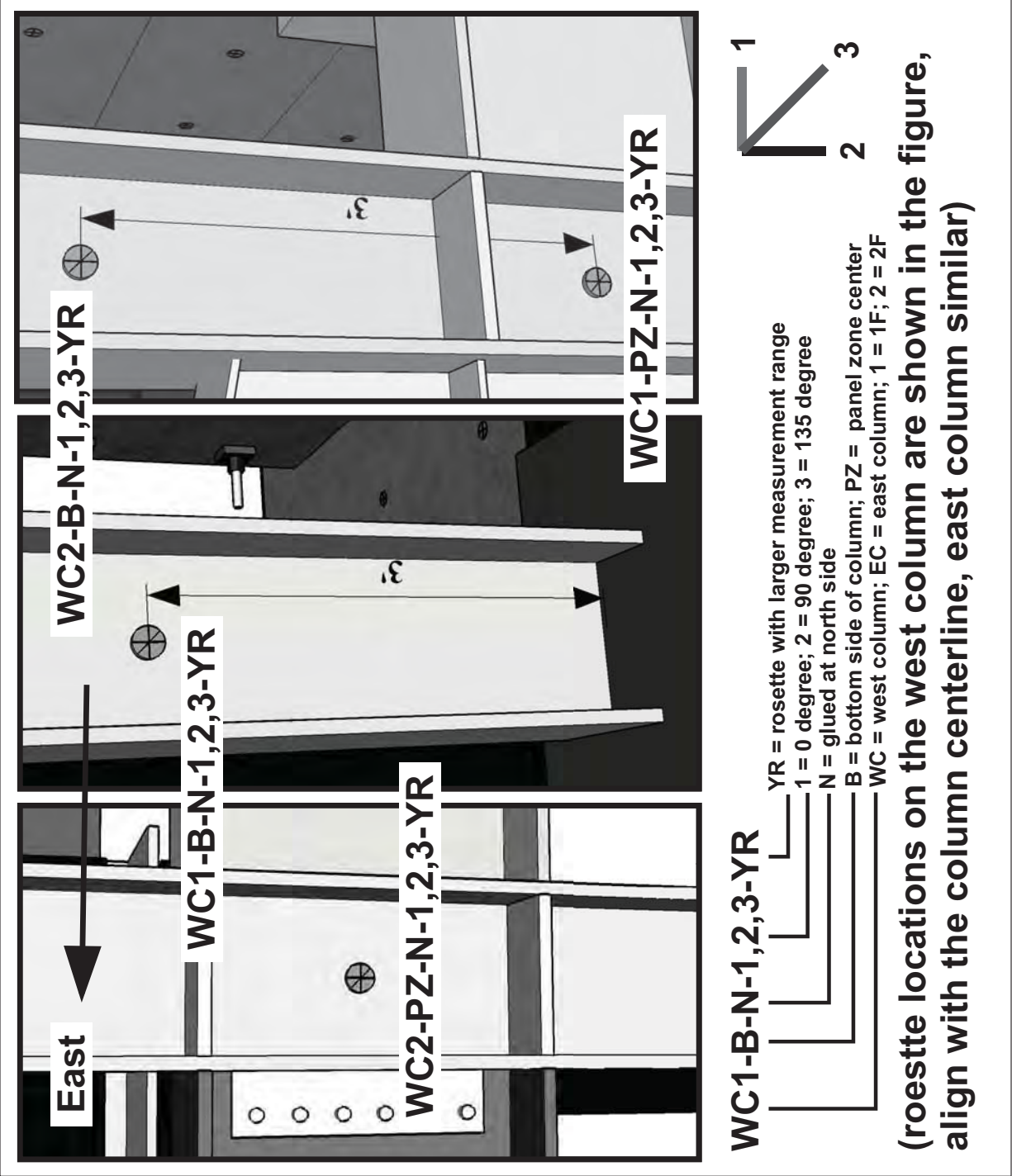
International Hybrid  
Simulation of  
Tomorrow's Braced  
Steel Frame  
Structures

University of California,  
Berkeley  
TCBF-B-4

PROJECT  
TCFB  
Mar 07, 2011  
DRAWN BY  
J.W. Lai  
TCBF-B-4  
PROJECT NO.

Sensor  
Locations

S-15







International Hybrid  
Simulation of  
Tomorrow's Braced  
Steel Frame  
Structures

University of California,  
Berkeley  
TCBF-B-4

PROJECT  
TCFB  
Mar 07, 2011  
ISSUE  
DRAWN BY  
J.W. Lai  
TCBF-B-4  
PROJECT NO.

Sensor  
Locations

S-16

**1F-E-TG-TL-1,2,3-N-YR**

**1F-E = east gusset plate**

**TG = top region**

**MG = middle region**

**BG = bottom region**

**TL = top left side**

**BL = bottom left side**

**TR = top right side**

**BR = bottom right side**

**TC = top center**

**BC = bottom center**

**1 = 0 degree (direction)**

**2 = 90 degree**

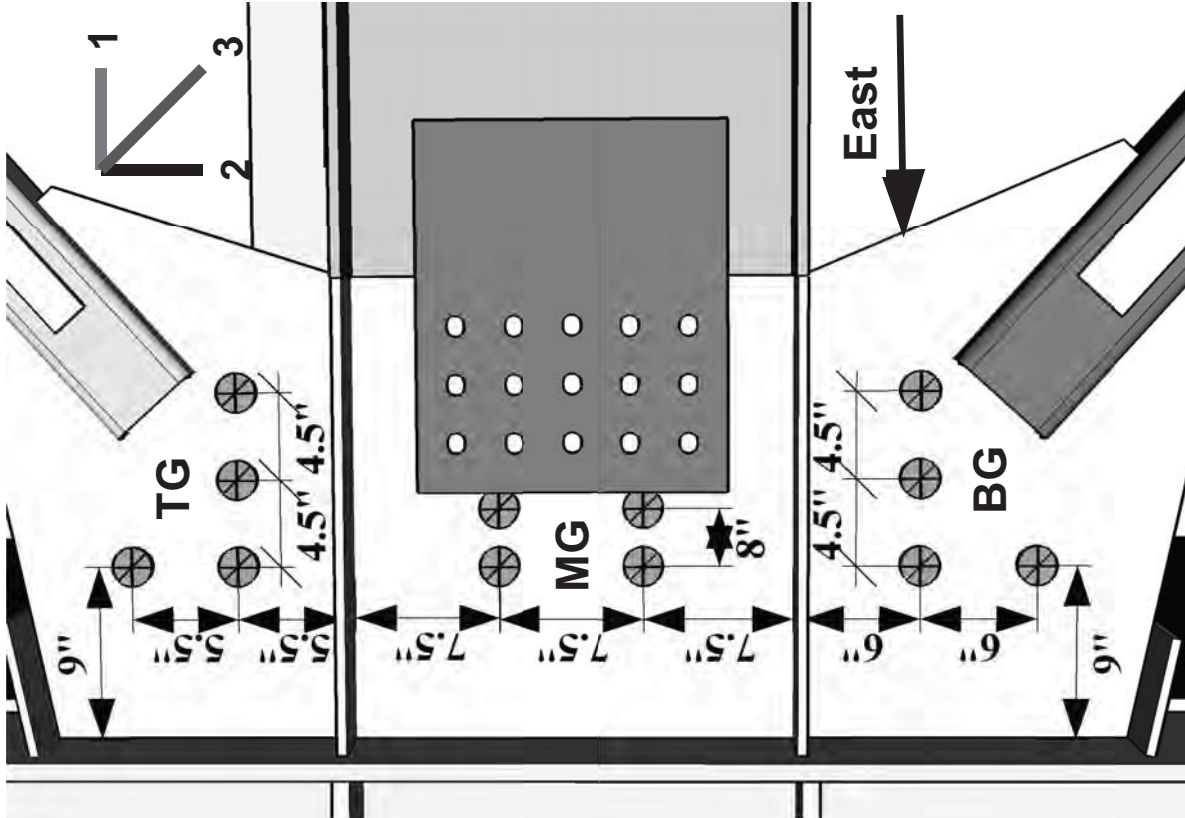
**3 = 135 degree**

**N = glued at north side**

**YR = rosette with larger**

**measurement range**

**(twelve rosette locations for the one-piece gusset plate, label keys are shown above)**





International Hybrid  
Simulation of  
Tomorrow's Braced  
Steel Frame  
Structures

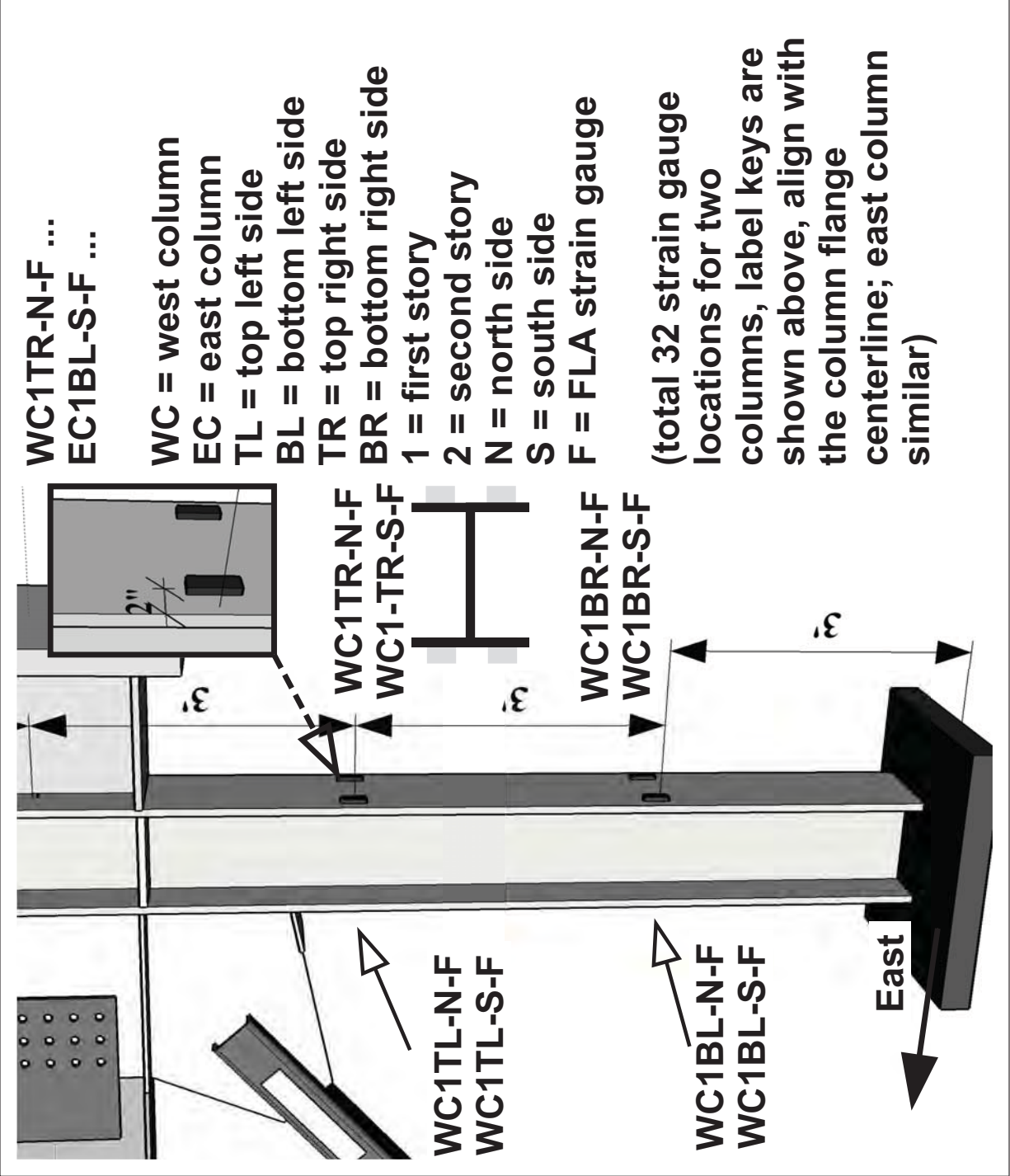
University of California,  
Berkeley  
TCBF-B-4

PROJECT  
TCFB  
Mar 07, 2011

ISSUE  
Mar 07, 2011  
DRAWN BY  
J.W. Lai

Sensor  
Locations

S-17





International Hybrid  
Simulation of  
Tomorrow's Braced  
Steel Frame  
Structures

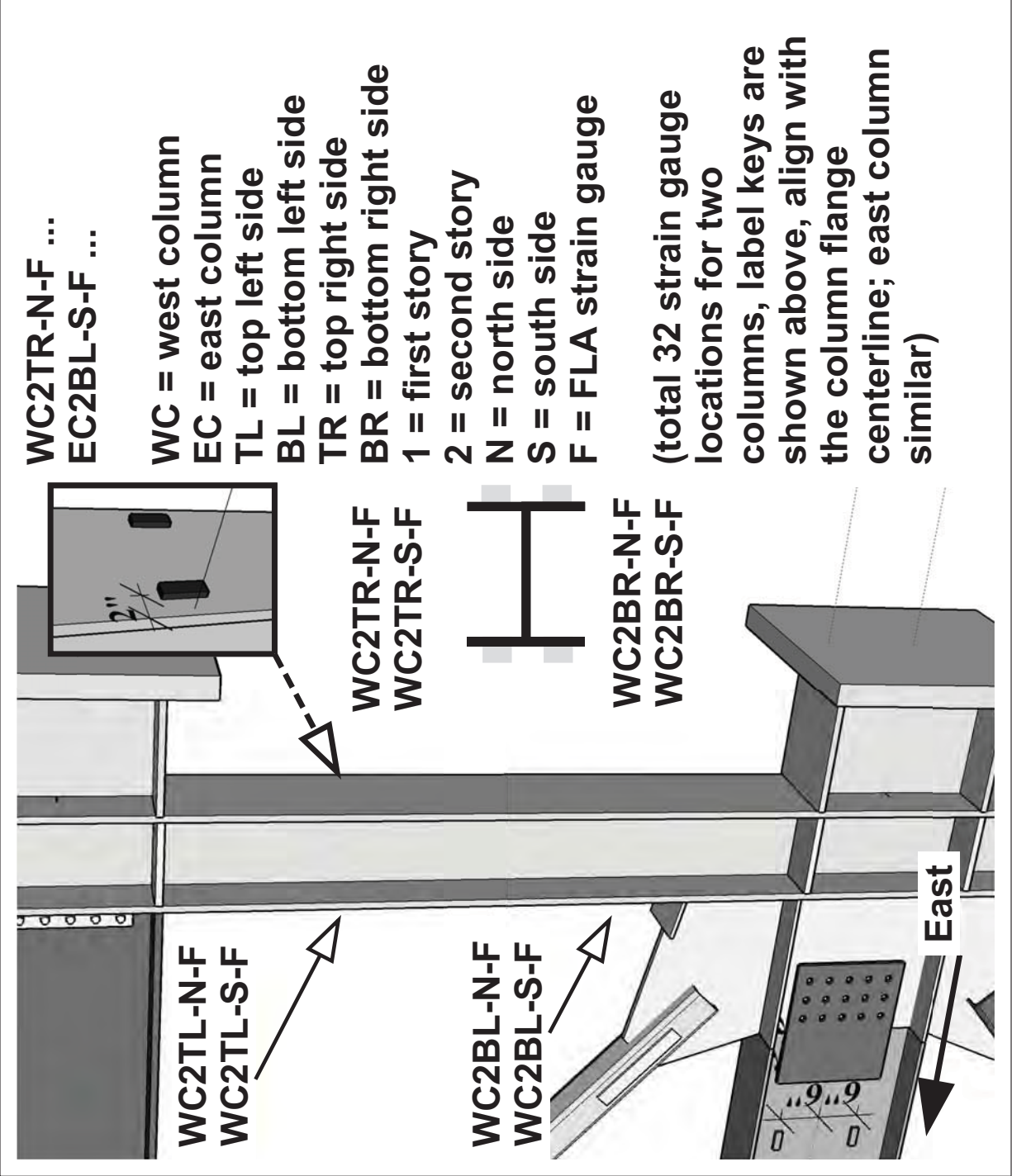
University of California,  
Berkeley  
TCBF-B-4

PROJECT  
TCFB  
Mar 07, 2011  
PROJECT NO.  
TCBF-B-4

ISSUE  
Mar 07, 2011  
DRAWN BY  
J.W. Lai

## Sensor Locations

**S-18**





International Hybrid  
Simulation of  
Tomorrow's Braced  
Steel Frame  
Structures

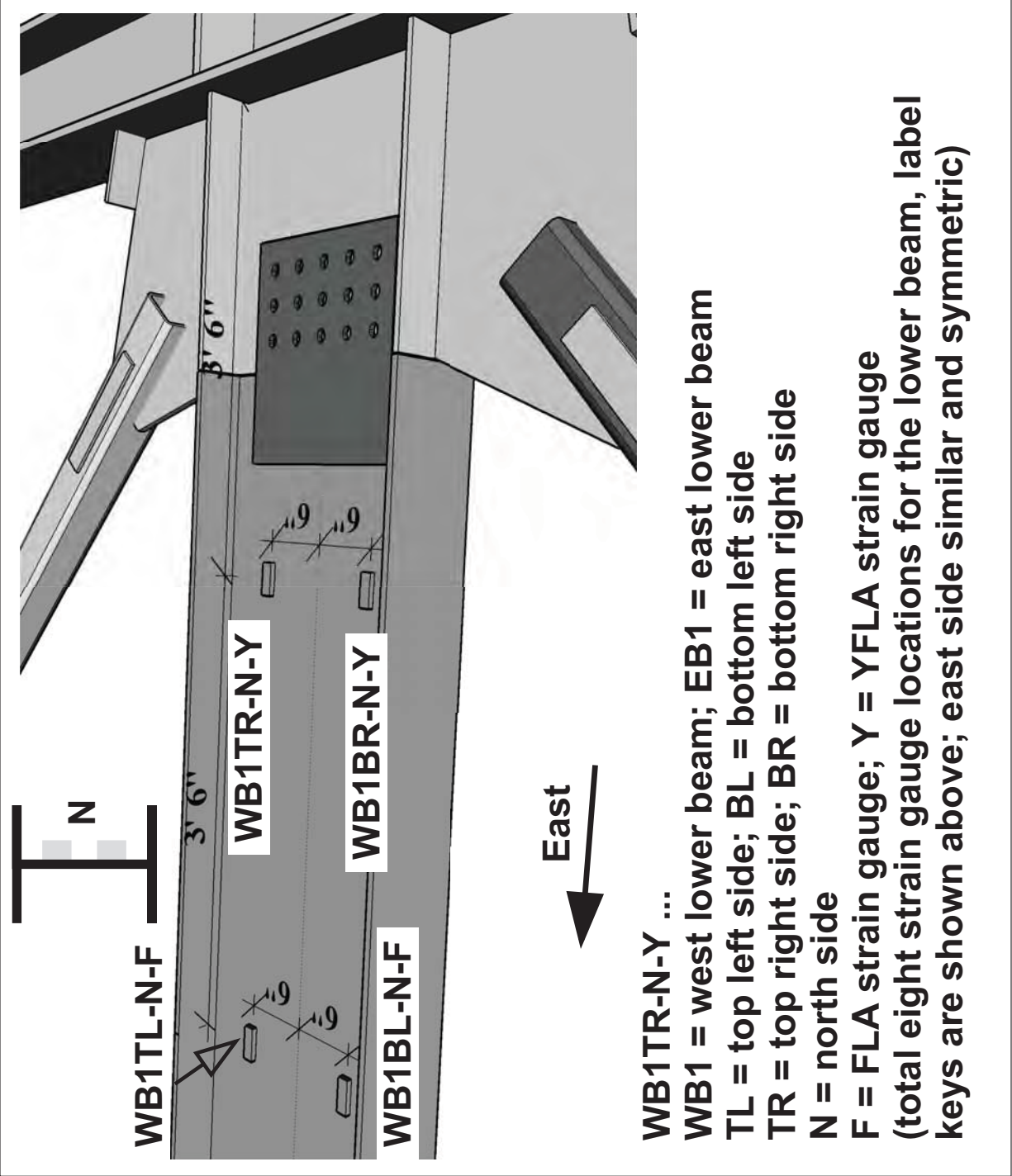
University of California,  
Berkeley  
TCBF-B-4

PROJECT  
TCFB  
Mar 07,  
2011

ISSUE  
Mar 07,  
2011  
DRAWN BY  
J.W. Lai

Sensor  
Locations

S-19





International Hybrid  
Simulation of  
Tomorrow's Braced  
Steel Frame  
Structures

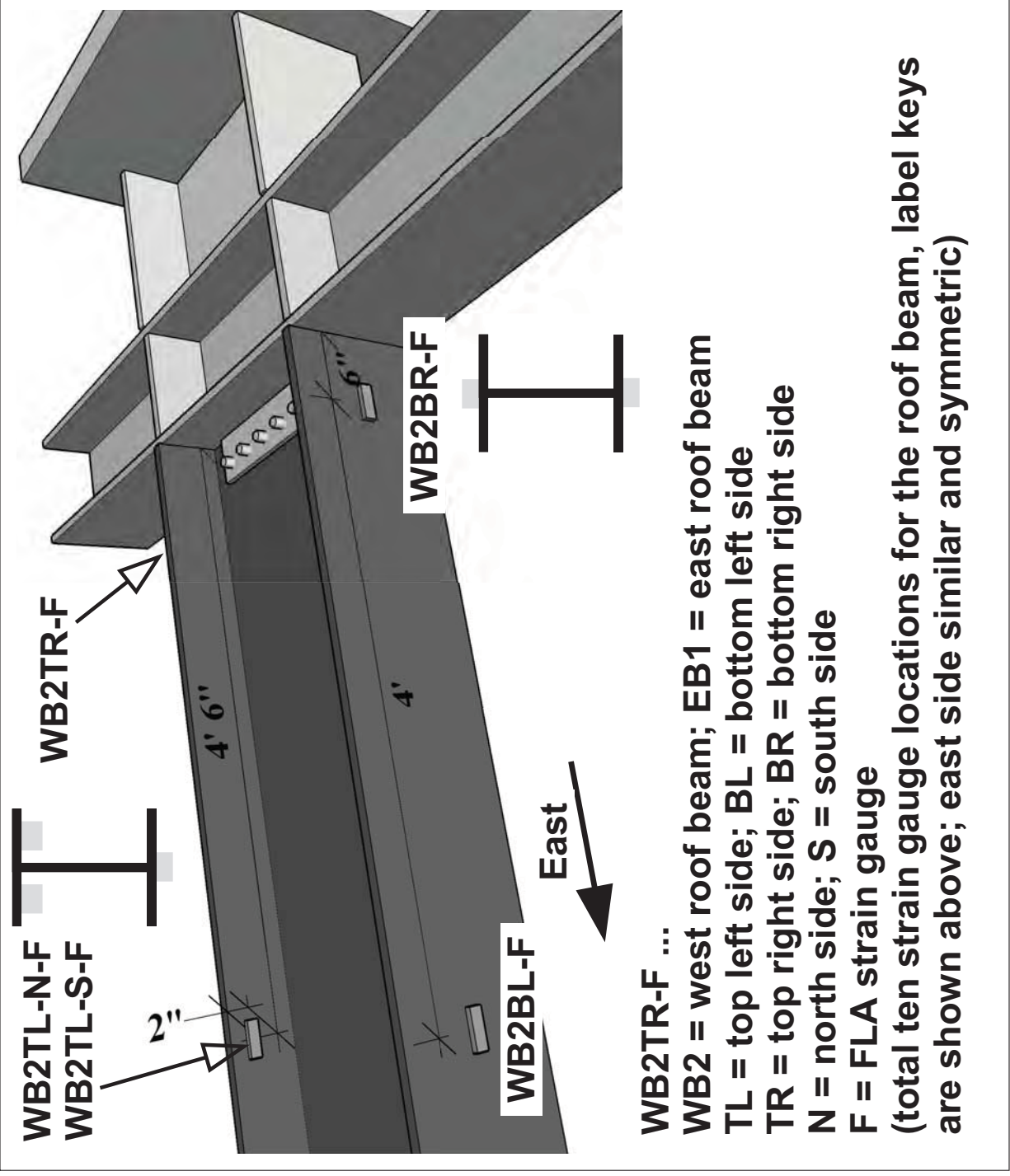
University of California,  
Berkeley  
TCBF-B-4

PROJECT  
TCFB  
Mar 07,  
2011

ISSUE  
Mar 07,  
2011  
DRAWN BY  
J.W. Lai

Sensor  
Locations

S-20





International Hybrid  
Simulation of  
Tomorrow's Braced  
Steel Frame  
Structures

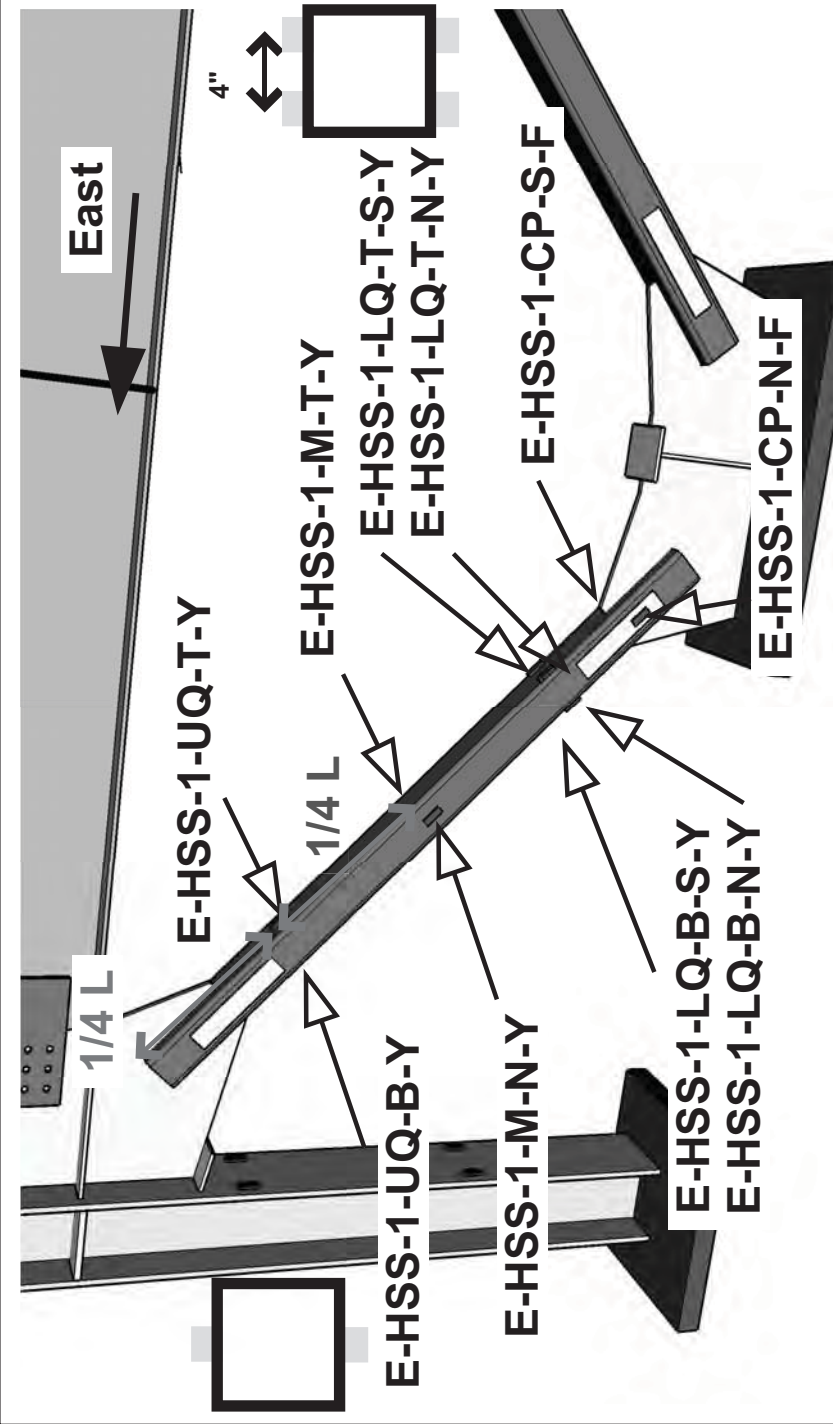
University of California,  
Berkeley  
TCBF-B-4

PROJECT  
TCFB  
Mar 07,  
2011

ISSUE  
Mar 07,  
2011  
DRAWN BY  
J.W. Lai

Sensor  
Locations

S.21



E-HSS = east HSS brace; W-HSS = west HSS brace; 1 = 1F  
 UQ = upper quarter point; LQ = lower quarter point; M = middle  
 T = top side; B = bottom side; CP = cover plate  
 N = north side; S = south side; L = length of HSS brace  
 F = FLA strain gauge; Y = YFLA strain gauge  
 (total ten strain gauge locations for each brace, label keys are  
 shown above; west side similar and symmetric)



International Hybrid  
Simulation of  
Tomorrow's Braced  
Steel Frame  
Structures

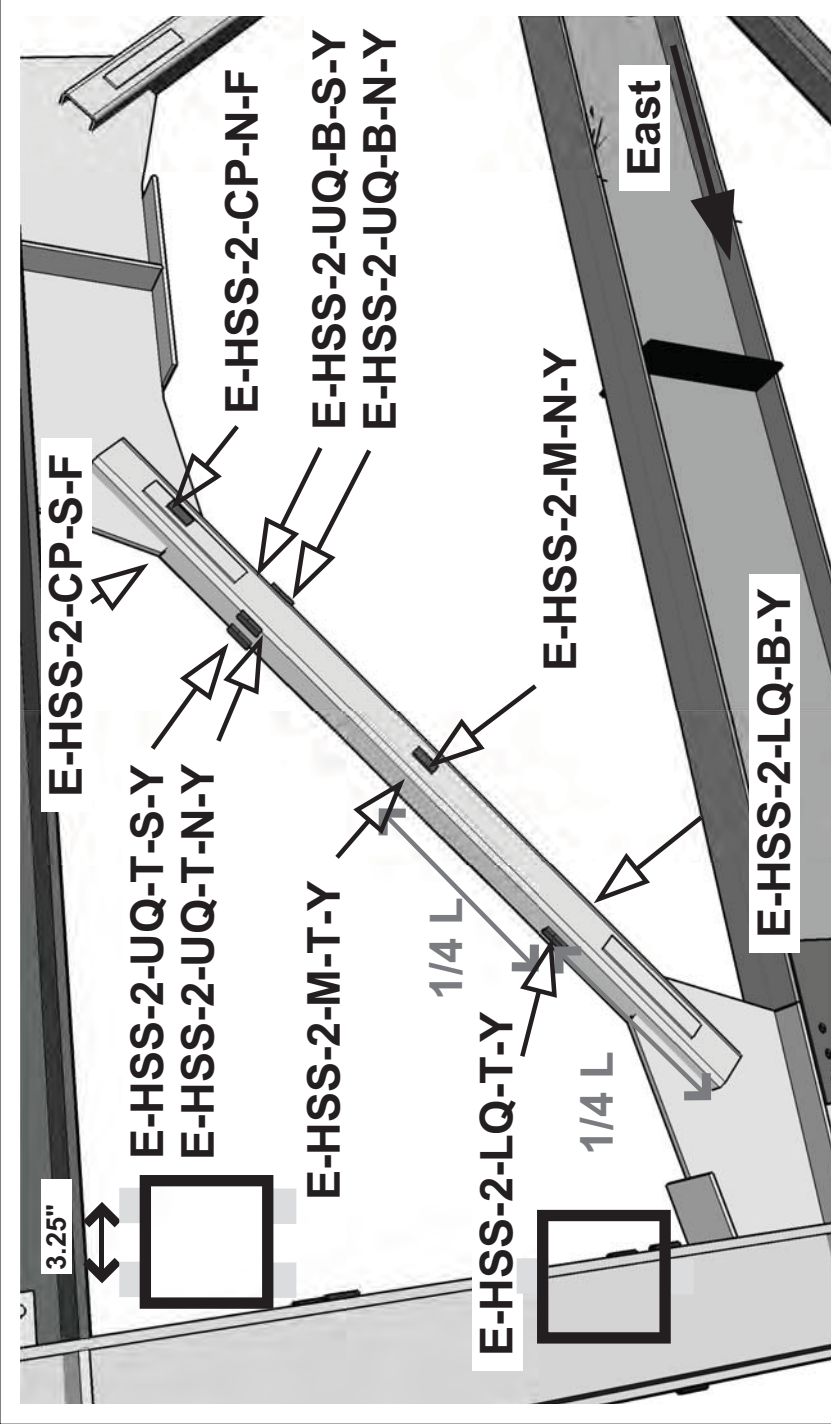
University of California,  
Berkeley  
TCBF-B-4

PROJECT  
TCFB  
Mar 07,  
2011

ISSUE  
Mar 07,  
2011  
DRAWN BY  
J.W. Lai

Sensor  
Locations

S.22



E-HSS = east HSS brace; W-HSS = west HSS brace; 2 = 2F  
 UQ = upper quarter point; LQ = lower quarter point; M = middle  
 T = top side; B = bottom side; CP = cover plate  
 N = north side; S = south side; L = length of HSS brace  
 F = FLA strain gauge; Y = YFLA strain gauge  
 (total ten strain gauge locations for each brace, label keys are  
 shown above; west side similar and symmetric)



International Hybrid  
Simulation of  
Tomorrow's Braced  
Steel Frame  
Structures

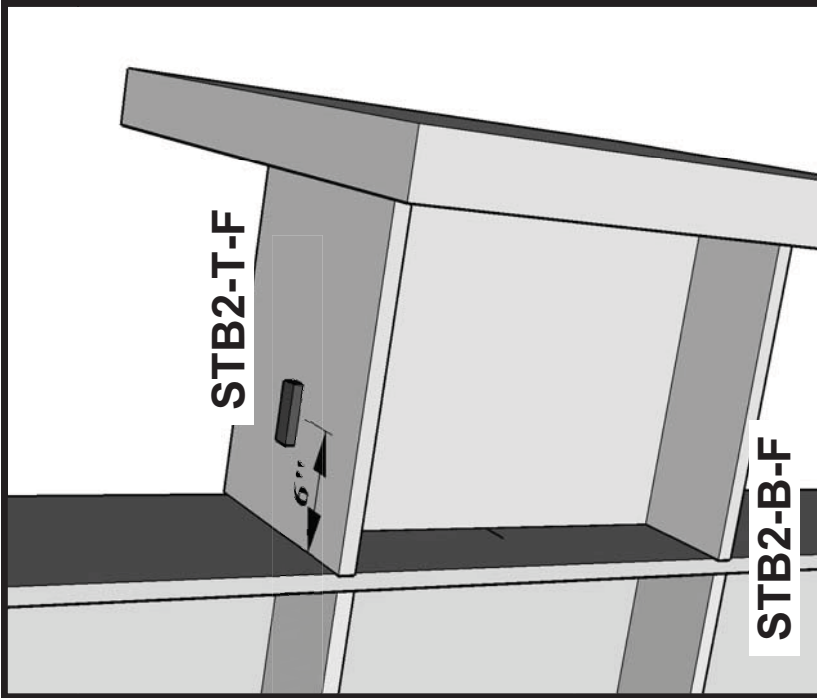
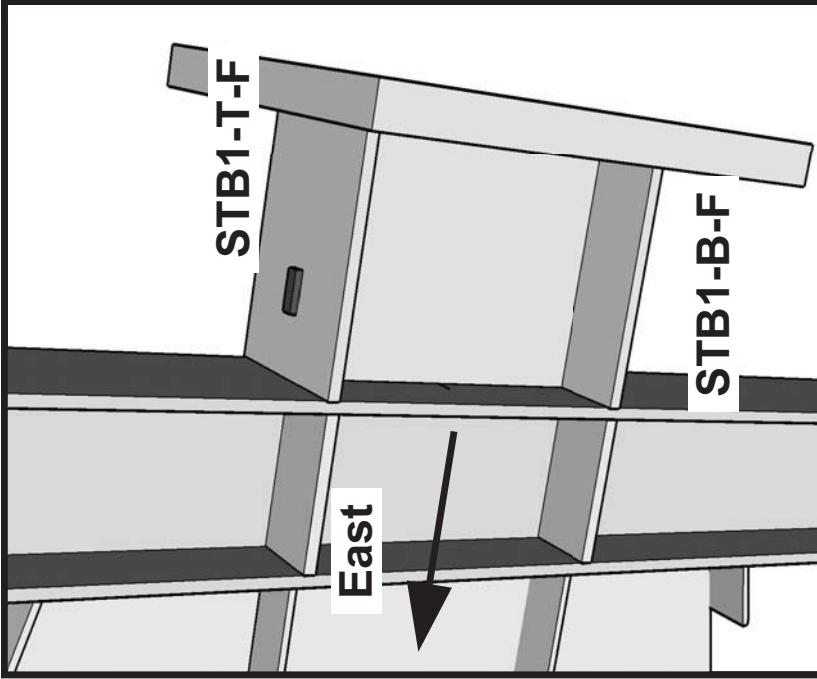
University of California,  
Berkeley  
TCBF-B-4

PROJECT  
TCFB  
PROJECT NO.  
TCBF-B-4

ISSUE  
Mar 07,  
2011  
DRAWN BY  
J.W. Lai

Sensor  
Locations

**S.23**



**STB = stub beam**

**1, 2 = first story or second story**

**T= top flange side; B = bottom flange side**

**F = FLA strain gauge**



**(two strain gauge locations for each stub beam at each floor level, align with flange centerline, label keys are shown above)**





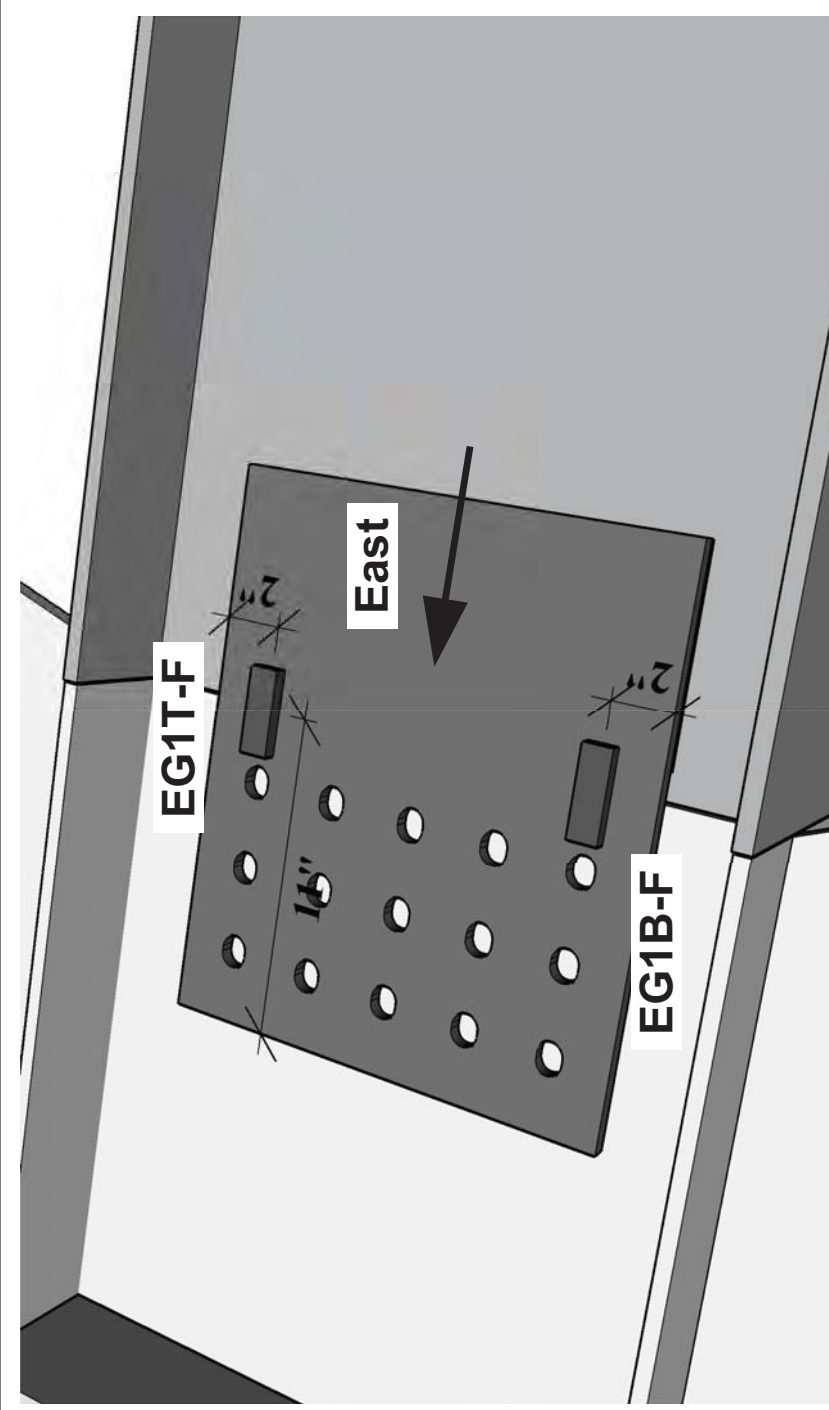
International Hybrid  
Simulation of  
Tomorrow's Braced  
Steel Frame  
Structures

University of California,  
Berkeley  
TCBF-B-4

PROJECT  
TCFB  
Mar 07,  
2011  
ISSUE  
DRAWN BY  
J.W. Lai  
PROJECT NO.  
TCBF-B-4

Sensor  
Locations

S.24



**EG1, WG1 = east or west side gusset splice**  
**T= top side; B = bottom side**  
**F = FLA strain gauge**

**(two strain gauge locations for each end of lower beam to gusset plate splice, align with the edge of lower beam, label keys are shown above, west end similar)**



International Hybrid  
Simulation of  
Tomorrow's Braced  
Steel Frame  
Structures

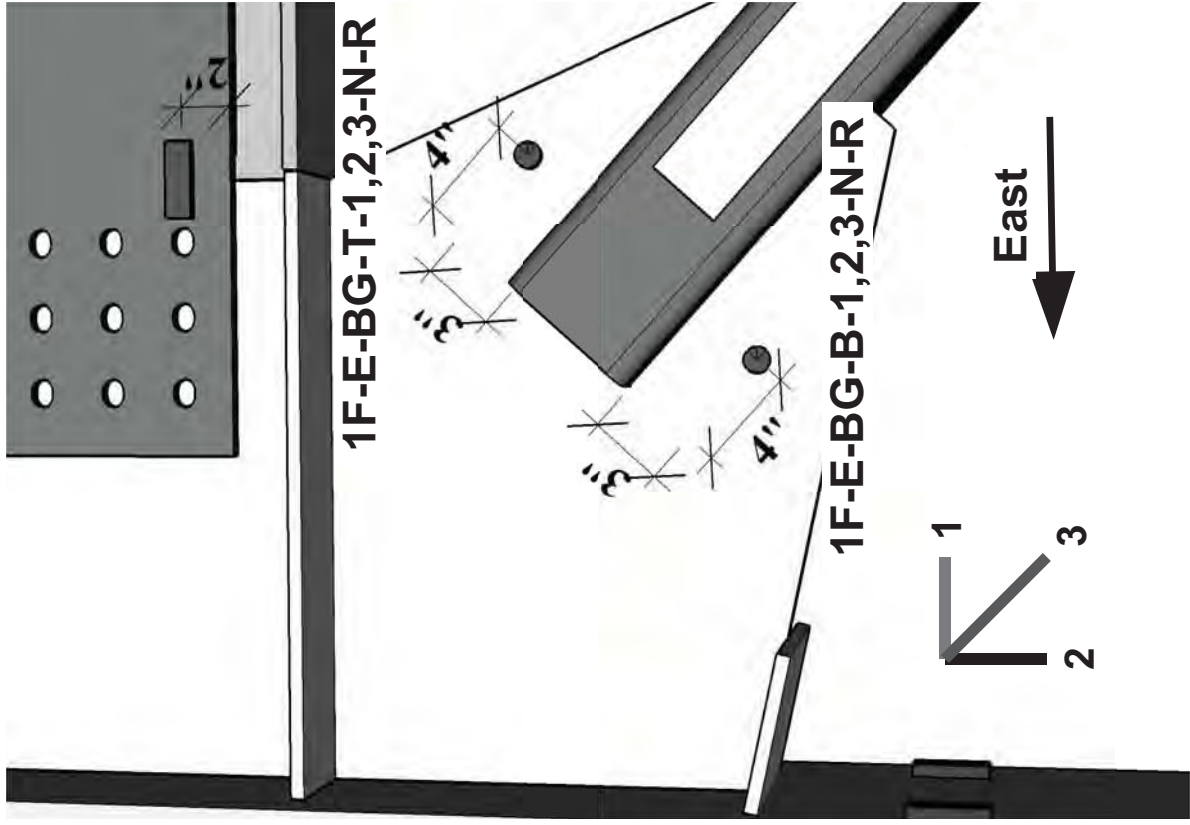
University of California,  
Berkeley  
TCBF-B-4

PROJECT  
TCFB  
Mar 07,  
2011  
ISSUE  
DRAWN BY  
J.W. Lai  
TCBF-B-4  
PROJECT NO.

Sensor  
Locations

S.25

**1F-E-BG-T-1,2,3-N-R**  
**1F-E** = east gusset plate  
**BG** = bottom region  
**T** = top side  
**B** = bottom side  
**1** = 0 degree (direction)  
**2** = 90 degree  
**3** = 135 degree  
**N** = glued at north side  
**R** = rosette with normal  
 measurement range  
 (two rosette locations  
 for this region, label  
 keys are shown above)



Channel	ID	Label	Device	Range	Serial No.	Cable No.	DAQ Box ID	Note	Column #
1	ST12	FB-Slip	stick	2"	2004NC01023	308	0:3:0	Novo 50 (recalibrated)	14
2	ST13	RRW-Slip-N	stick	2"	2009NC01016	309	0:3:1	Novo 50 (recalibrated)	15
3	ST14	RRW-Slip-S	stick	2"	2009NC01020	306	0:3:2	Novo 50 (recalibrated)	16
4	ST15	Act1-BK	stick	2"	2009NC01011	361	0:3:3	Novo 50 (recalibrated)	17
5	S5	E-HSS-1-UQ-T-F	strain gauge	-	-	5	0:1:0	1/4-Bridge	6
6	S6	E-HSS-1-UQ-B-F	strain gauge	-	-	6	0:1:1	1/4-Bridge	7
7	S7	E-HSS-1-M-N-Y	strain gauge	-	-	7	0:1:2	1/4-Bridge	8
8	S8	E-HSS-1-M-T-Y	strain gauge	-	-	8	0:1:3	1/4-Bridge	9
9	S9	E-HSS-1-LQ-T-N-F	strain gauge	-	-	9	0:2:0	1/4-Bridge	10
10	S10	E-HSS-1-LQ-T-S-F	strain gauge	-	-	10	0:2:1	1/4-Bridge	11
11	S11	E-HSS-1-LQ-B-N-F	strain gauge	-	-	11	0:2:2	1/4-Bridge	12
12	S12	E-HSS-1-LQ-B-S-F	strain gauge	-	-	12	0:2:3	1/4-Bridge	13
13	S13	E-HSS-1-CP-N-F	strain gauge	-	-	3	0:0:2	1/4-Bridge	4
14	S14	E-HSS-1-CP-S-F	strain gauge	-	-	4	0:0:3	1/4-Bridge	5
15	S15	EB1BL-N-Y	strain gauge	-	-	381	0:11:0	1/4-Bridge	46
16	S16	EB1TL-N-Y	strain gauge	-	-	380	0:10:3	1/4-Bridge	45
17	S17	EB1BR-N-F	strain gauge	-	-	204/70	1:1:1	1/4-Bridge	71
18	S18	EG1B-F	strain gauge	-	-	382	0:11:1	1/4-Bridge	47
19	S19	WB1BL-N-F	strain gauge	-	-	342/68	1:0:3	1/4-Bridge	69
20	S20	WG1B-F	strain gauge	-	-	322/69	1:1:0	1/4-Bridge	70
21	S21	WB1BR-N-Y	strain gauge	-	-	338/84	1:4:3	1/4-Bridge	85
22	S22	WB1TR-N-Y	strain gauge	-	-	325/57	0:14:0	1/4-Bridge	58
23	S23	W-HSS-1-CP-N-F	strain gauge	-	-	1	0:0:0	1/4-Bridge	2
24	S24	W-HSS-1-CP-S-F	strain gauge	-	-	2	0:0:1	1/4-Bridge	3
25	S25	W-HSS-1-LQ-T-N-F	strain gauge	-	-	25	0:6:0	1/4-Bridge	26
26	S26	W-HSS-1-LQ-T-S-F	strain gauge	-	-	26	0:6:1	1/4-Bridge	27
27	S27	W-HSS-1-LQ-B-N-F	strain gauge	-	-	27	0:6:2	1/4-Bridge	28
28	S28	W-HSS-1-LQ-B-S-F	strain gauge	-	-	28	0:6:3	1/4-Bridge	29
29	S29	W-HSS-1-M-N-Y	strain gauge	-	-	29	0:7:0	1/4-Bridge	30
30	S30	W-HSS-1-M-T-Y	strain gauge	-	-	30	0:7:1	1/4-Bridge	31
31	S31	W-HSS-1-UQ-T-F	strain gauge	-	-	31	0:7:2	Micro-Measurement	32
32	S32	W-HSS-1-UQ-B-F	strain gauge	-	-	32	0:7:3	Micro-Measurement	33
33	S33	WC1TL-S-F	strain gauge	-	-	95	1:7:2	1/4-Bridge	96
34	S34	WC1TR-S-F	strain gauge	-	-	93	1:7:0	1/4-Bridge	94
35	S35	WC1TL-N-F	strain gauge	-	-	94	1:7:1	1/4-Bridge	95
36	S36	WC1TR-N-F	strain gauge	-	-	92	1:6:3	1/4-Bridge	93

Channel	ID	Label	Device	Range	Serial No.	Cable No.	DAQ Box ID	Note	Column #
37	S37	EC2BL-S-F	strain gauge	-	-	390	0:9:2	1/4-Bridge	40
38	S38	EC2BR-S-F	strain gauge	-	-	391	0:9:3	1/4-Bridge	41
39	S39	EC2BL-N-F	strain gauge	-	-	376	0:10:0	1/4-Bridge	42
40	S40	EC2BR-N-F	strain gauge	-	-	377	0:10:1	1/4-Bridge	43
41	S41	EB2BL-F	strain gauge	-	-	378	0:10:2	1/4-Bridge	44
42	S42	EB2TL-F	strain gauge	-	-	200/348	2:4:3	1/4-Bridge	149
43	S43	EB2BR-F	strain gauge	-	-	197/145	2:4:0	1/4-Bridge	146
44	S44	EB2TR-S-F	strain gauge	-	-	199/147	2:4:2	1/4-Bridge	148
45	S45	E-HSS-2-LQ-T-F	strain gauge	-	-	48	0:11:3	1/4-Bridge	49
46	S46	E-HSS-2-LQ-B-F	strain gauge	-	-	392	0:12:0	1/4-Bridge	50
47	S47	E-HSS-2-M-N-Y	strain gauge	-	-	362	0:12:1	1/4-Bridge	51
48	S48	EB1TR-N-F	strain gauge	-	-	365	0:12:2	1/4-Bridge	52
49	S49	E-HSS-2-UQ-T-N-F	strain gauge	-	-	366	0:12:3	1/4-Bridge	53
50	S50	E-HSS-2-UQ-T-S-F	strain gauge	-	-	367	0:13:0	1/4-Bridge	54
51	S51	E-HSS-2-UQ-B-N-F	strain gauge	-	-	368	0:13:1	1/4-Bridge	55
52	S52	E-HSS-2-UQ-B-S-F	strain gauge	-	-	369	0:13:2	1/4-Bridge	56
53	S53	E-HSS-2-CP-N-F	strain gauge	-	-	370	0:13:3	1/4-Bridge	57
54	S54	E-HSS-2-CP-S-F	strain gauge	-	-	383	0:11:2	1/4-Bridge	48
55	S55	W-HSS-2-CP-N-F	strain gauge	-	-	324/58	0:14:1	1/4-Bridge	59
56	S56	W-HSS-2-CP-S-F	strain gauge	-	-	326/59	0:14:2	1/4-Bridge	60
57	S57	W-HSS-2-UQ-T-N-F	strain gauge	-	-	333/60	0:14:3	1/4-Bridge	61
58	S58	W-HSS-2-UQ-T-S-F	strain gauge	-	-	327/61	0:15:0	1/4-Bridge	62
59	S59	W-HSS-2-UQ-B-N-F	strain gauge	-	-	320/62	0:15:1	1/4-Bridge	63
60	S60	W-HSS-2-UQ-B-S-F	strain gauge	-	-	321/63	0:15:2	1/4-Bridge	64
61	S61	W-HSS-2-M-N-Y	strain gauge	-	-	322/64	0:15:3	1/4-Bridge	65
62	S62	WB1TL-N-F	strain gauge	-	-	203/65	1:0:0	1/4-Bridge	66
63	S63	W-HSS-2-LQ-T-F	strain gauge	-	-	315/66	1:0:1	1/4-Bridge	67
64	S64	W-HSS-2-LQ-B-F	strain gauge	-	-	343/67	1:0:2	1/4-Bridge	68
65	S65	WB2BL-F	strain gauge	-	-	346/137	2:2:0	1/4-Bridge	138
66	S66	WB2TL-S-F	strain gauge	-	-	328/138	2:2:1	1/4-Bridge	139
67	S67	WB2BR-F	strain gauge	-	-	201/71	1:1:2	1/4-Bridge	72
68	S68	WB2TR-F	strain gauge	-	-	345/140	2:2:3	1/4-Bridge	141
69	S69	WC2BL-N-F	strain gauge	-	-	316/73	1:2:0	1/4-Bridge	74
70	S70	WC2BR-N-F	strain gauge	-	-	349/74	1:2:1	1/4-Bridge	75
71	S71	WC2BL-S-F	strain gauge	-	-	351/75	1:2:2	1/4-Bridge	76
72	S72	WC2BR-S-F	strain gauge	-	-	318/76	1:2:3	1/4-Bridge	77

Channel	ID	Label	Device	Range	Serial No.	Cable No.	DAQ Box ID	Note	Column #
73	ST16	Act2-BK	stick	2"	2009NC01019	355	0:4:0	Novo 50 (recalibrated)	18
74	ST1	E-CB-Slip	stick	1"	2004NC01014	379	0:4:1	Novo 25 (recalibrated)	19
75	R73	STB2-T-F	strain gauge	-	-	396	0:4:2	1/4-Bridge	20
76	R2-1	EC1-PZ-N-1-YR	rosette	-	-	384	0:8:0	1/4-Bridge	34
77	R2-2	EC1-PZ-N-2-YR	rosette	-	-	385	0:8:1	1/4-Bridge	35
78	R2-3	EC1-PZ-N-3-YR	rosette	-	-	386	0:8:2	1/4-Bridge	36
79	R3-1	EC2-B-N-1-YR	rosette	-	-	387	0:8:3	1/4-Bridge	37
80	R3-2	EC2-B-N-2-YR	rosette	-	-	388	0:9:0	1/4-Bridge	38
81	R3-3	EC2-B-N-3-YR	rosette	-	-	389	0:9:1	1/4-Bridge	39
82	R4-1	EC2-PZ-N-1-YR	rosette	-	-	196/149	2:5:0	1/4-Bridge	150
83	R4-2	EC2-PZ-N-2-YR	rosette	-	-	198/150	2:5:1	1/4-Bridge	151
84	R4-3	EC2-PZ-N-3-YR	rosette	-	-	195/151	2:5:2	1/4-Bridge	152
85	R5-1	WC1-B-N-1-YR	rosette	-	-	89	1:6:0	1/4-Bridge	90
86	R5-2	WC1-B-N-2-YR	rosette	-	-	90	1:6:1	1/4-Bridge	91
87	R5-3	WC1-B-N-3-YR	rosette	-	-	91	1:6:2	1/4-Bridge	92
88	R6-1	WC1-PZ-N-1-YR	rosette	-	-	317/77	1:3:0	1/4-Bridge	78
89	R6-2	WC1-PZ-N-2-YR	rosette	-	-	350/78	1:3:1	1/4-Bridge	79
90	R6-3	WC1-PZ-N-3-YR	rosette	-	-	302/79	1:3:2	1/4-Bridge	80
91	R7-1	WC2-B-N-1-YR	rosette	-	-	301/80	1:3:3	1/4-Bridge	81
92	R7-2	WC2-B-N-2-YR	rosette	-	-	323/81	1:4:0	1/4-Bridge	82
93	R7-3	WC2-B-N-3-YR	rosette	-	-	336/82	1:4:1	1/4-Bridge	83
94	R8-1	WC2-PZ-N-1-YR	rosette	-	-	352/141	2:3:0	1/4-Bridge	142
95	R8-2	WC2-PZ-N-2-YR	rosette	-	-	319/142	2:3:1	1/4-Bridge	143
96	R8-3	WC2-PZ-N-3-YR	rosette	-	-	329/143	2:3:2	1/4-Bridge	144
97	R9-1	IF-E-BG-TL-1-N-YR	rosette	-	-	101	1:9:0	1/4-Bridge	102
98	R9-2	IF-E-BG-TL-2-N-YR	rosette	-	-	102	1:9:1	1/4-Bridge	103
99	R9-3	IF-E-BG-TL-3-N-YR	rosette	-	-	103	1:9:2	1/4-Bridge	104
100	R10-1	IF-E-BG-BL-1-N-YR	rosette	-	-	104	1:9:3	1/4-Bridge	105
101	R10-2	IF-E-BG-BL-2-N-YR	rosette	-	-	105	1:10:0	1/4-Bridge	106
102	R10-3	IF-E-BG-BL-3-N-YR	rosette	-	-	106	1:10:1	1/4-Bridge	107
103	R11-1	IF-E-BG-TR-1-N-YR	rosette	-	-	107	1:10:2	1/4-Bridge	108
104	R11-2	IF-E-BG-TR-2-N-YR	rosette	-	-	108	1:10:3	1/4-Bridge	109
105	R11-3	IF-E-BG-TR-3-N-YR	rosette	-	-	109	1:11:0	1/4-Bridge	110
106	R12-1	IF-E-BG-TC-1-N-YR	rosette	-	-	110	1:11:1	1/4-Bridge	111
107	R12-2	IF-E-BG-TC-2-N-YR	rosette	-	-	111	1:11:2	1/4-Bridge	112
108	R12-3	IF-E-BG-TC-3-N-YR	rosette	-	-	112	1:11:3	1/4-Bridge	113

Channel	ID	Label	Device	Range	Serial No.	Cable No.	DAQ Box ID	Note	Column #
109	R13-1	IF-E-MG-TL-1-N-YR	rosette	-	-	113	1:12:0	1/4-Bridge	114
110	R13-2	IF-E-MG-TL-2-N-YR	rosette	-	-	114	1:12:1	1/4-Bridge	115
111	R13-3	IF-E-MG-TL-3-N-YR	rosette	-	-	115	1:12:2	1/4-Bridge	116
112	R14-1	IF-E-MG-BL-1-N-YR	rosette	-	-	116	1:12:3	1/4-Bridge	117
113	R14-2	IF-E-MG-BL-2-N-YR	rosette	-	-	117	1:13:0	1/4-Bridge	118
114	R14-3	IF-E-MG-BL-3-N-YR	rosette	-	-	118	1:13:1	1/4-Bridge	119
115	R15-1	IF-E-MG-TR-1-N-YR	rosette	-	-	119	1:13:2	1/4-Bridge	120
116	R15-2	IF-E-MG-TR-2-N-YR	rosette	-	-	120	1:13:3	1/4-Bridge	121
117	R15-3	IF-E-MG-TR-3-N-YR	rosette	-	-	121	1:14:0	1/4-Bridge	122
118	R16-1	IF-E-MG-BR-1-N-YR	rosette	-	-	122	1:14:1	1/4-Bridge	123
119	R16-2	IF-E-MG-BR-2-N-YR	rosette	-	-	123	1:14:2	1/4-Bridge	124
120	R16-3	IF-E-MG-BR-3-N-YR	rosette	-	-	124	1:14:3	1/4-Bridge	125
121	R17-1	IF-E-TG-TL-1-N-YR	rosette	-	-	125	1:15:0	1/4-Bridge	126
122	R17-2	IF-E-TG-TL-2-N-YR	rosette	-	-	126	1:15:1	1/4-Bridge	127
123	R17-3	IF-E-TG-TL-3-N-YR	rosette	-	-	127	1:15:2	1/4-Bridge	128
124	R18-1	IF-E-TG-BL-1-N-YR	rosette	-	-	128	1:15:3	1/4-Bridge	129
125	R18-2	IF-E-TG-BL-2-N-YR	rosette	-	-	129	2:0:0	1/4-Bridge	130
126	R18-3	IF-E-TG-BL-3-N-YR	rosette	-	-	130	2:0:1	1/4-Bridge	131
127	R19-1	IF-E-TG-BC-1-N-YR	rosette	-	-	131	2:0:2	1/4-Bridge	132
128	R19-2	IF-E-TG-BC-2-N-YR	rosette	-	-	303	2:0:3	1/4-Bridge	133
129	R19-3	IF-E-TG-BC-3-N-YR	rosette	-	-	133	2:1:0	1/4-Bridge	134
130	R20-1	IF-E-TG-BR-1-N-YR	rosette	-	-	134	2:1:1	1/4-Bridge	135
131	R20-2	IF-E-TG-BR-2-N-YR	rosette	-	-	135	2:1:2	1/4-Bridge	136
132	R20-3	IF-E-TG-BR-3-N-YR	rosette	-	-	136	2:1:3	1/4-Bridge	137
133	WP07	IF-E-HSS-UQ-R-OD	wire pot	30"	2000NC51151	159	2:7:2	-	160
134	WP04	IF-E-HSS-M-R-OD	wire pot	40"	2005NC51006	156	2:6:3	-	157
135	WP02	IF-E-HSS-LQ-R-OD	wire pot	30"	2006NC51015	154	2:6:1	-	155
136	WP03	IF-E-HSS-UQ-L-OD	wire pot	30"	2006NC51012	155	2:6:2	-	156
137	WP05	IF-E-HSS-M-L-OD	wire pot	40"	2005NC01003	157	2:7:0	-	158
138	WP01	IF-E-HSS-LQ-L-OD	wire pot	30"	2006NC51014	153	2:6:0	-	154
139	WP06	IF-W-HSS-LQ-R-OD	wire pot	30"	2000NC51124	158	2:7:1	-	159
140	WP12	IF-W-HSS-M-R-OD	wire pot	40"	2005NC01008	164	2:8:3	-	165
141	WP09	IF-W-HSS-UQ-R-OD	wire pot	30"	2000NC51106	161	2:8:0	-	162
142	WP08	IF-W-HSS-LQ-L-OD	wire pot	30"	2006NC51016	160	2:7:3	-	161
143	WP11	IF-W-HSS-M-L-OD	wire pot	40"	2005NC01006	163	2:8:2	-	164
144	WP10	IF-W-HSS-UQ-L-OD	wire pot	40"	2005NC51005	162	2:8:1	(recalibrated)	163

Channel	ID	Label	Device	Range	Serial No.	Cable No.	DAQ Box ID	Note	Column #
145	WP14	2F-E-HSS-LQ-R-OD	wire pot	30"	2006NC51013	166/305	2:9:1	-	167
146	WP17	2F-E-HSS-M-R-OD	wire pot	40"	2005NC51002	169/308	2:10:0	-	170
147	WP13	2F-E-HSS-UQ-R-OD	wire pot	40"	2009NC01052	342	2:9:0	165/304 old cables N.G.	166
148	WP16	2F-E-HSS-LQ-L-OD	wire pot	30"	2000NC51125	168/307	2:9:3	-	169
149	WP18	2F-E-HSS-M-L-OD	wire pot	40"	2005NC51007	170/309	2:10:1	-	171
150	WP15	2F-E-HSS-UQ-L-OD	wire pot	30"	2000NC51105	167/306	2:9:2	-	168
151	WP22	2F-W-HSS-UQ-R-OD	wire pot	40"	2005NC01010	174/313	2:11:1	-	175
152	WP20	2F-W-HSS-M-R-OD	wire pot	40"	2005NC01009	172/311	2:10:3	-	173
153	WP24	2F-W-HSS-LQ-R-OD	wire pot	30"	2000NC51153	176/315	2:11:3	-	177
154	WP21	2F-W-HSS-UQ-L-OD	wire pot	40"	2005NC51010	173/312	2:11:0	-	174
155	WP19	2F-W-HSS-M-L-OD	wire pot	40"	2005NC01007	394	2:10:2	394 (171, 310 N.G.)	172
156	WP23	2F-W-HSS-LQ-L-OD	wire pot	30"	2000NC51111	175/314	2:11:2	-	176
157	WP25	1F-E-HSS-A-N	wire pot	40"	2005NC51009	177	2:12:0	-	178
158	WP26	1F-W-HSS-A-N	wire pot	40"	2005NC01004	178	2:12:1	-	179
159	WP27	2F-E-HSS-A-N	wire pot	40"	2005NC01001	300	2:14:0	-	183
160	WP28	2F-W-HSS-A-N	wire pot	40"	2000NC51131	399	2:14:1	(checked, not recalibrated)	184
161	-	not use	-	-	-	-	2:13:0	not use	-
162	-	not use	-	-	-	-	2:13:1	not use	-
163	-	not use	-	-	-	-	2:13:3	not use	-
164	ST17	WB1-RT	stick	4"	2009NC01008	307	2:13:2	Novo100 (recalibrated)	182
165	ST18	EB1-RT	stick	4"	2009NC01009	183	1:8:0	Novo100 (recalibrated)	98
166	ST19	EB1-RB	stick	4"	2009NC01001	184	1:8:1	Novo100 (recalibrated)	99
167	ST20	RRW-T-N	stick	4"	2004NC01037	318/86	1:8:2	Novo100 (recalibrated)	100
168	ST21	RRW-T-S	stick	4"	2004NC01038	319/395	1:8:3	Novo100 (recalibrated)	101
169	WP30	1F-C-G-TS-OD	wire pot	40"	2005NC01005	21	0:5:0	-	22
170	WP47	2F-W-HSS-A-S	wire pot	30"	2000NC51150	313	1:5:3	-	89
171	WP33	1F-E-HSS-A-S	wire pot	40"	2009NC01054	24	0:5:3	(recalibrated)	25
172	WP29	1F-W-HSS-A-S	wire pot	40"	2009NC01053	20	0:4:3	(recalibrated)	21
173	WP43	1F-E-BG-B-OD	wire pot	30"	2000NC51098	320	1:4:2	-	84
174	WP31	1F-C-B-BF-OD	wire pot	30"	2000NC51128	22	0:5:1	-	23
175	WP32	1F-C-B-CS-OD	wire pot	40"	2005NC51003	23	0:5:2	(recalibrated)	24
176	WP42	1F-W-BG-B-OD	wire pot	30"	2000NC51117	314	1:1:3	-	73
177	WP46	2F-E-HSS-A-S	wire pot	30"	2000NC51152	312	1:5:2	-	88
178	WP44	2F-C-B-BF-OD	wire pot	30"	2000NC51126	310	1:5:0	-	86
179	WP45	2F-C-G-BS-OD	wire pot	30"	2000NC51129	311	1:5:1	-	87
180	ST2	C-GB-Slip	stick	1"	2009NC01028	181	2:12:2	Novo 25 (recalibrated)	180

Channel	ID	Label	Device	Range	Serial No.	Cable No.	DAQ Box ID	Note	Column #
181	ST3	W-CB-Slip	stick	1"	2009NC01026	96	1:7:3	Novo 25 (recalibrated)	97
182	ST4	E-LC1-OD	stick	6"	2007NC01009	179	2:15:2	-	189
183	ST5	E-LC2-OD	stick	6"	2007NC01010	302	2:14:2	-	185
184	ST6	C-LC1-OD	stick	6"	2007NC01011	180	2:15:3	-	190
185	ST7	C-LC2-OD	stick	6"	2007NC51006	303	2:14:3	-	186
186	ST8	W-LC1-OD	stick	6"	2007NC51007	304	2:15:0	-	187
187	ST9	W-LC2-OD	stick	6"	2007NC51010	305	2:15:1	-	188
188	ST10	C-B1-VD	stick	4"	2007NC01006	144	2:3:3	-	145
189	ST11	C-B2-VD	stick	4"	2007NC01003	210	2:5:3	Novo100	153
190	ST22	WB1-RB	stick	4"	2009NC01004	316	2:2:2	Novo100 (recalibrated)	140
191	PT1	EC1-PZ-E-PT	Position Transducer	20"	-	323	2:4:1	Novo500	147
192	PT2	EC2-PZ-E-PT	Position Transducer	40"	-	182/363	2:12:3	Novo1000-22	181
193	A1	Act3disp	FLEX test	-	-	-	3:0:0	MTS-ST5	191
194	A2	Act3Force	Load Cell	-	-	-	3:0:1	MTS-ST5	192
195	A3	Act1dispFT	Position Transducer	40"	-	-	3:0:2	MTS-ST5	193
196	A4	Act2dispFT	Position Transducer	40"	-	-	3:0:3	MTS-ST5	194
197	A5	Act3dispFT	Position Transducer	40"	-	-	3:0:4	MTS-ST5	195
198	A6	Act4dispFT	Position Transducer	40"	-	-	3:0:5	MTS-ST5	196
199	A7	Act4disp	FLEX test	-	-	-	3:0:6	MTS-ST5	197
200	A8	Act4force	Load Cell	-	-	-	3:0:7	MTS-ST5	198
201	TG1	TriggerCanon	TriggerCanon	-	-	207	3:1:5	D-Space	204
202	TG2	TriggerLeica	TriggerLeica	-	-	208	3:1:6	D-Space	205
203	500	IRIGday-500	-	-	-	-	3:15:0	For time sync. (BNC to STS)	207
204	501	IRIGhour-501	-	-	-	-	3:15:1	For time sync. (BNC to STS)	208
205	502	IRIGmin-502	-	-	-	-	3:15:2	For time sync. (BNC to STS)	209
206	503	IRIGsec-503	-	-	-	-	3:15:3	For time sync. (BNC to STS)	210
207	504	IRIGmsec-504	-	-	-	-	3:15:4	For time sync. (BNC to STS)	211
208	505	IRIGusec-505	-	-	-	-	3:15:5	For time sync. (BNC to STS)	212
209	506	IRIGstatus-506	-	-	-	-	3:15:6	For time sync. (BNC to STS)	213



Channel	ID	Label	Device	Range	Serial No.	Cable No.	DAQ Box ID	Note	Column #
1	PS1	EC1BL-S-F	strain gauge	-	-	13	0:0:0	S1	2
2	PS2	EC1BR-S-F	strain gauge	-	-	14	0:0:1	S2	3
3	PS3	EC1TL-S-F	strain gauge	-	-	15	0:0:2	S3	4
4	PS4	EC1TR-S-F	strain gauge	-	-	16	0:0:3	S4	5
5	PS5	EB2TR-N-F	strain gauge	-	-	339/198A	0:0:4	S77	6
6	PS6	WB2TL-N-F	strain gauge	-	-	193	0:0:5	S78	7
7	PS7	EC1-B-N-1-R	rosette	-	-	17	0:0:6	R1-1 (Red)	8
8	PS8	EC1-B-N-2-R	rosette	-	-	18	0:0:7	R1-2 (White)	9
9	PS9	EC1-B-N-3-R	rosette	-	-	19	0:1:0	R1-3 (Green)	10
10	PS10	EC1BL-N-F	strain gauge	-	-	38	0:1:1	S79	11
11	PS11	EC1BR-N-F	strain gauge	-	-	40	0:1:2	S80	12
12	PS12	EC1TL-N-F	strain gauge	-	-	37	0:1:3	S81	13
13	PS13	EC1TR-N-F	strain gauge	-	-	39	0:1:4	S82	14
14	PS14	WC1BL-S-F	strain gauge	-	-	34	0:1:5	S83	15
15	PS15	WC1BR-S-F	strain gauge	-	-	33	0:1:6	S84	16
16	PS16	WC1BL-N-F	strain gauge	-	-	36	0:1:7	S85	17
17	PS17	WC1BR-N-F	strain gauge	-	-	35	0:2:0	S86	18
18	PS18	EC2TL-S-F	strain gauge	-	-	52	0:2:1	S87	19
19	PS19	EC2TR-S-F	strain gauge	-	-	51	0:2:2	S88	20
20	PS20	EC2TL-N-F	strain gauge	-	-	49	0:2:3	S89	21
21	PS21	EC2TR-N-F	strain gauge	-	-	50	0:2:4	S90	22
22	PS22	WC2TL-S-F	strain gauge	-	-	55	0:2:5	S91	23
23	PS23	WC2TR-S-F	strain gauge	-	-	56	0:2:6	S92	24
24	PS24	WC2TL-N-F	strain gauge	-	-	120C	0:2:7	S93	25
25	PS25	WC2TR-N-F	strain gauge	-	-	54	0:3:0	S94	26
26	PS26	E-HSS-2-M-T-Y	strain gauge	-	-	402	0:3:1	S95	27
27	PS27	1F-E-BG-B-1-N-R	strain gauge	-	-	44	0:3:2	S96	28
28	PS28	1F-E-BG-B-2-N-R	strain gauge	-	-	45	0:3:3	S97	29
29	PS29	1F-E-BG-B-3-N-R	strain gauge	-	-	46	0:3:4	S98	30
30	PS30	EGIT-F	strain gauge	-	-	47	0:3:5	S99	31
31	PS31	1F-E-BG-BR-1-N-R	rosette	-	-	41	0:4:4	R21-1 (Red)	32
32	PS32	1F-E-BG-BR-2-N-R	rosette	-	-	42	0:4:5	R21-2 (White)	33
33	PS33	1F-E-BG-BR-3-N-R	rosette	-	-	43	0:4:6	R21-3 (Green)	34
34	PS34	STB1-T-F	strain gauge	-	-	97	0:4:7	S74	35
35	PS35	STB1-B-F	strain gauge	-	-	98	0:5:0	S75	36
36	PS36	STB2-B-F	strain gauge	-	-	100	0:5:1	S76	37

Channel	ID	Label	Device	Range	Serial No.	Cable No.	DAQ Box ID	Note	Column #
37	PS37	WG1T-F	strain gauge	-	-	37C	0:5:3	(C for color coded cable)	38
38	PS38	W-HSS-2-M-T-Y	strain gauge	-	-	33C	0:5:7	(C for color coded cable)	39
39	73	IRIGday-73	-	-	-	-	0:9:0	For time sync. (BNC to STS)	40
40	74	IRIGhour-74	-	-	-	-	0:9:1	For time sync. (BNC to STS)	41
41	75	IRIGmin-75	-	-	-	-	0:9:2	For time sync. (BNC to STS)	42
42	76	IRIGsec-76	-	-	-	-	0:9:3	For time sync. (BNC to STS)	43
43	77	IRIGmsec-77	-	-	-	-	0:9:4	For time sync. (BNC to STS)	44
44	78	IRIGusec-78	-	-	-	-	0:9:5	For time sync. (BNC to STS)	45
45	79	IRIGstatus-79	-	-	-	-	0:9:6	For time sync. (BNC to STS)	46

---

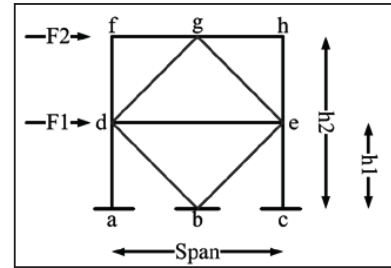
## **Appendix H**

### **TCBF-B-1 ~ TCBF-B-4 Specimen Design Calculation Sheets**

---

Title	TCBF-B-1 Specimen Design Calculation Sheet	Date	August 16, 2008
General		Page	1

Building height = 2 stories  
 Typical floor height = 9 ft  
 $F_{1, \max} = 300$  kip  
 $F_{2, \max} = 600$  kip  
 SR = 4 -  
 ratio = 0.8 -



#### Calculation Initialize

Items	values	units	Items	values	units
$F_1$	240	kip	$V_1$	720	kip
$F_2$	480	kip	$V_2$	480	kip
$h_1$	9	ft			
$h_2$	18	ft			
span	20	ft			(beam span)
$h$	9	ft			(typical floor height)
$M_{\text{base}}$	13500	kip-ft			
$P_{\text{column}}$	675	kip			
$L_{\text{brace}}$	13.45	ft			(work point to work point)
$E_s$	29000	ksi			

#### Notes

: input value

#### Materials

Members	Material Type	Fy (ksi)	Fu (ksi)	Ry	Rt	
Columns	ASTM A992	50	65	1.1	1.1	(Ref: Table I-6-1)  (HSS-Square)
Beams	ASTM A992	50	65	1.1	1.1	
Braces	ASTM A500B	46	58	1.4	1.3	
Plates 1	ASTM A36	36	58	1.3	1.2	
Bolts	A490	130	150	-	-	
Welds	E70XX	-	70	-	-	
Plates 2	ASTM A572 Gr.50	50	65	1.1	1.2	

#### Load Combinations

Per ASCE-7-2005

#### Basic Reference Codes

AISC Specification for Structural Steel Buildings (March 9, 2005)  
 AISC Seismic Provisions for Structural Steel Buildings (March 9, 2005)

Title	TCBF-B-1 Specimen Design Calculation Sheet		Date	August 16, 2008
2F-Brace			Page	2
$P_u =$	131.72	kip (compression)		
$L_{brace} =$	8.1	ft		
$k =$	1.0	-		
Try section	HSS5x5x5/16	(HSS-Square)		
$A_s =$	5.26	in <sup>2</sup>	$I_x =$	19.00 in <sup>4</sup>
$Z_x =$	9.16	in <sup>3</sup>	$I_y =$	19.00 in <sup>4</sup>
$b =$	5.00	in	$h =$	5.00 in
$t_{nom} =$	0.31	in	$t_{des} =$	0.291 in
$r_x =$	1.90	in		
$r_y =$	1.90	in		
$F_y$ (brace) =	46	ksi	$E_s =$	29000 ksi
$kL/r =$	51.05	-	Limit =	100.43 OK
$F_c =$	109.81	ksi	$0.44 F_y =$	20.24 ksi
$\phi =$	0.90	-		
$\phi P_n =$	182.74	kip (compression)	Check	OK
Check Compactness Seismically (AISC Seismic Provisions 2005, Sec 8.2b)				
$\lambda_{ps} =$	16.07	-	$b/t =$	14.20 OK
			$h/t =$	14.20 OK
				(Table I-8-1)
$\phi =$	0.90	-		
$\phi P_n =$	217.76	kip (tension)	Check	OK

$$Kl/r \leq 4\sqrt{E/F_y}$$

Title	TCBF-B-1 Specimen Design Calculation Sheet		Date	August 16, 2008	
1F-Brace			Page	3	
$P_u =$	249.37	kip (compression)			
$L_{brace} =$	9	ft			
$k =$	1.0	-			
Try section	HSS6x6x3/8 (HSS-Square)				
$A_s =$	7.58	in <sup>2</sup>	$I_x =$	39.50	in <sup>4</sup>
$Z_x =$	15.80	in <sup>3</sup>	$I_y =$	39.50	in <sup>4</sup>
$b =$	6.00	in	$h =$	6.00	in
$t_{nom} =$	0.38	in	$t_{des} =$	0.349	in
$r_x =$	2.28	in			
$r_y =$	2.28	in			
$F_y$ (brace) =	46	ksi	$E_s =$	29000	ksi
$kL/r =$	47.37	-	Limit =	100.43	OK
$F_c =$	127.55	ksi	$0.44 F_y =$	20.24	ksi
$\phi =$	0.90	-			
$\phi P_n =$	269.85	kip (compression)	Check	OK	
Check Compactness Seismically (AISC Seismic Provisions 2005, Sec 8.2b)					
$\lambda_{ps} =$	16.07	-	$b/t =$	14.20	OK
					(Table I-8-1)
			$h/t =$	14.20	OK
$\phi =$	0.90	-			
$\phi P_n =$	313.81	kip (tension)	Check	OK	

Title	TCBF-B-1 Specimen Design Calculation Sheet		Date	August 16, 2008	
2F	Brace to Gusset Plate Connection		Page	4	
Brace	HSS5x5x5/16				
$R_y F_y A_g =$	338.74	kip	$(T_u)$		
$F_u A_g =$	305.08	kip	$(P_u)$	$T_u/P_u =$	1.11 -
$R_y F_y =$	64.4	ksi			
$R_t F_u =$	75.4	ksi			
$U =$	0.9	-			
$\phi_t =$	0.75	( tensile rupture in net section )			
$A_n/A_g =$	1.27	( Net section reinforcement required! )			
$\phi_t =$	0.90	( tensile yield in gross section )			
$t_{gusset} =$	0.75	in	(estimated)	$F_y =$	50 ksi
$t_g =$	0.75	in	(use)	(gusset plate)	
				$F_u =$	65 ksi
$A_{cut} =$	0.51	in <sup>2</sup>			
$A_{net} =$	4.75	in <sup>2</sup>			
$A_e =$	5.99	in <sup>2</sup>	(Reinforcement required!)		
Reinforcement Plates					
$l =$	12	in	$B =$	5	in
$x_{bar} =$	1.875	in	$H =$	5	in
$U =$	0.84	-	$A_{e, req} =$	5.99	in <sup>2</sup>
$A_{reinf} =$	1.17	in <sup>2</sup>	$A_{net, req} =$	7.10	in <sup>2</sup>
	(both sides)				
$b_{reinf} =$	2	in	$t_{use} =$	0.625	in
$t_{req} =$	0.59	in	$L_{plate} =$	14	in
$F_{y, plate} =$	50	ksi	$R_y F_y A_g =$	68.75	kip
$L_{weld} =$	6	in	weld =	5	x 1/16 in (fillet)
$\phi R_n =$	83.51	kip	OK		
Brace Block Shear					
$t_{brace} =$	0.291	in			
$L_{req} =$	11.15	in	OK		
$L_{use} =$	12	in			
Brace to Gusset Plate Weld					
$L_{weld} =$	12	in			
weld =	6	x 1/16 in	(fillet)		
$\phi_b =$	0.75	-			

$F_{cxx} =$	70	ksi	
$F_w =$	42	ksi	
$\phi_b R_n =$	400.87	kip	OK
Gusset Plate Block Shear			
$A_{gv} =$	18	in <sup>2</sup>	
$A_{nt} =$	4.31	in <sup>2</sup>	
$U_{bs} =$	1	-	
$\phi =$	0.75	-	
$\phi R_n =$	615.23	kip	OK
Whitmore Effective Width			
$L_{whitmore} =$	20.59	in	(theoretical width)
$\phi =$	0.90	-	
$\phi R_n =$	694.86	kip	OK (check gross yield)



Title	TCBF-B-1 Specimen Design Calculation Sheet		Date	August 16, 2008	
1F	Brace to Gusset Plate Connection		Page	5	
Brace	HSS6x6x3/8				
$R_y F_y A_g =$	488.152	kip	$(T_u)$		
$F_u A_g =$	439.64	kip	$(P_u)$	$T_u/P_u =$	1.11 -
$R_y F_y =$	64.4	ksi			
$R_t F_u =$	75.4	ksi			
$U =$	0.9	-			
$\phi_t =$	0.75	( tensile rupture in net section )			
$A_n/A_g =$	1.27	( Net section reinforcement required! )			
$\phi_t =$	0.90	( tensile yield in gross section )			
$t_{gusset} =$	0.90	in	(estimated)	$F_y =$	50 ksi
$t_g =$	0.75	in	(use)	(gusset plate)	
				$F_u =$	65 ksi
$A_{cut} =$	0.61	in <sup>2</sup>			
$A_{net} =$	6.97	in <sup>2</sup>			
$A_e =$	8.63	in <sup>2</sup>	(reinforcement required)		
Reinforcement Plates					
$l =$	14	in	$B =$	6	in
$x_{bar} =$	2.25	in	$H =$	6	in
$U =$	0.84	-	$A_{e, req} =$	8.63	in <sup>2</sup>
$A_{reinf} =$	1.66	in <sup>2</sup>	(both sides)		
$b_{reinf} =$	3	in	$A_{net, req} =$	10.29	in <sup>2</sup>
$t_{req} =$	0.55	in	$t_{use} =$	0.625	in
$F_{y, plate} =$	50	ksi	$L_{plate} =$	16	in
$R_y F_y A_g =$	103.13	kip			
$L_{weld} =$	7	in	weld =	6	x 1/16 in (fillet)
$\phi R_n =$	116.92	kip	OK		
Brace Block Shear					
$t_{brace} =$	0.349	in			
$L_{req} =$	13.40	in	OK		
$L_{use} =$	14	in			
Brace to Gusset Plate Weld					
$L_{weld} =$	14	in			
weld =	7	x 1/16 in	(fillet)		
$\phi_b =$	0.75	-			

$F_{cxx} =$	70	ksi	
$F_w =$	42	ksi	
$\phi_b R_n =$	545.63	kip	OK
Gusset Plate Block Shear			
$A_{gv} =$	21	in <sup>2</sup>	
$A_{nt} =$	5.16	in <sup>2</sup>	
$U_{bs} =$	1	-	
$\phi =$	0.75	-	
$\phi R_n =$	723.87	kip	OK
Whitmore Effective Width			
$L_{whitmore} =$	23.90	in	(theoretical width)
$\phi =$	0.90	-	
$\phi R_n =$	806.55	kip	OK (check gross yield)

Title	TCBF-B-1 Specimen Design Calculation Sheet		Date	August 16, 2008	
2F	Roof Beam Design Check		Page	6	
$R_y F_y A_g =$	338.74	kip	$\theta =$	0.73	(rad) 42.0 (deg)
$0.3 P_n =$	60.91	kip	$\sin(\theta) =$	0.67	
			$\cos(\theta) =$	0.74	
$V =$	185.86	kip			
$H =$	297.06	kip			
$P_u =$	600.00	kip	(conservatively)		
$M_u =$	100.97	kip-ft	(revised from structural analysis)		
Try	w24x117				
$A_g =$	34.4	in <sup>2</sup>	$b_f =$	12.8	in
$I_x =$	3540	in <sup>4</sup>	$t_f =$	0.85	in
$I_y =$	297	in <sup>4</sup>	$d =$	24.3	in
$r_x =$	10.1	in	$t_w =$	0.55	in
$r_y =$	2.94	in	$F_y =$	50	ksi
$\lambda_{p1} =$	9.15		$b/t =$	7.53	Compact
$\lambda_{p2} =$	90.55		$h/t_w =$	41.09	Compact
$L_p =$	10.38	ft	$Z_x =$	327	in <sup>3</sup>
$c =$	1	-	$J =$	6.72	in <sup>4</sup>
$C_w =$	40800	in <sup>6</sup>	$h_o =$	23.45	in
$S_x =$	291	in <sup>3</sup>	$r_{ts} =$	3.46	in
$L_r =$	29.90	ft	Brace PT=	2	-
$L_b =$	10	ft	$C_b =$	1.0	(Conservatively)
$M_p =$	1362.5	kip-ft	$F_{cr} =$	248.50	ksi
$\phi_b =$	0.90	-	$M_n =$	1362.50	kip-ft (Need Check)
$\phi_b M_n =$	1226.25	kip-ft			
$kl/r =$	40.82	-	$k =$	1.0	-
$F_e =$	171.79	ksi	$0.44 F_y =$	22	ksi
$\phi_c =$	0.90	-			
$\phi_c P_n =$	1370.46	kip			
$P_u / \phi_c P_n =$	0.44	use (H1-1a)			
Check	0.51	OK			

Title	TCBF-B-1 Specimen Design Calculation Sheet			Date	August 16, 2008		
1F	Lower Beam Design Check			Page	7		
$R_y F_y A_g =$	488.15	kip	(1F)				
$R_y F_y A_g =$	338.74	kip	(2F)	$\theta =$	0.73	(rad)	42.0 (deg)
$0.3 P_n =$	89.95	kip	(1F)	$\sin(\theta) =$	0.67		
$0.3 P_n =$	60.91	kip	(2F)	$\cos(\theta) =$	0.74		
$V =$	285.81	kip					
$H =$	317.56	kip					
$P_u =$	317.56	kip	(conservatively)				
$M_u =$	170.85	kip-ft	(revised from structural analysis)				
Try	w24x68						
$A_g =$	20.1	in <sup>2</sup>		$b_f =$	8.97	in	
$I_x =$	1830	in <sup>4</sup>		$t_f =$	0.585	in	
$I_y =$	70.4	in <sup>4</sup>		$d =$	23.7	in	
$r_x =$	9.55	in		$t_w =$	0.415	in	
$r_y =$	1.87	in		$F_y =$	50	ksi	
$\lambda_{p1} =$	9.15			$b/t =$	7.67	Compact	
$\lambda_{p2} =$	90.55			$h/t_w =$	54.29	Compact	
$L_p =$	6.61	ft		$Z_x =$	177	in <sup>3</sup>	
$c =$	1	-		$J =$	1.87	in <sup>4</sup>	
$C_w =$	9430	in <sup>6</sup>		$h_o =$	23.12	in	
$S_x =$	154	in <sup>3</sup>		$r_{ts} =$	2.30	in	
$L_r =$	18.74	ft		Brace PT=	2	-	
$L_b =$	10	ft		$C_b =$	1.0	(Conservatively)	
$M_p =$	737.5	kip-ft		$F_{cr} =$	110.86	ksi	
$\phi_b =$	0.90	-		$M_n =$	656.87	kip-ft	OK
$\phi_b M_n =$	591.18	kip-ft					
$kl/r =$	64.17	-		$k =$	1.0	-	
$F_e =$	69.50	ksi		$0.44 F_y =$	22	ksi	
$\phi_c =$	0.90	-					
$\phi_c P_n =$	669.33	kip					
$P_u / \phi_c P_n =$	0.47	use (H1-1a)					
Check	0.73	OK					

Title	TCBF-B-1 Specimen Design Calculation Sheet		Date	August 16, 2008
2F	Column Design Check		Page	8
$P_u =$	42.58	kip	(revised from structural analysis)	
$M_u =$	126.56	kip-ft	(revised from structural analysis)	
$L_{column} =$	9	ft		
Try	w12x96			
$A_g =$	28.2	in <sup>2</sup>	$b_f =$	12.2 in
$I_x =$	833	in <sup>4</sup>	$t_f =$	0.9 in
$I_y =$	270	in <sup>4</sup>	$d =$	12.7 in
$r_x =$	5.44	in	$t_w =$	0.55 in
$r_y =$	3.09	in	$F_y =$	50 ksi
$\lambda_{p1} =$	7.22	-	$b/t =$	6.78 Compact
$\lambda_{p2} =$	71.71	-	$h/t_w =$	19.82 Compact
$L_p =$	10.91	ft	$Z_x =$	147 in <sup>3</sup>
$c =$	1	-	$J =$	6.85 in <sup>4</sup>
$C_w =$	9410	in <sup>6</sup>	$h_o =$	11.80 in
$S_x =$	131	in <sup>3</sup>	$r_{ts} =$	3.49 in
$L_r =$	40.86	ft	Brace PT=	0 -
$L_b =$	9	ft	$C_b =$	1.0 (Conservatively)
$M_p =$	612.5	kip-ft	$F_{cr} =$	344.49 ksi
$\phi_b =$	0.90	-	$M_n =$	612.50 kip-ft (Need Check)
$\phi_b M_n =$	551.25	kip-ft	$C_a =$	0.03 -
$kl/r =$	34.95	-	$k =$	1.0 -
$F_e =$	234.28	ksi	$0.44 F_y =$	22 ksi
$\phi_c =$	0.90	-		
$\phi_c P_n =$	1160.56	kip		
$P_u/\phi_c P_n =$	0.04	use (H1-1b)		
Check	0.25	OK		

Title	TCBF-B-1 Specimen Design Calculation Sheet		Date	August 16, 2008
1F	Column Design Check		Page	9
$P_u =$	484.19	kip	(revised from structural analysis)	
$M_u =$	274.18	kip-ft	(revised from structural analysis)	
$L_{column} =$	9	ft		
Try	w12x96			
$A_g =$	28.2	in <sup>2</sup>	$b_f =$	12.2 in
$I_x =$	833	in <sup>4</sup>	$t_f =$	0.9 in
$I_y =$	270	in <sup>4</sup>	$d =$	12.7 in
$r_x =$	5.44	in	$t_w =$	0.55 in
$r_y =$	3.09	in	$F_y =$	50 ksi
$\lambda_{p1} =$	7.22	-	$b/t =$	6.78 Compact
$\lambda_{p2} =$	52.56	-	$h/t_w =$	19.82 Compact
$L_p =$	10.91	ft	$Z_x =$	147 in <sup>3</sup>
$c =$	1	-	$J =$	6.85 in <sup>4</sup>
$C_w =$	9410	in <sup>6</sup>	$h_o =$	11.80 in
$S_x =$	131	in <sup>3</sup>	$r_{ts} =$	3.49 in
$L_r =$	40.86	ft	Brace PT=	0 -
$L_b =$	9	ft	$C_b =$	1.0 (Conservatively)
$M_p =$	612.5	kip-ft	$F_{cr} =$	344.49 ksi
$\phi_b =$	0.90	-	$M_n =$	612.50 kip-ft (Need Check)
$\phi_b M_n =$	551.25	kip-ft	$C_a =$	0.38 -
$kl/r =$	34.95	-	$k =$	1.0 -
$F_e =$	234.28	ksi	$0.44 F_y =$	22 ksi
$\phi_c =$	0.90	-		
$\phi_c P_n =$	1160.56	kip		
$P_u/\phi_c P_n =$	0.42	use (H1-1a)		
Check	0.86	OK		

Check Column Web Shear Stress

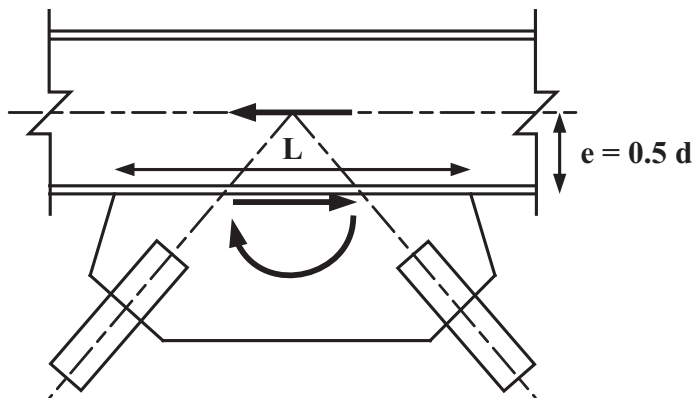
$M_p =$	7350	kip-in	
$L =$	96.15	in	
$V =$	152.89	kip	
$A_s =$	6.99	in <sup>2</sup>	$A_s = d*tw$
$S_v =$	21.89	ksi	
$S_{v, yield} =$	29.00	ksi	Elastic

Title	TCBF-B-1 Specimen Design Calculation Sheet		Date	August 16, 2008				
2F	Beam-Column Connection		Page	10				
Type	Bolted (WUF-B)							
H =	148.53	kip						
V =	92.93	kip						
M =	100.97	kip-ft (revised from structural analysis)						
$R_u =$	175.21	kip	$F_u =$	150	ksi			
Try $d_b =$	0.88	in	$F_{nv} =$	75	ksi (threads excluded)			
$A_b =$	0.60	in <sup>2</sup>	$N_b =$	6	bolts (in one row)			
$R_n =$	270.59	kip (bolt shear)	$L_{c\_ex} =$	1.5	in			
$\phi_b =$	0.75	-	$L_{c\_in} =$	3	in			
$\phi_b R_n =$	202.94	kip	OK					
$L_{c1} =$	1.03	in (edge clear distance)	$R_{n1} =$	46.41	kip			
$L_{c2} =$	2.06	in (clear distance)	$R_{n2} =$	236.25	kip			
t =	0.50	in (shear tab thickness)						
$R_n =$	1227.66	kip (combined bolt bearing)						
$\phi_b =$	0.75	-						
$\phi_b R_n =$	920.74	kip	OK					
$L_{tab} =$	18	in	$A_{s, tab} =$	9	in <sup>2</sup>	$R_n =$	524.79	kip
$w_{tab} =$	4.5	in	$F_{y, tab} =$	50	ksi	$P_{nt} =$	450.00	kip
			$F_{v, tab} =$	30.0	ksi	$P_{nv} =$	270.00	kip
			OK					
Weld	Fillet (shear tab)							
$F_{exx} =$	70	ksi	$R_n =$	334.06	kip			
$F_w =$	42	ksi	$\phi_b =$	0.75	-			
w =	5	x 1/16 inch	$\phi_b R_n =$	250.54	kip	OK		
$L_{weld} =$	18	in						
side =	2	sides						
Weld	CJP (top, bottom flanges)							
$b_f =$	12.8	in	$F_{y, bm} =$	50	ksi (base metal)			
$t_f =$	0.85	in	$M_n =$	1063.07	kip-ft	OK		
d =	24.3	in						
$t_w =$	0.55	in						



Check	Shear tab length, OK	
Check Block Shear		
Beam		
w24x117		
$A_{gv} =$	9.9	in <sup>2</sup>
$A_{gt} =$	1.925	in <sup>2</sup>
$A_{nv} =$	6.6	in <sup>2</sup>
$A_{nt} =$	1.65	in <sup>2</sup>
$U_{bs} =$	0.5	-
$\phi =$	0.75	-
$F_y =$	50	ksi
$F_u =$	65	ksi
$\phi R_n =$	233.27	kip
		OK
Shear Tab		
$A_{gv} =$	8.25	in <sup>2</sup>
$A_{gt} =$	1.5	in <sup>2</sup>
$A_{nv} =$	5.5	in <sup>2</sup>
$A_{nt} =$	1.25	in <sup>2</sup>
$U_{bs} =$	0.5	-
$\phi =$	0.75	-
$F_y =$	50	ksi
$F_u =$	65	ksi
$\phi R_n =$	191.34	kip
		OK

Title	TCBF-B-1 Specimen Design Calculation Sheet		Date	August 16, 2008	
2F	Braces to Beam Connection		Page	11	
Braces	HSS5x5x5/16				
T =	338.74	kip	$\sin(\theta) =$	0.669	
C =	312.69	kip	$\cos(\theta) =$	0.743	
e =	12.15	in			
Shear =	484.21	kip			
Tension =	169.56	kip			
Moment =	490.26	kip-ft			
$t_{\text{gusset}} =$	0.75	in			
L =	60	in			
$s_V =$	10.76	ksi			
$s_A =$	3.77	ksi			
$s_M =$	13.07	ksi			
$\phi =$	0.9	-			
$F_{y, \text{gusset}} =$	50	ksi			
Ratio =	0.56	OK			
$L_{\text{whitmore}} =$	20.59	in	$L_{\text{min}} =$	57.78	in (geometry limit) OK
$L_v =$	16	in	$L_{v, \text{min}} =$	15.30	in (geometry limit) OK
$w_{\text{up}} =$	10.29	in	$A_v =$	12	in <sup>2</sup>
$w_{\text{low}} =$	20.92	in	$P_u =$	226.61	kip
$\text{Whitm}_{\text{eff}} =$	20.59	in	$\phi R_n =$	324	kip OK
$\phi R_n =$	694.86	kip	OK		
Gusset Plate to Beam Flange					
Weld	Fillet				
$F_{\text{exx}} =$	70	ksi			
$F_w =$	42	ksi	$s_V =$	11.41	ksi
w =	8	x 1/16 inch	$s_M =$	13.87	ksi
$L_{\text{weld}} =$	60	in	$s_A =$	4.00	ksi
side =	2	sides	$f_{\text{peak}} =$	21.20	ksi
$t_{\text{eff}} =$	0.354	in	$f_{\text{avg}} =$	18.15	ksi
$\phi =$	0.75	-	$f_r =$	22.68	ksi
Ratio =	0.77	OK	Ratio =	0.72	OK
Check Beam Web					
width =	60	in	Beam	w24x117	



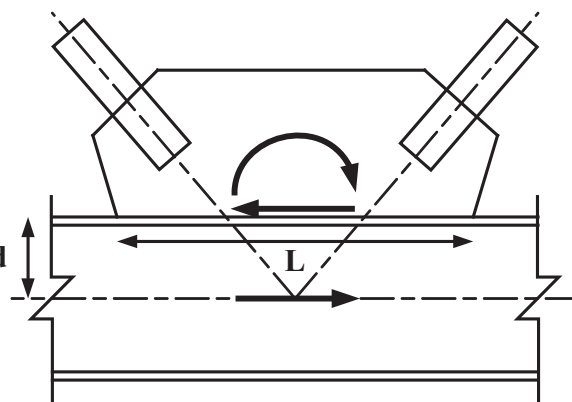
$R_u = 196.10$	kip	$d = 24.3$	in	$t_w = 0.55$	in
$N = 30$	in	$t_f = 0.85$	in	$F_{y, web} = 50$	ksi
$\phi = 0.75$	-	$R_n = 1060.63$	kip	$\phi R_n = 795.47$	kip
$k_{des} = 1.35$	in			(web crippling)	OK
$\phi = 1.00$	-	$R_n = 1010.63$	kip	$\phi R_n = 1010.63$	kip
				(web local yielding)	OK
Check Gusset Plate Buckling					
$L_{gb} = 17.68$	in	$kL/r = 98.0$	-	$L_c = 14.13$	in
$k = 1.2$	-	$F_e = 29.82$	ksi	$L_{c1} = 11.38$	in
$r = 0.217$	in	$0.44 F_y = 22$	ksi	$L_{c2} = 16.94$	in
$A_g = 15.44$	in <sup>2</sup>	$R_n = 382.72$	kip	$L_{max} = 24.06$	in
$\phi = 0.9$	-	$\phi R_n = 344.45$	kip	$L_{tip} = 21.88$	in
			OK	$L_{ave} = 17.68$	in
Free Edge Buckling					
$L_e = 15.63$	in				
$L_e/t_g = 20.83$	-				
Limit = 18.06	-	Edge stiffener required!			
Lateral Stability of Beam					
$M_r = 1498.75$	kip-ft	$Z = 327$	in <sup>3</sup>	$L_b = 10$	ft
$C_d = 1$	-	$h_o = 23.45$	in	$L_{pd} = 17.05$	ft
$P_{br} = 15.34$	kip	$\beta_{br} = 85.22$	kip/in	$n = 1$	OK
(Nodal)		(Nodal)		$C_b = 1$	-
$M_{br} = 17.985$	kip-ft				
$P_{br} = 9.20$	kip	(torsional)			
$\beta_T = 28842$	kip-in/rad	$\beta_{sec}$ not included			
$\beta_{br} = 52.45$	kip/in	(torsional)			
$\Delta = 0.18$	in				
Kicker					
L3x2x3/8					
$A_g = 1.73$	in <sup>2</sup>				
$L = 25$	in				
$k_{axial} = 2006.8$	kip/in				
$k = 1419$	kip/in	OK			

Title	TCBF-B-1 Specimen Design Calculation Sheet		Date	August 16, 2008	
1F	Beam-Column-Gusset Connections		Page	12	
Big Gusset Plate for Upper Floor Bracing and Lower Floor Bracing					
Sway to Right					
$F_{U2R} = 338.74$	kip	$\cos(\theta_U) = 0.743$			
$F_{L2R} = 461.74$	kip	$\cos(\theta_L) = 0.743$			
Sway to Left					
$F_{U2L} = 312.69$	kip				
$F_{L2L} = 488.15$	kip				
Beam	w24x68				
d	23.7	in			
$L_{c, \min}$	56.77	in			
Column	w12x96				
$e_c$	6.35	in			
$R_{beam}$	22.51	kip (downward)			
$L_{b, \min}$	15.99	in			
$L_{cu, \min}$	15.30	in			
$L_{cl, \min}$	17.76	in			
$t_g$	0.75	in			
$L_{cu} = 18$	in (use)	$F_{y, gusset} = 50$	ksi		
$L_{cl} = 18$	in (use)				
$L_c = 59.7$	in (use)				
$L_b = 23$	in (use)				
Sway to the Right					
$V_{U2R} = 226.61$	kip (upward)	$s_V = 11.46$	ksi		
$H_{U2R} = 251.79$	kip (rightward)	$s_M = 7.31$	ksi		
$V_{L2R} = 308.89$	kip (upward)	$s_A = 2.04$	ksi		
$H_{L2R} = 343.21$	kip (leftward)	Ratio = 0.49	-	OK	
$V_{total} = 512.98$	kip (upward)				
M = 271.45	kip-ft (counter-clockwise)				
Column-Side					
$V_{cu} = 154.67$	kip (downward)	$s_A = 5.11$	ksi		
$f_1 = 5.48$	kip/in (leftward)	$s_V = 11.46$	ksi		
$f_2 = 2.18$	kip/in (leftward)	$s_M = 2.20$	ksi		
$H_{cu} = 68.95$	kip (leftward)	Ratio = 0.47	-	OK	
Beam-Side					
$H_{bu} = 182.84$	kip (leftward)				
$V_{bu} = 71.94$	kip (downward)	$s_A = 4.17$	ksi		
$M_{cu} = 7.44$	kip-ft (counter-clockwise)	$s_V = 10.60$	ksi		

$M_{bu} = -118.93$	kip-ft	(clockwise)	$s_M = -21.58$	ksi	
			Ratio = 0.56	-	OK
$V_{cl} = 154.67$	kip	(downward)	$s_A = 5.11$	ksi	
$f_1 = 5.48$	kip/in	(rightward)	$s_V = 11.46$	ksi	
$f_3 = 2.18$	kip/in	(rightward)	$s_M = 2.20$	ksi	
$H_{cl} = 68.95$	kip	(rightward)	Ratio = 0.47	-	OK
$H_{bl} = 274.26$	kip	(rightward)			
$V_{bl} = 154.22$	kip	(downward)	$s_A = 8.94$	ksi	
$M_{bl} = 86.82$	kip-ft	(clockwise)	$s_V = 15.90$	ksi	
$M_{cl} = 7.44$	kip-ft	(counter-clockwise)	$s_M = 15.76$	ksi	
			Ratio = 0.82	-	OK
$V_{mid} = 156.39$	kip	(downward)	$s_A = 0.00$	ksi	
$M_{mid} = 10.02$	kip-ft	(counter-clockwise)	$s_V = 8.80$	ksi	
$H_{mid} = 0.00$	kip	(leftward)	$s_M = 1.71$	ksi	
			Ratio = 0.34	-	OK
Weld Size					
$f_v = 8.59$	kip/in				
$f_a = 4.98$	kip/in	(averaged)			
$f_b = 5.48$	kip/in				
$f_{peak} = 13.54$	kip/in				
$f_{avg} = 11.07$	kip/in				
$f_r = 13.84$	kip/in	13.84342			
D >=	4.97	x 1/16	(weld size)		
Use	6	x 1/16	(weld size)		

Title	TCBF-B-1 Specimen Design Calculation Sheet		Date	August 16, 2008			
1F	Lower Beam to Gusset Plate Splice		Page	13			
Web	Fillet welds with web plates						
Flange	CJP weld (T & B)						
$P_u =$	317.56	kip					
$t_f =$	0.59	in					
$b =$	8.97	in					
$A_s =$	5.25	in <sup>2</sup>					
$2 * A_s * F_y =$	524.75	kip	OK				
$R_{beam} =$	22.51	kip	(Gravity)				
$L_{tab} =$	20.375	in	$t =$	0.5	in		
$w_{tab} =$	8	in					
Weld	Fillet (shear tab)						
$F_{exx} =$	70	ksi	$R_n =$	315.96	kip		
$F_w =$	42	ksi	$\phi_b =$	0.75	-		
$w =$	6	x 1/16	inch	$\phi_b R_n =$	236.97	kip	OK
$L_{weld} =$	28.375	in					
side =	1	sides					
Shim Plate							
$L =$	20	in	$t =$	0.168	in	(shim as required)	
$w =$	4	in					
Weld	Fillet (shear tab)						
$F_{exx} =$	70	ksi	$R_n =$	139.26	kip		
$F_w =$	42	ksi	$\phi_b =$	0.75	-		
$w =$	2.68	x 1/16	inch	$\phi_b R_n =$	104.45	kip	OK
$L_{weld} =$	28	in	(3 sides)				
side =	1	sides					

Title	TCBF-B-1 Specimen Design Calculation Sheet		Date	August 16, 2008	
1F	Braces to Floor Beam Connection		Page	14	
Braces	HSS6x6x3/8				
T =	488.15	kip	$\sin(\theta) =$	0.669	
C =	461.74	kip	$\cos(\theta) =$	0.743	
e =	0	in			
Shear =	706.05	kip			
Tension =	242.31	kip			
Moment =	0.00	kip-ft			
$t_{gusset} =$	0.75	in			
L =	46	in			
$s_V =$	20.47	ksi			
$s_M =$	0.00	ksi			
$\phi =$	0.9	-			
$F_{y, gusset} =$	50	ksi			
Ratio =	0.80	OK			
whitmo =	23.90	in	$L_{min} =$	35.72	in (geometry limit) OK
$L_v =$	19	in	$L_{v, min} =$	17.76	in (geometry limit) OK
$w_{up} =$	11.95	in	$A_v =$	14.25	in <sup>2</sup>
$w_{low} =$	14.12	in	$P_u =$	326.56	kip
whit <sub>eff</sub> =	23.90	in	$\phi R_n =$	384.75	kip
$\phi R_n =$	806.55	kip	OK		OK
Weld	Fillet	(Gusset to beam flange)			
$F_{exx} =$	70	ksi			
$F_w =$	42	ksi			
w =	11	x 1/16	inch	$s_V =$	15.79 ksi
$L_{weld} =$	46	in		$s_M =$	0.00 ksi
side =	2	sides		$s_A =$	5.42 ksi
$t_{eff} =$	0.486	in			
$\phi =$	0.75	-			
Ratio =	0.89	OK			
Check Beam Web					
width =	46	in	Beam	w30x391	
$R_u =$	0.00	kip	d =	33.2	in $t_w =$ 1.36 in



$N =$	23	in	$t_f =$	2.44	in	$F_{y, web} =$	50	ksi
$\phi =$	0.75	-	$R_n =$	4450.60	kip	$\phi R_n =$	3337.95	kip
$k_{des} =$	3.23	in				(web crippling)		OK
$\phi =$	1.00	-	$R_n =$	2662.20	kip	$\phi R_n =$	2662.20	kip
						(web local yielding)		OK
Check Gusset Plate Buckling								
$L_{gb} =$	14.84	in	$kL/r =$	82.2	-	$L_c =$	15.88	in
$k =$	1.2	-	$F_e =$	42.32	ksi	$L_{c1} =$	18.06	in
$r =$	0.217	in	$0.44 F_y =$	22	ksi	$L_{c2} =$	12.56	in
$A_g =$	17.92	in <sup>2</sup>	$R_n =$	546.54	kip	$L_{max} =$	18.56	in
$\phi =$	0.9	-	$\phi R_n =$	491.88	kip	$L_{tip} =$	9.13	in
					OK	$L_{ave} =$	14.84	in
Free Edge Buckling								
$L_e =$	17.88	in						
$L_e/t_g =$	23.83	-						
Limit =	18.06	-	Edge stiffener required!					
Lateral Stability of Beam								
$M_r =$	6645.83	kip-ft	$Z =$	1450	in <sup>3</sup>	$L_b =$	10	ft
$C_d =$	1	-	$h_o =$	30.76	in	$L_{pd} =$	17.05	ft
$P_{br} =$	51.85	kip	$\beta_{br} =$	288.07	kip/in	$n =$	1	OK
(Nodal)			(Nodal)			$C_b =$	1	-
$M_{br} =$	79.75	kip-ft				$I_y =$	1550	in <sup>4</sup>
$P_{br} =$	31.11	kip	(torsional)					
$\beta_T =$	108666	kip-in/rad	$\beta_{sec}$ not included					
$\beta_{br} =$	114.85	kip/in	(torsional)					
$\Delta =$	0.27	in						



Title	TCBF-B-1 Specimen Design Calculation Sheet		Date	August 16, 2008	
1F	Column Base Plate Design Check		Page	15	
Column	w12x96				
$Z_x =$	147	in <sup>3</sup>	$L =$	96.15	in
$F_y =$	50	ksi	$V_{Mp} =$	152.89	kip
$M_p =$	7350	kip-in			
$P_u =$	484.19	kip	$d =$	12.7	in
$M_u =$	3290.12	kip-in	$b_f =$	12.2	in
$N =$	31.25	in	$f_{p, max} =$	36	ksi
$B =$	28	in			
$e =$	6.80	in	$q_{max} =$	1008	kip/in
$e_{cr} =$	15.38	in	(Small Moment)		
$Y =$	17.66	in			
$q =$	27.42	kip/in	OK		
$m =$	9.59	in			
$f_p =$	0.98	ksi			
$t_{p, req} =$	2.01	in	eq 3.3.14a (LRFD)		
$use =$	2.00	in			
All-thread-rods					
Type	ASTM A193 B7				
$d_{bolt} =$	1.125	in			
$F_u =$	125	ksi			
$F_y =$	105	ksi			
$F_{nt} =$	93.75	ksi			
$F_{nv} =$	50	ksi			
$A_b =$	0.99	in <sup>2</sup>			
$\phi =$	0.75	-			
$\phi R_n =$	69.89	kip	(tension)		
$\phi R_n =$	37.28	kip	(shear)		
$F_{PT} =$	86.98	kip	(minimum required pretension)		
$V_u =$	152.89	kip	(very conservative assumption)		
$M_u =$	7350	kip-in	(very conservative assumption)		
$P_u =$	600	kip	(very conservative assumption)		
$\mu =$	0.35	-	(class A surface)		
SF =	2	-	(safety factor for not having enough bolt pretension force)		

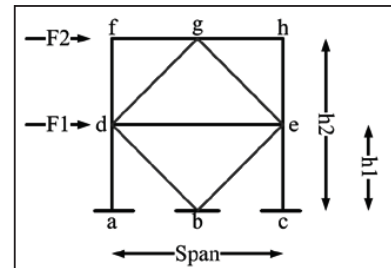
$N_V =$	10	bolts	(for friction shear)
$N_M =$	17	bolts	(for bending)
$N_T =$	9	bolts	(for uplifting)
$N_{\text{req, total}} =$	35	bolts	
use =	34	bolts	

Title	TCBF-B-1 Specimen Design Calculation Sheet			Date	August 8, 2009
2F	Stub Beam			Page	16
F1 =	300	kip	d =	24.3	in
F2 =	600	kip	t <sub>w</sub> =	0.55	in
L <sub>stub</sub> =	19	in	b =	12.8	in
Beam	w24x117		t <sub>f</sub> =	0.85	in
Column Dimension List					
Column	w12x96				
A <sub>g</sub> =	28.2	in <sup>2</sup>	b <sub>f</sub> =	12.2	in
I <sub>x</sub> =	833	in <sup>4</sup>	t <sub>f</sub> =	0.9	in
I <sub>y</sub> =	270	in <sup>4</sup>	d =	12.7	in
r <sub>x</sub> =	5.44	in	t <sub>w</sub> =	0.55	in
r <sub>y</sub> =	3.09	in	F <sub>y</sub> =	50	ksi
k <sub>des</sub> =	1.5	in	E <sub>s</sub> =	29000	ksi
Column Web Local Yielding					
N =	24.00	in			
R <sub>n</sub> =	866.25	kip			
φ =	1.00	-			
φR <sub>n</sub> =	866.25	kip	OK		
Column Web Crippling					
R <sub>n</sub> =	1382.366	kip			
φ =	0.75	-			
φR <sub>n</sub> =	1036.77	kip	OK		
Column Flange Local Bending					
R <sub>n</sub> =	253.13	kip	A <sub>web</sub> =	12.43	in <sup>2</sup>
			A <sub>s</sub> =	34.19	in <sup>2</sup>
φ =	0.90	-	A <sub>flange</sub> =	21.76	in <sup>2</sup>
φR <sub>n</sub> =	227.81	kip	F1 <sub>flange</sub> =	190.93	kip
			F2 <sub>flange</sub> =	381.87	kip
					Continue Plate Required!
Stub Beam Gross Yielding					
A <sub>s (beam)</sub> =	34.4	in <sup>2</sup>			
P <sub>y</sub> =	1720	kip	OK		

Title	TCBF-B-1 Specimen Design Calculation Sheet			Date	August 8, 2009
1F	Stub Beam			Page	17
$F_1 =$	300	kip	$d =$	23.7	in
$F_2 =$	600	kip	$t_w =$	0.415	in
$L_{stub} =$	19	in	$b =$	8.97	in
Beam	w24x68		$t_f =$	0.585	in
Column Dimension List					
Column	w12x96				
$A_g =$	28.2	in <sup>2</sup>	$b_f =$	12.2	in
$I_x =$	833	in <sup>4</sup>	$t_f =$	0.9	in
$I_y =$	270	in <sup>4</sup>	$d =$	12.7	in
$r_x =$	5.44	in	$t_w =$	0.55	in
$r_y =$	3.09	in	$F_y =$	50	ksi
$k_{des} =$	1.5	in	$E_s =$	29000	ksi
Column Web Local Yielding					
$N =$	24.00	in			
$R_n =$	866.25	kip			
$\phi =$	1.00	-			
$\phi R_n =$	866.25	kip	OK		
Column Web Crippling					
$R_n =$	1382.366	kip			
$\phi =$	0.75	-			
$\phi R_n =$	1036.77	kip	OK		
Column Flange Local Bending					
$R_n =$	253.13	kip	$A_{web} =$	9.35	in <sup>2</sup>
$\phi =$	0.90	-	$A_{flange} =$	10.49	in <sup>2</sup>
$\phi R_n =$	227.81	kip	$F1_{flange} =$	158.65	kip
			$F2_{flange} =$	317.31	kip
					OK
Stub Beam Gross Yielding					
$A_{s (beam)} =$	20.1	in <sup>2</sup>			
$P_y =$	1005	kip	OK		

Title	TCBF-B-2 Specimen Design Calculation Sheet	Date	May 27, 2009
General		Page	1

Building height = 2 stories  
 Typical floor height = 9 ft  
 $F_{1, \max} = 300$  kip  
 $F_{2, \max} = 600$  kip  
 SR = 4 -  
 ratio = 0.8 -



### Calculation Initialize

Items	values	units	Items	values	units
$F_1$	240	kip	$V_1$	720	kip
$F_2$	480	kip	$V_2$	480	kip
$h_1$	9	ft			
$h_2$	18	ft			
span	20	ft			(beam span)
$h$	9	ft			(typical floor height)
$M_{\text{base}}$	13500	kip-ft			
$P_{\text{column}}$	675	kip			
$L_{\text{brace}}$	13.45	ft			(work point to work point)
$E_s$	29000	ksi			

### Notes

: input value

### Materials

Members	Material Type	Fy (ksi)	Fu (ksi)	Ry	Rt	
Columns	ASTM A992	50	65	1.1	1.1	(Ref: Table I-6-1)  (HSS-Round)
Beams	ASTM A992	50	65	1.1	1.1	
Braces	ASTM A500B	42	58	1.4	1.3	
Plates 1	ASTM A36	36	58	1.3	1.2	
Bolts	A490	130	150	-	-	
Welds	E70XX	-	70	-	-	
Plates 2	ASTM A572 Gr.50	50	65	1.1	1.2	

### Load Combinations

Per ASCE-7-2005

### Basic Reference Codes

AISC Specification for Structural Steel Buildings (March 9, 2005)  
 AISC Seismic Provisions for Structural Steel Buildings (March 9, 2005)

Title	TCBF-B-2 Specimen Design Calculation Sheet		Date	May 27, 2009
2F-Brace			Page	2
$P_u =$	144.00	kip (compression)		
$L_{brace} =$	8.1	ft		
$k =$	1.0	-		
Try section	HSS5x.500	(HSS-Square)		
$A_s =$	6.62	in <sup>2</sup>	$I_x =$	17.20 in <sup>4</sup>
$Z_x =$	9.60	in <sup>3</sup>	$I_y =$	17.20 in <sup>4</sup>
OD =	5.00	in	OD =	5.00 in
$t_{nom} =$	0.50	in	$t_{des} =$	0.465 in
$r_x =$	1.61	in		
$r_y =$	1.61	in		
$F_y$ (brace) =	42	ksi	$E_s =$	29000 ksi
$kL/r =$	60.25	-	Limit =	105.11 OK
$F_c =$	78.85	ksi	$0.44 F_y =$	18.48 ksi
$\phi =$	0.90	-		
$\phi P_n =$	200.23	kip (compression)	Check	OK
Check Compactness Seismically (AISC Seismic Provisions 2005, Sec 8.2b)				
$\lambda_{ps} =$	16.82	-	$b/t =$	0.00 OK
			$h/t =$	0.00 OK
				(Table I-8-1)
$\phi =$	0.90	-		
$\phi P_n =$	250.24	kip (tension)	Check	OK

$$Kl/r \leq 4\sqrt{E/F_y}$$

Title	TCBF-B-2 Specimen Design Calculation Sheet		Date	May 27, 2009
1F-Brace			Page	3
$P_u =$	252.07	kip (compression)		
$L_{brace} =$	9	ft		
$k =$	1.0	-		
Try section	HSS6x.500	(HSS-Square)		
$A_s =$	8.09	in <sup>2</sup>	$I_x =$	31.20 in <sup>4</sup>
$Z_x =$	14.30	in <sup>3</sup>	$I_y =$	31.20 in <sup>4</sup>
OD =	6.00	in	OD =	6.00 in
$t_{nom} =$	0.50	in	$t_{des} =$	0.465 in
$r_x =$	1.96	in		
$r_y =$	1.96	in		
$F_y$ (brace) =	42	ksi	$E_s =$	29000 ksi
$kL/r =$	55.10	-	Limit =	105.11 OK
$F_c =$	94.26	ksi	$0.44 F_y =$	18.48 ksi
$\phi =$	0.90	-		
$\phi P_n =$	253.77	kip (compression)	Check	OK
Check Compactness Seismically (AISC Seismic Provisions 2005, Sec 8.2b)				
$\lambda_{ps} =$	16.82	-	$b/t =$	0.00 OK
			$h/t =$	0.00 OK
				(Table I-8-1)
$\phi =$	0.90	-		
$\phi P_n =$	305.80	kip (tension)	Check	OK

$$Kl/r \leq 4\sqrt{E/F_y}$$

Title	TCBF-B-2 Specimen Design Calculation Sheet		Date	May 27, 2009	
2F	Brace to Gusset Plate Connection		Page	4	
Brace	HSS5x.500				
$R_y F_y A_g =$	389.26	kip	$(T_u)$		
$F_u A_g =$	383.96	kip	$(P_u)$	$T_u/P_u =$	1.01 -
$R_y F_y =$	58.8	ksi			
$R_t F_u =$	75.4	ksi			
$U =$	0.9	-			
$\phi_t =$	0.75	( tensile rupture in net section )			
$A_n/A_g =$	1.16	( Net section reinforcement required! )			
$\phi_t =$	0.90	( tensile yield in gross section )			
$t_{gusset} =$	0.87	in	(estimated)	$F_y =$	50 ksi
$t_g =$	0.75	in	(use)	(gusset plate)	
				$F_u =$	65 ksi
$A_{cut} =$	0.81	in <sup>2</sup>			
$A_{net} =$	5.81	in <sup>2</sup>			
$A_e =$	6.88	in <sup>2</sup>	(Reinforcement required!)		
Reinforcement Plates					
$l =$	12	in	Section	HSS6x.500	
$x_{bar} =$	1.909859	in	OD =	6 in	ID = 5 in
$U =$	0.84	-	$A_{e, req} =$	6.88 in <sup>2</sup>	$A_{net, req} =$ 8.19 in <sup>2</sup>
$A_{reinf} =$	1.19	in <sup>2</sup>	(both sides)		
$b_{reinf} =$	2.38	in	$c_{reinf} =$	2.32 in	
$t_{req} =$	0.50	in	$b_{use} =$	2.5 in	$L_{plate} =$ 14 in
$F_{y, plate} =$	42	ksi	$R_y F_y A_g =$	73.50 kip	
$L_{weld} =$	6	in	weld =	5 x 1/16 in	(fillet)
$\phi R_n =$	83.51	kip	OK		
Brace Block Shear					
$t_{brace} =$	0.465	in			
$L_{req} =$	8.02	in	OK		
$L_{use} =$	12	in			
Brace to Gusset Plate Weld					
$L_{weld} =$	12	in			
weld =	6	x 1/16 in	(fillet)		
$\phi_b =$	0.75	-			



$F_{cxx} =$	70	ksi	
$F_w =$	42	ksi	
$\phi_b R_n =$	400.87	kip	OK
Gusset Plate Block Shear			
$A_{gv} =$	18	in <sup>2</sup>	
$A_{nt} =$	4.31	in <sup>2</sup>	
$U_{bs} =$	1	-	
$\phi =$	0.75	-	
$\phi R_n =$	615.23	kip	OK
Whitmore Effective Width			
$L_{whitmore} =$	21.59	in	(theoretical width)
$\phi =$	0.90	-	
$\phi R_n =$	728.61	kip	OK (check gross yield)

Title	TCBF-B-2 Specimen Design Calculation Sheet		Date	May 27, 2009	
1F	Brace to Gusset Plate Connection		Page	5	
Brace	HSS6x.500				
$R_y F_y A_g =$	475.692	kip	$(T_u)$		
$F_u A_g =$	469.22	kip	$(P_u)$	$T_u/P_u =$	1.01 -
$R_y F_y =$	58.8	ksi			
$R_t F_u =$	75.4	ksi			
$U =$	0.9	-			
$\phi_t =$	0.75	( tensile rupture in net section )			
$A_n/A_g =$	1.16	( Net section reinforcement required! )			
$\phi_t =$	0.90	( tensile yield in gross section )			
$t_{gusset} =$	0.88	in	(estimated)	$F_y =$	50 ksi
$t_g =$	0.75	in	(use)		(gusset plate)
				$F_u =$	65 ksi
$A_{cut} =$	0.81	in <sup>2</sup>			
$A_{net} =$	7.28	in <sup>2</sup>			
$A_e =$	8.41	in <sup>2</sup>	(reinforcement required)		
Reinforcement Plates					
$l =$	14	in	Section	HSS7x.500	
$x_{bar} =$	2.23	in	OD =	7 in	ID = 6 in
$U =$	0.84	-	$A_{e, req} =$	8.41 in <sup>2</sup>	$A_{net, req} =$ 10.00 in <sup>2</sup>
$A_{reinf} =$	1.36	in <sup>2</sup>	(both sides)		
$b_{reinf} =$	2.73	in	$c_{reinf} =$	2.66 in	
$t_{req} =$	0.50	in	$t_{use} =$	2.75 in	$L_{plate} =$ 16 in
$F_{y, plate} =$	42	ksi	$R_y F_y A_g =$	80.85 kip	
$L_{weld} =$	7	in	weld =	5 x 1/16 in	(fillet)
$\phi R_n =$	97.43	kip	OK		
Brace Block Shear					
$t_{brace} =$	0.465	in			
$L_{req} =$	9.80	in	OK		
$L_{use} =$	14	in			
Brace to Gusset Plate Weld					
$L_{weld} =$	14	in			
weld =	7	x 1/16 in	(fillet)		
$\phi_b =$	0.75	-			

$F_{cxx} =$	70	ksi	
$F_w =$	42	ksi	
$\phi_b R_n =$	545.63	kip	OK
Gusset Plate Block Shear			
$A_{gv} =$	21	in <sup>2</sup>	
$A_{nt} =$	5.16	in <sup>2</sup>	
$U_{bs} =$	1	-	
$\phi =$	0.75	-	
$\phi R_n =$	723.87	kip	OK
Whitmore Effective Width			
$L_{whitmore} =$	24.90	in	(theoretical width)
$\phi =$	0.90	-	
$\phi R_n =$	840.30	kip	OK (check gross yield)

Title	TCBF-B-2 Specimen Design Calculation Sheet		Date	May 27, 2009	
2F	Roof Beam Design Check		Page	6	
$R_y F_y A_g =$	389.26	kip	$\theta =$	0.73	(rad) 42.0 (deg)
$0.3 P_n =$	66.74	kip	$\sin(\theta) =$	0.67	
			$\cos(\theta) =$	0.74	
$V =$	215.75	kip			
$H =$	338.94	kip			
$P_u =$	600.00	kip	(conservatively)		
$M_u =$	88.57	kip-ft	(revised from structural analysis)		
Try	w24x117				
$A_g =$	34.4	in <sup>2</sup>	$b_f =$	12.8	in
$I_x =$	3540	in <sup>4</sup>	$t_f =$	0.85	in
$I_y =$	297	in <sup>4</sup>	$d =$	24.3	in
$r_x =$	10.1	in	$t_w =$	0.55	in
$r_y =$	2.94	in	$F_y =$	50	ksi
$\lambda_{p1} =$	9.15		$b/t =$	7.53	Compact
$\lambda_{p2} =$	90.55		$h/t_w =$	41.09	Compact
$L_p =$	10.38	ft	$Z_x =$	327	in <sup>3</sup>
$c =$	1	-	$J =$	6.72	in <sup>4</sup>
$C_w =$	40800	in <sup>6</sup>	$h_o =$	23.45	in
$S_x =$	291	in <sup>3</sup>	$r_{ts} =$	3.46	in
$L_r =$	29.90	ft	Brace PT=	2	-
$L_b =$	10	ft	$C_b =$	1.0	(Conservatively)
$M_p =$	1362.5	kip-ft	$F_{cr} =$	248.50	ksi
$\phi_b =$	0.90	-	$M_n =$	1362.50	kip-ft (Need Check)
$\phi_b M_n =$	1226.25	kip-ft			
$kl/r =$	40.82	-	$k =$	1.0	-
$F_e =$	171.79	ksi	$0.44 F_y =$	22	ksi
$\phi_c =$	0.90	-			
$\phi_c P_n =$	1370.46	kip			
$P_u / \phi_c P_n =$	0.44	use (H1-1a)			
Check	0.50	OK			

Title	TCBF-B-2 Specimen Design Calculation Sheet			Date	May 27, 2009		
1F	Lower Beam Design Check			Page	7		
$R_y F_y A_g =$	475.69	kip	(1F)				
$R_y F_y A_g =$	389.26	kip	(2F)	$\theta =$	0.73	(rad)	42.0 (deg)
$0.3 P_n =$	84.59	kip	(1F)	$\sin(\theta) =$	0.67		
$0.3 P_n =$	66.74	kip	(2F)	$\cos(\theta) =$	0.74		
$V =$	273.57	kip					
$H =$	303.97	kip					
$P_u =$	303.97	kip	(conservatively)				
$M_u =$	159.45	kip-ft	(revised from structural analysis)				
Try	w24x68						
$A_g =$	20.1	in <sup>2</sup>		$b_f =$	8.97	in	
$I_x =$	1830	in <sup>4</sup>		$t_f =$	0.585	in	
$I_y =$	70.4	in <sup>4</sup>		$d =$	23.7	in	
$r_x =$	9.55	in		$t_w =$	0.415	in	
$r_y =$	1.87	in		$F_y =$	50	ksi	
$\lambda_{p1} =$	9.15			$b/t =$	7.67	Compact	
$\lambda_{p2} =$	90.55			$h/t_w =$	54.29	Compact	
$L_p =$	6.61	ft		$Z_x =$	177	in <sup>3</sup>	
$c =$	1	-		$J =$	1.87	in <sup>4</sup>	
$C_w =$	9430	in <sup>6</sup>		$h_o =$	23.12	in	
$S_x =$	154	in <sup>3</sup>		$r_{ts} =$	2.30	in	
$L_r =$	18.74	ft		Brace PT =	2	-	
$L_b =$	10	ft		$C_b =$	1.0	(Conservatively)	
$M_p =$	737.5	kip-ft		$F_{cr} =$	110.86	ksi	
$\phi_b =$	0.90	-		$M_n =$	656.87	kip-ft	OK
$\phi_b M_n =$	591.18	kip-ft					
$kl/r =$	64.17	-		$k =$	1.0	-	
$F_e =$	69.50	ksi		$0.44 F_y =$	22	ksi	
$\phi_c =$	0.90	-					
$\phi_c P_n =$	669.33	kip					
$P_u / \phi_c P_n =$	0.45	use (H1-1a)					
Check	0.69	OK					

Title	TCBF-B-2 Specimen Design Calculation Sheet		Date	May 27, 2009
2F	Column Design Check		Page	8
$P_u =$	43.94	kip	(revised from structural analysis)	
$M_u =$	110.65	kip-ft	(revised from structural analysis)	
$L_{column} =$	9	ft		
Try	w12x96			
$A_g =$	28.2	in <sup>2</sup>	$b_f =$	12.2 in
$I_x =$	833	in <sup>4</sup>	$t_f =$	0.9 in
$I_y =$	270	in <sup>4</sup>	$d =$	12.7 in
$r_x =$	5.44	in	$t_w =$	0.55 in
$r_y =$	3.09	in	$F_y =$	50 ksi
$\lambda_{p1} =$	7.22	-	$b/t =$	6.78 Compact
$\lambda_{p2} =$	71.59	-	$h/t_w =$	19.82 Compact
$L_p =$	10.91	ft	$Z_x =$	147 in <sup>3</sup>
$c =$	1	-	$J =$	6.85 in <sup>4</sup>
$C_w =$	9410	in <sup>6</sup>	$h_o =$	11.80 in
$S_x =$	131	in <sup>3</sup>	$r_{ts} =$	3.49 in
$L_r =$	40.86	ft	Brace PT=	0 -
$L_b =$	9	ft	$C_b =$	1.0 (Conservatively)
$M_p =$	612.5	kip-ft	$F_{cr} =$	344.49 ksi
$\phi_b =$	0.90	-	$M_n =$	612.50 kip-ft (Need Check)
$\phi_b M_n =$	551.25	kip-ft	$C_a =$	0.03 -
$kl/r =$	34.95	-	$k =$	1.0 -
$F_e =$	234.28	ksi	$0.44 F_y =$	22 ksi
$\phi_c =$	0.90	-		
$\phi_c P_n =$	1160.56	kip		
$P_u/\phi_c P_n =$	0.04	use (H1-1b)		
Check	0.22	OK		

Title	TCBF-B-2 Specimen Design Calculation Sheet		Date	May 27, 2009
1F	Column Design Check		Page	9
$P_u =$	493.82	kip	(revised from structural analysis)	
$M_u =$	263.05	kip-ft	(revised from structural analysis)	
$L_{column} =$	9	ft		
Try	w12x96			
$A_g =$	28.2	in <sup>2</sup>	$b_f =$	12.2 in
$I_x =$	833	in <sup>4</sup>	$t_f =$	0.9 in
$I_y =$	270	in <sup>4</sup>	$d =$	12.7 in
$r_x =$	5.44	in	$t_w =$	0.55 in
$r_y =$	3.09	in	$F_y =$	50 ksi
$\lambda_{p1} =$	7.22	-	$b/t =$	6.78 Compact
$\lambda_{p2} =$	52.35	-	$h/t_w =$	19.82 Compact
$L_p =$	10.91	ft	$Z_x =$	147 in <sup>3</sup>
$c =$	1	-	$J =$	6.85 in <sup>4</sup>
$C_w =$	9410	in <sup>6</sup>	$h_o =$	11.80 in
$S_x =$	131	in <sup>3</sup>	$r_{ts} =$	3.49 in
$L_r =$	40.86	ft	Brace PT=	0 -
$L_b =$	9	ft	$C_b =$	1.0 (Conservatively)
$M_p =$	612.5	kip-ft	$F_{cr} =$	344.49 ksi
$\phi_b =$	0.90	-	$M_n =$	612.50 kip-ft (Need Check)
$\phi_b M_n =$	551.25	kip-ft	$C_a =$	0.39 -
$kl/r =$	34.95	-	$k =$	1.0 -
$F_e =$	234.28	ksi	$0.44 F_y =$	22 ksi
$\phi_c =$	0.90	-		
$\phi_c P_n =$	1160.56	kip		
$P_u/\phi_c P_n =$	0.43	use (H1-1a)		
Check	0.85	OK		

Check Column Web Shear Stress

$M_p =$	7350	kip-in	
$L =$	96.15	in	
$V =$	152.89	kip	
$A_s =$	6.99	in <sup>2</sup>	$A_s = d*tw$
$S_v =$	21.89	ksi	
$S_{v, yield} =$	29.00	ksi	Elastic



Title	TCBF-B-2 Specimen Design Calculation Sheet		Date	May 27, 2009				
2F	Beam-Column Connection		Page	10				
Type	Bolted (WUF-B)							
H =	169.47	kip						
V =	107.88	kip						
M =	88.57	kip-ft (revised from structural analysis)						
$R_u =$	200.89	kip	$F_u =$	150	ksi			
Try $d_b =$	0.88	in	$F_{nv} =$	75	ksi (threads excluded)			
$A_b =$	0.60	in <sup>2</sup>	$N_b =$	6	bolts (in one row)			
$R_n =$	270.59	kip (bolt shear)	$L_{c\_ex} =$	1.5	in			
$\phi_b =$	0.75	-	$L_{c\_in} =$	3	in			
$\phi_b R_n =$	202.94	kip	OK					
$L_{c1} =$	1.03	in (edge clear distance)	$R_{n1} =$	46.41	kip			
$L_{c2} =$	2.06	in (clear distance)	$R_{n2} =$	236.25	kip			
t =	0.50	in (shear tab thickness)						
$R_n =$	1227.66	kip (combined bolt bearing)						
$\phi_b =$	0.75	-						
$\phi_b R_n =$	920.74	kip	OK					
$L_{tab} =$	18	in	$A_{s, tab} =$	9	in <sup>2</sup>	$R_n =$	524.79	kip
$w_{tab} =$	4.5	in	$F_{y, tab} =$	50	ksi	$P_{nt} =$	450.00	kip
			$F_{v, tab} =$	30.0	ksi	$P_{nv} =$	270.00	kip
			OK					
Weld	Fillet (shear tab)							
$F_{exx} =$	70	ksi	$R_n =$	334.06	kip			
$F_w =$	42	ksi	$\phi_b =$	0.75	-			
w =	5	x 1/16 inch	$\phi_b R_n =$	250.54	kip	OK		
$L_{weld} =$	18	in						
side =	2	sides						
Weld	CJP (top, bottom flanges)							
$b_f =$	12.8	in	$F_{y, bm} =$	50	ksi (base metal)			
$t_f =$	0.85	in	$M_n =$	1063.07	kip-ft	OK		
d =	24.3	in						
$t_w =$	0.55	in						

Check	Shear tab length, OK	
Check Block Shear		
Beam		
w24x117		
$A_{gv} =$	9.9	in <sup>2</sup>
$A_{gt} =$	1.925	in <sup>2</sup>
$A_{nv} =$	6.6	in <sup>2</sup>
$A_{nt} =$	1.65	in <sup>2</sup>
$U_{bs} =$	0.5	-
$\phi =$	0.75	-
$F_y =$	50	ksi
$F_u =$	65	ksi
$\phi R_n =$	233.27	kip
		OK
Shear Tab		
$A_{gv} =$	8.25	in <sup>2</sup>
$A_{gt} =$	1.5	in <sup>2</sup>
$A_{nv} =$	5.5	in <sup>2</sup>
$A_{nt} =$	1.25	in <sup>2</sup>
$U_{bs} =$	0.5	-
$\phi =$	0.75	-
$F_y =$	50	ksi
$F_u =$	65	ksi
$\phi R_n =$	191.34	kip
		NG!

Title	TCBF-B-2 Specimen Design Calculation Sheet		Date	May 27, 2009
2F	Braces to Beam Connection		Page	11
Braces	HSS5x.500			
T =	389.26	kip	$\sin(\theta) =$	0.669
C =	342.61	kip	$\cos(\theta) =$	0.743
e =	12.15	in		
Shear =	543.99	kip		
Tension =	197.89	kip		
Moment =	550.79	kip-ft		
$t_{\text{gusset}} =$	0.75	in		
L =	60	in		
$s_V =$	12.09	ksi		
$s_A =$	4.40	ksi		
$s_M =$	14.69	ksi		
$\phi =$	0.9	-		
$F_{y, \text{gusset}} =$	50	ksi		
Ratio =	0.63	OK		
$L_{\text{whitmore}} =$	21.59	in	$L_{\text{min}} =$	59.27 in (geometry limit) OK
$L_v =$	16	in	$L_{v, \text{min}} =$	16.05 in (geometry limit) NG!
$w_{\text{up}} =$	10.79	in	$A_v =$	12 in <sup>2</sup>
$w_{\text{low}} =$	20.92	in	$P_u =$	260.40 kip
$\text{Whitm}_{\text{eff}} =$	21.59	in	$\phi R_n =$	324 kip OK
$\phi R_n =$	728.61	kip	OK	
Gusset Plate to Beam Flange				
Weld	Fillet			
$F_{\text{exx}} =$	70	ksi		
$F_w =$	42	ksi	$s_V =$	12.82 ksi
w =	8	x 1/16 inch	$s_M =$	15.58 ksi
$L_{\text{weld}} =$	60	in	$s_A =$	4.67 ksi
side =	2	sides	$f_{\text{peak}} =$	23.97 ksi
$t_{\text{eff}} =$	0.354	in	$f_{\text{avg}} =$	20.40 ksi
$\phi =$	0.75	-	$f_r =$	25.50 ksi
Ratio =	0.86	OK	Ratio =	0.81 OK
Check Beam Web				
width =	60	in	Beam	w24x117

$R_u = 220.32$	kip	$d = 24.3$	in	$t_w = 0.55$	in
$N = 30$	in	$t_f = 0.85$	in	$F_{y, web} = 50$	ksi
$\phi = 0.75$	-	$R_n = 1060.63$	kip	$\phi R_n = 795.47$	kip
$k_{des} = 1.35$	in			(web crippling)	OK
$\phi = 1.00$	-	$R_n = 1010.63$	kip	$\phi R_n = 1010.63$	kip
				(web local yielding)	OK
Check Gusset Plate Buckling					
$L_{gb} = 17.68$	in	$kL/r = 98.0$	-	$L_c = 14.13$	in
$k = 1.2$	-	$F_e = 29.82$	ksi	$L_{c1} = 11.38$	in
$r = 0.217$	in	$0.44 F_y = 22$	ksi	$L_{c2} = 16.94$	in
$A_g = 16.19$	in <sup>2</sup>	$R_n = 401.31$	kip	$L_{max} = 24.06$	in
$\phi = 0.9$	-	$\phi R_n = 361.18$	kip	$L_{tip} = 21.88$	in
			OK	$L_{ave} = 17.68$	in
Free Edge Buckling					
$L_e = 15.63$	in				
$L_e/t_g = 20.83$	-				
Limit = 18.06	-	Edge stiffener required!			
Lateral Stability of Beam					
$M_r = 1498.75$	kip-ft	$Z = 327$	in <sup>3</sup>	$L_b = 10$	ft
$C_d = 1$	-	$h_o = 23.45$	in	$L_{pd} = 17.05$	ft
$P_{br} = 15.34$	kip	$\beta_{br} = 85.22$	kip/in	$n = 1$	OK
(Nodal)		(Nodal)		$C_b = 1$	-
$M_{br} = 17.985$	kip-ft				
$P_{br} = 9.20$	kip	(torsional)			
$\beta_T = 28842$	kip-in/rad	$\beta_{sec}$ not included			
$\beta_{br} = 52.45$	kip/in	(torsional)			
$\Delta = 0.18$	in				
Kicker					
L3x2x3/8					
$A_g = 1.73$	in <sup>2</sup>				
$L = 25$	in				
$k_{axial} = 2006.8$	kip/in				
$k = 1419$	kip/in	OK			

Title	TCBF-B-2 Specimen Design Calculation Sheet		Date	May 27, 2009	
1F	Beam-Column-Gusset Connections		Page	12	
Big Gusset Plate for Upper Floor Bracing and Lower Floor Bracing					
Sway to Right					
$F_{U2R} = 389.26$ kip $F_{L2R} = 434.24$ kip	$\cos(\theta_U) = 0.743$ $\cos(\theta_L) = 0.743$				
Sway to Left					
$F_{U2L} = 342.61$ kip $F_{L2L} = 475.69$ kip Beam w24x68 $d = 23.7$ in $L_{c, \min} = 58.25$ in Column w12x96 $e_c = 6.35$ in $R_{beam} = 21.32$ kip (downward) $L_{b, \min} = 16.66$ in $L_{cu, \min} = 16.05$ in $L_{cl, \min} = 18.51$ in $t_g = 0.75$ in $L_{cu} = 18$ in (use) $L_{cl} = 18$ in (use) $L_c = 59.7$ in (use) $L_b = 23$ in (use)	$F_{y, gusset} = 50$ ksi				
Sway to the Right					
$V_{U2R} = 260.40$ kip (upward) $H_{U2R} = 289.33$ kip (rightward) $V_{L2R} = 290.49$ kip (upward) $H_{L2R} = 322.77$ kip (leftward) $V_{total} = 529.57$ kip (upward) $M = 280.23$ kip-ft (counter-clockwise)	$s_V = 11.83$ ksi $s_M = 7.55$ ksi $s_A = 0.75$ ksi Ratio = 0.49 - OK				
Column-Side					
$V_{cu} = 159.67$ kip (downward) $f_1 = 5.66$ kip/in (leftward) $f_2 = 2.25$ kip/in (leftward) $H_{cu} = 71.18$ kip (leftward)	$s_A = 5.27$ ksi $s_V = 11.83$ ksi $s_M = 2.28$ ksi Ratio = 0.49 - OK				
Beam-Side					
$H_{bu} = 218.16$ kip (leftward) $V_{bu} = 100.73$ kip (downward) $M_{cu} = 7.68$ kip-ft (counter-clockwise)	$s_A = 5.84$ ksi $s_V = 12.65$ ksi				

$M_{bu} = -112.45$	kip-ft	(clockwise)	$s_M = -20.41$	ksi	
			Ratio = 0.58	-	OK
$V_{cl} = 159.67$	kip	(downward)	$s_A = 5.27$	ksi	
$f_1 = 5.66$	kip/in	(rightward)	$s_V = 11.83$	ksi	
$f_3 = 2.25$	kip/in	(rightward)	$s_M = 2.28$	ksi	
$H_{cl} = 71.18$	kip	(rightward)	Ratio = 0.49	-	OK
$H_{bl} = 251.59$	kip	(rightward)			
$V_{bl} = 130.82$	kip	(downward)	$s_A = 7.58$	ksi	
$M_{bl} = 100.71$	kip-ft	(clockwise)	$s_V = 14.58$	ksi	
$M_{cl} = 7.68$	kip-ft	(counter-clockwise)	$s_M = 18.28$	ksi	
			Ratio = 0.80	-	OK
$V_{mid} = 161.44$	kip	(downward)	$s_A = 0.00$	ksi	
$M_{mid} = 10.34$	kip-ft	(counter-clockwise)	$s_V = 9.08$	ksi	
$H_{mid} = 0.00$	kip	(leftward)	$s_M = 1.77$	ksi	
			Ratio = 0.35	-	OK
Weld Size					
$f_v = 8.87$	kip/in				
$f_a = 5.13$	kip/in	(averaged)			
$f_b = 5.66$	kip/in				
$f_{peak} = 13.97$	kip/in				
$f_{avg} = 11.43$	kip/in				
$f_r = 14.28$	kip/in	14.283			
D >=	5.13	x 1/16	(weld size)		
Use	6	x 1/16	(weld size)		

Title	TCBF-B-2 Specimen Design Calculation Sheet		Date	May 27, 2009	
1F	Lower Beam to Gusset Plate Splice		Page	13	
Web	Fillet welds with web plates				
Flange	CJP weld (T & B)				
$P_u =$	303.97	kip			
$t_f =$	0.59	in			
$b =$	8.97	in			
$A_s =$	5.25	in <sup>2</sup>			
$2 * A_s * F_y =$	524.75	kip	OK		
$R_{beam} =$	21.32	kip	(Gravity)		
$L_{tab} =$	20.375	in	$t =$	0.5	in
$w_{tab} =$	8	in			
Weld	Fillet (shear tab)				
$F_{exx} =$	70	ksi	$R_n =$	315.96	kip
$F_w =$	42	ksi	$\phi_b =$	0.75	-
$w =$	6	x 1/16 inch	$\phi_b R_n =$	236.97	kip OK
$L_{weld} =$	28.375	in			
side =	1	sides			
Shim Plate					
$L =$	20	in	$t =$	0.168	in (shim as required)
$w =$	4	in			
Weld	Fillet (shear tab)				
$F_{exx} =$	70	ksi	$R_n =$	139.26	kip
$F_w =$	42	ksi	$\phi_b =$	0.75	-
$w =$	2.68	x 1/16 inch	$\phi_b R_n =$	104.45	kip OK
$L_{weld} =$	28	in (3 sides)			
side =	1	sides			

Title	TCBF-B-2 Specimen Design Calculation Sheet		Date	May 27, 2009
1F	Braces to Floor Beam Connection		Page	14
Braces	HSS6x.500			
T =	475.69	kip	$\sin(\theta) =$	0.669
C =	434.24	kip	$\cos(\theta) =$	0.743
e =	0	in		
Shear =	676.34	kip		
Tension =	239.00	kip		
Moment =	0.00	kip-ft		
$t_{gusset} =$	0.75	in		
L =	46	in		
$s_V =$	19.60	ksi		
$s_M =$	0.00	ksi		
$\phi =$	0.9	-		
$F_{y, gusset} =$	50	ksi		
Ratio =	0.77	OK		
whitmo =	24.90	in	$L_{min} =$	37.22 in (geometry limit) OK
$L_v =$	19	in	$L_{v, min} =$	18.51 in (geometry limit) OK
$w_{up} =$	12.45	in	$A_v =$	14.25 in <sup>2</sup>
$w_{low} =$	14.12	in	$P_u =$	318.22 kip
whit <sub>eff</sub> =	24.90	in	$\phi R_n =$	384.75 kip
$\phi R_n =$	840.30	kip	OK	OK
Weld	Fillet	(Gusset to beam flange)		
$F_{exx} =$	70	ksi		
$F_w =$	42	ksi		
w =	11	x 1/16 inch	$s_V =$	15.12 ksi
$L_{weld} =$	46	in	$s_M =$	0.00 ksi
side =	2	sides	$s_A =$	5.34 ksi
$t_{eff} =$	0.486	in		
$\phi =$	0.75	-		
Ratio =	0.85	OK		
Check Beam Web				
width =	46	in	Beam	w30x391
$R_u =$	0.00	kip	d =	33.2 in $t_w =$ 1.36 in



$N =$	23	in	$t_f =$	2.44	in	$F_{y, web} =$	50	ksi
$\phi =$	0.75	-	$R_n =$	4450.60	kip	$\phi R_n =$	3337.95	kip
$k_{des} =$	3.23	in				(web crippling)		OK
$\phi =$	1.00	-	$R_n =$	2662.20	kip	$\phi R_n =$	2662.20	kip
						(web local yielding)		OK
Check Gusset Plate Buckling								
$L_{gb} =$	14.84	in	$kL/r =$	82.2	-	$L_c =$	15.88	in
$k =$	1.2	-	$F_e =$	42.32	ksi	$L_{c1} =$	18.06	in
$r =$	0.217	in	$0.44 F_y =$	22	ksi	$L_{c2} =$	12.56	in
$A_g =$	18.67	in <sup>2</sup>	$R_n =$	569.41	kip	$L_{max} =$	18.56	in
$\phi =$	0.9	-	$\phi R_n =$	512.47	kip	$L_{tip} =$	9.13	in
					OK	$L_{ave} =$	14.84	in
Free Edge Buckling								
$L_e =$	17.88	in						
$L_e/t_g =$	23.83	-						
Limit =	18.06	-	Edge stiffener required!					
Lateral Stability of Beam								
$M_r =$	6645.83	kip-ft	$Z =$	1450	in <sup>3</sup>	$L_b =$	10	ft
$C_d =$	1	-	$h_o =$	30.76	in	$L_{pd} =$	17.05	ft
$P_{br} =$	51.85	kip	$\beta_{br} =$	288.07	kip/in	$n =$	1	OK
(Nodal)			(Nodal)			$C_b =$	1	-
$M_{br} =$	79.75	kip-ft				$I_y =$	1550	in <sup>4</sup>
$P_{br} =$	31.11	kip	(torsional)					
$\beta_T =$	108666	kip-in/rad	$\beta_{sec}$ not included					
$\beta_{br} =$	114.85	kip/in	(torsional)					
$\Delta =$	0.27	in						

Title	TCBF-B-2 Specimen Design Calculation Sheet		Date	May 27, 2009
1F	Column Base Plate Design Check		Page	15
Column	w12x96			
$Z_x =$	147	in <sup>3</sup>	$L =$	96.15 in
$F_y =$	50	ksi	$V_{Mp} =$	152.89 kip
$M_p =$	7350	kip-in		
$P_u =$	493.82	kip	$d =$	12.7 in
$M_u =$	3156.6	kip-in	$b_f =$	12.2 in
$N =$	31.25	in	$f_{p, max} =$	36 ksi
$B =$	28	in		
$e =$	6.39	in	$q_{max} =$	1008 kip/in
$e_{cr} =$	15.38	in	(Small Moment)	
$Y =$	18.47	in		
$q =$	26.74	kip/in	OK	
$m =$	9.59	in		
$f_p =$	0.96	ksi		
$t_{p, req} =$	1.99	in	eq 3.3.14a (LRFD)	
use =	2.00	in		
All-thread-rods				
Type	ASTM A193 B7			
$d_{bolt} =$	1.125	in		
$F_u =$	125	ksi		
$F_y =$	105	ksi		
$F_{nt} =$	93.75	ksi		
$F_{nv} =$	50	ksi		
$A_b =$	0.99	in <sup>2</sup>		
$\phi =$	0.75	-		
$\phi R_n =$	69.89	kip	(tension)	
$\phi R_n =$	37.28	kip	(shear)	
$F_{PT} =$	86.98	kip	(minimum required pretension)	
$V_u =$	152.89	kip	(very conservative assumption)	
$M_u =$	7350	kip-in	(very conservative assumption)	
$P_u =$	600	kip	(very conservative assumption)	
$\mu =$	0.35	-	(class A surface)	
SF =	2	-	(safety factor for not having enough bolt pretension force)	

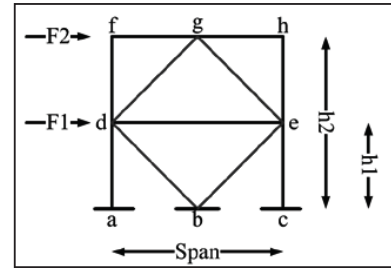
$N_V =$	10	bolts	(for friction shear)
$N_M =$	17	bolts	(for bending)
$N_T =$	9	bolts	(for uplifting)
$N_{\text{req, total}} =$	35	bolts	
use =	34	bolts	

Title	TCBF-B-2 Specimen Design Calculation Sheet			Date	May 27, 2009
2F	Stub Beam			Page	16
F1 =	300	kip	d =	24.3	in
F2 =	600	kip	t <sub>w</sub> =	0.55	in
L <sub>stub</sub> =	19	in	b =	12.8	in
Beam	w24x117		t <sub>f</sub> =	0.85	in
Column Dimension List					
Column	w12x96				
A <sub>g</sub> =	28.2	in <sup>2</sup>	b <sub>f</sub> =	12.2	in
I <sub>x</sub> =	833	in <sup>4</sup>	t <sub>f</sub> =	0.9	in
I <sub>y</sub> =	270	in <sup>4</sup>	d =	12.7	in
r <sub>x</sub> =	5.44	in	t <sub>w</sub> =	0.55	in
r <sub>y</sub> =	3.09	in	F <sub>y</sub> =	50	ksi
k <sub>des</sub> =	1.5	in	E <sub>s</sub> =	29000	ksi
Column Web Local Yielding					
N =	24.00	in			
R <sub>n</sub> =	866.25	kip			
φ =	1.00	-			
φR <sub>n</sub> =	866.25	kip	OK		
Column Web Crippling					
R <sub>n</sub> =	1382.366	kip			
φ =	0.75	-			
φR <sub>n</sub> =	1036.77	kip	OK		
Column Flange Local Bending					
R <sub>n</sub> =	253.13	kip	A <sub>web</sub> =	12.43	in <sup>2</sup>
			A <sub>s</sub> =	34.19	in <sup>2</sup>
φ =	0.90	-	A <sub>flange</sub> =	21.76	in <sup>2</sup>
φR <sub>n</sub> =	227.81	kip	F1 <sub>flange</sub> =	190.93	kip
			F2 <sub>flange</sub> =	381.87	kip
					Continue Plate Required!
Stub Beam Gross Yielding					
A <sub>s (beam)</sub> =	34.4	in <sup>2</sup>			
P <sub>y</sub> =	1720	kip	OK		

Title	TCBF-B-2 Specimen Design Calculation Sheet			Date	May 27, 2009
1F	Stub Beam			Page	17
$F_1 =$	300	kip	$d =$	23.7	in
$F_2 =$	600	kip	$t_w =$	0.415	in
$L_{stub} =$	19	in	$b =$	8.97	in
Beam	w24x68		$t_f =$	0.585	in
Column Dimension List					
Column	w12x96				
$A_g =$	28.2	in <sup>2</sup>	$b_f =$	12.2	in
$I_x =$	833	in <sup>4</sup>	$t_f =$	0.9	in
$I_y =$	270	in <sup>4</sup>	$d =$	12.7	in
$r_x =$	5.44	in	$t_w =$	0.55	in
$r_y =$	3.09	in	$F_y =$	50	ksi
$k_{des} =$	1.5	in	$E_s =$	29000	ksi
Column Web Local Yielding					
$N =$	24.00	in			
$R_n =$	866.25	kip			
$\phi =$	1.00	-			
$\phi R_n =$	866.25	kip	OK		
Column Web Crippling					
$R_n =$	1382.366	kip			
$\phi =$	0.75	-			
$\phi R_n =$	1036.77	kip	OK		
Column Flange Local Bending					
$R_n =$	253.13	kip	$A_{web} =$	9.35	in <sup>2</sup>
$\phi =$	0.90	-	$A_{flange} =$	10.49	in <sup>2</sup>
$\phi R_n =$	227.81	kip	$F1_{flange} =$	158.65	kip
			$F2_{flange} =$	317.31	kip
					OK
Stub Beam Gross Yielding					
$A_{s (beam)} =$	20.1	in <sup>2</sup>			
$P_y =$	1005	kip	OK		

Title	TCBF-B-3 Specimen Design Calculation Sheet	Date	May 28, 2009
General		Page	1

Building height = 2 stories  
 Typical floor height = 9 ft  
 $F_{1, \max} = 300$  kip  
 $F_{2, \max} = 600$  kip  
 SR = 4 -  
 ratio = 0.8 -



#### Calculation Initialize

Items	values	units	Items	values	units
$F_1$	240	kip	$V_1$	720	kip
$F_2$	480	kip	$V_2$	480	kip
$h_1$	9	ft			
$h_2$	18	ft			
span	20	ft			(beam span)
$h$	9	ft			(typical floor height)
$M_{\text{base}}$	13500	kip-ft			
$P_{\text{column}}$	675	kip			
$L_{\text{brace}}$	13.45	ft			(work point to work point)
$E_s$	29000	ksi			

#### Notes

: input value

#### Materials

Members	Material Type	Fy (ksi)	Fu (ksi)	Ry	Rt	
Columns	ASTM A992	50	65	1.1	1.1	(Ref: Table I-6-1)  (Wide Flange)
Beams	ASTM A992	50	65	1.1	1.1	
Braces	ASTM A992	50	65	1.1	1.1	
Plates 1	ASTM A36	36	58	1.3	1.2	
Bolts	A490	130	150	-	-	
Welds	E70XX	-	70	-	-	
Plates 2	ASTM A572 Gr.50	50	65	1.1	1.2	

#### Load Combinations

Per ASCE-7-2005

#### Basic Reference Codes

AISC Specification for Structural Steel Buildings (March 9, 2005)  
 AISC Seismic Provisions for Structural Steel Buildings (March 9, 2005)

Title	TCBF-B-3 Specimen Design Calculation Sheet		Date	May 28, 2009
2F-Brace			Page	2
$P_u =$	139.67	kip (compression)		
$L_{brace} =$	8.1	ft		
$k =$	1.0	-		
Try section	W8x21	(HSS-Square)		
$A_s =$	6.16	in <sup>2</sup>	$I_x =$	75.30 in <sup>4</sup>
$Z_x =$	20.40	in <sup>3</sup>	$I_y =$	75.30 in <sup>4</sup>
$b_f =$	5.27	in	$t_f =$	0.40 in
$d =$	8.28	in	$t_w =$	0.250 in
$r_x =$	3.49	in		
$r_y =$	1.26	in		
$F_y$ (brace) =	50	ksi	$E_s =$	29000 ksi
$kL/r =$	76.98	-	Limit =	96.33 OK
$F_c =$	48.29	ksi	$0.44 F_y =$	22 ksi
$\phi =$	0.90	-		
$\phi P_n =$	179.72	kip (compression)	Check	OK
Check Compactness Seismically (AISC Seismic Provisions 2005, Sec 8.2b)				
$\lambda_{ps} =$	7.22	-	$b_f / 2t =$	6.59 OK
$Ca =$	0.50	-		(Table I-8-1)
$\lambda_{ps} =$	35.88	-	$h / t_w =$	27.50 OK
$\phi =$	0.90	-		
$\phi P_n =$	277.20	kip (tension)	Check	OK

$$Kl/r \leq 4\sqrt{E/F_y}$$

Title	TCBF-B-3 Specimen Design Calculation Sheet		Date	May 28, 2009	
1F-Brace			Page	3	
$P_u =$	254.24	kip (compression)			
$L_{brace} =$	9	ft			
$k =$	1.0	-			
Try section	W8x28	(HSS-Square)			
$A_s =$	8.24	in <sup>2</sup>	$I_x =$	98.00	in <sup>4</sup>
$Z_x =$	27.20	in <sup>3</sup>	$I_y =$	98.00	in <sup>4</sup>
$b =$	6.54	in	$t_f =$	0.47	in
$d =$	8.06	in	$t_w =$	0.285	in
$r_x =$	3.45	in			
$r_y =$	1.62	in			
$F_y$ (brace) =	50	ksi	$E_s =$	29000	ksi
$kL/r =$	66.67	-	Limit =	96.33	OK
$F_c =$	64.40	ksi	$0.44 F_y =$	22	ksi
$\phi =$	0.90	-			
$\phi P_n =$	267.92	kip (compression)	Check	OK	
Check Compactness Seismically (AISC Seismic Provisions 2005, Sec 8.2b)					
$\lambda_{ps} =$	7.22	-	$b_f / 2t =$	7.03	OK
$Ca =$	0.69				(Table I-8-1)
$\lambda_{ps} =$	35.88	-	$h / t_w =$	22.30	OK
$\phi =$	0.90	-			
$\phi P_n =$	370.80	kip (tension)	Check	OK	

$$Kl/r \leq 4\sqrt{E/F_y}$$



Title	TCBF-B-3 Specimen Design Calculation Sheet		Date	May 28, 2009	
2F	Brace to Gusset Plate Connection		Page	4	
Brace	W8x21				
$R_y F_y A_g =$	338.80	kip	$(T_u)$		
$F_u A_g =$	400.40	kip	$(P_u)$	$T_u/P_u =$	0.85 -
$R_y F_y =$	55	ksi			
$R_t F_u =$	71.5	ksi			
$U =$	0.9	-			
$\phi_t =$	0.75	( tensile rupture in net section )			
$A_n/A_g =$	1.14	( Net section reinforcement required! )			
$\phi_t =$	0.90	( tensile yield in gross section )			
$t_{gusset} =$	0.71	in	(estimated)	$F_y =$	50 ksi
$t_g =$	0.75	in	(use)	(gusset plate)	
				$F_u =$	65 ksi
$A_{cut} =$	2.57	in <sup>2</sup>			
$A_{net} =$	3.59	in <sup>2</sup>			
$A_e =$	6.32	in <sup>2</sup>	(Reinforcement required!)		
Reinforcement Plates					
$l =$	12	in	$d =$	8.28	in
$U =$	1.00	-	$A_{e, req} =$	6.32	in <sup>2</sup>
$A_{reinf} =$	1.36	in <sup>2</sup>	(both sides)		$A_{net, req} =$
$b_{reinf} =$	4	in			6.32 in <sup>2</sup>
$t_{req} =$	0.47	in	$t_{use} =$	0.5	in
$F_{y, plate} =$	36	ksi	$R_y F_y A_g =$	93.60	kip
$L_{weld} =$	6	in	weld =	6	x 1/16 in (fillet)
$\phi R_n =$	100.22	kip	OK		
Brace Block Shear					
$t_{brace} =$	0.4	in			
$L_{req} =$	7.24	in	OK		
$L_{use} =$	12	in			
Brace to Gusset Plate Weld					
$L_{weld} =$	12	in			
weld =	6	x 1/16 in	(fillet)		
$\phi_b =$	0.75	-			

$F_{cxx} =$	70	ksi	
$F_w =$	42	ksi	
$\phi_b R_n =$	400.87	kip	OK
Gusset Plate Block Shear			
$A_{gv} =$	18	in <sup>2</sup>	
$A_{nt} =$	6.77	in <sup>2</sup>	
$U_{bs} =$	1	-	
$\phi =$	0.75	-	
$\phi R_n =$	735.16	kip	OK
Whitmore Effective Width			
$L_{whitmore} =$	23.87	in	(theoretical width)
$\phi =$	0.90	-	
$\phi R_n =$	805.56	kip	OK (check gross yield)
Brace Web Block Shear			
$A_{gv} =$	3	in <sup>2</sup>	
$A_{nt} =$	1.19	in <sup>2</sup>	
$U_{bs} =$	1	-	
$\phi =$	0.75	-	
$\phi R_n =$	125.39	kip	OK

Title	TCBF-B-3 Specimen Design Calculation Sheet		Date	May 28, 2009	
1F	Brace to Gusset Plate Connection		Page	5	
Brace	W8x28				
$R_y F_y A_g =$	453.2	kip	$(T_u)$		
$F_u A_g =$	535.6	kip	$(P_u)$	$T_u/P_u =$	0.85 -
$R_y F_y =$	55	ksi			
$R_t F_u =$	71.5	ksi			
$U =$	0.9	-			
$\phi_t =$	0.75	( tensile rupture in net section )			
$A_n/A_g =$	1.14	( Net section reinforcement required! )			
$\phi_t =$	0.90	( tensile yield in gross section )			
$t_{gusset} =$	0.77	in	(estimated)	$F_y =$	50 ksi
$t_g =$	0.75	in	(use)	(gusset plate)	
				$F_u =$	65 ksi
$A_{cut} =$	2.85	in <sup>2</sup>			
$A_{net} =$	5.39	in <sup>2</sup>			
$A_e =$	8.45	in <sup>2</sup>	(reinforcement required)		
Reinforcement Plates					
$l =$	14	in	$d =$	8.06	in
$U =$	1.00	-	$A_{e, req} =$	8.45	in <sup>2</sup>
$A_{reinf} =$	1.53	in <sup>2</sup>	(both sides)		
$b_{reinf} =$	4	in			
$t_{req} =$	0.53	in	$t_{use} =$	0.625	in
$F_{y, plate} =$	36	ksi	$R_y F_y A_g =$	99.00	kip
$L_{weld} =$	7	in	weld =	6	x 1/16 in (fillet)
$\phi R_n =$	116.92	kip	OK		
Brace Block Shear					
$t_{brace} =$	0.465	in			
$L_{req} =$	8.33	in	OK		
$L_{use} =$	14	in			
Brace to Gusset Plate Weld					
$L_{weld} =$	14	in			
weld =	7	x 1/16 in	(fillet)		
$\phi_b =$	0.75	-			

$F_{cxx} =$	70	ksi	
$F_w =$	42	ksi	
$\phi_b R_n =$	545.63	kip	OK
Gusset Plate Block Shear			
$A_{gv} =$	21	in <sup>2</sup>	
$A_{nt} =$	6.70	in <sup>2</sup>	
$U_{bs} =$	1	-	
$\phi =$	0.75	-	
$\phi R_n =$	799.19	kip	OK
Whitmore Effective Width			
$L_{whitmore} =$	25.96	in	(theoretical width)
$\phi =$	0.90	-	
$\phi R_n =$	876.08	kip	OK (check gross yield)
Brace Web Block Shear			
$A_{gv} =$	3.99	in <sup>2</sup>	
$A_{nt} =$	1.35	in <sup>2</sup>	
$U_{bs} =$	1	-	
$\phi =$	0.75	-	
$\phi R_n =$	155.77	kip	OK

Title	TCBF-B-3 Specimen Design Calculation Sheet		Date	May 28, 2009	
2F	Roof Beam Design Check		Page	6	
$R_y F_y A_g =$	338.80	kip	$\theta =$	0.73	(rad) 42.0 (deg)
$0.3 P_n =$	59.91	kip	$\sin(\theta) =$	0.67	
			$\cos(\theta) =$	0.74	
$V =$	186.57	kip			
$H =$	296.36	kip			
$P_u =$	600.00	kip	(conservatively)		
$M_u =$	92.46	kip-ft	(revised from structural analysis)		
Try	w24x117				
$A_g =$	34.4	in <sup>2</sup>	$b_f =$	12.8	in
$I_x =$	3540	in <sup>4</sup>	$t_f =$	0.85	in
$I_y =$	297	in <sup>4</sup>	$d =$	24.3	in
$r_x =$	10.1	in	$t_w =$	0.55	in
$r_y =$	2.94	in	$F_y =$	50	ksi
$\lambda_{p1} =$	9.15		$b/t =$	7.53	Compact
$\lambda_{p2} =$	90.55		$h/t_w =$	41.09	Compact
$L_p =$	10.38	ft	$Z_x =$	327	in <sup>3</sup>
$c =$	1	-	$J =$	6.72	in <sup>4</sup>
$C_w =$	40800	in <sup>6</sup>	$h_o =$	23.45	in
$S_x =$	291	in <sup>3</sup>	$r_{ts} =$	3.46	in
$L_r =$	29.90	ft	Brace PT=	2	-
$L_b =$	10	ft	$C_b =$	1.0	(Conservatively)
$M_p =$	1362.5	kip-ft	$F_{cr} =$	248.50	ksi
$\phi_b =$	0.90	-	$M_n =$	1362.50	kip-ft (Need Check)
$\phi_b M_n =$	1226.25	kip-ft			
$kl/r =$	40.82	-	$k =$	1.0	-
$F_e =$	171.79	ksi	$0.44 F_y =$	22	ksi
$\phi_c =$	0.90	-			
$\phi_c P_n =$	1370.46	kip			
$P_u / \phi_c P_n =$	0.44	use (H1-1a)			
Check	0.50	OK			

Title	TCBF-B-3 Specimen Design Calculation Sheet			Date	May 28, 2009	
1F	Lower Beam Design Check			Page	7	
$R_y F_y A_g =$	453.20	kip	(1F)			
$R_y F_y A_g =$	338.80	kip	(2F)	$\theta =$	0.73	(rad) 42.0 (deg)
$0.3 P_n =$	89.31	kip	(1F)	$\sin(\theta) =$	0.67	
$0.3 P_n =$	59.91	kip	(2F)	$\cos(\theta) =$	0.74	
$V =$	263.10	kip				
$H =$	292.33	kip				
$P_u =$	300.00	kip	(conservatively)			
$M_u =$	160.72	kip-ft	(revised from structural analysis)			
Try	w24x68					
$A_g =$	20.1	in <sup>2</sup>		$b_f =$	8.97	in
$I_x =$	1830	in <sup>4</sup>		$t_f =$	0.585	in
$I_y =$	70.4	in <sup>4</sup>		$d =$	23.7	in
$r_x =$	9.55	in		$t_w =$	0.415	in
$r_y =$	1.87	in		$F_y =$	50	ksi
$\lambda_{p1} =$	9.15			$b/t =$	7.67	Compact
$\lambda_{p2} =$	90.55			$h/t_w =$	54.29	Compact
$L_p =$	6.61	ft		$Z_x =$	177	in <sup>3</sup>
$c =$	1	-		$J =$	1.87	in <sup>4</sup>
$C_w =$	9430	in <sup>6</sup>		$h_o =$	23.12	in
$S_x =$	154	in <sup>3</sup>		$r_{ts} =$	2.30	in
$L_r =$	18.74	ft		Brace PT=	2	-
$L_b =$	10	ft		$C_b =$	1.0	(Conservatively)
$M_p =$	737.5	kip-ft		$F_{cr} =$	110.86	ksi
$\phi_b =$	0.90	-		$M_n =$	656.87	kip-ft
$\phi_b M_n =$	591.18	kip-ft				OK
$kl/r =$	64.17	-		$k =$	1.0	-
$F_e =$	69.50	ksi		$0.44 F_y =$	22	ksi
$\phi_c =$	0.90	-				
$\phi_c P_n =$	669.33	kip				
$P_u / \phi_c P_n =$	0.45	use (H1-1a)				
Check	0.69	OK				

Title	TCBF-B-3 Specimen Design Calculation Sheet		Date	May 28, 2009
2F	Column Design Check		Page	8
$P_u =$	43.55	kip	(revised from structural analysis)	
$M_u =$	115.54	kip-ft	(revised from structural analysis)	
$L_{column} =$	9	ft		
Try	w12x96			
$A_g =$	28.2	in <sup>2</sup>	$b_f =$	12.2 in
$I_x =$	833	in <sup>4</sup>	$t_f =$	0.9 in
$I_y =$	270	in <sup>4</sup>	$d =$	12.7 in
$r_x =$	5.44	in	$t_w =$	0.55 in
$r_y =$	3.09	in	$F_y =$	50 ksi
$\lambda_{p1} =$	7.22	-	$b/t =$	6.78 Compact
$\lambda_{p2} =$	71.62	-	$h/t_w =$	19.82 Compact
$L_p =$	10.91	ft	$Z_x =$	147 in <sup>3</sup>
$c =$	1	-	$J =$	6.85 in <sup>4</sup>
$C_w =$	9410	in <sup>6</sup>	$h_o =$	11.80 in
$S_x =$	131	in <sup>3</sup>	$r_{ts} =$	3.49 in
$L_r =$	40.86	ft	Brace PT=	0 -
$L_b =$	9	ft	$C_b =$	1.0 (Conservatively)
$M_p =$	612.5	kip-ft	$F_{cr} =$	344.49 ksi
$\phi_b =$	0.90	-	$M_n =$	612.50 kip-ft (Need Check)
$\phi_b M_n =$	551.25	kip-ft	$C_a =$	0.03 -
$kl/r =$	34.95	-	$k =$	1.0 -
$F_e =$	234.28	ksi	$0.44 F_y =$	22 ksi
$\phi_c =$	0.90	-		
$\phi_c P_n =$	1160.56	kip		
$P_u/\phi_c P_n =$	0.04	use (H1-1b)		
Check	0.23	OK		

Title	TCBF-B-3 Specimen Design Calculation Sheet		Date	May 28, 2009
1F	Column Design Check		Page	9
$P_u =$	492.31	kip	(revised from structural analysis)	
$M_u =$	259.53	kip-ft	(revised from structural analysis)	
$L_{column} =$	9	ft		
Try	w12x96			
$A_g =$	28.2	in <sup>2</sup>	$b_f =$	12.2 in
$I_x =$	833	in <sup>4</sup>	$t_f =$	0.9 in
$I_y =$	270	in <sup>4</sup>	$d =$	12.7 in
$r_x =$	5.44	in	$t_w =$	0.55 in
$r_y =$	3.09	in	$F_y =$	50 ksi
$\lambda_{p1} =$	7.22	-	$b/t =$	6.78 Compact
$\lambda_{p2} =$	52.38	-	$h/t_w =$	19.82 Compact
$L_p =$	10.91	ft	$Z_x =$	147 in <sup>3</sup>
$c =$	1	-	$J =$	6.85 in <sup>4</sup>
$C_w =$	9410	in <sup>6</sup>	$h_o =$	11.80 in
$S_x =$	131	in <sup>3</sup>	$r_{ts} =$	3.49 in
$L_r =$	40.86	ft	Brace PT=	0 -
$L_b =$	9	ft	$C_b =$	1.0 (Conservatively)
$M_p =$	612.5	kip-ft	$F_{cr} =$	344.49 ksi
$\phi_b =$	0.90	-	$M_n =$	612.50 kip-ft (Need Check)
$\phi_b M_n =$	551.25	kip-ft	$C_a =$	0.39 -
$kl/r =$	34.95	-	$k =$	1.0 -
$F_e =$	234.28	ksi	$0.44 F_y =$	22 ksi
$\phi_c =$	0.90	-		
$\phi_c P_n =$	1160.56	kip		
$P_u/\phi_c P_n =$	0.42	use (H1-1a)		
Check	0.84	OK		



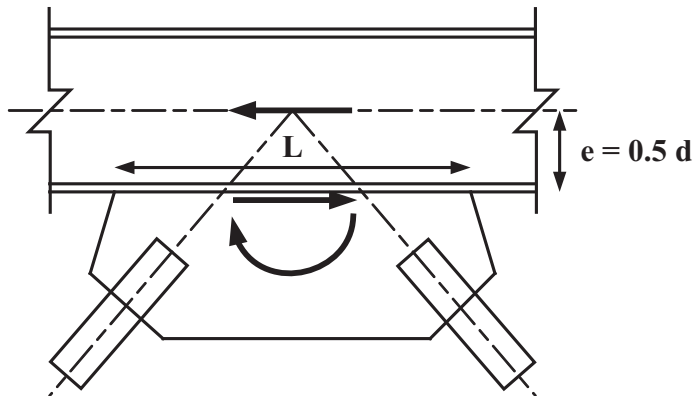
Check Column Web Shear Stress

$M_p =$	7350	kip-in	
$L =$	96.15	in	
$V =$	152.89	kip	
$A_s =$	6.99	in <sup>2</sup>	$A_s = d*tw$
$S_v =$	21.89	ksi	
$S_{v, yield} =$	29.00	ksi	Elastic

Title	TCBF-B-3 Specimen Design Calculation Sheet		Date	May 28, 2009				
2F	Beam-Column Connection		Page	10				
Type	Bolted (WUF-B)							
H =	148.18	kip						
V =	93.29	kip						
M =	92.46	kip-ft (revised from structural analysis)						
$R_u =$	175.10	kip						
Try $d_b =$	0.88	in	$F_u =$	150	ksi			
$A_b =$	0.60	in <sup>2</sup>	$F_{nv} =$	75	ksi (threads excluded)			
$N_b =$	6	bolts (in one row)						
$R_n =$	270.59	kip (bolt shear)	$L_{c\_ex} =$	1.5	in			
$\phi_b =$	0.75	-	$L_{c\_in} =$	3	in			
$\phi_b R_n =$	202.94	kip	OK					
$L_{c1} =$	1.03	in (edge clear distance)	$R_{n1} =$	46.41	kip			
$L_{c2} =$	2.06	in (clear distance)	$R_{n2} =$	236.25	kip			
t =	0.50	in (shear tab thickness)						
$R_n =$	1227.66	kip (combined bolt bearing)						
$\phi_b =$	0.75	-						
$\phi_b R_n =$	920.74	kip	OK					
$L_{tab} =$	18	in	$A_{s, tab} =$	9	in <sup>2</sup>	$R_n =$	524.79	kip
$w_{tab} =$	4.5	in	$F_{y, tab} =$	50	ksi	$P_{nt} =$	450.00	kip
			$F_{v, tab} =$	30.0	ksi	$P_{nv} =$	270.00	kip
			OK					
Weld	Fillet (shear tab)							
$F_{exx} =$	70	ksi	$R_n =$	334.06	kip			
$F_w =$	42	ksi	$\phi_b =$	0.75	-			
w =	5	x 1/16 inch	$\phi_b R_n =$	250.54	kip	OK		
$L_{weld} =$	18	in						
side =	2	sides						
Weld	CJP (top, bottom flanges)							
$b_f =$	12.8	in	$F_{y, bm} =$	50	ksi (base metal)			
$t_f =$	0.85	in	$M_n =$	1063.07	kip-ft	OK		
d =	24.3	in						
$t_w =$	0.55	in						

Check	Shear tab length, OK	
Check Block Shear		
Beam		
w24x117		
$A_{gv} =$	9.9	in <sup>2</sup>
$A_{gt} =$	1.925	in <sup>2</sup>
$A_{nv} =$	6.6	in <sup>2</sup>
$A_{nt} =$	1.65	in <sup>2</sup>
$U_{bs} =$	0.5	-
$\phi =$	0.75	-
$F_y =$	50	ksi
$F_u =$	65	ksi
$\phi R_n =$	233.27	kip
		OK
Shear Tab		
$A_{gv} =$	8.25	in <sup>2</sup>
$A_{gt} =$	1.5	in <sup>2</sup>
$A_{nv} =$	5.5	in <sup>2</sup>
$A_{nt} =$	1.25	in <sup>2</sup>
$U_{bs} =$	0.5	-
$\phi =$	0.75	-
$F_y =$	50	ksi
$F_u =$	65	ksi
$\phi R_n =$	191.34	kip
		OK

Title	TCBF-B-3 Specimen Design Calculation Sheet		Date	May 28, 2009	
2F	Braces to Beam Connection		Page	11	
Braces	W8x21				
T =	338.80	kip	$\sin(\theta) =$	0.669	
C =	241.62	kip	$\cos(\theta) =$	0.743	
e =	12.15	in			
Shear =	431.42	kip			
Tension =	182.56	kip			
Moment =	436.81	kip-ft			
$t_{\text{gusset}} =$	0.75	in			
L =	60	in			
$s_V =$	9.59	ksi			
$s_A =$	4.06	ksi			
$s_M =$	11.65	ksi			
$\phi =$	0.9	-			
$F_{y, \text{gusset}} =$	50	ksi			
Ratio =	0.51	OK			
$L_{\text{whitmore}} =$	23.87	in	$L_{\text{min}} =$	62.68	in (geometry limit) NG
$L_V =$	16	in	$L_{V, \text{min}} =$	17.74	in (geometry limit) NG!
$w_{\text{up}} =$	11.93	in	$A_V =$	12	$\text{in}^2$
$w_{\text{low}} =$	20.92	in	$P_u =$	226.65	kip
$\text{Whitm}_{\text{eff}} =$	23.87	in	$\phi R_n =$	324	kip OK
$\phi R_n =$	805.56	kip	OK		
Gusset Plate to Beam Flange					
Weld	Fillet				
$F_{\text{exx}} =$	70	ksi			
$F_w =$	42	ksi	$s_V =$	10.17	ksi
w =	8	x 1/16 inch	$s_M =$	12.36	ksi
$L_{\text{weld}} =$	60	in	$s_A =$	4.30	ksi
side =	2	sides	$f_{\text{peak}} =$	19.52	ksi
$t_{\text{eff}} =$	0.354	in	$f_{\text{avg}} =$	16.25	ksi
$\phi =$	0.75	-	$f_r =$	20.31	ksi
Ratio =	0.68	OK	Ratio =	0.64	OK
Check Beam Web					
width =	60	in	Beam	w24x117	



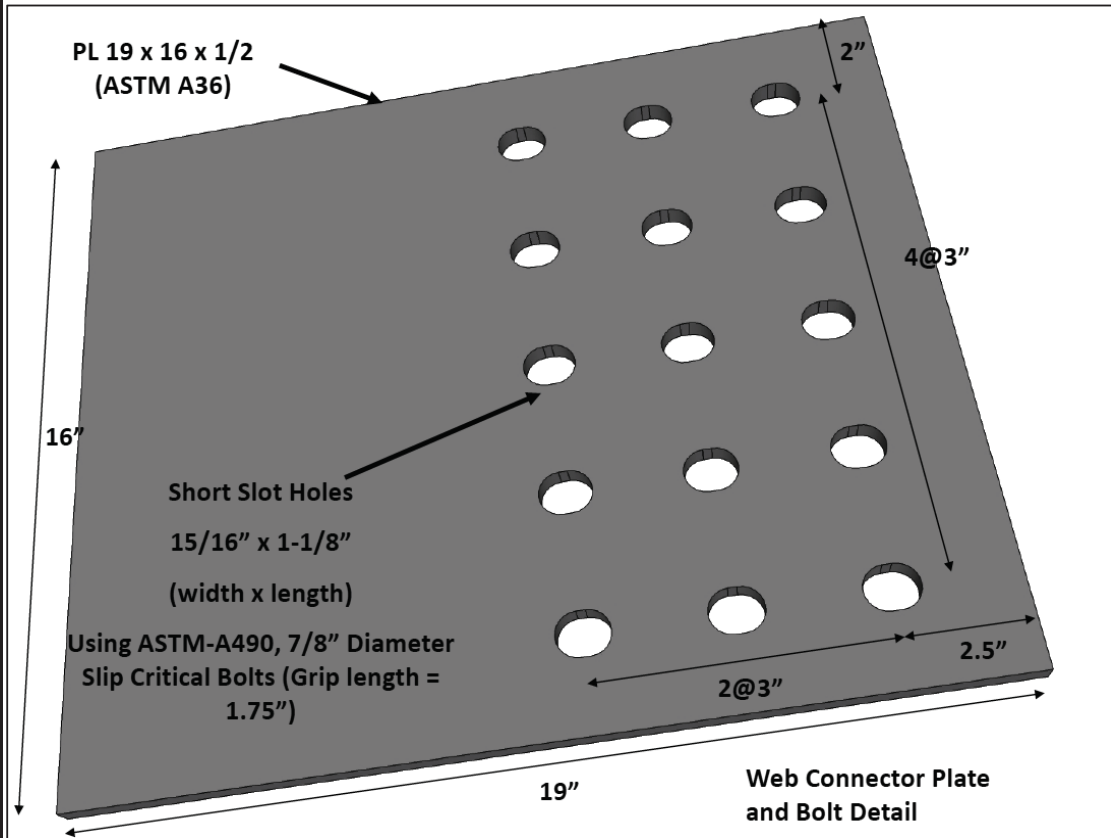
$R_u = 174.73$	kip	$d = 24.3$	in	$t_w = 0.55$	in
$N = 30$	in	$t_f = 0.85$	in	$F_{y, web} = 50$	ksi
$\phi = 0.75$	-	$R_n = 1060.63$	kip	$\phi R_n = 795.47$	kip
$k_{des} = 1.35$	in			(web crippling)	OK
$\phi = 1.00$	-	$R_n = 1010.63$	kip	$\phi R_n = 1010.63$	kip
				(web local yielding)	OK
Check Gusset Plate Buckling					
$L_{gb} = 17.68$	in	$kL/r = 98.0$	-	$L_c = 14.13$	in
$k = 1.2$	-	$F_e = 29.82$	ksi	$L_{c1} = 11.38$	in
$r = 0.217$	in	$0.44 F_y = 22$	ksi	$L_{c2} = 16.94$	in
$A_g = 17.90$	in <sup>2</sup>	$R_n = 443.70$	kip	$L_{max} = 24.06$	in
$\phi = 0.9$	-	$\phi R_n = 399.33$	kip	$L_{tip} = 21.88$	in
			OK	$L_{ave} = 17.68$	in
Free Edge Buckling					
$L_e = 15.63$	in				
$L_e/t_g = 20.83$	-				
Limit = 18.06	-	Edge stiffener required!			
Lateral Stability of Beam					
$M_r = 1498.75$	kip-ft	$Z = 327$	in <sup>3</sup>	$L_b = 10$	ft
$C_d = 1$	-	$h_o = 23.45$	in	$L_{pd} = 17.05$	ft
$P_{br} = 15.34$	kip	$\beta_{br} = 85.22$	kip/in	$n = 1$	OK
(Nodal)		(Nodal)		$C_b = 1$	-
$M_{br} = 17.985$	kip-ft				
$P_{br} = 9.20$	kip	(torsional)			
$\beta_T = 28842$	kip-in/rad	$\beta_{sec}$ not included			
$\beta_{br} = 52.45$	kip/in	(torsional)			
$\Delta = 0.18$	in				
Kicker					
L3x2x3/8					
$A_g = 1.73$	in <sup>2</sup>				
$L = 25$	in				
$k_{axial} = 2006.8$	kip/in				
$k = 1419$	kip/in	OK			

Title	TCBF-B-3 Specimen Design Calculation Sheet		Date	May 28, 2009	
1F	Beam-Column-Gusset Connections		Page	12	
Big Gusset Plate for Upper Floor Bracing and Lower Floor Bracing					
Sway to Right					
$F_{U2R} = 338.80$ kip $F_{L2R} = 360.20$ kip	$\cos(\theta_U) = 0.743$ $\cos(\theta_L) = 0.743$				
Sway to Left					
$F_{U2L} = 241.62$ kip $F_{L2L} = 453.20$ kip Beam w24x68 $d = 23.7$ in $L_{c, \min} = 60.74$ in Column w12x96 $e_c = 6.35$ in $R_{beam} = 21.45$ kip (downward) $L_{b, \min} = 17.36$ in $L_{cu, \min} = 17.74$ in $L_{cl, \min} = 19.29$ in $t_g = 0.75$ in $L_{cu} = 18$ in (use) $L_{cl} = 18$ in (use) $L_c = 59.7$ in (use) $L_b = 23$ in (use)	$F_{y, gusset} = 50$ ksi				
Sway to the Right					
$V_{U2R} = 226.65$ kip (upward) $H_{U2R} = 251.83$ kip (rightward) $V_{L2R} = 240.96$ kip (upward) $H_{L2R} = 267.73$ kip (leftward) $V_{total} = 446.16$ kip (upward) $M = 236.09$ kip-ft (counter-clockwise)	$s_V = 9.96$ ksi $s_M = 6.36$ ksi $s_A = 0.36$ ksi Ratio = 0.41 - OK				
Column-Side					
$V_{cu} = 134.52$ kip (downward) $f_1 = 4.77$ kip/in (leftward) $f_2 = 1.89$ kip/in (leftward) $H_{cu} = 59.96$ kip (leftward)	$s_A = 4.44$ ksi $s_V = 9.96$ ksi $s_M = 1.92$ ksi Ratio = 0.41 - OK				
Beam-Side					
$H_{bu} = 191.86$ kip (leftward) $V_{bu} = 92.13$ kip (downward) $M_{cu} = 6.47$ kip-ft (counter-clockwise)	$s_A = 5.34$ ksi $s_V = 11.12$ ksi				

$M_{bu} = -91.90$	kip-ft	(clockwise)	$s_M = -16.68$	ksi	
			Ratio = 0.50	-	OK
$V_{cl} = 134.52$	kip	(downward)	$s_A = 4.44$	ksi	
$f_1 = 4.77$	kip/in	(rightward)	$s_V = 9.96$	ksi	
$f_3 = 1.89$	kip/in	(rightward)	$s_M = 1.92$	ksi	
$H_{cl} = 59.96$	kip	(rightward)	Ratio = 0.41	-	OK
$H_{bl} = 207.77$	kip	(rightward)			
$V_{bl} = 106.44$	kip	(downward)	$s_A = 6.17$	ksi	
$M_{bl} = 86.32$	kip-ft	(clockwise)	$s_V = 12.04$	ksi	
$M_{cl} = 6.47$	kip-ft	(counter-clockwise)	$s_M = 15.66$	ksi	
			Ratio = 0.67	-	OK
$V_{mid} = 136.01$	kip	(downward)	$s_A = 0.00$	ksi	
$M_{mid} = 8.71$	kip-ft	(counter-clockwise)	$s_V = 7.65$	ksi	
$H_{mid} = 0.00$	kip	(leftward)	$s_M = 1.49$	ksi	
			Ratio = 0.30	-	OK
Weld Size					
$f_v = 7.47$	kip/in				
$f_a = 4.35$	kip/in	(averaged)			
$f_b = 4.77$	kip/in				
$f_{peak} = 11.79$	kip/in				
$f_{avg} = 9.64$	kip/in				
$f_r = 12.05$	kip/in	12.04781			
$D \geq 4.33$	x 1/16	(weld size)			
Use 6	x 1/16	(weld size)			

Title	TCBF-B-3 Specimen Design Calculation Sheet	Date	May 28, 2009
1F	Lower Beam to Gusset Plate Splice	Page	13

Web Fillet welds with web plates at one end and bolted to gusset plate  
 Flange free (no weld) (T & B)  
 $P_u = 300.00$  kip  
 $R_{beam} = 21.45$  kip (Gravity)



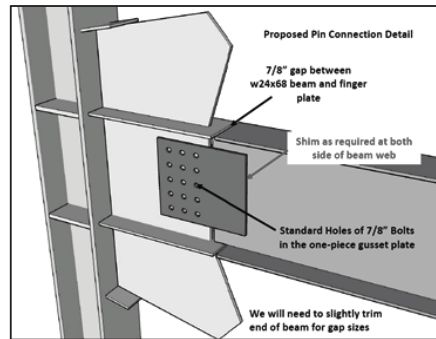
Fillet Weld at Beam Side

$L =$	16	in	$t_{shim} =$	0.168	in	(shim as required)
$w =$	7	in	$t_{splice} =$	0.500	in	
Weld	Fillet	(Splice plates)				
$F_{exx} =$	70	ksi	$R_n =$	779.47	kip	
$F_w =$	42	ksi	$\phi_b =$	0.75	-	
$w =$	7	x 1/16 inch	$\phi_b R_n =$	584.60	kip	OK
$L_{weld} =$	30	in				
side =	2	sides				



### Block Shear in Splice Plate

$F_y =$	36	ksi	
$F_u =$	58	ksi	
$\phi =$	0.75	-	
$A_{gv} =$	7	in <sup>2</sup>	
$A_{nt} =$	8	in <sup>2</sup>	
side =	2	sides	
$\phi R_n =$	1061.40	kip	OK



### Block Shear in Lower Beam Web

$F_y =$	50	ksi	
$F_u =$	65	ksi	
$\phi =$	0.75	-	
$A_{gv} =$	5.81	in <sup>2</sup>	
$A_{nt} =$	6.64	in <sup>2</sup>	
side =	1	sides	
$\phi R_n =$	493.64	kip	OK

### Bolt Strength Check

$L_{slot} =$	1.125	in	(short slot)
$d_{bolt} =$	0.875	in	(TC bolts)
$w_{slot} =$	0.9375	in	(short slot)
$\phi R_n =$	21.6	kip / per bolt	(LRFD)
$N_{bolt} =$	15	bolts	
$\phi R_n =$	324	kip	OK

### Block Shear in Gusset Plate

$F_y =$	50	ksi	
$F_u =$	65	ksi	
$\phi =$	0.75	-	
$A_{gv} =$	12.38	in <sup>2</sup>	
$A_{nt} =$	6.19	in <sup>2</sup>	
$A_{nv} =$	8.16	in <sup>2</sup>	
side =	1	sides	
$\phi R_n =$	540.21	kip	OK

Splice Plate Strength Check

$F_y =$	36	ksi		
$F_u =$	58	ksi		
$\phi =$	0.75	-		
$A_{gt} =$	8	in <sup>2</sup>		
$A_{nt} =$	5.66	in <sup>2</sup>		
side =	2	sides		
$\phi R_n =$	576.00	kip	OK	(gross yielding check)
$\phi R_n =$	492.09	kip	OK	(net section check)

Title	TCBF-B-3 Specimen Design Calculation Sheet		Date	May 28, 2009				
1F	Braces to Floor Beam Connection		Page	14				
Braces	W8x28							
T =	453.20	kip	$\sin(\theta) =$	0.669				
C =	360.20	kip	$\cos(\theta) =$	0.743				
e =	0	in						
Shear =	604.60	kip						
Tension =	237.46	kip						
Moment =	0.00	kip-ft						
$t_{gusset} =$	0.75	in						
L =	46	in						
$s_V =$	17.52	ksi						
$s_M =$	0.00	ksi						
$\phi =$	0.9	-						
$F_{y, gusset} =$	50	ksi						
Ratio =	0.69	OK						
whitmo =	25.96	in				$L_{min} =$	38.80	in (geometry limit) OK
$L_v =$	19	in				$L_{v, min} =$	19.29	in (geometry limit) NG!
$w_{up} =$	12.98	in				$A_v =$	14.25	in <sup>2</sup>
$w_{low} =$	14.12	in	$P_u =$	303.17	kip			
whit <sub>eff</sub> =	25.96	in	$\phi R_n =$	384.75	kip			
$\phi R_n =$	876.08	kip	OK	OK				
Weld	Fillet	(Gusset to beam flange)						
$F_{exx} =$	70	ksi						
$F_w =$	42	ksi						
w =	11	x 1/16 inch	$s_V =$	13.52	ksi			
$L_{weld} =$	46	in	$s_M =$	0.00	ksi			
side =	2	sides	$s_A =$	5.31	ksi			
$t_{eff} =$	0.486	in						
$\phi =$	0.75	-						
Ratio =	0.76	OK						
Check Beam Web								
width =	46	in	Beam	w30x391				
$R_u =$	0.00	kip	d =	33.2	in $t_w =$ 1.36 in			

$N =$	23	in	$t_f =$	2.44	in	$F_{y, web} =$	50	ksi
$\phi =$	0.75	-	$R_n =$	4450.60	kip	$\phi R_n =$	3337.95	kip
$k_{des} =$	3.23	in				(web crippling)		OK
$\phi =$	1.00	-	$R_n =$	2662.20	kip	$\phi R_n =$	2662.20	kip
						(web local yielding)		OK
Check Gusset Plate Buckling								
$L_{gb} =$	14.84	in	$kL/r =$	82.2	-	$L_c =$	15.88	in
$k =$	1.2	-	$F_e =$	42.32	ksi	$L_{c1} =$	18.06	in
$r =$	0.217	in	$0.44 F_y =$	22	ksi	$L_{c2} =$	12.56	in
$A_g =$	19.47	in <sup>2</sup>	$R_n =$	593.65	kip	$L_{max} =$	18.56	in
$\phi =$	0.9	-	$\phi R_n =$	534.29	kip	$L_{tip} =$	9.13	in
					OK	$L_{ave} =$	14.84	in
Free Edge Buckling								
$L_c =$	17.88	in						
$L_c/t_g =$	23.83	-						
Limit =	18.06	-	Edge stiffener required!					
Lateral Stability of Beam								
$M_r =$	6645.83	kip-ft	$Z =$	1450	in <sup>3</sup>	$L_b =$	10	ft
$C_d =$	1	-	$h_o =$	30.76	in	$L_{pd} =$	17.05	ft
$P_{br} =$	51.85	kip	$\beta_{br} =$	288.07	kip/in	$n =$	1	OK
(Nodal)			(Nodal)			$C_b =$	1	-
$M_{br} =$	79.75	kip-ft				$I_y =$	1550	in <sup>4</sup>
$P_{br} =$	31.11	kip	(torsional)					
$\beta_T =$	108666	kip-in/rad	$\beta_{sec}$ not included					
$\beta_{br} =$	114.85	kip/in	(torsional)					
$\Delta =$	0.27	in						

Title	TCBF-B-3 Specimen Design Calculation Sheet		Date	May 28, 2009
1F	Column Base Plate Design Check		Page	15
Column	w12x96			
$Z_x =$	147	in <sup>3</sup>	$L =$	96.15 in
$F_y =$	50	ksi	$V_{Mp} =$	152.89 kip
$M_p =$	7350	kip-in		
$P_u =$	492.31	kip	$d =$	12.7 in
$M_u =$	3114.35	kip-in	$b_f =$	12.2 in
$N =$	31.25	in	$f_{p, max} =$	36 ksi
$B =$	28	in		
$e =$	6.33	in	$q_{max} =$	1008 kip/in
$e_{cr} =$	15.38	in	(Small Moment)	
$Y =$	18.60	in		
$q =$	26.47	kip/in	OK	
$m =$	9.59	in		
$f_p =$	0.95	ksi		
$t_{p, req} =$	1.98	in	eq 3.3.14a (LRFD)	
use =	2.00	in		
All-thread-rods				
Type	ASTM A193 B7			
$d_{bolt} =$	1.125	in		
$F_u =$	125	ksi		
$F_y =$	105	ksi		
$F_{nt} =$	93.75	ksi		
$F_{nv} =$	50	ksi		
$A_b =$	0.99	in <sup>2</sup>		
$\phi =$	0.75	-		
$\phi R_n =$	69.89	kip	(tension)	
$\phi R_n =$	37.28	kip	(shear)	
$F_{PT} =$	86.98	kip	(minimum required pretension)	
$V_u =$	152.89	kip	(very conservative assumption)	
$M_u =$	7350	kip-in	(very conservative assumption)	
$P_u =$	600	kip	(very conservative assumption)	
$\mu =$	0.35	-	(class A surface)	
SF =	2	-	(safety factor for not having enough bolt pretension force)	

$N_V =$	10	bolts	(for friction shear)
$N_M =$	17	bolts	(for bending)
$N_T =$	9	bolts	(for uplifting)
$N_{\text{req, total}} =$	35	bolts	
use =	34	bolts	

Title	TCBF-B-3 Specimen Design Calculation Sheet			Date	May 28, 2009
2F	Stub Beam			Page	16
F1 =	300	kip	d =	24.3	in
F2 =	600	kip	t <sub>w</sub> =	0.55	in
L <sub>stub</sub> =	19	in	b =	12.8	in
Beam	w24x117		t <sub>f</sub> =	0.85	in
Column Dimension List					
Column	w12x96				
A <sub>g</sub> =	28.2	in <sup>2</sup>	b <sub>f</sub> =	12.2	in
I <sub>x</sub> =	833	in <sup>4</sup>	t <sub>f</sub> =	0.9	in
I <sub>y</sub> =	270	in <sup>4</sup>	d =	12.7	in
r <sub>x</sub> =	5.44	in	t <sub>w</sub> =	0.55	in
r <sub>y</sub> =	3.09	in	F <sub>y</sub> =	50	ksi
k <sub>des</sub> =	1.5	in	E <sub>s</sub> =	29000	ksi
Column Web Local Yielding					
N =	24.00	in			
R <sub>n</sub> =	866.25	kip			
φ =	1.00	-			
φR <sub>n</sub> =	866.25	kip	OK		
Column Web Crippling					
R <sub>n</sub> =	1382.366	kip			
φ =	0.75	-			
φR <sub>n</sub> =	1036.77	kip	OK		
Column Flange Local Bending					
R <sub>n</sub> =	253.13	kip	A <sub>web</sub> =	12.43	in <sup>2</sup>
			A <sub>s</sub> =	34.19	in <sup>2</sup>
φ =	0.90	-	A <sub>flange</sub> =	21.76	in <sup>2</sup>
φR <sub>n</sub> =	227.81	kip	F1 <sub>flange</sub> =	190.93	kip
			F2 <sub>flange</sub> =	381.87	kip
					Continue Plate Required!
Stub Beam Gross Yielding					
A <sub>s (beam)</sub> =	34.4	in <sup>2</sup>			
P <sub>y</sub> =	1720	kip	OK		

Title	TCBF-B-3 Specimen Design Calculation Sheet			Date	May 28, 2009
1F	Stub Beam			Page	17
$F_1 =$	300	kip	$d =$	23.7	in
$F_2 =$	600	kip	$t_w =$	0.415	in
$L_{stub} =$	19	in	$b =$	8.97	in
Beam	w24x68		$t_f =$	0.585	in
Column Dimension List					
Column	w12x96				
$A_g =$	28.2	in <sup>2</sup>	$b_f =$	12.2	in
$I_x =$	833	in <sup>4</sup>	$t_f =$	0.9	in
$I_y =$	270	in <sup>4</sup>	$d =$	12.7	in
$r_x =$	5.44	in	$t_w =$	0.55	in
$r_y =$	3.09	in	$F_y =$	50	ksi
$k_{des} =$	1.5	in	$E_s =$	29000	ksi
Column Web Local Yielding					
$N =$	24.00	in			
$R_n =$	866.25	kip			
$\phi =$	1.00	-			
$\phi R_n =$	866.25	kip	OK		
Column Web Crippling					
$R_n =$	1382.366	kip			
$\phi =$	0.75	-			
$\phi R_n =$	1036.77	kip	OK		
Column Flange Local Bending					
$R_n =$	253.13	kip	$A_{web} =$	9.35	in <sup>2</sup>
			$A_s =$	19.84	in <sup>2</sup>
$\phi =$	0.90	-	$A_{flange} =$	10.49	in <sup>2</sup>
$\phi R_n =$	227.81	kip	$F1_{flange} =$	158.65	kip
			$F2_{flange} =$	317.31	kip
					OK
Stub Beam Gross Yielding					
$A_{s (beam)} =$	20.1	in <sup>2</sup>			
$P_y =$	1005	kip	OK		



---

## **Appendix I**

### **Mill Certificate Report for TCBF-B-1 ~ 4 Specimen**

---

DATE	5/09/08
INVOICE NO.	227647
BILL OF LADING	907873
CUSTOMER NO.	7606
CUSTOMER P.O.	61060

**NUCOR-YAMATO STEEL CO.**  
P.O. BOX 1228 ■ BLYTHEVILLE, AR 72316

S  
H  
I  
P  
T  
O  
  
BROWN STRAUSS-STOCKTON  
4221 E MARIPOSA ROAD  
ROCKWELL TRACK 4  
STOCKTON, CA

**CERTIFIED MILL TEST REPORT**

100% MELTED AND MANUFACTURED IN U.S.A.  
All shapes produced by Nucor-Yamato Steel are cast and rolled to a fully killed and fine grain practice.

S  
P  
E  
C  
I  
F  
I  
C  
A  
T  
I  
O  
N  
S  
  
ASTM A992/A992M-06a A572/A572M GR50-06  
ASTM A709/A709M-07 GR50 (345)  
ASTM A709/A709M-07 GR50S (345S)  
ASTM A6/A6M-07

S  
O  
L  
D  
T  
O  
  
BROWN STRAUSS STEEL CO.  
2495 URAVAN STREET  
  
AURORA, CO 80011

ITEM #	ITEM DESCRIPTION	QTY	HEAT #	MECHANICAL PROPERTIES								CHEMICAL PROPERTIES										
				YIELD TO TENSILE RATIO	YIELD STRENGTH	TENSILE STRENGTH	ELONG	CHARPY IMPACT		C	Mn	P	S	Si	Cu	Ni	Cr	Mo	V	Cb	CE	
					PSI	PSI		%	TEMP													IMPACT ENERGY
					MPa	MPa		%	°F													FT-LBS
1	W12 - 79.0 35' W310 x117.0 10.668 M	2	313905	.77	56000	73000	26				.08	1.25	.013	.036	.30	.27	.10	.08	.02	.00	.022	.33
2	W12 - 79.0 35' W310 x117.0 10.668 M	1	313959	.76	56000	74000	27				.08	1.25	.017	.032	.30	.27	.09	.09	.02	.00	.024	.33
3	W12 - 79.0 55' W310 x117.0 16.764 M	1	313957	.76	58000	76000	26				.08	1.25	.017	.036	.32	.30	.09	.09	.02	.00	.024	.34
4	W12 - 79.0 55' W310 x117.0 16.764 M	2	314081	.76	57000	75000	25				.08	1.25	.015	.032	.30	.28	.12	.09	.02	.00	.024	.34
5	W12 - 79.0 56' W310 x117.0 17.069 M	3	313950	.78	56000	72000	27				.08	1.25	.020	.030	.30	.32	.11	.10	.03	.00	.024	.35
6	W12 - 96.0 45' W310 x143.0 13.716 M	3	313909	.77	57000	74000	27				.08	1.25	.021	.040	.25	.28	.09	.10	.02	.00	.021	.33
7	W12 - 96.0 55' W310 x143.0 16.764 M	3	313889	.77	57000	74000	27				.08	1.25	.019	.034	.29	.30	.11	.10	.03	.00	.024	.35
8	W12 - 96.0 60' W310 x143.0 18.288 M	1	313883	.76	57000	75000	25				.08	1.25	.016	.040	.31	.33	.11	.09	.03	.00	.023	.34
9	W12 - 96.0 60' W310 x143.0 18.288 M	2	313971	.74	56000	76000	27				.08	1.25	.016	.030	.29	.30	.09	.09	.02	.00	.022	.34

Form C-31 - Mn + Cu + Ni + V - 3.8 B - Approx. 2005

CARBON EQUIVALENT: CE = C(IIW) = C + Mn/6 + (Cr+Mo+V)/5 + (Ni+Cu)/15

Corrosion Index:  $CI = 0.0081[Cu] + 0.0016[Ni] + 1.305[Cr] + 1.405[S] + 7.205[Cu] + 0.1015[Mo] + 0.1015[P]$

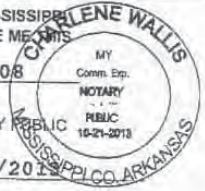
ELONGATION BASED ON 8.00 INCH GAUGE LENGTH

I hereby certify that the contents of this report are accurate and correct. All test results and operations performed by this material manufacturer are in compliance with the requirements of the material specifications listed in the Specifications Block above.

*David Linnell*  
QUALITY ASSURANCE

CUSTOMER COPY

STATE OF ARKANSAS COUNTY OF MISSISSIPPI  
SWORN TO AND SUBSCRIBED BEFORE ME THIS  
9 Day of 05/08  
*Charlene Wallis* NOTARY PUBLIC  
MY COMMISSION EXPIRES 10/21/2012



Bill To:  
 BROWN-STRAUSS STEEL  
 ACCOUNTS PAYABLE - STEEL  
 2495 DRAVAN STREET  
 AURORA  
 80011

Ship To: 121  
 BROWN STRAUSS STEEL  
 4221 EAST MARIPOSA ROAD  
 ROCKWELL TRACK #4  
 STOCKTON  
 95215

Order Date: 04/24/2008  
 PO No: 61391  
 Mill Order No: 3472634  
 Load No: 1206462  
 Manifest No: 1913453

CERTIFIED MATERIAL TEST REPORT  
 GERDAU AMERISTEEL  
 Midlothian Mill  
 GERDAU AMERISTEEL  
 300 Ward Road  
 Midlothian, TX 76065  
 (972) 775-8241

SIZE  
 0.28 X .038 X 101

GRADE  
 992/572-50

LENGTH  
 45 FT / 13.716 M

PRODUCT  
 WF BEAMS

SPECIFICATIONS  
 ASTM A6-05a, A992-06a, A572-06

HEAT NO: 22477490

CHEMICAL ANALYSIS													
C	Mn	P	S	Si	Cu	Ni	Cr	Mo	Sh	V	Al	Nb	CE
.09	.94	.018	.038	.28	.38	.10	.14	.029	.013	.002	.004	.013	.31

PHYSICAL PROPERTIES			
Yield Strength	Tensile Strength	Elongation	ROA
KSI	KSI	%	%
MPa	MPa		
54.2	71.7	25.4	
52.0	71.8	25.9	
		8 In	200 mm
		8 In	200 mm

9890  
 98901

J E A P

All manufacturing processes of this product, including electric arc melting and continuous casting, occurred in the U.S.A. CMTR complies with DIN EN 10204 3.1.B

"I hereby certify that the contents of this report are correct and accurate. All tests and operations performed by this material manufacturer or its sub-contractors, when applicable, are in compliance with the requirements of the material specifications and applicable purchaser designated requirements."

Signed: *Tom L. Harrington* Date: Jul. 12, 2008 Signed: \_\_\_\_\_ Date: \_\_\_\_\_  
 Tom L. Harrington: Quality Assurance Manager Notary Public (if applicable) Page: 1 of 1

**CERTIFIED MATERIAL TEST REPORT**

GERDAU AMERISTEEL  
 Petersburg Mill  
 GERDAU AMERISTEEL-25801 Hofheimer Way  
 Petersburg, VA 23803  
 (804) 524-2855

Order Date: 02/12/2008  
 PO No: 59471  
 Mill Order No: 3436184  
 Load No: 117346  
 Manifest No: 1885714

Ship To: 5  
 BROWN-STRAUSS STEEL  
 BROWN-STRAUSS STEEL  
 ZTS 3277100  
 SOUTH FONTANA

Bill To:  
 BROWN-STRAUSS STEEL  
 ACCOUNTS PAYABLE - STEEL  
 2495 URAVAN STREET  
 AURORA  
 80011

PRODUCT  
 WF BEAMS

LENGTH  
 60 FT / 18,288 M

GRADE  
 992/572-50

SIZE  
 W 24 X 117# / W610 X 174

ASTM A6-05a, A992-06a, A572-06  
 HEAT NO: 30406710

CHEMICAL ANALYSIS

C	Mn	P	S	Si	Cu	Ni	Cr	Mo	Sn	V	Al	Nb	CE
.07	1.13	.010	.033	.22	.30	.09	.07	.015	.015	.003	.004	.019	.3

PHYSICAL PROPERTIES

Yield Strength	Tensile Strength		Elongation	Gage Length	RCA
	KSI	MPa			
52.6	68.6	473.0	25.0	8 In	200 mm
52.2	68.4	471.6	25.6	8 In	200 mm

9890  
 98901

HVPL

All manufacturing processes of this product, including electric arc melting and continuous casting, occurred in the U.S.A. CMTR complies with DIN EN 10204 3.1.B

"I hereby certify that the contents of this report are correct and accurate. All tests and operations performed by this material manufacturer or its sub-contractors, when applicable, are in compliance with the requirements of the material specifications and applicable purchaser designated requirements."

Signed: Tom L. Harrington Date: Mar. 11, 2008 Signed: Notary Public (if applicable) Date: \_\_\_\_\_  
 Tom L. Harrington: Quality Assurance Manager Page: 2 of 2

# Test Certificate

Form (TC): Revision 1; Date 31 Oct 2000

12400 Highway 43 North, Axis, Alabama 36505

# SSAB

Customer:  
 GARY STEEL  
 CAO NAMASCO  
 500-500 COLONIAL CENTER PARKWA  
 ROSWELL,  
 GA 30076 1606

Customer P.O. No.: 6148242  
 Product Description: ASTM A572-50/M345(06)/A709-50/M345(06A)  
 Mill Order No.: 41-226583-11  
 Shipping Manifest: AR060408  
 Ship Date: 26 Jul 08  
 Cert Date: 26 Jul 08  
 Cert No: 081147198  
 ( Page 1 of 1 )

Size: 0.750 X 96.00 X 480.0 (IN)

Heat Id	Piece Id	Piece Dimensions	Tensiles			Charpy Impact Tests			Tst Dir (mm)	Tst Temp	Tst Dir	Tst Temp	B1)WTT
			Tst Loc	YS (PSI)	UTS (PSI)	%RA (PSI)	Average Hardness	Abs. Energy(FTL.B)					
M8G153	B08	0.750 X 96.00 (DISCRT)	1	58000	71000	26	T	1	2	3	Avg		

Heat Id	Chemical Analysis												
	C	Mn	P	S	SI	Tot Al	Cu	Ni	Cr	Mo	Co	V	Ti
M8G153-B08	.06	1.33	.011	.008	.32	.028	.25	.10	.14	.04	.029	.032	.018

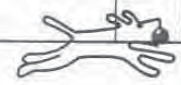
MERCURY IS NOT A METALLURGICAL COMPONENT OF THE STEEL AND NO MERCURY WAS INTENTIONALLY ADDED DURING THE MANUFACTURE OF THIS PRODUCT  
 -C3% MELTED AND MANUFACTURED IN THE USA, MTR DIN EN 2204 TYPE 3.1 COMPLIANT.  
 M8G153 B08 PAGES: 4, WGT: 39234

STOCK  
 PORTER

WE HEREBY CERTIFY THAT THIS MATERIAL WAS TESTED IN ACCORDANCE WITH THE APPROPRIATE SPECIFICATION

Cust Part # :

Jason Thomas  
 SSMR06147198





MILL CERTIFICATE ORIGINAL

M/C No. MC0000027692 Date 08/13/2008

THIS PIPE AND TUBE MADE IN U.S.A.

BL No. SH0000029199

Destination BROWN-STRAUSS STEEL INC-SIK

Supplier BROWN-STRAUSS STEEL INC-CO

MARUICHI AMERICAN CORPORATION

11529 GREENSTONE AVENUE

SANTA FE SPRINGS, CALIFORNIA

TEL: (562) 903-8600 FAX: (562) 903-8601

Table with columns: No of PCS, Hydrostatic Test, Chemical Composition (Ladle Analysis), Tensile Test, Bending Test, Flattening Test, Remarks. Rows 1-6 detailing ASTM A500 Grade B ERW Tubing specifications and test results.

We hereby certify that the material described herein conforms fully to the said specification.

Remarks:

J F Q D

9890 98901

MARUICHI AMERICAN CORPORATION

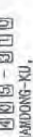
Signature and Quality Control stamp

bh

MILL TEST CERTIFICATE

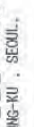


HISTEEL CO., LTD



HEAD OFFICE : 69BELOCK 4LOT, GOSANMONG, NAMJONG-KU, INCHON, KOREA

INCHON PLANT  
TEL : (032)815-6386-8  
FAX : (032)815-6389



SEOUL OFFICE : 57-9, CHUNGJU-RO 3-GA, JUNG-KU, SEOUL, KOREA

TEL : (02)273-2141-3  
FAX : (02)273-2157

*Star Jeffrey*

CUSTOMER : SEAH STEEL AMERICA, INC

CERTIFICATE NO : HIE2008-0121 PAGE : 4

DATE OF ISSUE : May. 15, 2008

L/C NO (P/O NO) : 98776

COMMODITY : ERW STEEL STRUCTURAL TUBING

SPECIFICATION : ASTM A500 GR. B

TYPE OF PIPE END	DIMENSION (OUTDIA. X THICK. X LENGTH)		QUAN-TITY (PCS)	WEIGHT (KG)	HYDRO-STATIC TEST	HEAT-NO.	TENSILE TEST		CHEMICAL COMPOSITION											IMPACT TEST																				
							YIELD STRENGTH	TENSILE STRENGTH	(EL)		C	Si	Mn	P	S	Cu	Ni	Cr	Mo	Nb	V	Ti	B	HARDNESS	Ceq	H	V													
									B	W																		%	%	HV	X1000	X1000	X1000	X1000	X1000	J	C			
*1	*2	*3	*4																																					
BPE	NB	6"x6"	X 0.313"	X 32'				54,806	65,101	30	H	6	3	53	14	5																								
BPE	NB	6"x6"	X 0.313"	X 36'				54,806	65,101	30	H	6	3	53	14	5																								
BPE	NB	6"x6"	X 0.375"	X 26'				46,397	66,986	28	H	14	3	68	9	6																								
BPE	NB	6"x6"	X 0.375"	X 28'				46,397	66,986	28	H	14	3	68	9	6																								
BPE	NB	6"x6"	X 0.375"	X 30'				46,397	66,986	28	H	14	3	68	9	6																								
BPE	NB	6"x6"	X 0.375"	X 32'				46,397	66,986	28	H	14	3	68	9	6																								
BPE	NB	6"x6"	X 0.375"	X 40'				46,397	66,986	28	H	14	3	68	9	6																								
BPE	NB	6"x6"	X 0.500"	X 26'				46,397	68,146	46	H	15	9	52	12	10																								
BPE	NB	6"x6"	X 0.500"	X 30'				46,397	68,146	46	H	15	9	52	12	10																								
BPE	NB	6"x6"	X 0.500"	X 32'				46,397	68,146	46	H	15	9	52	12	10																								
BPE	NB	6"x6"	X 0.500"	X 36'				46,397	68,146	46	H	15	9	52	12	10																								

*9	P	S	A	*10 VISUAL & DIMENSION TEST	*11 FLATTENING (B) TEST	*12 WELD DUCTILITY TEST	*13 NONDESTRUCTIVE TEST (U.T)	*14 DRIFT TEST	*15 FLARING TEST	*16 CRUSH TEST	*17 REVERSE FLATTENING TEST
				GOOD							
NOTE 1 *1 Type of pipe End											
				QPE :Galvanized Plain End Square-cut							
				BPFB :Black Plain End Beveled							
				BTC :Black Threaded & Coupled							
				BVJ :Black Victaulic Joint							
				ETC :Enamelled Threaded & Coupled							

\* 2 NB:Nominal Bore, OD:Outside Diameter  
\* 4 Unit (MMeter, F:Faet, I:Inch)  
\* 7 W : Weld Part  
\* 9 POST SEAM ANNEALING  
\* 12 Weld Ductility Test  
\* 15 Flaring Test  
\* 3 Unit (M:mm, I:inch)  
\* 6 Base Metal  
\* 8 H:Heat (Ladle) Analysis, P:Product Analysis  
\* 11 Flattening or Bending Test  
\* 14 Drift Test  
\* 17 Reverse Flattening Test

WE HEREBY CERTIFY THAT THE MATERIAL DESCRIBED HEREIN HAS BEEN ACCEPTED IN ACCORDANCE WITH THE PRESCRIBED SPECIFICATION AND ORDER

9890  
= 9890i

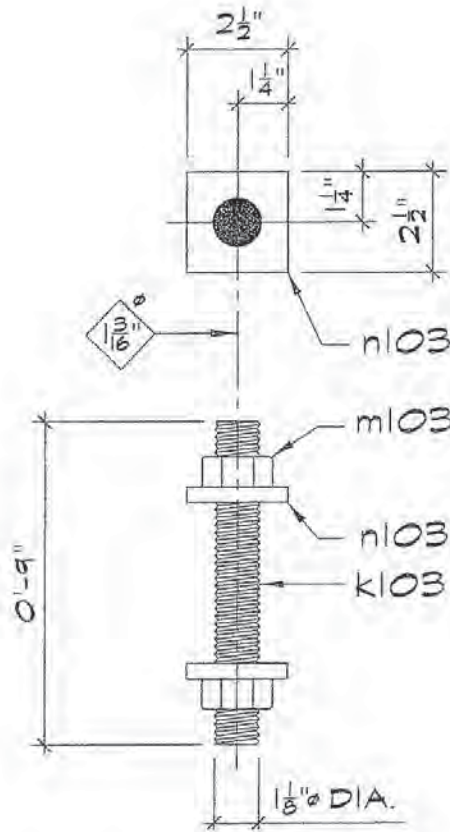
SUPERVISOR

INSPECTION MANAGER

HISTEEL CO., LTD

A4(210)

QTY	DESCRIPTION	LENGTH		MARK	MATERIAL	REMARKS	CODE	MO
		FT.	INCHES					
112	ANCHOR BOLT ASSY	-	-	D103				
112	1 1/8"Ø A193 ROD	0	9	K103	10	ALL THREAD ROD GR B7		
224	1 1/8"Ø NUT			m103	45	A194-2H		
224	PL 3/8"x2 1/2	0	2 1/2"	n103	2	A572-50	F H	



PURCHASE LENGTH : \_\_\_\_\_

PO # 98903  
Power Fastener

- APPROVED FOR PURCHASING
- FOR APPROVAL PRICING ONLY

MTO NO. :

REF. :

NO.	DATE	REVISION	BY	HOLES: AS NOTED	STOCKTON <input checked="" type="checkbox"/>
△	03/02/09	REVISED FOR FABRICATION	AEU		SAN BERNARDINO <input type="checkbox"/>
△	02/20/09	REVISED QUANTITY, ADDED GRADE	AEU	PAINT: NONE	

**Herrick**

SKETCH SHEET

ANCHOR BOLT BUYOUT DETAIL  
UNIVERSITY OF CALIFORNIA at BERKELEY  
BERKELEY, CA.

DRAWN AEU JOB NO. 9890  
CHECKED RA SHEET BO-103  
DATE 02/03/09

SHOP DATE : 1/13/09 LOAD NO. : \_\_\_\_\_

SHOP ISSUED : \_\_\_\_\_



# Certificate of Inspection

**POWER FASTENERS, INC.**      ISO 9001-2000 Reg# A1366US      Phone: 323-232-4362  
 PO BOX 512056  
 LOS ANGELES, CA 90051      Fax: 323-232-4367

**DESCRIPTION**    1-1/8"-7      **SPECIFICATION:** ASTM A193-04c B7  
 All Thread Rod      **PART #**      CUSTOM  
**LOT#**      40239

### PHYSICAL ANALYSIS

**SAMPLE SIZE:**    2 pcs      **TEMPERING TEMP.**    1310 Deg. F.      **TESTING STD.**    F606-98 / F1470

**TENSILE**      REQUIREMENT: 125,000    Psi    ACTUAL: 146    Psi    **HARDNESS**      REQUIREMENT: 35 HRC max    ACTUAL: 28 - 31 HRC

**YIELD 2% Off.**    REQUIREMENT: 81,000    Psi    ACTUAL: 133    Psi

**ELONGATION 2"**    REQUIREMENT: 14    %    ACTUAL: 22    %    **RED AREA**      REQUIREMENT: 50%    ACTUAL: 63%

### DIMENSIONAL ANALYSIS

**DIMENSIONAL**      **SAMPLE SIZE:**    8 pcs      **PASS**

**VISUAL:**      **SAMPLE SIZE:**    28 pcs      **PASS**

### CHEMICAL ANALYSIS

**MATERIAL TYPE:**      **HEAT #**    225082

C (.35-.53)	Mn (NR)	P	S	.040 Max.	Si	Cu	Ni	Cr	Mo	V	Nb	Al
0.41	0.86	0.01	0.021	0.23	0.21	0.09	0.85	0.21	0.024	0	0	0

Test values show represent the average of all tests taken.  
 We hereby certify that the data reflects the information as provided by the material supplier and/or our testing laboratory(s).  
 Mechanical testing performed using machine sample testing per ASTM F606.

**DATE:**      3/10/2009      **Inquiries can be directed to :**    QUALITY ASSURANCE REPRESENTATIVE  
**PO #**      98903      **POWER FASTENERS**      *[Signature]*  
 (see contact information above)

# Certificate of Inspection

**POWER FASTENERS, INC.**      **ISO 9001-2000 Reg# A1366US**      Phone: 323-232-4362  
 PO BOX 512056  
 LOS ANGELES, CA 90051      Fax: 323-232-4367

DESCRIPTION	1-1/8"-7 Heavy Hex Full Nut				SPECIFICATION: ASTM A563-04a Grade DH
LOT#	20082-5				PART # HH112CDH
					LOT SIZE: 12,800

### PHYSICAL ANALYSIS

**SAMPLE SIZE:** 20      **TEMPERING TEMP.** 900 Deg. F. Min.      **TESTING STD.** ASTM 563-04a-DH / F606  
**PROOF LOAD REQUIREMENT:** 133,525 LBS.      **ACTUAL:** PASS      **OK**      **PASS**

**HARDNESS REQUIREMENT:** 24-38 HRC      **ACTUAL:** 26-30 HRC      **PASS**

### DIMENSIONAL ANALYSIS

**DIMENSIONAL:**      **SAMPLE SIZE:** 20      **REQUIREMENT:** ANSIB 18.2.2      **PASS**

**APPEARANCE:**      **SAMPLE SIZE:** 20      **PASS**

### CHEMICAL ANALYSIS

**MATERIAL GRADE:** SAE C1045

C	Mn	P	S	Si	Cu	Ni	Cr	Mo	V	Nb	Al
0.45	0.64	0.023	0.016	0.22	0.01	0.01	0.01	0.01			

Marks: POW2H DH

**DATE:** 1/15/2008      **QUALITY ASSURANCE REPRESENTATIVE**  
**PO#:** 98903



**CMC Steel Texas**  
 PO Box 911  
 Seguin, TX 78155  
 (830) 372-8200

**CERTIFIED MILL TEST REPORT**  
 For Additional copies call (830) 372-8485

We hereby certify that the test results presented here  
 are accurate and conform to the reported grade  
*Daniel J. Schacht*  
 Quality Assurance Manager

HEAT NO:		SECTION:		GRADE:		WEIGHT/PCS:																												
254334		F 3x3/8x200"		ASTM A572-03a GRADE 50 TYPE 1		4.596 / 60																												
S O L D T O		S O L D T O		S O L D T O		S O L D T O																												
POWER FASTENERS INC P.O. BOX 2056 LOS ANGELES, CA 90051-		POWER FASTENERS PICK UP AT THE MILL SEGWIN TX 78155-		SHIP#: 101923/57		BOI#: 446134																												
INVENTORY #		INVENTORY #		CUST PO#: 18988-2		CUST PN#:																												
CHEMICAL ANALYSIS				MECHANICAL				TEST 1				TEST 2				TEST 3																		
%				YIELD STRENGTH				TENSILE STRENGTH				ELONGATION				REDUCTION OF AREA																		
C	MN	P	S	SI	CU	CR	NI	MO	CB	V	SN	B	TI	56.7KSI	76.6KSI	390.9MPA	528.2MPA	32%	32%	203MM														
JOMINY RESULTS - Rockwell C hardness at 1/16th inch increments																INCLUSION RATING																		
100% MELTED AND MANUFACTURED IN THE USA AND FREE OF MERCURY CONTAMINATION IN THE PROCESS																METHOD																		
REMARKS																TYPE																		
1																SIZE																		
2																A																		
3																B																		
4																C																		
5																D																		
6																T																		
7																H																		
8																T																		
9																H																		
10																T																		
11																H																		
12																T																		
13																H																		
14																T																		
15																H																		
16																T																		
17																H																		
18																T																		
19																H																		
20																T																		
21																H																		
22																T																		
23																H																		
24																T																		
25																H																		
26																T																		
27																H																		
28																T																		
29																H																		
30																T																		
31																H																		
32																T																		

	FIELD BOLTS				REMARKS	WEIGHT
	QUANTITY	DESCRIPTION	LENGTH			
			FT.	IN.		
2	31	7/8 A490 bolts	0	3	<i>Cardova PO # 98902</i>	34
2	19	7/8 A490 bolts	0	2 3/4		19
3	13	7/8 A490 bolts	0	2 1/2		12
4						
5						
6						
7						
8						
9						
10						
11						
12						
13						
14	69	7/8 HVY HEX NUTS				
15						
16	69	7/8 HVY WASHERS				5
17						
18						
19						
20						
21						
22						
23						
24						
25						
26						
27						
28						
29						
30						

*DC*  
*CV*  
*3/12/09*

NO.	DATE	REVISION	MADE BY	NO.	DATE	REVISION	MADE BY

**Herrick**

MISCELLANEOUS MATERIALS SUMMARY

STOCKTON   
SAN BERNARDINO

Field Bolts MADE BY: AEU JOB NO.: 9890  
 UC Berkeley Hybrid Bracings CHKD BY: \_\_\_\_\_ SHEET: MS-1  
 Berkeley Ca. DATE: 3/3/2009 WT: 70

SHOP DATE: 3/11/09 LOAD NO.: \_\_\_\_\_ SHOP ISSUE: \_\_\_\_\_

# NUCOR

LCT NO:  
244408APost Office Box 6100  
Saint Joe, Indiana 46785  
Telephone 260/337-1600

## FASTENER DIVISION

CUSTOMER NO/NAME  
163 CORDOVA BOLT INC  
TEST REPORT SERIAL# FB312231  
TEST REPORT ISSUE DATE 6/20/08  
DATE SHIPPED 9/02/08  
NAME OF LAB SAMPLER: STEVEN A. JENNINGS, LAB TECHNICIAN  
\*\*\*\*\*CERTIFIED MATERIAL TEST REPORT\*\*\*\*\*  
NUCOR PART NO QUANTITY LOT NO. DESCRIPTION  
165440 1500 244408A 7/8-9 X 3 A490 HVY HX  
MANUFACTURE DATE 6/03/08 STRUC SCREW PLAIN

NUCOR ORDER # 648314  
CUST PART #

CUSTOMER P.O. # 024959



--CHEMISTRY MATERIAL GRADE -4135MLV  
MATERIAL HEAT \*\*CHEMISTRY COMPOSITION (WT% HEAT ANALYSIS) BY MATERIAL SUPPLIER  
NUMBER NUMBER C MN P S SI CR MO V NUCOR STEEL - NEBRASKA  
RM024413 NU 844781 .34 .86 .011 .019 .25 .99 .16 .020 A2LA NO: 780.01 EXP: 2008-11-30  
MIN .30 FOR CHEMICAL TESTING  
MAX .48 .040 .040

--MECHANICAL PROPERTIES IN ACCORDANCE WITH ASTM A490-08a  
SURFACE CORE PROOF LOAD TENSILE STRENGTH  
HARDNESS HARDNESS 55450 LBS 10 DEG-WEDGE  
(R30N) (RC) (LBS) STRESS (PSI)  
N/A 33.3 PASS 74870 162056  
N/A 33.5 PASS 75240 162857  
N/A 33.0 PASS 73740 159610  
N/A 33.4  
AVERAGE VALUES FROM TESTS PRODUCTION LOT SIZE 5300 PCS  
33.3 74617 161508

--VISUAL INSPECTION IN ACCORDANCE WITH ASTM F788  
--WET MAGNETIC PARTICLE INSPECTION IN ACCORDANCE WITH ASTM A490-08a 4 PCS. SAMPLED LOT PASSED

--MICROHARDNESS TEST RESULT IN ACCORDANCE WITH SAE J121-99(HKN)  
POSITION 1. 365 2. 346 3. 361  
CARBURIZATION/DECARBURIZATION TEST IN ACCORDANCE WITH A490-08a LOT PASSED  
HEAT TREATMENT - AUSTENITIZED, OIL QUENCHED & TEMPERED (MIN 800 DEG F)

--DIMENSIONS PER ASME B16.2.6-2003  
CHARACTERISTIC #SAMPLES TESTED MINIMUM MAXIMUM  
Width Across Corners 8 1.6180 1.6290  
Grip Length 8 1.3700 1.4000  
Head Height 8 0.5600 0.5620  
Threads 8 PASS PASS

9890  
98902

ALL TESTS ARE IN ACCORDANCE WITH THE LATEST REVISIONS OF THE METHODS PRESCRIBED IN THE APPLICABLE SAE AND ASTM SPECIFICATIONS. THE SAMPLES TESTED CONFORM TO THE SPECIFICATIONS AS DESCRIBED/LISTED ABOVE AND WERE MANUFACTURED FREE OF MERCURY CONTAMINATION. NO HEATS TO WHICH BISMUTH, SELENIUM, TELLURIUM, OR LEAD WAS INTENTIONALLY ADDED HAVE BEEN USED TO PRODUCE THE BOLTS. THE STEEL WAS MELTED AND MANUFACTURED IN THE U.S.A. AND THE PRODUCT WAS MANUFACTURED AND TESTED IN THE U.S.A. WE CERTIFY THAT THIS DATA IS A TRUE REPRESENTATION OF INFORMATION PROVIDED BY THE MATERIAL SUPPLIER AND OUR TESTING LABORATORY. THIS CERTIFIED MATERIAL TEST REPORT RELATES ONLY TO THE ITEMS LISTED ON THIS DOCUMENT AND MAY NOT BE REPRODUCED EXCEPT IN FULL.



MECHANICAL FASTENER  
CERTIFICATE NO. A2LA 139-01  
EXPIRATION DATE 12/31/09

NUCOR FASTENER  
A DIVISION OF NUCOR CORPORATION

*James B. Galamas*  
JAMES GALAMAS  
TECHNICAL SERVICES MANAGER

# NUCOR

LOT NO.  
168404APost Office Box 6100  
Saint Joe, Indiana 46785  
Telephone 260/337-1600

## FASTENER DIVISION

CUSTOMER NO/NAME  
143 CORDOVA BOLT INC  
TEST REPORT SERIAL# FB214140  
TEST REPORT ISSUE DATE 8/22/03  
DATE SHIPPED 11/24/03  
NAME OF LAB SAMPLER: DARREN HARTZ, LAB TECHNICIAN  
\*\*\*\*\*CERTIFIED MATERIAL TEST REPORT\*\*\*\*\*  
NUCOR PART NO QUANTITY LOT NO. DESCRIPTION  
165430 2925 168404A 7/8-9 X 2 3/4 A490 HVY HX  
MANUFACTURE DATE 7/29/03 STRUC SCREW PLAIN



---CHEMISTRY MATERIAL GRADE -4135MOD  
MATERIAL HEAT \*\*\*CHEMISTRY COMPOSITION (WT% HEAT ANALYSIS) BY MATERIAL SUPPLIER  
NUMBER NUMBER C MN P S SI CR MO V INLAND STEEL  
RM020333 IN 391612 .34 .83 .008 .009 .23 .95 .16 .011 P. O. BOX 360518M  
MIN .30 PITTSBURGH, PA 15251  
MAX .48 .040 .040 A2LA NO: 111.01 EXP: 2004-12-31  
FOR CHEMICAL TESTING

---MECHANICAL PROPERTIES IN ACCORDANCE WITH ASTM A490-02  
SURFACE CORE PROOF LOAD TENSILE STRENGTH  
HARDNESS HARDNESS 55450 LBS 10 DEG-WEDGE  
(R30N) (RC) (LBS) STRESS (PSI)  
N/A 34.9 PASS 76502 165589  
N/A 35.3 PASS 76455 165487  
N/A 36.9 PASS 75924 164338  
N/A 35.0  
AVERAGE VALUES FROM TESTS PRODUCTION LOT SIZE 10000 PCS  
35.0 76294 165138

---NET MAGNETIC PARTICLE INSPECTION IN ACCORDANCE WITH ASTM A490 200 PCS. SAMPLED LOT PASSED

---MICROHARDNESS TEST RESULT IN ACCORDANCE WITH SAE J121(HKN)  
POSITION 1. 376 2. 379 3. 387  
CARBURIZATION/DECARBURIZATION TEST IN ACCORDANCE WITH A490 - LOT PASSED  
HEAT TREATMENT - AUSTENITIZED, OIL QUENCHED & TEMPERED (MIN 800 DEG F)

---DIMENSIONS PER ASME B18.2.6-1996  
CHARACTERISTIC #SAMPLES TESTED MINIMUM MAXIMUM  
Width Across Corners 8 1.6190 1.9300  
Grip Length 8 1.1100 1.1500  
Head Height 8 0.5460 0.5460  
Threads 8 PASS PASS

9890  
98902

ALL TESTS ARE IN ACCORDANCE WITH THE LATEST REVISIONS OF THE METHODS PRESCRIBED IN THE APPLICABLE SAE AND ASTM SPECIFICATIONS. THE SAMPLES TESTED CONFORM TO THE SPECIFICATIONS AS DESCRIBED/LISTED ABOVE AND WERE MANUFACTURED FREE OF MERCURY CONTAMINATION.  
THE STEEL WAS MELTED AND MANUFACTURED IN THE U.S.A. AND THE PRODUCT WAS MANUFACTURED AND TESTED IN THE U.S.A. WE CERTIFY THAT THIS DATA IS A TRUE REPRESENTATION OF INFORMATION PROVIDED BY THE MATERIAL SUPPLIER AND OUR TESTING LABORATORY. THIS CERTIFIED MATERIAL TEST REPORT RELATES ONLY TO THE ITEMS LISTED ON THIS DOCUMENT AND MAY NOT BE REPRODUCED EXCEPT IN FULL.



MECHANICAL FASTENER  
CERTIFICATE NO. A2LA 139-01  
EXPIRATION DATE 12/31/03

NUCOR FASTENER  
A DIVISION OF NUCOR CORPORATION

*Morton Schaffer*

MORTON SCHAFFER  
QUALITY ASSURANCE SUPERVISOR



LOT NO.  
243371A

Post Office Box 5100  
Saint Joe, Indiana 46785  
Telephone 260/337-1600

**FASTENER DIVISION**

CUSTOMER NO/NAME  
143 CORDOVA BOLT INC

TEST REPORT SERIAL# FB310961 NUCOR ORDER # 651058  
CUST PART #

TEST REPORT ISSUE DATE 6/13/08  
DATE SHIPPED 9/17/08 CUSTOMER P.O. # 025086

NAME OF LAB SAMPLER: Deann Moreno, LAB TECHNICIAN

\*\*\*\*\*CERTIFIED MATERIAL TEST REPORT\*\*\*\*\*

NUCOR PART NO QUANTITY LOT NO. DESCRIPTION  
165420 1400 243371A 7/8-9 X 2 1/2 A490 HVY HX  
MANUFACTURE DATE 6/10/08 STRUC SCREW PLAIN



--CHEMISTRY MATERIAL GRADE -4135MLV

MATERIAL NUMBER	HEAT NUMBER	CHEMISTRY COMPOSITION (WT% HEAT ANALYSIS) BY MATERIAL SUPPLIER									
		C	MN	P	S	SI	CR	MO	V	NUCOR STEEL - NEBRASKA	
RM024413	NU 844761	.34	.86	.011	.019	.25	.94	.16	.020	A2LA NO: 780.01 EXP: 2006-11-30	
		MIN .30								FOR CHEMICAL TESTING	
		MAX .48		.040	.040						

--MECHANICAL PROPERTIES IN ACCORDANCE WITH ASTM A490-08a

SURFACE HARDNESS (R30N)	CORE HARDNESS (RC)	PROOF LOAD 55450 LBS	TENSILE STRENGTH (LBS)	6 DEG-WEDGE STRESS (PSI)
N/A	34.9	PASS	76020	164545
N/A	34.4	PASS	75760	163983
N/A	35.4	PASS	76010	164524
N/A	35.1			
AVERAGE VALUES FROM TESTS		PRODUCTION LOT SIZE	32300 PCS	
35.0		75930	164351	

--VISUAL INSPECTION IN ACCORDANCE WITH ASTM F788  
 --WET MAGNETIC PARTICLE INSPECTION IN ACCORDANCE WITH ASTM A490-08a 4 PCS. SAMPLED LOT PASSED

--MICROHARDNESS TEST RESULT IN ACCORDANCE WITH SAE J121-99(HKN)  
 POSITION 1. 361 2. 376 3. 367  
 CARBURIZATION/DECARBURIZATION TEST IN ACCORDANCE WITH A490-08a LOT PASSED  
 HEAT TREATMENT - AUSTENITIZED, OIL QUENCHED & TEMPERED (MIN 800 DEG F)

--DIMENSIONS PER ASME B18.2.6-2003

CHARACTERISTIC	#SAMPLES TESTED	MINIMUM	MAXIMUM
Width Across Corners	8	1.6170	1.6230
Grip Length	8	0.8580	0.8730
Head Height	8	0.5560	0.5630
Threads	8	PASS	PASS

9890  
98902

ALL TESTS ARE IN ACCORDANCE WITH THE LATEST REVISIONS OF THE METHODS PRESCRIBED IN THE APPLICABLE SAE AND ASTM SPECIFICATIONS. THE SAMPLES TESTED CONFORM TO THE SPECIFICATIONS AS DESCRIBED/LISTED ABOVE AND WERE MANUFACTURED FREE OF MERCURY CONTAMINATION. NO HEATS TO WHICH BISMUTH, SELENIUM, TELLURIUM, OR LEAD WAS INTENTIONALLY ADDED HAVE BEEN USED TO PRODUCE THE BOLTS. THE STEEL WAS MELTED AND MANUFACTURED IN THE U.S.A. AND THE PRODUCT WAS MANUFACTURED AND TESTED IN THE U.S.A. WE CERTIFY THAT THIS DATA IS A TRUE REPRESENTATION OF INFORMATION PROVIDED BY THE MATERIAL SUPPLIER AND OUR TESTING LABORATORY. THIS CERTIFIED MATERIAL TEST REPORT RELATES ONLY TO THE ITEMS LISTED ON THIS DOCUMENT AND MAY NOT BE REPRODUCED EXCEPT IN FULL.



MECHANICAL FASTENER  
 CERTIFICATE NO. A2LA 139-01  
 EXPIRATION DATE 12/31/09

NUCOR FASTENER  
 A DIVISION OF NUCOR CORPORATION

*James B. Galamas*  
 JAMES GALAMAS  
 TECHNICAL SERVICES MANAGER



FACTORY : 601 YONGTAN-DONG, CHUNGLI-CITY,  
CHUNGCHENGBUK-DO, KOREA 380-250  
TEL : (043) 849 - 1114  
FAX : (043) 849 - 1234

FIELD OF TESTING : MECHANICAL TESTING  
LAB. ID. : 11883  
CERT. NO. : 882-01

STANDARD OF CERTIFIED : ISO/TS 18949, ISO 9001, ISO 14001  
CERT. NO. : TS-01899, AC-01899, EAC-01899  
PAGE 1/2

# INSPECTION CERTIFICATE

Customer : CORDOVA BOLT INC  
Description : ASTM A194 GR. 2H HEAVY HEX NUTS, PLAIN  
Grade : GR. 2H  
Size : 7/8-9UNC  
Marking : 2H, KPF LOGO  
Surface Condition : PLAIN  
Lot No. : F2K2317500  
Q'ty Shipped : 29,250 PCS

Certificate No. : J420081007057  
P/O No. : 024936  
L/C No. : CAD-CORDOVA BOLT  
Date Issued : 2008/10/07  
Date Shipped : 2008/10/13  
Date Tested : 2008/09/26  
Date Manufactured : 2008/09/19  
Specifications : ASTM A194/A194M - 04a

### 1. Chemical Composition (%)

Heat No.	C	Si	Mn	P	S	Cr	Ni	B	Cu	Ti	V	Al
Spec.	Min.	Max.	Min.	Max.	Max.	Min.	Max.	Max.	Max.	Max.	Max.	Max.
322455	43	21	70	18	15	9	1	6	22			

### 2. Macroetch Meel

Division	Surface Condition	Random Condition	Center Segregation	Spec. of Test Method
Results	S2	R2	C2	ASTM E381 -
Tested By	K. R. LEE			

### 3. Mechanical Properties

Division	Hardness		Specimen Tensile			Proof Load		Tensile Load	Sample Not Hardness 540°C/24hr	Impact Test	Sanding Test	Ball Penetration Hardness	Tap Hardness Fit Test	Decarburization Test By Hardness
	Surface	Core	Yield Strength	Elongation	Reduction of Area	Load	Elongation							
Unit	Min.	Max.	Min.	Max.	Min.	Max.	Min.	Max.	Min.	Max.	Average	Individual		
Spec.	Min.	Max.	Min.	Max.	Min.	Max.	Min.	Max.	Min.	Max.	Average	Individual		
Results	1	2	3	4	5	6	7	8	9	10	Avg.	Ind.		
	HRC	HRC	Yield	Elongation	Reduction of Area	Load	Elongation	HRC						
	24	35	31	31	30	80,850	1bf	39						
	31	31	31	31	30	6000	6000	29						
	31	31	31	31	30	6000	6000	29						
	31	31	31	31	30	6000	6000	29						
	31	31	31	31	30	6000	6000	29						
	31	31	31	31	30	6000	6000	29						
	31	31	31	31	30	6000	6000	29						
	31	31	31	31	30	6000	6000	29						
Tested By	G. Y. HWANG													
Spec. of Test Method	ASTM A370 -													

This is to certify that the above results are true and correct in every details

*G. Y. Hwang*

Chief of Quality Management Dept.

KPF





**TECHNICAL STAMPING, INC.**

50600 E. RUSSELL SCHMIDT BLVD.  
 CHESTERFIELD TWP., MI 48051  
 PH(586)948-3285 / FX(586)948-3286

**MATERIAL  
 CERTIFICATION**

CUSTOMER NAME			CUSTOMER ORDER NUMBER				DATE		
Cordova Bolt Inc.			24839				8/25/08		
PART NUMBER		CUSTOMER LOT NO.		LOT NUMBER		QUANTITY			
7/8" F436		87NWD3		0708-150		75,000			
STEEL GRADE	HEAT	C	MIN	P	S	SI	AL	REVISION	
SAE 1050	2143035	.53	.80	.007	.002	.051	.058	ASTM F-436-04	
SPECIFICATION		ACTUAL				GAUGE			
O.D -		1.719 - 1.781		1.752 - 1.755		CALIPER			
I.D -		.938 - .970		.954 - .957		CALIPER, PIN GAUGE			
THICKNESS-		.136 - .177		0.14		MICROMETER			
FLAT-		Max .010		.004		CALIPER			
HEAT TREAT -		38 - 45 HRC		42					
PLATING-				N / A					
OTHER				N / A					

WE HEARBY CERTIFY THIS PRODUCT WAS PRODUCED UNDER A ISO-9001:2000 QUALITY ASSURANCE SYSTEM, ISO-9001:2000 CERTIFICATION NUMBER-1265 - DATE OF REGIS. JAN. 3, 2003  
 ALL MATERIALS ARE MADE AND MELTED IN THE U.S.A. THIS PRODUCT WAS MANUFACTURED IN CHESTERFIELD, MICHIGAN, U.S.A. THIS PRODUCT CONFORMS TO ALL REQUIREMENTS  
 FOR WASHERS AS PRODUCED ACCORDING TO A.S.T.M. F-436-04. THE ABOVE TEST RESULTS APPLY ONLY TO THE ITEMS TESTED. THIS TEST REPORT MUST NOT BE REPRODUCED  
 EXCEPT IN FULL WITHOUT PRIOR WRITTEN APPROVAL.

9890  
 98902

AUTHORIZED SIGNATURE

CERTIFIED ISO 9001:2000

FIELD BOLTS						REMARKS <i>Cordova #D# 98902</i>	WEIGHT	
QUANTITY	DESCRIPTION	LENGTH		FT.	IN.			
2	4	3/4	A307 Bolts	0	6 1/2		5	
2	4	3/4	A307 Bolts	0	7 1/2		5	
3								
4								
5	8	3/4	A307 Hex Nuts					
6	8	3/4	A307 Washers				1	
7								
8	0							
9	0							
10	0							
11	0							
12	0							
13	0							
14	0							
15	0							
16	0							
17	0							
18	0							
19	0							
20	0							
21	0							
22	0							
23	0							
24	0							
25	0							
26	0							
27	0							
28	0							
29	0							
30	0					DOMESTIC ONLY		
NO.	DATE	REVISION		MADE BY	NO.	DATE	REVISION	MADE BY

**Herrick** MISCELLANEOUS MATERIALS SUMMARY STOCKTON  SAN BERNARDINO

Field Bolts MADE BY: AEU JOB NO.: 9890  
 U C Berkeley Hybrid Bracings CHKD BY: \_\_\_\_\_ SHEET: MS-2  
 Berkeley, CA DATE: 3/3/2009 WT: 11

SHOP DATE: 3/11/09 LOAD NO.: \_\_\_\_\_ SHOP ISSUE: \_\_\_\_\_



# Cordova Bolt, Inc.

5601 DOLLY AVENUE  
BUENA PARK, CA 90621  
(714) 739-7500

## CERTIFICATE OF CONFORMANCE Miscellaneous Materials

We certify, upon examination of the appropriate documents, records & specifications, that the material listed below conforms to applicable industry standards and that the manufacturing procedures for this material includes the required testing. Cordova Bolt, Inc. takes no part in the fabrication of this product and disclaims any responsibility for functional defects caused by the manufacturing process. Therefore, Cordova Bolt, Inc. expressly limits its responsibility to the replacement of defective parts.

Quantity	Description
4	3/4-10 X 6 1/2 NC A307A HEX MACH BOLT
4	3/4-10 X 7 1/2 NC A307A HEX MACH BOLT
8	3/4-10 HEX FINISH NUT
8	3/4-10 HEX FINISH NUT

Date: MARCH 6, 2009

Customer: THE HERRICK CORPORATION  
PO BOX 8429  
STOCKTON, CA 95208-0429

Customer Purchase Order No.: <sup>OB 9890</sup> 98902

Cordova Bolt Invoice No.: 689899-00

Signed:   
Quality Assurance Representative





BULL MOOSE TUBE ELKHART FACILITY  
CERTIFICATION OF TESTS

04/29/08  
Page 4 of 7

1819 Clarkson Rd.  
Chesterfield, Missouri 63017

BILL TO Herrick Corporation  
P.O. Box 8429  
Stockton CA 95208

SHIP TO HERRICK/STOCKTON STEEL  
BNSF C/O KEEP ON TRUCKING  
CCT / PORT OF STOCKTON, CA.  
BNSF DIRECT TRACK #9968  
STOCKTON CA

B/L Number 165180

Ship Via

TTPX\_804273

6" SQ X 0.500 HR X 42'													Order #	245951	
152.4 mm													Purchase Order #	24111	
ASTM A500-03 Grade B													Item #	115875 3840	
Ticket # = 59246072													P		
Heat # = 11974M08													YLD psi	TSN psi ELN %	
C	MN	P	S	AL	SI	CB	CU	CR	NI	VA					
.050	.730	.010	.006	.039	.011	.029	.030	.030	.020	.001		59850	68375	40	
6" SQ X 0.375 HR X 35'													Order #	245951	
152.4 mm													Purchase Order #	24111	
ASTM A500-03 Grade B													Item #	107858 3840	
Ticket # = 59246186													P		
Heat # = 11747M08													YLD psi	TSN psi ELN %	
C	MN	P	S	AL	SI	CB	CU	CR	NI	VA					
.060	.790	.013	.008	.032	.015	.032	.020	.030	.010	.002		64330	73501	34	
6" SQ X 0.375 HR X 35'													Order #	245951	
152.4 mm													Purchase Order #	24111	
ASTM A500-03 Grade B													Item #	107858 3840	
Ticket # = 59246191													P		
Heat # = L1084													YLD psi	TSN psi ELN %	
C	MN	P	S	AL	SI	CB	CU	CR	NI	VA					
.060	.630	.009	.008	.027	.020	.024	.170	.070	.080	0.000		58710	69163	37	
6" SQ X 0.250 HR X 34'													Order #	245951	
152.4 mm													Purchase Order #	24111	
ASTM A500-03 Grade B													Item #	101876 3840	
Ticket # = 59243265													P		
Heat # = L1069													YLD psi	TSN psi ELN %	
C	MN	P	S	AL	SI	CB	CU	CR	NI	VA					
.060	.770	.011	.012	.024	.030	.023	.170	.090	.070	.003		60960	72201	35	

Quality Manager: *Richard Long*

THIS WELDED STEEL TUBING IS MANUFACTURED IN THE UNITED STATES OF AMERICA AND HAS BEEN PRODUCED IN ACCORDANCE WITH THE STATED SPECIFICATION. LADLE CHEMISTRIES ARE REPORTED FROM DOCUMENTS PROVIDED BY THE SUPPLYING STEEL MILL. ANY PHYSICAL AND MECHANICAL TESTING RESULTS SHOWN ON THIS CERTIFICATION ARE CORRECT AS CONTAINED IN THE RECORDS OF THE COMPANY.



BULL MOOSE TUBE ELKHART FACILITY  
 CERTIFICATION OF TESTS

04/29/08  
 Page 7 of 7

1819 Clarkson Rd.  
 Chesterfield, Missouri 63017

**BILL TO** Herrick Corporation  
 P.O. Box 8429  
 Stockton CA 95208

**SHIP TO** HERRICK/STOCKTON STEEL  
 BNSF C/O KEEP ON TRUCKING  
 CGT / PORT OF STOCKTON, CA.  
 BNSF DIRECT TRACK #9968  
 STOCKTON CA

B/L Number 165180

Ship Via

TTPX\_804273

5" SQ X 0.312 HR X 38'				<b>Ladle Analysis and Physicals</b>								Order #	245962	
127.0 mm												Purchase Order #	24713	
ASTM A500-03 Grade B												Item #	111328 3200	
Ticket # = 59244860				Heat # = 23021M08								P		
C	MN	P	S	AL	SI	CB	CU	CR	NI	VA	YLD psi	TSN psi	ELN %	
.060	.780	.015	.009	.034	.011	.033	.040	.040	.020	.002	61970	72264	35	
5" SQ X 0.312 HR X 35'				<b>Ladle Analysis and Physicals</b>								Order #	245962	
127.0 mm												Purchase Order #	24713	
ASTM A500-03 Grade B												Item #	102245 3200	
Ticket # = 59244864				Heat # = 23021M08								P		
C	MN	P	S	AL	SI	CB	CU	CR	NI	VA	YLD psi	TSN psi	ELN %	
.060	.780	.015	.009	.034	.011	.033	.040	.040	.020	.002	61970	72264	35	

Quality Manager: *Richard Long*

THIS WELDED STEEL TUBING IS MANUFACTURED IN THE UNITED STATES OF AMERICA AND HAS BEEN PRODUCED IN ACCORDANCE WITH THE STATED SPECIFICATION. LADLE CHEMISTRIES ARE REPORTED FROM DOCUMENTS PROVIDED BY THE SUPPLYING STEEL MILL. ANY PHYSICAL AND MECHANICAL TESTING RESULTS SHOWN ON THIS CERTIFICATION ARE CORRECT AS CONTAINED IN THE RECORDS OF THE COMPANY.

DATE	3/21/07
INVOICE NO.	125455
BILL OF LADING	837798
CUSTOMER NO.	7950
CUSTOMER P.O.	\$ 22305-2230

**NUCOR-YAMATO STEEL CO.**  
P.O. BOX 1228 • BLYTHEVILLE, AR 72316

**CERTIFIED MILL TEST REPORT**

100% MELTED AND MANUFACTURED IN U.S.A.  
All shapes produced by Nucor-Yamato Steel are cast and rolled to a fully killed and fine grain practice.

S  
H  
I  
P  
T  
O  
  
SAN BERNARDINO STEEL  
C/O KEEP ON TRUCKING  
RANCHO CUCAMONGA, CA FOR TRK DEL TO  
SAN BERNARDINO, CA 92235

S  
P  
E  
C  
I  
F  
I  
C  
A  
T  
I  
O  
N  
S  
  
ASTM A992/A992M-06a A572/A572M GR50  
ASTM A709/A709M-03a GR50 (345)  
ASTM A709/A709M-03a GR50S (3456)  
ASTM A6/A6M-05a

S  
O  
L  
D  
T  
O  
  
HERRICK CORPORATION  
PO BOX 9125  
PLEASANTON, CA 94566

ITEM #	ITEM DESCRIPTION	QTY	HEAT #	MECHANICAL PROPERTIES						CHEMICAL PROPERTIES											CE	CI	
				YIELD TO TENSILE RATIO	YIELD STRENGTH	TENSILE STRENGTH	ELONG	CHARPY IMPACT		C	Mn	P	S	Si	Cu	Ni	Cr	Mo	V	Nb			Ti
					PSI	PSI		%	TEMP														
				MPa	MPa	%	* F	FT-LBS															
1	W08 - 24.0 51' W200 x 35.9 15.545 M	6	292513	.77	57000	74000	25					.08	1.12	.014	.035	.23	.30	.12	.13	.03	.00	.018	.33
				.76	56000	74000	23													.01	.18		
2	W08 - 28.0 50' W200 x 41.7 15.240 M	6	291731	.74	54000	73000	25					.07	1.20	.015	.030	.29	.25	.10	.12	.02	.00	.025	.32
				.74	55000	74000	23													.01	.16		
3	W08 - 28.0 50' W200 x 41.7 15.240 M	4	291733	.74	56000	76000	22					.07	1.20	.013	.030	.28	.23	.10	.09	.02	.00	.021	.31
				.74	56000	76000	23													.01	.15		
					386	524	22																
					386	524	23																

MTO  
4940

... LONGATION BASED ON 8.00 INCH GAUGE LENGTH

... hereby certify that the contents of this report are accurate and correct. All test results and operations performed by this material manufacturer are in compliance with the requirements of the material specifications, and when designated by the purchaser, meet the applicable specifications.

*Ray Linnell*  
QUALITY ASSURANCE

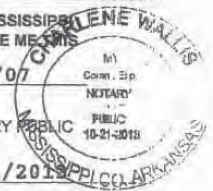
CUSTOMER COPY

STATE OF ARKANSAS COUNTY OF MISSISSIPPI  
SWORN TO AND SUBSCRIBED BEFORE ME

21 Day of 03/07

*Charlene Wallis* NOTARY PUBLIC

MY COMMISSION EXPIRES 10/21/2013



# MAANSHAN IRON AND STEEL COMPANY LIMITED

COMMODITY: HOT ROLLED STEEL WIDE FLANGE BEAMS  
 SPECIFICATION: W8, W10 AND W12 ACCORDING TO ASTM A992  
 W21 AND W18 ACCORDING TO ASTM A992 AND A572 GR 50

MILL'S TEST CERTIFICATE

W24.

PO 504604

CERTIFICATE NO.: 20070994-9  
 DATE: 2007-10-10

Size	Heat Number	Pieces	Weight □MT□	Chemical Analysis											Mechanical Properties						
				C	Si	Mn	P	S	Cr	Ni	Cu	V	Mo	Nb	Coq	Yield Strength R <sub>m</sub> (N/mm <sup>2</sup> )	Tensile Strength R <sub>m</sub> (N/mm <sup>2</sup> )	Elongation A <sub>500</sub> %			
24" x 76" x 45"	1070800540	9	13,950	0.17	0.21	1.26	0.019	0.015	0.020	0.010	0.010	0.010	0.010	0.010	0.020	0.360	395	510	520	28.0	27.5
24" x 76" x 45"	1070800541	3	4,650	0.17	0.21	1.19	0.018	0.017	0.010	0.010	0.010	0.010	0.010	0.010	0.020	0.360	400	520	515	27.0	28.5
24" x 76" x 50"	1070800536	14	24,108	0.15	0.21	1.23	0.022	0.017	0.030	0.010	0.010	0.010	0.010	0.020	0.370	385	525	530	27.5	27.3	
24" x 76" x 50"	1070800637	2	3,444	0.18	0.25	1.22	0.018	0.018	0.010	0.010	0.010	0.010	0.010	0.020	0.360	415	525	520	24.0	28.0	
24" x 76" x 55"	1070800642	4	7,578	0.16	0.25	1.20	0.024	0.018	0.020	0.010	0.010	0.010	0.010	0.020	0.370	415	530	525	28.5	28.5	
24" x 76" x 55"	1070800643	4	7,578	0.16	0.24	1.23	0.025	0.016	0.020	0.010	0.010	0.010	0.010	0.020	0.370	390	415	535	28.0	27.0	
24" x 84" x 40"	1070800635	18	37,208	0.16	0.21	1.28	0.023	0.017	0.030	0.010	0.010	0.010	0.010	0.020	0.360	405	525	525	27.0	27.0	
24" x 84" x 40"	1070800618	12	18,288	0.15	0.23	1.20	0.017	0.015	0.020	0.010	0.010	0.010	0.010	0.020	0.360	405	520	525	27.0	27.0	
24" x 84" x 45"	1070800616	11	18,885	0.16	0.22	1.23	0.017	0.025	0.010	0.010	0.010	0.010	0.010	0.020	0.370	385	400	515	28.5	29.0	
24" x 84" x 50"	1070800613	8	15,240	0.16	0.20	1.22	0.015	0.016	0.020	0.010	0.010	0.010	0.010	0.020	0.370	400	510	500	28.5	29.0	
24" x 84" x 55"	1070806030	9	16,884	0.16	0.20	1.26	0.029	0.031	0.010	0.010	0.010	0.010	0.010	0.020	0.380	385	390	510	27.0	27.0	
24" x 84" x 60"	1070800612	6	13,716	0.16	0.20	1.18	0.014	0.022	0.010	0.010	0.010	0.010	0.010	0.020	0.360	400	520	530	26.5	28.5	
24" x 94" x 35"	1070800602	1	1,484	0.15	0.21	1.18	0.015	0.024	0.020	0.010	0.010	0.010	0.010	0.020	0.360	400	535	540	28.0	27.0	
24" x 94" x 35"	1070800603	6	11,952	0.16	0.22	1.21	0.016	0.020	0.010	0.010	0.010	0.010	0.010	0.020	0.370	405	530	535	31.5	28.5	
24" x 94" x 40"	1070800598	6	13,058	0.16	0.22	1.24	0.015	0.022	0.030	0.010	0.010	0.010	0.010	0.020	0.360	405	530	530	26.5	28.0	
24" x 94" x 45"	1070800602	12	23,040	0.15	0.21	1.18	0.015	0.024	0.020	0.010	0.010	0.010	0.010	0.020	0.360	400	535	540	28.0	27.0	
24" x 94" x 50"	1070800685	5	10,670	0.15	0.22	1.18	0.022	0.018	0.020	0.010	0.010	0.010	0.010	0.020	0.360	430	540	546	27.5	27.0	
24" x 94" x 50"	1070800686	5	10,570	0.17	0.24	1.17	0.020	0.018	0.010	0.010	0.010	0.010	0.010	0.020	0.380	410	540	555	27.0	26.0	
24" x 94" x 55"	1070800591	3	7,041	0.17	0.23	1.23	0.021	0.016	0.030	0.010	0.010	0.010	0.010	0.020	0.380	400	585	545	28.0	26.0	
24" x 94" x 55"	1070800610	1	2,347	0.19	0.24	1.26	0.013	0.017	0.010	0.010	0.010	0.010	0.010	0.020	0.410	385	510	510	27.0	27.0	
24" x 94" x 55"	1070800611	5	11,735	0.15	0.23	1.21	0.018	0.020	0.020	0.010	0.010	0.010	0.010	0.020	0.360	385	515	515	28.5	28.0	
24" x 94" x 60"	1070800605	3	7,680	0.18	0.23	1.21	0.020	0.021	0.020	0.010	0.010	0.010	0.010	0.020	0.390	410	605	530	28.5	29.0	
24" x 94" x 60"	1070800608	3	7,680	0.17	0.21	1.17	0.014	0.018	0.020	0.010	0.010	0.010	0.010	0.020	0.370	385	400	505	29.0	29.5	
24" x 94" x 60"	1070800610	4	10,240	0.19	0.24	1.26	0.013	0.017	0.010	0.010	0.010	0.010	0.010	0.020	0.410	385	510	510	27.0	27.0	
8" x 18" x 35"	2070709654	66	18,744	0.17	0.24	1.30	0.023	0.016	0.020	0.010	0.010	0.010	0.010	0.020	0.400	435	435	575	30.0	28.0	
8" x 18" x 40"	2070710166	84	27,216	0.16	0.21	1.30	0.017	0.017	0.010	0.010	0.010	0.010	0.010	0.020	0.380	370	370	500	31.0	30.5	
8" x 18" x 45"	2070710000	16	5,840	0.16	0.24	1.22	0.013	0.024	0.020	0.010	0.010	0.010	0.010	0.024	0.010	0.380	430	430	565	31.0	30.0
8" x 18" x 50"	2070709447	48	19,440	0.15	0.21	1.24	0.019	0.020	0.030	0.010	0.010	0.010	0.010	0.024	0.010	0.370	430	435	575	28.5	30.0
8" x 18" x 60"	2070709664	42	20,412	0.16	0.24	1.26	0.022	0.024	0.020	0.010	0.010	0.010	0.010	0.025	0.010	0.380	365	365	540	35.0	34.0
8" x 21" x 40"	2070800012	7	2,674	0.15	0.23	1.25	0.026	0.020	0.030	0.010	0.010	0.010	0.010	0.020	0.010	0.370	375	405	540	33.0	33.5
8" x 21" x 40"	2070800013	8	3,438	0.16	0.24	1.22	0.022	0.019	0.020	0.010	0.010	0.010	0.010	0.020	0.010	0.370	370	405	535	30.0	33.5
8" x 21" x 50"	2070710335	14	6,678	0.17	0.22	1.33	0.030	0.026	0.020	0.010	0.010	0.010	0.010	0.030	0.010	0.400	365	365	520	30.5	32.5
8" x 21" x 60"	2070710300	7	4,004	0.15	0.26	1.26	0.019	0.019	0.040	0.010	0.010	0.010	0.010	0.026	0.010	0.360	360	370	525	30.0	31.0
8" x 21" x 80"	2070710311	17	9,724	0.19	0.24	1.36	0.028	0.020	0.020	0.010	0.010	0.010	0.010	0.028	0.010	0.430	370	375	545	33.0	33.0
10" x 12" x 35"	2070800008	1	0.191	0.21	1.11	0.023	0.016	0.030	0.030	0.020	0.010	0.010	0.010	0.017	0.010	0.360	390	400	510	31.0	37.0
10" x 12" x 35"	2070600010	2	0.382	0.16	0.23	1.14	0.021	0.019	0.020	0.020	0.010	0.010	0.010	0.014	0.010	0.350	410	400	525	29.0	30.0
10" x 12" x 35"	2070600011	1	0.161	0.15	0.20	1.13	0.025	0.018	0.020	0.010	0.010	0.010	0.010	0.016	0.010	0.350	410	425	540	28.5	28.0
10" x 12" x 35"	2070600012	2	0.382	0.16	0.23	1.14	0.023	0.017	0.020	0.010	0.010	0.010	0.010	0.017	0.010	0.360	370	410	530	30.0	27.5
10" x 12" x 35"	2070600013	1	0.191	0.16	0.23	1.13	0.021	0.017	0.020	0.010	0.010	0.010	0.010	0.015	0.010	0.350	400	425	510	28.5	28.5
10" x 12" x 35"	2070600014	1	0.161	0.16	0.20	1.11	0.018	0.013	0.020	0.010	0.010	0.010	0.010	0.014	0.010	0.360	425	420	530	28.0	29.0





Украина  
Ukraine

МАРИУПОЛЬСКИЙ МЕТАЛЛУРГИЧЕСКИЙ  
КОМБИНАТ ИМЕНА ИЛЬИЧА  
ILYICH IRON & STEEL WORKS OF MARIUPOLE

СЕРТИФИКАТ КАЧЕСТВА N  
QUALITY CERTIFICATE No 22558

От  
Date 11.07.2008

Лист 1  
Sheet 1

Из 1  
Of 1

Листов  
Sheets

87504, Г. Мариуполь, Ул. Левченко, 1. Телекс 115157 DEFO SU

Свидетельство о приемочных испытаниях

Inspection certificate

EN 10204-3.1

Контракт N 12EXH/001-07  
Contract No UF70107317

Заводской заказ N  
Manufacturer's work order No UF7-001073170327

Заказчик  
Customer SALLZITTER MANNESMANN INTERNATIONAL GmbH

Вароч N 66681354  
Specification No 317UF

Наименование товара  
Description of goods Прокат толстолистовой

Марка стали  
Grade of steel Стандарты ASTM A572/A572M-01

Gr. 50 TYPE 2

Состояние поставки  
Delivery condition Горячекатаный лист

Маркировка  
Marking Trade mark, Made in Ukraine, Grade of steel, Cast No, Test No, Lot 4, Dimensions in, Houston, One colour stroke red and one colour stroke green at both ends of the plate.

Клеймо  
Hard stamp Trade Mark, Grade of steel, Cast No

Размеры, дюйм  
Dimensions, inch

Толщина, дюйм  
Thickness, inch

Длина, дюйм  
Length, inch

Кол-во, шт.  
Number of pieces, pcs

Теоретическая масса, тн  
Theoretical mass, tn

284240 14857 1/2 96 240 10 14.820

284241 14855 3/4 96 240 2 4.446

284242 14856 1/2 96 240 23 34.086

284255 14862 1 96 240 4 11.852

39 65.204

Выплавка  
Steelmaking process Конвертерный способ производства

Made by the BOF process

Химический состав, %  
Chemical composition, %

Плавка Cast No	x100										x1000								
	C	Mn	Si	S	P	Cr	Ni	Cu	Ti	Al	As	N	Mo	V	Nb	Ca	B	Seg	Por
284240	18	107	21	10	25	5	2	2	6	27	2	6	3	47	4	-	-	36	-
284241	18	97	20	18	18	7	2	3	6	33	3	8	3	52	4	-	-	34	-
284242	20	105	22	12	15	3	2	2	4	29	3	6	2	49	4	-	-	38	-
284255	20	106	22	17	18	4	1	2	4	45	2	6	3	50	5	-	-	38	-

Lavchenko str. 1, Mariupol, 87504. Telex 115157 DEFO SU

Результаты испытаний

Размеры обр.  
Dimensions

Толщина/диаметр  
Thickness/diameter

Ширина  
Width

Напряжения обр.  
Tension

Темп. испит.  
Test temperature

Предел текучести  
Yield point

Предел прочности  
Tensile strength

Отн. удлинение  
Elongation

Отн. сужение  
Reduction of area

Тип надреза  
Notch type

Энергия удара  
Impact energy KV/KU

Энергия удара  
Impact energy KV/KU

Энергия удара  
Impact energy KV/KU

Энергия удара  
Impact energy KV/KU

Энергия удара  
Impact energy KV/KU

Энергия удара  
Impact energy KV/KU

Среднее значение  
Average value KV/KU

Классиф.  
Band test

Kor-na vna sost.

Л-пробитие/Longitudinal

д-пробитие/Transverse

Примечание / Note

Поставка соответствует условиям заказа. Осмотр поверхности без замечаний. Размеры проката в пределах допусков. Delivery conforms to conditions of the order. Surface examination without remarks. Rolled product dimensions within the tolerance limit.

It is hereby certified that the quality of goods mentioned in this certificate is in conformity with the standards and specifications.

Указанный в ласточке сертификате товар соответствует по качеству действующим стандартам и техническим условиям.

Подпись  
Signature

Подпись эксперта  
Expert's stamp

Подпись  
Signature

Подпись  
Signature

Подпись  
Signature

Подпись  
Signature

Подпись  
Signature

Подпись  
Signature

Подпись  
Signature

Подпись  
Signature

Подпись  
Signature

Подпись  
Signature

Подпись  
Signature

Подпись  
Signature

Подпись  
Signature

Подпись  
Signature

Подпись  
Signature

Подпись  
Signature

Подпись  
Signature

Подпись  
Signature

Подпись  
Signature

Подпись  
Signature

Подпись  
Signature

Подпись  
Signature

Подпись  
Signature

Подпись  
Signature

Подпись  
Signature

Подпись  
Signature

Подпись  
Signature

Подпись  
Signature

Подпись  
Signature

Подпись  
Signature

Подпись  
Signature

Подпись  
Signature

Подпись  
Signature

Подпись  
Signature

Atlas Tube Canada ULC  
 200 Clerk St.  
 Harrow, Ontario, Canada  
 NOR 1G0  
 Tel: 519-738-3541  
 Fax: 519-738-3537



Ref.B/L: 80349184  
 Date: 07.28.2009  
 Customer: 741

**Sold to**

Totten Tubes, Inc.  
 500 Danlee Street  
 AZUSA CA 91702-2341  
 USA

**MATERIAL TEST REPORT**

**Shipped to**

Totten Tubes, Inc.  
 500 Danlee Street  
 AZUSA CA 91702-2341  
 USA

Material: 5.000x500x42\*0\*(7x1).  
 Sales order: 486470

Material No: R050005004200  
 Purchase Order: 42808  
 Made in: Canada

Heat No	C	Mn	P	S	Si	Al	Cu	Cb	Mo	Ni	Cr	V	Ti
T82689	0.180	0.740	0.007	0.006	0.017	0.059	0.020	0.004	0.003	0.010	0.020	0.001	0.001
Bundle No	Yield		Tensile		Eln.2in		Certification				CE: 0.32		
M100871850	065881 Psi		072580 Psi		33.1 %		ASTM A500-07 GRADE B&C						

Material Note:  
 Sales Or.Note:

Material: 6.625x500x21\*0\*(2x1)PB  
 Sales order: 488857

Material No: R06625500  
 Purchase Order: 42532  
 Made in: Canada

Heat No	C	Mn	P	S	Si	Al	Cu	Cb	Mo	Ni	Cr	V	Ti
R83454	0.190	0.800	0.013	0.008	0.009	0.036	0.040	0.005	0.006	0.010	0.040	0.001	0.001
Bundle No	Yield		Tensile		Eln.2in		Certification				CE: 0.34		
0002167296	059650 Psi		071800 Psi		36.9 %		ASTM A500-07 GRADE B&C						

Material Note:  
 Sales Or.Note:

Material: 6.625x500x48\*0\*(15x1).  
 Sales order: 488857

Material No: R066255004800  
 Purchase Order: 42532  
 Made in: Canada

Heat No	C	Mn	P	S	Si	Al	Cu	Cb	Mo	Ni	Cr	V	Ti
R83455	0.190	0.780	0.013	0.006	0.009	0.036	0.030	0.005	0.005	0.020	0.030	0.001	0.001
Bundle No	Yield		Tensile		Eln.2in		Certification				CE: 0.33		
M100869166	067540 Psi		075920 Psi		30.9 %		ASTM A500-07 GRADE B&C						

Material Note:  
 Sales Or.Note:

9890  
 98904

*M. White*

Your P.C. # 989-04  
 Our Snipe # 97272  
 Covering lpc Ft.  
 A true copy from our records.  
 TOTTEN TUBES, INC.  
 M.T. a.c.

Authorized by Quality Assurance:  
 The results reported on this report represent the actual attributes of the material furnished and indicate full compliance with all applicable specification and contract requirements.  
 Calculated using the AWS D1.1 method.



42205



# Louisiana Steel, Inc.

## TEST CERTIFICATE

316 Jungermann Rd. St. Peters, MO 63376  
(636) 447-5255 fax (636) 447-6351

9890  
98904

DATE 6/23/09  
CERTIFICATE NO. 5004825  
SALES ORDER 6670  
MILL ORDER NO. 9621

PRODUCT ROUND TUBING  
SIZE 6.000 X .500  
SPECIFICATION ASTM A500 GR B

CUSTOMER Tottem Tubes Inc.  
500 Danlee Street  
Azusa CA 91702  
PO# 42305

### CHEMICAL ANALYSIS

HEAT NO.	C	Mn	P	S	Si	Ni	Cr	Mo	AJ	Cu	V
5378-6048	.20	.86	.016	.006	.030	.010	.030		.027	.030	.001

### PHYSICAL ANALYSIS

HEAT NO.	YIELD	TENSILE	ELONGATION	HARDNESS	FLATTENING	GRAIN SIZE	HEAT TREATMENT
5378-6048	68,100	77,600	33.0%		YES		

REMARKS

Your P.C. # 585-04  
 Our Shipper # 97272  
 Covering LAC  
 A true copy from our records.  
 TOTTEN TUBES, INC.  
 M.T. 19

WE HEREBY CERTIFY THAT THIS CERTIFICATE IS CORRECT AS CONTAINED IN OUR RECORDS.

QUALITY ASSURANCE MANAGER

ID: 935294

ArcelorMittal Burns Harbor Plate

QUALITY ASSURANCE  
REPORT OF TEST AND ANALYSIS

SHIPMENT NO. <b>802-38175</b>	DATE SHIPPED <b>08-28-08</b>	CAR OR VEHICLE NO. <b>EJE-EOLA-BNSF BN 621734</b>	PAGE <b>4</b>
S O L D I E R S : PRIMARY STEEL LLC GARY STEEL CO DIV 1699 W GRAND AVE OAKLAND CA 94607		S H I P T O : PRIMARY STEEL INC GARY STEEL CO DIV BNSF SIDING 690 OAKLAND CA	

S E R I A L N O T E	SERIAL NUMBER	PAT NO.	HEAT NUMBER	NO. PCS.	SIZE AND QUANTITY				WEIGHT	YIELD POINT	TENSILE STRENGTH	ELONG	RED
					THICKNESS	WIDTH OR DIA.	LENGTH						

INCHES INCHES INCHES POUNDS PSI PSI IN % %

QUALITY STEEL MELTED & MANUFACTURED IN THE U. S. A.  
TEST PERFORMED AT A ARCELORMITTAL APPROVED LABORATORY

PLATES - ASTM A709-07 GR 50 TYPE 2, ASTM A572-07 GR 50 TYPE 2 --- SHD MILL -  
MILL EDGE  
MFST - MILL EDGE - CUT LGTH ONLY MFST MILL SERIAL#  
LIFT MAX 20 TON UNLDG OH-PLATE HOOK LOAD MAX 185000 #

CO# 6147703 GH 843-2015D  
823B72300 4 3/4 96 360 29404 63100 88200 8 18  
62000 86900 8 20

PLATES - ASTM A709-03A GR 36, ASTM A 36-00A,  
ASME SA36 2004 EDITION  
MFST - MFST MILL SERIAL# LIFT MAX 20 TON UNLDG  
OH-PLATE HOOK LOAD MAX 185000 #

CO# 6153164 GH 843-2076H  
812C33280 1 1 1/2 96 240 9801 38600 67500 8 33

Q-QUENCH TEMPERATURE	T-TEMPERATURE	N-NORMALIZE TEMPERATURE
----------------------	---------------	-------------------------

SERIAL NUMBER	PAT NO.	HEAT NUMBER	HARD BHW	BEND	THICKNESS INCHES	TYPE	SIZE	DIR	TEST TEMP F	CHARPY IMPACT								
										ENERGY FT LBS			SHEAR(%)			LAT EXP MILS		
										1	2	3	1	2	3	1	2	3

HEAT NUMBER	CHEMICAL ANALYSIS															MCQUAD GRAIN SIZE
	C	Mn	P	S	Si	Cu	Ni	Cr	Mo	V	Ti	Al	B	Co	N	
823B72300	.19	1.30	.008	.005	.301	.022	.01	.02	.007	.060	.002	.034		.002	.009	.002
812C33280	.15	1.11	.008	.007	.188	.024	.02	.03	.008	.001	.002	.034	.0002	.002	.004	.004

I certify that the above results are a true and correct copy of actual results contained in records maintained by ArcelorMittal Burns Harbor and are in full compliance with the requirements of the specification cited above. This test report cannot be altered and must be transmitted intact with any subsequent third party test reports, if required.

SHIP TRIP TIME: \_\_\_\_\_ SUPV. QUALITY ASSURANCE: **D. W. ELWOOD** PER **WNK**



1770 Bill Sharp Boulevard, Muscatine, IA 52761-9412

# Test Certificate

Form TCI: Revision 1: Date: 31 Oct 2000

B20

<b>Customer:</b> GARY STEEL C/O NAMASCO 500-500 COLONIAL CENTER PARKWA ROSWELL GA 30076 1606		<b>Customer P.O. No.:</b> 22860 <b>Product Description:</b> ASTM A572-50/M345(06)/A709-50/M345(06A)		<b>Mill Order No.:</b> 41-196562-01 <b>Shipping Manifest:</b> MR046378	
<b>Ship Date:</b> 16 Oct 07 <b>Cert Date:</b> 16 Oct 07		<b>Ship Date:</b> 16 Oct 07 <b>Cert Date:</b> 16 Oct 07		<b>Cert No:</b> 061078029 (Page 1 of 1)	
<b>Size:</b> 0.500 X 96.00 X 480.0 (IN)					
Heat Id		Tensiles		Charpy Impact Tests	
Piece Id	Piece Dimensions	YS (PSI)	UTS (PSI)	%RA	Elong % 2in
D04	0.495 X 96.00 (DISCRD)	50000	67000	35	36
D05	0.495 X 96.00 (DISCRD)	59000	76000	36	36
Heat Id		Chemical Analysis		Average Hardness	
C	Mn	P	S	Si	Tot Al
A7J157	.06	1.33	.009	.004	.31
B7J635	.06	1.36	.010	.004	.31
Heat Id		Chemical Analysis		Average Hardness	
Cr	Ni	Cu	Mp	Ch	V
A7J157	.14	.19	.05	.001	.078
B7J635	.10	.18	.05	.001	.080
MERCURY IS NOT A METALLURGICAL COMPONENT OF THE STEEL AND NO MERCURY WAS INTENTIONALLY ADDED DURING THE MANUFACTURE OF THIS PRODUCT. .008 MELTET AND MANUFACTURED IN THE USA, MTR DIN EN-32C4 TYPE 3.1 COMPLIANT. B7J635 D05 PCS: 5, WGT: 32739 A7J157 D04 PCS: 10, WGT: 65468					
Primary Steel LLC CUSTOMER _____ CUSTOMER PO# _____					
WE HEREBY CERTIFY THAT THIS MATERIAL WAS TESTED IN ACCORDANCE WITH THE APPROPRIATE SPECIFICATION					
B. H. Wales SENIOR METALLURGIST - PRODUCT					



California Steel Industries  
14000 San Bernardino Ave.  
Fontana, California 92335

**CERTIFIED TEST REPORT**

CUSTOMER ORDER 93-CT2096-000	NO. NUMBER 01-2608-05	CERTIFICATION DATE 04/20/10	RR: UP210054	TALLY NUMBER HS 250845643 1/
BUYER PDM STEEL SERVICE CENTERS, INC. SUB. OF RELIANCE STEEL & ALUMINUM P.O. BOX 11188 FRESNO CA 93772		SHIP TO PDM STEEL SERVICE, INC. (PDF) FERALLOY CORPORATION 936 PERFORMANCE DRIVE STOCKTON CA 95206		

TEST REPORT MUST ACCOMPANY ALL LOADS - NO EXCEPTIONS.

END USE WAREHOUSE STOCK
PROD H.R. SHEET PROCESSED COIL (ME) - PRIME
SPEC ASTM-A-1011-08-CS-TYPE B

TR 1	INSPECTION MILL		
DESCRIPTION	COILS, PIECES OR BUNDLES	HEAT NUMBER	I certify that the material described herein has been manufactured and tested in accordance with the requirements of the referenced specification, and the test results conform to the specification requirements.   Chief - Laboratory Services  This steel is rolled, processed and substantially transformed in the USA.
.1310 x 72.0000 x COIL NOM ME	1 1	T48013 T48447	

MECHANICAL PROPERTIES							CHEMICAL ANALYSIS														05:12:13 04/19/10 MM		
HEAT OR LOT NUMBER	SLAB NUMBER	L O C	YIELD KSI	TENSILE STRENGTH KSI	% ELONGATION		BEND TEST																
					0.2	2		C	Mn	P	S	Si	Cu	Ni	Cr	Mo	Al	V	Co	Ti	B	N	
T48013								07	.39	012	010	015	01	00	02	00	043	001	000	001	0001	001	
T48447								08	.38	012	007	012	01	00	02	00	059	001	000	001	0001	002	
Material is RoHS compliant																							

**Bill To:** PDM - STOCKTON, CALIFORNIA  
 P.O. BOX 310  
 STOCKTON CA US  
 95201-0310

**Ship To: 1**  
 PDM STEEL SERVICE CENTER  
 3535 EAST MYRTLE STREET  
 SP SPUR# 8635  
 STOCKTON CA US  
 95205

**Order Date:** 02/28/2008  
 PO No: ST2422  
 Mill Order No: 3449307  
 Load No: 1204958  
 Manifest No: 1913726

**CERTIFIED MATERIAL TEST REPORT**  
 GERDAU AMERISTEEL  
 Petersburg Mill  
 GERDAUAMENSTEEL 25801 Hofheimer Way  
 Petersburg, VA 23803  
 (804)524-2855

**HEAT NO:** 30424590  
**SIZE:** W 24 X 117# / W610 X 174  
**GRADE:** 992/572-50  
**LENGTH:** 50 FT / 15.24 M  
**PRODUCT:** WF BEAMS

**ASTM A6-05a, A992-06a, A572-06**

CHEMICAL ANALYSIS														
	C	Mn	P	S	Si	Cu	Ni	Cr	Mo	Sn	V	Al	Nb	CE
	.10	1.19	.011	.029	.24	.28	.09	.08	.019	.011	.001	.002	.019	.34

**PHYSICAL PROPERTIES**

Yield Strength	KSI	MPa	Tensile Strength		Elongation		Bend Test	ROA	
			KSI	MPa	%	Gage Length			
51.7	356.5	70.8	70.8	488.1	1.231	7.94	25.0	8 In	200 mm
52.0	358.5	71.9	71.9	495.7	1.257	8.11	24.1	8 In	200 mm

All manufacturing processes of this product, including electric arc melting and continuous casting, occurred in the U.S.A. CMTR complies with DIN EN 10204 3.1.5

"I hereby certify that the contents of this report are correct and accurate. All tests and operations performed by this material manufacturer or its sub-contractors, when applicable, are in compliance with the requirements of the material specifications and applicable purchaser designated requirements."

Signed: Tom L. Harrington Date: Jul. 14, 2008 Signed: \_\_\_\_\_ Date: \_\_\_\_\_  
 Tom L. Harrington: Quality Assurance Manager Notary Public (if applicable)

NUCOR-YAMATO STEEL CO.

P O BOX 1228  
 BLYTHEVILLE AR 72316

DATE  
 9/29/09

CERTIFIED MILL TEST REPORT  
 100% MELTED AND MANUFACTURED IN U.S.A

All shapes produced by Nucor-Yamato Steel are cast and rolled to a fully killed and fine grain practice.

SOLD TO		SHIP TO		INVOICE	CUSTOMER NO.
P.D.M. SERVICE CENTER		P.D.M SERVICE CENTER - ST		316244	8911
PO BOX 310		P O BOX 310		BILL OF LADING	CUSTOMER P.O.
STOCKTON, CA 95201		3535 E. MYRTLE ST. STOCKTON, CA 95201		965314	ST 4212 FF
*1 SPECIFICATIONS GRADE: ASTM A709/A709M-09 GR50S (345S)      ASTM A992/A992M-06a A572/A572M GR50-07      ASTM A709/A709M-09 GR50 (345) ASTM A6/A6M-08a					

ITEM	ITEM DESCRIPTION	QTY	HEAT #	MECHANICAL PROPERTIES								CHEMICAL PROPERTIES															
				VIBES TO TENSILE HEAD	YIELD STRENGTH F <sub>y</sub> MPa	TENSILE STRENGTH F <sub>t</sub> MPa	ELONG % N	CHARTY IMPACT		C	Mn	P	S	Si	Cu	Ni	Cr	Mo	V	Cb	CE						
								TEMP F	IMPACT ENERGY FT-LBS																		
1	W12 - 96.0	2	338701	.75	55000	73000	26																				
	60'			.77	56000	73000	25																				
	W310 x143.0 18.288 M				379	503	26																				
2	W12 - 96.0	3	338703	.75	55000	73000	25																				
	60'			.78	56000	72000	26																				
	W310 x143.0 18.288 M				379	503	25																				
3	W12 -120.0	3	338688	.77	55000	71000	28																				
	60'			.76	55000	72000	27																				
	W310 x179.0 18.288 M				379	490	28																				
4	W12 -136.0	1	313022	.78	59000	76000	26																				
	50'			.76	58000	76000	26																				
	W310 x202.0 15.240 M				407	524	26																				
5	W12 -136.0	2	313024	.75	55000	73000	27																				
	50'			.76	55000	72000	27																				
	W310 x202.0 15.240 M				379	503	27																				

ELONGATION BASED ON 8.00 INCH GAUGE LENGTH  
 $P_{cm} = C + Si / 30 + Mn / 20 + Cu / 20 + Ni / 60 + Cr / 20 + Mo / 15 + V / 10 + 5B$  B-Approx. .0005  
 CARBON EQUIVALENT CE =  $C + Mn/6 + (Cr+Mo+V) / 5 + (Ni+Cu) / 15$   
 Corrosion Index:  $CI = 26.01(\%Cu) + 3.88(\%Ni) + 1.2(\%Cr) + 1.49(\%Si) + 17.28(\%P) - 7.29(\%Cu)(\%Ni) - 9.10(\%Ni)(\%P) - 33.39(\%Cu)^2$

I hereby certify that the contents of this report are accurate and correct. All test results and operations performed by this material manufacturer are in compliance with the requirements of the material specifications listed in the Specifications Block above.  
 GARY PENNELL  
 QUALITY ASSURANCE

STATE OF ARKANSAS  
 COUNTY OF MISSISSIPPI  
 SWORN TO AND SUBSCRIBED BEFORE ME THIS  
 Day of  
 NOTARY PUBLIC



**Mill Test Report**  
Page 2

Issuing Date : 01/19/2010 B/L No. : 250778 Our Order No. : 78436/13  
 Vehicle No: TTPX 805495 Sold To : RANGER STEEL SERVICES LP  
 Specification : 2.0000" x 96.000" x 240.000" 1225 NORTH LOOP W. STE 650  
 ASTM A572 Grade 50-07/ASTM A709 Grade 50-08a/AASHTO M270-50 HOUSTON, TX 77008  
 Type 2

Marking :

Heat No	C	Mn	P	S	SI	Cu	NI	Cr	Mo	Alto3	V	Nb	Ti	N	Ca	B	Sn	CEQ	PCMI
0500463	0.19	1.16	0.016	0.004	0.15	0.30	0.09	0.10	0.02	0.005	0.036	0.001	0.001	0.001	0.0002	0.0002	0.012	0.44	0.28
0500464	0.18	1.17	0.012	0.003	0.16	0.31	0.09	0.08	0.02	0.006	0.038	0.001	0.001	0.001	0.0003	0.0003	0.013	0.43	0.27

Plate Serial No	Pieces	Tens Dir.	Tensile Test		Elongation		Charpy Impacts		Temp (F)	Min Ave.	
			Yield (psi)	Tensile (psi)	% in 2"	% in 8"	Dir.	(ft-lb) shear			(ft-lb) shear
0500463-04	4	T	54,600	81,700	16.3	16.3	H-L	27.3	31.0	-20	25
			56,300	82,700	16.0	16.0	H-L	26.7	22.3	-20	25
						27.3	27.1	-20	25		
0500464-01	3	T	60,300	85,000	17.1	17.1	H-L	29.6	28.9	-20	25
			56,800	83,700	17.8	17.8	H-L	29.3	29.5	-20	25

A 2881-00019  
# 91625

RANGER STEEL  
QUALITY APPROVED

Manufactured to fully utilize practice by Electric Arc Furnace. Welding or weld repair was not performed on this material. Memory has not been used in the direct manufacturing of this material. Produced as continuous cast discrete plate as-rolled, unless otherwise noted in Specification.  
 Yield by 0.5EUL method unless otherwise specified. Ceq = C+(Mn/6)+(Cr+Ni+V/5)+(Cu+Ni/15)  
 Form = C+(S/0.004)+(P/0.002)+(Cu/20)+(Nb/5)+(Ti/5)+(V/10)+SE  
 Melted and manufactured in the USA. ISO 9001-2000 certified #0006461 by SRI Quality System Registrar #00665-09. PED 9729EC 72 Annex 1, Para. 4.3 Compliant.  
 DIN 50046 3, 1.9E6 10204 3, 1.9E6 10204 3, 1.2005 compliant. For ABS grades only. Quality Assurance certificate 06-IMPQA-383

T. A. Deppe  
F. A. Deppe, Metallurgist

01/25/2010 8:17:05 AM

A288U-0001V  
# 464400

<b>EVRAZ</b> Evraz Oregon Steel 14400 N. Riverside Blvd., Portland, Oregon 97203		<b>REPORT OF CHEMICAL/PHYSICAL TESTS</b>		CERTIFICATE NO. 1080475	DATE Feb 25, 2010	PAGE 2
<b>ISO 9001</b> REGISTERED PLATE MANUFACTURER		PDK STEEL SERVICE CENTER (FRESNO) ATTN: ACCOUNTS PAYABLE PO BOX 11188 FRESNO, CA 93772 USA		MAIL ORDER NO. 230629	DATE 02/25/2010	
THIS MATERIAL HAS BEEN MANUFACTURED, TESTED AND FOUND TO MEET THE SPECIFICATIONS AND PURCHASE ORDER REQUIREMENTS HSLA STRUCTURAL QUALITY PLATE ASTM A572-07 GRADE 50 ASTM A709-97B GRADE 50.		PITTSBURGH-DES MOINES / FRESNO ATTN: ACCOUNTS PAYABLE PO BOX 11188 FRESNO, CA 93772		CUSTOMER ORDER NO. 94-PP1041-003		
				SHIPMENT NO. 1080475	DATE 02/25/2010	
				CARRIER DHL PACIFIC		
				CAPTRUCK NO. DP262091		

PHYSICAL PROPERTIES									
HEAT NO.	DESCRIPTION	HEAT NO.	SLAB	YIELD PSI X 100	TENSILE PSI X 100	% ELONG 8" 2"	% RA	HARDNESS BHN	IMPACTS
5	0.6250 X 96.0000 X 240.000 PT# 1744250								
	3 PCS 12252 LBS	~ M13741		550	665 30				
	2 PCS 8168 LBS	~ M13742		575	690 27				
	29 PCS 79232 LBS TOTALS			550	705 25				
				580	705 24				

CHEMICAL ANALYSIS																	
HEAT NO.	C	Mn	P	S	Si	Cu	Ni	V	CS	Al	Cr	Mo	Ti	B	N	Cu	CE
M13741	.08	1.07	.010	.001	.25	.01	.01	.014	.030	.037	.01	.00	.002				.0034
M13742	.08	1.04	.010	.002	.26	.01	.01	.015	.031	.038	.01	.00	.002				.0022
HEATS INDICATED WITH (+) WERE MELTED & MANUFACTURED IN THE USA. HEATS INDICATED WITH (-) WERE ROLLED IN THE USA.																	
***** END OF REPORT *****																	

I certify the above to be correct as contained in the records of EVRAZ INC. NA By *A. K. ...* Technical Support Coordinator



# MATERIAL TEST REPORT

803

**SOLD TO:**  
STROCAL, INC.  
2324 NAVY DRIVE  
STOCKTON, CA

**SPECIFICATION:**  
ASTM A572-04 Grade 55

MILL ORDER	BILL OF LADING	CUSTOMER P.O. NO.	DATE
180503	225367	W74280A-803/REV	01/27/06

Unless otherwise specified, the following conditions apply: 1. Material is 100% melted and manufactured in the USA. 2. Mercury, radium or alpha source materials have not been used. 3. Test piece serial # represents actual plate tested, not necessarily plate shipped (except PVO where every plate is tested).

HEAT	CHEMICAL ANALYSIS											Acid Soluble			B		
	C	Mn	P	S	SI	Cu	Ni	Cr	Mo	Sn	Al	V	Nb	N		Acid Soluble AI	TI
1W380	0.15	1.42	0.023	0.022	0.35	0.48	0.19	0.18	0.048	0.019	0.009	0.110	0.003	0.011	0.009	0.003	0.0000
1W283	0.14	1.16	0.015	0.034	0.32	0.38	0.21	0.10	0.047	0.020	0.007	0.075	0.003	0.010	0.006	0.003	0.0000

HEAT	NO PCS	DIMENSION			TENSILE TESTS			IMPACT TESTS				
		GAUGE (IN)	WIDTH (IN)	LENGTH (IN)	TENSILE (KSI)	YIELD (KSI)	ELONG % IN	BEND TEMP (F)	TEST TEMP (F)	FT-LBS	MILS LAT EXP	% SHEAR
1W380	1	0.8750	96.0000	480.0000	95	67	23	2		1	2	3
1W283	1	0.8750	96.0000	480.0000	83	59	26	2		1	2	3

**OTHER TESTS / INFORMATION**

Fine Grain Practice  
Reported Yield Strength is from 0.2% offset Method

(Wgt. 175155 lbs) Page 4 (Tot Pcs: 13)

DAVID J. CERNAVA  
CHIEF METALLURGIST

*D. J. Cernava*

I CERTIFY THE ABOVE RESULTS TO BE CORRECT AS CONTAINED IN THE RECORDS OF THE CORPORATION

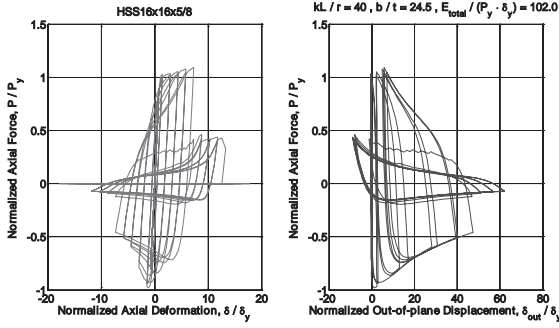
---

## **Appendix J**

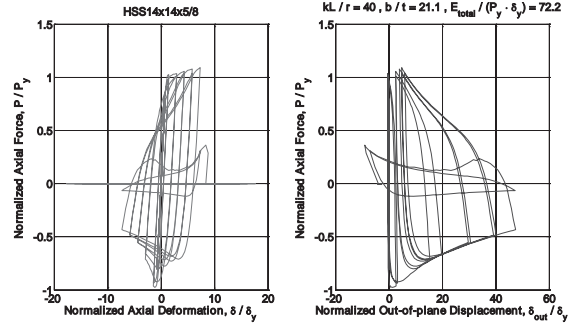
### **Response Plots of Square Hollow Structural Sections**

---

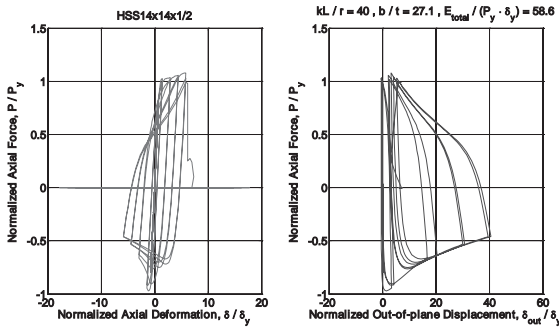
**(a)  $kL/r = 40$**



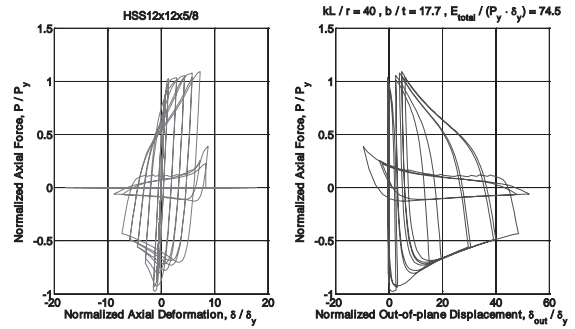
HSS 16 x 16 x 5/8 (kL/r = 40)



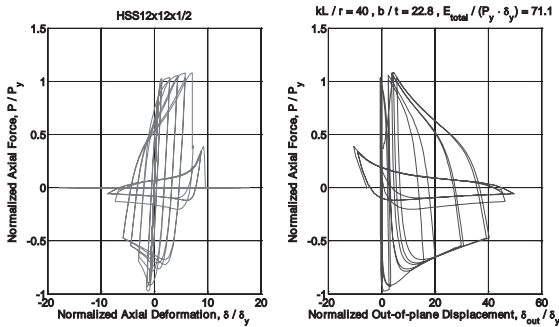
HSS 14 x 14 x 5/8 (kL/r = 40)



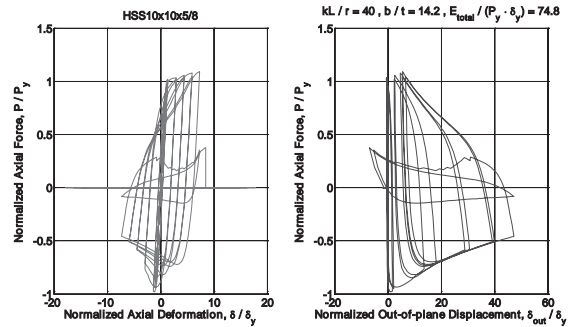
HSS 14 x 14 x 1/2 (kL/r = 40)



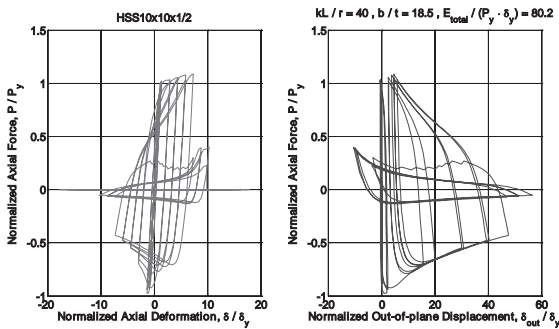
HSS 12 x 12 x 5/8 (kL/r = 40)



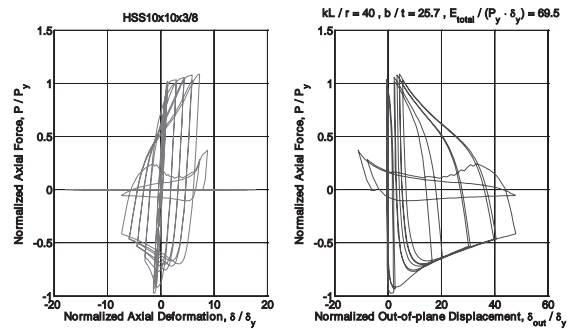
HSS 12 x 12 x 1/2 (kL/r = 40)



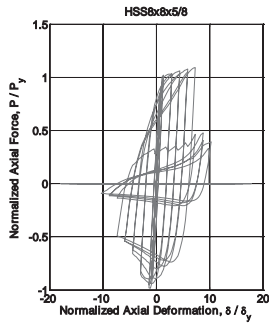
HSS 10 x 10 x 5/8 (kL/r = 40)



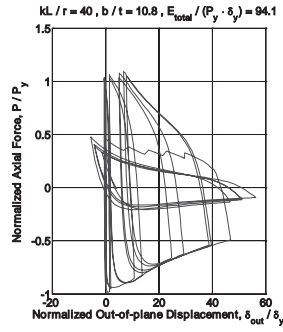
HSS 10 x 10 x 1/2 (kL/r = 40)



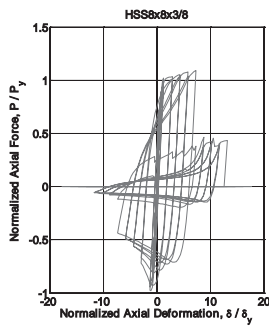
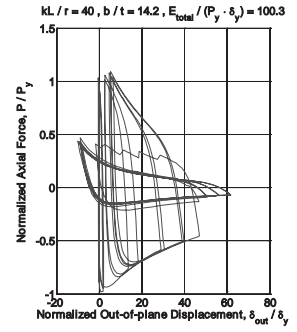
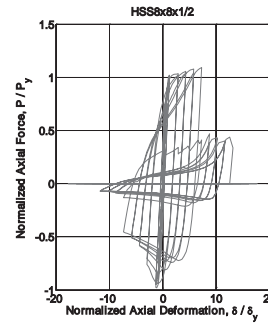
HSS 10 x 10 x 3/8 (kL/r = 40)



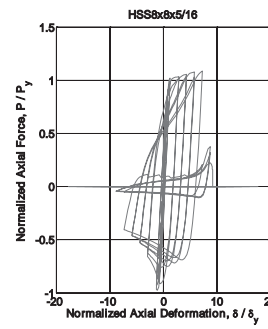
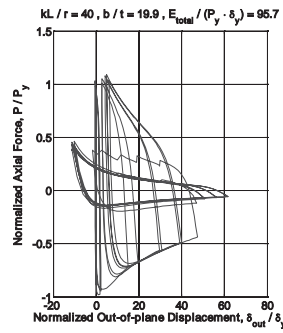
HSS 8 x 8 x 5/8 (kL/r = 40)



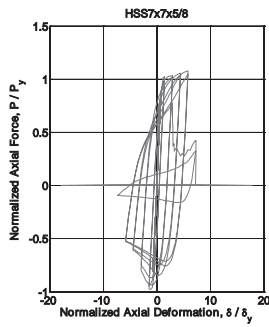
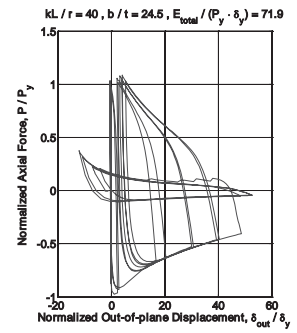
HSS 8 x 8 x 1/2 (kL/r = 40)



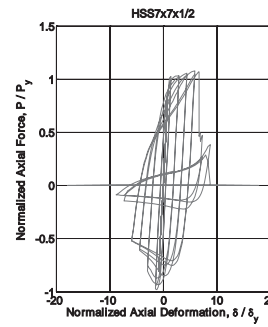
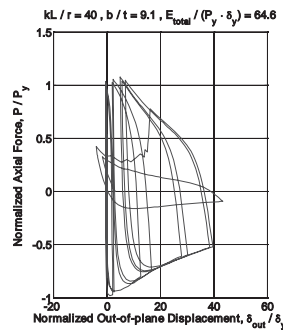
HSS 8 x 8 x 3/8 (kL/r = 40)



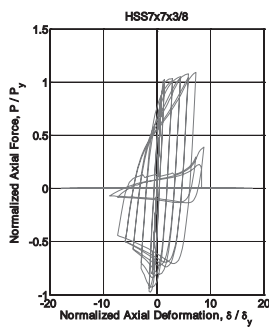
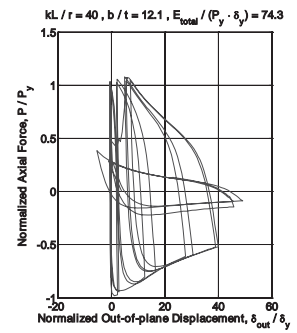
HSS 8 x 8 x 5/16 (kL/r = 40)



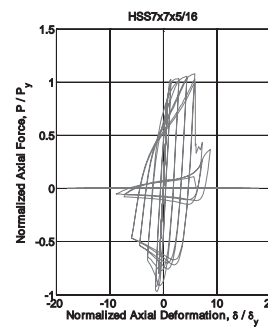
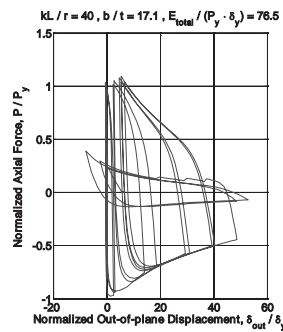
HSS 7 x 7 x 5/8 (kL/r = 40)



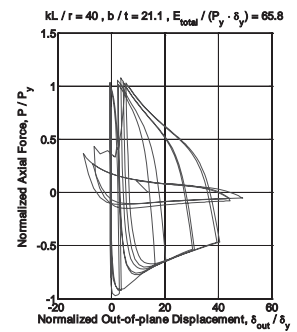
HSS 7 x 7 x 1/2 (kL/r = 40)

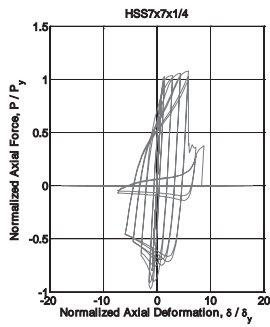


HSS 7 x 7 x 3/8 (kL/r = 40)

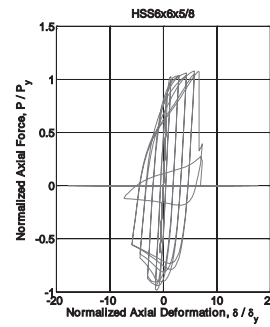
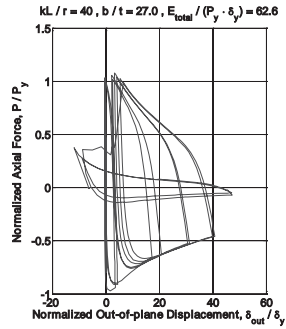


HSS 7 x 7 x 5/16 (kL/r = 40)

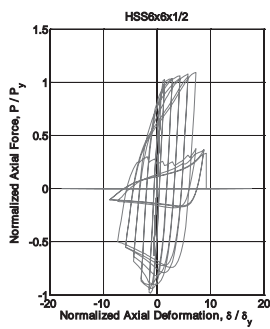
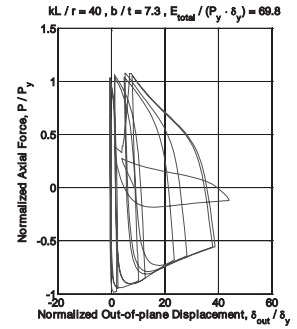




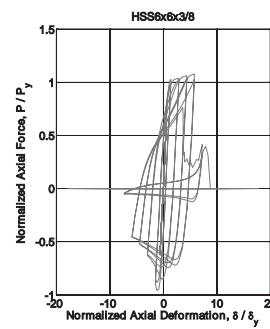
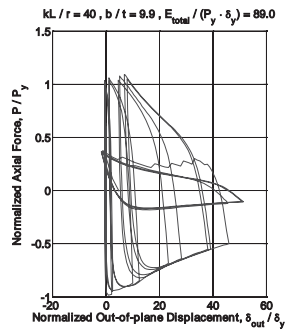
HSS 7 x 7 x 1/4 ( $kL/r = 40$ )



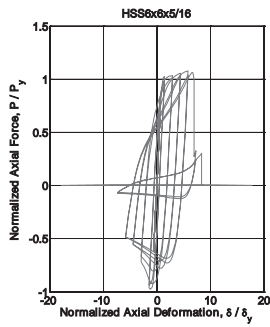
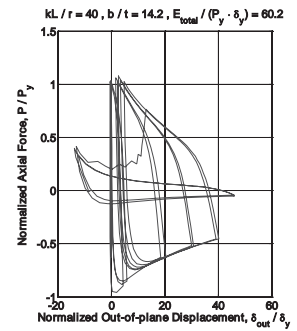
HSS 6 x 6 x 5/8 ( $kL/r = 40$ )



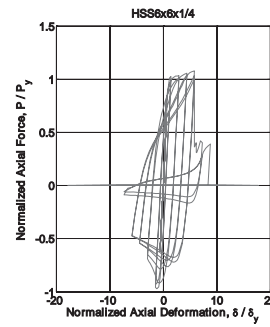
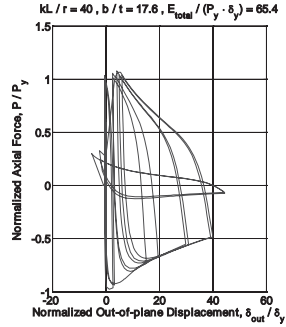
HSS 6 x 6 x 1/2 ( $kL/r = 40$ )



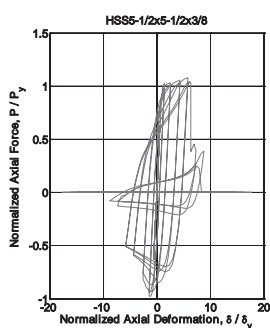
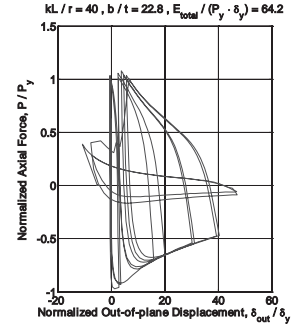
HSS 6 x 6 x 3/8 ( $kL/r = 40$ )



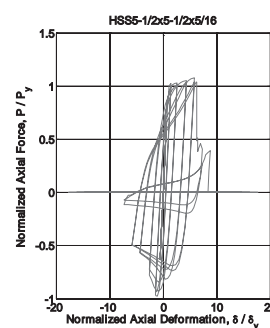
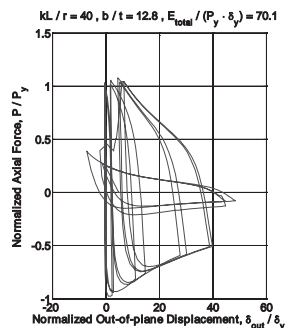
HSS 6 x 6 x 5/16 ( $kL/r = 40$ )



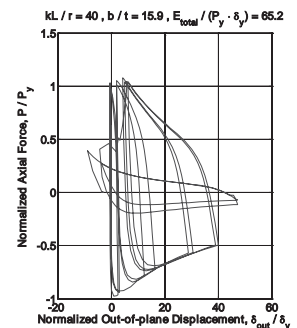
HSS 6 x 6 x 1/4 ( $kL/r = 40$ )



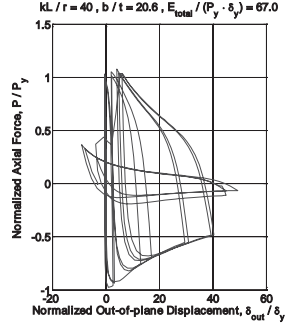
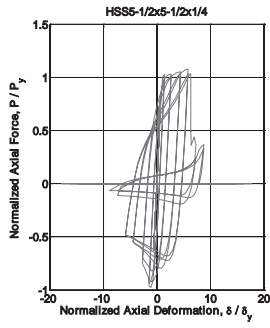
HSS 5-1/2 x 5-1/2 x 3/8 ( $kL/r = 40$ )



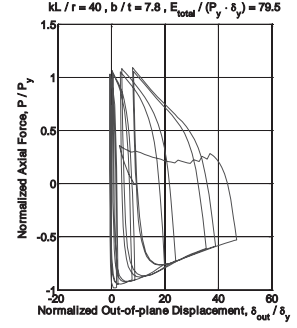
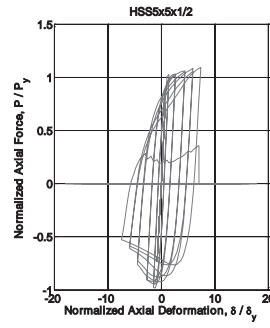
HSS 5-1/2 x 5-1/2 x 5/16 ( $kL/r = 40$ )



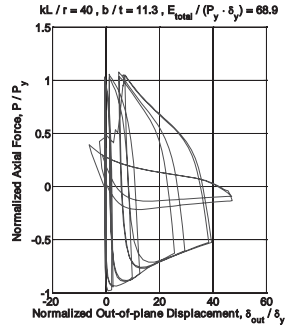
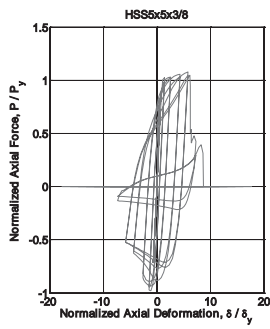




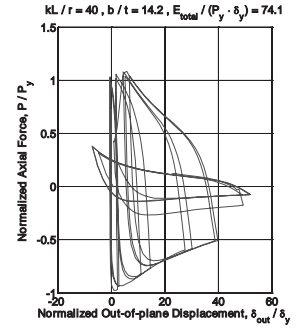
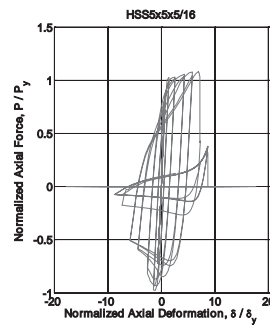
HSS 5-1/2 x 5-1/2 x 1/4 ( $kL/r = 40$ )



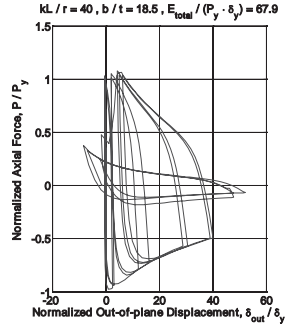
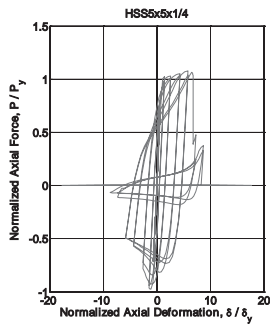
HSS 5 x 5 x 1/2 ( $kL/r = 40$ )



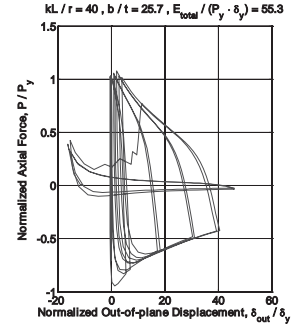
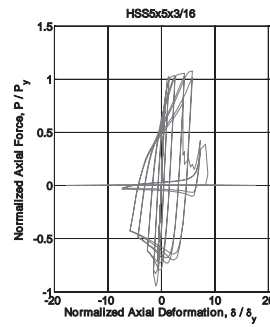
HSS 5 x 5 x 3/8 ( $kL/r = 40$ )



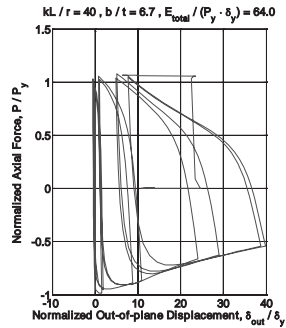
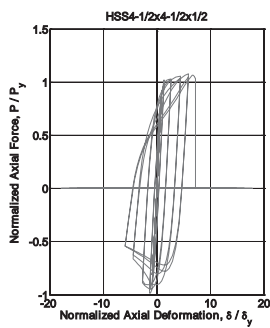
HSS 5 x 5 x 5/16 ( $kL/r = 40$ )



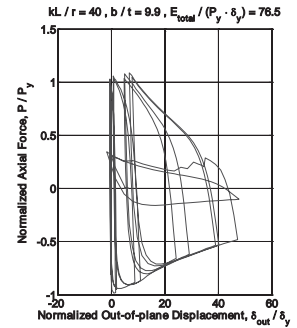
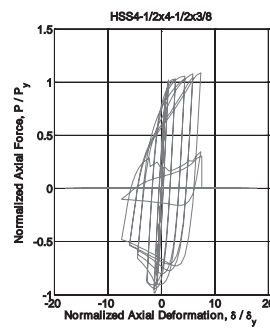
HSS 5 x 5 x 1/4 ( $kL/r = 40$ )



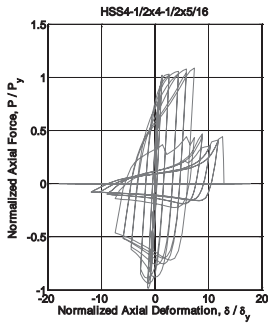
HSS 5 x 5 x 3/16 ( $kL/r = 40$ )



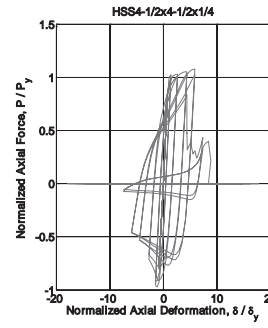
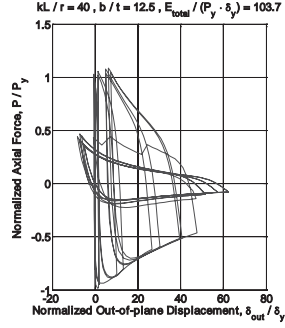
HSS 4-1/2 x 4-1/2 x 1/2 ( $kL/r = 40$ )



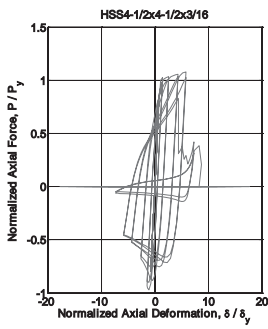
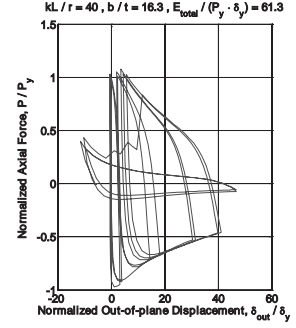
HSS 4-1/2 x 4-1/2 x 3/8 ( $kL/r = 40$ )



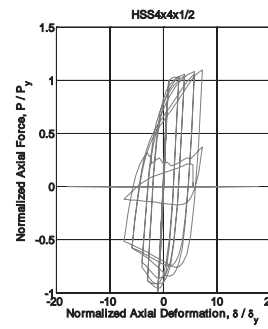
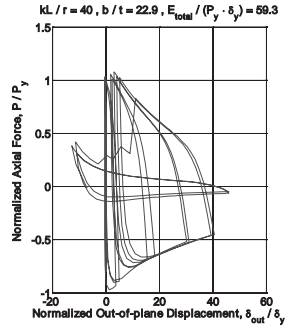
HSS 4-1/2 x 4-1/2 x 5/16 (kL/r = 40)



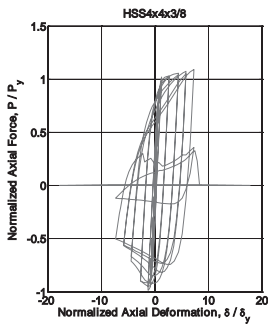
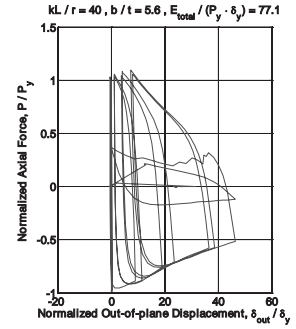
HSS 4-1/2 x 4-1/2 x 1/4 (kL/r = 40)



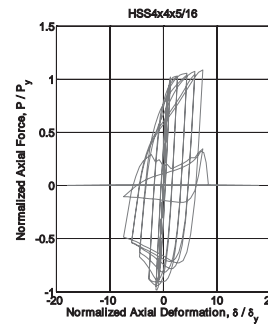
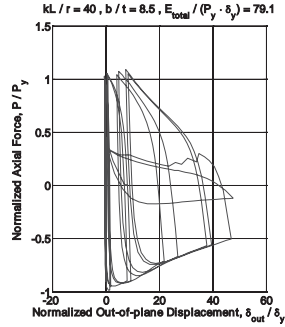
HSS 4-1/2 x 4-1/2 x 3/16 (kL/r = 40)



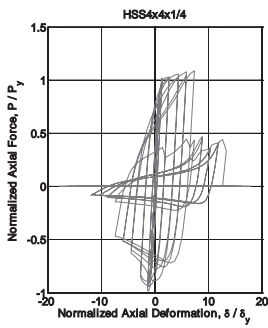
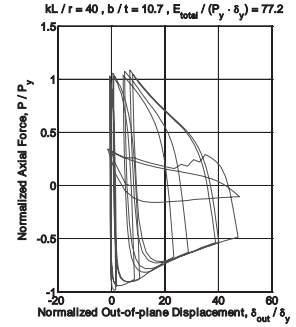
HSS 4 x 4 x 1/2 (kL/r = 40)



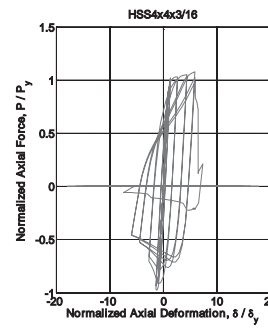
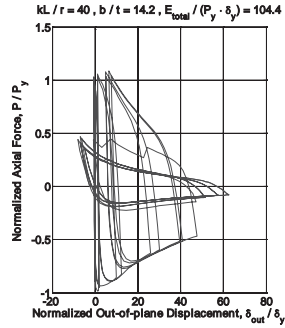
HSS 4 x 4 x 3/8 (kL/r = 40)



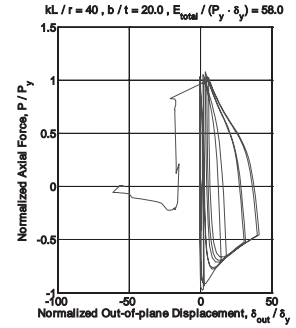
HSS 4 x 4 x 5/16 (kL/r = 40)



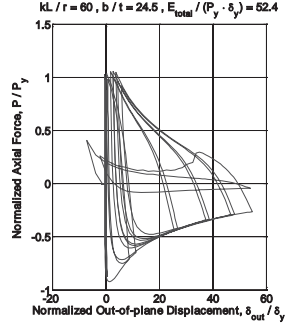
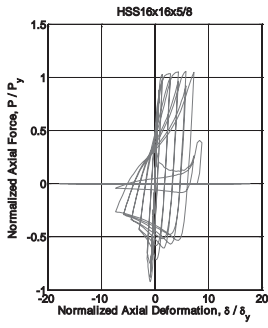
HSS 4 x 4 x 1/4 (kL/r = 40)



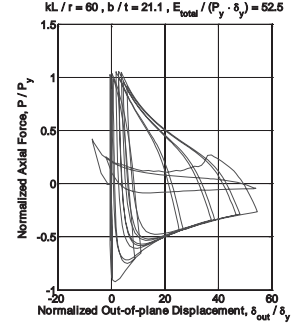
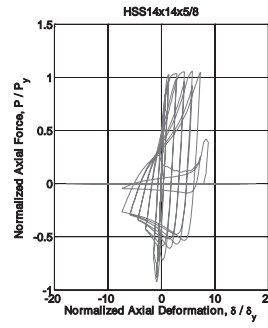
HSS 4 x 4 x 3/16 (kL/r = 40)



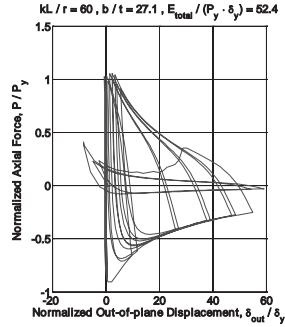
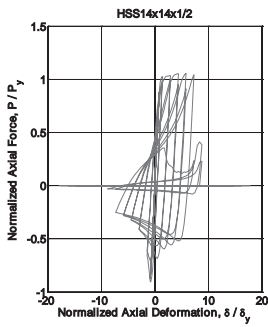
**(b)  $kL/r = 60$**



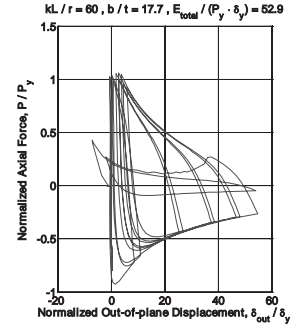
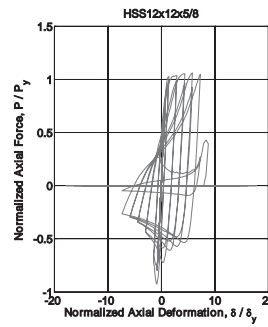
HSS 16 x 16 x 5/8 ( $kL/r = 60$ )



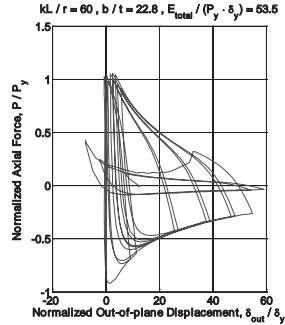
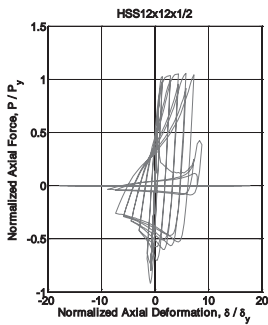
HSS 14 x 14 x 5/8 ( $kL/r = 60$ )



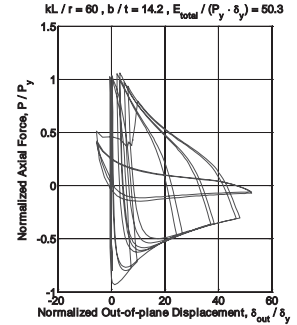
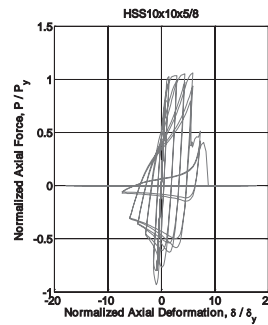
HSS 14 x 14 x 1/2 ( $kL/r = 60$ )



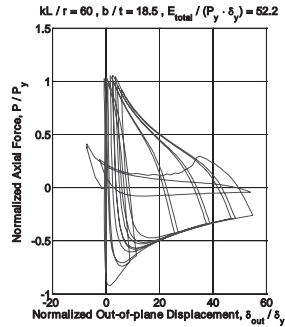
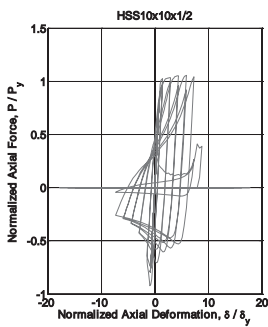
HSS 12 x 12 x 5/8 ( $kL/r = 60$ )



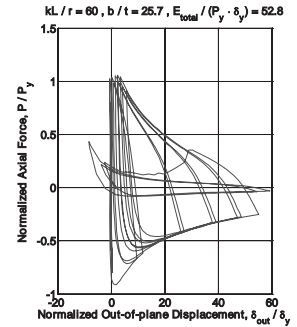
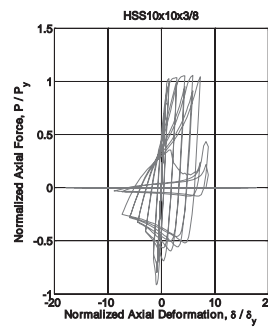
HSS 12 x 12 x 1/2 ( $kL/r = 60$ )



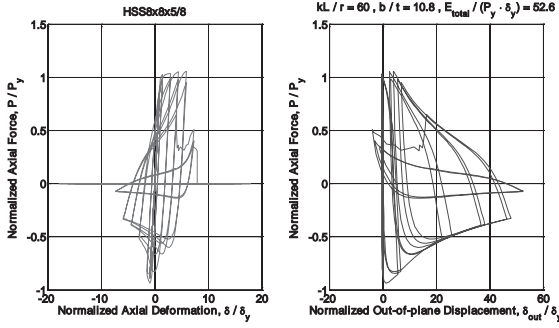
HSS 10 x 10 x 5/8 ( $kL/r = 60$ )



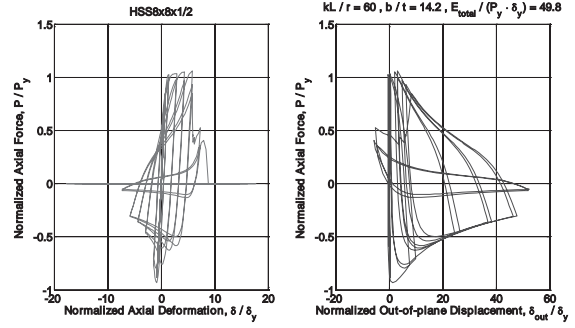
HSS 10 x 10 x 1/2 ( $kL/r = 60$ )



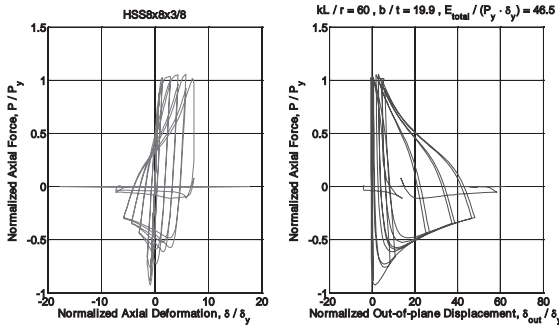
HSS 10 x 10 x 3/8 ( $kL/r = 60$ )



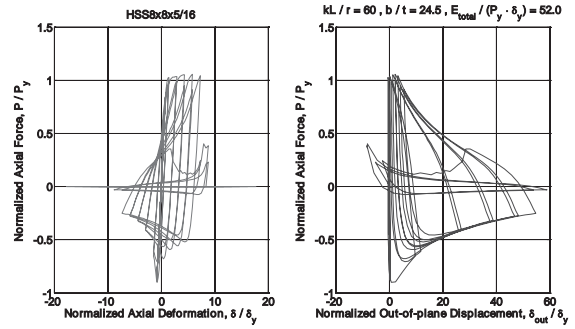
HSS 8 x 8 x 5/8 (kL/r = 60)



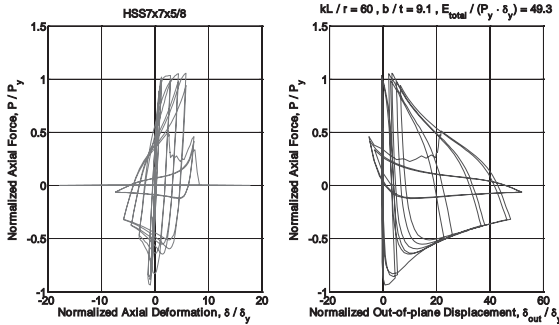
HSS 8 x 8 x 1/2 (kL/r = 60)



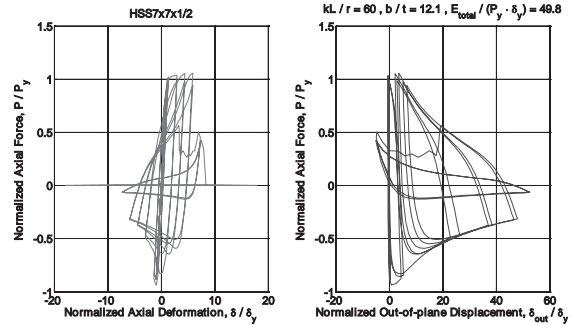
HSS 8 x 8 x 3/8 (kL/r = 60)



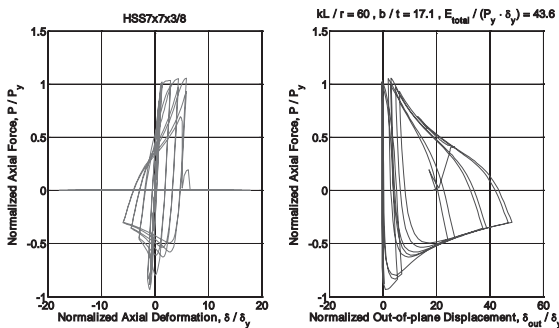
HSS 8 x 8 x 5/16 (kL/r = 60)



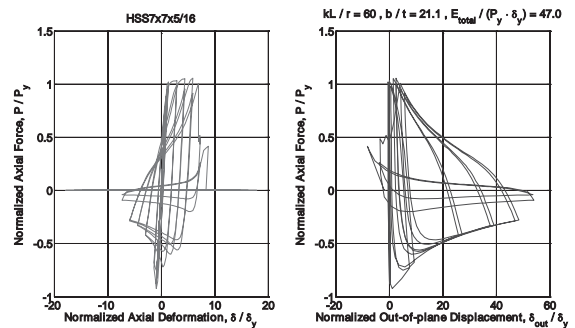
HSS 7 x 7 x 5/8 (kL/r = 60)



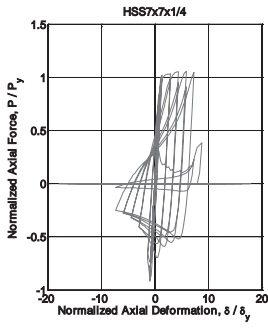
HSS 7 x 7 x 1/2 (kL/r = 60)



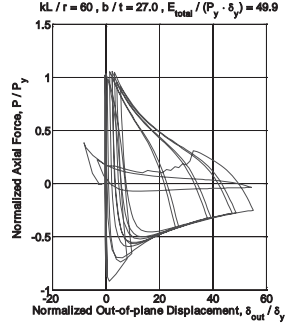
HSS 7 x 7 x 3/8 (kL/r = 60)



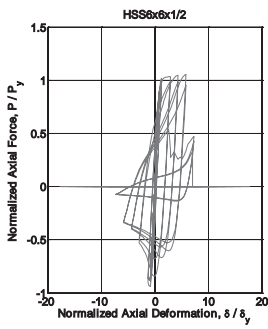
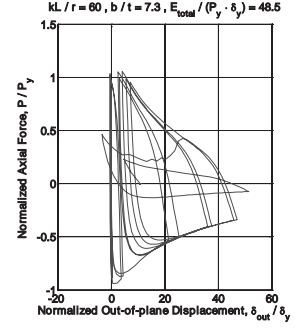
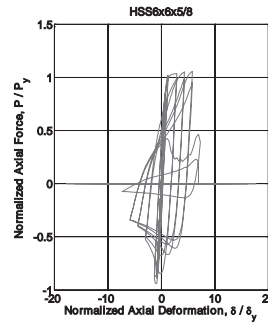
HSS 7 x 7 x 5/16 (kL/r = 60)



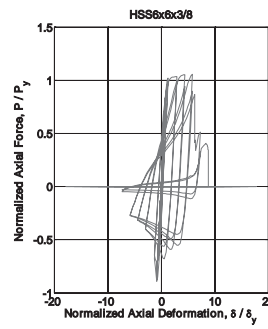
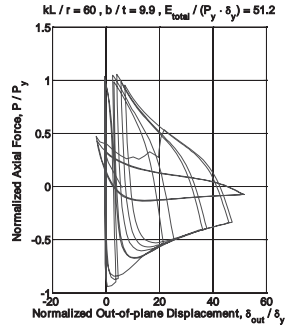
HSS 7 x 7 x 1/4 ( $kL/r = 60$ )



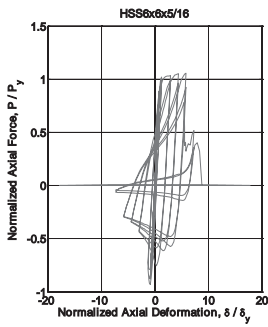
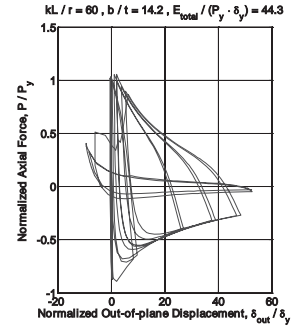
HSS 6 x 6 x 5/8 ( $kL/r = 60$ )



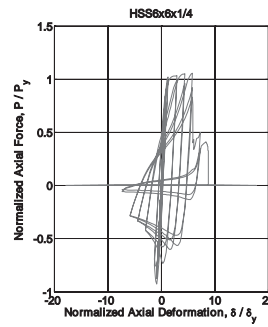
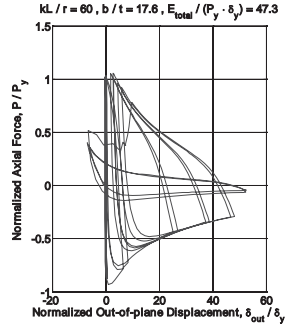
HSS 6 x 6 x 1/2 ( $kL/r = 60$ )



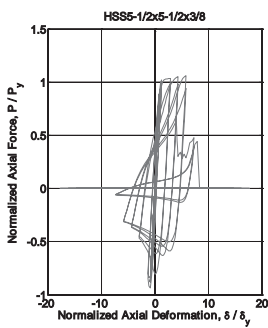
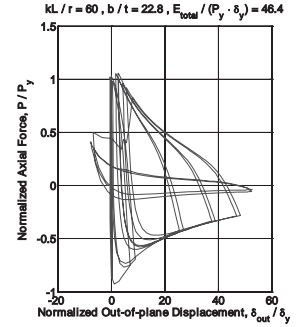
HSS 6 x 6 x 3/8 ( $kL/r = 60$ )



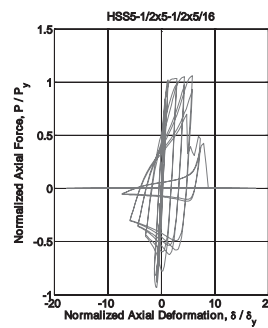
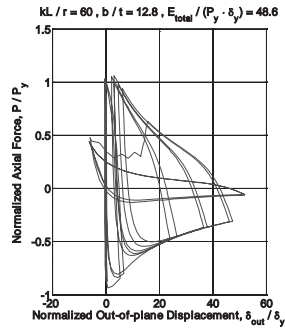
HSS 6 x 6 x 5/16 ( $kL/r = 60$ )



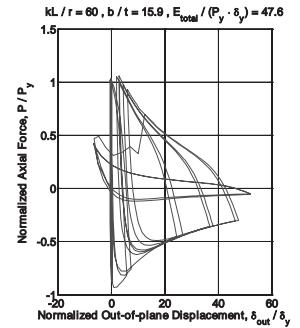
HSS 6 x 6 x 1/4 ( $kL/r = 60$ )

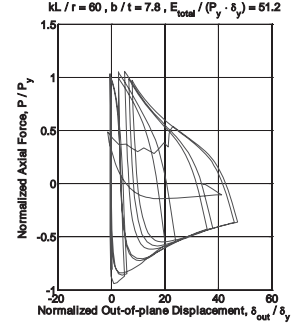
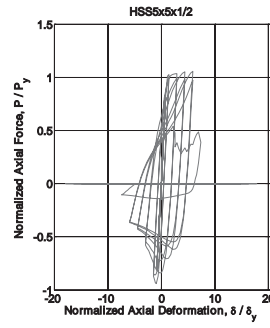
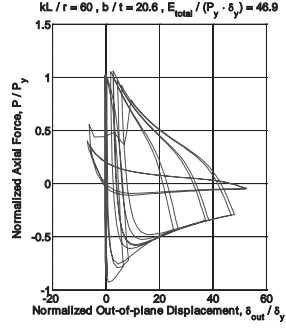
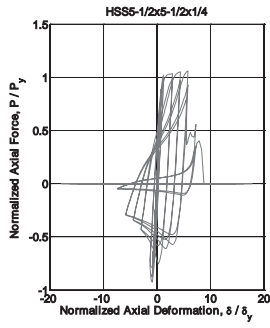


HSS 5-1/2 x 5-1/2 x 3/8 ( $kL/r = 60$ )



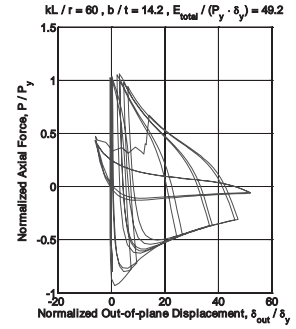
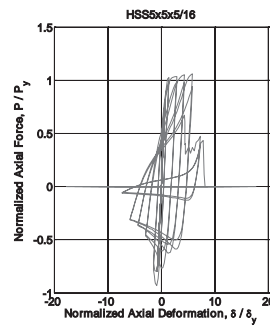
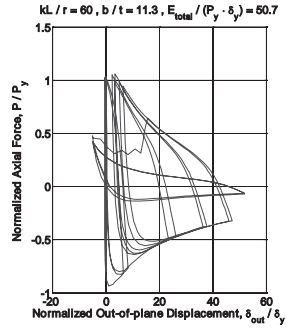
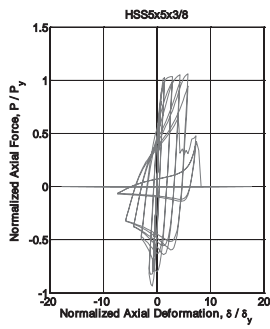
HSS 5-1/2 x 5-1/2 x 5/16 ( $kL/r = 60$ )





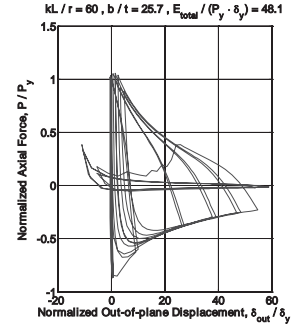
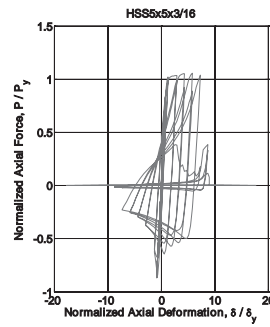
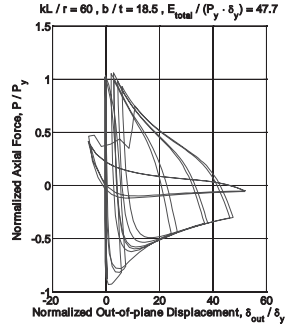
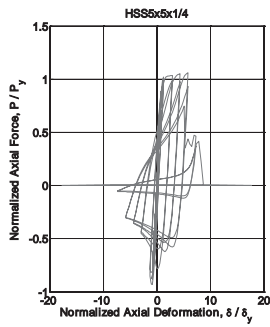
HSS 5-1/2 x 5-1/2 x 1/4 ( $kL/r = 60$ )

HSS 5 x 5 x 1/2 ( $kL/r = 60$ )



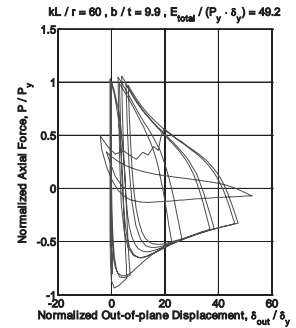
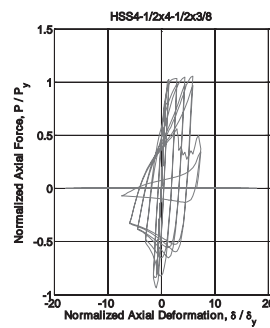
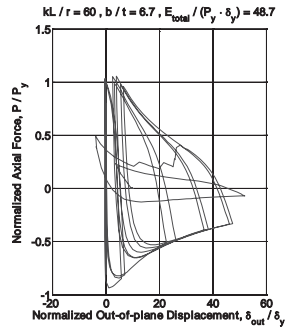
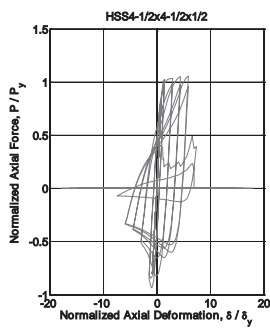
HSS 5 x 5 x 3/8 ( $kL/r = 60$ )

HSS 5 x 5 x 5/16 ( $kL/r = 60$ )



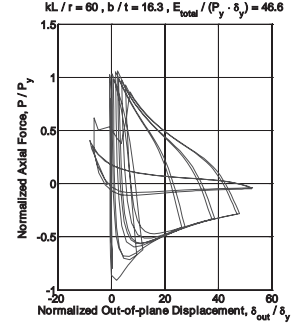
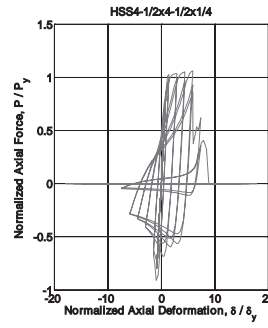
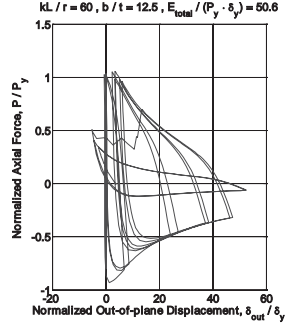
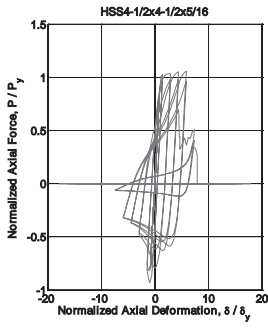
HSS 5 x 5 x 1/4 ( $kL/r = 60$ )

HSS 5 x 5 x 3/16 ( $kL/r = 60$ )



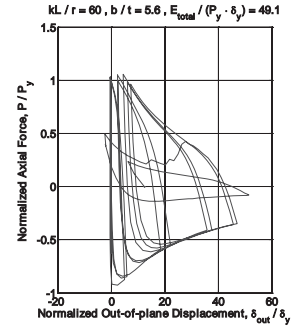
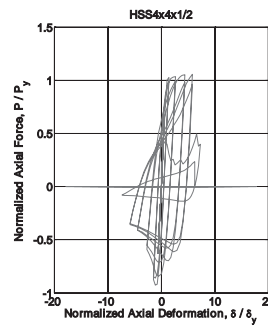
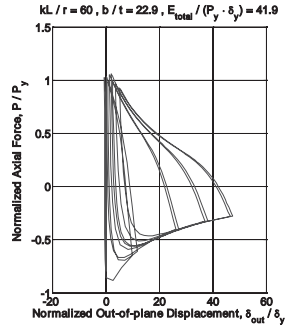
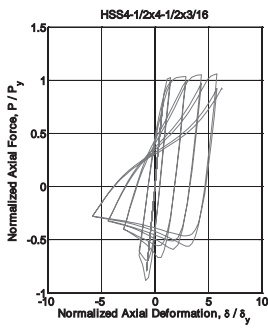
HSS 4-1/2 x 4-1/2 x 1/2 ( $kL/r = 60$ )

HSS 4-1/2 x 4-1/2 x 3/8 ( $kL/r = 60$ )



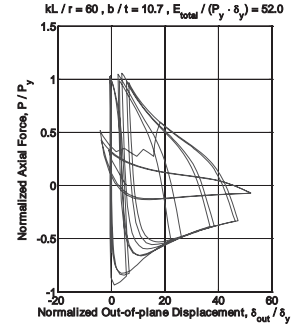
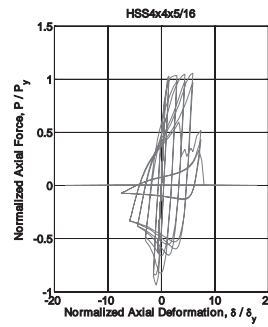
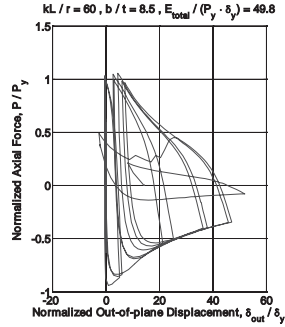
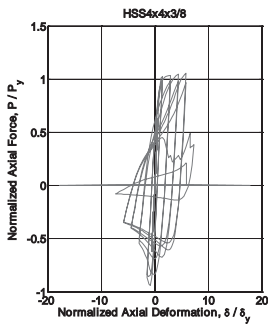
HSS 4-1/2 x 4-1/2 x 5/16 ( $kL/r = 60$ )

HSS 4-1/2 x 4-1/2 x 1/4 ( $kL/r = 60$ )



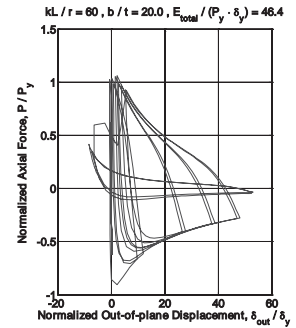
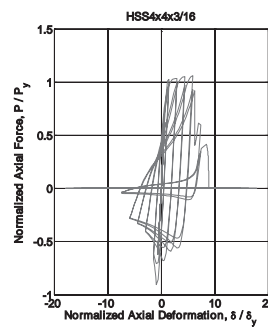
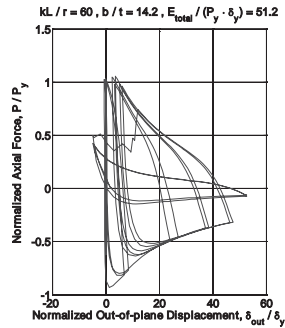
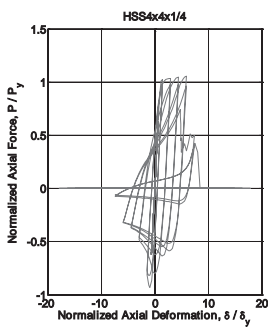
HSS 4-1/2 x 4-1/2 x 3/16 ( $kL/r = 60$ )

HSS 4 x 4 x 1/2 ( $kL/r = 60$ )



HSS 4 x 4 x 3/8 ( $kL/r = 60$ )

HSS 4 x 4 x 5/16 ( $kL/r = 60$ )

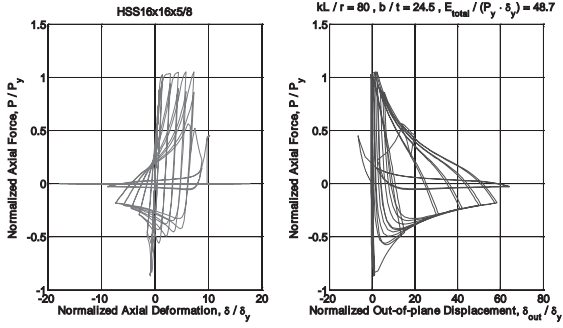


HSS 4 x 4 x 1/4 ( $kL/r = 60$ )

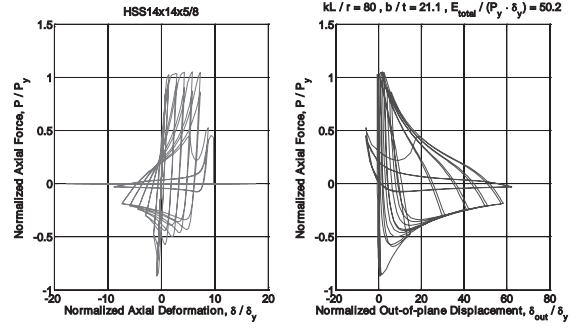
HSS 4 x 4 x 3/16 ( $kL/r = 60$ )



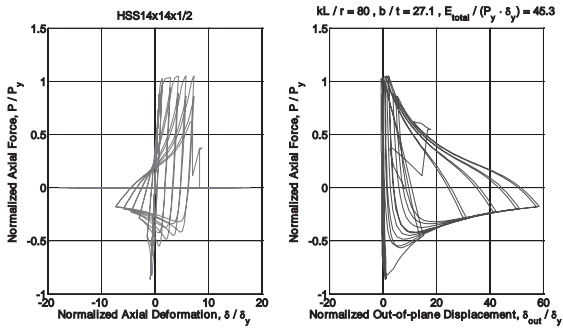
**(c)  $kL/r = 80$**



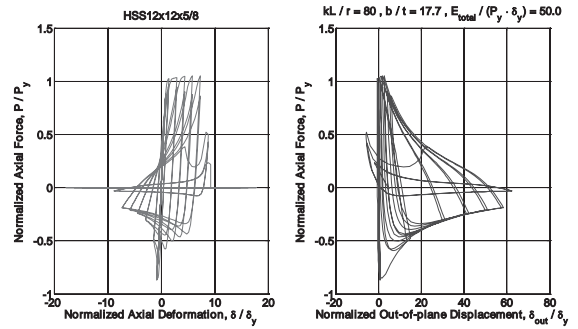
HSS 16 x 16 x 5/8 (kL/r = 80)



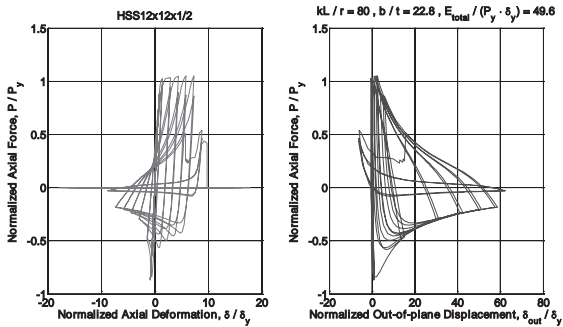
HSS 14 x 14 x 5/8 (kL/r = 80)



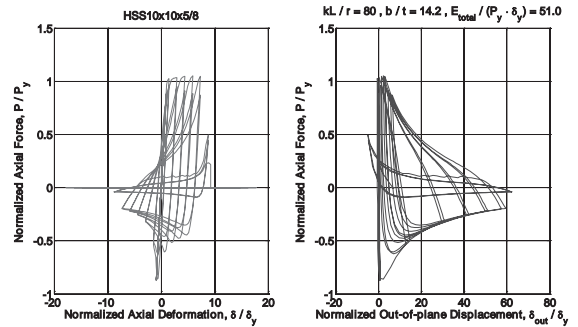
HSS 14 x 14 x 1/2 (kL/r = 80)



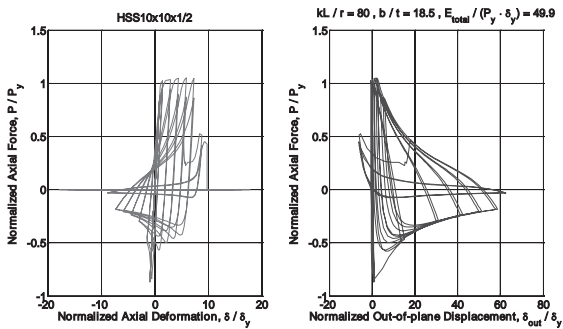
HSS 12 x 12 x 5/8 (kL/r = 80)



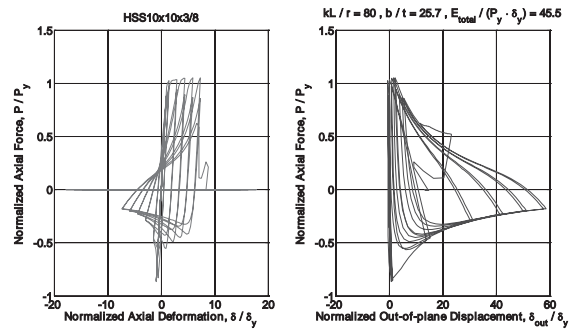
HSS 12 x 12 x 1/2 (kL/r = 80)



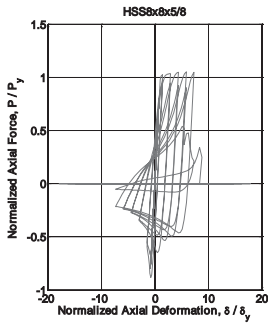
HSS 10 x 10 x 5/8 (kL/r = 80)



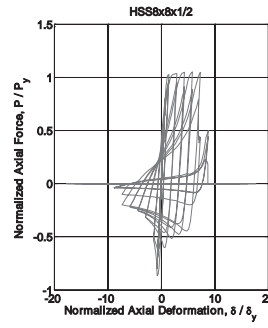
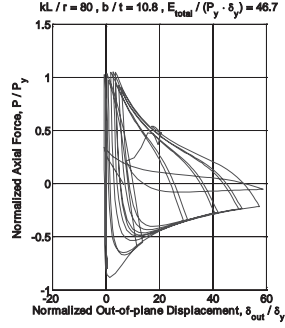
HSS 10 x 10 x 1/2 (kL/r = 80)



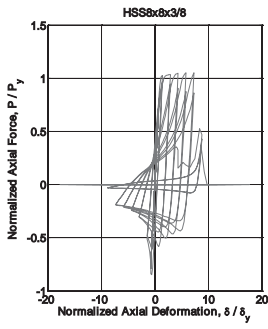
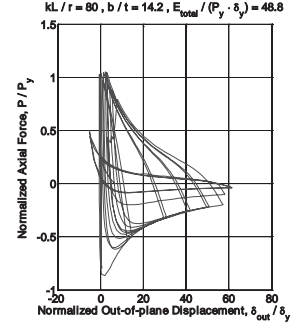
HSS 10 x 10 x 3/8 (kL/r = 80)



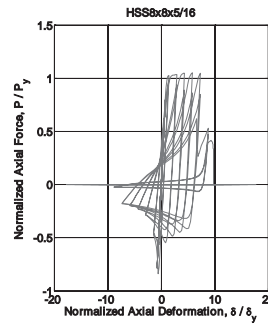
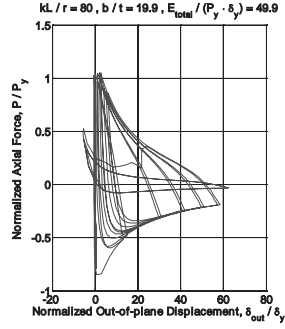
HSS 8 x 8 x 5/8 (kL/r = 80)



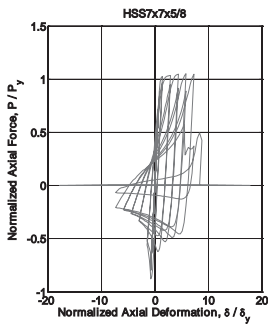
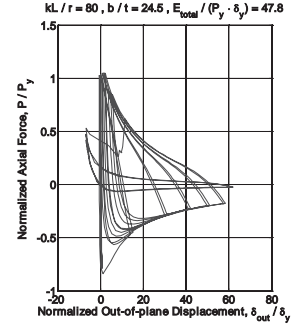
HSS 8 x 8 x 1/2 (kL/r = 80)



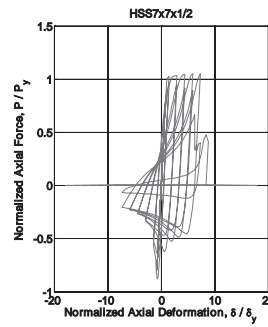
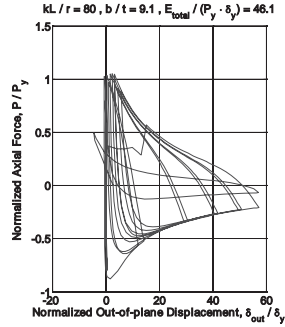
HSS 8 x 8 x 3/8 (kL/r = 80)



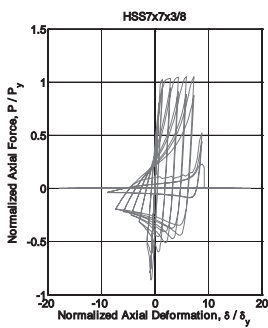
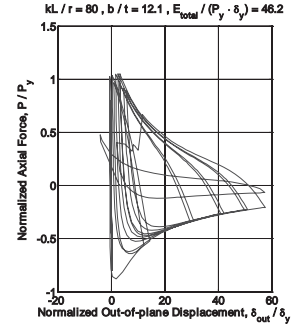
HSS 8 x 8 x 5/16 (kL/r = 80)



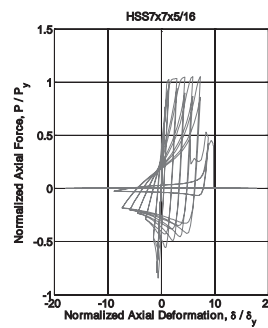
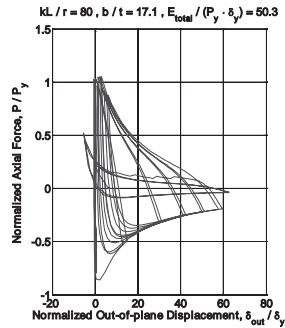
HSS 7 x 7 x 5/8 (kL/r = 80)



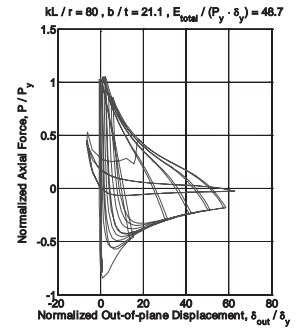
HSS 7 x 7 x 1/2 (kL/r = 80)

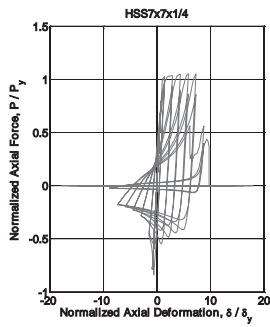


HSS 7 x 7 x 3/8 (kL/r = 80)

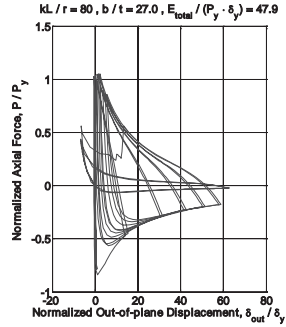


HSS 7 x 7 x 5/16 (kL/r = 80)

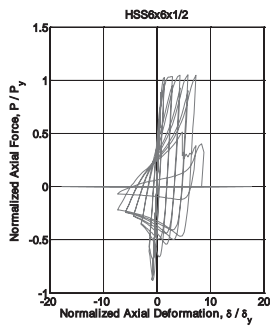
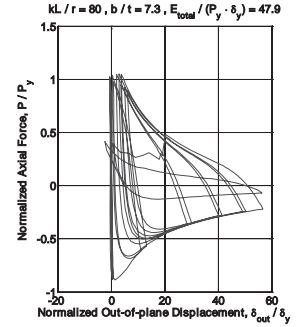
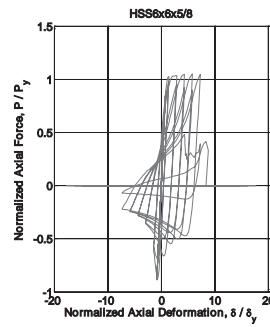




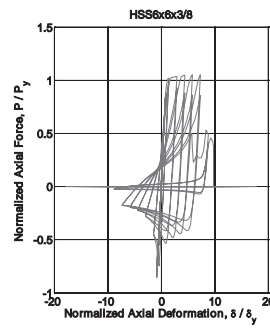
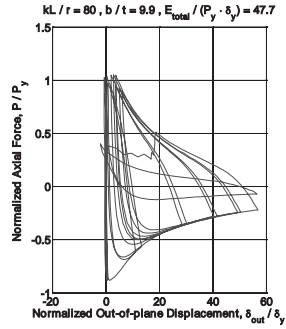
HSS 7 x 7 x 1/4 ( $kL/r = 80$ )



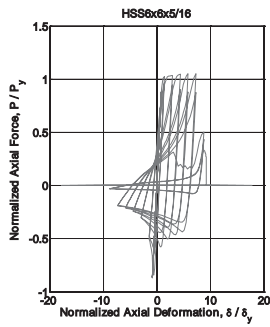
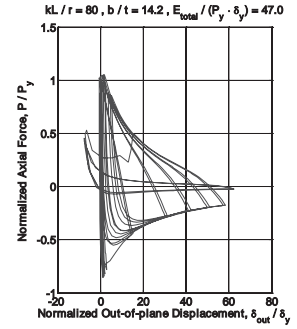
HSS 6 x 6 x 5/8 ( $kL/r = 80$ )



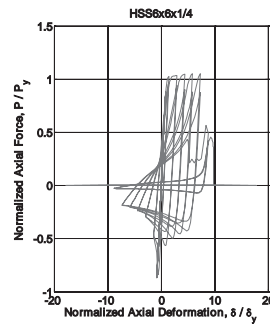
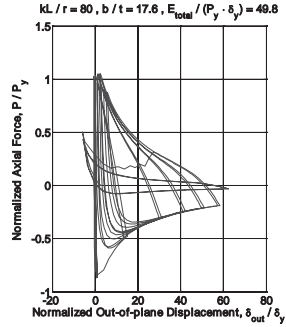
HSS 6 x 6 x 1/2 ( $kL/r = 80$ )



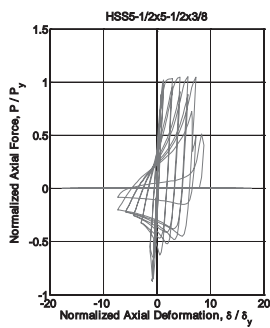
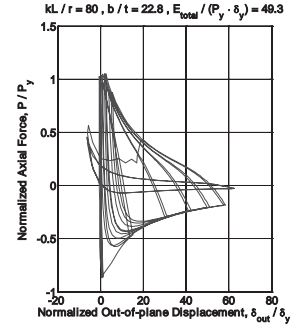
HSS 6 x 6 x 3/8 ( $kL/r = 80$ )



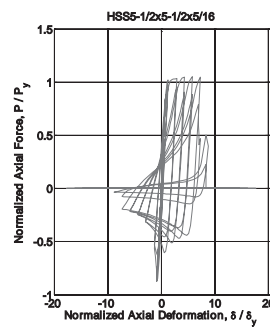
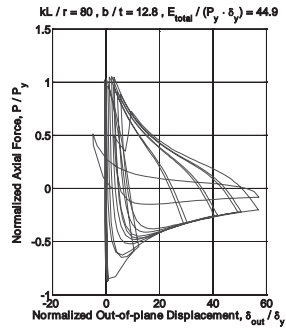
HSS 6 x 6 x 5/16 ( $kL/r = 80$ )



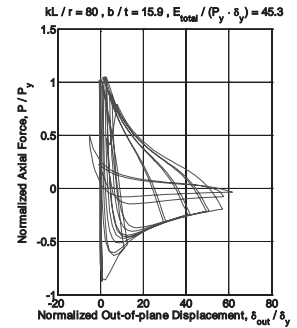
HSS 6 x 6 x 1/4 ( $kL/r = 80$ )

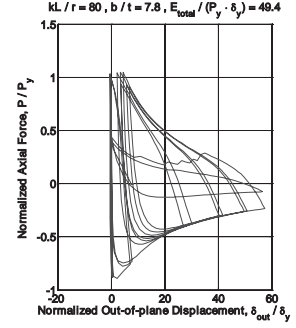
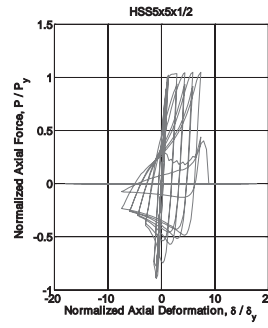
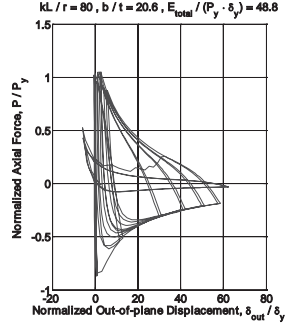
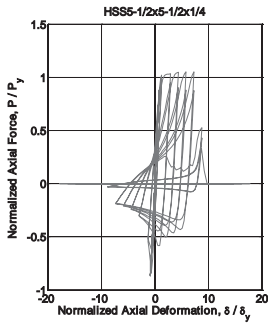


HSS 5-1/2 x 5-1/2 x 3/8 ( $kL/r = 80$ )



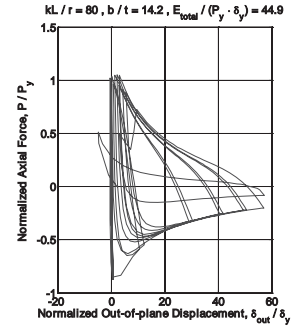
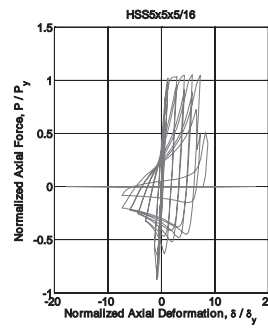
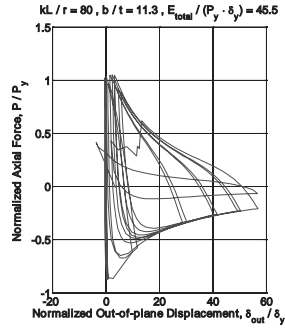
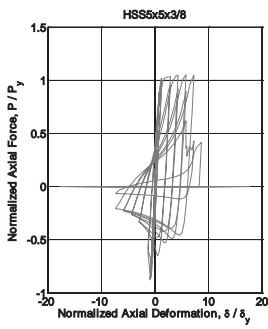
HSS 5-1/2 x 5-1/2 x 5/16 ( $kL/r = 80$ )





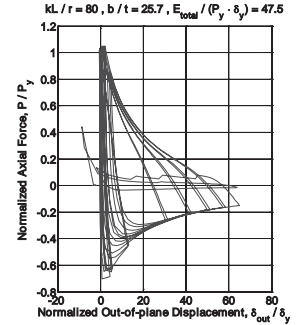
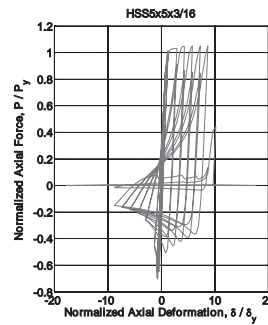
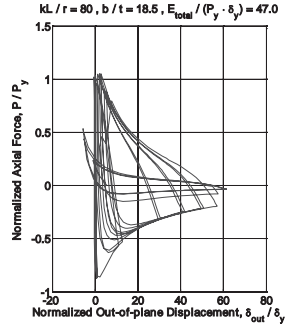
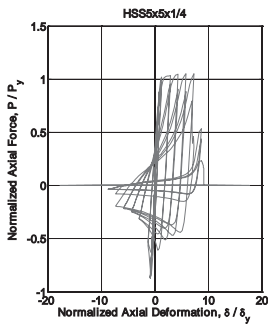
HSS 5-1/2 x 5-1/2 x 1/4 ( $kL/r = 80$ )

HSS 5 x 5 x 1/2 ( $kL/r = 80$ )



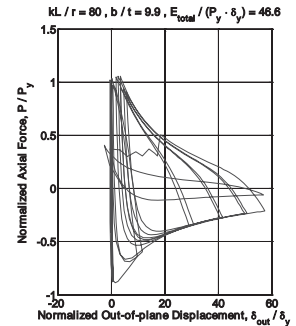
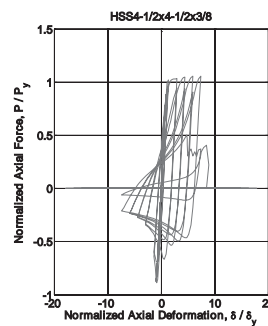
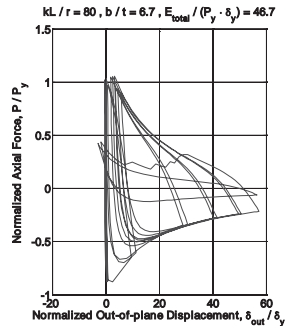
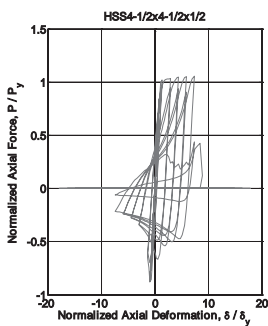
HSS 5 x 5 x 3/8 ( $kL/r = 80$ )

HSS 5 x 5 x 5/16 ( $kL/r = 80$ )



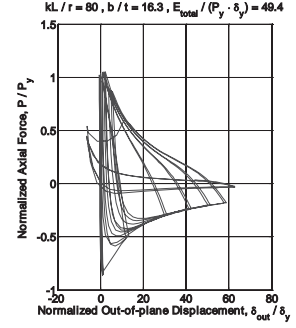
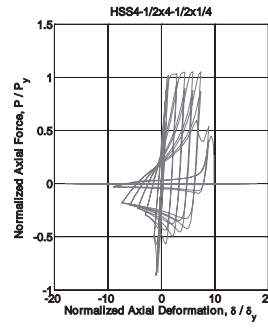
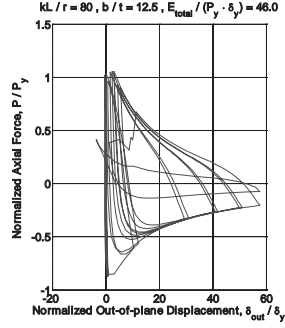
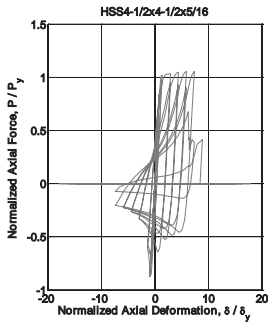
HSS 5 x 5 x 1/4 ( $kL/r = 80$ )

HSS 5 x 5 x 3/16 ( $kL/r = 80$ )



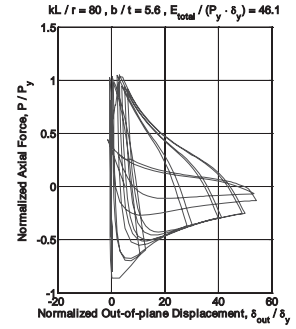
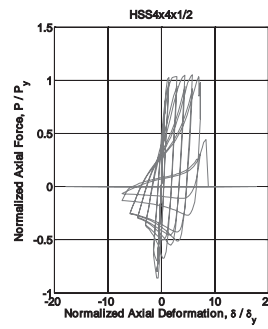
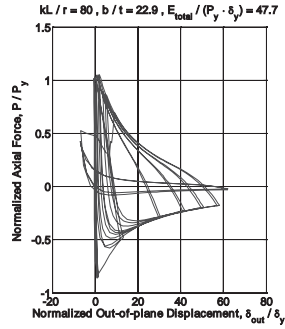
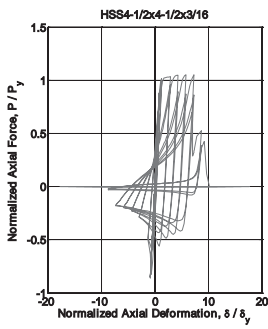
HSS 4-1/2 x 4-1/2 x 1/2 ( $kL/r = 80$ )

HSS 4-1/2 x 4-1/2 x 3/8 ( $kL/r = 80$ )



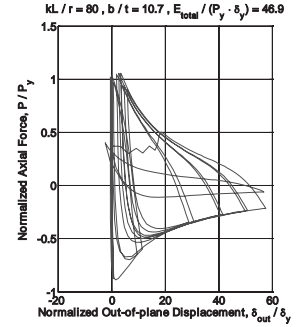
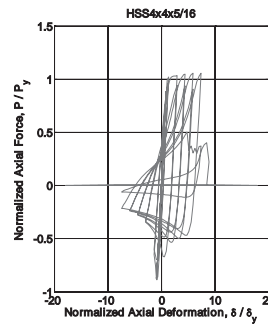
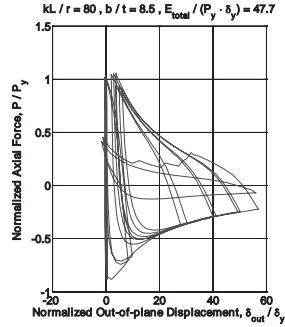
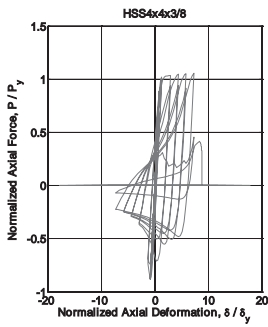
HSS 4-1/2 x 4-1/2 x 5/16 ( $kL/r = 80$ )

HSS 4-1/2 x 4-1/2 x 1/4 ( $kL/r = 80$ )



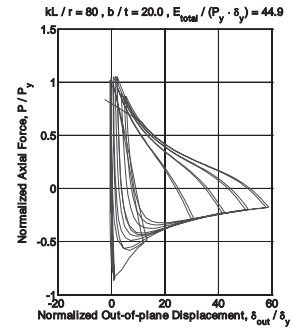
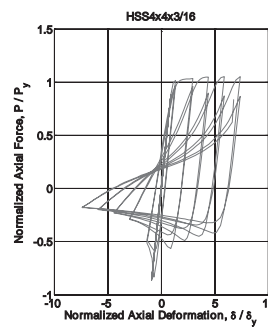
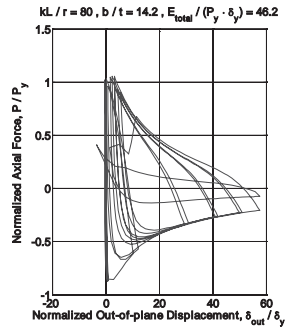
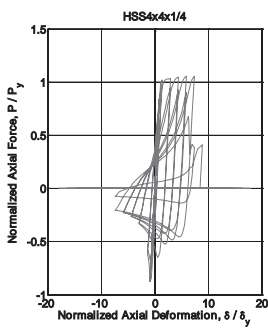
HSS 4-1/2 x 4-1/2 x 3/16 ( $kL/r = 80$ )

HSS 4 x 4 x 1/2 ( $kL/r = 80$ )



HSS 4 x 4 x 3/8 ( $kL/r = 80$ )

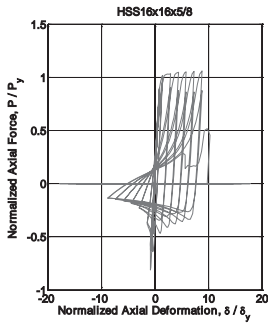
HSS 4 x 4 x 5/16 ( $kL/r = 80$ )



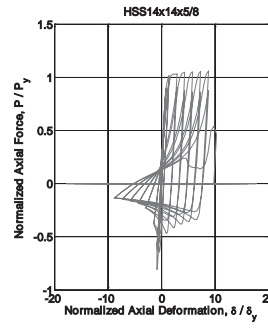
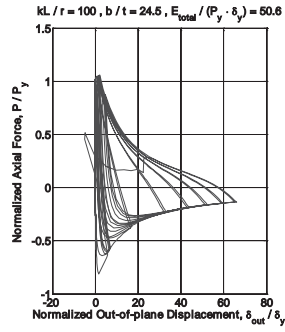
HSS 4 x 4 x 1/4 ( $kL/r = 80$ )

HSS 4 x 4 x 3/16 ( $kL/r = 80$ )

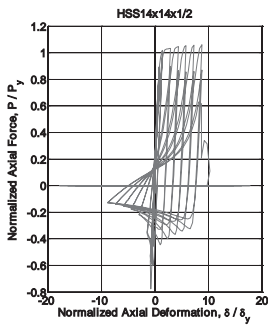
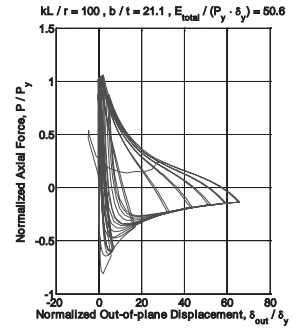
**(d)  $kL/r = 100$**



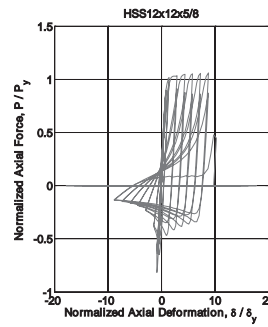
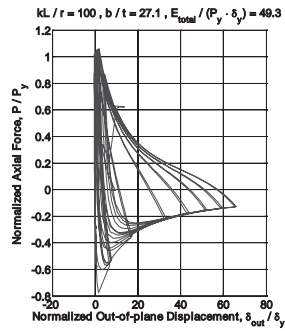
HSS 16 x 16 x 5/8 ( $kL/r = 100$ )



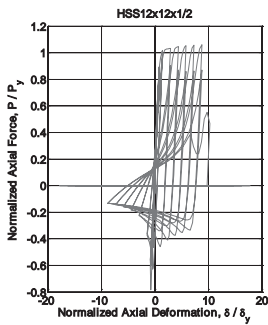
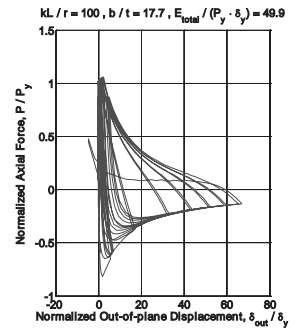
HSS 14 x 14 x 5/8 ( $kL/r = 100$ )



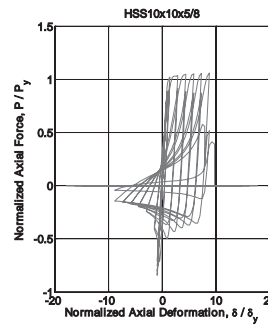
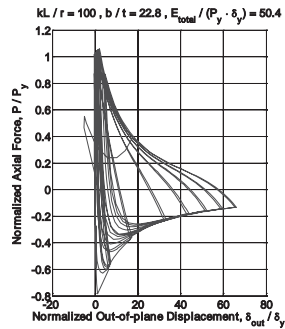
HSS 14 x 14 x 1/2 ( $kL/r = 100$ )



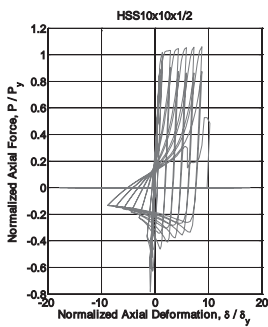
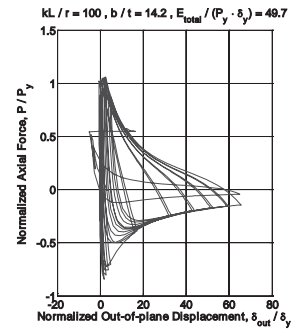
HSS 12 x 12 x 5/8 ( $kL/r = 100$ )



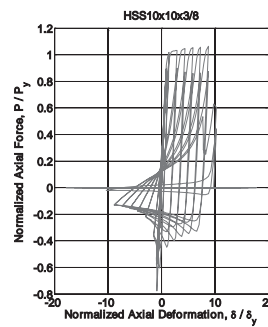
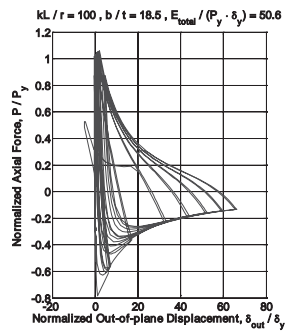
HSS 12 x 12 x 1/2 ( $kL/r = 100$ )



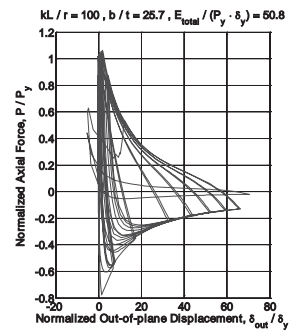
HSS 10 x 10 x 5/8 ( $kL/r = 100$ )



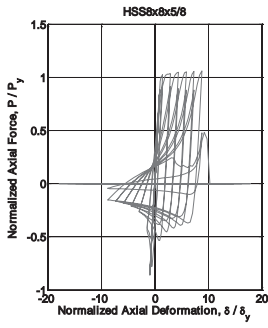
HSS 10 x 10 x 1/2 ( $kL/r = 100$ )



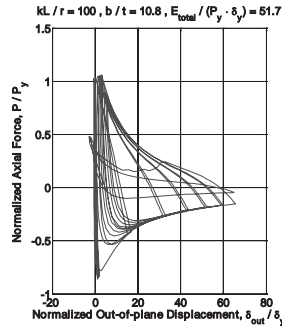
HSS 10 x 10 x 3/8 ( $kL/r = 100$ )



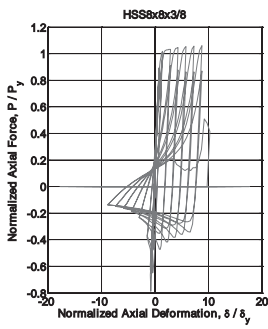
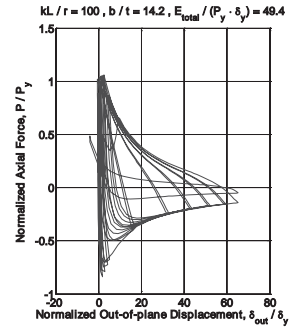
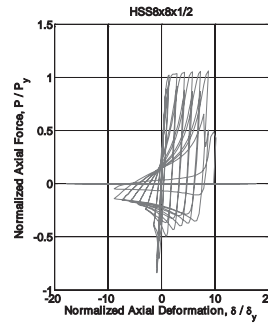




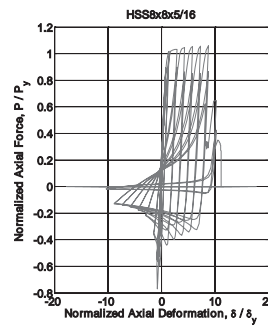
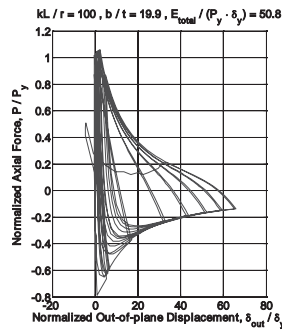
HSS 8 x 8 x 5/8 ( $kL/r = 100$ )



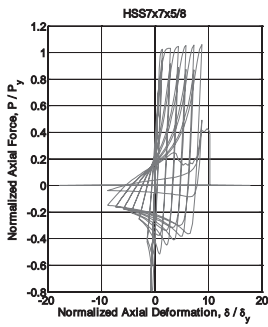
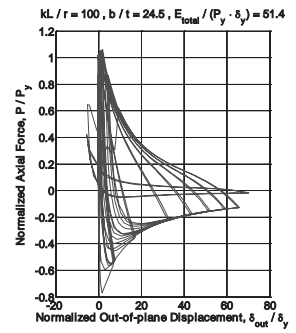
HSS 8 x 8 x 1/2 ( $kL/r = 100$ )



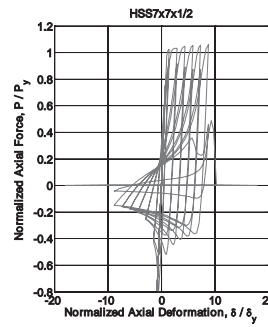
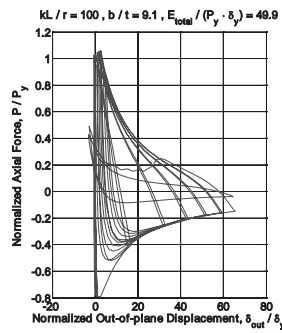
HSS 8 x 8 x 3/8 ( $kL/r = 100$ )



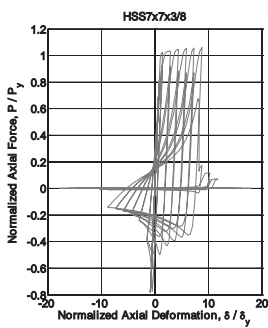
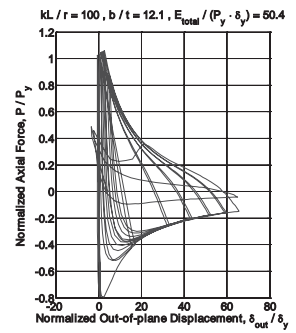
HSS 8 x 8 x 5/16 ( $kL/r = 100$ )



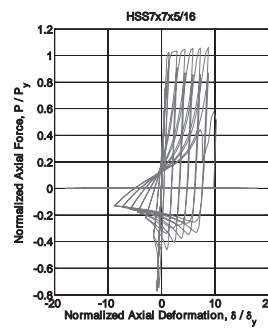
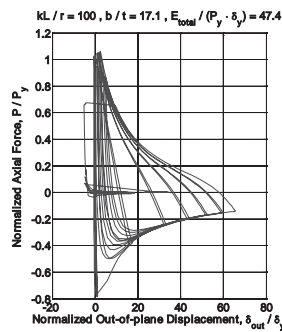
HSS 7 x 7 x 5/8 ( $kL/r = 100$ )



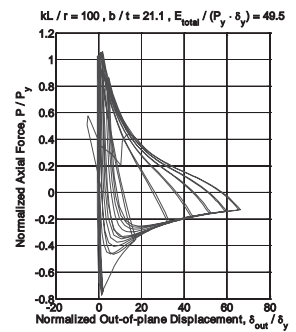
HSS 7 x 7 x 1/2 ( $kL/r = 100$ )

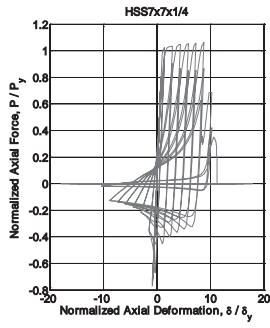


HSS 7 x 7 x 3/8 ( $kL/r = 100$ )

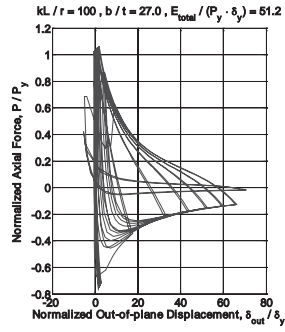


HSS 7 x 7 x 5/16 ( $kL/r = 100$ )

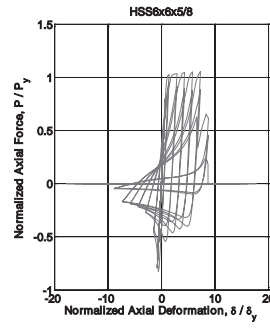




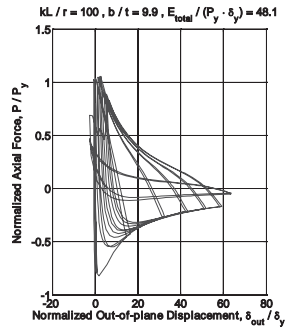
HSS 7 x 7 x 1/4 ( $kL/r = 100$ )



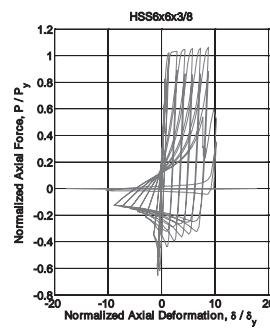
HSS 6 x 6 x 5/8 ( $kL/r = 100$ )



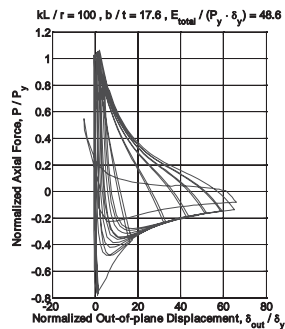
HSS 6 x 6 x 1/2 ( $kL/r = 100$ )



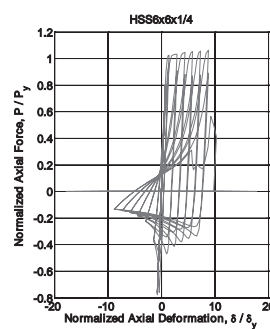
HSS 6 x 6 x 3/8 ( $kL/r = 100$ )



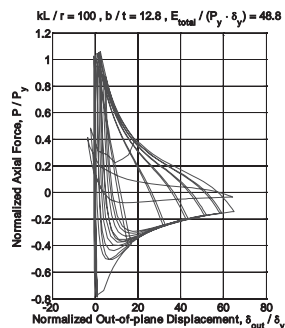
HSS 6 x 6 x 5/16 ( $kL/r = 100$ )



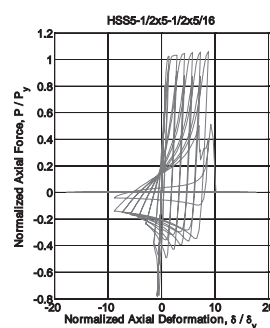
HSS 6 x 6 x 1/4 ( $kL/r = 100$ )

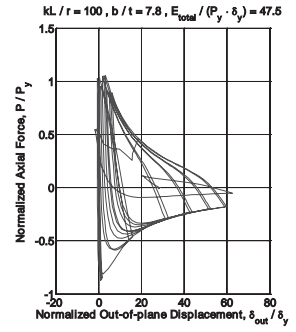
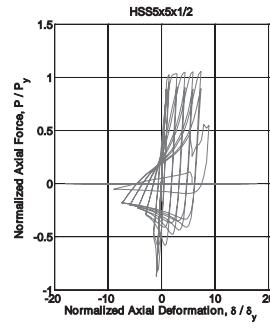
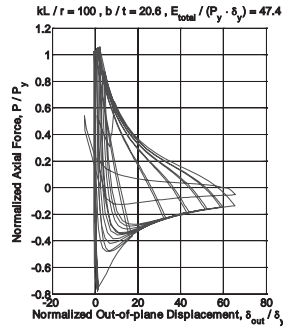
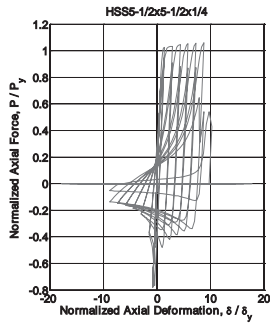


HSS 5-1/2 x 5-1/2 x 3/8 ( $kL/r = 100$ )



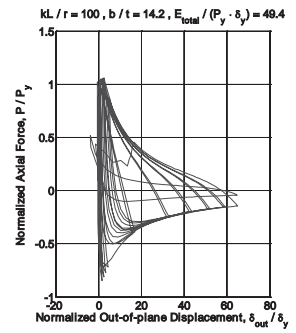
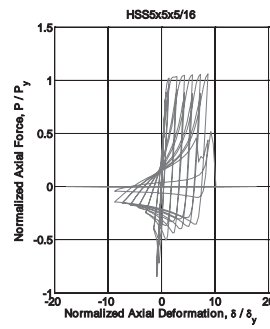
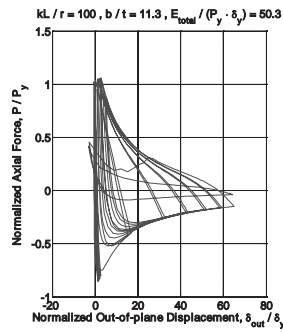
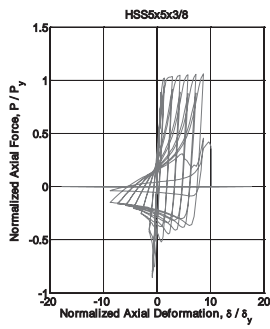
HSS 5-1/2 x 5-1/2 x 5/16 ( $kL/r = 100$ )





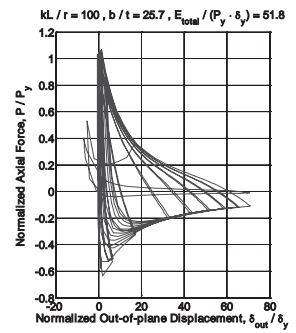
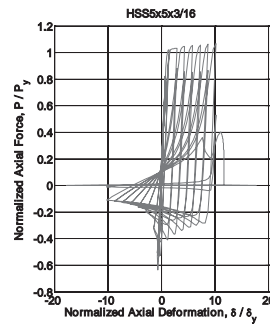
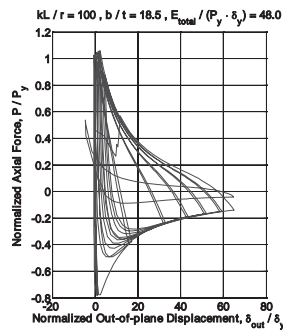
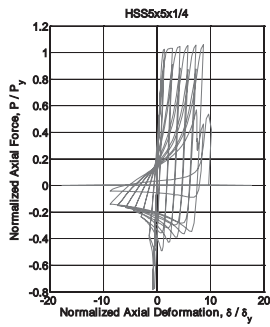
HSS 5-1/2 x 5-1/2 x 1/4 ( $kL/r = 100$ )

HSS 5 x 5 x 1/2 ( $kL/r = 100$ )



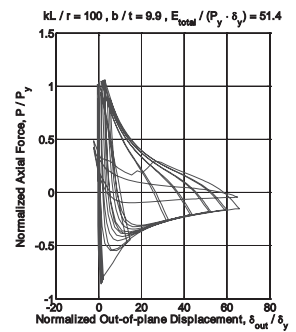
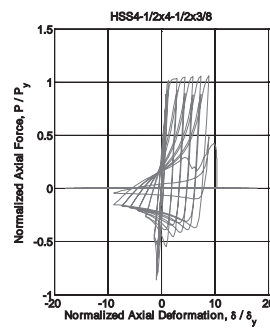
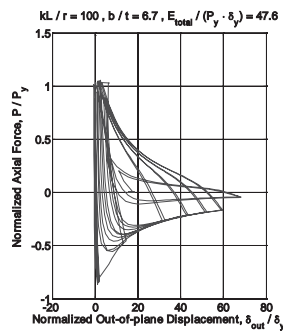
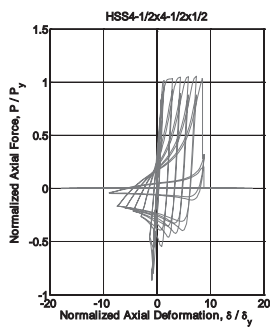
HSS 5 x 5 x 3/8 ( $kL/r = 100$ )

HSS 5 x 5 x 5/16 ( $kL/r = 100$ )



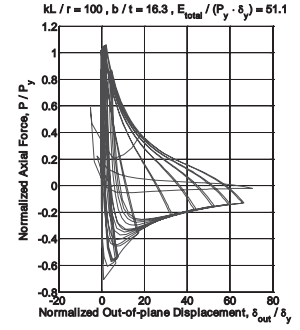
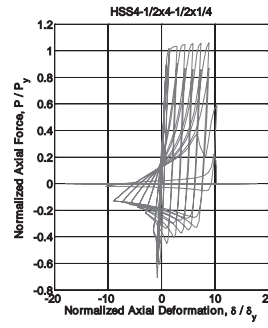
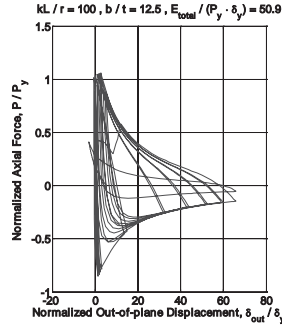
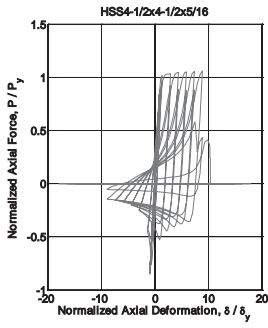
HSS 5 x 5 x 1/4 ( $kL/r = 100$ )

HSS 5 x 5 x 3/16 ( $kL/r = 100$ )



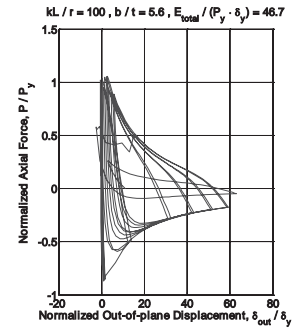
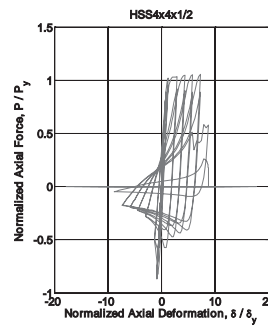
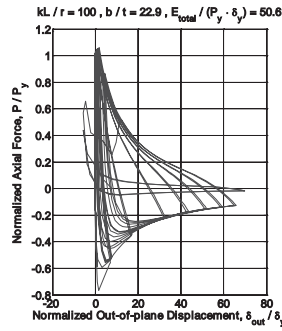
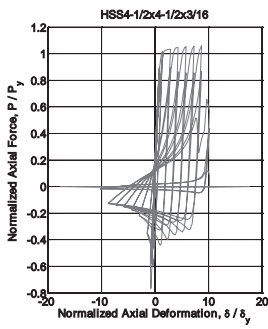
HSS 4-1/2 x 4-1/2 x 1/2 ( $kL/r = 100$ )

HSS 4-1/2 x 4-1/2 x 3/8 ( $kL/r = 100$ )



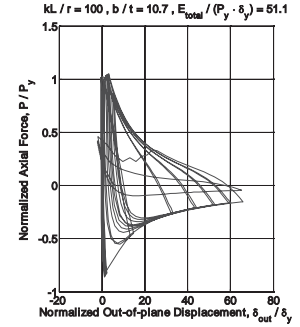
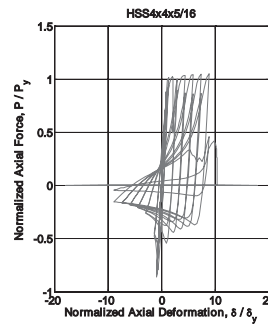
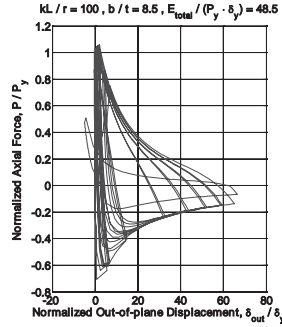
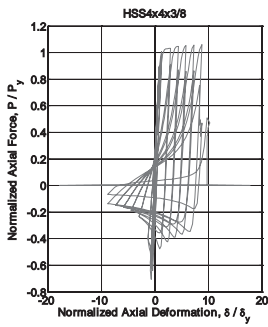
HSS 4-1/2 x 4-1/2 x 5/16 (kL/r = 100)

HSS 4-1/2 x 4-1/2 x 1/4 (kL/r = 100)



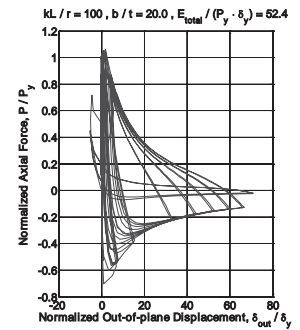
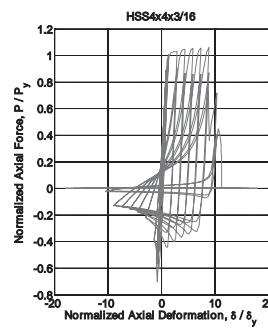
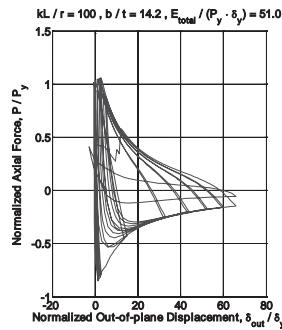
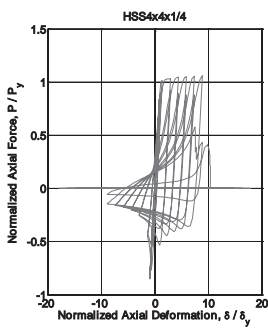
HSS 4-1/2 x 4-1/2 x 3/16 (kL/r = 100)

HSS 4 x 4 x 1/2 (kL/r = 100)



HSS 4 x 4 x 3/8 (kL/r = 100)

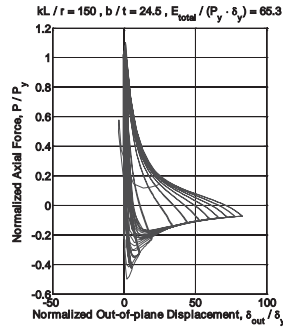
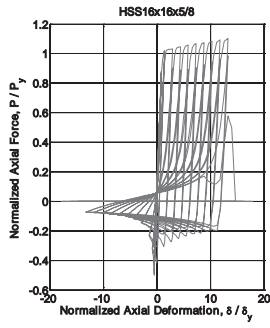
HSS 4 x 4 x 5/16 (kL/r = 100)



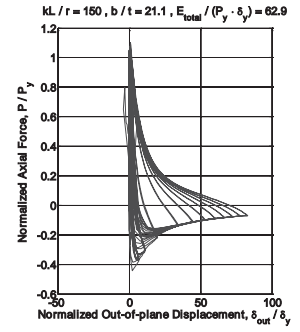
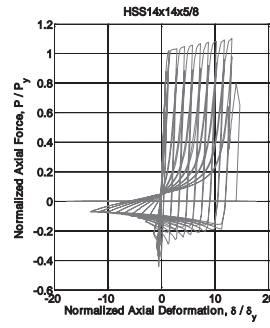
HSS 4 x 4 x 1/4 (kL/r = 100)

HSS 4 x 4 x 3/16 (kL/r = 100)

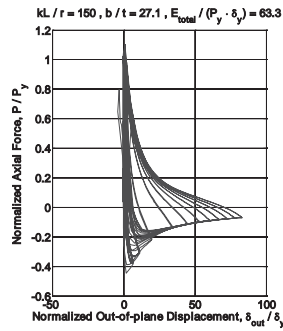
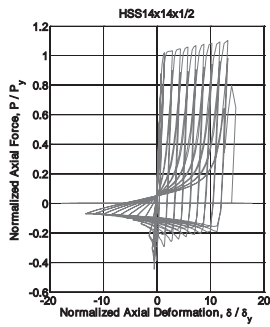
**(e)  $kL/r = 150$**



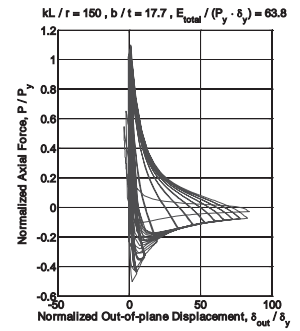
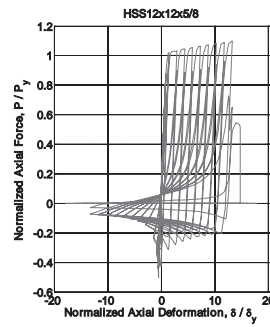
HSS 16 x 16 x 5/8 ( $kL/r = 150$ )



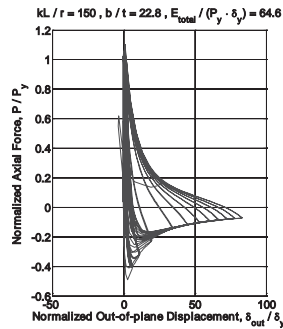
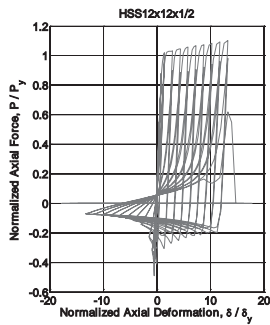
HSS 14 x 14 x 5/8 ( $kL/r = 150$ )



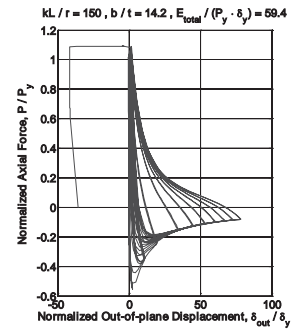
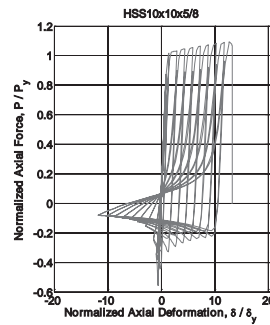
HSS 14 x 14 x 1/2 ( $kL/r = 150$ )



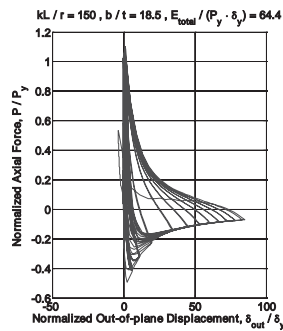
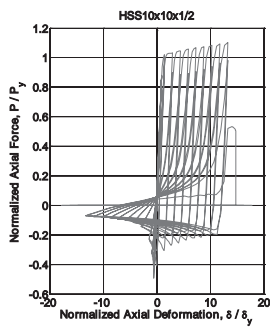
HSS 12 x 12 x 5/8 ( $kL/r = 150$ )



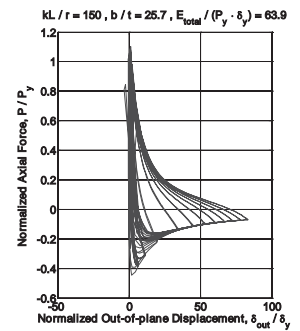
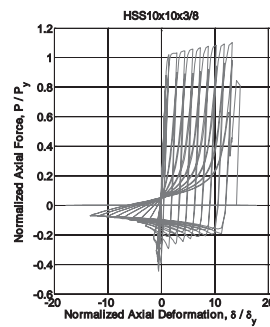
HSS 12 x 12 x 1/2 ( $kL/r = 150$ )



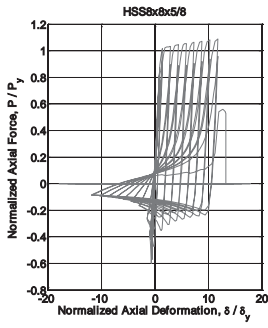
HSS 10 x 10 x 5/8 ( $kL/r = 150$ )



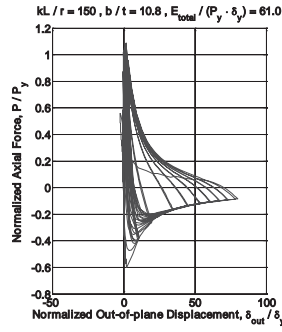
HSS 10 x 10 x 1/2 ( $kL/r = 150$ )



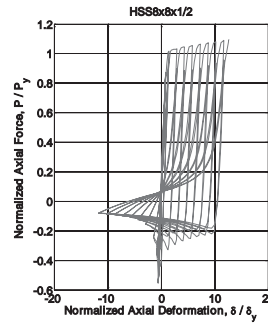
HSS 10 x 10 x 3/8 ( $kL/r = 150$ )



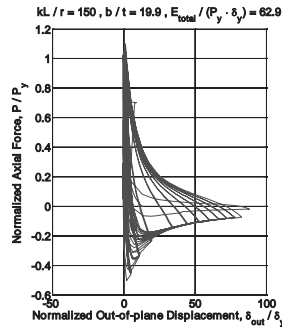
HSS 8 x 8 x 5/8 ( $kL/r = 150$ )



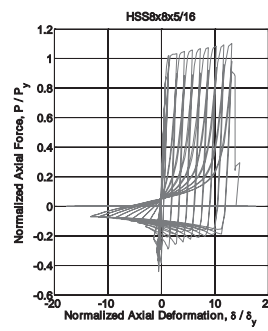
HSS 8 x 8 x 1/2 ( $kL/r = 150$ )



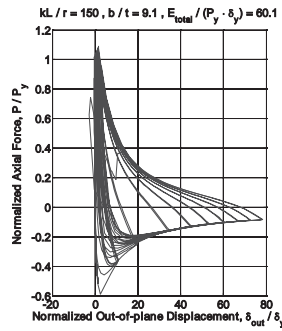
HSS 8 x 8 x 3/8 ( $kL/r = 150$ )



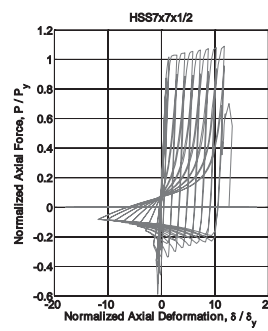
HSS 8 x 8 x 5/16 ( $kL/r = 150$ )



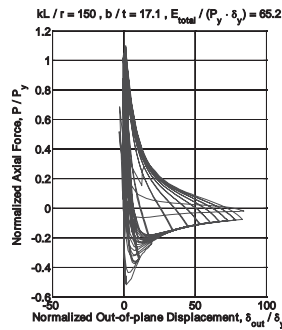
HSS 7 x 7 x 5/8 ( $kL/r = 150$ )



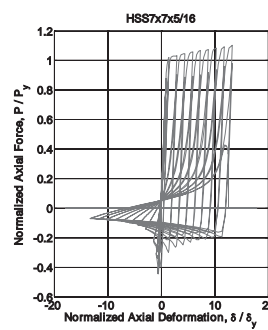
HSS 7 x 7 x 1/2 ( $kL/r = 150$ )

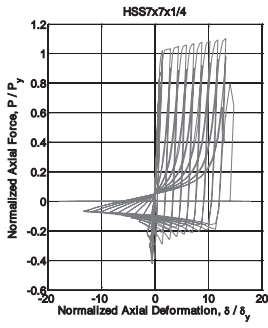


HSS 7 x 7 x 3/8 ( $kL/r = 150$ )

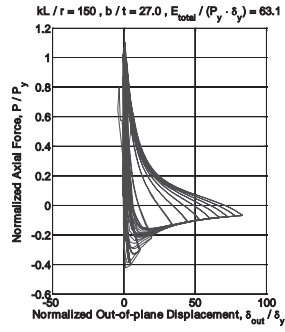


HSS 7 x 7 x 5/16 ( $kL/r = 150$ )

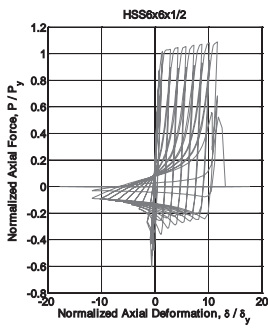
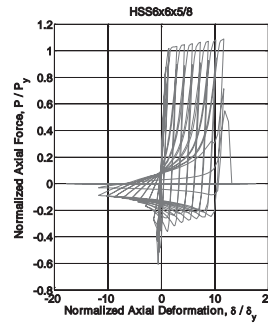




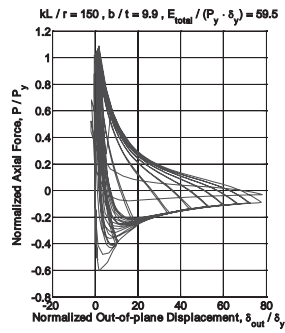
HSS 7 x 7 x 1/4 ( $kL/r = 150$ )



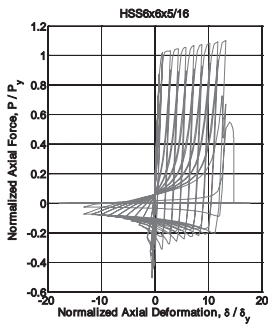
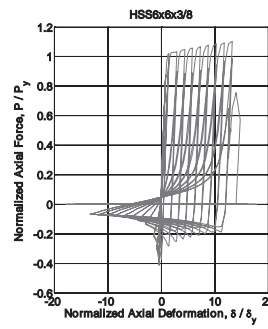
HSS 6 x 6 x 5/8 ( $kL/r = 150$ )



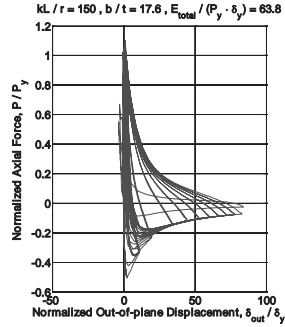
HSS 6 x 6 x 1/2 ( $kL/r = 150$ )



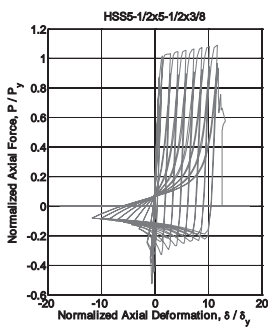
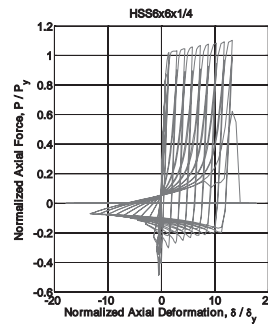
HSS 6 x 6 x 3/8 ( $kL/r = 150$ )



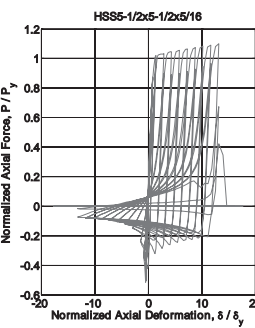
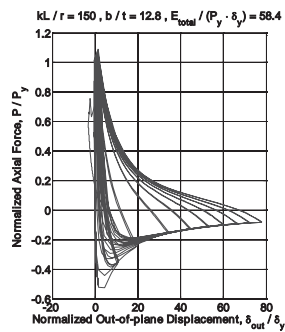
HSS 6 x 6 x 5/16 ( $kL/r = 150$ )



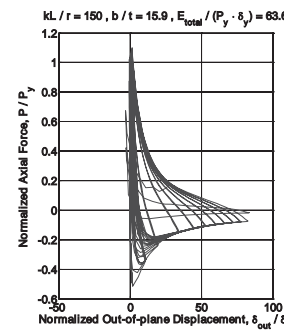
HSS 6 x 6 x 1/4 ( $kL/r = 150$ )



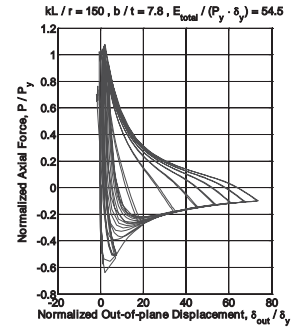
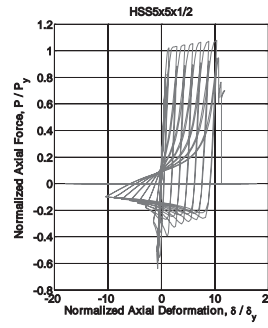
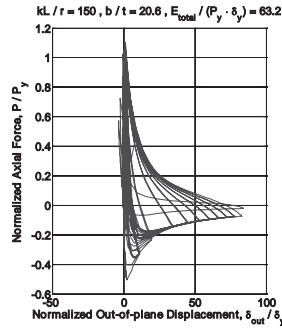
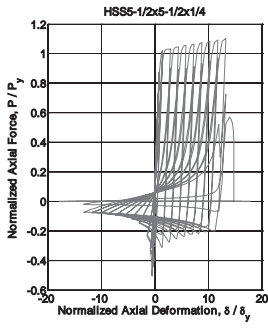
HSS 5-1/2 x 5-1/2 x 3/8 ( $kL/r = 150$ )



HSS 5-1/2 x 5-1/2 x 3/8 ( $kL/r = 150$ )

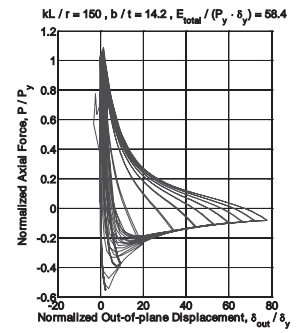
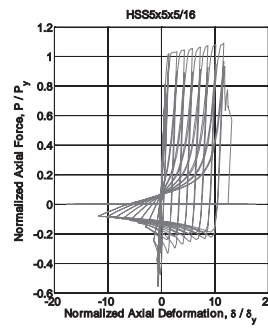
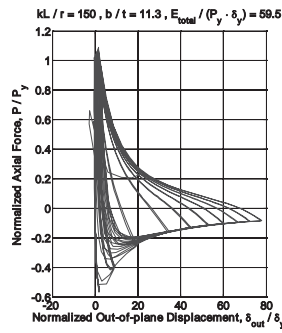
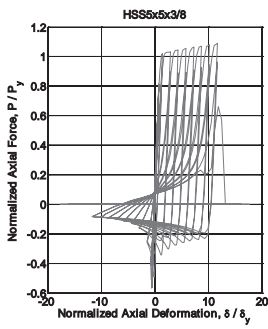






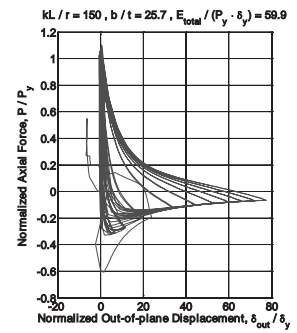
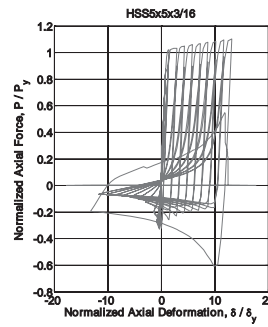
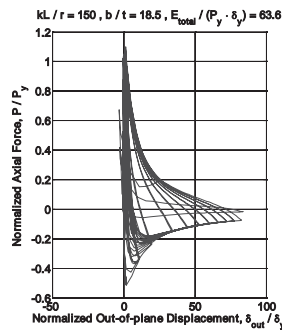
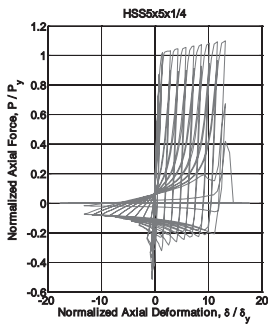
HSS 5-1/2 x 5-1/2 x 1/4 ( $kL/r = 150$ )

HSS 5 x 5 x 1/2 ( $kL/r = 150$ )



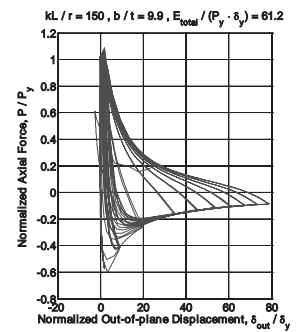
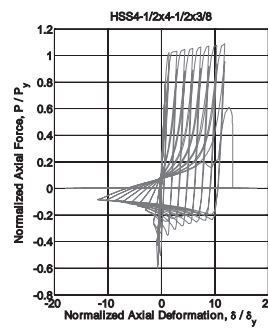
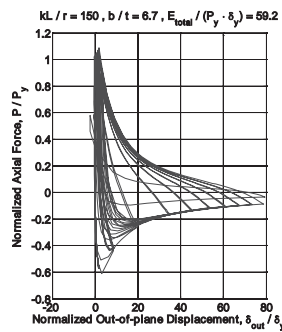
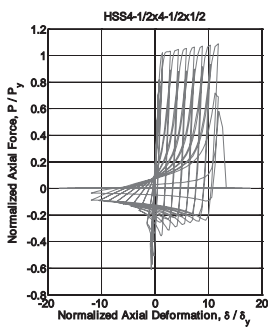
HSS 5 x 5 x 3/8 ( $kL/r = 150$ )

HSS 5 x 5 x 5/16 ( $kL/r = 150$ )



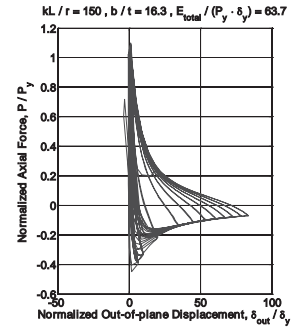
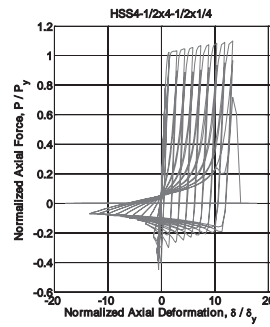
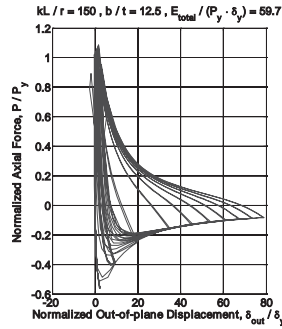
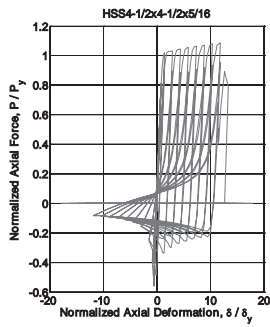
HSS 5 x 5 x 1/4 ( $kL/r = 150$ )

HSS 5 x 5 x 3/16 ( $kL/r = 150$ )



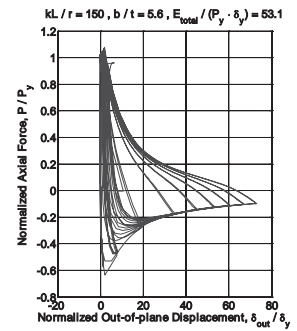
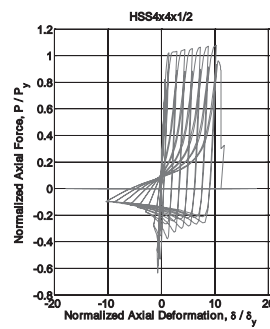
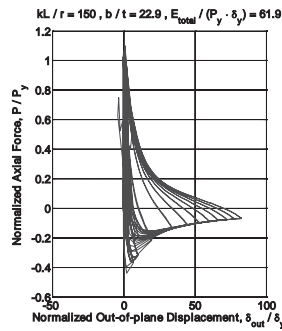
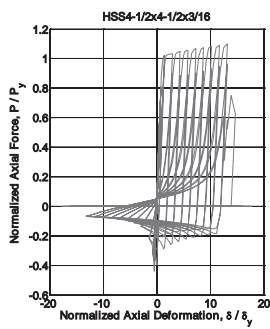
HSS 4-1/2 x 4-1/2 x 1/2 ( $kL/r = 150$ )

HSS 4-1/2 x 4-1/2 x 3/8 ( $kL/r = 150$ )



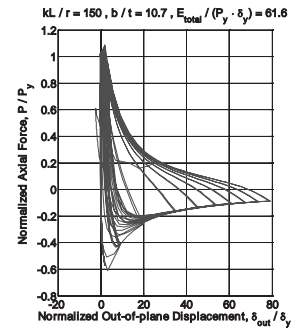
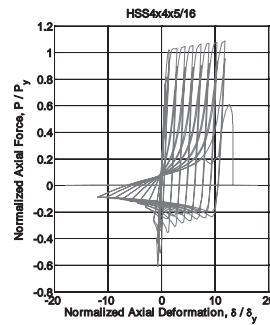
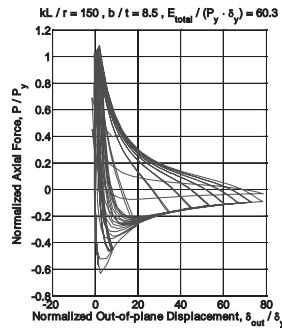
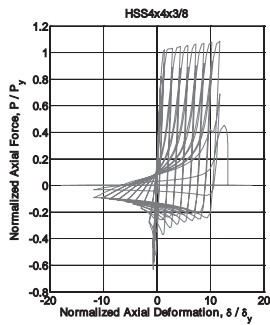
HSS 4-1/2 x 4-1/2 x 5/16 ( $kL/r = 150$ )

HSS 4-1/2 x 4-1/2 x 1/4 ( $kL/r = 150$ )



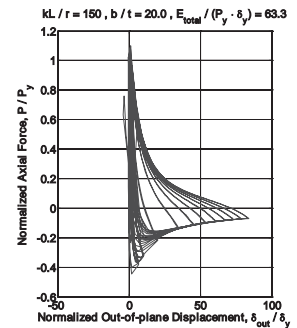
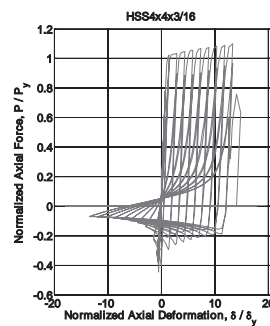
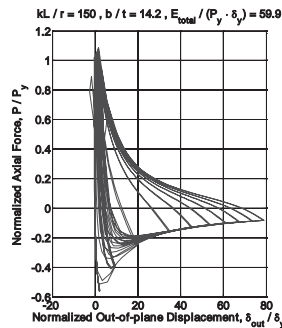
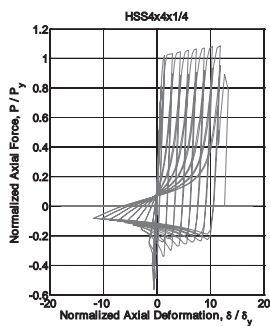
HSS 4-1/2 x 4-1/2 x 3/16 ( $kL/r = 150$ )

HSS 4 x 4 x 1/2 ( $kL/r = 150$ )



HSS 4 x 4 x 3/8 ( $kL/r = 150$ )

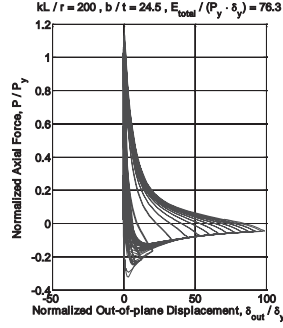
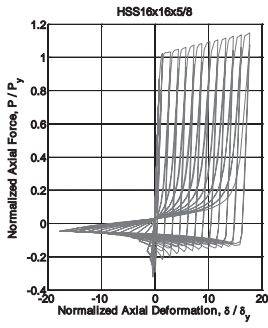
HSS 4 x 4 x 5/16 ( $kL/r = 150$ )



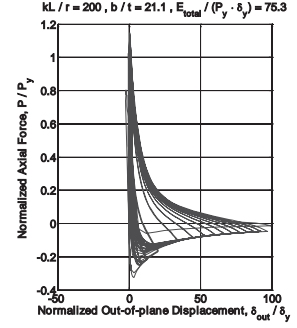
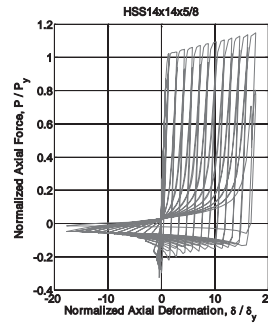
HSS 4 x 4 x 1/4 ( $kL/r = 150$ )

HSS 4 x 4 x 3/16 ( $kL/r = 150$ )

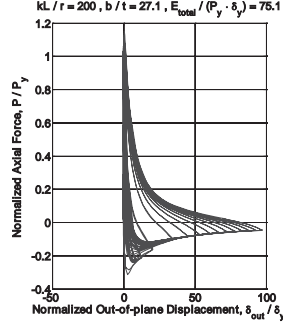
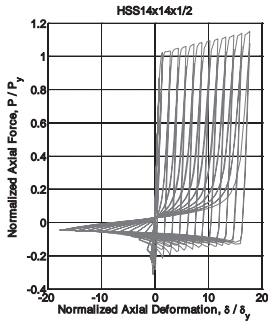
**(f)  $kL/r = 200$**



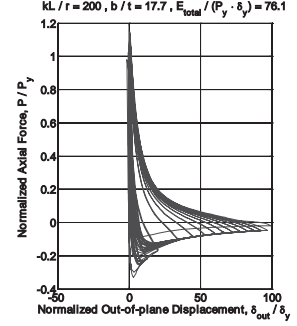
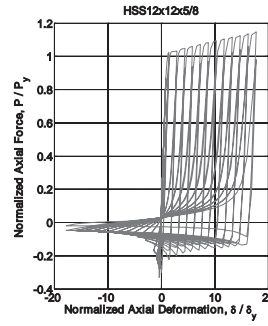
HSS 16 x 16 x 5/8 ( $kL/r = 200$ )



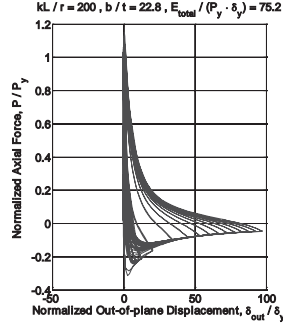
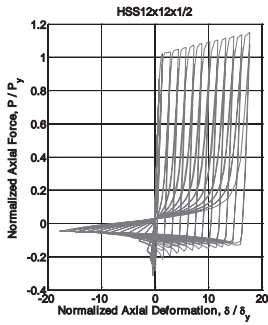
HSS 14 x 14 x 5/8 ( $kL/r = 200$ )



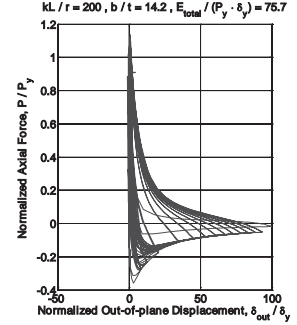
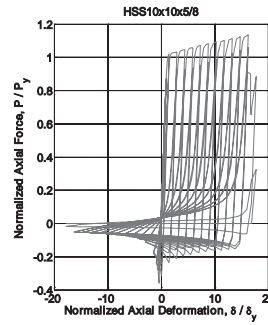
HSS 14 x 14 x 1/2 ( $kL/r = 200$ )



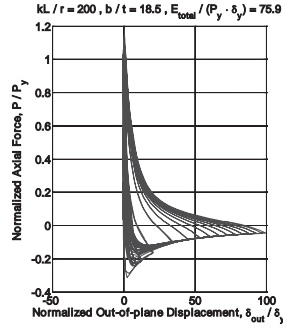
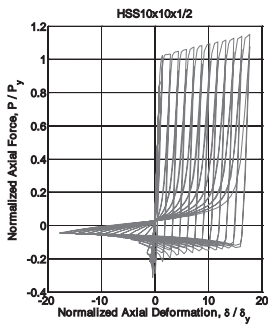
HSS 12 x 12 x 5/8 ( $kL/r = 200$ )



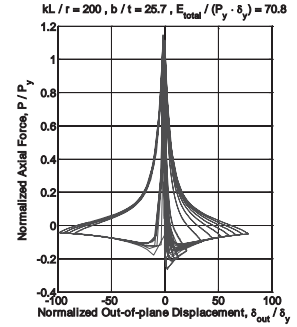
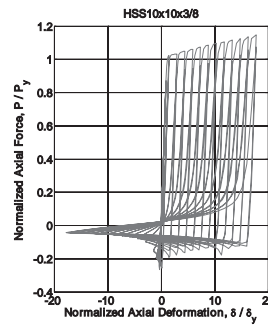
HSS 12 x 12 x 1/2 ( $kL/r = 200$ )



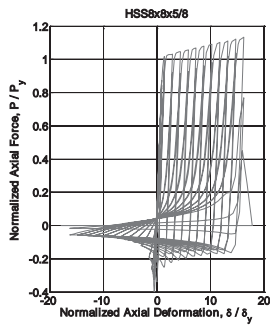
HSS 10 x 10 x 5/8 ( $kL/r = 200$ )



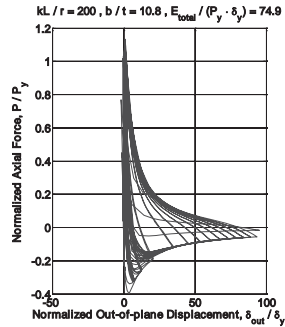
HSS 10 x 10 x 1/2 ( $kL/r = 200$ )



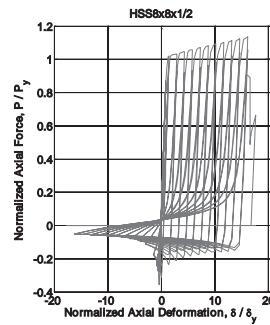
HSS 10 x 10 x 3/8 ( $kL/r = 200$ )



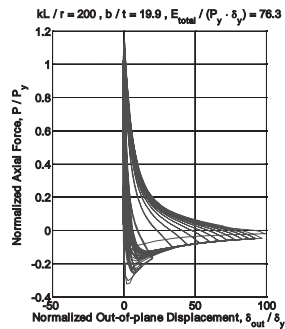
HSS 8 x 8 x 5/8 (kL/r = 200)



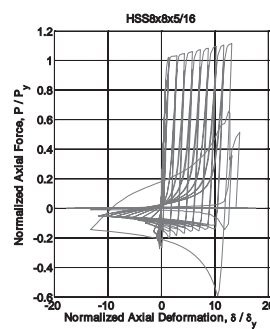
HSS 8 x 8 x 1/2 (kL/r = 200)



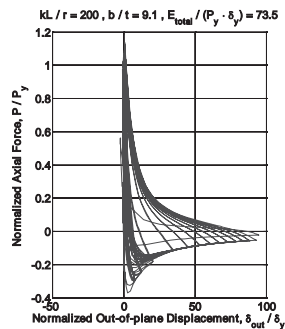
HSS 8 x 8 x 3/8 (kL/r = 200)



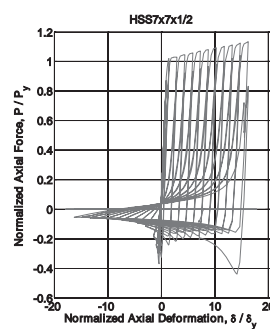
HSS 8 x 8 x 5/16 (kL/r = 200)



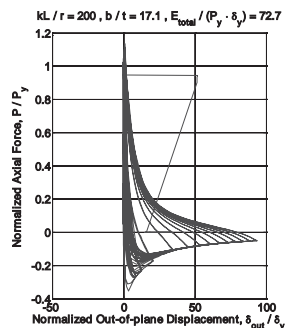
HSS 7 x 7 x 5/8 (kL/r = 200)



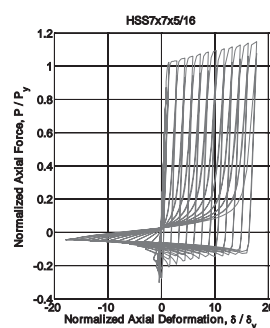
HSS 7 x 7 x 1/2 (kL/r = 200)

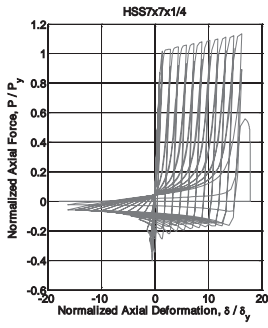


HSS 7 x 7 x 3/8 (kL/r = 200)

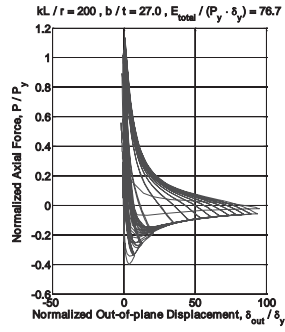


HSS 7 x 7 x 5/16 (kL/r = 200)

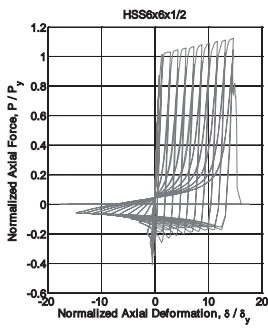
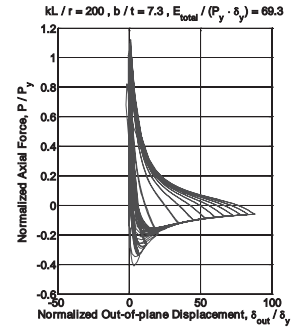
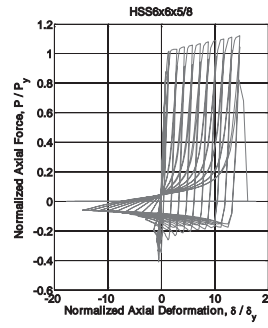




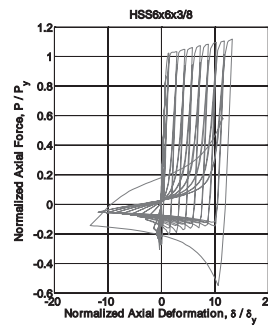
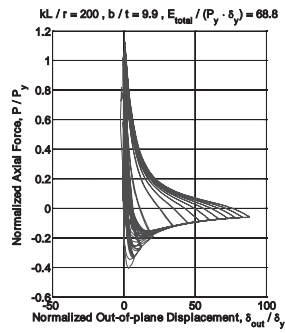
HSS 7 x 7 x 1/4 (kL/r = 200)



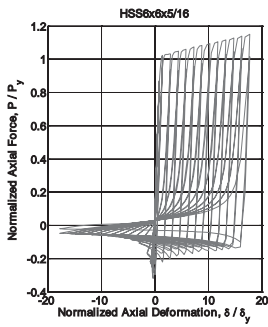
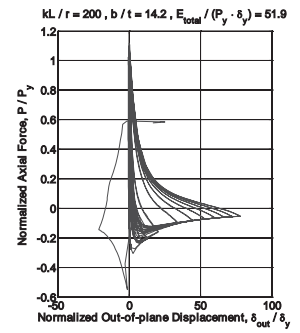
HSS 6 x 6 x 5/8 (kL/r = 200)



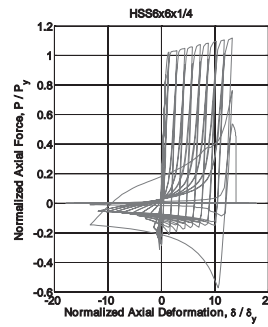
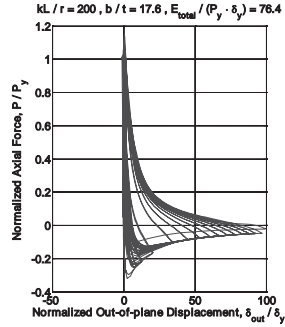
HSS 6 x 6 x 1/2 (kL/r = 200)



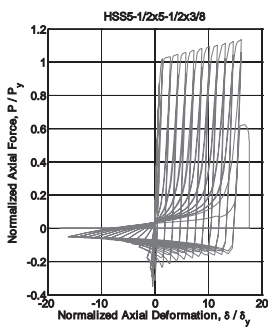
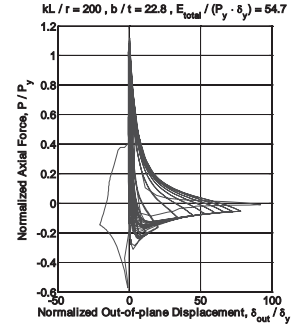
HSS 6 x 6 x 3/8 (kL/r = 200)



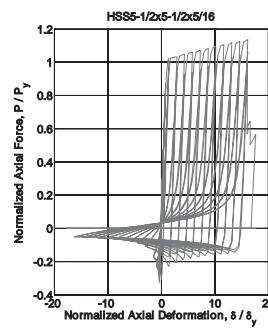
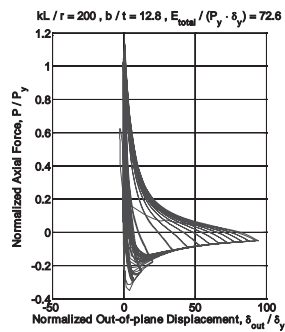
HSS 6 x 6 x 5/16 (kL/r = 200)



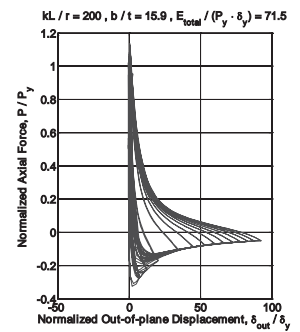
HSS 6 x 6 x 1/4 (kL/r = 200)

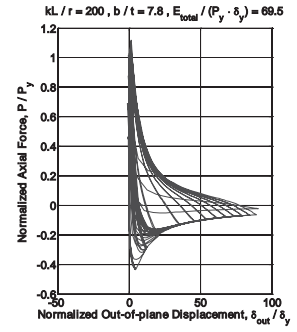
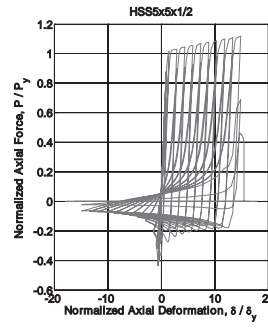
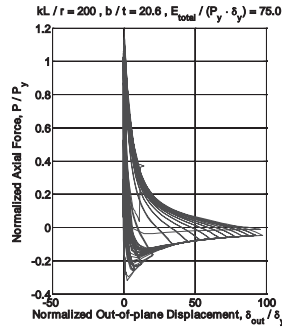
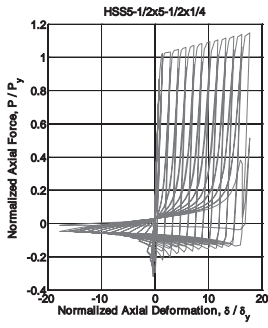


HSS 5-1/2 x 5-1/2 x 3/8 (kL/r = 200)



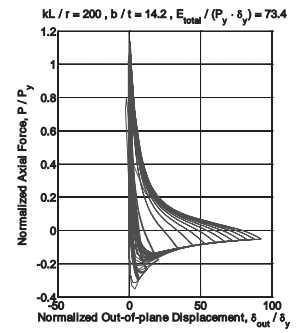
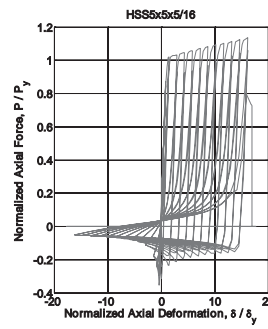
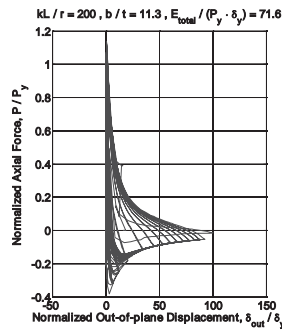
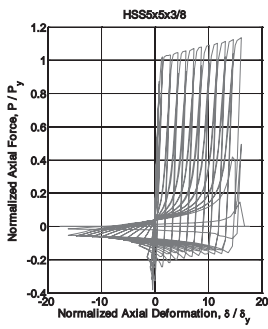
HSS 5-1/2 x 5-1/2 x 5/16 (kL/r = 200)





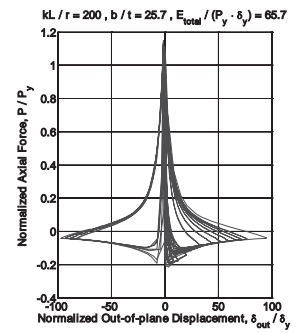
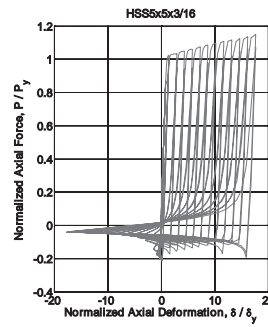
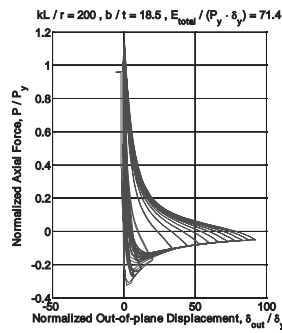
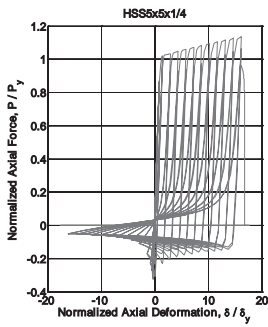
HSS 5-1/2 x 5-1/2 x 1/4 ( $kl/r = 200$ )

HSS 5 x 5 x 1/2 ( $kl/r = 200$ )



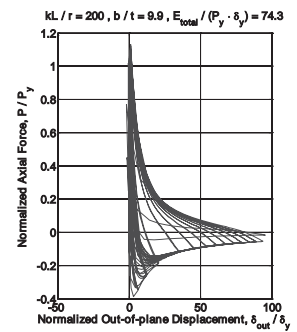
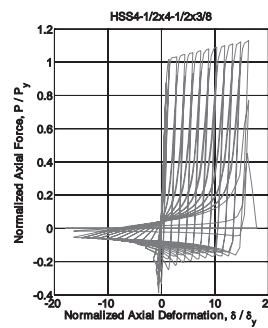
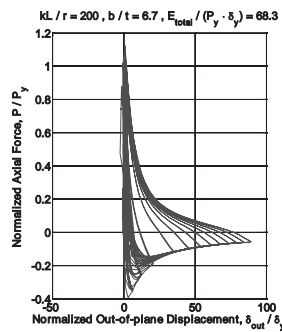
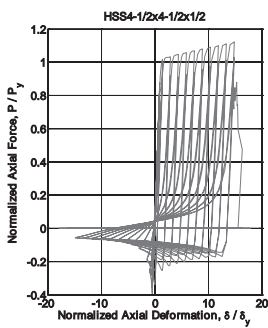
HSS 5 x 5 x 3/8 ( $kl/r = 200$ )

HSS 5 x 5 x 5/16 ( $kl/r = 200$ )



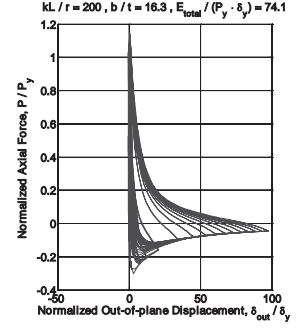
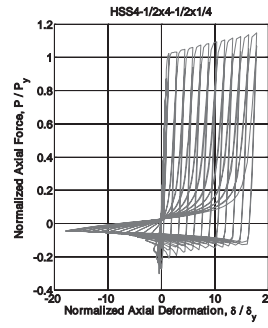
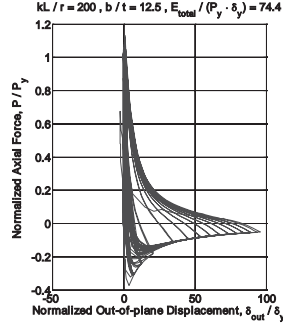
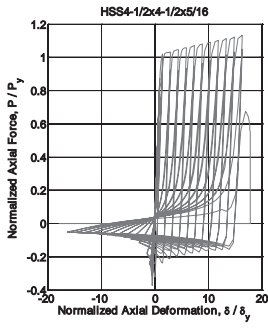
HSS 5 x 5 x 1/4 ( $kl/r = 200$ )

HSS 5 x 5 x 3/16 ( $kl/r = 200$ )



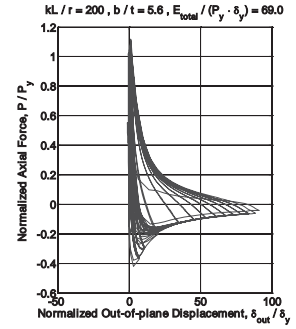
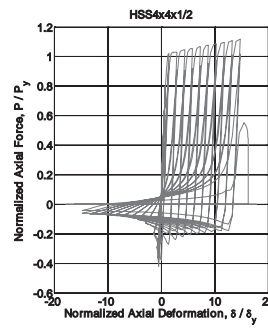
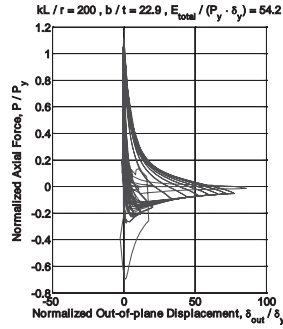
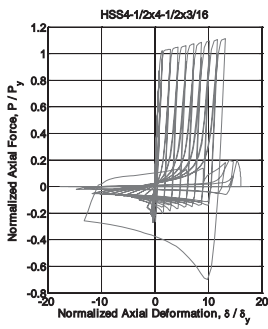
HSS 4-1/2 x 4-1/2 x 1/2 ( $kl/r = 200$ )

HSS 4-1/2 x 4-1/2 x 3/8 ( $kl/r = 200$ )



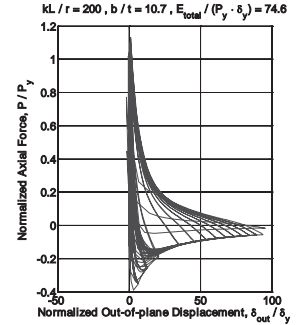
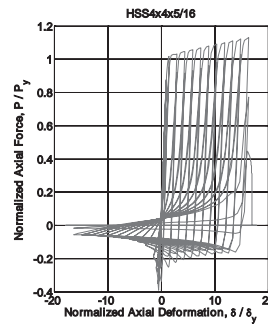
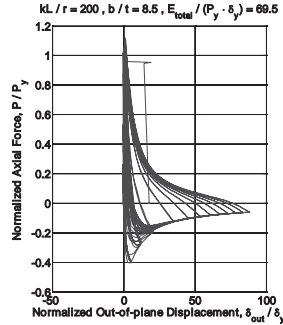
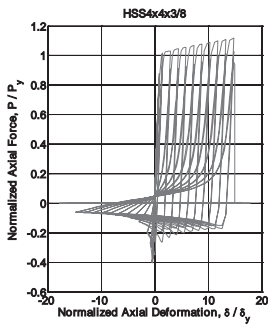
HSS 4-1/2 x 4-1/2 x 5/16 ( $kL/r = 200$ )

HSS 4-1/2 x 4-1/2 x 1/4 ( $kL/r = 200$ )



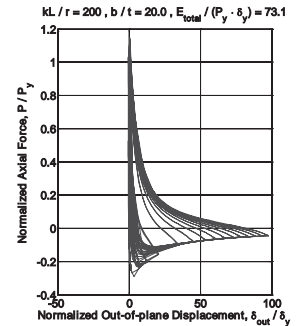
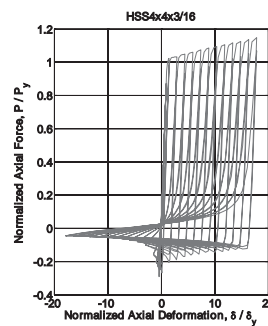
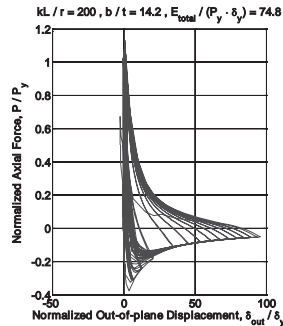
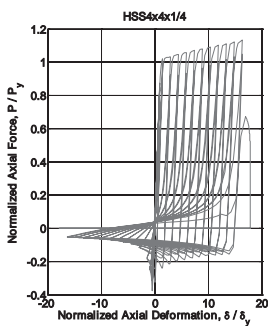
HSS 4-1/2 x 4-1/2 x 3/16 ( $kL/r = 200$ )

HSS 4 x 4 x 1/2 ( $kL/r = 200$ )



HSS 4 x 4 x 3/8 ( $kL/r = 200$ )

HSS 4 x 4 x 5/16 ( $kL/r = 200$ )



HSS 4 x 4 x 1/4 ( $kL/r = 200$ )

HSS 4 x 4 x 3/16 ( $kL/r = 200$ )